THE TECHNOLOGY OF ARTIFICIAL LIFT METHODS

Volume 4

Production Optimization
of Oil and Gas Wells
by Nodal* Systems Analysis

Kermit E. Brown

The University of Tulsa

contributing authors

Pudjo Sukarno
Jim Lea
Zelimir Schmidt
Dale R. Doty
Carl Granger
Lewis Ledlow
Joe Mach
Eduardo Proaño
A. Paul Szilas
Bashir Agena
Bob Tighe
Roberto Aguilera
Lewis Acevedo

* Mark of Flopetrol-Johnston-Schlumberger. Used in title and throughout this text with the express permission of Flopetrol-Johnston-Schlumberger.

PennWell Books
PennWell Publishing Company
Tulsa, Oklahoma

PennWell Publishing Company
1421 South Sheridan Road/P.O. Box 1260
Tulsa, Oklahoma, 74101

Library of Congress cataloging in publication data
(Revised for volume 4)

Brown, Kermit E.
The technology of artificial lift methods.

Includes bibliographical references and index.
CONTENTS: v. 1. Inflow performance, multiphase flow in pipes, the flowing well.—v. 2a. Introduction of artificial lift systems beam pumping.—[etc.]—v. 4. Production optimization of oil and gas wells by nodal systems analysis.
1. Oil wells—Artificial lift. 2. Pipe—Fluid dynamics. I. Title.

TN871.B819 622'.338 76-53201
ISBN 0-87814-031-X (v. 1)

Printed in the United States of America

3 4 5 88 87 86

Dedication

This book is dedicated to my mother, Mary Grossman Brown, and my father, John Wesley Brown. They have left this earth for their life beyond, and it will be a joyous time when I see them again. "Eye hath not seen, nor ear heard, neither have entered into the heart of man, the things which God has prepared for those that love Him." I Corinthians 2:9

Contents

Dedication v
Preface xv
Chapter 1 **Introduction, by Kermit E. Brown 1**

Chapter 2 **Inflow performance, by Pudjo Sukarno and Jim Lea 5**

2.1 Introduction 5

2.2 Inflow equations 5
2.21 Single-phase liquid flow (closed outer boundary and $\overline{P}_r$ known) 5
2.211 Estimating productivity index from limited information 12
2.22 Two-phase flow in the reservoir 13
2.221 Introduction 13
2.222 Vogel's equation 13
2.223 Combination single-phase liquid and two-phase flow 14
2.224 Standing's procedure for flow efficiency not equal to 1.0 18
2.225 Couto's procedure for FE not equal to one 23
2.226 Three- or four-point tests 24
2.227 The composite IPR curves 30
2.2271 The calculation of the flowing bottom-hole pressure at certain total flow rates for the composite IPR curves 30
2.2272 Calculation of the total flow rate at certain flowing bottom-hole pressures for the composite IPR curve 32
2.2273 Preliminary calculations to construct the composite IPR curves from the test data 32
2.2274 The composite IPR curves for the reservoir pressure below the bubble-point pressure 33
2.23 Preparation of future IPR curves 36
2.231 Fetkovich procedure 36
2.232 Combination Fetkovich and Vogel procedure for the preparation of future IPR curves 37
2.233 Standing's procedure for predicting future IPR curves 38
2.234 Couto's procedure 39
2.235 Pivot point method 39
2.236 Other methods of constructing future IPR curves 43
2.24 Transient IPR curves for oil flow 43
2.241 States of flow in the reservoir 43

2.3 Inflow relationships for gas wells 50
2.31 Four-point test on gas wells 60
2.32 Transient IPR curves for gas wells 61

2.4 IPR curves for fractured wells 63
2.41 Determining the performance of tight gas wells 63
2.42 Type curve matching 63
2.421 Post-frac testing 64
2.43 General procedure 64
Inflow curves for tight-formation gas wells 65
2.44 IPR computations 67
2.45 Character of tubing curves 69

Summary 69

References 70

Chapter 3 **Multiphase flow in pipes, by Kermit E. Brown, Zelimir Schmidt, and Dale R. Doty 71**

3.1 Introduction 71

3.2 Vertical multiphase flow 73
3.21 The use of vertical multiphase flow gradient curves 75

3.3 Horizontal multiphase flow 75
3.31 Introduction 75
3.32 The use of horizontal multiphase flow gradient curves 75

3.4 Inclined flow 75
3.41 Introduction 75
3.42 Directionally drilled wells 75
3.421 Correlations for directionally drilled wells 78
3.43 Multiphase flow correlations for inclined flow lines 78

3.5 Flow-through restrictions 78
3.51 Surface chokes 78
3.511 Multiphase flow through a choke 78
3.512 Gas flow through a choke 78

3.6 Two-phase flow in pipelines 81
3.61 Introduction 81
3.62 Steady-state pressure loss calculations 81
3.63 Liquid flow behavior predictions 83

Summary 85

References 85

Chapter 4 **Nodal systems analysis, by Kermit E. Brown, Dale R. Doty, Carl Granger, Lewis Ledlow, Joe Mach, Eduardo Proaño, Zelimir Schmidt, and A. Paul Szilas 87**

4.1 Introduction 87

4.2 Solution procedure for oil wells 89
4.21 Introduction 89
4.22 Solution at bottom of well (node 6 from Figure 4.3) 89
4.221 Constructing the IPR curve 90
4.222 Flowing one zone up two conduits 91
4.23 Solution at top of well 92
4.231 Introduction 92
4.232 Step-by-step solution procedure (refer also to Reference 2) 93
4.233 Why use the wellhead as solution position 93
4.24 Combination solution at bottom and top of well 94
4.241 Introduction 94
4.242 Solution procedure 94
4.25 Solution node at the separator 95
4.251 Introduction 95
4.252 Solution procedure for constant PI case 96
4.253 Why use the separator as the solution node 97
4.26 Solution node at the average reservoir pressure ($\bar{P}_r$) (constant PI case) 98
4.261 Introduction 98
4.262 Solution procedure 98
4.263 Why use $\bar{P}_r$ as a solution position 99
4.27 Tapered strings 100
4.271 Introduction 100
4.272 Solution procedure 101
4.28 Functional nodes 102
4.281 Introduction 102
4.282 Surface wellhead chokes 102
4.2821 Introduction 102
4.2822 ΔP solution for wellhead surface chokes 103
4.28221 Introduction 103

4.283 Safety valves 104
4.2831 Introduction 104
4.2832 Design procedure for the velocity-actuated safety valve 105
4.2833 Design procedure for the pressure-operated safety valve 110
4.2834 Summary on safety valves 111

4.3 Injection wells 112
4.31 Water injection wells 112
4.311 Introduction 112
4.312 Design procedure for a standard water injection well 112
4.313 Effect of variables for a water injection well 114
4.32 Gas-injection wells 117

4.4 Nodal analysis as applied to gas wells 118
4.41 Introduction 118
4.42 Summary and other variables 122
4.43 Gas well loading 123

4.5 Nodal analysis applied to gravel-packed oil and gas wells 124
4.51 Sand control 124
4.511 Introduction 124
4.512 Definition of sand control 124
4.513 Methods of sand control 124
4.52 Sand-control design criteria 125
4.521 Gravel-pack design criteria 125
4.522 Formation sand consolidation 131
4.5221 Types of formation and consolidation systems 131
4.523 Resin sand slurries 131
4.53 Solution procedure 132
4.531 Completion pressure-drop equations 134
4.532 Method of analysis 134
4.54 Bringing a gravel-packed well on production 145

4.6 Nodal analysis applied to a standard perforated well 149
4.61 Introduction 149
4.62 Open perforation pressure drop (oil wells) 150

4.7 Special pipeline problems 159
4.71 Introduction 159
4.72 Liquid-related problems 159
4.73 Pressure-drop prediction 159
4.74 Pressure gradient options 159
4.75 Choke pressure-drop predictions 159
4.76 Fluid property options 160
4.77 Slug characteristics prediction 160
4.78 Pigging characteristics prediction 160
4.79 Example cases 161

4.8 Production optimization for a complete ocean-floor optimization 169
4.81 Introduction 169
4.82 Solution procedure 170
4.821 Introduction 170
4.822 Individual wells 171
4.823 Vertical riser 171
4.824 Horizontal flow line 173
4.825 Flow line from the manifold to the wellhead 173
4.826 Final solution 173
4.8261 Approximate simple and direct solution 173
4.8262 Rigorous solution 175

4.9 Applying production optimization to a complete field-integrated oil-production system 178
4.91 Introduction 178
4.92 The concept of the field-integrated oil-production system (FIOPS) 178
4.93 Determination of the target 180
4.94 Selection of the components of the system 180
4.95 Numerical simulation of the subsystems 181
4.96 The analysis and the optimization of the system 182

References 183

Chapter 5 **Artificial lift, by Bashir Agena and Kermit E. Brown 185**

5.1 Introduction 185

5.2 Preparation of tubing intake (node outflow) curves for artificial lift systems 189
5.21 Introduction 189
5.22 Setting pump off bottom 190
5.23 Gas lift 191
5.231 Sensitivity analysis 197
5.2311 Introduction 197
5.2312 Effect of flow-line size 197
5.2313 Effect of tubing size 197
5.2314 Effect of separator pressure 197
5.2315 Effect of casing pressure 197
5.2316 Effect of water cut 198
5.2317 Effect of differential pressure 198
5.2318 Effect of mandrel spacing 199

5.3 Electric submersible pumps 199
5.31 Description of equipment 199
5.32 Pump performance curves 200
5.33 Pump intake curves 202
5.331 Pumping liquid only 203
5.3311 Procedure for the preparation of tubing intake curves for liquid only 203
5.332 Pumping liquid gas 205
5.3321 Determination of the number of stages 205
5.3322 Determination of horsepower 205
5.3323 Pump selection 205
5.3324 Procedure for the preparation of intake curves for wells pumping gas 205

5.4 Hydraulic pumps 210
5.41 Description of equipment 210
5.42 Power fluid systems 210
5.43 Tubing arrangements 211
5.44 P/E ratio 211
5.45 Pump displacement 211
5.46 Engine displacement 212
5.47 Pump friction 212
5.48 Pressure calculations 212
5.49 Horsepower 212
5.491 Pump intake curves 212
5.4911 Introduction 212
5.4912 Procedure for the preparation of tubing intake curves for liquid only 213
5.4913 Pumping liquid and gas 216
5.4914 Procedure for preparation of tubing intake curves for pumping gas and liquid 217
5.4915 Discussion of results 219

5.5 Jet pumps 220
5.51 Description of equipment 220
5.52 Cavitation 221
5.53 Power fluid rate and pressure 222
5.54 Horsepower 223
5.55 Pump intake curves 223
5.551 Pumping liquid only 223
5.5511 Introduction 223
5.5512 Procedure for the preparation of tubing intake curves for the jet pump 223
5.552 Pumping liquid and gas 226
5.5521 Introduction 226
5.5522 Procedure for the preparation of tubing intake curves for jet pump (pumping gas) 227

5.6 Beam pumps 230
5.61 General description 230
5.62 Pump intake curves 234
5.621 Introduction 234
5.622 Procedure for the preparation of tubing intake curves for sucker-rod pumps (liquid only) 235
5.623 Preparation of tubing intake curves for wells pumping gas and liquid 238
5.63 Discussion of results—sucker-rod pumping 244

5.7 Summary of results and comparisons 244

References 248

Chapter 6 **Gas well loading, by J. F. Lea and R. E. Tighe 249**

6.1 Natural flow from gas wells restricted by liquid loading 249
6.11 Compositional classification of gas reservoirs 249
6.111 Dry gas phase diagram 250
6.112 Gas condensate phase diagram 250
6.113 Volatile oils 250
6.114 Black oil 250
6.115 Tubing performance 251
6.12 Liquid loading-unloading conditions for gas wells 251
6.121 Liquid loading conditions 251
6.122 Conditions for natural flow 251
6.123 Predicting well performance and liquid loading conditions using inflow, outflow, and tubing performance curves 252
6.1234 Reducing wellhead pressure 253
6.1235 Tubing size effects 254
6.124 Detection of liquid loading—BHP estimates 254
6.1241 Calculated bottom-hole pressure—static gas column 254
6.1242 Flowing bottom-hole pressure 256
6.13 Vertical multiphase flow correlations for producing gas wells 257
6.131 Gas condensate well pressure drop prediction 257
6.132 Black-oil multiphase flow correlations for gas wells 259
6.133 Simplified models for predicting minimum gas velocity for liquid removal 259
6.134 Summary and conclusions 261
6.14 Other miscellaneous flowing well considerations 261
6.141 Pressure and rate cycling in gas wells 261
6.142 Intermitting operations 262

6.2 Plunger lift 262
6.21 Introduction 262
6.22 The plunger-lift-cycle description 262
6.23 Selection of wells for application of plunger lift 264
6.24 Plunger lift design calculations 265
6.241 Design calculations 265
6.25 Plunger lift equipment considerations 268
6.251 Plungers 268
6.252 Lubricators 268
6.253 Cycle controls 269
6.254 Casing size 270
6.255 Tubing seating nipple and standing valve 270
6.256 Tubing size 271
6.257 Tubing landing depth 271
6.26 Well symptom analysis 271

6.3 Foam unloading of gas wells 272
6.31 Introduction 272
6.32 Liquid removal process 273
6.321 Unloading techniques 273
6.33 Foam application selection 274
6.34 General information on foams 275
6.341 Foam generation 275
6.342 Foam stability 275

6.343 Surfactant types 276
6.344 Foaming tendency and surfactant behavior in brine-condensate mixtures 277
6.3441 Effect of condensate (aromatic) fraction on foaming tendency 277
6.3442 Effect of brine on foam tendency 279
6.35 Equipment considerations 279
6.351 Chemical injection equipment 279
6.352 Tubular goods sizing and landing position 279
6.353 Separation equipment 279
6.354 Instrumentation 280
6.36 Operating considerations 280
6.361 Surfactant selection 280
6.362 Well pressure cycling 280
6.363 Kicking off flow with surfactants 280
6.364 Chemical treatment problems 280

6.4 Other forms of assisted natural gas lift 281
6.41 Siphon-string gas-lift system 281
6.411 Cycle description 281
6.412 Applications 281
6.413 Design considerations 281
6.42 Subsurface liquid diverter—gas-lift system 282
6.421 Cycle description 282
6.422 Applications 283
6.423 Design considerations 284
6.43 Closed rotative gas-lift system 284
6.431 Cycle description 285
6.432 Application 285
6.433 Design considerations 285

6.5 Pumping methods 287
6.51 Introduction 287
6.52 Application guidelines for pumping systems 287
6.53 Rod pumps 288
6.531 Beam pumping units 288
6.532 Pneumatic pumping units 289
6.533 Hydraulic rod pumping units 289
6.54 Hydraulic jet pumps 290
6.55 Electric submersible pumps 292

References 293

Chapter 7 **Coning and fingering of water and gas, by Roberto Aguilera and Luis Acevedo 295**

7.1 Water and gas coning 295
7.11 Stable and unstable cones 295
7.12 Critical production rate 295
7.13 Coning in homogeneous reserves 295
7.131 Muskat and Arthur methods 295
7.132 Meyer and Gardner and Pirson methods 299
7.133 Craft and Hawkins method 301
7.134 Chaney et al. method 301
7.14 Coning in anisotropic reservoirs 306
7.141 Coning of gas and water 306
7.142 Chierici et al. method 306
7.143 Sobocinsky and Cornelius method 310
7.15 Water and gas coning in fractured reservoirs 312
7.151 Birks method 312
7.16 Remedial treatments for coning 316
7.161 Reduction of production rate 317
7.162 Infill drilling 317
7.163 Improvement of well productivity 317
7.164 Recompletions 317
7.165 Stop cocking 318
7.166 Oil injection 318
7.167 Artificial barriers 318

7.2 Water and gas fingering 318
7.21 Fingering in homogeneous reservoirs 319
7.211 Arthur method 319
7.212 Pirson method 320
7.22 Viscous fingering in water drives 320
7.221 Fingering in anisotropic reservoirs 321

References 327

Appendix 2.1 Working graphs 329

Appendix 4.1 Horizontal flowing pressure gradients 337

Appendix 4.2 Vertical flowing pressure gradients 365

Appendix 4.3 Design criteria for selecting velocity type subsurface safety valves 405

Appendix 4.4 Vertical injection pressure gradients 407

Appendix 4.5 Vertical flowing gas injection gradients 413

Appendix 4.6 Vertical flowing gas production gradients 417

Appendix 4.7 Equation summary 425

Appendix 4.8 Working graphs 429

Appendix 5.1 Calculation data 433

Index 443

Preface

Now we have Volume 4 (book 6) of *The Technology of Artificial Lift Methods*. This book, entitled "Production Optimization of Oil and Gas Wells by Nodal Systems Analysis," presents the latest material in order to properly design and optimize the flowing or artificial lift oil and gas wells. Starting from the separator, this involves the evaluation of each component in a production system, including the flow line, choke, tubing safety valve, downhole restrictions, artificial lift method, completion procedures (open-hole, standard perforations, or gravel-pack), well productivity, and average reservoir pressure. Future reservoir performance as well as channeling and coning are included. Numerous explanations and detailed examples explain each of these components. All components are then combined in order to optimize the system.

Total system examples such as ocean-floor completions are included. I have relied heavily on previously published work and want to thank the various societies and petroleum publishing companies as well as many individuals for permission to use their materials.

This book is the work of many authors, and I would like to thank each one individually for his contribution. I also want to thank the various companies that were willing to relinquish time to these authors. The following is a list of the various authors, the chapter that they wrote in full, or on which they assisted, and their respective companies.

Chapter 2—Inflow Performance
- Mr. Pudjo Sukarno, Ph.D. candidate, University of Tulsa
- Dr. Jim Lea, Amoco Production Research

Chapter 3—Multiphase Flow in Pipes
- Dr. Zelimir Schmidt, University of Tulsa
- Dr. Dale R. Doty, University of Tulsa

Chapter 4—Nodal Systems Analysis
- Dr. Dale R. Doty, University of Tulsa
- Mr. Carl Granger, Flopetrol-Johnston/ Schlumberger
- Mr. Lewis Ledlow, Conoco
- Mr. Joe Mach, Flopetrol-Johnston/ Schlumberger
- Mr. Eduardo Proaño, Flopetrol-Johnston/ Schlumberger
- Dr. Zelimir Schmidt, University of Tulsa
- Dr. A. Paul Szilas, University of Miskolc (Hungary)

Chapter 5—Artificial Lift
- Mr. Bashir Agena, Ph.D. candidate, University of Tulsa

Chapter 6—Gas Well Loading
- Dr. Jim Lea, Amoco Production Research
- Mr. Bob Tighe, Amoco Production Research

Chapter 7—Coning and Fingering of Water
- Dr. Roberto Aguilera, Consultants Ltd.
- Mr. Luis Acevedo, Consultants Ltd.

I also wish to acknowledge help received from Dr. Himanta Murkejee, for preparing the sensitivity plots on gas lift for Chapter 5; Betty Finnegan and Nelda Whipple, for assistance in typing; and Laura Passiglia, for her fine drafting work.

Sufficient pressure traverse curves are included in the appendices to work all the examples and class problems. Additional curves to cover practically any well in the world are found in Volumes 3a and 3b. Details on multiphase flow can be found in Volume 1, and all artificial lift methods can be found in Volumes 2a and 2b. Therefore, this text is not intended to replace any of the other books in this series but will stand on its own as a university textbook on production optimization or as a textbook for the practicing petroleum engineer.

Whew! This should be enough! I am now considering a novel and will try to crack the bestseller list. I have the plot, but not the time.

Thanks are due to my family and, in particular, to Katherine (my life-long traveling companion), for their encouragement, patience, and love.

Obviously, there is other material that should be included, but as the late Dr. Carl Gatlin said, "He who waits to include all up-to-date material in a book never publishes a book."

Thanks to all of you at PennWell for a job well done.

Kermit E. Brown

Chapter 1

Introduction

by Kermit Brown

The objective of this book is to set out the procedures for optimizing production from oil or gas wells. This is accomplished through a procedure known as Nodal Systems Analysis, sometimes called production systems analysis or production optimization. What does this mean? It is a procedure for determining that flow rate at which an oil or gas well will produce and then for evaluating the effect of various components, such as the tubing-string size, flow-line size, separator pressure, choke sites, safety valves, downhole restrictions, and well completion techniques including gravel packs and standard perforated wells. These components are then combined to optimize the entire system to obtain the most efficient objective flow rate. Each component is evaluated separately; then the entire system is combined to optimize the system effectively (Figures 1.1 and 1.2).

Many production systems are presently operating inefficiently; therefore, most can be improved significantly by careful analysis. It is not unusual to find flow lines that are too small and tubing sizes that are too large or too small. Also, many operators do not properly account for the severe heading or slugging that can occur in large flow lines. The frequency and size of large liquid slugs with followup slugs of gas can cause severe problems at the separation site. Ocean floor completions are extremely critical due to the very high costs to change tubing sizes or flow lines. Long flow lines laid on the ocean floor are almost prohibitive to replace; therefore, initial diameters must be correct. Also, the prediction of slug sizes and frequency of slugs is absolutely necessary in order to design separators and slug catchers properly.

In solving for the flow rates, the solution position can be taken at various nodes (locations), such as the bottom of the well, the top of the well, or the separator. The solution position is changed in order to illustrate the effect of certain components of the entire producing system. For example, if it is desirable to isolate the reservoir component, a node at the bottom of the hole is selected and the solution is taken at that position. A top-hole solution allows the flow line to be isolated and easily illustrates the effect of a change in flow-line size. The effect of a change in separator pressure can be illustrated by taking the solution point at the separator; then the separator pressure can be optimized based on possible compressor installations to elevate the gas pressure for sales or for rotative gas-lift systems.

Numerous operators immediately think in terms of *compression ratio* only when sizing compressors, which can cause a serious error in judgment especially in gas-lift operations. It is wise to remember that compressor horsepower is a function of both compression ratio and gas rate. Therefore, any increase in separator pressure—which controls compressor suction pressure—in order to decrease the compression ratio must be weighed against the decrease in production rate for the same gas volume or against additional gas volume required in order to maintain the same rate. Generally, an increase in separator pressure for the purpose of reducing the compression ratio will increase total compressor horsepower due to the additional gas volume needed to maintain the same flow rate.

An operator may intuitively decide to lower the separator pressure to increase the flow rate and later find that the rate did not change. Therefore, the producing system is restricted in some other component such as the flow line or tubing string. The importance of evaluating each component is very critical.

The decision to use wellhead separation as compared to separation of liquids and gas at a distant battery or separation point can be critical. For high productivity wells, any lowering of the wellhead pressure can materially increase the production rate. This change in rate can be approximated by taking 75% of the product of the change in wellhead pressure and productivity index. For example, a change in wellhead pressure from 300 to 100 psi for a well with a PI of 5 is (200)(5.0)(0.75), or 750 b/d.

Presently numerous completions have the option of laying one flow line to bring gas and liquid together to the separation facilities as compared to two separate lines—one for the liquid and one for the gas. The pres-

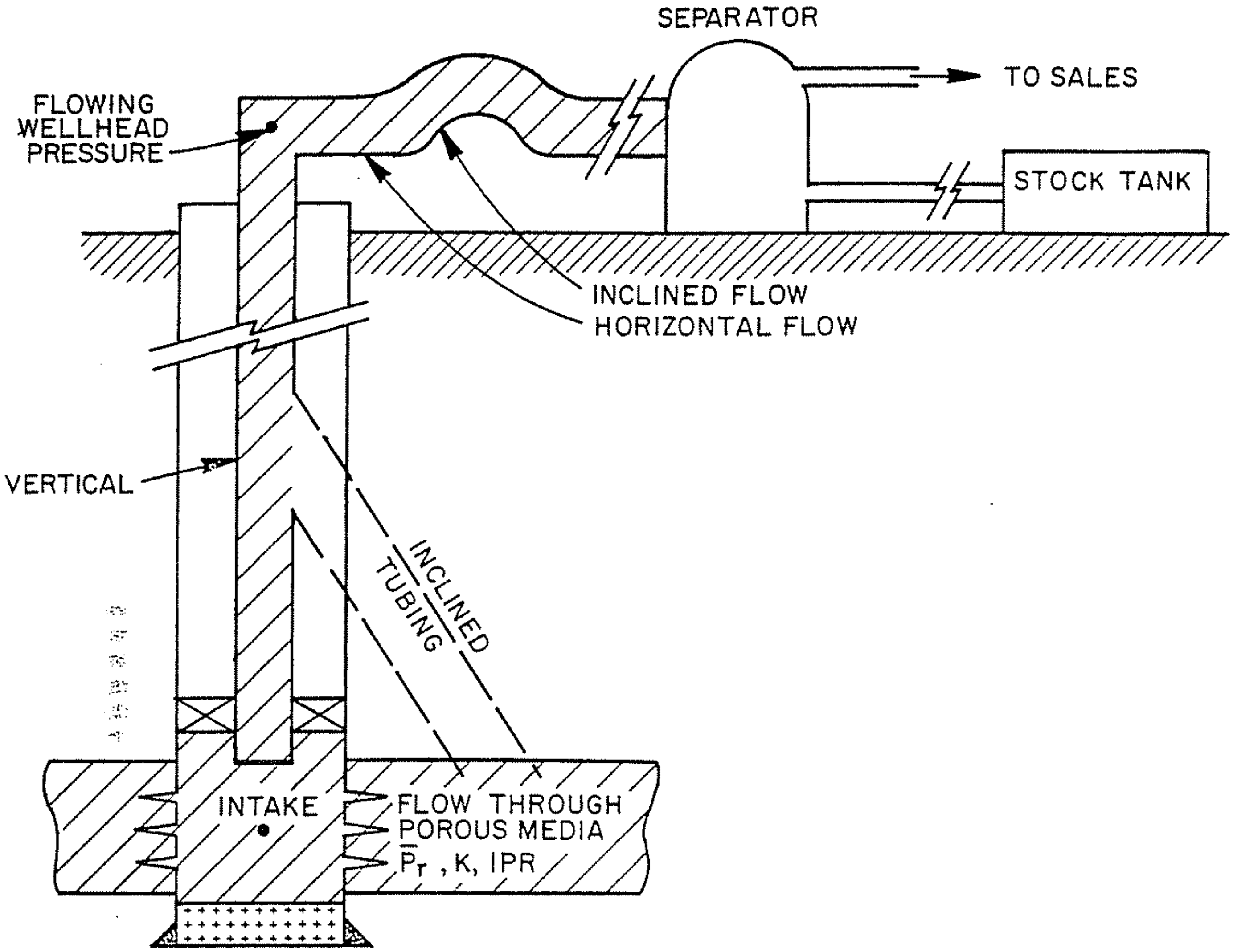

Figure 1.1 Complete Producing Simple System

sure loss in two parallel lines of the same size is much lower than in the multiphase flow line, and even two smaller lines will show less pressure loss. Therefore, the additional production gained by lowering the wellhead pressure must be economically evaluated against the cost of an additional flow line.

The manner in which a well is completed is also very important. For example, the number of perforations necessary to prevent excessive pressure loss across completions for gravel-packed and nongravel-packed oil or gas wells can also be evaluated by nodal analysis. It has been found that common perforation standards of four shots per foot (spf), and even two spf by some operators, may seriously restrict production rates on some wells. Perforation shot densities of 16 spf are common, and higher shot densities such as 24 spf or even open-hole completions are being practiced by many operators.

Some companies may set up a standard perforating shot density such as 4 spf without regard to the size of the perforated hole. For example, a standard large casing gun can shoot a 0.70–0.75-in. diameter hole, whereas a through-tubing gun shoots a 0.2–0.25-in. hole for the smaller tubing sizes. In checking out the areas it is found that 9 holes of 0.25-in. diameter are needed to give one hole a ¾-in. diameter. Obviously when using through-tubing guns in small tubing, it is very likely that an insufficient area to flow has been opened.

The importance of the perforating procedure is also very important. It appears that numerous wells, including some of the low flow rate pumping wells, may not be producing at capacity. Although the well may be pumping off and therefore indicating maximum production, there may still exist a pressure loss across the completion due to insufficient area open to flow. Some of these wells need to be reperforated, and several have shown increased production rates after doing so.

Many companies have now placed nodal analysis on computers, and others are planning to do so. A production systems graph is considered standard for each well file, and others are prepared when an analysis is to be made.

The nodal plot is a necessary tool in bringing a high flow rate gravel-packed well on production. The production rate and wellhead pressure can be used simultaneously to prevent excessive pressure loss across the gravel pack. Numerous gravel-packed completions are destroyed during the first 2–3 days of production. A proper systems analysis graph will prevent this. Some high-rate gas wells in the Gulf Coast may require a month to bring the rate up to the objective. This is

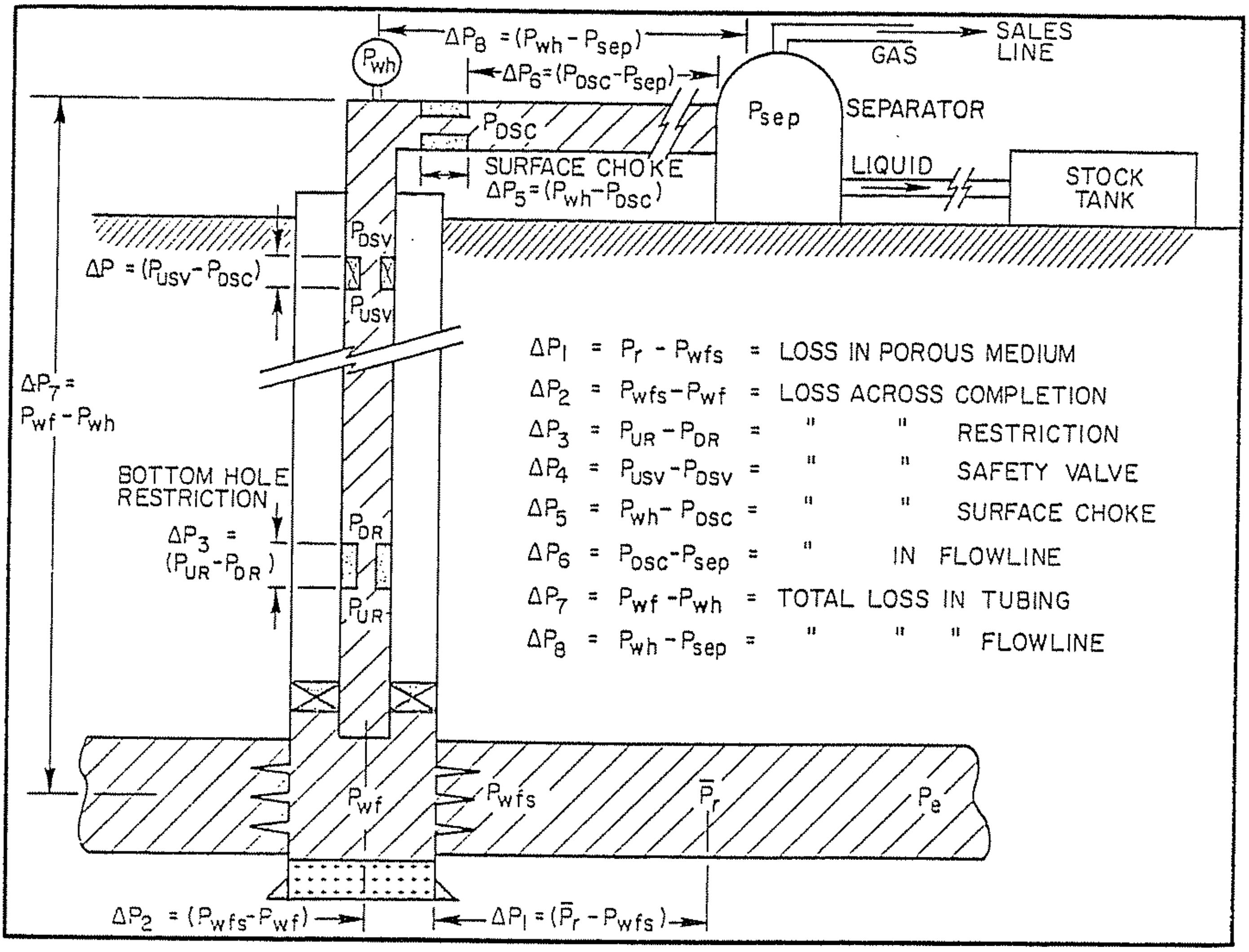

Figure 1.2 Pressure Losses in Complete System

nearly impossible without a good plot in order to follow the path of the production rate vs the pressure drop across the pack.

Good data on oil and gas wells are very important. Both conventional and sidewall cores can be in error in some cases.

A check of well capability against well productivity in many instances shows a well to be much better than its present rate indicates. These are wells that must be tested to verify Kh values or to determine skin or any other restrictions. The nodal analysis concept can be applied to drillstem tests to determine correct completion practices, including selection of pipe sizes.

The conception that nodal analysis can only be applied to high-rate wells is incorrect. Some of the most dramatic changes (percentage increase) have occurred on the weaker wells. For example, a specific field case showed that a well pumping 10 b/d with a relatively high gas-oil ratio (GOR) would flow 30 b/d by changing to a smaller tubing string.

The comparison of artificial lift methods, along with the selection of the correct lift method, is indeed a difficult problem. One of the most important criteria is the correct determination of flow rates by each artificial lift method. In order to do this, the preparation of tubing intake curves becomes a necessity. Chapter 5 shows the procedures for the preparation of these curves.

Combining tubing intake curves for artificial lift methods and inflow performance curves allows the selection of a lift method to meet the objective flow rate. The determination of when a well is expected to die and when artificial lift should be started can be properly evaluated. Many wells can be lifted at higher rates even though they are presently flowing.

One of the very serious problems existing in the petroleum industry is the depletion of gas wells. Eventually all of the gas energy in the world will be used since it is one of the cleanest and more economical sources of energy. However, the depletion of gas reservoirs may be a more difficult problem than that of oil wells. Gas wells that start making some liquids tend to load up and finally die, perhaps after extended periods of low production rates. All types of liquid removal methods have been tried on gas wells including sucker-rod pumps. It is not unusual to find a gas well on pump with the gas being produced up the annulus and the liquid being pumped up the tubing. This method of course has its problems in that gas lock of the pump is always a possibility. Chapter 6 on the various methods for removing liquid is quite thorough and should benefit gas well operations. Multiphase flow correla-

tions have been improved, and the prediction of gas well loading has become more accurate. This allows for more accurate sizing of tubing strings and for the selection of a good liquid removal technique.

The problem of coning or channeling gas or water is very serious and sometimes quite controversial. Numerous methods have been proposed to predict those flow rates at which coning and channeling become critical. This is discussed in complete detail in Chapter 7.

Well behavior is sometimes quite difficult to predict. An operator explained his flowing well as follows. At about 300 b/d the well made all oil. Any attempt to increase the rate increased the water percentage drastically. With a significant reduction in production rate, the well made mostly gas with about 20 b/d of oil. All of this was accomplished with a choke at the surface. All reasons were finally verified—some reservoir, some mechanical. What is your explanation?

Chapter 2

Inflow Performance

by Pudjo Sukarno and Jim Lea

2.1 INTRODUCTION

The preparation of IPR (inflow performance relationship) curves for oil and gas wells is extremely important in production systems analysis. Unless some idea of the productive capacity of a well can be established, the design and optimization of the piping system becomes very difficult.

This chapter presents the various procedures used by production engineers as shortcut procedures in the preparation of inflow curves. The best information available should always be used for the preparation of these curves. For example, if good reservoir-simulation models are available, they should be used in lieu of shortcut procedures.

2.2 INFLOW EQUATIONS

The use of Darcy's Law should always be considered in predicting flow rates from the reservoir into the wellbore. The following form of Darcy's Law can be used to predict any flow condition and is perfectly general for both oil and gas:

$$q = \frac{(\text{constant})\,(Kh)}{(\ln r_e/r_w)} \int_{P_{wf_s}}^{P_e} f(P)dP \qquad (2.1)$$

where:

K = absolute permeability
h = thickness of zone
r_e = radius of drainage
r_w = radius of wellbore
P_e = pressure at outer boundary
P_{wf_s} = sandface flowing pressure
$f(P)$ = some function of pressure

By making certain simplifying assumptions and setting certain boundary conditions, we can write Darcy's Law for specific conditions.

2.21 SINGLE-PHASE LIQUID FLOW (CLOSED OUTER BOUNDARY AND $\overline{P}_r$ KNOWN)

Darcy's Law for single-phase flow is as follows:

$$q_o = \frac{7.08 \times 10^{-3}\, k_o h(\overline{P}_r - P_{wf_s})}{\overline{\mu}_o\, \overline{B}_o(\ln r_e/r_w - 0.75 + S + a'q)} \qquad (2.2)$$

where:

k_o = effective permeability to oil (md)
h = effective feet of oil pay (ft)
$\overline{P}_r$ = average reservoir pressure (psia)
P_{wf_s} = wellbore sandface flowing pressure at center of perforations (psia)
q_o = oil flow rate (stb/d)
r_e = radius of drainage (ft)
r_w = radius of wellbore (ft)
S'' = total skin
$a'q$ = turbulent flow term (The a'q term is normally not significant for low-permeability wells and low flow rates.)
μ_o = viscosity (cp) at average pressure of $(P_r + P_{wf_s})/2$
B_o = formation volume factor at average pressure

Where possible, and even though tests may have been conducted on a well, Equation 2.2 should be used to determine whether a well is producing properly; that is, Equation 2.2 may show that a well is capable of much higher production rates as compared to tests on the well.

A brief discussion of each term of Equation 2.2 and where it may be obtained follows.

(1) *Permeability* (k). Permeability (k) normally is obtained from laboratory tests on conventional or sidewall cores. Sidewall cores may be misleading and, in general, will not check with conventional cores. For conventional core permeabilities greater than about 20 md, the sidewall core will give a lower value because of the crushing effect upon retrieving the core by impact into the wall of the drilled hole. For conventional core permeabilities less than 20 md, the sidewall core will give a higher value because the core fractures upon impact into the wall. Figure 2.1 verifies these results on 5,300 Gulf Coast samples taken by Core Laboratories Inc.

(2) *Thickness of producing zone* (h). The value h can be obtained from logging records or in some instances from drilling records and conventional cores where the entire zone has been cored. The letter h represents the entire thickness of the zone and not just the perforated interval; that is, Darcy's Law applies to flow in the reservoir and does not concern itself with the interval perforated. Any restriction caused by insufficient perforations is accounted for in the a'q term or may be part of total skin as measured from pressure buildup tests.

Also, h represents the vertical thickness of the formation even though the drilled hole may be at an angle

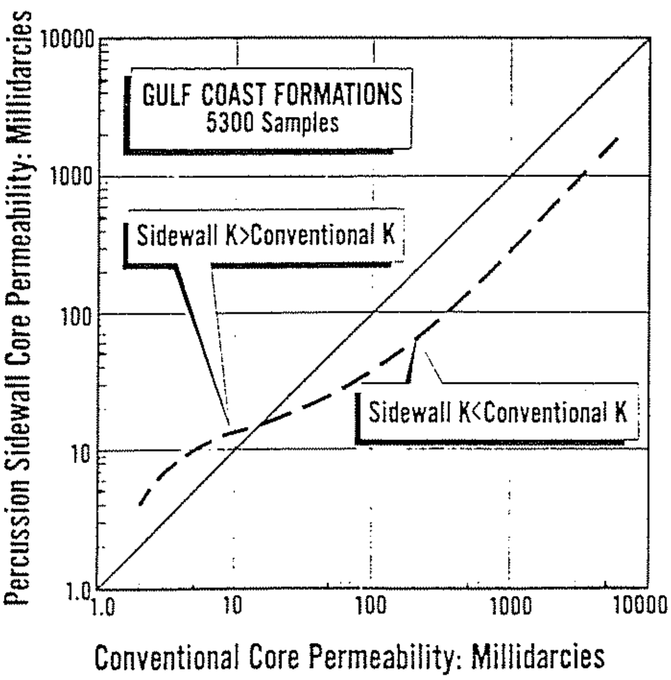

Figure 2.1 Comparison of Sidewall and Conventional Core Permeability (courtesy Core Laboratories Inc.)

through the zone. For oil zones underlain with water, the h for oil thickness only should be used.

(3) *Average reservoir pressure* ($\overline{P}_r$). The value of $\overline{P}_r$ is best obtained from buildup tests, but estimates may have to be made based on the best information available such as static fluid levels and offset wells.

(4) *Average viscosity* (μ). Pressure-volume-temperature (PVT) data may be available for viscosity determinations, but if not, Figures 2.2 and 2.3 may be used to obtain a value of viscosity. The value of gas in solution for the average pressure between $\overline{P}_r$ and P_{wf_s} should be used. It may be necessary to assume a value of P_{wf_s}. Gas in solution at average pressure should be used and not the producing GOR.

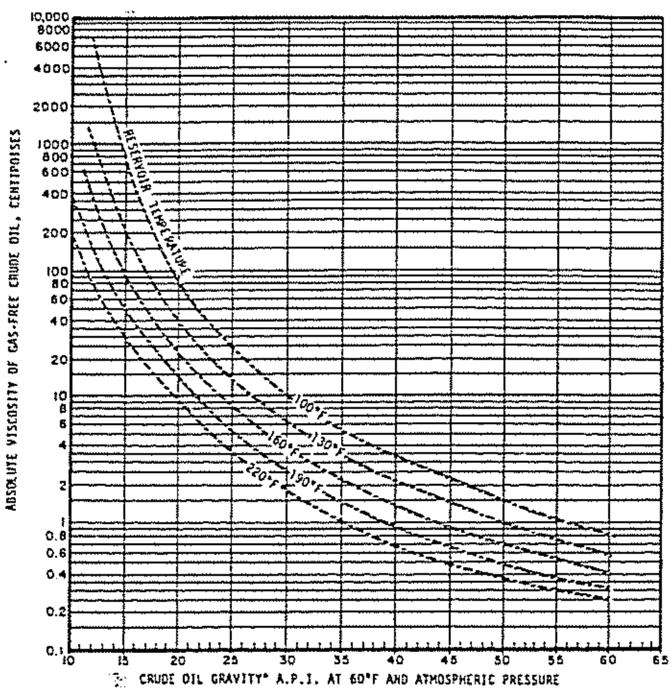

Figure 2.2 Viscosity of Gas-free Crude Oil (Working Copy on p. 330)

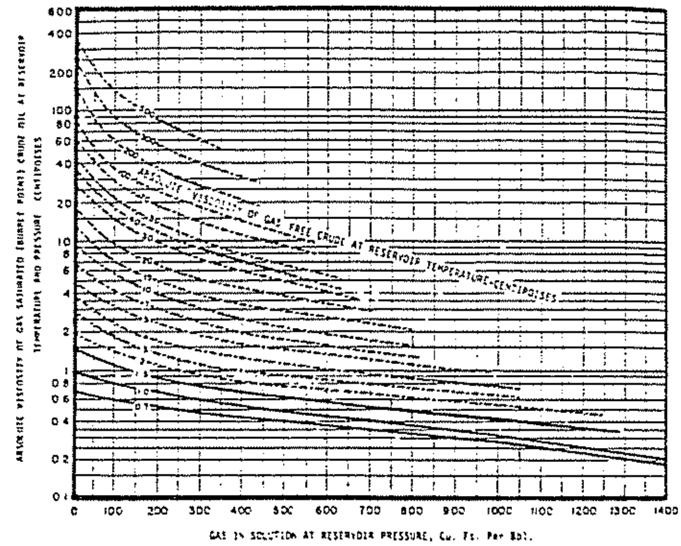

Figure 2.3 Viscosity of Gas-saturated Oil (Working Copy on p. 331)

(5) *Average oil formation volume factor* (B_o). To obtain the average formation volume factor, PVT data may be available. If not, either Standing's or Lasater's correlation is recommended. For Standing's correlation, the following equations are applicable:[1]

$$B_o = 0.972 + 0.000147\,F^{1.175} \tag{2.3}$$

$$F = R_s\left(\frac{\gamma_g}{\gamma_o}\right)^{0.5} + 1.25\,T \tag{2.4}$$

R_s = scf/bbl (in solution)

where:

$$R_s = \gamma_g\left\{\frac{\overline{P}}{18} \times \frac{10^{0.0125(API)}}{10^{0.00091(T)}}\right\}^{1/0.83} \tag{2.5}$$

$\overline{P}$ = average pressure (psi)

T = °F

Refer to Volume I, *Technology of Artificial Lift Methods,* pages 83–89 for additional information.[2]

Figure 2.4 is a nomograph for Standing's correlation to find R_s, after which B_o can be obtained from Figure 2.5. Figures 2.6, 2.7, and 2.8 can also be used. This represents Lasater's correlation and under certain conditions may be more accurate than Standing's correlation (generally better at higher °API).[3] The equation for Lasater's correlation is as follows:

$$R_s = \left[\frac{(379.3)(350)(\gamma_o)}{M_o}\right]\left(\frac{Y_g}{1 - Y_g}\right)C \tag{2.6}$$

where:

M_o = molecular weight (Figure 2.6)

Y_g can be obtained from Figure 2.7.

T = °R

Figure 2.8 shows a nomograph for Equation 2.6. The value of C is 1.0 unless a correction factor is necessary to make the equation check with actual field cases.

(6) *Radius of drainage* (r_e). Radius of drainage may be difficult to determine, but any error in its determination is dampened by taking the natural log of r_e/r_w. The value of r_e can be adjusted to take care of different

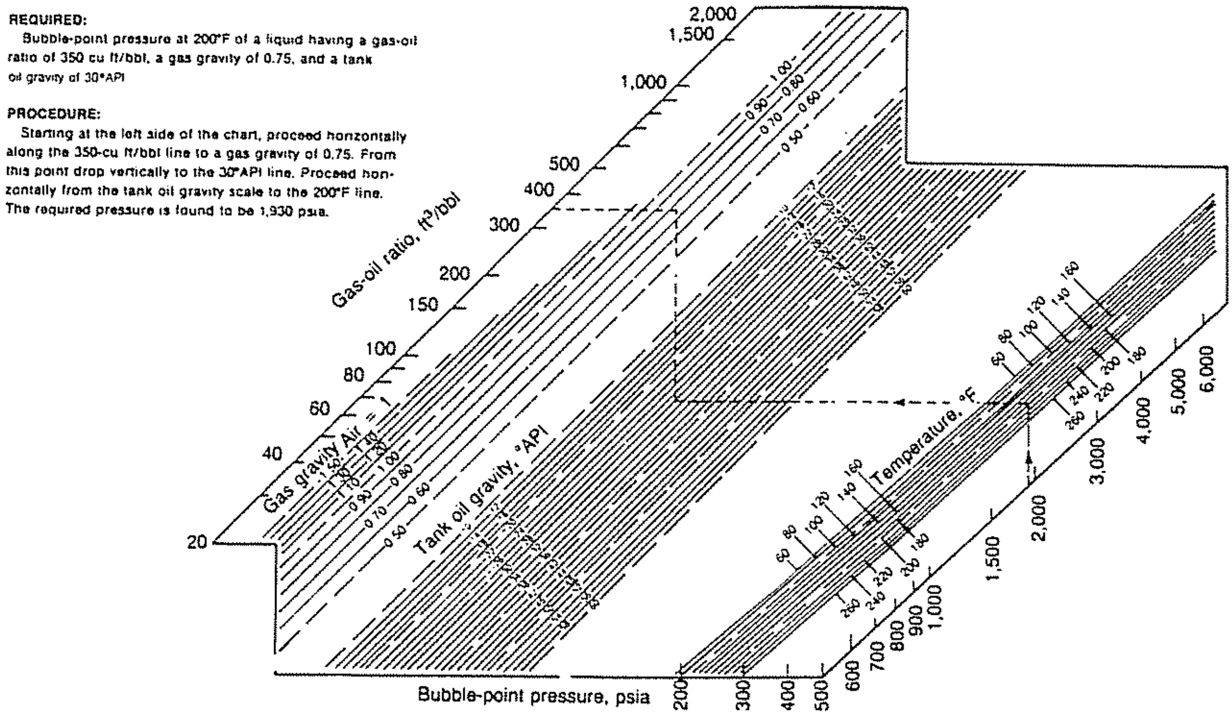

*Figure 2.4 Properties of Natural Hydrocarbon Mixtures of Gas and Liquid Bubble-Point Pressure (courtesy Chevron Research)**

shapes and well positions in a drainage area. Odeh,[4] using the work of Matthews and Russel,[5] suggested the following equation:

$$q_o = \frac{7.08 \times 10^{-3}\, kh(P_r - P_{wf})}{\bar{\mu}_o\, \bar{B}_o(\ln X - 3/4 + S)} \qquad (2.7)$$

where X is given in Figure 2.9.

Since the value of r_e is dampened considerably by taking the natural log of r_e/r_w, the establishment of an exact value of r_e is not critical. For example, if $r_w = 0.5$, the following values of $\ln r_e/r_w$ are obtained for various values of r_e:

Values of $\ln r_e/r_w$
$r_w = 0.5$ ft

r_e, ft	$\ln r_e/r_w$
500	6.9
1,000	7.6
2,000	8.29
5,000	9.2
10,000	9.9

Therefore, a relatively large error in r_e has only a minor effect on $\ln r_e/r_w$. Thus, for purposes in calculat-

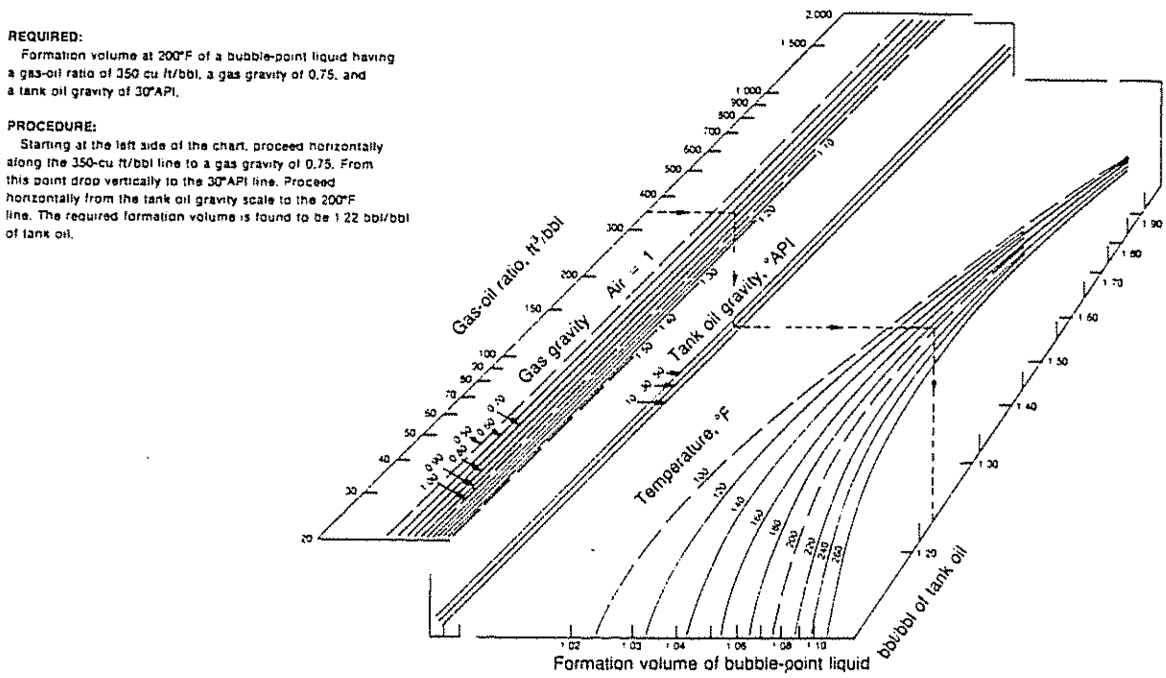

Figure 2.5 Properties of Natural Hydrocarbon Mixtures Formation Volume of Bubble-Point Liquid (courtesy Chevron Research)†

*** Working copies of figures are shown on pp. 332.**

† Working copies of figures are shown on pp. 428.

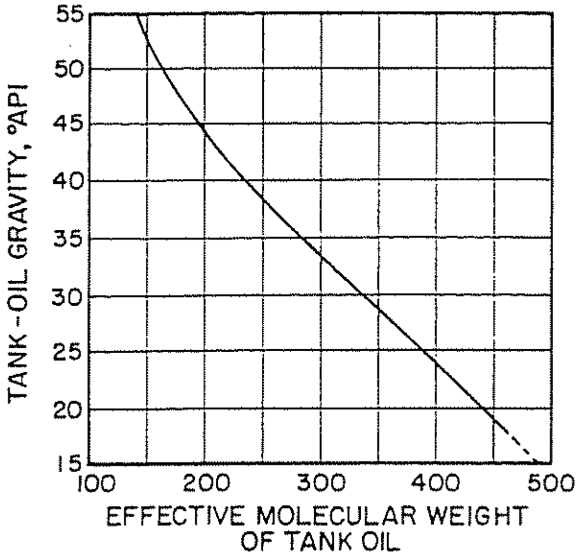

Figure 2.6 Molecular Weight vs °API (after Lasater)[3]

ing flow rates, there is no need to dwell at length in trying to determine an exact value for r_e. Of course, the best information available should be used in establishing r_e.

(7) *Radius of the drilled hole* (r_w). Do not use casing size for the radius of the drilled hole. The drilled hole size can be accurately determined by caliper surveys. If the surveys are not available, the bit size with which the hole was drilled can be used.

(8) *Total skin* (S''). For a first solution, assume skin = 0 to determine if the well is performing properly or to determine the well capability. The term S can be obtained from pressure buildup plots. The total value of S can include many factors:

(a) S' = physical damage such as mud infiltration
(b) $S(q,t)$ = a time- and rate-dependent skin
(c) S_p = a restriction for entry of fluids into the perforated hole

(9) *Turbulent flow* (aq). This term is generally negligible at low flow rates and for low-permeability wells. It may become significant at higher flow rates. A good policy is to check the value of aq at the maximum flow rate (P_{wf} = 0). If the value is low, it can be neglected. Jones, Blount, and Glaze showed that the equation could be written in the following form in order to account for turbulent flow:[6]

$$\overline{P}_r - P_{wf_s} = bq + aq^2 \tag{2.8}$$

where: a is = a' multiplied by $\dfrac{\overline{\mu}_o \overline{B}_o}{7.08 \times 10^{-3}\, k_o h}$

$$b = \frac{\overline{\mu}_o\, \overline{B}_o\, [\ln(0.472\, r_e/r_w) + S]}{1.127 \times 10^{-3}\, (2\pi\, kh)} \tag{2.9}$$

The value of a can be obtained from the following equation:

$$a = \frac{9.08 \times 10^{-13}\, \beta\, B_o^2}{4\pi^2\, h_p^2\, r_w}\, \rho_o \tag{2.10}$$

where:

a = turbulent flow coefficient

β is a turbulent velocity flow coefficient that can be obtained from Figure 2.10 or calculated by the equation:

$$\beta = \frac{2.33 \times 10^{10}}{k^{1.201}} \tag{2.11}$$

where:

μ = viscosity, cp
k = permeability, md
h = thickness, ft
h_p = perforated interval, ft
B_o = oil formation volume factor
ρ = density of fluid, lb_m/ft^3 (live oil)
S = skin effect excluding turbulence

Equation 2.8 is for single-phase liquid flow with a accounting for turbulence. a does not account for any two-phase flow, and the product aq will be small at low flow rates. It can become significant at very high rates. a is a function of permeability and the number of feet perforated. Figures 2.11 and 2.12 show the effect of permeability and perforation intervals (as a fraction of formation thickness). From these plots, the following can be noted

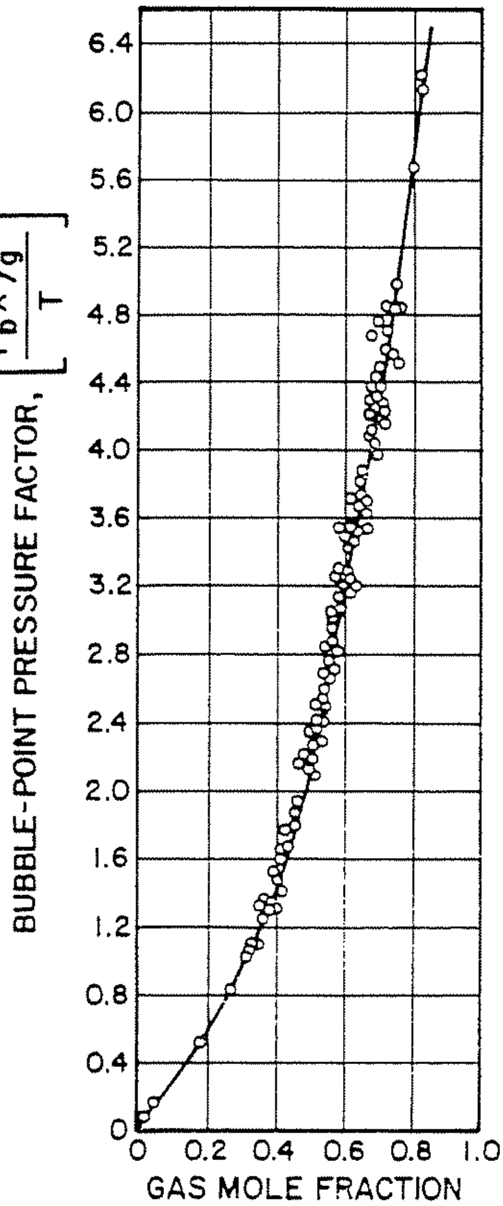

Figure 2.7 Bubble-Point Pressure Factor vs Gas Mole Fraction (after Lasater)[3]

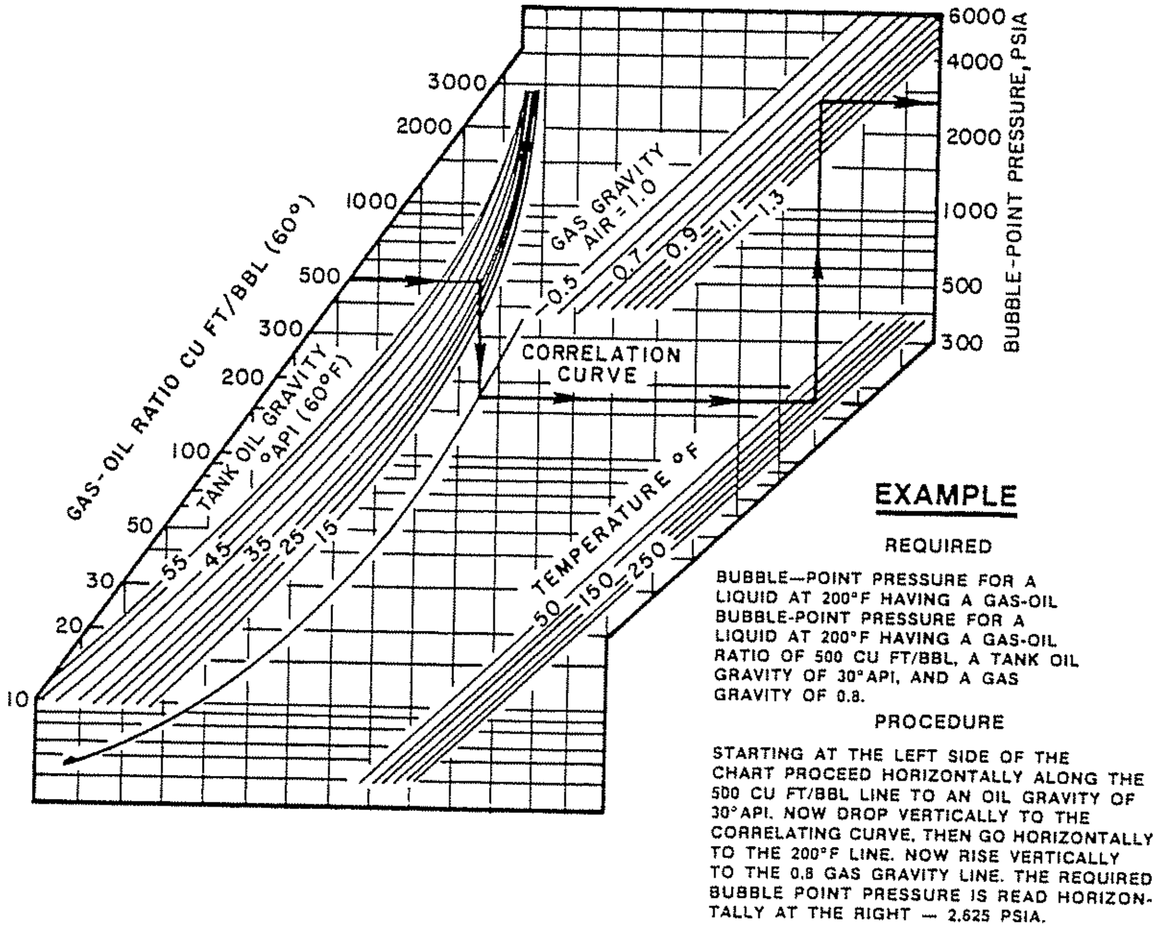

Figure 2.8 Bubble-Point Pressure (after Lasater)[3]

(1) For certain pressure ratios, (P_{wf}/P_r), the value of a'q increases with increasing permeability (Fig. 2.11).
(2) a'q will increase with decreasing perforation interval (Fig. 2.12).
(3) For low permeabilities, the effect of the perforation interval on a'q is small (Figure 2.12).

EXAMPLE PROBLEM #1

(Using Darcy's Law for pseudo-steady-state flow [single-phase liquid flow])

Given data:

$k_o = 30$ md	$\bar{P}_r = 3{,}000$ psia
$h = 40$ ft	$h_p = 10$ ft
°API = 30	GOR = 300 scf/bbl
$\bar{T}$ (reservoir) = 200°F	160-acre spacing
$\gamma_g = 0.7$	drilled hole size = 12¼ in.
(Produces all oil)	casing size = 7 in.

Calculate:

(1) the bubble-point flow rate for this well for a'q = 0
(2) the value of a'q at the bubble-point flow rate

Solution procedure:

Use Darcy's Law to determine q_b:

(1)
$$q_o = \frac{7.08 \times 10^{-3}\, kh(\bar{P}_r - P_{wf})}{\bar{\mu}_o \bar{B}_o (\ln r_e/r_w - 3/4 + S + a'q)} \qquad (2.2)$$

Assume $S = 0$
Assume $a'q = 0$

Then:

$$q_o = \frac{7.08 \times 10^{-3}\, kh(\bar{P}_r - P_{wf})}{\bar{\mu}_o \bar{B}_o (\ln r_e/r_w - 3/4)} \qquad (2.12)$$

Solution procedure:

(1) Obtain a value for $\bar{B}_o$ (average formation volume factor). Notice that the required B_o is for an average pressure between $\bar{P}_r$ and P_{wf}. A more rigorous solution could be obtained by taking B_o average for each increment. For this example, use an average pressure of $(\bar{P}_r + P_b)/2$.
(2) Determine bubble-point pressure from Figure 2.4 or Equation 2.4. This is found to be 1,800 psi.

Therefore, use $\bar{P} = \dfrac{3{,}000 + 1{,}800}{2} = 2{,}400$ psi,

which gives the average pressure for the constant J portion of the IPR curve.
(3) Determine $\bar{B}_o$ for $R_s = 300$ scf/bbl
Refer to Figure 2.5 or Equation 2.3 and obtain $\bar{B}_o = 1.19$. (See p. 428.)
(4) Determine the average viscosity
(a) Refer to Figure 2.2 to find that the viscosity of the gas-free oil is 2.1 cp.
(b) Refer to Figure 2.3 to determine the effect of gas in solution (300 scf/bbl) and note the final $\bar{\mu}_o = 0.96$ cp.
(5) Determine the effective r_e/r_w for a well located

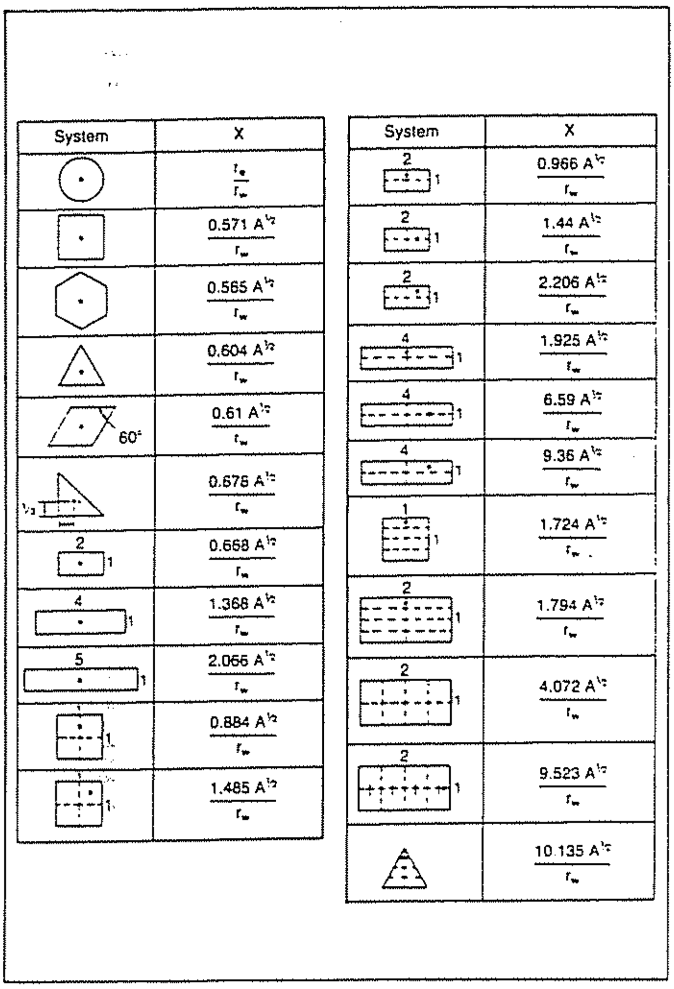

Figure 2.9 Factors for Different Shapes and Well Positions in a Drainage Area where A = Drainage Area of System Shown and $A^{1/2}/r_w$ is Dimensionless (after Mathews and Russel, courtesy SPE)[5]

in the center of 160 acres. Reference to Fig. 2.9 shows:

$$r_e/r_w = \frac{0.571A^{1/2}}{r_w} \tag{2.13}$$

where:

$$A = 43{,}560\,\frac{ft^2}{acre}\,(160\ acres) = 6{,}969{,}600\ ft^2$$

$$r_w = 12.25/2 = 6.125\ in. = 0.5104\ ft$$

$$r_e/r_w = \frac{0.571\,(6{,}969{,}600)^{1/2}}{0.5104} = 2{,}953$$

$$\ln r_e/r_w = 7.99$$

For this problem, r_e could be used as the radius of an equivalent circle with 160 acres to find πr_e^2 = (43,560)(160) or r_e = 1,489.45, and r_e/r_w = 2,918 where $\ln r_e/r_w$ = 7.9787. As can be seen, there is very little difference in the final $\ln r_e/r_w$ term. We are now ready to solve Equation 2.12 for the bubble-point flow rate:

$$q_b = \frac{7.08 \times 10^{-3}\,(30)(40)(3{,}000 - 1{,}800)}{(0.96)(1.19)(7.99 - 3/4 - 0)}$$

$$q_b = 1.027\,(3{,}000 - 1{,}800) = 1{,}232.6\ b/d$$

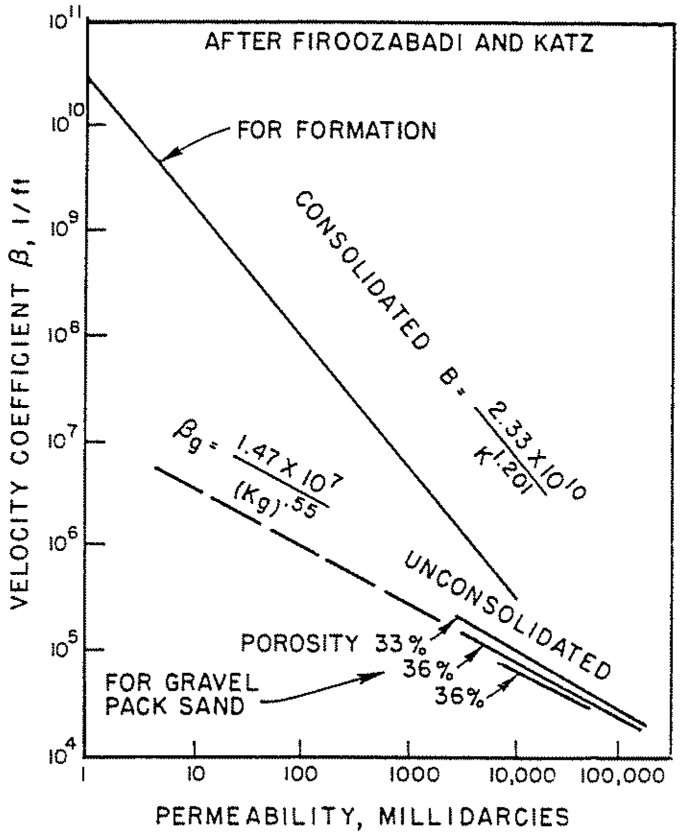

Figure 2.10 Correlation of β vs Permeability

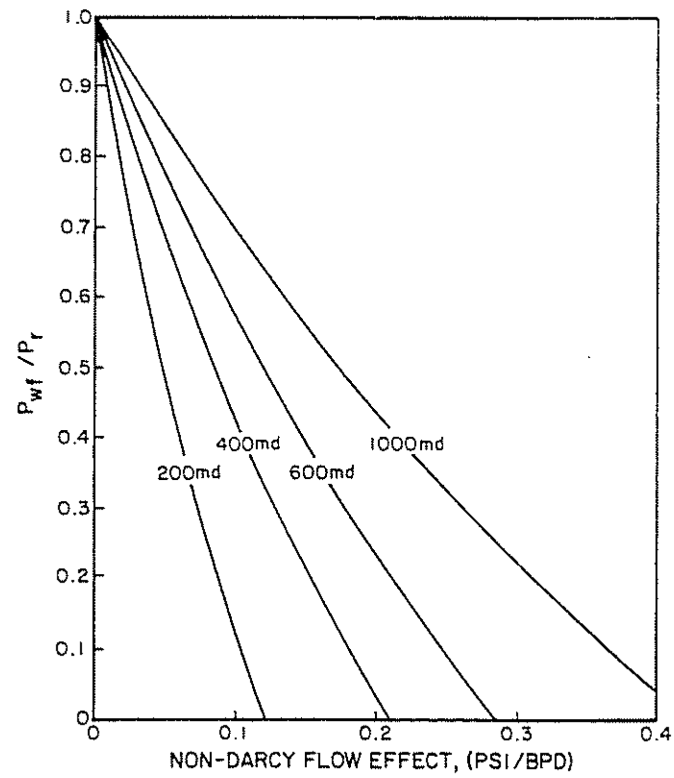

Figure 2.11 Effect of Permeability on Turbulent Term (aq) for Oil Flow (after Sukarno)[7]

where the J is 1.027 b/d per psi drawdown

(6) Find the flowing pressure at the bubble-point flow rate including the aq term:

$$q_b = 1.027\,(3{,}000 - 1{,}800) = 1{,}232.6\ b/d$$

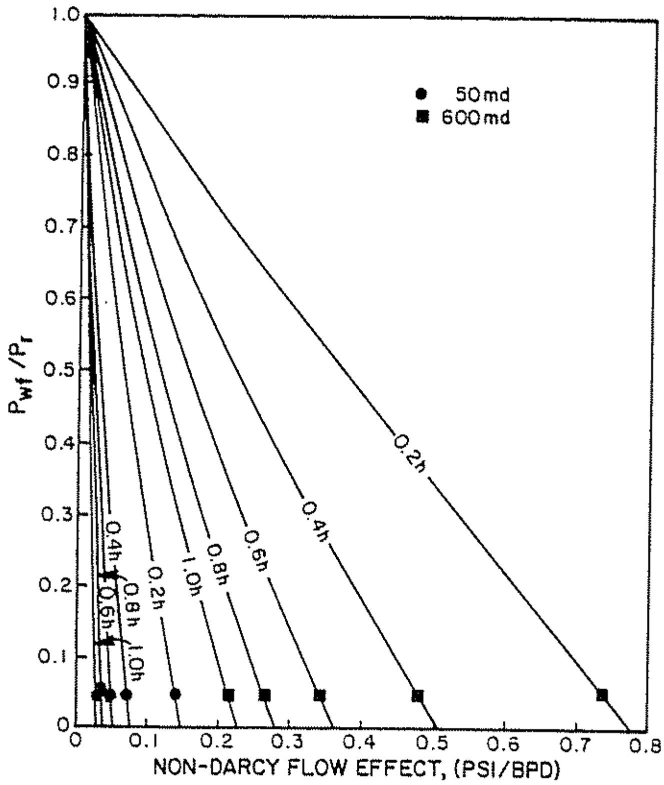

Figure 2.12 Effect of Permeability and Partial Penetration on Turbulence for Oil Flow (after Sukarno)[7]

The appropriate equation is as follows:

$$P_r - P_{wf} = bq + aq^2 \qquad (2.8)$$

where:

$$b = \frac{\mu_o B_o(\ln r_e/r_w - 3/4 + S)}{1.127 \times 10^{-3}(2\pi Kh)}$$

$$= \frac{(0.96)(1.19)(7.24)}{1.127 \times 10^{-3}(2\pi)(30)(40)} = 0.9737$$

$$a = \frac{9.08 \times 10^{-13} B_o^2\beta}{4\pi^2 h_p^2 r_w}\rho_o$$

$$\beta = \frac{2.33 \times 10^{10}}{k^{1.201}} = \frac{2.33 \times 10^{10}}{(30)^{1.201}}$$

$$= 3.92 \times 10^8$$

$$\rho_{do} = \gamma_o(62.4) = (0.876)(62.4) = 54.67\ lb_m/ft^3$$

$$a = \frac{9.08 \times 10^{-13}(3.92 \times 10^8)(1.19)^2(48.34)}{4\pi^2(10)^2(0.5104)}$$

$$a = 120.9 \times 10^{-7} = 1.21 \times 10^{-5}$$

Then:

$$P_r - P_{wf} = 0.9737\ q + 0.0000121\ q^2$$

Evaluating aq^2 at q_b = 1,232.6 b/d

$$aq^2 = 0.0000121(1{,}232.6)^2 = 18.38$$
$$P_r - P_{wf} = 0.9737(1{,}232.6) + 18.38$$
$$= 1{,}200.18 + 18.38 = 1{,}218.6$$
$$P_{wf} = 3{,}000 - 1{,}219 = 1{,}781\ psi$$

This compares to a value of P_{wf} = (3,000 − 1,232.6/1.027) = 1,800 psi when aq is not included.

$$\rho_{LIVE\ OIL} = \frac{\rho_{DEAD\ OIL} + \dfrac{0.0764\,\gamma_g R_s}{5.615}}{B_o}$$

$$= \frac{54.67 + \dfrac{0.0764(0.7)(300)}{5.615}}{1.19} = 48.34\ \frac{lb_m}{ft^3}$$

By including the aq term, an additional 21-psi drop in pressure is required at the bubble-point flow rate and for all practical purposes could be neglected for this example problem. The aq term is normally not considered below the bubble point because saturation effects must be accounted for and because a procedure such as Vogel's, which in itself accounts for all those effects that reduce the flow rate and which is principally a change in permeability to oil, is used.

CLASS PROBLEM #1a

Given data:

k_o = 50 md	P_r = 3,500 psia
h = 60 ft	hole size = 10¾ in.
GOR = 400 scf/bbl	γ_g = 0.65
T = 180°F	°API = 36
80-acre spacing	h_p = 20 ft

Calculate:

(1) the flow rate at the bubble-point pressure
(2) the value of the aq term at the bubble-point flow rate

CLASS PROBLEM #1b

Given data:

reservoir pressure = 3,750 psia
k_o = 150 md h = 10 ft
r_e = 1,290 ft r_w = 0.50 ft h_p = 10 ft
oil gravity = 45°API
bubble-point pressure = 2,800 psia
oil viscosity @ average pressure = 0.2954 cp
B_o @ average pressure = 1.5579 bbl/stb
skin effect = 0

Calculate:

(1) the flow rate at bubble-point pressure (by assuming S = 0 and aq = 0)
(2) the value of the aq term at the bubble-point flow rate by assuming h_p = h and h_p = 0.5(h)
(3) the flowing pressure at the bubble-point flow rate, including the aq term, by assuming h_p = h and h_p = 0.5(h)

CLASS PROBLEM #1c

Given data:

reservoir pressure = 4,150 psia
bubble-point pressure = 3,000 psia
k_o = 125 md h = 80 ft
γ_g = 0.65 h_p = 20 ft
oil gravity = 40°API
reservoir temperature = 190°F
hole diameter = 10¾ in.
spacing = 120 acres
skin effect = 0

Calculate:

(1) the flow rate for P_{wf} = 3,250 psia
 —by assuming aq = 0
 —by including the aq term
(2) the flow rate for P_{wf} = 3,500 psia
 —by assuming aq = 0
 —by including the aq term

CLASS PROBLEM #1d

Given data:

$P_r = 4{,}000$ psia $P_b = 2{,}900$ psia
$k_o = 195$ md $S = 0$
gravity of oil = 36°API
specific gravity of gas = 0.70
reservoir temperature = 200°F
$h = 90$ ft $h_p = 40$ ft
spacing = 180 acres
hole diameter = 10¾ in.

Calculate:

(1) the flow rate for $P_{wf} = 3{,}000$ psia
—by assuming aq = 0
—by including aq
(2) the flow rate for $P_{wf} = 3{,}250$ psia
—by assuming aq = 0
—by including aq

CLASS PROBLEM #1e

Given data:

$P_r = 3{,}900$ psia $P_b = 3{,}050$ psia
$k_o = 170$ md $h = 100$ ft
$r_e = 1{,}053$ ft $r_w = 0.33$ ft
gravity of oil = 40°API

Calculate:

(1) assuming S = 0 and aq = 0, calculate the flow rate for flowing pressure = 3,150 psia ($\overline{\mu}_o = 0.3532$ cp and $\overline{B}_o = 1.5008$ bbl/stb)
(2) the value of the aq term for flowing pressure = 3,150 psia by assuming $h_p = h$ and $h_p = 0.25(h)$
(3) the flowing pressure for the above flow rate (problem a), including aq term, by assuming $h_p = h$ and $h_p = 0.25(h)$

2.211 ESTIMATING THE PRODUCTIVITY INDEX FROM LIMITED INFORMATION

From Darcy's Law for oil flow:

$$q_o = \frac{7.08\, kh\, (P_r - P_{wf})}{\overline{\mu}_o \overline{B}_o (\ln r_e/r_w - 3/4 + S)} \tag{2.2}$$

where k is in darcies, assume that:

$$\ln r_e/r_w - 3/4 + S = 7.08$$

then:

$$q_o \simeq \frac{kh}{\mu_o\, B_o}\left[\Delta P\right] \tag{2.14}$$

or:

$$J \simeq \frac{kh}{\mu_o\, B_o} \tag{2.15}$$

An estimated value of PI can be obtained if we know k, h, B_o, and μ_o.

EXAMPLE PROBLEM: #2

Given data:

$k = 120$ md $= 0.120$ darcies
$h = 30$ ft
$\mu_o = 0.8$ cp
$B_o = 1.15$

Calculate:

$$J \simeq \frac{(0.120)(30)}{(0.8)(1.15)} = 3.9\, \frac{\text{b/d}}{\text{psi}}$$

There are other instances whereby we can estimate J by knowing only k and h. If we assume that the product of $\overline{\mu}_o\, \overline{B}_o = 1.0$, then

$$J \simeq kh \tag{2.16}$$

where k = darcies and h = ft.
For °API greater than 30, this approximation is normally valid.

EXAMPLE PROBLEM #3

Given data:

$k = 120$ md $= 0.120$ darcies
$h = 30$ ft

$$\text{estimated } J = kh = (0.120)(30) = 3.6\, \frac{\text{b/d}}{\text{psi}}$$

By knowing only k, h, and $\overline{P}_r$, a quick evaluation will show the productive capacity for either an oil or gas well. The following classification of kh values can be used to evaluate the potential of oil or gas wells.

For values of kh in md-ft:

(1) kh = 0–100 md-ft—not a very good well
(2) kh = 100–1,000 md-ft—good well
(3) kh = 1,000–5,000 md-ft—excellent well
(4) kh > 5,000 md-ft—will normally exceed piping system capacity when the kh value exceeds 5,000 md-ft. If the static reservoir pressure is high, this well is capable of producing just about any rate desired.

EXAMPLE PROBLEM #4

(4a) *Given data:*

Oil well:

$k = 20$ md
$h = 40$ ft
$\overline{P}_r = 2{,}600$ psi

Calculate:

evaluate this well

Solution procedure:

kh = (20)(40) = 800 md-ft or J = 0.8 Darcy-ft
q_{max} for constant J = 0.8(2,600 − 0) = 2,080 b/d

$$q_{max} \text{ for Vogel solution} = \frac{0.8(2{,}600 - 0)}{1.8} = 1{,}155 \text{ b/d}$$

This is a good well and shows a Vogel $q_{o_{max}}$ of 1,155 b/d, which is a minimum value depending upon the bubble-point pressure.

(4b) *Given data:*

Oil well:

$k = 200$ md $P_r = 4{,}000$ psia
$h = 100$ ft

Solution procedure:

$kh = (200)(100) = 20{,}000$ or $J = 20$

This is an excellent well for assumed constant J, $q_{o_{max}} = 20(4{,}000) - 0) = 80{,}000$ b/d

(4c) Given data:

$k = 600$ md $\quad P_r = 5{,}000$ psi
$h = 300$ ft

Solution procedure:

$kh = (300)(600) = 180{,}000$ or $J = 180$
$q_{max} = 180(5{,}000) = 900{,}000$ b/d

Obviously this well will produce at whatever rate you desire to obtain.

(4d) Given data:

$k = 5$ md $\quad P_r = 1{,}000$ psi
$h = 10$ ft

Solution procedure:

$kh = (5)(10) = 50$ md-ft

$$J = \frac{50}{1{,}000} = 0.05 \text{ b/d/psi}$$

$q_{max} = 0.05(1000 - 0) = 50$ b/d

This is not a good well and probably is below bubble-point pressure, giving a $q_{o_{max}}$ of $(50)/(1.8) = 28$ b/d. Production by artificial lift will probably be 15–20 b/d.

(4e) Given data:

Oil well:

$k = 300$ md
$h = 40$ ft
viscosity = 800 cp
$B_o = 1.15$
$P_r = 3{,}000$ psi

Solution procedure:

$kh = (300)(40) = 12{,}000$ md-ft
$J = 12$

kh > 5,000 indicates an excellent well. However, the high viscosity reduces the J on this well as follows:

$$J = \frac{(0.300)(40)}{(800)(1.15)} = 0.013 \text{ b/d/psi}$$

$q_{o_{max}} = 0.013(3{,}000 - 0) = 39$ b/d

For those wells having heavy crudes, the productivity is reduced drastically by the high viscosity.

Calculate:

CLASS PROBLEM #4a

Given data:

$k = 5$ md $\quad P_r = 2{,}000$ psi
oil well $\quad h = 20$ ft

Evaluate this well

CLASS PROBLEM #4b

Given data:

$k = 200$ md $\quad P_r = 3{,}500$ psi
oil well $\quad h = 40$ ft

Evaluate this well

CLASS PROBLEM #4c

Given data:

$k = 0.8$ md $\quad P_r = 6{,}000$ psia
oil well $\quad h = 30$ ft

Evaluate this well

CLASS PROBLEM #4d

Given data:

$k = 500$ md $\quad P_r = 4{,}000$ psia
oil well $\quad h = 200$ ft

Evaluate this well

CLASS PROBLEM #4e

Given data:

$k = 100$ md $\quad h = 50$ ft
viscosity = 350 cp $\quad P_r = 4{,}800$ psia
$B_o = 1.2$

Evaluate this well

2.22 TWO-PHASE FLOW IN THE RESERVOIR

2.221 INTRODUCTION

Again, refer back to the general Equation 2.1:

$$q = \frac{\text{Constant Kh}}{(\ln r_e/r_w)} \int_{P_{wf}}^{P_e} f(P)dP \qquad (2.1)$$

Assuming we know $\bar{P}_r$, $S = 0$, and $Dq = 0$; the outer boundary is closed; and $\bar{P}_r < P_b$, the following equation is valid:

$$q_o = \frac{7.08 \times 10^{-3}\,Kh}{(\ln r_e/r_w - 3/4)} \int_{P_{wf}}^{\bar{P}_r} \frac{k_{ro}}{\mu_o B_o} dP \qquad (2.17)$$

$\frac{k_{ro}}{\mu_o B_o}$ is then a function of pressure, and in turn, k_{ro} is a function of oil saturation. A typical plot of $\frac{k_{ro}}{\mu_o B_o}$ might appear as noted in Figure 2.13.

2.222 VOGEL'S EQUATION

A simplified solution to the two-phase flow problem was offered by Vogel.[8] In solving the equations of Weller,[9] Vogel gave the following general equation to account for two-phase flow in the reservoir (saturation effects):

$$q_o/q_{max} = 1 - 0.2\left(\frac{P_{wf}}{\bar{P}_r}\right) - 0.8\left(\frac{P_{wf}}{\bar{P}_r}\right)^2 \qquad (2.18)$$

He arrived at this equation from a computer solution to several solution-gas-drive reservoirs and for differ-

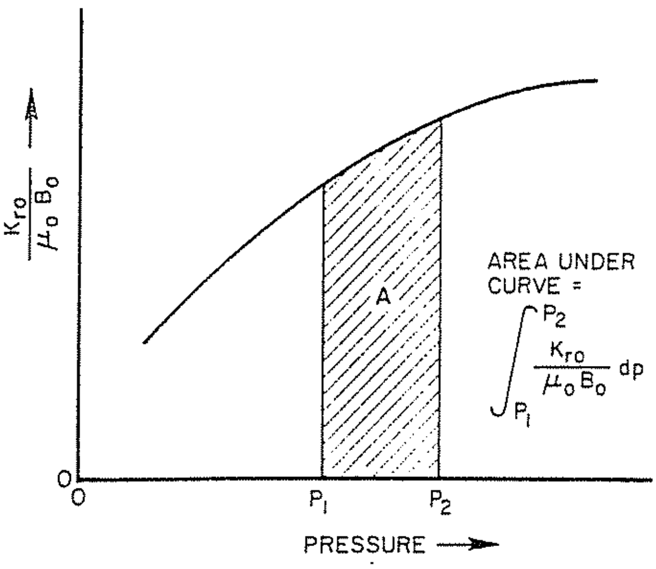

Figure 2.13 $\frac{K_{ro}}{\mu_o B_o}$ *vs Pressure*

ent fluid properties. Figure 2.14 may also be used to arrive at a solution. His solution has been found to be very good and is widely used in the prediction of IPR curves where two-phase flow exists (liquid and gas). It appears to work reasonably well for water percentages up to 50%.

EXAMPLE PROBLEM #5

Given data:

$P_r = 2{,}400$ psi
$q_o = 100$ b/d
$P_{wf} = 1{,}800$ psi

Calculate:

Determine $q_{o_{max}}$ using the equation:

$$q_o/q_{max} = 1 - 0.2\left(\frac{P_{wf}}{P_r}\right) - 0.8\left(\frac{P_{wf}}{P_r}\right)^2$$

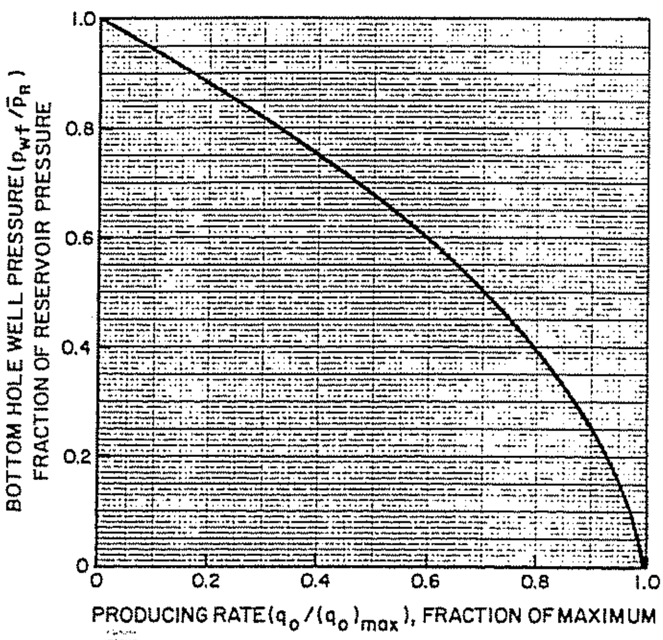

Figure 2.14—Inflow Performance Relationship for Solution-Gas Drive Reservoirs (after Vogel)[8] (Working Copy on p. 333)

Solving for $q_{o_{max}}$:

$$q_{o_{max}} = \frac{q_o}{1 - 0.2\left(\frac{P_{wf}}{P_r}\right) - 0.8\left(\frac{P_{wf}}{P_r}\right)^2} \tag{2.19}$$

$$q_{o_{max}} = \frac{100}{1 - 0.2\left(\frac{1{,}800}{2{,}400}\right) - 0.8\left(\frac{1{,}800}{2{,}400}\right)^2}$$

$$q_{o_{max}} = \frac{100}{[1 - 0.15 - 0.45]} = 250 \text{ b/d}$$

Find q_o for $P_{wf} = 800$ psi

$$q_o = q_{max}\left[1 - 0.2\frac{P_{wf}}{P_r} - 0.8\left(\frac{P_{wf}}{P_r}\right)^2\right]$$

$$q_o = 250\left[1 - 0.2\left(\frac{800}{2{,}400}\right) - 0.8\left(\frac{800}{2{,}400}\right)^2\right]$$

$$q_o = 250\,[1 - 0.06667 - 0.08889] = 211 \text{ b/d}$$

Other values of P_{wf} may be assumed in order to obtain sufficient points to plot an IPR curve.

Solution procedure using Figure 2.14:

$$\frac{P_{wf}}{P_r} = \frac{1{,}800}{2{,}400} = 0.75$$

Read from Figure 2.14:

$$q_o/q_{max} = 0.40 \text{ or } q_{max} = \frac{100}{0.4} = 250 \text{ b/d}$$

Vogel's equation may be solved directly for P_{wf} as follows:

$$P_{wf} = 0.125\,\bar{P}_r\left[-1 + \sqrt{81 - 80\,(q_o/q_{o_{max}})}\right] \tag{2.20}$$

CLASS PROBLEM #5a

Given data:

$P_r = 1{,}600$ psia $\quad P_b = 1{,}600$ psia
$q_o = 150$ b/d
$P_{wf} = 1{,}000$ psia

Calculate:

(1) $q_{o_{max}}$
(2) q_o for $P_{wf} = 600$ psia
(3) construct the IPR curve

CLASS PROBLEM #5b

Given data:

$P_r = 2{,}400$ psi $\quad P_b > P_r$
$q_o = 80$ b/d
$P_{wf} = 2{,}000$ psia

Calculate:

(1) $q_{o_{max}}$
(2) q_o for $P_{wf} = 1{,}500$ psia
(3) construct the IPR curve

2.223 COMBINATION SINGLE-PHASE LIQUID AND TWO-PHASE FLOW

Refer to Figure 2.15, then start again with the general equation:

$$q_o = \frac{7.08\ 10^{-3}\ Kh}{(\ln r_e/r_w - 3/4)}\int_{P_{wf}}^{\bar{P}_r} f(P)\,dP$$

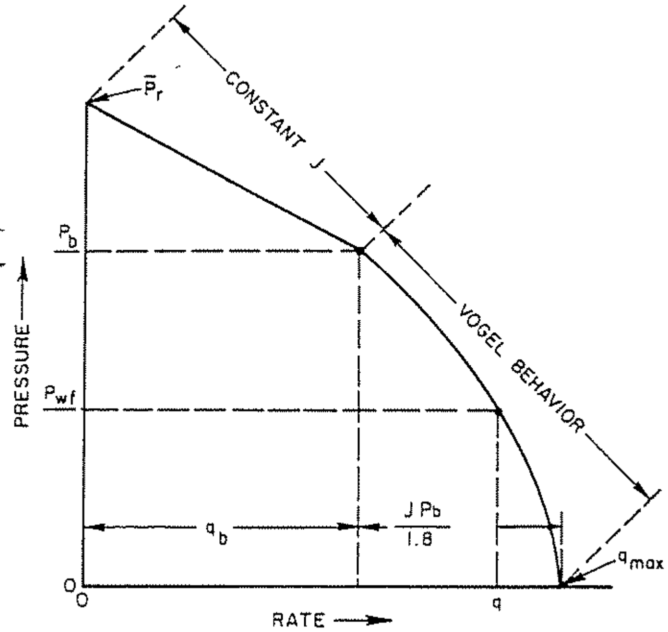

$$q_{max} = q_b - \frac{J P_b}{1.8}$$

$$q_b = J(\bar{P}_r - P_b)$$

$$q = q_b + (q_{max} - q_b)\left[1 - .2\frac{P_{wf}}{P_b} - .8\left(\frac{P_{wf}}{P_b}\right)^2\right]$$

Figure 2.15 Combination Constant PI and Vogel Behavior Case

In this case, $\int_{P_{wf}}^{P_r} f(P)dP$ is divided into two parts as follows:

$$\int_{P_{wf}}^{P_r} f(P)dP = \int_{P_b}^{\bar{P}_r} \frac{1}{\bar{\mu}_o \bar{B}_o} dP + \int_{P_{wf}}^{P_b} \frac{k_{ro}}{\mu_o B_o} dP \tag{2.21}$$

Be careful in attaching any physical significance to the above integrals because the flow from P_r to P_b must also pass through the region from P_b to P_{wf}. We can, however, use this analysis to obtain a total flow rate—that is, q_b from P_r to P_b plus q from P_b to P_{wf}.

The complete IPR curve can be constructed if we know the productivity index that exists at the bubble point.

The following relationship is very important concerning the two-phase flow section only:

$$\underset{(Vogel)}{\bar{q}_{max}} = \frac{q_{max}(J)}{1.8} \tag{2.22}$$

$$q_{max}(J) = J(P_b - 0) = J P_b$$

$$\underset{(Vogel)}{q_{max}} = \frac{J P_b}{1.8}$$

or:

$$J = \frac{q_{max}(1.8)}{P_b} \tag{2.23}$$

If we start with Vogel's equation:

$$q_o = q_{max}\left[1 - 0.2\frac{P_{wf}}{P_r} - 0.8\left(\frac{P_{wf}}{P_r}\right)^2\right]$$

and take the differential:

$$-\frac{dq}{dp_{wf}} = q_{max}\left[\frac{0.2}{P_r} + \frac{1.6 P_{wf}}{P_r^2}\right] \tag{2.24}$$

(P_R) $\quad P_r \approx P_{wf} \approx P_b$

$$J = \frac{0.2 P_r + 1.6 P_{wf}}{P_R^2} \approx \frac{(0.2 + 1.6)\cancel{P_b}}{P_b^{\cancel{2}}} = \frac{1.8}{P_b}$$

Taking the slope or J at $P_{wf} = P_b$, we have:

$$J = \frac{1.8\, q_{max}}{P_b} \tag{2.25}$$

or:

$$\underset{(Vogel)}{q_{max}} = \frac{J P_b}{1.8} \tag{2.26}$$

Although I am not certain where this work originated, I would like to give credit to both Eickmeier et al.[10] and Neeley.[11]

The following equations are applicable in constructing the complete IPR curve:

$$q_b = J(P_r - P_b) \tag{2.27}$$

$$q_{max} = q_b + \frac{J P_b}{1.8} \tag{2.28}$$

$$q = q_b + [q_{max} - q_b]\left[1 - 0.2\left(\frac{P_{wf}}{P_b}\right) - 0.8\left(\frac{P_{wf}}{P_b}\right)^2\right] \tag{2.29}$$

Therefore, if we know J, we can determine $q_{o_{max}}$, and by assuming other pressures, we can calculate the corresponding flow rates. J can be determined from a test on the well or from Darcy's Law. If the test is taken below the bubble-point pressure, we must first solve for J from the following equation:

$$J = \frac{q}{\bar{P}_r - P_b + \frac{P_b}{1.8}\left[1 - 0.2\left(\frac{P_{wf}}{P_b}\right) - 0.8\left(\frac{P_{wf}}{P_b}\right)^2\right]} \tag{2.30}$$

This equation is obtained by combining Equations 2.27, 2.28, and 2.29. Once J is determined, the complete IPR curve can be constructed as previously shown. J can be determined either from a test or by using Darcy's Law. If a test is given along with $\bar{P}_r$, J is calculated by the following equation:

$$J = \frac{q_{test}}{P_r - P_{wf}} \tag{2.31}$$

where:

$P_{wf} > P_b$

or J may be calculated from Darcy's Law:

$$J = \frac{7.08 \times 10^{-3}\, kh}{\bar{\mu}\,\bar{B}\,(\ln r_e/r_w - 3/4 + S)} \tag{2.32}$$

where:

$k = md,\ h = ft,\ \mu = cp$

EXAMPLE PROBLEM #6

Given data:

$P_r = 4{,}200$ psi
$J = 2.0$
$P_b = 3{,}000$ psi

Calculate:

(1) q_b
(2) q_{max}
(3) q for $P_{wf} = 1{,}500$ psi

Solution procedure:

(1) $q_b = J(P_r - P_b) = 2.0(4{,}200 - 3{,}000)$
$= 2{,}400$ b/d

(2) $q_{max} = q_b + \frac{J\,P_b}{1.8} = 2{,}400 + \frac{(2)(3{,}000)}{1.8}$
$= 2{,}400 + 3{,}333 = 5{,}733$ b/d

(3) Find: q_o for $P_{wf} = 1{,}500$ psia

$$q_o = q_b + \left[q_{max} - q_b\right]\left[1 - 0.2\left(\frac{P_{wf}}{P_b}\right) - 0.8\left(\frac{P_{wf}}{P_b}\right)^2\right]$$

$$q_o = 2{,}400 + [5{,}733 - 2{,}400]\left[1 - 0.2\left(\frac{1{,}500}{3{,}000}\right) - 0.8\left(\frac{1{,}500}{3{,}000}\right)^2\right]$$

$$q_o = 2{,}400 + (3{,}333)(0.7) = 4{,}733 \text{ b/d}$$

Other values of flowing pressure can be assumed, and the corresponding values of flow rate can be determined. From these, the IPR curve can be plotted.

EXAMPLE PROBLEM #7

Given data:

$P_r = 3{,}000$ psia
$P_b = 2{,}000$ psia (bubble point)
$k = 30$ md
$h = 60$ ft
$\overline{B}_o = 1.2$
$\overline{\mu}_o = 0.68$ cp
$r_e = 2{,}000$ ft
$r_w = 0.4$ ft
$S = 0$

Calculate:

(1) $q_{bubble\ point}$
(2) $q_{o_{max}}$ total if it follows Vogel's relationship below P_b
(3) q_o for a flowing pressure of:
 (a) 2,500 psia
 (b) 1,000 psia

Solution procedure:

For this solution, we must first obtain the J from Darcy's Law (Assume S = 0).

$$q_o = \frac{7.08\,kh \times 10^{-3}\,(P_r - P_{wf})}{\overline{B}_o\,\overline{\mu}_o\left(\ln\frac{r_e}{r_w} - \frac{3}{4} + S\right)}$$

$$q_b = J\,(P_r - P_{wf})$$

$$q_b = \left[\frac{(7.08)(30)(60)\times 10^{-3}}{(1.2)(0.68)\left(\ln\frac{2{,}000}{0.4} - 0.75 + 0\right)}\right](3{,}000 - 2{,}000) = 2.011(3{,}000 - 2{,}000) = 2{,}010.72 \text{ b/d}$$

where:

$$J = \frac{2{,}010.72}{3{,}000 - 2{,}000} = \frac{2{,}010.72}{1{,}000} = 2.011 \text{ b/d/psi}$$

$$q_{max} = q_b + \frac{J\,(P_b)}{1.8}$$

$$q_{max} = \left[2{,}010.72 + \frac{(2.011)(2{,}000)}{1.8}\right] = 4{,}245.32 \text{ b/d}$$

(a) Find q_o for $P_{wf} = 2{,}500$ psi:

$$q_o = J\,(P_r - P_{wf}) = 2.011\,(3{,}000 - 2{,}500) = 1{,}005.50 \text{ b/d}$$

(b) Find q for $P_{wf} = 1{,}000$ psi:

$P_{wf} = 1{,}000$ psia $< P_b$

$$q_o = q_b + (q_{max} - q_b)\left[1 - 0.2\left(\frac{P_{wf}}{P_b}\right) - 0.8\left(\frac{P_{wf}}{P_b}\right)^2\right]$$

$$q_o = 2{,}010.72 + (4{,}245.32 - 2{,}010.72) \times \left[1 - 0.2\left(\frac{1{,}000}{2{,}000}\right) - 0.8\left(\frac{1{,}000}{2{,}000}\right)^2\right]$$

$$= 3{,}574.94 \text{ b/d}$$

EXAMPLE PROBLEM #8

(For a test taken below the bubble-point pressure)

Given data:

$P_r = 4{,}000$ psia
$P_b = 3{,}000$ psia
$q_o = 600$ b/d for $P_{wf} = 2{,}000$ psia

Calculate:

(1) J
(2) q_b
(3) q_{max}
(4) q for $P_{wf} = 3{,}500$ psia
(5) q for $P_{wf} = 1{,}000$ psia

Solution procedure:

In order to solve this problem, first determine the productivity index that exists on the straight-line portion of the IPR curve. Equation 2.30 can be used.

(1) $$J = \frac{q}{P_r - P_b + \frac{P_b}{1.8}\left[(1 - 0.2\left(\frac{P_{wf}}{P_b}\right) - 0.8\left(\frac{P_{wf}}{P_b}\right)^2\right]}$$

$$J = \frac{600}{(4{,}000 - 3{,}000) + \frac{3{,}000}{1.8}\left[1 - 0.2\left(\frac{2{,}000}{3{,}000}\right) - 0.8\left(\frac{2{,}000}{3{,}000}\right)^2\right]}$$

$$J = \frac{600}{(1{,}000) + 1{,}667\,(0.511)} = 0.324\,\frac{\text{b/d}}{\text{psi}}$$

(2) $q_b = 0.324\,[4{,}000 - 3{,}000] = 324$ b/d

(3) $$q_{max} = q_b + \frac{J\,P_b}{1.8} = 324 + \frac{0.324\,(3{,}000)}{1.8} = 324 + 540 = 864 \text{ b/d}$$

(4) find q for $P_{wf} = 3{,}500$ psi

$$q = J\,(P_r - P_{wf}) = 0.324\,(4{,}000 - 3{,}500) = 162 \text{ b/d}$$

(5) find q for $P_{wf} = 1{,}000$ psi

$$q = q_b + [q_{max} - q_b]\left[1 - 0.2\left(\frac{P_{wf}}{P_b}\right) - 0.8\left(\frac{P_{wf}}{P_b}\right)^2\right]$$

$$= 324 + (540)\left[1 - 0.2\left(\frac{1{,}000}{3{,}000}\right) - 0.8\left(\frac{1{,}000}{3{,}000}\right)^2\right]$$

$$= 324 + 540\,(0.844) = 780 \text{ b/d}$$

Hasan[12] extended Vogel's equation for the combination of single-phase flow and two-phase flow conditions by using a similar procedure used by Standing.[13] The equation he obtained was:

$$\frac{J}{J^*} = \frac{P_b}{1.8(P_r - P_{wf})}\left\{1.8\left(\frac{P_r}{P_b}\right) - 0.8 - 0.2\left(\frac{P_{wf}}{P_b}\right) - 0.8\left(\frac{P_{wf}}{P_b}\right)^2\right\} \quad (2.33)$$

where:

P_r = reservoir pressure (above the bubble-point pressure)
J = the productivity index at flowing conditions below the bubble point
$J^* = \lim_{P_{wf} \to P_b} J$ = the productivity index above the bubble point

The procedure for determining IPR curves using Hasan's equation (Equation 2.33) is as follows:

(1) If the test is taken below the bubble-point pressure, calculate J at the test condition using the definition of productivity index; that is:

$$J = \frac{q_{o_{test}}}{P_r - P_{wf_{test}}}$$

Then, using Equation 2.33, calculate J^* and continue to step 3.

(2) If the test is taken above the bubble-point pressure, calculate J^* using the definition of productivity index; that is:

$$J^* = (q_o)/(P_r - P_{wf}) \text{ for } P_{wf} > P_b$$

(3) For a specific flowing pressure, calculate J using Equation 2.33.

(4) Calculate the flow rate for the flowing pressure of step 3 using the definition of productivity index.

EXAMPLE PROBLEM #9

Use the data from example problem #6 and solve it using Equation 2.33.

Solution procedure:

(1) $J^* = 2.0$:
$q_b = 2.0\,(4{,}200 - 3{,}000) = 2{,}400$ b/d

(2) $P_{wf} = 0$:

$$J = \frac{(2.0)(3{,}000)}{1.8\,(4{,}200 - 0)}\left\{1.8\left(\frac{4{,}200}{3{,}000}\right) - 0.8 - 0.2(0) - 0.8\,(0)^2\right\} = 1.365$$

$q_{max} = 1.365\,(4{,}200 - 0) = 5{,}733$ b/d

(3) $P_{wf} = 1{,}500$ psi:

$$J = \frac{(2.0)(3{,}000)}{1.8\,(4{,}200 - 1{,}500)}\left\{1.8\left(\frac{4{,}200}{3{,}000}\right) - 0.8 - 0.2\left(\frac{1{,}500}{3{,}000}\right) - 0.8\left(\frac{1{,}500}{3{,}000}\right)^2\right\} = 1.753$$

$q_o = 1.753\,(4{,}200 - 1{,}500) = 4{,}733$ b/d

EXAMPLE PROBLEM #10

Use the data from example problem #8 and, for the test taken below the bubble-point pressure, solve the problem using Equation 2.33.

Solution procedure:

(1) $J = \dfrac{600}{4{,}000 - 2{,}000} = 0.30$

$$J^* = 0.30 \Big/ \left[\frac{3{,}000}{1.8(4{,}000 - 2{,}000)}\left\{1.8\left(\frac{4{,}000}{3{,}000}\right) - 0.8 - 0.2\left(\frac{2{,}000}{3{,}000}\right) - 0.8\left(\frac{2{,}000}{3{,}000}\right)^2\right\}\right] = 0.324$$

(2) $q_b = 0.324(4{,}000 - 3{,}000) = 324.03$ b/d

(3) For $P_{wf} = 0$ psi:

$$J = \frac{0.324(3{,}000)}{1.8(4{,}000 - 0)}\left\{1.8\left(\frac{4{,}000}{3{,}000}\right) - 0.8 - 0.2(0) - 0.8(0)^2\right\} = 0.216$$

$q_{max} = 0.216(4{,}000 - 0) = 864.0$ b/d

(4) For $P_{wf} = 3{,}500$ psi (above the bubble point):

$q_o = J^*(P_r - P_{wf}) = 0.324(4{,}000 - 3{,}500)$
$= 162.0$ b/d

(5) For $P_{wf} = 1{,}000$ psi (below the bubble-point pressure):

$$J = \frac{0.324(3{,}000)}{1.8(4{,}000 - 1{,}000)}\left\{(1.8\left(\frac{4{,}000}{3{,}000}\right) - 0.8 - 0.2\left(\frac{1{,}000}{3{,}000}\right) - 0.8\left(\frac{1{,}000}{3{,}000}\right)^2\right\} = 0.260$$

$q_o = 0.260(4{,}000 - 1{,}000) = 780.0$ b/d

Other values of flowing pressure can be assumed from which the corresponding values of flow rate can be determined and the complete IPR curve can be plotted.

CLASS PROBLEM #10a

Given data:

$P_r = 3{,}100$ psia
$P_b = 2{,}200$ psia
$J = 1.65$

Calculate: (using an extension of Vogel's method and Hasan's equation)

(1) q_b
(2) q_{max}
(3) q for $P_{wf} = 1{,}000$ psi
(4) construct the IPR curve

CLASS PROBLEM #10b

Given data:

$P_r = 3{,}600$ psia	$k = 100$ md
$P_b = 2{,}800$ psia	$h = 40$ ft
°API = 30	140-acre spacing
Temperature = 190°F	10¾-in. diameter drilled hole
$\gamma_g = 0.7$	
GOR = 350 scf/bbl	S = 0

Calculate: (using an extension of Vogel's method and Hasan's equation)

(1) q_b
(2) q_{max}

(3) q for $P_{wf} = 2{,}000$ psia
(4) q for $P_{wf} = 1{,}000$ psia
(5) q for $P_{wf} = 3{,}100$ psia

CLASS PROBLEM #10c

Given data:

$P_r = 4{,}200$ psia
$P_b = 2{,}700$ psia

A test on this well shows 1,600 b/d for $P_{wf} = 1{,}700$ psia.

Calculate: (using an extension of Vogel's method and Hasan's equation)

(1) J
(2) q_b
(3) q_{max}
(4) q for $P_{wf} = 1{,}000$ psia
(5) construct the IPR curve

In the previous discussion, the pressure-dependent function was divided into two parts as shown in Equation 2.21. This equation assumes that the critical gas saturation as well as pressure at the critical gas saturation is reached rapidly as soon as the bubble point is reached.

Under a constant production rate for reservoirs that have initial reservoir pressure above the bubble point, the gas saturation builds rapidly to the critical gas saturation and remains constant. The high pressure drop in the vicinity of the wellbore causes the gas saturation to increase. This phenomenon can be drawn schematically as shown in Figure 2.16. Based on this fact, Hasan divides the pressure-dependent function into three parts as shown in Equation 2.34; that is:[12]

$$\int_{P_{wf}}^{P_r} f(P)\,dP = \int_{P_b}^{P_r} \frac{k_{ro}}{\mu_o B_o}\,dP + \int_{P_{Sg_c}}^{P_b} \frac{k_{ro}}{\mu_o B_o}\,dP + \int_{P_{wf}}^{P_{Sg_c}} \frac{k_{ro}}{\mu_o B_o}\,dP \qquad (2.34)$$

Assuming the relative permeability is a function of oil saturation only, Equation 2.34 can be simplified into:

$$\int_{P_{wf}}^{P_r} f(P)\,dP = \int_{P_b}^{P_r} \frac{1}{\mu_o B_o}\,dP + k_{rc}\int_{P_{Sg_c}}^{P_b} \frac{1}{\mu_o B_o}\,dP + \int_{P_{wf}}^{P_{Sg_c}} \frac{k_{ro}}{\mu_o B_o}\,dP \qquad (2.35)$$

Using the actual field data, Hasan made plots of calculated values of J/J^* (based on Equation 2.33 and Equation 2.21) vs P_{wf}/P_b as shown in Figure 2.17 and compared the results to the actual field performance.[14] The same thing was done using Equation 2.35, and the comparison of the results to the actual field performance is shown in Figure 2.18.

Based on these plots, Hasan concluded that Equation 2.35 yields the best agreement to the actual field performance. His work was for critical gas saturation between 10% and 13%.

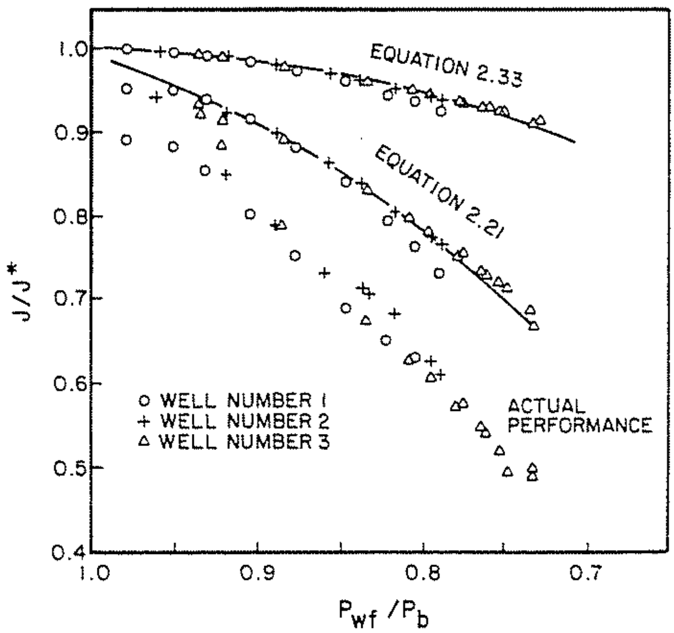

Figure 2.17 Comparison of the Values J/J Calculated using Equations 2.33 and 2.21 with Actual Field Performance (after Hasan)*[12]

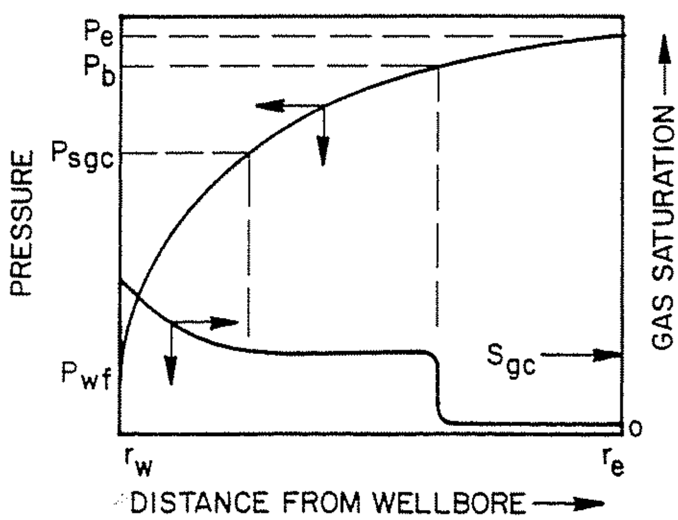

Figure 2.16 Pressure-Saturation Relationship (after Hasan)[12]

2.224 STANDING'S PROCEDURE FOR FLOW EFFICIENCY NOT EQUAL TO 1.0

Standing extended the work of Vogel to take care of those cases where FE ≠ 1.0.[13] Flow efficiency can be defined from Figure 2.19:

$$FE = \frac{P_r - P'_{wf}}{P_r - P_{wf}} \qquad (2.36)$$

where:

P'_{wf} = the equivalent undamaged flowing pressure
P_{wf} = actual flowing pressure
$\bar{P}_r$ = static reservoir pressure

Standing presented Figure 2.20 for use with FE values between 0.5 and 1.5. A necessary first step for this use is to determine $q_{o_{max}}$ for FE = 1.0, after which

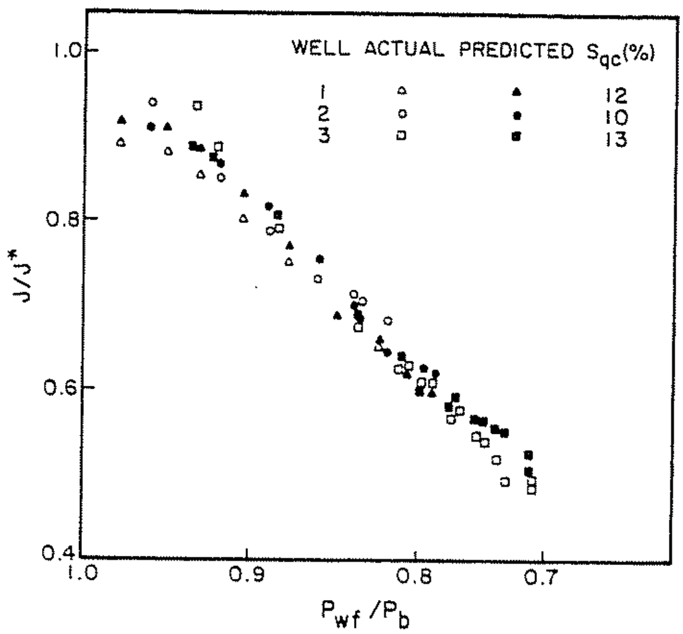

Figure 2.18 Comparison of the Values of J/J Calculated using Equation 2.35 with Actual Field Performance (after Hasan)[12]*

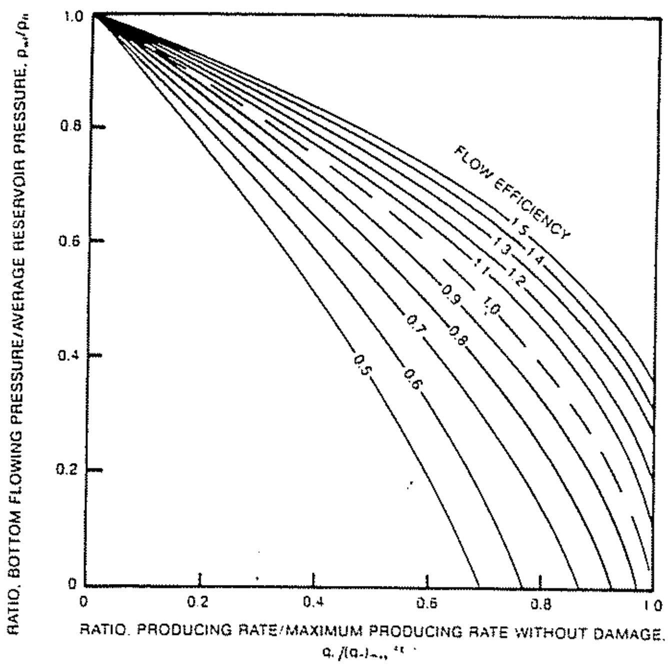

Figure 2.20 Standing's Correlation for Wells with FE Values not Equal to 1 (Working Copy on p. 334)

the flow rate can be determined for any flow efficiency and any flowing pressure. Therefore, an IPR curve may be constructed for flow efficiencies other than 1.0. The solution may also be obtained from the following equations:

Solving Equation 2.36 for P'_{wf} provides:

$$P'_{wf} = P_r - (P_r - P_{wf})FE \qquad (2.37)$$

Then, Vogel's equation can be used directly:

$$\underset{(FE = 1.00)}{q_o/q_{max}} = 1 - 0.2\left(\frac{P'_{wf}}{P_r}\right) - 0.8\left(\frac{P'_{wf}}{P_r}\right)^2 \qquad (2.38)$$

because P'_{wf} equals flowing pressure for FE = 1.00. In the use of Figure 2.20 and Vogel's equation, a problem develops for certain conditions of low flowing pressures and high FE values. For example, if the following data are known:

$P_r = 2{,}000$ psia
FE = 2.0
$P_{wf} = 500$ psi

then:

$$P'_{wf} = P_r - (P_r - P_{wf})FE \qquad (2.37)$$

$$P'_{wf} = 2{,}000 - (2{,}000 - 500)2 = -1{,}000 \text{ psi}$$

The negative value of 1,000 psi gives trouble in Vogel's original equation and will show a reduced flow rate as compared to positive values of P'_{wf}. Typical results are shown in Figure 2.21.

A more accurate solution can be obtained by chang-

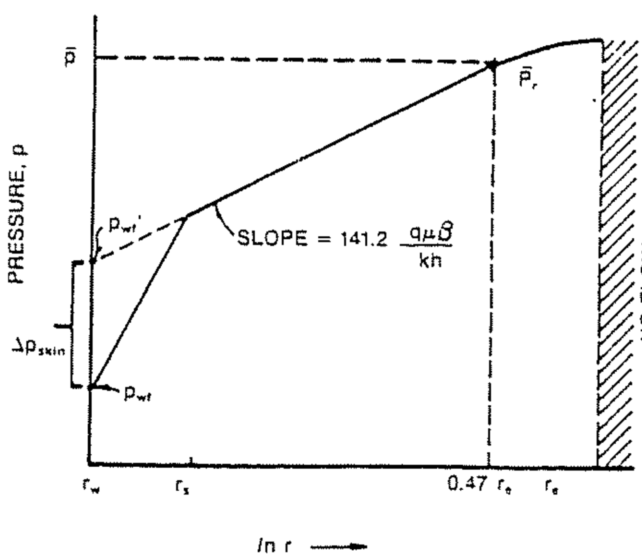

Figure 2.19 Pressure Profile of Damaged Wells Producing by Solution-Gas Drive (after Standing)[13]

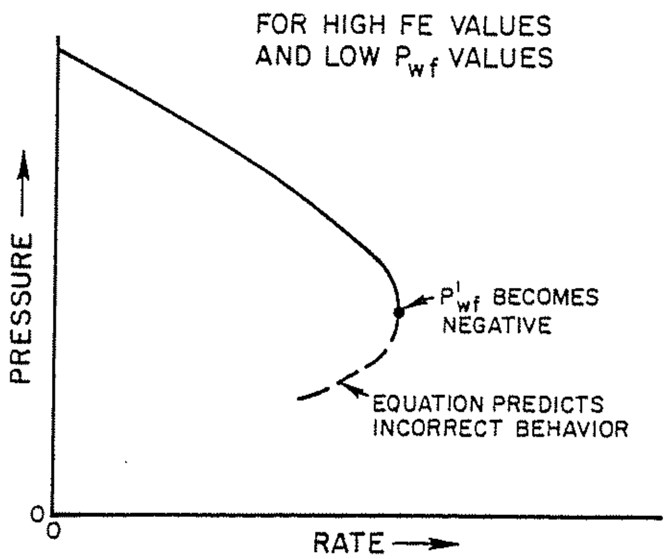

Figure 2.21 Errors from Extrapolating Standing's Work Outside of Its Range

ing the form of the equation. Two possibilities are suggested.

(1) The following equation was suggested by Harrison and will do equally well for positive or negative values of P'_{wf}.[14]

$$q_o/q_{max(FE=1.0)} = 1.2 - 0.2\, e^{(1.792\, P'_{wf}/P_r)} \qquad (2.39)$$

This equation may be used in place of Vogel's equation and works for either positive or negative values of P'_{wf}. However, it has been noted that it underpredicts the flow rates as compared to Vogel's equation.

(2) An equation of the following form may also be used:

$$q = J'_o\,(P_r^2 - P_{wf}^2)^n \qquad (2.40)$$

This equation is for a straight line on log-log paper. In order to use Equation 2.40, use Vogel's equation until negative values of P'_{wf} start. Note Figure 2.22 for a plot of P_{wf} vs q.

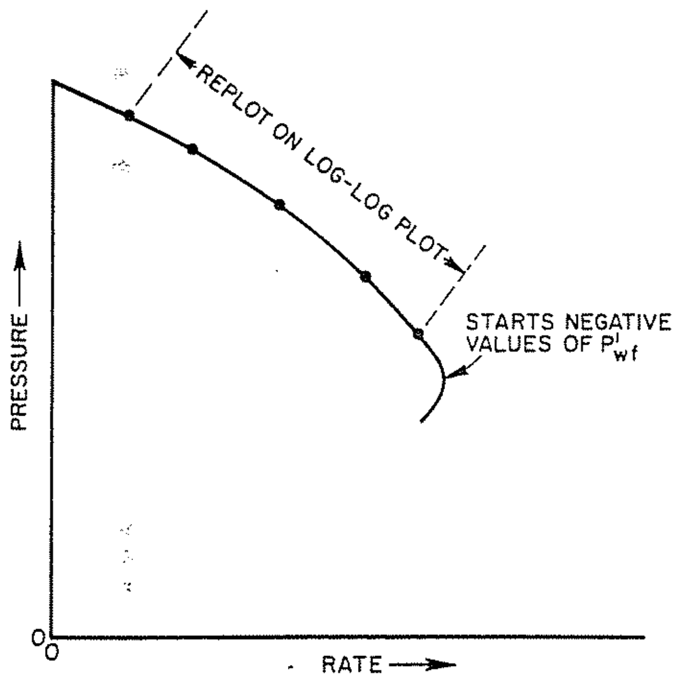

Figure 2.22 Plot of Flow Rate vs Pressure for Positive Values of P_{wf}'

Using only those values noted on the heavy line of Figure 2.22, these points are replotted on log-log paper as noted in Figure 2.23.

J'_o is the intercept on the q axis where $P_r^2 - P_{wf}^2 = 1.0$ and n = 1/slope. Once the values of n and J'_o have been determined, this equation may then be used to complete the IPR plot of pressure vs rate as noted in Figure 2.24.

A generalized plot by Harrison[14] is noted in Figure 2.25, which has been extended by use of Equation 2.40.

Figure 2.25 should be used when the FE value is out of the range of Standing's original plot and gives more accurate results than Equation 2.39.

EXAMPLE PROBLEM #11

(Standing's Procedure [using Figure 2.20])

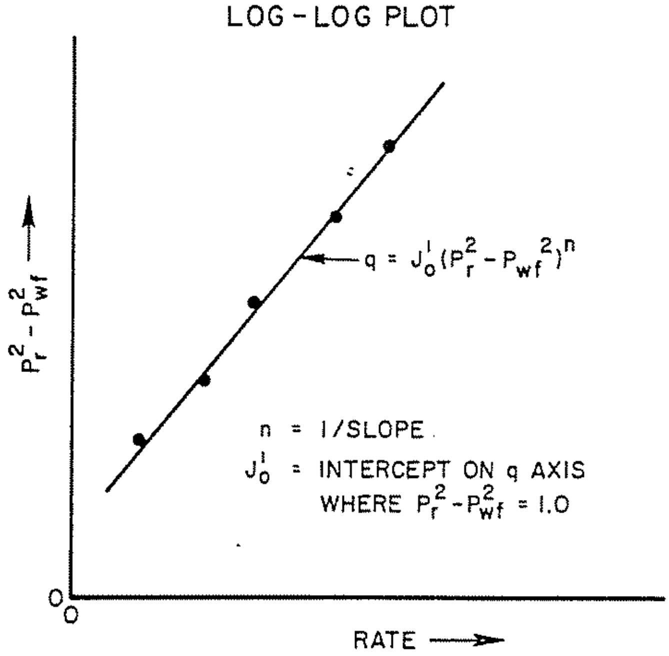

Figure 2.23 Replot of Figure 2.21

Given data:

P_r = 2,600 psia < P_b
test shows q = 500 b/d for P_{wf} = 1,800 psia
from buildup, the FE value = 0.6

Calculate:

(1) $q_{o_{max}}$ for FE = 1.0
(2) $q_{o_{max}}$ for FE = 0.6
(3) Find q_o for P_{wf} = 1,300 psia for FE = 0.6, 1.0, and 1.3

Solution procedure:

(1) Determine $q_{o_{max}}$ for FE = 1.0.

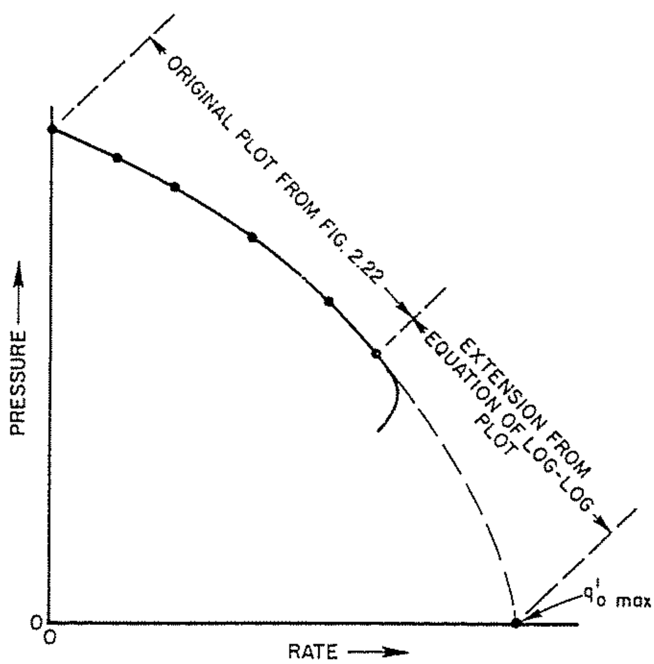

Figure 2.24 Extension of Figure 2.22 by Equation from Figure 2.23

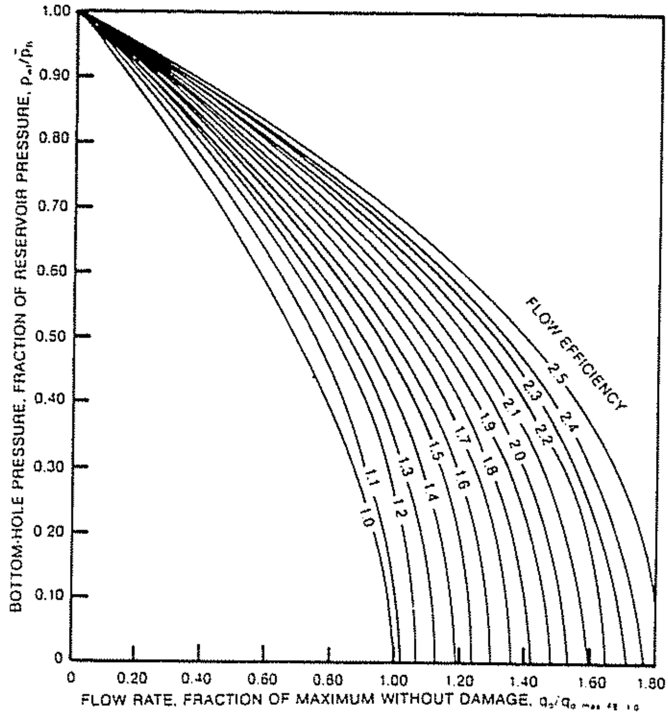

Figure 2.25 Harrison's Extension of Standing's Work to Include Other FE Values (Working Copy on p. 335)

$$P_{wf}/P_r = \frac{1,800}{2,600} = 0.692$$

From Figure 2.20, read $q_o/q_{max(FE=1.0)} = 0.3$, from which $q_{max}(FE = 1.0) = 1667$ b/d.

(2) Find q_{max} for FE = 0.6.

From Figure 2.20, read $q_o/q_{max(FE=1.0)} = 0.765$ where $P_{wf}/P_r = 0$. Then, q_{max} for FE = 0.6 = (0.765)(1,667 = 1,275 b/d.

(3) Find q_o for P_{wf} = 1,300 psia for FE = 0.6, 1.0, and 1.3.

$$\frac{1,300}{2,600} = 0.5$$

From Figure 2.20, read q_o/q_{max} for each FE value and then calculate the q_o values.

Results are noted in the following table:

FE value	$q_o/q_{max(FE=1.0)}$	q_{max} FE = 1.00	q_o
0.6	0.462	1,667	770
1.0	0.70	1,667	1,167
1.3	0.83	1,667	1,384

In order to construct three complete IPR curves for FE values of 0.6, 1.0, and 1.3, other values of P_{wf} can be assumed and corresponding values of q_o calculated for each FE value. A plot similar to Figure 2.26 will be obtained.

EXAMPLE PROBLEM #12

(Standing's Procedure [using Equations 2.37 and 2.38])

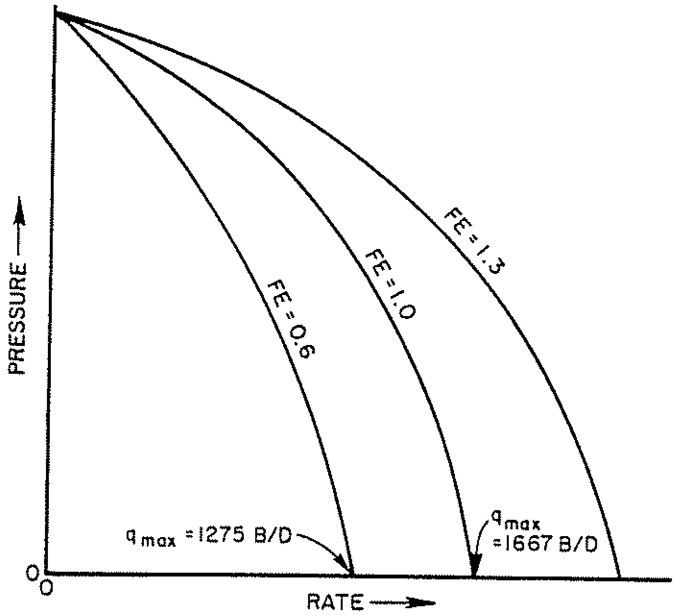

Figure 2.26 Typical IPR Curves for Varying FE Values

Given data: (same as example problem #11)

P_r = 2,600 psia
q_o = 500 b/d for P_{wf} = 1,800 psia
FE = 0.6

Calculate:

(1) $q_{o_{max}}$ for FE = 1.0
(2) $q_{o_{max}}$ for FE = 0.6
(3) Find q_o for P_{wf} = 1,300 psia and FE = 0.6, 1.0, and 1.3

Solution procedure:

(1) Find $q_{o_{max}}$ for FE = 1.0.

Find the equivalent test flowing pressure for FE = 1.0. From the equation:

$$P'_{wf} = P_r - (P_r - P_{wf})FE = 2,600 - (2,600 - 1,800)(0.6) = 2,120 \text{ psi}$$

From Vogel's equation:

$$q_{max} = \frac{q_o}{1 - 0.2\left(\frac{P'_{wf}}{P_r}\right) - 0.8\left(\frac{P'_{wf}}{P_r}\right)^2}$$

$$= \frac{500}{1 - 0.2\left(\frac{2,120}{2,600}\right) - 0.8\left(\frac{2,120}{2,600}\right)^2} = \frac{500}{0.305}$$

= 1,639 b/d (value from Figure 2.20 = 1,667)

(2) Find $q_{o_{max}}$ for FE = 0.6.

P_r = 2,600 $\qquad P_{wf} = 0$

P'_{wf} = 2,600 − (2,600 − 0)0.6 = 1,040 psi

$$q_o = q_{max}\left[1 - 0.2\left(\frac{P'_{wf}}{P_r}\right) - 0.8\left(\frac{P'_{wf}}{P_r}\right)^2\right]$$

$$q_o = 1,639\left[1 - 0.2\left(\frac{1,040}{2,600}\right) - 0.8\left(\frac{1,040}{2,600}\right)^2\right]$$

= 1,639(0.792) = 1,298 b/d

(3) Find q_o for P_{wf} = 1,300 psia and for FE = 0.6, 1.0, and 1.3.

(a) For FE = 0.6:

$$P'_{wf} = 2,600 - (2,600 - 1,300)0.6 = 1,820 \text{ psi}$$

$$q_o = 1,639\left[1 - 0.2\left(\frac{1,820}{2,600}\right) - 0.8\left(\frac{1,820}{2,600}\right)^2\right]$$

$$= 1,639(0.468) = 767 \text{ b/d}$$

(b) For FE = 1.0:

$$P'_{wf} = P_{wf} = 1,300 \text{ psia}$$

$$q_o = 1,639\left[1 - 0.2\left(\frac{1,300}{2,600}\right) - 0.8\left(\frac{1,300}{2,600}\right)^2\right]$$

$$= 1,639(0.7) = 1,147 \text{ b/d}$$

(c) For FE = 1.3:

$$P'_{wf} = 2,600 - (2,600 - 1,300)(1.3) = 910 \text{ psi}$$

$$q_o = 1,639\left[1 - 0.2\left(\frac{910}{2,600}\right) - 0.8\left(\frac{910}{2,600}\right)^2\right]$$

$$= 1,364 \text{ b/d}$$

EXAMPLE PROBLEM #13

Making use of Figure 2.25 prepared from an equation of the form:

$$q = Jo'(P_r^2 - P_{wf}^2)^n$$

Given data:

P_r = 2,000 psi
FE = 2.0
q_o = 1,200 b/d for P_{wf} = 500 psia

Calculate:

(1) q_{max} for FE = 1.0
(2) q_{max} for FE = 2.0
(3) q_o for P_{wf} = 1,000 psia and FE value of 2

Solution procedure:

(1) Find q_{max} for FE = 1.0:

$$\frac{P_{wf}}{P_r} = \frac{500}{2,000} = 0.25$$

Reading from FE = 2.0 curve:

$$q_o/q_{max(FE=1.0)} = 1.435 \text{ from Fig. 2.25}$$

$$\frac{200}{q_{max(FE=1.0)}} = 1.435$$

$$q_{max}(FE = 1.00) = \frac{1,200}{1.435} = 836 \text{ b/d}$$

(2) Find q_{max} for FE = 2.0

$$\frac{0}{P_r} = 0$$

Read 1.53 from Figure 2.25:

$$(1.53)(836) = 1,280 \text{ b/d}$$

(3) q_o for P_{wf} = 1,000 and FE = 2.0 and 2.5

$$\frac{1,000}{2,000} = 0.5$$

Read $q_o/q_{max(FE=1.0)}$ = 1.165 from FE = 2.0 curve and $q_o/q_{max(FE=1.0)}$ = 1.40 from FE = 2.5 curve:

$$(1.165)(836) = 974 \text{ b/d for FE} = 2.0$$

$$(1.4)(836) = 1,170 \text{ b/d for FE} = 2.5$$

EXAMPLE PROBLEM #14

(Where Standing's procedure gives negative value of P'_{wf})

Given data:

P_r = 2,000
FE = 2.0
q_o = 200 b/d for P_{wf} = 500 psia

Calculate:

(1) q_{max} for FE = 1.0
(2) q_{max} for FE = 2.0
(3) q_o for P_{wf} = 1,000 psia and FE = 2 and 3.

Solution procedure:

Try Standing's equation:

$$P'_{wf} = 2,000 - (2,000 - 500)(2) = -1,000 \text{ psi}$$

A negative P'_{wf} if used in Vogel's equation will show rates less than positive values—that is, a P_{wf} greater than 1,000 psi (that P_{wf} where P'_{wf} = 0)—and would result in a plot similar to Figure 2.21.

(1) Find q_{max} for FE = 1.0:

Using the equation developed by Harrison:

$$q_o/q_{max(FE=1.0)} = 1.2 - 0.2\,e^{1.792\,P'_{wf}/P_r}$$

$$P'_{wf} = 2,000 - (2,000 - 500)2 = -1,000 \text{ psi}$$

$$q_o/q_{max(FE=1.0)} = 1.2 - 0.2\,e^{1.792(-500/2,000)}$$

$$= 1.118 \text{ (where } e = 2.7183)$$

$$q_{max}(FE = 1.0) = (200)(1.118) = 178.8 \text{ b/d}$$

(2) Find q_{max} for FE = 2.0:

$$P'_{wf} = 2,000 - (2,000 - 0)2 = -2,000$$

$$\frac{q_o}{178.8} = 1.2 - 0.2\,e^{1.792(-2,000/2,000)} = 1.1665$$

$$q_o = (178.8)(1.1665) = 208.5 \text{ b/d}$$

(3) Find q_o for P_{wf} = 1,000 and FE = 2 and FE = 3:

(a) For FE = 2:

$$P'_{wf} = 2,000 - (2,000 - 1,000)2 = 0$$

$$q_o/178.8 = 1.2 - 0.2\,e^{1.792(0/2,000)} = 1.0$$

$$q_o = 178.8 \text{ b/d}$$

(b) For FE = 3.0:

$$P'_{wf} = 2,000 - (2,000 - 1,000)(3) = -1,000$$

$$q_o/178.8 = 1.2 - 0.2\,e^{1.792(-1,000/2,000)} = 1.19$$

$$q_o = (178.8)(1.19) = 212.7 \text{ b/d}$$

CLASS PROBLEM #14a

Given data:

P_r = 1,800 psia
FE = 0.7
q_o = 150 b/d for P_{wf} = 1,400 psia

Calculate: (using Standing's procedure and Figures 2.20 and 2.25)

(1) $q_{o_{max}}$ for FE = 1.0
(2) $q_{o_{max}}$ for FE = 0.7
(3) q_o for P_{wf} = 1,000 psia and FE = 0.7, 1.0, and 1.4

CLASS PROBLEM #14b

Given data:

$P_r = 1{,}900$ psia
FE = 2.2
$q_o = 300$ b/d for $P_{wf} = 800$ psia

Calculate: (using Standing's procedure and Figure 2.25)

(1) $q_{o_{max}}$ for FE = 1.0
(2) $q_{o_{max}}$ for FE = 2.0
(3) q_o for P_{wf} = 1,000 psia and FE = 1.0, 2.0, and 2.5

CLASS PROBLEM #14c

Given data:

$P_r = 2{,}000$ psia
FE = 0.6
$q_o = 200$ b/d for $P_{wf} = 1{,}600$ psia

Calculate: (using Standing's procedure and Figures 2.20 and 2.25)

(1) $q_{o_{max}}$ for FE = 1.0
(2) $q_{o_{max}}$ for FE = 0.6
(3) q_o for P_{wf} = 500 psia and FE = 0.6, 1.0, 2.0, and 2.5

2.225 COUTO'S PROCEDURE FOR FE NOT EQUAL TO ONE

Couto[15] manipulated Standing's equation for damaged wells (Equation 2.38) and applied it to the definition of productivity index proposed by Standing.[13] He arrived at an equation to predict present IPR curves and also future IPR curves. For circular drainage areas, his equation is:

$$q_o = 3.49(a)\frac{Kh}{\ln(0.472r_e/r_w)}P_r\left(\frac{k_{ro}}{\mu_o B_o}\right)(FE) \times (1-R)[1.8 - 0.8(FE)(1-R)] \qquad (2.41)$$

For noncircular drainage areas, the previous equation can be generalized into:

$$q_o = 3.49(a)\frac{Kh}{\ln X}P_r\left(\frac{k_{ro}}{\mu_o B_o}\right)(FE)(1-R) \times [1.8 - 0.8(FE)(1-R)] \qquad (2.42)$$

where:

a = unit conversion factor = 0.001127 for ft, psi, cp, md, and stb/d
X = shape factor as shown in Figure 2.9
$R = P_{wf}/P_r$

Equation (2.42) can be used to predict IPR curves at the present time or in the future at any flow efficiency and any stage of reservoir depletion. For FE values greater than 1, a similar result in Standing's method in predicting IPR curves will be obtained.

EXAMPLE PROBLEM #15

Given data:

reservoir pressure = 2,500 psi
B_o @ P_r = 1.319 stb/bbl
μ_o @ P_r = 0.5421 cp
k_o = 50 md
h = 50 ft
r_e = 1,500 ft
r_w = 0.25 ft

Calculate:

(1) the flow rate for P_{wf} = 1,000 psi
(2) the maximum flow rate at FE = 0.6 and FE = 1.2

Solution procedure:

(1) Using Equation (2.41) for FE = 0.6 and P_{wf} = 1,000 psi, the flow rate can be calculated as follows:

$$R = 1{,}000/2{,}500 = 0.4$$

$$\begin{aligned} q_o &= (3.49)(0.001127)\left(\frac{50}{\ln(0.472(1{,}500)/(0.25))}\right)(2{,}500) \\ &\quad\times\left(\frac{50}{0.5421(1.319)}\right)(0.6)(1-0.4)(1.8-0.8) \\ &\quad\times[(0.6)(1-0.4)] \\ &= (4{,}325.21)(0.6)(1-0.4)[1.8-0.8(0.6)(1-0.4)] \\ &= 2{,}354.30 \text{ stb/d} \end{aligned}$$

(2) The maximum flow rate for FE = 0.6 is as follows:

$$\begin{aligned} q_{max} &= (4{,}325.21)(0.6)(1-0)[1.8-0.8(0.6)(1-0)] \\ &= 3{,}425.56 \text{ stb/d} \end{aligned}$$

(3) For FE = 1.2, the flow rate at P_{wf} = 1,000 psi is as follows:

$$\begin{aligned} q_o &= (4{,}325.21)(1.2)(1-0.4)[1.8-0.8(1.2)(1-0.4)] \\ &= 3{,}811.72 \text{ stb/d} \end{aligned}$$

(4) Maximum flow rate: (for FE = 1.2)

$$\begin{aligned} q_{max} &= (4{,}325.21)(1.2)(1-0)[1.8-0.8(1.2)(1-0)] \\ &= 4{,}359.81 \text{ stb/d} \end{aligned}$$

CLASS PROBLEM #15a

Given data:

reservoir pressure = 2,200 psi
B_o @ P_r = 1.2807 bbl/stb
μ_o @ P_r = 0.5874 cp
k_o = 25 md
h = 40 ft
r_e = 1,200 ft
r_w = 0.33 ft

Calculate:

maximum flow rate and flow rate at P_{wf} = 1,250 psi for FE = 0.5 and 1.5

CLASS PROBLEM #15b

Given data:

P_r = 1,780 psia k_o = 40 md
h = 60 ft r_e = 1,290 ft

μ_o @ $P_r = 0.3598$ cp $r_w = 0.50$ ft
B_o @ $P_r = 1.3387$

Calculate:

(1) the flow rate for flowing pressure = 1,500 psi for FE = 0.4 and 2.0
(2) the maximum flow rate for FE = 0.4 and 2.0

CLASS PROBLEM #15c

Given data:

$P_r = 2{,}450$ psi $k_o = 150$ md
$r_e = 1{,}053$ ft $r_w = 0.33$ ft
μ_o @ $P_r = 0.9316$ cp B_o @ $P_r = 1.2317$
$h = 50$ ft

Calculate:

(1) the flow rate for $P_{wf} = 2{,}000$ psia and for FE = 0.75 and 2.50
(2) the maximum flow rate for FE = 0.75 and 2.50

2.226 THREE- OR FOUR-POINT TESTS

Fetkovich proposed that flow-after-flow or isochronal tests as used on gas wells could also be used on oil wells.[16] His justification for this was his assumption that a plot of $\frac{k_{ro}}{\mu_o B_o}$ vs pressure could be represented approximately by two straight-line segments as noted in Figure 2.27.

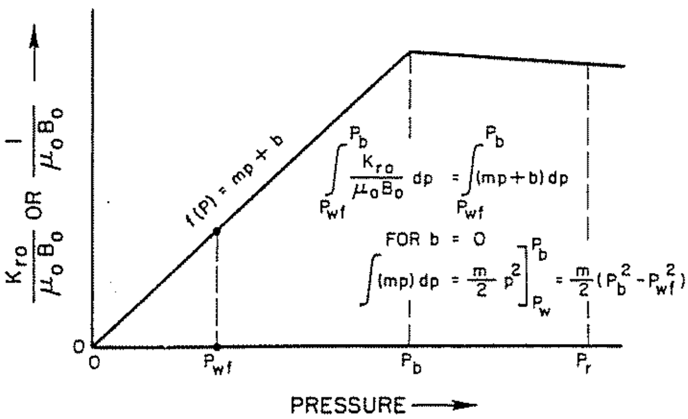

Figure 2.27 Fetkovich Plot of $\frac{K_{ro}}{\mu_o B_o}$ vs Pressure

By referring to Darcy's equation again:

$$q = \frac{(\text{constant})Kh}{(\ln r_e/r_w - 3/4 + S)} \int_{P_{wf}}^{P_r} f(P)\, dP \tag{2.1}$$

f(P) can be divided into two integrals:

$$f(P) = \int_{P_b}^{P_r} \frac{1}{\mu_o B_o} dP + \int_{P_{wf}}^{P_b} \frac{k_{ro}}{\mu_o B_o} dP \tag{2.43}$$

$$\int_{P_b}^{P_r} \frac{1}{\mu_o B_o} dP = \frac{1}{\bar{\mu}_o \bar{B}_o}(P_r - P_b) \tag{2.44}$$

$$\int_{P_{wf}}^{P_b} \frac{k_{ro}}{\mu_o B_o} dP = \int_{P_{wf}}^{P_b} (m_1 p + b_1)\, dP \tag{2.45}$$

where:

m_1 = the slope
b_1 = the intercept

If we assume further that $b_1 = 0$, then:

$$f(P) = \frac{m_1}{2}(P_b^2 - P_{wf}^2) \tag{2.46}$$

or:

$$q_{total} = \frac{(\text{constant})Kh}{(\ln r_e/r_w - 3/4 + S)} \times \left[\frac{1}{\bar{\mu}_o \bar{B}_o}(P_r - P_b) + \frac{m_1}{2}(P_b^2 - P_{wf}^2)\right] \tag{2.47}$$

Fetkovich suggested that we can represent this as follows:

$$q = J(P_r - P_b) + J'_o(P_b^2 - P_{wf}^2) \tag{2.48}$$

where:

$$J = \frac{7.08kh}{\bar{\mu}_o \bar{B}_o(\ln r_e/r_w - 3/4 + S)} \tag{2.49}$$

$$J'_o = \frac{7.08kh}{(\ln r_e/r_w - 3/4 + S)}\left[\left(\frac{k_{ro}}{\mu_o B_o}\right)_{P_r}\left(\frac{1}{2P_r}\right)\right] \tag{2.50}$$

where:

$$\text{slope } m_1 = \frac{k_{ro}}{\mu_o B_o} \Big/ P_r \tag{2.51}$$

He suggested that Equation 2.48 could be further generalized into the form:

$$q = J'_o(P_r^2 - P_{wf}^2)^n \tag{2.52}$$

This equation is in the same form used for gas wells; that is:

$$q = C(P_r^2 - P_{wf}^2)^n \tag{2.52}$$

where:

$$C = \frac{(\text{constant})kh}{\bar{\mu}\bar{T}\bar{Z}(\ln r_e/r_w - 3/4 + S)} \tag{2.53}$$

Equations 2.52 and 2.53 are straight lines on log-log paper, with both J'_o and C representing the intercept on the q axis (abscissa) where $P_r^2 - P_{wf}^2 = 1.0$ and n is 1/slope. Fetkovich presented numerous field cases for oil wells showing that Equation 2.53 represented accurately the inflow into the wellbore.

EXAMPLE PROBLEM #16

Given data: four-point oil well test:

$P_r = 2{,}500$ psia		$P_b = 3{,}000$
Test	q_o	P_{wf}
1	880	2,000
2	1,320	1,500
3	1,595	1,000
4	1,752	500

Calculate:

(1) value of exponent n
(2) value of J'_o
(3) absolute open flow potential (AOFP) or $q_{o_{max}}$
(4) q_o for $P_{wf} = 2{,}200$ psia

Solution procedure:

Refer to Figure 2.28 and note that a plot of $P_r^2 - P_{wf}^2$ vs q is required on log-log paper.

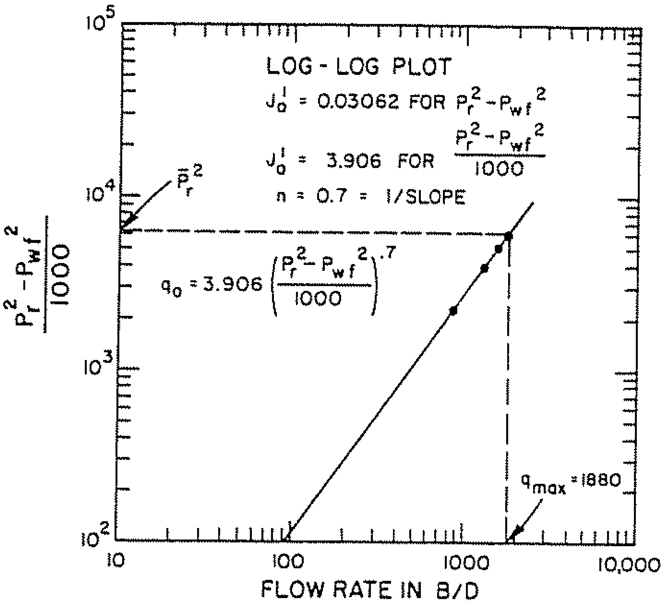

Figure 2.28 Four-Point Test Plot

(1) Prepare a table as follows:

q_o	P_{wf}	$(P_r^2 - P_{wf}^2) \times 10^3$*
880	2,000	2,250
1,320	1,500	4,000
1,595	1,000	5,250
1,752	500	6,000

* A choice can be made to plot in thousands if desired.

(a) Find the exponent n = 1/slope:

$$n = 0.70192$$

(b) Find J_o':

$$J_o' = 0.03062, \text{ or } J_o' = 3.906 \text{ for } \frac{P_r^2 - P_{wf}^2}{1,000}$$

(c) Find AOFP:

$$q_o = 0.03062(P_r^2 - P_{wf}^2)^{0.70192}$$

Use $P_{wf} = 0$:

$$q_{max} = 0.03062[2,500^2]^{0.70192}$$
$$q_{max} = 1,803.72 \text{ b/d}$$

Checking AOFP with the following equation:

$$q_{o_{max}} = 3.906\left[\frac{P_r^2 - 0^2}{1,000}\right]^{0.70192} = 1,803.58$$

or we obtain the same results as in part c.

(d) Find q_o for $P_{wf} = 2,200$ psia:

$$q_o = 0.03062(2,500^2 - 2,200^2)^{0.70192}$$
$$= 634.26 \text{ b/d}$$

CLASS PROBLEM #16a

Given data:

Flow-after-flow well test:
$\bar{P}_r = 3,000$ psia

q(b/d)	P_{wf} (psia)
80	2,987
200	2,949
400	2,863
1,000	2,449

Calculate:

(1) values of n and J_o' using Fetkovich's procedure
(2) the absolute open-flow potential ($q_{o_{max}}$)
(3) q_o for $P_{wf} = 1,000$ psia

CLASS PROBLEM #16b

Given data: Flow-after-flow well test:

$\bar{P}_r = 4,343$ psi

Test #	q_o	P_{wf}
1	372	4,313
2	724	4,288
3	1,403	4,242
4	2,767	4,154

Calculate:

(1) $q_{o_{max}}$
(2) the value of exponent n
(3) the value of constant J_o'
(4) q_o for $P_{wf} = 2,800$ psia and 1,500 psia

Jones, Blount, and Glaze suggest that radial flow for both oil and gas could be represented in another form in order to show whether near-wellbore restrictions exist.[6] The radial flow equation for oil is most commonly written as follows, except for the inclusion of the Dq term:

$$q_o = \frac{7.08 \times 10^{-3} kh(P_r - P_{wf})}{\bar{\mu}_o \bar{B}_o(\ln r_e/r_w - 3/4 + S + a'q)} \qquad (2.2)$$

It can be rearranged to appear as follows:

$$P_r - P_{wf} = \left[\frac{\mu B(\ln r_e/r_w - 3/4 + S)}{7.08 \times 10^{-3}(kh)}\right] q + \left(\frac{9.08 \times 10^{-13} \beta B_o^2 \rho}{4\pi^2 h_p^2 r_w}\right) q^2 \qquad (2.54)$$

If sufficient data is available, b and a can be calculated for use in Equation 2.54. If a three- or four-point flow rate test is available, b and a can be obtained from a plot. Equation 2.54 can be written in the form:

$$\frac{P_r - P_{wf}}{q} = aq + b$$

This can then be plotted as noted in Figure 2.29, which represents a straight line on regular coordinate paper.

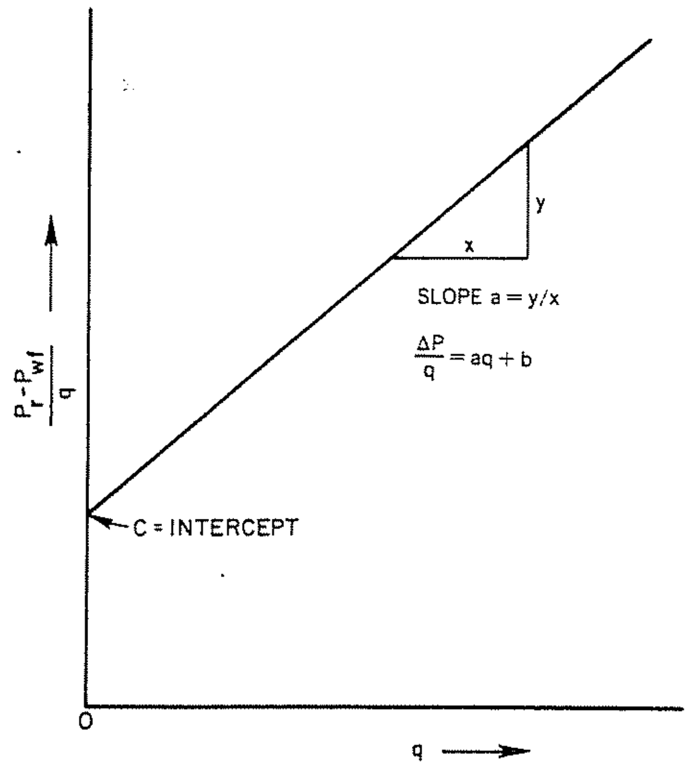

Figure 2.29 Typical Plot of Jones, Blount, and Glaze Equation[6]

From Equation 2.54, the values of b and a are as follows:

$$b = \frac{\mu_o B_o(\ln(r_e/r_w) - 0.75 + S)}{7.08 \times 10^{-3}\, kh} \qquad (2.55)$$

$$a = \frac{9.08 \times 10^{-13} \beta B_o^2 \rho}{4(\pi)^2 (h_p)^2\, r_w} \qquad (2.56)$$

If sufficient data are available, b and a can be calculated for use in Equation 2.54, by using Equations 2.55 and 2.56, respectively.

If a three- or four-point flow rate test is available, b and a can be obtained from the plot by using the following procedure (refer to Figure 2.29):

(1) From the test data, calculate $(P_r - P_{wf})/q$.
(2) Prepare the plot by placing the values of $(P_r - P_{wf})/q$ on the vertical axis and the flow rate on the horizontal axis.
(3) Plot the points and draw the best straight line.
(4) Extend the line to the left; the intercept of this line to the vertical axis is the value of b.
(5) From the plot, choose two arbitrary values of flow rate (q_{o_1} and q_{o_2}) and determine the corresponding values of $(P_r - P_{wf})/q_o$. The slope, a, can be calculated as follows:

$$a = \frac{(\Delta P/q_o)_1 - (\Delta P/q_o)_2}{q_{o_1} - q_{o_2}} \qquad (2.57)$$

Be sure to use two points on the line, not two data points.

A plot of the Jones, Blount, and Glaze equation using a three- or four-point flow rate test can be used to distinguish pressure losses caused by non-Darcy flow (Dq) from pressure losses caused by skin (S). This is an important factor in selecting the appropriate stimulation or remedial workover to improve productivity.

(1) the measured value b (obtained from the plot), which indicates damaged or undamaged conditions of the formation
(2) the measured value of a, which indicates the degree of turbulence in the well formation system
(3) the ratio of b′ to b—that is, b′/b—which is also a good indicator to determine pressure losses caused by non-Darcy flow

The value of b′ is determined by using the following equation:

$$b' = b + aq_{max} \qquad (2.58)$$

b′ can also be determined from the plot as the ordinate value of a $\Delta P/q$ vs q plot at maximum flow rate (that is, at $(P_r - O)/q_o$). The value of b is determined from the plot.

Figure 2.30 illustrates some possible conclusions that can be obtained from a plot of the Jones, Blount, and Glaze equation. Some conclusions can be drawn based on the plots by using indicators that were previously discussed as follows:

(1) If the value of b is low—less than 0.05—no formation damage occurs in the well. The degree of damage will increase with increasing values of b.
(2) If the value of b′/b is low—less than 2.0—little or no turbulence is occurring in the well formation system.
(3) If the values of b and b′/b are low, the well has a good completion.
(4) If the value of b is low and b′/b is high, stimulation is not recommended. The low productivity in the well is caused by an insufficient open-perforated area. Additional perforations would be recommended.
(5) If the value of b is high and b′/b is low, stimulation is recommended.

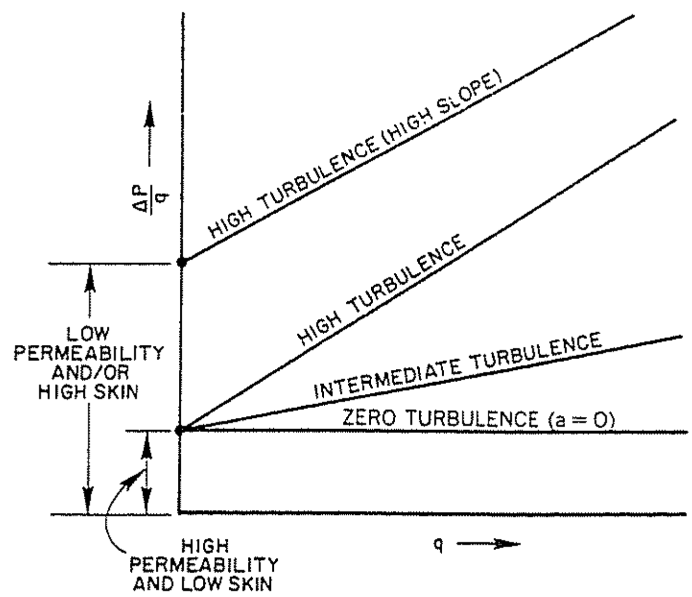

Figure 2.30 Interpretations of Various Well Tests by Jones, Blount, and Glaze Procedure[9]

EXAMPLE PROBLEM #17

(Jones, Blount, and Glaze procedure)

Given data: oil well test:

$P_r = 3{,}000$ psia

Test no.	q	P_{wf}
1	400	2,820
2	1,000	2,175
3	1,340	1,606
4	1,600	1,080

Plot in the form suggested by Jones, Blount, and Glaze. (Plot $\Delta P/q$ vs q on regular coordinate paper.) See Figure 2.29.

Calculate:

(1) a and b
(2) $q_{o_{max}}$ or AOFP
(3) q_o for $P_{wf} = 800$ psia

Solution procedure:

(1) Prepare table of q vs $\dfrac{\Delta P}{q}$

q	P_{wf}	$\dfrac{P_r - P_{wf}}{q}$
400	2,820	0.4500
1,000	2,175	0.8250
1,340	1,606	1.0403
1,600	1,080	1.200

(2) Determine the slope and intercept as noted on Figure 2.31. Then:

$$\frac{P_r - P_{wf}}{q_o} = 0.1997 + 0.000626\ q_o$$

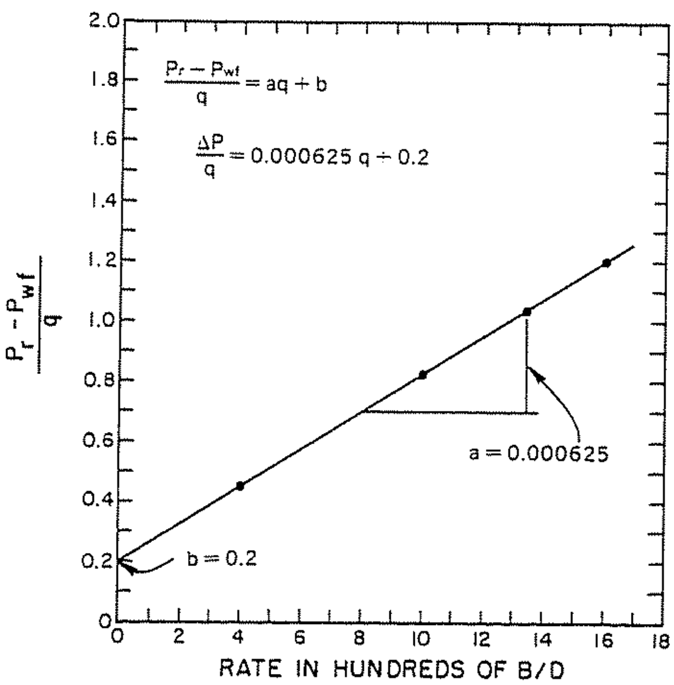

Figure 2.31 Solution to Example Problem #17

(a) $b = 0.1997$
$a = 0.000626$

(b) Find q_{max} (set $P_{wf} = 0$). Then:

$$\frac{3{,}000 - 0}{q_o} = 0.1997 + 0.000626\ (q_o)$$

$$3{,}000 = 0.1997\ q_o + 0.000626\ q_o^2$$

$$0.000626\ q_o^2 + 0.1997\ q_o - 3{,}000 = 0$$

Recall the solution to a quadratic equation:

$$q_o = \frac{-b \pm \sqrt{b^2 - 4\ ac}}{2\ a}$$

where:

$$a\ q^2 + bq + c = 0$$

where:

$a = 0.000626$
$b = 0.1997$
$c = -3{,}000$
$q_o = 2{,}035.44$ b/d
(Trial and error may also be used.)

(c) Find q_o for $P_{wf} = 800$ psi:

$$\frac{3{,}000 - 800}{q_o} = 0.1997 + 0.000626\ q_o$$

$$2{,}200 = 0.1997\ q_o + 0.000626\ q_o^2$$

$$0.000626\ q_o^2 + 0.1997\ q_o - 2{,}200 = 0$$

$$q_o = 1{,}721.94\ \text{bo/d}$$

EXAMPLE PROBLEM #18

(Jones, Blount, and Glaze plot interpretation)

Given data: oil well test:

Reservoir pressure = 4,750 psi

Test #	Flow rate	Flowing pressure
1	2,560	4,710
2	3,120	4,701.2
3	3,895	4,689
4	4,430	4,681

Calculate:

Plot $(P_r - P_{wf})/q_o$ vs q_o and make an interpretation of the plot.

Solution procedure:

(1) Calculate $(P_r - P_{wf})/q_o$ as follows:

Test #	q_o	P_{wf}	$(P_r - P_{wf})/q_o$
1	2,560	4,710	0.015625
2	3,120	4,701.2	0.015639
3	3,895	4,689	0.015659
4	4,430	4,681	0.015673

Plot $(P_r - P_{wf})/q_o$ vs q_o as shown in Figure 2.32.

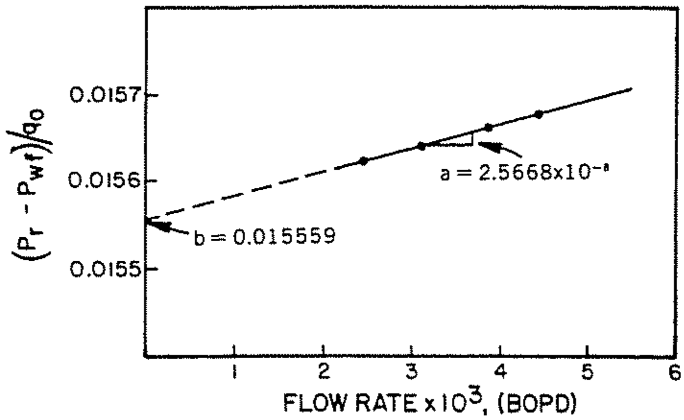

Figure 2.32 Plot of $(P_r - P_{wf})/q_o$ vs q_o for Example Problem #18

(2) From the plot:

$$b = 0.015559$$
$$a = 2.5668 \times 10^{-8}$$

(3) Thus:

$$(P_r - P_{wf})/q_o = 0.015559 + 2.5668 \times 10^{-8} q_o$$

Solve this equation for $P_{wf} = 0$ to obtain:

$$q_o = q_{max} = 222{,}806.09 \text{ bo/d}$$

(4) The value of $b' = (P_r - P_{wf})/q_o$ at $q_{max} = 0.0213$
(5) $b'/b = (0.0213)/(0.015559) = 1.3666$

Obviously, this high-rate well needs no remedial action.

EXAMPLE PROBLEM #19

(Jones, Blount, and Glaze plot interpretation)

Given data: four-point test:

Reservoir pressure = 4,250 psi

Test #	Flow rate	Flowing pressure
1	427	2,625
2	564	2,059
3	635	1,758
4	712	1,425

Calculate:

Plot $(P_r - P_{wf})/q_o$ vs q_o and interpret the plot.

Solution procedure:

(1) Prepare a table to calculate $(P_r - P_{wf})/q_o$ as follows:

Test #	q_o	P_{wf}	$(P_r - P_{wf})/q_o$
1	427	2,625	3.806
2	564	2,059	3.884
3	635	1,758	3.924
4	712	1,425	3.968

(2) Plot $(P_r - P_{wf})/q_o$ vs q_o as shown in Figure 2.33.

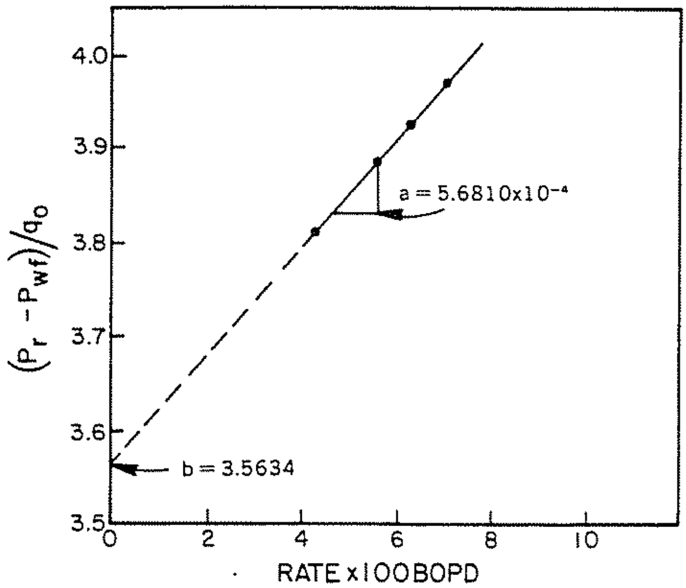

Figure 2.33 Plot of $(P_r - P_{wf})/q_o$ vs q_o for Example Problem #19

(3) From the plot:

$$b = 3.5634$$
$$a = 5.6810 \times 10^{-4}$$

(4) The Jones, Blount, and Glaze equation is:

$$(P_r - P_{wf})/q_o = 5.6810 \times 10^{-4} q_o + 3.5634$$

(5) To find the maximum flow rate, solve this equation by taking:

$$P_{wf} = 0$$
$$q_{max} = 1{,}025.14 \text{ bo/d}$$

(6) The value of $b' = 4.1458$
(7) The ratio of b' to b, $b'/b = 1.1634$

The low value of b'/b indicates low turbulence.

EXAMPLE PROBLEM #20

(Jones, Blount, and Glaze plot interpretation)

Given data: well test:

Reservoir pressure = 4,453 psi

Test #	Flow rate (bo/d)	Flowing pressure
1	545	4,427
2	672	4,418
3	746	4,412
4	822	4,405

Calculate:

(1) Plot $(P_r - P_{wf})/q_o$.
(2) Recommend ways to improve the productivity of the well.

Solution procedure:

(1) Prepare a table to calculate $(P_r - P_{wf})/q_o$ as follows:

Test #	q_o	P_{wf}	$(P_r - P_{wf})/q_o$
1	545	4,427	0.0477
2	672	4,418	0.0521
3	746	4,412	0.0550
4	822	4,405	0.0584

(2) Plot $(P_r - P_{wf})/q_o$ vs q_o as shown in Figure 2.34. From the plot:

$$b = 0.0266$$
$$a = 3.8369 \times 10^{-5}$$

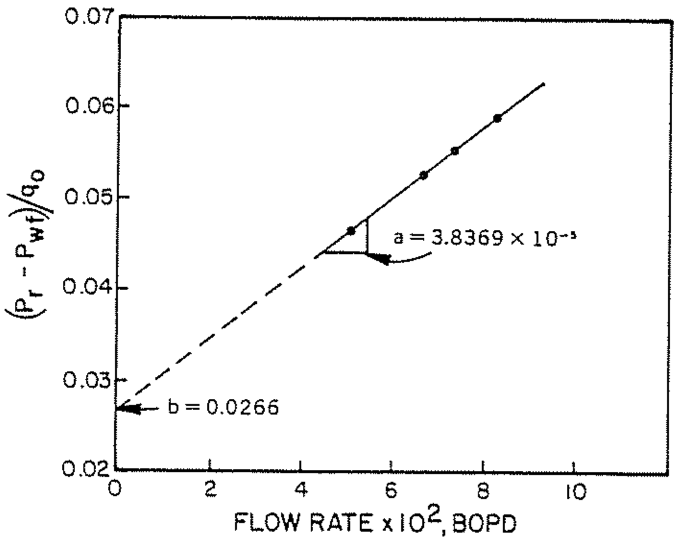

Figure 2.34 Plot of $(P_r - P_{wf})/q_o$ vs q_o for Example Problem #20

(3) Thus, Jones' equation is:

$$(P_r - P_{wf})/q_o = 3.8369 \times 10^{-5}\, q_o + 0.0266$$

(4) Using the previous equation, calculate maximum flow rate by taking $P_{wf} = 0$:

$$q_{max} = 10{,}431.93 \text{ bo/d}$$

The value of b' = 0.4269

(5) The ratio of b' to b, b'/b, = 16.05

This high value of b'/b indicates high turbulence, signifying the need for more area open to flow.

CLASS PROBLEM #20A

(Plot in Jones, Blount, and Glaze form)

Given data: (After Fetkovich)

P_r = 1,200 psia (oil well)

Test no.	P_{wf}	q_o
1	1,147	70
2	1,023	147
3	856	209
4	612	280
5	530	292

Calculate:

(1) Plot in the form suggested by Jones, Blount, and Glaze.
(2) Determine values of a and b.
(3) Find $q_{o_{max}}$.
(4) Compare your answer to a Fetkovich type of plot of the same data on page 42 of Volume 1, *The Technology of Artificial Lift Methods.*

CLASS PROBLEM #20b

(Plot in suggested Jones, Blount, and Glaze form)

Given data:

Reservoir pressure = 4,126 psia

Test #	Flow rate (bo/d)	Flowing pressure
1	4,245	3,939
2	3,824	3,959
3	3,540	3,972
4	3,090	3,992

Calculate:

Recommend ways to improve the productivity of this well, based on the plot of $(P_r - P_{wf})/q_o$ vs q_o.

CLASS PROBLEM #20c

Given data:

Reservoir pressure = 4,268 psia

Test #	Flow rate (bo/d)	Flowing pressure
1	1,248	3,511
2	954	3,704
3	708	3,859
4	612	3,917

Calculate:

Recommend ways to improve the productivity of this well.

CLASS PROBLEM #20d

Given data:

Reservoir pressure = 4,281 psia

Test#	Flow rate (bo/d)	Flowing pressure
1	3,579	3,673
2	2,786	3,897
3	2,432	3,980
4	1,950	4,078

Calculate:

Recommend ways to improve the productivity of this well.

CLASS PROBLEM #20e

Given data:

Reservoir pressure = 4,313 psia

Test #	Flow rate (bo/d)	Flowing pressure
1	527	3,335
2	475	3,507
3	348	3,857
4	295	3,974

Calculate:

Recommend ways to improve the productivity of this well.

CLASS PROBLEM #20f

Given data:

Reservoir pressure = 4,445 psia

Test #	Flow rate (bo/d)	Flowing pressure
1	4,327	4,334
2	3,965	4,343
3	3,274	4,361
4	2,945	4,369

Calculate:

Based on a plot of $(P_r - P_{wf})/q_o$ vs q_o, give your conclusions.

CLASS PROBLEM #20g

Given data:

Reservoir pressure = 4,594 psia

Test #	Flow rate (bo/d)	Flowing pressure
1	657	3,924
2	512	4,088
3	468	4,136
4	309	4,302

Calculate:

Recommend ways to improve the productivity of this well.

CLASS PROBLEM #20h

Given data:

Reservoir pressure = 3,581 psia

Test #	Flow rate (bo/d)	Flowing pressure
1	2,945	3,219
2	2,270	3,349
3	1,836	3,418
4	1,340	3,483

Calculate:

Recommend ways to improve the productivity of this well.

CLASS PROBLEM #20i

Given data:

Reservoir pressure = 3,900 psia

Test #	Flow rate (bo/d)	Flowing pressure
1	425	2,552
2	367	2,869
3	304	3,165
4	259	3,347

Calculate:

Recommend ways to improve the productivity of this well.

2.227 THE COMPOSITE IPR CURVES

The determination of the IPR curves, as previously discussed, was based on the assumption that no water was produced from the wells. The following method can be used to determine the IPR curves for oil wells producing water. This method was derived by Petrobras* based on the combination of Vogel's equation for oil flow and constant productivity index for water flow. The composite IPR curve is determined geometrically from those equations by considering the fractional flow of oil and water.

The equations to determine the composite IPR curves can be derived based on:

(1) the calculation of the flowing bottom-hole pressure at certain total flow rates
(2) the calculation of the total flow rate at certain flowing bottom-hole pressures

2.2271 THE CALCULATION OF THE FLOWING BOTTOM-HOLE PRESSURE AT CERTAIN TOTAL FLOW RATES FOR THE COMPOSITE IPR CURVES

Figure 2.35 is used to derive the equations to calculate the flowing bottom-hole pressure at certain total flow rates for a reservoir pressure greater than the bubble-point pressure. From Figure 2.35, the composite IPR curve can be divided into three intervals; that is:

(1) The interval between 0 and the flow rate at the bubble-point pressure ($0 < q_t < q_b$). In this interval,

* Solution given by Petrobras

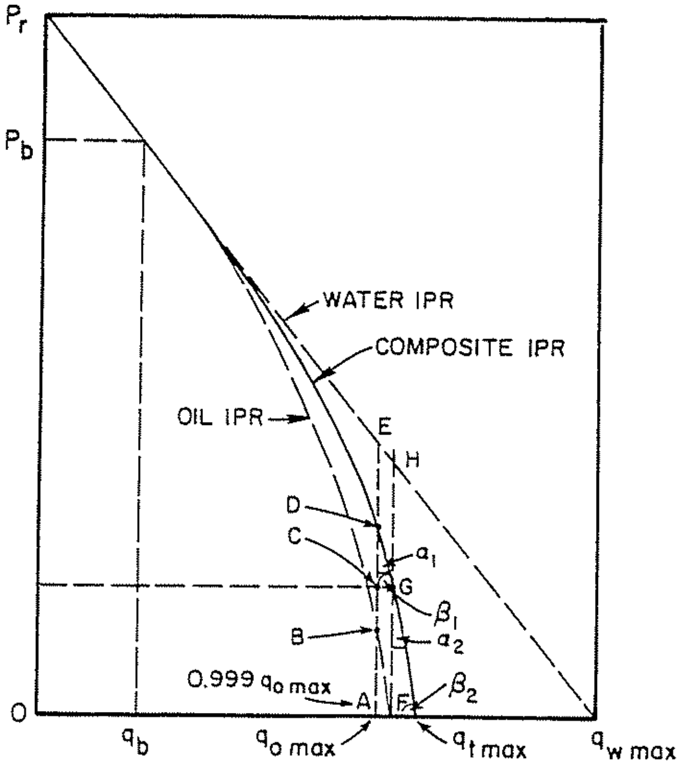

Figure 2.35 Composite IPR Curve

a linear relationship between flow rate and flowing pressure occurs, and the flowing bottom-hole pressure at the total flow rate can be determined as follows:

$$P_{wf} = P_r - \frac{q_t}{J} \tag{2.59}$$

(2) The interval between the flow rate at the bubble point to the maximum oil flow rate ($q_b < q_t < q_{o_{max}}$). At a total flow rate, the flowing bottom-hole pressure is defined by:

$$P_{wf} = F_o(P_{wf_{oil}}) + F_w(P_{wf_{water}}) \tag{2.60}$$

where:

F_o = oil fraction
$P_{wf_{oil}}$ = P_{wf} of oil IPR curve
F_w = water fraction
$P_{wf_{water}}$ = P_{wf} of water IRP curve

From Vogel's equation, $P_{wf_{oil}}$ can be calculated as follows:

$$P_{wf_{oil}} = 0.125(P_b)\left[-1 + \sqrt{81 - 80\left\{\frac{q_t - q_b}{q_{o_{max}} - q_b}\right\}}\right] \tag{2.61}$$

where:

$$q_{o_{max}} = q_b + \frac{JP_b}{1.8}$$

$$q_b = J(P_r - P_b)$$

From the constant productivity index, $P_{wf_{water}}$ can be calculated as follows:

$$P_{wf_{water}} = P_r - \frac{q_t}{J} \tag{2.62}$$

By substituting Equation 2.61 and Equation 2.62 into Equation 2.60, the flowing bottom-hole pressure at the total flow rate is:

$$P_{wf} = F_w\left(P_r - \frac{q_t}{J}\right) + F_o(0.125)P_b \times \left[-1 + \sqrt{81 - 80\left\{\frac{q_t - q_b}{q_{o_{max}} - q_b}\right\}}\right] \tag{2.63}$$

(3) The interval between the maximum oil flow rate and the maximum total flow rate, $q_{o_{max}} < q_t < q_{t_{max}}$. In this interval, the composite IPR curve would have a constant slope, since the curve is mostly affected by water production. So, tan β must be determined (refer to Figure. 2.35) for calculating the flowing bottom-hole pressure at a total flow rate as follows:

(a) Take a total flow rate that is very close to the maximum oil flow rate, i.e.:

$$q_t = 0.999\ q_{o_{max}}$$

(b) Since the difference between q_t and $q_{o_{max}}$ is very small, we can assume that $\alpha_2 = \alpha_1$ and $\beta_2 = \beta_1$ and the tangent of these angles can be calculated geometrically in the shaded triangle.

(c) From the shaded triangle,

$$\tan\beta_1 = CD/CG \qquad \tan\alpha_1 = CG/CD \tag{2.64}$$

CD is the difference between the flowing bottom-hole pressure at point D, P_{wf_D}, and the flowing bottom-hole pressure at point C, P_{wf_C}; that is:

$$CD = P_{wf_D} - P_{wf_C} \tag{2.65}$$

Point D lies on the composite IPR curve, so:

$$P_{wf_D} = F_o(P_{wf_{oil}}) + F_w(P_{wf_{water}})$$

Or, from Figure 2.35:

$$P_{wf_D} = F_o \times P_{wf_B} + F_w \times P_{wf_E}$$

$$P_{wf_B} = 0.125(P_b) \times \left[-1 + \sqrt{81 - 80\left\{\frac{0.999\ q_{o_{max}} - q_b}{q_{o_{max}} - q_b}\right\}}\right]$$

$$P_{wf_E} = P_r - \frac{0.999\ q_{o_{max}}}{J}$$

Therefore:

$$P_{wf_D} = F_w\left(P_r - \frac{0.999\ q_{o_{max}}}{J}\right) + F_o(0.125)P_b \times \left\{-1 + \sqrt{81 - 80\left\{\frac{0.999\ q_{o_{max}} - q_b}{q_{o_{max}} - q_b}\right\}}\right\} \tag{2.66}$$

From Figure 2.35, $P_{wf_C} = P_{wf_G}$ where G also lies on the composite IPR curve for $q_t = q_{o_{max}}$.

$$P_{wf_G} = F_o(P_{wf_{oil}}) + F_w(P_{wf_{water}})$$

At $q_t = q_{o_{max}}$, $P_{wf_{oil}} = 0$; therefore:

$$P_{wf_G} = F_w(P_{wf_{water}}) = F_w\left(P_r - \frac{q_{o_{max}}}{J}\right)$$

$$P_{wf_C} = P_{wf_G} = F_w\left(P_r - \frac{q_{o_{max}}}{J}\right) \tag{2.67}$$

Substituting Equations 2.66 and 2.67 into Equation 2.65 yields:

$$CD = P_{wf_D} - P_{wf_C}$$
$$= F_w\left(\frac{0.001\ q_{o_{max}}}{J}\right) + F_o(0.125)P_b\left[-1 + \sqrt{81 - 80\left\{\frac{0.999\ q_{o_{max}} - q_b}{q_{o_{max}} - q_b}\right\}}\right] \quad (2.68)$$

CG is the difference between q_t and $q_{o_{max}}$; therefore:

$$CG = q_{o_{max}} - 0.999\ q_{o_{max}} = 0.001\ q_{o_{max}} \quad (2.69)$$

Hence, from Equations 2.68 and 2.69, $\tan \alpha_1$ or $\tan \beta_1$ can be calculated.

The flowing bottom-hole pressure at flow rates between the maximum oil flow rate and the maximum total flow rate can be calculated by using the following equation:

$$P_{wf} = F_w\left(P_r - \frac{q_{o_{max}}}{J}\right) - \left(q_t - \frac{q_{o_{max}}}{J}\right)(\tan \beta) \quad (2.69)$$

The maximum total flow rate (for the composite IPR curve) can be calculated by using the following equation:

$$q_{t_{max}} = q_{o_{max}} + P_{wf_G}(\tan \alpha)$$

or:

$$q_{t_{max}} = q_{o_{max}} + F_w\left(P_r - \frac{q_{o_{max}}}{J}\right)(\tan \alpha) \quad (2.70)$$

2.2272 CALCULATION OF THE TOTAL FLOW RATE AT CERTAIN FLOWING BOTTOM-HOLE PRESSURES FOR THE COMPOSITE IPR CURVE

Refer to Figure 2.36, which shows that the composite IPR curve can be divided into three intervals, and in every interval, the total flow rate at certain flowing bottom-hole pressures can be calculated as follows:

(1) For pressures between reservoir pressure and the bubble-point pressure, $P_b < P_{wf} < P_r$, the total flow rate can be calculated by using the following equation:

$$q_t = J(P_r - P_{wf})$$

(2) For pressures between the bubble-point pressure and the flowing bottom-hole pressure where the oil flow rate is equal to the maximum rate—that is $P_{wf_G} < P_{wf} < P_b$—the total flow rate is:

$$q_t = \frac{-C + \sqrt{C^2 - 4B^2D}}{2B^2} \qquad \text{for } B \neq 0 \quad (2.71)$$

$$q_t = D/C \qquad \text{for } B = 0 \quad (2.72)$$

where:

$$A = \frac{P_{wf} + 0.125\ F_o P_b - F_w P_r}{0.125\ F_o P_b} \quad (2.73)$$

$$B = \frac{F_w}{0.125\ F_o P_b J} \quad (2.74)$$

$$C = 2(A)(B) + \frac{80}{q_{o_{max}} - q_b} \quad (2.75)$$

$$D = A^2 - (80)\frac{q_b}{q_{o_{max}} - q_b} - 81 \quad (2.76)$$

(3) For pressures between P_{wf_G} and 0—that is $0 < P_{wf} < P_{wf_G}$—the total flow rate is:

$$q_t = \frac{P_{wf_G} + q_{o_{max}}(\tan \beta) - P_{wf}}{\tan \beta} \quad (2.77)$$

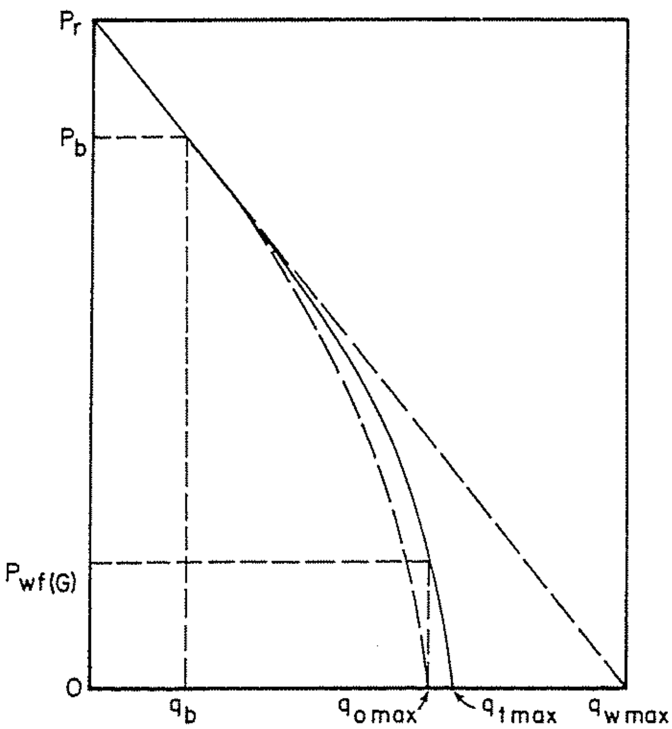

Figure 2.36 Composite IPR Curves

2.2273 PRELIMINARY CALCULATIONS TO CONSTRUCT THE COMPOSITE IPR CURVES FROM THE TEST DATA

The variables that are needed to construct the composite IPR curves are the reservoir pressure, the bubble-point pressure, the flowing bottom-hole pressure, the total flow rate, and the water fraction.

There are two possibilities that might occur; that is:

(1) When the flowing bottom-hole pressure of the test is greater than the bubble-point pressure ($P_{wf_T} > P_b$), the variables that are needed to construct the composite IPR curves can be calculated by using the following equations:

$$J = \frac{q_{t_{test}}}{P_r - P_{wf_{test}}} \quad (2.78)$$

$$q_b = J(P_r - P_b) \quad (2.79)$$

$$q_{o_{max}} = q_b + \frac{JP_b}{1.8} \quad (2.80)$$

$$q_{t_{max}} = q_{o_{max}} + F_w\left(P_r - \frac{q_{o_{max}}}{J}\right)(\tan \alpha) \quad (2.81)$$

where $\tan \alpha$ can be determined by applying Equation 2.64.

(2) The flowing bottom-hole pressure of the test is less than the bubble-point pressure, $P_{wf_{test}} < P_b$. For determining q_b, $q_{o_{max}}$, and $q_{t_{max}}$, the productivity

index J must be calculated. The following section shows the derivation of the equation to determine J at this condition. Refer to Figure 2.35.

$$q_t = F_o\,(q_{oB}) + F_w\,(q_{wD}) \qquad (2.82)$$

$$q_{oB} = q_b + (q_{o_{max}} - q_b)\left\{1 - 0.2\left(\frac{P_{wf_{test}}}{P_b}\right) - 0.8\left(\frac{P_{wf_{test}}}{P_b}\right)^2\right\}$$

if:

$$A = 1 - 0.2\left\{\frac{P_{wf_{test}}}{P_b}\right\} - 0.8\left\{\frac{P_{wf_{test}}}{P_b}\right\}^2$$

$$q_{oB} = q_b + (q_{o_{max}} - q_b)\,A$$

$$q_b = J(P_r - P_b)$$

$$q_{o_{max}} = q_b + \frac{P_b J}{1.8}$$

therefore:

$$q_{oB} = J(P_r - P_b) + \left\{q_b + \frac{JP_b}{1.8} - q_b\right\}A$$

$$q_{oB} = J(P_r - P_b) + \left(\frac{JP_b}{1.8}\right)A \qquad (2.83)$$

$$q_{wD} = J\,[P_r - P_{wf_{test}}] \qquad (2.84)$$

Substituting Equation 2.83 and Equation 2.84 into Equation 2.82 yields:

$$q_t = F_o\left\{J\left(P_r - P_b + \frac{P_b\,A}{1.8}\right)\right\} + F_w\,J\,[P_r - P_{wf_{test}}]$$

$$q_t = J\left[F_o\left\{P_r - P_b + \frac{P_b\,A}{1.8}\right\} + F_w[P_r - P_{wf_{test}}]\right]$$

$$J = \frac{q_{t_{test}}}{F_o\left\{P_r - P_b + \frac{P_b\,A}{1.8}\right\} + F_w[P_r - P_{wf_{test}}]} \qquad (2.86)$$

If J can be determined from Equation 2.86, q_b, $q_{o_{max}}$, and $q_{t_{max}}$ can be calculated by applying Equations 2.79, 2.80, and 2.81, respectively.

2.2274 THE COMPOSITE IPR CURVES FOR THE RESERVOIR PRESSURE BELOW THE BUBBLE-POINT PRESSURE

At this condition, the previous equations for constructing the composite IPR curves for the flowing pressure below the bubble-point pressure can be used by changing P_b to P_r, setting the value of q_b equal to 0, and using the same procedure.

EXAMPLE PROBLEM #21

(reservoir pressure greater than the bubble-point pressure)

Given data:

reservoir pressure = 2,550 psi
bubble-point pressure = 2,100 psi
Test data:
Flowing bottom-hole pressure = 2,300 psi
Flow rate (total), q_t = 500 b/d

Calculate:

Determine the composite IPR curves for F_w = 0.0, 0.25, 0.50, 0.75, and 1.0

Solution procedure:

(1) (Example for the preliminary calculations for F_w = 0.50)

Since $P_{wf_{test}} > P_b$:

$$J = \frac{500}{2{,}550 - 2{,}300} = 2.0 \text{ b/d/psi}$$

$$q_b = (2.0)(2{,}550 - 2{,}100) = 900 \text{ b/d}$$

$$q_{o_{max}} = 900 + \frac{(2.0)(2{,}100)}{1.8} = 3{,}233.33 \text{ b/d}$$

By applying Equation 2.68, CD can be calculated as follows:

$$CD = 0.50\,\frac{0.001(3{,}233.33)}{2.0} + 0.50(0.125)(2.100) \times\left\{-1 + \sqrt{81 - 80\left\{\frac{0.999(3{,}233.33 - 900)}{3{,}233.33 - 900}\right\}}\right\}$$
$$= 7.89$$

By using Equation 2.69, CG can be calculated as follows:

$$CG = 0.001\,(3{,}233.33) = 3.23$$
$$\tan\alpha = CG/CD = 3.23/7.89 = 0.41$$
$$\tan\beta = 1/\tan\alpha = 1/0.41 = 2.44$$

By using Equation 2.70, the maximum total flow rate is:

$$q_{t_{max}} = 3{,}233.33 + 0.50\left(2{,}550 - \frac{3{,}233.33}{2.0}\right)(0.41)$$
$$= 3{,}424.66 \text{ b/d}$$

(2) The calculation of P_{wf} at certain total flow rates is as follows:

For q_t = 600 b/d, $q_t > q_b$:

$$P_{wf} = P_r - \frac{q_t}{J} = 2{,}550 - (600/2.0) = 2{,}250 \text{ psi}$$

For q_t = 1,500 b/d, $q_b < q_t < q_{o_{mas}}$:

$$P_{wf} = 0.50\left(2{,}550 - \frac{1{,}500}{2.0}\right) + 0.50(0.125)(2{,}100) \times -1 + 81 - 80\,\frac{1{,}500 - 900}{3{,}233.33 - 900}$$
$$= 1{,}789.03 \text{ psi}$$

For q_t = 3,300 b/d, $q_{o_{max}} < q_t < q_{t_{max}}$:

$$P_{wf} = 0.50\left(2{,}550 - \frac{3{,}233.33}{2.0}\right) - 3{,}300 - 3{,}233.33(2.44) = 303.99 \text{ psi}$$

(3) The calculations of the total flow rates at certain flowing bottom-hole pressures are as follows:

(a) By using Equation 2.67, calculate the flowing bottom-hole pressure at $q_t = q_{o_{max}}$ = 3,233.33 b/d—that is:

$$P_{wf_G} = 0.50\left(2{,}550 - \frac{3{,}233.33}{2.0}\right) = 466.67 \text{ psi}$$

(b) For $P_{wf} = 2{,}400$ psi, $P_{wf} > P_b$:

$$q = 2.0(2{,}550 - 2{,}400) = 300 \text{ b/d}$$

For $P_{wf} = 1{,}500$ psi, $P_{wf_G} < P_{wf} < P_b$:

$$A = \frac{1{,}500 + 0.125(0.50)(2{,}100) - 0.50(2{,}550)}{0.125(0.50)(2{,}100)} = 2.71$$

$$B = \frac{0.50}{0.125(0.50)(2{,}100)(2)} = 0.001905$$

$$C = 2(2.71)(0.001905) + \frac{80}{3{,}233.33 - 900} = 0.04461$$

$$D = (2.71)^2 - 80\left\{\frac{900}{3{,}233.33 - 900}\right\} - 81 = -104.5131$$

$B \neq 0$, so:

$$q_t = \frac{-0.04461 + \sqrt{(0.04461)^2 - (4)(0.001905)^2(-104.5131)}}{2(0.001905)^2}$$

$$= 2013.13 \text{ b/d}$$

For $P_{wf} = 350$ psi, $P_{wf} < P_{wf_G}$:

$$q_t = \frac{466.67 + 3{,}233.33(2.44) - 350}{2.44} = 3{,}281.15 \text{ b/d}$$

(4) The results of the preliminary calculations for other values of F_w are shown in the following table:

	F_w				
	0.0	0.25	0.50	0.75	1.00
J	2.0	2.0	2.0	2.0	2.0
q_b	900.0	900.0	900.0	900.0	900.0
$q_{o_{max}}$	3,233.33	3,233.33	3,233.33	3,233.33	3,233.33
tan α	0.23	0.29	0.41	0.68	2.0
tan β	4.38	3.41	2.44	1.47	0.50
$q_{t_{max}}$	3,233.33	3,301.73	3,424.52	3,709.38	5,100.00
P_{wf_G}	0.00	233.33	466.67	700.0	—

(5) The results of the calculations of the total flow rates at the flowing bottom-hole pressures for every value of F_w are shown in the following table:

	q_t @ F_w				
P_{wf}	0	0.25	0.50	0.75	1.00
2,550	0	0	0	0	0
2,400	300	300	300	300	300
2,300	500	500	500	500	500
2,100	900	900	900	900	900
1,700	1,632	1,647	1,663	1,681	1,700
1,400	2,093	2,132	2,177	2,232	2,300
1,000	2,588	2,663	2,758	2,887	3,100
600	2,948	3,043	3,160	3,301	3,900
200	3,172	3,243	3,343	3,573	4,700
0	3,233	3,302	3,425	3,709	5,100

(6) The plot of the composite IPR curves is shown in Figure 2.37.

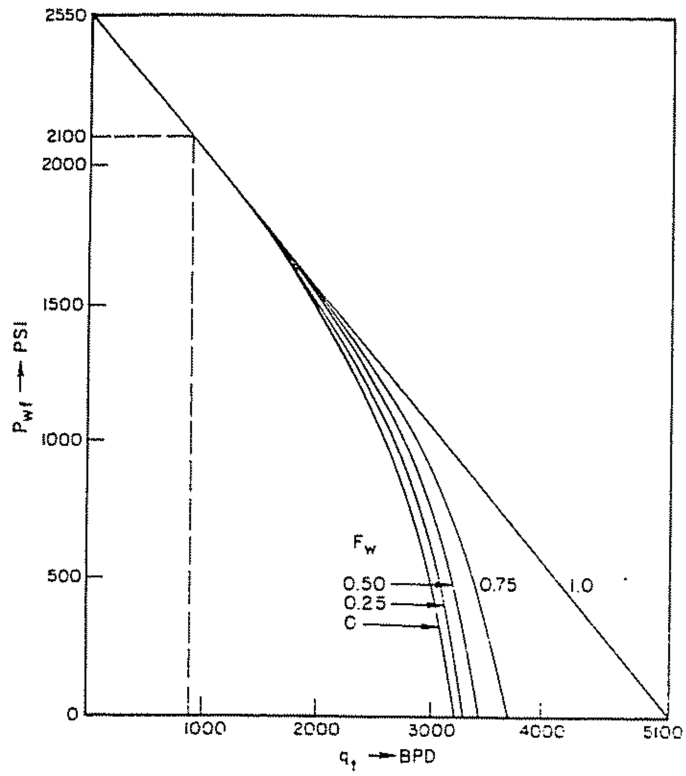

Figure 2.37 Composite IPR Curves for Example Problem #21

EXAMPLE PROBLEM #22

($P_{wf_{test}}$ is less than the bubble-point pressure)

Given data:

reservoir pressure = 2,800 psi
bubble-point pressure = 2,400 psi

test data:

$P_{wf_{test}} = 1{,}200$ psi
$q_{t_{test}} = 1{,}480$ b/d

Calculate:

Construct the composite IPR curve for $F_w = 0.50$.

Solution procedure:

(1) Preliminary calculation:

$$A = 1.0 - 0.2(1{,}200/2{,}400) - 0.8(1{,}200/2{,}400)^2$$
$$= 0.70$$

$$J = \frac{1{,}480}{0.50\left\{2{,}800 - 2{,}400 + \frac{2{,}400(0.70)}{1.8}\right\} + 0.50(2{,}800 - 1{,}200)}$$

$$J = 1.01$$

$$q_b = 1.01(2{,}800 - 2{,}400) = 403.64 \text{ b/d}$$

$$q_{o_{max}} = 403.64 + \frac{1.01(2{,}400)}{1.8} = 1{,}749.09 \text{ b/d}$$

Using Equation 2.64, tan $\alpha = 0.21$
tan $\beta = 4.84$

$$q_{t_{max}} = 1{,}749.09 + 0.50\left(2{,}800 - \frac{1{,}749.09}{1.01}\right)(0.21)$$
$$= 1{,}859.18 \text{ b/d}$$

(2) The flowing bottom-hole pressure vs total flow rate relationships are as follows:

P_{wf}	q_t
2,800	0
2,600	202
2,400	404
2,000	791
1,600	1,140
1,200	1,438
800	1,662
400	1,777
0	1,859

(3) The plot of the composite IPR curve is shown in Figure 2.38.

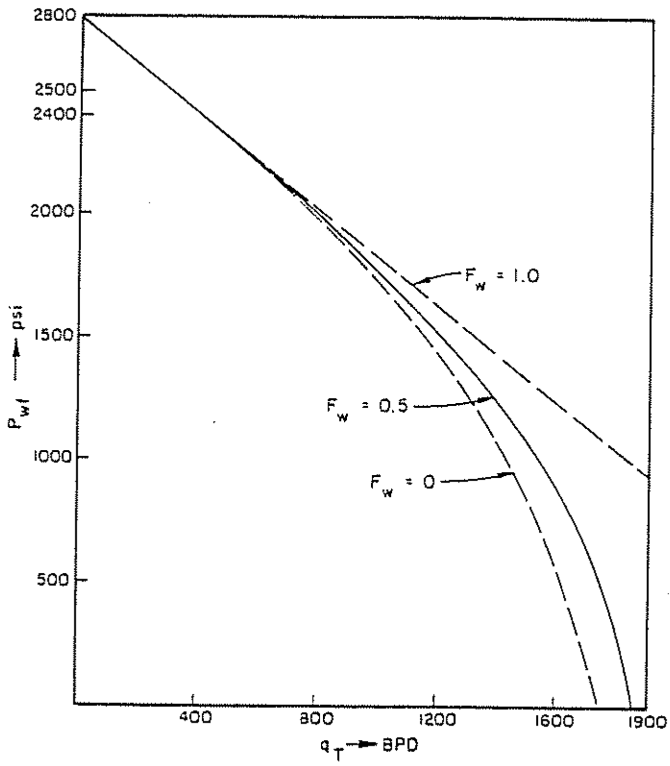

Figure 2.38 Composite IPR Curve for Example Problem #22

EXAMPLE PROBLEM #23

(reservoir pressure is below the bubble-point pressure)

Given data:

reservoir pressure = 2,250 psi
bubble-point pressure = 3,000 psi
test data:

$P_{wf_{test}}$ = 1,800 psi
$q_{t_{test}}$ = 900 b/d

Calculate:

Plot the composite IPR curves for F_w = 0.0, 0.25, 0.50, 0.75, and 1.00.

Solution procedure:

(1) The preliminary calculations for every value of F_w are made by using the same procedure as in example problem #21 except the values of $P_b = P_r$ and $q_b = 0$ must be set. The results are shown in the following table:

	F_w				
	0.0	0.25	0.50	0.75	1.00
J	2.20	2.14	2.09	2.05	2.00
$q_{o_{max}}$	2,743.90	2,678.57	2,616.28	2,556.82	—
tan α	0.25	0.31	0.43	0.69	2.00
tan β	4.02	3.21	2.35	1.45	0.50
$q_{t_{max}}$	2,743.90	2,756.55	2,829.27	3,075.67	4,500.00

(2) The relationship of the flow rate vs the flowing bottom-hole pressure for every value of F_w is tabulated as follows:

	q_t @ F_w				
P_{wf}	0	0.25	0.50	0.75	1.00
2,250	0	0	0	0	0
2,000	522	515	510	505	500
1,800	900	897	896	897	900
1,400	1,553	1,571	1,598	1,638	1,700
1,000	2,066	2,110	2,175	2,280	2,500
800	2,271	2,323	2,399	2,517	2,900
400	2,577	2,618	2,659	2,799	3,700
0	2,744	2,757	2,829	3,076	4,500

(3) The plot of the composite IPR curves for every value of F_w is shown in Figure 2.39.

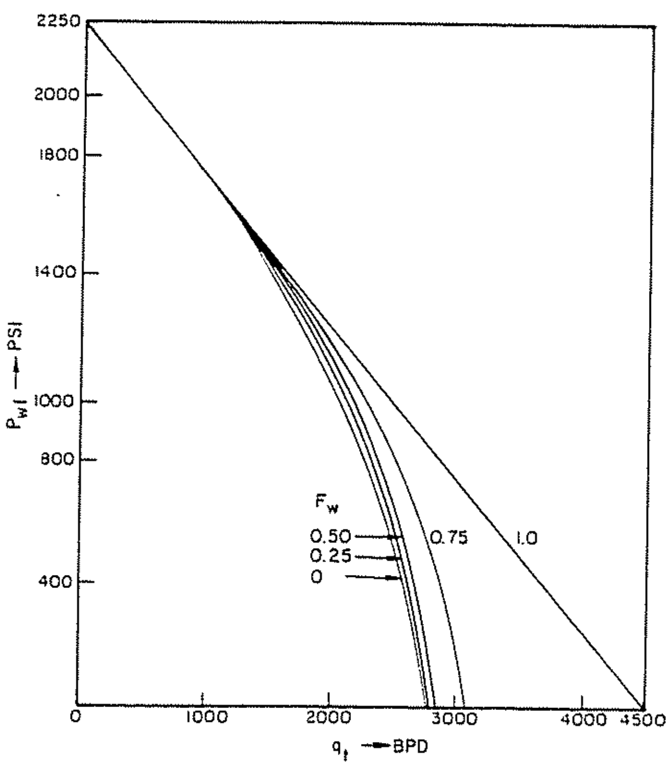

Figure 2.39 Composite IPR Curves for Example Problem #23

2.23 PREPARATION OF FUTURE IPR CURVES

The preparation of future IPR curves becomes very important in determining future production rates for both flowing and artificial lift wells. These IPR curves also represent a means of determining when a well is to be placed on artificial lift. They are necessary in looking at rate acceleration projects and comparing artificial lift methods.

Figure 2.40 represents a typical set of these curves.

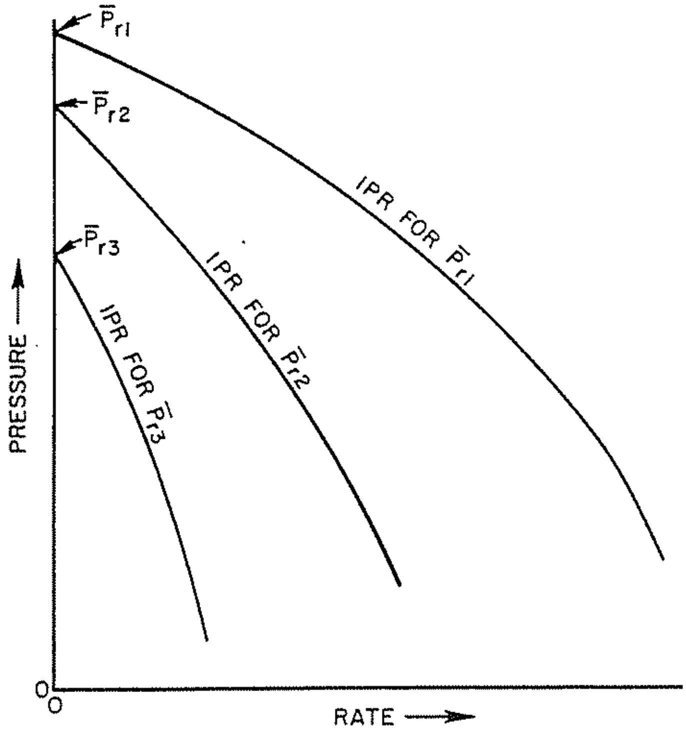

Figure 2.40 IPR Curves for Present and Future Reservoir Pressures

2.231 FETKOVICH PROCEDURE

In early years, Muskat noted that the productivity index on a well at time 1 could be related to the productivity of a well at time 2 by the following relationship:

$$\frac{J_1}{J_2} = \left(\frac{k_{ro}}{\mu_o B_o}\right)_1 \Bigg/ \left(\frac{k_{ro}}{\mu_o B_o}\right)_2 \tag{2.87}$$

Fetkovich noted that, in material balance calculations for solution gas drive reservoirs, k_{ro} was approximately linear with pressure.[16] He then wrote the following equation, which approximates the change in oil permeability with pressure depletion:

$$\frac{k(\overline{P}_r)}{k_i} = \frac{\overline{P}_r}{\overline{P}_{ri}} \tag{2.88}$$

or:

$$k_{ro}(\overline{P}_r) = \frac{\overline{P}_r}{\overline{P}_{ri}} \tag{2.89}$$

where k_{ro} is taken with respect to k_i and is defined at a vanishing ΔP (zero drawdown). He then constructed Figure 2.41, which defines a locus of values

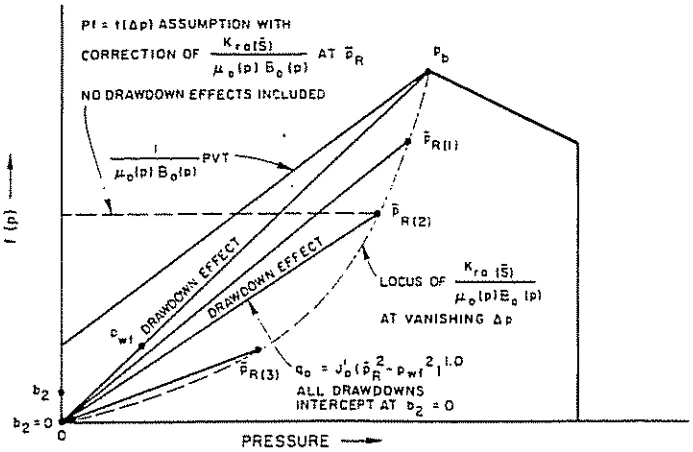

Figure 2.41 Fetkovich Plot of Locus of Values ($K_{ro}/\mu_o B_o$) vs Pressure

of $\left(\frac{k_{ro}}{\mu_o B_o}\right)_{\overline{P}_r}$ vs pressure at zero drawdown. Using his two equations:

$$q_{o_1} = J'_{o_1}(P_{r_1}{}^2 - P_{wf}{}^2)^n \tag{2.90}$$

which defines rate vs drawdown, and:

$$k_{ro}(\overline{P}_r) = \frac{\overline{P}_r}{P_{ri}} \tag{2.91}$$

which corrects for depletion, the final equation proposed by Fetkovich is obtained as follows:

$$q_o = J'_{o_1}\left(\frac{\overline{P}_{r_2}}{\overline{P}_{r_1}}\right)(\overline{P}_{r_2}{}^2 - P_{wf}{}^2)^n \tag{2.99}$$

If a three- or four-point flow test is being conducted at the present time, it is possible to predict IPR curves at other static reservoir pressures by use of Equation 2.99.

EXAMPLE PROBLEM #24

Given data (From example #16)

The equation describing this test was:

$$q_o = 3.906\left[\frac{(2{,}500)^2 - P_{wf}{}^2}{1{,}000}\right]^{0.70192}$$

Calculate:

(1) $q_{o_{max}}$ when P_r lowers to 1,800 psia
(2) q_o for P_{wf} = 800 psia when P_r = 1,800 psia

Solution procedure:

(1)
$$q_o = J'_{o_1}\left(\frac{P_{r_2}}{P_{r_1}}\right)[P_{r_2}^2 - P_{wf}^2]^n$$

For $P_r = 1800$ psi,

$$q_{max} = 3.906\left(\frac{1{,}800}{2{,}500}\right)\left[\frac{(1{,}800)^2 - 0}{1{,}000}\right]^{0.70192}$$

$= 819$ b/d

or:

$$q_o = 0.03062\left(\frac{1{,}800}{2{,}500}\right)[(1{,}800)^2 - 0]^{0.70192} = 819 \text{ b/d}$$

(2) Find q_o for $P_{wf} = 800$ psia when $P_r = 1{,}800$ psia:

$$q_o = 0.03062\left(\frac{1{,}800}{2{,}500}\right)[(1{,}800)^2 - (800)^2]^{0.70192}$$
$$= 702 \text{ b/d}$$

By assuming other values of P_{wf}, a complete IPR curve can be prepared for $P_r = 1{,}800$ psi. Also, other IPR curves can be prepared for other static pressures such as 1,500 psia, 1,000 psia, etc.

CLASS PROBLEM #24a

Using the data of class problem #16a, prepare future IPR curves for static pressures of 2,000 psia and 1,000 psia.

CLASS PROBLEM #24b

Using the data of class problem #16b, prepare future IPR curves for static pressures of 3,800, 3,000, and 2,400 psia.

2.232 COMBINATION FETKOVICH AND VOGEL PROCEDURE FOR THE PREPARATION OF FUTURE IPR CURVES

Eckmier noted that if we take the equations of Fetkovich for static pressure at time 1 and divide by the inflow equation for static pressure at time 2 we arrive at an equation for determining $q_{o_{max}}$ at time 2 after which we can use Vogel's equation directly for preparation of the IPR curve.[17]

$$q_{o_1} = J'_{o_1}(P_{r_1}{}^2 - P_{wf}{}^2)^n \qquad (2.100)$$

$$q_{o_2} = \left(\frac{P_{r_2}}{P_{r_1}}\right) J'_{o_1}(P_{r_2}{}^2 - P_{wf}{}^2)^n \qquad (2.101)$$

By solving for $q_{o_{max}}$ (setting $n = 1.0$ and $P_{wf} = 0$) and dividing Equation 2.100 by Equation 2.101, we have:

$$q_{o_{max_1}}/q_{o_{max_2}} = (\overline{P}_{r_1}/\overline{P}_{r_2})^3 \qquad (2.102)$$

Therefore, we need only one test at the present time from which we can obtain $q_{o_{max_1}}$. By knowing $q_{o_{max_1}}$ and $\overline{P}_{r_1}$, we can solve for $q_{o_{max_2}}$ at any other desired static pressure (P_{r_2}), and in turn, by using Vogel's equation, a complete IPR curve at time 2 (P_{r_2}) can be constructed.

EXAMPLE PROBLEM #25

Given data:

$P_r = 3{,}000$ psia ($P_b = 3{,}000$ psia)
A test shows $q = 200$ b/d at a flowing pressure of 2,500 psia.

Calculate:

(1) $q_{o_{max}}$ when the static pressure drops to 2,000 psia
(2) q_o for $P_r = 2{,}000$ psia and $P_{wf} = 1{,}000$ psia

Solution procedure:

(1) Solve for $q_{o_{max}}$ at $P_r = 3{,}000$ psia:

$$q_o/q_{max} = \left[1 - 0.2\left(\frac{P_{wf}}{P_r}\right) - 0.8\left(\frac{P_{wf}}{P_r}\right)^2\right]$$

$$q_{max} = \frac{200}{1 - 0.2\left(\frac{2{,}500}{3{,}000}\right) - 0.8\left(\frac{2{,}500}{3{,}000}\right)^2}$$

$$q_{max} = \frac{200}{0.28} = 720 \text{ b/d}$$

(2) Find q_{max} at $P_r = 2{,}000$ psia. Use the relationship:

$$\frac{q_{o_{max_1}}}{q_{o_{max_2}}} = \left(\frac{\overline{P}_{r_1}}{\overline{P}_{r_2}}\right)^3 = \left(\frac{3{,}000}{2{,}000}\right)^3 = 3.37$$

$$q_{o_{max_2}} = \frac{720}{3.37} = 213 \text{ b/d}$$

(3) Use Vogel's equation to find q_o for $P_{wf} = 1{,}000$ psia and $\overline{P}_r = 2{,}000$ psia:

$$q_{o_2} = q_{max_2}\left[1 - 0.2\left(\frac{P_{wf}}{P_r}\right) - 0.8\left(\frac{P_{wf}}{P_r}\right)^2\right]$$

$$= 213\left[1 - 0.2\left(\frac{1{,}000}{2{,}000}\right) - 0.8\left(\frac{1{,}000}{2{,}000}\right)^2\right] = 149 \text{ b/d}$$

CLASS PROBLEM #25a

Given data:

$P_r = 2{,}400$ psia ($P_b > 2{,}400$)
$FE = 1.0$
$q = 180$ b/d for $P_{wf} = 1{,}700$ psia

Calculate:

(1) $q_{o_{max}}$ when $\overline{P}_r$ drops to 1,800 psia
(2) q_o for $P_{wf} = 1{,}500$ psia, 1,000 psia, and 700 psia when the static pressure is 1,800 psia

CLASS PROBLEM #25b

Given data:

$P_r = 1{,}790$ psia ($P_b > 1{,}790$)
$q_o = 95$ b/d for $P_{wf} = 1{,}500$ psia
$FE = 1.0$

Calculate:

(1) the maximum flow rate when P_r drops to 1,600 psia
(2) the flow rate for $P_{wf} = 1{,}400$ psia, 1,200 psia, and 1,000 psia when the reservoir pressure is 1,600 psia

CLASS PROBLEM #25c

Given data:

$P_r = 2{,}850$ psia
$q_o = 685$ b/d for $P_{wf} = 2{,}100$ psia
$FE = 1.0$

Calculate:

(1) the maximum flow rate when P_r drops to 2,000 psia
(2) the flow rate for $P_{wf} = 1{,}800$ psia, 1,500 psia, and 1,200 psia when $P_r = 2{,}000$ psia

(3) the flow rate for $P_{wf} = 1{,}500$ psia, 1,200 psia, and 1,000 psia when $P_r = 1{,}800$ psia

2.233 STANDING'S PROCEDURE FOR PREDICTING FUTURE IPR CURVES

Standing used Vogel's equation in combination with Muskat's relationship concerning present and future productivity indices in presenting a method for predicting future inflow curves.[18] The procedure requires that we use material balance calculations in order to determine future saturations from which we can obtain k_{ro} values.

The following relationships are used:

$$\frac{J_p^*}{J_f^*} = \left(\frac{k_{ro}}{\mu_o B_o}\right)_p \Big/ \left(\frac{k_{ro}}{\mu_o B_o}\right)_f \quad (2.103)$$

$$q_o = q_{max}\left[1 - 0.2\left(\frac{P_{wf}}{P_r}\right) - 0.8\left(\frac{P_{wf}}{P_r}\right)^2\right] \quad (2.104)$$

$$q_{o_{max}\,Vogel} = \frac{q_{max_J}}{1.8} = \frac{J^*(P_r)}{1.8} \quad (2.105)$$

where:

$J^* = \lim J$ as $P_{wf} \longrightarrow P_r$

$$J = \frac{q_o}{P_r - P_{wf}} \quad (2.106)$$

$$J^* = \frac{1.8(q_{max})}{\overline{P}_r} \quad (2.107)$$

Vogel's equation can be rearranged:

$$q_o/q_{max} = \left(1 - \frac{P_{wf}}{P_r}\right)\left[1 + 0.8\left(\frac{P_{wf}}{P_r}\right)\right] \quad (2.108)$$

By substituting $q_o = J\,(P_r - P_{wf})$ into Equation 2.108 and solving for J, we have

$$J = \frac{q_{o_{max}}}{P_r}\left(1 + 0.8\frac{P_{wf}}{P_r}\right) \quad (2.109)$$

By dividing Equation 2.109 by Equation 2.107, we have:

$$\frac{J}{J^*} = \frac{1}{1.8}\left(1 + 0.8\frac{P_{wf}}{P_r}\right) \quad (2.110)$$

Substituting Equation 2.105 into 2.104, we have:

$$q_o = \frac{J^* P_r}{1.8}\left[1 - 0.2\left(\frac{P_{wf}}{P_r}\right) - 0.8\left(\frac{P_{wf}}{P_r}\right)^2\right] \quad (2.111)$$

where J^* for any future P_r is determined from:

$$J_f^* = J_p^*\left(\frac{k_{ro}}{\mu_o B_o}\right)_f \Big/ \left(\frac{k_{ro}}{\mu_o B_o}\right)_p \quad (2.112)$$

It is necessary to test the well at the present time so that P_r and the present value of J can be determined.

(1) Calculate the present value (J_p^*) from Equation 2.107, or J_p^* can be determined from Darcy's Law—that is:

$$J_p^* = \frac{7.08 \times 10^{-3}\,kh}{\overline{\mu}_o \overline{B}_o\left(\ln r_e/r_w - \frac{3}{4} + S\right)} \quad (2.113)$$

(2) Calculate the future value of J from the relationship:

$$J_f^* = J_p^*\left(\frac{k_{ro}}{\mu_o B_o}\right)_f \Big/ \left(\frac{k_{ro}}{\mu_o B_o}\right)_p \quad (2.114)$$

In order to use Equation 2.114, we need present and future values of k_{ro}, μ_o and B_o. Therefore, we need to apply material balance calculations in order to establish oil saturations vs $\overline{P}_r$ since k_{ro} is a function of oil saturations—which in turn is a function of static pressure. Standing suggested using the Tarner[19] gas depletion calculations for determining oil saturation. If k_{ro} values are not available, Standing also suggested that the work of A.T. Corey could be used to obtain values for k_{ro}:

$$k_{ro} = \left(\frac{S_L - S_{Lr}}{1 - S_{Lr}}\right)^n \quad (2.115)$$

where:

$S_L = S_o + S_{wi}$
$S_{Lr} = S_{or} + S_{wi}$

or:

$$k_{ro} = \left(\frac{S_o - S_{or}}{1 - S_{or} - S_{wi}}\right)^n \quad (2.116)$$

where n is approximately 4 for consolidated sandstones and nonvugular limestones. The value of n is less for unconsolidated sandstones.

EXAMPLE PROBLEM #26

Given data:

	Present condition	Future condition
reservoir pressure	2,500	2,000
flowing pressure	1,750	—
flow rate	2,024	—
flow efficiency	1.0	1.0
k_{ro}	0.80	0.75
k_{abs}	62.5	62.5
μ_o	0.5421	0.6229
B_o	1.3190	1.2562
r_e	1,500	1,500
r_w	0.25	0.25
h	50.0	50.0

Calculate:

the flow rate for $P_{wf} = 1{,}500$ psia and 1,000 psia when reservoir pressure drops to 2,000 psia

Solution procedure:

(1) Using Equation 2.106, calculate J:

$$J = \frac{q}{P_r - P_{wf}} = \frac{2{,}024}{2{,}500 - 1{,}750} = 2.70$$

$$q_{max} = \frac{2{,}024}{1.0 - 0.2\left(\frac{1{,}750}{2{,}500}\right) - 0.8\left(\frac{1{,}750}{2{,}500}\right)^2} = 4{,}325 \text{ b/d}$$

(2) Using Equation 2.107, calculate J_p^*, as follows:

$$J_p^* = \frac{(1.8)(4{,}325)}{2{,}500} = 3.11$$

(3) Using Equation 2.112, calculate J_f^*, as follows:

$$J_f^* = (3.11)\frac{\dfrac{0.75}{(0.6229)(1.2562)}}{\dfrac{0.80}{(0.5421)(1.3190)}} = 2.67$$

(4) Using Equation 2.111, calculate the flow rate for specific flowing pressures:

For $P_{wf} = 1{,}500$ psia @ $P_r = 2{,}000$ psia:

$$q_o = \frac{(2.67)(2{,}000)}{1.8}\left[1.0 - 0.2\left(\frac{1{,}500}{2{,}000}\right) - 0.8\left(\frac{1{,}500}{2{,}000}\right)^2\right] = 1{,}186 \text{ b/d}$$

For $P_{wf} = 1{,}000$ psia @ $P_r = 2{,}000$ psia:

$$q_o = \frac{(2.67)(2{,}000)}{1.8}\left[1.0 - 0.2\left(\frac{1{,}000}{2{,}000}\right) - 0.8\left(\frac{1{,}000}{2{,}000}\right)^2\right] = 2{,}075 \text{ b/d}$$

2.234 COUTO'S PROCEDURE

Couto's procedure, by using Equation 2.41 or 2.42, can also be used to predict future IPR curves if the relative permeability, the oil viscosity, and the formation volume factor at certain reservoir pressures in the future are known.

EXAMPLE PROBLEM #27

Given data:

Use data from example problem #23.

Calculate:

the flow rate for P_{wf} = 1,500 psia and 1,000 psia when reservoir pressure drops to 2,000 psia

Solution procedure:

(1) Using the data from example problem #26, Equation 2.41 can be simplified as follows:

$$q_o = (3.49)(0.001127)\left(\frac{(62.5)(50)}{\ln(0.472 \times 1{,}500/0.25)}\right) \times (2{,}500)\left(\frac{0.80}{(0.5421)(1.319)}\right)(1.0)(1.0 - R) \times [1.8 - 0.8(1.0)(1.0 - R)]$$
$$= 2{,}964.25(1.0 - R)[1.8 - 0.8(1.0 - R)]$$

(2) For P_{wf} = 1,500 psia and P_r = 2,000 psia:

$$R = 1{,}500/2{,}000 = 0.75$$
$$q_o = 2{,}964.25(1 - 0.75)[1.8 - 0.8(1 - 0.75)] = 1{,}186 \text{ b/d}$$

(3) For P_{wf} = 1,000 psi and P_r = 2,000 psia:

$$R = 1{,}000/2{,}000 = 0.5$$
$$q_o = 2{,}964.25(1 - 0.5)[1.8 - 0.8(1 - 0.5)] = 2{,}075 \text{ b/d}$$

CLASS PROBLEM #27a

Given data:

	Present condition	Future condition
reservoir pressure	2,210	1,850
flowing pressure	1,975	—
flow rate	1,032	—
flow efficiency	1	1
k_{ro}	0.42	0.25
k_{abs}	75	75
μ_o	0.3423	0.3745
B_o	1.3526	1.2939
r_e	1,053	1,053
r_w	0.33	0.33
h	70	70

Calculate:

Using Standing's and Couto's procedures, calculate flow rates for P_{wf} = 1,600 psia, 1,400 psia, and 1,000 psia when the reservoir static pressure = 1,850 psia.

CLASS PROBLEM #27b

Given data:

	Present condition	Future condition
reservoir pressure (psi)	2,895	2,375
flowing pressure (psi)	2,541	—
flow rate (b/d)	582	—
flow efficiency	1.0	1.0
k_{ro}	0.42	0.25
k_{abs}	65	65
μ_o, cp	0.2970	0.3298
B_o	1.4735	1.3806
r_e, ft	1,590	1,590
r_w, ft	0.33	0.33
h, ft	40	40

Calculate:

(1) Calculate flow rates for P_{wf} = 2,000 psi, 1,800 psi, and 1,500 psi when P_r = 2,375 psi by using Couto's procedure.
(2) By assuming FE = 1.0, calculate flow rates for P_{wf} = 2,000 psi, 1,800 psi, and 1,500 psi when P_r = 2,375 psi by using Standing's procedure.

CLASS PROBLEM #27c

Rework problem #27b, section (1) only, by assuming FE = 2.0.

2.235 PIVOT POINT METHOD

Uhri and Blount derived the pivot point method to predict future inflow performance relationship (IPR) curves by considering two IPR curves of a well, which represents the different stage of depletion of a solution-gas-drive reservoir.[20] This method can be applied

graphically or numerically by calculating the relationship between the productivity index, $(-dq_o/dP_{wf})$ at $P_{wf} = P_r$, and reservoir pressures.

The productivity index is determined by differentiating Vogel's equation, that is:

$$\frac{dq_o}{dP_{wf}} = \frac{q_{max}}{P_r}\left(-0.2 - 1.6\frac{P_{wf}}{P_r}\right) \tag{2.117}$$

For the maximum flow rate, $P_{wf} = 0.0$, and the equation becomes:

$$\frac{dq_o}{dP_{wf}} = 0.2\frac{q_{max}}{P_r} \tag{2.118}$$

and for $P_{wf} = P_r$:

$$\frac{dq_o}{dP_{wf}} = 1.8\frac{q_{max}}{P_r} \tag{2.119}$$

Based on Equations 2.118 and 2.119, the productivity index at $P_{wf} = P_r$ is equal to nine times the productivity index at $P_{wf} = 0.0$, or:

$$\left\{\frac{dq_o}{dP_{wf}}\right\}_{P_{wf}=P_r} = 9 \times \left\{\frac{dq_o}{dP_{wf}}\right\}_{P_{wf}=0} \tag{2.120}$$

To predict future inflow performance relationships, this method needs two flow tests at different times. One test can be in the past and one test at present, or both can be at different times in the past. Using these two flow tests and applying Equations 2.118, 2.119, and 2.120, the relationship between (dq_o/dP_{wf}) vs P_r can be obtained.

The following procedure is used to predict future IPR curves by using the pivot point method graphically (refer to Figure 2.42):

(1) Calculate the maximum flow rate from each flow test using Vogel's equation.
(2) For each flow test, calculate dq_o/dP_{wf} for $P_{wf} = 0$ and $P_{wf} = P_r$ using Equations 2.118 and 2.119.
(3) Draw the X-Y axis with dq_o/dP_{wf} as the vertical axis and P_{wf} as the horizontal axis.
(4) Plot the value of dq_o/dP_{wf} vs P_{wf} as shown in Figure 2.42 from the flow tests.

Point $P = dq_o/dP_{wf}$ at $P_{wf} = 0$ from first test
$Q = dq_o/dP_{wf}$ at $P_{wf} = P_r$ from first test
$R = dq_o/dP_{wf}$ at $P_{wf} = 0$ from second test
$S = dq_o/dP_{wf}$ at $P_{wf} = P_r$ from second test

(5) Draw a line between P-Q and R-S and extend these lines until both lines intersect. This intersection is called the pivot point—PP.
(6) If O is the point of origin, divide line OP (on the vertical axis) into several parts, for example into four parts—that is, P_1, P_2, and P_3—and draw lines from the pivot point (PP) to P_1, P_2, and P_3—that is, PP-P_1, PP-P_2, and PP-P_3—and then extend the lines far enough to incorporate the envelope.
(7) On the vertical or dq_o/dP_{wf} axis, determine points q_1, q_2, and q_3, where the distances Oq_1, Oq_2, and Oq_3 are determined, based on the value of OP_1, OP_2, and OP_3, respectively, by applying Equation 2.120; that is:

$$Oq_1 = OP_1 \times 9$$
$$Oq_2 = OP_2 \times 9$$
$$Oq_3 = OP_3 \times 9$$

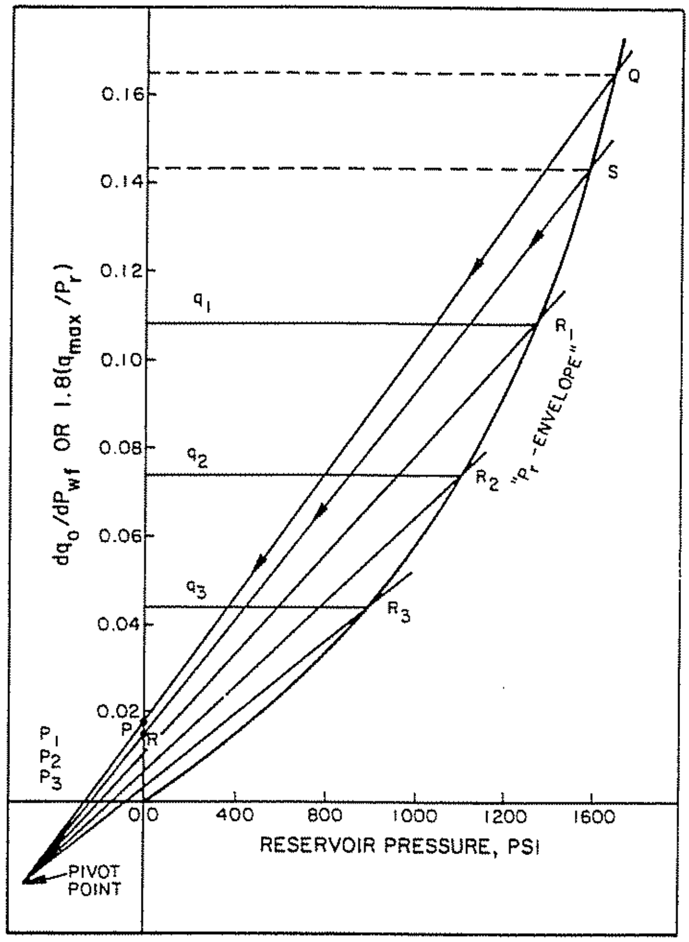

Figure 2.42 Illustration to Construct Reservoir Pressure Envelope using the Pivot Point Method

(8) From q_1, q_2, and q_3, draw horizontal lines until they intersect the extension of PP-P_1, PP-P_2, and PP-P_3, respectively, and obtain points R_1, R_2, and R_3.
(9) Connect points S, R_3, R_2, R_1, Q, and O. This curve is called the reservoir pressure envelope.
(10) If the horizontal axis is considered to be the reservoir pressure P_r, the vertical axis is 1.8 (q_{max}/P_r).
(11) Using the reservoir pressure envelope from step 9 and for certain values of reservoir pressure in the future, the value of 1.8 (q_{max}/P_r) can be determined; then the maximum flow rate can be calculated.
(12) An IPR curve into the future can be predicted by applying Vogel's equation based on the future reservoir pressure and the maximum flow rate from step 11.

Uhri and Blount also derived equations to predict IPR curves numerically,[20] which can be obtained in two ways, that is:

(1) numerical solution using the pivot point method
(2) numerical solution using the P_r-envelope equation

For the numerical solution approach using the pivot point, the following equations were derived:

$$P^*_{wf} = \frac{1/8\ [(q_{max})_2\, P_{r_1}{}^2 \times P_{r_2} - (q_{max})_1\, P_{r_2}{}^2 \times P_{r_1}]}{(q_{max})_1\, P_{r_2}{}^2 - (q_{max})_2\, P_{r_1}{}^2} \tag{2.121}$$

$$\left(-\frac{dq_o}{dP_{wf}}\right)^* = (q_{max})_1\left[\frac{0.2}{P_{r_1}} + 1.6\frac{P^*_{wf}}{P_{r_1}{}^2}\right] \quad (2.122)$$

$$\left(-\frac{dq_o}{dP_{wf}}\right)_f @ P_{wf} = 0 = \frac{\left(-\frac{dq_o}{dP_{wf}}\right)^*}{1 + 8\,(P^*_{wf}/P_{r_f})} \quad (2.123)$$

$$\left(-\frac{dq_o}{dP_{wf}}\right)_f @ P_{wf} = 0 = \frac{0.2(q_{max})_f}{P_{r_f}} \quad (2.124)$$

P^*_{wf} and $(-dq/dP_{wf})^*$ are the coordinates of the pivot point, and subscripts 1 and 2 refer to well tests 1 and 2, respectively; subscript f indicates a future curve's condition.

The following procedure may be followed to predict future IPR curves:

(1) By using Vogel's equation, calculate the maximum flow rate for both tests—that is, $(q_{max})_1$ and $(q_{max})_2$.
(2) By using Equation 2.121, calculate P^*_{wf}.
(3) Calculate $(-dq_o/dP_{wf})^*$ by using Equation 2.122.
(4) For a particular future reservoir pressure, calculate $\left(-\frac{dq_o}{dP_{wf}}\right)_f$ @ $P_{wf} = 0$, by using Equation 2.123.
(5) Based on the result in step 4, the maximum flow rate at a particular future reservoir pressure can be obtained by using Equation 2.124.
(6) The future IPR curve can be obtained by using Vogel's equation based on the values of P_{rf} and $(q_{max})_f$.

For the numerical solution approach using the P_r-envelope equation, Uhri and Blount derived an analytical expression for the P_r-envelope. The equation is:

$$\frac{q_{max}}{P_r} = \frac{A \times P_r}{P_r + n} \quad (2.125)$$

where A and n are constants for a particular well.

These constants can be determined by using the values of P_r and the maximum flow rate from the tests as follows:

$$A = \frac{P_{r_1} - P_{r_2}}{\frac{P_{r_1}{}^2}{(q_{max})_1} - \frac{P_{r2}{}^2}{(q_{max})_2}} \quad (2.126)$$

$$n = P_{r_1}\,[A\,P_{r_1}/(q_{max})_1 - 1] \quad (2.127)$$

The procedure to predict future IPR curves by using the P_r-envelope equation is as follows:

(1) By using Vogel's equation, determine the maximum flow rates for both tests.
(2) Calculate A and n by using Equations 2.126 and 2.127, respectively.
(3) Calculate the maximum flow rate for a particular future reservoir pressure by using Equation 2.125.
(4) By using Vogel's equation, obtain the IPR curve for a particular future reservoir pressure.

EXAMPLE PROBLEM #28

Given data: two well tests:

Test #	P_r	P_{wf}	q_o
1	1,900	1,650	511.60
2	1,750	1,575	290.92

Calculate:

(1) the maximum flow rate when the reservoir pressure drops to 1,600 psia
(2) the flow rate for $P_{wf} = 1{,}200$ psia when $P_r = 1{,}600$ psia

Solution procedure:

(1) Calculate the maximum flow rate from each test by using Vogel's equation; then calculate dq/dP_{wf} for $P_{wf} = 0$ and $P_{wf} = P_r$ by using Equations 2.118 and 2.119, respectively.

Test #	q_{max}	dq/dP_{wf} @ $P_{wf} = 0$	dq/dP_{wf} @ $P_{wf} = P_r$
1	2,294.26	0.2415	2.1735
2	1,691.40	0.1933	1.7397

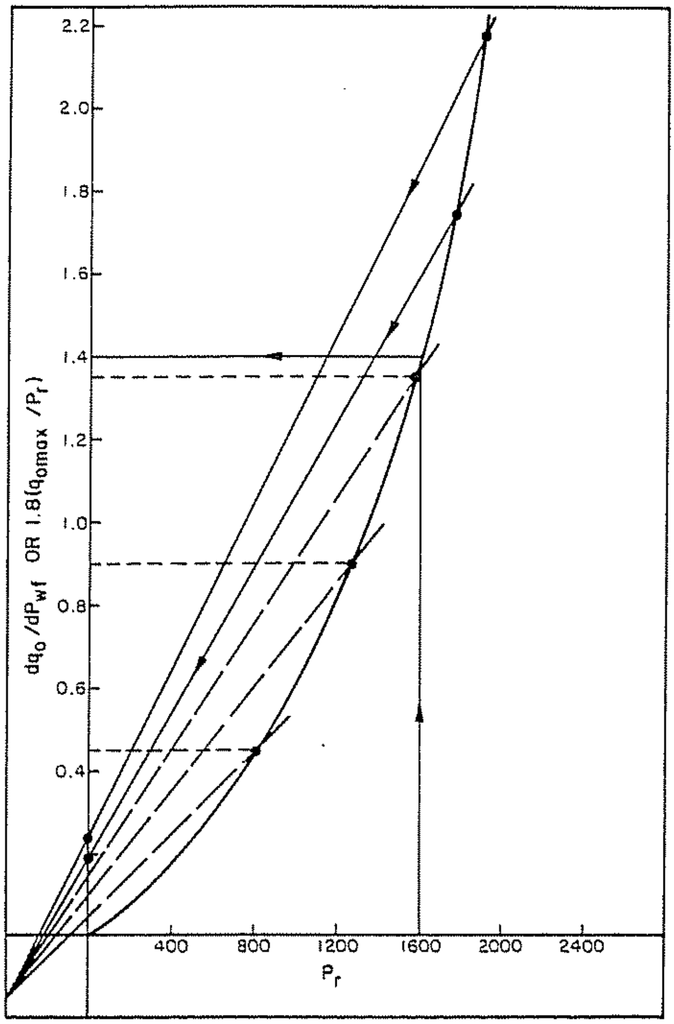

Figure 2.43 P_r Envelope for Example Problem #28

(2) Plot dq/dP_{wf} vs P_r and determine the pivot point as shown in Figure 2.43.
(3) Assume several values of dq/dP_{wf} @ $P_{wf} = 0$ and calculate dq/dP_{wf} @ $P_{wf} = P_r$ by using Equation 2.120 as follows:

dq/dP_{wf} @ $P_{wf}=0$ (assumed)	dq/dP_{wf} @ $P_{wf}=P_r$
0.15	1.35
0.10	0.90
0.05	0.45

(4) By using steps 6, 7, 8, and 9 of the procedure, draw the P_r-envelope as shown in Figure 2.43.
(5) Using the P_r-envelope, for P_r = 1,600 psia, the value of $1.8(q_{max})/P_r = 1.40$. The maximum flow rate is:

$$q_{max} = (1.40)(1{,}600)/1.8 = 1{,}244 \text{ bo/d}$$

(6) By using Vogel's equation, the flow rate for P_{wf} = 1,200 psia is:

$$q_o = 1{,}244\left[1.0 - 0.2\left(\frac{1{,}200}{1{,}600}\right) - 0.8\left(\frac{1{,}200}{1{,}600}\right)^2\right]$$
$$= 498 \text{ bo/d}$$

EXAMPLE PROBLEM #29

Given data (same as for example problem #28).

Calculate: (using the numerical solution proposed by Uhri and Blount).[20]

Solution procedure:

(1) Numerical solution using the pivot point method:

(a) Calculate the maximum flow rates for both tests:

Test #	P_r	q_{max}
1	1,900	2,294.26
2	1,750	1,691.40

(b) Calculate P^*_{wf} by using Equation 2.121 as follows:

$$P^*_{wf} = \frac{\tfrac{1}{8}[(1{,}691.40)(1{,}900)^2(1{,}750) - (2.294.26)(1{,}750)^2(1{,}900)]}{(2{,}294.26)(1{,}750)^2 - (1{,}691.40)(1{,}900)^2}$$
$$= -361.91$$

(c) Calculate $\left(-\frac{dq_o}{dP_{wf}}\right)^*$ by using Equation 2.122:

$$\left(-\frac{dq_o}{dP_{wf}}\right)^* = (2{,}294.26)$$
$$\times\left[0.2\frac{1}{1{,}900} + \frac{1.6(-361.91)}{(1{,}900)^2}\right]$$
$$= -0.1265$$

(d) Calculate $\left(-\frac{dq_o}{dP_{wf}}\right)_f$ @ $P_{wf} = 0$ by using Equation 2.123:

$$\left(-\frac{dq_o}{dP_{wf}}\right)_f = \frac{-0.1265}{1 + 8(-361.91/1{,}600)} = 0.1563$$

(e) Calculate the future maximum flow rate by using Equation 2.124:

$$0.1563 = 0.2\,(q_{max})_f/1{,}600$$
$$(q_{max})_f = \frac{0.153 \times 1{,}600}{0.2} = 1{,}250.14 \text{ b/d}$$

(f) The flow rate @ P_{wf} = 1,200 psi can be calculated by using Vogel's equation as follows:

$$q_o = 1{,}250.14\left[1 - 0.2\frac{1{,}200}{1{,}600} - 0.8\left(\frac{1{,}200}{1{,}600}\right)^2\right]$$
$$= 500 \text{ b/d}$$

(2) Numerical solution by using P_r-envelope equation:

(a) The maximum flow rates for both tests had been calculated previously.
(b) Calculate constant A, using Equation 2.126:

$$A = \frac{1{,}900 - 1{,}750}{\left[\frac{1{,}900^2}{2{,}294.26} - \frac{1{,}750^2}{1{,}691.46}\right]} = -0.6327$$

(c) Calculate constant n, using Equation 1.127:

$$n = 1{,}900\left[\left(\frac{-0.6327(1{,}900)}{2{,}294.26}\right) - 1\right] = -2{,}895.57$$

(d) The P_r-envelope equation is:

$$\frac{q_{max}}{P_r} = \frac{-0.6327\,P_r}{P_r - 2895.57}$$

(e) For Pr_f = 1,600 psi:

$$(q_{max})_f = \frac{1{,}600(-0.6327)(1{,}600)}{1{,}600 - 2{,}895.57} = 1{,}250.19 \text{ b/d}$$

(f) The flow rate at P_{wf} = 1,200 psi is 500 b/d (by using Vogel's equation).

CLASS PROBLEM #28a

Given data: two well tests:

Test #	P_r	P_{wf}	q_o
1	2,325	1,825	639
2	2,150	1,750	407

Calculate:

(1) the maximum flow rates when the reservoir pressures drop to 2,000 psia, 1,600 psia, and 1,200 psia
(2) the flow rates for flowing pressure = 900 psia when the reservoir pressures drop to 2,000 psia, 1,600 psia, and 1,200 psia

CLASS PROBLEM #28b

Given data: two tests were taken on a well:

Test #	P_r	P_{wf}	q_o
1	1,890	1,250	648
2	1,640	1,300	215

Calculate:

(1) the maximum flow rates when the reservoir pressures drop to 1,500 psia, 1,200 psia, and 1,100 psia
(2) the flow rates for flowing pressure = 950 psia when the reservoir pressures drop to 1,500 psia, 1,200 psia, and 1,100 psia

CLASS PROBLEM #28c

Given data: two well tests:

Test #	P_r	P_{wf}	q_o
1	2,250	1,800	501
2	2,010	1,700	217

Calculate:

(1) the maximum flow rates when the reservoir pressures drop to 1,900 psia, 1,750 psia, and 1,500 psia
(2) the flow rates for $P_{wf} = 1{,}000$ psia when the reservoir pressures = 1,900 psia, 1,750 psia, and 1,500 psia

CLASS PROBLEM #28d

Given data: two well tests:

Test #	P_r	P_{wf}	q_o
1	1,800	1,500	274
2	1,600	1,200	271

Calculate:

(1) the maximum flow rates when the reservoir pressures drop to 1,400 psia, 1,200 psia, and 1,000 psia
(2) the flow rates for $P_{wf} = 1{,}000$ psia when the reservoir pressures = 1,400 psia and 1,200 psia

2.236 OTHER METHODS OF CONSTRUCTING FUTURE IPR CURVES

Refer to pages 25 through 32 of Volume 1 of this series for work by Eckmier[17] and others in establishing future IPR curves.

2.24 TRANSIENT IPR CURVES FOR OIL FLOW

There are many wells with low permeability that require a long time period to reach pseudo-steady-state flow. It therefore becomes important to construct IPR curves at different times in order to predict the flow rate at these times.

2.241 STATES OF FLOW IN THE RESERVOIR

In a finite reservoir system, there are three states of flow (flow regimes):

(1) transient flow
(2) late transient flow
(3) pseudo-steady-state flow

These three states of flow are shown schematically by plotting flow rate vs time for a certain constant flowing pressure as shown in Figure 2.60.

Transient flow occurs for a certain time, and its pressure behavior is essentially the same as that of an infinite reservoir. As the time becomes larger, the pressure decline becomes a linear function of time; at this condition, pseudo-steady-state flow occurs. The flow period between the transient and pseudo-steady-state is called the late transient period in which, at the beginning of late transient period (or at the end of the transient period), the pressure drop caused by production has been felt at the drainage boundary of the well. At this condition, the IPR curves decrease as time increases.

At the end of the late transient period or when the pseudo-steady state is reached, the transient IPR curve is close to pseudo-steady-state IPR curves.

The duration of the transient period may be estimated from the following equation:

$$t_{tp} = \frac{\phi\, \mu_o\, C_t\, (r_e)^2}{0.002637\, k_o} \tag{2.128}$$

where t_{tp} = duration of transient period, hours.

The late transient period may be estimated by the following equation:

$$t_{ltp} = \frac{\phi\, \mu_o\, C_t\, (r_e)^2}{0.00088\, k_o} \tag{2.129}$$

Equation 2.129 was derived for a circular-shaped reservoir with an error percent of 0.01. To take care of some average errors in the shape factor, Ertle suggested using the following equation to estimate the late transient period:[21]

$$t_{ltp} = \frac{\phi\, \mu_o\, C_t\, (r_e)^2}{0.001055\, k_o} \tag{2.130}$$

For $t < t_{tp}$, the IPR curve can be calculated by using the following equation:

$$P_r - P_{wf} = \frac{162.6\, q_o\, \mu_o B_o}{k_o h}\left(\text{Log}\left(\frac{k_o t}{\phi \mu_o C_t (r_w)^2}\right) - 3.23 + 0.87S\right) \tag{2.131}$$

In the previous discussion, we learned how to approximate the value of μ_o and B_o if those values are not available from laboratory data. The following discussion shows how to approximate the value of the total system compressibility.

The total system compressibility, C_t, is defined by:

$$C_t = S_o\, C_o + S_g\, C_g + S_w\, C_w + C_f \tag{2.132}$$

where:

S_o = oil saturation, fraction
C_o = oil compressibility, psi^{-1}
S_g = gas saturation, fraction
C_g = gas compressibility, psi^{-1}
S_w = water saturation, fraction
C_w = water compressibility, psi^{-1}
C_f = formation or rock compressibility, psi^{-1}

Equation 2.132 is used for an undersaturated condition; that is, the pressure of the system is above the bubble-point pressure. For pressures below the bubble-point pressure, Equation 2.132 becomes:

$$C_t = S_o\, C_{oa} + S_g\, C_{ga} + S_w\, C_{wa} + C_f \qquad (2.133)$$

where C_{oa} and C_{wa} are the apparent compressibility of oil and water, respectively.

(1) *Oil compressibility at isothermal conditions.* For pressures above the bubble-point pressure, oil compressibility, C_o, is defined by:

$$C_o = -\frac{1}{B_o}\left(\frac{dB_o}{dP}\right) \qquad (2.134)$$

Equation 2.134 can be used to approximate the oil compressibility if the plot of B_o vs pressure from the laboratory data is available. If the plot is not available from laboratory data, C_o at undersaturated conditions can be approximated by using Trube's correlation:

$$C_o = -\frac{C_{Pr}}{P_{Pc}} \qquad (2.135)$$

where:

C_{Pr} = pseudo-reduced compressibility, which can be determined by using Figure 2.44
$T_{Pr} = T/T_{Pc}$ = pseudo-reduced temperature
T_{Pc} = pseudo-critical temperature
$P_{Pr} = P/P_{Pc}$ = pseudo-reduced pressure
P_{Pc} = pseudo-critical pressure

Pseudo-critical temperature and pseudo-critical pressure can be approximated by using the following equations:

$$T_{Pc} = 169 + 314\,\gamma_g \qquad (2.136)$$

$$P_{Pc} = 708.75 - 57.5\,\gamma_g \qquad (2.137)$$

For pressures below the bubble-point pressure, gas in solution should be considered for approximating the value of oil compressibility, and C_{oa} is defined by:

$$C_{oa} = -\frac{1}{B_o}\left(\frac{dB_o}{dP}\right) + \frac{B_g}{B_o}\left(\frac{dR_s}{dP}\right) \qquad (2.138)$$

Equation 2.138 is used if the plot of B_o vs pressure and R_s vs pressure are available from laboratory data. If those data are not available, C_{oa} can be approximated as follows:

(1) dR_s/dP can be approximated by using Figure 2.45 or estimated by using the following equation:

$$\frac{dR_s}{dP} = \frac{R_s}{0.83\,P + 21.75} \qquad (2.139)$$

(2) dB_o/dP can be evaluated as follows:

$$\frac{dB_o}{dP} \approx \frac{dR_s}{dP} \times \frac{dB_o}{dR_s} \qquad (2.140)$$

dB_o/dR_s can be estimated by using Figure 2.46 (°API of oil and gas gravity should be known)

(3) R_s and B_o are estimated by using Standing's correlations, Figure 2.4 and Figure 2.5, respectively.
(4) B_g is calculated by using the following equation.

$$B_g = 5.039 \times 10^{-3}\,\frac{Z\,T}{P} \qquad (2.141)$$

where:

Z = gas deviation factor
T = temperature, °R
P = pressure, psi

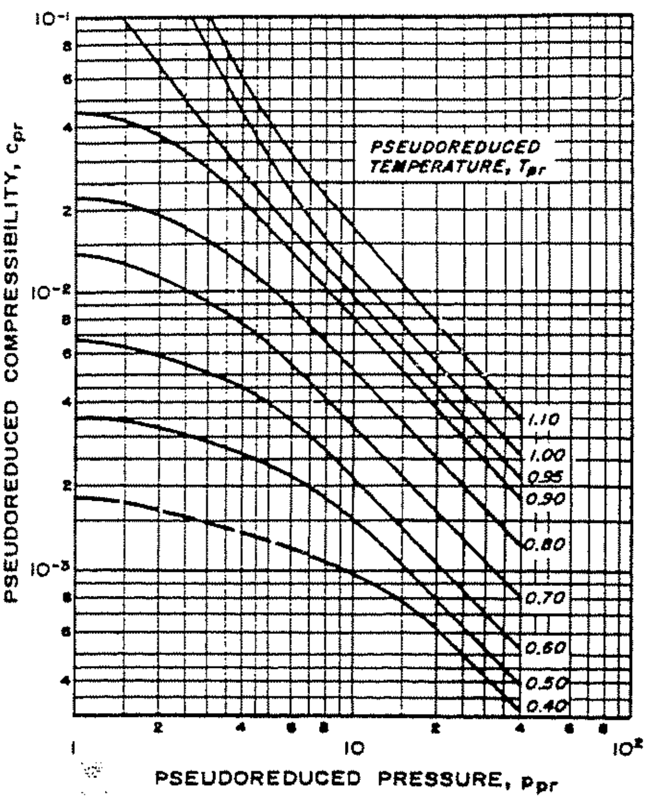

Figure 2.44 Correlation of Pseudo-reduced Compressibility for an Undersaturated Oil (after Trube)[22]

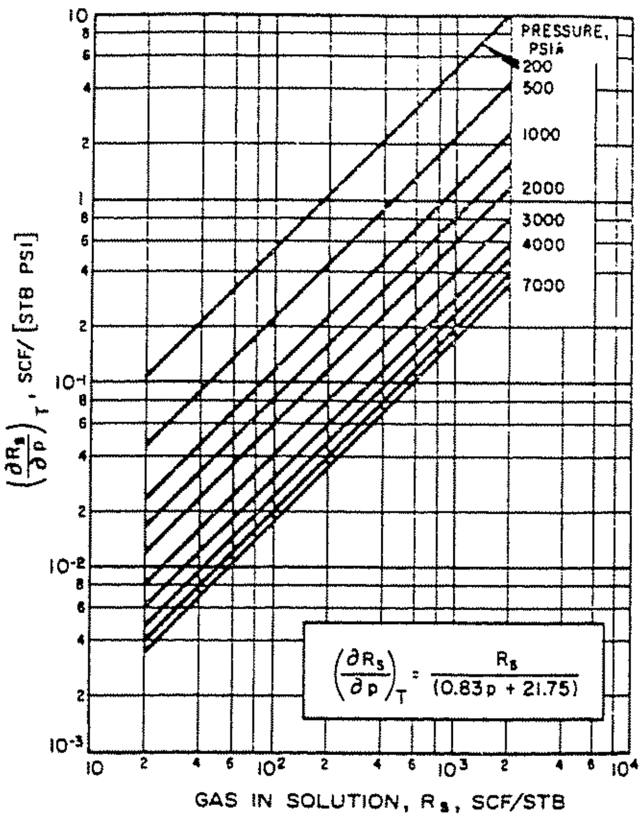

Figure 2.45 Change of Gas in Solution in Oil with Pressure vs Gas in Solution (after Ramey,[23] data of Standing[1])

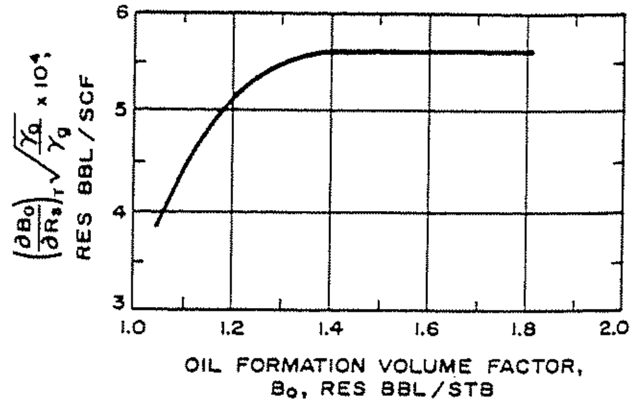

Figure 2.46 Change of Oil Formation Volume Factor with Gas in Solution vs Oil Formation Volume Factor (after Ramey)[23]

(2) *Gas compressibility.* Gas compressibility is defined as:

$$C_g = \frac{1}{P} - \frac{1}{Z}\left(\frac{dZ}{dP}\right) \tag{2.142}$$

In pseudo-reduced pressure and temperature terms, Equation 2.142 becomes:

$$C_g = \frac{1}{P_{Pc}}\left\{\frac{1}{P_{Pr}} - \frac{1}{Z}\left(\frac{dZ}{dP_{Pr}}\right)\right\} \tag{2.143}$$

For solving equation 2.143, the Z-factor chart can be used to evaluate (dZ/dP_{Pr}) and Z, and if P_{Pc} and T_{Pc} are not known, Equations 2.136 and 2.137 can be used. The gas compressibility can also be estimated by using the following equation:

$$C_g = \frac{C_{Pr}}{P_{Pc}} \tag{2.144}$$

where C_{Pr} = pseudo-reduced compressibility, which can be determined by using Figure 2.47 or Figure 2.48.

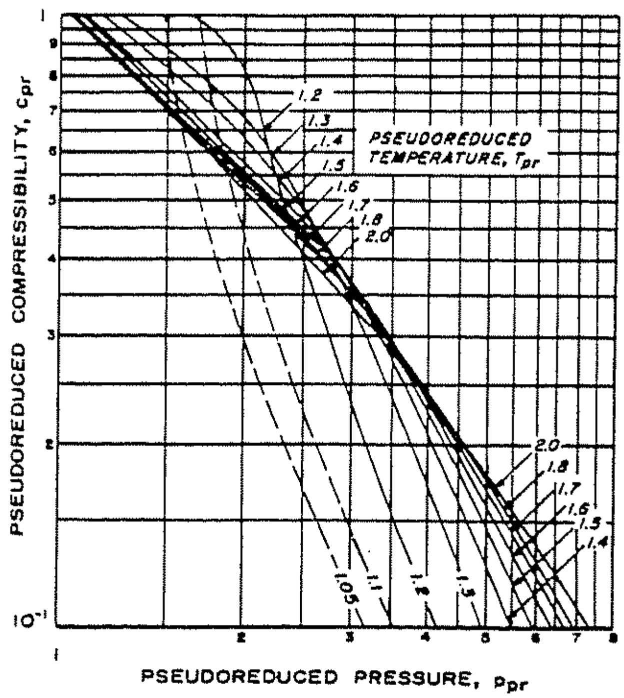

Figure 2.47 Correlation of Pseudo-reduced Compressibility for Natural Gases (after Trube)[24]

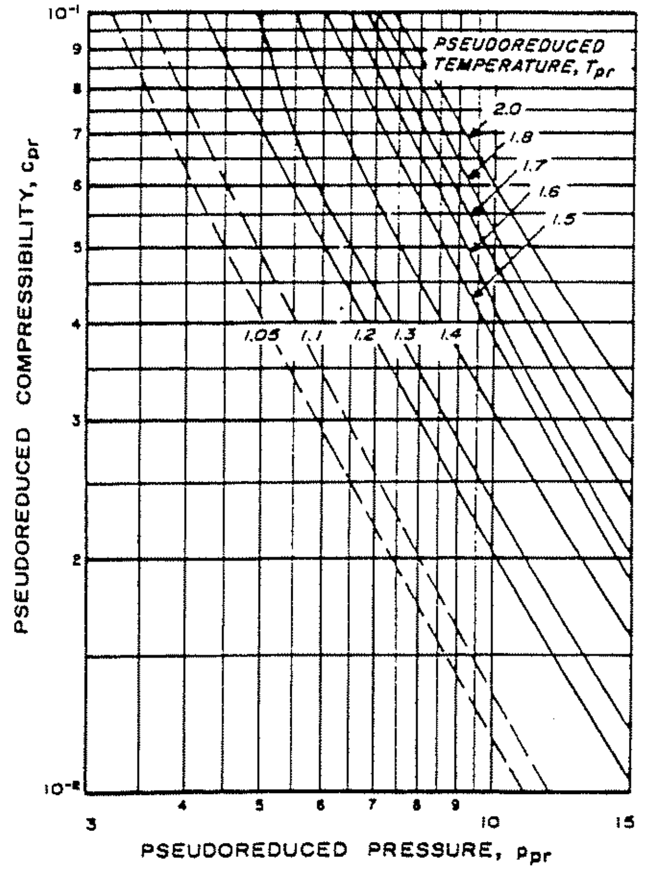

Figure 2.48 Correlation of Pseudo-reduced Compressibility for Natural Gases (after Trube)[24]

(3) *Water compressibility.* For pressures above the bubble point (for gas and water systems), the water compressibility can be estimated by using Figures 2.49 and 2.50. Long and Chierici recommended the following equation for pressures greater than the bubble-point pressure:[25]

$$C_w = (C_w)_{fn}[1 + 0.0088 \times 10^{-Kn}(R_{sw})] \tag{2.145}$$

where:

C_w = water compressibility at undersaturated condition, psi^{-1}

$(C_w)_{fn}$ = water compressibility of gas-free water (brine), containing n gram-equivalents of dissolved solids, psi^{-1}. This value can be determined by using Figures 2.49 and 2.50.

n = dissolved solid, gram-equivalent/liter, ppm/58,443.

K = Secenov's coefficient, which is determined by using Figure 2.51.

R_{sw} = gas solubility in distilled water, scf/bbl, which is determined by using Figure 2.52.

For pressures below the bubble point, water compressibility can be approximated by using the following equation:

$$C_{wa} = -\frac{1}{B_w}\frac{dB_w}{dP} + \frac{B_g}{B_w}\frac{dR_s}{dP} \tag{2.146}$$

where:

$\frac{1}{B_w}\frac{dB_w}{dP}$ is determined by using Figure 2.53 or Equation 2.145

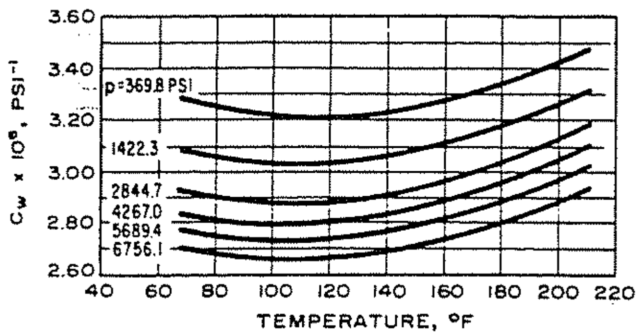

Figure 2.49a Average Compressibility of Distilled Water (after Long and Chierici)[25]

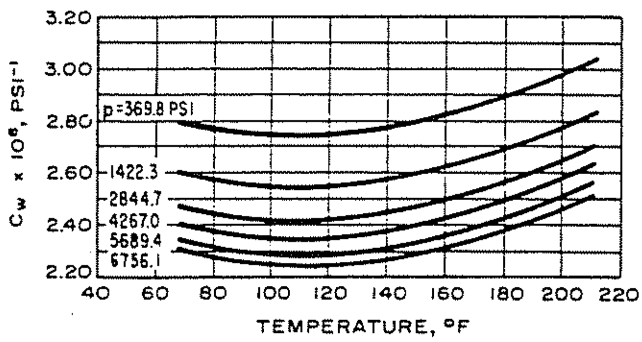

Figure 2.49b Average Compressibility of 100,000-ppm NaCl in Distilled Water (after Long and Chierici)[25]

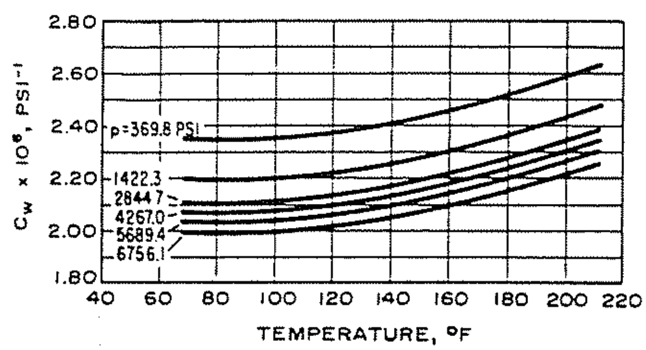

Figure 2.50a Average Compressibility of 200,000-ppm NaCl in Distilled Water (after Long and Chierici)[25]

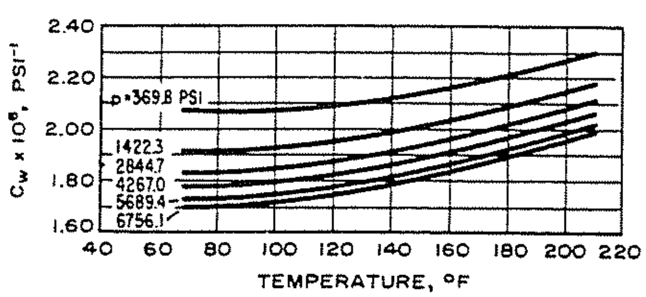

Figure 2.50b Average Compressibility of 300,000-ppm NaCl in Distilled Water (after Long and Chierici)[25]

$\frac{dR_{sw}}{dP}$ is determined by using Figure 2.54

B_g is calculated by applying Equation 2.141

B_w is determined by using Figure 2.55

(4) *Formation or rock compressibility.* Formation compressibility is defined by:

$$C_f = \frac{1}{V_p}\frac{dV_p}{dV} \tag{2.147}$$

For determining formation compressibility, correlations of Hall[27] and van der Knaap[28] have been used extensively, but according to Newman,[29] those correlations do not apply to a very wide range of reservoir rocks. Figures 2.56 through 2.59 are the plots between initial porosity, ϕ_i, vs pore volume (rock) compressibility at 75% lithostatic pressure based on the large number of samples studied by Newman. The lithostatic

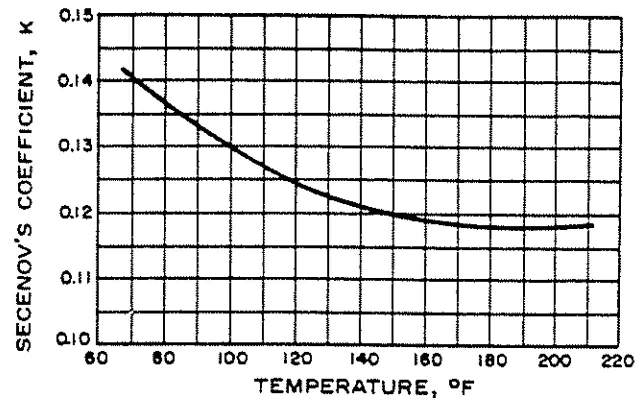

Figure 2.51 Secenov's Coefficient for Methane (after Long and Chierici)[25]

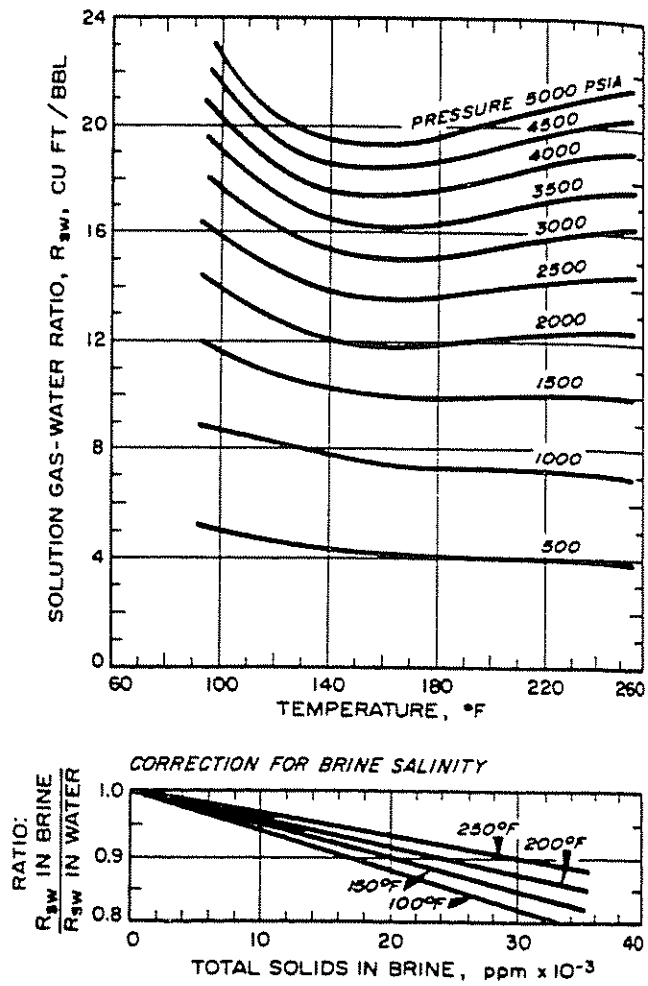

Figure 2.52 Solubility of Natural Gas in Water (after Dodson and Standing)[26]

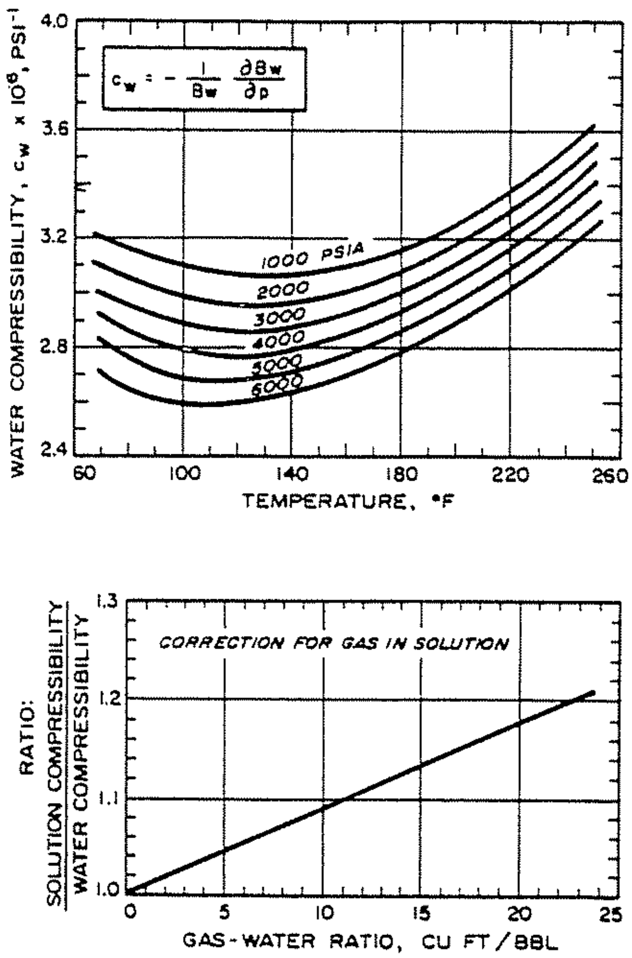

Figure 2.53 Effect of Dissolved Gas on Water Compressibility (after Dodson and Standing)[26]

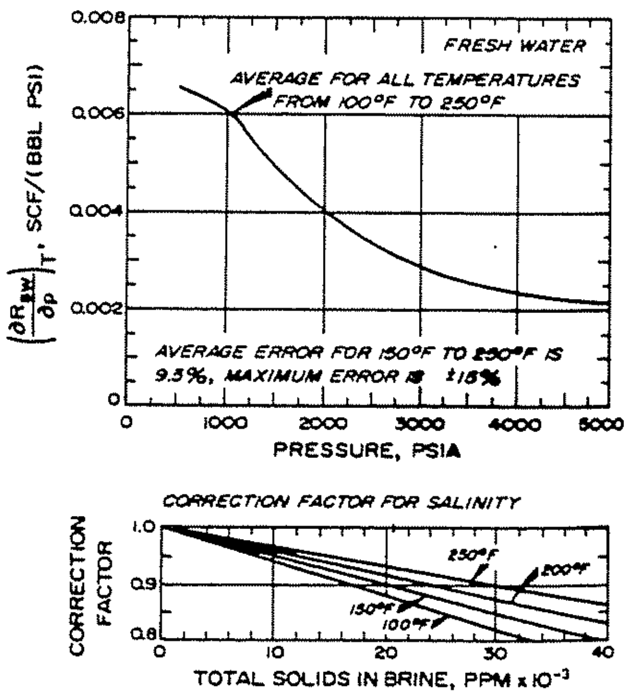

Figure 2.54 Change of Natural Gas in Solution in Formation Water with Pressure vs Pressure. Multiply $(\partial R_{sw}/\partial p)_T$ by the Correction Factor to Get Result for Brine (after Ramey,[3] data of Standing[1])

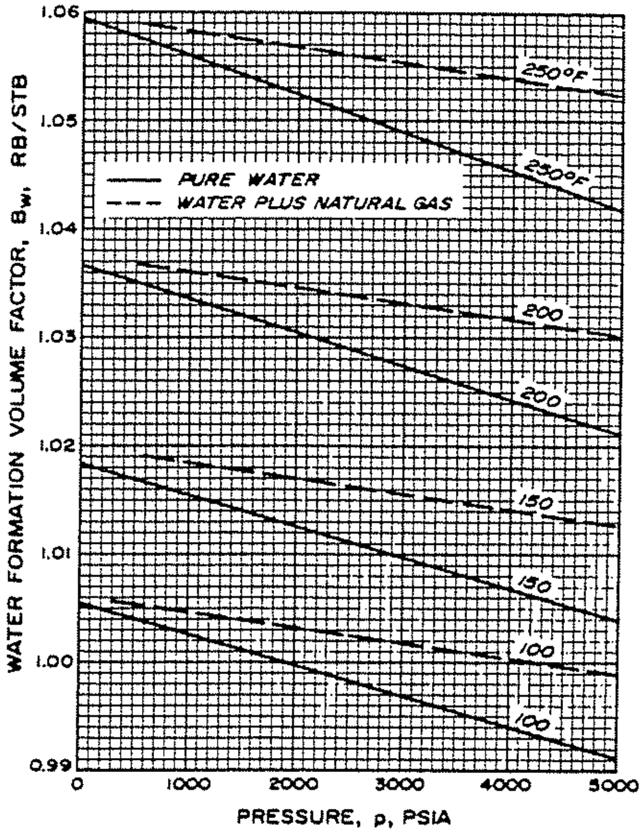

Figure 2.55 Formation Volume Factor of Pure Water and a Mixture of Natural Gas and Water (data of Dodson and Standing)[26]

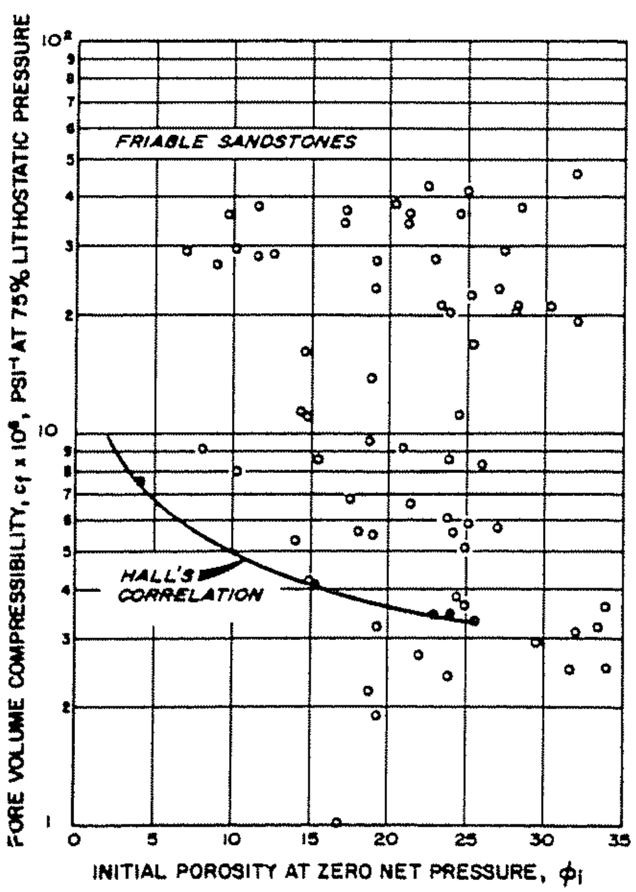

Figure 2.56 Pore-Volume Compressibility at 75% Lithostatic Pressure vs Initial Sample Porosity for Friable Sandstones (after Newman)[29]

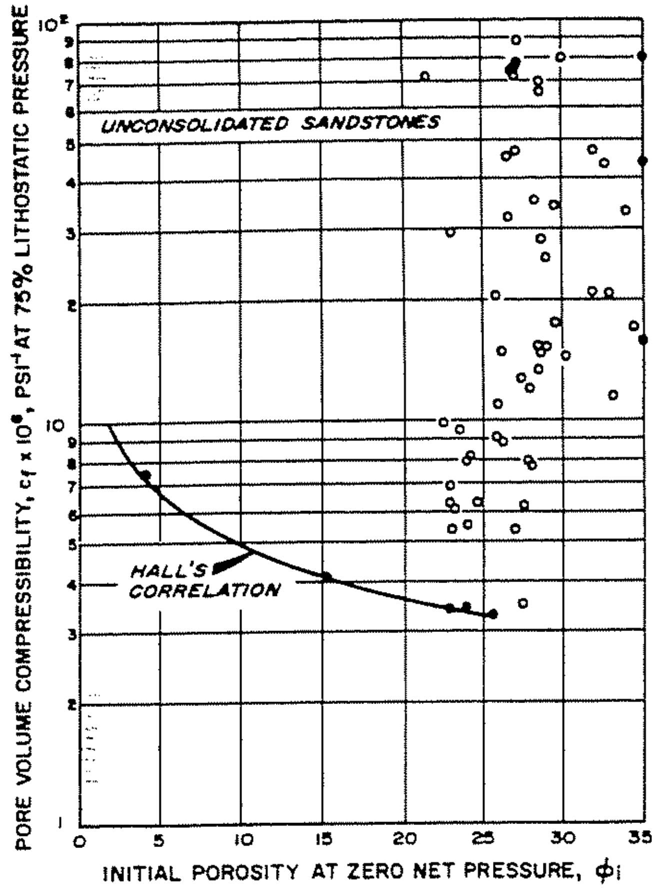

Figure 2.57 Pore-Volume Compressibility at 75% Lithostatic Pressure vs Initial Sample Porosity for Unconsolidated Sandstones (after Newman)[29]

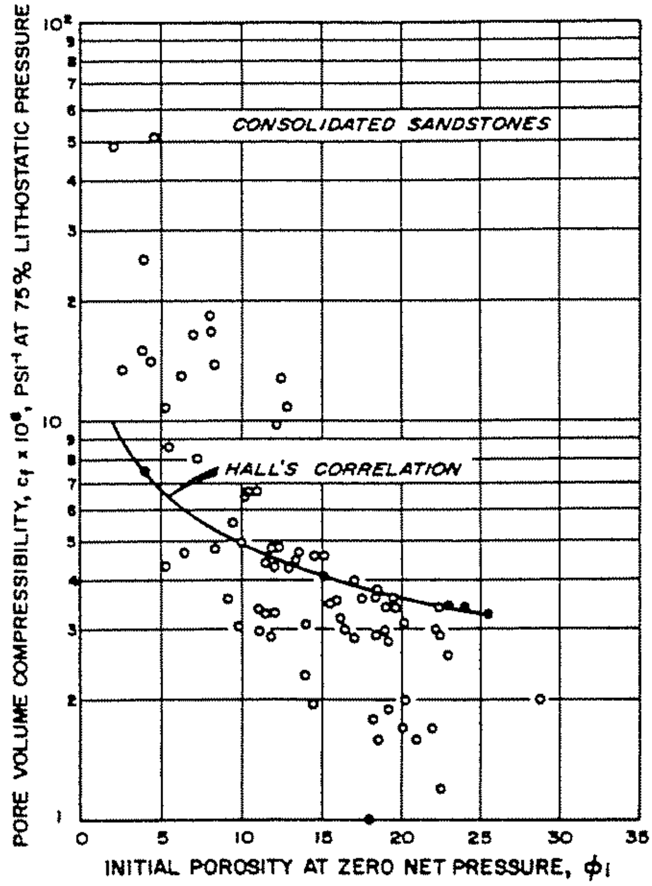

Figure 2.58 Pore-Volume Compressibility at 75% Lithostatic Pressure vs Initial Sample Porosity for Consolidated Sandstones (after Newman)[29]

pressure is reservoir depth multiplied by 1 psi/ft. From these plots, it can be concluded that Hall's and van der Knaap's correlations would not provide a good estimation. To obtain the best formation compressibility, it should be measured from a sample of reservoir rocks.

Knowing C_o, C_g, C_w, and C_f and also the gas, oil, and water saturation, the total compressibility can be calculated by using Equation 2.132 or 2.133.

EXAMPLE PROBLEM #29

(to estimate the decrement of the flow rate vs time at constant flowing pressure)

Given data:

$P_r = 3250$ psi	$T = 175°F$
$\phi = 0.14$	$k_o = 1.0$ md
$\gamma_g = 0.65$	$API = 30°$
$\mu_o = 0.8807$ cp	$B_o = 1.2586$
$r_e = 1{,}500$ ft	$r_w = 0.33$ ft
$h = 70$ ft	skin $= 0$
$C_t = 2.0 \times 10^6$ psi^{-1}	

Calculate:

(1) The transient period by using Equations 2.128, 2.129, and 2.130.
(2) Plot flow rate vs time for constant flowing pressure at 2,000 psi.

Solution procedure:

(1) The transient period calculation is figured by applying:

(a) Equation 2.128 as follows:

$$t_{tp} = \frac{(0.14)(0.8807)(2.0 \times 10^{-6})(1{,}500)^2}{0.002637\,(1)} = 210.41 \text{ hr}$$

(b) Equation 2.129 as follows:

$$t_{ltp} = \frac{(0.14)(0.8807)(2.0 \times 10^{-6})(1{,}500)^2}{0.00088\,(1)} = 630.50 \text{ hr}$$

(c) Equation 2.130 as follows:

$$t_{ltp} = \frac{(0.14)(0.8807)(2.0 \times 10^{-6})(1{,}500)^2}{0.001055\,(1)} = 525.92 \text{ hr}$$

(2) Plot flow rate vs time (hours) for a constant flowing pressure of 2000 psi as follows:

$$(3{,}250 - 2{,}000) = \frac{162.6(q_o)(0.8807)(1.2586)}{(1)(70)} \times \left[\log\left(\frac{(1)(t)}{(0.14)(0.8807)(2.0 \times 10^{-6})(0.33)^2}\right) - 3.23 + 0\right]$$

Simplifying the previous equation yields:

$$q_o = \frac{485.48}{\log(t) + 4.34}$$

By varying t from 1 to 700 hours, the plot of flow rate vs time can be made as shown in Figure 2.60.

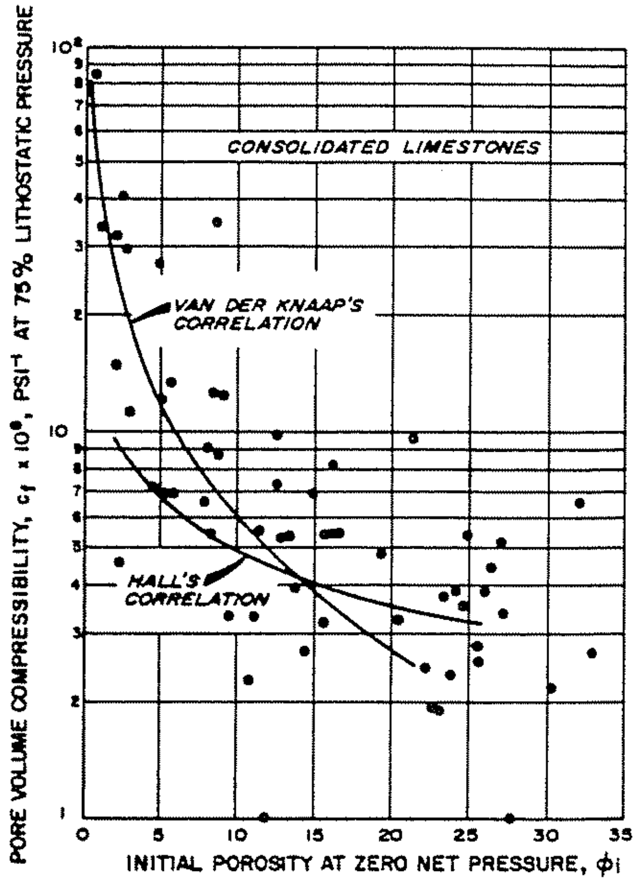

Figure 2.59 Pore-Volume Compressibility at 75% Lithostatic Pressure vs Initial Sample Porosity for Limestones (after Newman)[29]

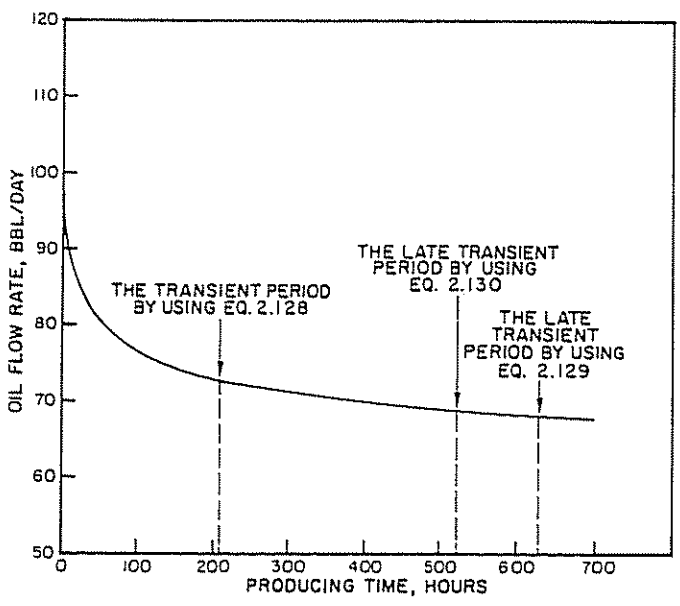

Figure 2.60 Flow Rate vs Producing Time at Constant Flowing Pressure (Example Problem 29)

EXAMPLE PROBLEM #30

Given data: Reservoir pressure = 2,000 psia

$k_o = 5$ md	$h = 50$ ft
$\mu_o = 0.4$ cp	$B_o = 1.2$
$\phi = 0.15$	$C_t = 2 \times 10^{-5}$ psi^{-1}
$r_e = 1{,}300$ ft	$r_w = 0.25$ ft
$S = 0$	$a'q = 0$

Calculate:

(1) The time needed to reach the pseudo-steady-state period.
(2) Prepare the IPR curves for t = 1 day, 2 days, 4 days, and at $t = t_{tp}$.
(3) Prepare the IPR curve at the pseudo-steady-state period by using Equation 2.2.

Solution procedure:

(1) By using Equation 2.128, t_{tp} can be calculated as follows:

$$t_{tp} = \frac{(0.15)(0.4)(2.0 \times 10^{-5})(1{,}300)^2}{0.002637\,(5)}$$
$$= 153.81 \text{ hours} = 6.41 \text{ days}$$

(2) For $t < t_{tp}$, the IPR curves can be calculated by using Equation 2.131 and for $t > t_{tp}$, the IPR curve can be calculated using Equation 2.2. The results are as follows:

Flowing pressure	Flow rate @ t, days				
	1	2	4	t_{tp}	Equation 2.2
2,000	0	0	0	0	0
1,600	214	204	195	189	189
1,200	429	408	390	378	378
800	643	613	585	567	567
400	858	817	779	756	756
0	1,072	1,021	974	945	945

The IPR curves are shown in Figure 2.61.

CLASS PROBLEM #30a

Given data:

$P_r = 4{,}790$ psia	
$\mu_o = 0.4964$ cp	$B_o = 1.4927$
$k_o = 2.0$ md	$\phi = 0.20$
$h = 80$ ft	$C_t = 0.5 \times 10^{-5}$ psi^{-1}
$r_e = 1{,}500$ ft	$r_w = 0.33$ ft
$S = 0$	$a'q = 0$

Calculate:

(1) The duration of the transient period.
(2) Plot the IPR curves for t = 2 days, 4 days, 6 days, and at $t = t_{tp}$.
(3) Plot the IPR curve for t = 20 days.

CLASS PROBLEM #30b

Given data:

$P_r = 2{,}500$ psia	
$\phi = 0.20$	$\mu_o = 0.4$ cp
$h = 100$ ft	$B_o = 1.25$ stb/bbl

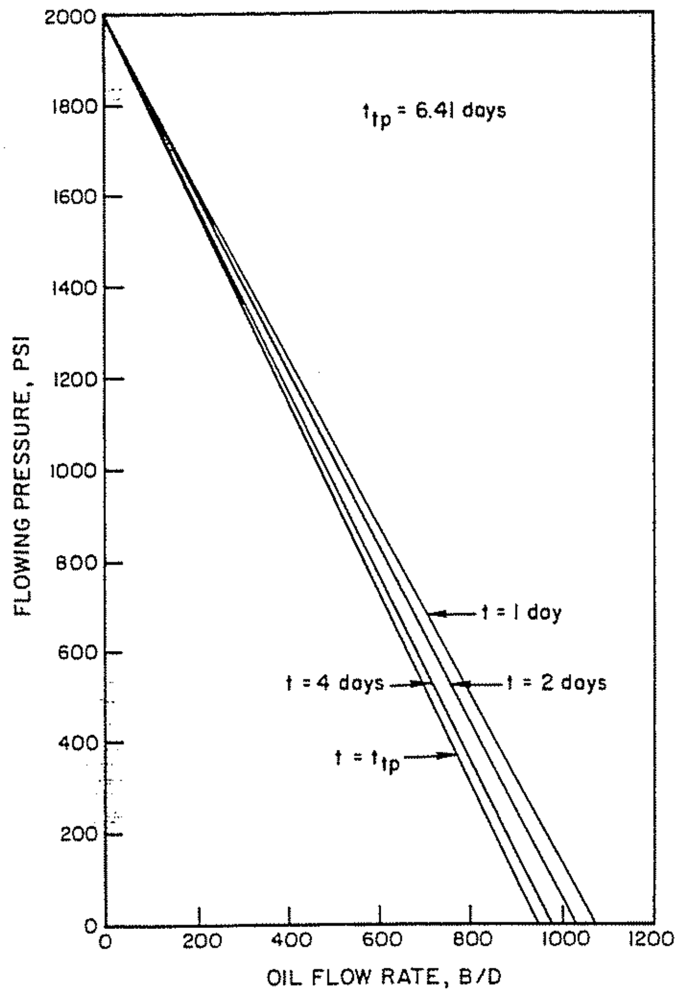

Figure 2.61 IPR Curves at Different Times during Transient Period

$r_w = 0.33$ ft $\quad C_t = 2.5 \times 10^{-5}$ psi^{-1}
$r_e = 1{,}500$ ft $\quad k = 1.0$ md
$S = 0 \quad a'q = 0$

Calculate:

(1) The time needed to reach the pseudo-steady-state period.
(2) Prepare the IPR curves for t = 10 days, 30 days, 50 days, and $t = t_{tp}$.
(3) Prepare the IPR curve for t = 100 days.

CLASS PROBLEM #30c

Given data:

$P_r = 3{,}570$ psia
$k_o = 0.9$ md $\quad \phi = 0.18$
$h = 70$ ft $\quad C_t = 1.75 \times 10^{-5}$ psi^{-1}
$B_o = 1.3567 \quad \mu_o = 0.6150$ cp
$r_e = 1{,}750$ ft $\quad r_w = 0.25$ ft
$S = 0 \quad a'q = 0$

Calculate:

(1) t_{tp}
(2) Prepare the IPR curves for t = 10 days, 40 days, 80 days, and at $t = t_{tp}$.
(3) Prepare the IPR curve for t = 150 days.

CLASS PROBLEM #30d

Given data:

$P_r = 3{,}225$ psia
$k_o = 0.5$ md $\quad \phi = 0.17$
$h = 90$ ft $\quad C_t = 2.0 \times 10^{-5}$ psi^{-1}
$B_o = 1.3209 \quad \mu_o = 0.6615$ cp
$r_e = 1{,}860$ ft $\quad r_w = 0.5$ ft
$S = 0 \quad a'q = 0$

Calculate:

(1) t_{tp}
(2) Prepare the IPR curves for t = 50 days, 100 days, 200 days, and $t = t_{tp}$.
(3) Prepare the IPR curve for t = 275 days.

2.3 INFLOW RELATIONSHIPS FOR GAS WELLS

Al-Hussainy and Ramey derived the real gas flow equation by solving the partial differential equation of real gas flow, which comes from the combination of the continuity equation and Darcy's Law for radial flow.[30] The solution of the partial differential equation, after applying the proper boundary conditions and by taking 14.7 psi and 60°F as pressure and temperature at standard conditions, respectively, is:

$$m(P_r) - m(P_{wf}) = \frac{1{,}637\, q_{sc}\, T}{kh}\left\{\log\left(\frac{kt}{\phi(\mu_g C_t)_i (r_w^2)}\right) - 3.23 + 0.87(S + a'q)\right\} \quad (2.148)$$

where:

q_{sc} = gas flow rate at standard condition, Mscf/day
T = reservoir temperature, °R
k = gas permeability of the formation, md
h = thickness of the gas zone, ft
t = producing time, hours
ϕ = porosity, fraction
$(\mu_g)_i$ = initial viscosity, cp
$(C_t)_i$ = initial total compressibility, psi^{-1}
r_w = wellbore radius, ft
S = skin effect, dimensionless
$a'q$ = non-Darcy flow term $= \dfrac{2.222 \times 10^{-15}\, \beta\, \gamma_g\, K}{\mu\, h_p r_w}$

$m(P)$ = pseudo-pressure function, psi^2/cp

Equation 2.148 can be applied to calculate pressures in a gas well that produces at a constant rate from an infinite reservoir or to calculate the flow rate at constant flowing pressure, including skin effect and the non-Darcy flow term for "short" producing times.

For long flowing (producing) times, Equation 2.148 becomes:

$$q_{sc} = \frac{703 \times 10^{-6}(kh)[m(P_r) - m(P_{wf})]}{T\,(\ln(r_e/r_w) - 0.75 + S + a'q)} \quad (2.149)$$

The pseudo-pressure function, m(P), is defined as follows:

$$m(P) = \int_{P_b}^{P} \frac{2P}{\mu_g Z}\, dP \quad (2.150)$$

where:

P_b = base pressure, psi
P = pressure, psi
μ_g = gas viscosity, cp
Z = gas compressibility factor, dimensionless

A typical plot of $(\mu_g Z)$ vs pressure is shown in Figure 2.62 (the plot is made for a gas gravity = 0.65 and a temperature from 150°F to 225°F) and in Figure 2.63 for a constant temperature (200°F) and gas gravities from 0.60 to 0.75. From those plots, it can be concluded that the values of $(\mu_g Z)$ will be constant for pressures between 0 to approximately 1,000 psi. Therefore, in this case, $(\mu_g Z)$ can be taken out of the integral, and the pseudo-pressure function can be defined by:

$$m(P) = \frac{2}{\overline{\mu}_g \overline{Z}} \int_{P_b}^{P} P\, dP \tag{2.151}$$

By solving the integral of Equation 2.151, the pseudo-pressure function becomes:

$$m(P) = \frac{1}{\overline{\mu}_g \overline{Z}} (P^2 - P_b^2) \tag{2.152}$$

where:

$\overline{\mu}_g$ = the average viscosity, cp
$\overline{Z}$ = the average gas compressibility

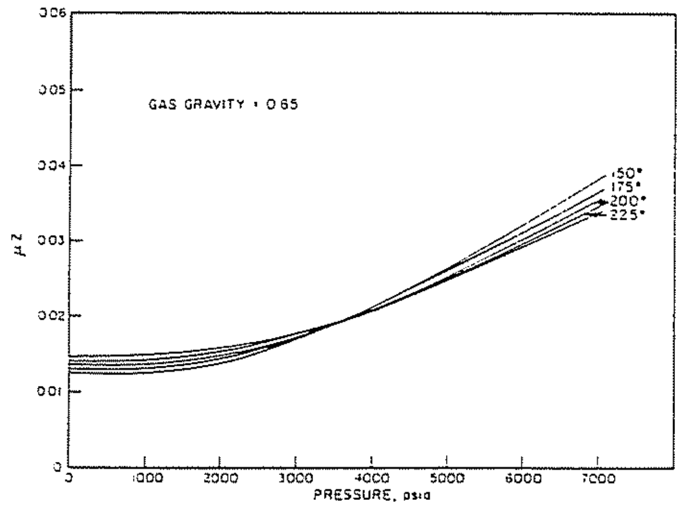

Figure 2.62 Plot of μZ vs Pressure ($\gamma_g = 0.65$)

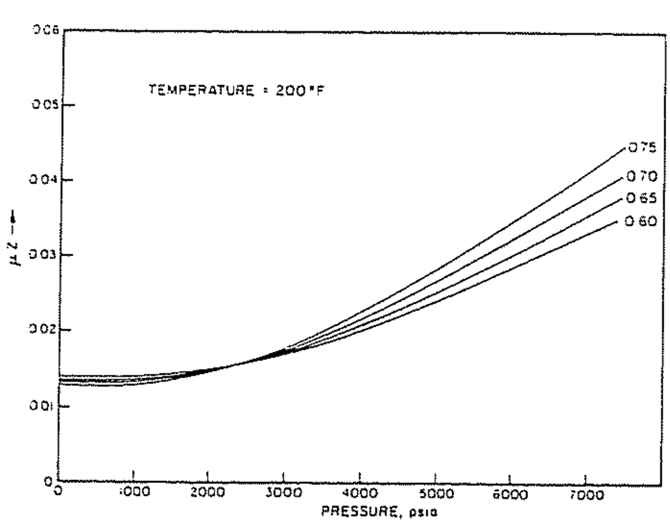

Figure 2.63 Plot of μZ vs Pressure for Constant Temperature

$\overline{\mu}$ and $\overline{Z}$ are evaluated at an average pressure, $\overline{P}$, where $\overline{P}$ is the root mean square pressure defined by:

$$\overline{P} = \left\{\frac{P^2 + P_b^2}{2}\right\}^{0.5} \tag{2.153}$$

By substituting Equation 2.152 into Equation 2.149, we obtain:

$$q_{sc} = \frac{703 \times 10^{-6}\, kh\, (P_r^2 - P_{wf}^2)}{T\, \overline{\mu}_g\, \overline{Z}\left(\ln \frac{r_e}{r_w} - 0.75 + S + a'q\right)} \tag{2.154}$$

From Figures 2.62 and 2.63, it is obvious that Equation 2.154 is valid for pressures below 1,000 psi, but several authors suggest that Equation 2.154 is valid for pressures below 2,500 psi. This is reasonable, since the plot between $2P^2/\mu_g Z$ vs pressure deviates from m(P) vs pressure at pressures greater than 2,500 psi, as shown in Figure 2.64 by the dashed line.

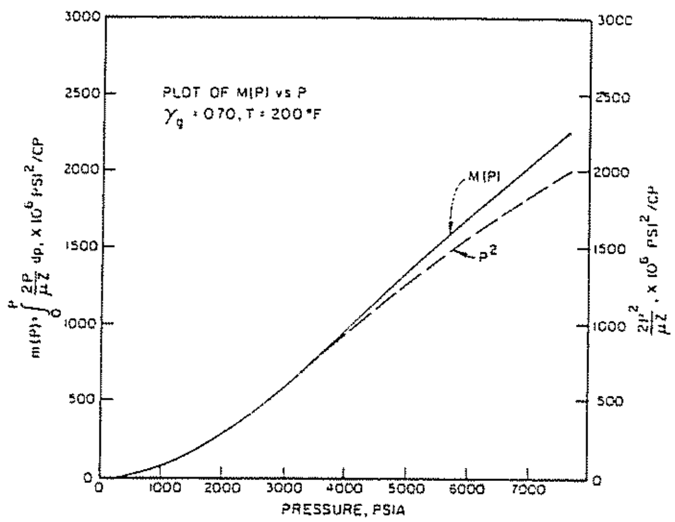

Figure 2.64 Plot of m(P) vs Pressure

At high pressure, Figures 2.62 and 2.63 show that the slope of the curves, $\Delta(\mu_g Z)/\Delta P$, are constant, so:

$$\frac{2P}{\mu_g Z} = \text{constant} = C \tag{2.155}$$

The pseudo-pressure function can be defined by:

$$m(P) = C \int_{P_b}^{P} dP \tag{2.156}$$

$$m(P) = C\,(P - P_b) \tag{2.157}$$

where $C = (2P_i)/(\mu_g Z)_i$

Substituting Equation 2.157 into Equation 2.149 yields:

$$q_{sc} = \frac{703 \times 10^{-6}\, kh\, C\, (P_r - P_{wf})}{T\,(\ln(r_e/r_w) - 0.75 + S + a'q)} \tag{2.158}$$

Equation 2.158 is valid for pressures above 5,000 psi.

The plot of $2P/\mu Z$ vs pressure for a gas gravity of 0.70 and a temperature of 200°F is shown in Figure 2.65. The shaded area is the difference of two values of the pseudo-pressure function—that is, m(5,000) − m(4,000)—and it can be calculated by integration. An analytical procedure such as the trapezoidal rule or the composite Simpson's rule for certain values of ΔP

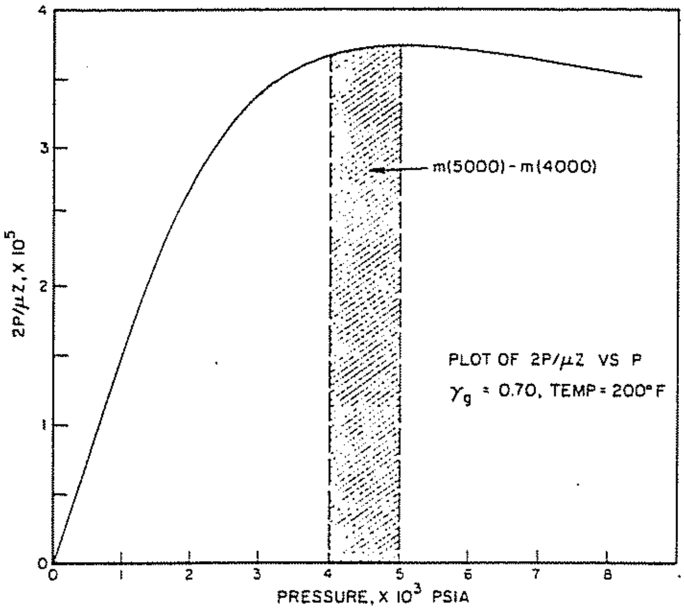

Figure 2.65 Plot of 2P/μZ vs Pressure

can be used to solve the integration and, of course, is easily handled by computer.

By using 0 as the base pressure and applying the composite Simpson's rule, the value of the pseudo-pressure function for some pressures can be calculated and plotted as shown in Figure 2.64.

Using a plot such as Figure 2.64, the value of m(P) at certain values of pressure can be obtained, and by applying Equation 2.149, the inflow performance relationship of a gas well can be calculated.

A quick estimate of AOFP for most medium-depth gas wells with low permeabilities less than about 7 md can be made with the following equation:

$$q_{AOFP} = 77 \times 10^{-7}\, kh\, (\overline{P}_r)^2$$

where:

$k = md$
$h = ft$
$q = Mcfd$
$\overline{P}_r = psia$

The following assumptions for this approximation have been made in Darcy's flow equation for gas:

$$q_{Mcfd} = \frac{703 \times 10^{-6}\, kh\, (P_r^2 - 0)}{\overline{\mu}_g\, \overline{T}\, \overline{Z}(\ln r_e/r_w - 3/4 + S + aq)}$$

Assume:

$\overline{Z} = 1.00$
$\overline{\mu}_g = 0.02$ cp
$\overline{T} = 200°F = 660°R$

$(\ln r_e/r_w - 3/4 + S + aq) = 7.03$

$$q_{Mcfd} = \frac{703 \times 10^{-6}\, (kh)(P_r)^2}{(0.02)(660)(7.03)} = 77 \times 10^{-7}\, kh(P_r)^2$$

For permeabilities of 100 divide by 2
For permeabilities of 600 divide by 4
These are for estimates only and should in no way replace accurate calculations.

Equation 2.154 can be rearranged into the following form:

$$P_r^2 - P_{wf_s}^2 = bq + aq^2 \qquad (2.159)$$

where:

$$b = \frac{1.424 \times 10^3 \mu_g TZ\,(\ln(r_e/r_w) - 0.75 + S)}{kh} \qquad (2.160)$$

$$a = \frac{3.166 \times 10^{-12} \beta\, \gamma_g Z\, T}{h_p^2\, r_w} \qquad (2.161)$$

In the paper by Jones, Blount, and Glaze, the flow rate is given in scfd instead of MSCF/D and hence:

$$b' = \frac{1.424\, \mu_g ZT(\ln r_e/r_w - 3/4 + S)}{kh} \qquad (2.162)$$

$$a' = \frac{3.16 \times 10^{-18}\, \beta \gamma_g ZT}{h_p^2 r_w} \qquad (2.163)$$

Also, we may choose to write the radial flow equation as follows:

$$q = \frac{703 \times 10^{-6}\, kh\, (P_r^2 - P_{wf_s}^2)}{\mu_g T\, Z(\ln r_e/r_w - 3/4 + S + a'q)} \qquad (2.164)$$

for q in Mcfd

The constant is 703×10^{-3} for scfd.

A brief discussion of each term and how it may be obtained follows:

(1) k—permeability to gas can be obtained from core analysis from either conventional or sidewall cores.
(2) h—thickness of producing zone is obtained from well logs.
(3) P_r—static pressure is obtained from buildup tests or from the best source available.
(4) $\overline{\mu}$—average viscosity. If lab tests are not available, numerous charts such as noted in Figures 2.66 and 2.67 are available. Lee's correlation is one of the better ones and his equation is as follows:

$$\mu_g = k \times 10^{-4} \exp(X\rho^y) \qquad (2.165)$$

where:

$$k = \frac{(9.4 + 0.02\, M)T^{1.5}}{209 + 19M + T} \qquad (2.166)$$

$$X = 3.5 + \frac{986}{T} + 0.01M \qquad (2.167)$$

$$y = 2.4 - 0.2X \qquad (2.168)$$

where:

$T = °R$
$\mu_g = cp$
$\rho = g/cm^3$ (in-situ density)
$M =$ molecular weight

* The gas density in g/cm^3 must be determined at in-situ conditions by the following equation:

$$\rho_g = 0.0433\, \frac{\gamma_g P}{ZT} \qquad (2.169)$$

Reference can be made to Volume 1 of this series for additional charts for obtaining gas viscosity.

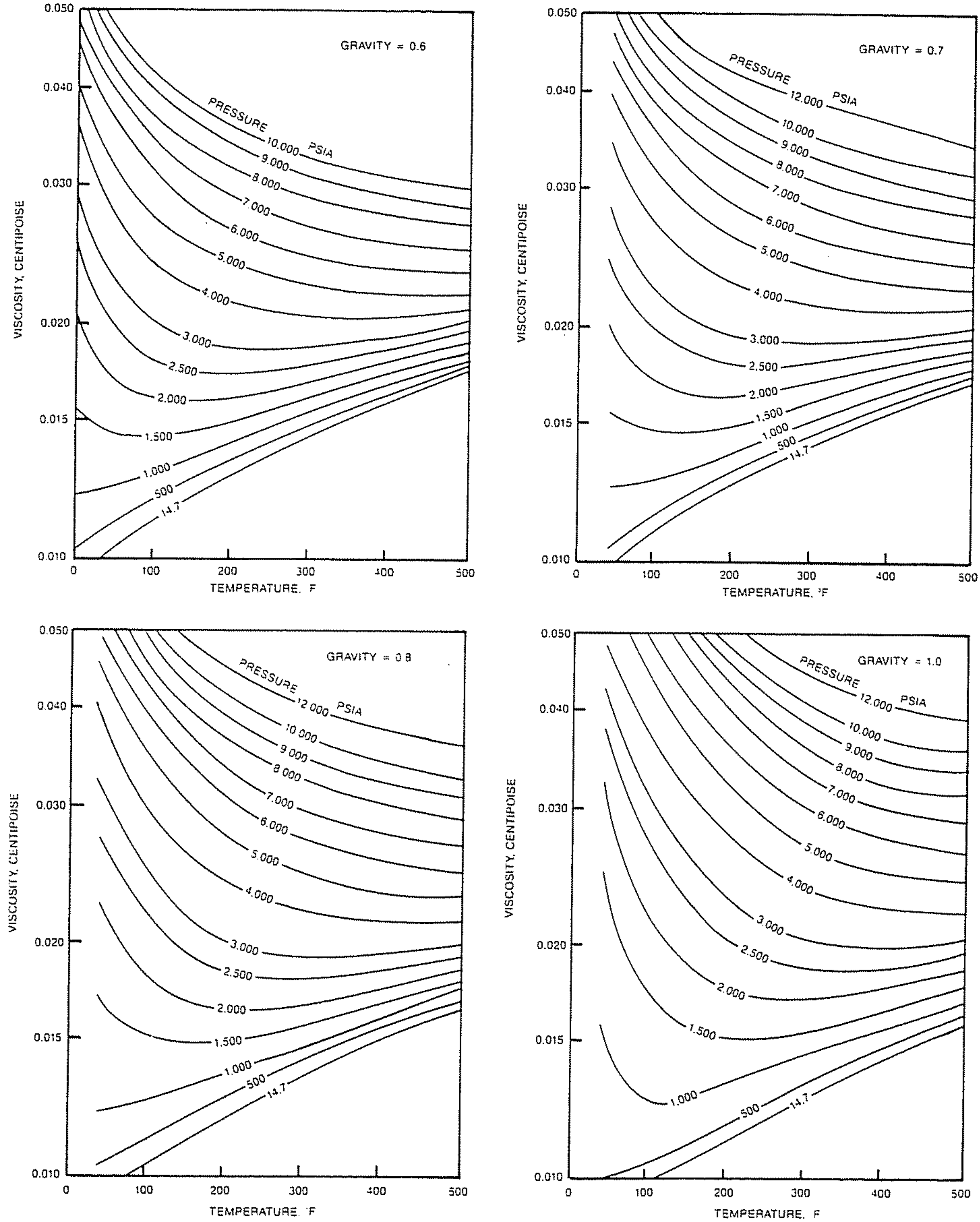

Figure 2.66 *Viscosity of Natural Gas (Charts Were Presented at Summer Session on "Flow of Natural Gas from Reservoirs," conducted by D.L. Katz and David Cornell, University of Michigan, College of Engineering, 1955)*

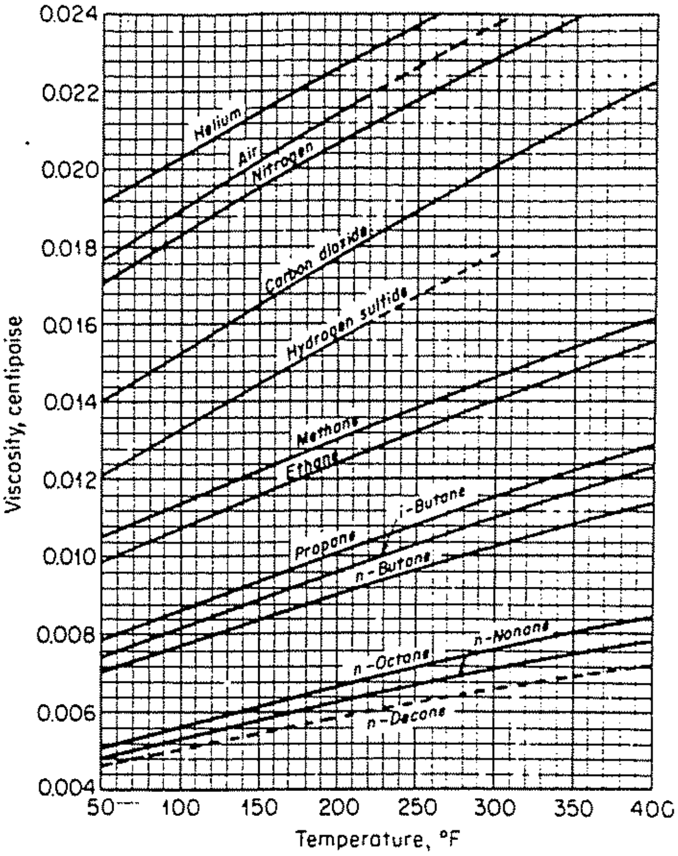

Figure 2.67a Viscosity of Natural Gases at Atmospheric Pressure (after Carr et al., courtesy AIME)[31]

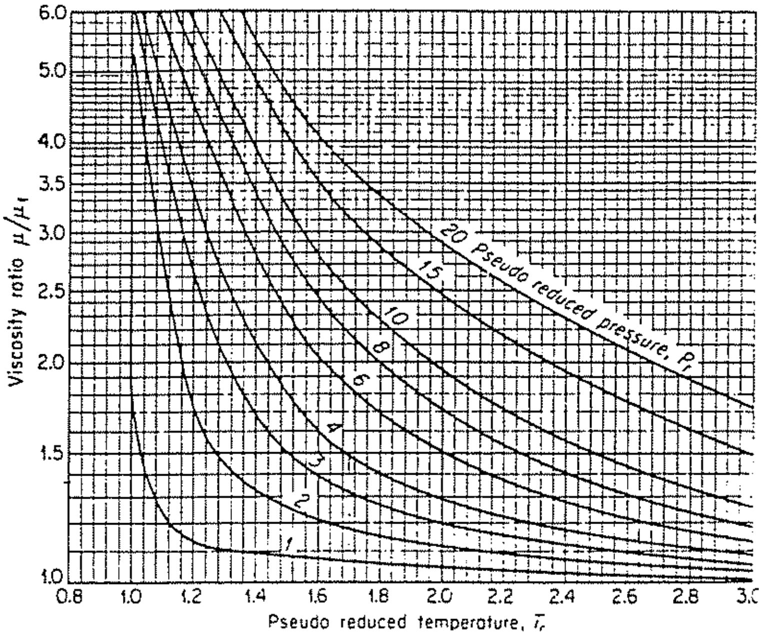

Figure 2.67b Viscosity Ratio vs Pseudo-reduced Temperature (after Carr et al.)[31]

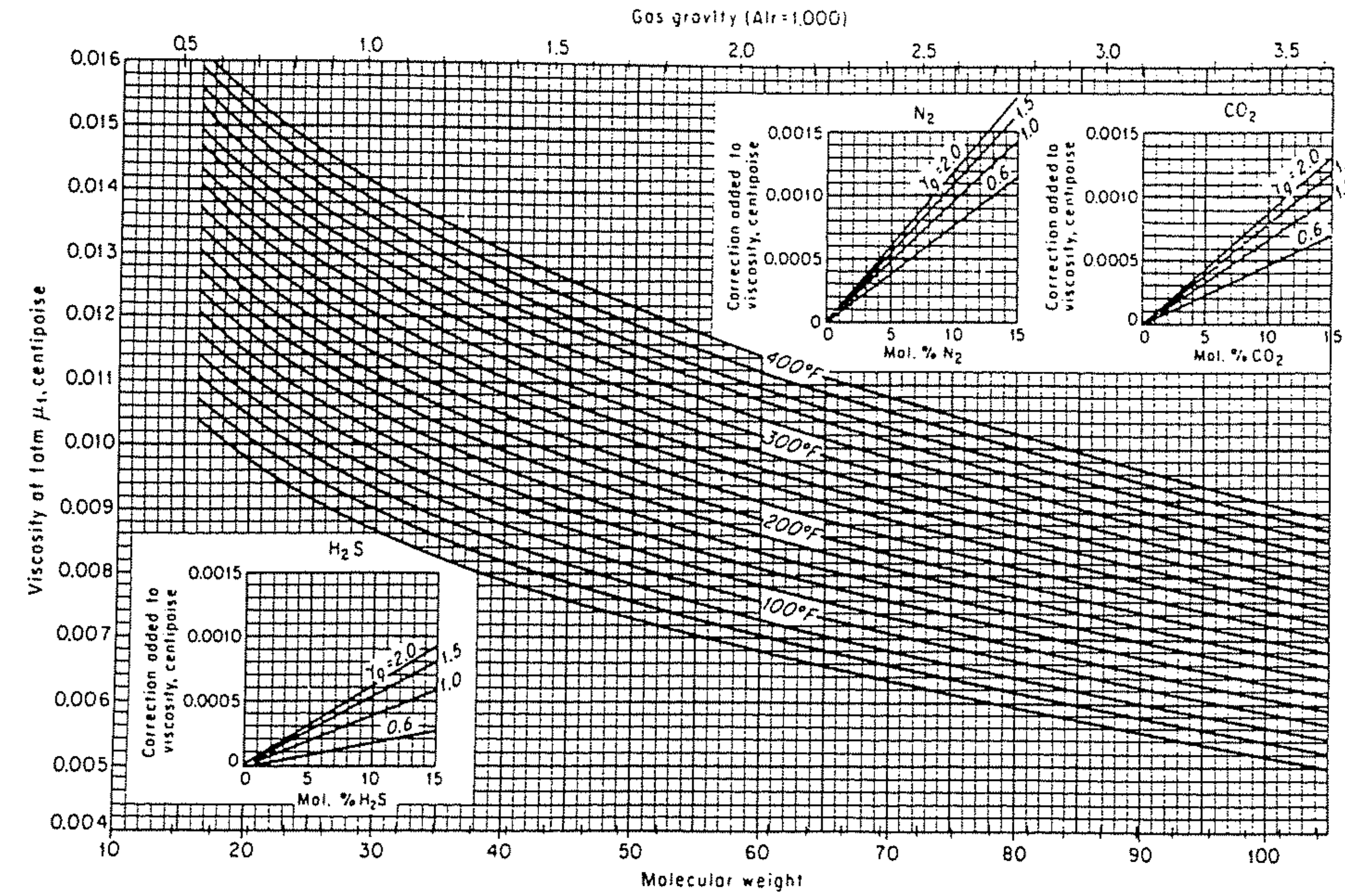

Figure 2.67c Viscosity of Paraffin Hydrocarbon Gases at 1 atm (after Carr et al., courtesy AIME)[31]

EXAMPLE CALCULATION FOR VISCOSITY

Given data:

$P = 3{,}000$ psia
$T = 200°F$
$M = 20$
$\gamma_g = 0.7$
$\mu_g = k \times 10^{-4} \exp(x\rho^y)$

$$k = \frac{9.4 + 0.02(20)(660)^{1.5}}{209 + 19(20) + 660} \times 10^{-4} = 133$$

$$X = 3.5 + \frac{986}{660} + 0.01(20) = 5.194$$

$$y = 2.4 - 0.2X = 2.4 - 0.2(5.194) = 1.36$$

$$\rho_g = 0.0433(0.7)\left(\frac{3{,}000}{(0.88)(660)}\right) = 0.1565 \text{ g/cm}^3$$

$$\mu_g = 133 \times 10^{-4}\, e^{(5.194)(0.1565)^{1.36}} = \underline{0.0201} \text{ cp}$$

This compares to a chart determination from Figure 2.66 of 0.0193 cp.

(5) Temperature—from measured values or from geothermal maps of the area.
(6) Compressibility factor—if PVT data are not available, charts such as Figures 2.68, 2.69, and 2.70 can be used. Numerous other charts can be found in Volume 1 of this series.
(7) r_e—the radius of drainage is the same as for oil wells based on spacing and shape.
(8) r_w—the radius of the wellbore is determined from caliper surveys or bit sizes.
(9) S—skin is determined from buildup tests
(10) D—the turbulence factor is calculated from Equation 2.161

EXAMPLE PROBLEM #31

Given data:

reservoir pressure = 5,100 psi
formation permeability = 15 md
drainage radius = 2,100 ft

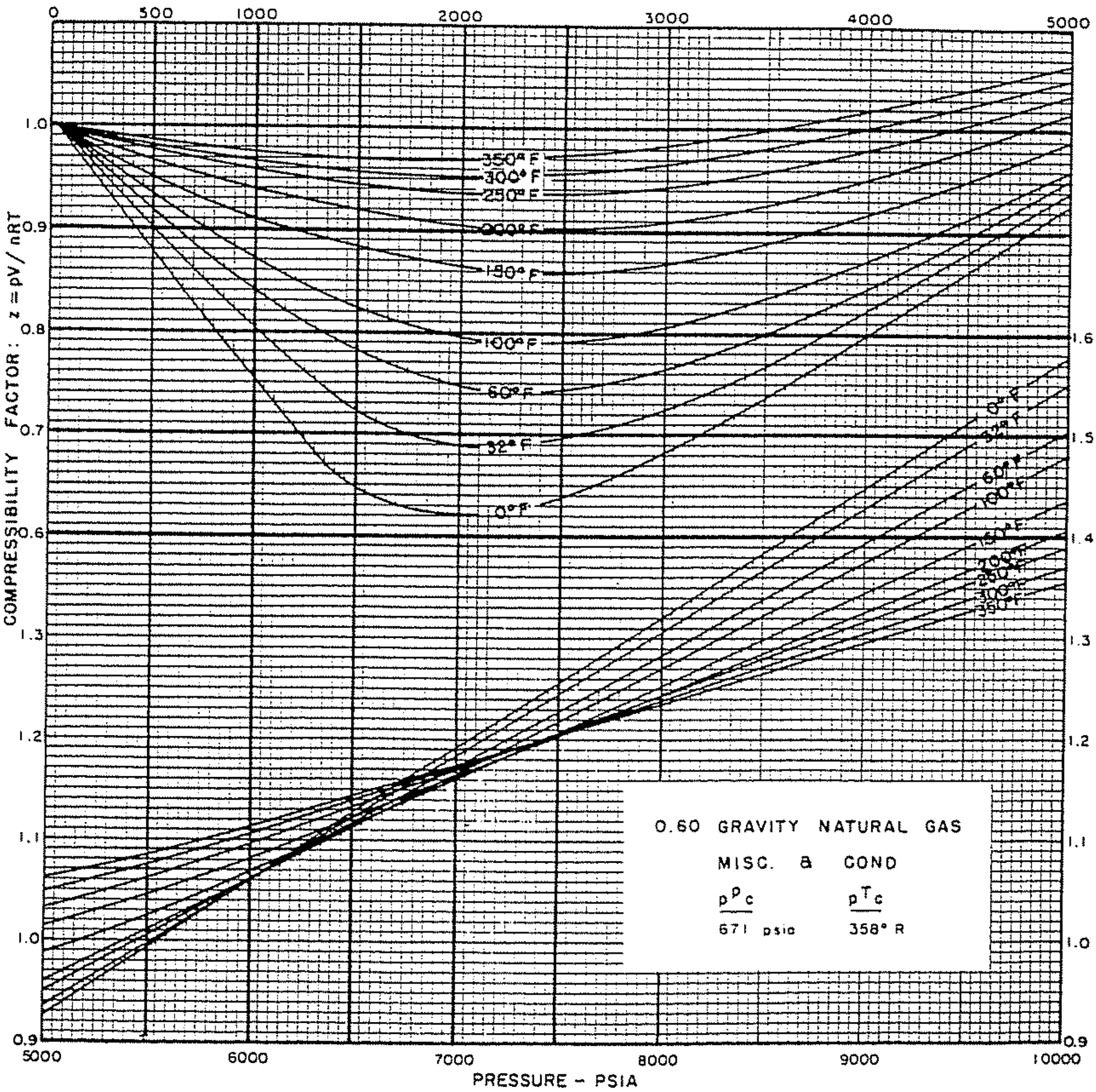

Figure 2.68 Compressibility Factors for a 0.60 Natural Gas (after Gatlin, courtesy API)[32]

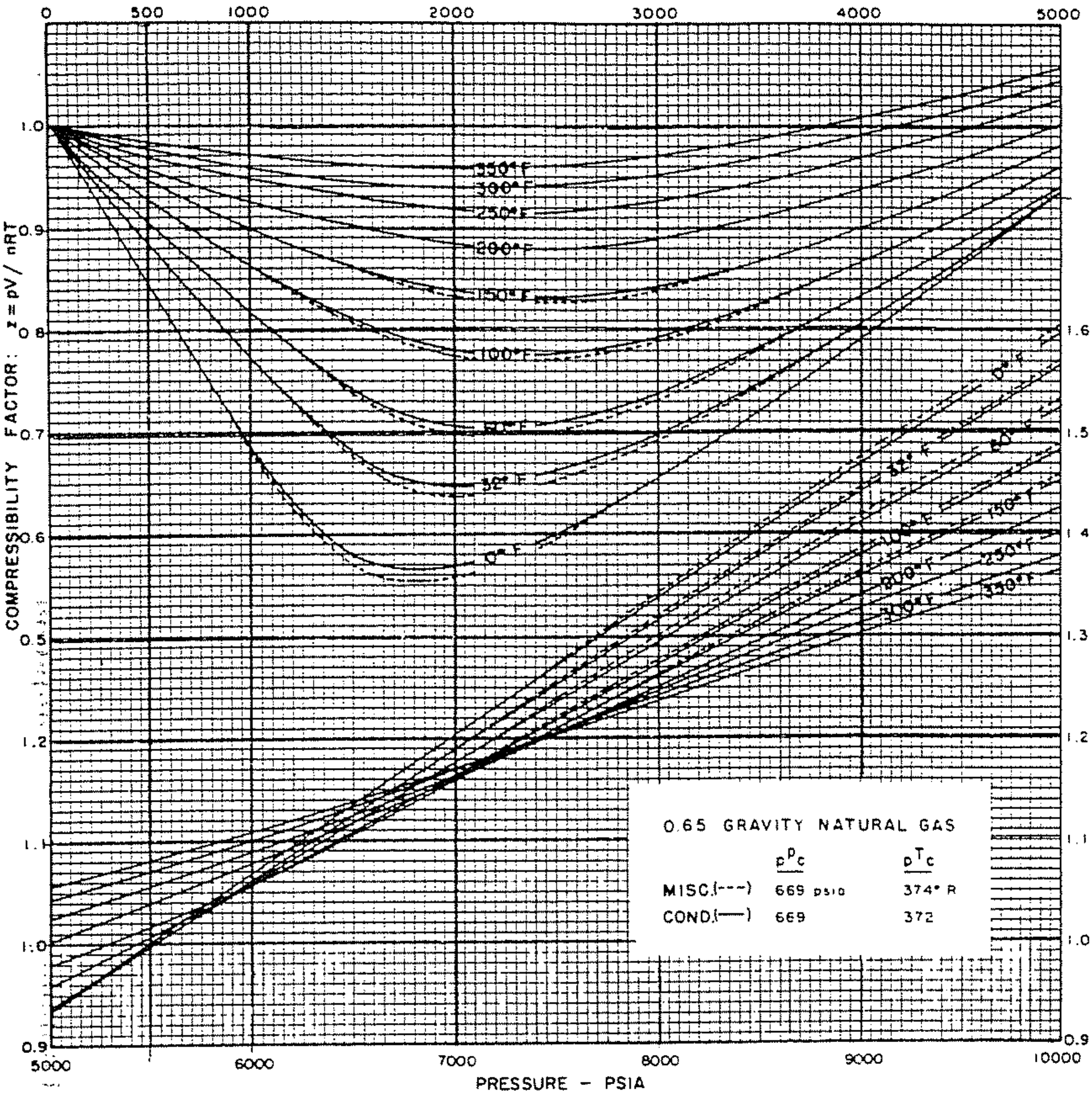

Figure 2.69 Compressibility Factors for a 0.65 Natural Gas (after Gatlin, courtesy API)[32]

wellbore radius = 0.45 ft
formation thickness = 30 ft
skin effect = 0
a'q = 0
P_{sc} = 14.7 psi
T_{sc} = 60°F
specific gravity of gas = 0.70
reservoir temperature = 200°F

Calculate:

Construct the IPR curves for this gas well by using Equations 2.149 and 2.154.

Solution procedure:

(1) By using a gas specific gravity of 0.70 and a temperature of 200°F and by applying the composite Simpson's rule, the plot of the pseudo-pressure function vs pressure can be drawn as shown in Figure 2.64.

The pressure vs gas flow rate relationship can be calculated as follows:

for: P_r = 5,100 psi, m(5,100) = 1,373.68 × 10^6 psi²/cp
P_{wf} = 5,000 psi, m(5,000) = 1,336.30 × 10^6 psi²/cp

Using Equation 2.179, the gas flow rate at P_{wf} = 5,000 psi can be calculated as follows:

$$q_{sc} = \frac{703 \times 10^{-6}(15)(30)(1{,}373.68 \times 10^6 - 1{,}336.30 \times 10^6)}{660(\ln(2{,}100/0.45) - 0.75 + 0)}$$

= 2327 Mscfd

Using the same procedure discussed previously, the pressure vs gas flow rate relationship can be calculated and the results are as follows:

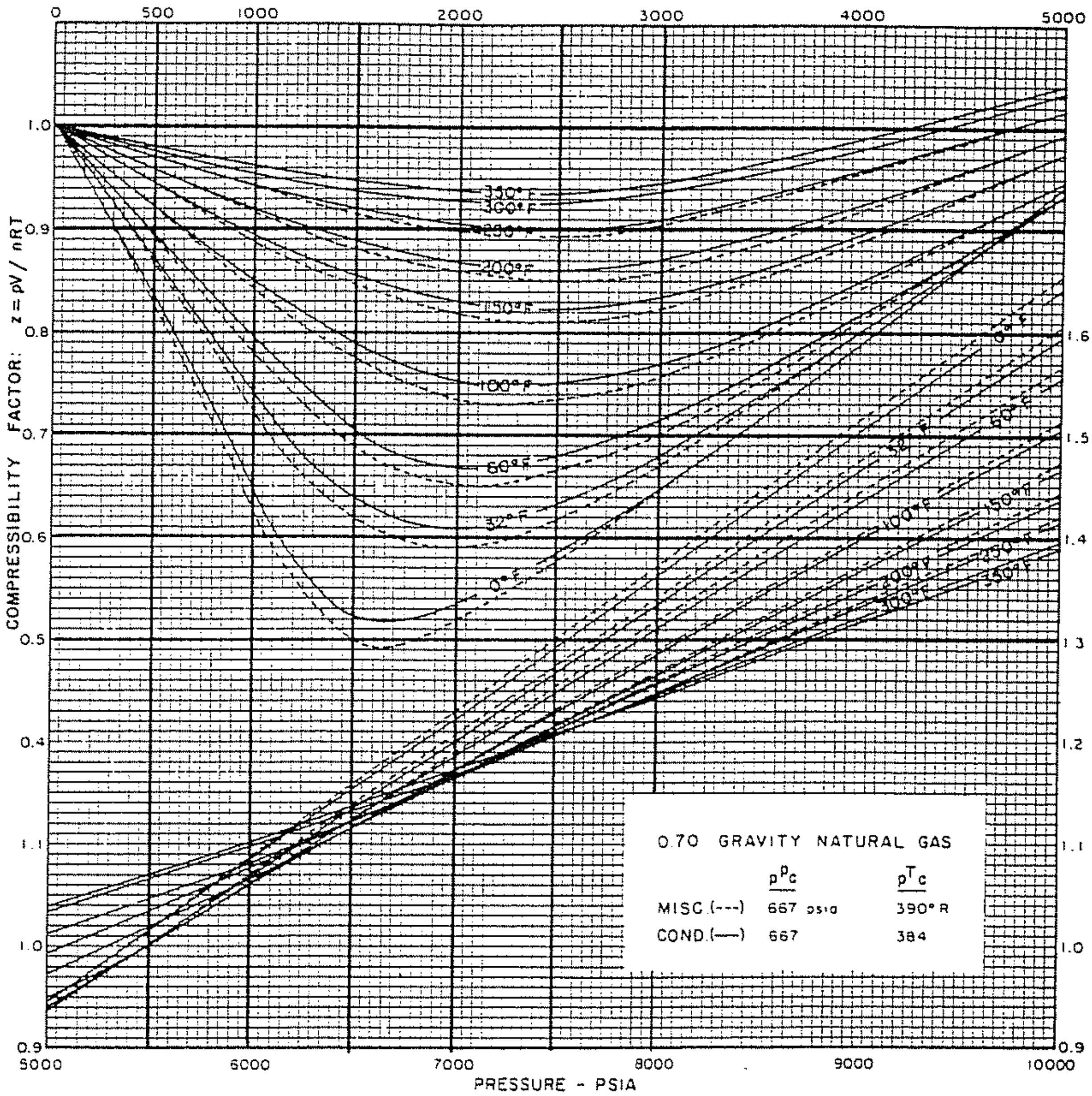

Figure 2.70 Compressibility Factors for a 0.70 Natural Gas (after Gatlin, courtesy API)[32]

P_{wf}	m(P) × 10^6	Δm(P) × 10^6	q (Mscf/d)
5,100	1,373.68	—	0
5,000	1,336.30	37.38	2,327
4,000	964.03	409.65	25,506
3,000	605.58	768.10	47,825
2,000	292.42	1,081.26	67,323
1,000	76.01	1,297.67	80,797
0	0	1,373.68	85,530

P_{wf}	$\overline{P}$	$\overline{Z}$	$\overline{\mu}_g$	q (Mscf/d)
5,100	—	—	—	0
5,000	5,050.25	0.9721	0.0278	2,325
4,000	4,583.12	0.9362	0.0262	25,382
3,000	4,183.90	0.9086	0.0248	46,951
2,000	3,873.62	0.8898	0.0237	64,915
1,000	3,674.92	0.8793	0.0230	76,916
0	3,606.25	0.8760	0.0227	81,354

P_{wf} vs q is plotted in Figure 2.71.

(2) The following table shows the results of the calculations of gas flow rate, which are accomplished by applying Equation 2.154 where $\overline{\mu}_g$ and $\overline{Z}$ are calculated at $\overline{P}$, the root mean square pressure, that is, Equation 2.153.

The plot of pressure vs flow rate is shown in Figure 2.71. Figure 2.71 also shows the IPR curves calculated by using Equations 2.158 and 2.154 and by assuming constant viscosity and gas compressibility, which are evaluated at reservoir pressure ($\mu_{gi} = 0.0280$ cp and $Z_i = 0.9761$) and also by using Equation 2.154, where μ_g and Z are evaluated at the average pressure—that

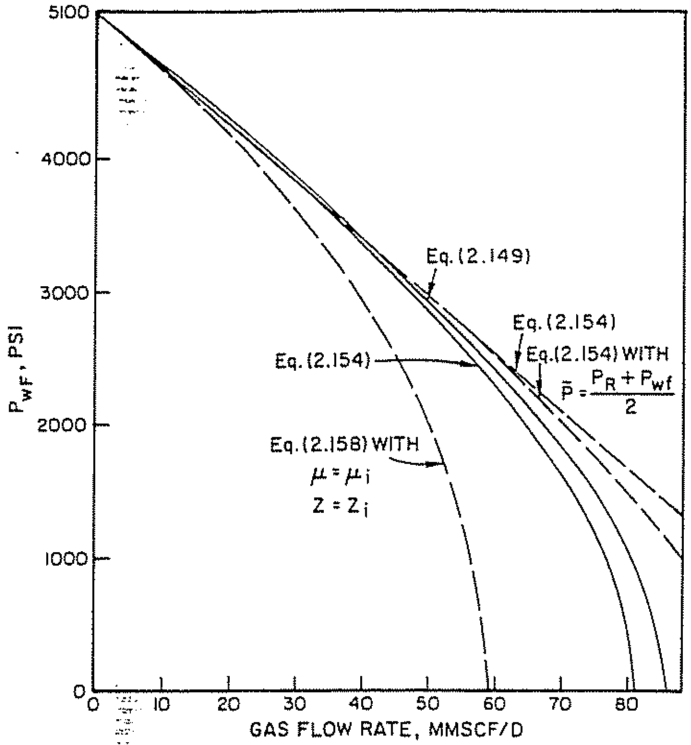

Figure 2.71 IPR Curves for a Gas Well for Example Problem #31

is, $\bar{P} = \frac{1}{2}(P_r + P_{wf})$. From Figure 2.71, it can be concluded that:

(1) By using the root mean square pressure to evaluate the gas viscosity and gas compressibility, the IPR curve calculated by using Equation 2.154 shows only a small difference compared to the IPR curve calculated by using Equation 2.149.
(2) By using the average pressure equal to $\frac{1}{2}(P_r + P_{wf})$ for evaluating gas viscosity and gas compressibility, the IPR curve calculated by using Equation 2.154, shows a large difference compared to the IPR curve calculated by using Equation 2.149.
(3) Equation 2.158 shows a large difference compared to the IPR curve calculated by using Equation 2.149.

EXAMPLE PROBLEM #32

(effect of including turbulent flow term)

Given data:

$\mu_g = 0.017$ cp	$T = 680°R$
$h = 40$ ft	$Z = 1.0$
$P_r = 5{,}000$ psia	640-acre spacing
$h_p = 10$ ft	10¾-in. drilled hole

The permeability is varied and values of 0.06, 6, and 600 md are worked for both conditions—that is, including the turbulence term and excluding the turbulence term.

Calculate:

Determine the flow rates for varying flowing pressures.

Solution procedure:

(1) For $k = 0.06$ md, the following equation was arrived at:

$$5{,}000^2 - P_{wf_s}{}^2 = \frac{1.424(0.017)(1.0)(680)}{0.06(40)}(8.05)q_g + \frac{3.16 \times 10^{-18}(1 \times 10^{12})(0.7)680}{100(0.4479)} q_g{}^2$$

$$= 55.23\, q_g + 3.358 \times 10^{-5}\, q_g{}^2$$

For 6 md, the following equation was arrived at:

$$5{,}000^2 - P_{wf_s}{}^2 = \frac{1.424(0.017)(1.0)(680)}{6(40)}(8.05)q_g + \frac{3.16 \times 10^{-18}(6.2 \times 10^9)(0.7)(680)}{100(0.4479)} q_g{}^2$$

$$5{,}000^2 - P_{wf_s}{}^2 = 0.5523 q_g + 2.08 \times 10^{-7} q_g{}^2$$

For 600 md, the following equation was used:

$$5{,}000^2 - P_{wf_s}{}^2 = \frac{1.424(0.017)(1.0)(680)}{600(40)} \times \left(\ln\frac{2{,}978.9}{0.4479} - \frac{3}{4}\right) q_g + \frac{3.16 \times 10^{-18}(2.3 \times 10^7)(0.7)(680)}{100(0.4479)} q_g{}^2$$

$$5{,}000^2 - P_{wf_s}{}^2 = 0.0055\, q_g + 7.7240 \times 10^{-10}\, q_g{}^2$$

The preceding equations are used to calculate flow rates for specific values of flowing pressures, and the results are shown in Table 2.1. Equation 2.154 was used to calculate flow rates for specific values of flowing pressures for every value of permeability by assuming $aq = 0$. The results are shown in Table 2.1. The plot of P_{wf} vs flow rate for every value of permeability, excluding or including the aq term, is shown in Figure 2.72.

TABLE 2.1
EFFECT OF THE TURBULENCE TERM IN A GAS WELL
(Example Probiem #32)

		Gas flow rate, Mcf/d					
		k = 0.06 md		k = 6.0 md		k = 600 md	
P_r	P_{wf}	aq = 0	aq ≠ 0	aq = 0	aq ≠ 0	aq = 0	aq ≠ 0
5,000	5,000	0	0	0	0	0	0
	4,000	162.95	149.39	16,294.97	5,380.81	1,629,497	104,428.77
	3,000	289.69	251.31	28,968.84	7,539.67	2,896,884	140,395.50
	2,000	380.22	318.55	38,021.61	8,803.84	3,802,160	161,351.82
	1,000	434.53	357.05	43,453.26	9,491.66	4,345,326	172,734.01
	0	452.64	369.61	45,263.82	9,711.41	4,526,381	176,368.15

Similar to oil flow, the effect of the permeability and perforation interval on the aq term can be seen in Figures 2.73 and 2.74. From these plots, it can be noted that:

(1) The value of aq increases with increasing permeability (Figure 2.73) for set values of pressure ratios.
(2) The value of the aq term increases with decreasing values of the perforated interval (Figure 2.74).
(3) For low permeabilities, the effect of the perforated interval to aq can normally be neglected.

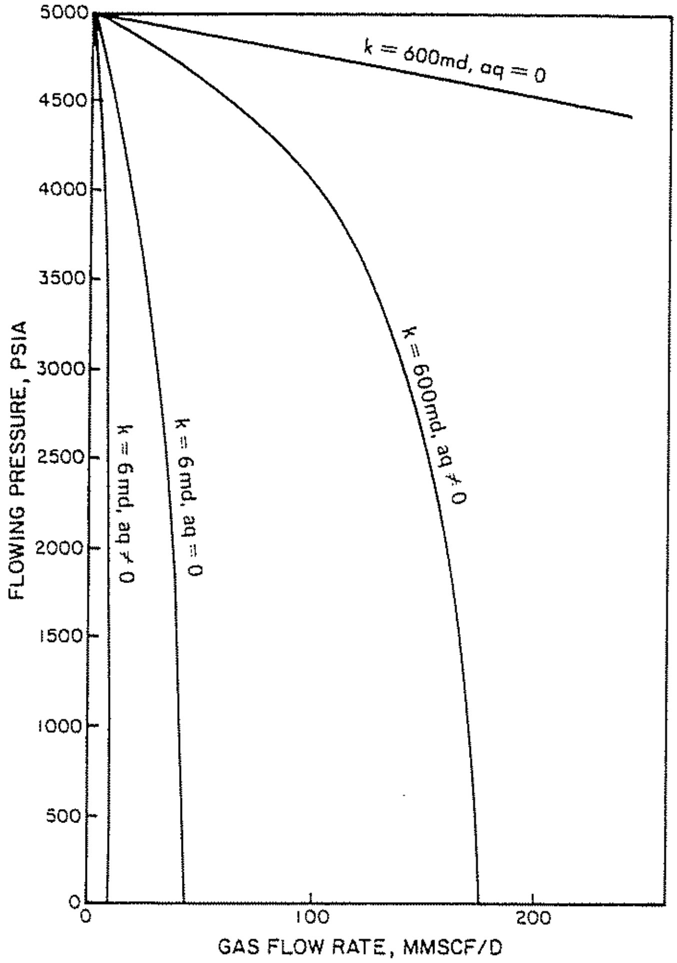

Figure 2.72 The Effect of aq Term on IPR Curves for Different Values of Permeability (Example Problem #32)

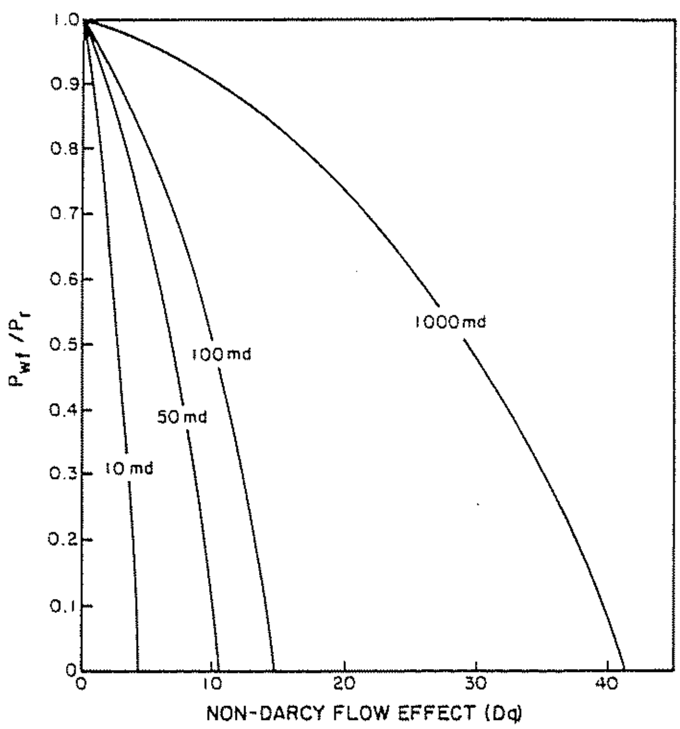

Figure 2.73 The Effects of Permeability on Turbulent Term (after Sukarno)[7]

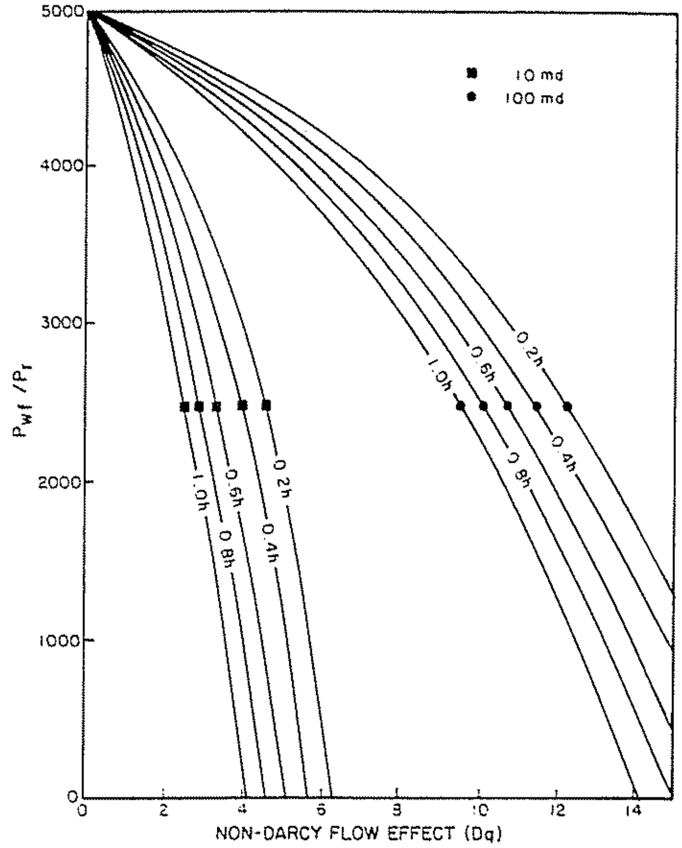

Figure 2.74 The Effects of Permeability and Partial Penetration to aq (after Sukarno)[7]

CLASS PROBLEM #32a

Given data: gas well:

$P_r = 4500$ psia	$k = 40$ md	$r_e = 1{,}500$ ft
$T = 220°F$	$h = 60$ ft	$r_w = 0.33$ ft
$h_p = 40$ ft	$\gamma_g = 0.65$	
$\mu_g = 0.0175$ cp	$Z = 0.8938$	
skin = 0		

Calculate:

(1) Prepare an IPR curve for this gas well by assuming aq = 0.
(2) Prepare an IPR curve for this gas well by including aq in the calculations.

CLASS PROBLEM #32b

Given data: gas well:

$P_r = 5{,}500$ psia	$k = 20$ md
$T = 250°F$	$h = 60$ ft
$\gamma_g = 0.70$	$\mu_g = 0.0194$ cp
$Z = 0.8927$	skin = 0.0
$r_e = 1{,}500$ ft	$r_w = 0.5$ ft

Calculate:

Prepare the IPR curves for this gas well by assuming:

(1) $h_p = 40$ ft
(2) $h_p = 20$ ft

Dq is included in the calculation.

CLASS PROBLEM #32c

Given data: gas well:

$P_r = 5{,}250$ psia $k = 10$ md
$T = 200°F$ $h = 100$ ft
$h_p = 50$ ft $\gamma_g = 0.70$
$r_e = 1{,}500$ ft $r_w = 0.4479$ ft
$\mu_g = 0.0191$ cp $Z = 0.8499$
skin = 0

Calculate:

Prepare the IPR curves for this gas well by:

(1) assuming aq = 0
(2) including aq in the calculations

CLASS PROBLEM #32d

Given data: gas well:

$P_r = 6{,}500$ psia $T = 200°F$ $r_e = 1{,}500$ ft
$h = 50$ ft $h_p = 30$ ft $r_w = 0.4479$ ft
$\gamma_g = 0.67$ $\mu_g = 0.0208$ cp
skin = 0 $Dq \neq 0$ $Z = 0.8743$

Calculate:

Prepare the IPR curves for this gas well:

(1) for k = 0.01 md
(2) for k = 1.0 md

2.31 FOUR-POINT TEST ON GAS WELLS

Multipoint well test procedures such as the flow-after-flow or isochronal four-point test can be plotted as suggested by Jones, Blount, and Glaze in order to properly analyze specific problems.

Equation 2.159 may be written in the form:

$$\frac{P_r^2 - P_{wf}^2}{q} = aq + b \tag{2.170}$$

The plot between $(P_r^2 - P_{wf}^2)/q$ vs q is a straight line on regular cartesian paper as noted in Figure 2.75.

Similar to oil wells, the slope of the plot indicates the degree of turbulent flow in the well formation system, and the intercept indicates the degree of formation damage. Jones et al. suggest the use of this plot to determine the presence of near-wellbore restrictions. They suggest that the maximum value of $\frac{P_r^2 - P_{wf}^2}{q}$ be obtained ($P_{wf} = 0$). Then, this should be compared to $\frac{P_r^2 - P_{wf}^2}{q}$ at the intercept b. If the maximum value (P_r^2/q) was two or three times greater than the value at the intercept, near-wellbore restrictions could be expected. This would most generally be caused by a lack of sufficient perforations in the well.

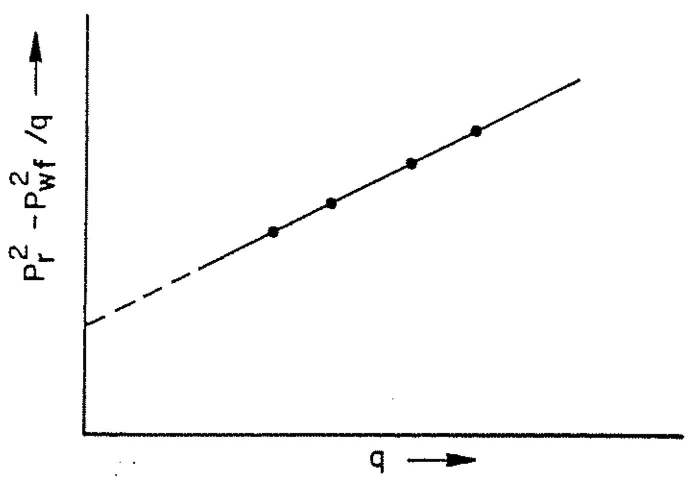

Figure 2.75 The Multipoint-Test Plot of a Gas Well

This case has been discussed for oil wells in Section 2.226 and is also applicable for gas wells. In addition, this type of analysis has been applied in the field by Himmatramka on twelve actual cases (six cases for gas wells) and has been found a valid method for making these determinations.[33]

The following example shows the application of Jones, Glaze, and Blount's equation to determine the presence of near-wellbore restrictions for a gas well.

EXAMPLE PROBLEM #33

Given data: four-point gas-well test:

reservoir pressure = 4,750 psia	
Flowing pressure, psia	Gas flow rate, MMscf/d
4,213	9.45
3,806	12.37
3,243	15.21
2,763	16.98

Calculate:

Recommend a way to improve the productivity of this well.

Solution procedure:

(1) Calculate $(P_r^2 - P_{wf}^2)/q$ as follows:

P_{wf}, psia	q_g, MMscf/d	$(P_r^2 - P_{wf}^2)/q$
4,213	9.45	0.5093
3,806	12.37	0.6529
3,243	15.21	0.7912
2,763	16.98	0.8792

(2) Plot $(P_r^2 - P_{wf}^2)/q$ vs q as shown in Figure 2.76. From the plot, obtain:

$b = 0.0454$
$a = 4.91 \times 10^{-6}$
maximum flow rate = 20.98 MMscf/d
$b' = 1.0754$
$b'/b = 23.69$

(3) Based on this analysis, it can be concluded that:

(a) The value of b is low (b = 0.0454)—that is, less than 0.05—so restrictions caused by skin effect are low.
(b) The value of b'/b is high (b'/b = 23.69)—that is, greater than 3.0—so the restrictions

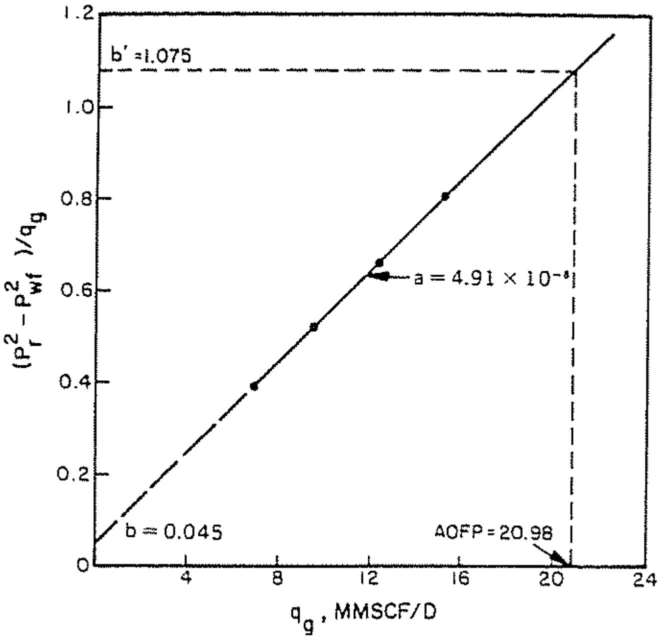

Figure 2.76 Plot of $(P_r^2 - P_{wf}^2)/q_g$ vs q_g (Example Problem #29)

caused by turbulence effects are occurring in the well. The turbulence effect is normally caused by a lack of sufficient perforations in the well.

(c) To improve the productivity of the well, additional perforations are recommended.

CLASS PROBLEM #33a

Given Data: four-point gas-well tests:

P_r = 4,900 psia	
Flowing pressure, psia	Gas flow rate, MMscf/d
4,505	125
3,954	245
3,637	298
3,439	327

Calculate:

Recommend ways to improve this well based on the tests.

CLASS PROBLEM #33b

Given data: four-point gas-well tests:

P_r = 4,140 psia	
Flowing pressure, psia	Gas flow rate, MMscf/d
3,957	15.7
3,794	22.3
3,608	27.9
3,266	35.6

Calculate:

Recommend ways to improve the productivity of this well.

CLASS PROBLEM #33c

Given data: four-point gas-well tests:

Reservoir pressure = 4,470 psia	
Flowing pressure, psia	Gas flow rate, MMscf/d
4,226	1.647
4,119	2.281
4,005	2.905
3,941	3.237

Calculate:

Recommend a way to improve the productivity of the gas well.

2.32 TRANSIENT IPR CURVES FOR GAS WELLS

The previous discussion mentioned that Equation 2.148 is the solution of the partial differential equation of real gas flow for "short" periods of flowing time. Equation 2.148 can be used to find the gas flow rate vs pressure relationship during the transient flow period.

For pressures below 2,500 psi, where $\mu_g Z$ can be assumed constant, Equation 2.148 becomes:

$$P_r^2 - P_{wf}^2 = \frac{1{,}637\, q_{sc} T \bar{\mu}_g \bar{Z}}{kh}\left[\log\left(\frac{kt}{\phi(\mu_g C_t)_i (r_w)^2}\right) - 3.23 + 0.87(S + a'q)\right] \quad (2.171)$$

The duration of the transient period can be calculated by applying Equations 2.128, 2.129, and 2.130, as noted in the discussion of the transient IPR curves for oil flow. The following example problem will show how to construct the IPR curve in a gas well during the transient period.

EXAMPLE PROBLEM #34

Given data:

$P_r = 5250$ psi $k = 0.01$ md $\mu_g = .023$ cp
$\phi = 0.12$ $h = 30$ ft
$r_e = 2{,}100$ ft $r_w = 0.45$ ft
$\gamma_g = 0.70$ $C_t = 2.0 \times 10^{-6}$ psi^{-1}
skin = 0 $a'q = 0$
reservoir temperature = 200°F

Calculate:

(1) The duration of the transient period and of the late transient period.
(2) Draw the IPR curves at t = 10 days, 48 days, 100 days, and at $t = t_{ltp} = 118$ days.

Solution procedure:

(1) Calculate the transient period by using Equation 2.128 and calculate the late transient periods by using Equations 2.129 and 2.130.

At pressure = 5,250 psi, $(\mu_g)_i = 0.028$ cp
Using Equation 2.128, the transient period can be calculated as follows:

$$t_{tp} = \frac{(0.12)(0.0284)(2.0 \times 10^{-6})(2{,}100)^2}{(0.002637)(0.01)}$$
$$= 1{,}141.37 \text{ hr} = 47.56 \text{ days}$$

Using Equation 2.129, the late transient period is:

$$t_{ltp} = \frac{(0.12)(0.0284)(2.0 \times 10^{-6})(2{,}100)^2}{(0.00088)(0.01)}$$
$$= 3{,}420.21 \text{ hr} = 142.51 \text{ days}$$

Based on Ertle's Equation (Equation 2.130)[21] the late transient period is:

$$t_{ltp} = \frac{(0.12)(0.0284)(2.0 \times 10^{-6})(2{,}100)^2}{(0.001055)(0.01)}$$
$$= 2{,}852.88 \text{ hr} = 118.87 \text{ days.}$$

(2) The pressure vs flow rate relationship at t = 10 days, 48 days, 100 days, and at the late transient periods can be calculated by using Equation 2.171, and the results are shown in the following table:

	Gas Flow Rate, Mscf/d				
Pressure	t = 10 days	t = 48 days	t = 100 days	t_{ltp} Eq. 2μg	t_{ltp} Eq. 2.130
5,250	0	0	0	0	0
5,000	4.32	3.88	3.70	3.66	3.62
4,000	21.37	19.19	18.32	18.13	17.93
3,000	37.25	33.46	31.94	31.60	31.25
2,000	50.47	45.33	43.27	42.81	42.34
1,000	59.35	53.30	50.88	50.34	49.79
0	62.48	56.12	53.57	53.00	52.42

The plot of the IPR curves is shown in Figure 2.77.

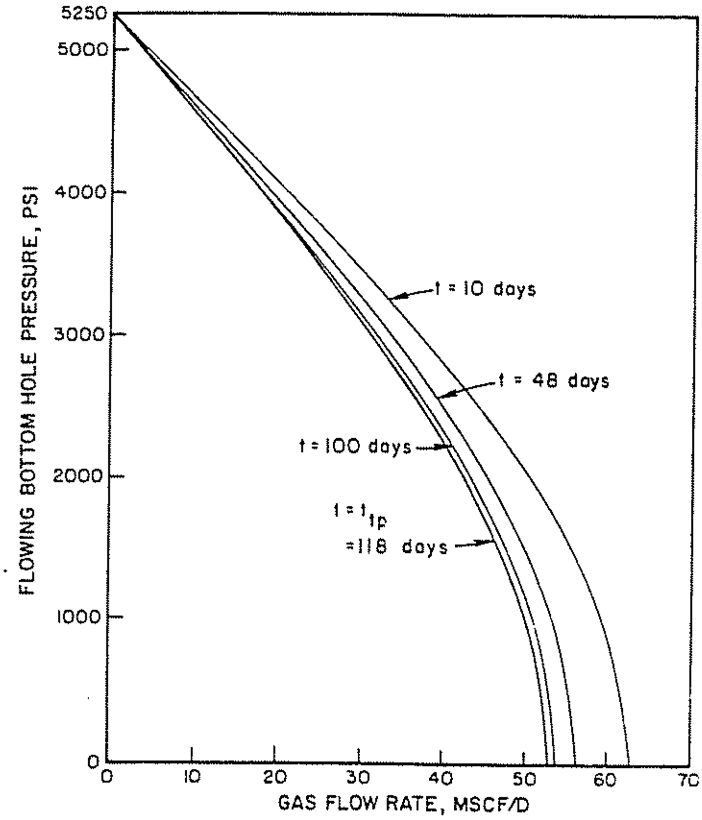

Figure 2.77 Transient IPR Curves for Example Problem #34

CLASS PROBLEM #34a

Given data:

$P_r = 6{,}050$ psi $\quad \mu_g = 0.0277$
$k = 0.1$ md $\quad Z = 1.0961$
$h = 10$ ft $\quad T = 240°F$
$r_e = 2{,}355$ ft $\quad \gamma_g = 0.65$
$r_w = 0.5$ ft $\quad \phi = 0.13$
skin = 2 $\quad C_t = 2 \times 10^{-6}$

Calculate:

(1) The duration of the transient period.
(2) Plot the IPR curves for t = 2 days, 6 days, and at pseudo-steady-state conditions.

CLASS PROBLEM #34b

Given data:

$P_r = 4{,}357$ psia $\quad Z = 0.9203$
$k = 0.25$ md $\quad \mu_g = 0.0258$
$h = 20$ ft $\quad T = 210°F$
$r_e = 1{,}750$ ft $\quad \gamma_g = 0.72$
$r_w = 0.4479$ $\quad \phi = 0.20$
skin = 4 $\quad C_t = 3.0 \times 10^{-5}$ psi^{-1}

Calculate:

(1) The duration of the transient period.
(2) Plot the IPR curves for t = 10 days, 20 days, and for pseudo-steady-state conditions.

CLASS PROBLEM #34c

Given data:

$P_r = 5{,}565$ psia $\quad \mu_g = 0.0294$
$k = 0.07$ md $\quad Z = 1.0146$
$h = 15$ ft $\quad T = 200°F$
$r_e = 1{,}500$ ft $\quad \gamma_g = 0.70$
$r_w = 0.5$ ft $\quad \phi = 0.15$
skin = −2 $\quad C_t = 2.8 \times 10^{-5}$

Calculate:

(1) The duration of the transient period.
(2) Plot the IPR curves for t = 20 days, 40 days, and at pseudo-steady-state conditions.

CLASS PROBLEM #34d

Given data:

$P_r = 4{,}870$ psia $\quad \mu_g = 0.0260$
$k = 0.04$ md $\quad Z = 0.9693$
$h = 25$ ft $\quad T = 220°F$
$r_e = 1{,}500$ ft $\quad \gamma_g = 0.68$
$r_w = 0.5$ ft $\quad \phi = 0.14$
skin = 0 $\quad C_t = 2.8 \times 10^{-5}$ psi^{-1}

Calculate:

(1) The duration of the transient period.
(2) Plot the IPR curves for t = 30 days, 60 days, and at pseudo-steady-state conditions.

2.4 IPR CURVES FOR FRACTURED WELLS,* BY DR. JIM LEA

2.41 DETERMINING THE PERFORMANCE OF TIGHT GAS WELLS

Most low-permeability gas wells (k = 0.1, 0.01, 0.001, and 0.0006 md) are more difficult to analyze because the long testing times required make it practically impossible to obtain stabilized test data. Because of this, multipoint well test procedures such as the flow-after-flow or isochronal four-point tests do not give useful information.

Since most low-permeability wells are fractured to obtain commercial production rates, the analysis of the tight-gas wells, of necessity, is broken into a *pre-frac* and a *post-frac* well testing period. For most low-permeability wells, testing the well before fracturing is necessary to obtain data on the interwell permeability, skin, and initial reservoir pressure.

These values are routinely found from semi-log analysis or by matching the buildup curve to type curves when the well is exhibiting "radial" flow or is in the transition to radial flow. However, once the well is fractured, the effective wellbore area increases tremendously, and it can become impossible to obtain radial flow data. The post-frac testing can be used to determine the increase in effective wellbore area caused by fracturing if the pre-frac data (primarily k and $\bar{P}_r$) was obtained. Then, if both pre-frac data (k, $\bar{P}_r$, and S) and post-frac data (X_f and S) are obtained, the user can input a reservoir model with the appropriate data and predict reservoir performance into the future.

Type curves may also be used. However, it is necessary to have a bottom-hole pressure to make predictions with a reservoir model. Many times, this pressure is assumed to be a constant for reservoir studies.

The thrust of this section is to determine how to predict gas-well production by considering liquids that accumulate during low-volume gas production. This means that the bottom-hole pressure (BHP) will change with time. The reservoir model (input with the pre- and post-frac data) or a type curve (reservoir model generated) becomes the tool for predicting when liquid loading will become a problem.

The use of the reservoir model or type curve is introduced later, but the concept is to generate IPR curves by plotting BHP vs rate on linear scales and then plot a tubing performance curve on the same plot. The intersection of the IPR or reservoir curve with the tubing performance curve indicates where the well will flow. IPR curves for future conditions intersected with tubing performance curves will predict when the well will experience liquid loading problems.

(1) *Pre-frac testing.* Pre-frac testing must be done to obtain values for k, S, and $\bar{P}_r$. The primary reason for testing before fracturing is to obtain data while the well is exhibiting radial flow. This will allow the user to perform a semi-log analysis of the data collected, which is the only way that k (permeability) of the reservoir can be calculated from transient well testing (with the exception of type-curve analysis) while the data is changing into radial flow. The general analysis is as follows:

(a) *General Procedure for Pre-Frac Testing.*

(1) Estimate time required for pressure buildup well test.
(2) Obtain test data.
(3) Make a type curve log ΔP, log Δt) to identify dominant flow mechanisms during different time periods of the test.
(4) If good radial flow data is present, use a semi-log plot to calculate S, kh, and P*; then calculate P_i.
(5) If data are just changing from storage or linear flow to radial flow, use the appropriate type curve to calculate Kh and S.

(b) *Dimensionless Type Curves.* An alternative to the conventional methods of making a log-log plot is to use a dimensionless type curve for an unfractured well as shown in Figure 2.78.[35] By plotting data on log-log paper of the same sized grid, it is possible to determine when storage ends and also when radial flow begins. Also, it is possible to obtain skin S if an approximate match of the data to the curves is made. The preferred method is to try to calculate the storage first and then make a match to obtain the appropriate skin and the value t_D (dimensionless time), which corresponds to a match point. From the match point, a kh can be found from the dimensionless pressure. However, since there may be several places on the curve where a match to data can be made, Figure 2.78 is primarily used by some analysts only to determine where radial flow begins; then semi-log analysis is used.

2.42 TYPE CURVE MATCHING[35]

(1) Select the theoretical type curve to be matched based on known well conditions (i.e., fractured well, unfractured well, constant pressure, constant production, etc.).
(2) Using a piece of transparent paper, overlay the scale of the theoretical type curve and trace the grid.
(3) Plot the data type curve on the overlay using the

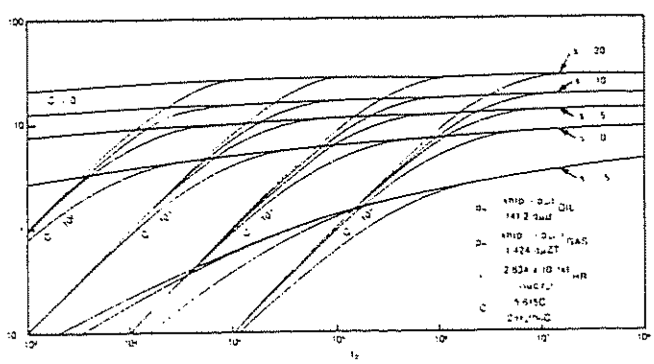

Figure 2.78 P_D *vs* t_D *for Well with Storage and Skin Effect (after Agarwal, Al-Hussainy, and Ramey)*[35] *(Working Copy on p. 336)*

* Adapted with permission from the *Oil and Gas Journal.*

underlying grid for scaling purposes. Temporarily ignore the curves plotted on the theoretical type curve.

(4) Keeping the horizontal and vertical grid lines on the data type curve parallel to the corresponding grid on the theoretical type curve, move the data type curve until a best match is obtained between the overlying data points and the underlying curve(s).

(5) Place a match-point mark on the data type curve at *any* known point (P_D, t_D) of the theoretical type curve. Though any point can be used, cycle intersections are convenient, and $P_D = t_D = 1$ is usually the most convenient.

(6) Replace the overlay to the position in which the data points were plotted.

Overlay: $\Delta p^2 = \Delta p_1$ $\quad$ Type curve: $P_D = 1$

$t = t_1$ $\quad$ $t_D = 1$

(8) Compute using Figure 2.78 as an example:

$$kh = (P_D)\frac{1{,}424\ q\mu_g ZT}{\Delta P_1{}^2}$$

$$\phi C_t = \frac{1}{t_D}\,\frac{0.000264kt_1}{\mu r_w{}^2}$$

where:

$\Delta p^2 = (p_i{}^2 - p_{wf}{}^2)$, ϕ = porosity

Note: These symbols are standard SPE nomenclature; see reference 35 for detailed definitions.

2.421 POST-FRAC TESTING

Post-frac testing involves testing a well with a tremendous increase in apparent wellbore area (A_w) caused by the large fracture face surfaces:

$$A_w = 4\,X_f h$$

where X_f = ½ the tip-to-tip fracture length.

For a fractured well, the test may cover times that include linear flow, transition, and radial flow or may last only through transition or possibly may exhibit only linear flow. If there is no radial flow, a type-curve match (less accurate than semi-log analysis) is required to obtain the kh of the well.

To illustrate why a fractured well may exhibit linear flow for a very long time, consider the criterion that t_D must be greater than 20 to get to radial flow. Then, for an unfractured well:

$$\Delta t(\text{hr}) = \frac{t_D\,\phi\mu_g C_t r_w{}^2}{0.000264k}$$

EXAMPLE TO DETERMINE Δt IN HRS:

Given data:

$t_D = 20$
$\phi = 0.05$
$\mu_g = 0.02$ cp
$C_t = 1. \times 10^{-5}$, psi^{-1} (total system compressibility)
$r_w = 0.3$ ft
$k = 0.1$ md

Solution procedure:

then:

$$\Delta t(\text{hr}) = \frac{(20)(0.05)(0.02)(0.5/5{,}000)(0.3)^2(3{,}600)}{(0.000264)(0.1)}$$

$$= 24.54 \text{ sec} = 0.0068 \text{ hr.}$$

for a fractured well, let r_w = 500 ft (effective radius after fracturing). Then:

$$\Delta t(\text{hr}) = 18{,}396 \text{ hrs} = 2.1 \text{ yrs.}$$

The above example shows how it may be impossible to get to any radial flow analysis and demonstrates the necessity of obtaining the permability before the well is fractured.

2.43 GENERAL PROCEDURE

When a well is fractured, there may or may not be a significant pressure drop along the fracture. A significant drop will give a low fracture flow capacity, F_{CD} This is determined by type-curve matching the data against Figure 2.79.[36] This curve is for constant wellbore pressure, which is near the way most tight gas wells are produced. If there is little pressure drop, the dimensionless fracture flow capacity F_{CD} will be large, on the order of 500.

$$\text{Dimensionless Fracture flow capacity} = \frac{k_f w}{kX_f}$$

where:

k_f = fracture permeability
w = fracture width
k = formation permeability
X_f = fracture ½ length

If the data indicates that there is significant pressure drop in the fracture, the analysis must proceed using this curve to obtain the fracture length from the t_{DX_f}

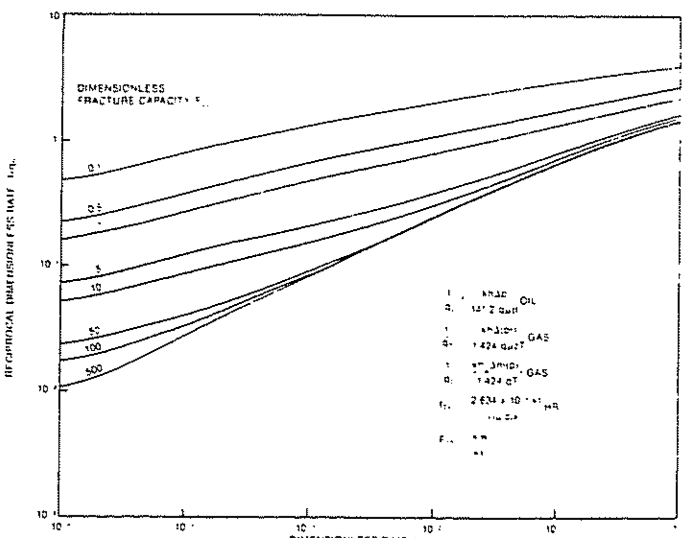

Figure 2.79 Log-Log Type Curves for Finite Capacity Vertical Fractures (Constant Wellbore Pressure) (after Agarwal, Carter, and Pollock)[36] (Working Copy on p. 336)

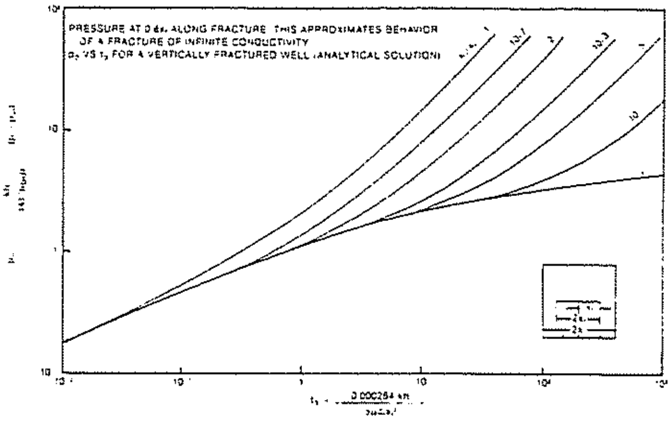

Figure 2.80 Propped Hydraulic Fractures

(dimensionless time on the abscissa) and the approximate kh from the $1/q_D$, which is the dimensionless reciprocal rate on the ordinate.

If the match on Figure 2.78 indicates approximate infinite fracture flow capacity, it is possible to use the type curve shown in Figure 2.80 for a fracture of infinite capacity. Also, conventional plots such as the square root plot (Figure 2.81) and the tandem square root plot (Figure 2.82) can be used for infinite capacity fracture data. The tandem square root plot has the advantage that it can be extrapolated to a P*, which will be the initial reservoir pressure P_i if the well has always flowed in linear flow. Also, the tandem square root plot will account for short flow times prior to shutin, whereas the square root plot requires an extended stabilized flow. Note that the square root plots allow the user to obtain only the product of $a_w\sqrt{k}$ (a_w = wellbore producing area) and does not uniquely identify the permeability.

2.431 INFLOW CURVES FOR TIGHT-FORMATION GAS WELLS

Because of low-permeability considerations, it is a very different problem to obtain a deliverability expression for a fractured low-permeability well than for a well in which stabilized data can be determined easily.

To review briefly, the normal expression for the deliverability of a gas well is the familiar back-pressure equation:

$$q = C(\overline{P}_r^2 - P_{wf}^2)^n$$

where:

q = rate of flow, Mcfd
C = a numerical coefficient characteristic of the particular well
$\overline{P}_r$ = shutin reservoir pressure, psia
n = numerical constant characteristic of the well

If a well has properties such that stabilized data can be collected within a short period of time, the procedure is to plot the data on a log-log plot of $(\overline{P}_r^2 - P_{wf}^2)$ vs q. The n value is determined from the slope, and the C value is determined from the horizontal displacement of test data on the graph.

However, if an excessive amount of time is required to obtain stabilized data, the isochronal or modified isochronal method[37] can be used to test the well and obtain a deliverability expression. The isochronal or modified isochronal well tests involve plotting nonstabilized data to obtain the slope (or n) and require at

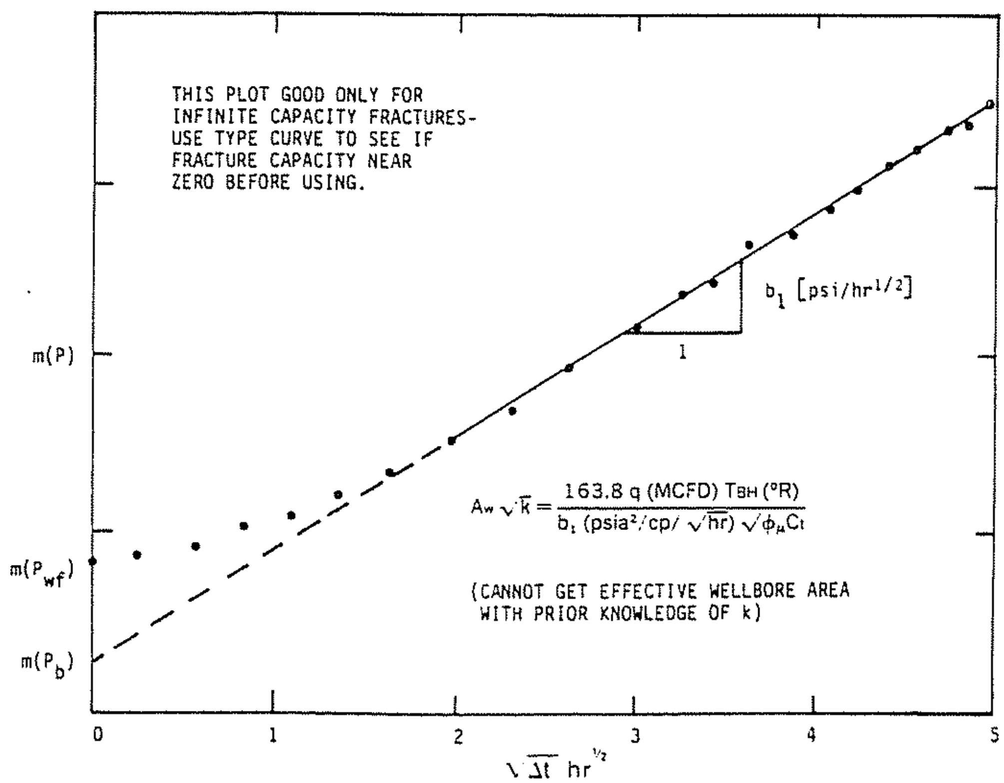

Figure 2.81 Typical Linear Flow Plot

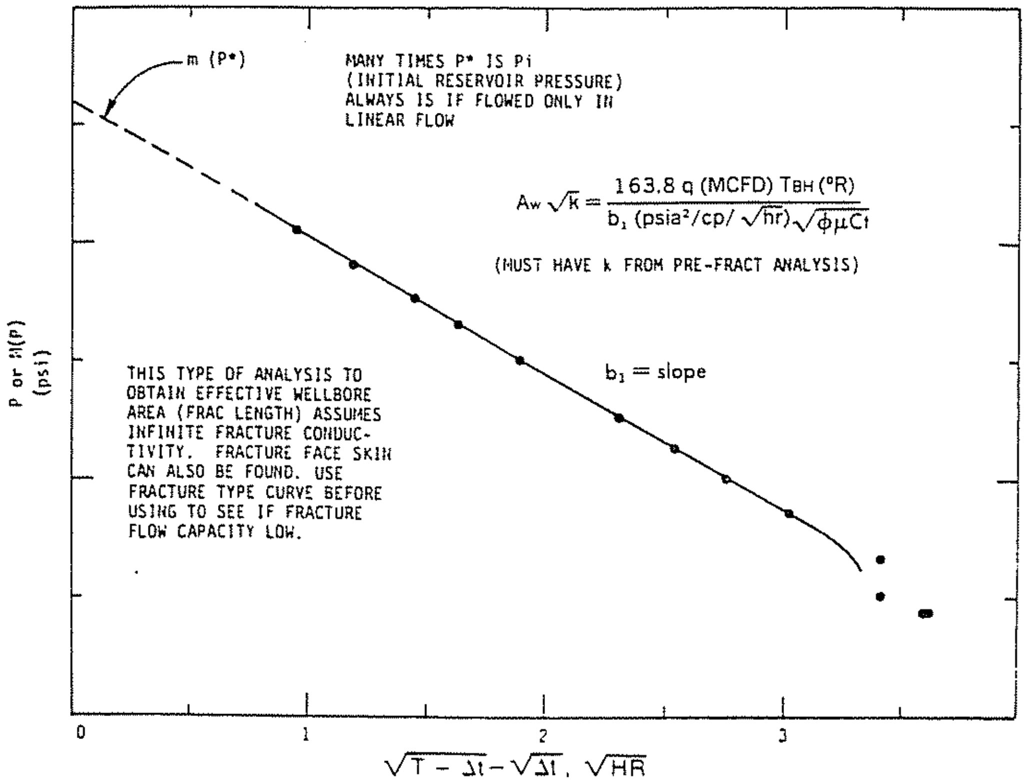

Figure 2.82 Example Tandem Square Root Buildup Plot

least one stabilized test value to evaluate the C constant.

For still lower permeability wells, nonstabilized data can be collected, and analytical methods[38] can be used to predict a "stabilized" point. This method has limited use because the expression obtained is valid only when the stabilization is predicted to occur.

However, an MHF (massive hydraulic fracture) low-permeability gas well will exhibit some type of flow because of the fracture (linear or linear with low-fracture conductivity) early in the well life and may not reach stabilization for years.

To illustrate how to obtain IPR curves for the MHF well, the following example is presented using a type curve to determine fracture conductivity of a given well. Then, as an extension of this example, the type curve will be used to generate a present and future IPR expression. The type curve that is used (Fig. 2.79) in the example is a constant pressure solution for a fractured well as a function of fracture flow capacity.[36]

EXAMPLE PROBLEM #35 (TO PREPARE IPR CURVES):

Given data (for type curve analysis and IPR construction):

initial reservoir pressure, pi, psi = 2,555
reservoir temperature, T, °R = 720
formation thickness, h, ft = 32
formation permeability, k, md
(permeability determined from semi-log analysis of the well before fracturing) = 0.0081
formation porosity, ϕ, (fraction of PV) = 0.107
total system compressibility, c_t, psi^{-1} = 2.34×10^{-4}
initial gas viscosity, μ_i, cp = 0.0195
difference between the initial and flowing pressures squared $(P_i^2 - P_{wf}^2)$, psi^2, = 6.28×10^6

AFTER-FRAC TESTS

Performance data

Time days	q(Mcfd)	1/q(Mcfd)$^{-1}$
20	625	1.6×10^{-3}
35	476	2.1×10^{-3}
50	408	2.45×10^{-3}
100	308	3.25×10^{-3}
150	250	4.00×10^{-3}
250	208	4.81×10^{-3}
300	172	5.21×10^{-3}

PVT Data
Reservoir temperature = 720°R

P, psi	Viscosity, cp	Z Factor
14.7	0.0141	1.000
600	0.0146	0.972
1,200	0.0153	0.9521
1,800	0.0164	0.9413
2,000	0.0178	0.9402
2,555	0.0195	0.9482

where:

F_{CD} = fracture flow capacity = $k_f w / k x_f$
w = fracture width, ft
k_f = fracture permeability, md
k = formation permeability, md
X_f = fracture half length, ft

$$F_{CD} = \frac{k_f w}{k X_f} = \text{dimensionless fracture flow capacity}$$

$$\frac{1}{q_D} = \frac{kh\Delta P^2}{1{,}424 q \mu_g Z T} = \text{reciprocal dimensionless rate (ordinate of Figure 2.79)}$$

where:

h = formation thickness
q = flow rate, Mcfd
μ_g = gas viscosity, cp
Z = real gas deviation factor
T = reservoir temperature, °R
$\Delta P^2 = P_i^2 - P_{wf}^2$, psia²
P_i = initial reservoir pressure, psia
P_{wf} = bottom-hole flowing pressure, psia

The type-curve abscissa is:

$$t_{DX_f} = \frac{2.634 \times 10^{-4} kt}{\phi\, (\mu_g C_t)_i\, x_f^2}$$

where

ϕ = formation porosity, fraction
$(\mu_g C_t)_i$ = viscosity-compressibility product at initial condition, cp /psi
t = flowing time, hr

Solution procedure:

The following steps for type-curve matching are repeated to determine the fracture flow capacity.[36]

(1) 1/q vs time data are plotted on tracing paper using the log-log scale of the type curves. Main X and Y axes also are drawn on the tracing paper. This plot is shown in Figure 2.83.
(2) Since formation flow capacity kh is known from a prefracturing buildup test and from semi-log analysis for a value of $1/q = 0.001$, the corresponding value of $1/q_D = 0.11$ is computed:

$$\frac{1}{q_D} = \frac{kh\Delta P^2}{1{,}424 q \mu_g Z T} = \frac{(0.0081)(32)(P_i^2 - P_{wf}^2)}{(1{,}424)(1{,}000)(0.0157)(0.95)(720)}$$

$$= \frac{1.69 \times 10^{-5}}{q}(P_i^2 - P_{wf}^2)$$

$$= 1.69 \times 10^{-5}(2{,}555^2 - 500^2) = 0.11$$

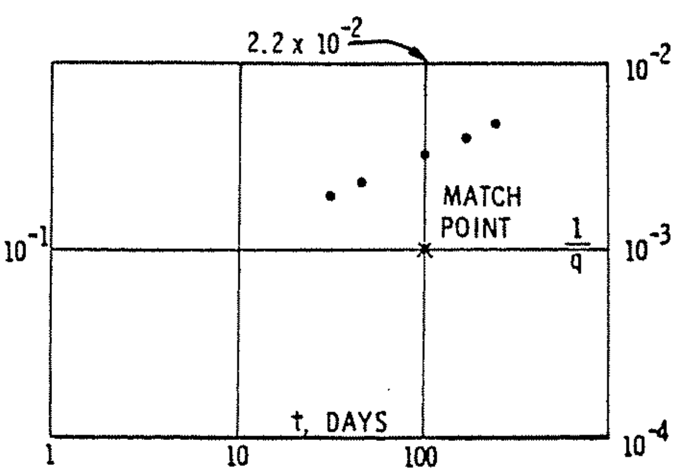

Figure 2.83 Type Curve Match (Example Problem)

Note that in this example, the μZ product is evaluated at $(P_i + P_{wf})/2$. To be more correct concerning the variations in μZ caused by steep pressure gradients in the reservoir, the m(p) (pseudo-pressure) form of the above equation could be used as opposed to the $\Delta P^2/\mu Z$ form used here. The pressure form is used here since it will be easier to illustrate the following IPR calculations without a relationship between m(P) and P as required when using pseudo-pressure.

The position of $1/q = 10^{-3}$ on the Y axis of the tracing paper is fixed in the relationship to $1/q_D = 0.11$ on the Y axis of the type-curve graph paper.

(3) The tracing paper is moved horizontally along the X axis until a match is obtained. The "match" is shown in Figure 2.84.
(4) A match point is chosen

where:

$$t = 100 \text{ days} = 2{,}400 \text{ hrs}$$
$$t_{DX_f} = 2.2 \times 10^{-2} \text{ @ } F_{CD} = 50$$

(5) Compute the fracture half length:

$$X_f^2 = \frac{(2.634 \times 10^{-4})kt}{\phi\, \mu_i C_i\, t_{DX_f}}$$

$$= \frac{(2.634 \times 10^{-4})(0.0081)(2{,}400)}{(0.107)(0.0195)(2.34 \times 10^{-4})(2.2 \times 10^{-2})}$$

$$= 476{,}710 \text{ ft}^2$$

$$X_f = 690 \text{ ft or } 2X_f \text{ (fracture length)} = 1{,}380 \text{ ft}$$

(6) Compute flow capacity of fracture:

$$k_f w = F_{CD}(kx_f) = 50\,(0.0081)(690) = 259 \text{ md ft}$$

2.44 IPR COMPUTATIONS

Now that the fracture length and flow capacity have been defined, it is possible to calculate future IPR expressions. The times at which it is desirable to calculate IPR curves are tabulated; then a corresponding T_{DX_f} is calculated. From T_{DX_f}, enter Figure 2.79 and at $F_{CD} = 50$, and find a corresponding $1/q_D$:

Flowing time (days)	T_{DX_f} = t(hr)/ 108,951(hr)	$1/q_D$ (from Fig. 2.79)
20	4.4×10^{-3}	0.104
182.5	4.02×10^{-2}	0.45
365	8.04×10^{-2}	0.62
730	1.61×10^{-1}	0.82
1,095	2.41×10^{-1}	0.92
1,460	3.22×10^{-1}	1.01
1,325	4.11×10^{-1}	1.13

With the above constants established, an expression for a deliverability curve at each $1/q_D$ (time) can be found:

$$q = \frac{1.65 \times 10^{-5}}{1/q_D}(P_i^2 - P_{wf}^2)$$

The coefficient in the above expression (1.65×10^{-5}) contains μZ, which is a function of pressure. An approximate average value of this quantity is used to obtain

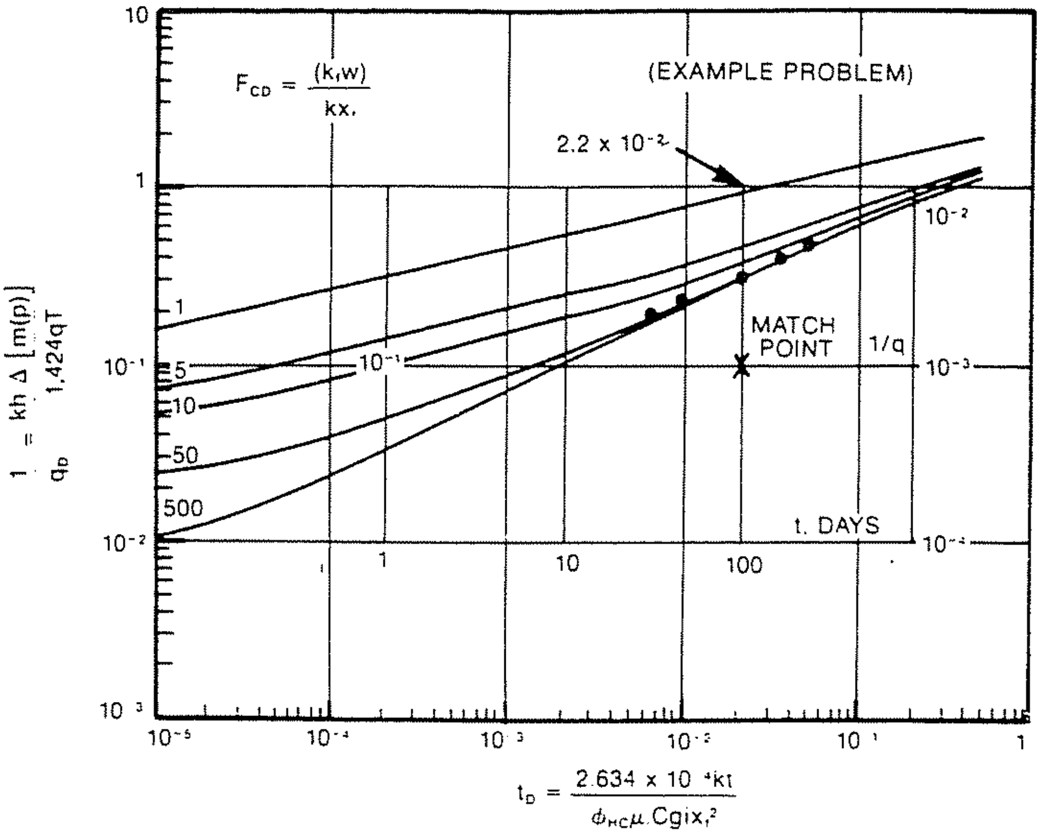

Figure 2.84 Type Curves for Finite Capacity Fractures

the constant for facilitating the example calculations so that it does not vary slightly as pressures change. After substituting the values of $1/q_D$ corresponding to given flowing times, rate vs pressure curves (IPR curves) can be found as shown in Figure 2.85 beginning at 20 days and extending to 60 months into the life of the reservoir.

Once these IPR curves are calculated, tubing performance or J curves can be plotted on the same graph

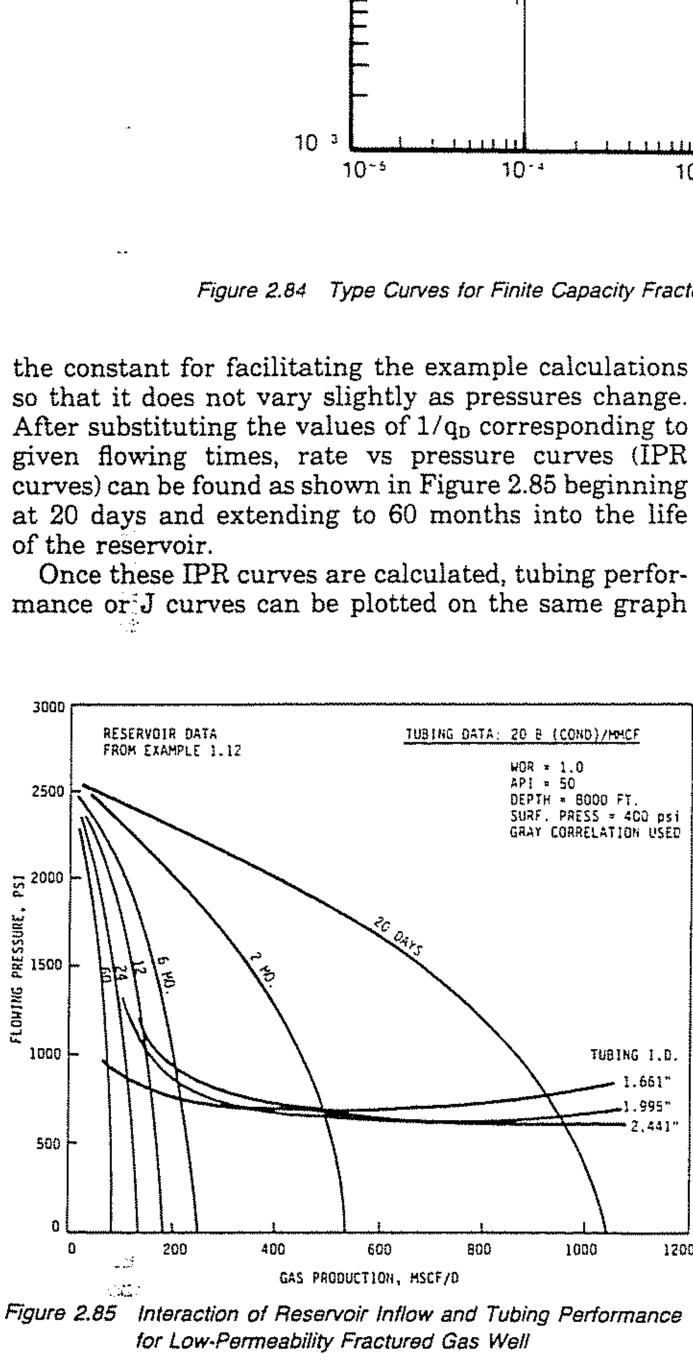

Figure 2.85 Interaction of Reservoir Inflow and Tubing Performance for Low-Permeability Fractured Gas Well

to indicate when the well may begin to load with liquids and cease to produce. The tubing performance curves shown in Figure 2.85 were calculated by using the Gray correlation[39] for condensate gas wells with 20 bbl/MMcf input as liquid condensate production.

Note that the IPR curves for the example tight gas well are very steep. This indicates that reducing the flowing bottom-hole pressure at any particular time would not increase the flow rate very much.

However, because of the sharp decline in production over the early life of the well, it is obvious that the well can experience severe loading conditions, leading to a total reduction in flow rate fairly early if, for instance, the tubing is too large.

Thus, the transient nature of the IPR curves is more significant than a slight change in bottom-hole pressure and the resulting PI (productivity index) effects.

These particular results show that a current reduction in flowing bottom-hole pressure (removal of some liquids in the wellbore) will not produce much of a gain in production. If deliquefication methods are not initiated at the appropriate time, the production can drop into a tubing performance area where liquids can continually accumulate and shut off production.

Figure 2.86 shows the production that might be expected over the life of the well (data from the example for preparing IPR curves) at a constant bottom-hole pressure (500 psi). But, if the actual case of liquid loading is considered, the production is calculated to cease in 2 years with the use of 1.995-in. ID tubing. This is indicated in Figure 2.85 by observing that the 1.995-in. tubing performance curve, if extended upward and to the left, would barely intersect, or be tangent to, the 24-month IPR curve. Further depletion beyond 24

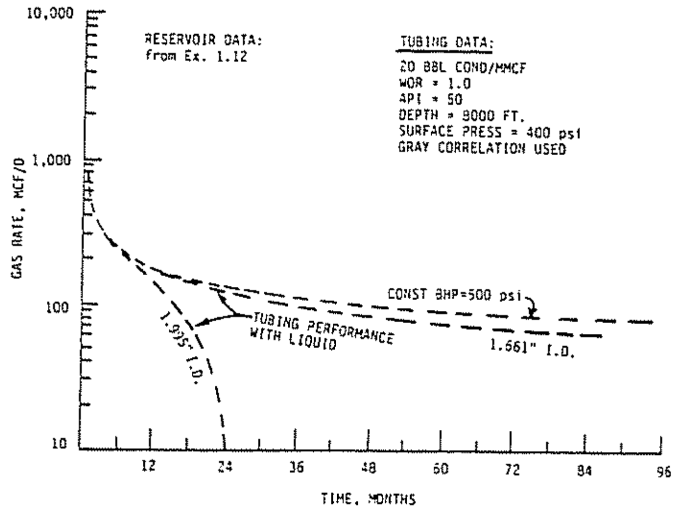

Figure 2.86 Projected Low-Permeability Fractured Gas-Well Production with Tubing Performance Considered

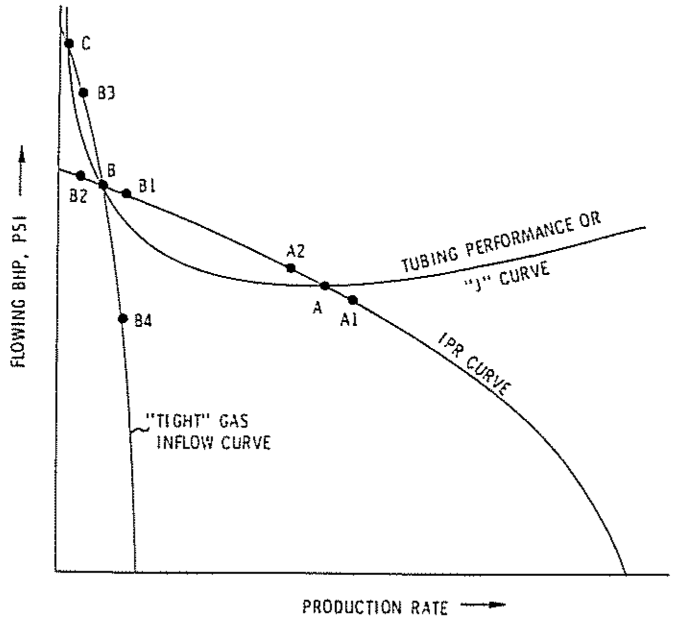

Figure 2.87 Liquid Loading Identified with Tubing and IPR Curves

months would result in no intersection of the tubing curve with the IPR curve, and no further production would occur.

However, use of the smaller tubing extends the life of the well to beyond 60 months.

This shows the importance of considering tubing performance when making reservoir projections.

A considerable amount of flowing well data is required to first make the required type-curve match and then project reservoir performance. Also, knowledge of the liquid/gas production is required. If the reservoir fluids and conditions do not match the conditions under which the type curve (Figure 2.79) was generated,[36] a reservoir simulator can be used to generate future IPR curves.

These should be calculated by finding rates at selected, fixed bottom-hole pressures as a function of time and plotting curves (Figure 2.85 along values with the same production times.

Further, a tubing performance relationship that matches field performance must be found to generate tubing performance curves.

Smaller tubing may be only a temporary solution, and consideration must be given to other methods of deliquefication such as plunger lift, which might require a larger diameter tubing string.

Note that a constant-pressure type curve was used with a tubing curve that was not completely constant pressure with time. In fact, near the loading condition, the tubing curve turns up sharply. It is felt that, since the tubing curve is fairly flat (constant pressure) before loading, this approach should give a good approximation to reality. However, if the tubing curve changes sharply with time, computer-generated curves, where each point of flow has the reservoir and tubing solution in agreement, may be necessary to obtain satisfactory results.

2.45 CHARACTER OF TUBING CURVES

For wells flowing gas and liquid, the tubing performance curve has a minimum flowing bottom-hole pressure as a function of rate, and as such, can cross an IPR curve in two locations such as point A and B (Figure 2.87)

Point A can be shown to be a stable flow point because, with slight fluctuations in flow rate, the flow point tends to return to point A. This is because, at A_1, the IPR curve has less available pressure than required by the tubing curve, so flow increases. By a similar argument, the tubing-IPR intersection at B is shown to be unstable. In fact, dry-tubing–IPR intersection to the left of the minimum in the J curve or tubing curve can be shown to be unstable.

However, for the steep tight-gas inflow curve, arguments similar to the above show that the tight-gas inflow–tubing curve intersection is stable even though it is to the left of the minimum in the J curve. Point C would have to be reached for unstable conditions with the tight-gas inflow curve. However, based on limited data, it seems that even with steep tight-gas inflow curves difficulties arise if the well is flowed to the left of the J curve. This may be caused by the slug flow pattern precipitating a more pronounced heading type of flow.

SUMMARY

The purpose of this chapter has been to show the various procedures used in the construction of IPR curves for both oil and gas wells. Our objective is to prepare these IPR curves using the best data and procedures available.

We have not attempted to discuss the more sophisticated reservoir simulation techniques. However, if reservoir models are readily available, they may be used in place of a less rigorous solution procedure.

IPR curves for gas condensate reservoirs and many wells producing from secondary and tertiary recovery projects are good examples of times when more sophisticated techniques are needed.

REFERENCES

1. Standing, M. B. *Volumetric and Phase Behavior of Oil Field Hydrocarbon Systems.* New York, New York: Reinhold Publishing Corp., 1952.
2. Brown K. E. *Technology of Artificial Lift Methods.* Vol. 1. Tulsa, Oklahoma: PennWell Publishing Co.
3. Lasater, J. A. "Bubble Point Pressure Correlation." *Transactions of the AIME* (1958), p. 379.
4. Odeh, A. S. "Pseudosteady-State Flow Equation and Productivity Index for a Well with Noncircular Drainage Area." *Journal of Petroleum Technology.*
5. Mathews, C. S. and D. G. Russel. *Pressure Build-up and Flow Tests in Wells.* Monograph Series. SPE of AIME, 1967, p. 110.
6. Jones, Loyd G., E. M. Blount, and O. H. Glaze. "Use of Short Term Multiple Rate Flow Tests to Predict Performance of Wells Having Turbulence." *SPE 6133.* SPE of AIME, 1976.
7. Sukarno, Pudjo. "Comparison of the Methods for Predicting Inflow Performance Relationship Curves." M.S. Thesis, University of Tulsa, 1982.
8. Vogel, J. V. "Inflow Performance Relationships for Solution Gas Drive Wells." *Journal of Petroleum Technology* (January 1968), p. 83–93.
9. Weller, W. T. "Reservoir Performance During Two-Phase Flow." *Journal of Petroleum Technology* (February 1966), p. 210–246.
10. Eickmeier, James R. Personal Communication.
11. Neeley, Bruce. Unpublished Work.
12. Hasan, M. "Oil Well Performance in the Presence of a Gas Phase." *SPE 7782.* SPE of AIME, 1979.
13. Standing, M. B. "Inflow Performance Relationships for Damaged Wells Producing by Solution Gas Drive Reservoirs." *Journal of Petroleum Technology* (November 1970), p. 1399–1400.
14. Harrison, David. Personal Communication.
15. Dias-Couto, Luiz Evanio and Michael Golan. "General Inflow Performance Relationship for Solution Gas Drive Reservoir." *Journal of Petroleum Technology* (February 1982), p. 285–288.
16. Fetkovich, M. J. "The Isochronal Testing of Oil Wells. *SPE 4529.* SPE of AIME.
17. Eickmeier, James R. "How to Accurately Predict Future Well Productivities." *World Oil* (May 1968), p. 99.
18. Standing, M. B. "Concerning the Calculation of Inflow Performance of Wells Producing from Solution Gas Drive Reservoirs." *Journal of Petroleum Technology* (September 1971), p. 1141–1142.
19. Tarner, J. "How Different Size Gas Cap and Pressure Maintenance Programs Affect Amount of Recoverable Oil." *Oil Weekly,* v. 144, no. 2 (June 12, 1944), p. 32–44.
20. Uhri, D. C. and E. M. Blount. "Pivot Point Method Quickly Predicts Well Performance." *World Oil* (May 1982), p. 153–164.
21. Ertle, Jim. Personal Communication.
22. Trube, Albert S. "Compressibility of Undersaturated Hydrocarbon Fluids." *Transactions of the AIME,* v. 210 (1957), p. 341–344.
23. Ramey, H. J. Jr. "Rapid Method of Estimating Reservoir Compressibility." *Journal of Petroleum Technology* (April 1964), p. 447–454.
24. Trube, Albert S. "Compressibility of Natural Gases." *Transactions of the AIME,* v. 210 (1957), p. 55–357.
25. Long, Giordano and Gianluigi Chierici. "Salt Content Changes Compressibility of Reservoir Brines." *Petroleum Engineer* (July 1961), p. B-25 to B-31.
26. Dodson, C. R. and M. B. Standing. "Pressure-Volume-Temperature and Solubility Relations for Natural-Gas-Water Mixtures." *API Drilling and Production Practice* (1944), p. 173–179.
27. Hall, Howard N. "Compressibility of Reservoir Rocks." *Transactions of the AIME,* v. 198 (1953), p. 309–311.
28. van der Knaap, W. "Nonlinear Behavior of Elastic Porous Media." *Transactions of the AIME,* v. 216 (1959), p. 179–187.
29. Newman, G. H. "Pore-Volume Compressibility of Consolidated, Friable, and Unconsolidated Reservoir Rocks Under Hydrostatic Loading." *Journal of Petroleum Technology* (Feburary 1973), p. 129–134.
30. Al-Hussainy, R. and H. J. Ramey. "Application of Real Gas Flow Theory to Well Testing and Deliverability Forecasting." *Journal of Petroleum Technology* (May 1966).
31. Carr, N. L., *et al.* "Viscosity of Hydrocarbon Gases under Pressure." *Transactions of the AIME.* 1954, p. 264.
32. Gatlin, Carl. *Petroleum Engineering, Drilling and Well Completion.* Englewood Cliffs: Prentice-Hall, 1960.
33. Himmatramka, Alok K. "Analysis of Productivity Reduction Due to Non-Darcy Flow and True Skin in Gravel-Packed Wells." *SPE 10084.* SPE of AIME, 1981.
34. Lea, Jim F. "Avoid Premature Liquid Loading in Tight Gas Wells by Using Prefac and Postfrac Test Data." *Oil and Gas Journal* (September 20, 1982), p. 123.
35. Agarwal, R. G., R. Al-Hussainy, and H. J. Ramey Jr. "An Investigation of Wellbore Storage and Skin Effect in Unsteady Liquid Flow: I. Analytical Treatment." *SPE Journal* (September 1970), p. 279–290.
36. Agarwal, R. G., R. D. Carter, and C. B. Pollock. "Evaluation and Performance Prediction of Low Permeability Gas Wells Stimulated by Massive Hydraulic Fracturing." *Journal of Petroleum Technology* (March 1979), p. 362.
37. Katz, K. L. et al. *Handbook of Natural Gas Engineering.* New York, New York: McGraw-Hill Book Co. Inc., 1959.
38. Brar, G. S. and K. Aziz. "The Analysis of Modified Isochronal Tests to Predict the Stabilized Deliverability of Gas Wells Without Using Stabilized Flow Data." *SPE 6134.* SPE of AIME, 1976.
39. Gray, H. E. "Vertical Flow Correlation in Gas Wells." In *User Manual for API 14B Subsurface Controlled Safety Valve Sizing Computer Program.* App. B. June 1974.
40. Alberta Energy Resources Conservation Board. *Theory and Practice of the Testing of Gas Wells.* 3d ed. 1975.
41. Aziz, K. and D. L. Flock. "Unsteady State Gas Flow—Use of Drawdown Data in the Prediction of Gas Well Behavior." *Journal of Canadian Petroleum Technology,* v. 2, no. 1.
42. Beal, Carlton, "The Viscosity of Air, Water, Natural Gas, Crude Oil and Its Associated Gases at Oil Field Temperatures and Pressures." *Transactions of the AIME,* v. 765 (1946), p. 94.
43. Cullender, M. H. "The Isochronal Method of Determining the Flow Characteristics of Gas Wells." *Transactions of the* AIME (1955).
44. Dake, L. P. *Fundamentals of Reservoir Engineering.* Elsevier Scientific Publishing Co., 1978.
45. Dietz. D. N. "Determination of Average Reservoir Pressure From Build-up Surveys." *Transactions of the AIME* (1965).
46. Earlougher, Robert C. Jr. *Advances in Well Test Analysis.* 2nd ed. Monograph 5. New York, New York: SPE of AIME, 1977.
47. Firoozabadi, A. and D. L. Katz. "An Analysis of High Velocity Gas Flow Through Porous Media." *Journal of Petroleum Technology* (February 1979), p. 211–216.
48. Greene, W. R. "Analyzing the Performance of Gas Wells." *25th Annual Southwestern Petroleum Short Course Proceedings.* Lubbock, Texas, 1978, p. 129–135.
49. Havelena, D. and A. S. Odeh. "The Material Balance as an Equation of a Straight Line." *Transactions of the AIME* (1963).
50. Horner, D. R. "Pressure Buildup in Wells." *3rd World Petroleum Congress.* Sect. II. p. 503–521.
51. Miller, C. C., A. E. Dyes, and C. A. Hutchinson. "The Estimation of Permeability and Reservoir Pressures from Bottom-Hole Pressure Build-up Characteristics." *Transactions of the AIME* (1950).
52. Muskat, M. *The Flow of Homogeneous Fluids Through Porous Media.* New York, New York: McGraw-Hill Book Co., 1957.
53. van Everdingen, A. F. and W. Hurst. "The Application of the LaPlace Transformation to Flow Problems in Reservoirs." *Transactions of the AIME* (1949).

Chapter 3

Multiphase Flow in Pipes

by Kermit E. Brown, Zelimir Schmidt, and Dale R. Doty

3.1 INTRODUCTION

A brief discussion of multiphase flow in pipes will be given in this chapter. The subject has been thoroughly covered in Volume 1 and in numerous other references.[1,2,3] However, a brief review and a discussion of the most important correlations is presented here.

The three principal components of the equation for predicting pressure loss in any fluid flow problem are

(1) elevation or static component
(2) friction component
(3) acceleration component

For vertical and inclined flow, the elevation component is normally the most important.

The equation for the flow of fluids in pipes, which is good for any fluid (single phase or multiphase), and for any angle (upward direction) of flow, (refer to Figure 3.1) states:

$$\text{Total Pressure Loss} = \text{Loss Caused by Elevation} + \text{Loss Caused by Friction} + \text{Loss Caused by Acceleration} \quad (3.1)$$

If we take the pressure loss (ΔP) that occurs over a distance (ΔZ), we can write an equation in terms of the pressure gradient commonly used in units of psi/ft:

$$\frac{dP}{dZ_{total}} = \frac{dP}{dZ_{elev}} + \frac{dP}{dZ_{friction}} + \frac{dP}{dZ_{acceleration}} \quad (3.2)$$

The elevation component is taken over the vertical distance only with friction, and acceleration is taken over the entire length.

A more specific equation for single-phase flow that represents all terms may be written as follows:

$$\frac{dP}{dZ_{total}} = (g/g_c)\,\rho \sin\theta + \frac{f\rho v^2}{2g_c d} + \frac{\rho v dv}{g_c dZ} \quad (3.3)$$

For multiphase flow, this may be written:

$$\frac{dP}{dZ_{total}} = \frac{g}{g_c}\rho_m \sin\theta + \frac{f_m \rho_m v_m^2}{2g_c d} + \frac{\rho_m V_m (dv_m)}{g_c (dZ)} \quad (3.4)$$

where:

ρ = density
v = velocity
d = pipe diameter
g = acceleration caused by gravity
g_c = conversion factor
f = friction factor
dP/dZ = pressure gradient
m = mixture properties

The elevation component for vertical or inclined flow is by far the most important of all three components. For vertical flow, it generally contributes greater than 80% of the total loss and may range from 70 to 98%. It is also the most difficult to properly evaluate because so many variables have an effect on it. It is the principal component that causes wells to load up and die. One of the easiest ways to visualize its importance is in the loading of gas wells. Many low-flow-rate gas wells, if making some liquid, will eventually accumulate sufficient liquid to cause the well to die or flow at very low flow rates. The prediction of when to expect this to occur in gas wells is quite difficult and complex and is discussed in detail in Chapter 6.

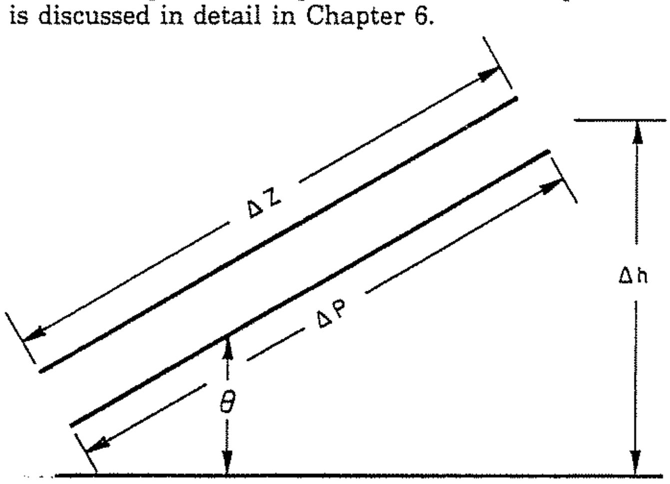

Figure 3.1 General Flow Schematic

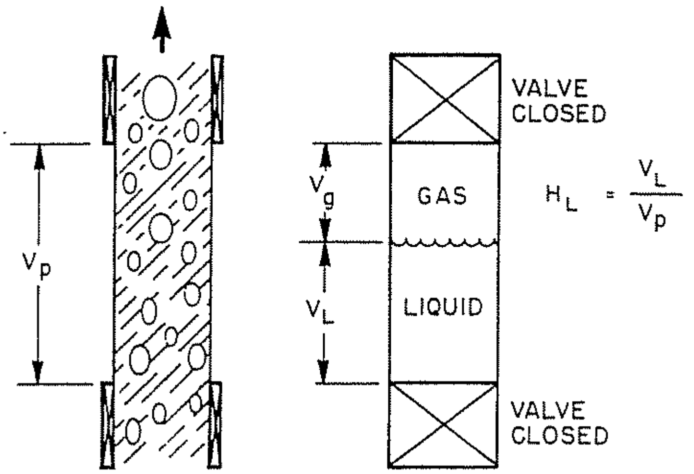

Figure 3.2 Holdup Illustration

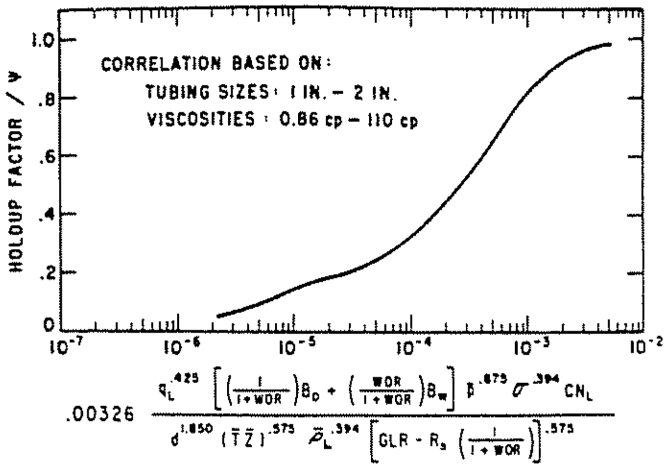

Figure 3.3 Holdup Correlation (after Hagedorn and Brown)[4]

In order to determine the elevation component, it is necessary to determine the density of the mixture in a static condition. In order to do this, we must be able to determine that fractional part of the pipe occupied by liquid and that fractional part of the pipe occupied by gas. Refer to Figure 3.2. That part of the pipe occupied by liquid is called holdup (H_L) and will vary from the top to the bottom of the well, as well as varying with numerous factors such as liquid rate, gas rate, viscosity, etc., as noted in Figure 3.3. Figure 3.3 represents the Hagedorn and Brown correlation for predicting the holdup value.[4] Once H_L is determined, the density can be readily calculated:

$$\rho_m = \rho_L(H_L) + \rho_g(1 - H_L) \tag{3.5}$$

where:

$\rho_m = lb_m/ft^3$

The gradient in psi/ft is $\rho_m/144$ and represents the elevation gradient component at one set of conditions.

The friction component can vary from the rather complex correlations of Ros[5] to the simplified correlations of others such as Hagedorn.[4] Refer to Figure 3.4 for Hagedorn's correlation. Hagedorn used a standard Darcy-Weisbach plot but incorporated a two-phase Reynolds number—that is:

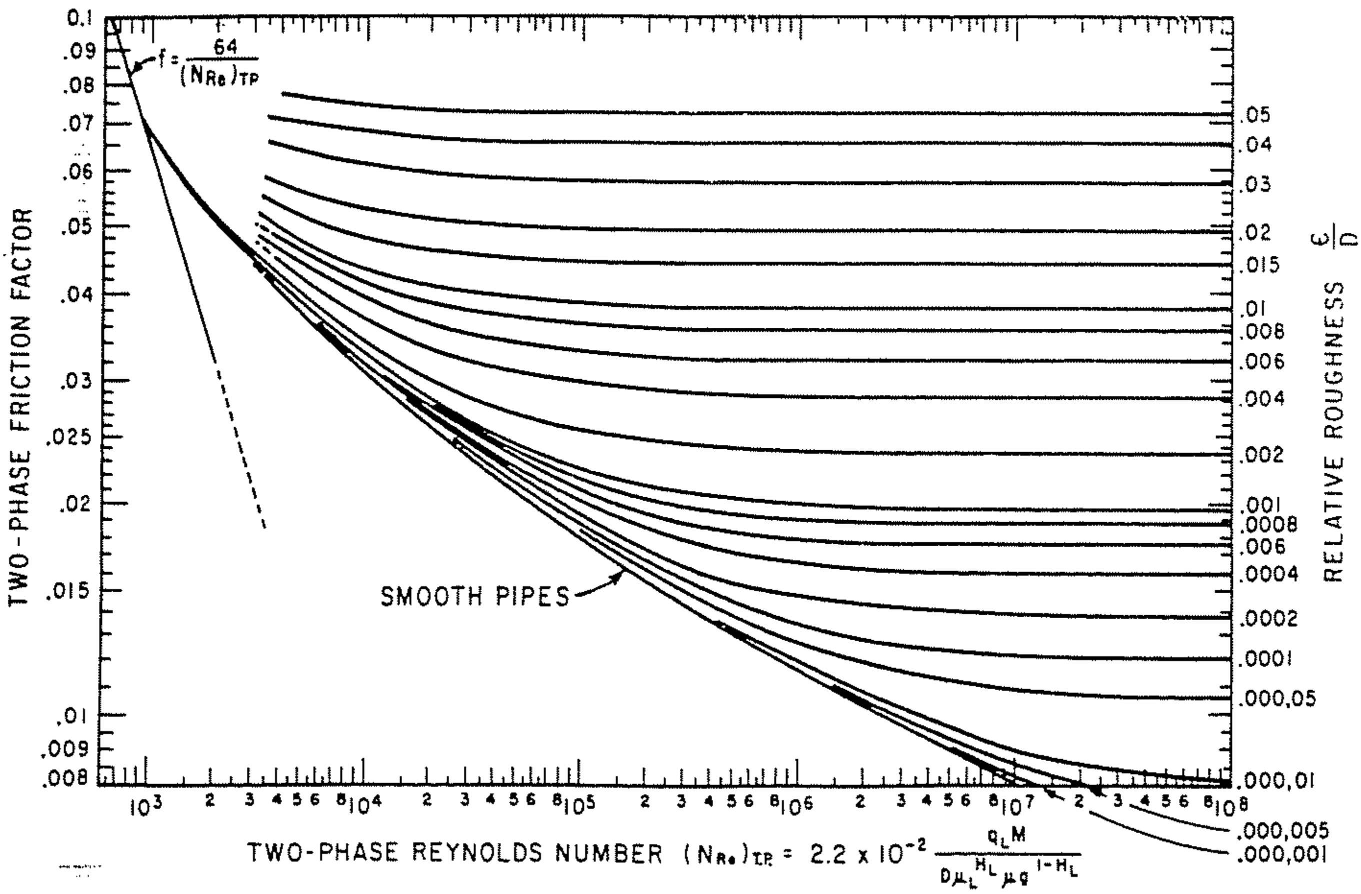

Figure 3.4 Friction-Factor Correlation (after Hagedorn and Brown)[4]

$$N_{Re} = \frac{dv_m\rho_m}{\mu_m} = 2.2 \times 10^{-2} \frac{q_{Lm}}{d\, \mu_L{}^{H_L}\mu_g{}^{(1-H_L)}} \quad (3.6)$$

Mixture properties are used to determine N_{Re}. The most significant one is viscosity. Refer to Volume 1, *Technology of Artificial Lift Methods*, for more detailed discussions on viscosity.[1] The viscosity of a mixture of liquid and gas has no meaning because the two phases are in reality separated. The most common method for determining mixture viscosity is to take the average viscosity based on that portion of the pipe occupied by each phase—that is:

$$\mu_m = \mu_L H_L + \mu_g(1 - H_L) \quad (3.7)$$

and:

$$\mu_L = F_0\mu_0 + F_w\mu_w$$

where:

F_0 = fraction, oil
F_w = fraction, water
μ_L = viscosity, liquid
μ_g = viscosity, gas
μ_m = viscosity, mixture
H_L = holdup

However, other methods for determining μ_m are used such as the one by Hagedorn where:

$$\mu_m = \mu_L{}^{H_L}\mu_g{}^{(1-H_L)} \quad (3.8)$$

None of these methods give a true mixture viscosity.

Emulsions are a complete and separate problem, and even after additional research, the correct prediction of pressure loss for emulsified flow leaves much to be desired.

A rather serious problem is that viscosity also affects the holdup term. Therefore, true holdup values as a function of viscosity may be questionable. Although the true friction loss and the true elevation loss may not be quite correct, the sum of the two-plus acceleration losses may give the correct total loss, which is what we are striving for.

Frictional losses may comprise from 1 to 30% of the total pressure loss. Very low rates such as 100,000 scfd of gas in 1.995-in. ID tubing have very little frictional loss, but 3,000 b/d of oil with a gas-oil ratio of 1,000 scf/bbl have very high frictional loss in 1.995-in. ID tubing.

The third component is the acceleration term, which sometimes is referred to as the kinetic energy term. It constitutes a velocity-squared term and is based on a changing velocity that must occur between various positions in the pipe—that is, Δv_m^2. In about 98% of the actual field cases, this term approaches zero but can be significant in some instances, showing up to 10% of the total pressure loss. In those cases of low pressure and hence low densities and high gas volumes or high gas-oil ratios, a rapid change in velocity is occurring and the acceleration component may become significant. It should always be included in any computer calculations. Only one final equation is shown here—that is, the one by Hagedorn and Brown.[4]

$$144\frac{\Delta P}{\Delta Z} = \frac{g}{g_c}\bar{\rho}_m \sin\theta + \frac{fw^2}{2.9652 \times 10^{11} d^5 \bar{\rho}_m} + \bar{\rho}_m \frac{\Delta\left(\frac{v_m^2}{2g_c}\right)}{\Delta Z} \quad (3.9)$$

where:

$\bar{\rho}_m = \bar{\rho}_L H_L + \bar{\rho}_g(1 - H_L)$
$\frac{\Delta P}{\Delta Z}$ = psi/ft
$g/g_c = 1.00$
w = mass flow rate, lb_m/day
d = pipe ID, ft
$\bar{\rho}_m$ = average density, lb_m/ft^3
v_m = mixture velocity, ft/sec

Refer to Volume 1, *Technology of Artificial Lift Methods*, by K. E. Brown for complete details and example problems on this and other procedures for calculating pressure losses.[1]

Notice that the two principal unknowns in Equation 3.9 are density (ρ_m) and friction factor (f). In order to calculate ρ_m, we must know holdup (H_L), and this is obtained from Figure 3.3. The friction factor is obtained from Figure 3.4. Increments of length or pressure are then assumed and the average gradient determined from which the correct distance between any two pressure points is determined.

3.2 VERTICAL MULTIPHASE FLOW

For vertical multiphase flow, the general equation reduces to:

$$\frac{dP}{dh_{total}} = \rho_m + \frac{f_m\rho_m v_m^2}{2g_c d} + \frac{\rho_m v_m dv_m}{g_c dh} \quad (3.10)$$

For Hagedorn's equation we can write:

$$144\frac{\Delta P}{\Delta h} = \bar{\rho}_m + \frac{fw^2}{2.9652 \times 10^{11} d^5 \bar{\rho}_m} + \bar{\rho}_m \frac{\Delta\left(\frac{v_m^2}{2g_c}\right)}{\Delta h} \quad (3.11)$$

Again, the principal unknowns are $\bar{\rho}_m$ and f.

The correlations that are most widely used at the present time are listed as follows:

(1) for vertical multiphase flow (oil wells)
 (a) Hagedorn and Brown[4]
 (b) Duns and Ros[6]
 (c) Ros and Gray[7]
 Modification of original work of Ros and Duns and Ros:
 (d) Orkiszewski[8]
 (e) Beggs and Brill[9]
 (f) Aziz[2]

There are numerous other correlations, but the previous six are used more widely than all others.

(2) for vertical flow (dry gas wells)
 (a) Cullender, Smith, and Poettman[10]
(3) for vertical flow (wet gas wells)
 (a) Ros and Gray[7]—available through the API; handles both water and condensate production
 (b) Beggs and Brill[9]—has been found to be good for gas wells with gas-liquid ratios less than 50,000 to 75,000 scf/bbl and does reasonably well for relatively dry gas wells.

By assuming various flow rates, a "tubing intake" curve can be prepared. Figure 3.5 shows a plot of pres-

sures at the entry of the tubing string vs flow rates. This may also be called a "node outflow" pressure curve. It is equally important for both oil and gas wells. Its shape will differ depending upon the correlation used, with the Ros and Gray[7] correlation being recommended for gas wells making liquid.

Figure 3.5 is an extremely important plot because it shows the critical rates below which the flow in the tubing becomes unstable and a loading in the tubing string can be expected. Another manner in which to visualize this is that the gas is slipping past the liquid and therefore the liquid falls back. As the rate decreases, the pressure required at the entry of the tubing continues to increase.

For a particular well, the tubing intake curve and inflow performance curve must be analyzed together. The following series of figures shows the significance of the tubing entry or node outflow curve.

Figure 3.6 shows a condition of stable flow caused by the IPR and tubing entry curve crossing to the right of the critical point.

Figure 3.7 shows a condition whereby the tubing entry curve crosses the IPR curve at two positions. The well will flow at position 2 to the right of the critical point and will exhibit stable flow at this position. The flow at position 1 will not occur on this well unless the operator purposely places it in this position by choking the well back, and when he does this, he is shifting the position of the tubing entry curve. Note Figure 3.8. Here, the IPR curve is not shifted for a particular set of conditions; therefore, we can only shift the tubing entry curve, and this will kill the well.

Notice that as the choke size decreases, the wellhead pressure P_{wh} increases and hence the tubing entry pres-

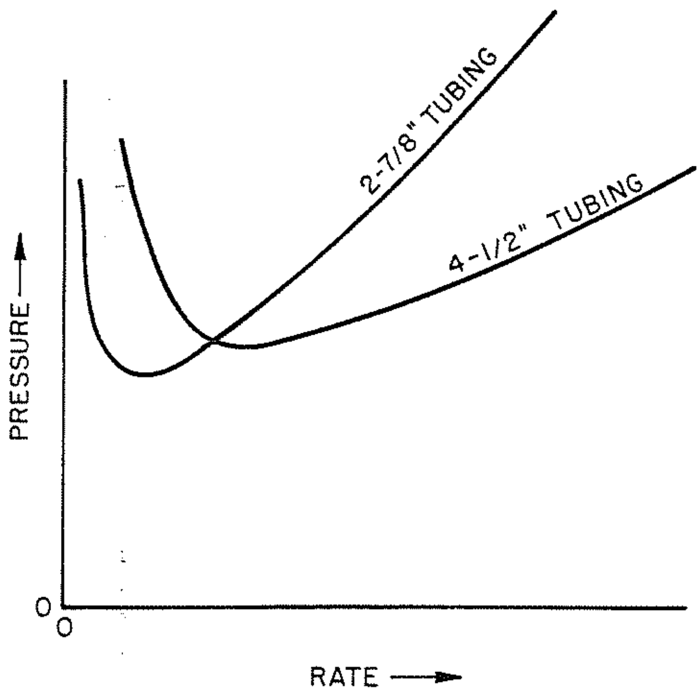

Figure 3.5 Typical Intake Curves

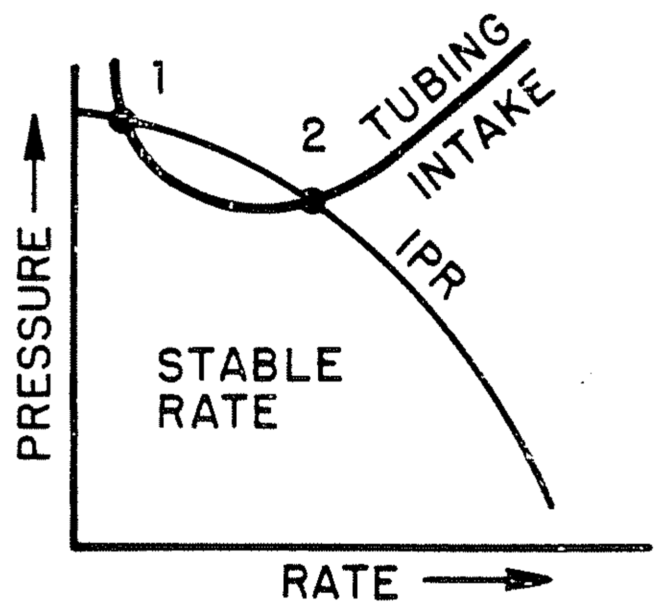

Figure 3.7 Well Flowing at Position 2

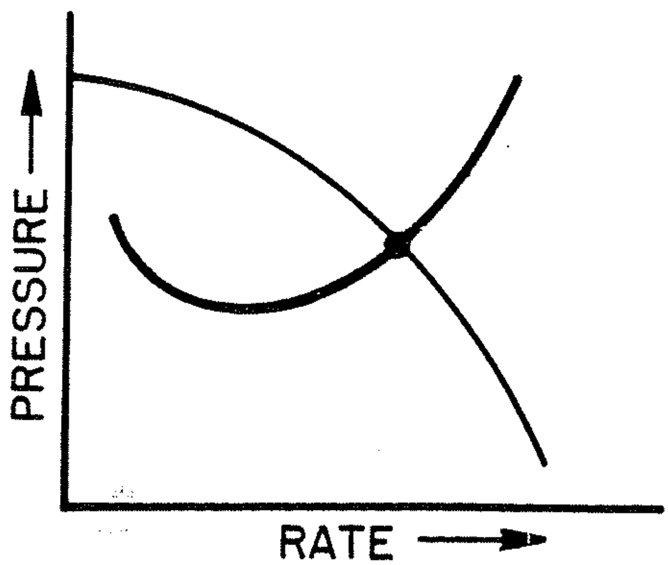

Figure 3.6 Stable Flow

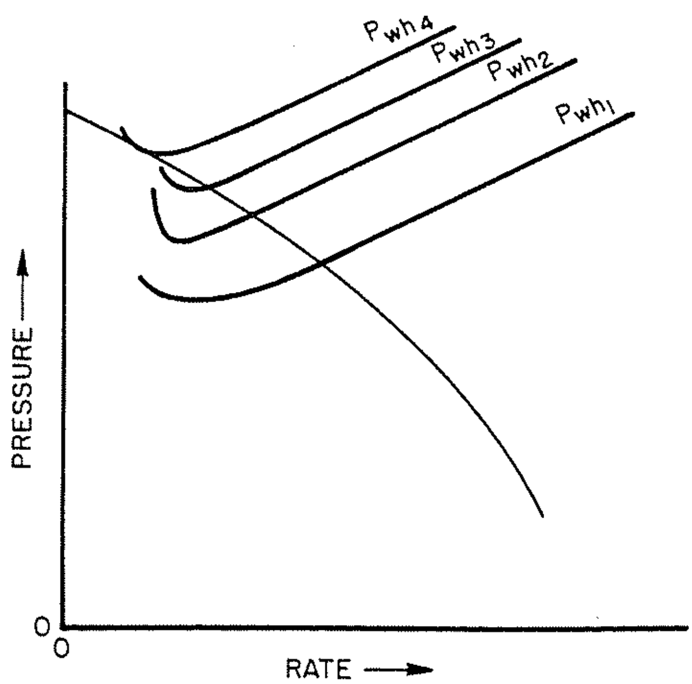

Figure 3.8 How Choking Shifts the Intake Curve and Finally Kills the Well

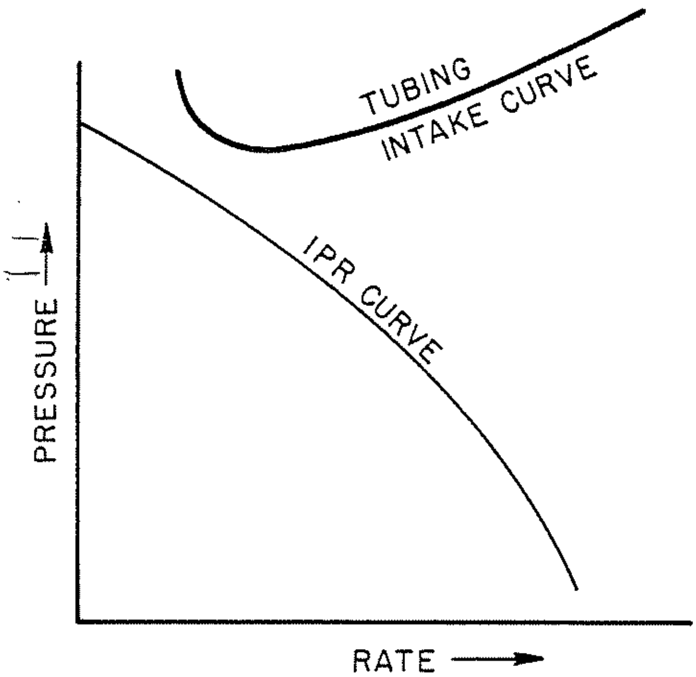

Figure 3.9 Dead Well

sure increases. Finally, upon reaching P_{wh_4}, the well is dead and is very likely to be dead at P_{wh_3}.

Figure 3.9 shows a condition whereby the well is dead because the IPR and tubing entry curve do not intersect.

3.21 THE USE OF VERTICAL MULTIPHASE FLOW GRADIENT CURVES

Refer to Volume 1, *Technology of Artificial Lift Methods*, pages 158–166, for numerous examples in the use of these curves.[1] Refer to Volumes 3a and 3b, *Technology of Artificial Lift Methods*, for numerous gradient curves of all types.[11]

Only two examples are shown in this section, and they are the same as those shown in Volume 3a.

Refer to Figures 3.10 and 3.11 for further explanations.

3.3 HORIZONTAL MULTIPHASE FLOW

3.31 INTRODUCTION

For horizontal flow, the general equation reduces to:

$$\frac{dP}{dL} = \frac{f_m \rho_m v_m^2}{2g_c d} + \frac{\rho_m v_m dv_m}{g_c dL} \tag{3.12}$$

The elevation component drops out since no fluids are to be lifted vertically. Mathematically, $\sin \theta = 0$ at zero angle in Equation 3.3.

If the acceleration terms are neglected, we have the rather simple equation:

$$\frac{dP}{dL} = \frac{f_m \rho_m v_m^2}{2g_c d}$$

The principal unknowns in this equation are the density and the friction factor. It is then important to have a good holdup correlation for horizontal flow as well as a good friction factor correlation.

One of the best horizontal multiphase flow correlations has been found to be the one of Beggs and Brill.[3] It covers the entire range of rates and pipe sizes and was originally intended to be good for any angle of flow as well as for vertical flow. Field experience has shown it to be one of the best for horizontal flow.

Some of the other correlations that are quite often used are those of Dukler,[12] Eaton et al.,[13] Lockhart and Martinelli,[14] and Baker.[15] Baker's correlation was used almost exclusively in the past by numerous companies and is still used with some modifications. Various modifications of the Lockhart and Martinelli correlation are also used by several companies.

One of the best holdup correlations was the one proposed by Eaton et al.[13] (Figure 3.12). Excellent results have been obtained by using Eaton's holdup correlation in conjunction with Dukler's correlation—that is, using Dukler's procedure but substituting Eaton's holdup correlation for the one proposed by Dukler.

3.32 THE USE OF HORIZONTAL MULTIPHASE FLOW GRADIENT CURVES

Refer to Volume 1, *Technology of Artificial Lift Methods*, pages 191–196, for numerous examples in the use of horizontal multiphase flow gradient curves.[1]

Only one example is shown here, and it is the same one shown in Volume 3a.

Refer to Figure 3.13 and note that, if the separation pressure is known, the wellhead pressure can be determined and vice versa.

3.4 INCLINED FLOW

3.41 INTRODUCTION

There are numerous cases whereby the tubing string deviates from the vertical and/or where the flow line deviates from the horizontal. This causes a more difficult solution to the multiphase flow problem. There have been numerous attempts to solve the inclined flow problems, but there is still much work that needs to be done in resolving this problem. The most recent work of Beggs and Brill[9] appears to offer the most promise. Beggs and Brill conducted laboratory experimental work in small pipes for various angles of flow (both upward and downward from the horizontal). Our experience has shown that they offer the best solution for inclined flow lines. Their correlation, along with specific examples, can be found in reference 1.

The Flanigan correlation also is used quite often for inclined flow—in particular for larger lines and gas transmission lines. Complete details, along with example problems, can be found in reference 1.

3.42 DIRECTIONALLY DRILLED WELLS

More and more directional wells are being drilled from offshore platforms and even from numerous land wells in the Arctic and in other places such as manmade islands. Some companies are suggesting that we drill more wells from central locations, thereby reducing overall costs. Angles greater that 60° from the vertical are fairly common, and angles greater than 70°

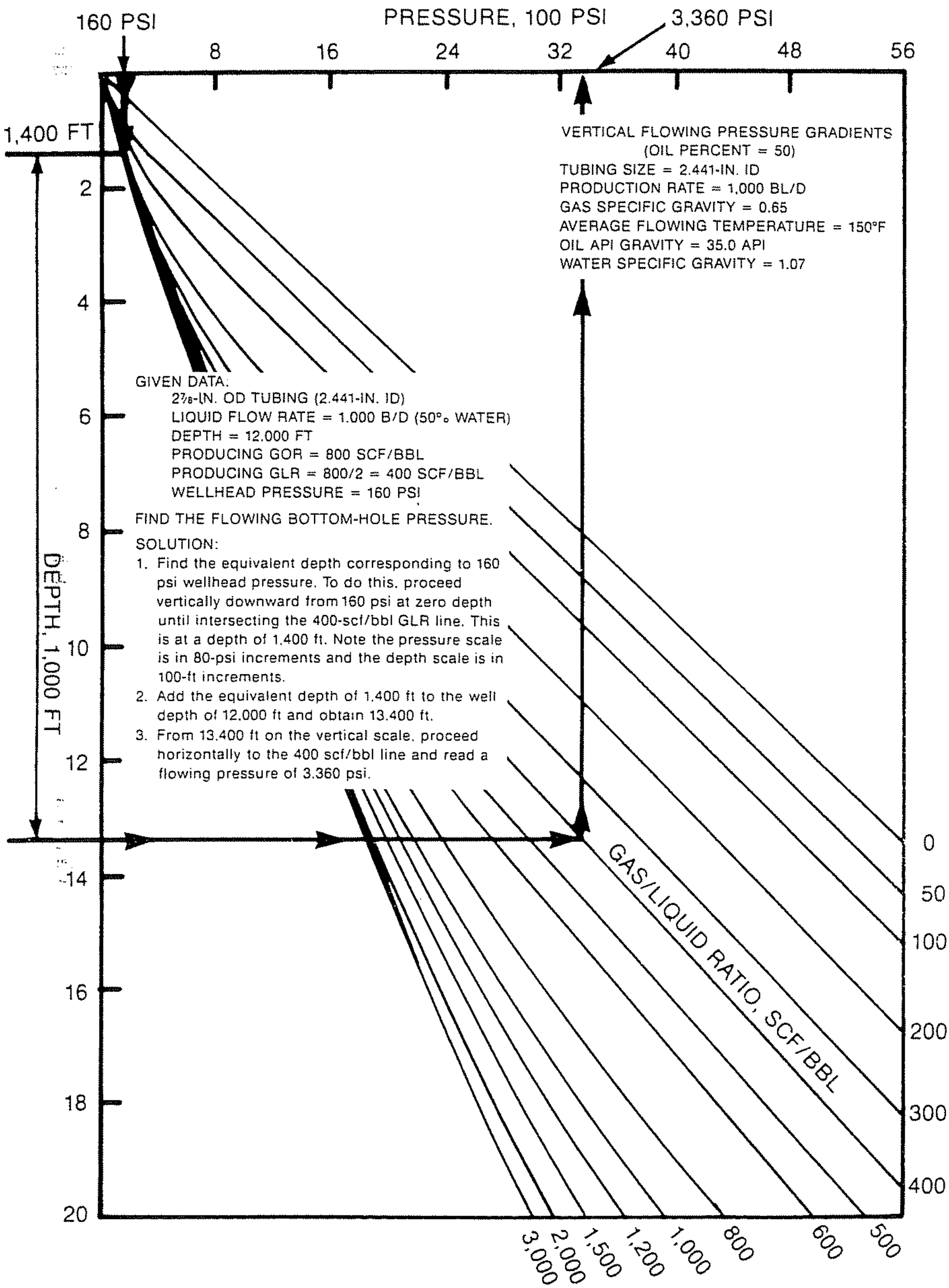

Figure 3.10 How to Find the Flowing Bottom-Hole Pressure

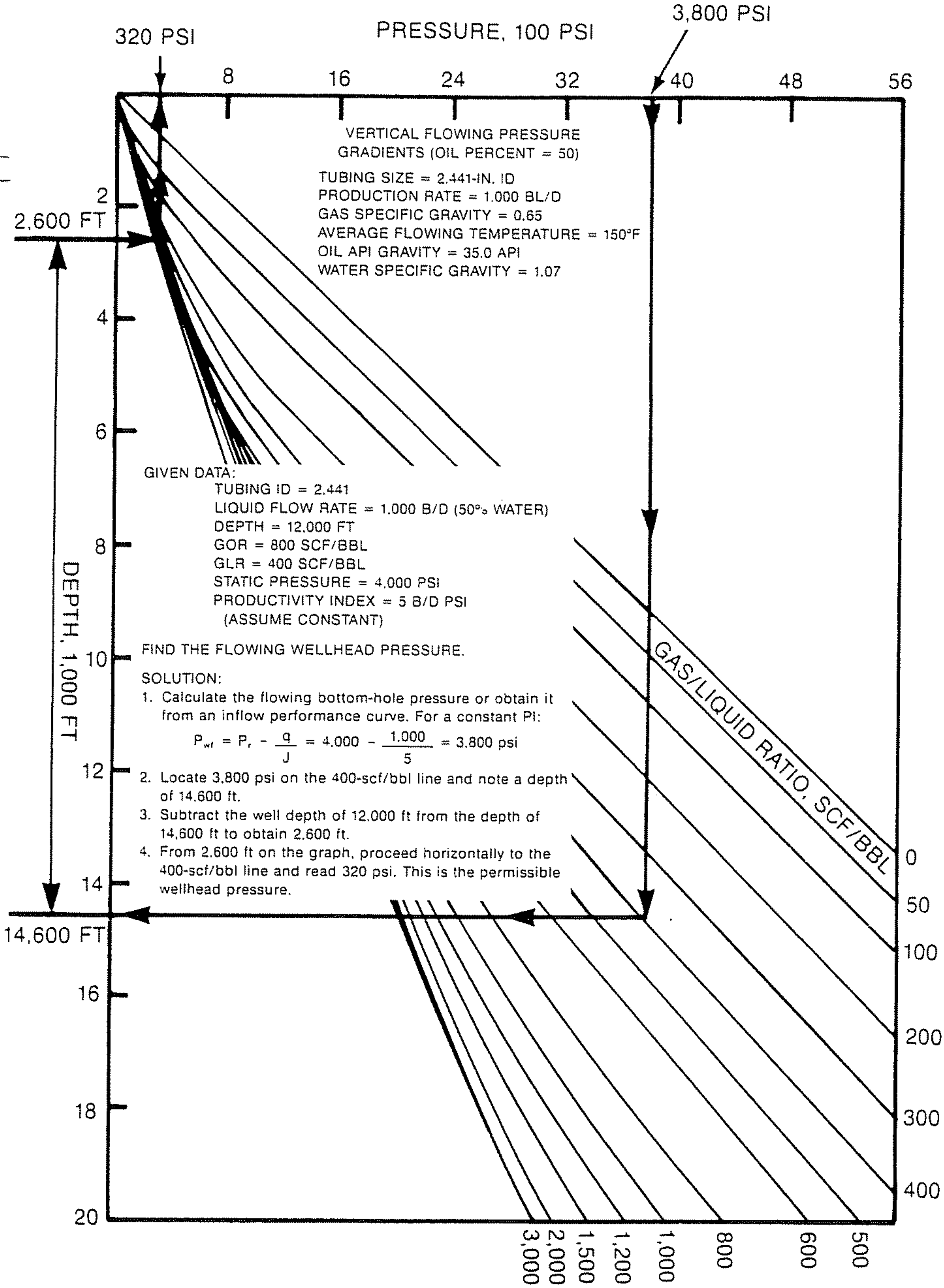

Figure 3.11 How to Find the Flowing Wellhead Pressure

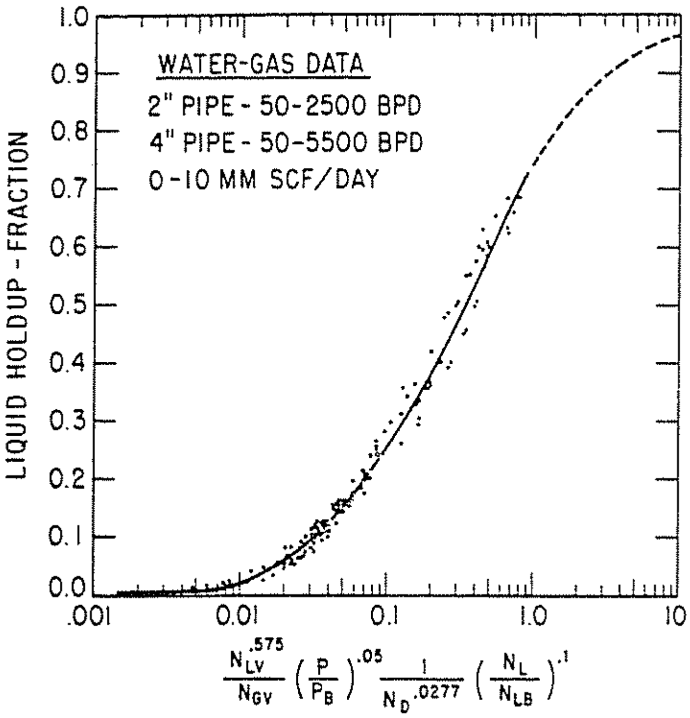

Figure 3.12 Holdup Correlation for Horizontal Flow (after Eaton et al.)[12]

have been drilled. However, additional careful planning should be done in extending these wells too far from the vertical. For example, some wells with an overall deviation of between 60–70° can be expected to produce 30–35% less than a vertical well to the same formation for the same tubing size. In addition, artificial lift problems are increased drastically, with some lift methods being ruled out completely. For good planning, the production engineer, the reservoir engineer, and the drilling engineer should get together in establishing drilling and completion programs. Highly deviated wells should be analyzed to see if the objective flow rate can be obtained with the planned casing and tubing sizes under consideration.

3.421 CORRELATIONS FOR DIRECTIONALLY DRILLED WELLS

It is recommended that the multiphase flow correlation be used in the form of Equation 3.4:

$$\frac{dP}{dZ_{total}} = \underbrace{(g/g_c)\rho_m \sin\theta}_{\text{(elevation)}} + \underbrace{\frac{f_m \rho_m v_m^2}{2g_c d}}_{\text{(friction)}} + \underbrace{\frac{\rho_m v_m dv_m}{g_c dZ}}_{\text{(acceleration)}} \quad (3.4)$$

where:

$$\rho_m = \rho_L H_L + \rho_g(1 - H_L) \quad (3.5)$$

f_m = mixture energy loss factor

As can be seen, the elevation component is converted to vertical distance only, whereas friction and acceleration are taken over the entire length of the piping system. The reliability of this method depends mostly upon the correct determination of H_L.

Reasonable reliability has been obtained by using a vertical flow holdup correlation such as Figure 3.3 as proposed by Hagedorn. This can be expected to be reliable up to about 35–40° deviation from the vertical after which the holdup values for directional flow begin to deviate from vertical flow values. Hagedorn's equation would then appear as noted in Equation 3.11.

$$\frac{\Delta P}{\Delta Z_{total}} = \frac{g}{g_c}\bar{\rho}_m \sin\theta + \frac{fw^2}{2.9652 \times 10^{11} d^5 \bar{\rho}_m} + \bar{\rho}_m \frac{\Delta\left(\frac{v_m^2}{2g_c}\right)}{\Delta Z} \quad (3.11)$$

Other correlations such as those of Orkiszewski, Ros,[5] etc., could be handled in the same manner. The greatest error comes from assuming that the holdup (H_L) is the same for directional flow and vertical flow.

The next best approach to the problem is to use the correlation of Beggs and Brill, which gives a holdup value for each angle of flow.[9] This should be the best procedure to use. However, when using the published work of Beggs and Brill, it appears that most of the calculated pressure losses will be higher than the true values. In other words, lower rates will be predicted than obtainable when using this correlation, but it is always consistent.

The improved correlation of Beggs and Brill gives good results. Figure 3.14 shows the effect of the angle of deviation on the flowing pressure-traverse. Figure 3.15 shows the effect of the angle of deviation on flow rate for a gas lift well.

3.43 MULTIPHASE FLOW CORRELATIONS FOR INCLINED FLOW LINES

The best correlation for inclined multiphase flow in flow lines appears to be the one by Beggs and Brill.[9] It covers the complete range of angles of inclination, including both upward and downward flow. It also appears to handle flow in larger transmission lines as well as condensate flow when an adequate compositional model is used. Adequate example problems can be found in Volume 1, *Technology of Artificial Lift Methods,* along with a complete discussion of their correlation.[1]

The correlation that has been most widely used in past years has been the one of Flanigan,[16] and it is still used extensively by several companies although several modifications may be included. It is probably the simplest solution to the inclined flow problem and may be used in conjunction with any good horizontal flow correlation such as the one by Beggs and Brill,[9] Dukler,[12] etc. A holdup correction factor is obtained based on superficial gas velocity, which accounts for both upslope energy loss and downslope recovery in one factor.

3.5 FLOW-THROUGH RESTRICTIONS

3.51 SURFACE CHOKES

3.511 MULTIPHASE FLOW THROUGH A CHOKE

The equation most commonly used for multiphase flow through surface chokes is the one by Gilbert, which was based on field data:[17]

$$P_{wh} = \frac{435\,(GLR)^{0.546}}{(d)^{1.89}}\, q \quad (3.13)$$

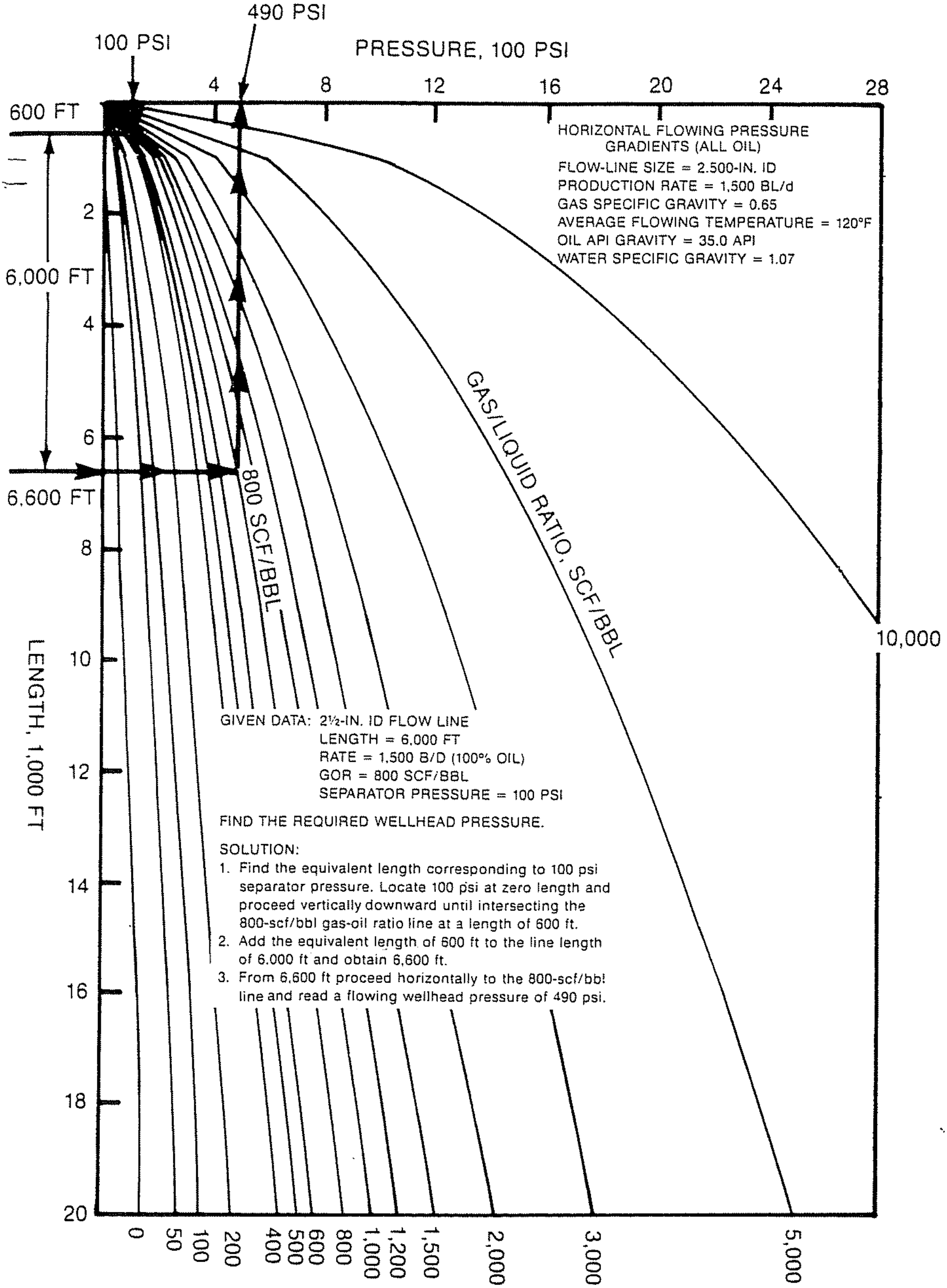

Figure 3.13 Horizontal Multiphase Flow to Find Flowing Wellhead Pressure

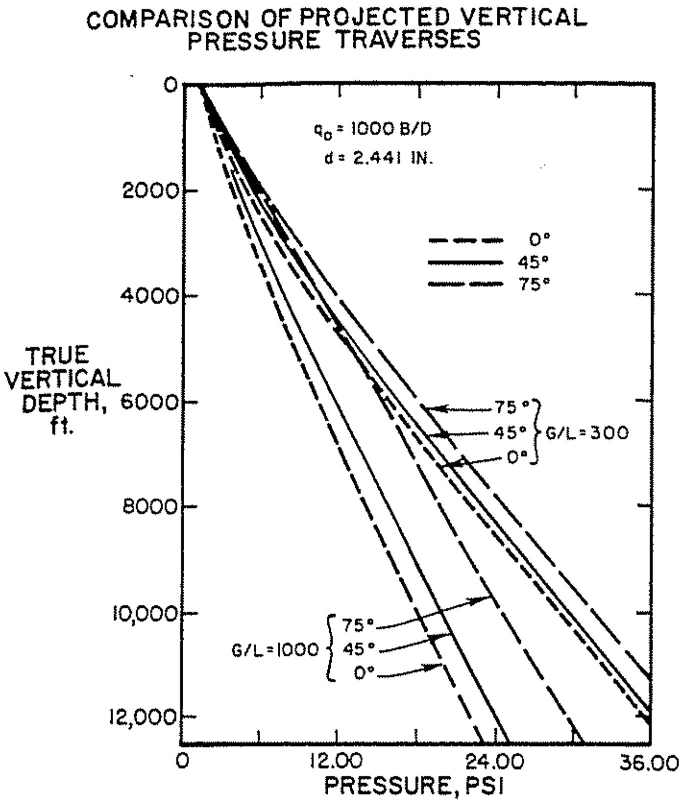

Figure 3.14 Comparison of Projected Vertical Pressure Traverses

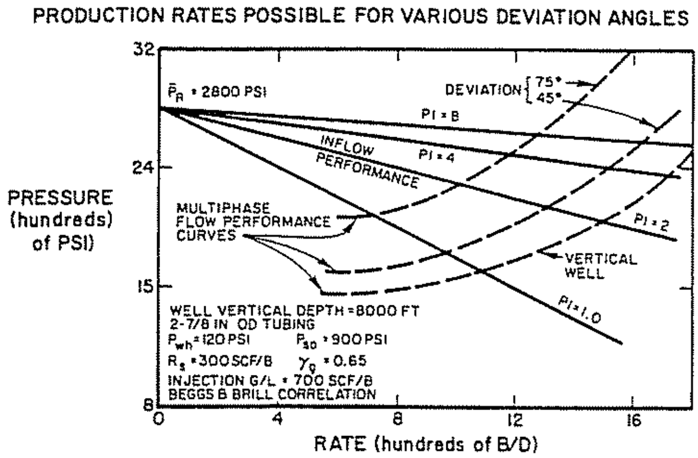

Figure 3.15 Production Rates Possible for Various Deviation Angles

where:

P_{wh} = wellhead pressure (psia)
GLR = gas-liquid ratio (Mcf/bbl)
q = flow rate (b/d)
d = choke diameter (64*ths* of an inch)

3.512 GAS FLOW THROUGH A CHOKE

Texas A & I University published research work in 1946 that it had conducted concerning gas flow through the Thornhill-Craven standard 6-in.-long positive flow bean.[18] The flow coefficients were found to be:

Nominal choke dia., in.	Average flow coefficient, C	Average discharge coefficient, C_d
⅛	5.65	0.7602
3/16	13.39	0.8049
¼	24.57	0.8324
5/16	38.48	0.8322
⅜	55.85	0.8324
7/16	75.56	0.8275
½	98.07	0.8278
⅝	152.26	0.8198
¾	224.62	0.8399

Note that the discharge coefficients become essentially constant at 0.830 for sizes greater than 3/16 in.

The above coefficients are used in the equations:

$$q = \frac{C\,P_u}{\sqrt{\gamma_g T}}$$

and:

$$q = \frac{605.37\,C_d\,A\,P_u}{\sqrt{\gamma_g T}} \tag{3.14}$$

where:

q = Mcfd at 14.65 psia and 60°F
C = flow coefficient
C_d = coefficient of discharge
P_u = pressure upstream of choke, psia
A = area of choke, in.²
γ_g = specific gravity of gas
T = temperature (absolute)

The basic formula for gas flow through an orifice is as follows:

$$q = \frac{155.5 C_d\,A\,P_u \sqrt{2g\,\frac{K}{K-1}\,(R^{2/K} - R^{(K+1/K)})}}{\sqrt{\gamma_g T}} \tag{3.15}$$

where:

g = acceleration of gravity
K = C_p/C_v = ratio of specific heats at constant pressure and constant volume
P_D = downstream pressure (psia)
R = ratio $P_D/P_u \geqq R_o$
R_o = critical flow pressure ratio

$$R_o = \left(\frac{2}{K+1}\right)^{(K/K-1)}$$

Using air as a basis:

$$K = 1.41$$
$$R_o = 0.5266$$

and:

$$q = \frac{605.37\,C_d\,A\,P_u}{\sqrt{\gamma_g T}} \tag{3.16}$$

This equation is valid as long as the downstream pressure is less than approximately one-half of the upstream pressure.

3.6 TWO-PHASE FLOW IN PIPELINES, BY DR. ZELIMIR SCHMIDT AND DR. DALE R. DOTY

3.61 INTRODUCTION

There are numerous production systems whereby pressure losses as well as heading and slugging in pipelines become very important. Large production lines such as those in the Prudhoe Bay area or ocean-floor completion lines such as those in the North Sea offer specific examples of large lines for two-phase flow.

The pigging of these lines may also become important, and calculations for pigging become critical.

The effects of riser pipes on offshore platforms become critical in predicting slugging in horizontal lines. Calculations as to slug sizes and frequency are critical in designing separation facilities to handle the large separated slugs of gas and liquid.

This section presents a discussion and a manner of solution to this problem.

3.62 STEADY-STATE PRESSURE LOSS CALCULATIONS

The prediction of pressure gradients, liquid holdups, and flow patterns for pipelines that are transporting both a gas and liquid phase is a common problem in the petroleum industry. Such two-phase flow occurs frequently in well tubing and in flow lines. The flow can be vertical, inclined, or horizontal, and the resulting interaction between phases can create a number of different possible flow patterns. Figure 3.16 displays the commonly accepted two-phase flow patterns. Flow pattern, along with pipe inclination, liquid holdup, fluid composition, flow rates, and fluid physical properties, determines the nature of the pressure loss along the length of the pipeline. Because the exact effect of each of these factors in determining the pressure loss is not theoretically known, physical correlations combined with the pressure-loss equation are required to solve practical problems. The results that follow are also valid for single-phase flow.

(1) *Steady-State Continuity Equation.* The theoretical basis for determining pressure loss results from combining the physical laws of conservation of mass and momentum.

Under steady-state conditions, the conservation of mass for a pipeline segment of length ΔL (See Figure 3.17) can be expressed as:

Rate of mass transport across position 1
= rate of mass transport across position 2.

In terms of the two-phase density (ρ) and the two-phase velocity (v) at positions 1 and 2, the conservation of mass can be expressed as:

$$\rho_1 A\, v_1 = \rho_2 A\, v_2 \qquad (3.17)$$

where it is assumed that ρ and v are constant across the cross-sectional area (A) of the pipe. Dividing this equation by ΔL and taking the limit as ΔL goes to zero yields the steady-state continuity equation:

$$\frac{d(\rho v)}{dL} = 0 \qquad (3.18)$$

(2) *Steady-State Pressure Loss Equation.* Under steady-state conditions, the momentum in a pipe seg-

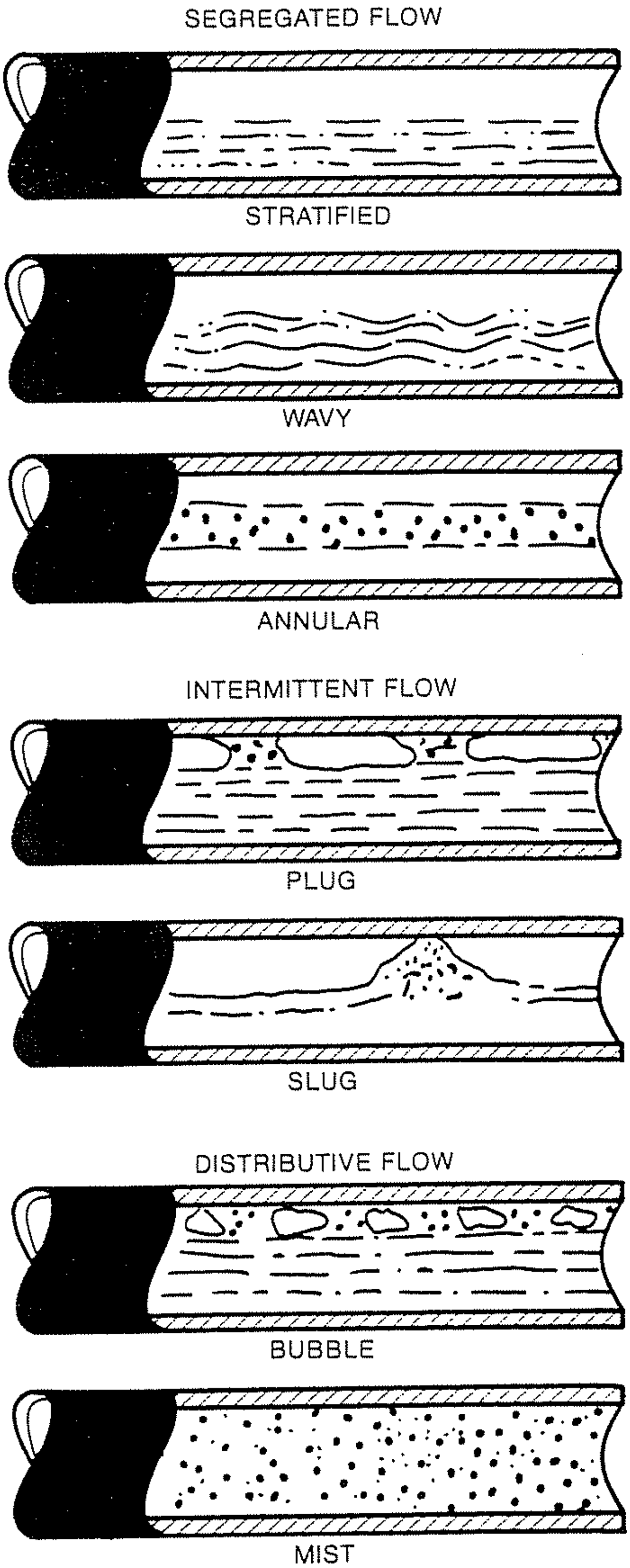

Figure 3.16 Schematic Diagram of Possible Flow Patterns in Two-Phase Pipelines

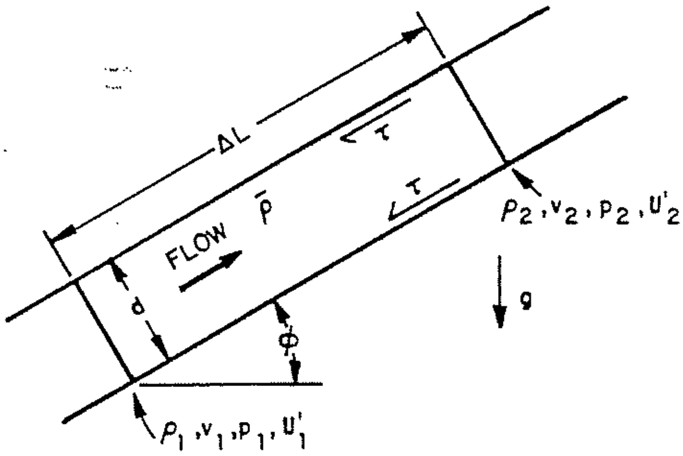

Figure 3.17 Flow in a Pipe Segment

ment of length ΔL does not change; therefore, the conservation of the linear momentum can be expressed as:

Rate of momentum transport across position 1
− Rate of momentum transport across position 2
+ the sum of the forces acting on the fluid = 0

In terms of the variables defined in Figure 3.17, this equation can be expressed as:

$$\left(\frac{\rho_1 v_1}{g_c}\right)(A\, v_1) - \left(\frac{\rho_2 v_2}{g_c}\right)(A\, v_2) + P_1 A - P_2 A - \frac{g}{g_c}\bar{\rho}\sin\theta\, A\, \Delta L - \tau(\pi\, d\, \Delta L) = 0 \quad (3.19)$$

where τ is the two-phase wall shear stress. Dividing this equation by ΔL and A and taking the limit as ΔL goes to zero yields:

$$-\frac{d}{dL}\left(\frac{\rho\, v^2}{g_c}\right) - \frac{dP}{dL} - \frac{g}{g_c}\rho\sin\theta - \tau\frac{\pi d}{A} = 0 \quad (3.20)$$

Differentiating $\rho\, v^2$ and using the continuity equation gives:

$$\frac{dP}{dL} = -\frac{\rho\, v}{g_c}\frac{dv}{dL} - \frac{g}{g_c}\rho\sin\theta - \tau\left(\frac{\pi d}{A}\right) \quad (3.21)$$

It is traditional to view this equation as a pressure *loss* equation. Therefore, the total pressure loss is considered to be composed of acceleration, elevation, and friction components:

$$\left(\frac{dP}{dL}\right)_{total} = \left(\frac{dP}{dL}\right)_{acceleration} + \left(\frac{dP}{dL}\right)_{elevation} + \left(\frac{dP}{dL}\right)_{friction}$$

This equation is more difficult to apply than it would appear from a first examination. The difficulty arises from the fact that both the two-phase velocity and density are not truly constant across the pipe cross section. Also, the two-phase velocity and density are complicated by the fact that, for most flow patterns, the gas and the liquid phases are not moving with the same actual velocity. This "slippage" between phases implies that, in addition to the gas and liquid mass flow rates, a knowledge of the liquid and gas holdups is required to determine the two-phase velocity and density. This, along with additional information, must be supplied by external correlations.

(3) *Two-phase correlations.* Use of the pressure loss equation requires a determination of two-phase velocity, density, and wall shear stress. In order to simplify the wall shear stress term τ, it is traditional to introduce a dimensionless Moody friction factor (f) defined as the ratio of four times the two-phase wall shear to the two-phase kinetic energy per unit volume:

$$f = 4\frac{\tau}{(\rho\, v^2/2\, g_c)} \quad (3.22)$$

In terms of the two-phase friction factor, the pressure loss equation can be expressed as:

$$\left(\frac{dP}{dL}\right)_{total} = -\frac{\rho v}{g_c}\frac{dv}{dL} - \frac{g}{g_c}\rho\sin\theta - \frac{f\,\rho\, v^2}{2\, g_c\, d} \quad (3.23)$$

The problem of calculating the two-phase pressure loss has been reduced to integrating the pressure loss along the length of the pipeline. This can be accomplished only when proper values can be assigned to ρ, v, and f. As observed earlier, the definition of ρ, v, and f for each portion of the pipeline depends upon the steady-state gas and liquid flow rates, the nature of the flow pattern, liquid holdup, and the fluid physical properties for each phase. It is the purpose of two-phase flow correlations to define the relationship between these variables.

The two-phase flow correlations commonly used are the Dukler-Eaton[13] and the Beggs and Brill[9] correlations. The Dukler-Eaton correlation was developed for horizontal flow in pipelines and gives reasonably good results for pressure loss and liquid holdup predictions. However, the Dukler-Eaton correlation does not directly take the flow pattern into consideration.

The Beggs and Brill correlation removes this shortcoming by including the flow pattern in the pressure drop and liquid holdup calculations. Moreover, the correlation was developed for any pipeline inclination. When compared to the Dukler-Eaton correlation, the Beggs and Brill correlation tends to slightly underpredict pressure losses, and the Dukler-Eaton tends to slightly overpredict pressure losses.

It is very important to accurately define the flow pattern, since the pressure loss calculation is flow-regime dependent. The different flow patterns arise from different physical distributions of gas and liquid in the pipeline. A schematic diagram of possible flow patterns for pipelines is shown in Figure 3.16. Various "maps" are available for predicting the flow pattern from the gas and liquid flow rates, the pipeline inclination, and the fluid physical properties, and each pressure loss correlation uses its own map. The Mandhane et al.[19] map shown in Figure 3.18 is probably the most widely used map for predicting flow pattern because flow pattern can be predicted from a knowledge of the gas and liquid flow rates. The pipeline outlet flow pattern under steady-state flow is of interest, since slug flow can require special liquid storage facilities. The flow-pattern maps commonly used are the Mandhane map, the Beggs map,[9] and the Mukherjee map.[20] The use of more than one map serves as a method of cross-referencing.

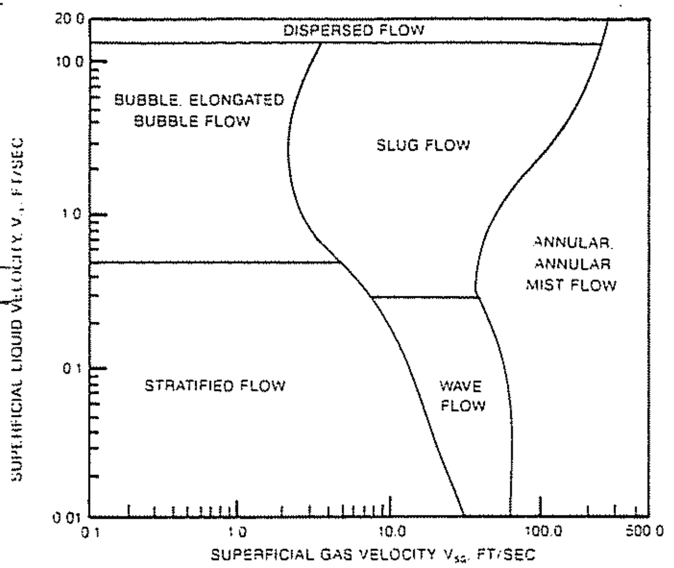

Figure 3.18 Flow Pattern Map for Two-Phase Pipelines (after Mandhane et al.)[6]

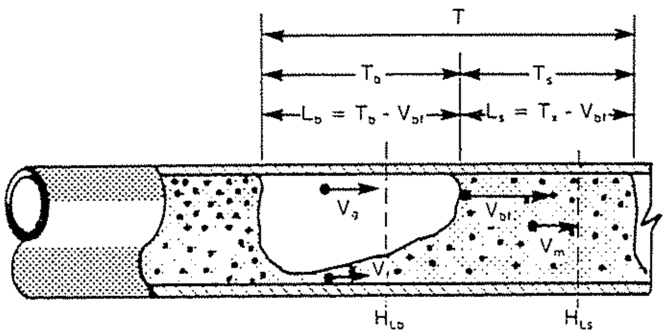

T = PERIOD
T_s = LIQUID SLUG RESIDENCE TIME
T_b = GAS BUBBLE RESIDENCE TIME
L_s = LIQUID SLUG LENGTH
L_b = GAS BUBBLE LENGTH
V_g = GAS VELOCITY
V_f = LIQUID FILM VELOCITY
V_{bf} = GAS BUBBLE VELOCITY
V_m = MIXTURE VELOCITY
H_{Ls} = LIQUID HOLDUP IN LIQUID SLUG
H_{Lb} = LIQUID HOLDUP IN GAS BUBBLE

Figure 3.19 Schematic of an Idealized Liquid Slug and Gas Bubble—Slug Unit

3.63 LIQUID FLOW BEHAVIOR PREDICTIONS

Calculations have been performed for two separate cases that can result in liquid slugs flowing out of the pipeline. These include normal slug flow and pigging. The calculations for each case are different and are given in the following sections.

(1) *Normal slug flow.* When steady-state flow occurs in a pipeline, time-averaged gas and liquid mass flow rates are constant at the inlet and outlet of the pipeline. If slug flow occurs, instantaneous flow rates and pressures are not constant, and liquid slugs and following gas bubbles vary in velocity and length in a random way. Proper design of separators must account for random slug flow and be based on the flow characteristics of slugs.

Figure 3.19 shows a schematic diagram of a slug flow model in a horizontal pipe.[21] The model is composed of a gas bubble and a liquid slug containing many small bubbles. The hydrodynamic model was developed using the following assumptions:

(1) Small gas bubbles and liquid in the liquid slug travel with the same velocity.
(2) Liquid film does not contain any gas bubbles.
(3) Negligible liquid droplets occur in the gas bubble.

To develop a relationship among variables, an overall mass balance for the liquid in the slug unit of length $(L_b + L_s)$ in Figure 3.19 was used. The mass of liquid that flows out of the pipe during one period T is the sum of the mass of the liquid in the liquid slug m_{L_s} and in the liquid film m_{L_f}. However, as the slug flows out of the pipe with a velocity v_m, the gas bubble following the liquid slug overruns or bypasses part of the liquid slug. The portion of liquid that is overrun will not flow out with the slug. The mass balance can be expressed as:

$$m_{L_t} = m_{L_s} + m_{L_f} - m_{L_o} \tag{3.24}$$

where:

$$m_{L_t} = v_{sL}\, T\, A\, \rho_L$$
$$m_{L_s} = v_{bf} T_s\, A\, H_{Ls}\, \rho_L$$
$$m_{L_f} = v_{bf} T_b\, A\, H_{Lb}\, \rho_L$$
$$m_{L_o} = (v_{bf} - v_m)\, T\, A\, H_{Ls}\, \rho_L$$

Substituting the mass equations into Equation 3.24 and solving for v_{sL} gives:

$$v_{sL} = v_{bf}\frac{T_s}{T} H_{Ls} + v_{bf}\frac{T_b}{T} H_{Lb} - (v_{bf} - v_m) H_{Ls} \tag{3.25}$$

A similar development for mass conservation of gas phase results in:

$$m_{gt} = m_{gb} + m_{gs} - m_{go} \tag{3.26}$$

where:

$$m_{gt} = v_{sg}\, T\, A\, \rho_g$$
$$m_{gb} = v_{bf}\, T_b\, A\,(1 - H_{Lb})\, \rho_g$$
$$m_{gs} = v_b\, T_s\, A\,(1 - H_{Ls})\, \rho_g$$
$$m_{go} = (v_{bf} - v_m)\, T\, A\,(1 - H_{Ls})\, \rho_g$$

Substituting the mass equations into Equation 3.26 and solving for v_{sg} gives:

$$v_{sg} = v_{bf}\frac{T_b}{T}(1 - H_{Lb}) + v_{bf}\frac{T_s}{T}(1 - H_{Ls}) - (v_{bf} - v_m)(1 - H_{Ls}) \tag{3.27}$$

Consider a coordinate system that travels in the pipe with the velocity of the nose of the gas bubble, v_{bf}. Continuity considerations on the gas phase across the liquid slug and the gas bubble result in:

$$(v_{bf} - v_m)\, A\,(1 - H_{Ls})\, \rho_g = (v_{bf} - v_g)\, A\,(1 - H_{Lb})\, \rho_g \tag{3.28}$$

Solving for v_g gives:

$$v_g = v_{bf} - (v_{bf} - v_m)\frac{1 - H_{Ls}}{1 - H_{Lb}} \tag{3.29}$$

A similar development for continuity consideration on the liquid phase results in:

$$(v_{bf} - v_m) A H_{Ls} \rho_L = (v_{bf} - v_f) A H_{Lb} \rho_L \quad (3.30)$$

Solving for the liquid film velocity gives:

$$v_f = (v_m - v_{bf}) \frac{H_{Ls}}{H_{Lb}} + v_{bf} \quad (3.31)$$

The time average liquid holdup, H_L, can be expressed in terms of the liquid holdup and the period of the liquid slug and gas bubble. Thus:

$$H_L T = H_{Ls} T_s + H_{Lb} T_b \quad (3.32)$$

Combining Equations 3.32 and 3.25 and solving for v_{bf} gives:

$$v_{bf} = \frac{v_{sL} - v_m H_{Ls}}{H_L - H_{Ls}} \quad (3.33)$$

Variables v_f, v_g, and v_{bf} are uniquely defined with Equations 3.29, 3.31, and 3.33. Combining Equations 3.25 and 3.32 results in an equation that does not contain T_b or T_s. Thus, a new equation must be developed for either T_b or T_s. The average liquid slug length is related to the liquid slug residence time or period by:

$$T_s = \frac{\bar{L}_s}{v_{bf}} \quad (3.34)$$

Equations 3.27, 3.29, 3.31, 3.33, and 3.34 must be solved to obtain values of v_f, v_g, v_{bf}, T_s, and T_b. To solve these equations, it is necessary to have empirical correlations for H_L, H_{Ls}, H_{Lb} and $\bar{L}_s$. Experimental data were available from two Tulsa University test facilities. The tests were conducted in 2-in. pipe with the Piping Components Facility and in 1½-in. pipe with the Inclined Flow Facility. Kerosene and air were used for fluids, and liquid holdup was measured with a capacitance sensor and associated electronics. Data collected included one hundred tests for H_L and approximately fifty tests each for H_{Ls} and H_{Lb}. The following empirical correlations were developed using v_{sL} and v_{sg} as independent variables:

$$H_{Lb} = 1.0 - 0.01 \exp [a + b \ln v_{sg} + c(\ln v_{sg})^2] \quad (3.35)$$

where:

$$a = 4.47108 - 0.13691\ v_{sL}$$
$$b = -0.05831 + 0.08070\ v_{sL}$$
$$c = 0.02124 - 0.01169\ v_{sL}$$

$$H_{Ls} = 1.0 - 0.01 \exp [a + b \ln v_{sg} + c (\ln v_{sg})^2] \quad (3.36)$$

where:

$$a = -0.52728 + 0.43839\ v_{sL}$$
$$b = 2.01451 - 0.17878\ v_{sL}$$
$$c = -0.20271 + 0.01819\ v_{sL}$$

$$H_L = 1.0 - 0.01 \exp [a + b \ln v_{sg} + c (\ln v_{sg})^2] \quad (3.37)$$

where:

$$a = 4.27143 - 0.26172\ v_{sL}$$
$$b = 0.06495 + 0.12992\ v_{sL}$$
$$c = 0.00406 - 0.01826\ v_{sL}$$

An empirical correlation for the average slug length was developed using data from the Prudhoe Bay field of Alaska.[22] The data were collected on 16- and 12-in. two-phase pipelines. The slug length was found to be log-normally distributed with a homogeneous variance of 0.3. A linear regression analysis of experimental average liquid slug lengths resulted in the following correlation.

$$\bar{L}_s = \exp [-2.663 + 5.441 (\ln d)^{0.5} + 0.059 \ln v_m] \quad (3.38)$$

During production of a liquid slug from a pipeline, the liquid slug and film are continuously overrun by the faster moving gas bubble. Thus, not all of the slug length in the pipeline is produced. The total liquid volume produced from the pipeline in time T is defined by:

$$V_{LP} = v_{sL} T A \quad (3.39)$$

Distribution of this liquid is not uniform in the pipe, and part comes from the liquid slug and part from the liquid film beneath the gas bubble. The liquid produced from the liquid slug during time T_s is:

$$V_{LsP} = v_m T_s A H_{Ls} \quad (3.40)$$

The liquid produced from the liquid film during time T_b is the difference between V_{LP} and V_{Lsp} and can also be calculated from:

$$V_{LfP} = v_f T_b A H_{Lb} \quad (3.41)$$

The volume of the liquid slug in the pipeline, which is not totally produced because of gas-bubble overrun, is defined by:

$$V_{Ls} = v_{bf} T_s A H_{Ls} \quad (3.42)$$

The difference between V_{Ls} and V_{LsP} will not be produced with the slug. The total liquid in a slug unit (liquid slug and gas bubble) shown in Figure 3.19 is given as:

$$V_{LT} = v_{bf} T_b A H_{Lb} + v_{bf} T_s A H_{Ls} \quad (3.43)$$

This volume is greater than V_{LP} because of the overrunning phenomenon.

(2) *Pigging*. When gas and liquid flow into a pipeline, density differences tend to separate the phases. The gas flows more rapidly, leaving the liquid to flow along the bottom of the pipe at a much lower velocity. The liquid is moved because of the viscous drag of the gas on the free liquid surface.

Liquid holdup in a pipeline is primarily a function of liquid and gas volumetric flow rates and pipeline configuration. The liquid holdup contained in a pipeline, for a constant liquid flow rate, decreases rapidly with increasing gas flow rates. At higher gas flow rates when annular or mist flow prevails, liquid holdup approaches asymptotically a value of the no-slip holdup. The liquid holdup always increases with an increase in liquid flow rate. When gas and liquid flow in hilly terrain pipelines, liquid holdup increases in the uphill sections and decreases in the downhill sections. As a result of this, liquid tends to accumulate in the low spots or valleys of the pipeline.

The pressure drop in a pipeline increases as liquid holdup increases. The pipeline efficiency is therefore inversely proportional to the liquid holdup. In order to increase the efficiency of a pipeline, liquid holdup must be reduced. This can be accomplished by pigging the line at regular intervals using rubber spheres inflated to the desired diameter. The major variable dur-

ing pigging is the volume of liquid that will be removed by a sphere. Liquid separation or storage volume at the sphere receiving end must be capable of handling the maximum size of slug. The velocity with which the liquid slug exits the pipe is assumed to be that of the sphere. Assuming 100% removal efficiency of a sphere and that all liquid removed by the sphere is in the form of a continuous slug, the volume can be estimated by integrating the difference between the liquid holdup and the no-slip holdup in the pipeline. This additional liquid volume to be handled by slug catchers can be estimated from:

$$\begin{aligned} V_L &= A \int_0^L (H_L - v_{sL}/v_m)\, dX \\ &\approx A \sum_{i=1}^{n} (\overline{H}_L\, \Delta X - \overline{v}_{sL}/\overline{v}_m\, \Delta X) \end{aligned} \tag{3.44}$$

Thus, the pipeline is divided into n calculation length increments, and average liquid holdup and no-slip holdup are determined for each increment. Summing the liquid volumes in all calculation increments using Equation 3.44 yields an estimate of the total liquid volume swept by a sphere.

A more rigorous estimate of the liquid slug volume can be obtained by developing an expression that performs a volumetric balance at the time the slug formed by the sphere first reaches the outlet end of the pipeline. The volume of liquid swept from the inlet to the sphere location, X, must be equal to the void volume ahead of the sphere that would exist, assuming steady-state flow without spheres. Thus:

$$A \int_0^X (H_L - \lambda_L)\, dX = A \int_X^L (1 - H_L)\, dX \tag{3.45}$$

Equation 3.45 would require a numerical solution. However, some simplifications can be made. Comparison of H_L and λ_T values from inlet to outlet in steady-state flow shows that very little change occurs in either variable. Equation 3.45 then becomes:

$$A\,(H_L - \lambda_L)\, X = A\,(1 - H_L)(L - X)$$

Algebraic simplification yields an expression for slug length:

$$L_s = L - X = L \left[\frac{H_L - \lambda_L}{1 - \lambda_L}\right]$$

Comparison with Equation 3.44 suggests that a more accurate estimate can be obtained from:

$$L_s = \frac{5.614\, V_L}{A\,(1 - \lambda_L)} \tag{3.46}$$

where:

V_L = liquid volume, bbl
λ_L is based on outlet conditions

The time required to produce the liquid slug can be calculated from:

$$T_{Pr} = \frac{L_s}{v_{sg}} \tag{3.47}$$

The time required for the liquid slug to reach the outlet after introducing a sphere at the inlet is:

$$T = \frac{L - L_s}{v_{sg}} \tag{3.48}$$

The assumption of 100% removal efficiency is not possible in a pipeline. As the sphere travels, some amount of liquid will be bypassed. The amount of liquid slipping past the sphere will affect the velocity of the sphere, the outlet liquid velocity, and the slug length.

SUMMARY

There are numerous areas whereby additional study is needed in the area of multiphase flow.

Emulsions are a very difficult problem, and the prediction of when emulsions can be expected to form is questionable. Once an emulsion exists, the prediction of pressure loss becomes more complex and questionable.

Present-day correlations also give trouble in handling viscous crudes. The principal correlations available fail to predict accurate results and give widely varying answers.

The prediction of well loading also leaves much to be desired, with the Ros and Gray correlation appearing reasonably good for condensate wells that may also produce some water. The principal multiphase flow correlations give widely varying results.

REFERENCES

1. Brown, Kermit E. and H. D. Beggs. *Technology of Artificial Lift Methods.* Vol. 1. Tulsa, Oklahoma: PennWell Books, 1980.
2. Aziz, K., G. W. Govier, and M. Fogarasi. "Pressure Drop in Wells Producing Oil and Gas." *Journal of Canadian Petroleum Technology* (July–September 1972), pp. 38–48.
3. Brill, J. P. and H. D. Beggs. *Two-Phase Flow in Pipes.* Tulsa: University of Tulsa, 1978.
4. Hagedorn, Alton R. and Kermit E. Brown. "Experimental Study of Pressure Gradients Occurring During Continuous Two-Phase Flow in Small Diameter Vertical Conduits." *Journal of Petroleum Technology* (April 1965), p. 475.
5. Ros, N. C. J. "Simultaneous Flow of Gas and Liquid as Encountered in Well Tubing." *Journal of Petroleum Technology,* 13 (October 1961), p. 1037.
6. Duns, H. Jr. and N. C. J. Ros. "Vertical Flow of Gas and Liquid Mixtures in Wells." *6th World Petroleum Congress,* Frankfurt, Germany.
7. Gray, H. E. "Vertical Flow Correlations in Gas Wells." *User Manual for API 14B Subsurface Controlled Safety Valve Sizing Computer Program.* App. B. June, 1974.
8. Orkiszewski, J. "Predicting Two-Phase Pressure Drops in Vertical Pipe." *Journal of Petroleum Technology* (June 1967).
9. Beggs, H. D. and J. P. Brill. "A Study of Two Phase Flow in Inclined Pipes." *Journal of Petroleum Technology* (May 1973), p. 607.
10. Katz, Donald L. et al. *Handbook of Natural Gas Engineering.* New York, New York: McGraw Hill Book Co., 1959, pp. 309–312.
11. Brown, K. E. *Technology of Artificial Lift Methods.* Vols. 3a and 3b. Tulsa, Oklahoma: PennWell Books, 1980.
12. Dukler, A. E., et al. "Gas-Liquid Flow in Pipelines." *Research Results.* Vol. 1. American Gas Association, American Petroleum Institute, May 1969.
13. Eaton, B. A. et al. "The Prediction of Flow Patterns, Liquid Holdup and Pressure Losses Occurring During Continuous Two-Phase Flow in Horizontal Pipelines." *Transactions of the AIME* (1966).
14. Lockhart, R. W. and R. C. Martinelli. "Proposed Correlation of Data for Isothermal Two-Phase, Two-Component Flow in Pipes." *Chemical Engineering Progress,* v. 45, N-1 (January 1949), pp. 39–48.
15. Baker, Ovid. "Design of Pipelines for the Simultaneous Flow of Oil and Gas." *Oil and Gas Journal,* 53 (1954), pp. 185–195.
16. Flanigan, Orin. "Effect of Uphill Flow on Pressure Drop in Design of Two-Phase Gathering Systems." *Oil and Gas Journal* (March 10, 1958), p. 132.

17. Gilbert, W. E. "Flowing and Gas-Lift Well Performance." *Drilling and Production Practice.* API, 1954, p. 143.
18. Texas A & I University. *Report on the Calibration of Positive Flow Beans.* Kingsville, Texas, 1946.
19. Mandhane, J. M. et al. "A Flow Pattern Map for Gas-Liquid Flow in Horizontal Pipes." *International Journal of Multiphase Flow,* 1 (1974), pp. 537–553.
20. Mukherjee, H. "An Experimental Study of Inclined Two-Phase Flow." Diss., University of Tulsa, 1979.
21. Schmidt, Z. "Experimental Study of Two-Phase Slug Flow in a Pipeline-Riser Pipe System." Diss., University of Tulsa, 1977.
22. Brill, J. P. et al. "Analysis of Two-Phase Tests in Large Diameter Prudhoe Bay Field Flowlines." *SPE 8305.* SPE Annual Fall Meeting, September, 1979.
23. Baker, O. et al. "Gas-Liquid Flow in Pipelines." *Design Manual.* Vol. 2. AGA-API Project NX-28, October 1970.
24. Corteville, T. et al. "Two-Phase Flow Key to Offshore Line Design." *Oil and Gas Journal* (August 10, 1981), pp. 71–75.
25. Cunlife, R. S. "Prediction of Condensate Flow Rates in Large Diameter High Pressure Wet Gas Pipelines." *APEA Journal* (1978), p. 171.
26. Kreith, F. *Principles of Heat Transfer.* New York, New York: Intext Education Publishers, 1973.
27. Vohra, I. R. et al. "Comparison of Liquid Holdup and Friction Factor Correlations for Gas-Liquid Flow in Horizontal Pipes." *Journal of Petroleum Technology* (May 1975), pp. 564–567.

Chapter **4**

Nodal systems analysis

by Kermit E. Brown, Dale R. Doty, Carl Granger, Lewis Ledlow, Joe Mach, Eduardo Proaño, Zelimir Schmidt, and A. Paul Szilas

4.1 INTRODUCTION

The objective of nodal systems analysis is to combine the various components of the oil or gas well in order to predict flow rates and to optimize the various components in the system. This approach was discussed by Mach, Proaño, and Brown and is given here essentially the same as in the original paper (copyright SPE of AIME):[1]

An approach is presented for applying systems analysis to the complete well system, from the outer boundary of the reservoir to the sand face, across the perforations and completion section to the tubing intake, and up the tubing string, including any restrictions and downhole safety valves, the surface choke, the flow line and separator.

Figure 4.1 shows a schematic of a simple producing system. This system consists of three sections or modules:

(1) flow through porous medium
(2) flow through vertical or directional conduit
(3) flow through horizontal pipe or inclined flow line

Figure 4.2 shows the various pressure losses that can occur in the more complex system from the reservoir to the separator. Beginning from the reservoir, these are noted as:

$\Delta P_1 = \bar{P}_r - P_{wf_s}$ = pressure loss in porous medium
$\Delta P_2 = P_{wf_s} - P_{wf}$ = pressure loss across completion
$\Delta P_3 = P_{UR} - P_{DR}$ = pressure loss across regulator, choke, or tubing nipple
$\Delta P_4 = P_{USV} - P_{DSV}$ = pressure loss across safety valve
$\Delta P_5 = P_{wh} - P_{DSC}$ = pressure loss across surface choke
$\Delta P_6 = P_{DSC} - P_{SEP}$ = pressure loss in surface flow line
$\Delta P_7 = P_{wf} - P_{wh}$ = total pressure loss in tubing string, which includes ΔP_3 and ΔP_4
$\Delta_8 = P_{wh} - P_{SEP}$ = total loss in surface flow line, including surface choke

The various well configurations may vary from the very simple system of Figure 4.1 to the more complex system of Figure 4.2 or any combination thereof, and present-day completions more realistically include the various configurations of Figure 4.2 (especially offshore).

This chapter will discuss the manner in which to interrelate the various pressure losses. In particular, the ability of the well to produce fluids will be interfaced with the ability of the piping system to handle these fluids. The manner in which to treat the effect of the various components will be shown by a nodal concept.

In order to solve the total-producing-system problems, nodes are placed to segment the portion defined by different equations or correlations.

Figure 4.3 has been prepared showing locations of the various nodes. This figure is the same as Figure 4.2 except only the node positions are shown. A node is classified as functional when a pressure differential exists across it and the pressure or flow-rate response can be represented by some mathematical or physical function. More realistically, we will refer to a node at the bottom of the well, at the top of the well, etc., as a solution node. These two solution positions were discussed by Brown and Beggs.[2]

Node 1 represents the separator pressure, which is usually regulated at a constant value; however, some separator pressures do change with rate and should be properly accounted for. There are two positions whereby the pressures are not functions of flow rates. These are $\bar{P}_r$ at node 8 and P_{SEP} at node 1. For this reason, any trial-and-error solution to the total system problem must be started at node 1 (P_{SEP}), node 8 ($\bar{P}_r$), or both node 1 and 8 if an intermediate node such as 3 or 6 is selected as the solution node. Once the solution node is selected, the pressure drops or gains from the starting point are added until the solution node is reached. Example problems are worked to show the nodal system approach. For example, the flow rate possible can be determined by utilizing node 8 ($\bar{P}_r$), node

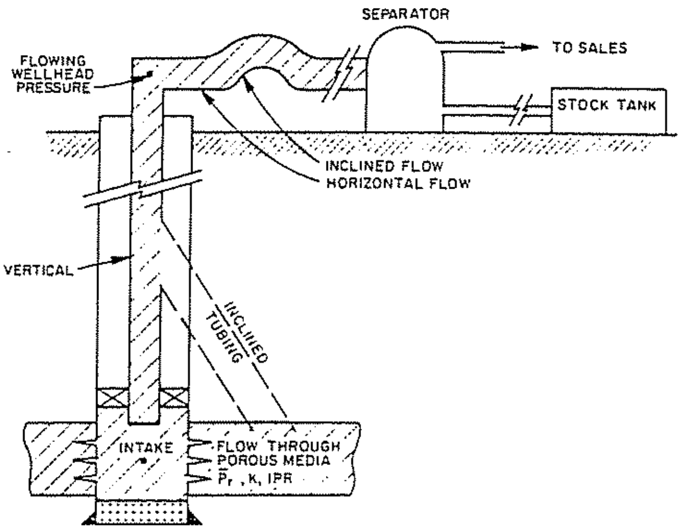

Figure 4.1 Complete Producing System

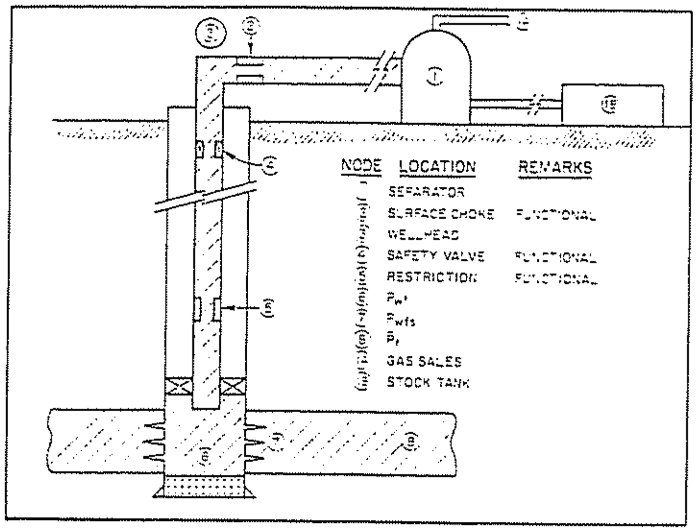

Figure 4.3 Location of Various Nodes (after Mach, Proaño, and Brown,[1] © SPE of AIME)

6 (P_{wf}), node 3 (P_{wh}), and node 1, (P_{sep}) or other positions. The node selected depends upon which component we want to isolate for evaluation. The effect of tapered strings, surface chokes, and safety valves can also be evaluated in this manner.

In summary, a nodal approach is presented in order to effectively evaluate a complete producing system. All of the components in the well, starting from the static pressure ($\bar{P}_r$) and ending at the separator, are considered. This includes flow through the porous me-

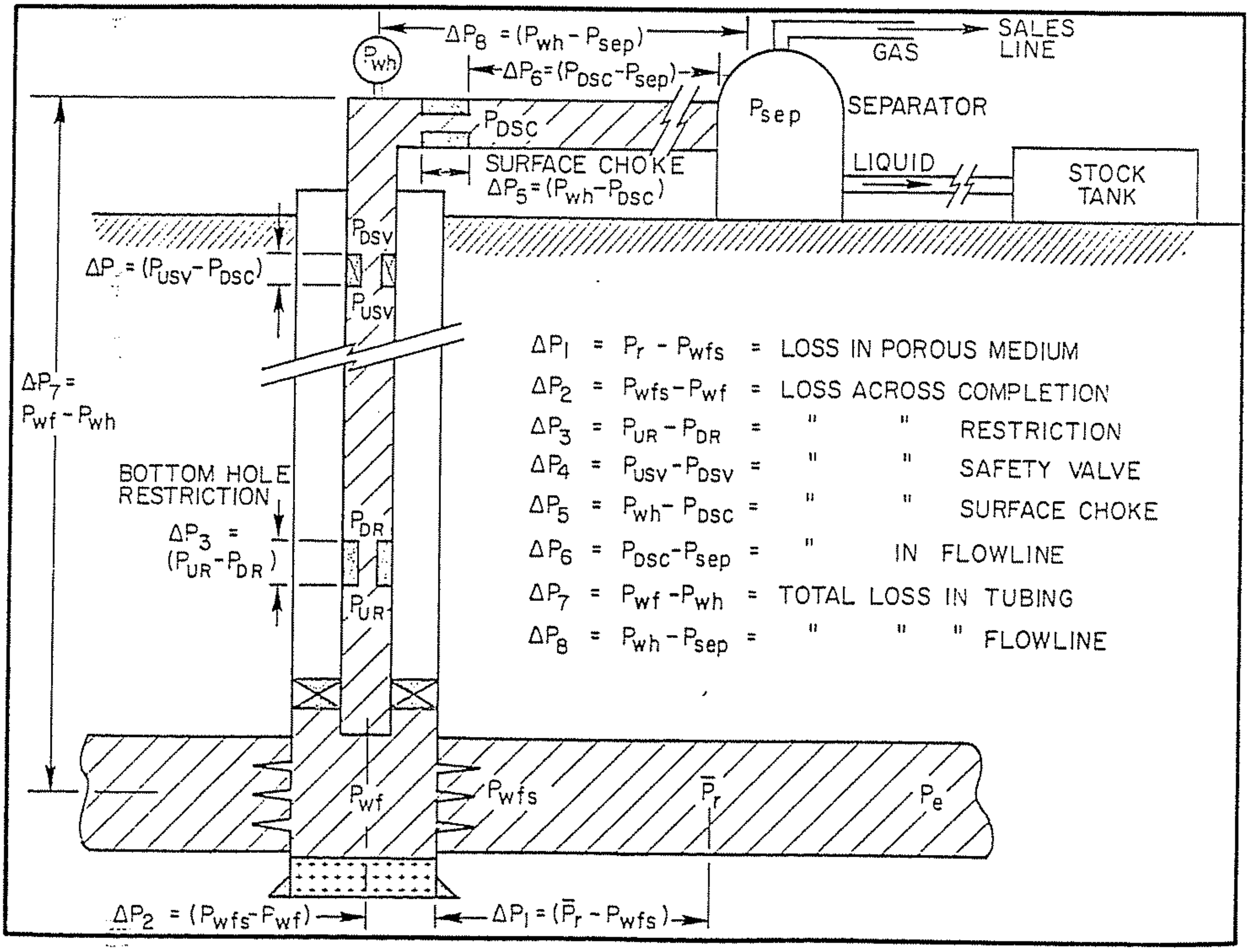

Figure 4.2 Pressure Losses in Complete System (after Mach, Proaño, and Brown,[1] © SPE of AIME)

dium, flow across the perforations and completion, flow up the tubing string with passage through a possible downhole restriction and safety valve, and flow in the horizontal flow line with passage through a surface choke and on to the separator.

Various positions are selected for solution nodes, and the pressure losses are converged on that point from both directions. Nodes can be effectively selected to show better the effect of certain variables such as inflow ability, perforations, restrictions, safety valves, surface chokes, tubing strings, flow lines, and separator pressures.

The appropriate multiphase flow correlations and equations for restrictions, chokes, etc., must be incorporated in the solution.

An effective means of analyzing an existing well, making recommended changes, or planning properly for a new well can be accomplished by the nodal system analysis. This procedure offers a means to more economically optimize producing wells.

4.2. SOLUTION PROCEDURE FOR OIL WELLS

4.21 INTRODUCTION

In order to best illustrate the solution procedure, the following example was presented by Mach, Proaño, and Brown[1] and will be worked by taking the solution node at several different positions.

EXAMPLE PROBLEM (OIL WELL)

Given Data (flowing oil well):

separator pressure: 100 psi	$\gamma_g = 0.65$
flow line: 2-in., 3,000 ft long	°API = 35
WOR: 0	T = 140°F
depth: 5,000 ft mid perf.	tubing size, 2⅜-in OD
GOR: 400/scf/bbl	$\overline{P}_r$: 2200 psi
productivity index = 1.0	

A simple system such as shown in Figure 4.4 is assumed.

For purpose of illustration only let us assume that a constant J of 1.0 exists for all flowing pressures

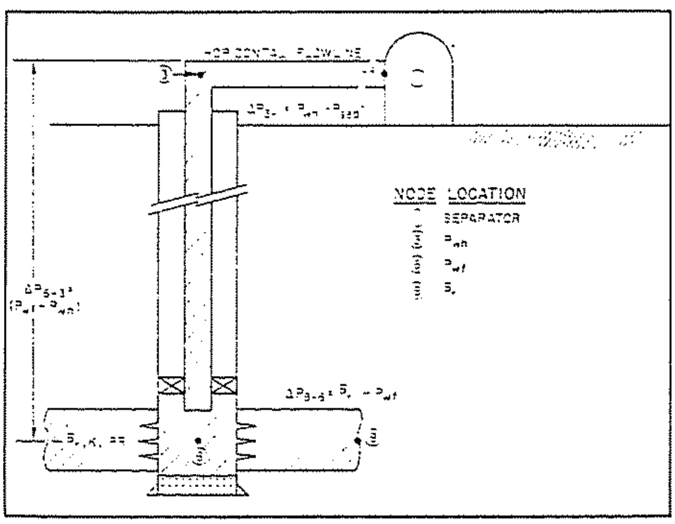

Figure 4.4 Nodes for Simple Producing System (after Mach, Proaño, and Brown,[1] © SPE of AIME)

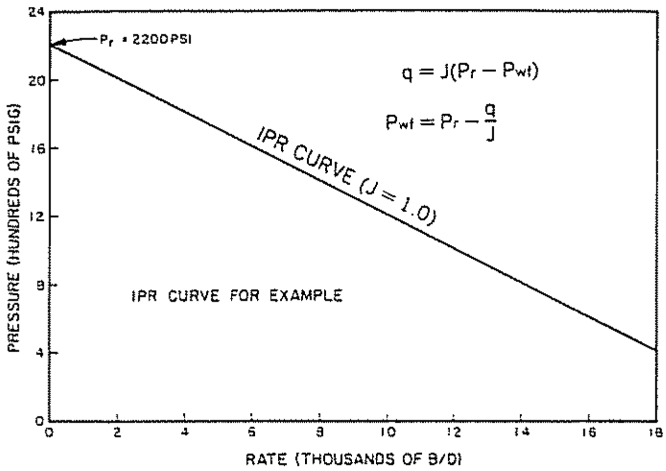

Figure 4.5 IPR Curve for Example Problem (Constant J = 1.0)

for this well. In reality, we know that two-phase flow will occur below the bubble-point pressure of 1,800 psi found from Figure 2.14. However, for the flow rates obtainable with 2⅜-in. OD tubing, the rates will differ very little from a straight-line J plot as compared to a Vogel solution (see Figure 4.5). In order to apply the constant J plus Vogel solution, we will assume a constant J of 1.0 from 2,200 psi, to 1,800 psia (bubble point) and a Vogel curve behavior from 1,800 to zero pressure.

$$q_{max} = q_b + \frac{JP_b}{1.8} = 1.0(2{,}200 - 1{,}800) + \frac{(1.0)(1{,}800)}{1.8}$$
$$= 400 + 1{,}000 = 1{,}400 \text{ b/d}$$

or for the constant J case, $q_{max} = 1.0(2{,}200 - 0) = 2{,}200$ b/d. Other pressures are assumed, and the IPR curve is constructed as noted in Figure 4.6.

For purposes of illustration, we will show the constant J solution for simplification in working the problem in most cases.

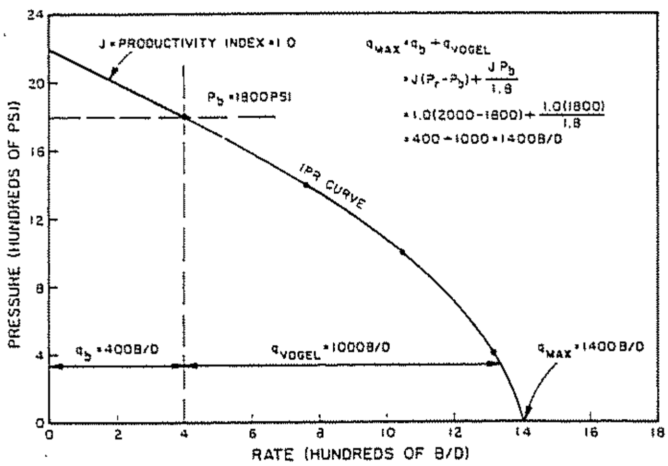

Figure 4.6 IPR Curve for Example Problem (Vogel Solution)

4.22 SOLUTION AT BOTTOM OF WELL (NODE 6 FROM FIGURE 4.3)

Probably the most common solution position is at the bottom of the well—that is, at the center of the

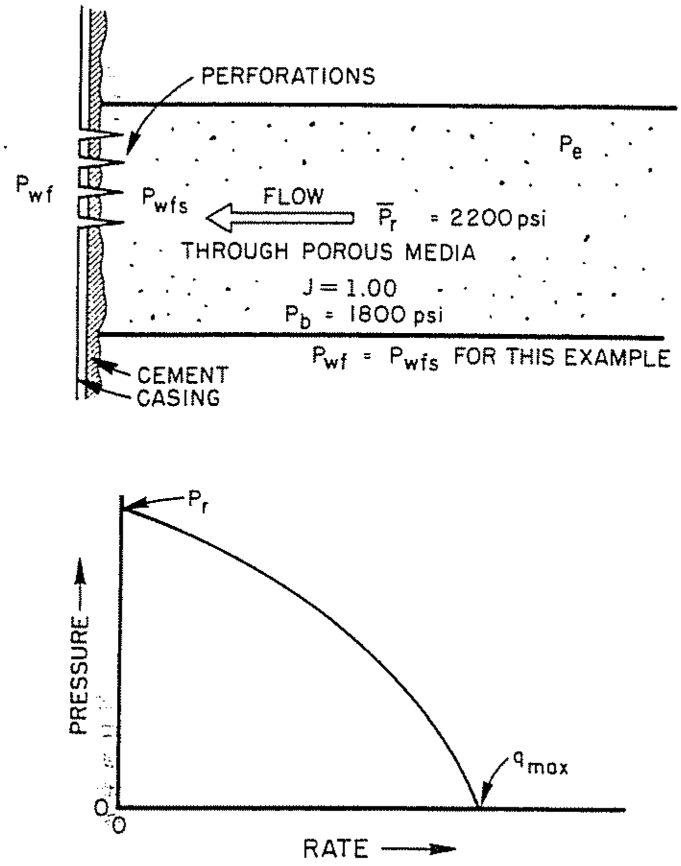

Figure 4.7 Reservoir Component

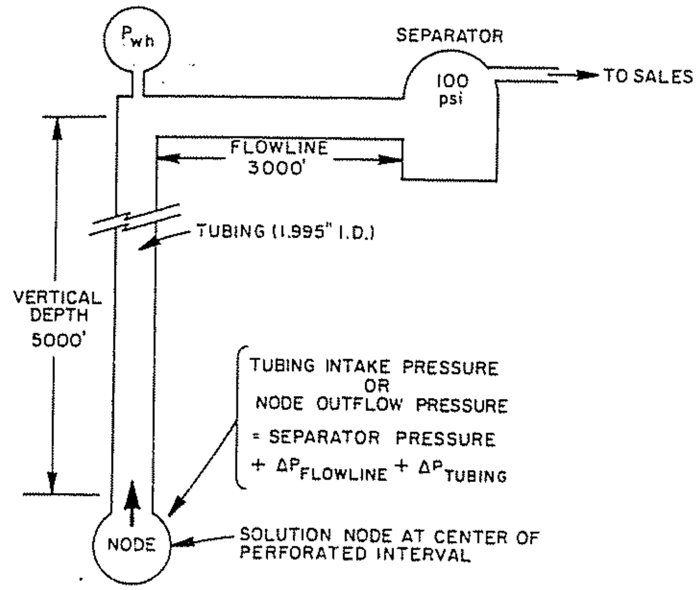

Figure 4.8 Piping for Simple System

borehole at the center of the perforated interval (node 6 from Figure 4.3).

In order to solve for the flow rate at this solution position, the entire system is divided into two components, the reservoir or well capability component and the total piping system component. Refer to Figure 4.7, which shows the reservoir component and Figure 4.5, which shows a plot of the reservoir or IPR curve for example problem 4.1.

Figure 4.8 shows the piping system component. For our example, it is assumed that no restrictions exist, and therefore we have only the flow line and tubing pressure losses.

4.221 CONSTRUCTING THE IPR CURVE

For the constant J case, this is relatively simple. Assume a flow rate and determine the corresponding flowing pressure. Then, extend a straight line between the static pressure of 2,200 psi at zero rate to the calculated point. For example, at a rate of 1,000 b/d, the flowing pressure is $P_{wf} = P_r - q/J = 2{,}000 - \frac{1{,}000}{1} =$ 1,200 psi. Note Figure 4.5, which shows the constant J assumption, and then Figure 4.6, which shows the more realistic Vogel solution. The same solution procedure would apply for either case—that is, constant J or Vogel.

In order to work this problem, a table should be prepared showing the various losses existing in the separate components.

Step-by-Step Solution Procedure

(1) Assume several flow rates and construct the IPR curve as noted in Figure 4.5 by solving for the corresponding pressures. The constant J equation is applicable in Figure 4.5, and Vogel's equation is applicable for pressures less than 1,800 psi for Figure 4.6.

For example, assume q = 200 b/d. Then, $P_{wf} = P_r - q/J = 2{,}200 - \frac{200}{1} = 2{,}000$ psi, and for 400 b/d, the value of P_{wf} is $2{,}000 - \frac{400}{1} = 1{,}800$ psi. For pressures less than 1,800 psi and for Figure 4.6, we will use Vogel's equation to calculate the flowing pressures. By solving Vogel's equation for P_{wf} we have:

$$P_{wf} = 0.125\overline{P}_r\,[-1 + \sqrt{81 - 80\,(q_o/q_{o_{max}})}]$$

In our case, $\overline{P}_r = P_b$ for the Vogel section. As an example for $q_o = 1{,}000$ b/d, the Vogel section is $q_{Vogel} = 1{,}000 - 400 = 600$ b/d where $q_b = 1.0\,(2{,}200 - 1{,}800) = 400$ b/d.

$$P_{wf} = 0.125\,(1{,}800)\left[-1 + \sqrt{81 - 80\left(\frac{600}{1{,}000}\right)}\right]$$

$$= 1{,}067 \text{ psi}$$

$$q_{total} = q_b + q_{Vogel} = 400 + 600 = 1{,}000 \text{ b/d}$$

Table 4.1 shows the rates vs flowing pressures for both solutions.

TABLE 4.1

Assumed rate, b/d	P_{wf} for constant J, psi	P_{wf} for Vogel, psi
200	2,000	2,000
400	1,800	1,800
600	1,600	1,590
800	1,400	1,350
1,000	1,200	1,067
1,500	700	—

(2) Assume several flow rates and obtain the required wellhead pressures necessary to move the fluids through the horizontal flow line to the separator using an appropriate multiphase flow correlation (See Appendix 4.1 for gradient curves.) Table 4.2 shows these results:

TABLE 4.2

Assumed rate, b/d	P_{wh} (required horiz), psi
200	115
400	140
600	180
800	230
1,000	275
1,500	420

(3) Using the same assumed flow rates as step 2 and the corresponding wellhead pressures, determine the required tubing intake (node outflow) pressures from the appropriate multiphase flow correlations. (See Appendix 4.2 for gradient curves.) Table 4.3 shows these results.

TABLE 4.3

Assumed rate b/d	P_{wh} horizontal, psi	Tubing intake pressure (node outflow), psi
200	115	750
400	140	880
600	180	1,030
800	230	1,225
1,000	275	1,370
1,500	420	1,840

(4) Plot the tubing intake (node outflow) pressures of step 3 vs the node inflow pressures of step 1. The intersection of these two curves shows the flow rate to be 900 b/d for the constant J case and 870 b/d for the Vogel IPR case. Refer to Figure 4.9a. It should be emphasized that this is "the rate" possible for this system. It is not a maximum, minimum, or optimum but is the rate at which this well will produce for the piping system installed. The rate can be changed only by changing something in the system—that is, pipe sizes, choke, separator pressure—or by shifting the IPR curve through stimulation treatment. This procedure is also given in Reference 2.

4.222 FLOWING ONE ZONE UP TWO CONDUITS

Combination tubing flow would be handled in the same manner. There are occasions where some wells are produced up two parallel tubing strings, a concentric string such as 1 in. inside of 2⅞-in. tubing and even 3½-in. tubing and a 3½-in. × 9⅝-in. annular flow-in combination.

The solution procedure starting from a common wellhead pressure or from the separator pressure into one

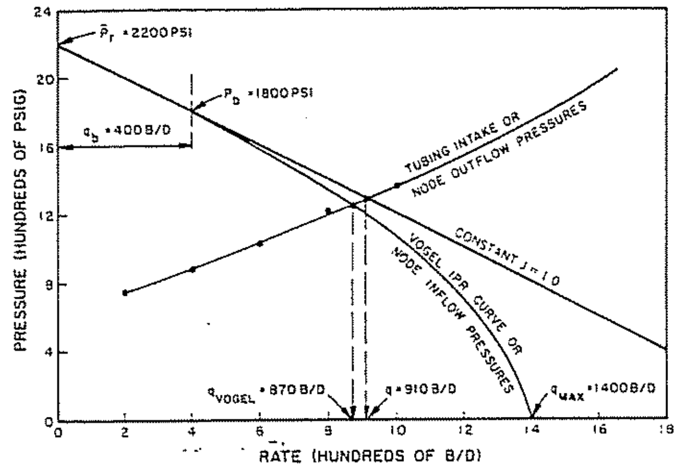

Figure 4.9a Solution at Bottom of Well (Center of Perforated Interval)

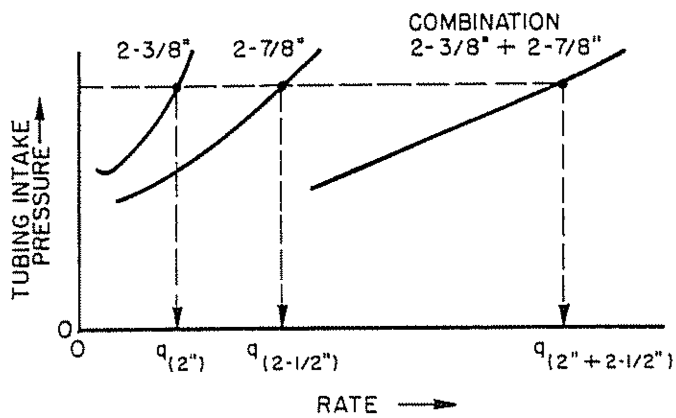

Figure 4.9b Flow Through Parallel Tubing Strings

common system for either concentric or parallel tubing conduits is as follows:

(1) Assume various flow rates.
(2) Determine tubing intake (node outflow) pressures independently for each string.
(3) Plot the tubing intake pressures vs rate as noted in Figure 4.9b.
(4) For the same pressure, total the flow rates from each flow conduit.
(5) Plot the total flow rates vs tubing pressure as noted in Figure 4.9b.
(6) The final solution procedure to determine flow rate can be obtained by plotting the appropriate IPR curve on Figure 4.9b as explained in section 4.22.

Why select the bottom of the well as the solution position? Notice that the reservoir component has been isolated from the piping system. Therefore, if a change in average reservoir pressure such as dropping from 2,200 psi to 1,800 psi within 1 year and on to 1,200 psi in 2 years is anticipated, we can immediately see the change in flow rates that will occur by constructing the IPR curve, beginning with a static pressure of 1,800 psi and 1,200 psi respectively (refer to Figure 4.10). Corresponding rates are noted in Table 4.4.

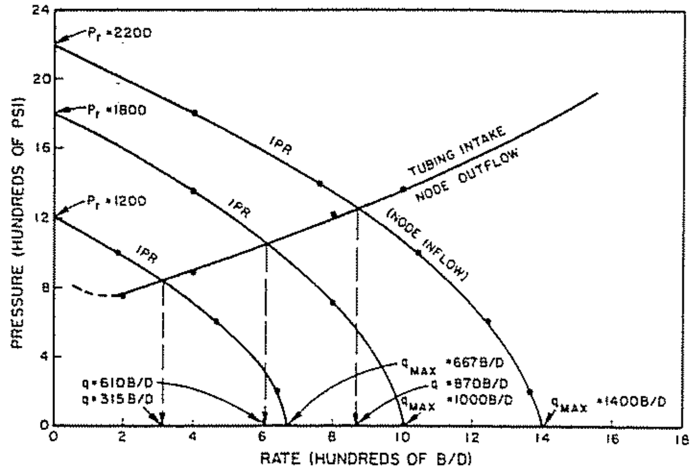

Figure 4.10 Prediction of Future Flow Rates (Vogel Solution)

TABLE 4.4

P_r, psia	q, b/d
2,200	870
1,800	610
1,200	315

The assumption is made that the gas-oil ratio (GOR) remains constant at 400 scf/bbl. Practical field cases normally show a change in GOR with depletion and, hence, the construction of a new tubing intake curve.

The IPR curve for 1,200 psi was constructed from Vogel's equation, having first determined $q_{o_{max}}$ by the relationship:

$$\frac{q_{o_{max}} \text{ at } 1{,}800 \text{ psi}}{q_{o_{max}} \text{ at } 1{,}200 \text{ psi}} = \left(\frac{1{,}800}{1{,}200}\right)^3$$

There are other cases whereby a solution at the bottom of the well is the best to illustrate the effect of certain variables. One of these is to show the differences in flow rate expected by stimulating a well or by removing damage. Refer to Figure 4.11, which shows an example of a well having an original flow efficiency of 0.4, a flow efficiency of 1.0 (all damage removed), and a flow efficiency of 1.4 obtained by stimulating the well.

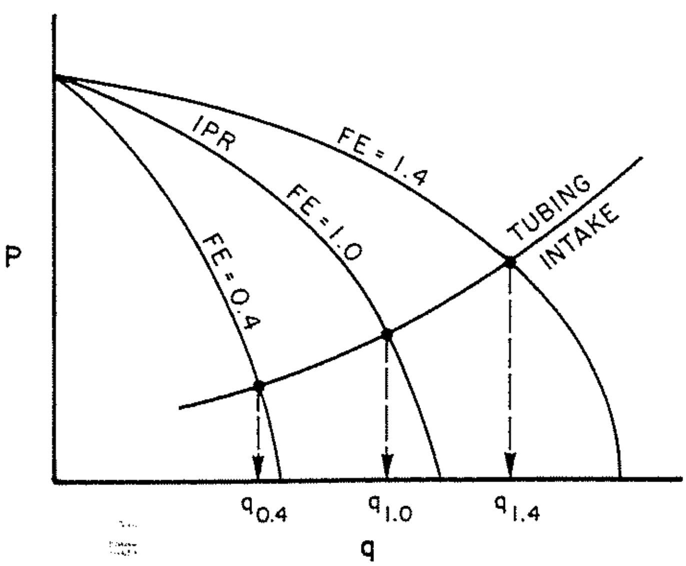

Figure 4.11 Effect of Well Improvement on Flow Rate

Another case is one of showing the effect of transient IPR curves on the same well. Depending upon reservoir characteristics, this shifting of the IPR can occur with time for the same well in the same reservoir and will finally reach stabilized flow. This time of stabilized flow can be calculated as discussed in Chapter 2 (see Figure 4.12.

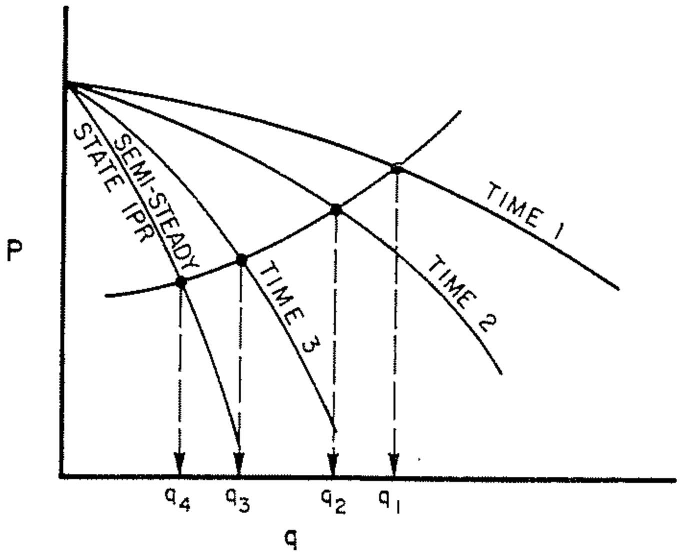

Figure 4.12 Effect of Transient IPR's

4.23 SOLUTION AT TOP OF WELL

4.231 INTRODUCTION

The next-most-common solution position is at the top of the well—that is, at the Christmas tree. The entire system is again divided into two components in order to solve for the flow rate. The separator and flow line are considered as one component (Figure 4.13)

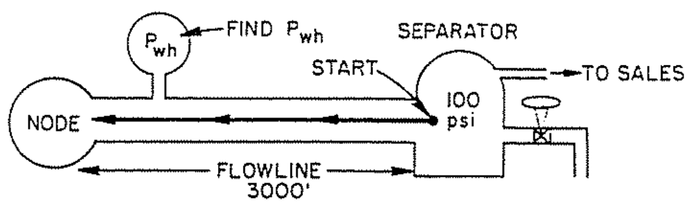

Figure 4.13 Flow Line and Separator Component

and the reservoir and tubing string as the other component (Figure 4.14). Start at both end positions. In Figure 4.13, start with separator pressure and find the wellhead pressures necessary to move the assumed flow rates through the flow line and to the separator. In Figure 4.14, start at $\overline{P}_r$, assume a flow rate, proceed to the center of the wellbore to obtain P_{wf} using the appropriate IPR plot or equation, and using that pres-

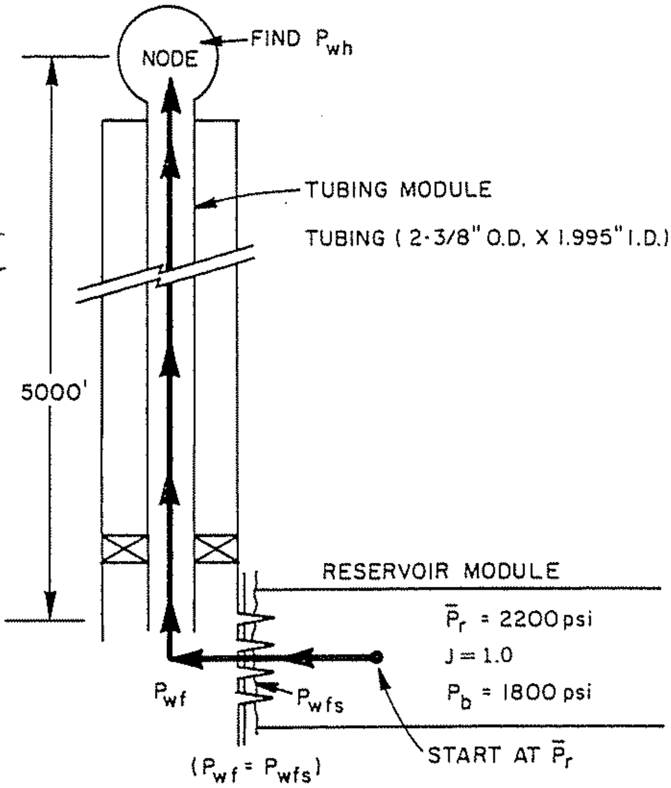

Figure 4.14 Tubing and Reservoir Component

sure, proceed to the top of the tubing string to find the wellhead pressure necessary for a set flow rate.

4.232 STEP-BY-STEP SOLUTION PROCEDURE (REFER ALSO TO REFERENCE 2)

(1) Assume several flow rates as before: 200, 400, 600, 800, 1,000, and 1,500 b/d.
(2) Start with the separator pressure and find the required wellhead pressures to move the fluids through 3,000 ft of 2-in. flow line. This will be the node outflow pressure at the solution position. These values, which can be found in Table 4.2, represent the solution to the flow-line component of the problem.
(3) Using the same assumed flow rates and starting from $\bar{P}_r$, find the corresponding flowing pressures for the reservoir to produce these rates. These values have also been previously determined and shown in Table 4.1.
(4) Using the flowing pressures obtained from step 3, determine the permissible (allowable) wellhead pressure for these flow rates—node inflow pressures. Note that these wellhead pressures control the flow rate of the well. An appropriate vertical multiphase flow correlation should be used. Gradient curves from Appendix 4.2 were used in this case. Refer to Table 4.5 for these results.
(5) Plot wellhead pressures of step 2 vs wellhead pressures of step 4 to obtain the flow rate. Refer to Figure 4.15a and b. The intersection of these two wellhead pressure curves gives the flow rate of 900 b/d and 870 b/d for the constant J and Vogel solutions.

TABLE 4.5
PERMISSIBLE WELLHEAD PRESSURES VS RATES

Assumed rate, b/d	P_{wf} Vogel	P_{wh} Vogel	P_{wf} constant J	P_{wh} constant J
200	2,000	610	2,000	610
400	1,800	540	1,800	540
600	1,590	440	1,600	450
800	1,350	300	1,400	330
1,000	1,067	100	1,200	180
1,400	0	—	800	—
1,500	0	—	700	—

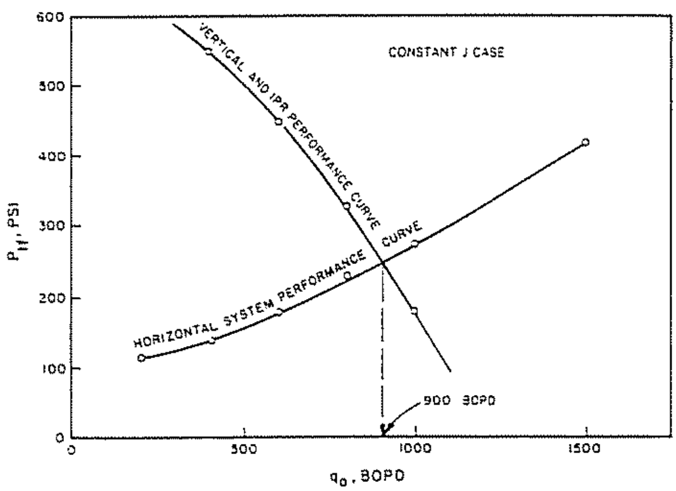

Figure 4.15a Wellhead Pressure Solution

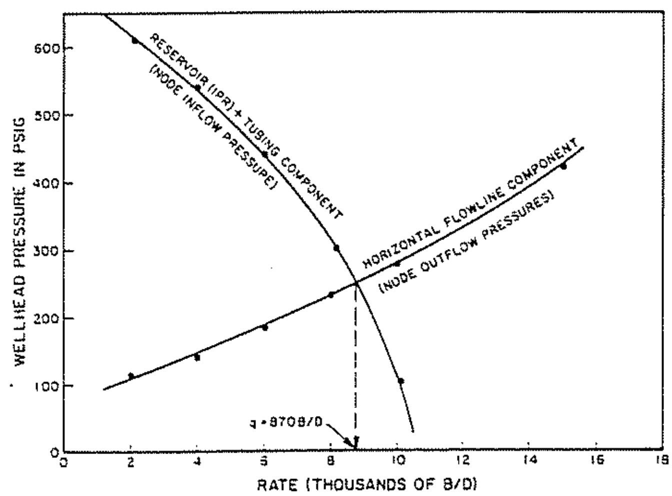

Figure 4.15b Wellhead Pressure Solution (Vogel IPR)

4.233 WHY USE THE WELLHEAD AS SOLUTION POSITION

By taking the solution at the wellhead, the flow line is isolated, and therefore it is easy to show the effect of changing the flow line size. Reference to Figure 4.16 shows the flow rate possible from this well by utilizing a 3-in. flow line. See Appendix 4.1. This rate is found to be 1,020 b/d as compared to 900 b/d for the 2-in. flow line. Notice also that the 3-in. flow line is relatively flat for all rates, indicating that friction is not excessive in this line, even at the higher rates. There is no need to evaluate a larger line size such as 4 in. since the

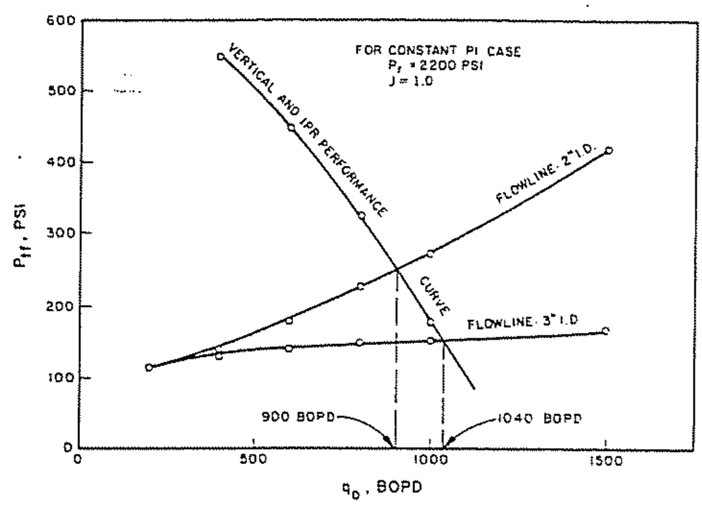

Figure 4.16 Effect of Change in Flow Line Size

3-in. line is sufficiently large to maximize the rate. Figure 4.17a shows a plot whereby several flow-line sizes and several tubing sizes can be evaluated on one plot. The intersections show rates possible for various combinations of flow-line and tubing sizes.

Figure 4.17b shows how to solve the problem of parallel flow lines. For example, if we want to use a 2-in. flow line in parallel with a 3-in. flow line, reference

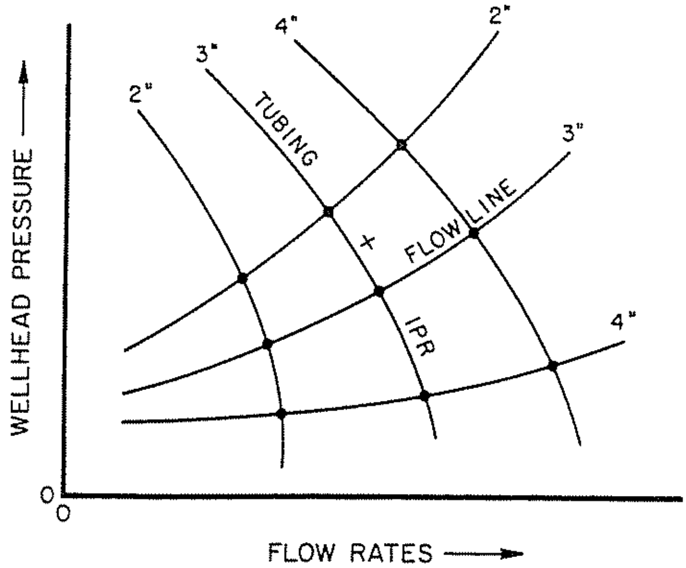

Figure 4.17a Wellhead Solution for Several Combinations of Flow-Line and Tubing Sizes

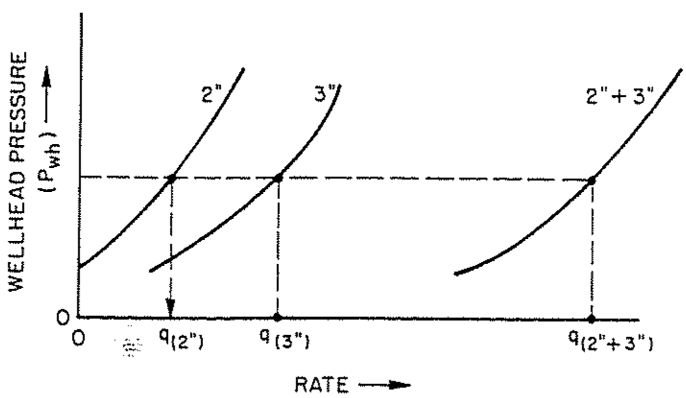

Figure 4.17b Solution for Parallel Flow Lines

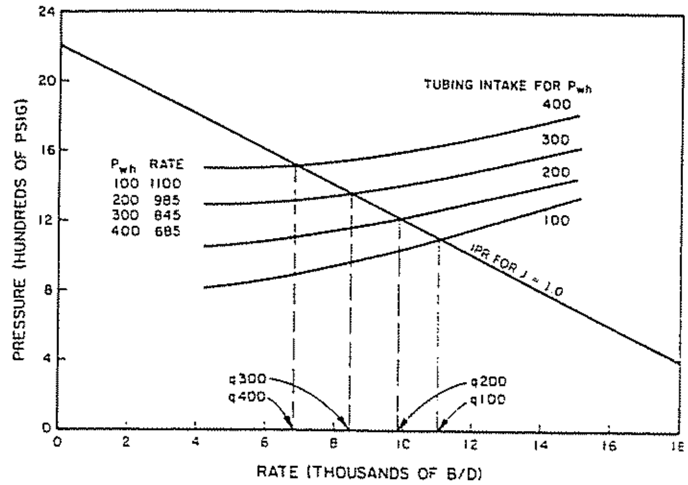

Figure 4.18 Solution Node at Bottom of Well for Varying Wellhead Pressures

should be made to Figure 4.17b. Each line is plotted separately by assuming flow rates and determining the required wellhead pressures independently of each other.

The flow rates for each line size are totaled for various wellhead pressures and then plotted as the total rate from both lines vs wellhead pressure.

A rate can be determined for a particular well by plotting the combination of IPR plus tubing curve on the same plot as described in Section 4.23.

4.24 COMBINATION SOLUTION AT BOTTOM AND TOP OF WELL

4.241 INTRODUCTION

Another solution procedure that is used quite often is shown in Figures 4.18 and 4.19. The final result appears the same as in Figure 4.15a for the solution at the wellhead. The difference is that the wellhead pressure vs flow rate was determined in a different manner.

4.242 SOLUTION PROCEDURE

The manner of solution is as follows for the constant J case:

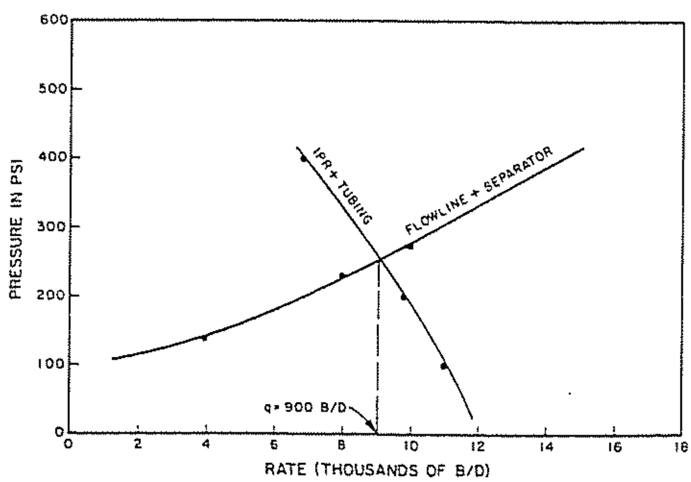

Figure 4.19 Solution Node at Wellhead With Data Taken From Figure 4.18.

(1) Assume various wellhead pressures such as 100, 200, 300, and 400 psi.
(2) For each wellhead pressure, assume various flow rates such as 400, 600, 800, 1,000, 1,200, and 1,500 b/d.
(3) Determine the tubing intake pressure for each wellhead pressure for the various assumed flow rates.
(4) Prepare a pressure–flow-rate diagram as noted in Figure 4.18 for the various wellhead pressures.
(5) Note the flow rates at the intersection of the tubing intake curves for each wellhead pressure with the IPR curve.
(6) Replot wellhead pressure vs rate as noted in Figure 4.19.
(7) Complete the solution by plotting the wellhead pressures required for the horizontal flow line as noted in Figure 4.19.

The advantage to this solution is that we obtain both a bottom-hole and wellhead solution with a minimum amount of effort. If we have a changing reservoir condition such as a drop in static pressure to 1,800 psi and a J change to 0.75 as noted in Figure 4.20, this IPR curve can be placed on the same plot with no changes for the tubing intake curves unless a change in the gas-oil ratio occurs and/or the well begins to produce some water.

Flow rates vs wellhead pressures can be obtained from Figure 4.20 and placed on Figure 4.21 to obtain a wellhead pressure solution for changing IPR curves. The wellhead pressure solution easily permits the opportunity to observe the effect of changing flow-line sizes.

4.25 SOLUTION NODE AT THE SEPARATOR

4.251 INTRODUCTION

The selection of the separator pressure is critical when designing a rotative gas-lift system or when the gas pressure from the separator must be increased to flow into a higher pressure system such as a sales line or another gathering system. The separator pressure controls the suction pressure to the compressor and is directly related to compressor horsepower (HP) requirements. For example, if we assume that we have

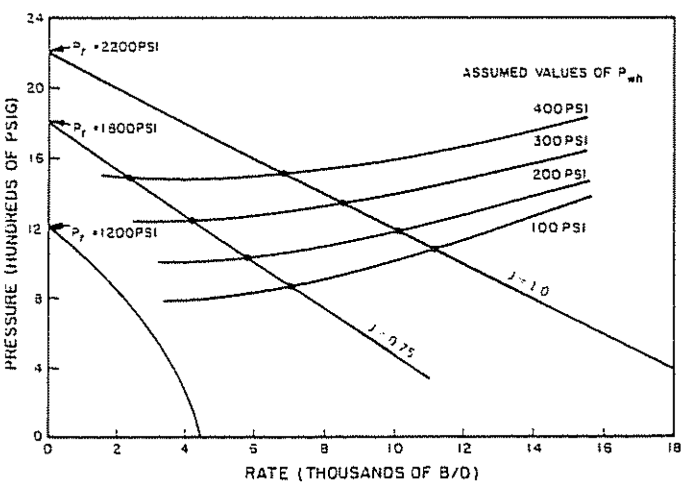

Figure 4.20 Solution Node at Bottom of Well for Varying Wellhead Pressure and Changing IPR Curves

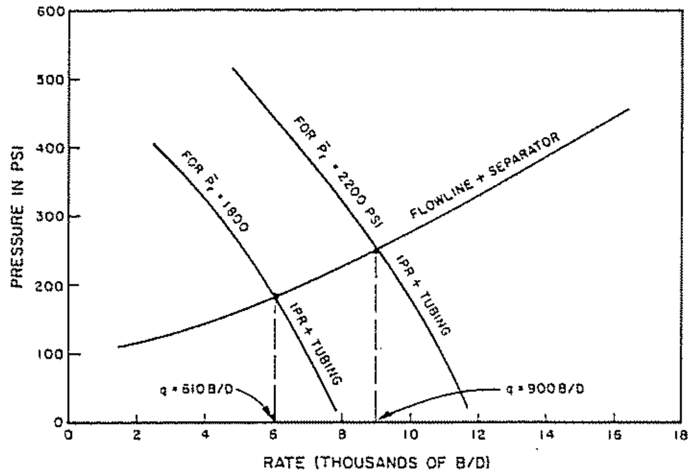

Figure 4.21 Solution Node at Wellhead With Data Taken From Figure 4.20

1 million scfd of gas that we want to place into a 1,000-psia system, the horsepower can be estimated in the following manner:

$$HP = 23\,(R)^{1/n}\,(n)\,(q)$$

where:

$$R = \text{compression ratio} = \frac{\text{press discharge}_{\text{absolute}}}{\text{press suction}_{\text{absolute}}}$$

n = number of stages
q = standard cubic feet per day in millions (for R between 4.5 and 20, use two stages)

Let us assume suction pressures of 100, 200, and 300 psi, respectively. For 100 psia:

$$R = \frac{1{,}000}{100} = 10\ (2\ \text{stages})$$

$$HP = (23)(10)^{1/2}(2)(1) = 145.5\ \text{HP}$$

For 200 psia suction:

$$R = \frac{1{,}000}{200} = 5\ (2\ \text{stages})$$

$$HP = (23)(5^{1/2}(2)(1) = 102.8\ \text{HP}$$

For 300 psia suction:

$$R = \frac{1{,}000}{300} = 3.33\ (1\ \text{stage})$$

$$HP = 23\,(3.33)(1) = 76.6\ \text{HP}$$

Table 4.6 shows the compressor horsepower needed per million scfd vs separator pressure.

TABLE 4.6

Separator pressure, psi	HP
50	205.7
100	145.5
200	102.8
300	76.6
400	57.5
500	46

However, the separator pressure should not be indiscriminately lowered or increased without performing systems analysis on the entire piping system and, in particular, on the flow line. An intuitive thought that a lowering of the separator pressure will greatly increase the rate may not be true at all. There are numerous cases whereby a lowering of the separator pressure (even 200–300 psi) fails to change the production rate—even on a very high productivity well. The reason for this is that the flow line or the tubing may be serving as the restriction.

On low-productivity wells, the reservoir itself can be the restriction, and a change in separator pressure will have little effect on production rate since additional drawdown in pressure offers little increase in production.

Gas-lift wells are a separate problem, and horsepower requirements are not controlled entirely by separator pressure. In gas lift, if a lowering of the separator pressure does in fact lower the wellhead pressure, the same rate can be obtained with less injection gas. Compressor horsepower is a function of both compression ratio and gas volume.

4.252 SOLUTION PROCEDURE FOR CONSTANT J CASE

The solution procedure at the separator sets one of the end positions (separator) as the solution position. Since the separator pressure in itself is not normally a variable with rate, it is considered to be constant at 100 psi. There can be some cases where the separator pressure may vary with rate, and it can be properly accounted for in the solution procedure if necessary. Figure 4.22 shows the path taken in obtaining the solution.

(1) Assume various flow rates such as 200, 400, 600, 800, 1,000, and 1,500 b/d.
(2) Start with the other end position at $\bar{P}_r$ and determine the flowing bottom-hole pressures necessary for the well to produce the assumed flow rates. These values have been previously determined and noted in Table 4.1.

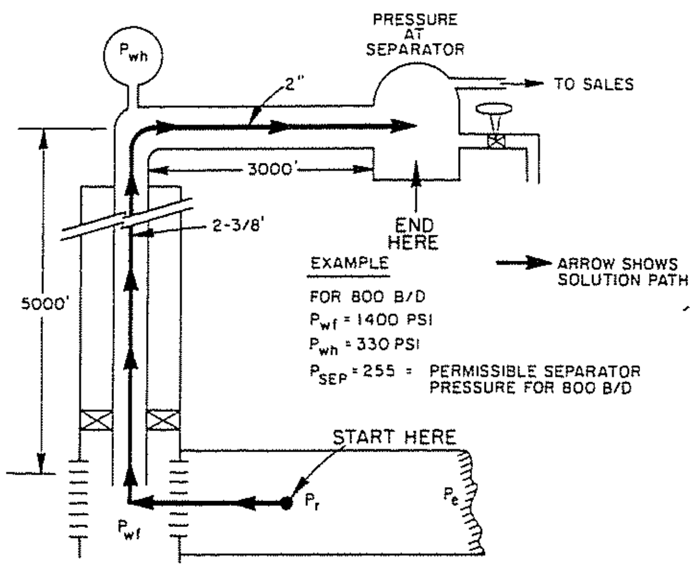

Figure 4.22 Solution Position at Separator

(3) Start with the P_{wf} values of step 2 as tubing intake pressures and find the corresponding wellhead pressures from a vertical multiphase flow correlation. This has been determined previously and noted in Table 4.5.
(4) Starting with the wellhead pressures of step 3, find the corresponding permissible separator pressures for each rate, disregarding the fact that the separator pressure is constant at 100 psi. Table 4.7 represents the complete sequence of pressures determined.

TABLE 4.7

Assumed rate	P_{wf}	P_{wh} (vertical)	Separator pressure
200	2,000	610	595
400	1,800	540	525
600	1,600	450	410
800	1,400	330	255
1,000	1,200	180	—
1,500	700	—	—

(5) Plot the separator pressure vs rate as shown in Figure 4.23, drawing the constant separator pressure line of 100 psi. The intersection of these two

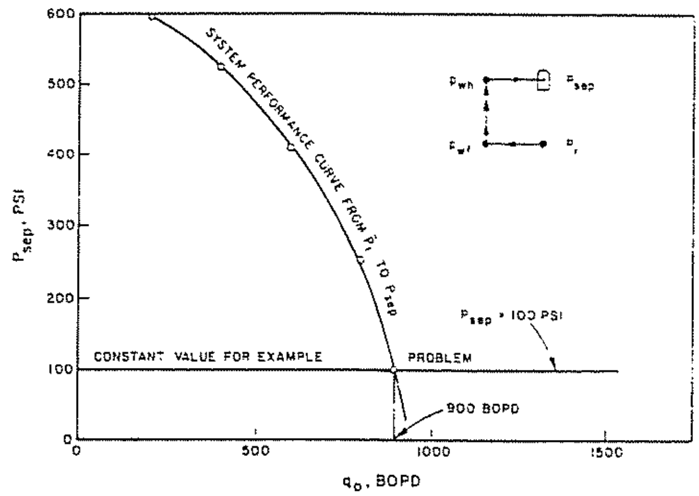

Figure 4.23 Solution to Example Problem Taken at Separator

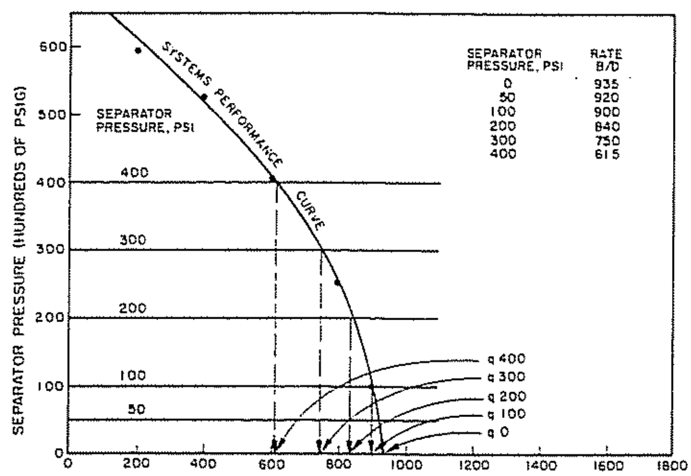

Figure 4.24 Effect of Separator Pressure—Example Problem

lines shows the flow rate to be 900 b/d. Regardless of the solution position, the rate will be the same at 900 b/d.

The rate for other separator pressures can be determined very quickly by noting the intersection of various separator pressure horizontal lines with the total systems performance line. Refer to Figure 4.24 to note the rates possible for other separator pressures. These results are noted in Table 4.8.

TABLE 4.8

Separator pressure, psi	Rate, b/d
0	935
50	920
100	900
200	840
300	750
400	615

Note that no significant increase in production occurs from dropping the separator pressure below 100 psi. The reason for this is that the flow line is becoming the restriction for this system.

4.253 WHY USE THE SEPARATOR AS THE SOLUTION NODE

By taking the solution position at the separator, it is quite easy to visualize the effect of the separator pressure on the flow rate. This change in rate, if any, is influenced by the total system, including the well productive capability (IPR curves) and tubing and flow-line sizes and lengths. Refer to Figure 4.25 for four different well systems. It is obvious that well A shows a significant increase in production as the separator pressure is lowered but that well D shows essentially no change in production with a lowering of the separator pressure. Each well must be analyzed individually in order to optimize properly.

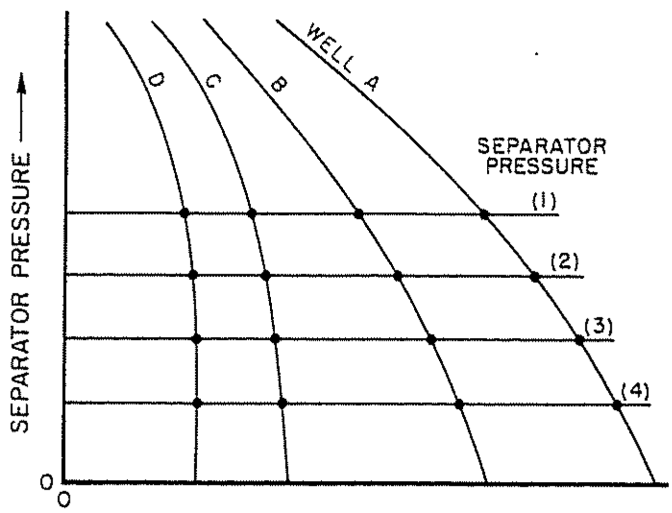

Figure 4.25 Effect of Separator on the Flow Rate for Four Wells

In all cases, the final criteria for separator pressure selection is one of economics, even in those cases where stage separation is considered.

As a word of caution, the flow-line size should always be analyzed prior to making a final selection of the separator pressure. There are field cases whereby changing the flow line will show greater changes in rate than changing the separator pressure.

For example, let us assume the following conditions:

Given data:

2-in. flow line	$q = 1{,}000$ b/d
6,000 ft long	GLR = 2,000 scf/bbl

Find the required wellhead pressures for varying separator pressures.

The results are noted in Table 4.9.

TABLE 4.9

Separator pressure, psi	Required wellhead, psi
50	860
100	860
200	885
300	930
600	1,090

Note that a change in separator pressure from 50 to 100 psi would have no effect on the rate, and an increase in separator pressure to 200 psi requires only an additional 25 psi at the wellhead.

This example illustrates that a lowering of the separator pressure will not necessarily increase the flow rate. However, for the very same conditions, a change in the flow-line size for the same problem has a decided effect on the wellhead pressure as noted in Table 4.10.

TABLE 4.10

Flow-line size	Separator pressure	P_{wh}
2 in.	100	860
3 in.	100	310
4 in.	100	180

This example illustrates the importance of analyzing each component separately and then combining the components for analysis of the total system.

In the following example, we note that a change in separator pressure will indeed lower the wellhead pressure quite significantly.

For example, let us assume that we have 4,000 ft of 2-in. flow line producing 1,000 b/d with a GLR of 1,000 scf/bbl into a separator pressure of 300 psia. What change in wellhead pressure can be obtained by lowering the separator pressure to 100 psia? Let us check the wellhead pressure necessary for the same conditions for both 3-in. and 4-in. ID flow lines. Refer to Table 4.11 for these results.

TABLE 4.11

Separator pressure psi	Line size	P_{wh}
300	2 in.	580
200	2 in.	530
100	2 in.	485
300	3 in.	340
200	3 in.	260
100	3 in.	200
300	4 in.	320
200	4 in.	225
100	4 in.	135

For this example, a change in separator pressure shows a significant change in wellhead pressure—in particular for the larger flow lines. This shows that, if the flow line is large, a change in separator pressure does indeed show a change in wellhead pressure.

4.26 SOLUTION NODE AT THE AVERAGE RESERVOIR PRESSURE ($\bar{P}_r$) (CONSTANT J CASE)

4.261 INTRODUCTION

Although this solution node position may be of less practical value than some of the other positions, it is shown here in order to illustrate that the same flow rate can be obtained regardless of the solution position. The position does allow a simple illustration of the effect of changing $\bar{P}_r$ values, but other changing variables such as gas-liquid ratios and water cut are not included in this example. However, these variables could be included where applicable. It is quite likely that, as $\bar{P}_r$ decreases, the gas-oil ratio will increase up to a point, after which it will decrease for a solution-gas-drive reservoir.

For the solution at $\bar{P}_r$, we start at the other end position (separator pressure) and proceed all the way to $\bar{P}_r$ by summing all pressure losses to that position (see Figure 4.26).

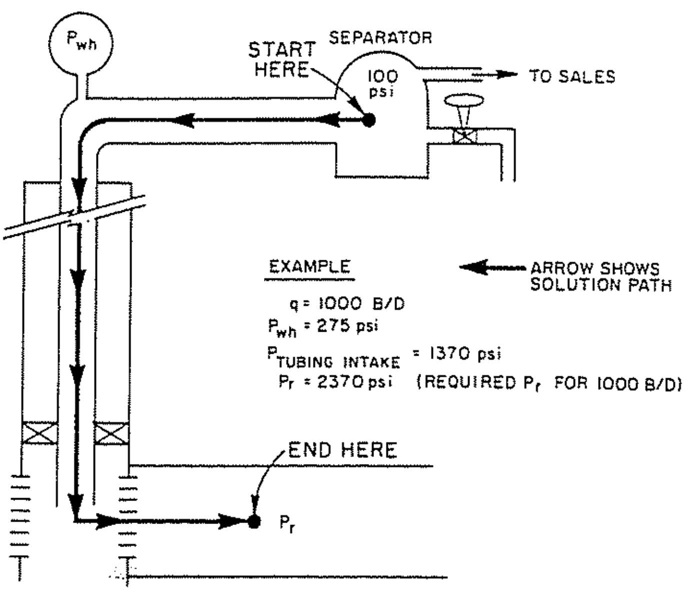

Figure 4.26 Solution Position at $\bar{P}_r$

4.262 SOLUTION PROCEDURE

(1) Assume various flow rates such as 200, 400, 600, 800, 1,000, and 1,500 b/d.

(2) Starting with the separator pressure of 100 psi, find the required wellhead pressures to move the fluids to the separator from an appropriate multiphase flow correlation.

This has already been determined in Table 4.2.

(3) Using the wellhead pressures from step 2 and using an appropriate vertical multiphase flow correlation, determine the values of tubing intake pressure for the assumed rates. This was determined previously in Table 4.3.

(4) Starting with the tubing intake pressure of step 3, find the required $\bar{P}_r$ values for each assumed flow rate for the constant J case. The quotation for the constant J case is:

$$\bar{P}_r = P_{wf} + q/J$$

For example, at q = 1,000 b/d:

$$\bar{P}_r = 1{,}370 + \frac{1{,}000}{1} = 2{,}370 \text{ psi}$$

All of the results are tabulated in Table 4.12.

TABLE 4.12
(Data for Solution at $\bar{P}_r$)

Assumed rate	P_{wh}	Tubing intake	$\bar{P}_r$
200	115	750	950
400	140	880	1,280
600	180	1,031	1,630
800	230	1,220	2,020
1,000	275	1,370	2,370
1,500	420	1,840	3,340

For the case where Vogel's IPR curve was applicable. Vogel's equation could be used to solve for $\bar{P}_r$ for those rates giving pressures below the bubble point.

Refer to Figure 4.27 for the $\bar{P}_r$ solution for the constant J case. Again, the same flow rate of 900 b/d is obtained.

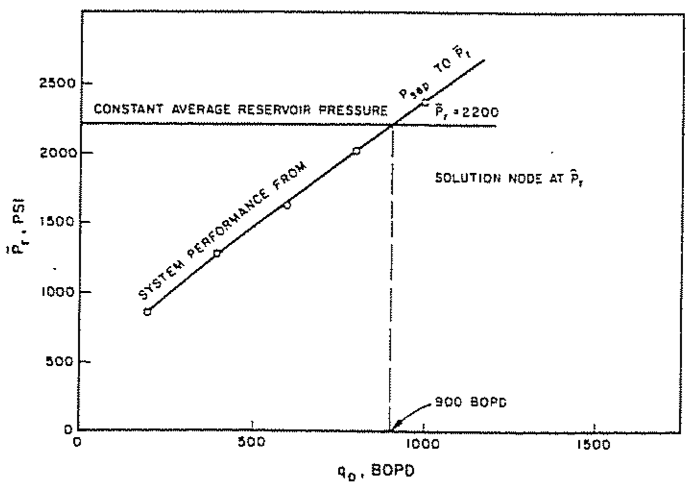

Figure 4.27 Solution to Example Problem at $\bar{P}_r$

4.263 WHY USE $\bar{P}_r$ AS A SOLUTION POSITION

By taking the solution position at $\bar{P}_r$, we can immediately determine the flow rate for other average reservoir pressures. However, this solution assumes no change in the producing gas-oil ratio or water cut from the well. Referring to Figure 4.28 shows rates possible at various average reservoir pressures. Rates vs $\bar{P}_r$ are tabulated in Table 4.13.

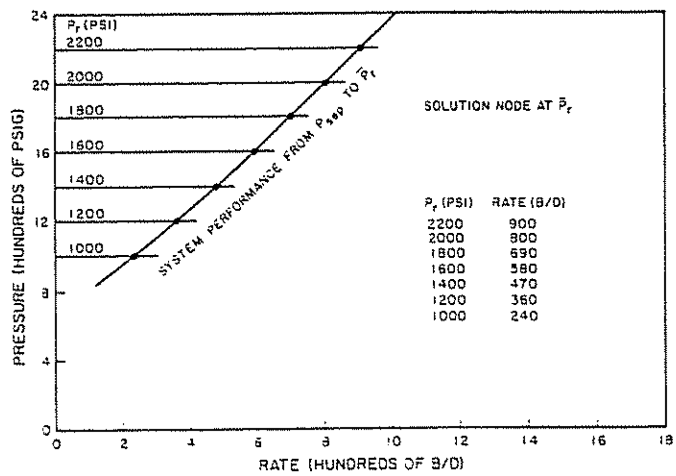

Figure 4.28 Effect of Changing $\bar{P}_r$

TABLE 4.13

$\bar{P}_r$, psi	Rate, b/d
2,200	900
2,000	800
1,800	690
1,600	580
1,400	470
1,200	360
1,000	240

The practicality of this solution may be questionable since, under normal conditions, the GOR also changes as the static reservoir pressure drops, hence requiring a new total-systems curve each time.

CLASS PROBLEM #1

Given data: (oil well)

40-acre spacing	$\gamma_g = 0.7$
$P_r = 1{,}200$ psi	$k = 1.0$ md
$T = 130°F$	$h = 30$ ft
depth = 6,000 ft	

Present conditions:

2⅜-in. OD tubing
1,500 ft of 2-in. flow line
separator pressure = 30 psi
5½-in. casing to T.D.
7½-in. hole size
40°API crude (all oil)
GOR = 5,000 scf/bbl
Well now on beam pump producing 10 b/d with gas locking problems.

Calculate:

(1) Evaluate this well.
(2) Check to see if it will flow.
(3) Recommend a tubing size.

CLASS PROBLEM #2

Given data: (oil well)

depth = 10,000 ft
h = 40 ft
Pr = 5,600 psi
160-acre spacing
T = 230°F
oil gravity = 35°API
GOR = 600 scf/bbl
gas gravity = 0.7
k = 80 md

Present conditions:

7-in. casing
tubing = 2⅞ in.
flow line = 2,000 ft of 2½ in.
sales-line pressure = 600 psi
drilled with 9¾-in. bit

Note: Present test shows 400 b/d for a wellhead pressure of 1,000 psi.

Calculate:

(1) Evaluate this well.
(2) Prepare an IPR curve by Darcy's Law and by test.
(3) Why the difference?

CLASS PROBLEM #3

Given data: (oil well)

8,000 ft of 2⅞-in. tubing
3,000 ft of 2½-in. flow line
separator pressure = 100 psi
35°API oil gravity

h = 30 ft	k = 140 md
T = 170°F	gas gravity = 0.7
GOR = 500 scf/bbl	160-acre spacing
$P_r = 3{,}400$ psi	casing size = 7 in.
hole size = 10¾ in.	

Note: P_r will be 2,000 psi in 2 years, and water cut will be 50% and finally 90%, with P_r staying at 2,000 psia (*well will be gas lifted at this time with retrievable valves*).

Calculate:

(1) Evaluate this well.
(2) Select tubing size based on mandrel OD. Assume casing ID = 6 in. Assume gas pressure sufficiently high to inject gas around bottom of tubing.

Constant J case for water cut = 90% and Vogel solution at 50% may be assumed.

MANDREL SIZES

Tubing OD	Valve size	Mandrel OD*
2⅜ in.	1 in.	4.250
2⅜ in.	1½ in.	4.750
2⅞ in.	1 in.	4.750
2⅞ in.	1½ in.	5.407
3½ in.	1 in.	5.546
3½ in.	1½ in.	6.031
4½ in.	1 in.	6.505
5½ in.	1 in.	7.988

* Does not represent exact sizes of all manufacturers. A slim-line 4-in. mandrel is available for 7-in. casing.

CLASS PROBLEM #4

Given data: (oil well)

well depth = 14,000 ft	
2⅜-in. tubing	
P_r = 5,000 psia	7-in. casing
h = 50 ft	k = 200 md
T = 250°F	160-acre spacing
GOR = 700 scf/bbl	8½-in. hole
gas gravity = 0.7	40°API

Present conditions:

Test shows 500 b/d on gas lift with P_{wh} = 450 psig

Calculate:

(1) Evaluate this well.
(2) Check test against Darcy's Law.
(3) Will the well flow at 50% water cut?

CLASS PROBLEM #5

Given data: (oil well)

P_r = 4,600	GOR = 400 scf/bbl
k_o = 600 md	T = 195°F
h = 160 ft	depth = 8,775 ft
WOR = 0	oil gravity = 40°API
gas gravity = 0.7	perf. interval = 60 ft
8½-in. hole	8 spf (0.4-in. dia. hole)
640-acre spacing	1,500 ft of 4-in. flow
3½-in. tubing	line separator
casing = 7-in. (6.184-in. ID)	pressure = 80 psi

P_r drops to 3,000 in 2 years and GOR = 600 scf/bbl with no water.

Calculate:

(1) Evaluate this well.
(2) Find rates now and in the future.
(3) Make any recommendations.

CLASS PROBLEM #6

Given data:

well depth = 6,000 TVD or 8,000 ft MD
h = 40 ft
k = 60 md
P_r = 3,600 psi
T = 165°F
GOR = 500 scf/bbl
API = 35°
gas gravity = 0.65
separator pressure = 100 psi (short flow line)
160-acre spacing
casing = 13⅜ in.
hole size = 16 in.
tubing size = 3½ in.

where:

MD = measured tubing length
TVD = true vertical depth

Calculate:

(1) Evaluate this well and make any recommended changes.
(2) Find the flow rate for 3½-in. tubing and other flow configurations. Assume annular flow is permitted.

4.27 TAPERED STRINGS

4.271 INTRODUCTION

There are numerous reasons why tapered strings may be run in a well, but the principal one involves the use of a liner in the completion string of casing. Numerous completions, especially in deeper wells, make use of a liner in the lower section of the well. The liner restricts the size of tubing that can be run, but the larger casing above the liner setting position permits a larger string of tubing to be run from the top of the liner to the surface. This type of nodal analysis permits an easy solution to determine the effect of different sizes of tubing above the liner.

Assume that, for the previously worked example problem, it is necessary to set a liner from near 3,500 ft through the producing zone at 5,000 ft and that the liner ID is such that 2⅜-in. tubing is the largest size tubing that can be installed. The problem is to investigate the possible production rate increases by installing larger than 2⅜-in. tubing above the liner from 3,500 ft to the surface. Refer to Figure 4.29.

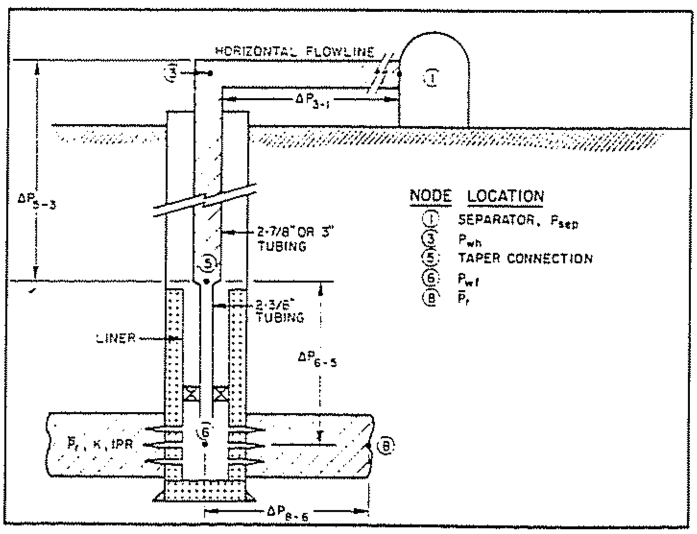

Figure 4.29 Tapered Strings

4.272 SOLUTION PROCEDURE

In order to solve this problem, the solution node is taken at the position of the taper—that is, 3,500 ft down the well at the top of the liner. Assume that the option of running 2⅞-in. OD, 3½-in. OD, or 2⅜-in. OD tubing from that position to the surface exists. Reference to Figure 4.30 shows the solution path. Starting at each end position—that is, P_{sep} and $\overline{P}_r$—converge on the tapered position from both directions. Starting from $\overline{P}_r$, calculate P_{wf} from the inflow equation; then, from vertical flow calculations, determine the pressure at the bottom of the taper (below taper component). Then, starting at the separator pressure, obtain P_{wh} from a horizontal flow correlation and proceed to the top of the taper using a vertical multiphase flow correlation (above taper component). The system has been divided into two components, a below-taper and an above-taper component, and was originally presented in reference 1.

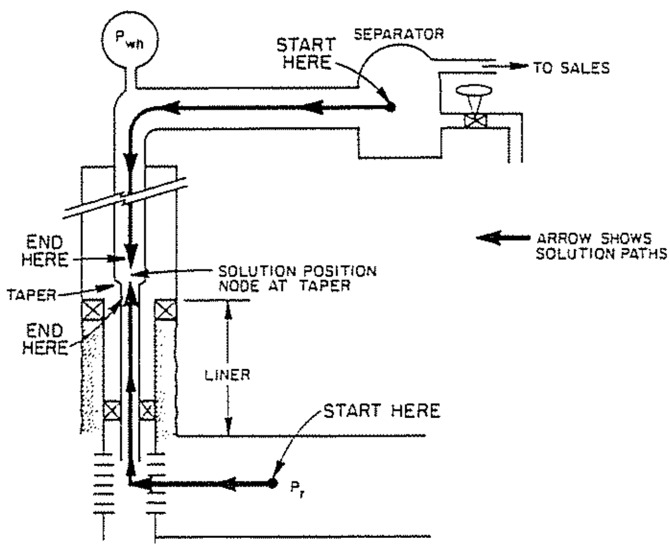

Figure 4.30 Tapered String Solution

Step-by-step procedure:

(1) Assume rates of 200, 400, 600, 800, 1,000, and 1,500 b/d.

(2) Starting with the above taper component, obtain the wellhead pressures for each assumed flow rate. This has been determined previously in Table 4.2.

(3) Starting with each assumed rate and the corresponding wellhead pressure, determine the pressure at the top of the taper for both 2⅞-in. and 3½-in. tubing, which represents 3,500 ft of tubing to that point. This information is tabulated in Table 4.14.

(4) Starting with the below-taper component at P_r, obtain the flowing pressures at the bottom of the well using the appropriate IPR curve or calculation. These are noted in Table 4.1.

(5) Starting from the P_{wf} of step 4 and for the assumed rates, obtain the below-taper pressures from an appropriate multiphase flow correlation. This represents 1,500 ft of 2⅜-in. OD tubing. These values are tabulated in Table 4.15.

TABLE 4.14
PRESSURES AT TAPER TOP

Assumed q, b/d	P_{wh}, psi	Pressure at top of taper: 2⅞-in. OD tubing	Pressure at top of taper: 3½-in. OD tubing
200	115	475	420
400	140	500	475
600	180	600	560
800	230	718	660
1,000	275	820	780
1,500	420	970	900

TABLE 4.15

Assumed q, b/d	P_{wf}, psi	Pressure below taper, psi
200	2,000	1,400
400	1,800	1,300
600	1,600	1,170
800	1,400	1,000
1,000	1,200	820
1,500	700	360

(6) Plot the above-taper pressures of step 3 vs the below-taper pressures of step 5, as noted in Figure 4.31.

The intersection of the two performance curves at the taper connection predict a flow rate of 1,020 bo/d for 2⅞-in. OD tubing and 1,045 bo/d for 3½-in. OD tubing. For 2⅜-in. OD tubing, the predicted rate was 900 bo/d. Notice that the increase in rate from 2⅜-in. OD to 2⅞-in. OD tubing is much greater than the increase in rate from 2⅞ in. to 3½ in.

It is recommended that 2⅞-in. tubing be used above the taper because, as the pressure decreases and the rate falls off, the 3½-in. tubing may become too large and cause unstable flow (heading) and loading because of gas slippage past the liquid. This problem could have been solved by placing the solution node at any point in the system. However, this approach can simplify

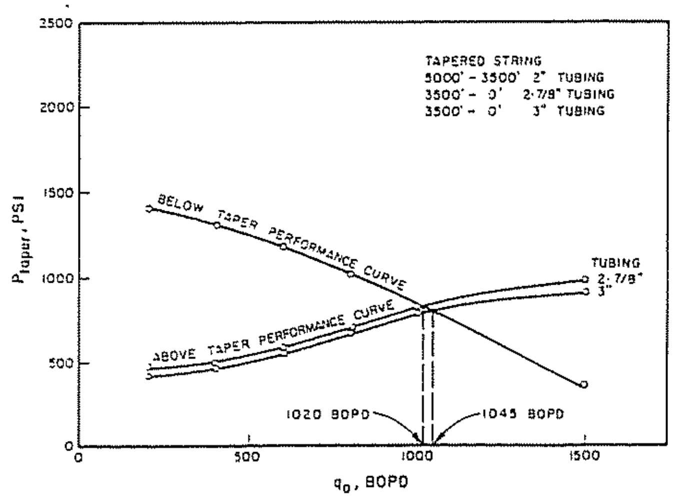

Figure 4.31 Tapered String Solution

the procedure depending on the manner in which the curves or computer programs available are formulated. This same procedure could be used if a change in flowline configuration occurs at some point along the path of the horizontal system.

4.28 FUNCTIONAL NODES

4.281 INTRODUCTION

In the previous discussions, it has been assumed that no pressure discontinuity exists across the solution node. However, in a total producing system, there is usually at least one point or node where this assumption is not true. When a pressure differential exists across a node, that node is termed a "functional node" since the pressure flow rate response can be represented by some physical or mathematical function. A functional node is one where an immediate pressure loss occurs in a short distance. Figure 4.2 shows examples of some common system parameters that are functional nodes.

There are many surface or downhole tools or completion methods that could create pressure drops with flow rates as those shown in Figure 4.2. Some of these are surface chokes, safety valves, downhole chokes, regulators, gravel-packed completions, and normal perforated completions.

It is important to notice that, for each restriction placed in the system shown in Figure 4.2, the calculation of pressure loss across that node as a function of flow rate is represented by the same general form; that is, ΔP is some function of rate.

4.282 SURFACE WELLHEAD CHOKES

4.2821 INTRODUCTION

Refer to Figure 4.32, which physically describes a well with a surface choke installed. The most common formula used for calculations concerning multiphase flow through surface chokes is the one offered by Gilbert.[3] Numerous other correlations are available,

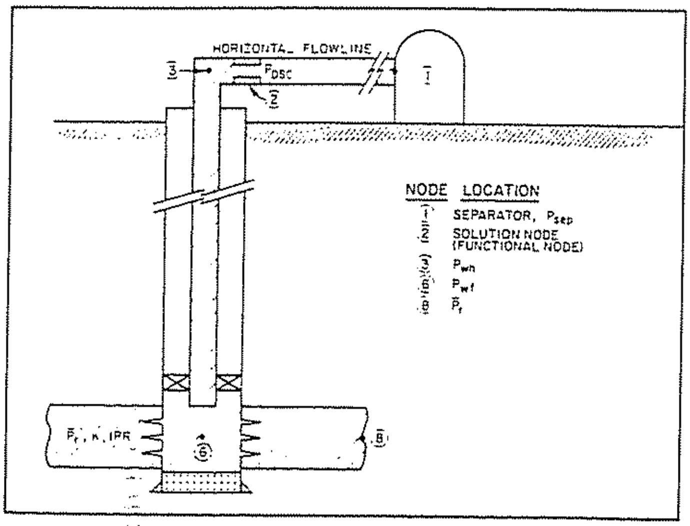

Figure 4.32 Surface Choke Problem

and these are discussed by Brown and Beggs.[2] Gilbert's equation is as follows:

$$P_{wh} = \frac{435\, R^{0.546}(q)}{S^{1.89}}$$

where:

P_{wh} = wellhead pressure, psig
R = gas-liquid ratio, Mcf/bbl
q = flow rate, b/d
S = choke beam diameter, 64*ths* of an inch

Notice that the downstream pressure is not included in this equation; that is, the equation is independent of the downstream pressure. Gilbert developed his equation from field data in California, and he found his equation to be valid as long as the downstream pressure was less than 70% of the upstream pressure—that is, $P_D/P_{wh} \le 0.7$. His equation has been found to give reasonable results and certainly is accurate enough for a first sizing of choke-beam requirements.

Therefore, in order to correctly size a choke beam, all that is needed is the necessary wellhead pressure for a set flow rate. Assume that, for the previous example problem, an objective flow rate of 600 b/d is desired. It is necessary to refer to Figure 4.15a, which shows the solution position at the top of the well. In Figure 4.15a, permissible wellhead pressures for certain flow rates have been plotted. The wellhead pressures required for the horizontal line do not enter into the calculations except to check the validity of the equation—that is, $P_D/P_{wh} \le 0.7$. Therefore, the objective flow rate is 600 b/d. The P_{wh} value necessary to allow this rate is 450 psig.

Solving the equation for S:

$$S^{1.89} = \frac{435\, R^{0.546}(q)}{P_{wh}}$$

$$S = \left[\frac{435\, R^{0.546}(q)}{P_{wh}}\right]^{1/1.89}$$

$$S = \left[\frac{(435)(0.4)^{0.546}(600)}{450}\right]^{1/1.89}$$

$$= 22.2/64ths \text{ of an in.}$$

The nearest standard bean size would be used, or the exact size could be set with an adjustable choke.

Recall that the unrestricted rate for this well is 900 b/d. Table 4.16 shows the various choke sizes needed for the assumed flow rates.

TABLE 4.16

Assumed q, b/d	P_{wh} for assumed rate, psi	Choke size, 64*ths* of in.	P_{wh} horiz., psi	$\frac{P_D}{P_{wh}}$
200	610	12.4	115	0.188—(O.K.)
400	540	17.9	140	0.259—(O.K.)
600	450	22.2	180	0.4—(O.K.)
800	330	25.9	230	0.697—(O.K.)

Note that the choke sizes calculated for 200, 400, 600, and 800 b/d are all valid by using Gilbert's equation; that is, $P_D/P_w \le 0.7$ in all cases, with 800 b/d being very close with a P_D/P_{wh} value of 0.697.

4.2822 ΔP SOLUTION FOR WELLHEAD SURFACE CHOKES

4.28221 INTRODUCTION

Referring to Figure 4.33 shows the solution paths. In this solution, the differential available at the wellhead is utilized in order to solve the choke problem and determine flow rates possible for different choke sizes. The differentials created at the wellhead can be obtained from the wellhead solution as previously described in section 4.23 (refer to Figure 4.15a).

Solution procedure:

(1) Assume various flow rates; determine the wellhead pressures necessary to move the fluids to the separator; then determine the allowable wellhead pressures for the assumed flow rates as set out in Section 4.23.
(2) Plot wellhead pressures vs rates and note ΔP's at different flow rates (see Figure 4.34).

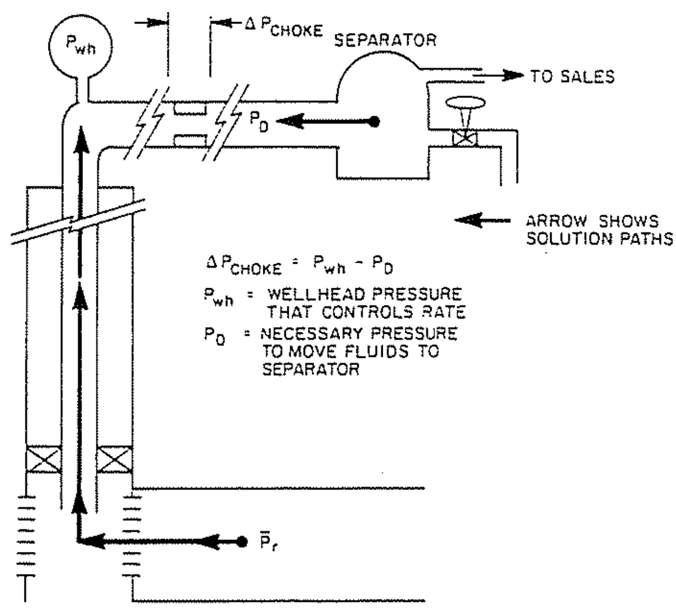

Figure 4.33 Solution Paths for Surface Choke

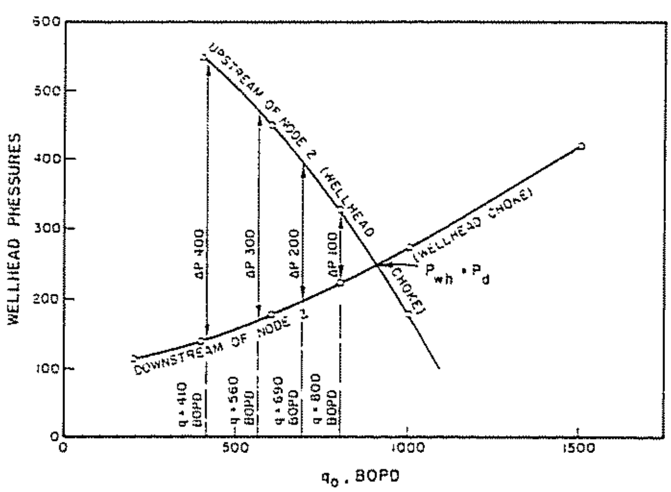

Figure 4.34 Surface Choke Evaluation

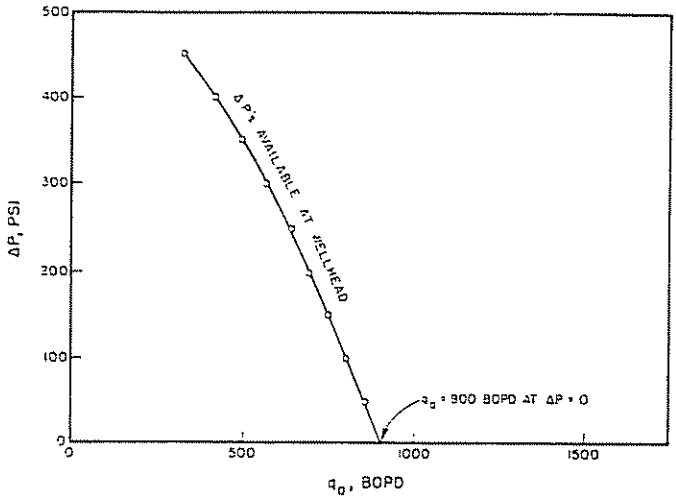

Figure 4.35 Total Systems Performance Curve for Surface Choke Problem

(3) Re-plot the ΔP values from Figure 4.34 in the form shown in Figure 4.35.
(4) From an appropriate choke formula, assume various flow rates and determine the corresponding wellhead pressures.

For this example, use the same equation as in the paper by Mach, Proaño, and Brown:[1]

$$P_{wh} = \frac{500\, R^{0.5}(q)}{S^2}$$

This is a modification of Gilbert's equation and uses the same units. The following choke sizes are checked for flow rates possible: 16/64, 20/64, 24/64, and 28/64. Table 4.17 shows the resulting calculations, including the ΔP values between the wellhead pressure required to move the assumed rates through the choke and the necessary downstream pressure to move the fluids to the separator. The downstream pressures are taken from Figure 4.15a.

Gilbert's equation can be adjusted quite easily to

TABLE 4.17
ΔP vs RATE FOR DIFFERENT CHOKE SIZES

Choke size	Assumed rate, b/d	P_D from horiz. correl., psi	P_{wh} from choke eq., psi	P_D/P_{wh}	ΔP across choke, psi
16/64	300	128	370	0.35	242
	400	140	484	0.28	354
	500	160	617	0.26	457
	600	180	741	0.24	561
20/64	300	128	237	0.54	109
	500	160	395	0.41	235
	700	200	553	0.36	353
	900	250	711	0.35	461
24/64	500	160	274	0.58	114
	700	200	384	0.52	184
	900	250	494	0.51	244
	1,100	300	603	0.50	303
28/64	800	227	322	0.70	95
	1,000	275	403	0.68	128
	1,200	330	484	0.68	154

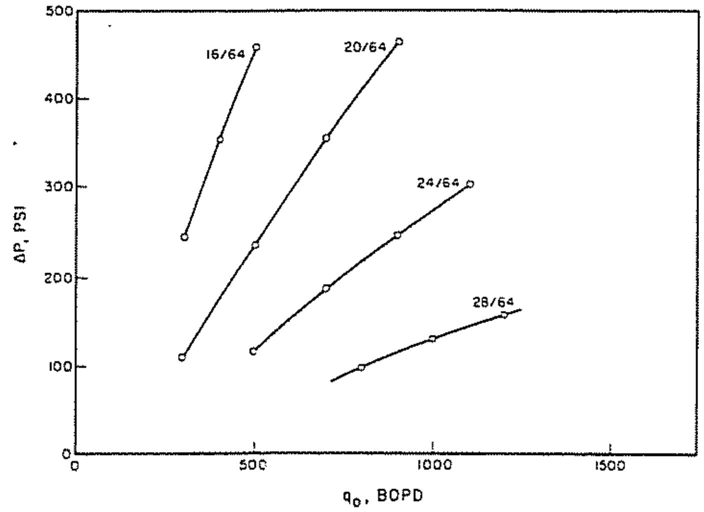

Figure 4.36 Choke Bean Performance

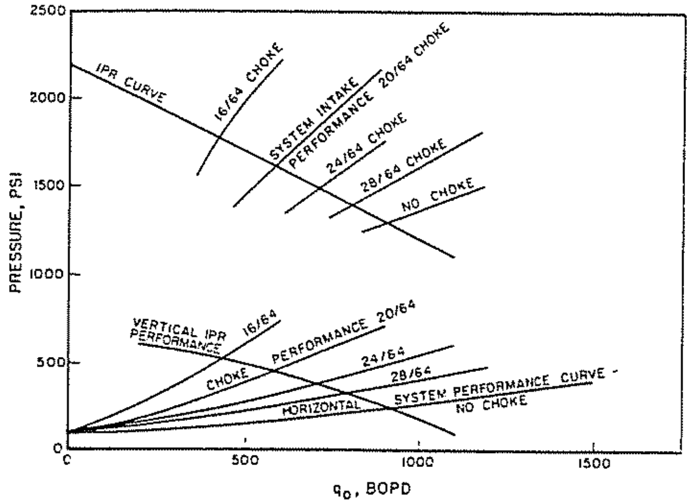

Figure 4.38 Surface Choke Evaluation

more closely reproduce data from a particular well or field.

The ΔP's calculated are unique to the example system since the downstream pressures were calculated for the example system. Notice that in each case a check was made to ensure $P_D/P_{wh} \leq 0.7$ so that Gilbert's equation would apply. If this is not the case, a subcritical flow equation must be used to calculate ΔP across the choke.

(5) From Table 4.17, plot the ΔP's for each choke as shown in Figure 4.36.

(6) Overlay the results of Figures 4.35 and 4.36 as shown in Figure 4.37.

Figure 4.37 displays the total system performance for different wellhead choke sizes. The system performance curves show the "required" ΔP for various flow rates considering the entire system from reservoir to separator. The choke performance curves show the "created" ΔP for various flow rates considering choke performance for different choke sizes. The intersection points of the created and required ΔP's represent the flow rates possible. For example, the rate will drop from 900 bo/d to 715 bo/d with the installation of a 24/64 wellhead choke.

Figure 4.38 shows another presentation that is often used to evaluate wellhead chokes. The solution is shown at the bottom of the well at the top of Figure 4.38. In this case, the solution is obtained by starting at the separator and proceding all the way to the bottom of the tubing and on to the center of the perforated interval to find the tubing intake pressure.

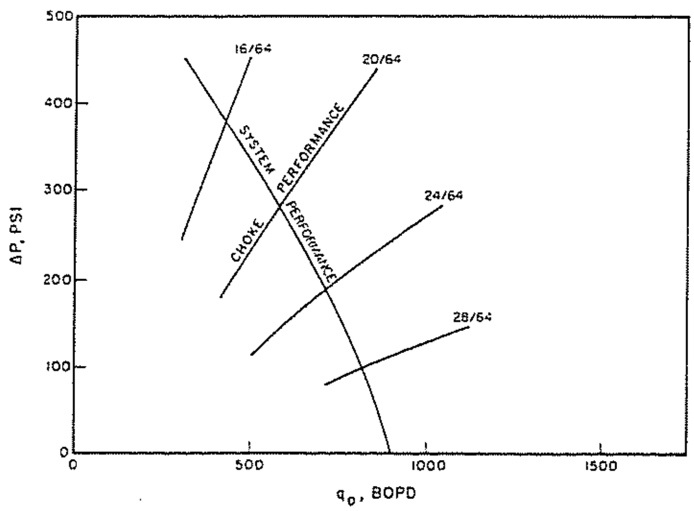

Figure 4.37 Systems Performance for Various Wellhead Chokes

The solution at the bottom of Figure 4.38 shows allowable wellhead pressures (P_{wh} values necessary for certain rates) plotted against the horizontal performance curves, which include the choke.

All three solution positions will give the same answer.

The secret to sizing chokes is to remember that the wellhead pressure controls the flow rate. The choke is merely a means of setting and controlling the wellhead pressure.

The various reports that are seen in the morning paper and numerous company reports always bother us a little when they say "well #A-22 came in producing 600 b/d on a 14/64 choke." From that bit of information, it is difficult to know whether the well is any good. Now, if the report says "well #A-22 came in producing 600 b/d with a wellhead pressure of 2,500 psi," it is obviously an excellent well. However, if it says "well #A-22 came in at 600 b/d with 100 psi wellhead pressure," it may be a much weaker well. The wellhead pressure has much more significance than the choke size, and it controls the flow rate.

4.283 SAFETY VALVES

4.2831 INTRODUCTION

There are several types of downhole safety valves that are presently being run in oil and gas wells in the United States as well as in other countries. These valves can be divided into two categories—that is, surface-controlled safety valves and subsurface-controlled safety valves. These safety valves, normally with ID's less than the tubing in which they are installed, create certain pressure losses in the flow stream. The surface-controlled safety valves can be installed as fully open valves, but most of these must be tubing retrievable in order to have the same ID as the tubing. Presently, some valves are retrievable and still fully open. The surface-controlled safety valve is normally retrievable

by wire line, which means that it offers a restriction to flow across it. The fully open valve can be made to accept a restricted wire-line valve if and when it becomes necessary.

The subsurface-controlled safety valves are of two types: (1) velocity- or differential-controlled valves and (2) pressure-actuated valves (similar to a gas-lift valve).

The following design procedure is for any safety valve that serves as a restriction in the tubing string but is specifically applicable for a safety valve that requires a differential pressure to close.

4.2832 DESIGN PROCEDURE FOR THE VELOCITY-ACTUATED SAFETY VALVE

Refer to Figure 4.39 for a physical picture of the location of a safety valve. This position varies and may change from one manufacturer to the next based on certain pressure requirements. The following procedures were given by Mach, Proaño, and Brown and are essentially the same as found in the original paper (copyright SPE of AIME).[4]

The safety-valve location is considered a node (solution position), and pressures are converged on it from both directions (refer to Figure 4.40). The pressure under the safety valve is a combination of the inflow performance curve (ability of well to produce) and the vertical multiphase pressure drop from the bottom of the well to the bottom of the safety valve. This defines the pressure under the safety valve (upstream pressure) for various flow rates from the well. Figure 4.41 shows the emergency condition. The pressure just above the safety valve (downstream pressure) is a combination of the horizontal and vertical multiphase pressure drop from the separator to the top of the safety valve. Emergency response curves can be constructed to represent the pressure above the safety valve under emergency conditions. This pressure is the vertical multiphase pressure drop from a selected emergency wellhead pressure to the top of the safety valve. Then, how the well will respond for different sized chokes in the safety valve for both normal and emergency conditions is determined.

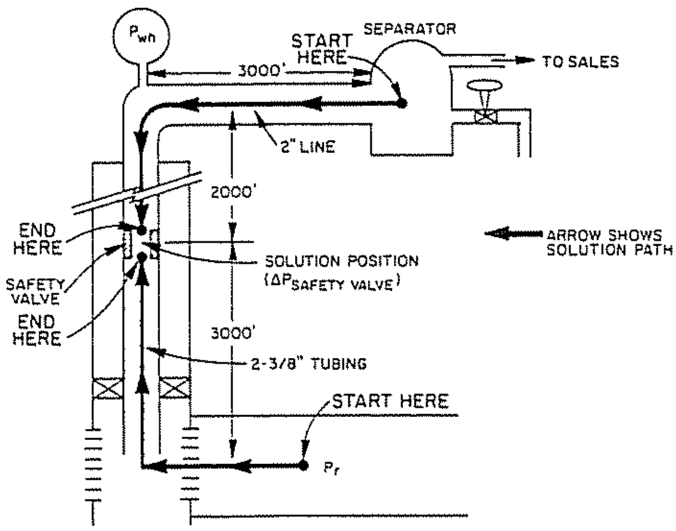

Figure 4.40 Safety Valve Normal Operations

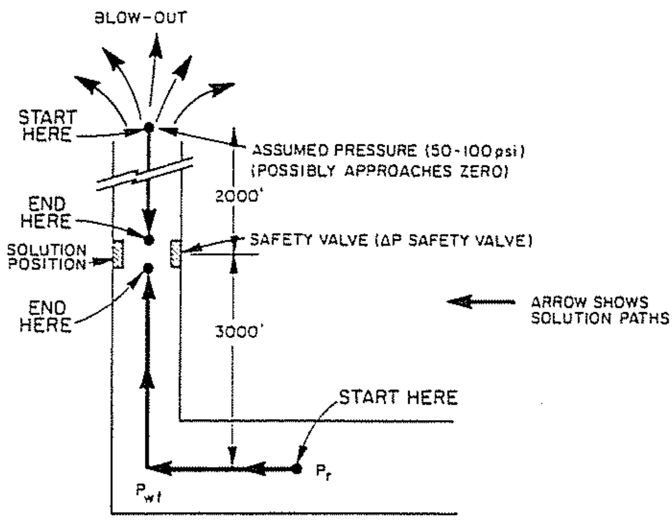

Figure 4.41 Safety Valve Emergency Conditions

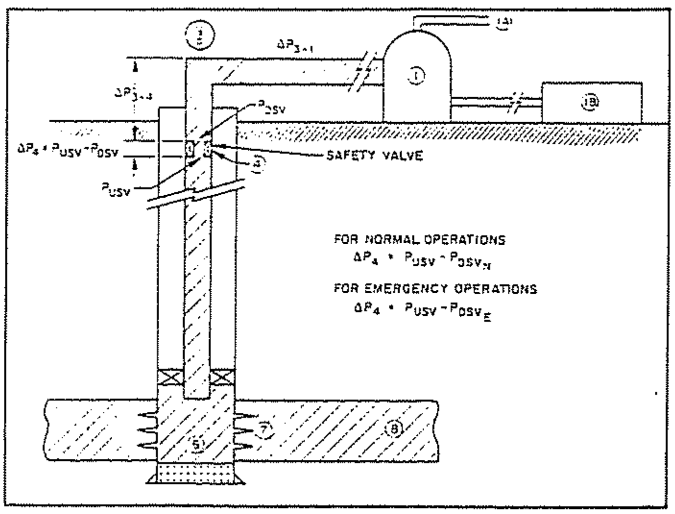

Figure 4.39 Safety Valve Solution

The solution to determine pressure loss across the velocity- or differential-controlled safety valve is similar to the surface-choke solution. A determination of flow rates possible vs differential pressures created at the safety-valve position is first determined. Then, based on differential requirements to actuate the safety valve, a proper orifice size for the safety valve can be selected.

The same example problem as worked in Section 4.2 will be used to install a safety valve, and this data is given again at this point.

EXAMPLE PROBLEM (VELOCITY-ACTUATED SAFETY VALVE)

Given data: flowing oil well. safety valve placed at 2,000 ft

separator pressure = 100 psi
flow line = 2 in., 3,000 ft long
WOR: 0
depth = 5,000 ft to center of perforation
GOR = 400 scf/bbl
$\bar{P}_r$ = 2,200 psi
IPR = J = 1.0 b/d/psi (assume constant)
tubing size = 2⅜ in.

The solution node is taken at the safety-valve location (2,000 ft from the top). The solution is given for both a velocity-actuated safety valve and a pressure-operated safety valve. The velocity or differential safety valve (commonly called "storm choke") is the one that has the most restriction to flow. The purpose of this section is to cover the procedure for the correct sizing of the velocity and the pressure-operated safety valves. Where possible, the velocity type of safety valves are being replaced by surface-controlled safety valves. However, there are numerous velocity valves still installed, and under certain well conditions, some velocity valves continue to be installed. The flow through the standard surface-controlled safety valve creates relatively low pressure losses in most cases. Therefore, a condition of subsonic or subcritical flow exists, although subsonic flow for a gas-oil mixture is not well defined.

In this example, it is assumed that no other restrictions are in the system. The pressure losses must be determined for both emergency and normal conditions. A little difficulty is experienced in predicting that wellhead pressure at which emergency conditions occur. For example, if the Christmas tree is completely sheared off, the well would be flowing to atmospheric pressure. However, some debris may always be present thereby creating some back pressure. In the example well, it is noted that, under normal operating conditions at 900 b/d, a wellhead pressure of 245 psig is present. Therefore, it would probably be wise to set the velocity type of valve to close on a wellhead pressure between 50 and 100 psig or even higher, depending upon the degree of safety desired. Normally, a valve set to close at a pressure lower than 50 psig is not recommended under any circumstances. However, Mach, Proaño, and Brown worked this example using atmospheric pressure (zero pressure) at the wellhead, and this solution is presented here.[4]

Step-by-step procedure (normal operations)

(1) Assume flow rates of 200, 400, 600, 800, 1,000, and 1,500 b/d.

(2) For normal operations, start at the separator pressure of 100 psig and proceed through the horizontal flow line to the top of the safety valve at 2,000 ft down the well. Table 4.18 shows these results.

(3) Starting with $\overline{P}_r$ and the assumed flow rates, determine the flowing bottom-hole pressures and

TABLE 4.18
NORMAL OPERATIONS

Assumed q, b/d	Horizontal multiphase flow P_{sep}, psi	ΔP_{1-3}, psi	P_{wh}, psi	Vertical multiphase flow ΔP_{3-4}, psi	P_{DSV}, psi
200	100	15	115	195	310
400	100	40	140	230	370
600	100	80	180	270	450
800	100	130	230	320	550
1,000	100	175	275	355	630
1,500	100	320	420	470	890

then proceed upward to the bottom of the safety valve, 3,000 ft up the hole. These results are noted in Table 4.19 where P_{USV} = the pressure at the bottom of the safety valve or the pressure upstream of the safety valve.

TABLE 4.19
NORMAL OPERATIONS

Assumed q, b/d	$\overline{P}_r$, psi	From P1 ΔP_{8-6}, psi	$P_{wf} = P_6$, psi	Vertical multiphase flow ΔP_{6-4}, psi	P_{USV}, psi
200	2,200	200	2,000	990	1,010
400	2,200	400	1,800	890	910
600	2,200	600	1,600	790	810
800	2,200	800	1,400	730	670
1,000	2,200	1,000	1,200	680	520
1,500	2,200	1,500	700	660	40

(4) Plot the pressures on top of the safety valve (P_{USV}) of step 2 vs the pressures downstream of the safety valve (P_{DSV}) as noted in Figure 4.42. The intersection of these two curves again shows 900 b/d. In other words, we have solved for the flow rate from this well by taking a solution position 2,000 ft from the top.

Step-by-step procedure (emergency conditions)

Assume that the wellhead is completely sheared off and that the well is blowing to atmospheric pressure (zero psig). By way of caution, take the emergency wellhead pressure to be 50 psig or greater, using common sense based on the wellhead producing pressure at the objective flow rate. (Do not use zero as used in this illustrative example.)

(1) Assume flow rates of 200, 400, 600, 800, 1,000, and 1,500 b/d.

(2) For emergency conditions and assuming P_{wh} = 0, find the pressure at the top of the safety valve (P_{DSV}) at 2,000 ft. These values are tabulated in Table 4.16.

(3) This step is the same as step 3 from normal operations. Starting with $\overline{P}_r$, determine the flowing bottom-hole pressures and then proceed upward to the bottom of the safety valve, 3,000 ft up the hole. These results have already been tabulated in Table 4.19.

(4) Plot the pressures on top of the safety valve for emergency conditions vs the pressures below the safety valve as noted in Table 4.20 and Figure 4.42. This shows an emergency flow rate of 1,200 b/d at the intersection of these two curves.

As a word of caution, safety valves sometimes are set on a rate equivalent to some percentage increase in production such as 125–150%. In this case, the rate of increase from normal (900 b/d) to maximum (1,200 b/d) is 133%, and this is the absolute maximum rate from this well with zero wellhead pressure. Therefore, a setting on a percentage increase greater than 133% would never allow the safety valve to close.

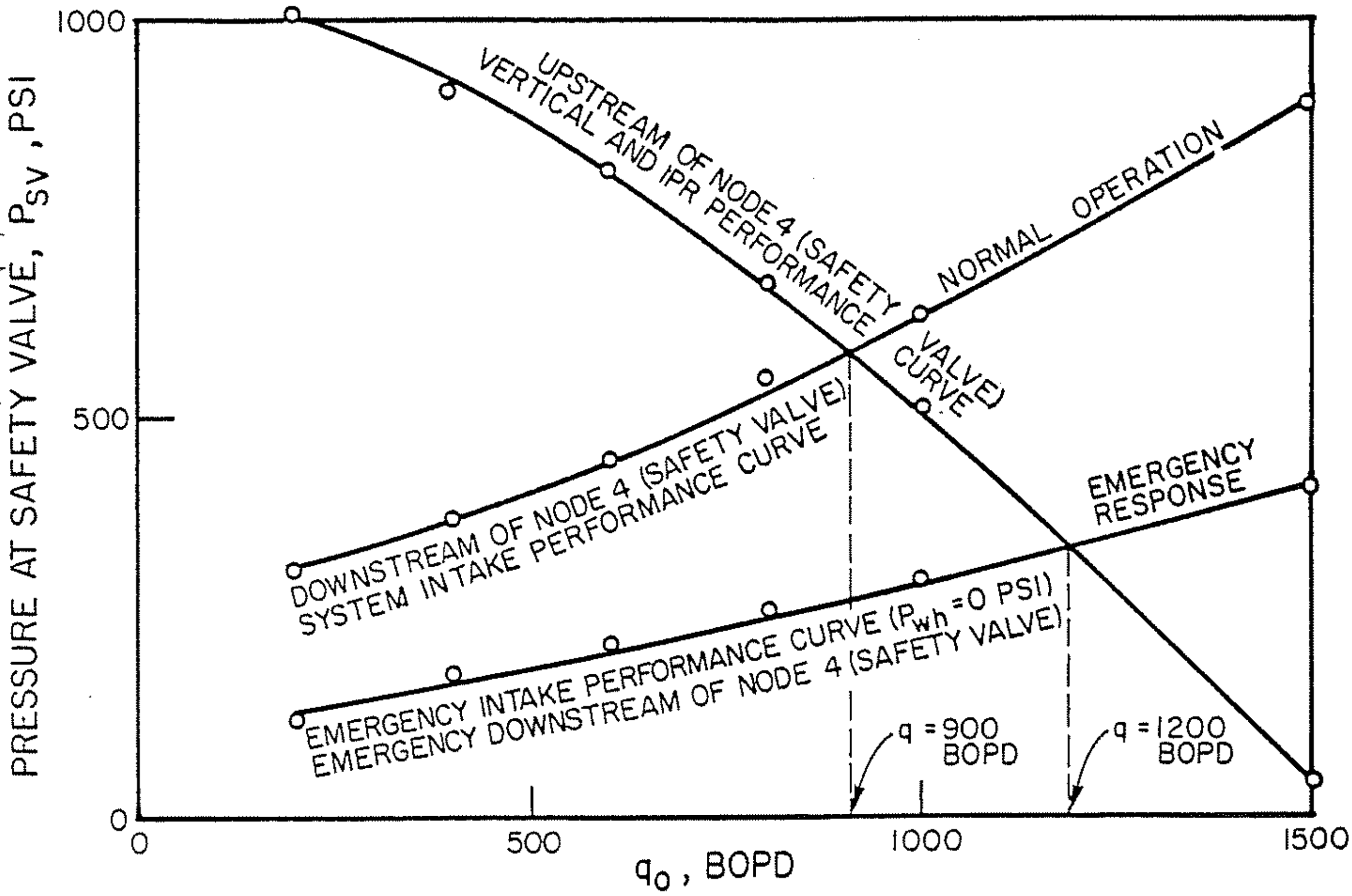

Figure 4.42 Pressures Above and Below Safety Valve for Different Rates

TABLE 4.20
EMERGENCY CONDITIONS

Assumed q, b/d	P_{wh}, psi	Vertical multiphase flow $\Delta P_{3-4} = P_{DSV}$, psi
200	0	120
400	0	180
600	0	215
800	0	260
1,000	0	295
1,500	0	410

(5) Determine the flow rates from this well for certain differential pressures (ΔP's) that exist at the safety-valve location (node 4) for both normal and emergency operations. Refer to Figures 4.43 and 4.44, respectively. These values of ΔP are tabulated in Tables 4.21 and 4.22, respectively.

(6) Plot ΔP vs rate as noted in Figure 4.45 for both normal and emergency conditions.

(7) The next step becomes rather complex in that an appropriate equation for predicting pressure loss across a safety valve (choke restrictions) must be used. In some instances, this pressure loss is low, and subsonic flow conditions exist. Various models have been proposed to predict subcritical two-phase flow pressure drop across restrictions. The main models were proposed by the University of Tulsa,[5] *API-14B*,[6] Ashford and Pierce,[7] and Fortunati.[8] A thorough review on some of the limitations of these models and their applicability to experimental data is given by Proaño[9] and Roman-Lazo.[10] Pressure-loss calculations and orifice settings for this example are determined, with the correlations presented by Beggs.[5] These procedures and an example problem have been reproduced by permission in Appendix 4.3.

By use of the appropriate equation, calculate the pressure drop across the safety valve for several choke sizes within the range of sizes expected to be used.

(8) Plot the ΔP values obtained across the various choke sizes with the ΔP values of Figure 4.45 (see Figure 4.46). Notice that Figure 4.46 shows only the 10, 12, 16, 20, 32, and 64/64ths of an inch choke sizes. The ΔP values for both emergency and normal conditions are plotted. Figure 4.46 shows the flow rates possible for both normal and emergency conditions. Figure 4.46 permits the logical selection of an orifice that, installed in the safety valve, will permit closure under emergency conditions and will remain open under normal conditions. Mach, Proaño, and Brown noted that the proper selection of the safety valve orifice should meet the following criteria:[4]

(a) The valve must close when an emergency situation exists.

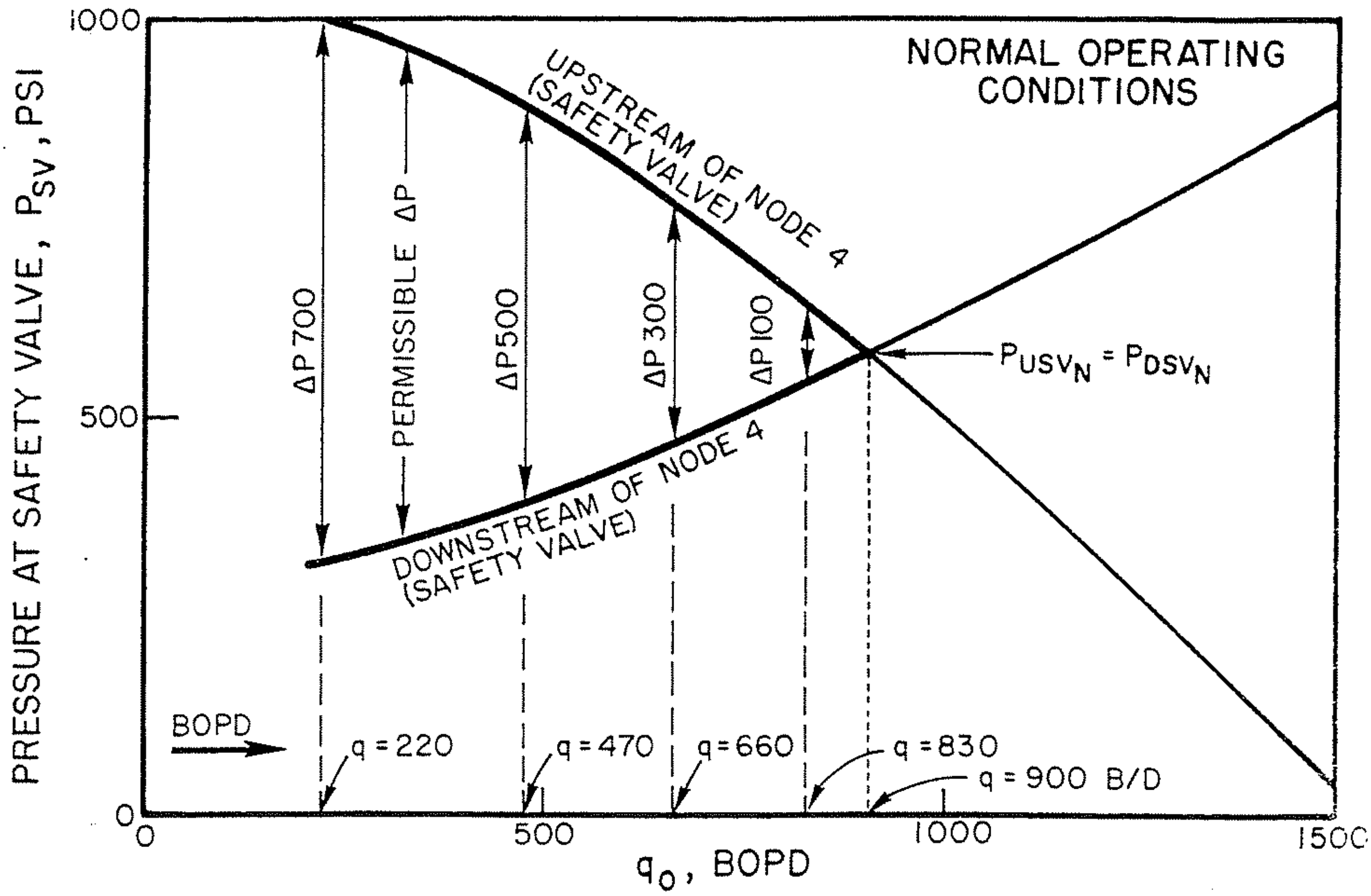

Figure 4.43 Permissible Pressure Drops (ΔP) That Exist at Node 4 vs Rates

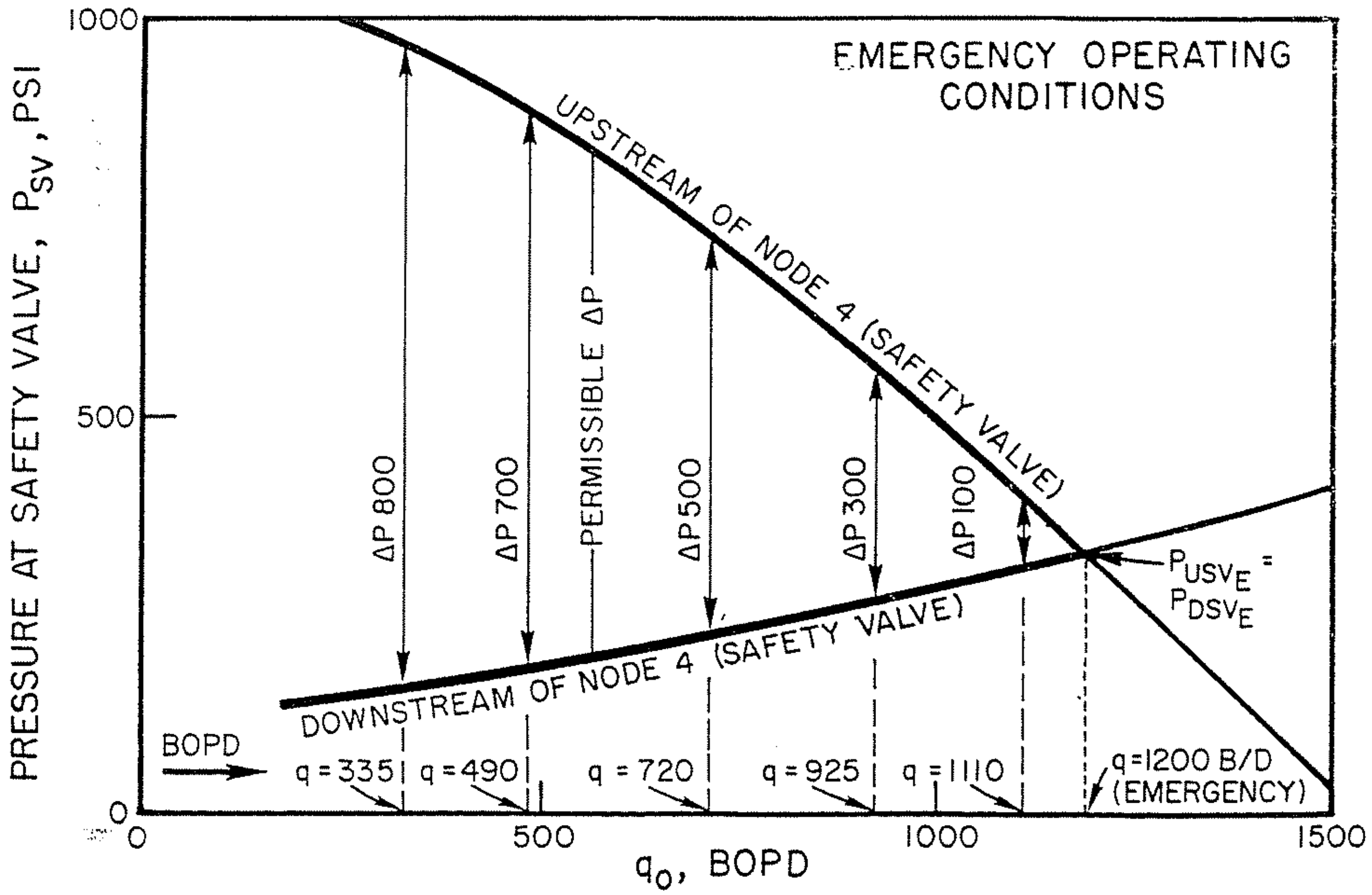

Figure 4.44 Permissible Pressure Drops (ΔP) That Exist at Node 4 vs Rates

TABLE 4.21
VALUES OF ΔP vs q FOR NORMAL OPERATIONS

$\Delta P = P_{USV} - P_{DSV_N}$, psi	Rate, b/d
100	830
200	750
300	660
400	570
500	470
600	350
700	220

TABLE 4.22
VALUES OF ΔP vs q FOR EMERGENCY OPERATIONS

$\Delta P = P_{USV} - P_{DSV_E}$, psi	Rate, b/d
100	1,100
200	1,020
300	925
400	830
500	720
600	610
700	490
800	335
900	120

(b) The valve should not inadvertently close during normal operations.
(c) As large an orifice as possible should be selected so that the reduction in production rate from the normal unrestricted rate of 900 b/d is minimized.

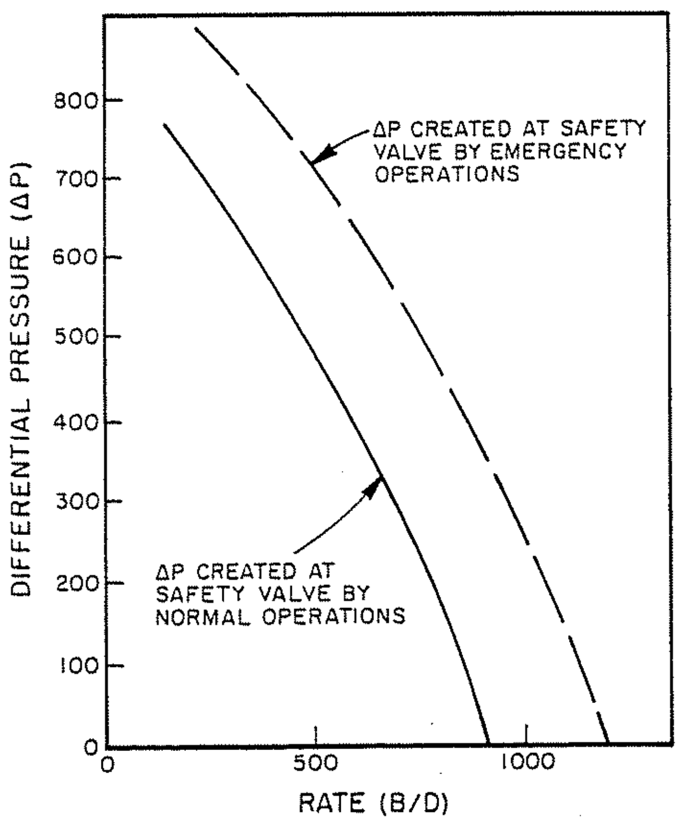

Figure 4.45 Differential Pressure vs Rate

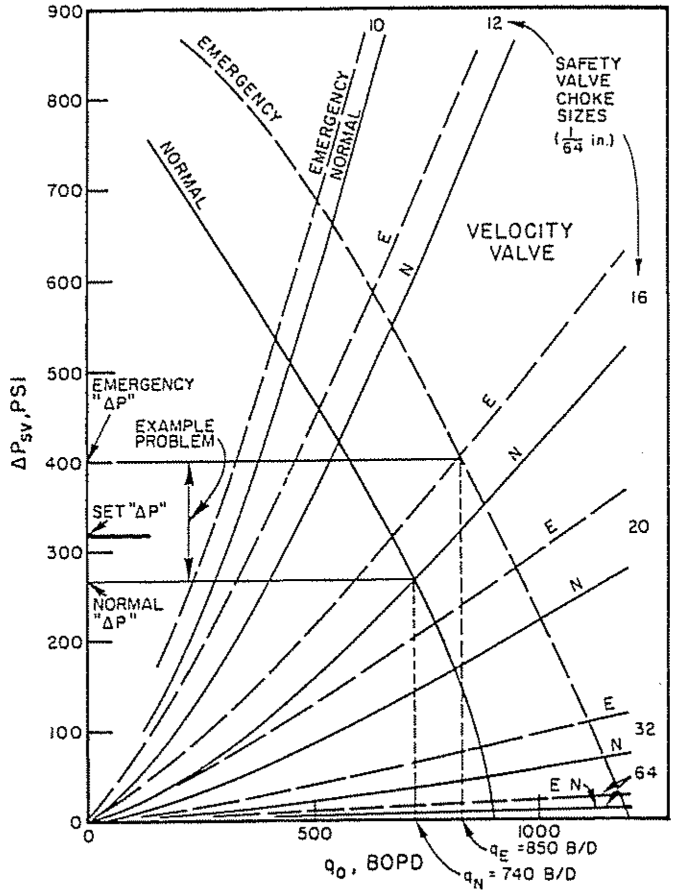

Figure 4.46 Flow Rate vs ΔP for Different Choke Sizes Under Normal and Emergency Conditions

There is no set procedure for selecting the final orifice size. To some extent, this may depend upon personal or company policy and philosophy. Some cases may dictate a greater safety factor in making certain that a potentially hazardous well will definitely "close in" on a predetermined lowering of the wellhead pressure. Mach, Proaño, and Brown noted that the selection of the final orifice size will depend upon:[4]

(1) known accuracy of the multiphase flow correlations used in a certain area
(2) known fluctuations in wellhead pressure caused by chokes, long flow lines, changing sales-line pressures, etc.
(3) changing reservoir parameters such as water cut, permeability, reservoir pressure, etc.

As a guideline, it is recommended that the closing differential be selected at least 75 psi below the expected emergency differential. This is done to assure valve closure during an emergency condition. To minimize the nuisance of premature closures, it is recommended that the closing differential be selected at least 75 psi above the expected normal differential. These requirements mean that the orifice size selected must create at least 150 psi more pressure drop under emergency conditions than under normal conditions. Notice from Figure 4.46 that a 16/64 bean fits this requirement; therefore, for this example well, a 16/64 bean size is selected with a closing differential set at 325 psi. The following information is obtained from Figure 4.46:

(1) safety valve orifice size: 16/64
(2) closing ΔP to be set in valve: 325 psi
(3) emergency flow rate: 825 bo/d
(4) emergency ΔP across safety valve: 400 psi
(5) normal flow rate: 720 bo/d
(6) normal ΔP across safety valve: 260 psi
(7) normal flow rate with no safety valve in well: 900 bo/d
(8) emergency flow rate with no safety valve in well: 1,200 bo/d

The preparation of Figure 4.46 has made the selection much easier, and as a matter of fact, it would have been impossible to make a logical selection without Figure 4.46. Notice that both the 10/64 and 12/64 orifices restrict the flow rate rather drastically, whereas the 20/64 and larger fail to create enough working differential across the orifice for good selection, although with luck a 20/64 might be made to work satisfactorily but would leave little room for error and changing well conditions.

It is also very important to set the emergency wellhead pressure at a value sufficiently high to always obtain closure. This should be some value greater than zero but not so close to normal wellhead pressure that premature closing occurs.

4.2833 DESIGN PROCEDURE FOR THE PRESSURE-OPERATED SAFETY VALVE

The pressure-operated safety valve operates on the same principle as a gas-lift valve. It has a pressure-charged dome or spring that requires a predetermined pressure to hold the valve open. Therefore, under normal operating conditions and with a set wellhead pressure of 245 psig at 900 b/d, there would be sufficient pressure at 2,000 ft in the tubing string to hold the valve open. An obvious choice is to select the largest orifice or seat size available for a particular tubing size. A 1-in. 64/64-in. valve is available for 2⅜-in. OD tubing.

This pressure valve closes on a decrease in pressure at the valve location. Under emergency conditions, the wellhead pressure lowers and immediately lowers the pressure in the tubing at the safety valve location at 2,000 ft.

Even though a decrease in wellhead pressure will generally cause an increase in flow rate, the additional pressure drop in the tubing caused by the increased flow rate is usually much less than the lowering of the wellhead pressure from the normal flowing wellhead pressure to the emergency wellhead pressure. This, of course, must be checked by constructing appropriate pressure traverses for both conditions.

EXAMPLE PROBLEM (REFER TO REFERENCE 4)

Given data:

Same as Example Problem for velocity valve. Safety valve placed at 2,000 ft with 64/64-in. restriction.

Steps 1 through 7 are the same as for the velocity valve except only a 64/64-in. choke need be evaluated in step 7.

(8) Plot the ΔP values as noted in Figure 4.47. Again, the normal and emergency flow rates can be obtained as well as the pressure drops for both normal and emergency conditions.
(9) Construct pressure traverses for both the normal and emergency conditions as noted in Figure 4.48. The data from Table 4.23 is available from appropriate figures or tables.

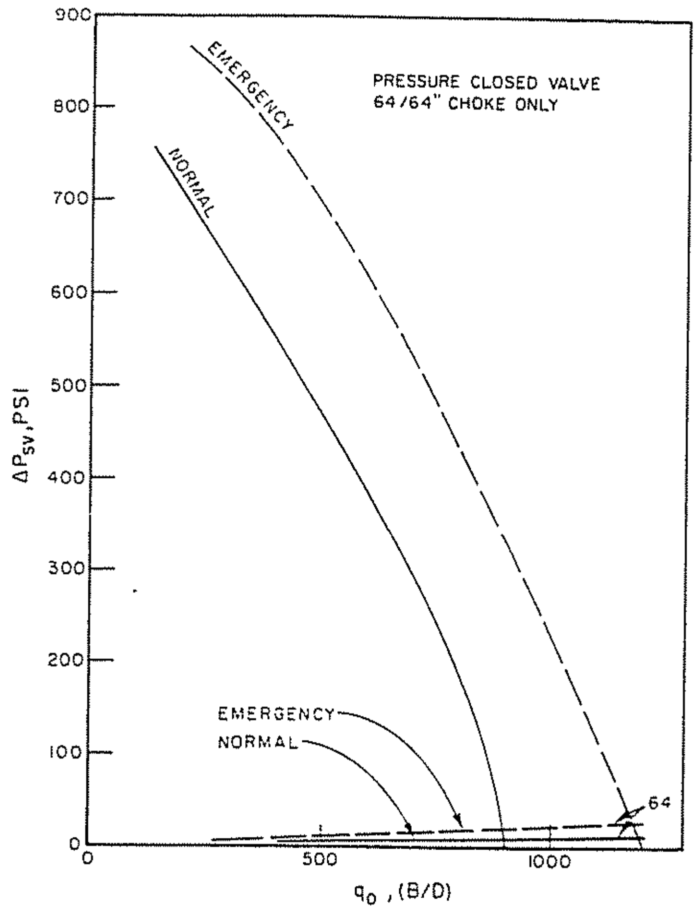

Figure 4.47 Flow Rate vs ΔP for Emergency and Normal Conditions

As with the velocity valve, the selection of the closing pressure should meet the following criteria:

(1) The valve must close when an emergency condition occurs.
(2) The valve should not close prematurely during normal operations.

The selection depends on:

(1) known accuracy of the multiphase flow correlations used in certain areas
(2) known fluctuations in wellhead pressure caused by chokes, long flow lines, changing sales-line pressures, etc.
(3) changing reservoir parameters such as water cut, permeability, reservoir pressure, etc.

In general, it is recommended that the closing pressure be selected at least 75 psi above the emergency pressure and below the normal pressure at the valve location. These selections can be logically made by checking Figure 4.48 and noting the two pressure traverses. Also, caution must be exercised to keep the valve from prematurely closing. In some cases, this may require a smaller orifice.

If there is sufficient difference between the normal and emergency pressures at the valve, it is recom-

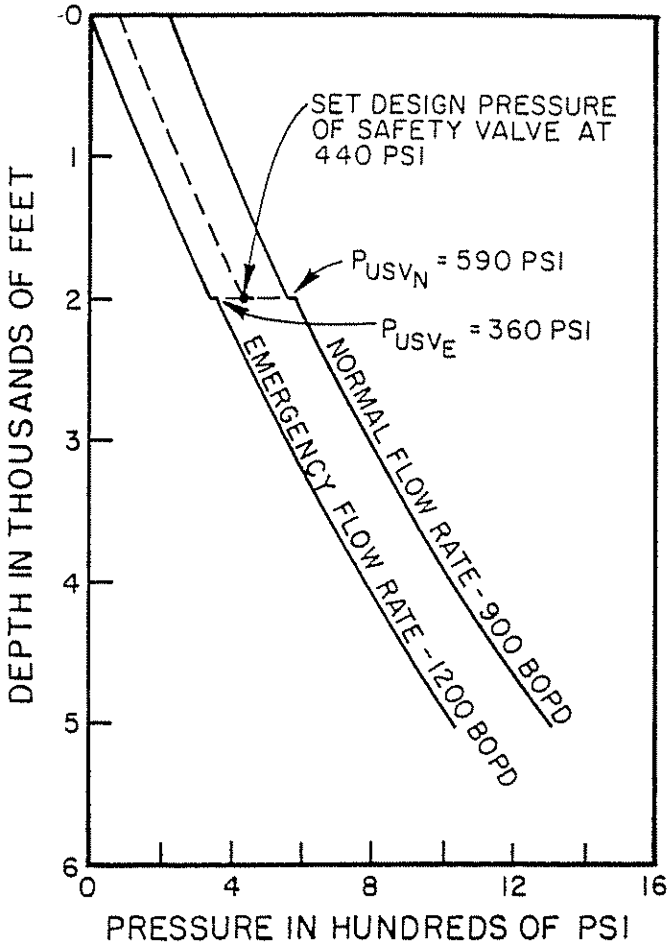

Figure 4.48 Vertical Flowing Pressure vs Depth Traverse for Pressure Valve

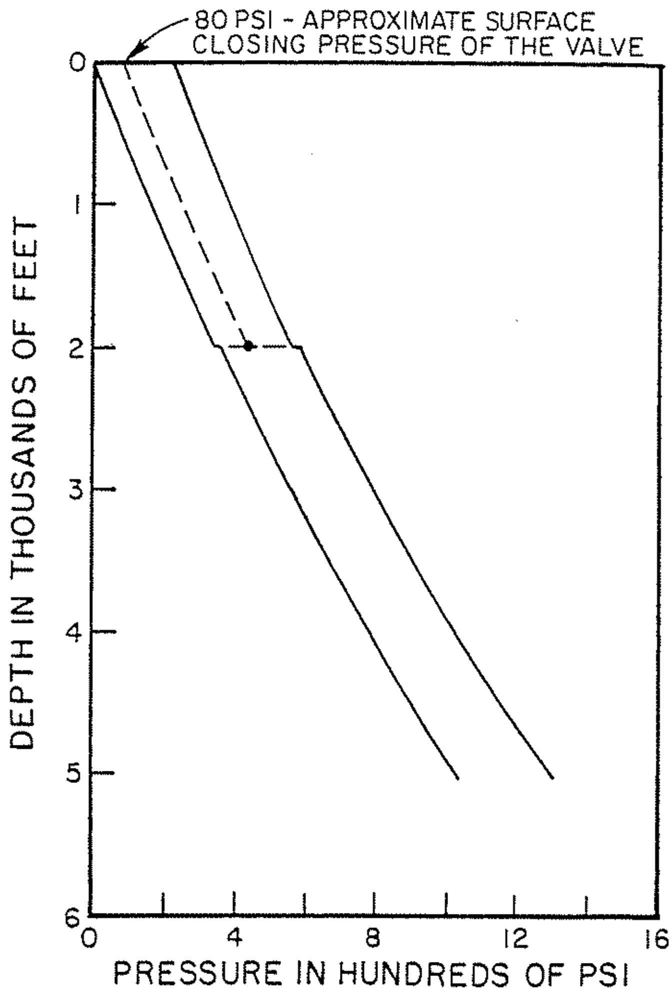

Figure 4.49 Surface Closing Pressure of Pressure Valve

TABLE 4.23

Normal conditions	Emergency conditions
$q_o = 900$ b/d	$q_o = 1{,}200$ b/d
$P_{wh} = 255$ psi	$P_{wh} = 0$ (assumed)
ΔP safety valve = 8 psi	ΔP safety valve = 23 psi
$P_{wf} = 1{,}300$ psi	$P_{wf} = 1{,}000$ psi
$P_{above\ s.v.} = 582$ psi	$P_{above\ s.v.} = 337$ psi
$P_{below\ s.v.} = 590$ psi	$P_{below\ s.v.} = 360$ psi

mended that the closing pressure of the valve be set halfway between these two pressures. In some cases, it may be advantageous to set the closing pressure of the valve closer to the emergency or normal pressure, depending upon the objective. For example, if the reservoir pressure is declining rapidly in a well, it may be better to set the valve closer to the emergency pressure so that the valve will function longer before a readjustment of the set closing pressure is necessary.

Figure 4.49 shows the approximate surface wellhead pressure of 80 psi at which the pressure valve would close. Additional safety could be gained by setting the valve to close at a wellhead pressure nearer the normal pressure of 245 psi, such as 120 or 150 psi. Do not permit the wellhead pressure to drop below 50 psi before closure, and more realistically, not below 120–150 psi.

4.2834 SUMMARY ON SAFETY VALVES

A disadvantage of the velocity type of valve is that it is a normally open valve. This means that a differential caused by increased flow rates under an emergency situation must occur before the valve will close. The reservoir pressure must be monitored to make sure the well deliverability potential remains high enough to close the safety valve under emergency conditions.

The pressure-closed valve generally does not have the disadvantages of the velocity valve and is a normally closed valve. As the reservoir pressure declines, the normal pressure caused by the well at the valve will move closer and closer to the set closing pressure of the valve. Finally, the valve will close under normal conditions if the system pressure is lower than the surface closing pressure of the valve. At this time, it will be necessary to pull the valve and reset it at a lower pressure to continue to produce the well.

Many of the new safety valves are, of course, the surface-controlled valves, but the majority of these still offer restrictions to flow similar to a normal choke. Most of them operate at low pressure drops and therefore require subsonic flow equations. Recent innovations in safety valves show a design whereby a fully open valve is achieved, with the actuating device being retrievable by wire line. Also, safety valves that will close on the annulus are available.

4.3 INJECTION WELLS

Nodal systems analysis can be applied to both water and gas injection wells in order to determine optimum injection rates, correct tubing sizes, and completion techniques, and as a diagnostic tool.

4.31 WATER INJECTION WELLS

4.311 INTRODUCTION

There are numerous wells that are being used to inject water for waterflood purposes or as water disposal wells. The proper design of these wells is very important economically because new wells may be required to inject the objective water rates. In other cases, some producing or abandoned wells may be converted to injection wells.

After a period of time, these wells generally start showing a decrease in injection rate, principally because of partial plugging near the wellbore. Therefore, provision is made to backwash many of these wells. This is generally done by installing gas-lift valves and producing the well in a normal production manner until it has cleaned up properly and will again take water as an injection well.

If this well is completed in an unconsolidated sand, it may also have to be gravel packed in order to backwash properly without excessive sand production. Therefore, it is not unusual to find a gravel-packed water injection well. This must be properly designed to permit water injection at the objective rate as well as to permit proper backwashing at sometimes rather high differentials to remove those deposits, particles, etc., that have reduced the injection rates.

4.312 DESIGN PROCEDURE FOR A STANDARD WATER INJECTION WELL

(1) Prepare the IPR curve in the normal manner by making use of Darcy's Law:

$$q_{inj} = \frac{7.08 \times 10^{-3} k_w h (\Delta P)}{\bar{\mu}_w \bar{B}_w (\ln r_e/r_w - 3/4 + S)}$$

where:

k_w = md
h = ft
q = b/d
μ_w = cp

This equation appears the same as Darcy's law for flow into the wellbore except that ΔP must be added to the average reservoir pressure. An injection productivity index can be calculated; then, the equation appears as follows:

$$q_{inj} = J_{inj}\, \Delta P$$

This is a linear relationship for single-phase water flow. Assume values of ΔP and calculate the corresponding rates. Then, plot q vs ($P_r + \Delta P$). Obtain a figure similar to Figure 4.50.

The fracture pressure should not be exceeded, and this point is noted in Figure 4.50. If the fracture gradient for a particular well is not known, it can be estimated; it seldom exceeds a gradient of 0.8 psi/ft and is more likely to be on the order of 0.7 psi/ft. That is, the fracture gradient for a normal well can be estimated to be (0.7) (10,000) = 7,000 psi for a 10,000-ft well.

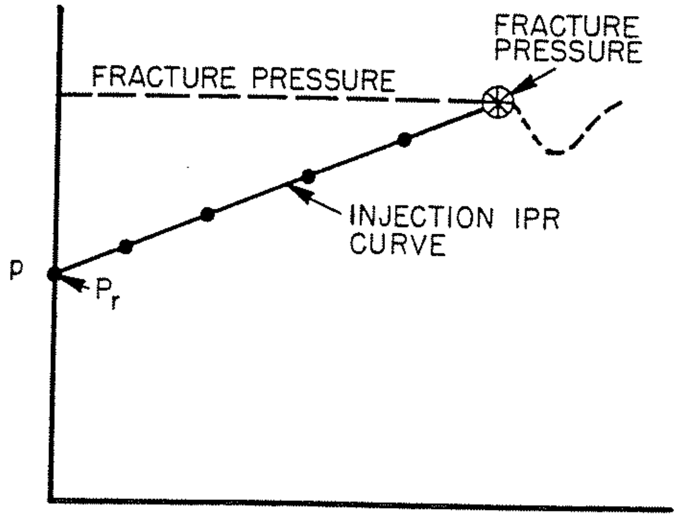

Figure 4.50 Construction of Water Injection IPR Curve

(2) Construct the tubing discharge curves as noted in Figure 4.51. These curves are analogous to the tubing intake curves for a producing well. However, for water injection curves, the friction is subtracted from the elevation component (static gradient). That is, the total pressure at the discharge of the tubing (assumed to be at the center of the perforations) is the elevation component minus the friction component, with acceleration normally being negligible for water flow only. If the tubing is less than two or three joints from the center of the perforated interval, it can be assumed to project to the center of the interval. Less friction will occur in the casing interval as compared to the tubing, and any long length of casing should be properly accounted for. By assuming tubing all the way, a slightly lower pressure and, hence, slightly lower injection rate will be predicted. A typical set of gradient curves for water injection is noted in Figure 4.52, including

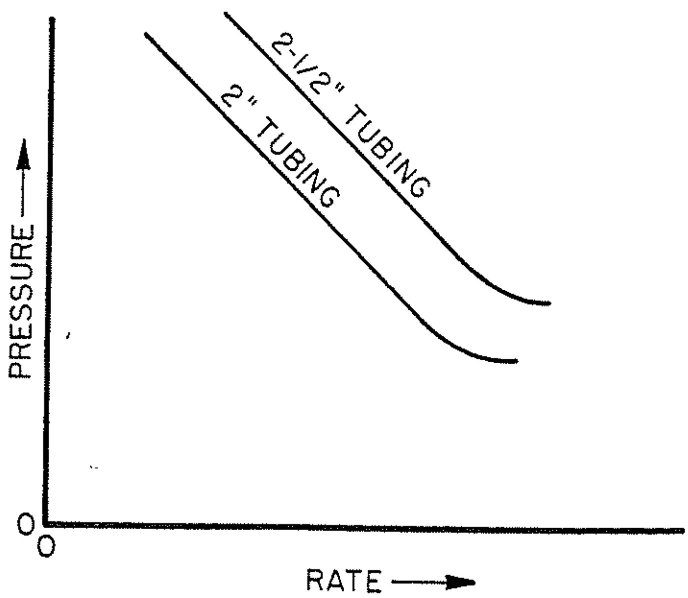

Figure 4.51 Tubing Discharge Curves for Water Injection Well

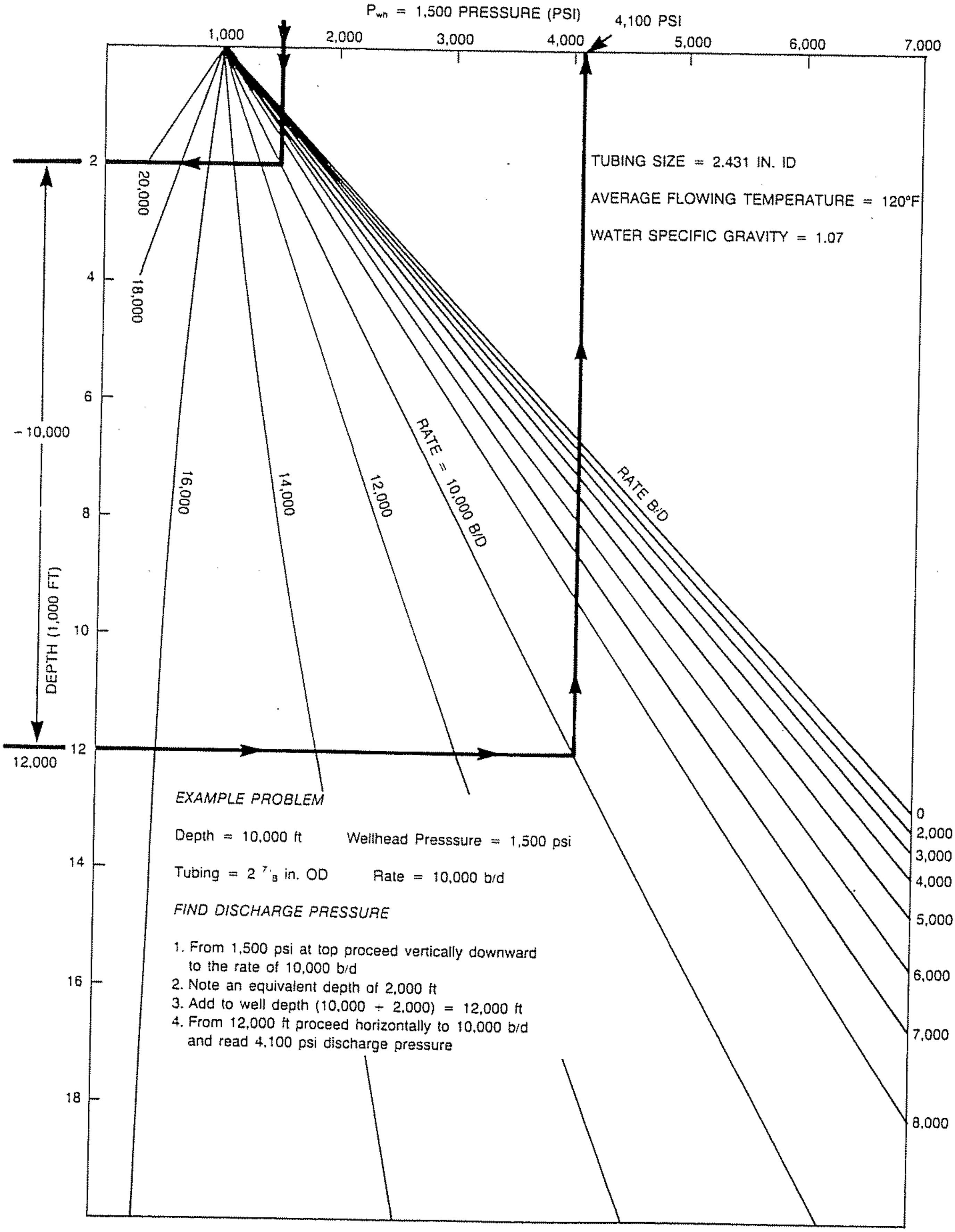

Figure 4.52 Typical Water-Injection Curves with Example Problem

an example problem. A complete set of curves for several tubing sizes can be found in Volume 3b of this textbook series. (Also see Appendix 4.4.)

(3) The injection IPR curves of step 1 and tubing discharge curves of step 2 are combined in the same manner as for a flowing well, as shown in Figure 4.53. The intersection of these curves shows the injection rate possible for this well.

A gravel-packed water injection well can be handled in the same manner as a producing well. The loss across the pack can be included in the IPR curve, or a ΔP plot such as Figure 4.54 can be prepared.

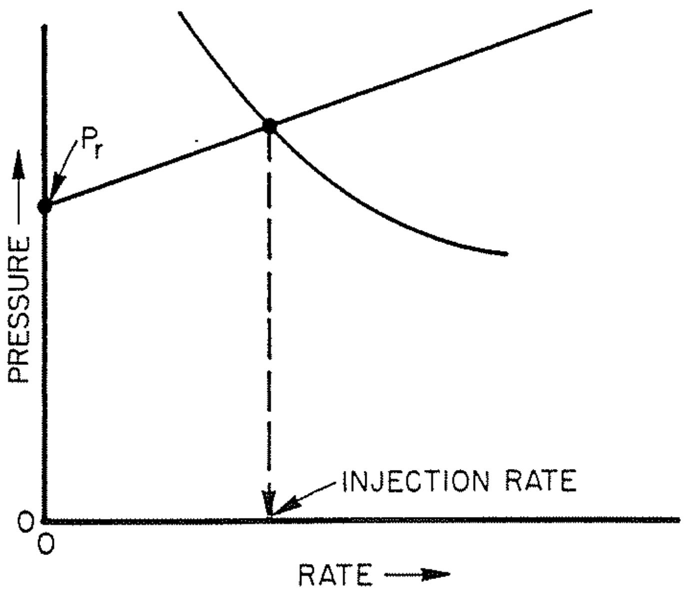

Figure 4.53 Combined IPR and Tubing Discharge Curves for Rate Prediction of Water Injection Well

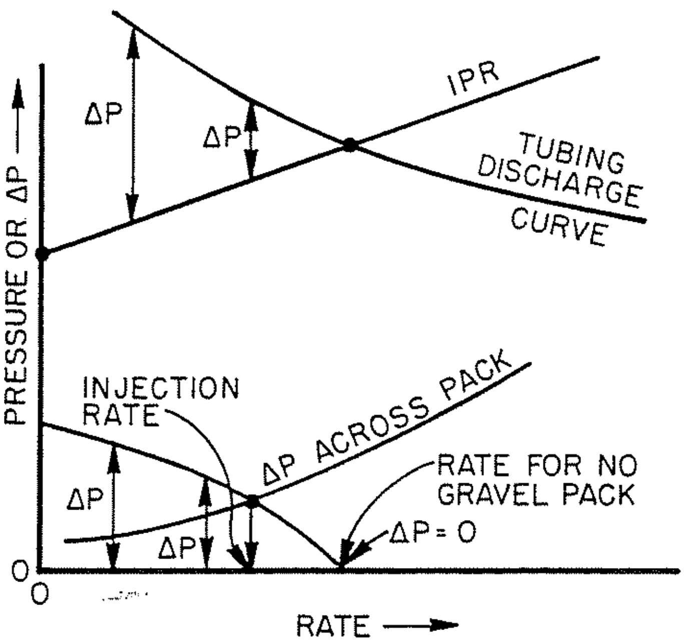

Figure 4.54 Solution for Gravel-Packed Water Injection Well

4.313 EFFECT OF VARIABLES FOR A WATER INJECTION WELL

A nodal systems analysis graph similar to Figure 4.53 can be used to look at the effect of such variables as wellhead pressure, tubing size, injection surface flow-line length, surface injection pump pressure, and perforation shot density for both gravel-packed and non-gravel-packed wells.

The systems graph can also be used as a diagnostic tool in determining when to backwash or acidize an injection well to increase the injection rate.

(1) *Effect of Surface Injection Wellhead Pressure.* A plot similar to Figure 4.55 can be prepared to show the effect of wellhead injection pressure and to aid in the selection of pump discharge pressure and pump horsepower. This plot is quite easily prepared by assuming various wellhead pressures and determining the corresponding tubing discharge curves.

(2) *Effect of Tubing Sizes.* The effect of tubing sizes can be shown in a plot similar to Figure 4.56. The

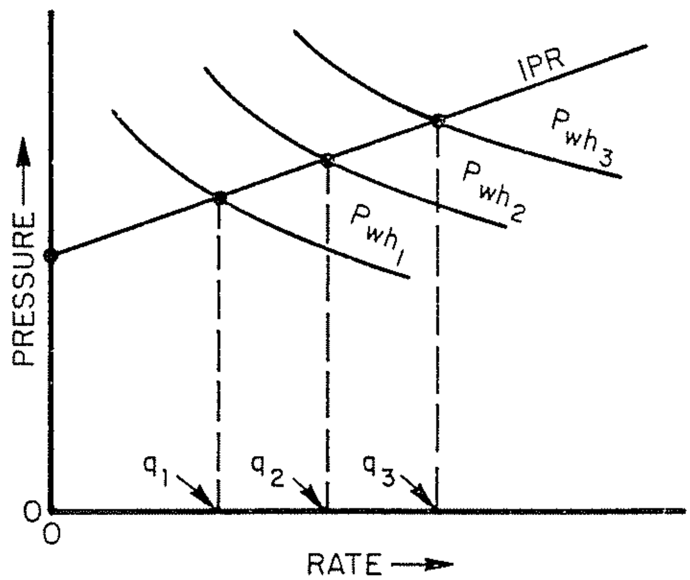

Figure 4.55 Effect of Surface Injection Wellhead Pressure

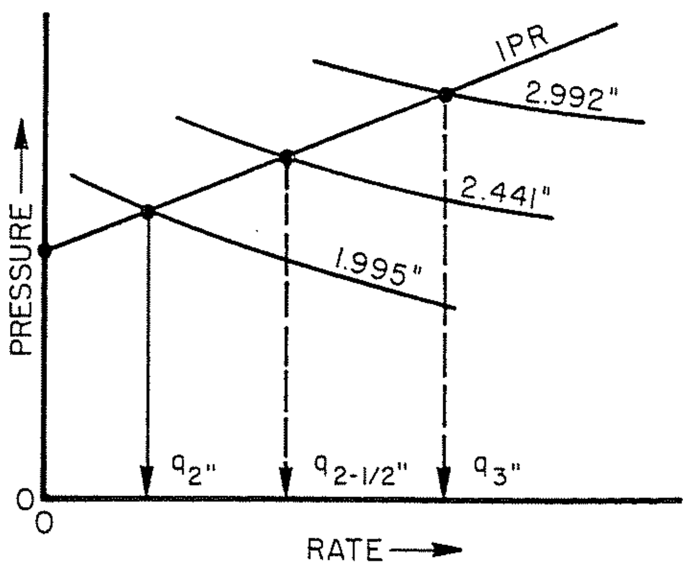

Figure 4.56 Effect of Tubing Sizes on Water Injection Well

correct tubing-size selection can then be made in order to obtain the objective flow rate.

(3) *Effect of Static Reservoir Pressure.* If a waterflood project is started on a depleted reservoir with a relatively low static pressure, the injection rate vs $\bar{P}_r$ may be important; this is noted in Figure 4.57.

Eventually at reservoir fill-up, the original reservoir will be reached or exceeded, depending upon reservoir withdrawals at that time. In order to construct IPR curves during these transient times—that is, until the water bank has reached r_e—an interative procedure could be employed that would properly account for all variables.

(4) *Effect of Flow-line Size.* If a long, small flow line is required to bring the water to the injection well, its effect can be significant in that excessive pressure loss caused by friction will occur in the flow line.

The effect of flow-line sizes could be evaluated in the same manner as for a naturally flowing well by taking the solution point at the wellhead or at the bottom of the well.

The following procedure would be followed for a wellhead pressure solution (see Figure 4.58):

(1) Assume various flow rates.
(2) Starting with the surface pump discharge pressure, determine the wellhead pressure for each assumed rate. This will be just opposite that of a flowing well in that wellhead pressure will be less as the rate increases because of increased frictional losses from the pump to the wellhead.
(3) Plot P_{wh} vs rate as noted in Figure 4.58.
(4) Starting from $\bar{P}_r$, determine the pressure at the center of the wellbore for injecting the various flow rates or read these values from the IPR curves.
(5) Using the pressures of step 4, determine the required wellhead pressure for each rate.
(6) Plot the required wellhead pressures of step 5 on Figure 4.58. The intersection of the curve of step 3 and step 6 gives the injection rate for this well.

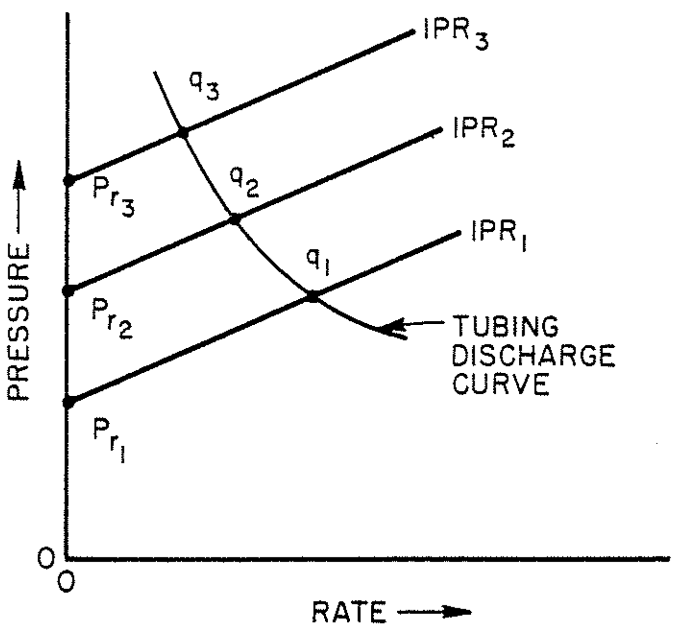

Figure 4.57 Effect of Increase in Static Reservoir Pressure

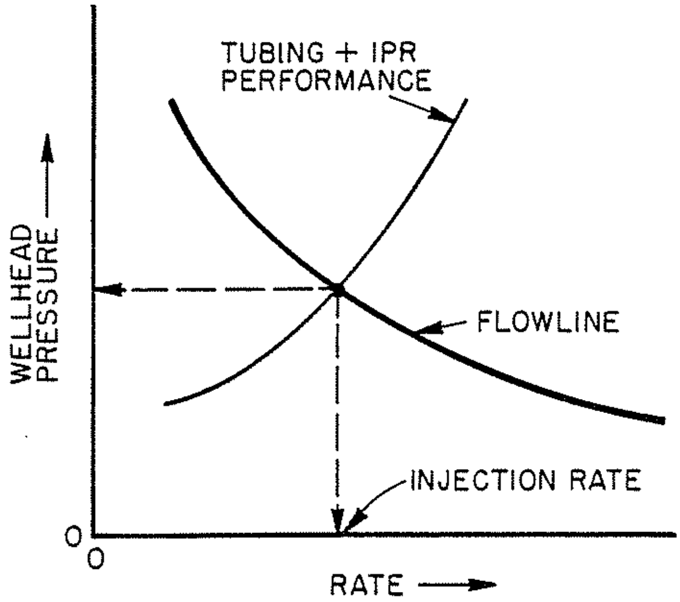

Figure 4.58 Wellhead Solution for Water Injection Well

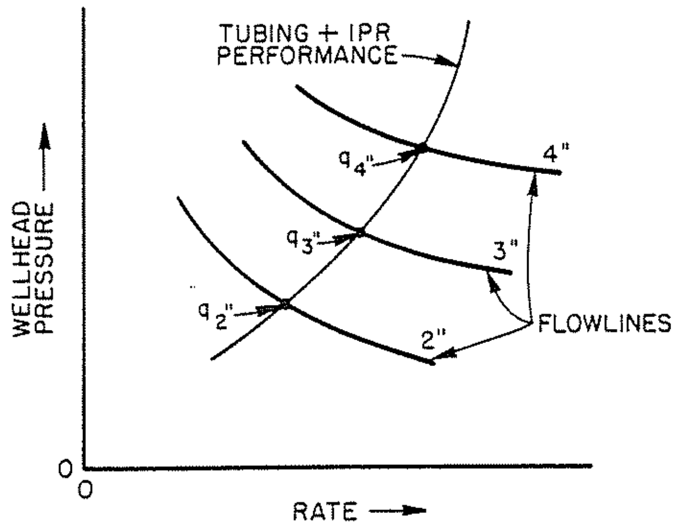

Figure 4.59 Effect of Flow-Line Sizes

The wellhead pressure solution permits the isolation of the flow line from the rest of the system and larger flow lines can be easily evaluated as shown in Figure 4.59.

EXAMPLE PROBLEM FOR WATER INJECTION (See Figure 4.60)

Given data:

well depth = 10,000 ft
k = 70 md
h = 30 ft (all perforated)
7⅝-in. casing 9⅞-in. hole 2⅞-in. tubing
T = 190°F
r_e = 2,000 ft
$\bar{P}_r$ = 5,000 psi (at fill-up)

A normal fracture gradient of 0.7 psi/ft is expected. The pump is to be located at the wellsite; hence,

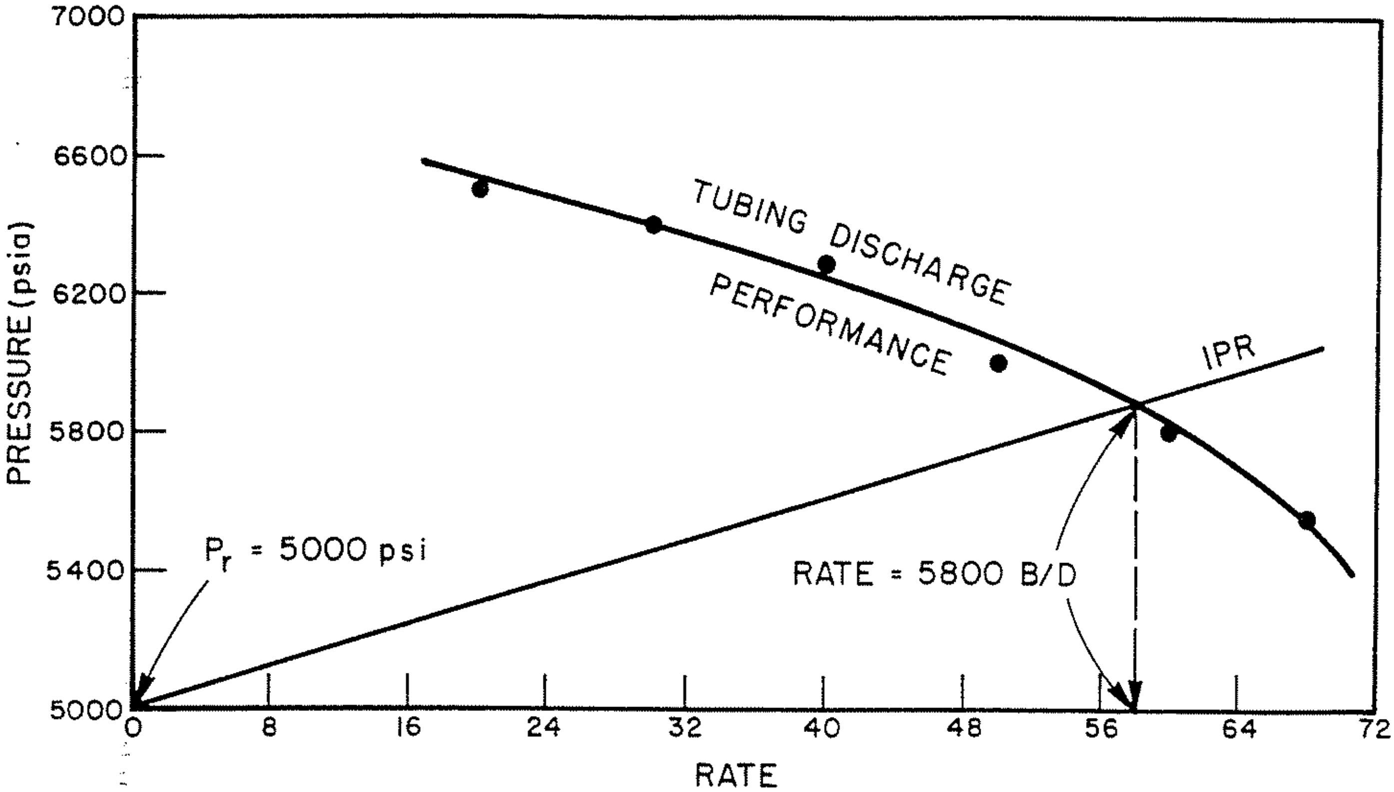

Figure 4.60 Example Water Injection Well Problem

no flow line is required—salt water of a specific gravity of 1.07 is to be injected.

Calculate:

(1) Determine the injection rate for this well for a wellhead pressure of 2,000 psi. Refer to Figure 4.4(2) for tubing injection curves for internally plastic-coated 2⅞-in. OD tubing (ID = 2.431 in.).

Solution procedure:

(1) Prepare the IPR curve using Darcy's Law.

$$q_w = \frac{7.08 \times 10^{-3} k_w h(\Delta P)}{\overline{\mu}_w \overline{B}_w(\ln r_e/r_w - 3/4 + S)}$$

Assume S = 0 and B_w = 1.0 (essentially noncompressible). μ_w can be found from Figure 4.61 and is noted to be 0.3 cp.

$$r_w = \frac{9.875}{2(12)} = 0.41 \text{ ft}$$

Assume values of q and solve for ΔP

$$\Delta P = \frac{q_w \mu_w B_w \left(\ln \frac{r_e}{r_w} - 3/4\right)}{7.08 \times 10^{-3} k_w h}$$

$$\Delta P = \frac{(0.3)(1.0)\left(\ln \frac{2{,}000}{0.41} - 3/4\right)}{7.08 \times 10^{-3}(70)(30)}(q) = 0.1562q$$

$$\Delta P = 0.1562\, q$$

where:
q = flow rate, b/d
ΔP = pressure change, psi

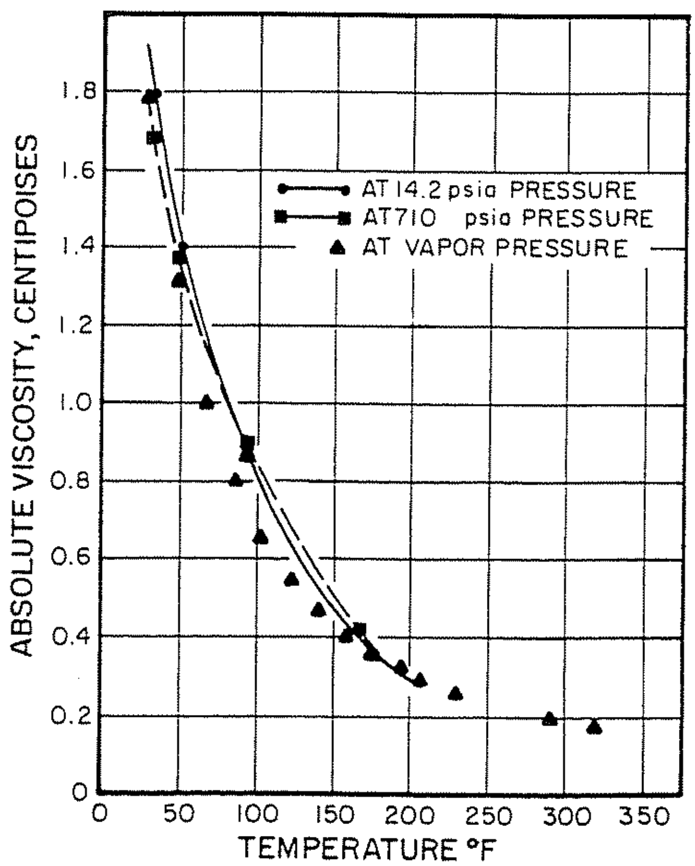

Figure 4.61 Water Viscosity

Add values of ΔP to $\bar{P}_r$ to obtain P_{wf} and prepare Table 4.24.

TABLE 4.24

q	ΔP	$P_{wf} = P_r + \Delta P$
100	15.62	5,016
200	31.24	5,031
400	62.48	5,062
600	93.72	5,094
800	124.96	5,125
1,000	156.2	5,156
1,500	234.3	5,234
2,000	312.4	5,312
3,000	468.6	5,469
5,000	781	5,781
10,000	1,562	6,562

Using data from Table 4.24, plot the IPR curve not to exceed the frac gradient pressure of 0.7 psi/ft (10,000 ft) = 7,000 psi.

(2) Determine tubing discharge pressures from Figure 4.4(2). Pressures may be read directly at 10,000 ft on the graph because both the well and graph start at the top with 2,000 psi. Prepare Table 4.25 of rate vs discharge pressure.

TABLE 4.25

Assumed q	Tubing discharge pressure, psi
2,000	6,510
3,000	6,400
4,000	6,300
5,000	6,050
6,000	5,820
7,000	5,570
8,000	5,290
10,000	4,530

(3) Plot the tubing discharge pressures vs rate on Figure 4.60.

(4) The intersection of the IPR and tubing discharge curve shows the rate to be 5,800 b/d.

Other tubing sizes and other wellhead pressures can be placed on the same plot.

4.32 GAS-INJECTION WELLS

Gas-injection wells can be handled in the same manner as water-injection wells.

Solution procedure:

(1) Calculate P_{wf} from Darcy's Law or from the appropriate back-pressure equation.

(2) Determine ΔP required for an assumed rate and add it to $\bar{P}_r$ to find a P_{wf} that is greater than $\bar{P}_r$.

(3) Assume other rates and determine corresponding P_{wf} valves. Plot the IPR curve.

(4) From the appropriate gas-injection curves or from an appropriate gas-injection equation, determine tubing discharge pressures vs rate.

(5) On the same figure, plot to obtain the injection rate.

CLASS PROBLEM #1

Work the example problem for water injection for a wellhead pressure of 1,000 psi.

CLASS PROBLEM #2

Work the class problem for 3½-in. OD and 4½-in. OD tubing, which is 2.982-in. ID and 3.948-in. ID, respectively.

CLASS PROBLEM #3

Given data:

depth = 8,000 ft
P_r = 3,280 psi at fill-up
P_{wh} = 1,500 psi
2⅞-in. OD tubing
k_w = 50 md
h = 10 ft
T = 160°F
γ_w = 1.07
160-acre spacing
10¾-in. drilled hole
frac gradient = 0.67 psi/ft

Calculate:

Determine the injection rate into this well for:

(a) 2⅞-in. tubing
(b) P_{wh} = 2,000 and 2⅞-in. tubing
(c) tubing = 3.948-in. ID and P_{wh} = 1,500 psi

CLASS PROBLEM #4

Given data:

k_w = 800 md
h = 60 ft
T = 200°F
depth = 10,000 ft
P_r = 4,460 psi
240-acre spacing
γ_w = 1.07
12¼-in. drilled hole
P_{wh} = 2,000 psi

Calculate:

Determine the injection rate for 3.948-in. tubing.

CLASS PROBLEM #5

Given data (gas injection well):

k = 120 md
h = 30 ft
T = 220°F
γ_g = 0.7
640-acre spacing
hole size = 10¾-in.
P_r = 3,200 psia
assume S = 0
tubing size = 2⅞ in. (2.441-in. ID) (Appendix)
depth = 9,000 ft
wellhead pressure = 1,000 psig ?

5000psig.

Calculate:

Find the injection rate.

CLASS PROBLEM #6

Same as problem #5 except k = 300 md.

CLASS PROBLEM #7

Same as problem #5 except tubing size = 1.995-in ID.

4.4 NODAL ANALYSIS AS APPLIED TO GAS WELLS

4.41 INTRODUCTION

The same procedure used for oil wells can be applied to gas wells. It is recommended that the turbulence term be included for gas well analysis although its effect is normally negligible at low permeabilities (less than 1 md).

The producing system for a gas well can be divided into the same components as for an oil well—that is, the reservoir, the vertical or directional conduit, surface flow line, and the separator pressure.

The separator pressure for a gas well has particular significance since the gas is normally being placed into some sales outlet such as a 1,000-psi sales line. The operator is faced with the problem of determining whether he wishes to maintain a separator pressure sufficiently high to put gas directly into the sales line or buy a compressor (lower the separator pressure to try and increase the rate) to raise the pressure in order to place the gas into the sales line. This problem becomes one involving economic considerations, and the cost of compression must be weighed against increased production.

The gas-well analysis can be best illustrated by an example problem.

EXAMPLE PROBLEM (GAS WELL)

Given data:

$P_r = 5{,}200$ psi	$k = 45$ md
depth = 10,000 ft	$h = 30$ ft
$\gamma_g = 0.7$	perforated interval = 20 ft
$T = 210°F$	320-acre spacing
assume $S = 0$	10¾-in. drilled hole

7-in. casing
2⅞-in. OD × 2.441-in. ID tubing
sales line pressure = 800 psi
short flow line with negligible pressure loss

Calculate:

Determine the flow rate from this well for a wellhead pressure of 1,000 psi (sufficiently high to put the gas into the sales line). Assume no pressure loss across the completion.

Solution procedure:

The well will be divided into two components:

(1) reservoir component
(2) tubing component

The solution position will be taken at the bottom of the well.

(1) Prepare the IPR curve

The Jones, Blount, and Glaze form of Darcy's Law will be used. Jones, Blount, and Glaze gave this equation in the following form:[11]

$$P_r^2 - P_{wf_s}^2 = aq^2 + bq \tag{4.11}$$

where:

$$a = \frac{3.166 \times 10^{-6}\beta\, \gamma_g\, Z\, T}{h_p^2\, r_w} \tag{4.12}$$

$$b = \frac{1.424 \times 10^{6}\, \mu_g\, Z\, T}{kh}(\ln r_e/r_w - 3/4 + S) \tag{4.13}$$

where:

q = flow rate, MMscfd
h = thickness of zone, ft
h_p = perforated interval, ft
T = °R
r_w = radius of wellbore, ft
r_e = radius of drainage, ft
μ_g = cp
k = md
$\beta = \dfrac{2.33 \times 10^{10}}{k^{1.201}} = \text{ft}^{-1}$

By assuming values of pressure or rate, Table 4.26 was prepared:

TABLE 4.26

Rate, MMscfd	Pressure, psia
3	5,150
6	5,100
9	5,050
17	4,900
22	4,800
33	4,500
42	4,250
49	4,000
72	3,000
88	2,000
98	1,000
103 (AOFP)	0

As a matter of interest, if Darcy's Law is used without the turbulence term, Table 4.27 shows the results.

TABLE 4.27

Rate, MMscfd	Pressure, psia
14	5,000
83	4,000
150	3,000
213	2,000
267	1,000
305 (AOFP)	0

There is, of course, a large difference in the absolute open-flow potential: 305 million as com-

pared to 103 MMscfd. However, the difference is less critical at the projected rate of approximately 30 MMscfd for 2.441-in. ID tubing. It is recommended that the turbulence term always be included.

The data of Table 4.26 is plotted in Figure 4.62 but only to a rate scale of 50 million since the projected rate for the particular pipe size will be less.

(2) Prepare tubing intake curves.

Refer to Figure 4.63. Other gradient curves can be found in Appendix 4.5 and Volume 3b of this book series. Table 4.28 shows rates vs tubing intake pressures for a wellhead pressure of 1,000 psi and a tubing size of 2.441-in. ID.

(3) Plot the data of step 2, (Table 4.28) on Figure 4.62.

(4) Note the intersection of the IPR and tubing intake curves showing a rate of 28.6 MMscfd.

EXAMPLE PROBLEM (FEASIBILITY OF A COMPRESSOR)

The operator has an option of lowering the wellhead pressure to 200 psi and buying a compressor. If the present static pressure of 5,200 psi can be maintained for 1 year, determine the feasibility of this option. The following additional information is needed:

Given data:

compressor HP = $23\ (R)^{1/n} n(q)$

where:

q = MMscfd
R = compression ratio
n = no. of stages

compressor fuel usage = 240 (HP) scfd
initial compressor installation cost = \$900/HP
maintenance and operating costs for 1 year = \$15,000
price for gas = \$5/mcf

Solution procedure (option 1):

(1) Determining tubing intake pressures for a wellhead pressure of 200 psi. Refer to Figure 4.64 and prepare Table 4.29.

(2) Plot the rate vs tubing intake pressures of Table 4.29 on Figure 4.65.

(3) The intersection of the tubing intake and IPR curve shows a rate of 29.3 MMscfd.

(4) Determine the difference in rate between a wellhead pressure of 1,000 psi and 200 psi. The difference is 29.3 − 28.6 = 700,000 scfd.

(5) Determine the compressor costs to handle 29.3 MMscfd with a suction pressure of 200 psia and a discharge pressure of 1,000 psia. Compressor HP can be estimated as follows:

$$\text{HP} = 23\ (R)^{1/n}(n)\ (q\ \text{MMscfd})$$

$$= (23)\left(\frac{1{,}000}{200}\right)^{1/2}(2)(29.3) = 3{,}013\ \text{HP}$$

$$R = \frac{1{,}000}{200} = 5\ (\text{use two stages})$$

For R > 4.5 use two stages.
For R > 20 use three stages.

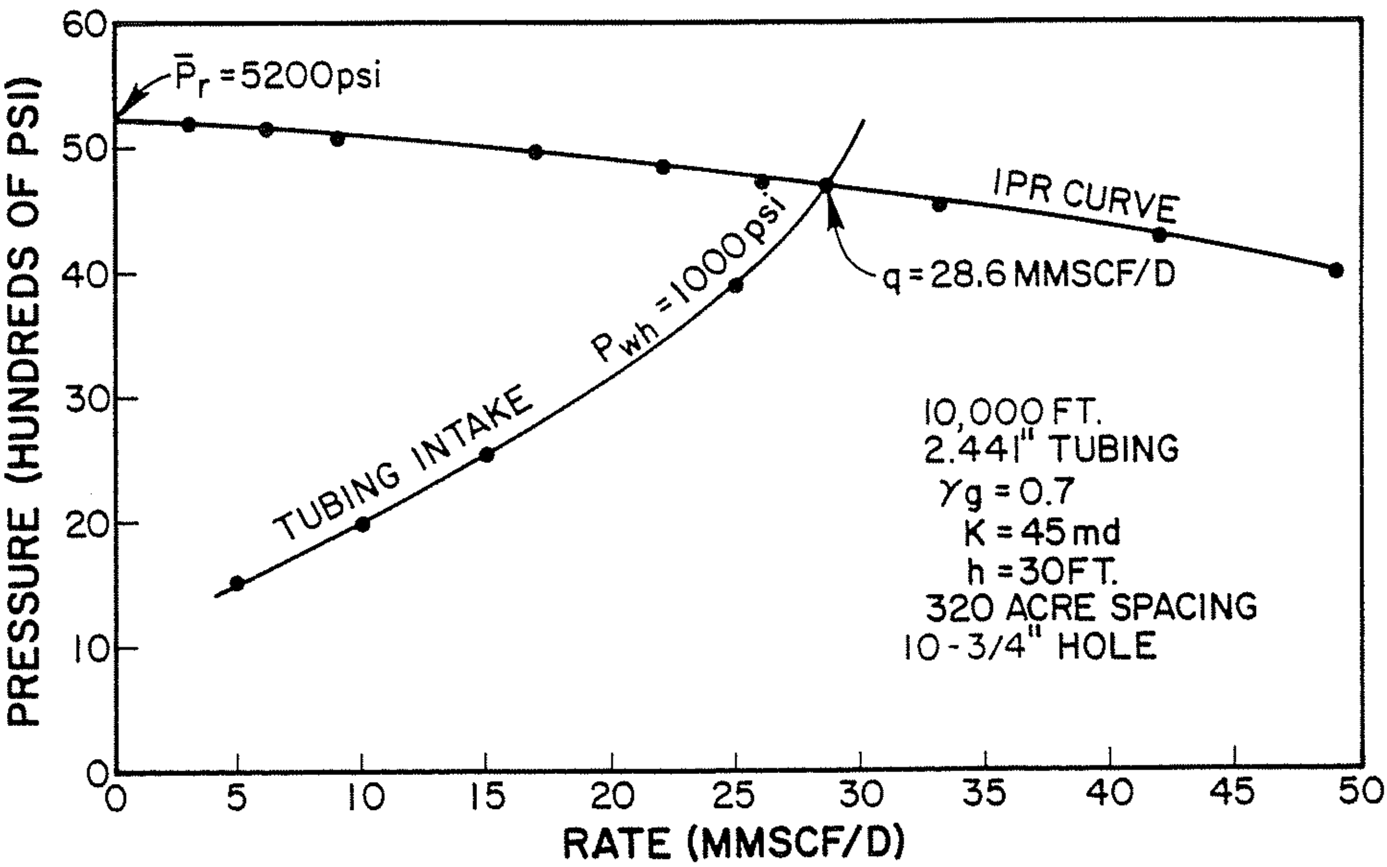

Figure 4.62 Predicting Flow Rate for a Gas Well

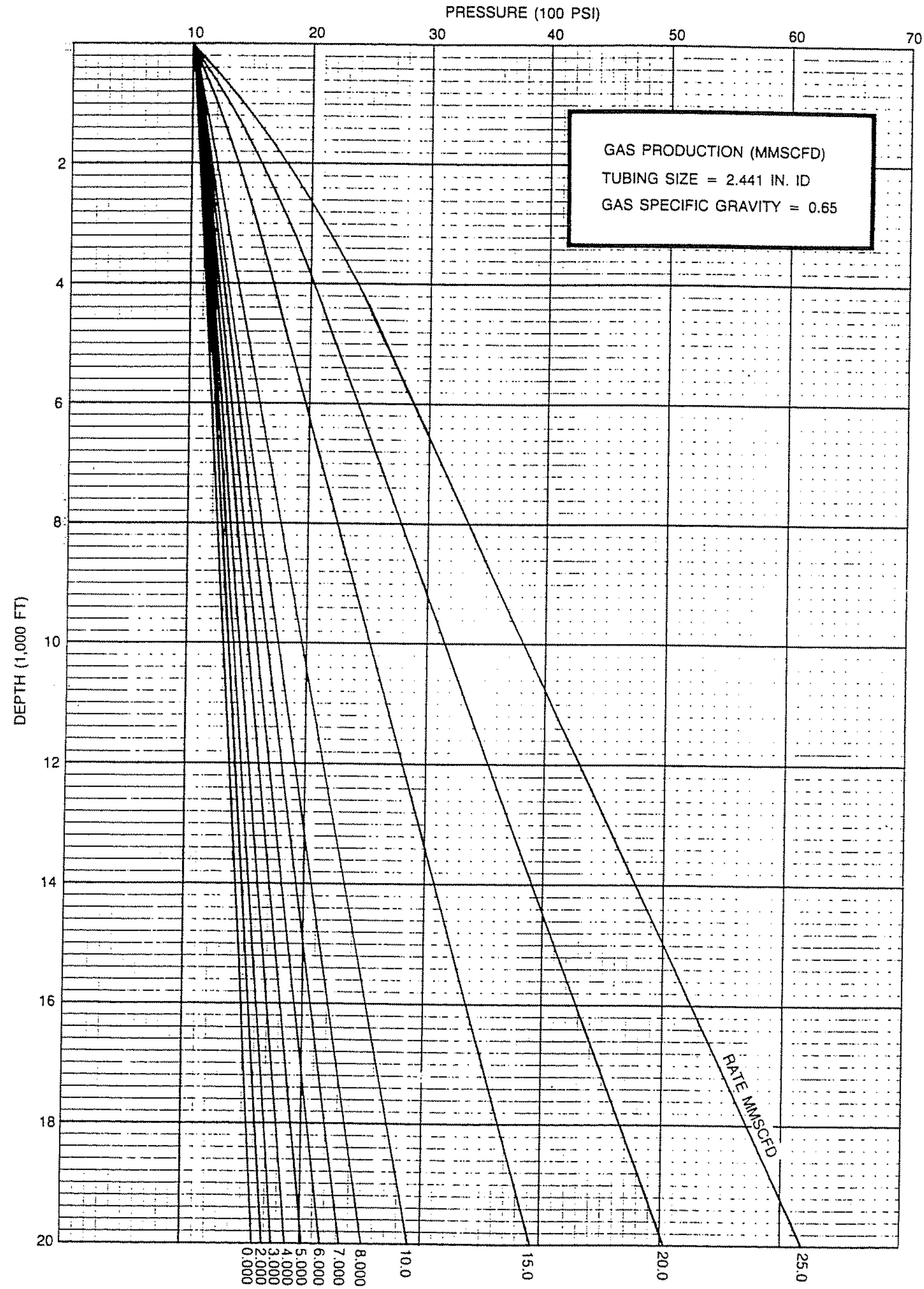

Figure 4.63 Vertical Flowing Gas Gradients (Gas Production, MMscfd; Tubing Size, 2.441-in. ID; Gas Specific Gravity, 0.65)

TABLE 4.28

Assumed rate, MMscfd	Tubing intake pressure, psi
5	1,500
10	1,950
15	2,530
20	3,180
25	3,820

The cost of 3,013 HP = (3,013)(900) \$2,711,700.

Additional return on gas
= (\$5/Mcf)(700 Mcfd)(365 days/year)
= \$1,277,500/year.

Fuel usage = (240)(3,013) = 723,120 scfd.

The compressor uses more fuel than the gain in rate per day.

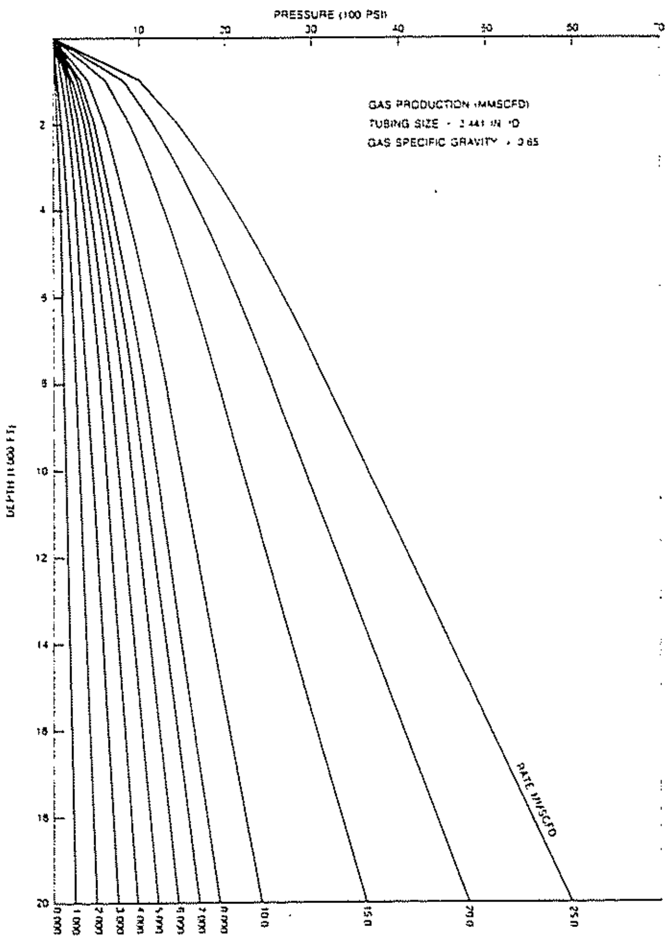

Figure 4.64 Vertical Flowing Gas Gradients (Gas Production, MMscfd; Tubing Size, 2.441-in. ID; Gas Specific Gravity, 0.65) (Working Copy on p. 430)

TABLE 4.29

Rate, MMscfd	Tubing intake pressure, psig
5	800
10	1,550
15	2,275
20	3,000
25	3,700

In option 1, obviously, it is not profitable to lower the wellhead pressure from 1,000 psi to 200 psi. However, in some cases, this may be a profitable consideration and each case must be evaluated.

Solution procedure (option 2):

Let us assume that a sales-line pressure of 2,650 psi exists and that it is necessary to place the gas into this line. One option is to carry a wellhead pressure of approximately 3,000 psi and flow directly into the line or to lower the wellhead pressure to 1,000 psi and compress the gas to place it into the line.

(1) Prepare tubing intake curves for a wellhead pressure of 3,000 psi (see Table 4.30).
(2) Plot the tubing intake pressures of step 1 on Figure 4.65 along with the data for a wellhead pressure of 1,000 psi and 200 psi. Note that the rate for a wellhead pressure of 3,000 psi is 21 MMscfd as compared to 28.6 MMscfd for a wellhead pressure of 1,000 psi. The difference is 28.6 − 21 = 7.6 MMscfd.
(3) Determine the cost of compression for 28.6 MMscfd from 1,000 psi to 3,000 psi.

$$R = \frac{3,000}{1,000} = 3 \text{ (use 1 stage)}$$

$$HP = (23)(3)(1)(28.6) = 1,973.4 \text{ HP}$$

$$\text{original cost} = (\$900)(1,973.4) = \$1,776,000$$

$$\text{fuel} = (240)(1973.4) = 473,616 \text{ scfd}$$

fuel usage per year

$$= (473,616) \times (365) = 1.728 \times 10^{8} \text{ scf/year}$$

fuel cost per year

$$= (\$5)\left(\frac{1.728 \times 10^{8}}{1,000}\right) = \$864,000/\text{year}$$

$$\text{maintenance} = \$15,000/\text{year}$$

Total cost for 1st year, including total initial cost = \$2,655,000

(4) Determine the additional income per year based on an increased daily rate of 7.6 MMscfd.

$$\frac{7,600,000}{1,000}(5)(365) = \$13,870,000$$

(5) Determine gain or loss in income per year.

Gain = 13,870,000 − 2,655,000 = \$11,215,000

In this instance, it would be profitable to lower the wellhead pressure to 1,000 psi and buy a compressor. By assuming several wellhead pressures, the optimum economic wellhead pressure can be determined.

EXAMPLE PROBLEM (EFFECT OF TUBING SIZES)

Other tubing sizes can be placed on the same plot. For example, find the flow rate possible with 2.992-in. ID tubing (3.5-in. OD)

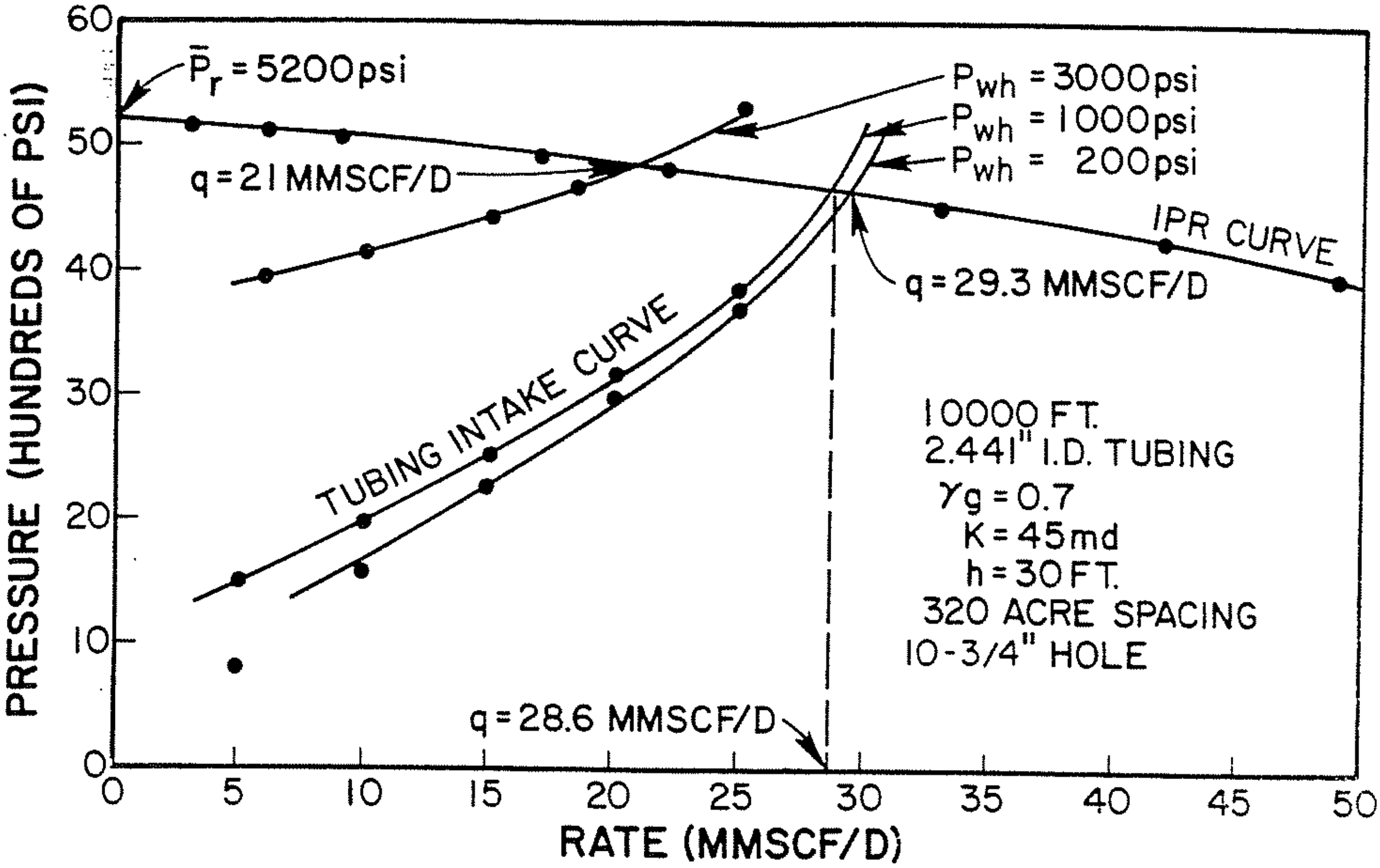

Figure 4.65 Effect of Wellhead Pressure

TABLE 4.30

q, MMscfd	Tubing intake pressure, psi
6	3,950
10	4,110
15	4,420
20	4,830
25	5,320

Solution procedure:

(1) From Figure 4.66, prepare a table of flow rates vs tubing intake pressures for a wellhead pressure of 1,000 psi (see Table 4.31).
(2) Plot the tubing intake pressures of step 1 on Figure 4.67 with the IPR Curve.
(3) Note the rate of 45.6 MMscfd for 2.992-in. ID tubing as compared to 28.6 MMscfd for 2.441-in. tubing.

TABLE 4.31

Rate, MMscfd	Tubing intake pressure, psig
10	1,550
15	1,820
20	2,160
25	2,500
30	2,890
35	3,250
40	3,650
50	4,460

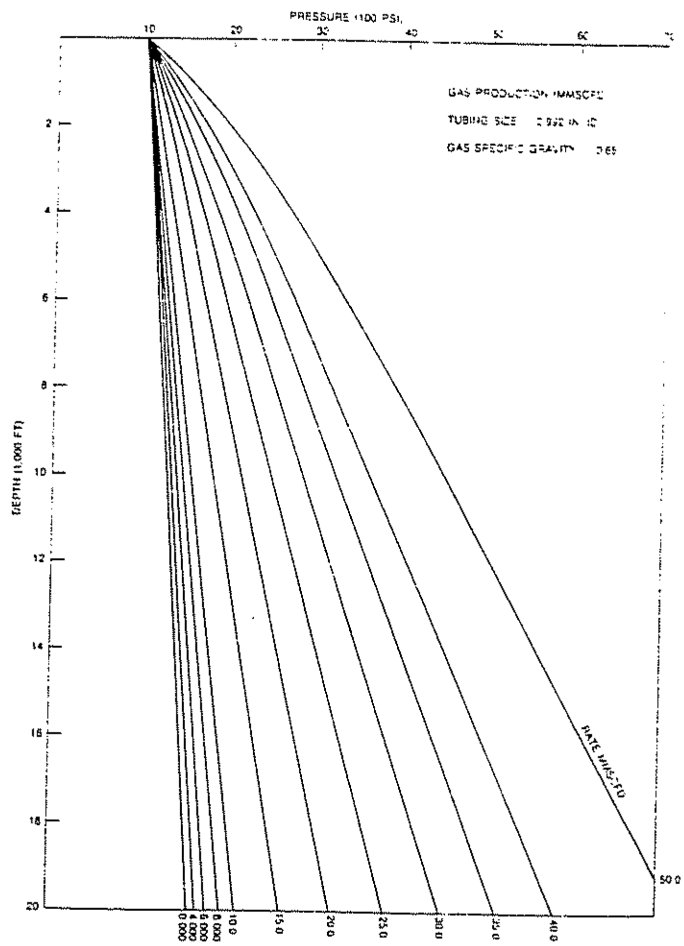

Figure 4.66 Vertical Flowing Gas Gradients (Gas Production, MMscfd; Tubing Size, 2.992-in. ID; Gas Specific Gravity, 0.65) (Working Copy on p. 431)

Other tubing sizes can be placed on the same or similar graphs, but large sizes will require a changing of the rate scale.

4.42 SUMMARY AND OTHER VARIABLES

Other options such as decreasing static bottom-hole pressure, flow lines, annular flow, etc., can be analyzed in the same manner. The same procedures applied to the oil well example of section 4.2 can be applied to gas wells.

Additional sections show the effect of perforation restrictions for both gravel-pack and non-gravel-packed wells.

4.43 GAS WELL LOADING

Refer to Chapter 6 for a complete discussion of gas well loading.

CLASS PROBLEM #1

Given data:

well depth = 12,000 ft	h = 30 ft
640-acre spacing	T = 240°F
P_r = 7,000 psi	price of gas = $4/Mcf
k = 0.03 md	
gas gravity = 0.65	
5½-in. casing in 8¾-in. hole	
sales-line pressure = 800 psi	

Use a short flow line.

Note: Fracturing shows skin (S) = −4 typical for this area.
(Cost = $150,000)
Casing already set on well.
P_r drops approximately 1,000 psi/year.

Calculate:

(1) Make recommendations as to tubing sizes (refer to Volume 3b).
 (a) Assume no loading problem.
 (b) Assume that loading may occur (see Chapter 7).
(2) Would you fracture the well?
(3) Would you lower wellhead pressure to 200 psi and buy a compressor or set the wellhead pressure at 1,000 psi to put gas directly into the flow line?

CLASS PROBLEM #2

Given data:

Use same data as problem 1 except k = 30 md and sales-line pressure is 2,000 psi.

Calculate:

(1) Recommend tubing sizes.
(2) Recommend wellhead pressure of 2,400 psi or 1,000 psi and a compressor.

CLASS PROBLEM #3

Given data:

well depth = 16,000 ft on 1,280-acre spacing
P_r = 10,000 psia

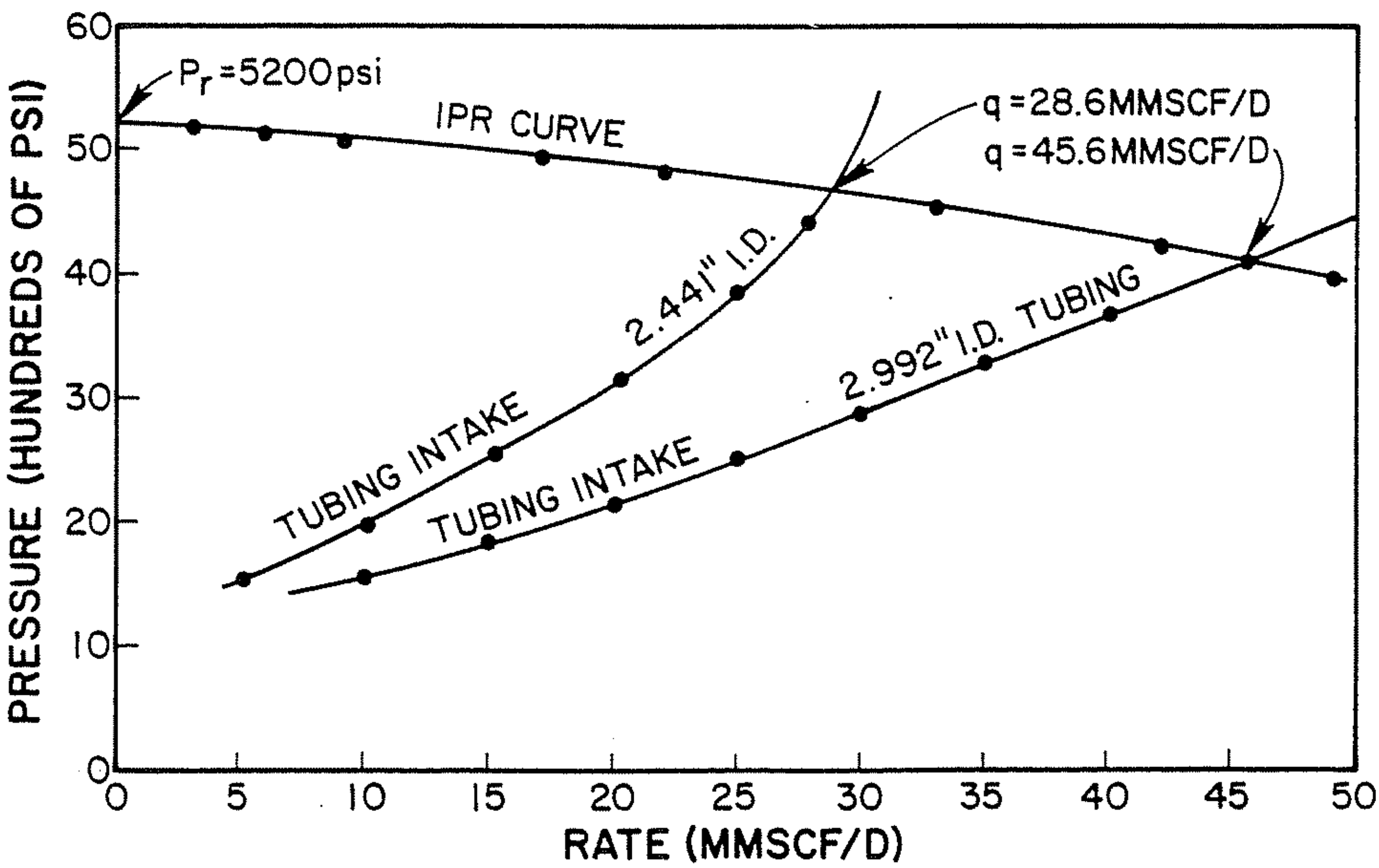

Figure 4.67 Effect of Tubing Sizes

k = 120 md
h = 80 ft
T = 290°F
gas gravity = 0.7
7-in. casing in 9⅞-in. hole

Present conditions:

short flow line
separator pressure = 1,000 psi
sales line = 900 psi
(some water and condensate anticipated—limestone formation)

Note: P_r drops 500 psi/year

Calculate:

Recommend:
(1) tubing size
(2) wellhead pressure

CLASS PROBLEM #4

Given data:

$P_r = 4{,}200$ psi	k = 10 md
depth = 8,000 ft	h = 60 ft
$\gamma_g = 0.6$	7-in. casing
T = 170°F	8½-in. drilled hole
320-acre spacing	wellhead pressure = 600 psi

can obtain S = −4 by frac
gas price = $3.50/Mcf

Calculate:

Recommend:
(1) whether to frac
(2) tubing size

4.5 NODAL ANALYSIS APPLIED TO GRAVEL-PACKED OIL AND GAS WELLS BY LEWIS LEDLOW AND CARL GRANGER

4.51 SAND CONTROL

4.511 INTRODUCTION

Sand production has long been associated with oil or gas production in Miocene and younger formations. Recently, sand production has been observed at depths of 17–22,000 ft in the Tuscaloosa trend and at depths of 17,000 ft offshore of Louisiana. Previously, sand production was thought to be nonexistent at depths greater than 10,000 ft.

Sand production becomes a production problem when it reduces or stops hydrocarbon production, erodes surface and downhole equipment, or causes disposal problems or casing collapse.

The elimination of allowable production, the development of better completion practices, and the systems analysis approach to evaluating well completions have increased the productivity of sand-control completions.

4.512 DEFINITION OF SAND CONTROL

Successful sand control is stopping the production of load-bearing solids while maintaining efficient fluids production. Stopping sand production is easy. Just set a cement plug or shut the well in. The difficult part is maintaining an efficient completion—one that will flow at or near its non-sand-controlled rate with little or no pressure drop across the completion. Shutting in or choking the well back is not considered successful sand control because it reduces the production. Stopping the production of load-bearing solids does not necessarily mean that formation material will not be produced. In the Gulf Coast, the practical limit for sand production is 0.1% (600 lb/1,000 bbl) as measured in a shakeout.

4.513 METHODS OF SAND CONTROL

The basic methods of sand control as practiced today are:

(1) *Gravel Packing.* Gravel-pack-sand-laden fluids are pumped into a well around a screen or liner. This creates a downhole filter that allows the formation sand to bridge on the gravel-pack sand, preventing formation sand from flowing but allowing oil or gas production (refer to Figure 4.68).

(2) *Formation Sand Consolidation.* A series of chemicals are pumped sequentially into the formation for formation sand consolidation. These chemicals react to consolidate or strengthen the formation. Refer to Figure 4.69 for idealized and probable results.

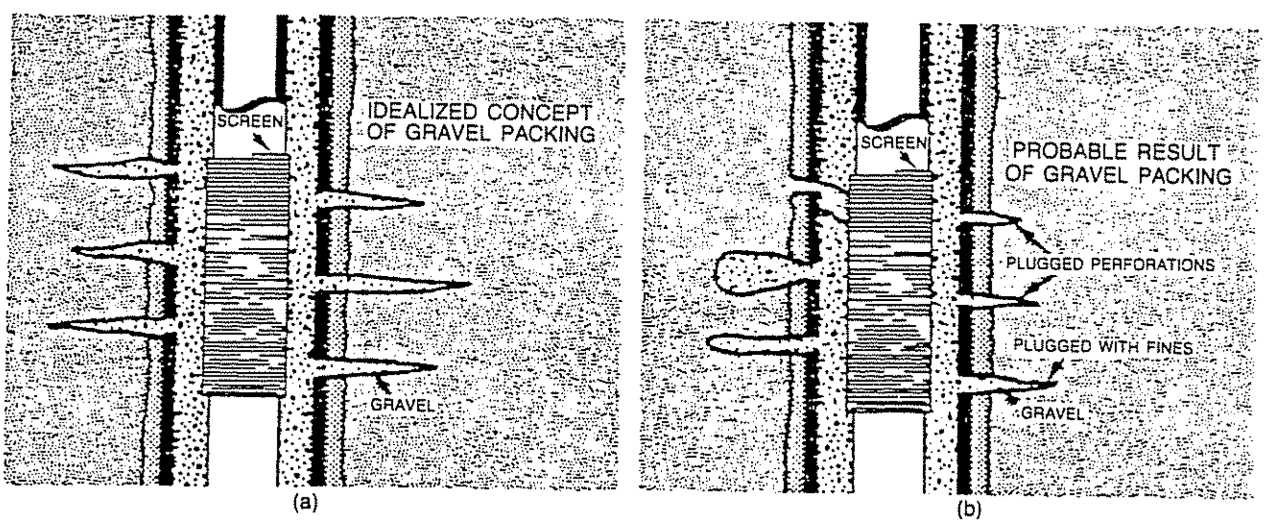

Figure 4.68a Idealized Concept of Gravel Packing With 4.68b Showing the Probable Field Result

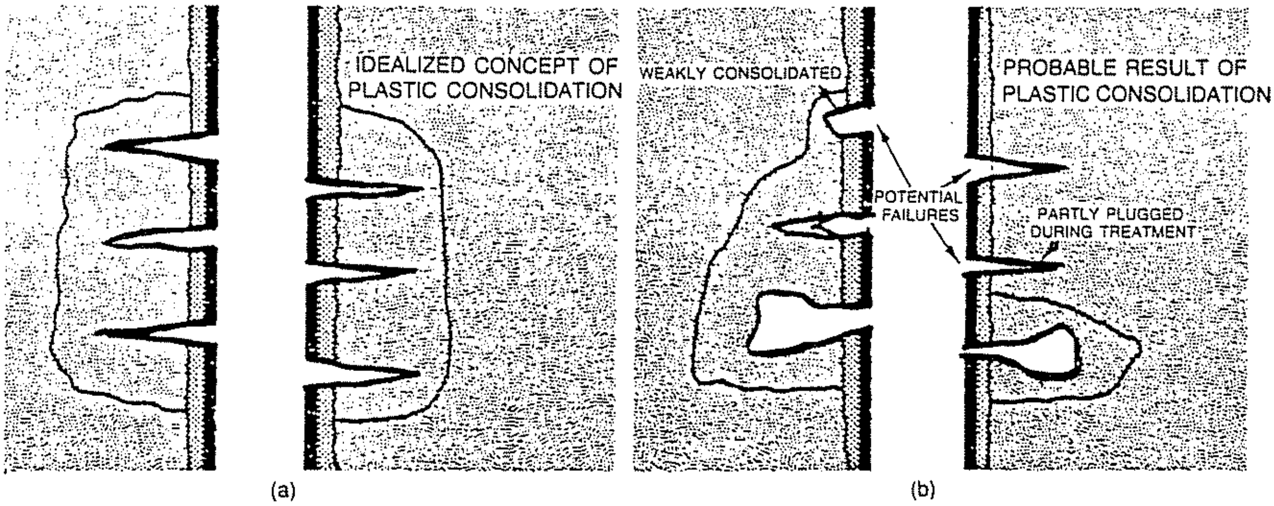

Figure 4.69 Formation Sand Consolidation

(3) *Resin Sand Slurries.* A resin slurry consisting of plastic and gravel-pack sand or precoated gravel is pumped into a well, allowed to cure, and then drilled out, leaving the perforation tunnels packed with the plastic-coated gravel. Refer to Figure 4.70 for idealized and probable results.

4.52 SAND-CONTROL DESIGN CRITERIA

4.521 GRAVEL-PACK DESIGN CRITERIA

The first step in designing a gravel pack is obtaining a sample of formation material. Commonly available methods of obtaining formation samples are listed below in order of preference:

(1) rubber-sleeve core
(2) conventional core
(3) sidewall core
(4) bailed sample
(5) produced sample

Rubber-sleeve or conventional cores are the best and are the most representative samples that can be obtained. They are also the most expensive and difficult to obtain. Because of the added expense, they are rarely used in designing gravel packs. The taking of rubber-sleeve or conventional cores should be encouraged, especially in development wells, because they will provide sufficient sample material to perform X-ray diffraction, acid solubility, and related mineralogy work. They are necessary to design better completions.

Sidewall cores are the most readily available and are taken on an electric line tool prior to running the production casing through the completion interval. These cores are easy to obtain, and it is recommended that two sets be taken. One of these sets can be used by the geologists for their analysis and one set can be used for sand control, sieve analysis, X-ray diffraction, SEM (scanning electron micrographs), and acid solubility. These sidewall cores should be taken at 1-ft intervals throughout the entire producing interval. Sand from a sidewall core is generally smaller than the true formation sand. This is caused by compression when the sidewall core barrels are fired into the formation. However, this factor can be taken into account when designing a gravel pack.

Bailed or produced samples are not truly representative, but they are better than no samples. Sand from bailed samples is usually larger than the formation sand but may be smaller, depending on how the sample

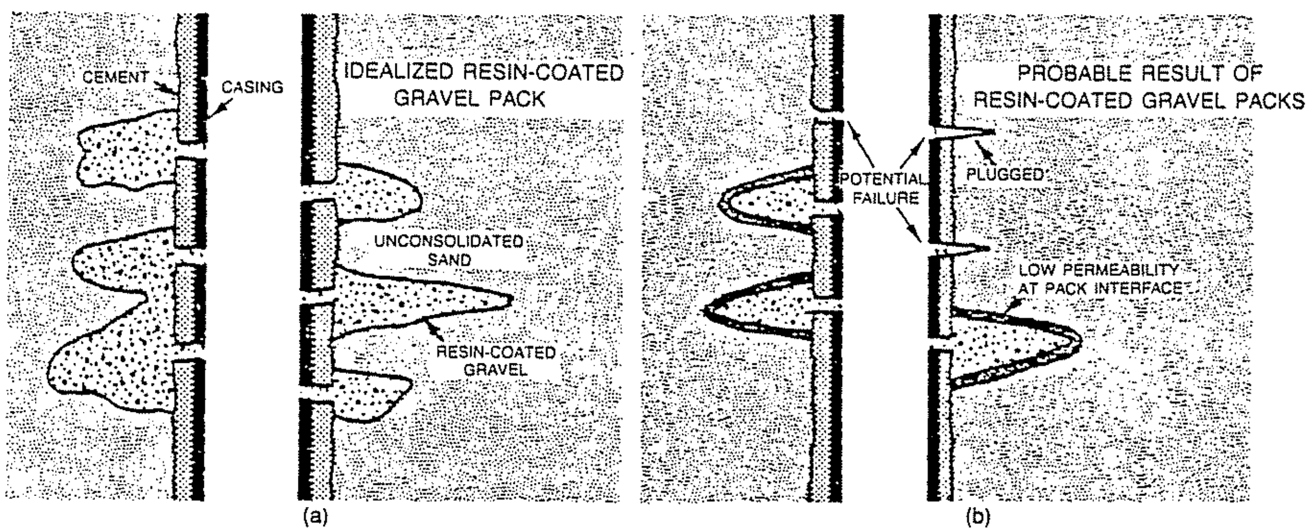

Figure 4.70 Resin Sand Slurries

is obtained. If the well was shut in for a long period of time and the first bailed fill is analyzed, the particles will be the smallest because they will be the last particles to settle out of a column of fluid. However, if fill taken and analyzed from the plugged tubing is from one of the last bailers, the sample may be larger than the formation sand because these particles were heavier and bigger and they were the first particles to settle out of the column of fluid. This should be taken into account when designing a gravel pack based on bailed samples.

Produced samples are just as poor because they are generally eroded and are usually smaller than the formation sand, and the location from which these samples are taken can affect the size distribution. When designing a gravel pack based on bailed or produced samples, it is better to design one on the conservative side.

(1) *Gravel Size Determination.* To determine gravel size, a sieve analysis of the sand should be performed. Preliminary steps include washing the sample with solvents to remove any residual hydrocarbons and then disaggregating and drying to allow dry sieve analysis. The sample is then sieved and separated, and the weight percent retained is measured. Then, the cumulative weight percent retained is determined for each screen size. After the sieve analysis, the 50% point is determined by plotting the cumulative weight percent vs the grain size on logarithmic probability paper. This grain diameter is then multiplied by five or six and becomes the median grain diameter for the selected gravel. An example of such a sieve analysis plot is illustrated in Figure 4.71.

Figure 4.72 is a graphic representation of the sizes as determined from the 50%. These methods are based on the work of Saucier, who determined the practical optimum size diameter ratio between the formation sand and a gravel-pack sand.[12] A graphic representation of this is illustrated in Figure 4.73. It is important to note that when the gravel size diameter ratio between the formation sand and gravel-pack sand is less than five or six, no sand is produced. When the formation sand–gravel-pack sand diameter ratio is between six and twelve, formation sand can migrate into the gravel pack, partially plug it, and reduce its permeability. When the formation–gravel-pack sand diameter ratio is greater than twelve, sand formation material

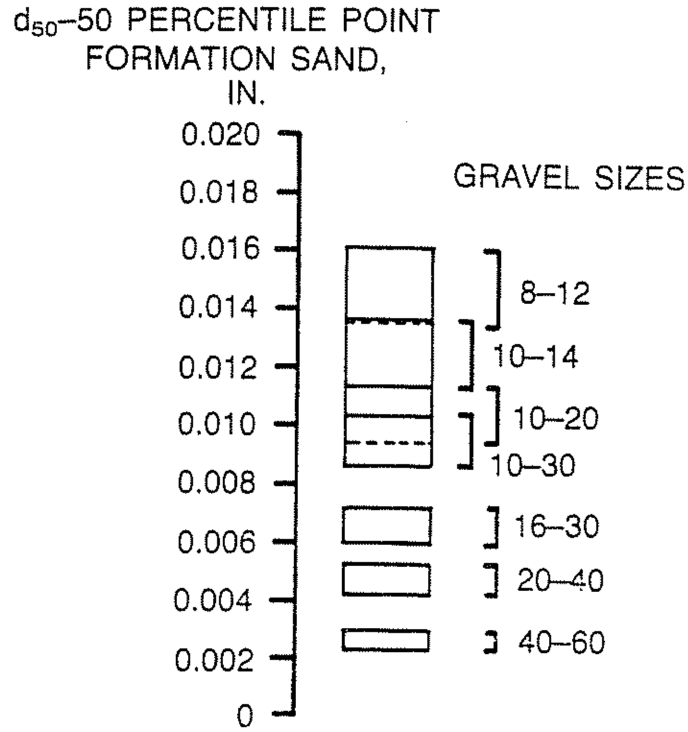

Figure 4.72 Recommended Commercial Gravel Sizes

can freely flow through the gravel pack and allow the screen or liner as well as downhole and surface equipment to be cut out. Earlier work by Coberly demonstrated these diameter ratios;[13] however, these determinations were not directly applied. Figure 4.73 illustrates that the diameter ratio of the formation sand must be smaller than 6.5 times the diameter of the gravel-pack sand.

(2) *Gravel Selection.* Gravel size should be very specific. It is critical that the correct size of gravel be ordered and received. This will allow the correct diameter ratio to be achieved. Confusion arises when "mesh" and not U.S. mesh or Tyler mesh is used to specify gravel size. In different parts of the world, as many as ten different classifications of gravel sizes are used. It is important that the ratio of gravel-pack-sand diameter to formation-sand diameter be maintained at five or six, whether measured in U.S. mesh, inches, or millimeters.

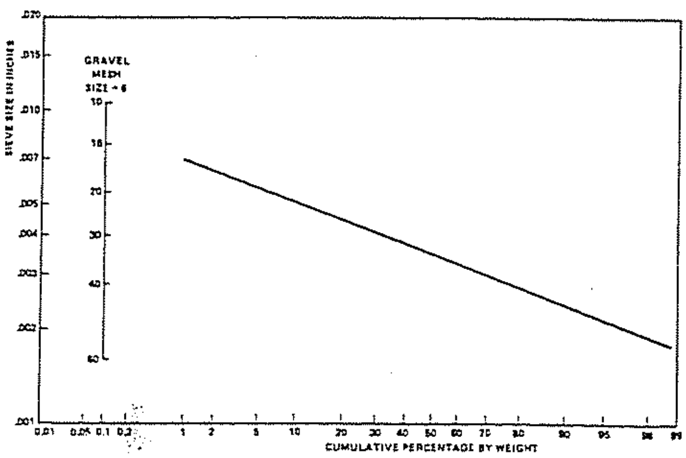

Figure 4.71 Logarithmic Probability Plot of Sieve Analysis

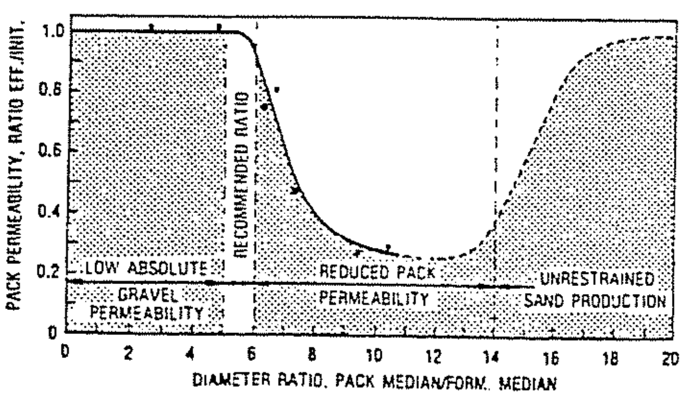

Figure 4.73 Graphic Representation of Gravel Sizes

The proper selection and quality control of gravels used in gravel packing is essential. All gravels used in sand control should "meet or exceed API specifications." These specifications include:

(1) high quartz content (96–100%)
(2) well-roundedness (sphericity and roundness 0.6 or greater)
(3) no more than 2% less the size range or 4% total of the specified size range
(4) acid solubility less than 1% in 12% hydrochloric by 3% hydrofluoric in 1 hr at 72°F

The commonly available gravels include:

12–20 U.S. mesh
20–30 U.S. mesh
20–40 U.S. mesh
30–40 U.S. mesh
40–50 U.S. mesh
40–60 U.S. mesh
50–70 U.S. mesh

(3) *Screen Slot Size.* The screen slot size should be as large as possible and still retain all of the gravel-pack sand. Flow area or inlet area on slotted liners is much more critical than inlet area on stainless-steel, all-welded screens. With all-welded screens, flow rates as high as 500 b/d/ft of screen result in pressure drops of only 3–5 psi.

(4) *Selection of Screens.* The type of screen or liner used to complete a gravel-packed well is largely determined by the economics and productivity of the well. There are three basic types of screens and liners used to gravel pack wells in the oil industry (refer to Figure 4.74). They are listed below, in order of preference:

(1) All-welded, stainless-steel pipe base—these offer the most resistance to corrosion, longest life, and the greatest inlet area.
(2) Wire-wrapped pipe base—these may be ribbed, Gru-v-cut or wrapped directly on the pipe base. The wire is held in place by welds or solder beads. This type is more susceptible to corrosion and is more difficult to remove during workover operations. It also has a higher pressure drop caused by reduced inlet area.
(3) Slotted liners—these are generally used on long intervals with low productivity or when the economics do not justify an all-weld or a wire-wrapped screen. Slotted liners are very susceptible to corrosion and have a smaller flow area than either all-welded or wire-wrapped screens. This restricted flow area creates high pressure drops and increases the probability of plugging with fines and debris. Their use should be discouraged.

Quality control for screens and liners is essential. The lack of quality control can allow the gravel to be produced, resulting in a cut-out screen or liner and a major workover. Use an automobile feeler gauge to check the spacing. Check the spacing every foot and reject the screen if the spacing is *greater* than 0.001 in. over the specification or if 20% of the spacings are less than 0.002 in. under size.

(5) *Screen Diameters.* In a cased hole, ¾ to 1 in. of *radial* space between the screen and casing should be provided for gravel. This allows enough volume for the gravel to flow freely, and bridges or holidays do

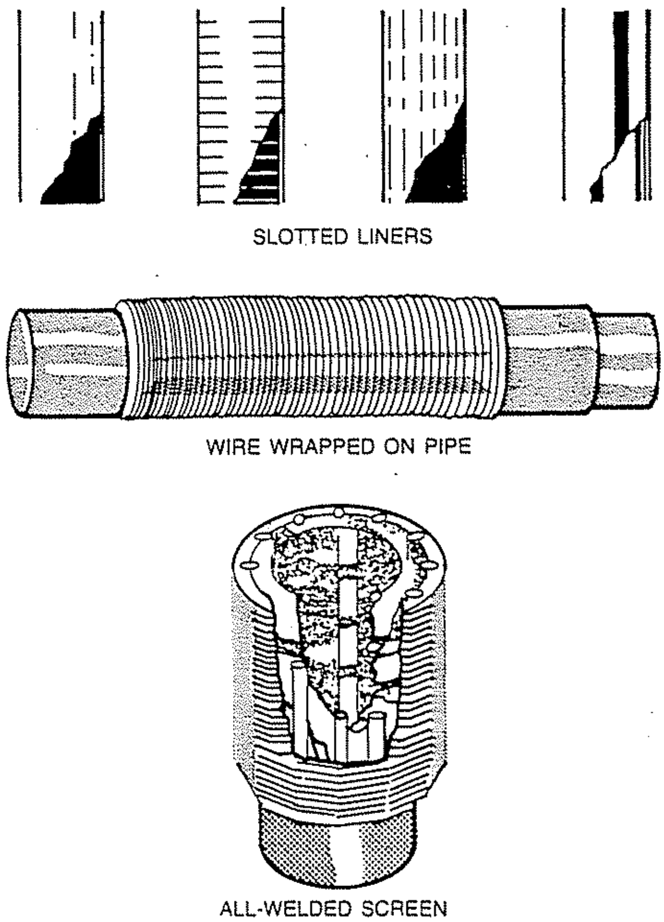

Figure 4.74 Liners and Screens

not form in the pack. It also provides adequate space for a washover tool if the screen needs to be removed in the future. The following table can be used as a guide for screen diameters inside cased holes.

Casing size			Maximum Screen diameter	
OD, in.	Wt, lb.	ID, in.	Pipe OD, in.	Wire OD, in.
4	9.5	3.548	1	1.815
4½	11.6	4	1¼	2.160
5	18	4.276	1½	2.400
5½	17	4.892	2⅜	2.875
6⅝	24	5.921	3½	4
7	29	6.184	4	4.500
7⅝	33.7	6.765	4	5.500
9⅝	47	8.681	5½	6

In an open-hole completion, a minimum of 2 in. of radial clearance should be provided between the screen and the hole. This will allow for some hole irregularities.

(6) *Screen Centralizers.* Centralizers are an essential part of successful gravel packing (refer to Figure 4.75). Uncentralized screens and liners can be positioned next to a perforation, which prevents gravel

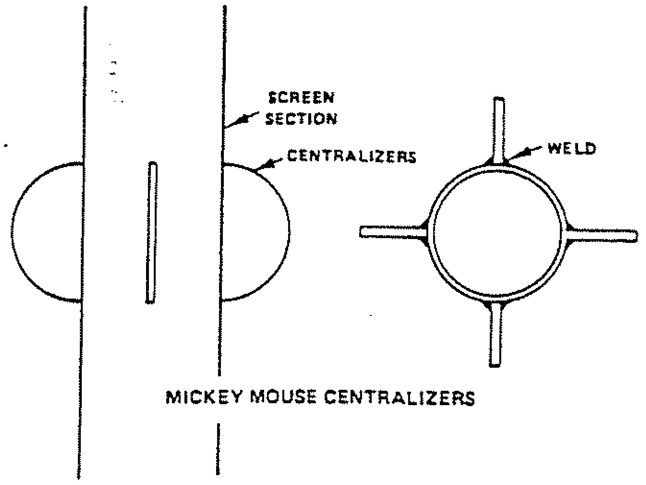

Figure 4.75 Centralizers

from entering that perforation. Also, *if* flow occurs through that perforation, the formation sand will erode a hole in the screen or liner. Some general guidelines for centralizer placements are:

(1) 0–30° angle of deviation every 15 ft
(2) 30–45° angle of deviation every 10 ft
(3) greater than 45° angle of deviation every 5 ft

Centralizers should be weld-on, blade types for casing and bow types for open hole. The use of bolt-on aluminum centralizers should be eliminated because they are very susceptible to wear while going in the hole and are 100% soluble in 15% hydrochloric acid.

(7) *Well Preparation for Sand Control.* A well that has been properly prepared for sand control should be clean—clean enough to store drinking water. Anything less than this increases the probability of formation damage and decreases the chances of success. The practice of successful sand control is like riding a multistage rocket to the moon: if one stage fails to fire or, in the case of sand control, one step is neglected, you don't get there. This intricate attention to detail makes sand-control completions the most difficult to successfully complete.

The following is an example of a procedure that can be modified to fit most gravel-pack wells.

Completion procedure:

Oil-Field Nomenclature Used in This Completion Procedure

MI—Move in
RU—Rig up
GIH—Go in hole
PU—Pick up
POOH—Pull out of hole
EOT—End of tubing
GP—Gravel pack
DE—Diatomaceous earth
HEC—Hydroxy ethyl cellulose
Pickle—Clean tubing with acid
BOP—Blowout preventer

(1) MI and RU on well no. ____.
(2) Install BOP with 2⅞-in. pipe runs and the Hydril. Test the Hydril to 250/3,000 psi and BOP to 250/500 psi.
(3) GIH with 2⅞-in. workstring with ____-in. bit (full gauge) and tandem scrapers. Make sure the jets are removed.

Note: Pipe dope should be applied to the pin end only. A 1-in. or smaller brush should be used. *Do not dope collars.*

(4) Make two complete circulations of ____ bbl with drilling mud. Treat to reduce the yield point and gel strength.
(5) Prepare a 40-bbl Phase I spacer of 3% caustic soda and seawater (10 ppb). Prepare a 40-bbl Phase II sand scrub (1 lb HEC and 45 lb blast sand/bbl seawater).
(6) Flush and clean all pits, lines, solids control equipment, and pumps. Circulate seawater with 3 lb/bbl caustic soda and discard. Circulate seawater through the entire system. Drain tank pits and lines. Scrub and rinse.
(7) Displace drilling mud with seawater; rotate and reciprocate. Make two complete circulations (____ bbl) *after* all the mud is displaced.
(8) Displace seawater with the Phase I spacer followed by Phase II. Pump rate should be the *maximum* possible (2–8 bbl/min).
(9) Follow rear spacer with filtered seawater. Filter seawater to 2 microns or less *and* less than 100 ppm solids with DE filter unit and downstream guard filter.

Note: All fluids from this point on should be filtered to less than 100 ppm into the suction pit. Ppm is determined by turbidmeter.

(10) Displace out all spacers and discard them.
(11) Circulate one complete circulation of ____ ppg ____ completion fluid through the DE filter unit.
(12) RU wire line. Run necessary logs.
(13) Make wire-line gauge ring and junk basket run to ____ ft.
(14) Set ____ model sump packer at ____ ft.
(15) PU and GIH with tubing-conveyed perforating gun made up of a Baker Retrievamatic packer or a Halliburton Champ III.
(16) RU wire line. Run gamma ray for depth control.
(17) RU, test head and choke manifold; test to ____ psi.
(18) Circulate a 20-bbl HEC pill (5 lb/bbl) down the tubing so that the pill is spotted immediately above the packer.
(19) Displace the pill with a lighter fluid down the tubing to achieve a 500-psi underbalance of formation pressure.
(20) Set and test packer.
(21) Open the Hydril and fill the hole. Station a person to watch the fluid level. The fluid level should remain constant. Report immediately any rise or fall in fluid level.
(22) Drop the bar to fire the gun. When the gun fires, decrease the choke while maintaining fluid flow to the surface. Flow a minimum of 2–3 tubing volumes (____ bbl). Shut the choke.
(23) Check the casing fluid level, which should be constant.

(24) Circulate, then kill the pump through the fillup line to ensure the pump is primed.
(25) Pick up and unset the packer. The annulus fluid level should fall and then be filled by the pump.
(26) Shut down, kill the pump, and check the annulus fluid level. If the fluid level remains constant, go to step 13. If the fluid level falls, resume pumping in the fill-up line. If fluid level rises, close the Hydril and begin kill procedures.

Note: If the well needs to be killed, circulate down the casing and up the workstring.

(27) Close the Hydril. Immediately open the choke; simultaneously, begin pumping down the annulus and circulating up the workstring until the well is dead. Adjust the completion fluid weight as required.
(28) Stop pumping and check for pressure, flow, or fluid loss.
(29) POOH at 2,500 ft/hr (0.7 ft/sec). Fill hole every 5 stands.
(30) PU and run in GP assembly 2,500 ft/hr.
(31) Sting into sump packer and pull 6–8,000 lb above PU weight.
(32) Break circulation by reversing down the casing and returning up the workstring. This will remove any excess pipe dope.
(33) Set and test GP packer.
(34) Establish the injection rate (1 bbl/min @ 1,000 psi surface); release from the packer; locate and mark circulating and squeeze positions.
(35) Pickle the workstring by circulating the following: 10 bbl HEC (2.5 ppb); 500 gal of 15% hydrochloric with corrosion inhibitor; surfactant; 30 lb of EDTA per 5,000 ft of workstring; and 10 bbl HEC (2.5 ppb). Circulate acid to within 500 ft of EOT; then reverse out and discard.
(36) Pump GP slurry, 10 bbl pad, and slurry (65 lb at HEC/1,000 gal and sand 300 lb bbl). Displace with completion fluid at 500 ft/min. No rear pad required.
(37) Circulate until lower telltale is covered. Slack off and squeeze until sandout of 5,000-psi surface pressure occurs. If long, stroke the tool, pick up, and sand out on production screen.
(38) Continue pressure up cycles until bleedoff is less than 500 psi in 5 min. Reverse out and retest. If the pack does not retest, mix a ____-bbl slurry and repeat until leakoff is less than 500 psi in 5 min.
(39) POOH at 2,500 ft/hr with a GP crossover tool assembly.
(40) Rig up the wire line and run a GP log.
(41) If no voids are present, proceed with completion. If voids are present, transmit logs and wait for instructions.

Careful attention to selecting the best perforating techniques and to properly caring for and maintaining the completion fluids has the greatest effect on sand control success (refer to the above sections for a detailed discussion). Perforating for sand control is affected more by inlet area (perforation diameter) than by depth of penetration. Select the largest diameter perforation possible. The number of shots per foot required can be determined by using the procedure outlined in the next section.

Once these large diameter perforations are made, they must be cleaned out. Underbalanced perforating has proved to be the best method of cleaning perforations.

The following guidelines can be considered when selecting a method to clean out these perforations.

Guidelines for Perforation Cleanout

(1) Wash Tool
  (a) Cup Type
    (i) 4-cup minimum
    (ii) Large bypass area
    (iii) Shear-out ball seat that allows full opening for spotting pills or killing the well
    (iv) Rubber durometer based on BHT
    (v) Cup spacing 6 in. (12-in. max.)
    (vi) Proper pressure rating, especially in 9⅝ in.
    (vii) Wash rate as fast as possible without exceeding the pressure limitations of the tubing, tool, pumps, or casing; 2–3 BPM minimum, use 10 bbl/setting
  (b) Packer Type
    (i) Rubber durometer based on BHT
    (ii) Pump-out shear type of ball assembly that allows full opening for spotting pills or killing the well
    (iii) Fluid control valve, which allows the packer to unset should the well go on "vacuum"
    (iv) Wash rate as fast as possible without exceeding the pressure limitations of the tubing, tool, pumps, or casing; 2–3 BPM minimum, use 10 bbl/setting
(2) Surge Tool
  (a) One gal/perforation or 10 gal/ft max.
(3) Tubing Run Perforation
  (a) Use a packer with a large internal bypass (Retrievamatic, Champ Model 14)
  (b) Use a test head and choke manifold
  (c) Preplan for disposal or burning of well fluids
  (d) Spot 20–50 bbl of a 5-ppb HEC pill immediately above the packer
  (e) Flow 2–3 tubing volumes
  (f) Use a sump packer with as much rathole as possible
  (g) Fill annulus before and after firing the gun
  (h) Fill the tubing with a fluid that will give an underbalance wellbore condition; 500–1,000 psi
  (i) Hold pressure on tubing after flow; pressure up on casing; then pick up to release the packer
  (j) Kill the well by circulating *down* the casing and *up* the tubing
  (k) Circulate and adjust completion fluid weight until the well is under control
  (l) POOH at 2,500 ft/hr or less (0.7 ft/sec); fill the hole every 5 stands or less

(8) *Gravel placement procedures.* The main placement procedures consist of either a circulating pack, a squeeze pack, or a combination (see Figure 4.76).

(9) *Circulating pack.* A circulating pack uses a crossover tool and a wash pipe to place gravel around the

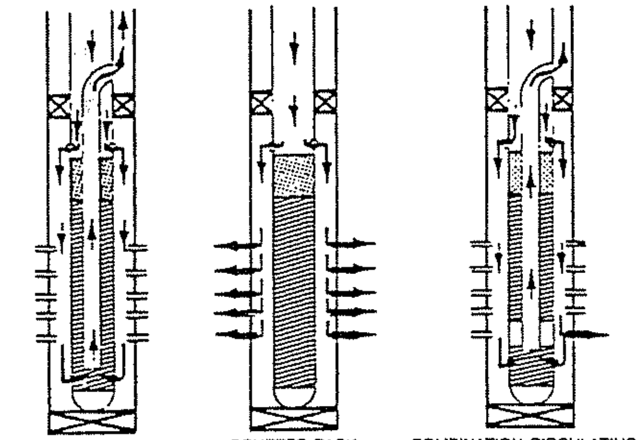

Figure 4.76 Gravel Placement Procedure

screen or liner. Gravel is pumped down the tubing and out the crossover port. Returns are taken through the screen or through a telltale screen until a sandout is obtained. This method is not very efficient in placing gravel through perforations. This method is most effective in open-hole gravel packs and longer intervals.

(10) *Squeeze pack.* With the squeeze-pack method, the gravel-pack slurry is pumped into the formation and around the screen with *no* returns taken through the screen. This continues until a sandout is obtained. This method is very efficient in placing gravel through the perforations but is limited to intervals of 45 ft or less.

(11) *Combination squeeze and circulate.* This method is the best and most versatile method to use. The slurry is circulated in place with returns taken through the lower telltale. When a calculated volume is pumped or a pressure increase is observed, the tool is placed in the squeeze position until a sandout is obtained. The tool may now be placed in the upper circulation position with returns taken through the production screen until a sandout is obtained. The sequence may be repeated until an adequate volume of gravel is pumped.

(12) *Selection of slurry volume and blank circulating pack.*

(1) Overlap the perforations with a minimum of 5 ft on either side.
(2) Run the screen all the way to the bottom; *eliminate* blank or pup joints below the screen.
(3) Run a *minimum* of 90 ft of blank when space permits.
(4) Pump a sand volume contained in a slurry volume sufficient to completely cover the screen and give a reservoir of 60 ft when the gravel has settled.

(13) *Squeeze pack.*

(1) Overlap the perforations with a minimum of 5 ft on either side.
(2) Run the screen all the way to the bottom; *eliminate* blank or pup joints below the screen.
(3) Pump a slurry volume that contains a sufficient volume of gravel to cover the screen, yield a 60-ft reservoir, and also allow ¼–½ ft^3/ft of perforation into the formation.
(4) A general rule is to allow four times as much blank as screen for a 15-ppg sand slurry and five times as much blank as screen for a 10-ppg sand slurry.

(14) *Gravel-pack fluids.* Successful sand control and high-permeability completions have been achieved using slurries of high-viscosity fluids with high gravel concentrations. This gravel-packing technique packs gravel outside the wellbore to establish a region of high permeability. The gravel-packing technique has shown a high degree of success in field applications and evaluation.

Conventional gravel-packing treatments use ½ to 1 lb of gravel per gallon of nonviscous carrying fluid. usually filtered salt water or oil. This technique requires the fluid to be pumped at a rate of 3 to 6 bbl/min to prevent the gravel from falling out of the fluid or bridging on the perforations. These high fluid velocities in conjunction with the low gravel concentration result in a very efficient sand-blasting effect.

The consequent mixing of formation sand and gravel results in a region of low permeability around the wellbore. This reduced permeability results in the production impairment observed after gravel packing with conventional techniques.

Gravel-packing systems have been developed that permit placement of the gravel outside the perforations and that establish a highly permeable filter around the wellbore.

The slurry-pack technique with high gravel concentrations in a viscous carrying fluid has the following characteristics:

(1) The technique minimizes mixing of formation sand and gravel because:
  (a) The viscous carrier fluid forces the loose formation sand away from the wellbore to restress the formation.
  (b) The high gravel concentration in the viscous carrier fluid, along with low pump rates, permits a large amount of gravel to get to the formation at the same time.
  (c) The sand-blasting effect on the formation is reduced by pumping at slow rates.
(2) Better gravel suspending properties of the viscous fluids provide good radial and vertical distribution of the pack.
(3) The smaller amounts of fluid and the higher concentrations of gravel reduce the amount of fluid squeezed into the formation. This reduces the chances of creating undesirable chemical changes, saturation changes, or other types of formation damage.

The gravel-packing fluid should be free of any solids and should be chosen to be compatible with the formation. The amount of slurry should be determined by length of interval, history of the well, and previous experience with wells in the same area.

Clean, nondamaging fluids should always be used in well preparations. Any particles in the fluid may be trapped in the formation sand by the gravel pack. This can cause considerable permeability impairment, resulting in low production.

The slurry is usually mixed with 10–15 lb of gravel per gallon of carrier fluid. A typical 10-bbl slurry will

contain 250–280 gal of high-viscosity fluid (HEC) and 3,000–3,800 lb of gravel. Most jobs will be done mixing 10-bbl batches of slurry. A mixing tank equipped with a screw or paddle will be required. The base fluid and additives are added to the tank with the screw turning. This gives a fluid with some viscosity. With the screw turning, the sand is added, and the fluid is complexed. Slurries with gravel concentrations as high as 20 lb/gal of fluid have been mixed successfully.

A skid-mounted centrifugal pump should be used to pump the slurry from the mixing tank to the triplex pumps. The centrifugal pump's suction should be kept as short as possible—less than 6 ft—and should be as large as possible, usually 4 in.

4.522 FORMATION SAND CONSOLIDATION

The objective of formation sand consolidation treatments is to increase the strength of the formation sand around the wellbore such that an economic, sand-free production rate can be maintained. This is accomplished by pumping a series of chemicals sequentially into the formation. These chemicals react and precipitate to form a cement to hold the formation sand in place.

Permeability to oil is reduced because the resin occupies some of the pore space and the resin surface is oil wet. If the well is properly prepared and the formation sand consolidation system properly applied, the productivity is not seriously affected. However, a sloppy job can and does effectively seal a well with an impermeable mass.

Conoco has applied various plastics to more than one hundred zones in the Gulf Coast area with a success ratio of 87%. It is important to note that success or failure of consolidation treatments appeared to be related more to formation characteristics, well completion, and workover techniques than to the particular brand of plastic employed.

The following are formation sand consolidation advantages:

(1) Formation sand consolidation is best applied with concentric tubing (workover rig not required).
(2) The wellbore is left unobstructed.
(3) There are no casing-size limitations.
(4) Wells that have produced sand can be worked over without shutting in the whole platform or waiting on a rig to move on the platform.

The following are formation sand consolidation disadvantages:

(1) Effective placement in zones over 15 ft in length is difficult and expensive.
(2) The expense is \$2,000–\$8,000/ft of zone treated.
(3) Specialized personnel are required to perform the treatment.
(4) It requires complicated mixing.

In spite of the problems associated with formation sand consolidation, if a candidate well is correctly picked, the well properly prepared, and the system correctly applied, economic, productive wells can be completed. Formation sand consolidation is viewed as the first method to use when a well cannot be gravel packed.

4.5221 TYPES OF FORMATION SAND CONSOLIDATION SYSTEMS

There are two broad categories of resin systems.

(1) *Internally catalyzed systems.* The catalyst for these systems is included in the resin solution; its reaction is time and temperature dependent. Internally catalyzed systems react like cement. There is a definite working time, and when this time is exceeded, the resin will set. If the resin is properly placed in the formation, this presents no problem. However, if the resin is in the tubing or surface equipment it will set and cause serious problems.

(2) *Externally catalyzed systems.* For these systems, the catalyst is placed in an overflush, which is pumped following the resin with a spacer in between. The resin bonds to the formation sand, and the overflush contacts it in the formation to cause the reaction. This method has an indefinite pump time as long as the solutions do not become mixed before entering the formation. One drawback to this system is that the overflush must contact the resin in the formation to cause the reaction. If some of the perforations do not take overflush, the resin will not be catalyzed.

The following are characteristics of successful formation sand consolidation:

(1) a clean well free of rust, dirt, pipe dope, etc.
(2) clean fluids
(3) clean surface equipment (pumps and tanks)
(4) concentric tubing
  (a) is cleaner
  (b) has better displacement control
(5) compatible wellbore and rathole fluids
(6) short zone and clean sand with uniform permeability
(7) properly mixed and compatible fluids
(8) good supervision

Table 4.32 is a list of the currently available formation sand consolidation systems with some of the more important characteristics of each listed.

4.523 RESIN SAND SLURRIES

Resin-coated gravel systems use gravel that is precoated with a consolidating resin. It is pumped into the formation and forms a permeable, man-made sandstone filter around the wellbore.

The resulting consolidated pack mechancially restrains the formation sand. In remedial treatments, this can restress the formation around a well that had previously produced sand. This excess sand slurry left in the wellbore is usually drilled out.

Resin-coated gravels can be used with or without a screen liner. Without a screen liner, the resin-coated gravel can be applied to older sand-producing wells; to wells that have a restriction that prevents running a screen liner; or where screen liners are undesirable, such as in the upper zone of a multiple completion.

The gravel that receives the resin coating must be sized just as accurately as in a good gravel-pack design. The same advice for sieve analysis and gravel-size determination applies. This procedure is described in the gravel-pack section.

TABLE 4.32
AVAILABLE SYSTEMS FOR FORMATION SAND CONSOLIDATION

Trade name	Developer	Suppliers	Type of plastic	Temperature range, °F	Activator location	Dirty sand (10% clay)	Waiting time, hours
Santrol	B.J. Hughes	B.J. Hughes	Epoxy	100–220°	Resin solution	Recommended	1–18
1. Sand-Bond V 2. Sand-Bond VI	Conoco	Completion Services	Phenolic-furfuryl 1. Water base 2. Oil base	100–300°	Overflush	Recommended	6
K-200	Dowell	Dowell	Phenol resin	60–275°	Overflush	Recommended	8–12
K-90	Dowell	Dowell	Phenol-formaldehyde	180–280°	Resin solution	Not recommended over 20% clay	24
K86-K87C	Dowell	Dowell	Phenol-formaldehyde	110–205°	Resin solution	Not recommended over 20% clay	24
Epoxy II	Exxon Production Research	Completion Services Dowell Halliburton	Epoxy	100–230°	Overflush	Recommended	24
1. Sand-Bond III 2. Sanset, Enriched Sanset	Exxon Production Research (Base catalyzed plastic)	1. Completion Services 2. Halliburton	Phenol-formaldehyde	120–200°	Resin solution	Recommended	24
Sanfix	Halliburton	Halliburton	Furan	60–235°	Overflush	Recommended	1–16
Enriched Sanfix	Halliburton	Halliburton	Furan	Up to 350°	Overflush	Not recommended	1–16
Hydrofix	Halliburton	Halliburton	Furan, water base	80–240°	Overflush	Recommended	1–16
Eposand 112	Shell	B.J. Hughes, Completion Services, Dowell, Halliburton, Baker, Sand Control	Epoxy	110–200°	Resin solution	Recommended	4–6

There are three types of resin-coated-gravel systems in use:

(1) the internally catalyzed liquid-epoxy systems
(2) the externally catalyzed Furan systems
(3) the phenolic-resin-coated gravel systems, Super Sand and Baker Bond

The following are advantages of resin-sand slurry:

(1) leaves wellbore open
(2) less expensive than sand/gravel pack followed by formation sand consolidation
(3) best applied with concentric tubing (major workover not required)
(4) less affected by length of interval than formation sand consolidation
(5) no casing-size limitations

The following are disadvantages of resin-sand slurry:

(1) requires specialized personnel
(2) requires complicated mixing equipment
(3) placement time critical in internally catalyzed systems
(4) subject to contamination by wellbore fluids

The same characteristics of successful formation sand consolidation apply to resin-sand slurries.

Table 4.33 lists the currently available resin-sand slurries systems with some of the important characteristics of each.

4.53 SOLUTION PROCEDURE

Having established that a gravel pack must succeed in both stopping sand production and allowing formation fluids to flow through it, we will now consider how to design and evaluate a gravel pack's efficiency in being invisible to formation fluids. We shall observe that designing and placing a gravel pack in such a way can extend a gravel pack's useful life as well as to help it fulfill its sand-stopping role. Figure 4.77 shows the overall picture of a gravel pack and a possible solution position.

Let us examine the path taken by fluids as they go from the formation through the properly placed gravel pack and into the screen and liner (Figure 4.78). The fluids must travel through the formation to the near-wellbore region. In order to get into the screen and liner, they must enter a perforation tunnel, travel through the gravel pack, and then travel into the screen with the perforated or slotted liner. In order to evaluate this flow in terms of nodal analysis, we must be able to account for the pressure losses caused

TABLE 4.33
AVAILABLE SYSTEMS FOR CONSOLIDATED GRAVEL/SAND PACKING

Trade name	Developer	Suppliers	Type of plastic	Type of process	Temperature range, °F	Overflush	Displacing or circulating fluids	Waiting time, hours
Slick San-stop	B.J. Hughes	B.J. Hughes	Epoxy	Internally catalyzed	80–200°	None	Diesel or brine	2–8
Comp-Perm	Completion Services	Completion Services	Epoxy	Internally catalyzed	100–220°	None	Diesel or brine	8
Sandlock IV	Dowell	Dowell	Epoxy	Internally catalyzed oil base	80–180°	None	Diesel or brine	6–24
Sandlock V	Dowell	Dowell	Epoxy	Internally catalyzed water base	80–180°	None	Diesel or brine	6–24
Hydrocon	Halliburton	Halliburton	Furan	Overflush catalyzed	80–240°	1. Spacer-brine w/surfactant 2. Overflush-aqueous acid w/surfactant		1–16
Conpac	Halliburton	Halliburton	Furan	Overflush activated	80–300°	1. Spacer-diesel w/surfactant 2. Overflush-oil soluble acid in diesel		1–16
Conpac II H	Halliburton	Halliburton	Furan	Internally activated	80–240°	None	N.S.	8–48
Baker Bond	Exxon	Baker Sand Control	Phenolic	Internally	100–400°	None	None	2–48
Super Sand	Exxon	All	Phenolic	Internally	100–400°	None	None	2–48

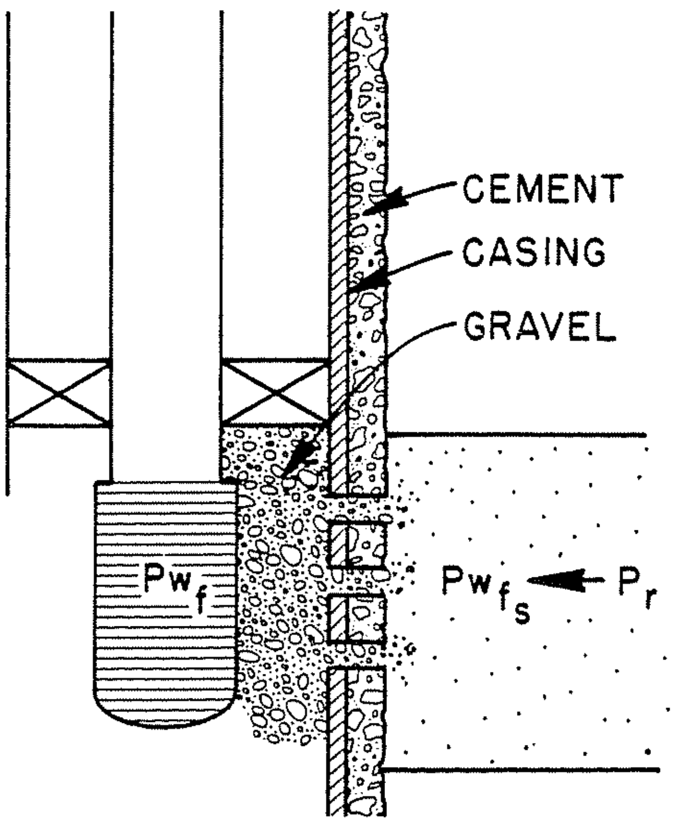

Figure 4.77 Gravel-Pack Schematic

by obstructions in this path. Fortunately, there are equations available to describe the pressure losses, whether the gravel pack is open or cased hole. By making use of equations that consider turbulence encountered during flow through a porous medium for both linear and radial flow regimes, it is possible to calculate and predict the pressure drop across a gravel pack.

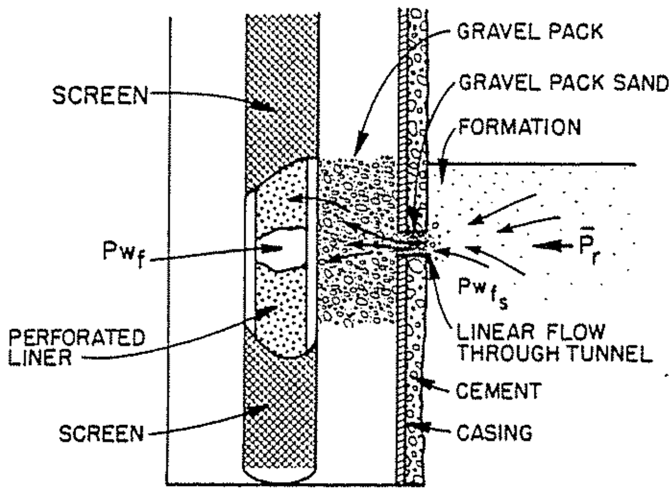

Figure 4.78 Flow Path Through a Gravel-Packed Well

The following equations, which are adapted from Jones, Blount, and Glaze have been used with success in predicting pressure drop across gravel packs for both oil and gas wells.[11]

4.531 COMPLETION PRESSURE-DROP EQUATIONS (GRAVEL-PACKED WELLS)

(1) *For Oil Wells:*

$$P_{wf_s} - P_{wf} = \Delta P = aq^2 + bq \quad (4.14)$$

$$\Delta P = \frac{9.08 \times 10^{-13}\, \beta\, B_o^2 \rho_o\, L}{A^2}(q^2) + \frac{\mu_o\, B_o\, L}{1.127 \times 10^{-13}\, k_G A}(q) \quad (4.15)$$

where:

$$a = \frac{9.08 \times 10^{-13} \beta\, B_o^2\, \rho_o\, L}{A^2} \quad (4.16)$$

$$b = \frac{\mu_o B_o\, L}{1.127 \times 10^{-3}\, k_G A} \quad (4.17)$$

q = flow rate, b/d
P_{wf} = pressure, well flowing (wellbore), psi
P_{wf_s} = flowing bottom-hole pressure at sandface, psi
β = turbulence coefficient, ft^{-1}
For gravel, the equation for β is:

$$\beta = \frac{1.47 \times 10^7}{k_G^{0.55}}$$

B_o = formation volume factor, rub/stb
ρ_o = oil density, lb/ft^3
L = length of linear flow path, ft
A = total area open to flow, ft^2
(A = area of 1 perforation × shot density × perforated interval)
k_G = permeability of gravel, md

(2) *For Gas Wells:*

$$P_{wf_s}^2 - P_{wf}^2 = aq^2 + bq \quad (4.18)$$

$$P_{wf_s}^2 - P_{wf}^2 = \frac{1.247 \times 10^{-10}\, \beta\, \gamma_g\, TZL}{A^2} q^2 + \frac{8.93 \times 10^3\, \mu_g TZL}{k_G A} q \quad (4.19)$$

where:

$$a = \frac{1.247 \times 10^{-10} \beta\, \gamma_g\, TZL}{A^2} \quad (4.20)$$

$$b = \frac{8.93 \times 10^3\, \mu_g TZL}{k_G A} \quad (4.21)$$

q = flow rate, Mcfd
P_{wf_s} = flowing bottom-hole pressure at sandface, psia
P_{wf} = flowing bottom-hole pressure in wellbore, psia
β = turbulence factor, ft^{-1}

$$\beta = \frac{1.47 \times 10^7}{k_G^{0.55}}$$

γ_g = gas specific gravity (dimensionless)
T = temperature, °R (°F + 460)
Z = supercompressibility (dimensionless)
L = linear flow path
A = total area open to flow
(A = area of 1 perforation × shot density × perforated interval)
μ_g = gas viscosity, cp

Making use of the previous equations in a nodal analysis will allow us to predict the pressure drop across a gravel pack with reasonable accuracy.

4.532 METHOD OF ANALYSIS

The gravel-pack nodal analysis is handled by treating the gravel pack as a functional node (a node whose length perpendicular to flow is small). Its effects can, in this manner, be isolated for direct examination. Isolation of the gravel pack's effects on flow is useful for planning (one can calculate and plot the effect of varying the parameters of the pack) and for evaluating a gravel pack's performance *post-facto.*

The general and most common procedure for either an oil or gas well is given as follows:

(1) Plot an IPR curve (Figure 4.79).
(2) Plot a tubing intake curve (Figure 4.80).
(3) Transfer ΔP between the IPR and tubing curve (Figure 4.81).
(4) Using the appropriate equation, calculate ΔP across the gravel pack and plot on Figure 4.82.
(5) Evaluate other shot densities or other variables as noted in Figure 4.83.

The pressure drop caused by the gravel pack can, of course, be incorporated into either of the two principal lines in a nodal analysis should one wish to isolate another part of the system.

Figure 4.84 shows how the ΔP across the pack can be incorporated into the IPR curve.

Figure 4.85 shows how the ΔP gravel pack can be included in the tubing curve.

The most common solution is the one that isolates the gravel pack and is the one to be used in this section.

In order to isolate the effects of the gravel pack, first analyze the system using the completion as the

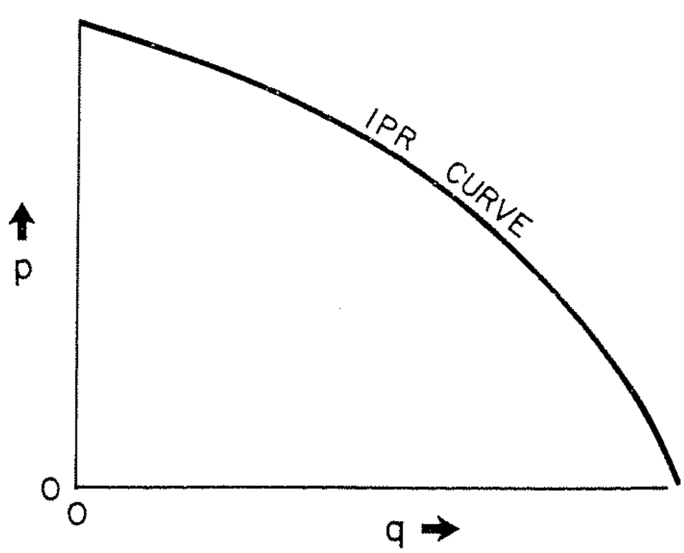

Figure 4.79 Constructed IPR Curve

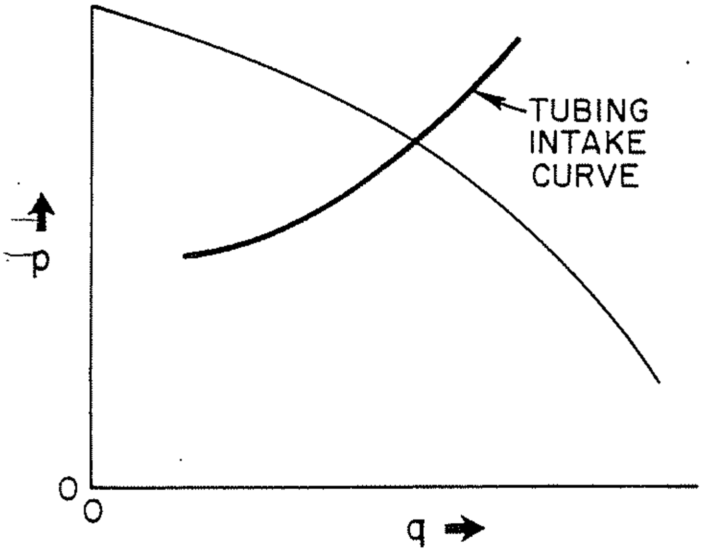

Figure 4.80 Constructed Tubing Intake Curve

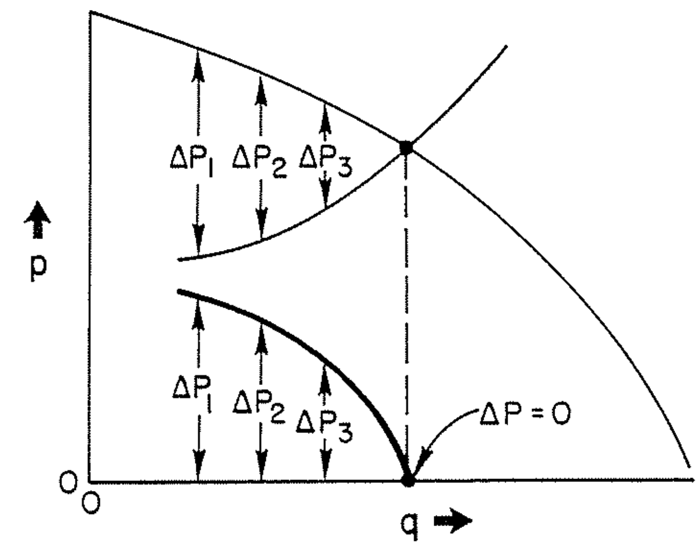

Figure 4.81 Transfer ΔP

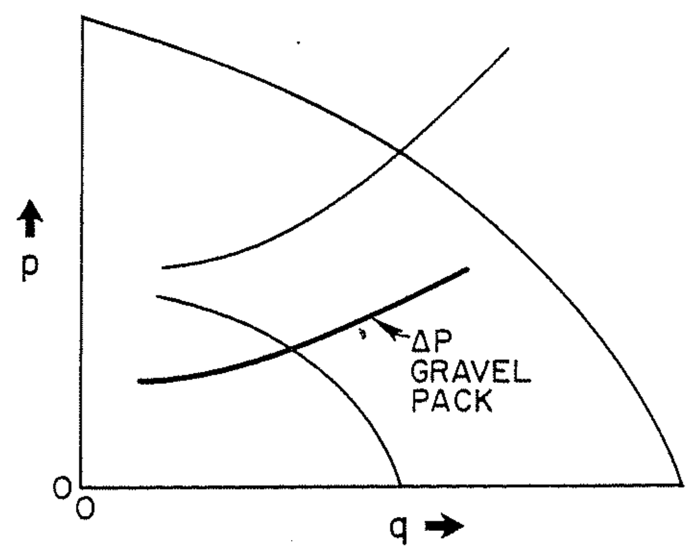

Figure 4.82 Constructed ΔP Across Gravel Pack

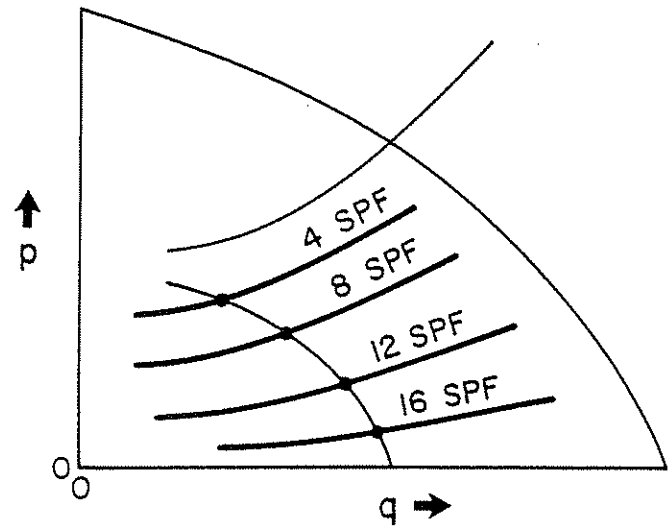

Figure 4.83 Evaluation of Various Shot Densities

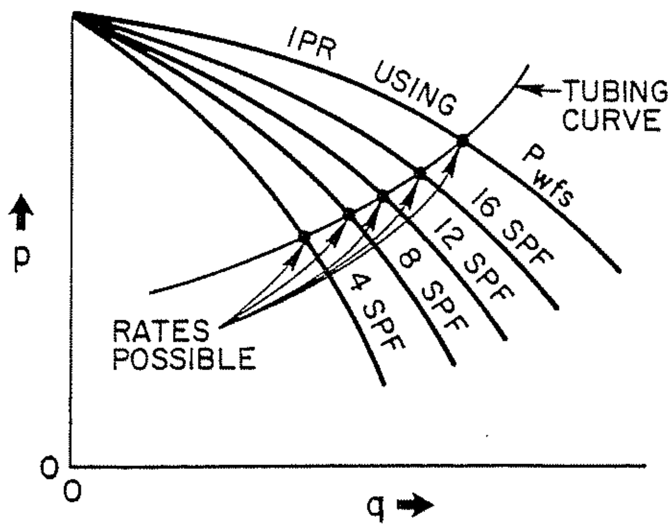

Figure 4.84 Gravel-Pack Solution by Including ΔP Completion in IPR Curve

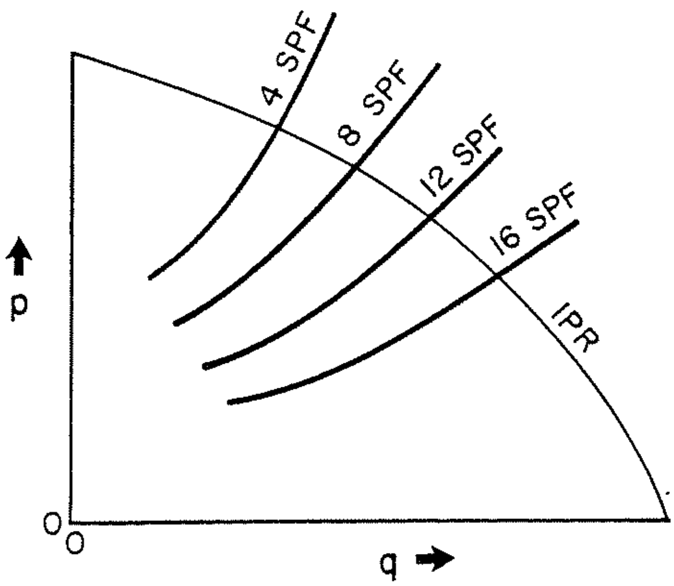

Figure 4.85 Solution Including ΔP Completion in the Tubing Performance Curve

solution point, initially leaving out the gravel pack. Having completed this, plot the pressure drop (ΔP) vs rate (q) relationship for the well system. Finally, plot the pressure drop vs rate relationship for the gravel pack on the same graph, using the same scale. The intersection of the pressure-drop system curve and the pressure-drop curve for the gravel pack will show the rate at which the system will produce and the magnitude of the pressure drop across the completion.

This procedure can be best illustrated by working an example problem for both gas and oil.

GAS WELL EXAMPLE

Given data: (gas well):

$\overline{P}_r = 4{,}000$ psi	$P_{wh} = 1{,}000$ psi
depth = 12,000 ft	$\gamma_g = 0.6$
k = 300 md	40–60 gravel
h = 20 ft	$k_G = 45{,}000$ md
$h_p = 10$ ft	4 spf
$r_e = 1{,}500$ ft	diameter = 0.73 in.
$r_w = 0.411$ ft	screen = 4-in. OD
9.875-in. hole	2.441-in. ID tubing
casing = 7⅝ in.	T = 220°F

This is a good well of high permeability; the values of viscosity (μ_g) and compressibility (Z) will be taken at pressures near the static pressure and are found to be 0.021 cp (μ_g) and 0.965 (Z), respectively.

Solution procedure:

(1) Construct the IPR Curve (see Figure 4.86).

The Jones, Blount, and Glaze equation is repeated again at this point:

$$\overline{P}_r^2 - P_{wf_s}^2 = aq^2 + bq \qquad (4.18)$$

$$\overline{P}_r^2 - P_{wf_s}^2 = \frac{3.16 \times 10^{-12} \beta \gamma_g TZ}{h_p^2 r_w} q^2 + \frac{1.424 \times 10^3 \mu_g TZ[\ln(0.472\, r_e/r_w) + S]}{k_g h} q \qquad (4.22)$$

$$AOF = \frac{-b \pm \sqrt{b^2 + 4a(\overline{P}_r^2)}}{2a} \qquad (4.23)$$

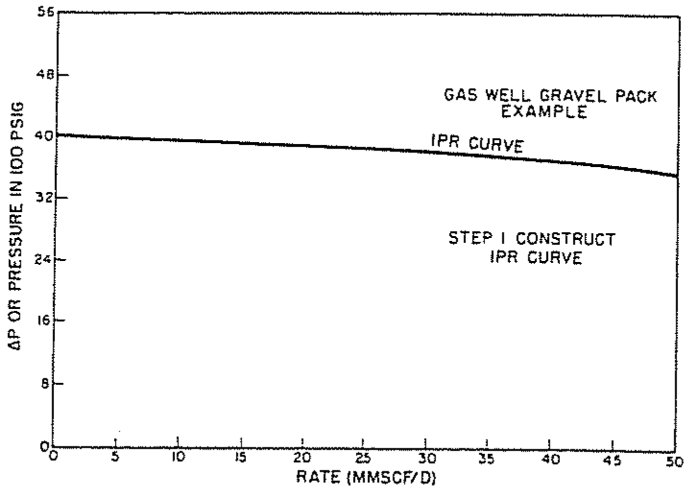

Figure 4.86 Construction of IPR Curve; Gas Well Gravel-Pack Example; Step 1, Construct IPR Curve

where:

$$a = \frac{3.16 \times 10^{-12} \beta \gamma_g TZ}{h_p^2 r_w} \qquad (4.24)$$

$$b = \{1.424 \times 10^3 \mu_g TZ \times [\ln(0.472\, r_e/r_w) + S]\}/kh \qquad (4.25)$$

q = flow rate, Mcfd
a = turbulence term
b = Darcy flow term
$\overline{P}_r$ = reservoir pressure (shut-in bottom-hole pressure), psia
P_{wf_s} = sandface flowing bottom-hole pressure, psia
β = turbulence coefficient, ft^{-1}

$$\beta = \frac{2.33 \times 10^{10}}{k^{1.201}}$$

γ_g = gas specific gravity (dimensionless)
T = reservoir temperature, °R (°F + 460)
Z = supercompressibility (dimensionless)
h_p = perforated interval, ft
μ_g = gas viscosity, cp
r_e = drainage radius, ft
r_w = wellbore radius, ft

Note that we have substituted P_{wf_s} for P_{wf} in this equation. This is because the gravel pack will cause a pressure drop. The pressure in the wellbore (P_{wf}) will not be the same as that at the sandface (P_{wf_s}).

Because the absolute open flow is so large compared to rates common to gas wells in the United States, we shall therefore set the limit of our graph at 50 million scfd for constructing the IPR. We shall find it useful to tabulate the data before plotting. The values calculated are:

$a = 7.47 \times 10^{-4}$
$b = 24.37$
$\beta = 2.47 \times 10^7$

Substituting in the appropriate values, the absolute open flow potential (AOFP) is found to be 130.94 MMscfd.

Figure 4.86 is constructed based on a scale to properly illustrate the objective flow rate, and Table 4.34 shows the data used.

TABLE 4.34

q, MMscfd	P_{wf_s}
5	3,982
10	3,960
15	3,933
20	3,900
25	3,860
30	3,820
35	3,772
40	3,719
45	3,659
50	3,594

(2) Next, construct the curves that describe the pressure vs rate relationship in the tubing. Making use of the Cullender and Smith correlation for

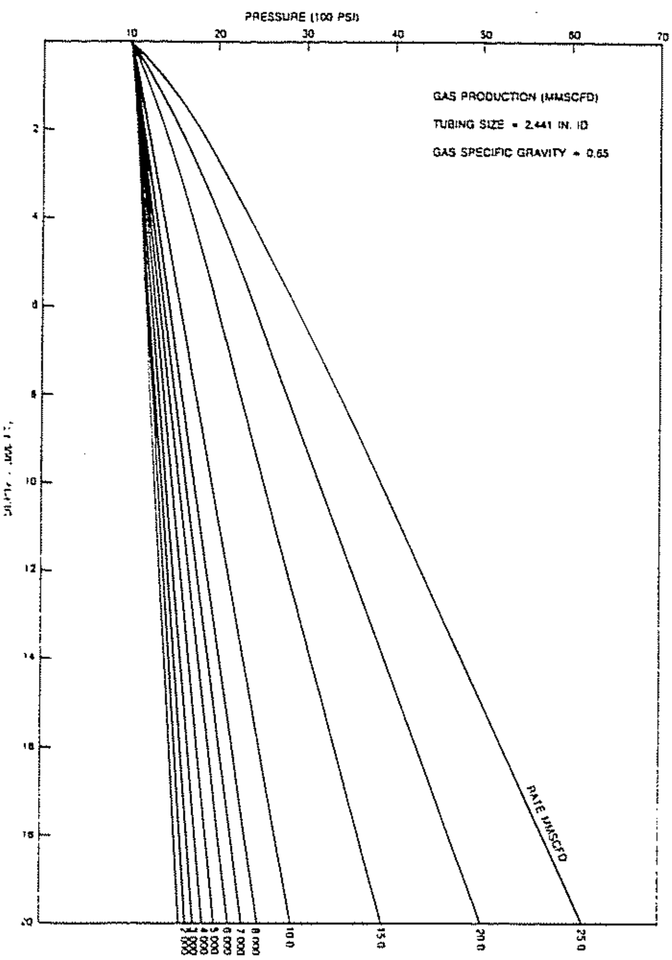

Figure 4.87 Vertical Flowing Gas Gradients (Gas Production, MMscfd; Tubing Size, 2.441-in. ID; Gas Specific Gravity, 0.65) (Working Copy on p. 432)

2⅞-in. (2.441-in. ID) tubing and 1,000-psi wellhead pressure (P_{wh}), we can construct a table of the necessary bottom-hole flowing pressure (P_{wf}) for each considered rate.

Refer to Figure 4.87 for the appropriate gradient curves used in this example. Table 4.35 shows these results.

TABLE 4.35
TUBING INTAKE PRESSURES

q, millions	Pressure, psig
25	4,300
20	3,550
15	2,800
10	2,130
5	1,600

This data is then plotted on Figure 4.88 to reveal an intersection at 22.5 MMscfd. This intersection indicates the rate at which the system would produce if there were no pressure drop across the completion. The P_{wf_s} value at the intersection is the sandface pressure at which the reservoir will produce this rate. We must now evaluate the pressure drop across the completion.

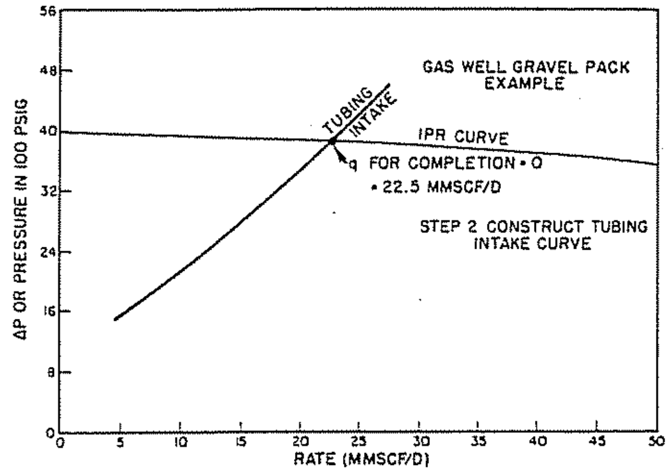

Figure 4.88 Tubing Intake Curve; Gas Well Gravel-Pack Example; Step 2, Construct Tubing Intake Curve

(3) The next step is to transfer the ΔP between the IPR and tubing intake curve (see Figure 4.89). To do this, calculate and plot the pressure drop (ΔP) of the system less the gravel pack by subtracting the tubing curve pressures from the IPR curve pressures for several rates and then plotting them on the same graph as a pressure drop vs rate diagram. Again, it is advisable to construct a table in order to keep all the data in order (Figure 4.89).

(4) To calculate and plot ΔP across the completion, we shall now turn our attention to the pressure drop across the gravel pack. Using the linear flow equations as given by Jones, Blount, and Glaze, we will be able to do this with some degree of accuracy.[11]

Fluids moving through the reservoir to the wellbore move in a radial flow regime; that is, the area normal (perpendicular) to flow is decreasing. When fluids begin to enter the gravel-packed wellbore, they move into the linear flow regime (the area normal to flow is constant). Let us discuss some of the variables that are different

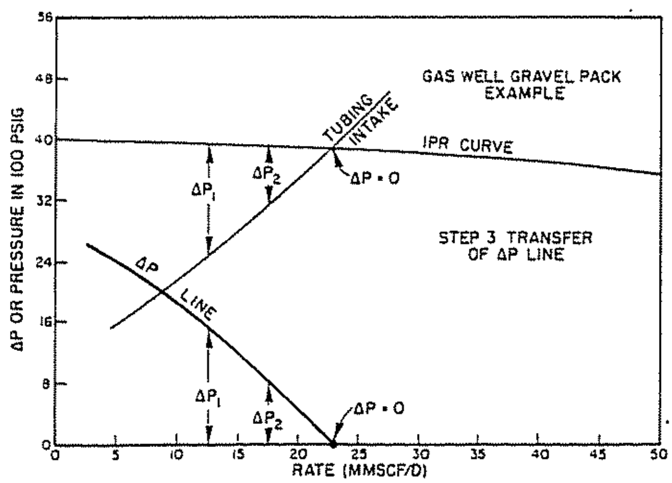

Figure 4.89 Transfer of ΔP; Gas Well Gravel-Pack Example; Step 3, Transfer of the ΔP Line

in these equations from those in the radial flow equations. Refer to Figures 4.90a and 4.90b.

The first unfamiliar variable is L (tunnel length). This variable is the length of the linear flow path in feet. The length of the linear flow path in unconsolidated formations is measured from the outer edge of the cement sheath (hole radius) to the OD of the screen and liner (Figure 4.90). It is assumed that insufficient consolidation is in the formation sand to allow for a discrete tunnel to exist in the formation proper. This is probably a sound assumption, especially since

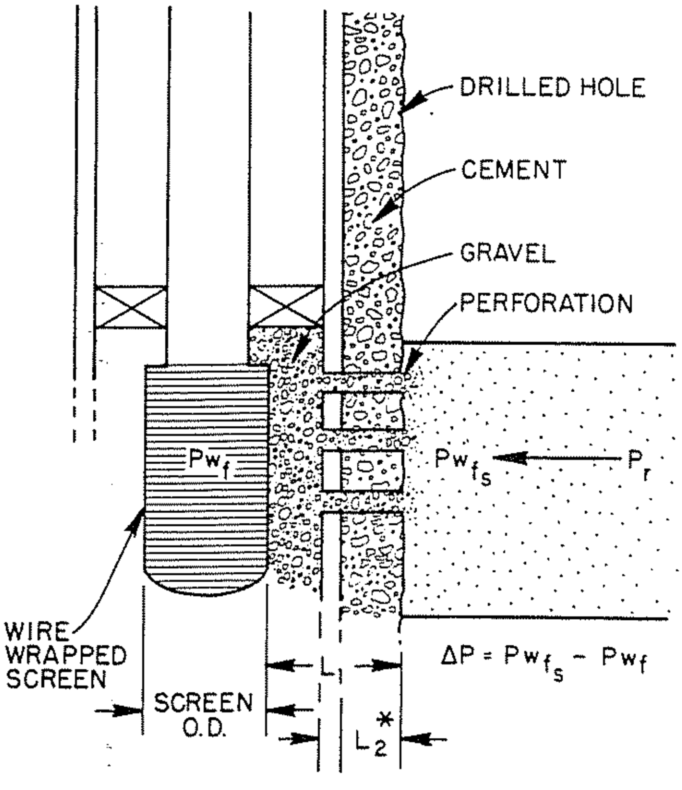

Figure 4.90a Gravel-Pack Schematic

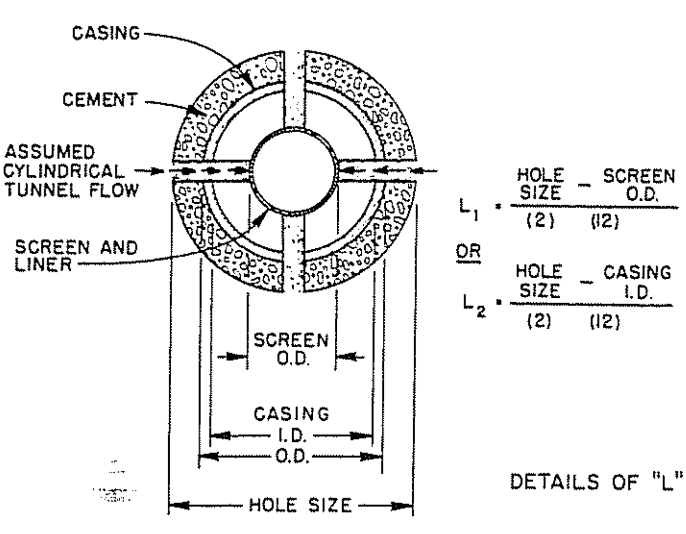

Figure 4.90b Details of "L"

perforations are usually cleaned by washing or surging the formation.

Some investigators say that fluids return to a radial flow regime once inside the casing (Figure 4.90) and therefore measure the length of linear flow path from the outside of the cement sheath to the casing ID. It has been this investigator's experience that measuring the linear flow path from the outer cement sheath to the screen OD will somewhat overpredict the pressure drop of a perforation tunnel. This means that it will underpredict the rate for a given flowing pressure and may mean a prediction of a higher-than-absolutely-necessary shot density. Conversely, measuring the linear flow path from the cement sheath to the casing ID will have the opposite effect upon an evaluation of the gravel pack's performance.

For evaluation of this example and for general application of nodal analysis, we recommend the former method—measuring the L (linear flow path) from the cement sheath to the screen OD—because it is much less expensive to shoot a few more shots than necessary before a gravel pack than to pull the pack and reperforate after a pack has been placed or to lose production or to have a gravel pack fail because of an excessive pressure drop.

By examining the equation, we can see that minimizing the magnitude of L can help to minimize the pressure drop in the gravel pack. In order to do this, use the largest screen and liner that can be washed over easily, should it become necessary to do so. To that end, an annular space of 0.75 to 1.25 in. (Figure 4.90) is considered optimum. This size of annulus between the screen and casing is sufficient to allow for placement of sand using modern viscous slurry methods, is ample for controlling sand production, and is still small enough to minimize the effects of the length of the linear flow path and its related pressure drop. When the L cannot be optimized because of mechanical or hole-condition reasons, the effects of L can be overcome by increasing the area open to flow.

The next unfamiliar term is A. This term is the total area open to flow, which means the area of one perforation multiplied by the number of perforations open. In this and all design examples, assume 100% efficiency in perforating until sufficient field experience is gained to revise the efficiency in each operator's field. Perforation efficiency of 70% should be achieved, but as low as 30% have been reported.

While permeability is not a new term, a short discussion of gravel permeability is in order. Gravel permeabilities were obtained from various gravel-packing and gravel-supply companies. A consensus of permeabilities was obtained, used, and published for various commonly used gravels. When those initially published permeabilities were applied in the equations, they proved, with experience, to be consistently underpredictive of pressure drop. It was then discovered that the permeabilities being used were the absolute

permeabilities of those gravels to air at low pressure. When tested, the gravel was also very, very clean, a condition often sought but rarely obtained in the field. Since in-situ conditions for a gravel pack are quite different from those in a laboratory, the gravel permeabilities used in predicting pressure drop were revised downward until they more nearly reflected the in-situ condition. Extensive data for comparison were available for 20–40 and 40–60 gravel only—other commercial gravels not being widely used on the Gulf Coast, where the evaluations were made. The results are listed below:

Gravel Size	Permeability
20–40 mesh	100,000 md
40–60 mesh	45,000 md

While it is somewhat risky to make an inference about the effective permeability of other gravel sizes based on these two gravel sizes, reducing the permeability to air of other gravel sizes by 50% may be a realistic beginning estimate that can be revised when field experience indicates what it should be.

(4) For the implementing step, ΔP across completion, first calculate the gravel-pack pressure drop by calculating the values of the a and b terms in the Jones equation. All of the necessary data can be found in the well data given earlier or can be easily calculated from the given data. Look first at the a term:

$$P_{wf_s}^2 - P_{wf}^2 = \frac{1.247 \times 10^{-10}\, \beta\, \gamma_g\, TZL}{A^2} q^2 + \frac{8.93 \times 10^3\, \mu_g TZL}{k_G A} q \quad (4.18)$$

where:

$$a = \frac{1.247 \times 10^{-10}\, \beta\, \gamma_g\, TZL}{A^2} \quad (4.20)$$

$$b = \frac{8.93 \times 10^3\, \mu_g TZL}{k_G A} \quad (4.21)$$

Now that the necessary terms are gathered together, plug them into the equation and calculate the value of a:

$L = 0.245$ ft
$\beta_g = 4.056 \times 10^4$
$A = 0.116$ ft^2

$$a = [1.247 \times 10^{-10}(4.056 \times 10^4) \times (0.6)(680)(0.965)(0.245)]/(0.116)^2 = 0.0361$$

Next, calculate the b term, first gathering the necessary variables:

$$b = \frac{8.93 \times 10^3\, \mu_g TZL}{k_G A} = \frac{8.93 \times 10^3(0.021)(680)(0.965)(0.245)}{(45{,}000)(0.116)} = 5.78$$

Note that these values are to be used for q in Mcfd.

The general equation now is:

$$P_{wf_s}^2 - P_{wf}^2 = 0.0361\, q^2 + 5.78\, q$$

This equation can be solved for P_{wf} as follows:

$$P_{wf} = \sqrt{(P_{wf_s})^2 - (0.0361 q^2 + 5.78 q)}$$

This equation allows us to assume several rates and calculate the corresponding value for P_{wf}. If the rate used is too large, the value under the radical will become negative. The meaning of this in the real world is that there simply is not enough energy at the sandface to allow that rate to cross the gravel pack. The equation requires a P_{wf_s} for each assumed rate. If we do not have the P_{wf_s} for the particular rate to be evaluated from the IPR table, we must use the IPR equation to calculate the P_{wf_s} for that rate.

The radial flow equation is used first to obtain P_{wf_s}. Then, the linear flow equation is used to obtain P_{wf}. The ΔP that we are interested in is $P_{wf_s} - P_{wf}$ for various assumed rates.

These values are shown in Tables 4.36, 4.37, 4.38, and 4.39 for several different conditions.

TABLE 4.36
4 SPF AND 10-FT PERFORATED

q, MMscfd	P_{wf_s}	P_{wf}	ΔP
5	3,982	3,863	119
10	3,960	3,467	493
15	3,933	2,696	1,237
20	3,900	809	3,011
25	3,863	—	—
30	3,821	—	—
35	3,773	—	—
40	3,719	—	—
45	3,659	—	—
50	3,594	—	—

Plot this data as noted on Figure 4.91.

TABLE 4.37
4 SPF AND 20-FT PERFORATED

q, MMscfd	P_{wf_s}*	P_{wf}	ΔP
5	3,984	3,954	30
10	3,967	3,848	119
15	3,949	3,677	272
20	3,929	3,431	498
25	3,908	3,093	815
30	3,886	2,627	1,259
35	3,862	1,942	1,920
40	3,837	428	3,409
45	3,811	—	—
50	3,783	—	—

* Note that P_{wf_s} values change slightly as compared to 10-ft perforated because of the h_p^2 term in the denominator of the a coefficient.

TABLE 4.38
8 SPF AND 10-FT PERFORATED

q, MMscfd	P_{wf_s}	P_{wf}	ΔP
5	3,982	3,952	30
10	3,960	3,841	119
15	3,933	3,660	273
20	3,900	3,398	502
25	3,860	3,032	828
30	3,820	2,528	1,292
35	3,772	1,756	2,515
40	3,719	—	—
45	3,659	—	—
50	3,594	—	—

where:

$L = 0.245$
$\beta = 4.056 \times 10^4$
$A = 0.233$ ft^2
$a = 9.015 \times 10^{-3}$
$b = 2.879$

TABLE 4.39
16 SPF AND 20-FT PERFORATED

q, MMscfd	P_{wf_s}	P_{wf}	ΔP
5	3,984	3,982	2
10	3,967	3,959	8
15	3,949	3,932	17
20	3,929	3,898	31
25	3,908	3,860	48
30	3,886	3,817	69
35	3,862	3,758	94
40	3,837	3,714	123
45	3,811	3,654	157
50	3,783	3,587	196
80	3,585	3,031	554

where:

$A = 0.93$ ft^2
$a = 5.63 \times 10^{-4}$
$b = 0.720$

We now have a complete plot of the system ΔP vs the completion ΔP. This plot yields two very valuable pieces of information: the rate at

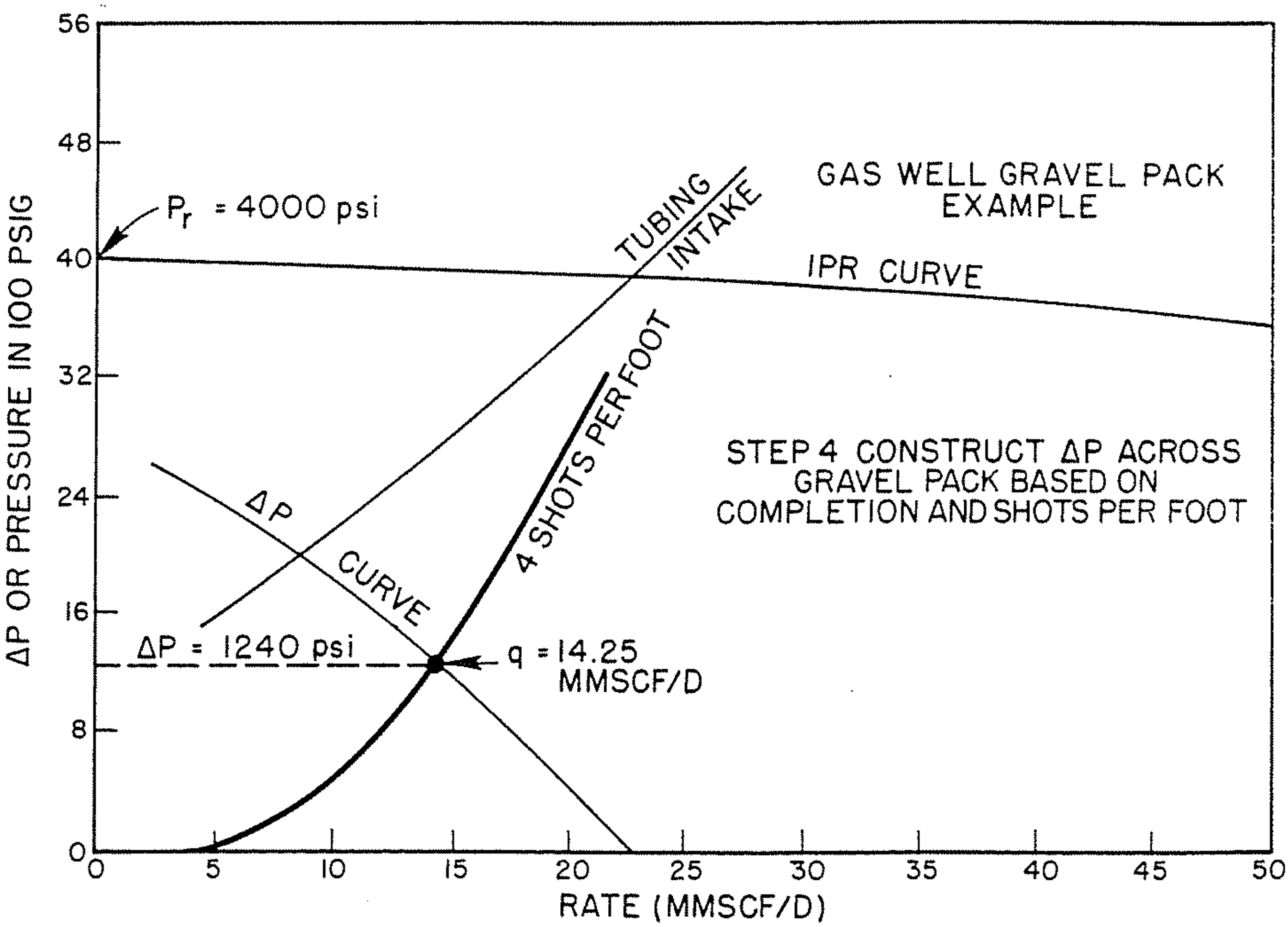

Figure 4.91 Final Plot for 4 spf; Gas Well Gravel-Pack Example; Step 4, Construct ΔP Across Gravel Pack Based on Completion and Shots Per Foot

which the total system (including the gravel pack) will produce and the magnitude of the pressure drop across the completion—in this case, the gravel pack.

It is now time for us to decide whether other shot density calculations are necessary. During the time in which nodal analysis has been used to evaluate gravel packs, it has been shown that a pressure drop of 200 psi or less is an excellent limit to plan for and operate under. None of the many people who have applied this technology has complained of a failure of his gravel pack when the pressure drop has been kept to or below the 200-psi limit. The only real force with which to move either fines or the gravel itself, leading to cutting out the screen and failure of the pack, is the velocity associated with a large pressure drop. The 200-psi limit was picked more or less randomly and has been shown to be somewhat conservative. Some operators have increased the upper limit of the pressure drop to 300–500 psi, depending on the degree of confidence they have in their gravel packing-procedures in general.

In our current example, the pressure drop across the pack with 4 spf is 1,240 psi. This much pressure drop is not acceptable, even to the most liberal of operators. It would, therefore, behoove us to examine some other shot densities or consider increasing the perforated interval or a combination of both. The parameter that we are actually changing by changing shot density or perforated interval—or even gun size—is the total area open to flow. We shall evaluate a change in both shot density and perforated interval for our current example problem.

First, let us extend the perforated interval to 20 ft. In order to evaluate the effects of this, we need only recalculate the a and b terms from our previous equations and follow the same procedure as before. This information is shown in Table 4.37 and plotted on Figure 4.92.

Once again, plotting this data on our original graph, we see that the rate at which the system will produce is increased to 20 million scfd, and the pressure drop across the pack has decreased to 440 psi.

Next, examine the effects of increasing the shot density to 8 spf with 10-ft open and 16 spf with 20-ft open. Once again, calculate the new a and b values and tabulate the data. Note Tables 4.38 and 4.39.

Now, again plot this data on the original plot (Figure 4.92). This shows that the well system will make 22 MMscf with a very low ΔP across the completion. Since both the increased shot density and the increased perforated interval are

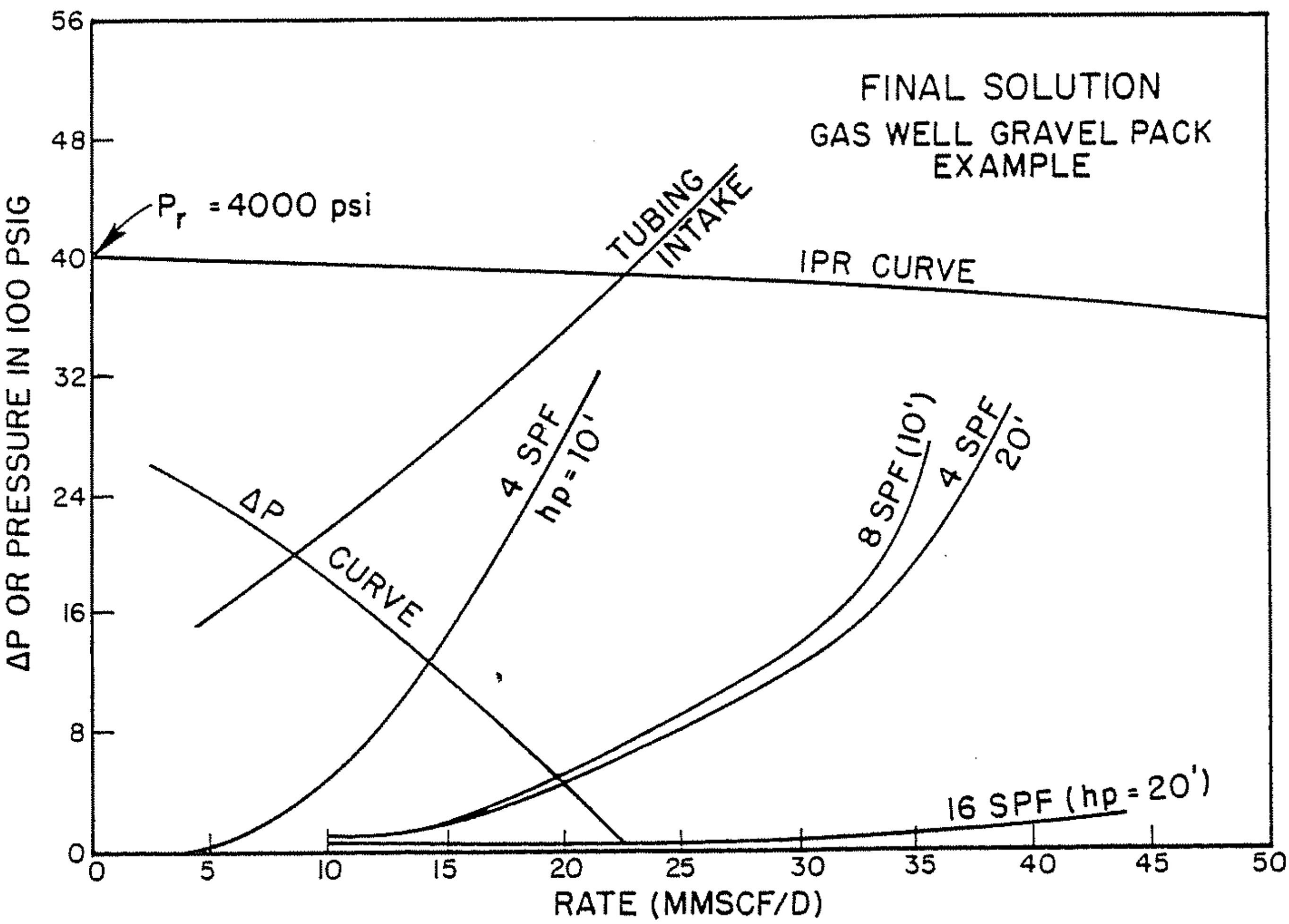

Figure 4.92 Final Solution; Gas Well Gravel-Pack Example

acceptable in terms of the pressure drop across the gravel pack, the operator must choose which course is better for him, either operationally or for reservoir considerations (e.g., the presence of a water contact near the producing interval). The operator is now able to make a decision about perforating this interval, which allows him to obtain the objective rate, keep the pressure drop across the gravel pack to an acceptable level, and allow for other considerations such as the presence of water near the producing interval. Additionally, these decisions are made in advance of the actual completion and, as has been shown through industry experience, can be made with reasonable assurance of both accuracy and achievability. This is a great boon to those who have to design gravel packs with longevity or high rates or both as an objective. The chances of picking exactly the proper combination of shot density, perforated interval, and size of perforation entry hole without the benefit of these types of calculations is small indeed. An analysis of this type can give more assurance to the kinds of expensive decisions that we make when writing out the well programs and gravel-pack designs.

$$\rho_o = \frac{\rho_{\text{dead oil}} + \dfrac{.0764(\gamma_g)Rs}{5.61}}{B_o}$$

OIL WELL EXAMPLE

We shall now turn our attention to an oil well. The procedure for the analysis is identical to that for gas wells. We must still choose the completion as the solution point of our analysis and then proceed to construct IPR and tubing curves. The construction of these two curves, the system ΔP curve, and the curve describing the pressure drop across the gravel pack should proceed in the same way whether one is working an oil well or a gas well. Only the particular equations are different.

Given data:

$P_{wh} = 280$ psi	4-in. tubing
$\overline{P}_r = 3{,}500$ psi	35°API($\rho = 43.9\ lb_m/ft^3$
depth = 8,000 ft	(all oil)
$r_e = 1{,}500$ ft	$\gamma_g = 0.65$
$k_o = 170$ md	$T = 190°F$
$h = 25$ ft	GOR = 600 scf/bbl
$hp = 15$ ft	shot with 4 spf
perforation hole diameter	= 0.51 in. dia. hole
drilled hole size = 12¼ in.	$P_b = 2{,}830$ psi
casing = 9⅝ in.	$B_o = 1.33$
OD screen = 5½ in.	$\mu_o = 0.54$ cp
$r_w = 0.51$ ft	
40–60 gravel (45,000 md)	

where Rs = solution GOR (see page 306, vol. 1 of this series)

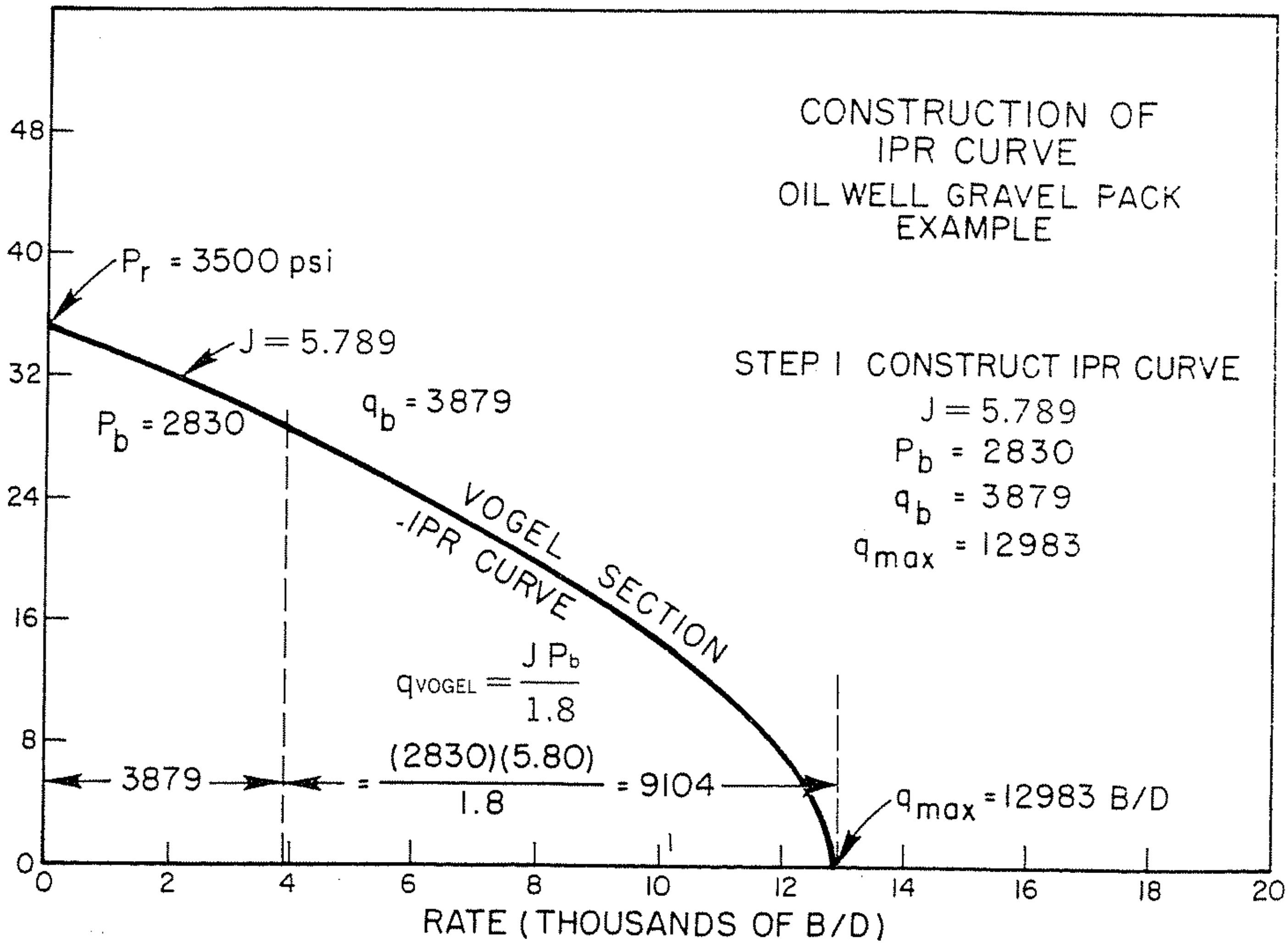

Figure 4.93 Construction of IPR Curve; Oil Well Gravel-Pack Example; Step 1, Construct IPR Curve

Solution procedure:

(1) Construct the IPR curve using Darcy's Law:

$$q_o = \frac{7.08(10^{-3})kh\,[P_r - P_b]}{\overline{\mu}_o \overline{B}_o (\ln r_e/r_w - 3/4 + 0} \qquad (5.26)$$

$$J = \frac{7.08\,(10^{-3})\,kh}{\overline{\mu}_o \overline{B}_o (\ln r_e/r_w - 3/4)} = 5.789 \qquad (5.27)$$

$$q_b = 5.789\,(3{,}500 - 2{,}830) = 3{,}879 \text{ b/d}$$

$$q_{max} = q_b + \frac{J\,P_b}{1.8} = 12{,}983 \text{ b/d}$$

Density of oil = 43.9 lb_m/ft^3
Refer to Figure 4.93 for the IPR curve.

Table 4.40 shows data plotted for the IPR curve.

TABLE 4.40

q, b/d	P_{wf_s}
5,691	2,500
8,059	2,000
9,972	1,500
11,430	1,000
12,434	500

(2) Construct the tubing intake curves for 4½-in. OD tubing and for a wellhead pressure of 280 psi (refer to Appendix 4.2). The data of Table 4.41 is used.

TABLE 4.41

q, b/d	Tubing intake pressure
4,000	1,640
6,000	1,860
8,000	2,120

Refer to Figure 4.94 and note a rate of 7,500 b/d for zero pressure drop across the completion.

(3) Transfer the ΔP curve (see Figure 4.95).

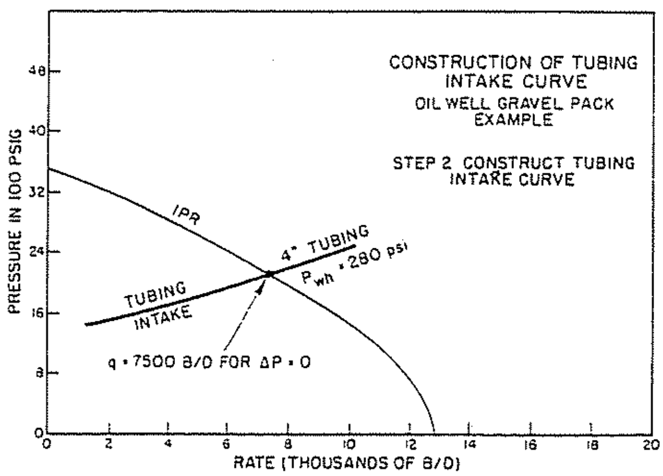

Figure 4.94 Construction of Tubing Intake Curve; Oil Well Gravel-Pack Example; Step 2, Construct Tubing Intake Curve

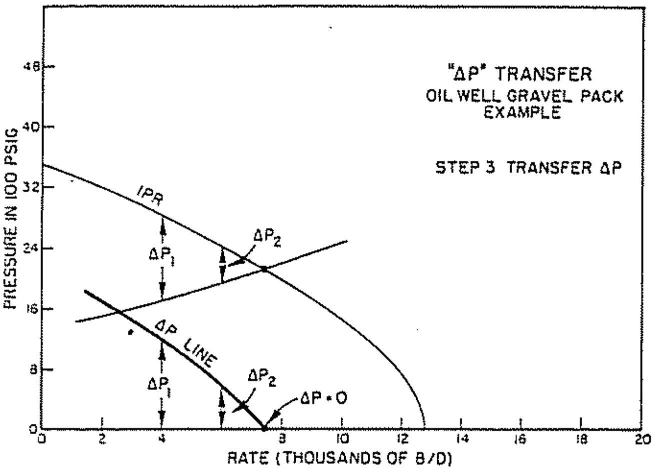

Figure 4.95 ΔP Transfer; Oil Well Gravel-Pack Example; Step 3, Transfer ΔP

(4) Calculate ΔP across the gravel pack for 4 spf and 0.51-in. diameter holes using the following equations as suggested by Jones, Blount, and Glaze.[11]

$$P_{wf_s} - P_{wf} = \Delta P = a\,q^2 + b\,q \qquad (4.14)$$

$$\Delta P = \frac{9.08 \times 10^{-13}\,\beta\,B_o^2\,\rho_o\,L}{A^2}(q^2) + \frac{\mu_o\,B_o\,L}{1.127 \times 10^{-3}\,k_G A}(q) \qquad (4.15)$$

where:

$$a = \frac{9.08 \times 10^{-13}\,\beta\,B_o^2\,\rho_o\,L}{A^2} \qquad (4.16)$$

$$b = \frac{\mu_o\,B_o\,L}{1.127 \times 10^{-3}\,K_G A} \qquad (4.17)$$

q = flow rate, b/d
P_{wf} = pressure, well flowing (wellbore), psi
P_{wf_s} = flowing bottom-hole pressure at sand-face, psi
β = turbulence coefficient, ft^{-1}
For gravel, the equation for β is:

$$\beta = \frac{1.47 \times 10^7}{k_G^{0.55}}$$

B_o = formation volume factor, rb/stb
ρ = oil density, lb/ft^3
L = length of linear flow path, ft
A = total area open to flow, ft^2
(A = area of 1 perforation × shot density × perforated interval)
k_G = permeability of gravel, md

An examination of these equations will reveal that there is only one term that is unfamiliar to us. We have seen all of these terms except the density term (ρ). The β term is the same for both oil and gas. The ρ_o term is the oil density in lb_m/cu ft. If this term is not known, it may be approximated by using the nomograph found on page 306 of Volume 1 of this series of books.

As before with the gas well example, we begin calculations for the gravel-pack pressure drop by calculating the value of the a and b terms. Also,

ΔP may be solved for directly since no pressure-squared term is involved.

Table 4.42 shows these results for 4 spf and 15-ft perforated:

$L = 0.281$ ft
$A = 0.085$ ft^2
$\beta = 4.056 \times 10^4$
$a = 1.11 \times 10^{-4}$
$b = 0.0468$

TABLE 4.42

Assumed q, b/d	ΔP
200	14
500	51
1,500	320
2,000	538
3,000	1,139
4,000	1,953
6,000	4,277
8,000	—
10,000	—

These results are shown on Figure 4.96 with a rate of 3,500 b/d but a ΔP of 1,400 psi, which is too high across the gravel pack.

(5) Calculate ΔP for other shot densities.

Table 4.43 shows these results for 8, 12, and 16 spf for 15-ft perforated:

TABLE 4.43

	8 spf	12 spf	16 spf
	$A = 0.17$ ft^2, $a = 2.77 \times 10^{-5}$, $b = 0.0234$	$A = 0.255$ ft^2, $a = 1.233 \times 10^{-5}$, $b = 0.0156$	$A = 0.34$ ft^2, $a = 6.938 \times 10^{-6}$, $b = 0.0117$
q, b/d	ΔP, psi	ΔP, psi	ΔP, psi
200	6	4	3
500	19	11	8
1,500	97	51	33
2,000	158	82	51
3,000	320	158	98
4,000	538	260	158
6	1,139	538	320
8	1,953	914	538
10	3,009	1,389	811
12	4,277	1,963	1,139

These ΔP values are then plotted in Figure 4.97. As before, we plot the tabulated data on the same graph, which already has the IPR, tubing

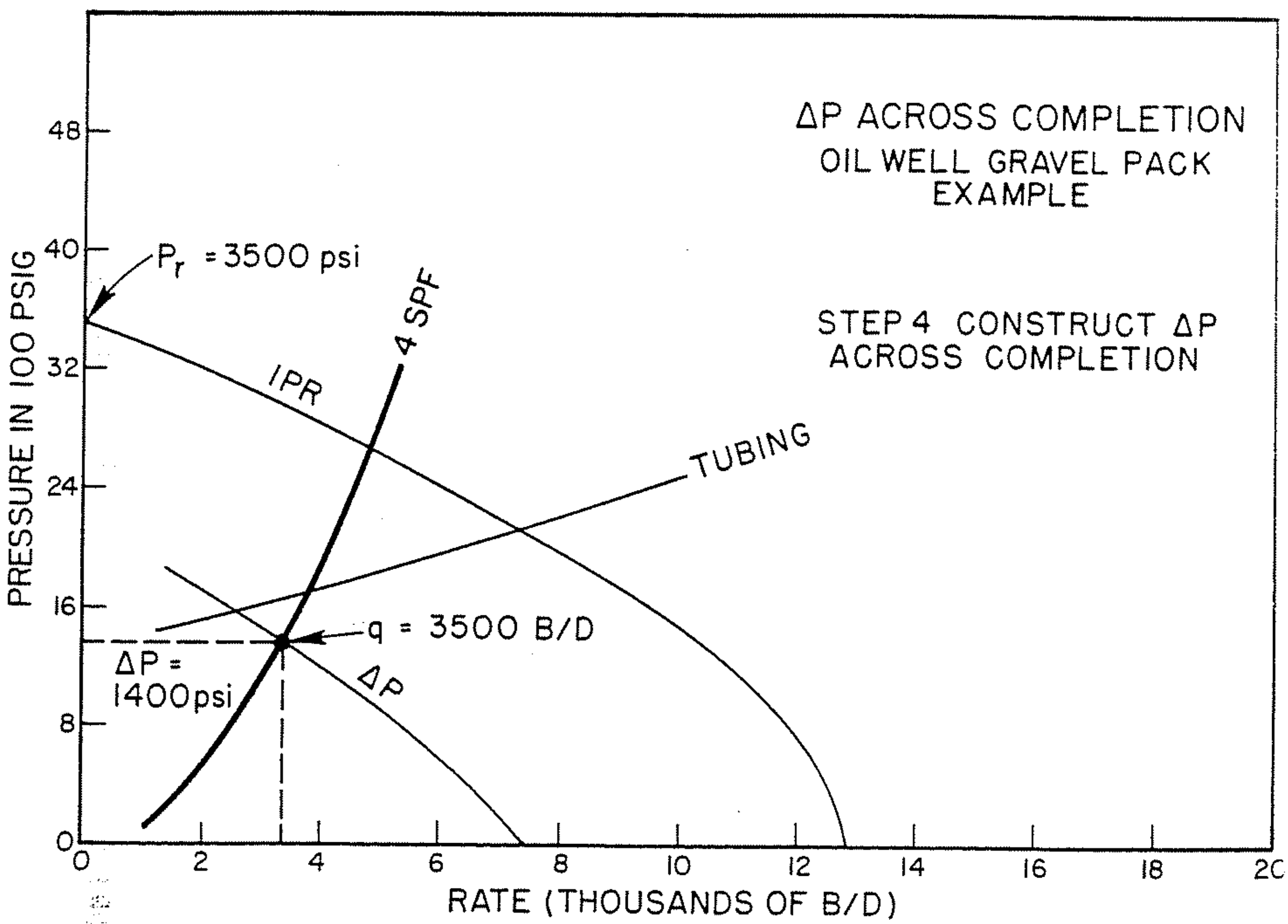

Figure 4.96 ΔP Across Completion; Oil Well Gravel-Pack Example; Step 4, Construct ΔP Across Completion

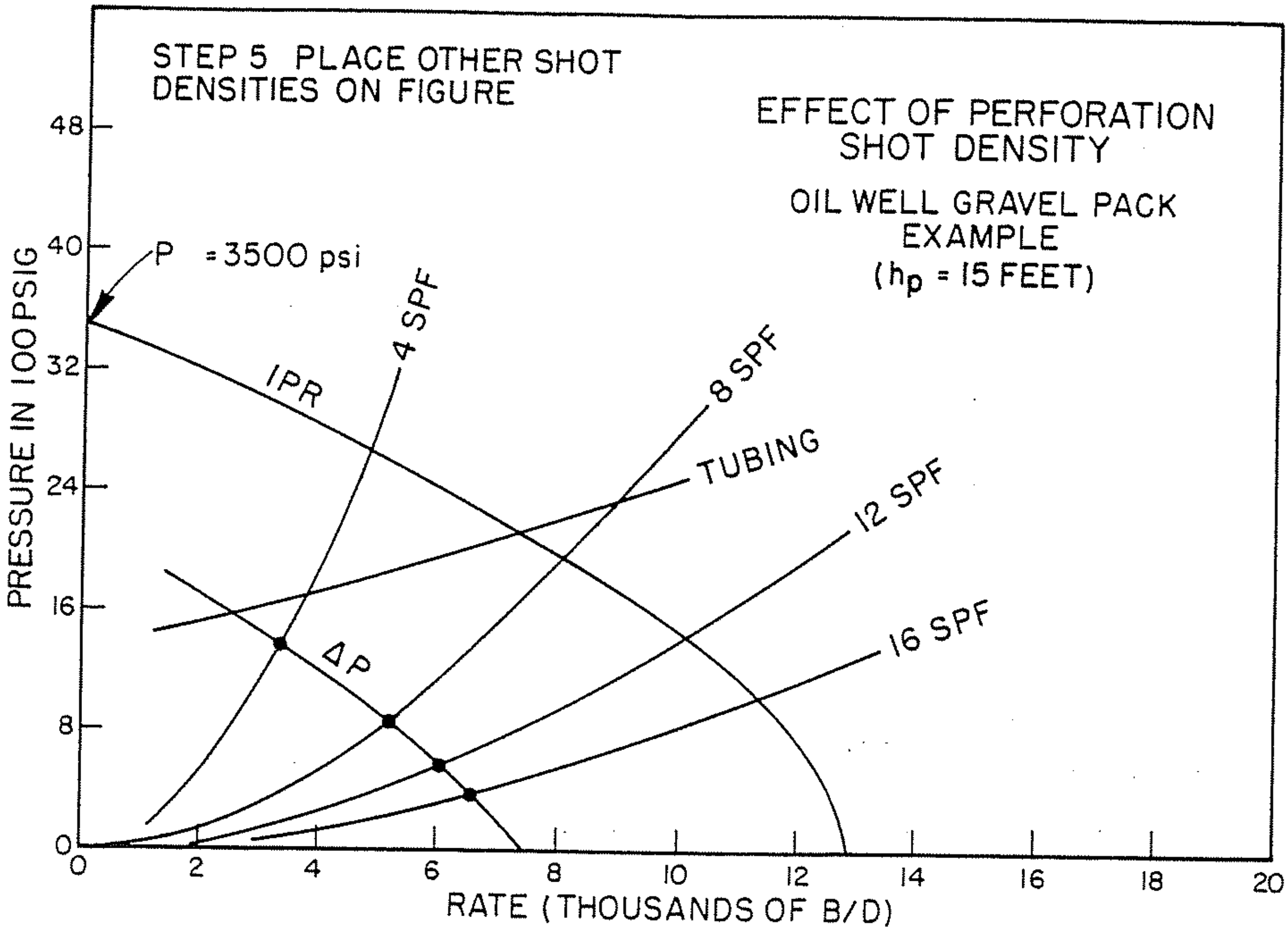

Figure 4.97 Effect of Perforation Shot Density; Oil Well Gravel-Pack Example (h_p = 15 ft)

and system pressure-drop curves (Figure 4.97). The intersection of the system pressure-drop curve and the gravel-pack pressure-drop curves shows two very valuable pieces of information: the rate at which our complete system will produce and the drop across the gravel pack. As with the gas well, we should try to keep the drop across the pack somewhere between 200–500 psi, depending upon field experience. In our example, the chosen shot density of 4 spf and perforated interval of 15 ft do not result in a satisfactory drop across the gravel pack. Therefore, new shot densities with the same perforated interval are examined.

These results are shown in Figure 4.97, and if we are interested in a high rate, we need 16 spf for 6,500 b/d, giving a ΔP of 380 psi. Additional intervals greater than 15 ft may also be opened if permissible.

4.54 BRINGING A GRAVEL-PACKED WELL ON PRODUCTION

In bringing a gravel-packed well on production, certain precautions should be taken. If not, all the gravel may be produced out at the surface. The idea is to bring the well on slowly and keep the differential low across the pack during this time.

It is necessary to make a nodal plot such as Figure 4.98 before opening the well up. Some companies may take as long as a month to bring the well up to the objective flow rate. Let us assume that the objective flow rate for the well of Figure 4.98 is 40 MMscfd, and the operator prefers not to exceed a 250-psi differential across the gravel pack.

Mark the intersection of 40 MMscfd and 250 psi on Figure 4.98. Note that the wellhead pressure should be 2,500 psi and that this requires a perforation shot density of 8 spf. The well is then completed and perforated in this manner. Depending upon company philosophy and field experience, a safety factor in perforating can be utilized in the completion; that is, to assure 8 spf, a recommended 12 spf would not be unreasonable.

The final flow rate of 40 MMscfd should occur with 2,500-psi wellhead pressure. Therefore, the rate and wellhead pressure should both be monitored very closely in bringing the well on production. The accuracy of the measuring meter and the pressure gauges (preferably a pen recorder) should be verified before start-up.

Stepwise procedure:

(1) Open the well on a low rate such as 5 MMscfd or less and monitor the wellhead pressure. For 5 MMscfd, the wellhead pressure should not be less than 4,000 psi. Therefore, an attempt should

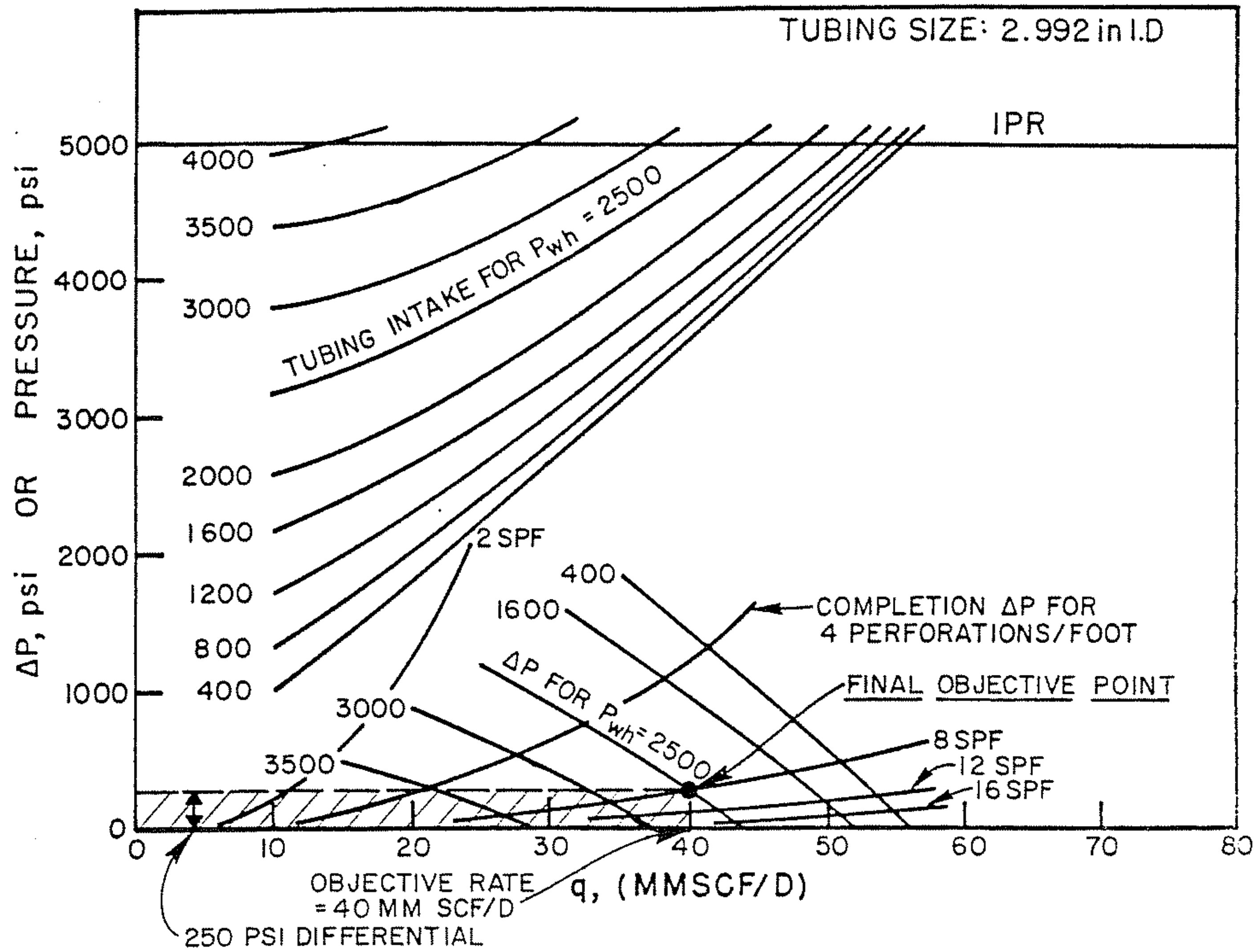

Figure 4.98 Final Nodal Plot Showing ΔP Pack = 250 psi

be made to obtain 5 MMscfd, but the wellhead pressure should not be allowed to drop below 4,000 psi. Keeping the wellhead pressure at 4,000 psi or above assures a low ΔP across the pack regardless of the rate.

Two possibilities can occur at this time:

(a) The rate of 5 MMscfd is obtained with a high wellhead pressure greater than 4,000 psi. This would be a good indicator that everything is okay and that ΔP across the pack is low.

(b) The wellhead pressure is maintained at 4,000 psi, but the rate is only 2 MMscfd. This indicates a problem, but no conclusions should be made until further testing.

Continued procedure option for good completion (Figure. 4.99):

(2) Allow a reasonable production time of 8 to 24 hours; then open the well up to 10 MMscfd, but again monitor the wellhead pressure very closely. Do not allow the wellhead pressure to drop below 3,750 psi. This again assures a ΔP of 200 psi or less across the pack. Assume that all is well and that the rate of 10 MMscfd is being obtained with a wellhead pressure of 4,000 psi.

(3) After a reasonable production time, open the well up in increments of 5 MMscfd and continually monitor the wellhead pressure. For example, at 20 MMscfd, the wellhead pressure should not be less than 3,500 psi.

(4) Continue this process of opening up by increments of rate until reaching the objective of 40 MMscfd. Note Figure 4.99 for a line of points labeled good operation.

Procedure option for a problem well (refer to Figure 4.100):

Assume that an attempt was made to reach 5 MMscfd but that a wellhead pressure of 4,000 psi allowed only 2 MMscfd.

(2) Allow the well to produce perhaps several days to observe what happens to either the rate or the wellhead pressure. Perhaps some cleaning or settling down of the well is possible. If all is okay after a few days—that is, the rate has increased to 5 MMscfd—proceed in the previous manner described. If the well continues to produce at a low rate, an attempt should be made to obtain additional points to more clearly define the problem.

(3) Open the well up to 5 or 6 MMscfd and observe

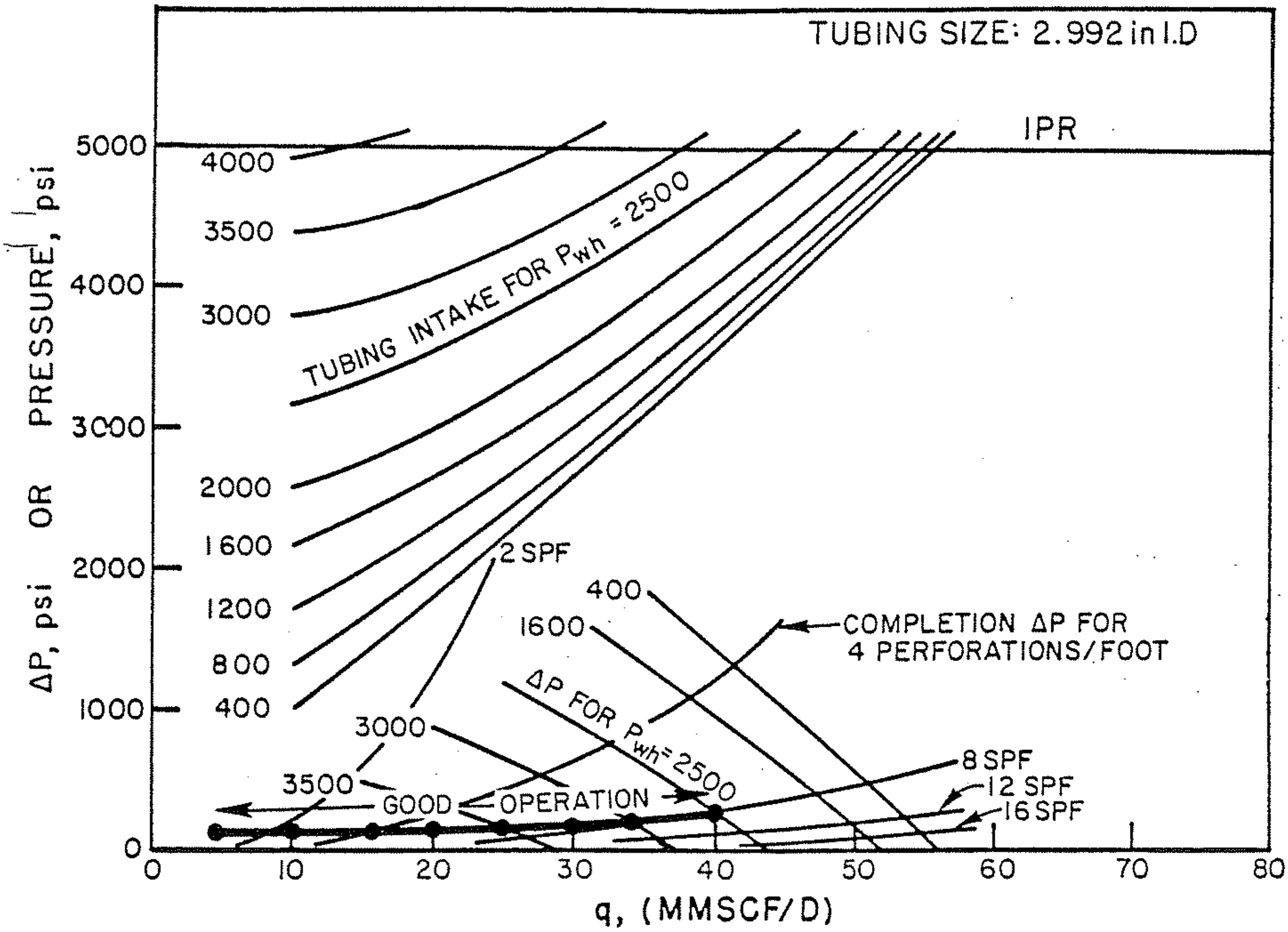

Figure 4.99 Path of Good Completion

the wellhead pressure. Mark this point on the graph. Assume that $P_{wh} = 3{,}500$ psi for 5 MMscfd. This indicates a relatively high ΔP of 600 psi across the pack (Figure 4.100).

(4) Another higher rate of as much as 10 MMscfd may be attempted, depending upon field experience and good judgment. However, a ΔP of 1,000 psi or greater across the pack begins to reach a point of pack failure.

(5) Observe all the points on Figure 4.100 for the bad well.

(6) Before destruction of the pack, some alternatives can be taken. An acidizing job may be reasonable at this time. Several field cases have shown significant improvement after acidizing. Patience becomes important. Be sure to give the well ample time and opportunity to clean up and settle down. A month's time would be reasonable in bringing the well up to the objective rate. See Figure 4.100 for a problem case. Another problem case is noted in Figure 4.101, but not as serious as shown in Figure 4.100.

Special cases:

If a straight line is being drawn such as noted in Figure 4.102, but a higher than desired ΔP is indicated, it could be an error in the measured $\bar{P}_r$. One field case actually verified this.

As a final word of caution, a high-rate well of this type should not be brought on production without a good systems analysis and design plot to monitor the production path.

A good paper for study on this subject was presented by Crouch and Pack.[14] Other good information on gravel packing can be found in references 15 through 19.

CLASS PROBLEM #1

Given data: (oil well)

k = 35 md	T = 160°F
gas gravity = 0.65	h = 60 ft
depth = 5,400 ft	GOR = 400 scf/bbl
P_r = 2,700 psi	36° API
hole size = 9⅞-in. bit	120-acre spacing
casing = 7 in.	
tubing = 2⅜ in.	
flow line: 1,500 ft of 2-in.	
separator pressure = 200 psi	

Calculate:

(1) Use 40–60 gravel and evaluate the completion; screen size = 4½-in. OD.

Note: The well presently has 20 ft of perforations with 4 spf and 0.31-in. diameter holes.

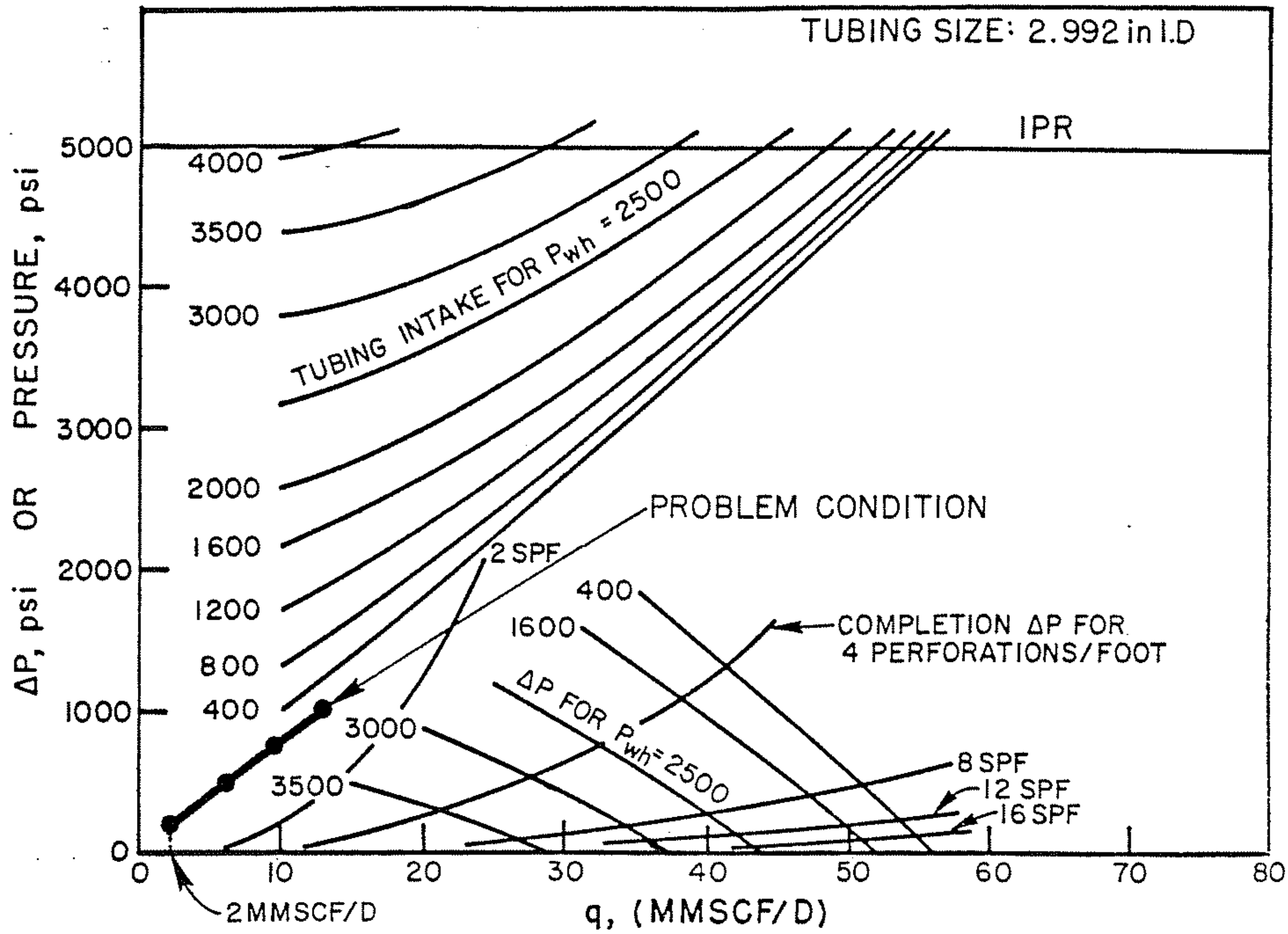

Figure 4.100 Path of Problem Completion

(2) Recommend other shot densities.
(3) Recommend other tubing or flow-line sizes.

CLASS PROBLEM #2

Given data: (oil well)

well depth = 10,000 ft
h = 60 ft
P_r = 4,000 psi
r_e = 2,000 ft
oil gravity = 35° API
GOR = 500 scf/bbl
k = 200 md
gas gravity = 0.6
T = 200°F
tubing = 2⅞ in.
casing = 7⅝ in.
hole size = 10¾ in.
separator pressure = 120 psi
4,000 ft of 2½-in. flow line
Well currently completed in 20 ft of perforated interval with 4 spf of 0.41-in. diameter hole
Use 40–60 gravel and 4½-in. OD screen

Calculate:

(1) Recommend a good completion.
(2) Recommend other tubing or flow-line sizes.

CLASS PROBLEM #3

Given data: (oil well)

well depth = 10,000 ft
h = 120 ft
k = 500 md
P_r = 5,000 psi
h_p = 60 ft
GOR = 600 scf/bbl
oil gravity = 38° API
gas gravity = 0.70
T = 240°F
casing = 7 in.
sep. pressure = 100 psi
20–40 gravel (100 darcies)
r_e = 1,500 ft
r_w = 0.51 ft
flow line = 4,000 ft

Note: Water will increase to 50% in 2 years, with P_r dropping to 4,000 psia. Make recommendations with possibility of gas lift in mind (use retrievable valves).

Calculate:

Recommend both flow-line and tubing sizes as well as shot density and casing-gun size.

CLASS PROBLEM #4

Given data: (gas well)

h = 35 ft
h_p = 15 ft
(short flow line—offshore)
P_r = 2,430 psi
bit = 9⅞ in.
8 spf
depth = 4,800 ft
320-acre spacing
screen = 2⅞ in.
γ_g = 0.65
T = 136°F
k = 1,000 md
tubing = 2⅞ in. – csg.
sales-line pressure = 900 psi
5-in. gun used for perforating (0.7-in. diameter hole)
use 20–40 mesh gravel (k = 100,000 md)

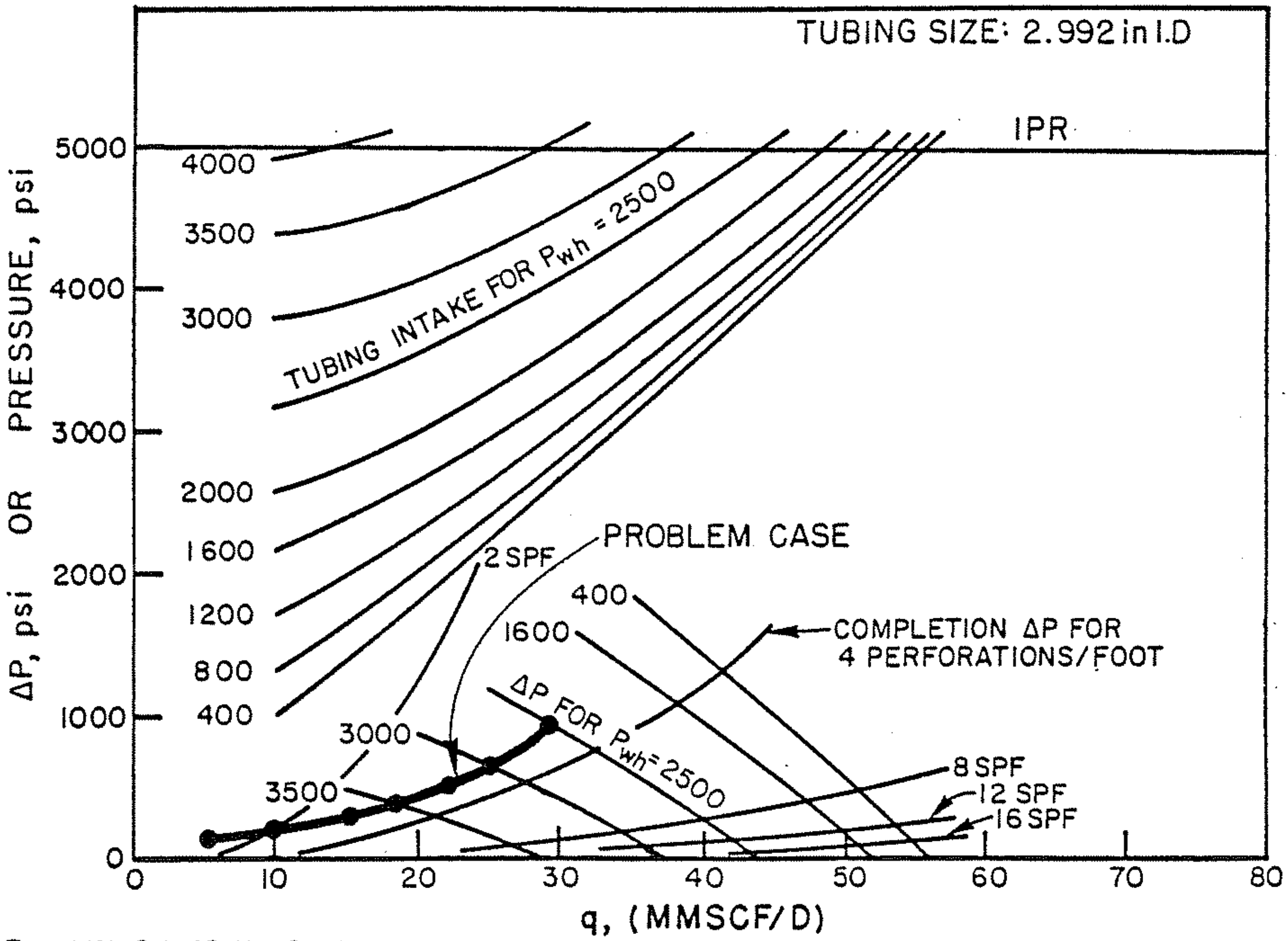

Figure 4.101 Path of Problem Completion

Calculate:

(1) Determine flow rate and ΔP gravel pack.
(2) Recommend a good shot density.
(3) Recommend a good shot density for 3.958-in. tubing.

CLASS PROBLEM #5

Given data: (gas well)

depth = 8,000 ft	$\gamma_g = 0.65$
P_r = 5,400 psi	T = 210°F
2⅞-in. OD tubing	9⅝-in. casing
k = 500 md	640-acre spacing
h = 40 ft	h_p = 12 ft
hole size = 12¼ in.	4-in. screen and liner
40–60 gravel	

sales-line pressure = 500 psi presently perforated with 4 spf (¾-in. hole)

Use a wellhead pressure sufficient to place gas in the sales line.

Calculate:

(1) Find flow rate and ΔP gravel pack.
(2) Check 8, 12, and 16 spf.
(3) Check 20 ft, 30 ft, and 40 ft perforated for 8 spf.

4.6 NODAL ANALYSIS APPLIED TO A STANDARD PERFORATED WELL, BY CARL GRANGER AND KERMIT BROWN

4.61 INTRODUCTION

A publication by Dr. Harry McLeod has given a practical approach to the evaluation of a standard perforated well.[20] It has been shown that a compacted, damaged zone occurs around a perforated tunnel in normal perforation conditions. It should be emphasized that this problem differs from gravel-packed wells in that, for gravel-packed wells, we are dealing with an unconsolidated formation and, hence, are interested in area open to flow. For the tight-rock formations, we are not only interested in area open to flow, but also in the length of perforated tunnel. Both have an effect on the flow rate into the wellbore. Figure 4.103 shows a typical perforated tunnel and the nomenclature used in this analysis.

In order to analyze the effects of this perforation and its flow capacity, several sound assumptions have been made based on the work of numerous authors.

Refer to Figure 4.104, which shows that, by turning the perforation 90°, it can be treated as a miniature wellbore. Furthermore, it has been assumed in this analysis that there is no damaged zone around the wellbore. Several other assumptions are made here such as:

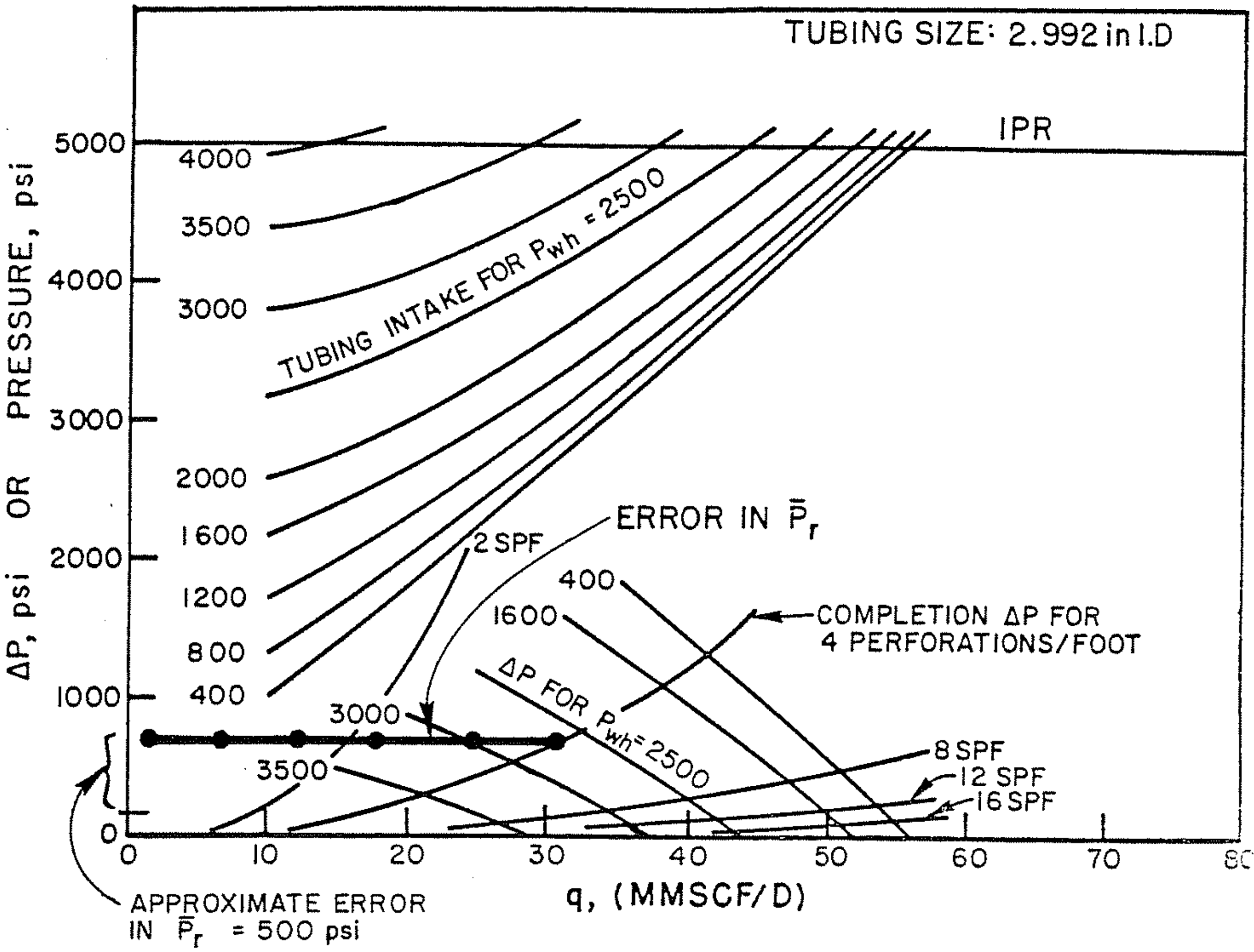

Figure 4.102 Error in $\bar{P}_r$

(1) The permeability of the crushed or compacted zone is:
   (a) 10% of formation permeability if perforated overbalanced.
   (b) 40% of formation permeability if perforated underbalanced. McLeod gave a range of values.

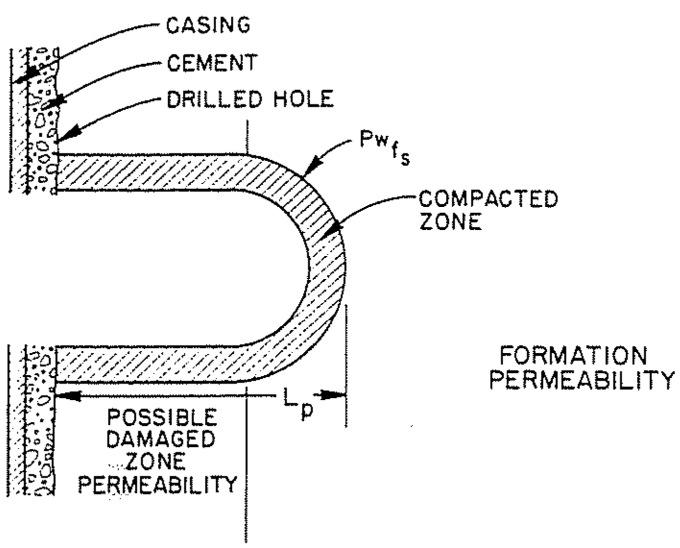

Figure 4.103 Typical Perforated Hole

(2) The thickness of the crushed zone is ½ in.
(3) The small wellbore can be treated as an infinite reservoir; that is, p_{wf_s} remains constant at the edge of the compacted zone, thus eliminating the $-\frac{3}{4}$ of Darcy's Law for a closed outer boundary.
(4) The equation presented by Jones, Blount, and Glaze can be used to evaluate the pressure loss across these perforations.[11]

The Jones, Blount, and Glaze equations have been modified as follows:

4.62 OPEN PERFORATION PRESSURE DROP

(Oil Wells):

$$P_{wf_s} - P_{wf} = aq^2 + bq = \Delta P \tag{4.28}$$

$$\Delta P = \left(\frac{2.30 \times 10^{-14}\beta\, B_o^2 \rho_o \left(\frac{1}{r_p} - \frac{1}{r_c}\right)}{L_p^2}\right) q^2 + \left(\frac{\mu_o B_o (\ln r_c/r_p)}{7.08 \times 10^{-3} L_p\, k_p}\right) q \tag{4.29}$$

where:

$$a = \frac{2.30 \times 10^{-14}\beta\, B_o^2\, \rho_o \left(\frac{1}{r_p} - \frac{1}{r_c}\right)}{L_p^2} \tag{4.30}$$

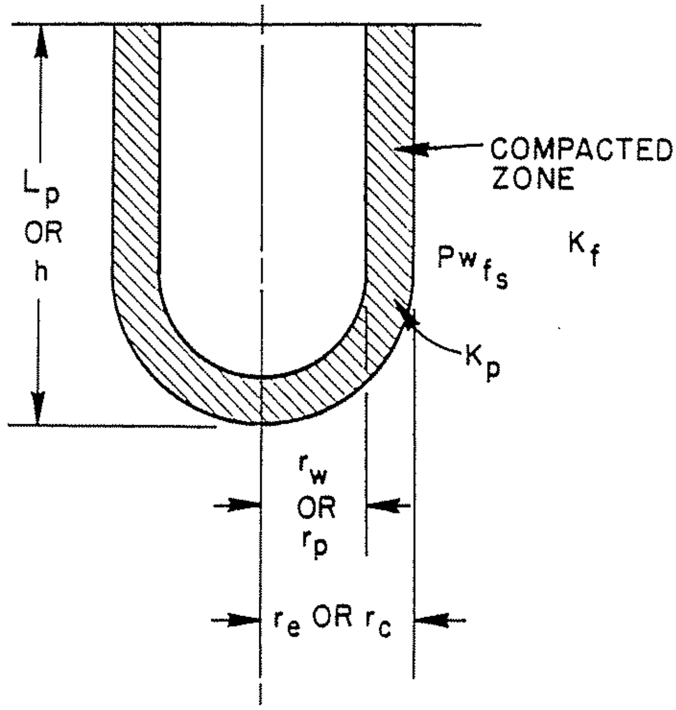

Figure 4.104 Perforated Hole Turned 90°

$$b = \frac{\mu_o B_o (\ln r_c/r_p)}{7.08 \times 10^{-3} L_p k_p} \quad (4.31)$$

q_o = flow rate/perforation (q/perforation), b/d

β = turbulence factor, ft^{-1}

$$\beta = \frac{2.33 \times 10^{10}}{k_p^{1.201}}$$

B_o = formation volume factor, rub/stb

ρ_o = oil density, lb/ft^3

L_p = perforation tunnel length, ft

μ_o = oil viscosity, cp

k_p = permeability of compacted zone, md
 = 0.1k formation if shot overbalanced
 0.4k formation if shot underbalanced

r_p = radius of perforation tunnel, ft

r_c = radius of compact zone, ft $\left(r_c = r_p + \frac{.5}{12}, \text{ft}\right)$

(Gas Wells):

$$P_{wf_s}^2 - P_{wf}^2 = aq^2 + bq \quad (4.32)$$

$$P_{wf_s}^2 - P_{wf}^2 = \left(\frac{3.16 \times 10^{-12} \beta\, \gamma_g TZ\left(\frac{1}{r_p} - \frac{1}{r_c}\right)}{L_p^2}\right) q^2 + \left(\frac{1.424 \times 10^3 \mu_g TZ (\ln r_c/r_p)}{k_p L_p}\right) q \quad (4.33)$$

where:

$$a = \frac{3.16 \times 10^{-12} \beta\, \gamma TZ\left(\frac{1}{r_p} - \frac{1}{r_c}\right)}{L_p^2} \quad (4.34)$$

$$b = \frac{1.424 \times 10^3 \mu_g TZ (\ln r_c/r_p)}{k_p L_p} \quad (4.35)$$

q = flow rate/perforation (q/perforation), Mcfd

β = turbulence factor, ft^{-1}

$$\beta = \frac{2.33 \times 10^{10}}{k_p^{1.201}}$$

γ_g = gas specific gravity (dimensionless)

T = temperature, °R (°F + 460)

Z = supercompressibility factor (dimensionless)

r_c = radius of compact zone, ft
 ($r_c = r_p + 0.5/12$, ft)

r_p = radius of perforation, ft

L_p = perforation tunnel length, ft (see Table 4.44)

μ_g = gas viscosity, cp

k_p = permeability of compacted zone, md
 = 0.1k formation if shot overbalanced
 0.4k formation if shot underbalanced

Table 4.44 has been prepared showing perforation data.

TABLE 4.44
PERFORATING GUN DATA

Gun size	Casing	Perforation diameter, in., avg.	Penetration,* in. avg.	Penetration,* in. longest
Retrievable through tubing				
1⅜ in.	4½ csg	0.21	3.03	3.30
1 9/16 in.	5½ csg	0.24	4.7	5.48
1 11/16 in.	4½–5½ csg	0.24	4.8	5.50
2 in.	4½–5½ csg	0.32	6.5	8.15
2⅛ in.	2⅞ tbg–4½ csg	0.33	7.2	8.15
2⅝ in.	4½ csg	0.36	10.36	10.36
Expendable through tubing				
1⅛ in.	4½ csg	0.19	3.15	3.15
1¼ in.	2⅜ tbg	0.30	3.91	3.91
1⅜ in.		0.30	5.1	5.35
1 11/16 in.	2⅞ tbg–5½ csg	0.34	6	8.19
2 1/16 in.	5½–7 csg	0.42	8.2	8.6
2⅛ in.	2⅞ tbg–5½ csg	0.39	7.7	8.6
Retrievable casing guns				
2¾ in.	4½ csg	0.38	10.55	10.5
2⅞ in.	4½ csg	0.37	10.63	10.6
3⅛ in.	4½ csg	0.42	8.6	11.1
3⅜ in.	4½ csg	0.36	9.1	10.8
3⅝ in.	4½ & 5½ csg	0.39	8.9	12.8
4 in.	5½–9⅝ csg	0.51	10.6	13.5
5 in.	6¾–9⅝ csg	0.73	12.33	13.6

* Penetration length measured from ID of casing

Two example problems will be worked—one for a gas well and one for an oil well.

GAS WELL EXAMPLE

Given data:

k = 5 md	2⅜-in. tubing
P_r = 4,000 psi	p_{wh} = 1,500 psi
r_e = 1,500 ft	4-in. casing gun
r_w = 0.411 ft	depth = 10,000 ft
h = 20 ft	hole size = 9⅞-in.
h_p = 10 ft	γ_g = 0.6
7⅝-in. casing	T = 220°F

shot = 2 spf—overbalanced
given perforation tunnel length = 10.6 in. (length

from drilled hole to end of perforation)
Diameter of perforated hole = 0.51 in.

Calculate:

Assume P average $= \frac{4{,}000 + 1{,}000}{2} = 2{,}500$ psi (Use closes increments for a computer solution to evaluate $Z = 0.921$)
$\mu_g = 0.018$ cp

Stepwise procedure:

(1) Construct the IPR curve. Use the Jones, Blount, and Glaze equation (see Figure. 4.105).

$$\beta = 3.37 \times 10^9$$
$$a = 0.097$$
$$b = 1{,}196$$
$$\text{AOFP} = 8.071 \text{ MMscfd}$$

(2) Plot the tubing intake curve on Figure 4.105. These results are shown on Figure 4.106. It is noted that q = 5.5 MMscfd for a $\Delta P = 0$ across the completion.
(3) Transfer the ΔP as noted in Figure 4.107.
(4) Determine the ΔP across the perforations using the appropriate equation. Several things are due an explanation here.
(5) Refer to Figure 4.108 and note that L_p is 10.6 in., or 0.883 ft. The perforation tunnel length (L_p) as listed in Table 4.44 represents the length from the casing ID to the end of the tunnel. L_p as used in the equation is the length from the drilled hole or calipered hole to the end of the perforation. For this example, the perforation length was given from the service company as being 12.1 in. The calculated L_p is:

$$L_p = 12.1 - \frac{\text{hole size} - \text{casing ID}}{2}$$
$$= 12.1 - \frac{9.875 - 6.875}{2} = 10.6 \text{ in.}$$

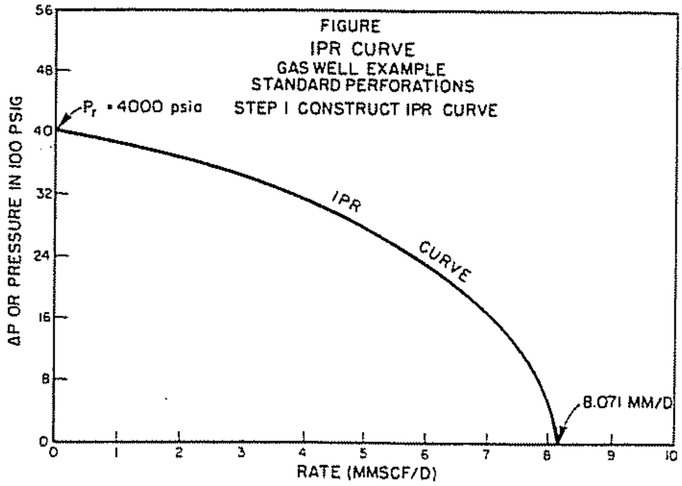

Figure 4.105 IPR Curve; Gas Well Example, Standard Perforations; Step 1, Construct IPR Curve

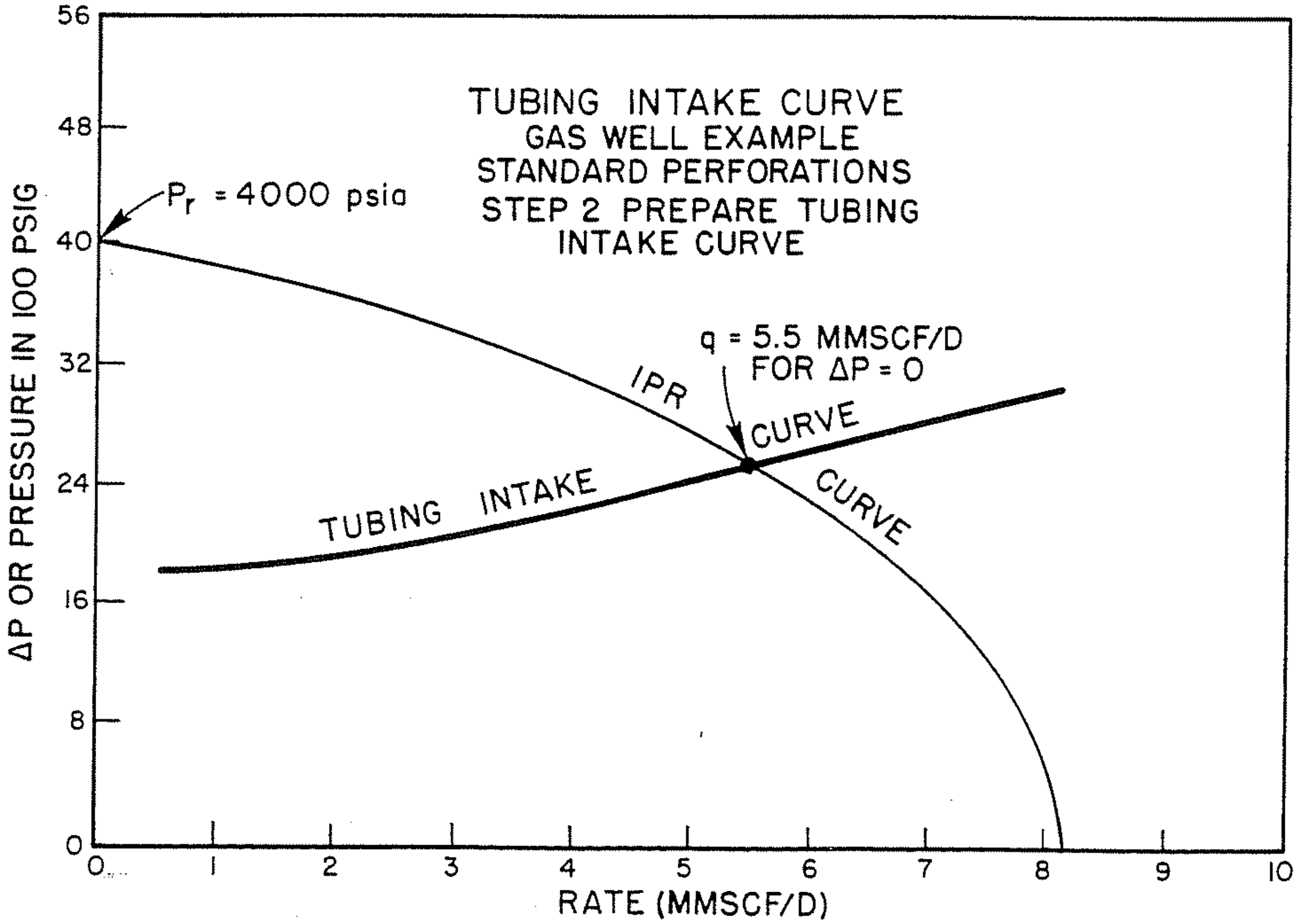

Figure 4.106 Tubing Intake Curve; Gas Well Example, Standard Perforations; Step 2, Prepare Tubing Intake Curve

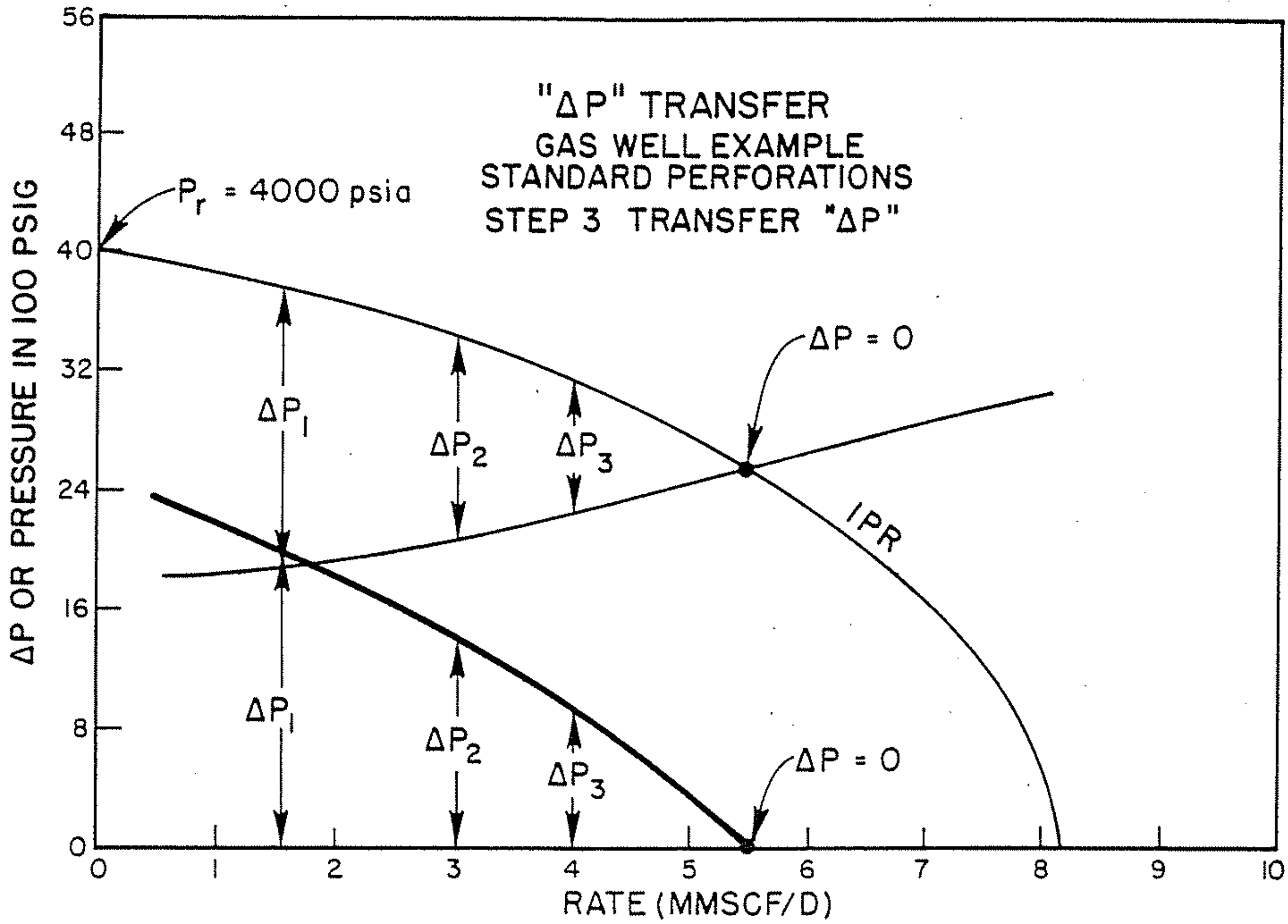

Figure 4.107 ΔP Transfer; Gas Well Example, Standard Perforations; Step 3, Transfer ΔP

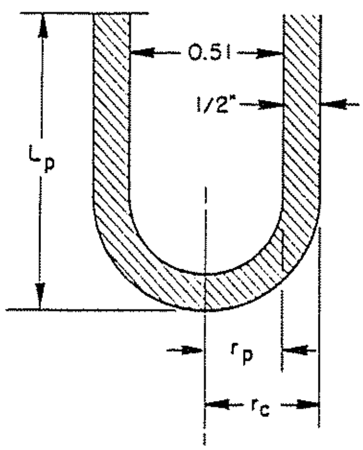

$$r_p = \frac{(0.51)}{2\,(12)} = 0.021 \text{ feet}$$

$$r_c = r_p + 1/2 \text{ inch}$$

$$= 0.021 + \frac{0.5}{12}$$

$$= 0.063 \text{ feet}$$

$$L_p = \frac{10.6}{12} = 0.883 \text{ feet}$$

Figure 4.108 Details of Perforated Hole

(6) $r_p = 0.021$ ft, and $r_c = 0.063$ ft.
(7) β is the β for the crushed zone, which has a permeability of $0.1(5) = 0.5$ md:

$$\beta = 5.36 \times 10^{10}$$

Using Equation 4.33, we find:

$a = 2{,}541$
$b = 39{,}471$

It is better to set up Table 4.45 as follows. We have used a total flow rate to determine P_{wf_s} but will divide this rate equally among the total perforated interval to obtain the flow rate through each perforation since the equation to find P_{wf} is based on one perforation. The equation must be solved for P_{wf}:

$$P_{wf} = \sqrt{P_{wf_s}^{\,2} - (bq + aq^2)}$$

The q used in the above equation is the q per perforation and is Mcfd/perforation. However, P_{wf_s} has been determined from the Jones, Blount, and Glaze radial flow equation,[11] and q for this equation is the total flow rate in Mcfd.

TABLE 4.45
2 spf OVERBALANCED (20 holes)

Total q, Mcfd	P_{wf_s}	q/perforation	ΔP
200	3,969	10	83
400	3,938	20	236
600	3,905	30	473
800	3,870	40	850
1,000	3,835	50	1,309
1,100	3,817	55	1,646
1,200	3,798	60	2,093

This information is then plotted on Figure 4.109 along with 4 spf for an underbalanced condition.

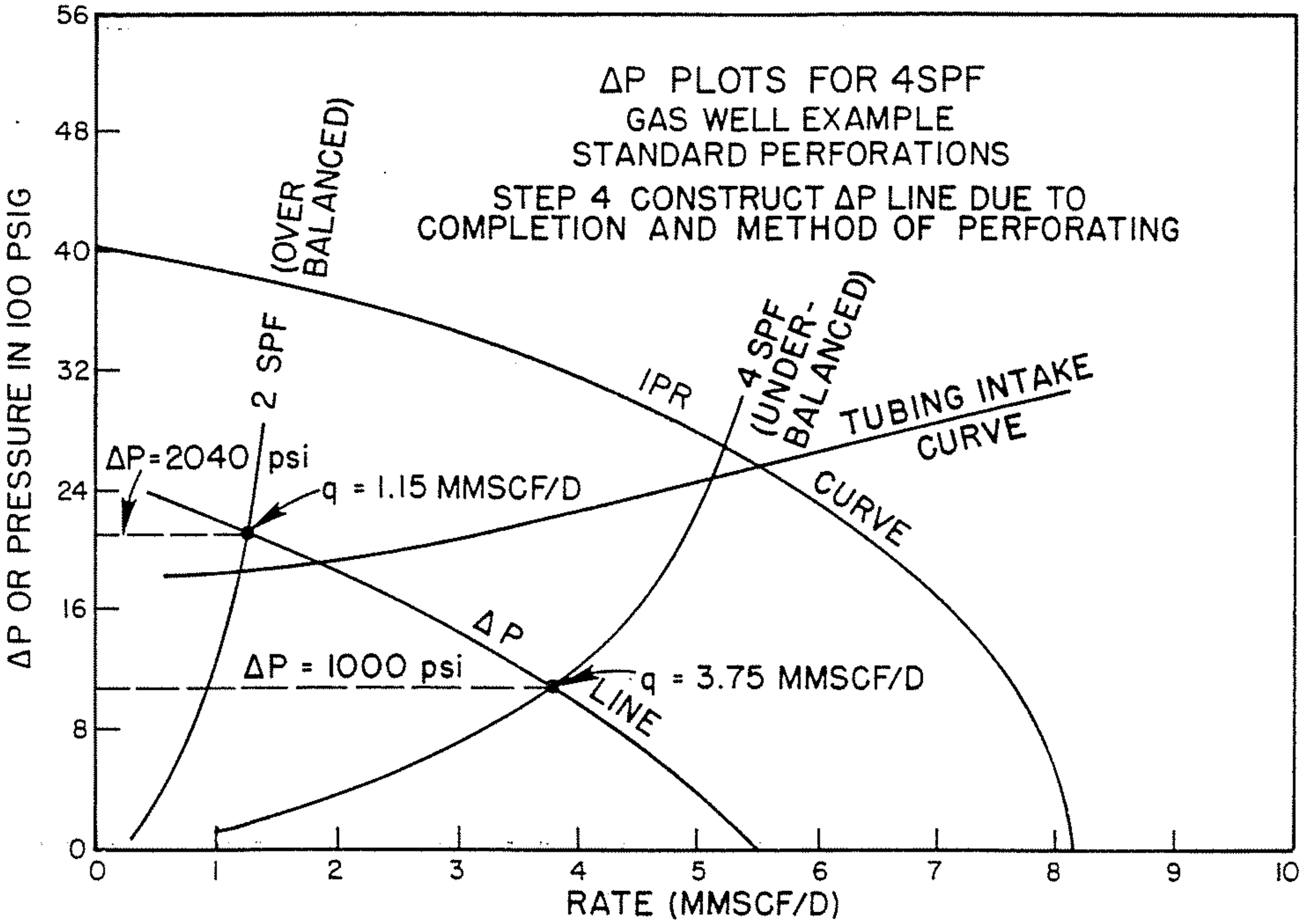

Figure 4.109 ΔP Plots for 4 spf; Gas Well Example, Standard Perforations; Step 4, Construct ΔP Line Caused by Completion and Method of Perforating

Refer to Figure 4.110 for other conditions, which shows that 8 spf underbalanced gives a much higher flow rate. Table 4.46 shows the rates possible for several conditions.

Obviously, we are much better off perforating underbalanced, and this emphasizes the results of eliminating the damaged or crushed zone by acidizing or by other means.

OIL WELL EXAMPLE

When an oil well example is worked out, the procedure is the same as for a gas well.

Given data:

$k = 5$ md	35° API
$P_r = 3{,}500$ psi	$\gamma_g = 0.65$
$r_e = 1{,}500$ ft	$T = 190°F$
$h = 25$ ft	GOR = 600 scf/bbl
2 spf	$P_{wh} = 200$ psi
$h_p = 15$ ft	depth = 6,000 ft
hole size = 8.750 in.	$P_b = 2{,}830$ psi
5½-in. casing	$B_o = 1.33$
2⅞-in. OD tubing	$\mu_o = 0.54$ cp
	$r_w = 0.36$ ft

Shoot overbalanced with a 4-in. casing gun (hole size = 0.51 in.).

IPR

$J = 0.162$ b/d psi above P_b
$q_b = 109$ b/d
$q_{max} = 364$ b/d

The following additional information is available:

$k_c = 0.1(5) = 0.5$ md
tunnel length = 10.6 in. = 0.883 ft (net formation tunnel length)
$r_p = 0.021$ ft $a = 3.82$
$r_c = 0.063$ ft $b = 249.43$
$\beta = 5.36 \times 10^{10}$

Calculate:

The appropriate equations are used for oil flow, and ΔP can be solved for directly:

$$\beta = \frac{2.33 \times 10^{10}}{k_p^{1.201}}$$

$$\Delta P = a\,q^2 + bq = P_{wf_s} - P_{wf} \tag{4.28}$$

$$a = \frac{2.30 \times 10^{-14}\,\beta\,B_o^2\rho_o\left(\dfrac{1}{r_p} - \dfrac{1}{r_c}\right)}{L_p^2} \tag{4.30}$$

$$b = \frac{\mu_o\,B_o\,\ln\,(r_c/r_p)}{7.08 \times 10^{-3}\,k_p\,L_p} \tag{4.31}$$

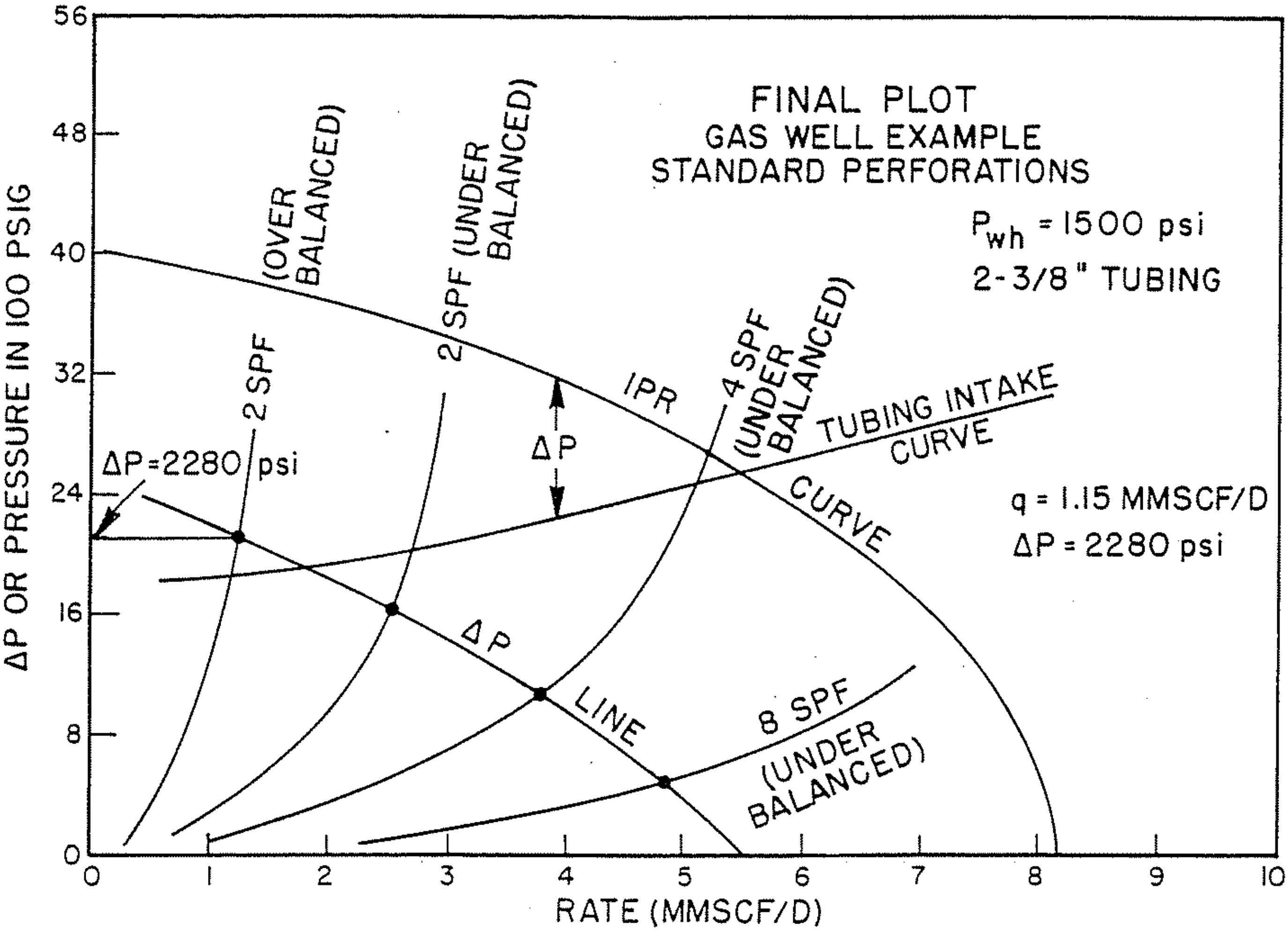

Figure 4.110 Final Plot; Gas Well Example, Standard Perforations

TABLE 4.46

spf	Condition	Rate	ΔP, psi
2	Overbalanced	1.2	2,280
2	Underbalanced	2.5	1,600
4	Underbalanced	3.75	1,200
8	Underbalanced	4.8	420

The sequence to the solution of this problem is shown in Figures 4.111, 4.112, 4.113, 4.114, and 4.115.

Figure 4.115 shows the final plot from which perforation decisions can be made. Table 4.47 shows these results.

This well should be perforated underbalanced because 2 spf underbalanced produces the same rate as 8 spf overbalanced. Finally, 8 spf underbalanced produces 320 b/d, which is near the maximum of 364 b/d. This also points out the fact that perforations should be cleaned up in some appropriate manner.

TABLE 4.47

spf	Perforation condition	q, b/d	ΔP, psi
2	Overbalanced	175	1,600
2	Underbalanced	285	600
4	Overbalanced	240	1,040
8	Overbalanced	285	600
8	Underbalanced	320	180

CLASS PROBLEM #1 (GAS WELL)

Given data:

k = 10 md	2⅞-in. tubing
P_r = 4,600 psia	(2.441-in. ID)
320-acre spacing	h = 30 ft
7-in. casing	h_p = 15 ft
10¾-in. hole	wellhead pressure = 1,000 psi
γ_g = 0.7	depth = 9,000 ft
T = 180°F	

diameter perforated hole = 0.42 in.
length of perforated tunnel = 8.2 in. (net)
4 spf underbalanced

Calculate:

(1) Determine flow rate and ΔP across completion
(2) Determine rate and ΔP for 8, 12, and 16 spf

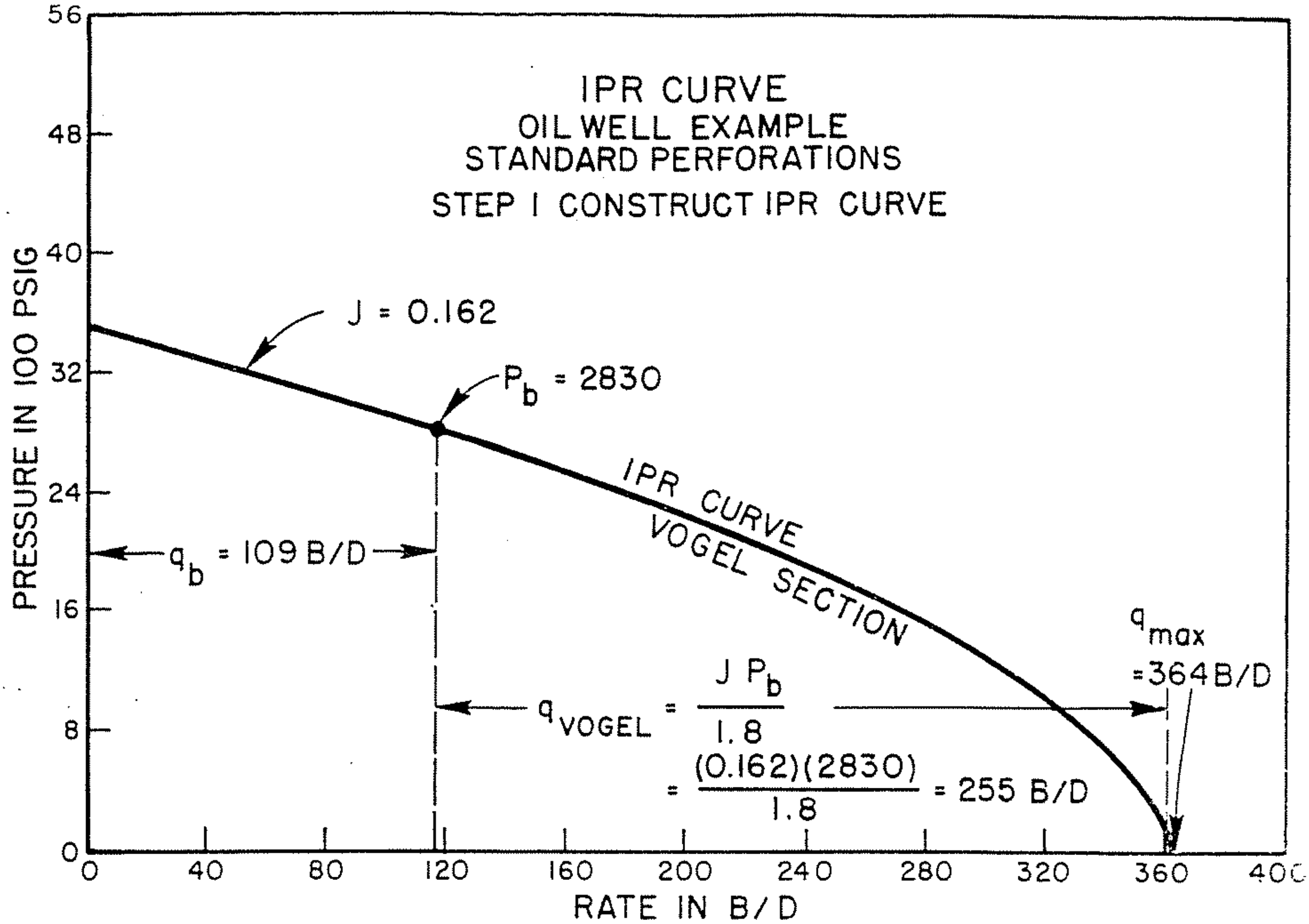

Figure 4.111 IPR Curve, Oil Well Example, Standard Perforations; Step 1, Construct IPR Curve

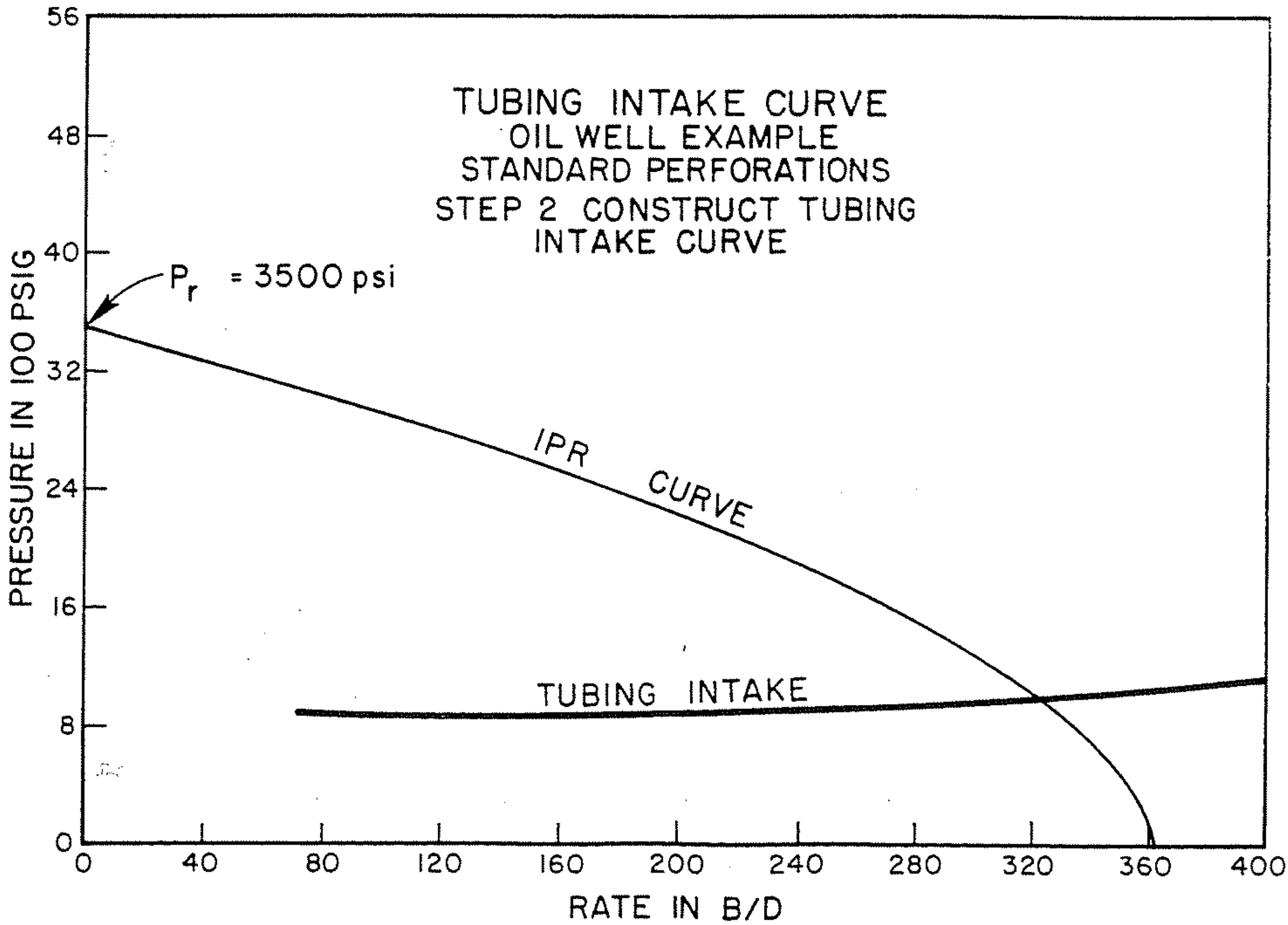

Figure 4.112 Tubing Intake Curve; Oil Well Example, Standard Perforations; Step 2, Construct Tubing Intake Curve

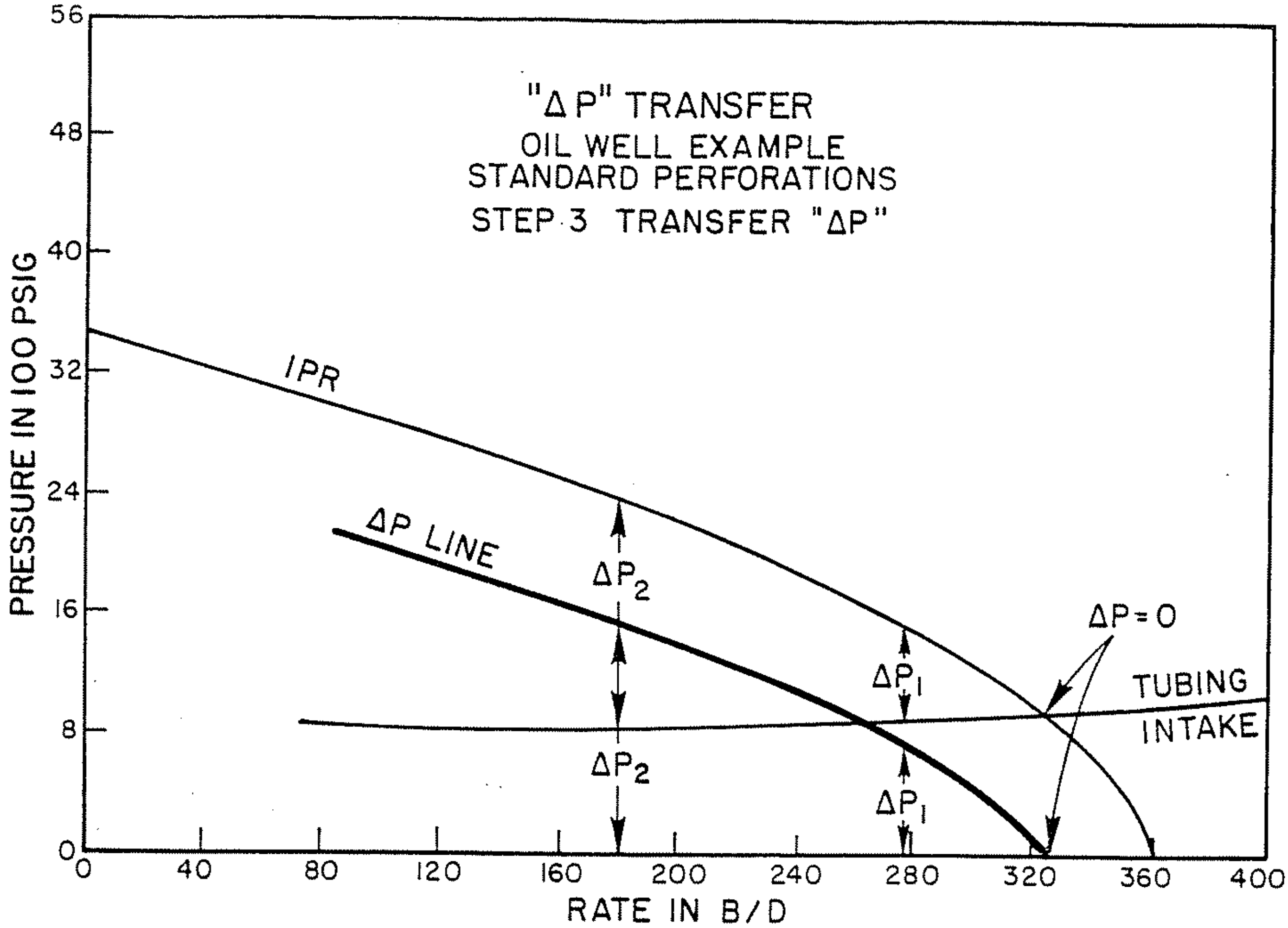

Figure 4.113 ΔP Transfer; Oil Well Example, Standard Perforations; Step 3, Transfer ΔP

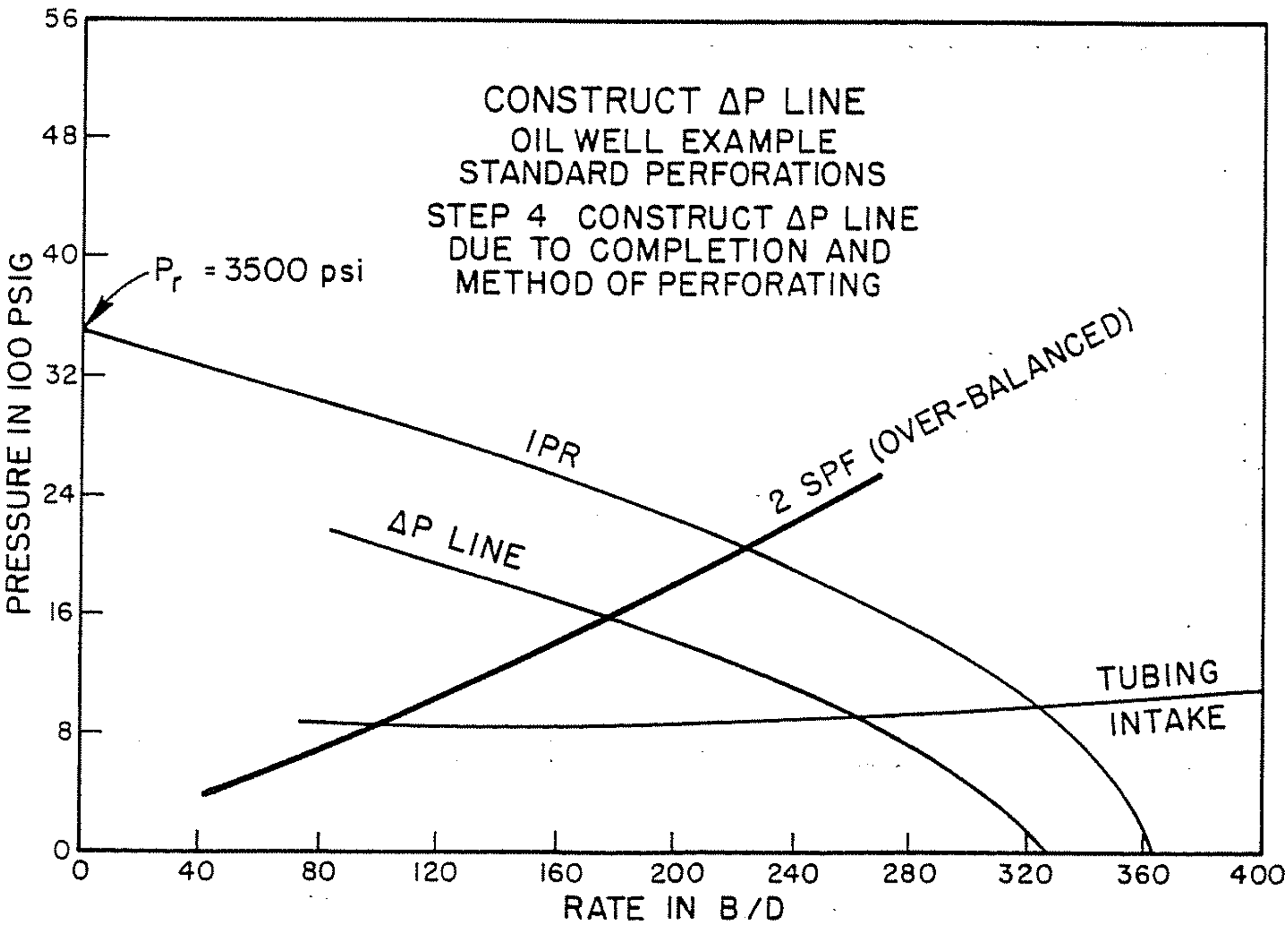

Figure 4.114 Construct ΔP Line; Oil Well Example, Standard Perforations; Step 4, Construct ΔP Line Caused by Completion and Method of Perforating

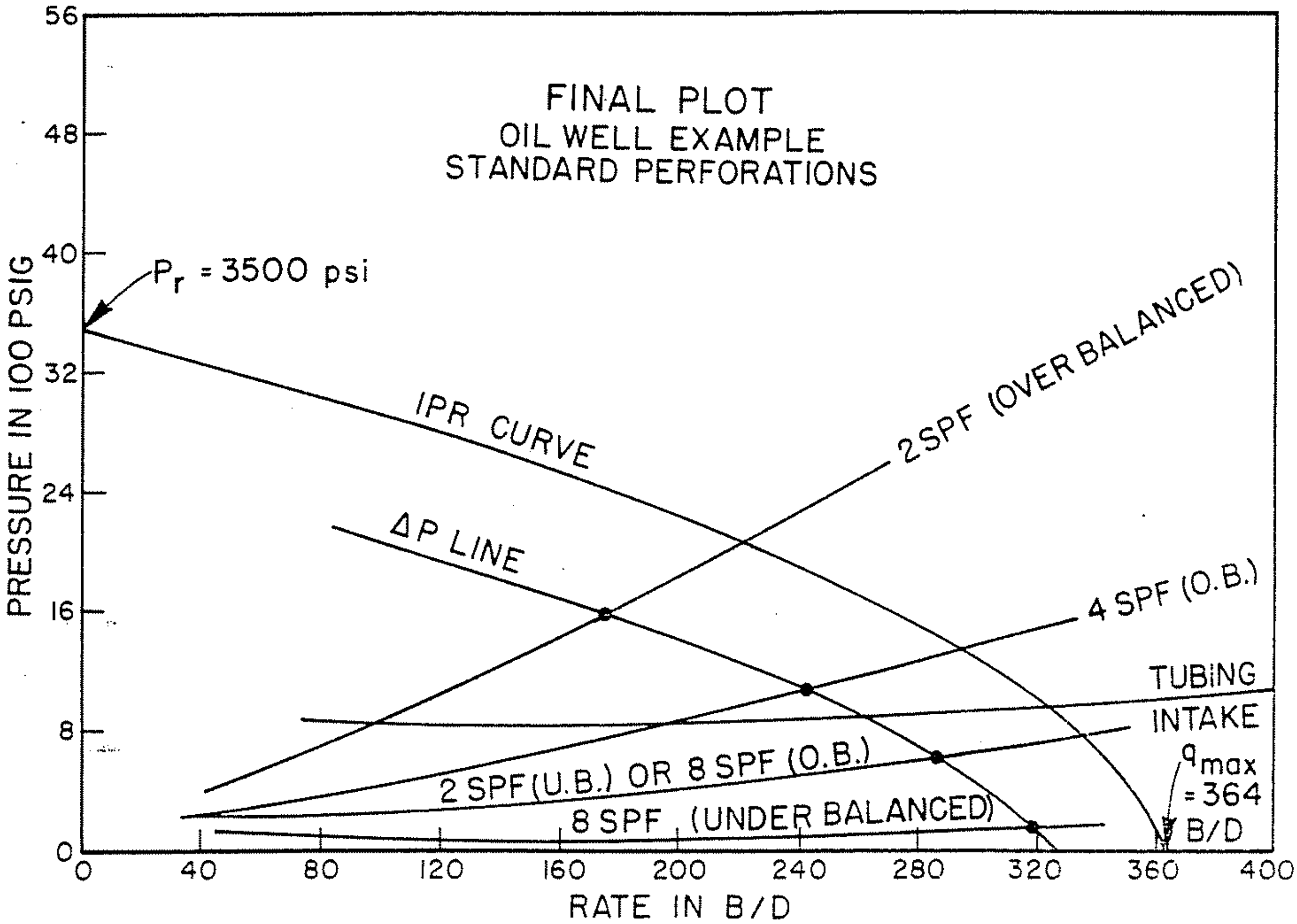

Figure 4.115 Final Plot; Oil Well Example, Standard Perforations

CLASS PROBLEM #2 (GAS WELL)

$k = 3.5$ md	2.992-in. tubing
$h = 82$ ft	7-in. casing
$h_p = 40$ ft	12¼-in. hole
640-acre spacing	$T = 200°F$
depth = 10,000 ft	$P_r = 5{,}200$ psia

$\gamma_g = 0.7$
wellhead pressure = 1,500 psi
diameter, perforation = 0.51 in.
length, tunnel = 12 in. (net)
2 spf overbalanced

Calculate:

(1) Find the present flow rate and ΔP completion
(2) Evaluate the following:

1 2 spf underbalanced
2 4 spf underbalanced
3 8 spf underbalanced
4 12 spf underbalanced
5 16 spf underbalanced
6 8 spf overbalanced
7 16 spf overbalanced
8 effect of 3.98-in. ID tubing

CLASS PROBLEM #3 (OIL WELL)

$k = 8$ md	60-acre spacing
$h = 15$ ft	5½-in. casing
$h_p = 10$ ft	1.995-in. ID tubing (2⅜-in. OD)
$P_r = 2{,}400$ psi	produces all oil
depth = 8,000 ft	$T = 178°F$
GOR = 600 scf/bbl	$\gamma_g = 0.65$
hole size = 8¾ in.	°API = 40
$P_{wh} = 160$ psi	hole = 0.38 in.

depth = 8,000 ft
shot overbalanced with 2 spf diameter perforated length, perforated tunnel = 10.55 in.

Calculate:

(1) Find the flow rate and ΔP completion.
(2) Evaluate the following:

1 4 spf overbalanced
2 8 spf overbalanced
3 16 spf overbalanced
4 4 spf underbalanced
5 8 spf underbalanced
6 16 spf underbalanced

CLASS PROBLEM #4 (OIL WELL)

$k = 30$ md	120-acre spacing
$h = 80$ ft	7-in. casing
$h_p = 50$ ft	2.441-in. ID tubing
$P_r = 4{,}000$ psia	produces all oil

depth = 9,000 ft $T = 195°F$
GOR = 400 scf/bbl   38°API
hole size = 10¾ in. $\gamma_g = 0.7$
$P_{wf} = 120$ psi
shot with 4 spf underbalanced
diameter, perforated hole = 0.24 in.
length, perforated tunnel = 4.8 in.

Calculate:

(1) Present rate and ΔP completion
(2) Evaluate:

1–8 spf underbalanced
2–16 spf underbalanced

4.7 SPECIAL PIPELINE PROBLEMS, BY DR. ZELIMIR SCHMIDT AND DR. DALE DOTY

4.71 INTRODUCTION

The design of large pipelines for transmission lines or for production lines can be quite complex. An optimum must be reached between pressure losses occurring in the line and the slugging and heading action of alternate slugs of liquid and gas. The larger lines will exhibit lower pressure losses but will have greater slugging and heading, whereas the smaller lines will reduce the slugging and heading but will create more pressure loss for the same flow rate of liquid and gas.

There are essentially three types of problems that arise in pipeline design with regard to the flow capacity of a pipeline. These are:

(1) determining the pressure drop for specified flow rates, pipe size, and the presence of restrictions such as chokes
(2) determining flow rates for a specified pipe size and maximum pressure drop
(3) determining the pipe size required for specified flow rates and pressure drop

4.72 LIQUID-RELATED PROBLEMS

Liquid handling problems caused principally by the fact that the gas often flows faster than the liquid and liquid is "held up" in the pipeline are very common in pipeline flow. This often causes the flow to develop a pattern of alternating slugs of gas and liquid and, in some cases, can overload the separation facilities at the pipeline outlet. This problem is compounded if the pipeline is not horizontal because liquid will tend to accumulate in low spots and then be discharged as long slugs.

4.73 PRESSURE-DROP PREDICTION

The general equation for calculating the pressure gradient dP/dL, which exists at a point in a pipeline, requires the evaluation of two primary unknowns. These are the fraction of the pipe occupied by liquid, which is called the liquid holdup, and the two-phase friction factor. Once the pressure gradient at a point is known, the pressure drop, ΔP, occurring over a finite length of pipe, ΔL, can be calculated from:

$$\Delta P = \Delta L\ (dP/dL)$$

The calculation procedure consists of dividing the pipe into increments short enough that average values of all the parameters used in the pressure gradient equation can be assumed constant in that increment.

Calculation of the pressure gradient in an increment requires not only values for liquid holdup and friction factor, but also values for any fluid properties that are functions of pressure and temperature.

Many correlations have been published for estimating the pressure losses when gas and liquid flow simultaneously in horizontal or inclined pipes. Most of these correlations have been found to be unreliable beyond the range of variables considered in developing the correlation. In general, all correlations exhibit weaknesses in some areas. To overcome this, several correlations have been combined into a single hybrid model. This approach, although successful in some cases, results occasionally in unrealistic estimates of pressure drop and liquid volume in the pipeline.

There are a number of studies in which empirical correlations have been evaluated. Vohra, Marcano, and Brill evaluated liquid holdup and friction factor correlations for horizontal flow.[21] The study revealed that the Eaton et al.[22] and the Beggs and Brill[23] liquid holdup correlations are the most reliable. The Dukler et al.[24] and the Beggs and Brill friction factor correlations have been found by the same study to be the most reliable. Gould and Ramsey[25] indicated that the Beggs and Brill correlation gave excellent results in large-diameter pipelines. A study on a large-diameter pipeline by Cunlife[26] reported that the closest results on liquid holdup were obtained by Eaton's correlation. The same conclusion was drawn by a recent study on an experimental facility by Carterville et al.[27]

The Dukler correlation was developed for horizontal flow. To account for the pressure loss caused by hills, this equation is combined with the Flanigan[28] correlation. This hybrid correlation often overpredicts the pressure loss caused by hills since it ignores pressure recovery in the downhill section.

The most common equation for gas transmission pipelines is the Panhandle equation. To account for the presence of hills, this equation is coupled with the Flanigan correlation.

4.74 PRESSURE GRADIENT OPTIONS

Good programs allow the user to select from several methods to calculate the pressure gradient occurring in a pipe increment. Some of these are:

(1) Beggs and Brill
(2) Dukler et al. and Flanigan with Dukler et al. holdup
(3) Dukler et al. and Flanigan with Eaton et al. holdup
(4) Panhandle and Flanigan

4.75 CHOKE PRESSURE-DROP PREDICTIONS

The flow of fluids through chokes is a common occurrence in the petroleum and natural gas industry. The basic function of a choke is to maintain a desired flow rate by imposing a back pressure on the formation.

It is a standard oil-field practice to choose a choke in such a way that a small variation in the downstream

pressure does not affect the upstream pressure and thus the well's performance. This implies that fluid flow through the choke is at the velocity of sound. This flow is usually called "critical" or sonic flow. On the other hand, if the velocity through the choke becomes less than the sonic velocity, the upstream pressure is affected by the downstream pressure. This type of flow is called "subcritical" flow.

If a choke exists in the pipeline, a good program normally calculates the pressure drop across the choke for both critical and subcritical flow conditions. Two good correlations used are those of Gilbert[29] and Ashford and Pierce.[30]

4.76 FLUID PROPERTY OPTIONS

The fluid properties existing in a pipe increment at a given pressure and temperature can be calculated by one of two methods. For most cases, the so-called black-oil model is adequate, but for volatile oils and condensates, a compositional model will give better results.

The normally accepted correlations and options used for calculating the various fluid properties for the black oil model are given in Table 4.48.

TABLE 4.48
SUMMARY OF FLUID PROPERTY OPTIONS

Property	Source
Oil formation volume factor (below bubble-point pressure)	Standing[35] Vasquez and Beggs[36]
Oil formation volume factor (above bubble-point pressure)	Vasquez and Beggs[36]
Water formation volume factor	Keenan and Keyes[37]
Solution gas-water ratio	Culbertson and McKetta[38]
Solution gas-oil ratio	Lasater[39] Standing[35] Vasquez and Beggs[36]
Gas viscosity	Lee et al.[40]
Oil viscosity (above bubble point)	Vasquez and Beggs[36]
Oil viscosity (below bubble point)	Beggs and Robinson[41]
Water viscosity	Van Wingen[42]
Gas compressibility factor	Yarborough and Hall[43]
Oil-gas surface tension	Baker and Swerdloff[44]
Water-gas surface tension	Hough[45]

If the compositional model for handling fluid properties is chosen, all of the necessary fluid properties, as functions of pressure and temperature, are calculated using a flash program.

The feed composition that can be handled can be specified in the form of hydrocarbons ranging from methane to octane and impurities. The heavier hydrocarbons, usually referred to as C_{7+}, are treated on the basis of their boiling point, BP. This approach was found to give much more reliable results than simply replacing the heavier fractions by a single component.

The feed composition can normally be entered as mol fraction, mol percent, or as number of mols.

Good correlations for equilibrium constants are those developed either by Usdin and McAuliffe[31] or by Canfield.[32]

4.77 SLUG CHARACTERISTICS PREDICTION

The basic model used to predict slug characteristics was developed by Hubbard.[33] This model was tested and modified using field data from Prudhoe Bay oil field.[34] The basic modifications are the incorporation of empirical correlation for liquid holdups in the liquid slug and in the film and the average holdup in a slug unit. An empirical correlation for slug length in the pipeline was also developed.

If slug flow is occurring at the outlet of the pipeline, slug characteristics can be calculated. All necessary information for sizing separation facilities can be determined. The variables of special significance are the volume of liquid produced from the liquid slug, the time during which the slug is produced, and the time between two slugs.

4.78 PIGGING CHARACTERISTICS PREDICTION

Pigging characteristics can be best predicted using the McDonald and Baker model.[46] Assuming 100% removal efficiency of a sphere and that all liquid removed by the sphere is in the form of a continuous slug, the slug volume can be estimated by integrating the difference between the liquid holdup and the no-slip holdup in the pipeline. Referring to the data of example 1A in Table 4.49a, the no-slip liquid volume in the pipe is 322 bbl and the liquid holdup volume predicted by Eaton is 660 bbl. Therefore, the liquid slug volume swept by the sphere, V_L, is 660 − 322 = 338 bbl. This volume is the additional volume that the production facility has to handle during pigging.

The time required to produce the liquid slug can be roughly estimated from:

$$T_{pr} \approx \frac{5.614\ V_L}{A\left(1 - \frac{v_{SL}}{v_{SL} + v_{Sg}}\right) v_{Sg}} \tag{4.37}$$

Solving for Table 4.49a, we have:

$$T_{pr} \approx \frac{5.614\ (338)}{0.737\left(1 - \frac{1.8}{1.8 + 12.5}\right) 12.5} = 235 \text{ sec}$$

An additional problem arises in offshore gathering lines that terminate with a vertical riser pipe. When slug flow is present in either a pipeline or the riser pipe, severe pressure fluctuation at the pipeline outlet might occur.

One of the most common methods for handling liquid slugs is to place accumulators called slug catchers upstream of the gas-liquid separator. These slug catchers must be capable of containing the largest slug anticipated and be able to drain fast enough to be ready for the next slug. This requires the calculation of the following slugging characteristics:

(1) liquid slug and gas-bubble lengths in a pipeline
(2) liquid slug and bubble residence times
(3) liquid volume produced from the slug
(4) liquid volume produced from the film
(5) liquid slug velocity
(6) liquid film velocity
(7) actual gas velocity in the bubble
(8) pressure fluctuation at the pipeline outlet if a riser exists

All of these characteristics can be determined if the flow pattern at the outlet condition is in the slugging regime.

Another important fact that has to be considered in slug catcher design is the amount of liquid swept by a sphere during pigging a pipeline. Pigging is a common procedure in pipelines. It is mainly performed to increase pipeline efficiency and to remove scale. Liquid volumes swept with this technique are usually much larger than those produced during the normal slug flow.

Liquid inventory of a pipeline (i.e., the volume swept by a sphere) can be calculated for each case, regardless of the flow pattern present in the pipeline.

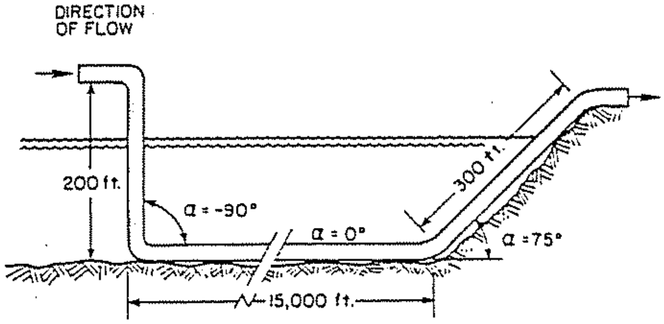

Figure 4.116 Pipeline Geometry for Examples 3 and 4

4.79 EXAMPLE CASES

Seven examples are shown. Each problem example is preceded by a listing of input data used in the problem. The problems do not represent an actual pipeline design, and a complete design study could involve many computer runs utilizing several of the available options. Refer to Figures 4.116 and 4.117 for the pipeline geometry of these examples. Refer to Tables 4.49a and b through 4.55a and b for the various example cases.

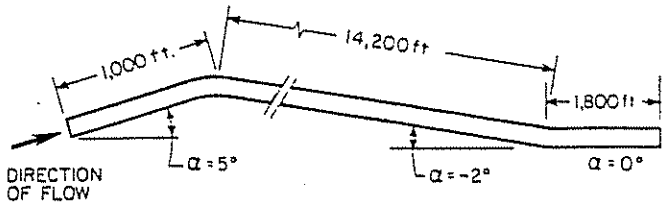

Figure 4.117 Pipeline Geometry for Examples 1A, 1B, 2, 5, and 6

TABLE 4.49A

Input Data For Example 1A

*** Example 1A: black oil—Beggs & Brill—calc. in direction of flow ***

100030070101100

20,000	10,000	0	40	0.6	0	
232.08	0	70	60	11.626	17,000	0.0028
1,000	3,200	6,200	9,200	12,200	15,200	17,000
5	−2	0				
1,000	15,200	17,000				

Output For Example 1A

Pipeline Pressure Traverse

*** Example 1A: black oil—Beggs & Brill—calc. in direction of flow ***

Oil flow rate, stb/d =	20,000
Water flow rate, stb/d =	0
Gas flow rate, Mscf/d =	10,000
Gas-liquid ratio, scf/stb =	500
Gas gravity, (air = 1) =	0.600
Oil gravity, °API =	40
Upstream temp, °F =	70
Downstream temp, °F =	60
Initial pressure, psia =	232.08
Pipe ID, in. =	11.626

Pressure gradient calculated by Beggs-Brill method

Distance, ft	Pressure, psia	Flow pattern			Holdup (fraction)				Liquid volume, bbl			
		Beggs	Mandane	Mukherjee	No slip	Beggs	Tuffp	Eaton	No slip	Beggs	Tuffp	Eaton
0	232.08	intermittent	slug	slug								
1,000	219.35	intermittent	slug	slug	0.164	0.289	0.292	0.320	21.531	37.917	38.287	41.978
3,200	213.56	intermittent	slug	slug	0.158	0.151	0.284	0.312	45.517	43.664	82.027	90.021
6,200	205.02	intermittent	slug	slug	0.153	0.149	0.278	0.306	60.181	58.537	109.572	120.643
9,200	195.60	intermittent	slug	slug	0.147	0.145	0.271	0.299	57.784	57.244	106.596	117.860
12,200	185.12	intermittent	slug	slug	0.140	0.142	0.262	0.291	55.096	55.767	103.148	114.609
15,200	173.34	intermittent	slug	slug	0.132	0.137	0.252	0.281	52.051	54.060	99.095	110.759
17,000	164.70	intermittent	slug	slug	0.125	0.269	0.242	0.272	29.535	63.527	57.106	64.204

TABLE 4.49B
EXAMPLE 1A

FINAL RESULT
****

Distance, ft	Pressure, psia	Flow pattern			Holdup (fraction)				Liquid volume, bbl			
		Beggs	Mandane	Mukherjee	No Slip	Beggs	Tuffp	Eaton	No Slip	Beggs	Tuffp	Eaton
17,000	164.70	intermittent	slug	slug	0.125	0.269	0.242	0.272	29.535	63.527	57.106	64.204
		Total liquid volume in pipeline, bbl							321.695	370.717	595.830	660.074
		Final calculated pressure, psia							164.70			

Conditions at Pipeline Outlet for Slug Flow

	Average slug unit	Maximum slug unit
Liquid slug length, L_s, ft	474.65	2,538.28
Gas-bubble length, L_b, ft	2,374.66	12,698.80
Liquid slug residence time, T_s, sec	26.54	141.92
Gas-bubble residence time, T_b, sec	132.77	709.99
Gas-bubble velocity, v_{bl}, ft/sec	17.89	17.89
Liquid-film velocity, v_f, ft/sec	1.28	1.28
Gas velocity, v_g, ft/sec	16.56	16.56
Liquid holdup, H_L	0.2416	0.2416
Liquid holdup in liquid slug, H_{Ls}	0.6840	0.6840
Liquid holdup in gas bubble, H_{Lb}	0.1474	0.1474
Volume of liquid produced during $T_s + T_b$, V_{Lp}, bbl	37.40	200.01
Volume of liquid produced from the liquid slug, V_{Lsp}, bbl	34.11	182.39
Volume of liquid produced from the liquid film, V_{Lfp}, bbl	3.30	17.62
Volume of liquid in liquid slug in pipeline, V_{Ls}, bbl	42.63	227.96
Volume of liquid in a slug unit in pipeline, V_{LT}, bbl	300.64	1,607.69
Superficial gas velocity, v_{sg}, ft/sec	12.521	
Superficial liquid velocity, v_{sL}, ft/sec	1.788	
Gas velocity number, N_{gv}	28.938	
Liquid velocity number, N_{Lv}	4.133	

TABLE 4.50A

Input Data For Example 1B

*** Example 1B: Black oil—Dukler & Eaton—Calc. in direction of flow ***
300030070101000

20,000	10,000	0	40	0.6	0	
232.08	0	70	60	11.626	17,000	0.0028
1,000	3,200	6,200	9,200	12,200	15,200	17,000
5	−2	0				
1,000	15,200	17,000				

Output For Example 1B

Pipeline Pressure Traverse
*** Example 1B: Black oil—Dukler & Eaton—Calc. in direction of flow ***

Oil flow rate, stb/d =	20,000
Water flow rate, stb/d =	0
Gas flow rate, Mscfd =	10,000
Gas-liquid ratio, scf/stb =	500
Gas gravity, (air = 1) =	0.600
Oil gravity, °API =	40
Upstream temp, °F =	70
Downstream temp, °F =	60
Initial pressure, psia =	232.08
Pipe ID, in. =	11.626

Pressure gradient calculated by Dukl-Flan-Eaton method

Distance, ft	Pressure, psia	Flow pattern			Holdup (fraction)				Liquid volume, bbl			
		Beggs	Mandane	Mukherjee	No slip	Beggs	Tuffp	Eaton	No slip	Beggs	Tuffp	Eaton
0	232.08	intermittent	slug	slug								
1,000	220.88	intermittent	slug	slug	0.165	0.315	0.292	0.320	21.603	41.384	38.372	42.077
3,200	213.37	intermittent	slug	slug	0.158	0.280	0.285	0.312	45.654	80.844	82.193	90.213
6,200	202.66	intermittent	slug	slug	0.152	0.274	0.277	0.305	59.820	107.845	109.121	120.128
9,200	191.33	intermittent	slug	slug	0.144	0.266	0.268	0.296	56.845	104.865	105.388	116.497
12,200	179.27	intermittent	slug	slug	0.136	0.258	0.257	0.286	53.657	101.600	101.229	112.470
15,200	166.33	intermittent	slug	slug	0.127	0.249	0.245	0.274	50.213	97.985	96.538	107.955
17,000	158.06	intermittent	slug	slug	0.120	0.263	0.234	0.264	28.359	62.076	55.404	62.367

TABLE 4.50B
EXAMPLE 1B

FINAL RESULT

Distance, ft	Pressure, psia	Flow pattern			Holdup (fraction)				Liquid volume, bbl			
		Beggs	Mandane	Mukherjee	No slip	Beggs	Tuffp	Eaton	No slip	Beggs	Tuffp	Eaton
17,000	158.06	intermittent	slug	slug	0.120	0.263	0.234	0.264	28.359	62.076	55.404	62.367
		Total liquid volume in pipeline, bbs							316.151	596.597	588.245	651.707
		Final calculated pressure, psia							158.06			

Conditions at pipeline outlet for slug flow

	Average slug unit	Maximum slug unit
Liquid slug length, L_s, ft	475.75	2,544.23
Gas bubble length, L_b, ft	2,430.78	12,999.42
Liquid slug residence time, T_s, sec	25.56	136.69
Gas bubble residence time, T_b, sec	130.59	698.38
Gas bubble velocity, v_{bf}, ft/sec	18.61	18.61
Liquid film velocity, v_f, ft/sec	1.24	1.24
Gas velocity, v_g, ft/sec	17.19	17.19
Liquid holdup, H_L	0.2344	0.2344
Liquid holdup in liquid slug, H_{Ls}	0.6720	0.6720
Liquid holdup in gas bubble, H_{Lb}	0.1440	0.1440
Volume of liquid produced during $T_s + T_b$, V_{Lp}, bbl	36.63	195.91
Volume of liquid produced from the liquid slug, V_{Lsp}, bbl	33.58	179.59
Volume of liquid produced from the liquid film, V_{Lfp}, bbl	3.05	16.33
Volume of liquid in liquid slug in pipeline, V_{Ls}, bbl	41.98	224.48
Volume of liquid in a slug unit in pipeline, V_{LT}, bbl	299.95	1,604.07
Superficial gas velocity, v_{sg}, ft/sec	13.104	
Superficial liquid velocity, v_{sL}, ft/sec	1.787	
Gas velocity number, N_{gv}	30.249	
Liquid velocity number, N_{Lv}	4.124	

TABLE 4.51A

Input Data For Example 2

*** Example 2: black oil model—calculate in direction against flow ***

100030070101100

20,000	10,000	0	40	0.6	0	
0	164.7	70	60	11.626	17,000	0.0028
1,000	3,200	6,200	9,200	12,200	15,200	17,000
5	−2	0				
1,000	15,200	17,000				

Output For Example 2

Pipeline Pressure Traverse

*** Example 2: black oil model—calc. in direction against flow ***

Oil flow rate, stb/d =	20,000
Water flow rate, stb/d =	0
Gas flow rate, Mscf/d =	10,000
Gas-liquid ratio, scf/stb =	500
Gas gravity, (air = 1) =	0.600
Oil gravity, °API =	40
Upstream temp, °F =	70
Downstream temp, °F =	60
Initial pressure, psia =	164.70
Pipe ID, in. =	11.626

Pressure gradient calculated by Beggs-Brill method

Distance, ft	Pressure, psia	Flow pattern			Holdup (fraction)				Liquid volume, bbl			
		Beggs	Mandane	Mukherjee	No slip	Beggs	Tuffp	Eaton	No slip	Beggs	Tuffp	Eaton
17,000	164.70	intermittent	slug	slug								
15,200	173.34	intermittent	slug	slug	0.125	0.269	0.242	0.272	29.534	63.527	57.105	64.203
12,200	185.12	intermittent	slug	slug	0.132	0.137	0.252	0.281	52.049	54.058	99.092	110.755
9,200	195.60	intermittent	slug	slug	0.140	0.142	0.262	0.291	55.095	55.767	103.148	114.608
6,200	205.02	intermittent	slug	slug	0.147	0.145	0.271	0.299	57.784	57.244	106.595	117.860
3,200	213.56	intermittent	slug	slug	0.153	0.149	0.278	0.306	60.180	58.537	109.571	120.642
1,000	219.35	intermittent	slug	slug	0.158	0.151	0.284	0.312	45.517	43.664	82.027	90.022
0	232.08	intermittent	slug	slug	0.164	0.289	0.292	0.320	21.531	37.917	38.287	41.978

TABLE 4.51B
EXAMPLE 2

FINAL RESULT
****

Distance, ft	Pressure, psia	Flow pattern			Holdup (fraction)				Liquid volume, bbl			
		Beggs	Mandane	Mukherjee	No slip	Beggs	Tuffp	Eaton	No slip	Beggs	Tuffp	Eaton
0	232.08	intermittent	slug	slug	0.164	0.289	0.292	0.320	21.531	37.917	38.287	41.978
		Total liquid volume in pipeline, bbl							321.690	370.713	595.823	660.067
		Final calculated pressure, psia							232.08			

Conditions at pipeline outlet for slug flow

	Average slug unit	Maximum slug unit
Liquid slug length, L_s, ft	474.66	2,538.28
Gas bubble length, L_b, ft	2,374.69	12,698.96
Liquid slug residence time, T_s, sec	26.54	141.91
Gas bubble residence time, T_b, sec	132.77	709.99
Gas bubble velocity, v_{bf}, ft/sec	17.89	17.89
Liquid film velocity, v_f, ft/sec	1.28	1.28
Gas velocity, v_g, ft/sec	16.56	16.56
Liquid holdup, H_L	0.2416	0.2416
Liquid holdup in liquid slug, H_{Ls}	0.6840	0.6840
Liquid holdup in gas bubble, H_{Lb}	0.1474	0.1474
Volume of liquid produced during $T_s + T_b$, V_{Lp}, bbl	37.40	200.01
Volume of liquid produced from the liquid slug, V_{Lsp}, bbl	34.11	182.39
Volume of liquid produced from the liquid film, V_{Lfp}, bbl	3.30	17.62
Volume of liquid in liquid slug in pipeline, V_{Ls}, bbl	42.63	227.98
Volume of liquid in a slug unit in pipeline, V_{LT}, bbl	300.64	1,607.69
Superficial gas velocity, v_{sg}, ft/sec	12.521	
Superficial liquid velocity, v_{sL}, ft/sec	1.788	
Gas velocity number, N_{gv}	28.939	
Liquid velocity number, N_{Lv}	4.133	

TABLE 4.52A

Input Data For Example 3

```
*** Example 3: black oil model—with riser ***
100030070101110
20,000     10,000       0      40        0.6        0
     0      164.7      70      60     11.626   15,500      0.0028
   200      3,200   6,200   9,200     12,200   15,200     15,500
   −90          0      75
   200     15,200  15,500
 289.8
```

Output For Example 3

Pipeline Pressure Traverse
*** Example 3: black oil model—with riser ***

Oil flow rate, stb/d =	20,000
Water flow rate, stb/d =	0
Gas flow rate, Mscf/d =	10,000
Gas-liquid ratio, scf/stb =	500
Gas gravity, (air = 1) =	0.600
Oil gravity, °API =	40
Upstream temp, °F =	70
Dowstream temp, °F =	60
Initial pressure, psia =	164.70
Pipe ID, in. =	11.626

Pressure gradient calculated by Beggs-Brill method

Distance, ft	Pressure, psia	Flow pattern			Holdup (fraction)				Liquid volume, bbl			
		Beggs	Mandane	Mukherjee	No slip	Beggs	Tuffp	Eaton	No slip	Beggs	Tuffp	Eaton
15,500	164.70	intermittent	slug	slug								
15,200	193.35	intermittent	slug	slug	0.132	0.256	0.252	0.283	5.212	10.069	9.925	11.165
12,200	205.73	intermittent	slug	slug	0.147	0.295	0.271	0.304	57.912	116.135	106.875	119.804
9,200	217.30	intermittent	slug	slug	0.155	0.304	0.282	0.314	61.156	119.787	110.886	123.654
6,200	228.19	intermittent	slug	slug	0.163	0.313	0.291	0.323	64.173	123.108	114.484	127.113
3,200	238.51	intermittent	slug	slug	0.170	0.320	0.299	0.331	67.000	126.158	117.746	130.217
200	248.34	intermittent	slug	slug	0.177	0.327	0.306	0.338	69.655	128.971	120.722	133.014
0	241.36	intermittent	slug	slug	0.178	0.101	0.307	0.338	4.664	2.650	8.069	8.869

TABLE 4.52B
EXAMPLE 3

FINAL RESULT
****

Distance, ft	Pressure, psia	Flow pattern			Holdup (fraction)				Liquid volume, bbl			
		Beggs	Mandane	Mukherjee	No slip	Beggs	Tuffp	Eaton	No slip	Beggs	Tuffp	Eaton
0	241.36	intermittent	slug	slug	0.178	0.101	0.307	0.338	4.664	2.650	8.069	8.869
		Total liquid volume in pipeline, bbl							329.772	626.878	588.706	653.835
		Final calculated pressure, psia							241.36			

Conditions at Pipeline Outlet for Slug Flow

	Average slug unit	Maximum slug unit
Liquid slug length, L_s, ft	432.25	2,307.53
Gas bubble length, L_b, ft	2,095.80	11,188.34
Liquid slug residence time, T_s, sec	25.57	136.51
Gas bubble residence time, T_b, sec	123.98	661.86
Gas bubble velocity, v_{bf}, ft/sec	16.90	16.90
Liquid film velocity, v_f, ft/sec	1.34	1.34
Gas velocity, v_g, ft/sec	15.71	15.71
Liquid holdup, H_L	0.2520	0.2520
Liquid holdup in liquid slug, H_{Ls}	0.7009	0.7009
Liquid holdup in gas bubble, H_{Lb}	0.1522	0.1522
Volume of liquid produced during $T_s + T_b$, V_{Lp}, bbl	35.14	187.59
Volume of liquid produced from the liquid slug, V_{Lsp}, bbl	31.82	169.88
Volume of liquid produced from the liquid film, V_{Lfp}, bbl	3.32	17.71
Volume of liquid in liquid slug in pipeline, V_{Ls}, bbl	39.78	212.36
Volume of liquid in a slug unit in pipeline, V_{LT}, bbl	274.97	1,467.94
Superficial gas velocity, v_{sg}, ft/sec	11.734	
Superficial liquid velocity, v_{sL}, ft/sec	1.789	
Gas velocity number, N_{gv}	27.172	
Liquid velocity number, N_{Lv}	4.144	
The expected pressure fluctuations at the bottom of the riser pipe are psi	57.09	

TABLE 4.53A

Input Data For Example 4

```
*** Example 4: composition model—with riser ***
110030070000110
0208130
0102030405060708091023 2425
    127.11    3,826.53    1,280.13    1,028.68    428.38    526.90    328.33    340.94
    233.79      634.61       56.97        0.03      0.01
    450         800          60          70
2,500,000
      0         464.7        70          60       11.626    15,500      0.0028
    200       3,200       6,200       9,200     12,200      15,200     15,500
    -90           0          75
    200      15,200      15,500
    289.8
```

Output For Example 4

Pipeline Pressure Traverse
*** Example 4: compositional model—with riser ***

Mass flow rate, lbm/d =	2,500,000
Upstream temp, °F =	70
Downstream temp, °F =	60
Initial pressure, psia =	464.70
Pipe ID, in. =	11.626

Pressure gradient calculated by Beggs—Brill method

TABLE 4.53A (Cont.)

Distance, ft	Pressure, psia	Flow pattern: Beggs	Mandane	Mukherjee	Holdup (fraction): No slip	Beggs	Tuffp	Eaton	Liquid volume, bbl: No slip	Beggs	Tuffp	Eaton
15,500	464.70	intermittent	slug	slug								
15,200	505.40	intermittent	slug	slug	0.140	0.544	0.337	0.265	5.500	21.409	13.264	10.442
12,200	506.92	intermittent	slug	slug	0.149	0.340	0.346	0.276	58.563	133.890	136.378	108.863
9,200	508.44	intermittent	slug	slug	0.147	0.338	0.345	0.274	57.974	133.143	135.828	108.108
6,200	509.98	intermittent	slug	slug	0.146	0.336	0.343	0.273	57.399	132.413	135.290	107.370
3,200	511.53	intermittent	slug	slug	0.144	0.334	0.342	0.271	56.838	131.699	134.764	106.646
200	513.08	intermittent	slug	slug	0.143	0.333	0.341	0.269	56.290	131.002	134.247	105.939
0	506.96	intermittent	slug	slug	0.141	0.071	0.339	0.266	3.698	1.858	8.895	6.994

TABLE 4.53B
EXAMPLE 4

FINAL RESULT
****

Distance, ft	Pressure, psia	Flow pattern: Beggs	Mandane	Mukherjee	Holdup (fraction): No slip	Beggs	Tuffp	Eaton	Liquid volume, bbl: No slip	Beggs	Tuffp	Eaton
0	506.96	intermittent	slug	stratified	0.141	0.071	0.339	0.266	3.698	1.858	8.895	6.994
		Total liquid volume in pipeline, bbl							296.263	685.414	698.666	554.362
		The final calculated pressure, psia							506.96			

Conditions at Pipeline Outlet for Slug Flow

	Average slug unit	Maximum slug unit
Liquid slug length, L_s, ft	406.55	2,167.72
Gas bubble length, L_b, ft	2,299.80	12,262.47
Liquid slug residence time, T_s, sec	55.93	298.23
Gas bubble residence time, T_b, sec	316.40	1,687.04
Gas bubble velocity, v_{bf}, ft/sec	7.27	7.27
Liquid film velocity, v_f, ft/sec	0.19	0.19
Gas velocity, v_g, ft/sec	7.08	7.08
Liquid holdup, H_L	0.3367	0.3367
Liquid holdup in liquid slug, H_{Ls}	0.8950	0.8950
Liquid holdup in gas bubble, H_{Lb}	0.1839	0.1839
Volume of liquid produced during $T_s + T_b$, V_{Lp}, bbl	39.69	211.65
Volume of liquid produced from the liquid slug, V_{Lsp}, bbl	38.22	203.80
Volume of liquid produced from the liquid film, V_{Lfp}, bbl	1.47	7.85
Volume of liquid in liquid slug in pipeline, V_{Ls}, bbl	47.78	254.75
Volume of liquid in a slug unit in pipeline, V_{LT}, bbl	359.53	1,916.99
Superficial gas velocity, v_{sg}, ft/sec	5.003	
Superficial liquid velocity, v_{sL}, ft/sec	0.812	
Gas velocity number, N_{gv}	13.874	
Liquid velocity number, N_{Lv}	2.252	
The expected pressure fluctuations at the bottom of the riser pipe are psi	47.79	

TABLE 4.54A

Input Data for Example 5

*** Example 5: black oil model—with choke ***
100030070101101

1,000	500	0	40	0.6	0		
0	164.7	70	60	3.026	17,000		0.0028
1,000	3,200	6,200	9,200	12,200	15,200	17,000	
5	−2	0					
1,000	15,200	17,000					
0,321							

TABLE 4.54A (Cont.)

Output for Example 5

Pipeline Pressure Traverse
*** Example 5: black oil model—with choke ***

Oil flow rate, stb/d =	1,000
Water flow rate, stb/d =	0
Gas flow rate, Mscfd =	500
Gas-liquid ratio, scf/stb =	500
Gas gravity, (air = 1) =	0.600
Oil gravity, API =	40
Upstream temp, °F =	70
Downstream temp, °F =	60
Initial pressure, psia =	164.70
Pipe ID, in. =	3.026
Choke size in 64th of inch =	32 at inlet

Pressure gradient calculated by Beggs-Brill Method

Distance, ft	Pressure, psia	Flow pattern			Holdup (fraction)				Liquid volume, bbl			
		Beggs	Mandane	Mukherjee	No slip	Beggs	Tuffp	Eaton	No slip	Beggs	Tuffp	Eaton
17,000	164.70	intermittent	slug	slug								
15,200	190.48	intermittent	slug	slug	0.131	0.273	0.280	0.311	2.101	4.368	4.483	4.985
12,200	230.74	intermittent	slug	slug	0.155	0.151	0.309	0.347	4.132	4.039	8.252	9.249
9,200	263.71	intermittent	slug	slug	0.181	0.165	0.338	0.382	4.827	4.398	9.014	10.184
6,200	291.83	intermittent	slug	slug	0.202	0.175	0.359	0.408	5.401	4.680	9.585	10.891
3,200	316.43	intermittent	slug	slug	0.221	0.184	0.376	0.429	5.890	4.911	10.037	11.458
1,000	332.70	intermittent	slug	slug	0.235	0.191	0.388	0.445	4.594	3.728	7.602	8.706
0	516.66	intermittent	slug	slug	0.247	0.370	0.399	0.459	2.198	3.290	3.548	4.079

TABLE 4.54B
EXAMPLE 5

FINAL RESULT

Distance, ft	Pressure, psia	Flow pattern			Holdup (fraction)				Liquid volume, bbl			
		Beggs	Mandane	Mukherjee	No slip	Beggs	Tuffp	Eaton	No slip	Beggs	Tuffp	Eaton
0	516.66	intermittent	slug	slug	0.247	0.370	0.399	0.459	2.198	3.290	3.548	4.079
		Total liquid volume in pipeline, bbl							29.143	29.414	52.521	59.552
		The final calculated pressure, psia							516.66			
		The pressure drop across the choke, psi							164.68	Subcritical flow		

Note: Inlet pressure has been increased for pressure drop across choke.

Conditions at Pipeline Outlet for Slug Flow

	Average slug unit	Maximum slug unit
Liquid slug length, L_s, ft	37.76	161.07
Gas bubble length, L_b, ft	208.43	888.98
Liquid slug residence time, T_s, sec	3.00	12.80
Gas bubble residence time, T_b, sec	16.56	70.64
Gas bubble velocity, v_{bf}, ft/sec	12.58	12.58
Liquid film velocity, v_f, ft/sec	0.77	0.77
Gas velocity, v_g, ft/sec	11.93	11.93
Liquid holdup, H_L	0.2800	0.2800
Liquid holdup in liquid slug, H_{Ls}	0.7850	0.7850
Liquid holdup in gas bubble, H_{Lb}	0.1672	0.1672
Volume of liquid produced during $T_s + T_b$, V_{Lp}, bbl	0.23	0.98
Volume of liquid produced from the liquid slug, V_{Lsp}, bbl	0.21	0.90
Volume of liquid produced from the liquid film, V_{Lfp}, bbl	0.02	0.08
Volume of liquid in liquid slug in pipeline, V_{Ls}, bbl	0.26	1.12
Volume of liquid in a slug unit in pipeline, V_{LT}, bbl	2.00	8.55
Superficial gas velocity, v_{sg}, ft/sec	8.747	
Superficial liquid velocity, v_{sL}, ft/sec	1.321	
Gas velocity number, N_{gv}	20.248	
Liquid velocity number, N_{Lv}	3.058	

TABLE 4.55A

Input Data for Example 6

```
*** Example 6: compositional model—with choke ***
110030070000101
0208130
01020304050607080910232425
   127.11    3,826.53    1,280.13    1,028.68    428.38    526.90    328.33    340.94
   233.79      634.61       56.97        0.03      0.01
   450         800          60           70
170,000
     0         464.7        70           60         3.026    17,000      0.0028
 1,000       3,200       6,200        9,200      12,200     15,200     17,000
     5          −2           0
 1,000      15,200      17,000
   322
```

Output for Example 6

Pipeline Pressure Traverse
*** Example 6: compositional model—with choke ***

Mass flowrate, lbm/d =	170,000
Upstream temp, °F =	70
Downstream temp, °F =	60
Initial pressure, psia =	464.70
Pipe ID, in. =	3.026
Choke size in 64*th* of in. =	32 at outlet

Pressure gradient calculated by Beggs-Brill method

Distance, ft	Pressure, psia	Flow pattern			Holdup (fraction)				Liquid volume, bbl			
		Beggs	Mandane	Mukherjee	No slip	Beggs	Tuffp	Eaton	No slip	Beggs	Tuffp	Eaton
17,000	495.60	intermittent	slug	slug								
15,200	500.52	intermittent	slug	slug	0.146	0.294	0.343	0.279	2.332	4.713	5.488	4.464
12,200	505.84	intermittent	slug	slug	0.146	0.145	0.344	0.280	3.909	3.881	9.172	7.466
9,200	511.12	intermittent	slug	slug	0.147	0.146	0.344	0.280	3.919	3.886	9.185	7.477
6,200	516.35	intermittent	slug	slug	0.147	0.146	0.345	0.281	3.929	3.892	9.198	7.488
3,200	521.53	intermittent	slug	slug	0.148	0.146	0.345	0.281	3.940	3.898	9.212	7.500
1,000	525.30	intermittent	slug	slug	0.148	0.146	0.346	0.281	2.896	2.862	6.765	5.508
0	534.98	intermittent	slug	slug	0.150	0.284	0.348	0.284	1.335	2.529	3.094	2.527

TABLE 4.55B
EXAMPLE 6

FINAL RESULT
****

Distance, ft	Pressure, psia	Flow pattern			Holdup (fraction)				Liquid volume, bbl			
		Beggs	Mandane	Mukherjee	No slip	Beggs	Tuffp	Eaton	No slip	Beggs	Tuffp	Eaton
0	534.98	intermittent	slug	slug	0.150	0.284	0.348	0.284	1.335	2.529	3.094	2.527
		Total liquid volume in pipeline, bbl							22.261	25.662	52.113	42.429
		Final calculated pressure, psia							534.98			
		The pressure drop across the choke, psi							30.90	Subcritical flow		

Note: Outlet pressure has been increased for pressure drop across choke.

TABLE 4.55B (Cont.)

Conditions at Pipeline Outlet for Slug Flow

	Average slug unit	Maximum slug unit
Liquid slug length, L_s, ft	36.83	155.98
Gas bubble length, L_b, ft	200.30	848.34
Liquid slug residence time, T_s, sec	5.23	22.14
Gas bubble residence time, T_b, sec	28.43	120.41
Gas bubble velocity, v_{bf}, ft/sec	7.05	7.05
Liquid film velocity, v_f, ft/sec	0.21	0.21
Gas velocity, v_g, ft/sec	6.87	6.87
Liquid holdup, H_L	0.3428	0.3428
Liquid holdup in liquid slug, H_{Ls}	0.8998	0.8998
Liquid holdup in gas bubble, H_{Lb}	0.1856	0.1856
Volume of liquid produced during $T_s + T_b$, V_{Lp}, bbl	0.25	1.04
Volume of liquid produced from the liquid slug, V_{Lsp}, bbl	0.24	1.00
Volume of liquid produced from the liquid film, V_{Lfp}, bbl	0.01	0.04
Volume of liquid in liquid slug in pipeline, V_{Ls}, bbl	0.29	1.25
Volume of liquid in a slug unit in pipeline, V_{LT}, bbl	2.15	9.11
Superficial gas velocity, v_{sg}, ft/sec	4.815	
Superficial liquid velocity, v_{sL}, ft/sec	0.821	
Gas velocity number, N_{gv}	13.401	
Liquid velocity number, N_{Lv}	2.285	

The "final result" table for each case gives pertinent information such as liquid slug length and volume, liquid slug and gas-bubble residence time, etc. The results are given using the correlation of Beggs and Brill, Mundane, Mukhurjee, Tuffp, and Eaton. Any significant differences can then be evaluated.

NOMENCLATURE FOR SECTION 4.7

Variable	*Description*
A	Area of pipe
BP	Boiling point
H_L	Liquid holdup
H_{Lb}	Liquid holdup in bubble
H_{Ls}	Liquid holdup in slug
L	Length
L_b	Length of bubble
L_s	Length of slug
P	Pressure
T	Temperature, time
T_{pr}	Production time
T_b	Gas bubble residence time
T_s	Liquid slug residence time
V_L	Volume of liquid removed by pig
V_{Lfp}	Volume of liquid produced from liquid film
V_{Lp}	Volume of liquid produced from a slug unit
V_{Ls}	Volume of liquid in slug
V_{Lsp}	Volume of liquid produced from the slug unit
V_{LT}	Volume of liquid in a plug unit
v	Velocity
v_{bf}	Gas bubble front velocity
v_f	Liquid film velocity
v_{sg}	Superficial gas velocity
v_{sL}	Superficial liquid velocity
XP	pressure psia
XT	Temperature, °F
XSGF	Specific gravity of free gas
XRHOL	Liquid density, lbm/ft³
XVISL	Liquid velocity, cp
XSUR	Surface tension, dyne/cm
XVSL	Liquid in situ volume, ft³/lbm of feed
XVSG	Gas in situ volume, ft³/lbm of feed
XZ	Z factor

4.8 PRODUCTION OPTIMIZATION FOR A COMPLETE OCEAN-FLOOR COMPLETION

4.81 INTRODUCTION

The following hypothetical case and data are considered representative of several areas of the world where ocean-floor completions are considered (see Figure 4.118).

(1) *Riser pipe.*

Separator pressure = 50 psig–300 psig
Vertical riser height = 600 ft
Riser pipe size = 12.5-in. ID–16-in. ID

(2) *Horizontal flow line.*

Length = 8 mi
Size = 12.5-in. ID–16-in. ID

(3) *Individual well data.*

Depth = 9,500 ft
Deviation = 45°F (average)
Static reservoir pressure = 3,500 psi
J = 5–10 b/d/psi
Temperature = 200°F
R_s = 100 scf/bbl
Gas specific gravity = 0.8
Water cut = 50%
°API = 32
Casing = 9⅝ in.

(4) *Ocean-floor equipment.* Anywhere from ten to fifteen wells are to produce into a common manifold. All production from the manifold enters a common

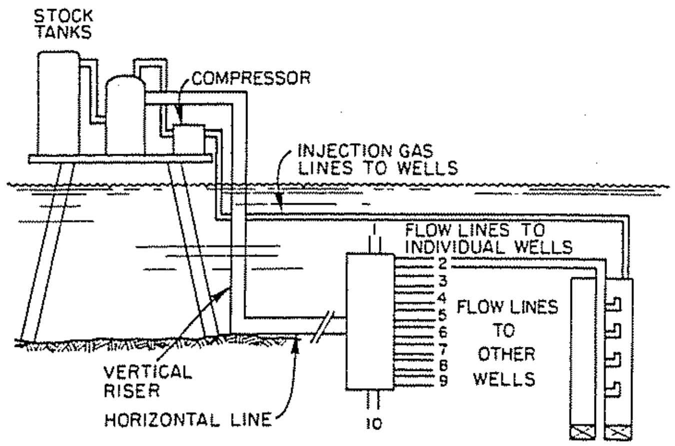

Figure 4.118 Ocean-Floor Completion

flow line, which is located on the ocean floor and travels in a horizontal manner for 8 mi.

(5) *Vertical riser and surface platform.* The fluids then encounter a 600-ft vertical riser and finally arrive at the top of a platform above sea level for separation.

(6) *Required production analysis.* The wells are to be placed on continuous-flow gas lift. For gas lift, a rotative compressor system is required, and therefore an optimum separator pressure is desired. Each component is to be analyzed individually and then combined in order to predict total rates from a group of wells. The following questions must be answered:

(1) What separator pressure is optimum?
(2) What must the separator size be in order to absorb any slugs created in the system?
(3) Will slug catchers be necessary?
(4) What size of vertical riser should be installed and at what angle from the vertical?
(5) What size of horizontal flow line is necessary to minimize back pressure and yet minimize slug formation?
(6) How does the vertical riser, in combination with the horizontal flow line, affect the size and frequency of slugs of liquid and gas?
(7) What wellhead pressure is to be expected at each well and how does it affect the flow rate from each well?

4.82 SOLUTION PROCEDURE

4.821 INTRODUCTION

A trial-and-error solution exists for this system and is more complex for the gas-lift system than for either a flowing or a pumping system.

Although the total system (every component) must eventually be combined, it is important to look at each component separately in the beginning.

Each component is listed as follows:

(1) separator pressures (try ranges of 50 to 300 psi)
(2) vertical risers (Try 8-in. to 16-in. diameter—may use in parallel)

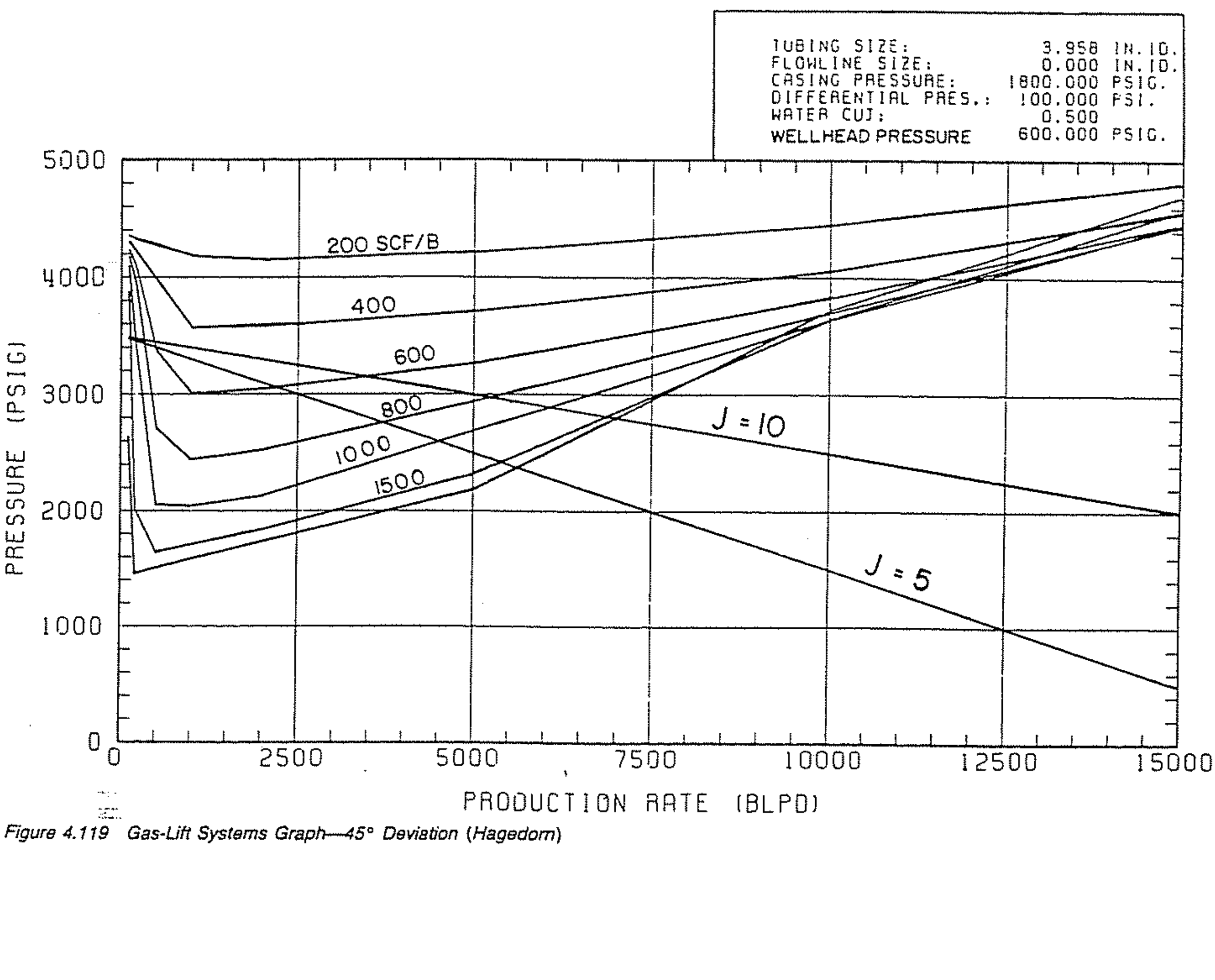

Figure 4.119 Gas-Lift Systems Graph—45° Deviation (Hagedorn)

(3) horizontal flow line (Try 8-in. to 16-in. diameter—may use in parallel)
(4) flow lines from manifold to wellhead (try 4-in. to 6-in.)
(5) individual wells (try 2.441-in. ID to 4.590-in. ID tubing sizes)

Gas lift becomes more complex since the volume of injected gas becomes another unknown in properly optimizing the system (refer to chapter 5).

4.822 INDIVIDUAL WELLS

By starting with the individual wells and using wellhead pressure as a sensitivity variable, a good idea of the total flow rate into the manifold can be obtained. If maximum rate is the objective, the better wells will be equipped with the larger tubing sizes.

A sequence of plots such as Figure 4.119 is made for different wellhead pressures. This plot is for 600 psig. A sensitivity plot such as Figure 4.120 shows rates vs wellhead pressures. This type of plot must be made for each well and for present and future times; that is, such things as anticipated water production increase, changing static reservoir pressure, and inflow performance must be analyzed.

Figure 4.121 is also prepared for each wellhead pressure to show gas volumes needed.

At this time, an estimate of the average wellhead pressure is made in order to obtain an estimate of the total flow rate into the manifold systems. A total field rate will be determined later.

For example, if the wellhead pressure is selected as 600 psi, the flow rate from Figure 4.121 (PI = 5) is 5,500 b/d. If this represents an average well, a total flow rate of 55,000 b/d from 10 wells can be assumed. A range of flow rates between 40,000 and 60,000 can now be used to evaluate the pressure losses in the vertical riser and the horizontal flow line. The pressure loss from the wellhead to the manifold also can be evaluated by the assumed rate from each well. This initial solution only gives approximations and ideas as to the range of sizes of pipes to consider. Exact solutions are given later.

4.823 VERTICAL RISER

The vertical riser can be treated as a separate component. Separator pressures of between 50 and 300 psi are to be evaluated, as well as pipe sizes between 8 and 16 in. Figure 4.122 shows a typical example for a 600-ft vertical riser of 12.5-in. ID and a separator pressure of 50 psi. The plot shows pressure at the bottom of the riser vs flow rate with the gas-liquid ratio (GLR) as a parameter.

The exit pressure from the horizontal line can be selected for different rates and different gas-liquid ratios. For example, if the rate is 50,000 b/d, the pressure at the bottom of the riser for a gas-liquid ratio of 1,000 scf/bbl is 125 psig.

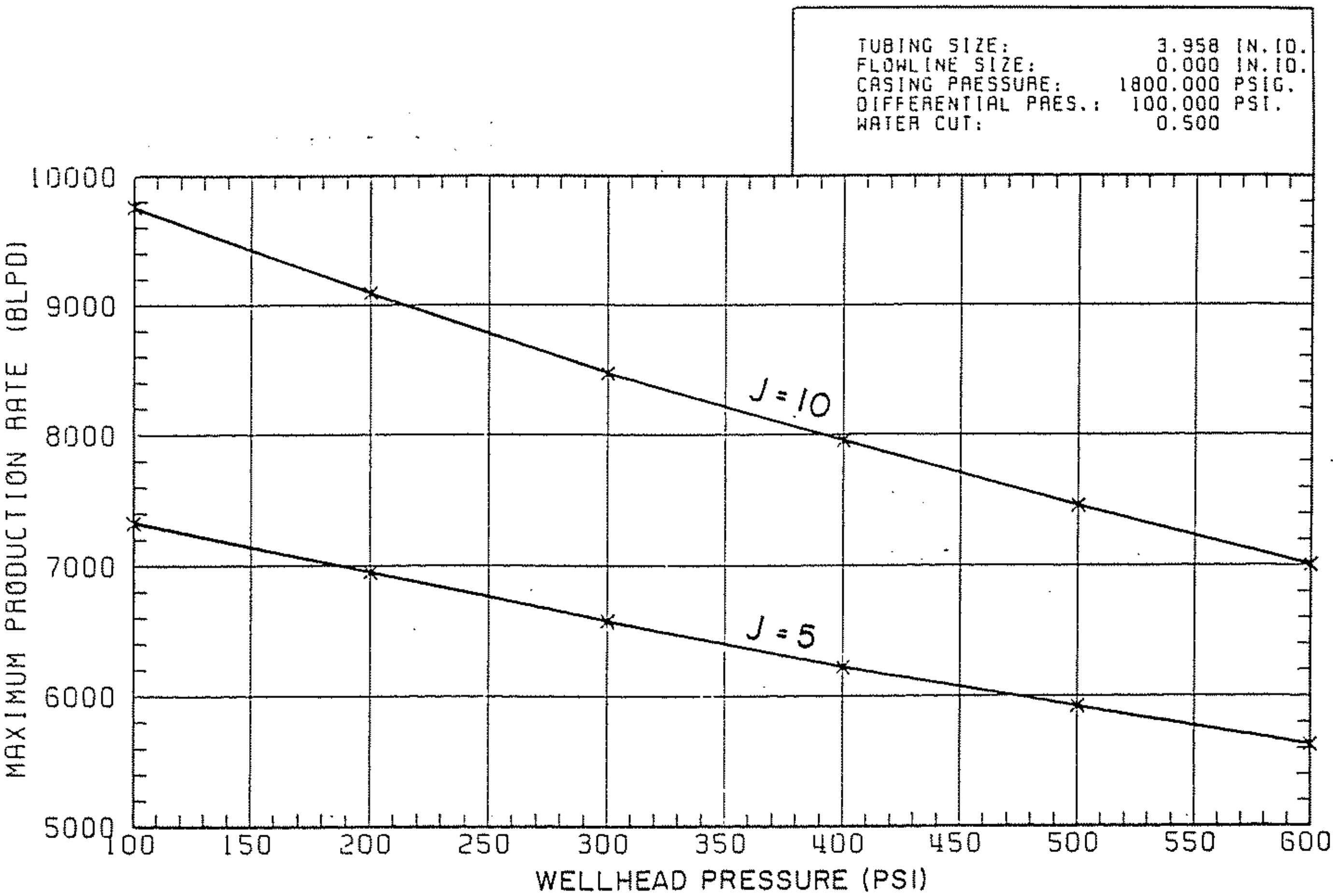

Figure 4.120 Effect of Wellhead Pressure—45° Deviation (Hagedorn)

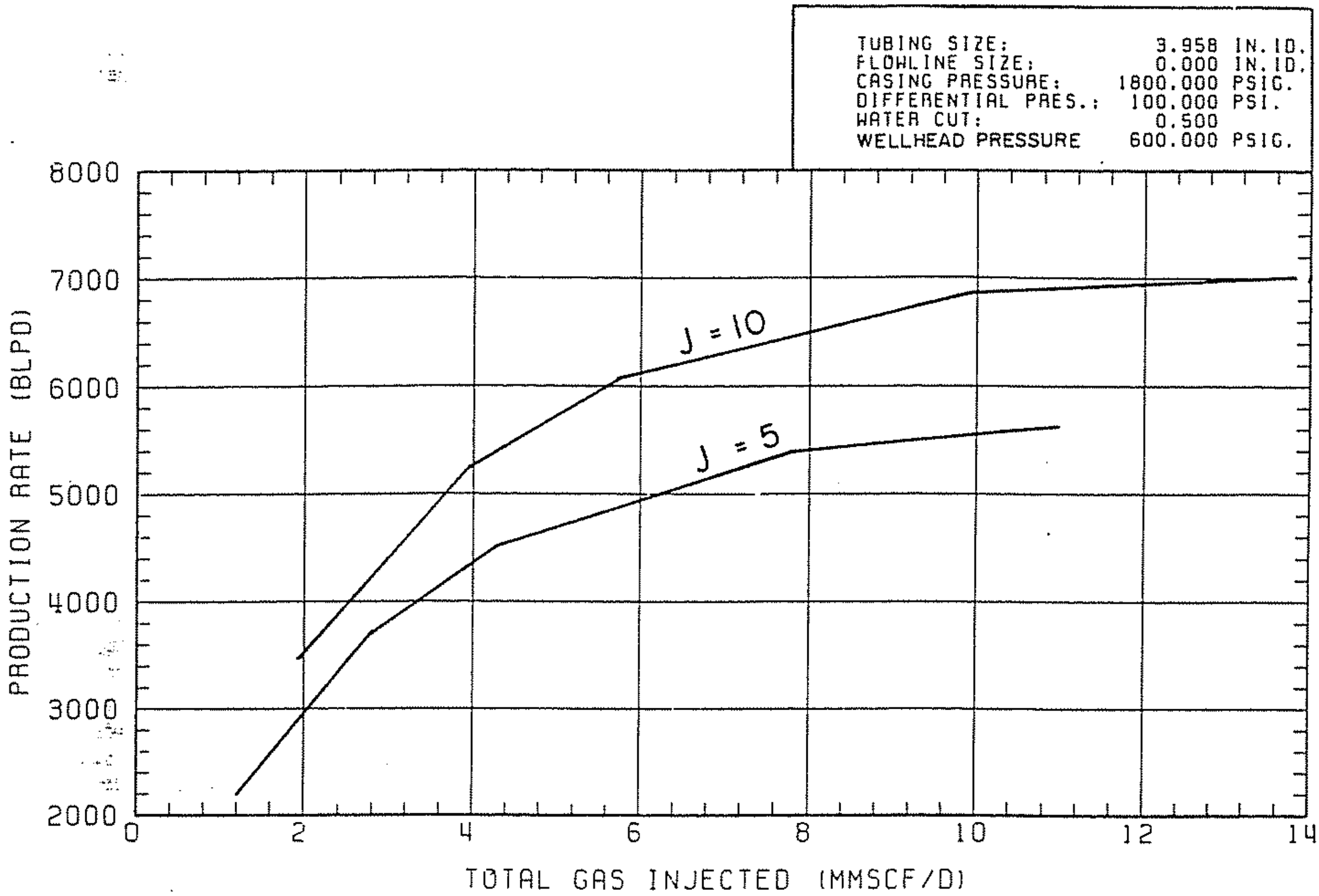

Figure 4.121 Gas-Lift Performance Curves—45° Deviation (Hagedorn)

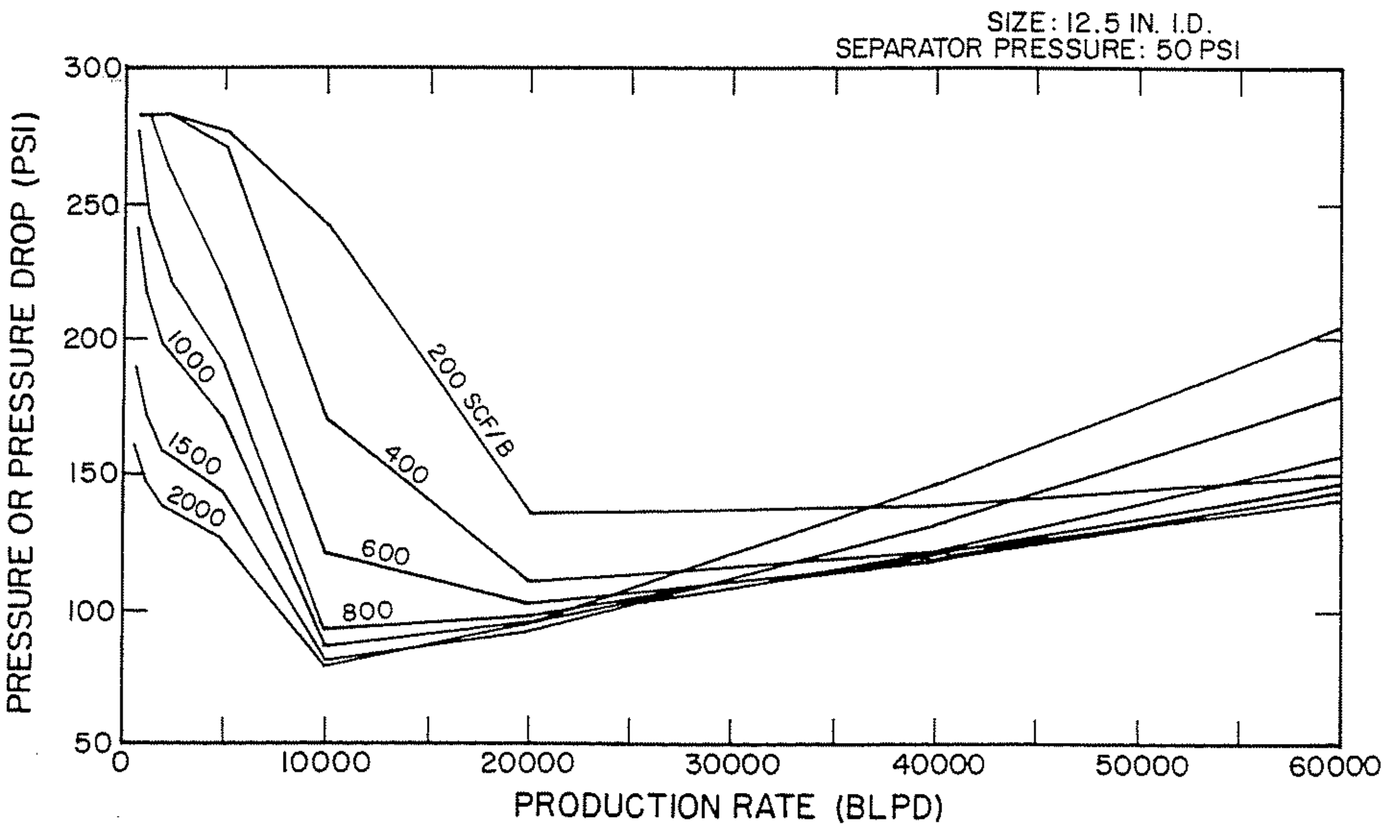

Figure 4.122 Riser Inlet Pressure (Hagedorn) Water Cut, 0

4.824 HORIZONTAL FLOW LINE

The horizontal flow line can also be treated as a separate component by assuming a reasonable exit pressure from observing Figure 4.122, and the exit pressure can be treated as a sensitivity variable. For example, Figure 4.123 shows inlet pressures vs flow rate for an exit pressure of 100 psig and with the gas-liquid ratio as a variable. For example, for a flow rate of 50,000 b/d and a gas-liquid ratio of 1,000 scf/bbl, the inlet pressure to the flow line, which is the manifold pressure, is found to be 900 psig. Other values can be selected for other conditions.

4.825 FLOW LINE FROM THE MANIFOLD TO THE WELLHEAD

The flow line from the manifold to the wellhead can now be evaluated for each well. A typical plot for a manifold pressure of 500 psi is noted in Figure 4.124 for 2,000 ft of flow line. For 5,000 b/d, a 4-in. flow line, and a GLR of 1,000 scf/bbl, p_{wh} is found to be 540 psig. Other manifold pressures can be evaluated.

4.826 FINAL SOLUTION

Now that a good idea has been established as to the design of each component and anticipated rates, the entire system is analyzed as one component to solve for the flow rate and the optimum gas injection volume.

Several things are noted in this system that become critical. For example, the pressure loss in the 12.5-in. horizontal line appears excessive for rates greater than 25,000 b/d and for GLR's in excess of 1,000 b/d. Therefore, larger line sizes should be evaluated. The riser pipe should be as large as the flow line and is also changed accordingly.

A trial-and-error procedure can now be started to obtain the total rate expected from a group of ten wells. A solution position (node) taken at the manifold appears attractive in this case (Figure 4.125).

The following solution procedure is adequate, although other solution procedures can be followed.

4.8261 APPROXIMATE SIMPLE AND DIRECT SOLUTION

The following solution assumes unlimited gas is available and that each producing well will receive the same injection gas-liquid ratio. The error in this solution exists in the assumption that each well will receive the same injection GLR. A more rigorous solution is presented in the next section.

The solution position (node) is to be taken at the manifold (refer to Figure 4.125). (See Chapter 5, gas lift section)

(1) Assume several total flow rates for the total well system such as 10,000, 20,000, 30,000, 40,000, and 50,000 b/d.
(2) Assume several total gas liquid ratios such as 400, 600, 800, 1,000, 1,500, and 2,000 scf/bbl. This includes solution plus injection gas.
(3) Starting from the separator pressure of say 50 psi, determine the manifold pressure for each rate and each GLR by calculating the pressure drop in the riser and in the horizontal flow line. A figure such as Figure 4.126 will result, showing rate vs manifold pressure for each GLR for 50 = psi separator pressure and a 12.5-in. ID line. Figure 4.127

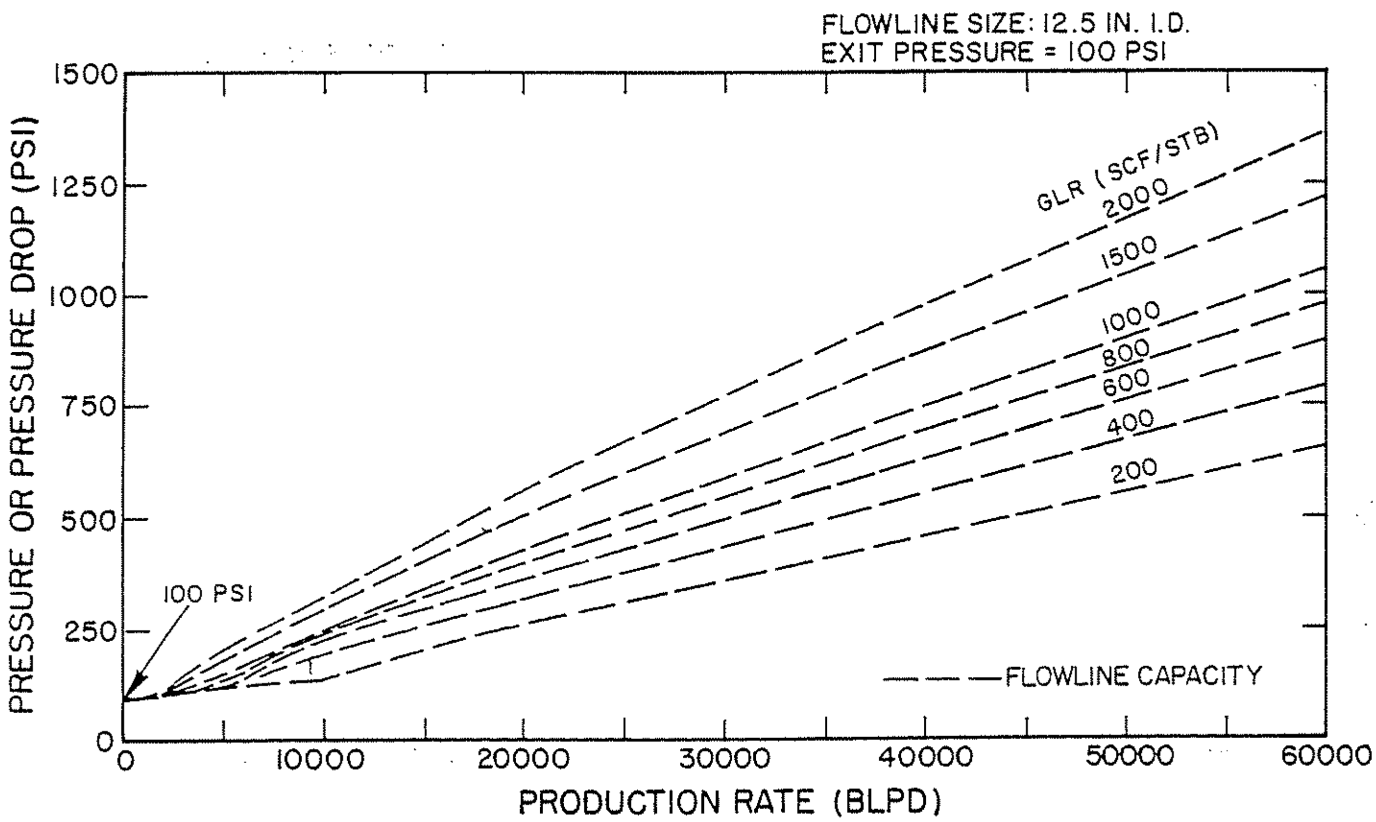

Figure 4.123 Horizontal Flow-Line Inlet Pressures

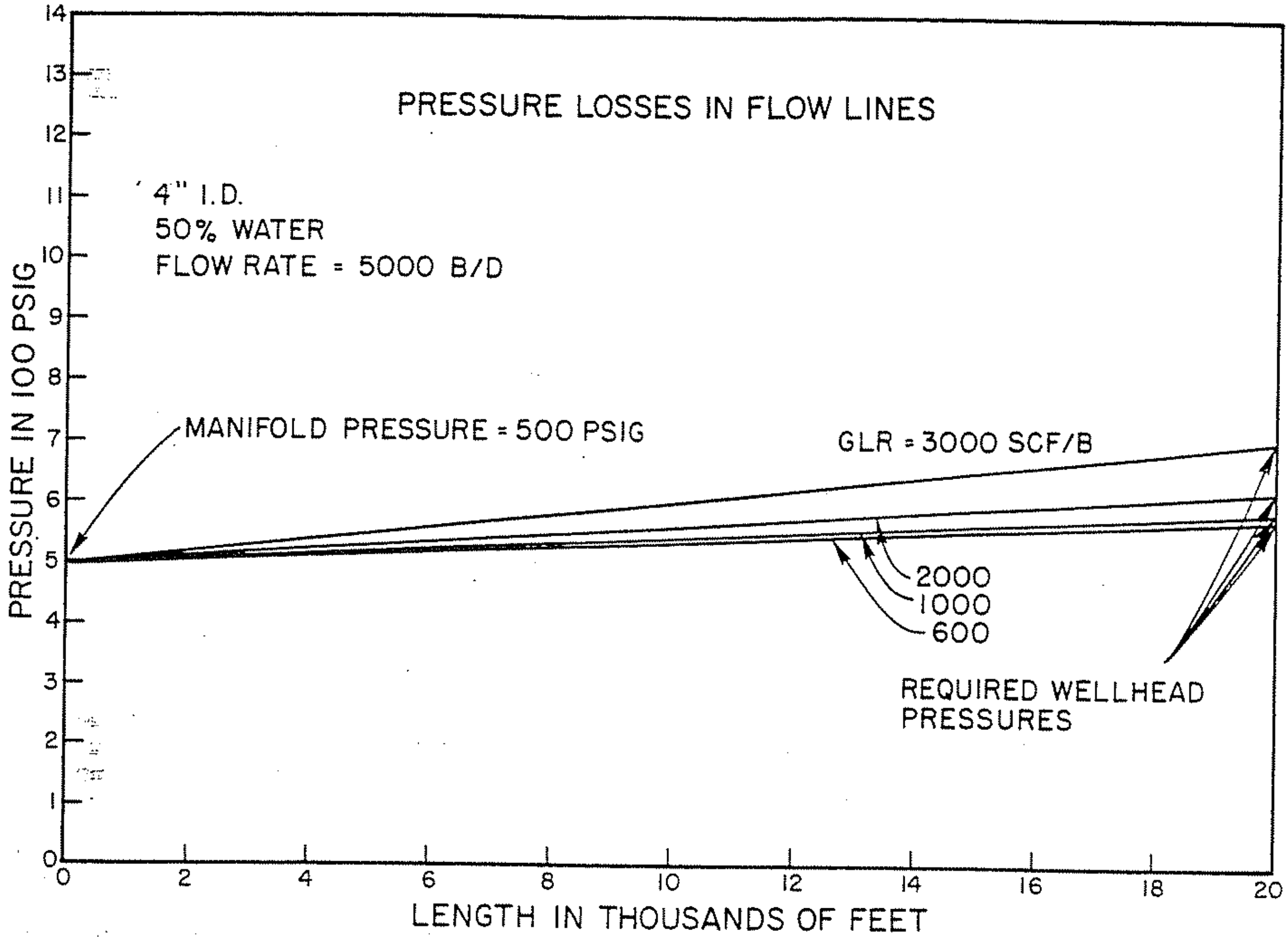

Figure 4.124 Pressure Losses in Flow Lines

shows a 14.5-in. ID line, and Figure 4.128 shows a 12.5-in. and 8-in. line in parallel.

(4) Start now with each individual well and assume several flow rates such as 2,000, 4,000, 6,000, and 8,000 b/d.

(5) Assume several total gas-liquid ratios (injection + solution gas) such as 400, 600, 800, 1,000, 1,500, and 2,000 scf/bbl.

(6) Starting from $\overline{P}_r$ for each well and for one assumed rate such as 2,000 b/d and one assumed total GLR, proceed all the way to the manifold to find the permissible manifold pressure for this rate and GLR.

(7) Repeat step 6 for each rate and for each GLR.

(8) Prepare a plot such as Figure 4.129, which shows

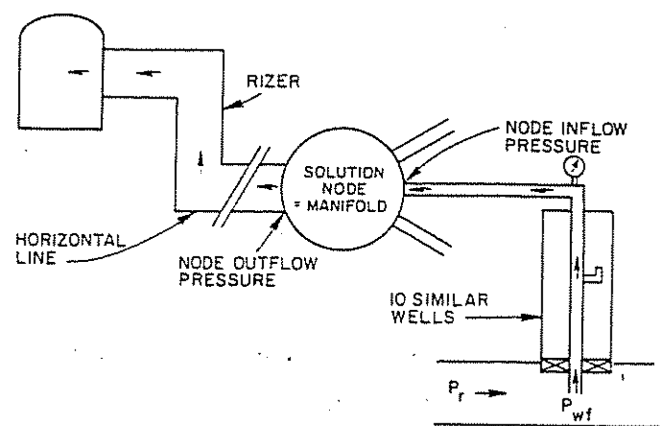

Figure 4.125 Ocean-Floor Completion Node Taken at Manifold

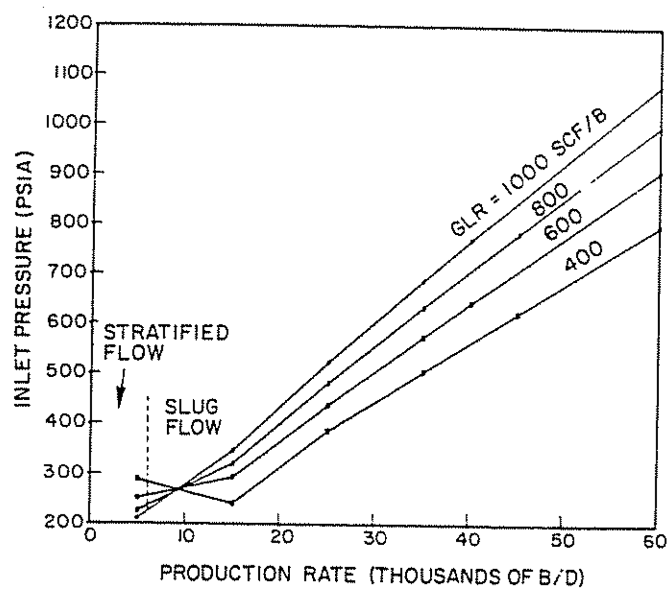

Figure 4.126 Predicted Inlet Pressure vs Production Rate and GLR for a 12.5-in. ID Pipeline Riser Pipe With a Separator Pressure of 50 psig

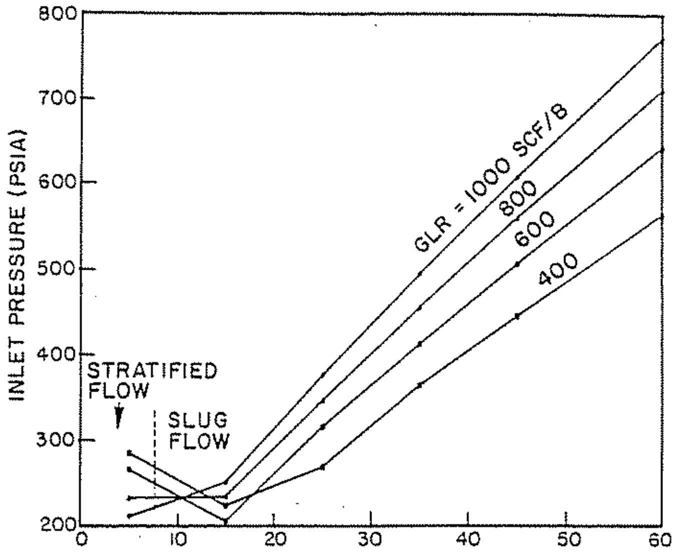

Figure 4.127 Predicted Inlet Pressure vs Production Rate and GLR for a 14.5-in. ID Pipeline Riser Pipe With a Separator Pressure of 50 psig

manifold pressure vs rate for each assumed GLR. Do this for each well.

(9) Assume several manifold pressures such as 300, 400, 600, 800, and 1,000 psi.

(10) For each manifold pressure of step 9, obtain the total field rate from all wells for each assumed GLR.

(11) Plot the total rate vs manifold pressure for each GLR on Figure 4.126, resulting in Figure 4.130. This is not the optimum solution but will give an approximate answer.

4.8262 RIGOROUS SOLUTION

It must be kept in mind that one wellhead pressure and one GLR exists for each well required to obtain

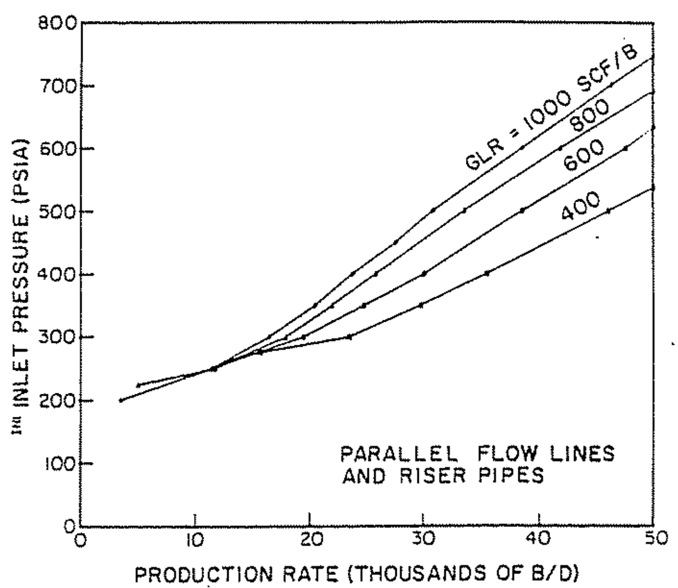

Figure 4.128 Predicted Inlet Pressure vs Production Rate and GLR for 8-and 12.5-in. ID Parallel Lines with a Separator Pressure of 50 psig

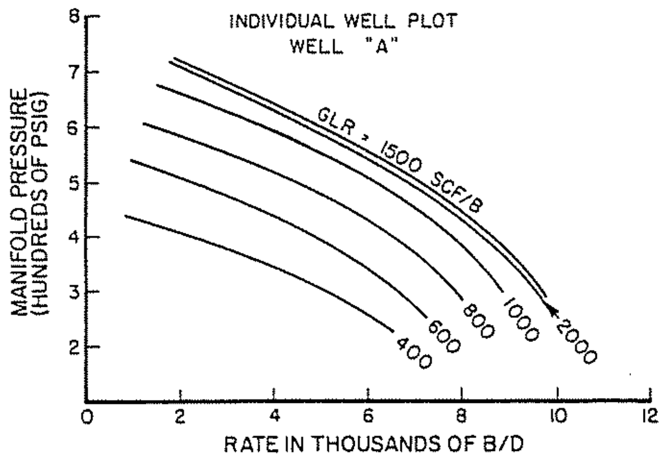

Figure 4.129 Manifold Pressure vs Rate for Each Well

the maximum flow rate from each well. If unlimited gas is available, this is also the optimum rate and GLR for each well.

If limited gas only is available, the gas must be allocated properly to each well in order to maximize the field rate.

(1) *Unlimited gas available.* For the first case, assume that unlimited gas is available.

The gas required to maximize the rate from each well is not necessarily the gas volume required to maximize the rate for the total system. When all gas enters the manifold, a certain manifold pressure is required to move the total rate from all wells to the separator. As noted in Figure 4.126, as the total GLR increases, the manifold pressure increases for each rate. Therefore, the summation of total gas volumes from each well must be optimized against the manifold pressure to move the fluids to the separator for that gas volume. Therefore, an optimum gas volume exists, which is usually less than the gas volume required to maximize the rate from each well.

Therefore, the objective is to find that total gas injection volume to maximize the rate, taking into account the outflow pressure from the manifold, which also depends on rate and GLR.

(2) *Rigorous solution procedure.* The solution node is taken at the manifold as in the previous simple solution. The first three steps are the same as given in the simple solution and are repeated here.

(1) Assume several total flow rates such as 10,000, 20,000, 30,000, 40,000, and 50,000 b/d.

(2) Assume several total GLR's such as 400, 600, 800, 1,000, 1,500, and 2,000 scf/bbl.

(3) Starting from the separator, proceed down the riser and through the horizontal line to find the manifold pressure for each assumed rate and each assumed GLR. Plot as shown in Figure 4.131.

(4) Construct gas-lift performance curves for each well with manifold pressure as a parameter (see Figure 4.132).

(5) Select the maximum rate and the corresponding gas injection rate for each manifold pressure and for each well. This represents the maximum rate possible from each well for each manifold pressure, assuming that the manifold pressure coin-

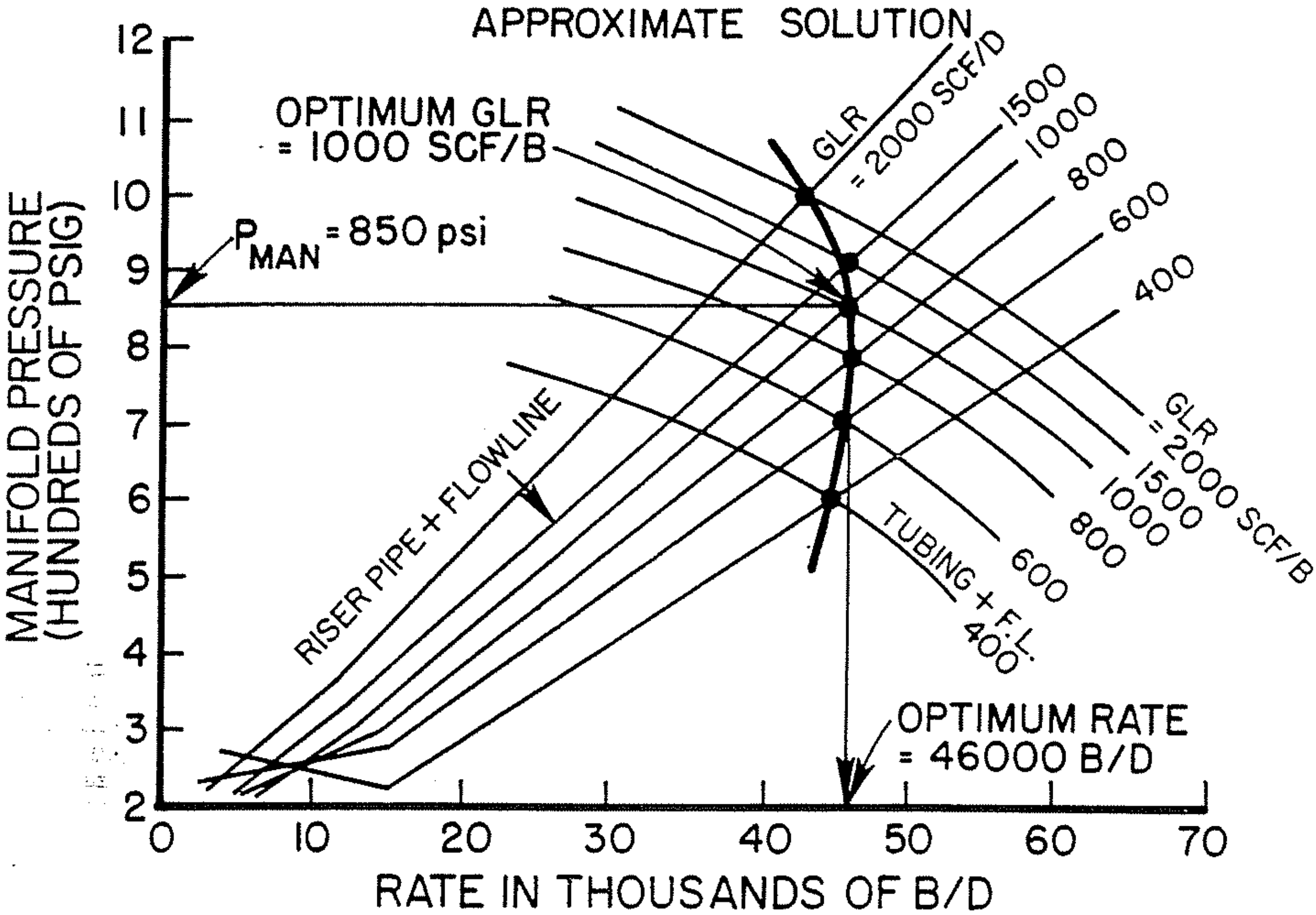

Figure 4.130 Approximate Solution at Manifold

cides with the manifold pressure necessary to move the total rate of gas and liquid to the separator from the manifold.

(6) Total the flow rates and the gas injection rates from each well for each equal manifold pressure. Based on total flow rate, convert the gas injection rate to total GLR's, taking into account solution GLR's from each well to obtain total GLR's. Tabulate this data.

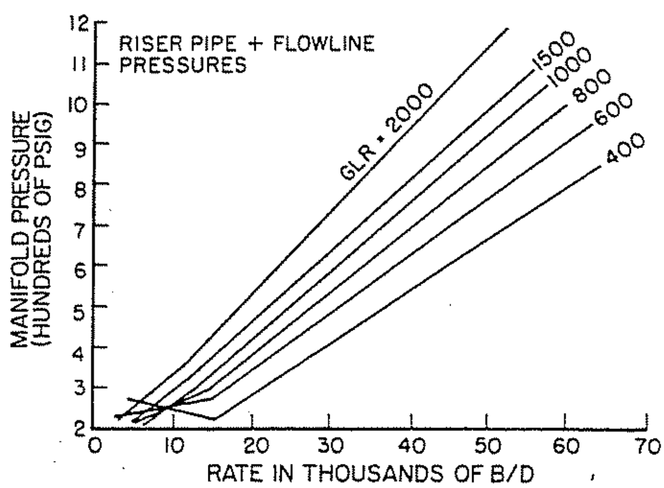

Figure 4.131 Manifold Pressure vs Rates Through Flow Line and Riser Pipe

(7) Start decreasing the amount of total injection gas to the system. This step can be accomplished by starting from the total injection gas needed to maximize total flow rate. Reduce the total injection gas by 5 or 10%. Keep in mind that maximum oil flow rate is the objective. Therefore, the gas-lift performance curves must be used in this case and $\Delta q_o/\Delta q_{inj}$ must be checked for each well and each total allocated injection gas. Some obvious things will occur in this solution. The better wells may retain the required injection gas to maximize their rate, whereas some of the weaker wells may take a high reduction in injection gas.

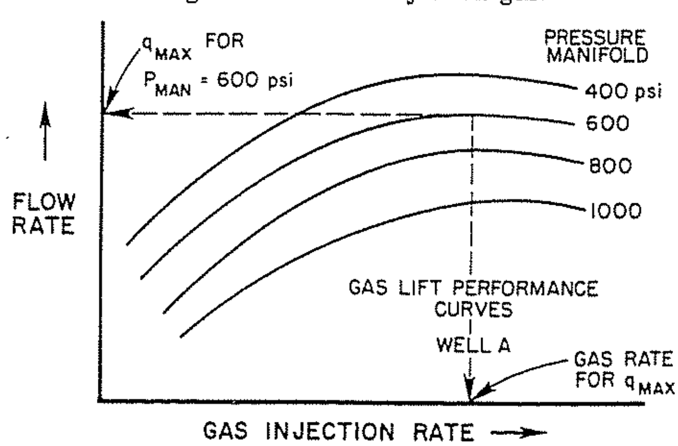

Figure 4.132 Gas-Lift Performance Curves

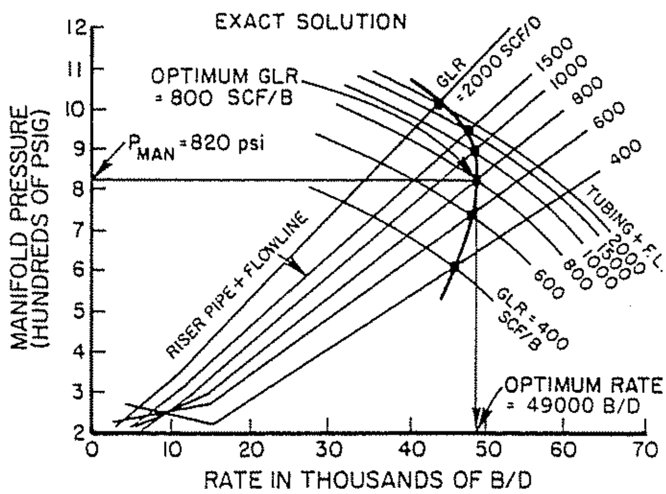

Figure 4.133 Rigorous Solution at Manifold

Finally, maximize the total rate for the assumed total injection gas.

(8) Repeat step 7 to make additional reductions in total injection gas to approximately 50% of the total gas needed for maximum production of the field.

(9) Determine total rates for each case—that is, each manifold pressure, each assumed total gas, and each total GLR.

(10) Plot all points on Figure 4.131, resulting in Figure 4.133, from which the maximum rate can be selected along with the optimum GLR and manifold pressure.

(3) *Slugging and heading caused by vertical riser and long, large diameter flow line.* The previous example showed design based on pressure loss calculations only. It did not account for the flow of slugs of liquid and gas and for the fluctuation in pressure that can be anticipated. However, in field practice this must be properly accounted for so that appropriate large separators and/or slug catchers can be designed in order to permit adequate safety in handling the liquids.

Reference to Chapter 3 shows the appropriate equations. Section 4.7 of Chapter 4 shows various examples and the expected results.

EXAMPLE PROBLEM

Tables 4.56, 4.57 and 4.58 show the results for this example for a 12.5-in. riser and horizontal line. Table 4.56 shows typical results for this problem for a flow rate of 30,000 b/d (all oil) at a gas-liquid ratio of 1,000 scf/bbl. Table 4.56 also shows the flow according to Beggs, Mandane, and Mukherjee with holdup and liquid volumes shown by Beggs, Tuffp and Eaton.

Table 4.57 shows the conditions at the pipeline outlet, with the principal factors of importance being the maximum volume of liquid in a slug unit of 304.78 bbl and the pressure fluctuation of 72.85 psi.

Table 4.58 summarizes all pertinent information for different flow rates and different gas-liquid ratios. Design must be made for the maximum slug sizes expected since one of the maximum slugs will occur frequently.

This portion of the study becomes very important because it gives data that allow for proper design of

TABLE 4.56

CASE 2

Oil flow rate, stb/d =	30,000
Water flow rate, stb/d =	0
Gas flow rate, Mscf/d =	30,000
Gas-liquid ratio, scf/stb =	1,000
Gas gravity, (air = 1) =	0.800
Oil gravity, °API =	32
Upstream temp, °F =	45
Downstream temp, °F =	45
Initial pressure, psia =	64.70
Pipe ID, in. =	12.500

Pressure gradient calculated by Beggs-Brill method

Distance, ft	Pressure, psia	Flow pattern			Holdup (fraction)				Liquid volume, bbl			
		Beggs	Mandane	Mukherjee	No slip	Beggs	Tuffp	Eaton	No slip	Beggs	Tuffp	Eaton
42,840	64.70	intermittent	slug	mist	—	—	—	—	—	—	—	—
42,240	123.78	intermittent	slug	mist	0.037	0.123	0.045	0.117	3.411	11.225	4.082	10.652
38,016	228.34	intermittent	slug	mist	0.071	0.194	0.122	0.204	45.820	124.392	78.309	133.662
33,792	297.81	intermittent	slug	mist	0.110	0.247	0.190	0.277	70.277	158.650	121.386	177.369
29,568	353.35	intermittent	slug	mist	0.138	0.282	0.232	0.322	85.496	180.563	148.792	206.144
25,344	400.86	intermittent	slug	mist	0.162	0.309	0.263	0.355	103.832	198.053	168.886	227.913
21,120	442.96	intermittent	slug	mist	0.183	0.331	0.289	0.383	117.407	212.379	185.155	245.769
16,896	481.10	intermittent	slug	mist	0.202	0.351	0.310	0.407	129.713	224.745	198.907	261.045
12,672	516.12	intermittent	slug	mist	0.221	0.368	0.330	0.429	141.504	236.125	211.542	275.071
8,448	548.67	intermittent	slug	mist	0.237	0.384	0.346	0.448	152.220	246.115	222.091	287.530
4,224	579.21	intermittent	slug	mist	0.253	0.398	0.362	0.466	162.315	255.249	231.803	298.551
0	608.04	intermittent	slug	mist	0.268	0.411	0.375	0.481	171.380	263.678	240.578	303.373

TABLE 4.57

FINAL RESULT
****

Distance, ft	Pressure, psia	Flow pattern: Beggs	Flow pattern: Mandane	Flow pattern: Mukherjee	Holdup (fraction): No slip	Holdup (fraction): Beggs	Holdup (fraction): Tuffp	Holdup (fraction): Eaton	Liquid volume, bbl: No slip	Liquid volume, bbl: Beggs	Liquid volume, bbl: Tuffp	Liquid volume, bbl: Eaton
0	608.04	Intermittent	Slug	MIST	0.268	0.411	0.375	0.481	171.880	263.675	240.678	303.573
		Total liquid volume in pipeline, bbl							1,186.574	2,111.482	1,811.929	2,423.181
		The final calculated pressure, psia							608.04			

Conditions at Pipeline Outlet for Slug Flow

	Average slug unit	Maximum slug unit
Liquid slug length, L_s, ft	487.49	2,652.52
Gas bubble length, L_b, ft	2,157.19	11,737.73
Liquid slug residence time, T_s, sec	12.05	65.58
Gas bubble residence time, T_b, sec	53.34	290.21
Gas bubble velocity, v_{bf}, ft/sec	40.45	40.45
Liquid film velocity, v_f, ft/sec	0	0
Gas velocity, v_g, ft/sec	35.29	35.29
Liquid holdup, H_L	0.1221	0.1221
Liquid holdup in liquid slug, H_{Ls}	0.4118	0.4118
Liquid holdup in gas bubble, H_{Lb}	0.0870	0.0780
Volume of liquid produced during $T_s + T_b$, V_{Lp}, bbl	22.95	124.88
Volume of liquid produced from the liquid slug, V_{Lsp}, bbl	22.95	124.58
Volume of liquid produced from the liquid film, V_{Lfp}, bbl	0	0
Volume of liquid in liquid slug in pipeline, V_{Ls}, bbl	30.47	165.80
Volume of liquid in a slug unit in pipeline, V_{LT}, bbl	56.01	304.78
Superficial gas velocity, v_{sg}, ft/sec	30.044	
Superficial liquid velocity, v_{sL}, ft/sec	2.312	
Gas velocity number, N_{gv}	69.223	
Liquid velocity number, N_{Lv}	5.328	
The expected pressure fluctuations at the bottom of the riser pipe are psi	72.85	

separators and slug catchers in order to prevent any overflow of oil or liquid. It also shows the pressure fluctuation expected, and this fluctuation will influence the selection of gas-lift valves and control equipment.

4.9 APPLYING PRODUCTION OPTIMIZATION TO A COMPLETE FIELD-INTEGRATED OIL-PRODUCTION SYSTEM K, BY A. PAUL SZILAS*

4.91 INTRODUCTION

It is generally accepted and seems to be obvious to every petroleum engineer that the oil- and gas-bearing subsurface reservoir can be considered a system from both a material and a hydraulic point of view. This concept is used very effectively by reservoir engineers in everyday practice, calculating, for example, the ultimate oil recovery under the assumption of various recovery methods. This system planning terminates, in most of the cases, at the bottom of the wells, which means the number, places, and sometimes production forecast of the wells are fixed, but generally, the reservoir engineering project does not include technical or economic data referring to the well and surface production equipment. The selection and operation program of this equipment is quite loosely bound to the reservoir engineering project and mostly consists of a series of isolated problem solutions.

* Previously published in *Oil & Gas Journal.*

It is easy to see, however, that the reservoir engineering project can employ different kinds and combinations of surface and subsurface equipment. One of these technically possible configurations is economically the best—the optimum solution. For its implementation, it is necessary to apply system considerations not only to reservoir recovery planning but also to production-equipment planning.

4.92 THE CONCEPT OF THE FIELD-INTEGRATED OIL-PRODUCTION SYSTEM (FIOPS)

No system exists that can not be influenced by some other system, whether natural or manmade. In the strict sense of the word, there is no absolutely independent system. We can select, however, a configuration of elements to create a system such that its dependence on other elements or other systems is either unambiguously determinable or negligible. What guidelines can help us determine the range of a group of system-creating elements?

Let us suppose we have two relatively small technical systems. The operational characteristics of both of them can be optimized. The result is, compared to a non-optimized "customary" solution, an economical gain. By unifying the two systems in consideration, we receive a new, larger, generally more complex system. The common operation of the two original systems

TABLE 4.58
DATA SUMMARY FOR THE 12.5-IN. DIAMETER PIPELINE, SEPARATOR PRESSURE = 50 PSIG

Case	Q_o, stb/d	Q_w, stb/d	GLR, scf/stb	Inlet pressure, psia	Pipeline pressure fluctuations, psi	Average produced slug volume, bbl	Average slug production time, sec	Average produced film volume, bbl	Average film production time, sec	Average slug frequency, 1/sec	Maximum produced slug volume, bbl	Maximum slug production time, sec	Maximum produced film volume, bbl	Maximum film production time, sec
1	30,000	0	600	508	96	31.24	17	1.65	77	0.0106	169.97	95	8.99	416
2	30,000	0	1,000	608	73	22.95	12	0	53	0.0154	124.88	66	0	290
3	30,000	0	1,500	712	58	16.27	9	0	37	0.0217	88.51	51	0	201
4	40,000	0	600	644	86	28.29	15	1.59	48	0.0159	153.91	84	8.66	263
5	40,000	0	1,000	771	65	21.04	11	0	34	0.0222	114.48	60	0	184
6	40,000	0	1,500	902	53	15.82	9	0	25	0.0294	86.10	48	0	135
7	60,000	0	600	911	72	24.19	14	1.47	23	0.0270	131.61	74	7.99	123
8	60,000	0	1,000	1,084	56	18.96	10	0	16	0.0385	103.14	55	0	90
9A	60,000	0	1,500	1,259	46	15.19	8	0	13	0.0476	82.65	45	0	70
19	15,000	15,000	600	490	105	30.76	17	1.41	75	0.0109	167.37	92	7.65	410
20	15,000	15,000	1,000	586	80	22.12	12	0	52	0.0156	120.35	64	0	282
21	15,000	15,000	1,500	686	62	15.37	9	0	35	0.0227	83.62	49	0	191
22	20,000	20,000	600	625	94	27.63	15	1.26	47	0.0161	150.32	81	6.88	257
23	20,000	20,000	1,000	747	71	20.05	11	0	32	0.0233	109.08	57	0	177
24	20,000	20,000	1,500	874	57	14.96	8	0	24	0.0313	81.38	46	0	128
25	30,000	30,000	600	892	78	23.38	13	1.12	22	0.0286	127.24	71	6.07	120
26	30,000	30,000	1,000	1,059	60	18.05	10	0	16	0.0385	98.19	53	0	87
27A	30,000	30,000	1,500	1,228	50	14.47	8	0	13	0.0476	78.72	43	0	69

(subsystems) can produce new characteristic properties and, therefore, new possibilities for a higher level of optimization. This system-enlarging procedure is synergistic if the economic gain obtained by the optimization of the enlarged system is greater than the sum of the gains of the two subsystems optimized separately. The possibility of a higher profit has to stimulate us to model larger and larger systems and to study their characteristics, the methods of optimization, and the attainable gain. The steps that should be followed are:

(1) determination of the target
(2) selection and numerical simulation of the components of the system
(3) analysis of the system
(4) synthesis and optimization of the whole system

4.93 DETERMINATION OF THE TARGET

The basis of a field-integrated oil-production system (FIOPS) must be the reservoir-engineering project containing the number, place, and production forecast of the wells. The FIOPS obtains the most economical and best technical solution of the project. In most cases, a number of reservoir-engineering projects can be developed according to various applicable recovery methods that give different ultimate recoveries. All of them must join an optimum production project, giving a perfect technical solution with minimum production costs. One of these singular optimum solutions will be the overall optimum and should be implemented.

The exact FIOPS planning assumes a reliable reservoir engineering forecast based on information about the static and dynamic characteristics of the reservoir. In the beginning period of field production, only a limited number of data are available, causing uncertainty in forecasting. In the course of production life, the amount of information is continuously increasing. We have to adjust to this reality and develop a means:

(1) to determine the final date of flowing production
(2) to model the operation of different production methods
(3) to evaluate the production spoke. (We call this fundamental subsystem a production spoke because it is a more or less radial element of a roughly circular oil- and gas-gathering area consisting of the series-connected reservoir area, well, flow line, and separator.)
(4) to calculate production costs related to a fixed-date planning method that will permit periodic corrections. This could happen yearly, for example. With the new information, we can improve the production project optimization by readjusting the parts of the project that are not fixed.

4.94 SELECTION OF THE COMPONENTS OF THE SYSTEM

Figure 4.134 is a schematic representation of the components of the FIOPS and the relation between them. In vertex 1 of the tetrahedron, it is assumed that m different reservoir engineering projects exist. At vertex 2, we have to determine the technically suitable and economically best production method and to order the application of the appropriate equipment.

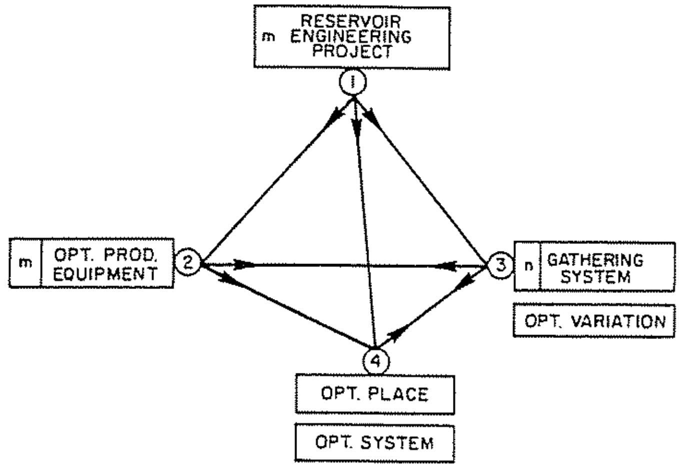

Figure 4.134 Schematic Representation of Various Components

At vertex 3, we assume n different gathering system types (e.g., open or closed types, hand-operated or automated). At vertex 4, we have to determine the optimum number and place of the gathering stations and the optimum locations of the flow lines and transport lines. The arrows represent the influence of one vertex on the others. It is easy to see that, in this assumption, vertices 2, 3, and 4 have no feedback to vertex 1, whereas a mutual influence exists between vertices 2–3 and 3–4. An iterative process in planning is, therefore, necessary.

For simplicity, it is assumed but not separately symbolized, that the reservoir-engineering project contains the equipment of secondary and tertiary recovery, too, if they are available.

The FIOPS is also influenced from other "outer" systems and factors (see Figure 4.135). Some of these are technical equipment or systems and can be assumed as enlarged parts of our FIOPS (e.g., transport of oil and gas and oil and gas processing). Some of the influencing factors are prescriptions (e.g. for safety or environmental protection) or can be given constraints (available hardware and software; the possibility of using other energy sources; and import oil and gas prices), but the economical influence is more or less numerically definable. There are also political and national economic factors with instant or long-term influence on these economic considerations.

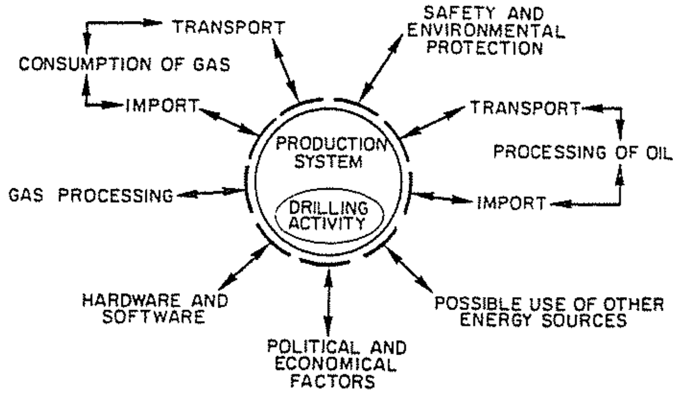

Figure 4.135 Outer Systems and Factors

Some parts of the production system for which the optimum solution is not influenced by the other components of the system can exist. We see in the FIOPS circle an oval area: this is the symbol of the drilling activity. It seems obvious that, for a given well size, the less the initial investment, the higher the savings in the implementation of FIOPS. This is the reason that this component is symbolized differently from the other influencing factors—systems.

4.95 NUMERICAL SIMULATION OF THE SUBSYSTEMS

At vertex 2, we have to choose the technically feasible well-production methods and calculate their production costs. For this target, we must have reliable numerical methods.

These preparatory problems are practically solved by a number of researchers. At Tulsa University, Professor Brown and his co-workers have made a very important contribution to the development of multiphase pressure-drop calculations valid in vertical, horizontal, and inclined pipes and to the development of production optimization analysis methods for numerical simulation of the production spoke. My co-worker and I have been dealing for some time with these problems, too. These methods describe the flow behavior of a one-well system and assume time-invariant inflow parameters. For determination of the vertex 2 problem, it is necessary to take into account the time variable production characteristics of the wells and the fact that there are a group of wells in a gathering area having different flow characteristics and that they influence each other.

In Figure 4.136, well-production data (q_o, daily rate of flow; R, gas-oil ratio; P_{wf}, flowing bottom-hole pressure; and P_{wh}, flowing wellhead pressure) are represented as a function of production life given by the reservoir-engineering project. Taking into account these data curves, K and K_{cum} in Figure 4.137 show the production costs as a function of production life for two different production methods (K is the yearly production cost, and K_{cum}, the cumulated production cost from the start of artificial lifting). It is assumed that both of the artificial lifting methods are capable of producing the prescribed daily production rate during the whole production life. We can see the yearly (specific) production costs of method I before date t_a. Thereafter, the same costs for method II, are less. The K_{cum} curves show us that method II gives smaller overall production costs related to the whole production life of the well.

Figure 4.138 represents the schedule of singular equipment for production method I and II mentioned before (denoted for simplicity purposes without M only) for a thirteen-well oil field. It is assumed that the inflow forecast data are given in Figure 4.136 for all the wells. The wells are scheduled according to the start of production. The start-date points are connected by the t_o curve. The t_a line connects the terminal points of flowing production or, in other words, the start points of artificial lifting. We will assume the use of both methods I and II. M-I is used from t_a until t_b and M-II from t_b until the end of the production life, t_c. If M-I equipment is a beam type of sucker-rod pump, the working life of the equipment can be much longer than the time period t_a-t_b belonging to one well. Therefore, the equipment must be moved from the well when time t_b is reached to another well in the (t_a-t_b) time period, that needs pumping equipment for artificial lift; that is, M-I_1 equipment (denoted in Figure 4.138 by I_1) is to be moved to well 7 and will work on this well further as equipment $I_{1.7}$.

Some corrections are visible regarding the moving time. Sometimes, the M-I equipment should not be moved exactly on the t_b date of the well and then only if another well has a justifiable demand. Let us assume that M-II equipment is for intermittent gas lift. The working life of this equipment is relatively short. Between t_b and t_c, therefore, sometimes more M-II equipment is needed. The data of the forecasted changes are signed by ch.

Such a schedule should not be assumed as a rigidly fixed order. This is a forecast only. By the aid of this forecast we can determine:

(1) the technically feasible and economically optimum production equipment
(2) the overall production costs
(3) the number, application order, and first cost demand of the required production equipment

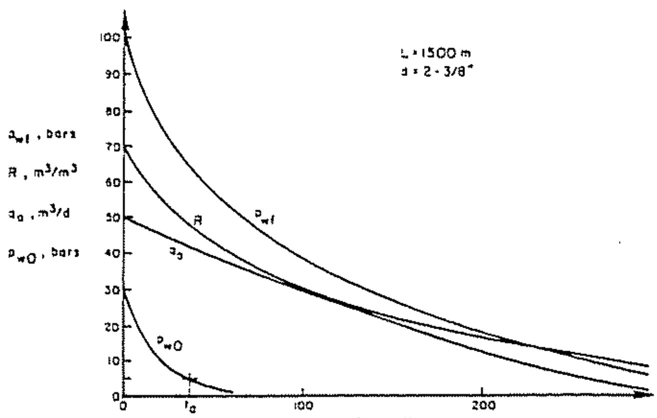

Figure 4.136 Production Data vs Time

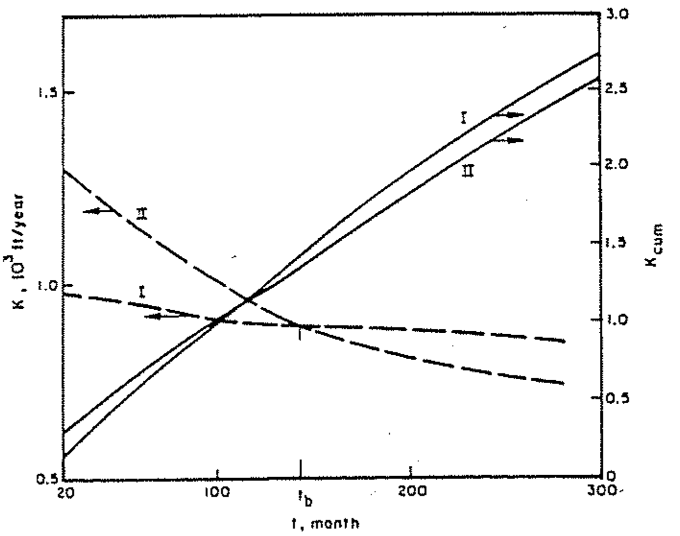

Figure 4.137 Costs vs Production Life

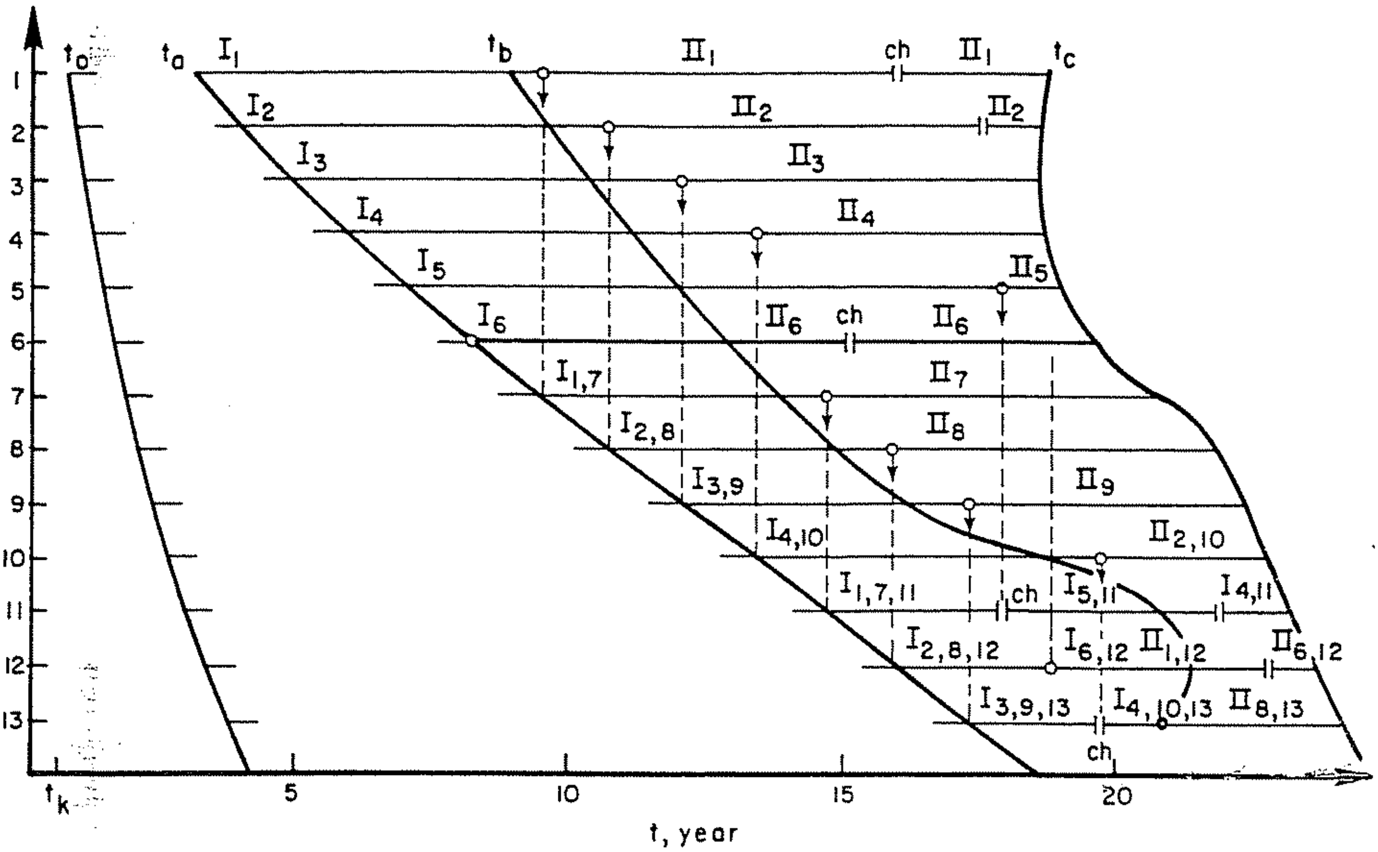

Figure 4.138 Schedule of Equipment

This optimization method was adopted for a new Hungarian 132 well oil field. All reservoir engineering projections were conducted first. Technically, both sucker rod-pumping and gas lifting were feasible to produce the required daily rates. The analysis has shown that overall production costs will be about $5 million less if gas lift is used instead of sucker-rod pumping. The optimum equipment and operational characteristics were chosen to give the minimum production costs within a method.

At vertex 3, different types of gathering systems and different operating characteristics (e.g. separator pressures) have to be assumed, and the common operation with different assumed production methods (vertex 2) should be technically and economically evaluated. The elaboration of a suitable calculation method is in progress.

At vertex 4, our task is to determine the optimum number and place of the well gathering stations, the optimum place of the main tank farm and LACT equipment, and the optimum trace of all flow lines and transport lines. The first step is to devise a planning method by which we can determine the optimum trace of a line between two given points, taking into account all the important characteristics of the surface area (type of soil, vegetation, prohibited territories, roads, rivers, etc.). Then, the investment cost of some existing long pipelines is compared with that of the optimum trace pipelines between the same two limiting points. The saving in first cost is 1.7–7.6% if the optimum trace pipelines are used. This method, which is based on dynamic programming, has been systematically used since 1980.

We have devised, thereafter, a computerized planning method for determining the gathering system with minimum investment. A considerable amount of information is needed for planning: the coordinates of the wells, the characteristics of the oil-field surface territory with respect to specific line-laying costs, prescriptions for lines (e.g. allowed maximum lengths of flow lines, pipe diameters, specific costs of the lines), and costs of gathering stations with respect to the number of hooked wells. We have compared the investment cost of the gathering system of an existing Hungarian oil field with the optimized system. The difference was about 30%. Figure 4.139 represents an example optimized gathering system map.

We should take into account, of course, that in most of the cases the amount of information about the future oil field is limited. Therefore, data for a totally perfect plan are not available. It is believed, however, that the savings, based on incomplete initial data, which are corrected automatically year to year, can be significant.

4.96 THE ANALYSIS AND THE OPTIMIZATION OF THE SYSTEM

The fundamental basis of the FIOPS system is the reservoir engineering project. We should achieve this with a minimum overall investment cost, taking into account the other influencing circumstances. The plan-

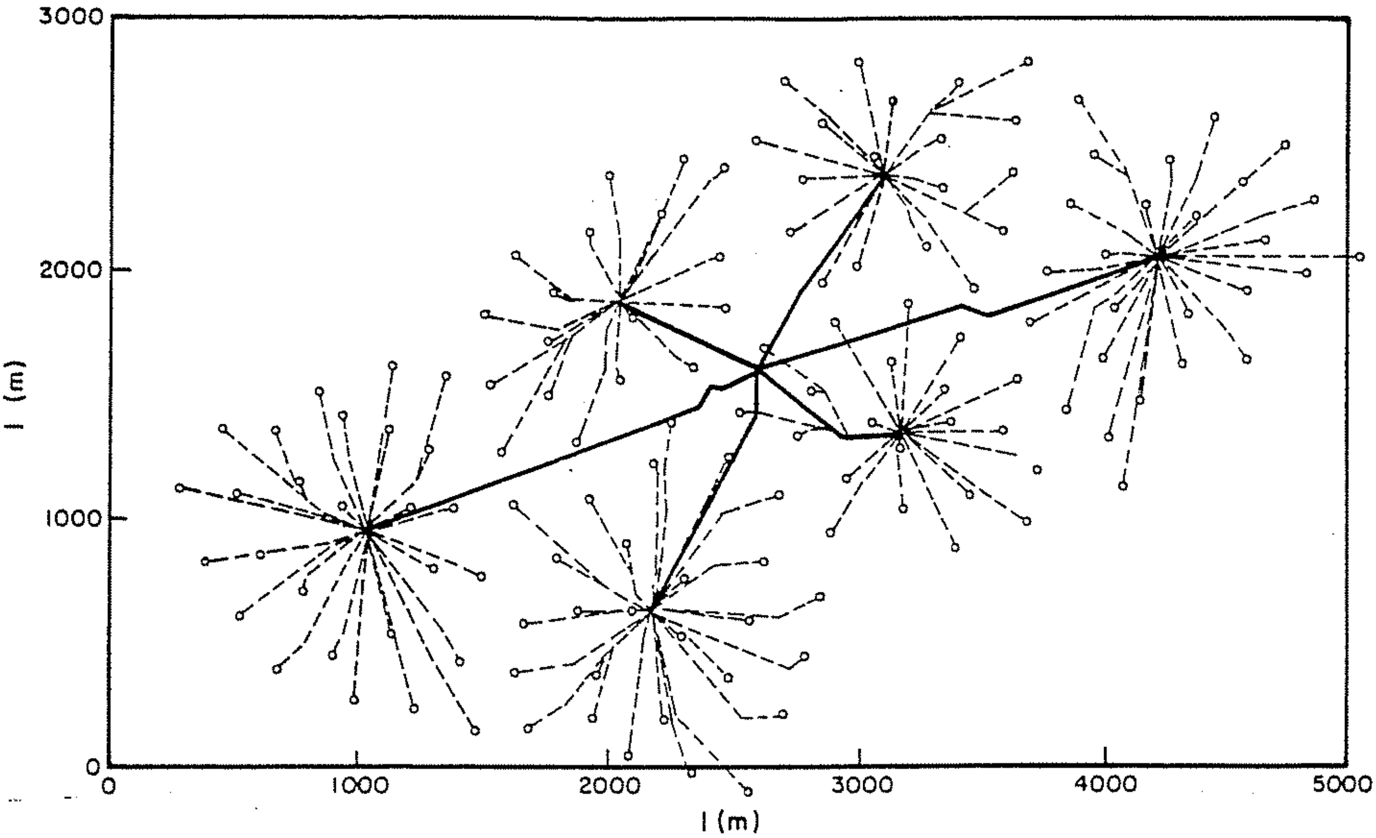

Figure 4.139 Optimized Gathering System Map

ning with respect to investments and operative conditions should be flexible, giving a possible systematic improvement.

The target of optimization of subsystem 2 is to select and schedule production equipment, giving a minimum overall production cost. The target of the optimization of subsystem 4 is to construct a gathering system with minimum first costs.

The next problems to be solved are a suitable planning method for vertex 3 and optimizing the common operation of all the vertices of the tetrahedron.

The FIOPS is, to a certain extent, a reality. It is a planning method for oil-production subsystems. It may be regarded, on the other hand, as the start of a new planning idea that should be developed by the aid of considerable additional work by many researchers.

REFERENCES

1. Mach, Joe, Eduardo Proaño, and Kermit E. Brown. "A Nodal Approach for Applying Systems Analysis to the Flowing and Artificial Lift Oil or Gas Well." *SPE 8025.*
2. Brown, Kermit E. and H. D. Beggs. *Technology of Artificial Lift Methods.* Vol. 1. Tulsa, Oklahoma: PennWell Books, 1980.
3. Gilbert, W. E. "Flowing and Gas-Lift Well Performance." *API Drilling and Production Practice* (1943), 143.
4. Mach, Joe, Eduardo Proaño, and Kermit E. Brown. "Application of Production Systems Analysis to the Design of Subsurface Closed Safety Valves (SSCSV)." *SPE 8730.*
5. Beggs, H. D. et al. "Design Criteria for Selecting Velocity Type Subsurface Safety Valves." *ASME-80-Pet-52.* New Orleans, Louisiana, February 1980.
6. *API 14B Subsurface Controlled Subsurface Safety Valve Sizing Computer Program. API Manual 14BM.* 1st ed., Section B4. June 1974.
7. Ashford, F. E. and P. E. Pierce. "Determining Multipurpose Pressure Drops and Flow Capacities in Down-Hole Safety Valves." *Transactions of the AIME* (1975), 1145.
8. Fortunati, F. "Two-Phase Flow Through Wellhead Chokes." *SPE 3472.* SPE of AIME, May 16–18, 1972.
9. Proaño, E. A. "Experimental Study of Two-Phase Flow Through Otis J Valve Chokes." M.S. Thesis, The University of Tulsa, 1976.
10. Roman-Lazo, C. E. "Experimental Study of Two-Phase Flow Through Camco A-3 Valve Chokes." M.S. Thesis, The University of Tulsa, 1976.
11. Jones, Loyd G., E. M. Blount, and C. E. Glaze. "Use of Short Term Multiple Rate Flow Tests to Predict Performance of Wells Having Turbulence." *SPE 6133.* SPE of AIME, October 3–6, 1976.
12. Saucier, R. J. "Gravel Pack Design Considerations." *SPE 4030.* SPE of AIME, October 8–11, 1972.
13. Coberly, C. J. *Selection of Screen Openings for Unconsolidated Sands. API Drilling and Production Practice* (1937).
14. Crouch, E. C. and K. J. Pack. "Systems Analysis Use for the Design and Evaluation of High-Rate Gas Wells." *SPE 9424.* SPE of AIME, September 21–24, 1980.
15. Zwolle, Simon and David R. Davies. "Gravel Packing Sand Quality—A Quantitative Study." *Journal of Petroleum Technology* (June 1983).
16. Boulet, P. D. "Gravel for Sand Control: A Study of Quality Control." *Journal of Petroleum Technology* (February 1979), 164–68.
17. Sparlin, D. D. "Sand and Gravel—A Study of Their Permeabilities." *SPE 4772.* SPE of AIME, February 7–8, 1974.
18. Rittenhouse, G. "A Visual Method of Estimating Two-Dimensional Spericity." *Journal of Sedimentary Petroleum,* 13 (1943), 79–81.
19. Krumbein, W. C. and L. L. Sloss. *Stratigraphy and Sedimentation.* Freeman and Co., 1953.
20. McLeod, Harry O. Jr. "The Effect of Perforating Conditions on Well Performance." *Journal of Petroleum Technology* (January 1983).
21. Vohra, I. R., N. Marcano, and J. P. Brill. "Comparison of Liquid Holdup Correlations for Gas-Liquid Flow in Horizontal Pipes." *SPE 4690.* SPE of AIME, October, 1973.
22. Eaton, B. A. et al. "The Prediction of Flow Patterns, Liquid Holdup and Pressure Losses Occurring During Continuous Two-Phase Flow in Horizontal Pipelines." Transactions of the AIME (1967), 815.

23. Beggs, H. D. and J. P. Brill. "A Study of Two-Phase Flow in Inclined Pipes." *Transactions of the AIME* (1973), 607.
24. Dukler, A. E. et al. "Gas-Liquid Flow in Pipelines." *Research Results*. Vol. 1. AGA-API Project NX-28, May 1969.
25. Gould, T. L. and E. L. Ramsey. "Design of Offshore Gas Pipelines Accounting for Two-Phase Flow." *SPE 4844*. SPE of AIME, May 1974.
26. Cunlife, R. S. "Prediction of Condensate Flow Rates in Large Diameter High Pressure Wet Gas Pipelines." *APEA Journal* (1978), 171.
27. Carterville, T. et al. "Two-Phase Flow Key to Offshore Line Design." *Oil and Gas Journal* (August 10, 1981), 71–75.
28. Flanigan, O. "Effect of Uphill Flow on Pressure Drop in Design of Two-Phase Gathering Systems." *Oil and Gas Journal*, 56 (March 10, 1958), 132.
29. Gilbert, W. E. "Flowing and Gas-Lift Well Performance." *API Drilling and Production Practice* (1954), 126.
30. Ashford, F. E. and P. E. Pierce. "The Determination of Multiphase Pressure Drops and Flow Capacities in Down-Hole Safety Valves (Storm Chokes)." *SPE 5161*. SPE of AIME, October 1974.
31. Usdin, E. and J. C. McAuliffe. "A One Parameter Family of Equations of State." *Chemical Engineering Science* (1976), 1077–1084.
32. Canfield, F. B. "Estimate K-Values With the Computer." *Hydro. Proceedings*, 50 (April 1971), 137–138.
33. Hubbard, M. G. "An Analysis of Horizontal Gas-Liquid Slug Flow." Ph.D. Dissertation, University of Houston, 1965.
34. Brill, J. P. et al. "Analysis of Two-Phase Tests in Large Diameter Prudhoe Bay Field Flowlines." *SPE 8305*. SPE of AIME, September 1979.
35. Standing, M. B. "A General Pressure-Volume-Temperature Correlation—For Mixtures of California Oils and Greases." *API Drilling and Production Practice* (1947), 275.
36. Vasquez, A. M. E. and H. D. Beggs. "Correlations for Fluid Physical Property Predictions." *SPE 6719*. SPE of AIME, October 9–12, 1977.
37. Keenan, J. H. and F. G. Keyes. *Thermodynamic Properties of Steam*. New York, New York: John Wiley & Sons Inc., 1936.
38. Culbertson, O. L. and J. J. McKetta. "Solubility of Methane in Water at Pressures to 10,000 psia." *Transactions of the AIME* (1951), 223.
39. Lasater, J. A. "Bubble Point Pressure Correlation." *Transactions of the AIME* (1958), 379.
40. Lee, A. L. et al. "The Viscosity of Natural Gases." *Transactions of the AIME* (1966), 997.
41. Beggs, H. D. and J. R. Robinson. "Estimating the Viscosity of Crude Oil Systems." *Journal of Petroleum Technology* (September 1975), 1140.
42. Van Wingen. *Secondary Recovery of Oil in the United States*. API, 1950, p. 127.
43. Yarborough, L. and K. R. Hall. "How to Solve Equation of State for Z-Factors." *Oil and Gas Journal* (February 18, 1974), 86.
44. Baker, O. and W. Swerdloff. "Finding Surface Tension of Hydrocarbon Liquids." *Oil and Gas Journal* (January 2, 1956), 125.
45. Hough, E. W. et al. "Interfacial Tensions at Reservoir Pressures and Temperatures; Apparatus and the Water-Methane System." *Transactions of the AIME* (1951), 57.
46. McDonald, A. E. and O. Baker. "A Method of Calculating Multiphase Flow in Pipe Lines Using Rubber Spheres to Control Liquid Holdup." *API Drilling and Production Practice* (1964), 56.

Chapter 5

Artificial lift

by Bashir Agena and Kermit E. Brown

5.1 INTRODUCTION*

The objective of this chapter on artificial lift is to show how to apply nodal systems analysis to design, optimize, and analyze artificial lift systems.

The first objective is to determine the flow rate by each method of lift. Although rate does not represent the only criteria in making a final lift selection, it normally represents the most important one.

Brown gave an overview of artificial lift systems, and a portion of his paper is reproduced by permission.[1]

> In the design of artificial lift systems for a well, it is recommended that it be initially treated as if it were a flowing well; that is, a production systems graph should be prepared to see if the well is capable of flowing and, if so, at what rate. The artificial lift analysis can be placed on the same plot. Numerous flowing wells will show increased flow rates by placing them on artificial lift.
>
> The purpose of any artificial lift system is to create a predetermined tubing intake pressure such that the reservoir may respond and produce the objective flow rate. The design and analysis of any lifting system can be divided into two main components. The first is the reservoir component (inflow performance relationship) which represents the well's ability to produce fluids. The second component represents the entire piping and artificial lift system. This includes the separator, flow line, flow-line restrictions such as chokes, tubing string, tubing string restrictions such as safety valves and the artificial lift mechanism itself. Tubing intake pressures can then be determined for varying flow rates and when this intake curve is placed on the same plot as the IPR curve, the rate for a particular lift method can be determined.

Figure 5.1 shows a typical system graph of the rates possible by different artificial lift methods. The procedures by which the tubing intake (node outflow) curves can be prepared are given in detail in this chapter.

The procedure for the flowing well has been covered thoroughly in Chapter 4. By way of review, Figure 5.2 shows a naturally flowing well under stable flow conditions. Note that the tubing intake curve crosses the IPR curve at a stable point; that is, the tubing intake curve shows a positive slope (upward to the right) at the intersection point.

Figure 5.3 shows a dead well in that the tubing intake curve fails to intersect the IPR curve. This well must have some type of artificial lift to shift the tubing intake curve to the right, making it intersect the IPR curve. This can be accomplished by utilization of the appropriate artificial lift method.

The various artificial lift methods have been covered in complete detail in Volume 2 of this textbook series.[2] However, the manner of preparation of tubing intake curves has not been adequately covered for all the lift methods except gas lift, which is covered in detail in Volume 2a.[3]

That a well may be capable of flowing naturally does not mean that artificial lift should not be considered. Many wells are capable of producing much higher rates when placed on artificial lift, and this is done quite often for rate acceleration projects or where a competitive situation exists.

(1) *Mechanical pumping systems.* There are numerous artificial lift systems that utilize downhole mechanical pumps to displace the liquid to the surface. The three principal ones are sucker-rod, hydraulic, and electrical centrifugal pumps. Numerous modifications of the sucker-rod pump are available. The manner in which the sucker rods are surface actuated varies from the use of a beam unit to a hydraulic system to a winch type of unit. Although the downhole pumps show numerous variations, their objective is the same—to displace the fluids to the surface. Fluid entry is achieved by creating certain tubing intake pressures.

The pump may or may not be located at the bottom of the well. Some installations have pumps located on bottom because the objective is to create as much drawdown in pressure as possible in order to obtain maxi-

* All tables numbered 5A appear in Appendix 5.1.

mum production rates. This is particularly true in stripper-well production and in nearly all cases for rates less than 100–150 b/d.

There are numerous other installations where the pump is set off bottom and may be only 2,000 to 3,000 ft from the top in some wells. For example, a high-productivity well with high bottom-hole pressure may utilize an electrical submersible centrifugal pump at a relatively shallow depth, even in a deep well.

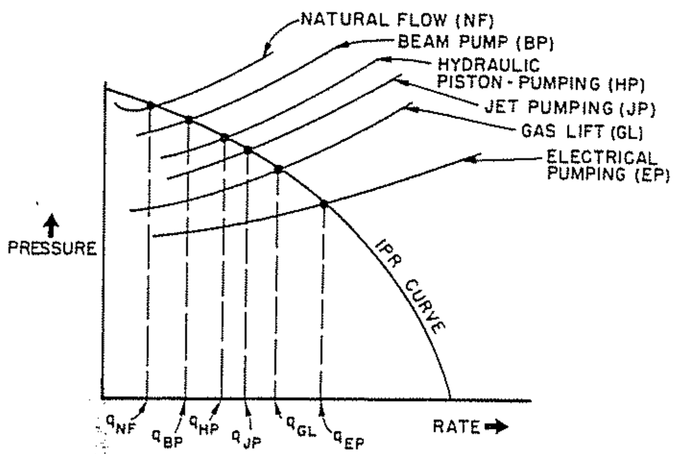

Figure 5.1 Tubing Intake Curves for Artificial Lift Systems

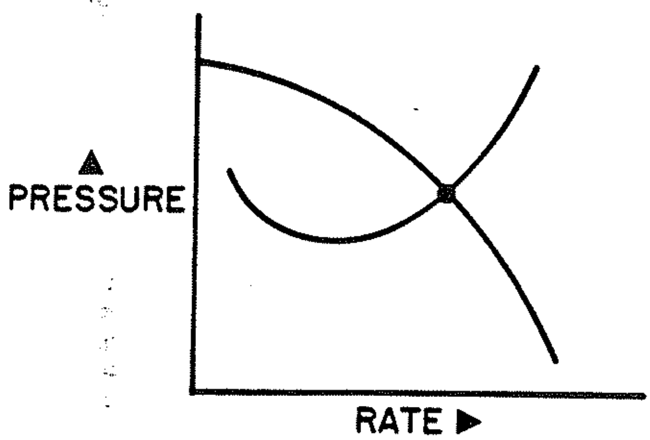

Figure 5.2 Stable Flow

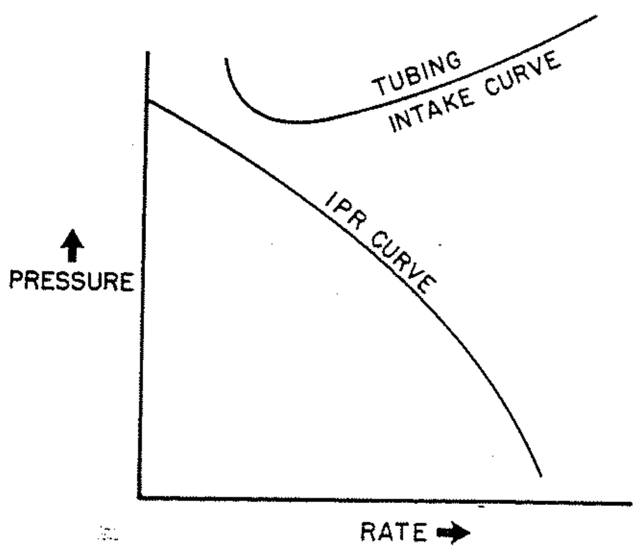

Figure 5.3 Dead Well

The intake tubing curves are easier to prepare when the pump is set on bottom. The principal reason for this is that the pump intake and tubing intake pressures are the same. When the pump is up from bottom, the pump intake and tubing intake pressures are different. The tubing intake pressure being defined is that pressure at the center of the perforated interval necessary to move the fluids to the stock tank. This pressure should not be confused with the flowing bottom-hole pressure required by the reservoir to produce a certain rate, although where these two pressures coincide sets the flow rate. The pump intake pressure is the pressure at the entry of the pump and may differ considerably from the tubing intake pressure depending on pump location.

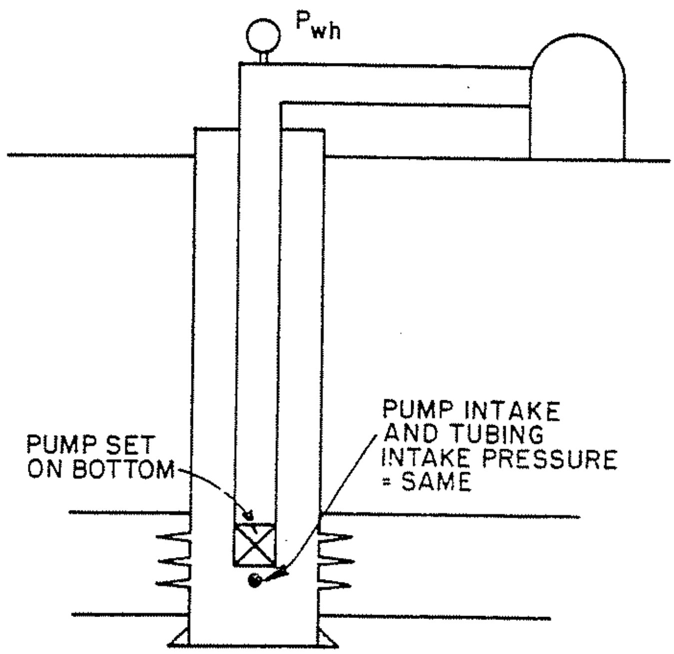

Figure 5.4a Pump Set on Bottom

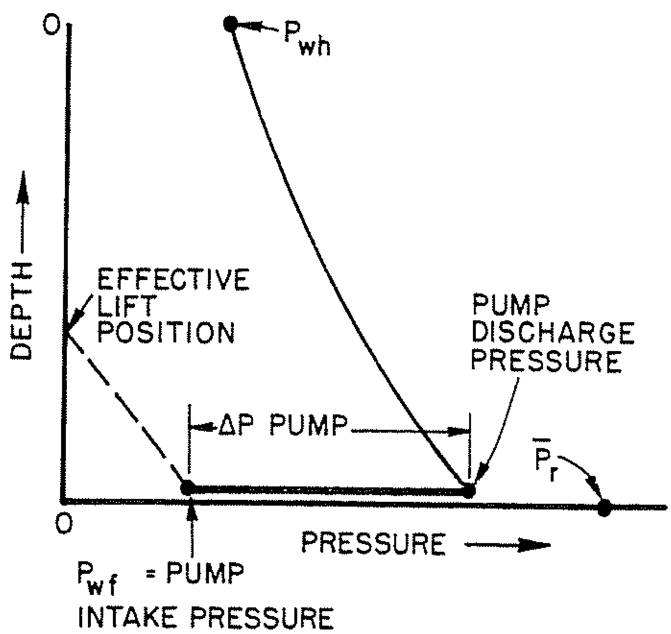

Figure 5.4b Pressure Traverses for Pump on Bottom

Figure 5.4a shows a typical pump installation whereby the pump is set on bottom. Figure 5.4b shows the pressure traverses for the pump on bottom.

Figure 5.5a shows an installation whereby the pump is set upward from bottom. Note the location of the pump intake pressure and the tubing intake pressure (node outflow pressure). Figure 5.5b is shown to explain this concept in detail. Note that casing flow exists from the center of the perforations upward to the pump intake. By knowing the pump intake pressure, we can extend this to bottom and determine the tubing intake (node outflow) pressure.

A term that is quite often misunderstood is "effective lift." For example, a pump may be set at 10,000 ft but may be lifting only from 7,000 ft. Therefore, if the assumption is made that the pump is having to lift from its setting depth, the unit may be designed for greater horsepower than required (note Figure 5.4b).

An extension of the flowing bottom-hole pressure upward from bottom until it intersects the depth line on a depth (ordinate) vs pressure plot locates the position of effective lift. This is the depth at which the flowing bottom-hole pressure is capable of supporting the production rate. Another way of visualizing effective lift is that it is the depth at which the pump could be set and pump the same flow rate if zero pressure existed at the intake of the pump. This can be illustrated with a simple example.

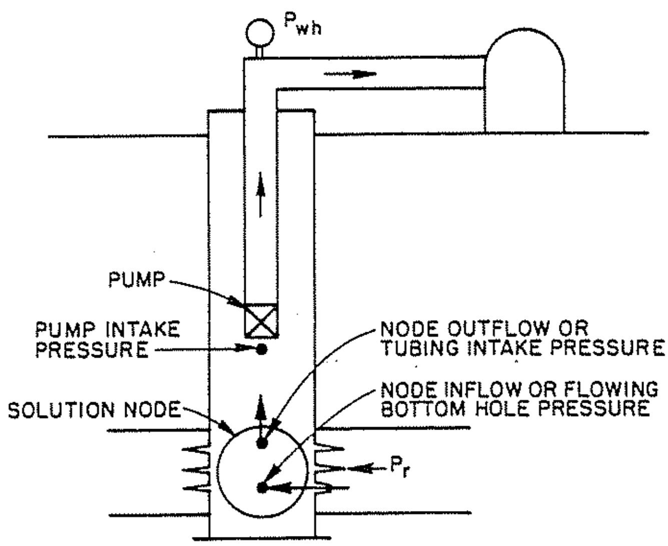

Figure 5.5a Pump Set Upward From Bottom

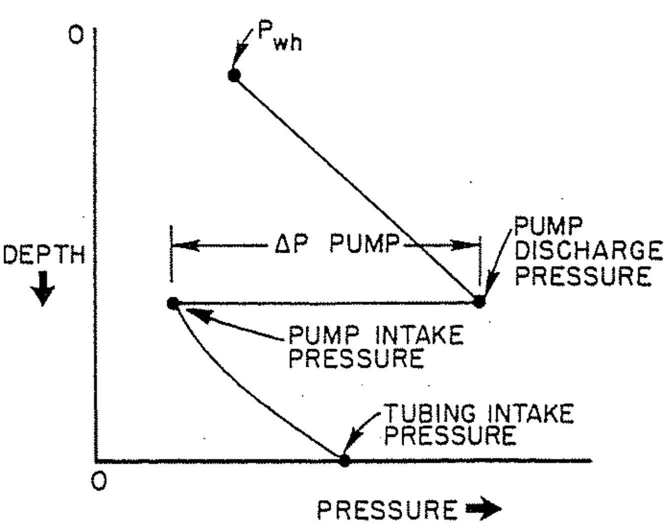

Figure 5.5b Pressure Traverse for Pumping System

Assume that salt water is being produced for a waterflood project. Assume that the gradient of this water is 0.50 psi/ft, which includes friction of movement. The additional data is known about this well:

P_r = 2,400 psi	depth = 8,000 ft
J = 4	desired rate = 3,200 b/d

The required flowing bottom-hole pressure is $2{,}400 - \frac{3{,}200}{4} = 1{,}600$ psi. The flowing bottom-hole pressure is capable of supporting the flowing salt water to a height of 1,600/0.5 = 3,200 ft. The depth from the surface to this point is 8,000 − 3,200 = 4,800 ft. The effective lift point is 4,800 ft from the surface. Therefore, if the well was only 4,800 ft deep and had zero wellhead pressure, it would flow naturally at a rate of 3,200 b/d. Or, if we set the pump at 4,800 ft and created zero intake pressure at that position, the well would pump 3,200 b/d. If the wellhead flowing presure is 100 psi, the pump must discharge at a pressure of 100 + 4,800(0.50) = 100 + 2,400 = 2,500 psi. This is also the ΔP that the pump must create for $\Delta P = (P_d - 0) =$ 2,500 psi.

Now, if we choose to set the pump on bottom at 8,000 ft, the tubing intake and pump intake pressure are the same and are equal to 1,600 psi. However, the pump discharges at 100 + 8,000(0.5) = 4,100 psi. The ΔP that the pump must create is, however, the same and is 4,100 − 1,600 = 2,500 psi. Therefore, the same pump would produce the same 3,200-b/d rate regardless of whether it was set at 4,800 ft or 8,000 ft. In actual practice, we would set the pump deeper than 4,800 ft in order to maintain some submergence over the pump (perhaps at 5,200 ft). Regardless of the position at which the pump is set, it must create the same ΔP and hence requires the same horsepower.

The multiphase flow well is slightly different, and the following example is given. If a well is 10,000 ft deep, has a static pressure of 2,000 psi, J = 2 (assumed constant), gas-liquid ratio = 300 scf/bbl, wellhead pressure = 120 psi, and is completed with 2⅜-in. OD tubing, what is the depth of effective life for a rate of 1,000 b/d for all oil? The flowing bottom-hole pressure required for the well to yield this rate is $2{,}000 - \frac{1{,}000}{2} = 1{,}000$ psi. The effective lift point is that depth at which the flowing bottom-hole pressure is capable of supporting the fluids in the tubing string. The appropriate multiphase flow correlation shows this to be 5,000 ft from bottom or at a depth of 5,000 ft. Figure 5.6 shows typical curves. Theoretically, a pumping system could be set at 5,000 ft, and by creating zero intake pressure at that point, the objective flow rate could be obtained. The discharge head above the pump would

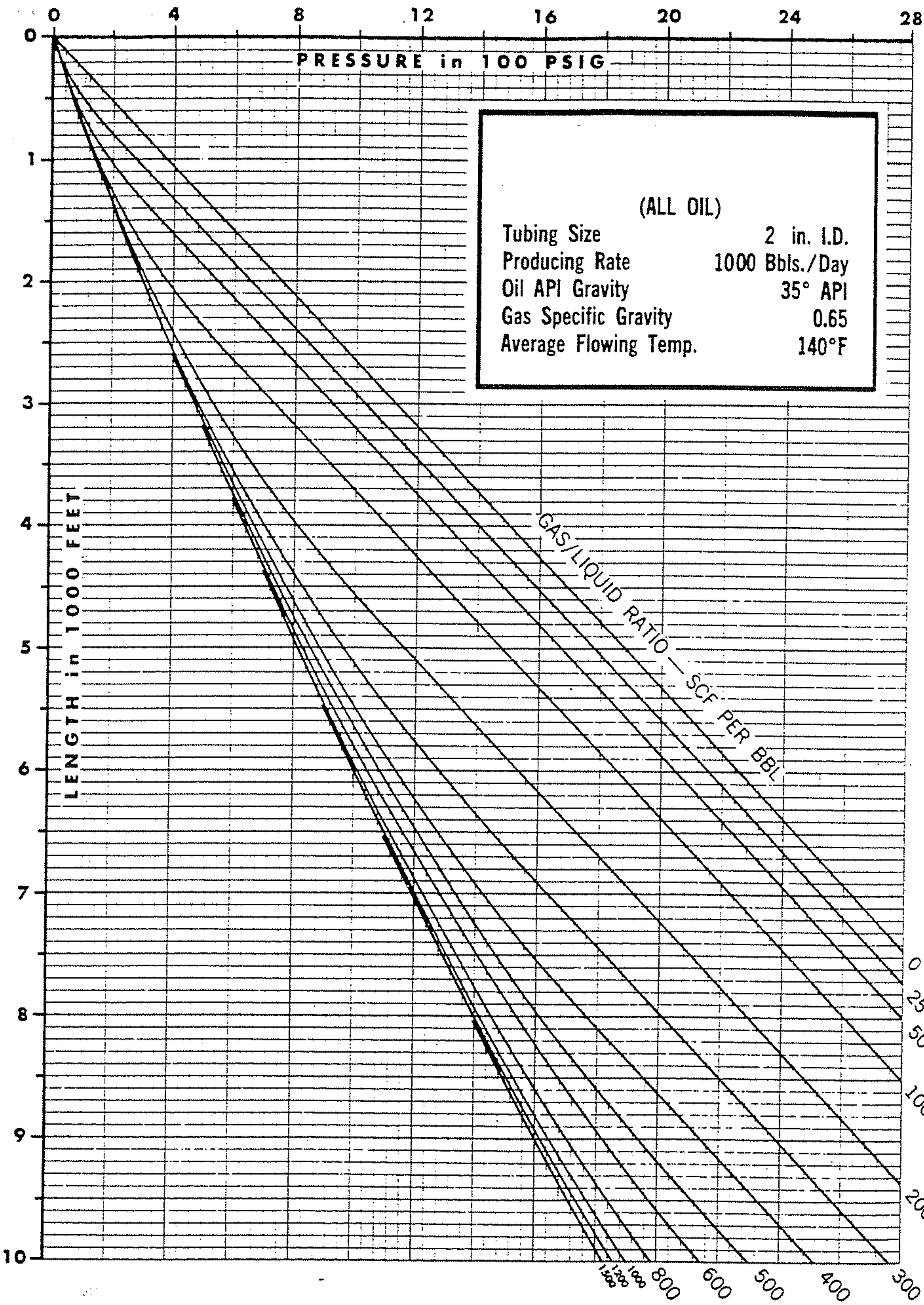

Figure 5.6 Vertical Flowing Pressure Gradients (All Oil)

then consist of all head and pressure losses above 5,000 ft such as tubing loss, flow-line loss, and separator pressure and is approximately 950 psi. If this well was only 5,000 ft deep, it would flow 1,000 b/d of oil with zero pressure at the wellhead. Therefore, in this 10,000-ft well, the pump only has to work or lift from 5,000 ft, even though the pump is normally set deeper.

If we assume that the pumping system is located at 10,000 ft (on bottom), the pump only has to lift from the effective lift point of 5,000 ft. Another way to visualize this concept is to note that the pump must create a certain discharge pressure to overcome all pressure losses and head above the effective lift point, which is also the ΔP that the pump must create if set at the effective lift point. If we assume for this example that all gas (300 scf/bbl is being pumped, the discharge pressure is approximately 950 psi for a wellhead pressure of 120 psi as determined from an appropriate multiphase flow correlation. This discharge pressure increases as more gas is vented because gas is no longer available for lightening the pressure traverse above the pump.

There are numerous reasons for setting a pump either below or near the effective lift point. Obviously, the pump should be submerged enough to allow entry pressure high enough to prevent cavitation and overcome any entry loss restrictions such as those that may exist across a downhole gas separator. Submergence in feet is defined as the fluid level in the annulus above the pump under operating conditions. The desireability of creating low pump intake pressures may restrict some pumping systems, and a general rule of 150- to 300-ft pump submergence for oil wells pumping gas will restrict some pumps. The handling of lower free gas volumes through the pump makes the deeper setting positions more attractive.

High-volume oil wells using electrical pumps generally may require more submergence, whereas very low-volume oil wells using sucker-rod pumps may require very little submergence and may reach pump-off condition (no submergence) in some cases. Where feasible, a submergence of 150 to 300 ft on pumping wells is considered a good value for eliminating pump problems and preventing undue repair work. This may not be possible in some cases where the static pressure is extremely low, and as low as 50 ft and even complete pump-off have been used.

Higher temperatures at greater depths may also encourage higher setting depths, although the handling of additional free gas may discourage it. The cost may be greater to set the same unit to a greater depth. This means more cable for electrical pumps, more sucker rods for sucker-rod pumps, and more parallel tubing for some hydraulic pumping systems. The principal advantage to lower pump settings is that the total volumetric intake flow rate is less because of higher intake pressures and reduced free-gas volumes.

In order to determine the intake rates to be handled by pumps, it is necessary to prepare IPR curves to include total volumetric flow rates. The standard IPR curve shows a plot of stock-tank barrels of liquid per day vs flowing bottom-hole pressure. This does not include the increased oil volume caused by gas in solution nor does it include the volume of free gas that the pump must handle.

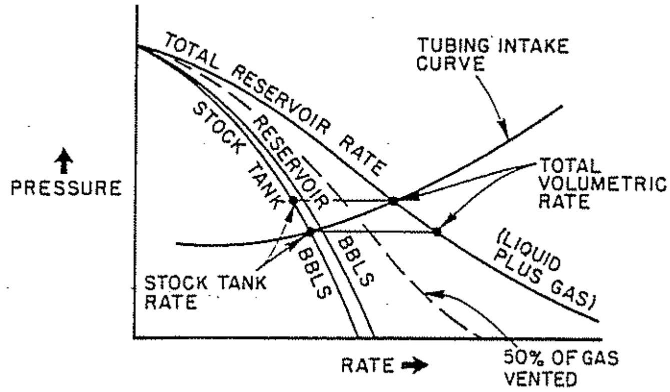

Figure 5.7 IPR Curves for Total Fluid Production Including Gas

Refer to Figure 5.7, which shows a typical pressure-flow rate diagram, including IPR curves for stock-tank barrels, reservoir barrels, and total reservoir volumetric rates including free gas. Under some completions such as offshore installations where the venting of gas may not be feasible, it is necessary for the pump to handle the total volumetric rate of oil, water, and gas. The pump must be large enough to handle the entire volume of fluids, including free gas.

Also, designing a pump to have the capacity to handle the extra gas volume does not mean that the pump will behave as if it is handling that equivalent volume of liquid. Numerous other problems may occur such as gas locking and liquid pounding for sucker-rod pumps, decreased pump efficiency for electrical pumps, increased piston leakage for hydraulic and sucker-rod pumps, and decreased efficiency for jet pumps for what amounts to a sort of gas restriction in the throat of the jet. The only benefit in bringing free gas through a pump is a lowering of the discharge pressure.

5.2 PREPARATION OF TUBING INTAKE (NODE OUTFLOW) CURVES FOR ARTIFICIAL LIFT SYSTEMS

5.21 INTRODUCTION

The manner of preparing tubing intake curves and, hence, determining flow rates is presented in this section. The same general procedure that was used for the flowing well as discussed in Chapter 4 applies. Gas lift is the easiest of the lift methods for preparing intake curves because of its similarity to the flowing well. The only difference is that the formation gas-oil ratio is supplemented with additional injection gas. For the case in which gas is injected around the bottom of the tubing, the procedure is identical to that of a flowing well except for the change in total gas-liquid ratio.

The pumping systems become more difficult and are presented after gas lift. The pump on bottom and pump off bottom represent two different cases that will be presented.

In order to illustrate the preparation of tubing intake curves, two example problems will be worked for all lift methods. In addition, one other problem is worked for gas lift. The data for these examples are listed in Table 5.1.

TABLE 5.1
WELL, FLUID, RESERVOIR, AND LIFT-SYSTEM DATA USED IN EXAMPLE CALCULATIONS FOR WELLS #1 AND #2

	Well #1	Well #2
Depth, ft	8,000	7,600
Casing size, in.	7	5½
Tubing size, in.	2⅞	2⅜
Wellhead pressure, psi	120	80
Wellhead temperature, °F	110	110
°API	35	40
γ_{osc}	0.85	0.83
γ_{gsc}	0.70	0.65
water cut	50%	0
γ_{wsc}	1.074	—
GOR, scf/stbo	400	200
P_b, psi	1,820	940
$\overline{P}_r$, psi	1,920	1,500
J (above P_b), stbl/d/psi	5	0.4
q_{max}, stbl/d	6,267	400
Flowing temperature, °F	170	167

It is assumed that, for gas lift, sufficient pressure is available to inject around the bottom of the tubing string. However, for gas-lift operations, well #1 will be worked for the inclusion of a 4,000-ft long, 2½-in. flow line. For each lift system, two cases were considered:

(1) pumping only liquid
(2) pumping gas with the liquid

For both cases, it is assumed that the lift system is set at the bottom of the well and that the wellhead pressure and the size of the flow conduits are fixed. For case 2, it is assumed that all associated gas is pumped with the liquid. Other assumptions are mentioned where applicable. The following variables affecting the rate are briefly discussed.

(1) *Volume factor.* When pumping gas (especially free gas) by means of an artificial lift system, it is important to predict the total volume of the produced fluid rate (including free gas) at any condition of pressure and temperature. This total volume, not just the liquid rate, determines the number of stages for an electric submersible pump,[4] the power fluid rate for a hydraulic or a jet pump,[5,6] and the pump speed and the stroke length for a beam pump.[7,8] The percentage of the free gas to be handled by the pumping mechanism also must be considered. However, the rather difficult problem of downhole gas separation[4] is not considered in this study.

The volume of 1 stb of liquid plus associated gas (hereafter referred to as the volume factor) at any pressure and temperature is given by:

$$VF = (wc)B_w + (1 - wc)B_o + [GLR - (1 - wc)R_s - (wc)R_{sw}]B_g \tag{5.1}$$

Since it is common practice to ignore R_{sw} and to take B_w as unity,[9,10,11,12,13] the above equation reduces to:

$$VF = wc + (1 - wc)B_o + [GLR - (1 - wc)R_s]B_g \tag{5.2}$$

If a certain percentage of the gas is to be vented before it enters the lift system, Equation 5.1 must be modified to:[4]

$$VF = wc + (1 - wc)B_o + GIP[GLR - (1 - wc)R_s]B_g \tag{5.3}$$

where GIP is the percentage of gas passing through the lift system. Brown et al.[4] referred to GIP as "percentage of gas ingestion." Calculation of VF with 100% GIP is made for the two fluids shown in Table 5.1. Results of the calculations are shown in Tables 5A.1 and 5A.2 in the appendix.

It should be mentioned that some texts refer to the reciprocal of VF as "volumetric efficiency."[5,6,7] In reality, VF has nothing to do with efficiency in regard to the mechanics of the system. It is simply a multiplier to account for the variation of the produced fluid rate with pressure and temperature.

The total volume of the produced fluid rate (liquid plus gas) at any conditions of pressure and temperature is, then:

$$V = q_{sc}\, VF \tag{5.4}$$

For flowing bottom-hole pressure above the bubble point, the IPR is described by the following linear relationship:[14]

$$q_{sc} = J(\overline{P}_r - P_{wf}) \tag{5.5}$$

As P_{wf} declines below the bubble point, nonlinearity in the IPR becomes apparent. For this case, the IPR is given by the familiar Vogel's equation:[15]

$$\frac{q_{sc}}{q_{max}} = 1 - 0.2\left(\frac{P_{wf}}{\overline{P}_r}\right) - 0.8\left(\frac{P_{wf}}{\overline{P}_r}\right)^2 \tag{5.6}$$

Sometimes, it is useful to prepare IPR curves on the basis of total barrels of produced fluid, including gas. This can be accomplished by multiplying q_{sc} in Equations 5.5 or 5.6 by VF evaluated at the flowing bottom-hole pressure and temperature from Equation 5.2.

Calculating IPR's in stbl/d and in b/d was carried out for the two wells shown in Table 5.1. Results of the calculations are shown in Tables 5A.3 and 5A.4 in the appendix. The production rate in stbl/d (column 2) was obtained from Equation 5.5 for pressures above the bubble point and from Equation 5.6 for pressures below the bubble point. The volume factor (column 3) was determined at the flowing bottom-hole pressure and temperature from Equation 5.2. The rate in stbl/d was multiplied by VF to obtain the rate in b/d (column 4). P_{wf} was plotted vs q_{sc} and V in Figures 5.8 and 5.9. The lower curve represents the stbl/d IPR, and the upper curve represents the b/d IPR. Of course, it may or may not be necessary to produce all free gas through the tubing. Venting of gas is essential for some wells.

5.22 SETTING PUMP OFF BOTTOM

The procedure for the preparation of tubing intake curves when the pump is set above the bottom of the well is not presented in this chapter. Once the pump intake pressure is determined for a pump up the hole, an appropriate flow correlation is used to establish the intake pressure opposite the perforations. Normally, this will be flow up the casing until reaching the intake

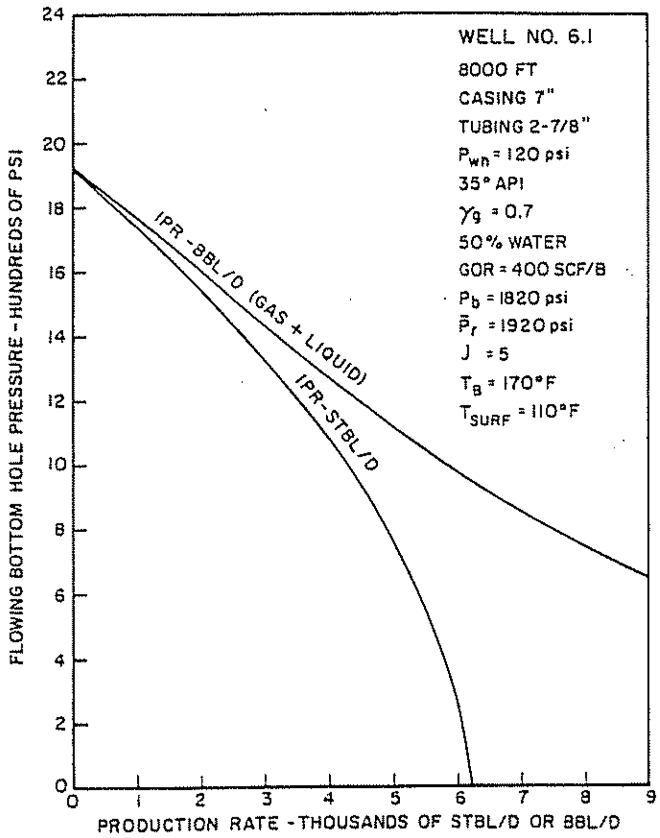

Figure 5.8 Inflow Performance Relationships for Well #1

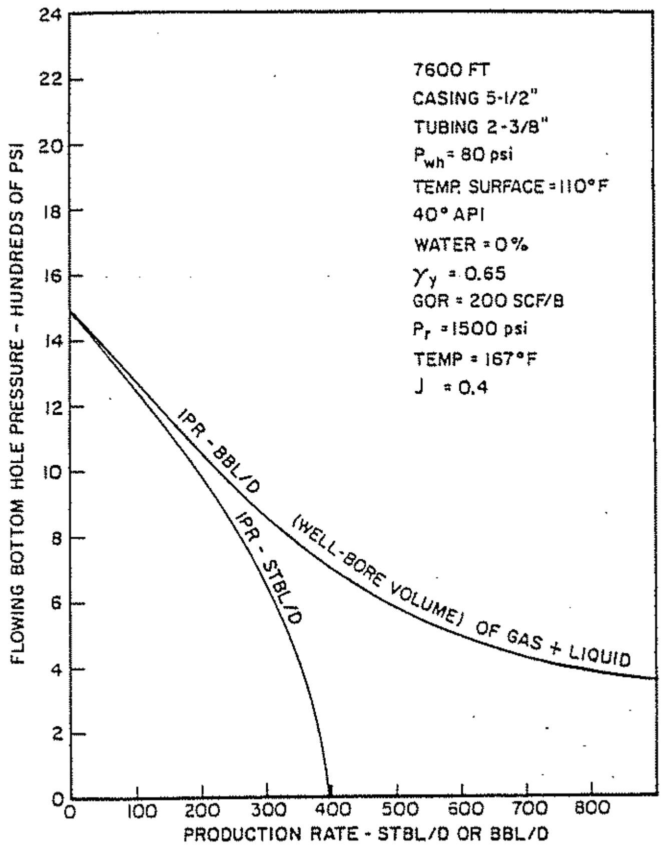

Figure 5.9 Inflow Performance Relationships for Well #2

of the pump. Therefore, the procedure is not that much more difficult.

5.23 GAS LIFT

Gas lift is presented in a rather brief form since it is discussed in complete detail in Volume 2a of this book series.[3]

EXAMPLE PROBLEM

The following step-wise procedure includes a 4,000-ft flow line:

Given data:

$J = 5$	GOR = 400 scf/bbl
2⅞-in. OD tubing	depth = 8,000 ft
7-in. casing	$\gamma_{gsc} = 0.7$
°API = 35	50% water
separator pressure = 80 psi	$P_{so} = 900$ psi
	$\bar{P} = 1{,}920$ psig

flow line = 2½ in. by 4,000 ft long
T = 170°F at 8,000 ft

Note that 4,000 ft of 2½-in. flow line has been added to well #1 for this gas-lift example. The line pressure available at the wellsite is 1,000 psi.

It is assumed that 900-psi pressure is available at the surface after reaching the operating gas-lift valve. Figure 5.10 represents the two components necessary to solve this problem. The solution position is taken at the bottom, and the system is divided into two components:

(1) the piping system
(2) the reservoir component

These two components are handled separately and then combined to make rate predictions.

Solution procedure (bottom of well):

(1) Construct the IPR curve as noted in Figure 5.8. This procedure is described in Chapter 2.
(2) Construct tubing intake curves for varying injection gas-liquid ratios. Because of the flow line,

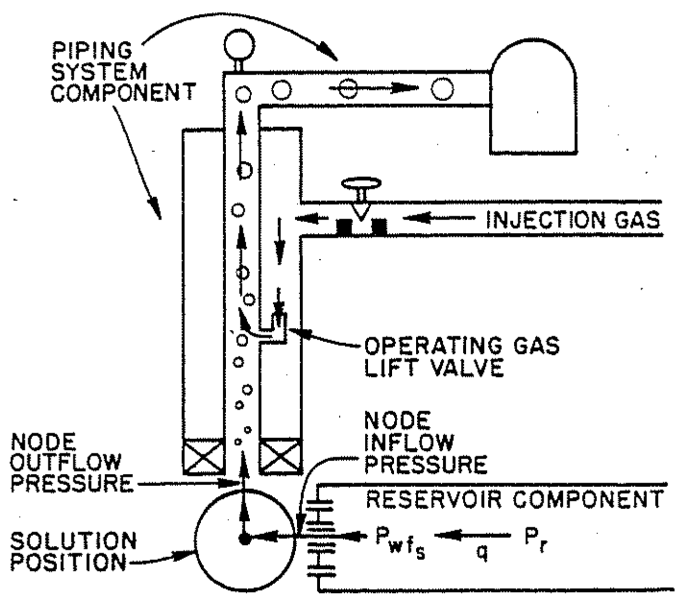

Figure 5.10 Components for Gas-Lift Solution

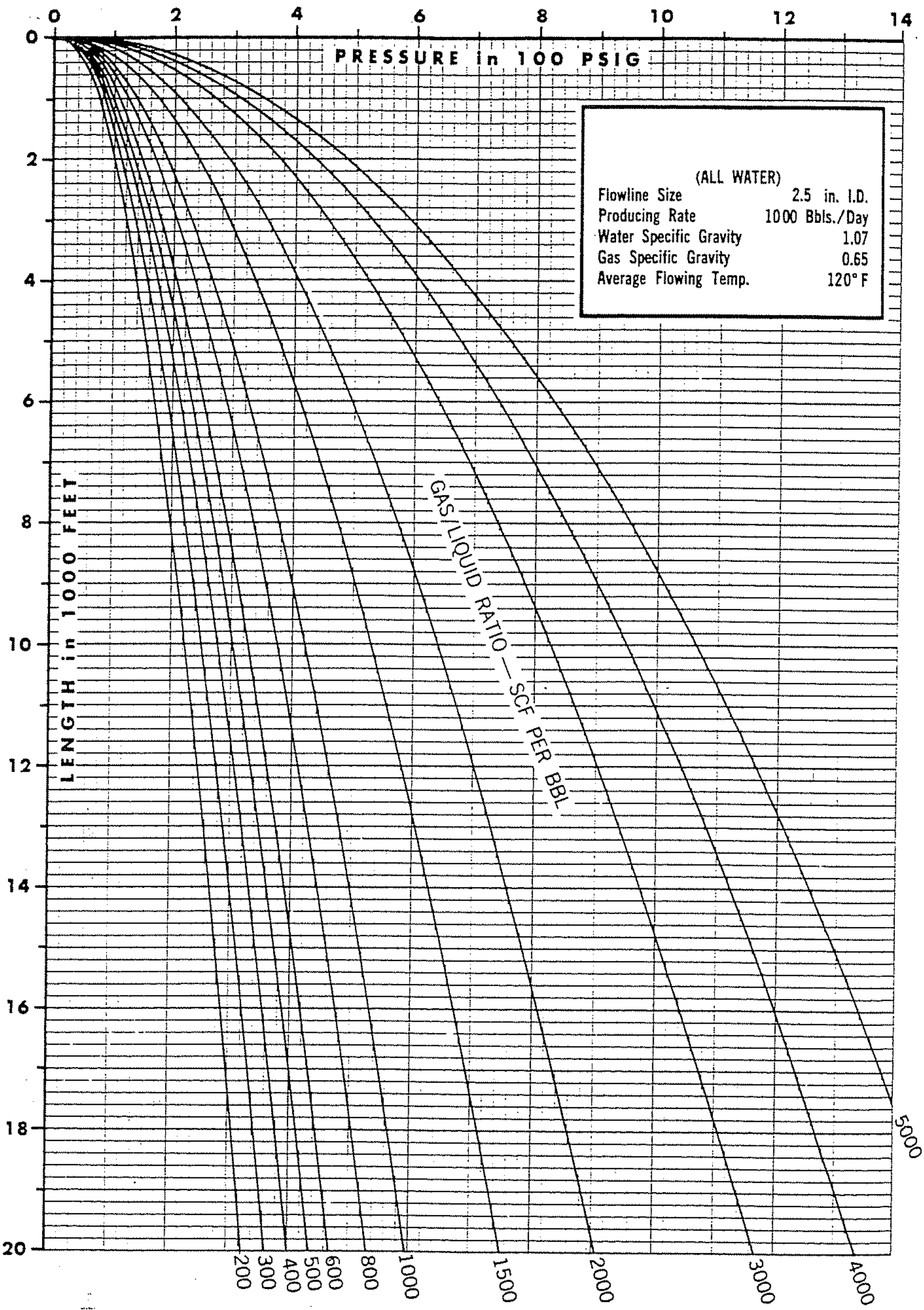

Figure 5.11 Horizontal Flowing Pressure Gradients (All Water)

the injection gas-liquid ratio becomes another unknown in this solution.

(a) Assume several rates such as 600, 800, 1,000, and 1,200 b/d.
(b) Assume several total gas-liquid ratios such as 600, 800, 1,000, and 1,500 scf/bbl that are to be used with each assumed flow rate.
(c) For each rate, such as 1,000 b/d, and for each assumed GLR, determine the wellhead pressures from an appropriate horizontal multiphase flow correlation. These are noted in Table 5.2, and the Eaton solution is used (see Figure 5.11).

TABLE 5.2
WELLHEAD PRESSURES VS RATE AND GLR

Assumed rate, b/d	GLR	(Eaton) P_{wh}
1,000	600	215
1,000	800	240
1,000	1,000	270
1,000	1,500	340

(d) Using the same rates and GLR's of step c, determine the tubing intake pressures. Use the wellhead pressures found in step c. This step becomes more involved than for the flowing well in that supplementary gas is injected into the tubing string. The following steps detail this solution. Computer solutions that simplify these calculations are available.
   (i) On a sheet of rectangular graph paper, prepare a scale equal to gradient curves that you may be using, or if on computer, you may set the scale (see Figure 5.12).
   (ii) Mark P_{so} = 900 psi at the top and draw in the gas gradient line. If high gas injection rates are expected, friction should be properly accounted for. For annular injection, the dynamic and static gas gradients will be essentially equal, and Figure 5.13 may be used. This is found to be 23.6 psi/1,000 ft for our problem, giving ($23.6 \times 81 = 189$ psia additional pressure at 8,000 ft). Mark 1,089 psi at 8,000 ft and draw a line from 900 psi at the top to 1,089 psi at 8,000 ft.
   (iii) Use a ΔP of 100 psi for this problem. Refer to reference 3.
   (iv) Using, for example, the GLR of 600 scf/bbl and 1,000 b/d (see Figure 5.14), construct the pressure traverse for 1,000 b/d and 600 scf/bbl downward from the wellhead pressure of 215 psi until intersecting the ΔP line (Figure 5.15). This occurs at 4,450 ft.
   (v) From the intersection depth of step 3 (4,450 ft), construct the formation GLR line of 200 scf/bbl downward to total depth, giving a tubing intake pressure at 8,000 ft of 2,200 psi.
   (vi) Repeat the same procedure for the other assumed GLR's of 800, 1,000, and 1,500 scf/bbl. Note that the 1,500 scf/bbl is shown in Figure 5.15 and gives a tubing intake pressure of 2,440 psi, starting at the surface with a wellhead pressure of 340 psi. Each GLR must start with the respective required wellhead pressure as determined in step 2c.
   (vii) Repeat steps iv through vi for the other assumed rates of 600, 800, and 1,200 b/d.

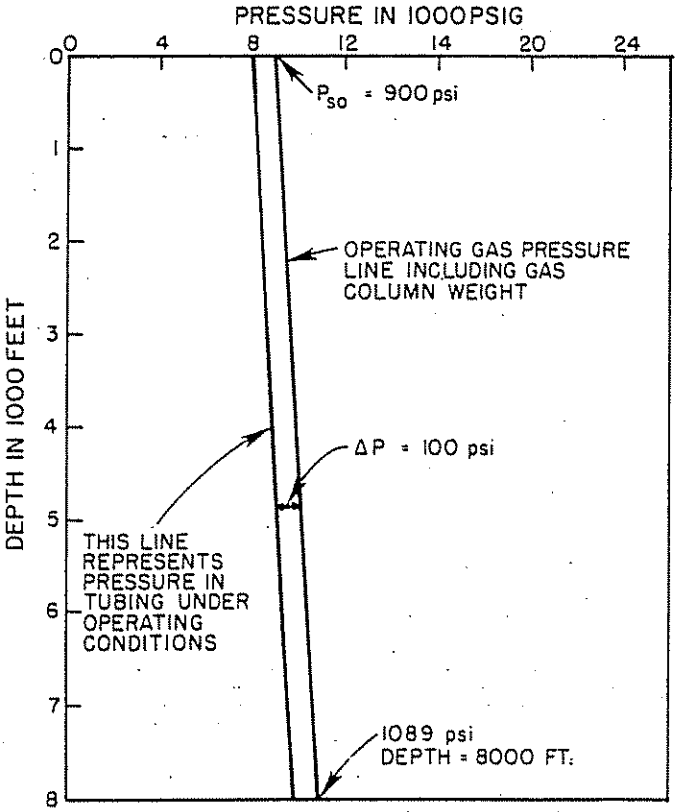

Figure 5.12 Steps 1,2, and 3 of Gas-Lift Solution

(3) A final plot such as in Figures 5.16a and b, which are computer plots with GLR's of 400, 500, 600, 700, 800, 900, 1,000, 1,200, 1,500, and 2,000 scf/bbl, is made, and the rate is noted to be 675 b/d. Figure 5.16a shows only four total gas-liquid ratios as compared to ten for Figure 5.16b.
(4) From Figure 5.16, we prepare a gas-lift performance curve as noted in Figure 5.17, which is the basic curve needed for gas-lift optimization.

Solution procedure (top of well):

Although the solution position is normally taken at the bottom of the well, it can also be taken at other positions, and one commonly used position is at the top of the well. If the solution point is taken at the bottom of the well, we can separate out the well capability. Therefore, if we are interested in looking at several IPR's at different average reservoir pressures, the node at the bottom of the well is the best solution point. The tubing intake pressure curve then represents the entire piping system, including separator pressure, flow line, any restrictions, and the tubing.

By taking the solution at the surface, we have isolated the flow line. One curve represents the separator

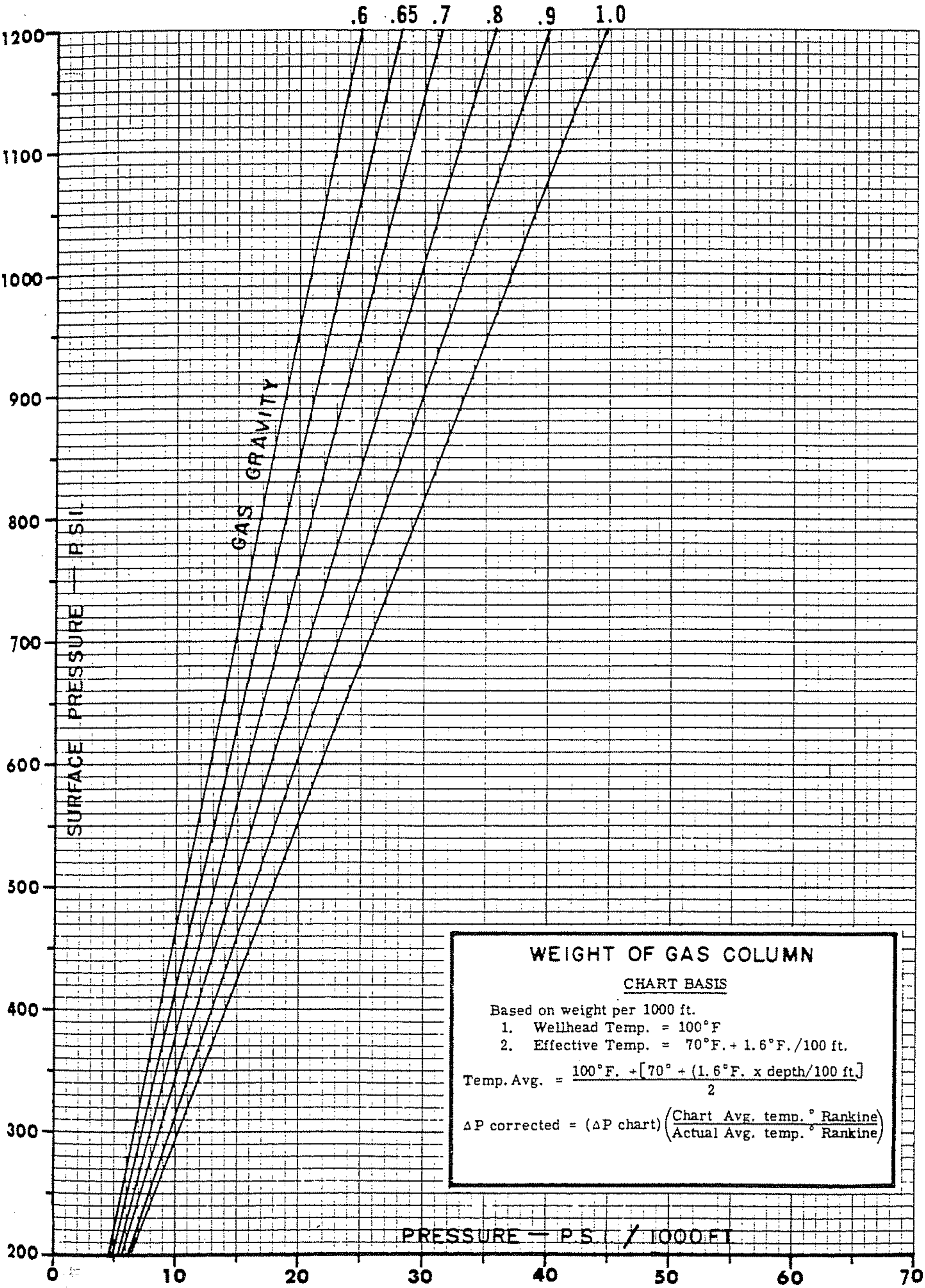

Figure 5.13 Static Gas Column Pressure (courtesy of Otis Engineering Corp)

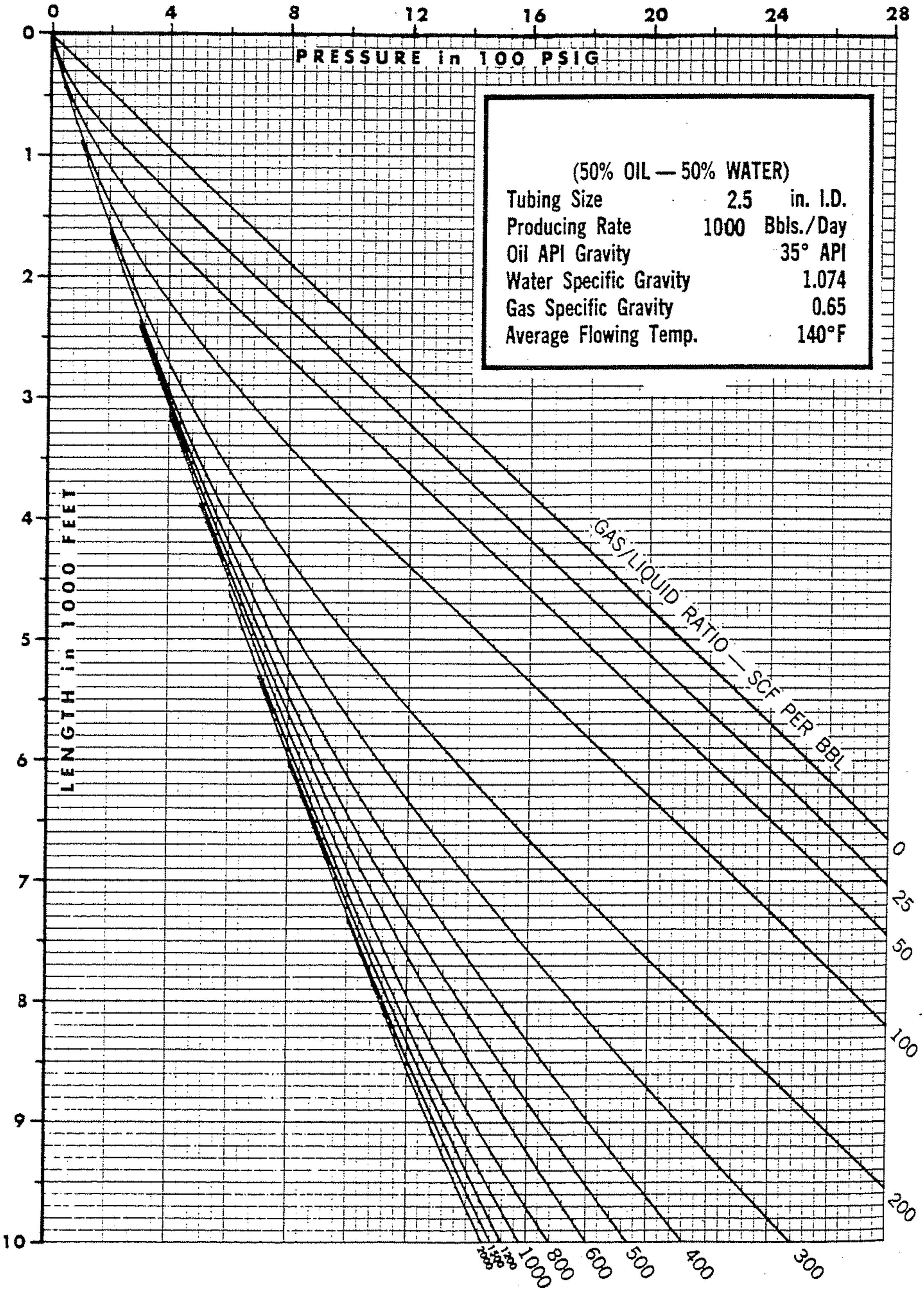

Figure 5.14 Vertical Flowing Pressure Gradients (50% Oil—50% Water)

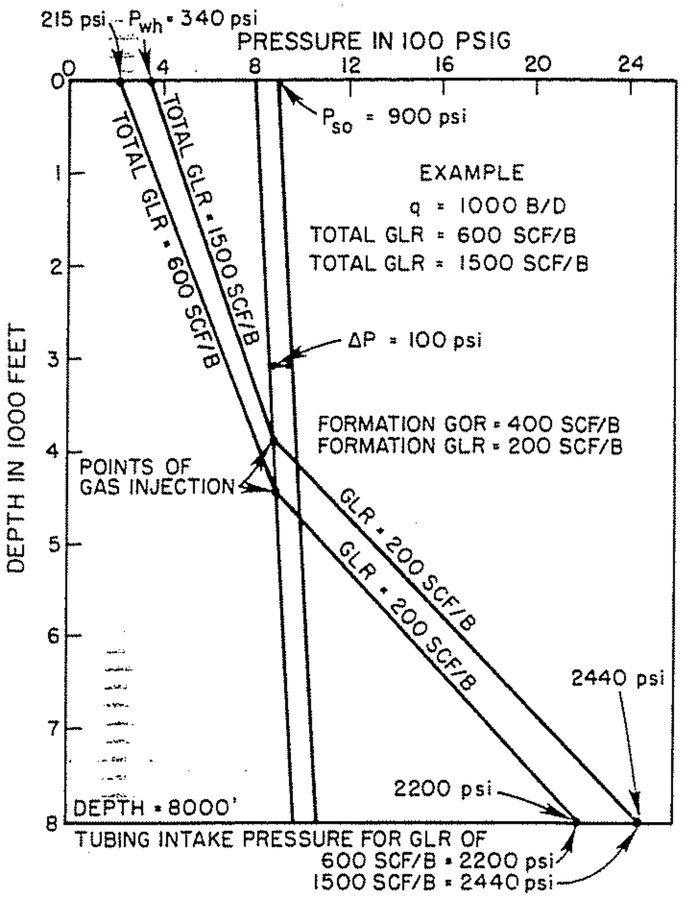

Figure 5.15 Gas-Lift Example Solution

pressure and flow line, whereas the other curve incorporates the tubing string and IPR of the well. If computer plots are available, both solutions may be advisable. In other cases, a personal preference may develop for one or the other. Numerous examples for solutions at the top of the well can be found in reference 3.

Figures 5.18a and b show the solution of this same example problem at the wellhead. Note that wellhead pressure is plotted against rate. Figure 5.18a shows only four GLR's, whereas Figure 5.18b shows nine.

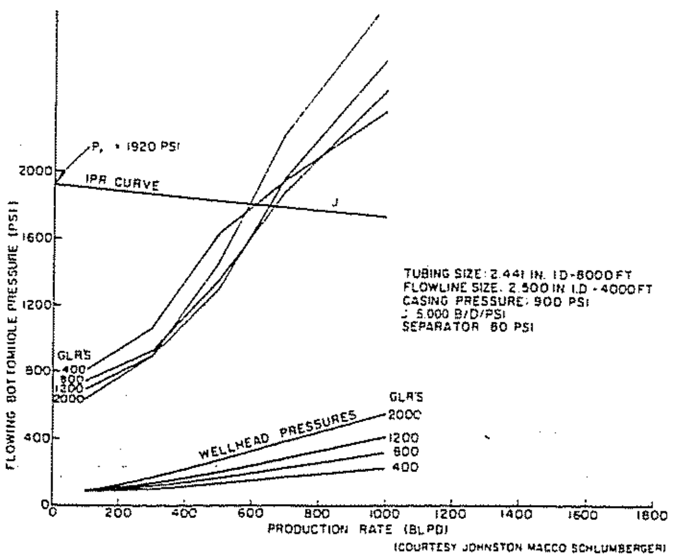

Figure 5.16a Gas-Lift Solution Node at Bottom of Well

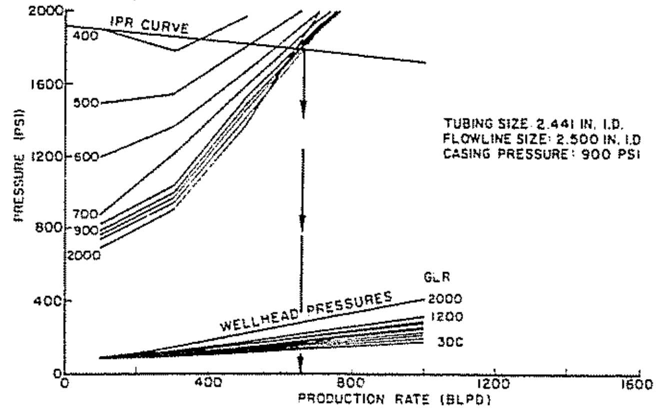

Figure 5.16b Gas-Lift Solution Node at Bottom of Well

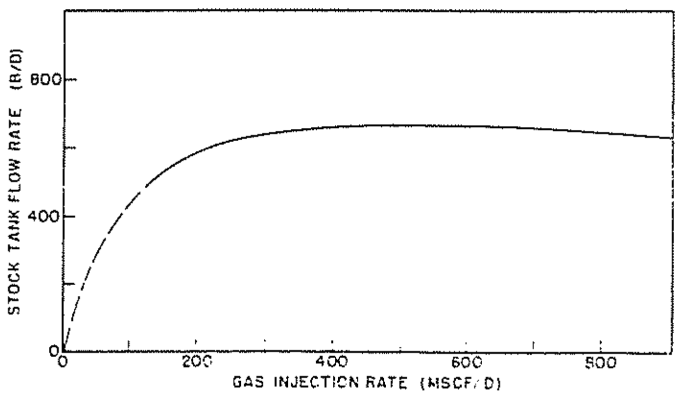

Figure 5.17 Gas-Lift Performance Curve

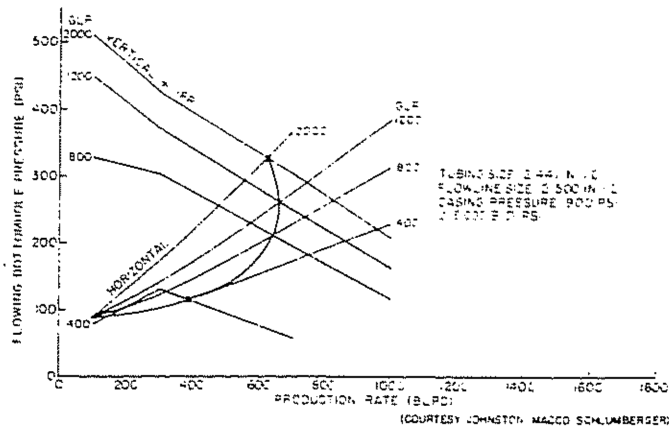

Figure 5.18a Solution Node at Top of Well

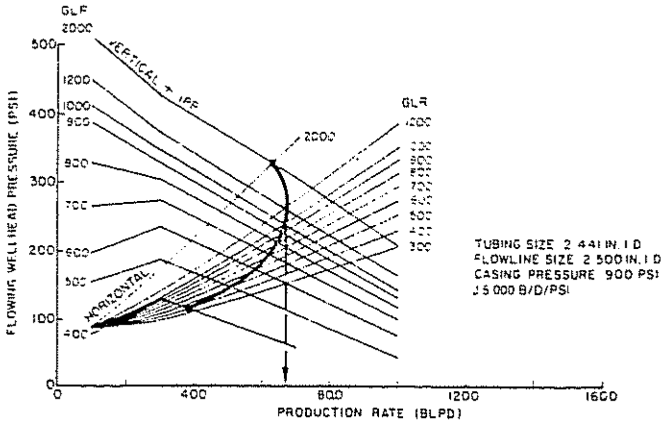

Figure 5.18b Gas-Lift Solution Node at Top of Well

Note that the maximum rate is found by connecting the intersection points of equal gas-liquid ratio lines. The rate is again found to be 675 b/d, and for a total gas-liquid ratio of 1,000 scf/bbl, the injection gas-liquid ratio is (1,000 − 200) = 800 scf/bbl.

A gas lift performance curve such as Figure 5.17 can also be prepared from Figure 5.18.

5.231 SENSITIVITY ANALYSIS

5.2311 INTRODUCTION

Nodal analysis can be successfully used to study the effect of all components in both the initial design and analysis of gas-lift installations. As was explained in Chapter 4 for the flowing well, the gas-lift well can be handled in the same way. As noted, the solution position to solve for the flow rate can be taken at either the bottom of the well (center of the perforated interval) or the top of the well. Both solution positions will predict the same rate, but one or the other may serve to isolate certain components of the entire system.

A sensitivity analysis can be computed to determine the effect of certain variables. Several unknowns are involved in the gas-lift problem. If we select the following constant values, (1) depth, (2) inflow productivity, (3) tubing size, (4) flow-line size, (5) separator pressure, (6) solution GOR, (7) surface injection pressure, and (8) $\overline{P}_r$, our unknowns are (1) flow rate, (2) injection gas volume, (3) wellhead pressure, (4) flowing bottom-hole pressure, (5) tubing intake pressure (may be same as 4 if sufficiently close to the pay zone), (6) depth of the point of gas injection, and (7) operating differential. The operating differential controls the rate as well as spacing and has been adequately discussed by Brown and Mach.[3] An operating differential of 100 psi has been selected for examples in this paper.

In designing a new system, we may want to select different values of (1) surface injection pressure, (2) separator pressure, (3) tubing sizes, and (4) flow-line sizes. Several systems graphs may be necessary to make logical decisions on different parameters. One of the most important parameters is the injection gas-liquid ratio. An often-used assumption is that the objective pressure gradient traverse in the tubing string is the one obtained using sufficient gas to attain the minimum gradient for a constant wellhead pressure. This can lead to serious errors in injection gas volume calculations. As this gas reaches the surface, we must have sufficient pressure at the wellhead to move the fluids to the separator. Any additional gas causes this pressure to increase and, hence, reduces production. Sufficiently large flow lines may allow us to approach the minimum pressure traverse in the tubing string, but generally, the optimum GLR for maximum rate will be approximately one-half that GLR necessary to reach the minimum pressure traverse in the tubing string.

Various sensitivity plots were made and they are discussed in the following sections.

5.2312 EFFECT OF FLOW-LINE SIZE

One of the quickest and most economical ways to increase flow rate is to change out the surface flow

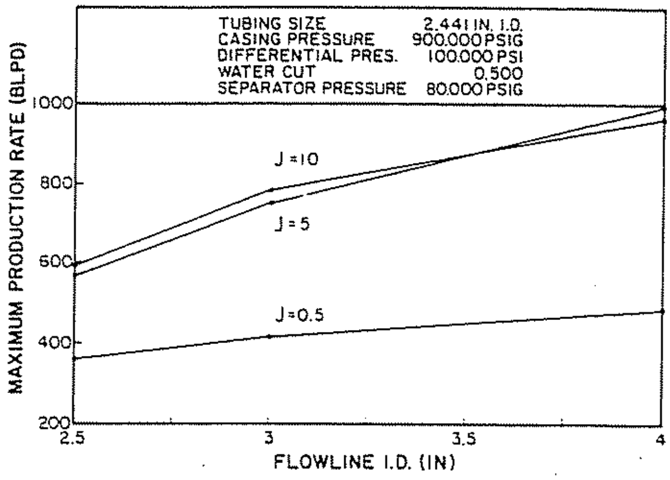

Figure 5.19 Effect of Flow-Line Size (courtesy of Johnston-Macco/Schlumberger)

line. This effect is shown in Figure 5.19 for lines between 2½ and 4 in. in diameter and for J's of 0.5, 5, and 10.

5.2313 EFFECT OF TUBING SIZE

Figure 5.20 shows the effect of tubing sizes. As tubing sizes are changed, the flow line should in turn be changed. For example, Figure 5.21 shows the rate to be 2,350 b/d for a 4-in. flow line in conjunction with a 4½-in. OD (3.958-in. ID) tubing size.

5.2314 EFFECT OF SEPARATOR PRESSURE

The separator pressure becomes very important in rotative gas-lift installations. Depending upon system conditions, a lowering of the separator pressure may or may not have much effect on the flow rate. Figure 5.22 shows these effects.

5.2315 EFFECT OF CASING PRESSURE

Figure 5.23 shows the effect of casing pressure on rate. An almost linear increase in rate for the higher J cases is noted as the pressure increases.

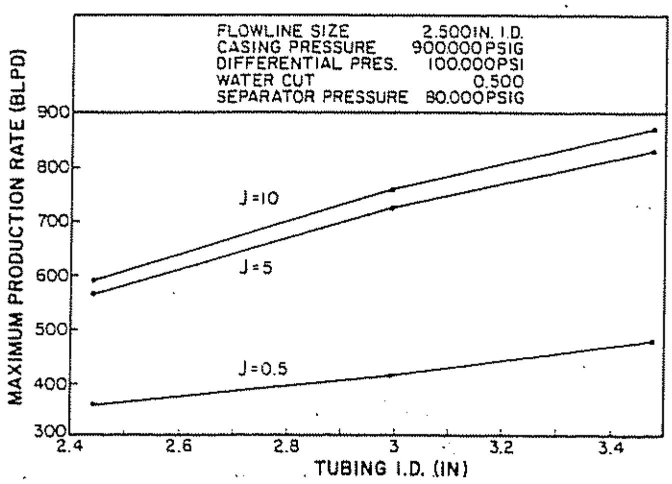

Figure 5.20 Effect of Tubing Size (courtesy of Johnston-Macco/Schlumberger)

Figure 5.24 shows that, as the pressure is increased in an unlimited manner, gas eventually goes around the bottom of the tubing and no further increase is noted.

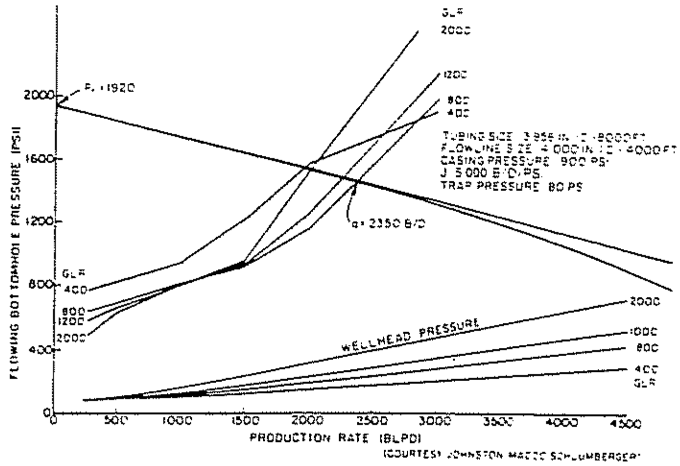

Figure 5.21 Systems Graph Showing Effect of Tubing Size (courtesy of Johnston-Macco/Schlumberger)

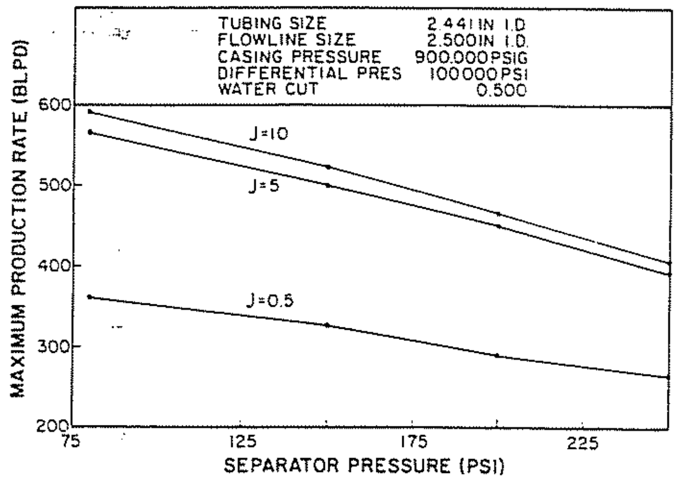

Figure 5.22 Effect of Separator Pressure (courtesy of Johnston-Macco/Schlumberger)

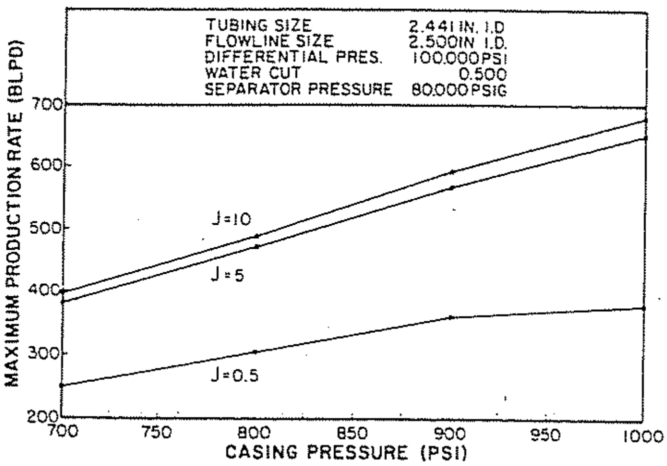

Figure 5.23 Effect of Casing Pressure (courtesy of Johnston-Macco/Schlumberger)

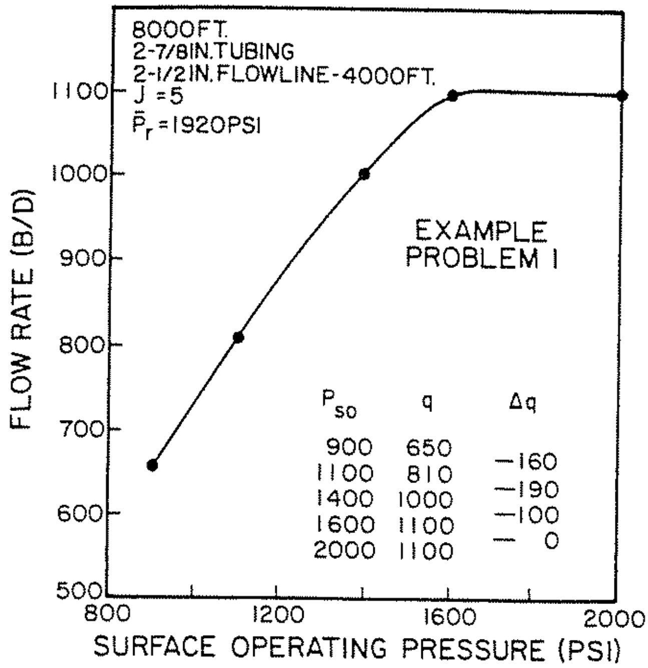

Figure 5.24 Effect of Injection Pressure

5.2316 EFFECT OF WATER CUT

Figure 5.25 has been prepared to show the effect of water cut. There are two effects from increased water. One is the heavier density of the water as compared to oil, but the principal effect is caused by the lowering of the solution gas-liquid ratio below the point of gas injection. Therefore, for wells with low surface injection pressure, there will be a greater decrease in flow rates than for wells with higher injection pressures as the water cut increases. If gas is going around bottom, there may be little effect of water cut if the GLR is maintained constant.

5.2317 EFFECT OF DIFFERENTIAL PRESSURE

The differential pressure that is selected for the solution depends on many factors and has been adequately discussed by Brown and Mach.[3] As can be seen in Figure 5.26, operating differential has a decided effect on

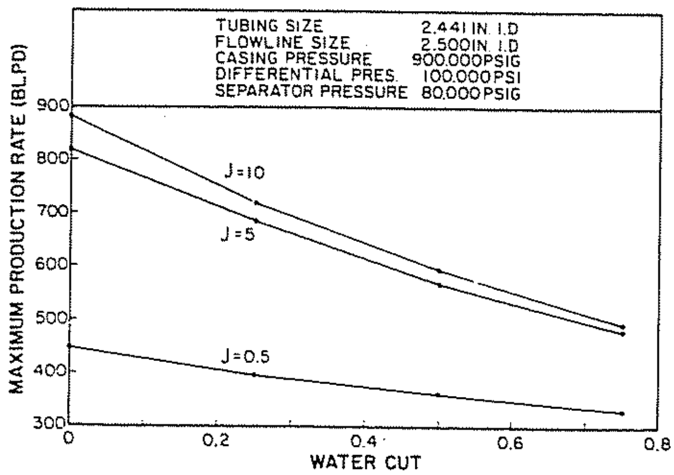

Figure 5.25 Effect of Water Cut (courtesy Johnston-Macco/Schlumberger)

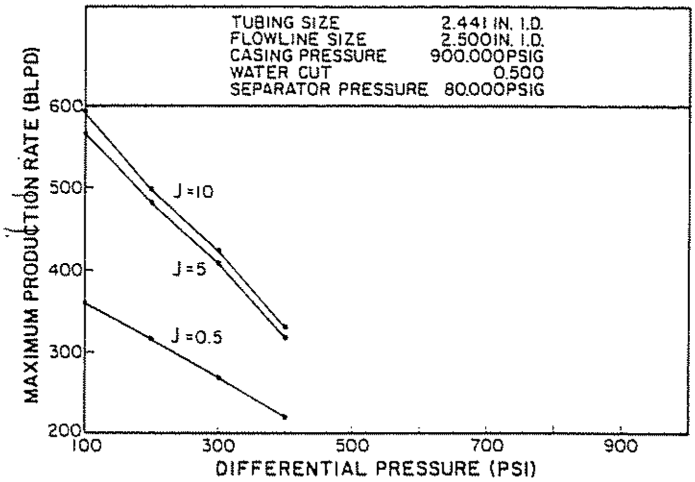

Figure 5.26 Effect of Operating Differential (courtesy Johnston-Macco/Schlumberger)

the rate. As the pressure differential between tubing and casing pressure increases, the flow rate decreases because in fact the mandrel spacing changes as discussed in Section 5.2328.

5.2318 EFFECT OF MANDREL SPACING

The operating differential of Figure 5.26 and the mandrel spacing of Figure 5.27 are directly related. One controls the other. Once the operating differential is selected, the mandrel spacing in and around the point of gas injection is fixed at a value equal to operating differential divided by the gradient of the fluid. For example, if $\Delta P = 100$ psi and the fluid gradient is 0.40 psi/ft, the spacing must be $\frac{100}{0.40} = 250$ ft or less.

EXAMPLE PROBLEM, WELLS #1 AND #2

The example wells of Table 5.1 were also worked. The principal difference between these two problems and the previous gas-lift example is that a constant wellhead pressure of 120 psig for well #1 and 80 psig for well #2 was used. Also, it was assumed that gas was being injected around the bottom of the tubing

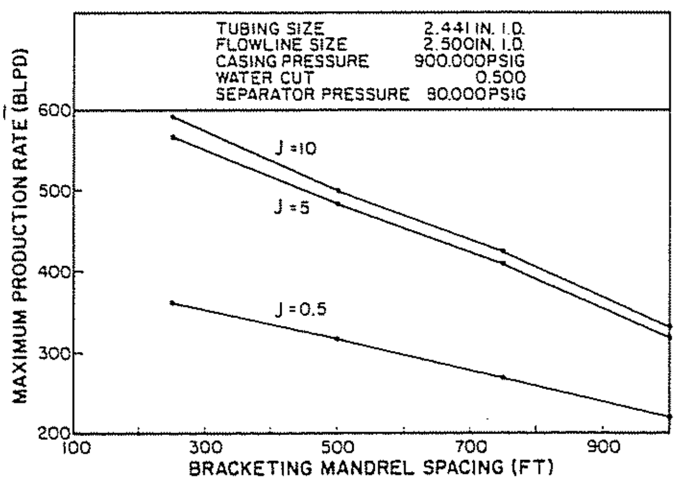

Figure 5.27 Effect of Mandrel Spacing (courtesy Johnston-Macco/Schlumberger)

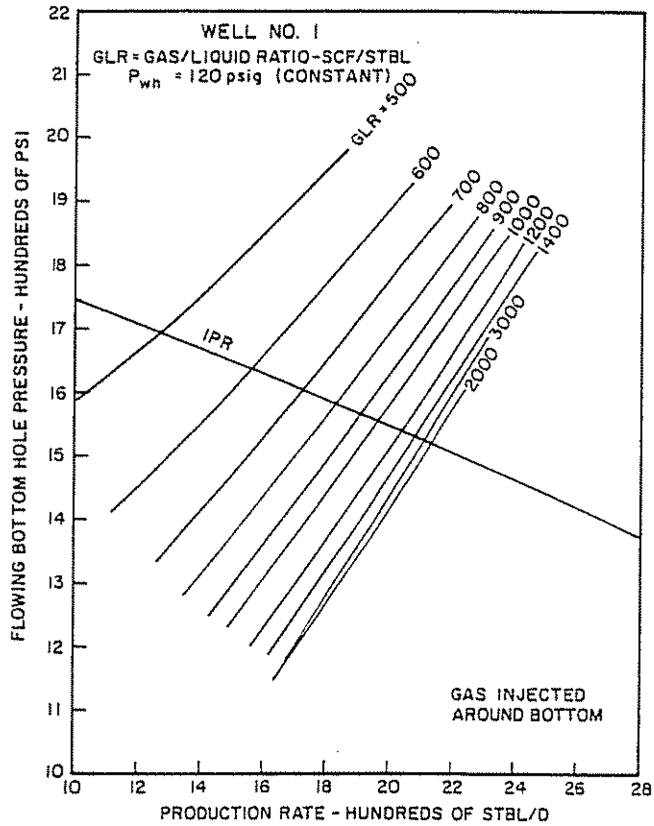

Figure 5.28 Tubing Intake Curves for Gas Lifting Well #1

string. Figure 5.28 shows these results for well #1, indicating a maximum rate of 2,000 b/d. For 900-psi casing pressure, the well will make only 1,000 b/d.

Figure 5.29 shows the gas-lift performance curves for this well from which an economic, optimum gas injection rate can be selected based on oil rate vs gas injection rate.

Figure 5.30 shows the results for well #2, indicating a maximum rate of 365 b/d. Figure 5.31 shows the gas-lift performance curve for this well from which an economic, optimum rate can be selected.

5.3 ELECTRIC SUBMERSIBLE PUMPS

5.31 DESCRIPTION OF EQUIPMENT

A typical submersible pumping unit consists of an electric motor, a seal section, an intake section, a multistage centrifugal pump, an electrical cable, a surface-installed switchboard, a junction box, and transformers. Additional miscellaneous components include means of securing the cable alongside the tubing and wellhead supports. Optional equipment may include a pressure sentry for sensing bottom-hole pressure and temperature, check and bleeder valves, etc.

The electric motor turns at a relatively constant speed, and the pump and the motor are directly coupled with a protector or seal section in between. Power is transmitted to the subsurface equipment through a three-conductor electric cable, which is strapped to the tubing. The fluid enters the pump at the intake section and is discharged into the tubing in which the unit is run into the well.

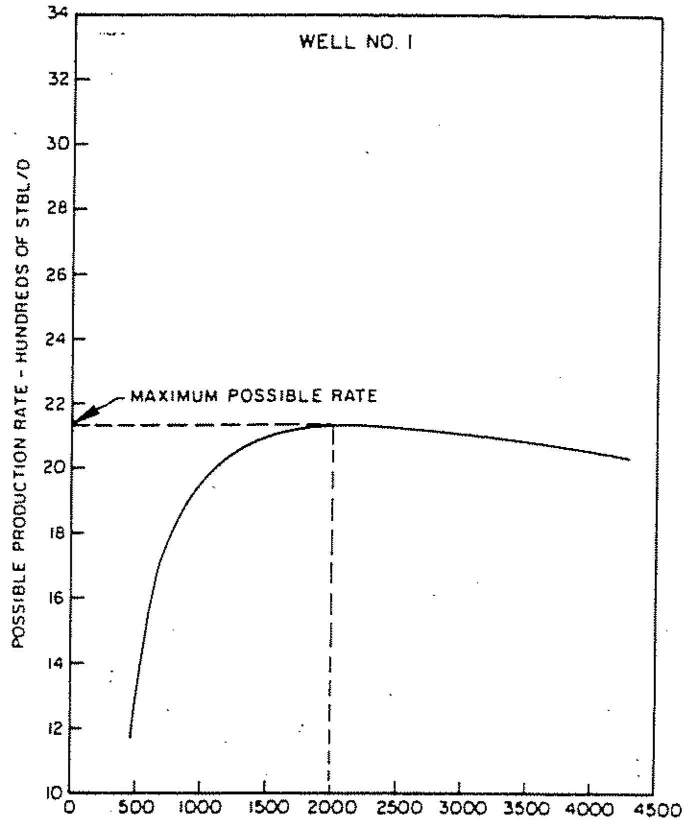

Figure 5.29 Possible Production Rate by Gas Lift vs Gas-Liquid Ratio for Well #1

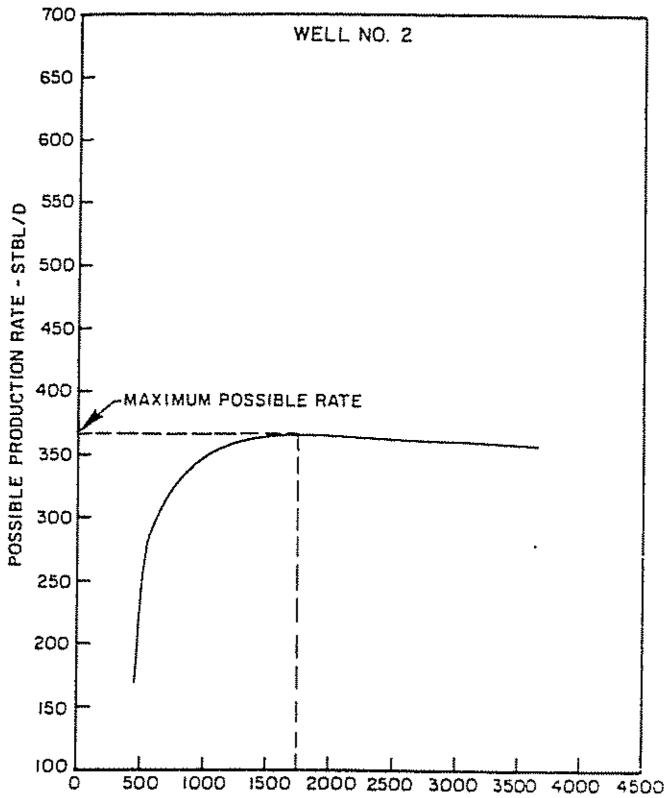

Figure 5.31 Possible Production Rate by Gas Lift vs Gas-Liquid Ratio for Well #2

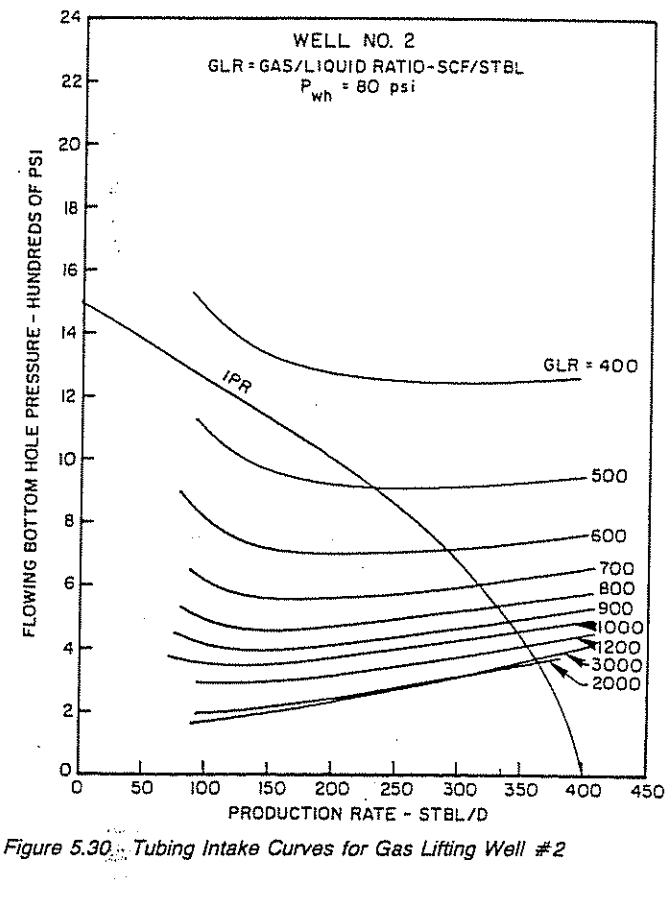

Figure 5.30 Tubing Intake Curves for Gas Lifting Well #2

The pump performs at highest efficiency when pumping liquid only. It can and does handle free gas along with the liquid. The manner in which the pump handles gas is not completely understood; however, high volumes of free gas are known to cause a very inefficient operation.

5.32 PUMP PERFORMANCE CURVES

The performance curves of several pump models were presented by Brown et al.[4] Pumps are divided into groups according to the minimum casing size into which the pump can be run. But even within the same group, each pump performs differently.

The performance curves of a submersible electrical pump (Figures 5.32 and 5.33) represent the variation of head, horsepower, and efficiency with capacity. Capacity refers to the volume of the produced fluid rate, which may include free and/or dissolved gas. These curves are for a fixed power cycle—normally 50 or 60 cycle—and can be changed with variable frequency controllers.

The head (in feet per stage) developed by a centrifugal pump is the same regardless of the type or specific gravity of the fluid pumped. But when converting this head to pressure, it must be multiplied by the gradient of the fluid in question. Therefore, the following can be stated:[4]

(pressure developed by pump) = (head per stage) × (gradient of fluid) × (number of stages)

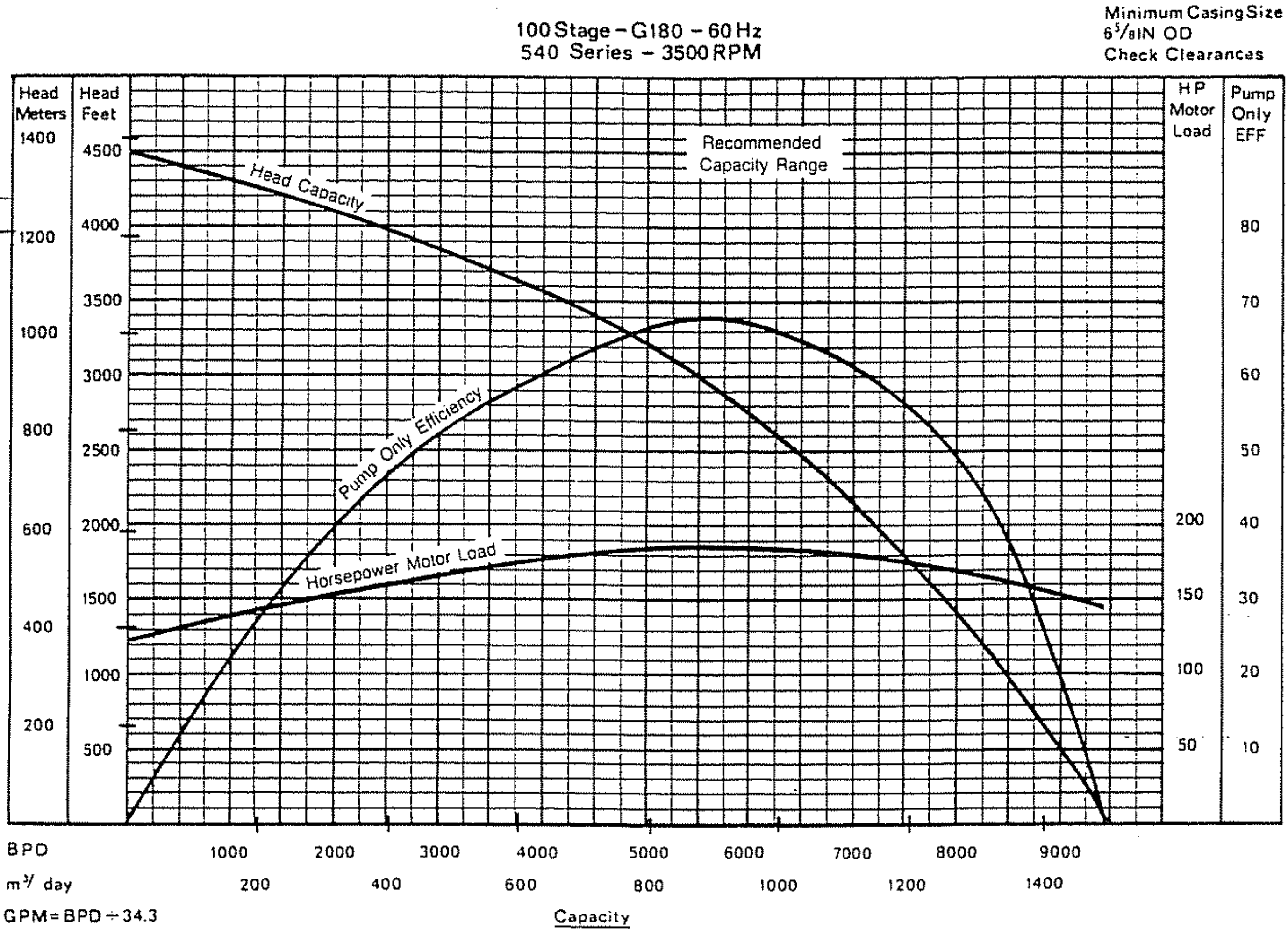

Figure 5.32 Performance Curves for Electrical Submersible Pump (after Brown et al.)[4]

When pumping gas with the liquid, the capacity and, consequently, the head per stage as well as the gradient vary as the pressure of the fluid is elevated from the intake value P_3 to the discharge value P_2. Thus, the above equation can be written as follows:

$$dP = h(V) \times G_f(V) \times d(St) \qquad (5.7)$$

where:

dP = the differential pressure developed by the pump, psi
h = the head per stage, ft/stage
G_f = the gradient of the pumped fluid, psi/ft
$d(St)$ = the differential number of stages

Note that parentheses are included to indicate that h and G_f are functions of the capacity V, which is given by Equation 5.4.

The gradient of the fluid at any pressure and temperature is given by:

$$G_f(V) = 0.433\ \gamma_f(V) \qquad (5.8)$$

but:

$$\gamma_f(V) = \frac{W}{350V}$$

where W is the weight of the capacity V at any pressure and temperature, which is equal to the weight at standard conditions. Hence:

$$\gamma_f(V) = \frac{q_{sc}\,\rho_{fsc}}{350V} \qquad (5.9)$$

Substituting Equation 5.9 into Equation 5.8 gives:

$$G_f(V) = \left(\frac{0.433}{350}\right)\frac{q_{sc}\,\rho_{fsc}}{V} \qquad (5.10)$$

ρ_{fsc} is the weight of 1 bbl of liquid plus pumped gas (per 1 bbl of liquid) at standard conditions, or:

$$\rho_{fsc} = 350\ wc\ \gamma_{wsc} + 350(1 - wc)\gamma_{osc} + (GIP)(GLR)\rho_{gsc} \qquad (5.11)$$

where ρ_{gsc} is the density of gas (in lb/scf) at standard conditions.

Substituting Equation 5.10 into Equation 5.7 gives:

$$d(St) = \left(\frac{350}{0.433\ q_{sc}\,\rho_{fsc}}\right)\frac{V}{h(V)}\,dP \qquad (5.12)$$

The total number of stages is obtained by integrating the above equation between the intake and the discharge pressures:

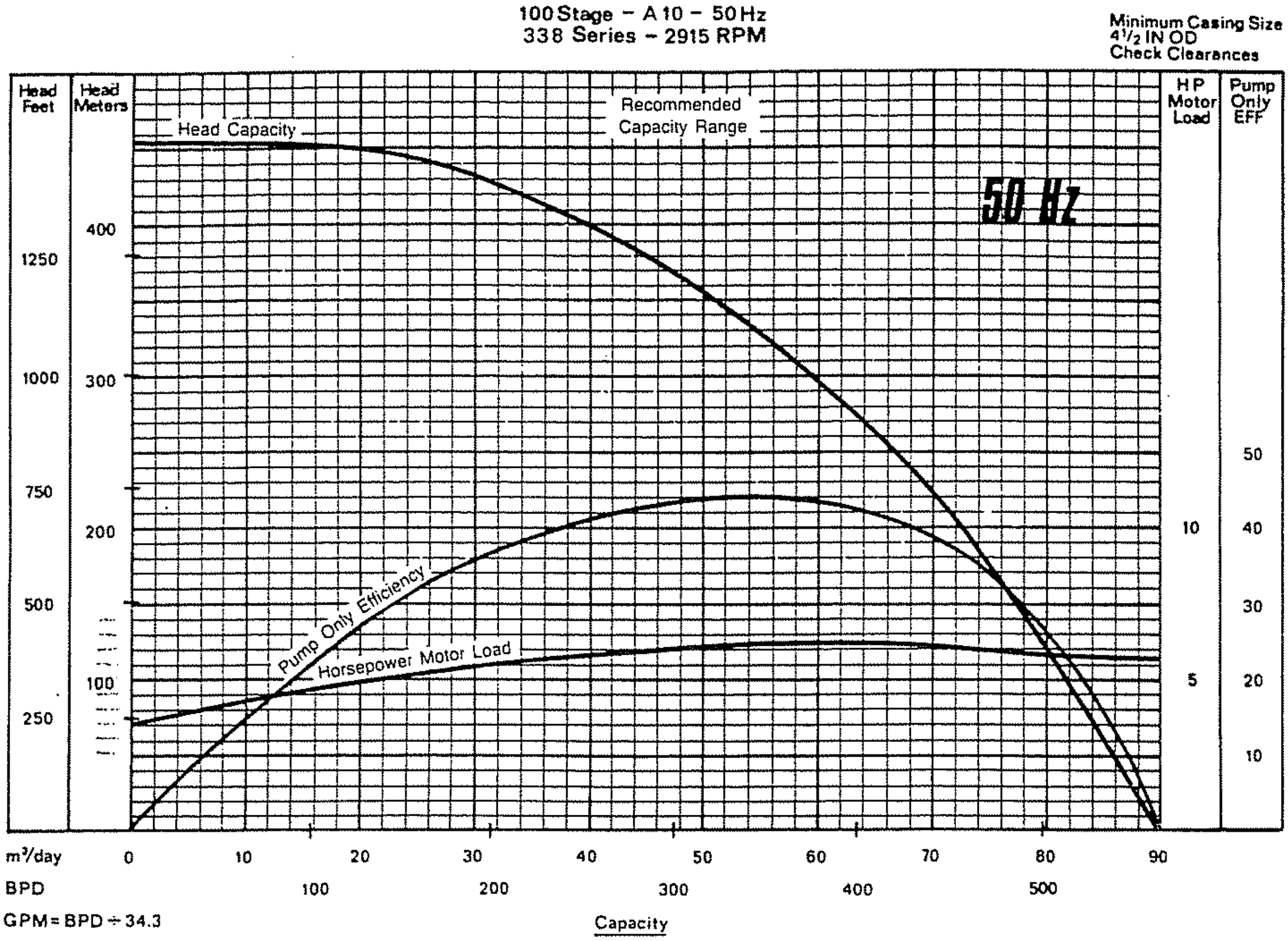

Figure 5.33 Performance Curves for Electrical Submersible Pump (after Brown et al.)[4]

$$\int_o^{St} d(St) = \left(\frac{350}{0.433\ q_{sc}\ \rho_{fsc}}\right)\int_{P_3}^{P_2}\frac{V}{h(V)}\,dP$$

or:

$$St = \left(\frac{808.3141}{q_{sc}\ \rho_{fsc}}\right)\int_{P_3}^{P_2}\frac{V}{h(V)}\,dP \tag{5.13}$$

Horsepower. The pump performance curves (Figures 5.32 and 5.33) give the horsepower per stage based on a fluid specific gravity equal to 1.0. This horsepower must be multiplied by the specific gravity of the fluid under consideration. Thus, the following can be stated:[4]

(horsepower requirements) = (horsepower per stage) × (specific gravity of fluid) × (number of stages)

Since the horsepower per stage, the specific gravity of the fluid, and the number of stages depend on the capacity V, which varies between the intake and the discharge pressures, the above equation can be written as follows:

$$d(HP) = hp(V) \times \gamma_f(V) \times d(St) \tag{5.14}$$

Substituting Equations 5.9 and 5.12 into the above equation gives:

$$d(HP) = \left(\frac{1}{0.433}\right)\frac{hp(V)}{h(V)}\,dP \tag{5.15}$$

The total horsepower requirement is obtained by integrating the above equation between the intake and the discharge pressures:

$$\int_o^{HP} d(HP) = \left(\frac{1}{0.433}\right)\int_{P_3}^{P_2}\frac{hp(V)}{h(V)}\,dP$$

or:

$$HP = \left(\frac{1}{0.433}\right)\int_{P_3}^{P_2}\frac{hp(V)}{h(V)}\,dP \tag{5.16}$$

For each pump, there is a capacity range within which the pump performs at or near its peak efficiency (see Figures 5.32 and 5.33). The volume range of the selected rate between the intake and the discharge pressures should, therefore, remain within the efficiency range of the pump. This range, of course, can be changed by using a variable frequency controller.

5.33 PUMP INTAKE CURVES

Predicting intake curves for submersible pumps is considered for two cases: (1) pumping only liquid, and (2) pumping liquid and gas. For both cases, it is assumed that the pump is set at the bottom of the well and that the wellhead pressure and the tubing size are fixed. For case 2, it is assumed that all associated gas

is pumped with the liquid. The sensitivity variable selected is the number of stages. As will be seen later, predicting intake curves for an electric submersible pump is direct for case 1 and indirect for case 2.

5.331 PUMPING LIQUID ONLY

Since liquids are only slightly compressible, the volume of the production rate can be considered constant and equal to the surface rate q_{sc}. Hence, the head per stage will also be constant, and Equation 5.13 can be integrated to give:

$$St = \left(\frac{808.3141}{\rho_{fsc}\, h}\right)(P_2 - P_3) \qquad (5.17)$$

Solving Equation 5.17 for P_3 gives:

$$P_3 = P_2 - \left(\frac{\rho_{fsc}\, h}{808.3141}\right) St \qquad (5.18)$$

Equation 5.16 also can be integrated to give:

$$HP = \left(\frac{1}{0.433}\right)\frac{hp}{h}(P_2 - P_3) \qquad (5.19)$$

Substituting Equation 5.17 into the above equation yields:

$$HP = hp\ \gamma_{fsc}\ St \qquad (5.20)$$

(1) *Pump selection.* As previously mentioned, pump selection is limited by the casing size. Another constraint is the desired production rate. If the objective is to maximize the production rate, the proper procedure is to select a pump whose efficiency range includes rates that are close to the maximum rate of the well.

5.3311 PROCEDURE FOR THE PREPARATION OF TUBING INTAKE CURVES FOR LIQUID ONLY

A step-wise procedure for predicting intake curves for the case when only liquid is pumped follows. This procedure is illustrated with a following example. Results of the calculations are shown in Figures 5.34, 5.35, 5.36, and 5.37.

(1) Select a suitable pump as dictated by the casing size and the flow capacity of the well.
(2) Calculate ρ_{fsc} from Equation 5.11 (GLR = 0) and γ_{fsc} from Equation 5.9 ($V = q_{sc}$).
(3) Assume various production rates and, for each of these rates, do the following:
   (a) Read the head per stage from the pump performance curves and calculate the quantity ($\rho_{fsc}h$/808.3141).
   (b) Determine the required discharge pressure from a pressure gradient correlation.
   (c) Assume various numbers of stages and, for each of these numbers, calculate the intake pressure from Equation 5.18.
(4) Plot the intake pressures vs rate for each assumed number of stages on the same graph as the IPR curve and to the same scale (see Figures 5.34 and 5.36).
(5) Read the rates at the intersection of the pump intake curves with the IPR curve.
(6) For each rate, read the horsepower per stage from

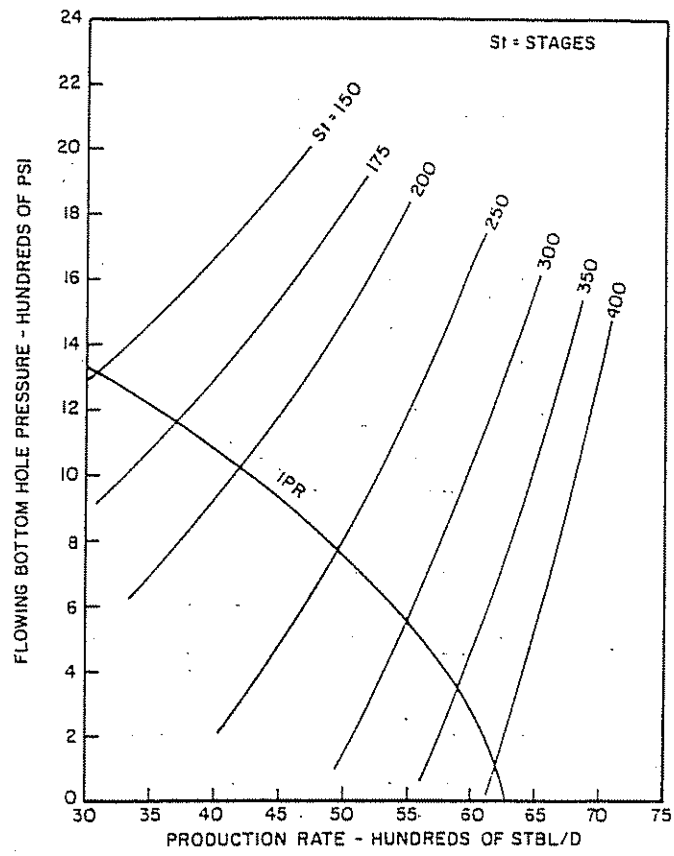

Figure 5.34 Intake Curves for an Electric Submersible Pump in Well #1 (Pumping Liquid)

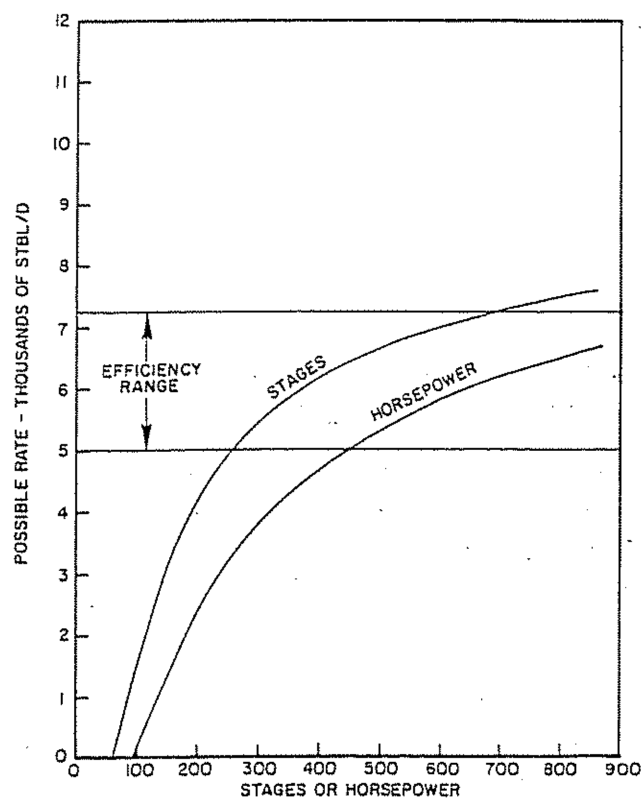

Figure 5.35 Possible Production Rate by Electric Pumping vs Stages and Horsepower for Well #1 (Pumping Liquid)

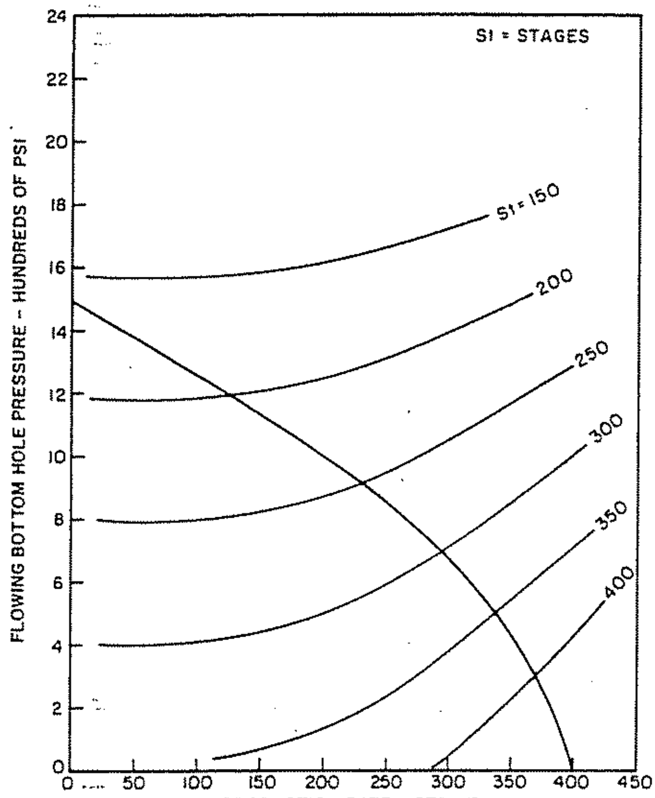

Figure 5.36 Intake Curves for an Electric Submersible Pump in Well #2 (Pumping Liquid)

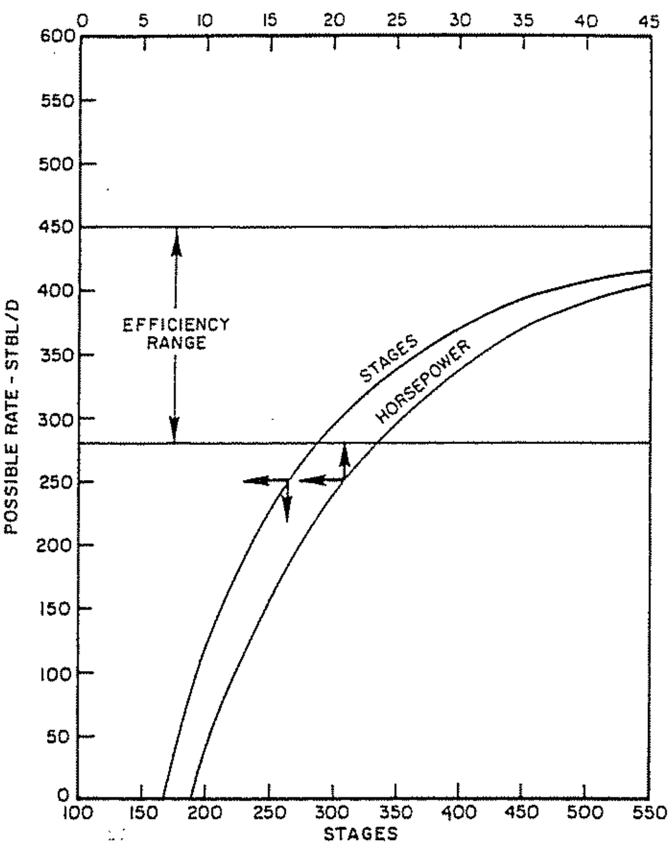

Figure 5.37 Possible Production Rate by Electric Pumping vs St and HP for Well #2 (Pumping Liquid)

the pump performance curves; then calculate the total horsepower requirement from Equation 5.20.

(7) Plot the rates vs the number of stages and horsepower requirements. Impose the efficiency range of the pump on the same graph (Figures 5.35 and 5.37).

(8) Select a suitable rate.

(2) *Rate selection.* Whether pumping only liquid or pumping gas with the liquid, the selected rate must satisfy the following criteria:

(1) Its volume range between the intake and the discharge pressures must remain within the efficiency range of the pump.

(2) It must be economically feasible.

As the number of stages and, consequently, the production rate increase, the effect of friction in the tubing string becomes significant, causing the discharge pressure to increase. As a result, the gain in the production rate per one stage continues to diminish until it becomes insignificant.

EXAMPLE PROBLEMS

To illustrate the procedure for pumping liquid only, calculations are made for the two example problems. The pump is set at the bottom of the well, and the wellhead pressure as well as the tubing size are fixed.

EXAMPLE WELL #1 FOR ELECTRICAL SUBMERSIBLE PUMPS (LIQUID ONLY)

Since the pump is set at the bottom of the well, the pump intake pressure is equal to the flowing bottom-hole pressure; hence, the stbl/d IPR shown in Figure 5.8 is applicable.

There are several pumps that can be used in a well with 7-in. casing. But since the objective is to maximize the production rate, a pump with an efficiency range that includes rates that are close to the maximum rate of the well will be selected. The performance curves for this pump are shown in Figure 5.32.

Equation 5.11 gives:

$$\rho_{fsc} = (0.5)(350)(1.074) + (0.5)(350)(0.85)$$
$$= 336.7 \text{lb/stbl}$$

Since liquids are essentially incompressible, V can be considered constant and equal to q_{sc}. For this case, Equation 5.9 reduces to:

$$\gamma_{fsc} = \frac{\rho_{fsc}}{350} = \frac{336.7}{350} = 0.962$$

With these values of ρ_{fsc} and γ_{fsc}, Equations 5.18 and 5.20 become:

$$P_3 = P_2 - 0.4165 h \, St \quad (5.21)$$

$$HP = (0.962) hp \, St \quad (5.22)$$

By assuming flow rates, P_2 can be determined from a pressure gradient correlation and h from the pump performance curves. By assuming St, P_3 and HP can be calculated from Equations 5.21 and 5.22. In doing so, the pump efficiency range will be ignored in order to show the effect of friction. Later, in rate selection, the pump efficiency will be considered.

For 3,000 stbl/d:

$P_2 = 3{,}679$ psi (pressure gradient correlation)
$h = 38.3$ ft/stage (Fig. 5.32)

Then Equation 5.21 becomes:

$$P_3 = 3{,}679 - 15.952\ St \qquad (5.23)$$

Assuming St and calculating P_3 from the above equation, we obtain:

St	P_3
150	1,286
175	887
200	489
250	−309

The same procedure is carried out for other assumed rates. Results of these calculations are shown in Table 5A.5 of Appendix 5. The obtained intake pressure was plotted vs q_{sc} for the various assumed number of stages (see Fig. 5.34). The stbl/d IPR was plotted to the same scale on the same graph. The rates are noted at the intersections of the pump intake curves with the IPR curve. For example, the well can produce 3,075 stbl/d with 150 stages. For this rate, Figure 5.32 shows the head per stage to be 1.66. The total horsepower requirement is calculated from Equation 5.22 as follows:

$$HP = (0.962)(1.66)(150) = 240\ HP$$

The same procedure was carried out for other rates. Results of these calculations are shown in Table 5A.6 (Appendix 5). The rate q_p was plotted vs St and HP in Figure 5.35. The pump efficiency range (5,000–7,250 stbl/d) was imposed on the same figure.

Inspection of Figure 5.35 indicates that, beyond 7,500 stbl/d, the number of stages as well as the horsepower requirement increases very fast without any significant gain in the production rate.

A good choice in this case is 6,000 stbl/d because this rate allows a reasonable drawdown and operates the pump near its peak efficiency (see Fig. 5.32). For 6,000 stbl/d, the discharge pressure is 4,487 psi, the number of stages is 367 (Fig. 5.35), and the horsepower requirement is 640 (Fig. 5.35).

EXAMPLE PROBLEM #2 (LIQUID ONLY)

The same type of calculations previously made for well #1 were carried out for well #2. The most suitable pump was found to be that shown in Figure 5.33. Results of calculations are shown in Tables 5A.7 and 5A.8 of Appendix 5.

The data of Table 5A.7 were plotted along with the stbl/d IPR curve in Figure 5.36. The horsepower requirement for the rates (obtained from Figure 5.36) is shown in Table 5A.8. Figure 5.37 is a plot of q_p vs St and HP. The selected rate is 375 stbl/d for which the number of stages and the horsepower requirements are 410 and 36, respectively. The required discharge pressure is 2,740 psi.

5.332 PUMPING LIQUID AND GAS

Because of the high compressibility of gas, the volume of the produced fluid rate V may undergo a significant variation as the pressure of the fluid changes from the intake value to the discharge value. At any pressure point between the intake and the discharge, the volume factor is determined from Equation 5.2 if all gas is pumped with the liquid or Equation 5.3 if a certain percentage of the gas is vented. In either case, the volume of the flow rate is given by Equation 5.4.

5.3321 DETERMINATION OF THE NUMBER OF STAGES

Because V and, consequently, h vary as the fluid passes through the pump, direct integration of Equation 5.13 is possible only if the integrand $V/h(V)$ can be reduced to a simple function of pressure. But this is difficult because VF is a very complicated function of pressure (see Equation 5.2). For this reason, numerical integration methods are recommended.

The existence of gas at the intake section of the pump implies that the intake pressure is below the bubble point of the crude (saturated crude). If that is the case and if the required discharge pressure is above the bubble point, Equation 5.13 should be broken down into two integrals as follows:

$$St = \frac{A}{q_{sc}}\int_{P_3}^{P_b} \frac{V}{h(V)}\,dP + \frac{A}{q_{sc}}\int_{P_b}^{P_2} \frac{V}{h(V)}\,dP \qquad (5.24)$$

where $A = 808.3141/\rho_{fsc}$ = constant (5.25)

For performing numerical integration, Equation 5.24 can be written in a more convenient form as follows:

$$St = \frac{A}{q_{sc}}\sum_{i=1}^{m} \frac{\overline{V}_i}{\overline{h}_i}\Delta P_{3,i} + \frac{A}{q_{sc}}\sum_{j=m}^{n} \frac{\overline{V}_j}{\overline{h}_j}\Delta P_{3,j} \qquad (5.26)$$

where:

$P_{3,i}$ = any intake pressure above the bubble point
$P_{3,j}$ = any intake pressure below the bubble point
$P_{3,0}$ = discharge pressure (P_2)
$P_{3,m}$ = bubble-point pressure (P_b)
$\Delta P_{3,i} = P_{3,i-1} - P_{3,i}$
$\Delta P_{3,j} = P_{3,j-1} - P_{3,j}$
$\overline{V}_i/\overline{h}_i$ and $\overline{V}_j/\overline{h}_j$ = average quantities evaluated at the average pressures $\overline{P}_{3,i}$ and $\overline{P}_{3,j}$, respectively

where:

$$\overline{P}_{3,i} = (P_{3,i-1} + P_{3,i})/2$$

and

$$\overline{P}_{3,j} = (P_{3,j-1} + P_{3,j})/2$$

The main reason for breaking down the number of stages into two summations is the fact that V and, consequently, h undergo only slight change above the bubble point; hence, $\Delta P_{3,i}$ can be taken much larger than $\Delta P_{3,j}$. In fact, satisfactory results are obtained even if ΔP_3 is taken as the difference between P_b and P_2 and the quantity $\overline{V}/\overline{h}$ is evaluated at the midpoint.

When using a computer solution, it is easier to divide the interval between the intake and the discharge pres-

sures into equal increments by taking ΔP_3 constant. For this case, Equation 5.26 can be written as:

$$St_i = \sum_{i=1}^{n} \left(\frac{A\Delta P_3}{q_{sc}}\right)\frac{\bar{V}_i}{\bar{h}_i} \qquad (5.27)$$

where:

$$P_{3,0} = \text{discharge pressure } (P_2) \qquad (5.28)$$
$$P_{3,n} = \text{intake pressure } (P_3) \qquad (5.29)$$
$$n = (P_2 - P_3)/\Delta P_3 \qquad (5.30)$$
$$P_{3,i} = P_{3,i-1} - \Delta P_3 \qquad (5.31)$$

The quantity $\bar{V}_i/\bar{h}_i$ is evaluated at the average pressure given by:

$$\bar{P}_{3,i} = (P_{3,i-1} + P_{3,i})/2 \qquad (5.32)$$

In reality, any pressure $P_{3,i}$ can be considered an intake pressure. To illustrate this point, Equation 5.27 can be written in the following form:

$$St_i = \sum_{i=1}^{n} \Delta(St)_i \qquad (5.33)$$

where:

$$\Delta(St)_i = \left(\frac{A\Delta P_3}{q_{sc}}\right)\frac{\bar{V}_i}{\bar{h}_i} \qquad (5.34)$$

Therefore, in order to obtain an intake pressure $P_{3,1}$, we have:

$$St_1 = \Delta(St)_1 = \left(\frac{A\Delta P_3}{q_{sc}}\right)\frac{\bar{V}_1}{\bar{h}_1} \qquad (5.35)$$

In order to obtain $P_{3,2}$, we have:

$$St_2 = \Delta(St)_1 + \Delta(St)_2 = \frac{A\Delta P_3}{q_{sc}}\left(\frac{\bar{V}_1}{\bar{h}_1} + \frac{\bar{V}_2}{\bar{h}_2}\right) \qquad (5.36)$$

And in order to obtain $P_{3,n}$, we have:

$$St_n = \Delta(St)_1 + \Delta(St)_2 + \ldots + \Delta(St)_n = \left(\frac{A\Delta P_3}{q_{sc}}\right)\left(\frac{\bar{V}_1}{\bar{h}_1} + \frac{\bar{V}_2}{\bar{h}_2} + \ldots + \frac{\bar{V}_n}{\bar{h}_n}\right) \qquad (5.37)$$

5.3322 DETERMINATION OF HORSEPOWER

The horsepower requirement is obtained by integrating Equation 5.16 between the intake and the discharge pressures. Since the integrand hp(V)/h(V) cannot be reduced to a simple function of pressure, direct integration is not possible, and numerical methods must be used.

If the interval between the intake and the discharge pressure is divided into equal increments by taking ΔP_3 constant, Equation 5.16 can be written as follows:

$$HP_i = \sum_{i=1}^{n}\left(\frac{\Delta P_3}{0.433}\right)\frac{\bar{h}p_i}{\bar{h}_i} \qquad (5.38)$$

where all subscripted variables are as defined by Equations 5.28–5.32.

If $\Delta(HP)_i$ is defined as:

$$\Delta(HP)_i = \left(\frac{\Delta P_3}{0.433}\right)\frac{\bar{h}p_i}{\bar{h}_i} \qquad (5.39)$$

then Equation 5.38 can be written as:

$$HP_i = \sum_{i=1}^{n} \Delta(HP)_i \qquad (5.40)$$

5.3323 PUMP SELECTION

As mentioned previously, pump selection is limited by the casing size and the flow capacity of the well. Another constraint that must be taken into account when pumping gas with the liquid is the volume range of the flow rate. Because of the high compressibility of gas, the difference between the intake and the discharge volumes may be too great to be contained within the efficiency range of one pump. For this reason, the following procedure for pump selection is suggested:

(1) Prepare IPR curves in stbl/d and b/d to the same scale on the same graph.
(2) Enter the b/d IPR curve at the upper limit of the efficiency range of several pumps that are suitable from a casing-size standpoint. Move horizontally to the stbl/d IPR curve and read the intake rate in stbl/d.
(3) For each intake rate determined in step 2, do the following:
    (a) Determine the required discharge pressure from a two-phase flow correlation.
    (b) Calculate VF at the discharge pressure from Equation 5.2 or Equation 5.3; then calculate the discharge volume from Equation 5.4.
(4) Select the pump for which the discharge volume is greater than or equal to the lower limit of its efficiency range.

Note: if more than one pump is found to be suitable, choose the one with the highest capacity.

5.3324 PROCEDURE FOR THE PREPARATION OF INTAKE CURVES FOR WELLS PUMPING GAS

A step-wise procedure for predicting tubing intake curves for the case in which gas is with the liquid is given as follows: The procedure is illustrated with examples.

(1) Select a suitable pump as outlined previously.
(2) Calculate ρ_{fsc} from Equation 5.11 and calculate the constant A from Equation 5.25.
(3) Assume several production rates in stbl/d and, for each of these rates, do the following:
    (a) Determine the required discharge pressure $(P_{3,0})$ from a two-phase flow correlation.
    (b) Choose ΔP_3 and calculate the quantity $(A\Delta P_3/q_{sc})$.
    (c) Calculate $P_{3,1}$ from Equation 5.31 and $\bar{P}_{3,1}$ from Equation 5.32.
    (d) Determine $\overline{VF}_1$ at $\bar{P}_{3,1}$ from Equation 5.2; then calculate $\bar{V}_1$ from Equation 5.4.
    (e) Read $\bar{h}_1$ at $\bar{V}_1$ from the pump performance curves.
    (f) Calculate the required number of stages to obtain the intake pressure $P_{3,1}$ from Equation 5.27.
    (g) Repeat steps c–f for $P_{3,2}$, $P_{3,3}$, through $P_{3,i}$ until a convenient intake pressure is reached. Tabulate the intake pressure vs the number of stages.

(4) By interpolation or plotting, obtain intake pressures for the assumed rates for an identical number of stages.
(5) Plot the intake pressure (obtained in step 4) vs the assumed production rates for the various number of stages. Plot the stbl/d IPR curve to the same scale on the same graph.
(6) Read the rates at the intersection of the pump intake curves with the IPR curve.
(7) For each rate, calculate the horsepower requirement from Equation 5.38.

Note: Calculation of horsepower requirements is similar to the calculation of the number of stages.

(8) Plot the rate vs the number of stages and horsepower requirements. Impose the efficiency range of the pump on the same graph.
(9) Select a suitable rate (see C2 in Section 5.3311).

EXAMPLE PROBLEM #1

For this solution, refer to Figures 5.38 and 5.39. Since the pump is set at the bottom of the well and all gas is pumped with the liquid, the IPR curves of Figure 5.8 and the volume factor data of Table 5A.1 (Appendix 5) are applicable.

As for the liquid case, there are several pumps that can be used in a well with 7-in. casing. But before selecting any pump, it must be made certain that the discharge volume of the upper limit of the efficiency range of the pump is greater than or equal to the lower limit of the efficiency range. Using the procedure described previously, the following can be obtained:

Pump #	Upper limit, bbl/d	Upper limit, stbl/d	P_2	Vol. of upper limit @ P_2, b/d	Lower limit, b/d
1	4,500	3,550	3,357	3,926	3,200
2	6,400	4,500	3,698	4,973	4,400
3	7,250	4,800	3,808	5,303	5,000

Since the volume of the upper limit at P_2 is greater than the lower limit for all pumps shown above, any of these pumps can be used. Since the objective in this case is to maximize the production rate, use the pump of Figure 5.32. This will control the selection.

Enter the b/d IPR curve (Fig. 5.8) at a rate slightly higher than the lower limit of the efficiency range of the selected pump, say, 5,250 stbl/d; then move horizontally to the stbl/d IPR to obtain 3,975 stbl/d. The required discharge pressure for 3,975 stbl/d is 3,505 psi, at which VF is 1.1055 bbl/stbl. The discharge volume is then 3,975 × 1.1055 or 4,395 b/d. Since 4,395 b/d is less than the lower limit (5,000 b/d), the same calculation should be made for rates higher than 5,250 b/d until a discharge volume higher than or equal to 5,000 b/d is obtained. However, since the pump efficiency at 4,395 b/d is still okay in this case (Fig. 5.32), the obtained rate of 3,975 stbl/d will be taken as the lower limit of the efficiency range of the pump.

The gas density at standard conditions is given by:

$$\rho_{gsc} = (0.0763)\gamma_{gsc} = (0.0763)(0.7) = 0.0534 \text{ lb/scf}$$

Then, Equation 5.11 gives:

$$\rho_{fsc} = (350)(0.5)(0.074) + (350)(1-0.5)(0.85) + (200)(0.0534) = 347.4 \text{ lb/stbl}$$

and Equation 5.25 gives:

$$A = 808.3141/347.4 = 2.327$$

Equation 5.27 can be written as:

$$St_i = \sum_{i=1}^{n} (A\Delta P_3)\frac{\overline{VF}_i}{\bar{h}_i} \qquad (5.41)$$

where:

$$\overline{V}_i = q_{sc}\overline{VF}_i \qquad (5.42)$$

With the obtained value of A and if ΔP_3 is taken to be 50 psi, Equation 5.41 becomes:

$$St_i = \sum_{i=1}^{n} (116.35)\frac{\overline{VF}_i}{\bar{h}_i} \qquad (5.43)$$

and Equation 5.38 becomes:

$$HP_i = \sum_{i=1}^{n} (115.47)\frac{\bar{h}p_i}{\bar{h}_i} \qquad (5.44)$$

Therefore, by assuming a liquid surface rate, the number of stages required to obtain any intake pressure $P_{3,i}$ can be obtained from Equation 5.43. The pump efficiency will be ignored in order to show the effects of friction and pumping gas with the liquid but will be considered when dealing with rate selection.

For 3,000 stbl/d:

$$P_{3,0} = P_2 = 3{,}178 \text{ psi (two-phase flow correlation)}$$

@ $i = 1$:

$$P_{3,1} = 3{,}178 - 50 = 3{,}128 \text{ psi (Eq. 5.31)}$$

$$\overline{P}_{3,1} = \frac{3{,}178 + 3{,}128}{2} = 3{,}153 \text{ psi (Eq. 5.32)}$$

@ $\overline{P}_{3,1}$:

$$\overline{VF}_1 = 1.1066 \text{ bbl/stbl (Eq. 5.2)}$$

Then:

$$\overline{V}_1 = (3{,}000)(1.1066) = 3{,}319 \text{ b/d (Eq. 5.42)}$$

@ $\overline{V}_1$:

$$\bar{h}_1 = 37.5 \text{ ft/stage (Fig. 5.32)}$$

Then, Equation 5.43 gives:

$$St_1 = \Delta St_1 = (116.35)\left(\frac{1.1066}{37.5}\right) = 3.4 \text{ stages}$$

@ $i = 2$:

$$P_{3,2} = 3{,}128 - 50 = 3{,}078 \text{ psi}$$

$$\overline{P}_{3,2} = \frac{3{,}128 + 3{,}078}{2} = 3{,}103 \text{ psi}$$

@ $\overline{P}_{3,2}$:

$$\overline{VF}_2 = 1.1068 \text{ bbl/stbl}$$

Then:

$$\overline{V}_2 = (3{,}000)(1.1068) = 3{,}320 \text{ b/d}$$

@ $\overline{V}_2$:

$$\bar{h}_2 = 37.5 \text{ ft/stage}$$

Then:

$$\Delta St_2 = (116.35)\left(\frac{1.1068}{37.5}\right) = 3.4 \text{ stages}$$

and:

$$St_2 = \Delta St_1 + \Delta St_2 = 3.4 + 3.4 = 6.8 \text{ stages}$$

The above calculations for 3,000 stbl/d were continued until an intake pressure of 328 psi was reached (Table 5A.9—Appendix 5). Note that ΔSt_i is essentially constant for pressures above the bubble point.

Interpolation of the data in Table 5A.9 (Appendix 5) between St_i and $P_{3,i}$ gives the following:

St	P_3
150	1,080
175	816
200	602
250	348

A similar procedure was carried out for other assumed rates. Results of the calculations are shown in Table 5A.10. The obtained intake pressure was plotted vs q_{sc} for the various number of stages in Figure 5.38. The stbl/d and the b/d IPR's were plotted to the same scale on the same graph. The possible rates are found at the intersection of the pump intake curves with the stbl/d IPR. For example, the well can produce 3,370 stbl/d with 150 stages. For 3,370 stbl/d:

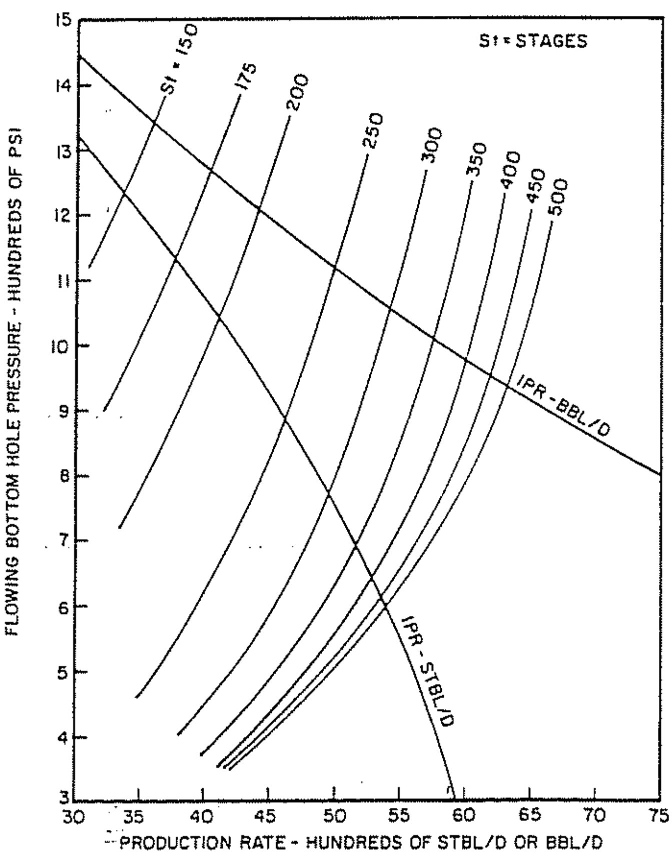

Figure 5.38 Intake Curves for an Electric Submersible Pump in Well #1 (Pumping Liquid and Gas)

$$P_3 = P_{3,n} = 1{,}238 \text{ psi (IPR curve)}$$

and:

$$P_2 = P_{3,0} = 3{,}298 \text{ psi (two-phase flow correlation)}$$

The horsepower requirement is calculated in the same manner as was done for the number of stages. For example:

@ $i = 1$:

$$P_{3,1} = 3{,}298 - 50 = 3{,}248 \text{ psi (Eq. 5.31)}$$

$$\bar{P}_{3,1} = \frac{3{,}298 + 3{,}248}{2} = 3{,}273 \text{ psi (Eq. 5.32)}$$

@ $\bar{P}_{3,1}$:

$$\overline{VF}_1 = 1.1062 \text{ bbl/stbl (Eq. 5.2)}$$

then:

$$\bar{V}_1 = (3{,}370)(1.1062) = 3{,}728 \text{ b/d (Eq. 5.42)}$$

@ $\bar{V}_1$:

$$\overline{hp}_1 = 1.73 \text{ HP/stage (Fig. 5.32)}$$

and:

$$\bar{h}_1 = 36.3 \text{ ft/stage (Fig. 5.32)}$$

Then Equation 5.44 gives:

$$HP_1 = (115.47)\left(\frac{1.73}{36.3}\right) = 5.49 \text{ HP}$$

@ $i = 2$:

$$P_{3,2} = 3{,}248 - 50 = 3{,}198 \text{ psi}$$

$$\bar{P}_{3,2} = \frac{3{,}248 + 3{,}198}{2} = 3{,}223 \text{ psi}$$

@ $\bar{P}_{3,2}$:

$$\overline{VF}_2 = 1.1064 \text{ bbl/stbl}$$

then:

$$\bar{V}_2 = 3{,}729 \text{ b/d}$$

@ $\bar{V}_2$:

$$\overline{hp}_2 = 1.73 \text{ HP/stage}$$

and:

$$\bar{h}_2 = 36.3 \text{ ft/stage}$$

then:

$$HP_2 = (115.47)\left(\frac{1.73}{36.3}\right) + (115.47)\left(\frac{1.73}{36.3}\right) = 10.98 \text{ HP}$$

The preceding calculations for 3,370 stbl/d were continued in Table 5A.11 until the required intake pressure (1,238 psi) was reached. Note that ΔHP_i is essentially constant for pressures above or slightly below the bubble point.

The same procedure was carried out for other possible rates. Results of calculations are shown in Table 5A.12. Possible rate q_p was plotted vs St and HP in Figure 5.39. The efficiency range of the pump (3,975–4,800 stbl/d) was imposed on the same figure.

Inspection of Figure 5.39 shows that, beyond 5,375 stbl/d, the number of stages as well as the horsepower requirement increase very fast without significant gain in the production rate. But 5,375 stbl/d cannot be se-

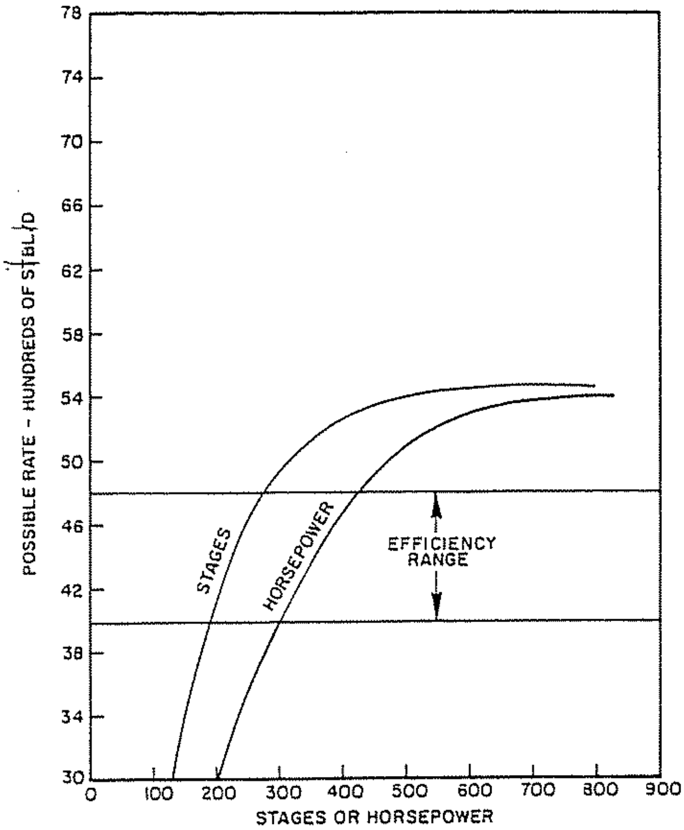

Figure 5.39 Possible Production Rate by Electric Pumping vs St and HP for Well #1 (Pumping Liquid and Gas)

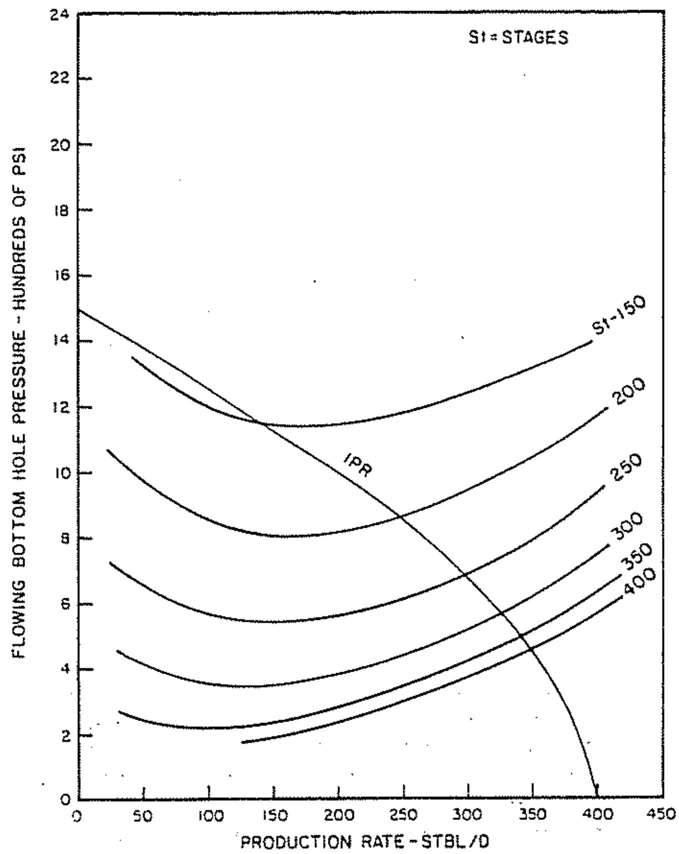

Figure 5.40 Intake Curves for an Electric Submersible Pump in Well #2 (Pumping Liquid and Gas)

lected since it is outside of the efficiency range of the pump. Clearly, the choice in this case should be the upper limit of the efficiency range (4,800 stbl/d). This rate requires 275 stages and 425 HP (Figure 5.39). The discharge pressure is 3,808 psi.

EXAMPLE PROBLEM #2

The same general procedure for pumping gas on well #2 was applied. The results are shown in Figures 5.40 and 5.41, with calculations shown in Tables 5A.13 and 5A.14 in Appendix 5.

Discussion of results for electrical pumping. Results of the calculations for both liquid and gas are shown in Figures 5.34 through 5.41. Whether pumping only liquid (Figs. 5.35 and 5.37) or pumping gas with the liquid (Figs. 5.39 and 5.41), it is evident that the gain in the production rate per one stage diminishes as the rate increases. This is attributed to the effect of friction loss in the tubing string, which works to increase the discharge pressure. Note that the effect of friction loss for well #2 is minor because of the low rates associated with this well.

Comparing Figure 5.34 to Figure 5.38 or Figure 5.36 to Figure 5.40 shows that, for intake pressures above or slightly below the bubble point (1,820 psi for the crude of well #1 and 940 psi for the crude of well #2), higher production rates can be obtained by pumping gas with the liquid. The reason is that the volume of the produced fluid rate and, consequently, the head per stage developed by the pump remain essentially constant in that range of pressure. However, the dis-

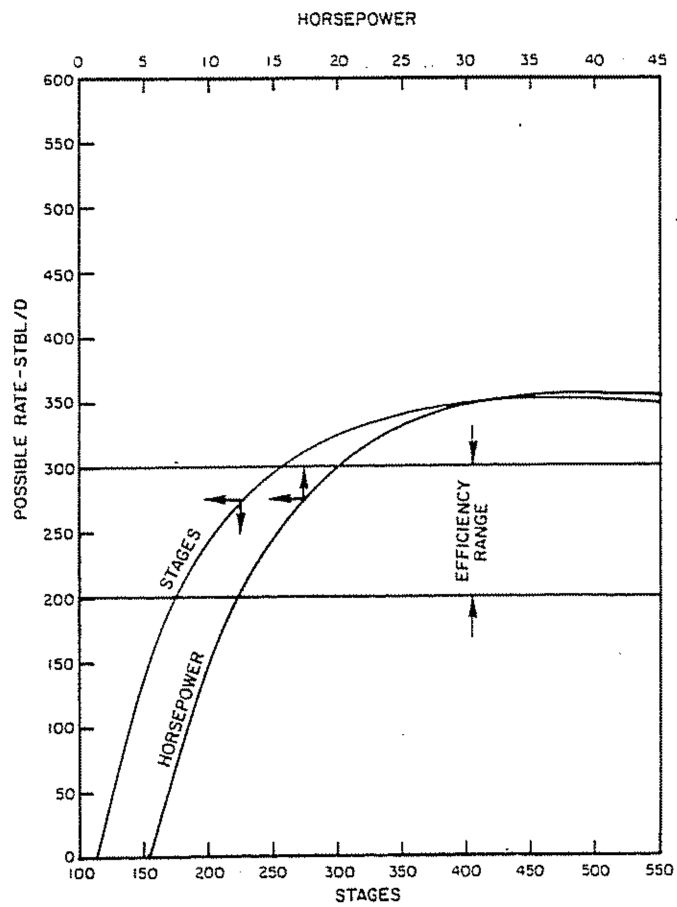

Figure 5.41 Possible Production Rate by Electric Pumping vs St and HP for Well #2 (Pumping Liquid and Gas)

charge pressure is reduced by the existence of gas in the tubing.

As the intake pressure drops below the bubble point, the fluids (especially free gas) expand, causing a significant increase in the volume of the produced fluid rate which, in turn, causes the head per stage developed by the pump to decline (see Figs. 5.32 and 5.33). As a result, the gain in the production rate per one stage declines much faster than in the case where pumping only liquid. For example, 300 stbl/d can be gained from well #1 by increasing the number of stages from 350 to 400 when pumping only liquid (Fig. 5.34), while the gain for the same increase in the number of stages is only 125 stbl/d when pumping gas with the liquid (Fig. 5.38).

5.4 HYDRAULIC PUMPS

5.41 DESCRIPTION OF EQUIPMENT

A subsurface hydraulic piston pump is a closely coupled reciprocating engine and pump. High-pressure power fluid is directed to the engine through one conduit, and spent power fluid is directed to the surface either through the same conduit with the produced fluid or through a separate conduit. The engine is normally referred to as the engine end of the pump, and the pump as the pump end of the pump.[5]

There is a variety of pump models; each is unique in its design of the engine end and/or pump end. However, the principle is the same for all pump models. Wilson[16] and Brown and Wilson[5] discussed basic aspects of hydraulic pumping. Tables 5.3, 5.4, 5.5, and 5.6 are some of the specification tables that are used in designing subsurface pumps.

5.42 POWER FLUID SYSTEMS

There are two basic types of power fluid systems:

(1) the closed power fluid (CPF) system in which the surface and subsurface power fluid stays in a closed conduit and does not mix with the produced fluid (Figure 5.42a)

(2) the open power fluid (OPF) system in which the power fluid mixes with the production fluid downhole and returns to the surface as commingled power fluid and production (Fig. 5.42b)

The power fluid is either water or oil. The choice of power fluid and/or power fluid system depends on a number of factors. Brown and Wilson discussed these factors in detail;[5] however, it is worth mentioning here

TABLE 5.3
SPECIFICATIONS FOR KOBE E PUMPS (AFTER WILSON)[16]

Pump size or description	P/E ratio	Displacement: At rated speed	Displacement: b/d per SPM, Eng.	Displacement: b/d per SPM, Pump	Max. rated speed spm
2 × 1⅜	1.152	1,311	18.35	21.15	62
2½ × 1¾	1.146	2,397	37.35	42.81	56
3 × 2⅛	1.142	4,015	66.32	75.76	53

TABLE 5.4
SPECIFICATIONS FOR KOBE A PUMPS (AFTER WILSON)[16]

Pump size or description	P/E ratio	Displacement: At rated speed	Displacement: b/d per SPM, Eng.	Displacement: b/d per SPM, Pump	Max. rated speed, spm
2 × 1–13/16	0.545	139	2.15	1.15	121
2 × 1–1	1.000	254	2.15	2.10	121
2 × 1–1 3/16	1.546	393	2.15	3.25	121
2 × 1 3/16–1	0.647	254	3.30	2.10	121
2 × 1 3/16–1 3/16	1.000	393	3.30	3.25	121
2½ × 1¼–1	0.520	256	5.02	2.56	100
2½ × 1¼–1⅛	0.746	367	5.02	3.67	100
2½ × 1¼–1¼	1.000	492	5.02	4.92	100
2½ × 1¼–1 7/16	1.431	703	5.02	7.03	100
2½ × 1 7/16–1¼	0.700	492	7.13	4.92	100
2½ × 1 7/16–1 7/16	1.000	703	7.13	7.03	100
3 × 1½–1¼	0.592	486	9.61	5.59	87
3 × 1½–1⅜	0.787	646	9.61	7.43	87
3 × 1½–1½	1.000	821	9.61	9.44	87
3 × 1½–1¾	1.480	1,218	9.61	14.00	87
3 × 1¾–1½	0.676	821	14.17	9.44	87
3 × 1¾–1¾	1.000	1,218	14.17	14.00	87
4 × 2–1¾	0.687	1,108	21.44	14.40	77
4 × 2–2	1.000	1,617	21.44	21.00	77
4 × 2–2⅜	1.541	2,502	21.44	32.50	77
4 × 2⅜–2	0.649	1,617	32.94	21.00	77
4 × 2⅜–2⅜	1.000	2,502	32.94	32.50	77

TABLE 5.5
SPECIFICATIONS FOR KOBE D PUMPS (AFTER WILSON)[16]

Pump size or description	P/E ratio	Displacement: At rated speed	Displacement: b/d per SPM, Eng.	Displacement: b/d per SPM, Pump	Max. rated speed, spm
2 × 1 3/16 × 1⅜–1 3/16 × 1 3/16	0.802	751	7.79	6.21	121
2 × 1 3/16 × 1⅜–1⅜ × 1 3/16	0.976	913	7.79	7.55	121
2 × 1 3/16 × 1⅜–1⅜ × 1⅜	1.150	1,076	7.79	8.90	121
2½ × 1 7/16 × 1¾–1½ × 1½	0.813	1,452	17.99	14.52	100
2½ × 1 7/16 × 1¾–1¾ × 1½	0.976	1,794	17.99	17.94	100
2½ × 1 7/16 × 1¾–1¾ × 1¾	1.196	2,136	17.99	21.36	100
3 × 1¾ × 2⅛–1⅞ × 1⅞	0.882	2,726	35.74	31.34	87
3 × 1¾ × 2⅛–2⅛ × 1⅞	1.039	3,213	35.74	36.94	87
3 × 1¾ × 2⅛–2⅛ × 2⅛	1.197	3,700	35.74	42.53	87

TABLE 5.6
SPECIFICATIONS FOR FLUID-PACKED VFR PUMPS (AFTER WILSON)[16]

Pump size or description	P/E ratio	Displacement: At rated speed	Displacement: b/d per SPM, Eng.	Displacement: b/d per SPM, Pump	Max. rated speed, spm
VFR 20161613	0.54	444	6.86	2.96	150
VFR 20161616	0.81	673	6.86	4.49	150
VFR 25202015	0.41	630	15.16	5.25	120
VFR 25202017	0.56	858	15.16	7.15	120
VFR 25202020	0.73	1,119	15.16	9.33	120

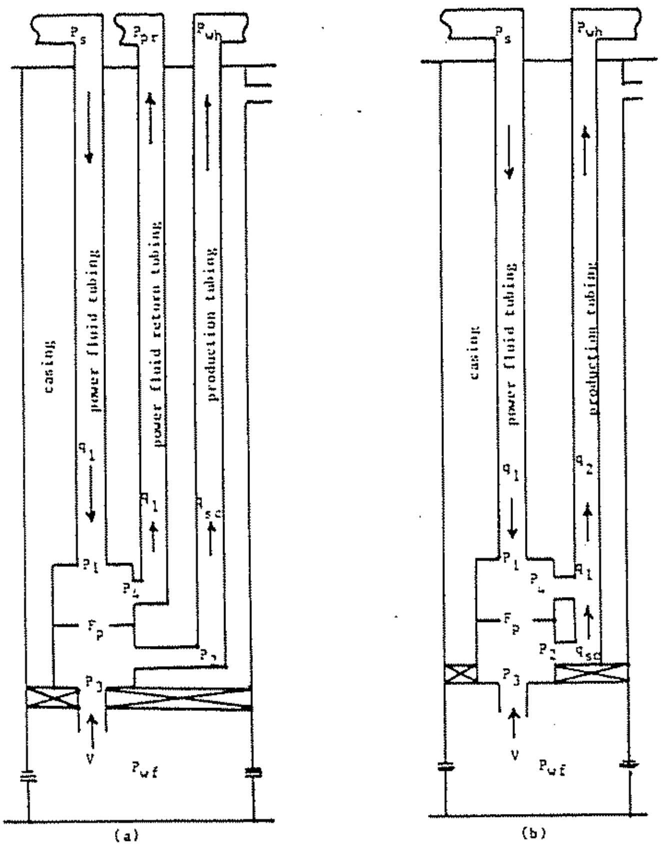

Figure 5.42 Pressures Affecting a Hydraulic Pump: (a) CPF, (b) OPF

P_1 = *power fluid pressure, psi* q_1 = *power fluid rate, stbl/d*
P_2 = *pump discharge pressure, psi* q_{sc} = *production rate, stbl/d*
$P_3 = P_{wf}$ = *intake pressure, psi* V = *intake volume, b/d*
P_4 = *engine discharge pressure, psi*
Note: *For an OPF system:*
P_s = *surface operating pressure, psi* $p_2 = P_4$
P_{pr} = *power return back pressure, psi* $q_2 = q_{sc} + q_1$
P_{wh} = *Wellhead pressure, psi*

that it is common practice to circulate part of the produced oil as a power fluid.

5.43 TUBING ARRANGEMENTS

When the pump is attached to the power fluid tubing and lowered into the well by that tubing, it is called a fixed type of pump. When the pump fits inside the power fluid tubing and is free to be circulated to the bottom and back out to the surface again, it is called a free type of pump.[16] Either type can be a CPF or an OPF system, but the main difference is that the free pump size is limited by the tubing size, while any fixed pump size is adaptable to the tubing, provided that the pump fits inside the casing. The first column of the specification tables (Tables 5.3, 5.4, 5.5, and 5.6) lists the pump sizes, which also identify the tubing size that the pump will run in.

5.44 P/E RATIO

The second column of the specification tables lists the ratio (called the P/E ratio) of the net pump piston area to the net engine piston area, or:

$$P/E = \frac{A_p - A_r}{A_e - A_r} \tag{5.45}$$

where:

A_p = area of pump piston, in.^{2}
A_e = area of engine piston, in.^{2}
A_r = area of rod, in.^{2}

The P/E ratio is related to the surface pressure required for a given lift. To limit the surface pressure to the generally acceptable maximum of 4,000 psi, the following maximum value is recommended:[18]

$$(P/E)_{max} = 10{,}000/NL \tag{5.46}$$

where:

NL = the net lift in ft given by:

$$NL = D_p - (P_3/G_f) \tag{5.47}$$

D_p = the pump setting depth, ft
P_3 = the pump intake pressure, psi
G_f = the flowing gradient of the fluid in the production conduit, psi/ft

In the special case in which the pump is set at the bottom of the well, Equation 5.47 becomes:

$$NL = D - (P_{wf}/G_f) \tag{5.48}$$

where:

D = well depth, ft
P_{wf} = flowing bottom-hole pressure, psi

Generally speaking, and especially for deep wells with low bottom-hole pressures, P_{wf}/G_f is small compared to D and, therefore, can be neglected.[5,16]

Usually, when more than one pump size can be used, the one with the greatest lift capability (lowest P/E ratio) is chosen. This will reduce the surface operating pressure, thereby reducing slippage in the bottom-hole pump.

5.45 PUMP DISPLACEMENT

The third column of the specification tables lists the maximum pump displacement based on the maximum rated speed (last column). The fourth column shows the pump displacement in b/d/spm. The production rate in b/d is, therefore, given by:[5]

$$q_3'' = q_3'N \tag{5.49}$$

where:

q_3' = pump displacement, b/d/spm
N = pump speed, spm

Normally, q_3'' is referred to as the theoretical production rate. It is equal to the actual production rate only if the pump operates at 100% efficiency. Good design practice is to use 85% pump efficiency and to select a pump that will operate below 85% of its rated speed.[5,16] Hence:

$$V = q_3''\eta_p \tag{5.50}$$

Substituting Equation 5.49 into the last equation gives:

$$V = q_3'N\eta_p \tag{5.51}$$

where η_p is the pump end efficiency.

V in Equation 5.51 is the volume of the produced fluid rate (liquid plus gas) at the intake pressure and, therefore, would be equal to the surface rate only if the fluid is considered incompressible, such as liquids are. If the pump is handling gas with the liquid, V must be calculated from Equation 5.4.

5.46 ENGINE DISPLACEMENT

Because the engine is coupled to the pump, the engine piston moves at the same speed as the pump piston. The theoretical power fluid rate is, then, given by:[5]

$$q_1'' = q_1' N \qquad (5.52)$$

where q_1' is the engine displacement in stbl/d/spm (column 3 in the specification tables).

The engine-end efficiency is the ratio of the theoretical rate to the actual rate,[5] or

$$\eta_e = q_1''/q_1$$

Substituting Equation 5.52 into the last equation gives:

$$q_1 = q_1' N/\eta_e \qquad (5.53)$$

where:

q_1 = the actual power fluid rate required to produce an actual fluid rate V

η_e = the engine-end efficiency, estimated at about 90%[5.16]

5.47 PUMP FRICTION

The pressure required to operate a hydraulic pump under no-load conditions is shown in Figure 5.43. The chart shows the mechanical and hydraulic friction in the pump. This friction depends on the pump type, percentage of rated speed, and viscosity of the power fluid.

5.48 PRESSURE CALCULATIONS

The various pressures involved in a CPF and in an OPF system are shown in Figure 5.42. The pressure available to drive the engine is P_1, while the engine must discharge against P_4. The pump end must discharge against P_2 while being filled with P_3. This force balance is shown as follows:

$$-P_1A_r - P_4(A_e - A_r) + P_1(A_e - A_r) - P_2(A_p - A_r) + P_3(A_p - A_r) + P_1A_r = 0$$

or:

$$(P_1 - P_4)(A_e - A_r) - (P_2 - P_3)(A_p - A_r) = 0$$

or:

$$P_1 - P_4 - (P_2 - P_3)\left(\frac{A_p - A_r}{A_e - A_r}\right) = 0 \qquad (5.54)$$

Pump friction must be subtracted from the last equation. Hence,

$$P_1 - P_4 - (P_2 - P_3)\left(\frac{A_p - A_r}{A_e - A_r}\right) - F_p = 0 \qquad (5.55)$$

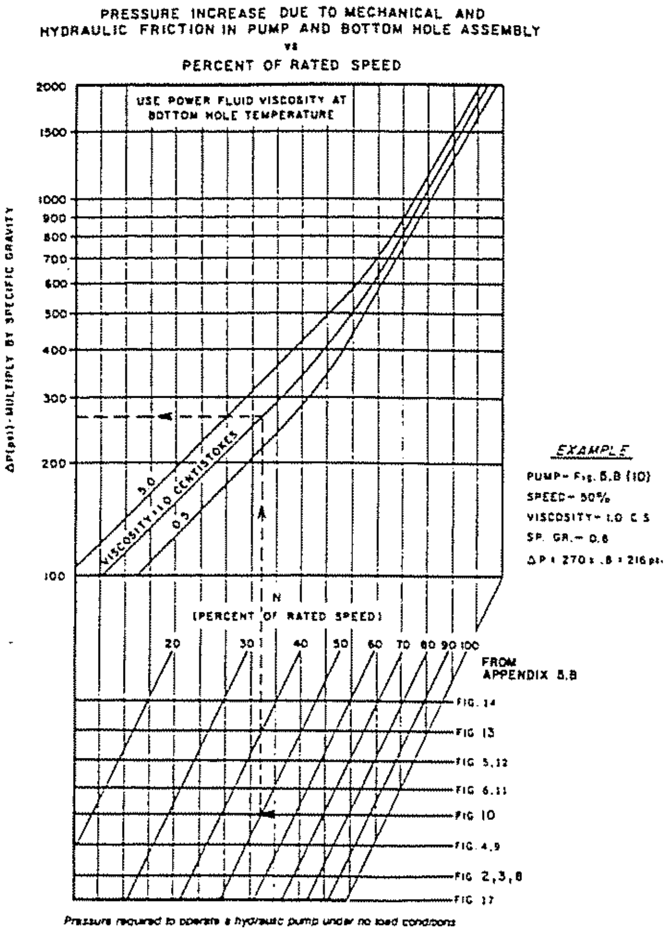

Figure 5.43 Pressure Required to Operate a Hydraulic Pump Under No-Load Conditions

Substituting Equation 5.45 into the last equation gives:

$$P_1 - P_4 - (P_2 - P_3)(P/E) - F_p = 0 \qquad (5.56)$$

Equation 5.56 is equally valid for an OPF system and a CPF system. In an OPF system, however, P_4 is identical to P_2. Thus, Equation 5.56 can be written as:

$$P_1 - P_2 - (P_2 - P_3)(P/E) - F_p = 0 \qquad (5.57)$$

5.49 HORSEPOWER

The horsepower requirement is estimated from the following equation:[5]

$$HP = 1.7 \times 10^{-5}\, q_1\, P_s \qquad (5.58)$$

5.491 PUMP INTAKE CURVES

5.4911 INTRODUCTION

Predicting intake curves for hydraulic pumps is considered for two cases: (1) pumping only liquid and (2) pumping gas with the liquid. For both cases, it is assumed that the pump is set at the bottom of the well and that the wellhead pressure and the flow-path size are fixed. For case 2, it is assumed that all associated gas is pumped with the liquid. The sensitivity variable selected for this lift system is the power fluid pressure.

As will be seen later, predicting intake curves for a hydraulic pump is direct for case 1 and indirect for case 2.

(1) *Pumping liquid.* Since liquids are only slightly compressible, V in Equation 5.51 can be considered constant and equal to the surface rate q_{sc}, or:

$$q_{sc} = q'_3\, N\, \eta_p$$

or:

$$N = q_{sc}/q'_3\, \eta_p \qquad (5.59)$$

In this case, the wellhead pressure, the surface return back pressure, the flow-path size, and the discharge pressures are fixed for each rate. This leaves only P_1 as a variable. Solving Equations 5.56 and 5.57 for P_3 gives:

For CPF systems:

$$P_3 = \left[P_2 + \left(\frac{P_4 + F_p}{P/E}\right)\right] - \frac{P_1}{(P/E)} \qquad (5.60)$$

For OPF systems:

$$P_3 = \left[P_2 + \left(\frac{P_2 + F_p}{P/E}\right)\right] - \frac{P_1}{(P/E)} \qquad (5.61)$$

Note: If the pump is set at the bottom of the well, such as in this case, P_3 will be equal to P_{wf}.

(2) *Pump selection.* As previously mentioned, the pump size is limited by the tubing size (free type) or by the casing size (fixed type). Another restriction is that the P/E ratio of the pump should not exceed $(P/E)_{max}$ given by Equation 5.46. In the event that more than one pump is found to be suitable and the surface operating pressure is fixed, the following procedure is recommended.

(1) For each pump, assume a production rate and do the following:
  (a) Calculate N from Equation 5.59. Then, calculate q_1 from Equation 5.53. Determine the percent of rated speed.
  (b) Determine the power fluid pressure and the discharge pressure(s) from a pressure gradient correlation.
  (c) Determine F_p from Figure 5.43.
  (d) Calculate P_3 from Equation 5.60 or Equation 5.61.
  (e) Repeat steps a–d for other assumed rates.
(2) Plot P_3 vs rate for each pump. Plot the stbl/d IPR curve to the same scale on the same graph (see Figure 5.44).
(3) Read the rate for each pump at the intersection of its intake curve with the IPR curve.
(4) For each rate, calculate N from Equation 5.59, q_1 from Equation 5.53, and HP from Equation 5.58.
(5) Select a pump on the basis of economics.

Note: The rate for the selected pump should not exceed 85% of its displacement at rated speed.[5.16]

Because of the difference in the P/E ratio and the power fluid rate, the plots prepared in step 2 above will overlap (Figure 5.44); hence, pump choice will depend on the well productivity (position of the IPR curve). Another limitation that may influence pump selection is the availability of power fluid and/or horsepower. If the objective is to maximize the production rate, the pump that yields the highest rate should be selected.

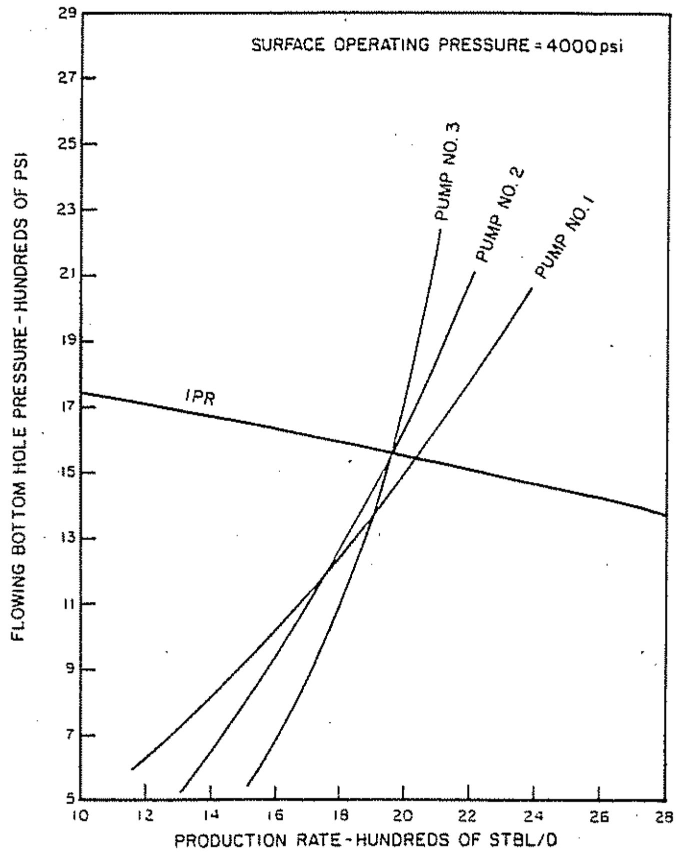

Figure 5.44 Intake Curves for Various Hydraulic Pumps in Well #1 (Pumping Liquid)

5.4912 PROCEDURE FOR THE PREPARATION OF TUBING INTAKE CURVES FOR LIQUID ONLY

In order to show the effect of friction, it is necessary to relax the limit on the surface operating pressure.

(1) Decide on the type of power fluid (water or oil) and the type of power fluid system (CPF or OPF).
(2) Select a suitable pump.
(3) Assume a production rate and do the following:
  (a) Calculate N from Equation 5.59. Then calculate q_1 from Equation 5.53. Determine the percent of rated speed.
  (b) Determine the required discharge pressure(s) from a pressure gradient correlation.
  (c) Determine F_p from Figure 5.43.
  (d) Assume various power fluid pressures and calculate P_3 from equation 5.60 or Equation 5.61.
  (e) Repeat steps a–d for other assumed rates.
(4) Plot P_3 vs rate for each assumed power fluid pressure. Plot the stbl/d IPR curve to the same scale on the graph.
(5) Read the possible rates at the intersection of the pump intake curves with the IPR curve.
(6) For each possible rate, calculate q_1. Then, determine the surface operating pressure. Calculate HP from Equation 5.58.
(7) Plot the rate vs q_1, P_s, and HP. Impose 85% of

the pump displacement at rated speed on the same graph.
(8) Select an optimum rate.

EXAMPLE WELL #1 (LIQUID ONLY)

Well, fluid, and reservoir data are shown in Table 5.1. A fixed type of hydraulic pump with an OPF system is set at the bottom of the well. The solution is shown in Figure 5.45.

Since the pump is set at the bottom of the well, the intake pressure of the pump is equal to the flowing bottom-hole pressure; hence, the stbl/d IPR curve shown in Figure 5.8 is applicable.

If P_{wf}/G_f is ignored, Equation 5.48 gives a net lift of 8,000 ft. Then, Equation 5.46 gives:

$$(P/E)_{max} = 10{,}000/8{,}000 = 1.25$$

Inspection of the specification tables (Tables 5.3–5.6) shows several pumps with P/E ratios that are less than $(P/E)_{max}$. The choice between these pumps is therefore limited only by the casing size and the productivity of the well. For such a high-productivity well, three candidates (high-capacity pumps) with a significant difference in the P/E ratio and power fluid requirement will be considered. These pumps will be numbered 1, 2, and 3:

Pump	Table	P/E	Displ. at rated speed	q_3'	q_1'	Max. rated speed
#1	1(#3)	1.142	4,015	75.76	66.32	53
#2	2(#22)	1.000	2,502	32.50	32.94	77
#3	3(#7)	0.882	2,726	31.34	35.74	87

For pump #1, assume $\eta_p = 85\%$ and $\eta_e = 90\%$. Then, Equations 5.59, 5.53, and 5.61 become, respectively:

$$N = q_{sc}/(75.76)(0.85) = q_{sc}/64.4 \qquad (5.62)$$

$$q_1 = (66.32)\,N/0.9 = 73.69\,N \qquad (5.63)$$

$$P_3 = P_2 + \left(\frac{P_2 + F_p}{1.142}\right) - \frac{P_1}{1.142} \qquad (5.64)$$

If a surface liquid rate of, say, 1,000 stbl/d is assumed, Equation 5.62 gives:

$$N = 1{,}000/64.4 = 15.53 \text{ spm}$$

Hence, Equation 5.63 yields:

$$q_1 = (73.69(15.53) = 1{,}144 \text{ stbo/d}$$

$$\% \text{ of rated speed } (\%RS) = (15.53)(100)/53 = 29.3$$

For 29.3% rated speed, Figure 5.43 shows:

$$F_p = (195)(0.85) = 166 \text{ psi}$$

The total liquid rate in the production tubing is 1,000 + 1,144 = 2,144 of which 1,644 bbl are oil and 500 bbl are water. For this rate:

$$P_2 = 3{,}325 \text{ psi (pressure gradient correlation)}$$

With a power fluid rate of 1,144 stbo/d and if the surface operating pressure is fixed at 4,000 psi, then:

$$P_1 = 6{,}761 \text{ psi (pressure gradient correlation)}$$

Then, Equation 5.64 gives:

$$P_3 = 3{,}325 + \left(\frac{3{,}325 + 166}{1.142}\right) - \frac{6{,}761}{1.142} = 462 \text{ psi}$$

Similarly, the following can be obtained for the same pump with other assumed rates:

q_{sc}	N	%RS	F_p	q_1	P_2	P_1	P_3
1,200	19	35	205	1,371	3,387	6,741	629
1,400	22	41	244	1,602	3,459	6,721	815
1,600	25	47	279	1,831	3,541	6,702	1,017
1,800	28	53	323	2,060	3,633	6,683	1,245
2,000	31	59	378	2,289	3,735	6,663	1,502
2,200	34	64	440	2,517	3,848	6,644	1,764
2,400	37	70	506	2,746	3,971	6,625	2,089

The intake pressure P_3 was plotted vs q_{sc} in Figure 5.44. The IPR curve was plotted to the same scale in the same figure.

The same type of calculations with 4,000 psi surface operating pressure was carried out for pump #2 and pump #3. Results of the calculations also were plotted in Figure 5.44. Note that the plots of Figure 5.44 overlap because of the difference in the P/E ratio and the power fluid rate.

For this particular well and with 4,000-psi surface operating pressure, the possible rates, power fluid rates, percent of rated speed, and horsepower requirements for each pump are as follows:

Pump	q_p	%RS	q_1	HP
#1	2,030	59.5	2,323	158
#2	1,960	92.1	2,596	177
#3	1,950	84.1	2,907	196

Pump #2 is not recommended since its percent of rated speed is higher than 85%. Pump #1 should be selected over pump #3 because it yields a higher production rate, requires less power fluid rate (less horsepower at the surface), and its percent of rated speed is much lower.

If 4,000 psi is the maximum allowable surface operating pressure and the production rate is to be optimized for the selected pump, the pump performance should be studied for pressures less than or equal to 4,000 psi. But, in order to illustrate the effect of friction, the limit on the surface operating pressure must be relaxed, in which case there will be no limit on the power fluid pressure.

For an assumed production rate of, say, 200 stbl/d, Equation 5.62 gives:

$$N = 200/64.4 = 3.11 \text{ spm}$$

Then:

$$\%RS = (3.11)(100)/53 = 5.86$$

For 5.86% of rated speed, Figure 5.43 shows:

$$F_p = 110 \text{ psi}$$

Equation 5.63 gives:

$$q_1 = (73.69)(3.11) = 229 \text{ stbo/d}$$

The total liquid rate in the production tubing is then 200 + 229 = 429 stbl/d of which 329 stb are oil and 100 stb are water. For this rate:

$P_2 = 3{,}179$ psi (pressure gradient correlation)

If a power fluid pressure of, say, 4,500 psi is assumed, Equation 5.64 yields:

$$P_3 = 3{,}179 + \left(\frac{3{,}179 + 110}{1.142}\right) - \frac{4{,}500}{1.142} = 2{,}119 \text{ psi}$$

Similarly, the following can be obtained for the same rate of 200 stbl/d with other assumed power fluid pressures:

P_1	P_3
5,000	1,681
5,500	1,245
6,000	805
6,500	367

The same type of calculations were carried out for other assumed rates. Results of the calculations are shown in Table 5A.15. Intake pressure P_3 was plotted vs q_{sc} for the various power fluid pressures in Figure 5.45. The stbl/d IPR curve was plotted to the same scale on the same graph. The possible rates are found at the intersection of the pump intake curves with the IPR curve. For example, the well can produce 650 stbl/d with a power fluid pressure of 5,000 psi. For this rate, Equation 5.62 gives:

$$N = 650/64.4 = 10 \text{ spm}$$

Then, Equation 5.63 yields:

$$q_1 = (73.69)(10) = 744 \text{ stbo/d}$$

For 5,000 psi power fluid pressure and a power fluid rate of 744 stbo/d:

$P_s = 2{,}221$ psi (pressure gradient correlation)

Then, Equation 5.58 gives:

$$HP = (1.7 \times 10^{-5})(744)(2{,}221) = 28 \text{ HP}$$

The same type of calculations were carried out for other possible rates. Results of calculations are shown in Table 5A.16. Possible rate q_p was plotted vs q_1, P_s, and HP in Figure 5.46. The allowable pump displacement (4,015 × 0.85 = 3,413 stbl/d) was imposed on the same figure.

It is evident from Figure 5.46 that, beyond 4,000 stbl/d, the surface operating pressure as well as the horsepower requirement increase very quickly without any significant gain in the production rate. Hence, this rate would be selected if it was within the allowable

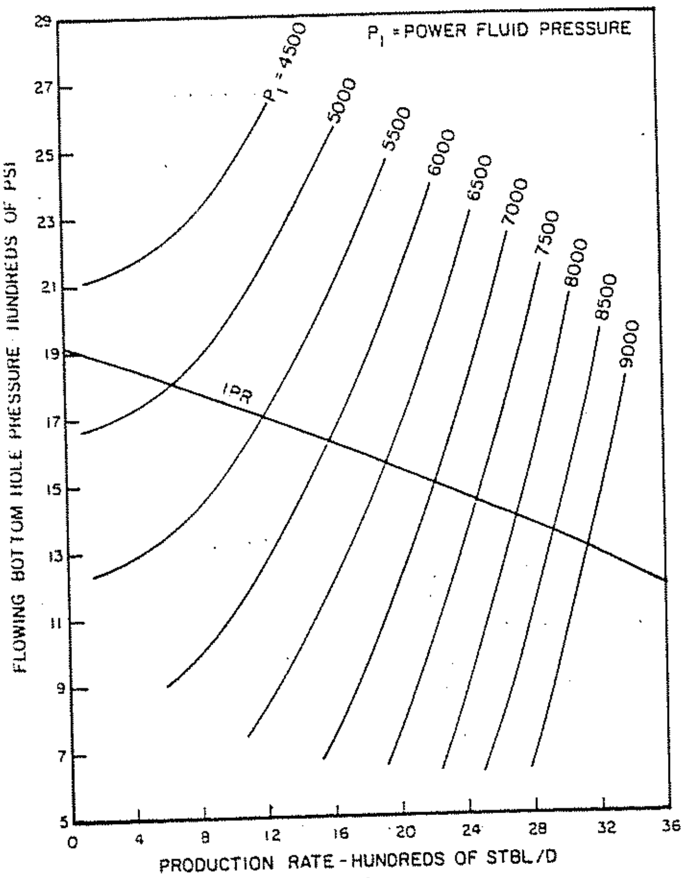

Figure 5.45 Intake Curves for a Hydraulic Pump in Well #1 (Pumping Liquid)

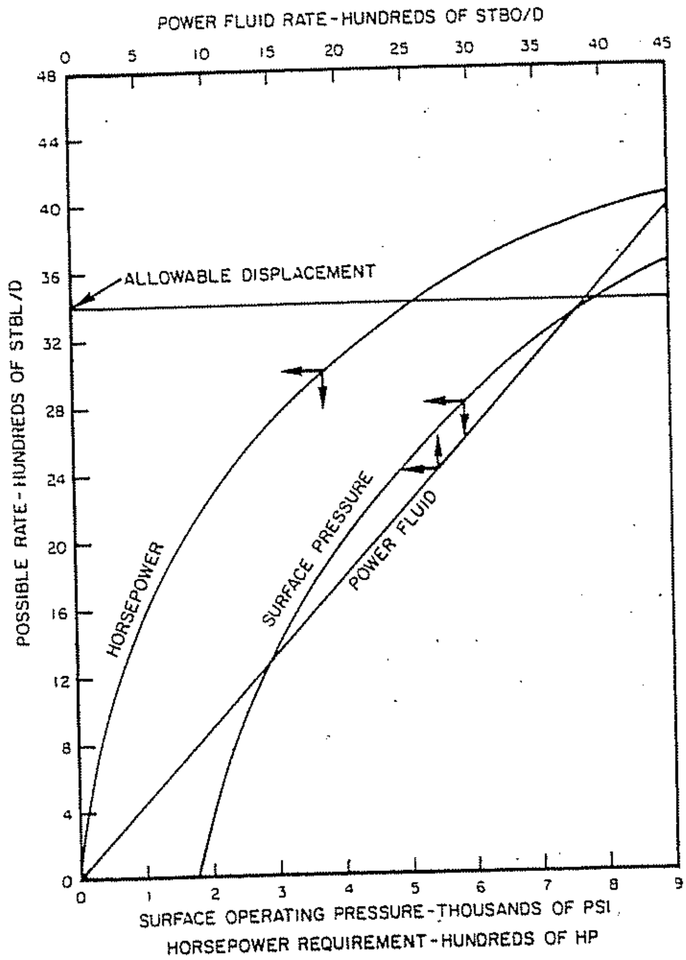

Figure 5.46 Possible Production Rate by Hydraulic Pumping vs HP, P_s, and q_1 for Well #1 (Pumping Liquid)

pump displacement on one hand and if there was no limit to the surface operating pressure on the other hand. In this case, however, the practical limit of 4,000-psi surface operating pressure will be used. With this pressure, the well can produce 1,975 stbl/d for which the power fluid rate is 2,260 stbo/d and the horsepower requirement is 154 HP (see Figure 5.46).

EXAMPLE WELL #2 (LIQUID ONLY)

Example well #2 was worked by the same procedure, and results are shown in Figures 5.47 and 5.48, which utilize the data of Tables 5A.17 and 5A.18. The horsepower requirements for the rates (obtained from Figure 5.47) are shown in Table 5A.18. Figure 5.48 is a plot of q_p vs HP, P_s, and q_1. The selected rate is 375 stbl/d (allowable pump displacement). For this rate, the horsepower requirements, the surface operating pressure, and the power fluid rate are 43.5, 2,250, and 1,135, respectively (see Figure 5.48).

5.4913 PUMPING LIQUID AND GAS

Because of the high compressibility of gas, V cannot be considered constant but must be determined at the intake pressure from Equation 5.4. Hence, Equation 5.51 becomes:

$$q_{sc}\ VF = q_3'\ N\ \eta_p$$

or:

$$N = q_{sc}\ VF / q_3'\ \eta_p \qquad (5.65)$$

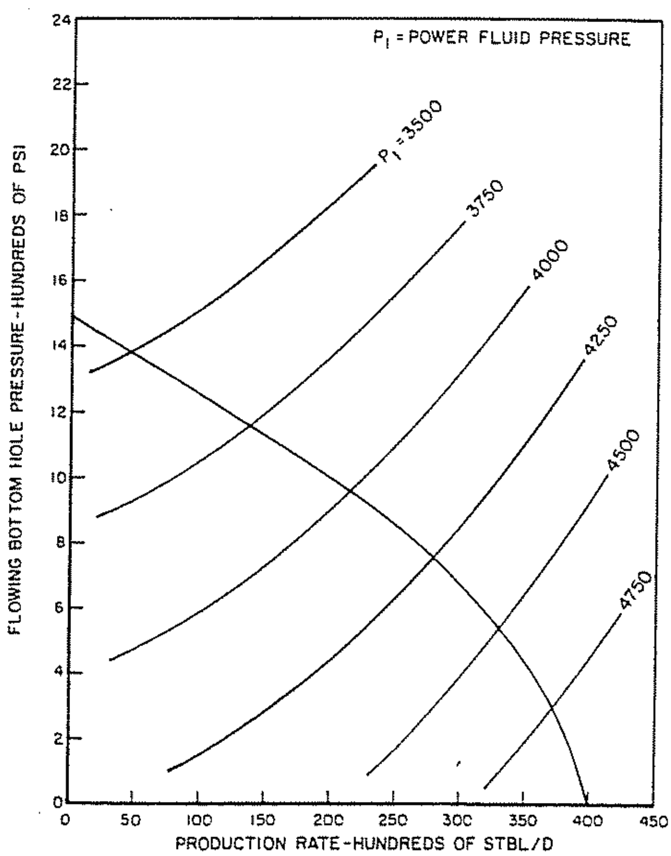

Figure 5.47 Intake Curves for a Hydraulic Pump in Well #2 (Pumping Liquid)

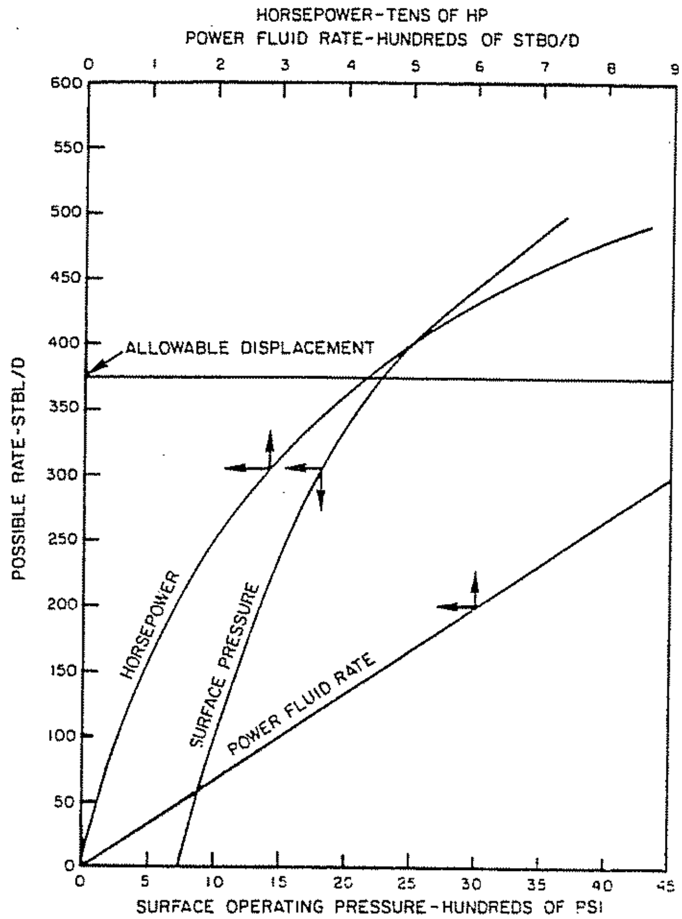

Figure 5.48 Possible Production Rate by Hydraulic Pumping vs HP, P_s, and q_1 for Well #2 (Pumping Liquid)

where VF is determined at the intake pressure from Equation 5.3.

For an OPF system using oil as the power fluid, the total liquid rate, the gas-oil ratio, and the water cut in the production column are as follows:

$$q_2 = q_1 + q_{sc} \qquad (5.66)$$

$$GOR_2 = \frac{q_{sc}\ GLR}{q_1 + q_{sc}(1 - wc)} \qquad (5.67)$$

and:

$$wc_2 = \frac{q_{sc}\ wc}{q_2} \qquad (5.68)$$

respectively. For a CPF system, the gas-oil ratio and the water cut in the production column are constant.

Unlike the case when pumping only liquid, predicting intake curves for the liquid-gas case is somewhat indirect. This is because the intake pressure must be known in advance in order to estimate VF. Since the surface power return back pressure and the wellhead pressure are assumed to be fixed, the discharge pressures also will be fixed for the same rate. Hence, the power fluid pressure cannot be assumed as was done for the liquid case but must be calculated from either Equation 5.56 or Equation 5.57 since it is the only unknown left in those equations. In order to facilitate plotting of intake curves, it is therefore necessary to obtain intake pressures for the production rates for

identical power fluid pressures. This can be accomplished either by making a plot of P_3 vs P_1 for each rate or by interpolation.

Solving Equations 5.56 and 5.57 for P_1 gives:

For CPF Systems:

$$P_1 = P_4 + (P_2 - P_3)(P/E) + F_p \quad (5.69)$$

For OPF Systems:

$$P_1 = P_2 + (P_2 - P_3)(P/E) + F_p \quad (5.70)$$

Pump selection. In addition to the tubing or casing size, the other factors that influence pump selection are the P/E ratio and the difference in the power fluid requirements. Because of the existence of gas in this case, the difference in the power fluid requirements will be higher than the liquid case. Hence, the pump that would be used for the liquid case would be used for the liquid-gas case.

5.4914 PROCEDURE FOR PREPARATION OF TUBING INTAKE CURVES FOR PUMPING GAS AND LIQUID

As for the case when pumping only liquid, the limit on the surface operating pressure is relaxed. The stepwise procedure is given as follows. This procedure is illustrated with examples.

(1) Decide on the type of power fluid (oil or water) and the type of power fluid system (CPF or OPF).
(2) Select a suitable pump.
(3) Assume various production rates in stbl/d and, for each of these rates, do the following:
  (a) Assume an intake pressure.
  (b) Determine VF at the assumed intake pressure from Equation 5.3.
  (c) Calculate N from Equation 5.65. Then, calculate q_1 from Equation 5.53.
  (d) Determine the percent of rated speed. Then, determine F_p from Equation 5.43.
  (e) Determine the required discharge pressure(s) from a two-phase flow correlation.
  (f) Calculate the power fluid pressure from Equation 5.69 or Equation 5.70.
  (g) Repeat steps b–f for other assumed intake pressures.
(4) By interpolation or plotting, obtain intake pressures for the assumed production rates for identical power fluid pressures.
(5) Plot the intake pressure (obtained in step 4) vs rate for the various power fluid pressures. Plot the stbl/d IPR curve to the same scale on the same graph.
(6) Read the possible rates at the intersection of the pump intake curves with the IPR curve.
(7) For each possible rate, calculate q_1. Then, determine the surface operating pressure. Calculate HP from Equation 5.58.
(8) Plot the possible rate vs P_1, P_s, and HP. Impose 85% of the pump displacement at rated speed on the same graph.
(9) Select an optimum rate.

Rate selection. Whether pumping only liquid or pumping gas with the liquid, the selected rate must be

(1) within 85% of the pump displacement at rated speed
(2) economically feasible

As the power fluid pressure and, consequently, the production rate as well as the power fluid rate increase, the effect of friction loss in the flow conduits begins to manifest itself. As a result, the gain in the production rate per 1 HP continues to diminish until it becomes insignificant.

EXAMPLE PROBLEM #1

Since the pump is set at the bottom of the well and all gas is pumped with the liquid, the IPR curves of Figure 5.8 and the volume factor data of Table 5A.1 are applicable. Refer to Figures 5.49 and 5.50 for the solution.

For the liquid case, pump #1 was selected over pump #3 because, for the same surface operating pressure, it gave a higher production rate, required a lower power fluid rate, and its percent of rated speed was lower. The difference in the production rates of both pumps was attributed to the difference in the power fluid rate which, in turn, made the effect of friction for pump #3 higher than that for pump #1. Because of the existence of gas in this case, the difference in the power fluid rate will be even higher; hence, pump #1 will again be selected.

In order to show the effects of friction and pumping gas with the liquid and to maximize the production

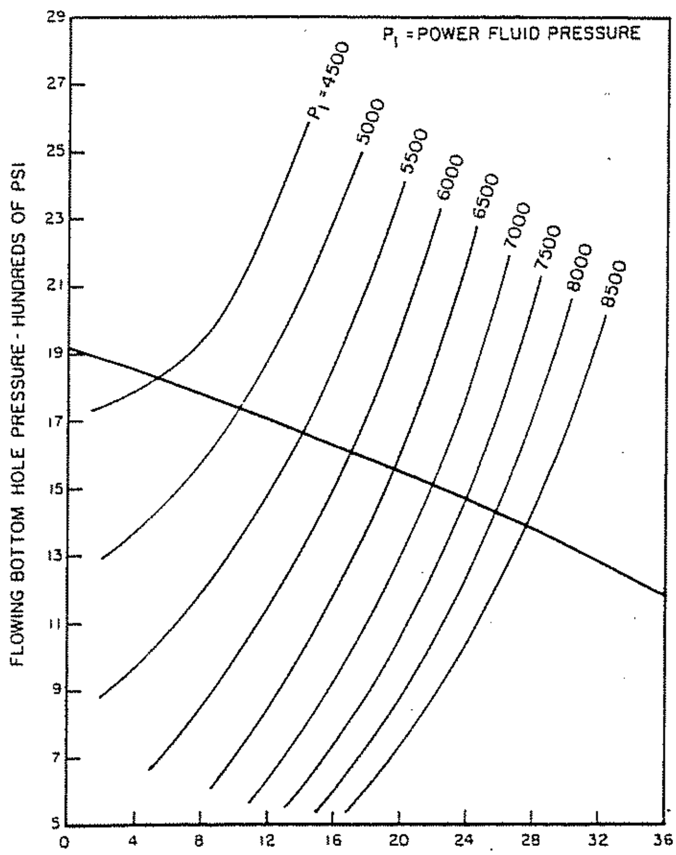

Figure 5.49 Intake Curves for a Hydraulic Pump in Well #1 (Pumping Liquid and Gas)

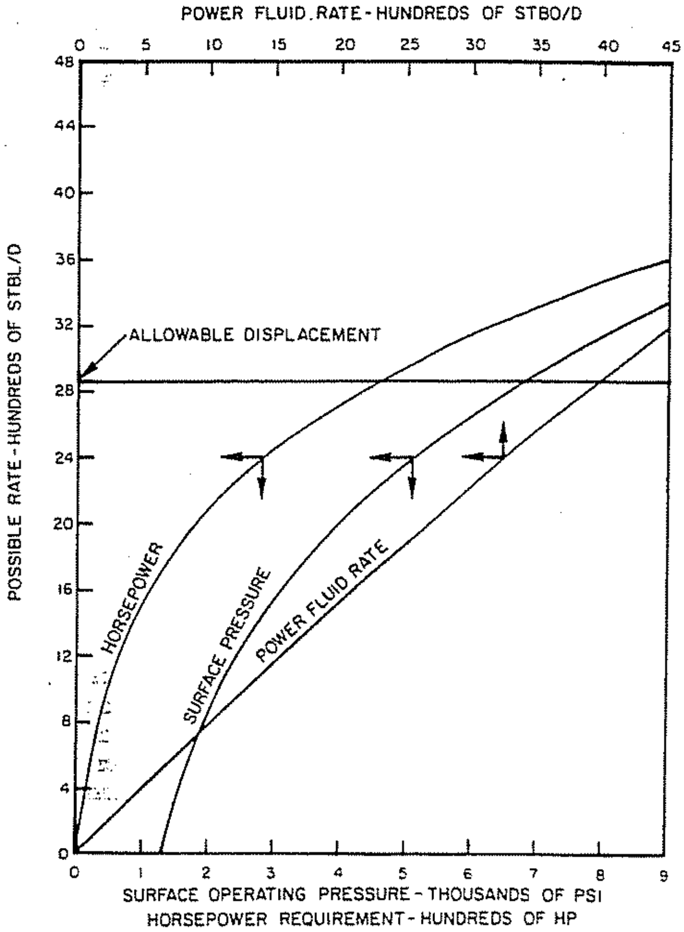

Figure 5.50 Possible Production Rate by Hydraulic Pumping vs HP, P_s, and q_1 for Well #1 (Pumping Liquid and Gas)

rate for the selected pump, the limit on the surface operating pressure will be relaxed.

Assume:

$$\eta_p = 85\% \text{ and } \eta_e = 90\%$$

Then Equations 5.65 and 5.53 become:

$$N = q_{sc}\, VF/(75.76 \times 0.85) = q_{sc}\, VF/64.4 \quad (5.71)$$

and:

$$q_1 = (66.32)\, N/0.9 = 73.69\, N \quad (5.72)$$

For the fluid of well #1, Equations 5.66, 5.67, and 5.68 become:

$$q_2 = q_1 + q_{sc} \quad (5.73)$$

$$GOR_2 = \frac{200\, q_{sc}}{q_1 + 0.5\, q_{sc}} \quad (5.74)$$

and:

$$wc_2 = \frac{0.5\, q_{sc}}{q_2} \quad (5.75)$$

The P/E ratio for pump #1 is 1.142; hence, Equation 5.70 becomes:

$$P_1 = P_2 + 1.142(P_2 - P_3) + F_p \quad (5.76)$$

If a surface liquid rate of, say, 400 stbl/d and an intake pressure of, say, 200 psi are assumed, then:

$$VF = 3.9210 \text{ bbl/stbl (Table 5A.2 @ 200 psi)}$$
$$N = (400)(3.9210)/64.4 = 24.36 \text{ spm (Equation 5.71)}$$
$$\%RS = (24.36)(100)/53 = 45.95$$

For 45.95% of rated speed, Figure 5.43 shows:

$$F_p = 273 \text{ psi}$$
$$q_1 = (73.69)(24.36) = 1{,}795 \text{ stbo/d (Eq. 5.72)}$$
$$q_2 = 1{,}795 + 400 = 2{,}195 \text{ stbl/d (Eq. 5.73)}$$
$$GOR_2 = \frac{(200)(400)}{1{,}795 + 200} = 40 \text{ scf/stbo (Eq. 5.74)}$$
$$wc_2 = \frac{(0.5)(400)}{2{,}195} = 9\% \text{ (Eq. 5.75)}$$

With a 2,195-stbl/d liquid rate, 40-scf/stbo GOR, 9% water cut, and the well and fluid data of Table 5.1, a two-phase flow correlation shows:

$$P_2 = 3{,}175 \text{ psi}$$

Then, Equation 5.76 gives:

$$P_1 = 3{,}175 + (1.142)(3{,}175 - 200) + 273 = 6{,}846 \text{ psi}$$

Similar calculations were made for the same rate of 400 stbl/d with other assumed intake pressures. Table 5A.19 shows continuation of the above calculations. Interpolating Table 5A.19 gives:

P_1	P_3
4,500	1,795
5,000	1,375
5,500	971
6,000	607
6,500	317

The same type of calculations were carried out for other rates. Results of calculations are shown in Table 5A.20. Intake pressure P_3 was plotted vs q_{sc} for the various power fluid pressures in Figure 5.49. The stbl/d IPR curve was plotted to the same scale in the same figure. The possible rates are found at the intersection of the pump intake curves with the IPR curve. For example, the well can produce 530 stbl/d with a power fluid pressure of 4,500 psi. The intake pressure for 530 stbl/d is 1,830 psi at which:

$$VF = 1.1150 \text{ bbl/stbl (Table 5A.2 @ 1,830 psi)}$$

Then:

$$N = (530)(1.1150)/64.4 = 9.18 \text{ spm (Eq. 5.71)}$$

and:

$$q_1 = (73.69)(9.18) = 676 \text{ stbo/d (Eq. 5.72)}$$

For 676 stbo/d power fluid rate and 4,500 psi power fluid pressure:

$$P_s = 1{,}659 \text{ psi (pressure gradient correlation)}$$

Then Equation 5.58 gives:

$$HP = (1.7 \times 10^{-5})(1{,}659)(676) = 19.1 \text{ HP}$$

The same type of calculation was made for other rates. Results of calculations are shown in Table 5A.21. Possible rate q_p was plotted vs q_1, P_s, and HP in Figure 5.50.

The allowable pump displacement (4,015 × 0.85 = 3,413 b/d) in this case refers to the volume of liquid plus gas at the intake pressure. It can be converted to stbl/d by entering the b/d IPR curve (Figure 5.8) at 3,413 b/d and then moving horizontally to the stbl/d IPR curve to obtain 2,850 stbl/d. This rate was imposed on Figure 5.50.

It is evident from Figure 5.50 that, beyond 3,600 stbl/d, the surface operating pressure as well as the horsepower requirement increase very fast without significant gain in the production rate. Hence, this rate would be selected if it was within the allowable pump displacement on one hand and if there was no limit to the surface operating pressure on the other hand. In this case, however, the practical limit of 4,000-psi surface operating pressure will be used. With this pressure, the well can produce 2,010 stbl/d, which is higher than that obtained previously for the liquid case (1,975 stbl/d). For 2,010 stbl/d, the power fluid rate is 2,680 stbo/d, and the horsepower is 180 HP (Figure 5.50).

EXAMPLE PROBLEM #2

Well, fluid, and reservoir are shown in Table 5.1. Calculation of VF with 100% GIP was made in the Appendix (Table 5A.2). IPR's in stbl/d and in b/d are shown in Figure 5.9.

The same type of calculations previously made for well #1 were carried out for this well. The most appropriate pump was found to be that shown in Table 5.6 (pump #1). Results of calculations are shown in Tables 5A.22 and 5A.23.

The data of Table 5A.22 were plotted in Figure 5.51. The stbl/d IPR curve was plotted to the same scale in the same figure. The horsepower requirements for the possible rates (obtained from Figure 5.51) are shown in Table 5A.23. Figure 5.52 is a plot of q_p vs HP, P_s, and q_1. The selected rate is 290 stbl/d (allowable pump displacement). For this rate, the horsepower requirements, the surface operating pressure, and the power fluid rate are 51, 2,550, and 1,085, respectively (see Figure 5.52).

5.434 DISCUSSION OF RESULTS

Whether pumping only liquid (Figures 5.46 and 5.48) or pumping gas with the liquid (Figures 5.50 and 5.52), it is evident that the gain in the production rate per 1 HP diminishes as the rate increases. This is attributed to the effect of friction loss in the flow conduits, which works to increase the discharge pressure and reduce the power fluid pressure. Note that the effect of friction loss in well #2 is minor because of the low rates associated with this well.

Comparing Figure 5.45 to Figure 5.49 or Figure 5.47 to Figure 5.51 shows that, for intake pressures above or slightly below the bubble point (1,820 psi for the crude of well #1 and 940 psi for the crude of well #2), higher production rates can be obtained by pumping a small volume of gas with the liquid. The reason is that existence of gas in the production column re-

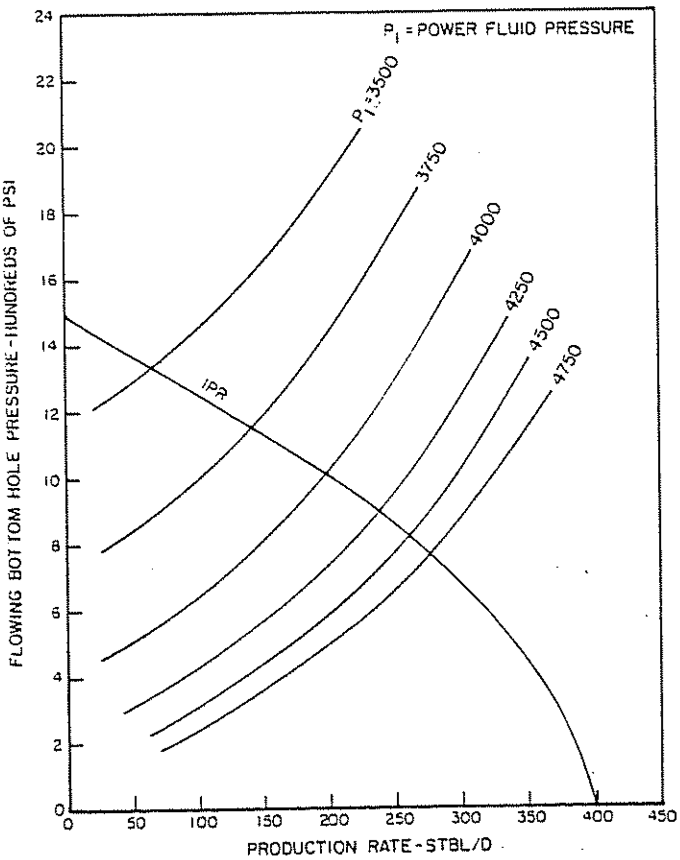

Figure 5.51 Intake Curves for a Hydraulic Pump in Well #2 (Pumping Liquid and Gas)

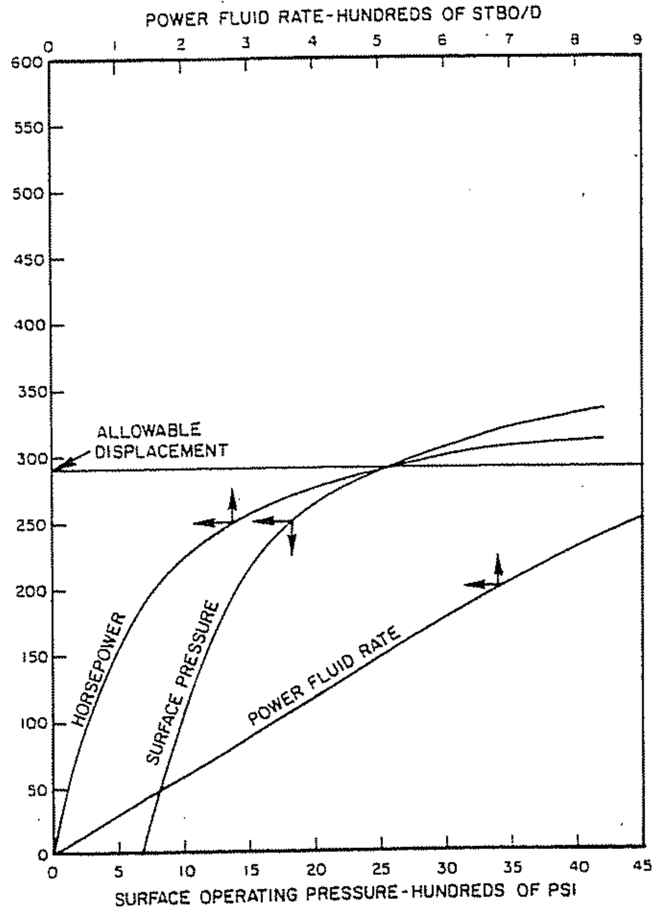

Figure 5.52 Possible Production Rate by Hydraulic Pumping vs HP, P_s, and q_1 for Well #2 (Pumping Liquid and Gas)

duces the discharge pressure below the level needed for the case in which there is no gas. However, as the intake pressure drops below the bubble point, a large expansion in the volume of the produced fluid rate takes place, causing a significant increase in the power fluid rate. High production (liquid) rates combined with still higher power fluid rates cause a continuous decline in the GLR in the production column and a continuous increase in the friction loss. Eventually, the discharge pressure will exceed that required for the case when pumping only liquid, and the opposite effect takes place.

5.5 JET PUMPS

5.51 DESCRIPTION OF EQUIPMENT

A typical example of a subsurface jet pump is shown in Figure 5.53 with details in Figure 5.54. The power fluid enters the top of the pump from the tubing and passes through the nozzle, where virtually all of the total pressure of the power fluid is converted to a velocity head. The jet from the nozzle discharges into the production inlet chamber, which is connected to the pump intake for formation fluids. The production fluid is entrained by the power fluid, and the combined fluids enter the throat of the pump.

In the confines of the throat, which is always of larger diameter than the nozzle, complete mixing of the power fluid and the production fluid takes place. During this process, the power fluid loses momentum and energy while the production fluid gains momentum and energy. The resultant mixed fluid exiting the throat has sufficient total head to flow against the production return column gradient. Much of this total head, however, is still in the form of a velocity head. The final working section of the jet pump is, therefore, a carefully shaped diffuser section of expanding area that converts the velocity head to a static head greater than the static column head, allowing flow to the surface.[6]

(1) *Dimensionless area.* The ratio of the nozzle area to the total area of the throat (Figure 5.54) is called the area ratio, or:[6]

$$R = A_j/A_t \tag{5.77}$$

(2) *Dimensionless flow rate.* The dimensionless flow rate is defined by:

$$M = V/q_1 \tag{5.78}$$

where:

V = the volume of the produced fluid rate (liquid plus gas)
q_i = the power fluid rate

V is determined at the intake pressure from Equation 5.54. When pumping slightly compressible fluids such as liquids, it can be considered constant and equal to the surface rate.

(3) *Dimensionless head.* The dimensionless head is defined as the ratio of the pressure increase experienced by the production fluid to the pressure loss suffered by the power fluid (refer to Figures 5.54 and 5.55):

$$H = (P_2 - P_3)/P_1 - P_2) \tag{5.79}$$

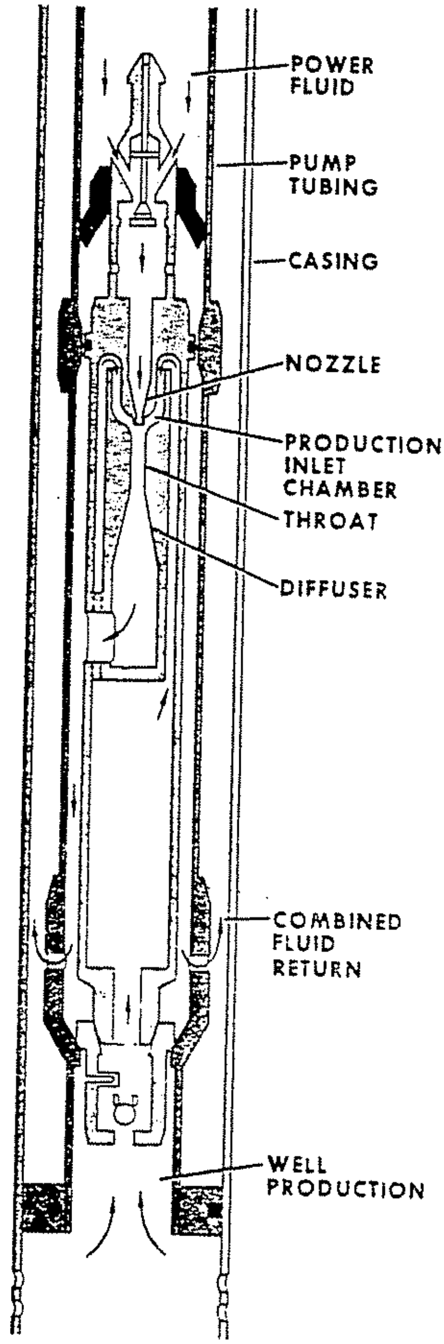

Figure 5.53 Jet Free Pump

where:

P_1 = power fluid pressure
P_2 = discharge pressure
P_3 = intake pressure

Development of Equation 5.79 is based on Lorenz's mixing-loss model, which involves converting the velocity head to a pressure head.[6]

(4) *Efficiency.* The efficiency of a jet pump is defined as the ratio of the power added to the produced fluid to the power lost by the power fluid.[6] The power added to the production fluid is:

$$(HP)_3 \;\alpha\; V(P_2 - P_3) \tag{5.80}$$

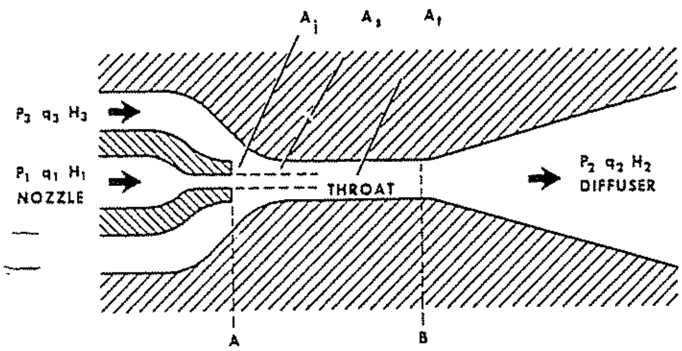

Figure 5.54 Jet Free Pump Nomenclature

P_1 = *power fluid pressure, psi*	q_1 = *power fluid rate, stbl/d*
P_2 = *discharge pressure, psi*	q_2 = *total liquid rate in return column, stbl/d*
P_3 = *intake pressure, psi*	V = *intake volume, b/d*
A_j = *nozzle area, in.²*	A_s = *net throat area, in.²*
A_t = *total throat area, in.²*	

The power lost by the power fluid is:

$$(HP)_1 \ \alpha \ q_1(P_1 - P_2) \qquad (5.81)$$

Then, the efficiency is:

$$\eta_p = \frac{(HP)_3}{(HP)_1} = \left(\frac{V}{q_1}\right)\left(\frac{P_2 - P_3}{P_1 - P_2}\right) \qquad (5.82)$$

Substituting Equations 5.78 and 5.79 into the above equation gives:

$$\eta_p = MH \qquad (5.83)$$

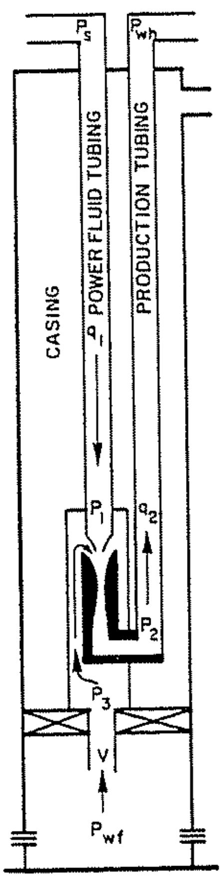

P_1 = POWER FLUID PRESSURE, psi
P_2 = DISCHARGE PRESSURE, psi
P_3 = P_{wf} = INTAKE PRESSURE, psi
P_s = SURFACE OPERATING PRESSURE, psi
P_{wh} = WELLHEAD PRESSURE, psi
q_1 = POWER FLUID RATE, STBL/D
q_2 = TOTAL LIQUID RATE IN PRODUCTION TUBING, STBL/D
V = INTAKE VOLUME, BBL/D

Figure 5.55 Jet Pump Schematic

(5) *Dimensionless performance curves.* The performance of geometrically similar jet pumps operating at the same Reynolds number is described by Equations 5.77, 5.78, 5.79, and 5.83. A plot of these equations showing H and η_p vs M for several values of R is shown in Figure 5.56. The area ratios selected cover the range from a relatively high head, low-flow-rate pump (A ratio, R = 0.410) to a relatively low head, high-flow-rate pump (E ratio, R = 0.168).

It is good field practice to attempt to operate the pump at its peak efficiency. For this case, the M and H ratios will be fixed; hence, Equations 5.78 and 5.79 become:

$$q_1 = V/M_p \qquad (5.84)$$

and:

$$P_3 = (1 + H_p)P_2 - H_pP_1 \qquad (5.85)$$

where M_p and H_p are the peak efficiency flow ratio and the peak efficiency head ratio, respectively.

5.52 CAVITATION

If pressure P_3 at the entrance to the throat is reduced below the vapor pressure of the fluid being pumped, cavitation will result. Attempts to lower P_3 below the vapor pressure by increasing the power fluid pressure will simply lead to greater vapor volumes in the suction fluid. The collapse of the cavitation bubbles in the throat of the pump causes severe damage because of shock waves and high-velocity microjets resulting from asymmetrical bubble collapse. For these reasons, predicting the cavitation limit is important in applying jet pumps.[6]

If the vapor pressure is considered to be zero, the cavitation limit can be estimated from the following equation:

$$M_c = \frac{1-R}{R}\sqrt{1+K_j}\sqrt{\frac{P_3}{I_c(P_1 - P_3) + P_3}} \qquad (5.86)$$

where:

K_j = the nozzle-loss coefficient
I_c = a cavitation index

Numerous tests by different investigators have placed the value of I_c between 0.8 and 1.67, with 1.35 being a conservative design value.[6] Similar tests have shown that 0.15 is representative of K_j in a typical jet pump. With these values of I_c and K_j, Equation 5.86 becomes:

$$M_c = (1.0724)\left(\frac{1-R}{R}\right)\sqrt{\frac{P_3}{1.35(P_1 - P_3) + P_3}} \qquad (5.87)$$

Operation at M values below M_c will be noncavitating. Attempts to increase M beyond M_c will lead to cavitation at the throat entrance, and the pump performance will deviate from the expected H-M performance curve (Figure 5.56).

As will be seen later, construction of an intake curve for a jet pump will be based on assuming P_1 and calculating P_3 from Equation 5.85 for a fixed value of P_2. Since M_c is independent of P_2 (see Equation 5.87), as P_1 increases and, consequently, P_3 decreases, M_c will decrease until it reaches the operating M, which in this case is equal to M_p. Therefore, Equation 5.87 can

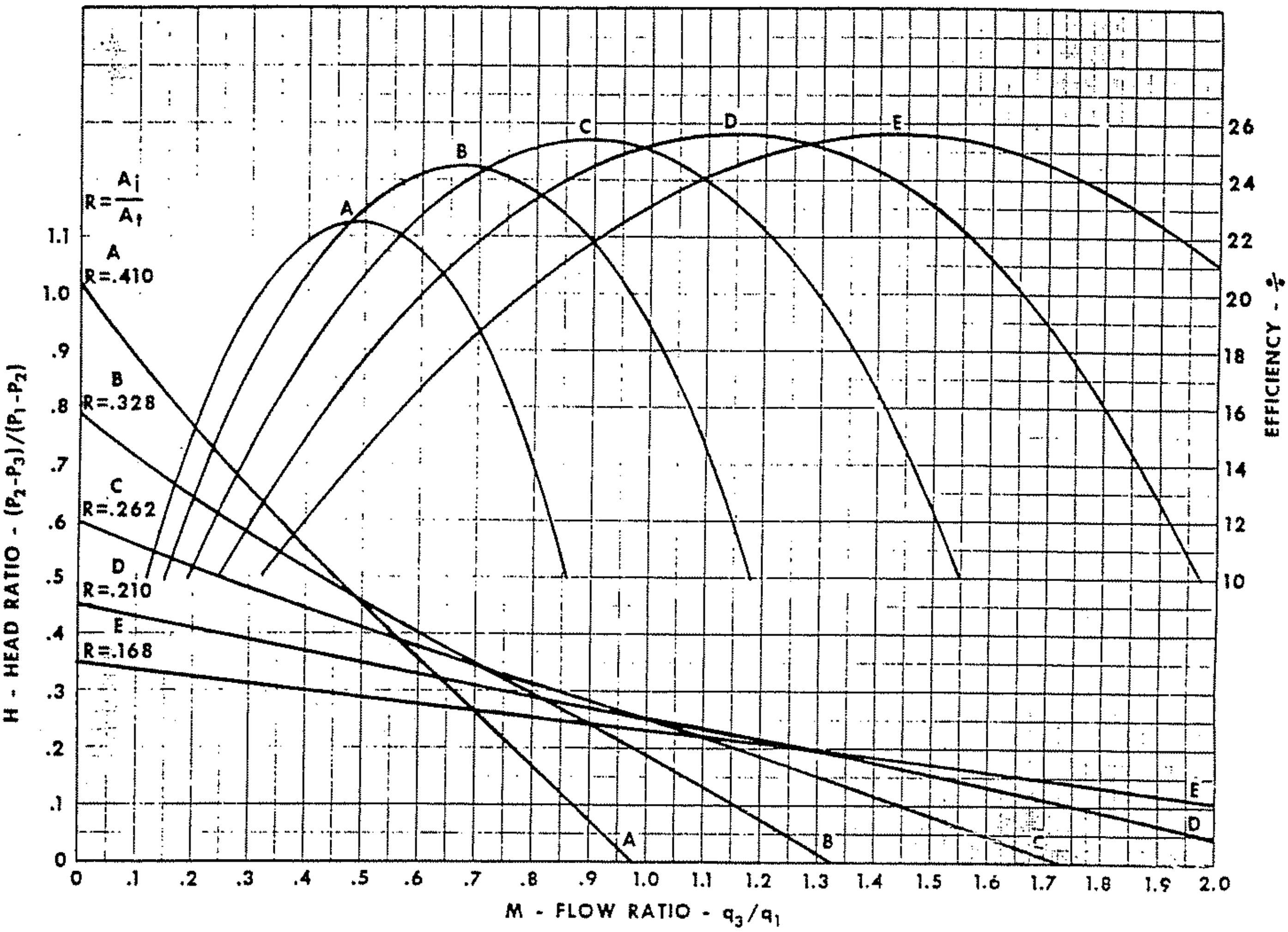

Figure 5.56 Jet Pump—H vs M and Efficiency (after Brown and Petrie)[6]

be solved for the minimum value of P_3 below which cavitation takes place. In doing so, Equation 5.87 is written in the following form:

$$\frac{P_3}{1.35(P_1 - P_3) + P_3} = \left[\frac{R\,M_p}{1.0724(1 - R)}\right]^2 \tag{5.88}$$

For the same pump, the right-hand side of the above equation is constant and will be denoted as B:

$$B = \left[\frac{R\,M_p}{1.0724(1 - R)}\right]^2 \tag{5.89}$$

Then:

$$P_c = \left(\frac{1.35B}{1 + 1.35B - B}\right) P_1 \tag{5.90}$$

where P_c is the cavitating intake pressure.

The coefficient of P_1 in the above equation is constant and will be denoted C:

$$C = \frac{1.35B}{1 + 1.35B - B} \tag{5.91}$$

Then

$$P_c = C\,P_1 \tag{5.92}$$

5.53 POWER FLUID RATE AND PRESSURE

Similar to hydraulic pumps, jet pumps utilize either water or oil as a power fluid. The actual power fluid rate is a function of the pressure P_1 and P_3, the flow area of the nozzle A_j, and the specific gravity of the power fluid γ_1. When everything is measured in common oil-field units, the power fluid rate can be estimated from the following equation:[6]

$$q_1 = 1{,}214.5\,A_j\sqrt{\frac{P_1 - P_3}{\gamma_1}} \tag{5.93}$$

where:

q_1 is in stbl/d
P_1 and P_3 are in psi
A_j is in in.^{2}

Since q_1 is normally known from the M ratio (Eq. 5.78), the above equation should be solved for A_j:

$$A_j = \frac{q_1}{1{,}214.5}\sqrt{\frac{\gamma_1}{P_1 - P_3}} \tag{5.94}$$

Once A_j is determined from Equation 5.94, it must be corrected for the available nozzle sizes. Brown and

Petrie discussed nozzle and throat design for field application.[6]

Higher power fluid pressures are desirable since they result in lower intake pressures and, consequently, higher production rates. Attempts to obtain higher drawdowns by increasing P_1, however, may eventually lead to cavitation on one hand and excessive surface operating pressures on the other hand. In normal operations, the surface operating pressure should not exceed 4,000 psi.[6]

5.54 HORSEPOWER

The horsepower requirement is estimated from the following equation:[5]

$$HP = 1.7 \times 10^{-5} q_1 P_s \qquad (5.95)$$

where P_s is the surface operating pressure in psi.

5.55 PUMP INTAKE CURVES

A procedure for predicting intake curves is considered for two cases: (1) pumping only liquid and (2) pumping gas with the liquid. For both cases, it is assumed that the pump is set at the bottom of the well, the wellhead pressure and size of the flow path are fixed, and the pump is operated at its peak efficiency. For case 2, it is assumed that all associated gas is pumped with the liquid. The sensitivity variable selected for this lift system is the power fluid pressure. As will be seen later, predicting intake curves for a jet pump is direct for case 1 and indirect for case 2.

5.551 PUMPING LIQUID ONLY

5.5511 INTRODUCTION

Liquids are only slightly compressible; hence, V in Equation 5.84 can be considered constant and equal to the surface rate:

$$q_1 = q_{sc}/M_p \qquad (5.96)$$

It should be kept in mind that, since the pump is set at the bottom of the well, the intake pressure in Equation 5.85 is equal to the flowing bottom-hole pressure.

For assumed surface production rates, q_1 can be calculated from Equation 5.96; then, the total liquid rate in the production column, which is necessary to determine P_2, will be known. Having determined P_2 and by assuming various power fluid pressures, the intake pressure can be determined from Equation 5.85. These are the bases for constructing intake curves for jet pumps.

Pump selection. Generally speaking, a high head pump such as that associated with the A or B ratio would be employed in a deep well with a high lift. On the other hand, a high-flow-rate pump, such as that associated with the D or E ratio, would be employed in a shallow well with a low lift. But the most appropriate pump for a specific well will remain unknown until the performance of several pump ratios is investigated in light of the reservoir performance. A proper procedure for pump selection follows.

(1) Establish a surface operating pressure.
(2) Read R, M_p, and H_p for several pump ratios from Figure 5.56. For each pump ratio, do the following:
   (a) Assume a production rate.
   (b) Calculate q_1 from Equation 5.96.
   (c) Determine the power fluid pressure and the discharge pressure from a pressure gradient correlation.
   (d) Calculate the intake pressure from Equation 5.85.
   (e) Repeat steps b–d for other assumed production rates.
(3) Plot the intake pressure vs rate for each pump ratio. Plot the stbl/d IPR curve to the same scale on the same graph.
(4) Read the possible rates for each pump at the intersection of its intake curve with the IPR curve.
(5) For each possible rate, calculate q_1 from Equation 5.96; then determine the horsepower requirements from Equation 5.95.
(6) Select a suitable pump on the basis of economical considerations.

Because of the difference in the M_p and H_p ratios, the plots prepared in step 3 above will overlap; hence, pump choice will depend on the position of the IPR curve. Another constraint that may influence pump selection is the availability of power fluid and/or horsepower. If the objective is to maximize the production rate, the pump that yields the highest rate should be selected.

5.5512 PROCEDURE FOR THE PREPARATION OF TUBING INTAKE CURVES FOR THE JET PUMP

In order to show the effect of friction, it is necessary to relax the limit on the surface operating pressure.

(1) Select a suitable pump ratio.
(2) Read M_p and H_p from Figure. 5.56 for the selected pump.
(3) Assume a production rate and do the following:
   (a) Calculate q_1 from Equation 5.96.
   (b) Determine P_2 from a pressure gradient correlation.
   (c) Assume various power fluid pressures and, for each of these pressures, calculate P_3 from Equation 5.85.
   (d) Repeat steps a–c for other assumed production rates.
(4) Plot P_3 vs rate for the various assumed power fluid pressures. Plot the stbl/d IPR curve to the same scale on the same graph.
(5) Calculate B from Equation 5.89; then, calculate C from Equation 5.91. Determine the cavitating intake pressure from Equation 5.92. Mark the cavitation points at the intersection of the cavitating intake pressure (horizontal line) with the respective intake curve. Draw a smooth curve through the cavitation points.
(6) Read the possible rates at the intersection of the pump intake curves with the IPR curve. Read the cavitation limit rate at the intersection of the cavitation curve with the IPR curve.
(7) For each possible rate, calculate the power fluid

rate; then, determine P_s and calculate HP from Equation 5.95.

(8) Plot the possible rate vs P_s, HP, and q_1. Impose the cavitation limit rate on the same plot.

(9) Select a suitable rate.

EXAMPLE PROBLEM #1 (PUMPING LIQUID ONLY)

Well, reservoir, and fluid data are shown in Table 5.1. IPR's in stbl/d and in b/d are shown in Figure 5.8. For the solution, refer to Figures 5.57, 5.58 and 5.59.

Since the pump is set at the bottom of the well, the intake pressure is identical to the flowing bottom-hole pressure; hence, the stbl/d IPR shown in Figure 5.8 is applicable.

For the A ratio pump, the peak efficiency flow ratio is 0.475, and the peak efficiency head ratio also is 0.475 (Figure 5.56). Hence, Equations 5.96 and 5.85 become:

$$q_1 = q_{sc}/0.475 \tag{5.97}$$

and

$$P_3 = 1.475\ P_2 - 0.475\ P_1 \tag{5.98}$$

Since R is 0.41:

$$B = \left[\frac{(0.41)(0.475)}{1.0724(1-0.41)}\right]^2 = 0.0947 \tag{5.89}$$

and

$$C = \frac{(1.35)(0.0947)}{1 + (1.35)(0.0947) - 0.0947} = 0.1237 \tag{5.91}$$

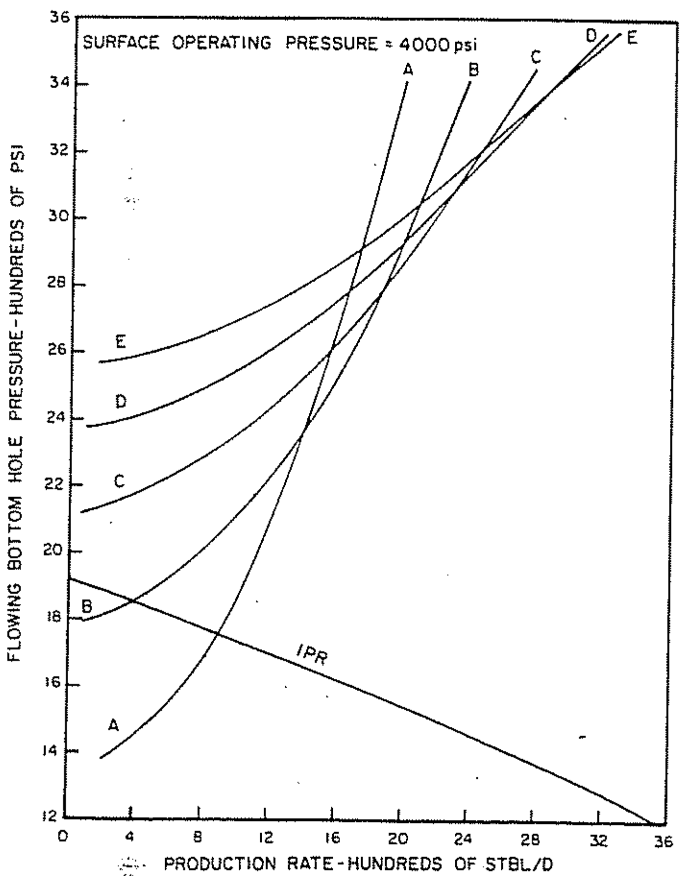

Figure 5.57 Intake Curves for Various Jet Pumps in Well #1 (Pumping Liquid)

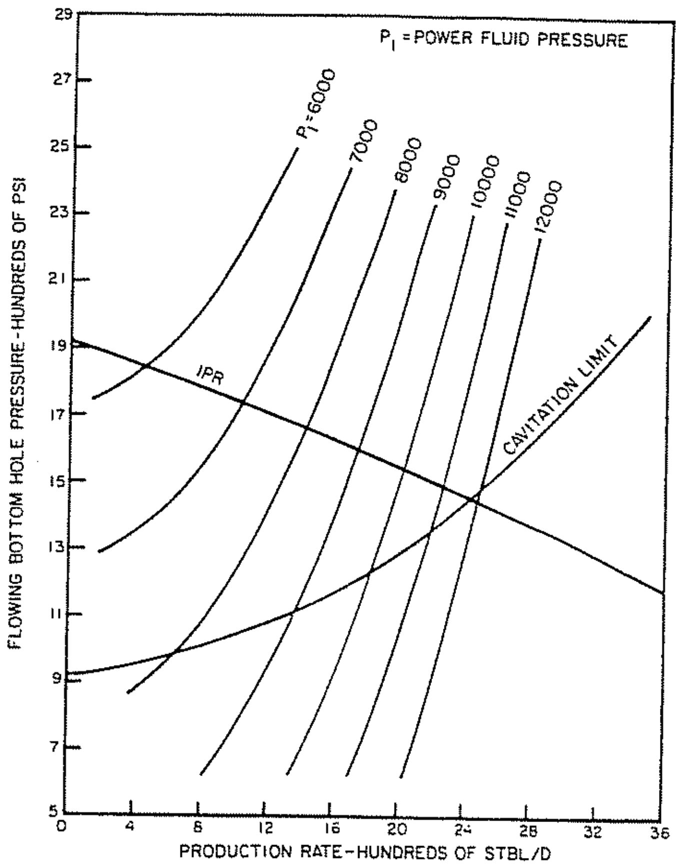

Figure 5.58 Intake Curves for a Jet Pump in Well #1 (Pumping Liquid)

With the obtained value of C, Equation 5.92 becomes:

$$P_c = 0.1237\ P_1 \tag{5.99}$$

If a production rate of, say, 200 stbl/d is assumed, Equation 5.97 gives:

$$q_1 = 200/0.475 = 421 \text{ stbo/d}$$

The total liquid rate in the return column is then 200 + 421 or 621 stbl/d of which 521 bbl are oil and 100 bbl are water. The required discharge pressure for this rate is:

$P_2 = 3{,}129$ psi (pressure gradient correlation)

With a surface operating pressure of, say, 4,000 psi, the power fluid pressure is:

$P_1 = 6{,}824$ psi (pressure gradient correlation)

Then Equation 5.98 gives:

$$P_3 = (1.475)\ (3{,}129) - (0.475)\ (6{,}824) = 1{,}374 \text{ psi}$$

Similarly, the following can be obtained for other assumed production rates:

q_{sc}	q_1	P_2	P_1	P_3
400	842	3,169	6,787	1,451
600	1,263	3,231	6,750	1,560
800	1,684	3,314	6,714	1,699
1,000	2,105	3,417	6,679	1,868
1,200	2,526	3,542	6,644	2,069
1,400	2,947	3,688	6,452	2,375
1,600	3,368	3,855	6,350	2,670
1,800	3,789	4,044	6,238	3,002
2,000	4,211	4,256	6,119	3,372

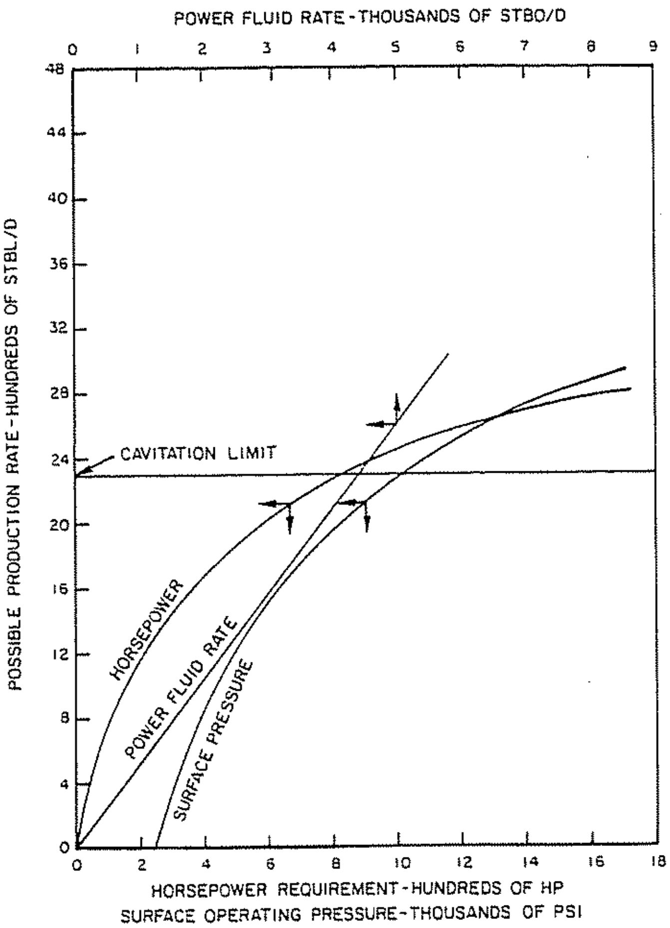

Figure 5.59 Possible Production Rate by Jet Pumping vs HP, P_s, and q_1 for Well #1 (Pumping Liquid)

Intake pressure P_3 was plotted vs q_{sc} in Figure 5.57. The stbl/d IPR was plotted to the same scale in the same figure.

The same type of calculations were made for the other pump ratios. Results of calculations also were plotted in Figure 5.57. Note that the plots overlap because of the difference in the flow and head ratios. It is evident that, within the limit of 4,000-psi surface operating pressure, the A ratio pump should be selected since it yields a higher production rate than the B ratio pump, while no flow is associated with the C, D, or E ratio pumps.

For the A ratio pump, the well can produce 900 stbl/d with 4,000 = psi surface operating pressure (Figure 5.57). If 4,000 psi is the maximum allowable surface operating pressure and optimization of the production rate is desired, the pump performance should be studied for pressures that are less than 4,000 psi. But in order to illustrate the effect of friction and to show the cavitation zone, the limit on the surface operating pressure must be relaxed, in which case there will be no limit on the power fluid pressure.

For an assumed production rate of 200 stbl/d, the discharge pressure was previously determined as 3,129 psi. Then, if a power fluid pressure of, say, 6,000 psi is assumed, Equation 5.98 gives:

$$P_3 = (1.475)(3{,}129) - (0.475)(6{,}000) = 1{,}765 \text{ psi}$$

Similarly, the following can be obtained for the same rate of 200 stbl/d with other assumed power fluid pressures:

P_1	P_3
7,000	1,290
8,000	815
9,000	340

The same type of calculations were made for other assumed rates. Results of the calculations are shown in Table 5A.24. Intake pressure P_3 was plotted vs q_{sc} for the various power fluid pressures in Figure 5.58. The stbl/d IPR was plotted to the same scale in the same figure.

The intake pressure below which cavitation takes place is calculated from Equation 5.99:

P_1	P_c
8,000	990
9,000	1,113
10,000	1,237
11,000	1,361
12,000	1,484

Cavitation points were marked at the intersection of the P_c line (horizontal) with the respective intake curve; then a smooth curve was drawn through these points (see Figure 5.58). Operation of the pump should be anywhere above the cavitation curve and limited only by the power fluid (surface operating) pressure.

The possible rates are the intersections of the pump intake curves with the IPR curve. For example, the well can produce 450 stbl/d with a power fluid pressure of 6,000 psi. The required power fluid rate for this rate is:

$$q_1 = 450/0.475 = 947 \text{ stbo/d (Eq. 5.97)}$$

For 6,000-psi power fluid pressure and a 947-stbo/d power fluid rate:

$$P_s = 3{,}198 \text{ psi (pressure gradient correlation)}$$

Then Equation 5.95 gives:

$$HP = (1.7 \times 10^{-5})(947)(3{,}198) = 52 \text{ HP}$$

Similar calculations were made for other rates. Results of the calculations are shown in Table 5A.25. Possible rate q_p was plotted vs HP, P_s, and q_1 in Figure 5.59. The cavitation limit rate, which is about 2,300 stbl/d (see Figure 5.58), was imposed on the same figure.

It is evident from Figure 5.59 that, beyond 2,800 stbl/d, the surface operating pressure as well as the horsepower requirements increase very quickly without any significant gain in the production rate. This rate would be selected if it was noncavitating on one hand and if there was no limit to the surface operating pressure on the other hand. In this case, the practical limit of 4,000-psi surface operating pressure is used. With this pressure, the well can produce 880 stbl/d (see Figure 5.59). Then:

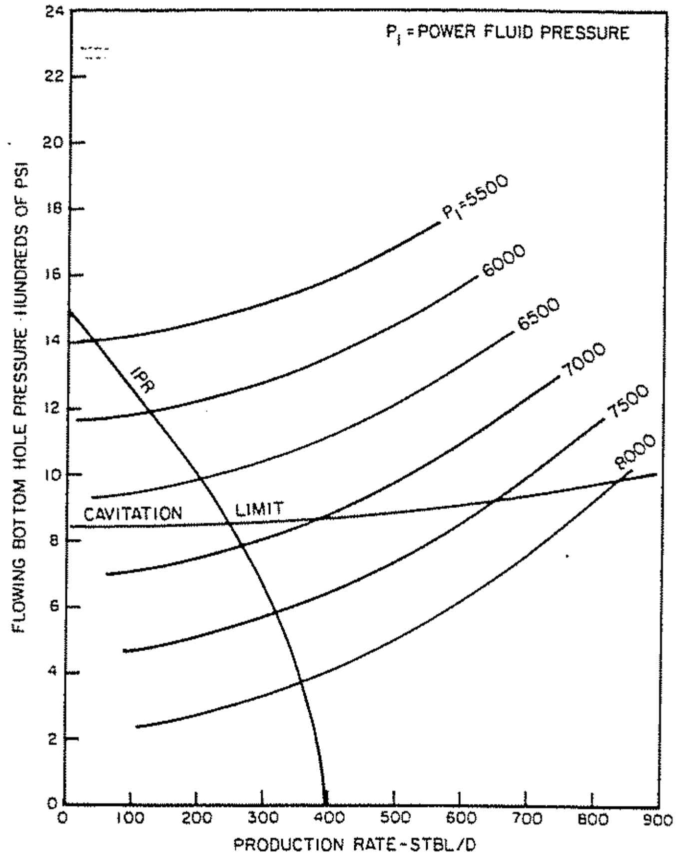

Figure 5.60 Intake Curves for a Jet Pump in Well #2 (Pumping Liquid)

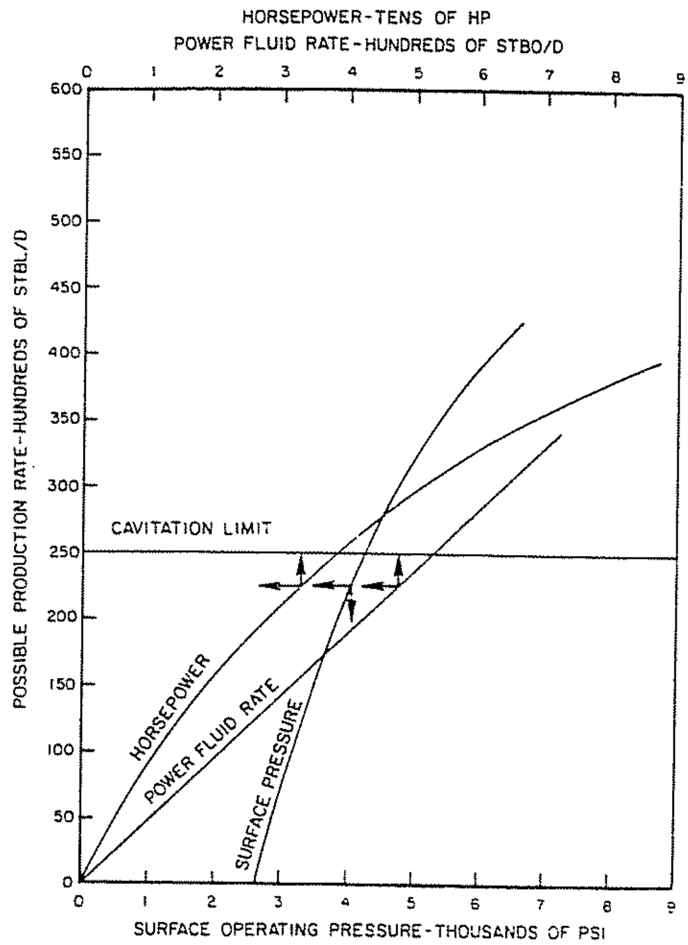

Figure 5.61 Possible Production Rates by Jet Pumping vs Horsepower, P_s, and q_1 for Well #2 (Pumping Liquid)

$q_1 = 880/0.475 = 1{,}853$ stbo/d (Eq. 5.97)
HP $= (1.7 \times 10^{-5})(1{,}853)(4{,}000) = 112$ HP (Eq. 5.95)
$P_1 = 6{,}700$ psi (pressure gradient correlation)
$P_3 = 1{,}770$ psi (Figure 5.58)

Hence, Equation 5.94 gives:

$$A_j = \frac{1{,}853}{1{,}214.5}\sqrt{\frac{0.85}{6{,}700 - 1{,}770}} = 0.02 \text{ in.}^2$$

Note: A_j must be corrected for the available nozzle sizes (see Ref. 14).

EXAMPLE PROBLEM #2 (LIQUID ONLY)

Refer to Figures 5.60 and 5.61.

Well, fluid, and reservoir data are shown in Table 5.1. IPR's in stbl/d and in b/d are shown in Figure 5.9.

The same type of calculations previously made for well #1 were made for this well. The most appropriate pump was found to be the A ratio pump. Results of the calculations are shown in Tables 5A.26 and 5A.27.

The data of Table 5A.26 were plotted in Figure 5.60. The stbl/d IPR was plotted to the same scale on the same graph. The horsepower requirements for the possible rates are shown in Table 5A.27. Figure 5.61 is a plot of q_p vs P_s, HP, and q_1. The selected rate is 220 stbl/d (4,000-psi surface operating pressure). For this rate, the horsepower requirement, the power fluid rate, and the power fluid pressure are 32 HP, 465 stbo/d, and 6,600 psi, respectively. The nozzle area, which is subject to correction, is 0.0046 in.^{2}

5.552 PUMPING LIQUID AND GAS

5.5521 INTRODUCTION

Because of the high compressibility of gas, V in Equation 5.84 cannot be considered constant as was done for the liquid case but should be determined at the intake pressure from Equation 5.4. Hence, Equation 5.84 becomes:

$$q_1 = q_{sc}\, VF/M_p \quad (5.100)$$

where VF is the volume factor estimated at the intake pressure from Equation 5.2.

For a jet pump using oil as the power fluid, the total liquid rate, the gas-oil ratio, and the water cut in the return column are as follows:

$$q_2 = q_1 + q_{sc} \quad (5.101)$$

$$GOR_2 = \frac{q_{sc}\, GLR}{q_1 + q_{sc}(1 - wc)} \quad (5.102)$$

$$wc_2 = \frac{q_{sc}\, wc}{q_2} \quad (5.103)$$

Unlike the case for pumping only liquid, predicting intake curves for the liquid and free gas is somewhat indirect. This is because the intake pressure must be known in order to determine VF. Since the wellhead pressure is fixed, the discharge pressure also will be

fixed for each rate. Hence, the power fluid pressure cannot be assumed as was done for the liquid case but must be calculated from Equation 5.85 since it is the only unknown left in that equation. In order to facilitate plotting of intake curves, it is therefore necessary to obtain intake pressures for the assumed production rates for identical power fluid pressures. This can be accomplished either by making a plot of P_3 vs P_1 for each rate or by interpolating.

Solving Equation 5.85 for P_1 gives:

$$P_1 = \frac{(1 + H_p)P_2 - P_3}{H_p} \qquad (5.104)$$

(1) *Pump selection.* As mentioned previously, the two factors that influence pump selection are the flow and head ratios. The difference in the flow ratio is a measure of the difference in the power fluid rate. Because of the existence of gas in this case, the difference in the power fluid rate will be higher than in the case when pumping only liquid. Hence, the pump that would be employed for the liquid case would be employed in this case.

5.5522 PROCEDURE FOR PREPARING TUBING INTAKE CURVES FOR JET PUMP (PUMPING GAS)

As was done for the liquid case, the limit on the surface operating pressure will be relaxed, so there will be no limit on the power fluid pressure. The stepwise procedure is as follows:

(1) Select a suitable pump.
(2) Assume various liquid rates, and for each of these rates, do the following:
  (a) Assume an intake pressure.
  (b) Determine VF at the assumed intake pressure from Equation 5.2.
  (c) Calculate q_1 from Equation 5.100.
  (d) Calculate q_2, GOR_2, and wc_2 from Equations 5.101, 5.102, and 5.103.
  (e) Determine P_2 from a two-phase flow correlation.
  (f) Calculate P_1 from Equation 5.104.
  (g) Repeat steps b–f for other assumed intake pressures.
(3) By interpolating or plotting, obtain intake pressures for the assumed production rates for identical power fluid pressures.
(4) Plot the intake pressure (obtained in step 3) vs rate for the various power fluid pressures. Plot the stbl/d curve to the same scale on the graph.
(5) Calculate B from Equation 5.89; then, calculate C from Equation 5.91. Determine the cavitating intake pressure for each power fluid pressure from Equation 5.92. Mark the cavitation points at the intersection of the cavitating intake pressure (horizontal line) with the respective intake curve. Draw a smooth curve through the cavitation points.
(6) Read the possible rates at the intersection of the pump intake curves with the IPR curve. Read the cavitation limit rate at the intersection of the cavitation curve with the IPR curve.
(7) For each possible rate, calculate the power fluid rate; then, determine P_s and calculate HP from Equation 5.95.
(8) Plot the possible rate vs q_1, P_s, and HP. Impose the cavitation limit rate on the same graph.
(9) Select a suitable rate.

(2) *Rate selection.* Whether pumping only liquid or pumping gas with the liquid, the selected rate must be:

(1) noncavitating
(2) economically feasible

As the power fluid pressure and, consequently, the production rate as well as the power fluid rate increase, the effect of friction loss in the flow conduits begins to manifest itself. As a result, the gain in the production rate per 1 HP continues to diminish until it becomes insignificant.

EXAMPLE WELL #1

Refer to Figures 5.62 and 5.63.

Since the pump is set at the bottom of the well and all gas is pumped, the IPR curves of Figure 5.8 and the volume factor data of Table 5A.1 are applicable.

For the liquid case, the A ratio pump was selected because it gave the highest production rate. The same pump will be used in this case. At peak efficiency, Equations 5.100 and 5.104 become:

$$q_1 = q_{sc}\,VF/0.475 \qquad (5.105)$$

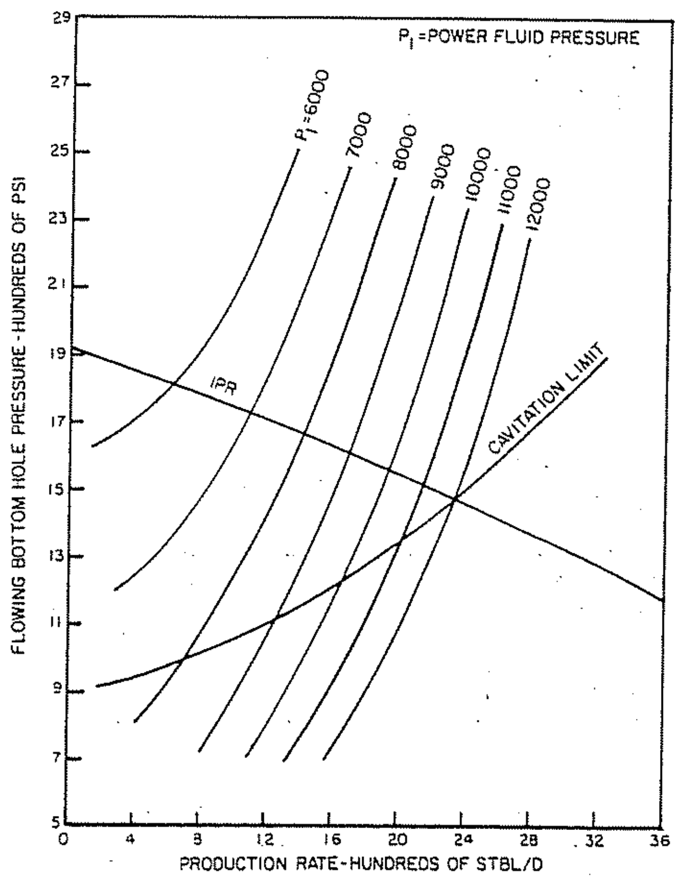

Figure 5.62 Intake Curves for a Jet Pump in Well #1 (Pumping Liquid and Gas)

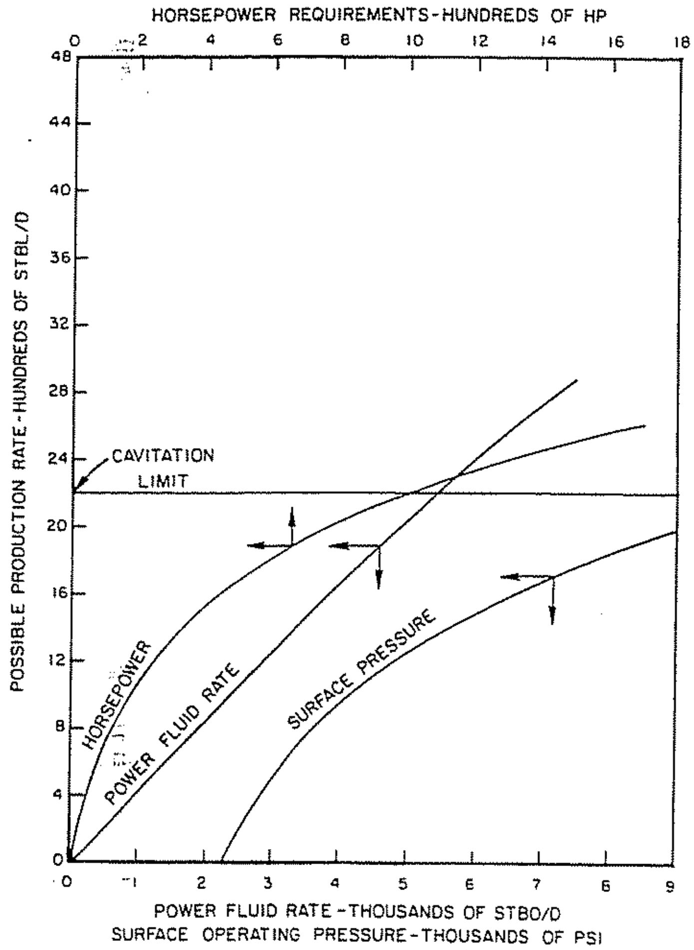

Figure 5.63 Possible Production Rate by Jet Pumping vs HP, P_s, and q_1 for Well #1 (Pumping Liquid and Gas)

and

$$P_1 = \frac{1.475\ P_2 - P_3}{0.475} \qquad (5.106)$$

For the fluid of well #1, Equations 5.101, 5.102, and 5.103 become:

$$q_2 = q_1 + q_{sc} \qquad (5.107)$$

$$GOR_2 = \frac{200\ q_{sc}}{q_1 + 0.5\ q_{sc}} \qquad (5.108)$$

and

$$wc_2 = \frac{0.5\ q_{sc}}{q_2} \qquad (5.109)$$

If a liquid surface rate of, say, 200 stbl/d and an intake pressure of, say, 500 psi are assumed, then:

VF = 1.9899 bbl/stbl (Table 5A.1 @ 500 psi)

$q_1 = (200)(1.9899)/0.475 = 838$ stbo/d (Eq. 5.105)

$$GOR_2 = \frac{(200)(200)}{838 + (0.5)(200)} = 43 \text{ scf/stbo (Eq. 5.108)}$$

$$wc_2 = \frac{(0.5)(200)}{1{,}038} = 0.096 \text{ (Eq. 5.109)}$$

For a liquid rate of 1,038 stbl/d, a gas-oil ratio of 43 scf/stbo, and a water cut of 0.096:

$P_2 = 3{,}066$ psi (two-phase flow correlation)

Then, Equation 5.106 gives:

$$P_1 = \frac{(1.475)(3{,}066) - 500}{0.475} = 8{,}467 \text{ psi}$$

A similar procedure was carried out for the same rate—200 stbl/d—with other assumed intake pressures. Results of the calculations are shown in Table 5A.28. Interpolating Table 5A.28 gives:

P_1	P_3
6,000	1,639
7,000	1,176
8,000	711

The same type of calculations were made for other assumed rates. Results of the calculations are shown in Table 5A.29. Intake pressure P_3 was plotted vs q_{sc} for the various power fluid pressures in Figure 5.62. The stbl/d IPR was plotted to the same scale in the same figure.

If the vapor pressure is assumed to be zero, the cavitating intake pressure is the same as that calculated previously for the liquid case. The cavitation curve of Figure 5.58 was reproduced in Figure 5.62. Operation of the pump should be anywhere above the cavitation zone and limited only by the power fluid (surface operating) pressure.

The possible rates are the intersection of the pump intake curves with the IPR curve. For example, the well can produce 630 stbl/d with a power fluid pressure of 6,000 psi (see Fig. 5.62). The intake pressure for this rate is 1,815 psi, at which VF is 1.1162 (Table 5A.1). Hence, Equation 5.105 gives:

$q_1 = (630)(1.1162)/0.475 = 1{,}480$ stbo/d

For a power fluid rate of 1,480 stbo/d and a power fluid pressure of 6,000 psi:

$P_s = 3{,}233$ psi (pressure gradient correlation)

Then Equation 5.95 gives:

$HP = (1.7 \times 10^{-5})(1{,}480)(3{,}233) = 81$ HP

Similar calculations were made for other possible rates. Results of the calculations are shown in Table 5A.30. Possible rate q_p was plotted vs P_s, HP, and q_1 in Figure 5.63. The cavitation limit rate (2,200 stbl/d) was imposed on the same figure.

Inspection of Figure 5.63 shows that, beyond 2,600 stbl/d, the surface operating pressure as well as the horsepower requirements increase very quickly without any significant gain in the production rate. This rate would be selected if it was noncavitating and if there was no limit to the surface operating pressure. In this case, operation of the pump up to the practical limit of 4,000 psi surface operating pressure will be allowed. With this pressure, the well can produce 950 stbl/d (Figure 5.63), which is greater than that obtained previously for the liquid case (880 stbl/d). For 950 stbl/d:

$q_1 = 2{,}250$ stbo/d (Figure 5.63)
HP = 160 HP (Figure 5.63)
$P_3 = 1{,}755$ psi (Figure 5.62)
$P_1 = 6{,}600$ psi (determined)

Then:

$$A_j = \frac{2{,}250}{1{,}214.5}\sqrt{\frac{0.85}{6{,}600 - 1{,}755}} = 0.025 \text{ in.}^2$$

EXAMPLE PROBLEM #2 (PUMPING GAS)

Well fluid and reservoir data are shown in Table 5.1. Calculation of VF with 100% GIP was made in Table 5A.2 (Appendix 5). IPR's in stbl/d and in b/d are shown in Figure 5.9.

The same type of calculations previously made for well #1 were made for this well. The most appropriate pump was found to be the A ratio pump. Results of the calculations are shown in Tables 5A.31 and 5A.32 (Appendix 5).

The data of Table 5A.31 were plotted in Figure 5.64. The stbl/d IPR was plotted to the same scale in the same figure. The horsepower requirements for the possible rates (obtained from Figure 5.64) are shown in Table 5A.32. Figure 5.65 is a plot of q_p vs P_s, HP, and q_1. The selected rate is 250 stbl/d (4,000-psi surface operating pressure). For this rate, the horsepower requirements, the power fluid rate, and the power fluid pressure are 44 HP, 610 stbo/d, and 6,550 psi, respectively. The nozzle area, which is subject to correction, is 0.0061 in.^{2}

Discussion of results. Results of the calculations are shown in Figures 5.58–5.65.

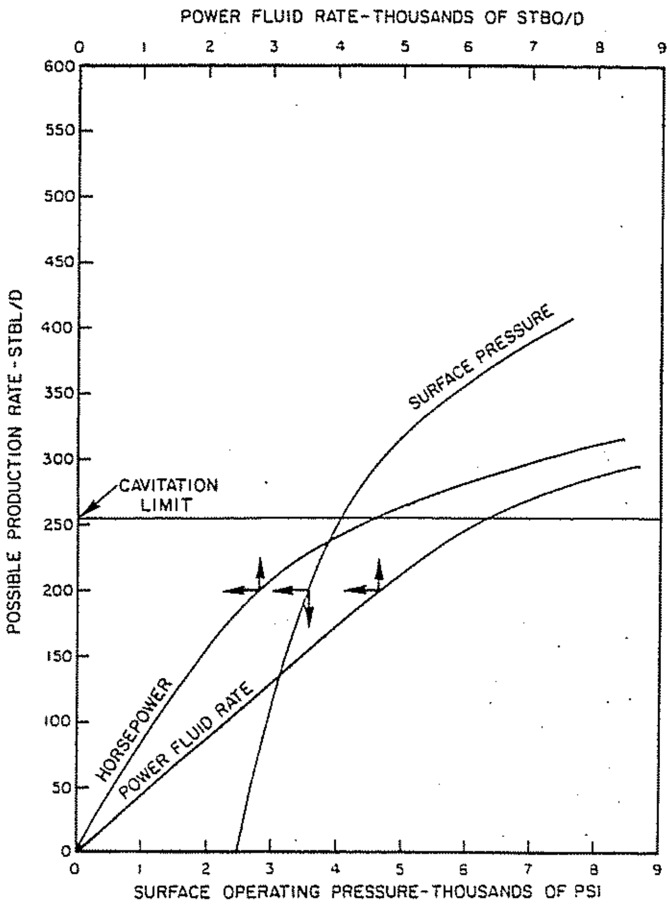

Figure 5.65 Possible Production Rate by Jet Pumping vs HP, P_s, and q_1 for Well #2 (Pumping Liquid and Gas)

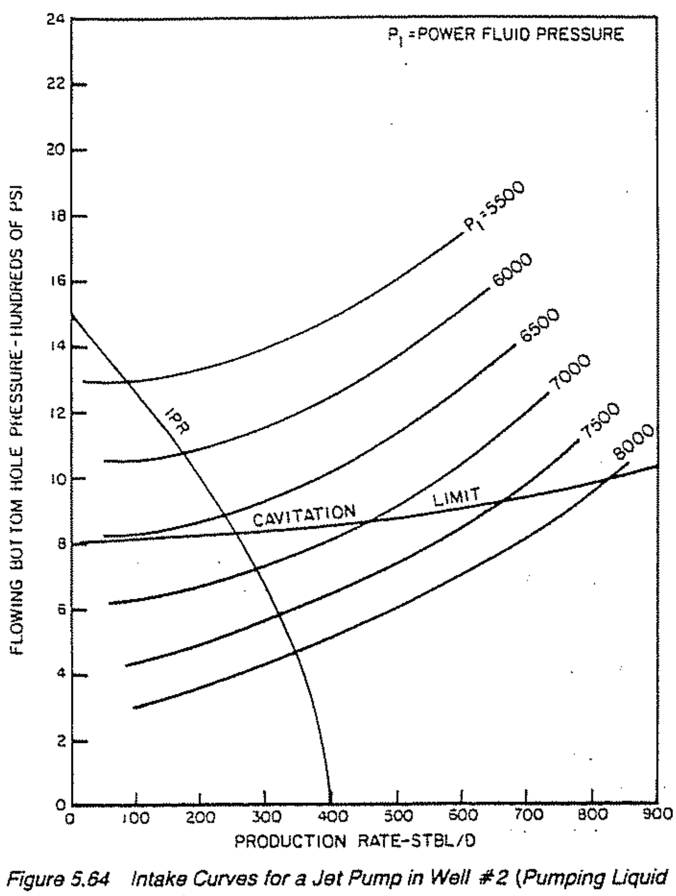

Figure 5.64 Intake Curves for a Jet Pump in Well #2 (Pumping Liquid and Gas)

Whether pumping only liquid (Figures 5.59 and 5.61) or pumping gas with liquid (Figures 5.63 and 5.65), it is evident that the gain in the production rate per 1 HP diminishes as the rate increases. This is attributed to the effect of friction loss in the flow conduits, which works to increase the discharge pressure and to reduce the power fluid pressure. Note that the effect of friction loss is minor for well #2 because of the low rates associated with this well.

Comparing Figure 5.58 to Figure 5.62 or Figure 5.60 to Figure 5.64 shows that, for intake pressures above or slightly below the bubble point (1,820 psi for the crude of well #1 and 940 psi for the crude of well #2), higher production rates can be obtained by pumping some gas with the liquid. The reason is that existence of gas in the production column reduces the discharge pressure below the level needed for the case where there is no gas. However, as the intake pressure drops below the bubble point, a large expansion in the volume of the produced fluid rate takes place, causing a significant increase in the power fluid rate. High production (liquid) rates combined with still higher power fluid rates cause a continuous decline in the GLR in the production column and a continuous increase in the friction loss. Eventually, the discharge pressure will exceed that required for the case when pumping only liquid and the opposite effect takes place.

5.6 BEAM PUMPS

5.61 GENERAL DESCRIPTION

A typical beam pumping unit consists of five parts (see Figures 5.66 and 5.67):[7]

(1) the prime mover, which furnishes the necessary power to the system

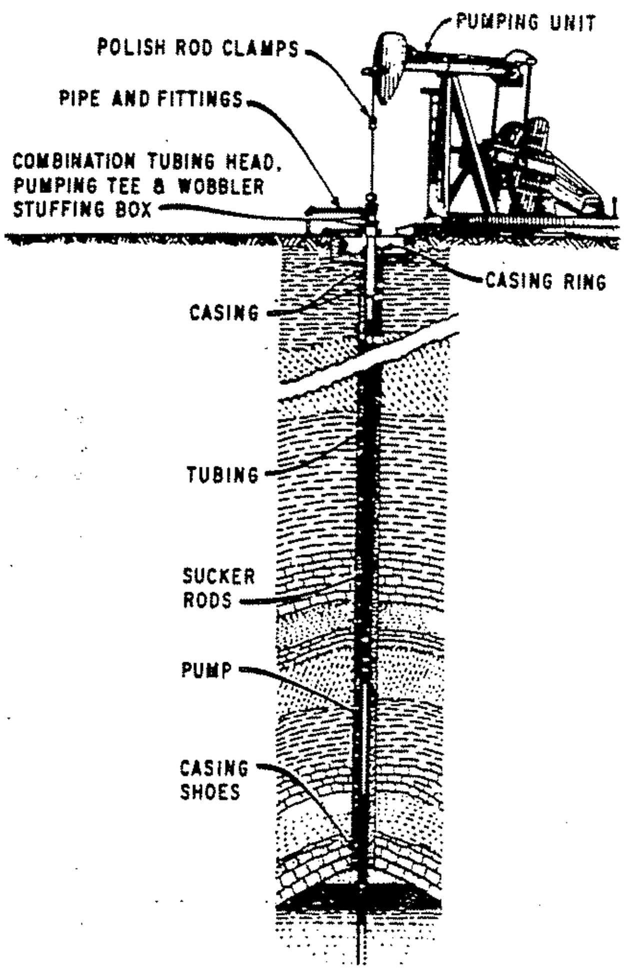

Figure 5.66 Beam Pumping Unit

(2) the power transmission unit or speed reducer
(3) the surface pumping equipment, which changes the rotating motion of the prime mover into oscillating linear pumping motion
(4) the sucker-rod string, which transmits the surface pumping motion and power to the subsurface pump; also included is the necessary string of tubing and/ or casing within which the sucker rods operate and which conducts the pumped fluid from the pump to the surface
(5) the subsurface sucker-rod-driven pump

(1) *Surface pumping unit.* The surface pumping unit (Figure 5.67), which is designated the beam pumping unit, includes items 1, 2, and 3 mentioned in Section 5.61. Brown, Day, and Byrd presented detailed discussion of each of these components.[7]

All beam types of pumping unit geometries fall into two distinct classes: (1) the class I lever system, which has its speed (gear) reducer rear-mounted with the fulcrum at midbeam, and is represented by the conventional unit (Figure 5.68a), and (2) the class III lever system, a push-up geometry with its speed reducer front-mounted, which is represented by the air-balanced (Figure 5.68b) and Lufkin Mark II (Figure 5.68c) units, in which the fulcrum is located at the rear of the beam.

Figure 5.67 shows the arrangement of the surface equipment for a typical conventional unit. The rotary motion of the crank arm is converted into oscillating motion by means of the walking beam. The crank arm is connected to the walking beam by means of the pitman arm, and the walking beam is supported by the Sampson post and the saddle bearing.

The horse's head and the bridle (or the hanger cable arrangement) are used to ensure that the pull on the sucker-rod string is vertical at all times so that no bending moment is applied to that part of the sucker-rod string above the stuffing box. The polished rod and stuffing-box combination is used to maintain a good fluid seal at the surface.

Such beam pumping units are available in a wide range of sizes. Stroke lengths vary from 12 to 240 in. The stroke length for any particular unit can be varied,

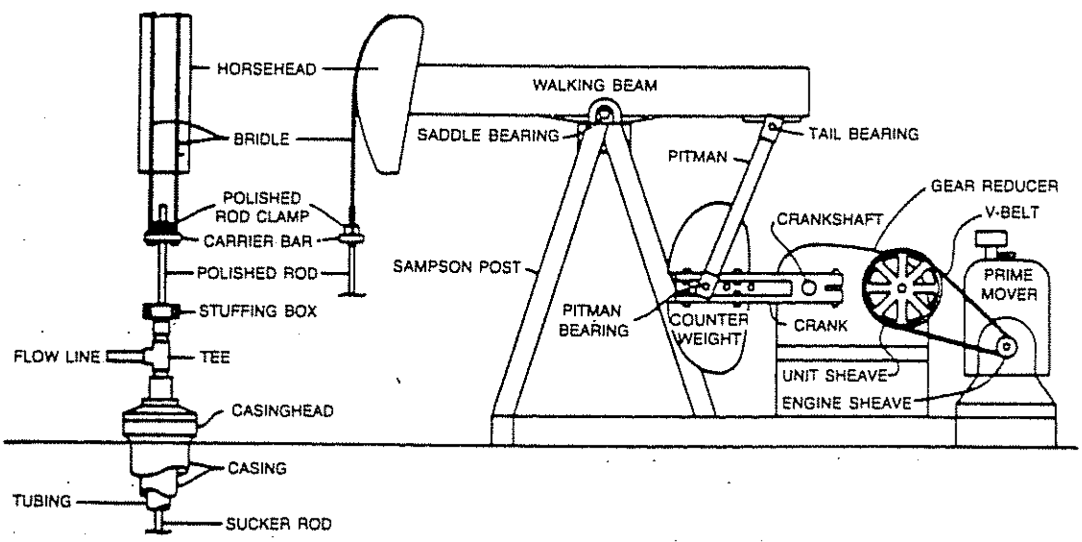

Figure 5.67 Surface Equipment of a Beam Pumping Unit

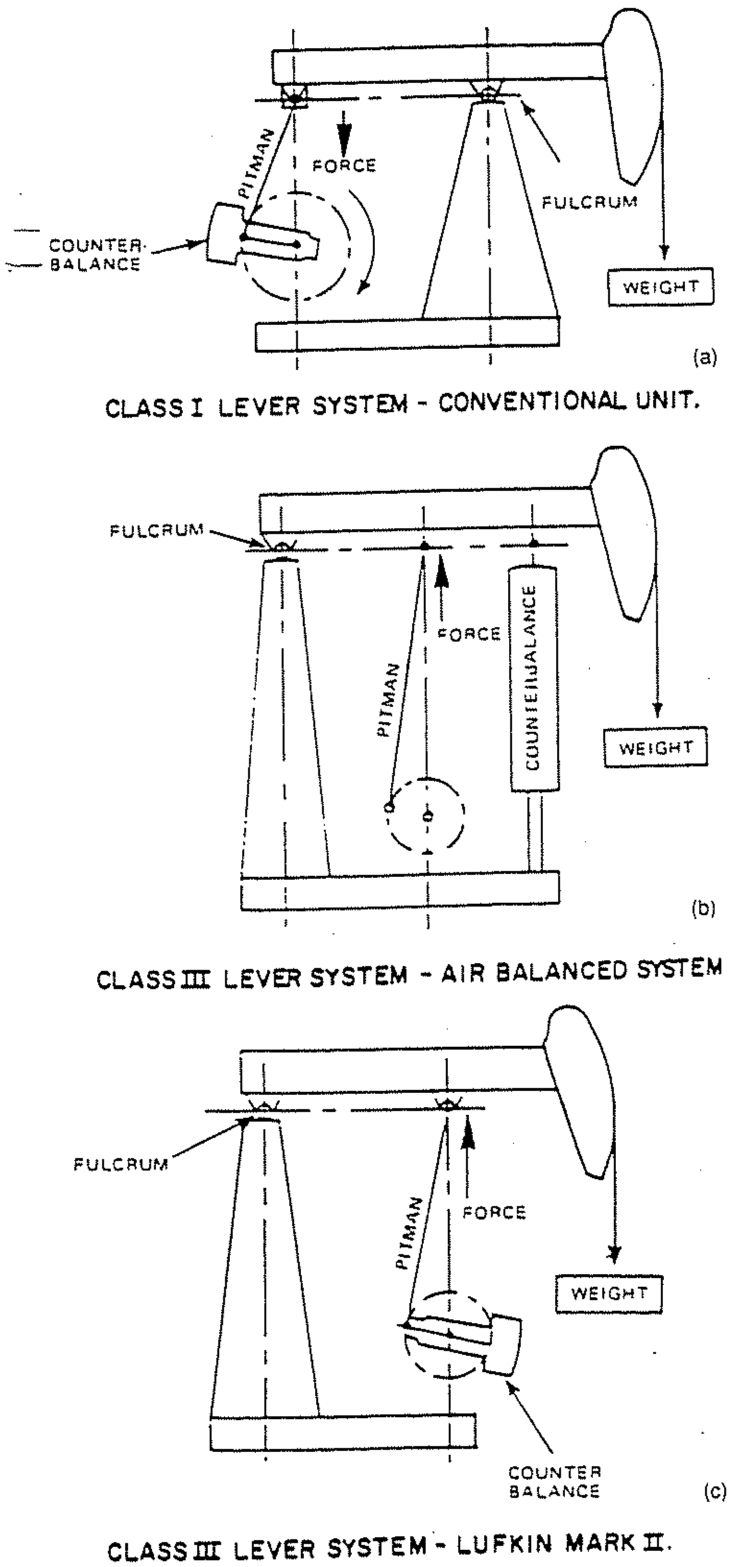

Figure 5.68 Geometries of a Beam Pumping Unit

with three or more different lengths being possible. These different strokes can be achieved by varying the position of the pitman connection to the crank. Rod and structural ratings are expressed in terms of maximum polished rod loads, which can vary from 3,000 to over 42,000 lb.

(2) *Sucker-rod string.* The sucker-rod string is a complex vibratory system that transmits energy from the surface equipment to the subsurface pump. Selection of a suitable sucker-rod string depends on the well depth and operating conditions. For well depths greater than 3,500 ft, it is common practice to use a tapered rod string that consists of different lengths of different rod sizes. The percentage of each rod size can be determined from Table 5.7.

The smallest rods are placed at the bottom of the string where the load on the string is minimum, and the largest rods are placed at the top of the string where the load on the string is maximum. The minimum and maximum loads expected during the pumping cycle must be determined as accurately as possible to design or select suitable surface equipment to handle these loads.[7]

The maximum stress at the top of the entire rod string is the peak polished rod load (denoted PPRL and discussed in a following section) divided by the cross-sectional area of the top section of the rods:[7]

$$\sigma_{max} = \frac{PPRL}{A_{tr}} \tag{5.110}$$

The minimum stress at the top rod is the minimum polished rod load (denoted MPRL and also discussed in a following section) divided by the cross-sectional area of the top rod:[7]

$$\sigma_{min} = \frac{MPRL}{A_{tr}} \tag{5.111}$$

The maximum stress is related to the minimum stress by the following equation:[7]

$$\sigma_{max} = \left(\frac{T}{4} + 0.5625\ \sigma_{min}\right) SF \tag{5.112}$$

where:

T = the minimum tensile strength for the rods (90,000 psi for API Grade C rods and 115,000 psi for API Grade D rods)

SF = a service factor that depends on the type of rods and the operating conditions

Table 5.8 lists approximate values of SF.

TABLE 5.8
SERVICE FACTORS (AFTER BROWN, DAY, AND BYRD)[7]

Service	API C	API D
Noncorrosive	1.00	1.00
Salt water	0.65	0.90
Hydrogen sulfide	0.50	0.70

Equation 5.112 gives the maximum allowable range of stress between σ_{min} and σ_{max}. In that equation, σ_{max} must not exceed the maximum allowable stress for steel (30,000 to 40,000 psi):

$$\sigma_{max} \le \sigma_a$$
$$30{,}000 \le \sigma_a \le 40{,}000 \tag{5.113}$$

(3) *Subsurface pump.* The subsurface pump (Figure 5.69a) consists of four essential elements:[7,8]

TABLE 5.7
ROD AND PUMP DATA (AFTER BROWN, DAY, AND BYRD)[7]

1	2	3	4	5	6	7	8	9	10	11
Rod* no.	Plunger diam., in.	Rod weight, lb/ft	Elastic constant, in./lb-ft E_r	Frequency factor, F_c	Rod string, % of each size 1⅛	1	⅞	¾	⅝	½
44	All	0.726	1.990×10^{-6}	1.000	—	—	—	—	—	100.0
54	1.06	0.908	1.668×10^{-6}	1.138	—	—	—	—	44.6	55.4
54	1.25	0.929	1.633×10^{-6}	1.140	—	—	—	—	49.5	50.5
54	1.50	0.957	1.584×10^{-6}	1.137	—	—	—	—	55.4	43.6
54	1.75	0.990	1.525×10^{-6}	1.122	—	—	—	—	64.6	35.4
54	2.00	1.027	1.460×10^{-6}	1.095	—	—	—	—	73.7	26.3
54	2.25	1.067	1.391×10^{-6}	1.061	—	—	—	—	83.4	16.6
54	2.50	1.108	1.318×10^{-6}	1.023	—	—	—	—	93.5	6.5
55	All	1.135	1.270×10^{-6}	1.000	—	—	—	—	100.0	—
64	1.06	1.164	1.382×10^{-6}	1.229	—	—	—	33.3	33.1	33.5
64	1.25	1.211	1.319×10^{-6}	1.215	—	—	—	37.2	35.9	26.9
64	1.50	1.275	1.232×10^{-6}	1.184	—	—	—	42.3	40.4	17.3
64	1.75	1.341	1.141×10^{-6}	1.145	—	—	—	47.4	45.2	7.4
65	1.06	1.307	1.138×10^{-6}	1.098	—	—	—	34.4	65.6	—
65	1.25	1.321	1.127×10^{-6}	1.104	—	—	—	37.3	62.7	—
65	1.50	1.343	1.110×10^{-6}	1.110	—	—	—	41.8	58.2	—
65	1.75	1.369	1.090×10^{-6}	1.114	—	—	—	46.9	53.1	—
65	2.00	1.394	1.070×10^{-6}	1.114	—	—	—	52.0	48.0	—
65	2.25	1.426	1.045×10^{-6}	1.110	—	—	—	58.4	41.6	—
65	2.50	1.460	1.018×10^{-6}	1.099	—	—	—	65.2	34.8	—
65	2.75	1.497	0.990×10^{-6}	1.082	—	—	—	72.5	27.5	—
65	3.25	1.574	0.930×10^{-6}	1.037	—	—	—	88.1	11.9	—
66	All	1.634	0.883×10^{-6}	1.000	—	—	—	100.0	—	—
75	1.06	1.566	0.997×10^{-6}	1.191	—	—	27.0	27.4	45.6	—
75	1.25	1.604	0.973×10^{-6}	1.193	—	—	29.4	29.8	40.8	—
75	1.50	1.664	0.935×10^{-6}	1.189	—	—	33.3	33.3	33.3	—
75	1.75	1.732	0.892×10^{-6}	1.174	—	—	37.8	37.0	25.1	—
75	2.00	1.803	0.847×10^{-6}	1.151	—	—	42.4	41.3	16.3	—
75	2.25	1.875	0.801×10^{-6}	1.121	—	—	46.9	45.8	7.2	—
76	1.06	1.802	0.816×10^{-6}	1.072	—	—	28.5	71.5	—	—
76	1.25	1.814	0.812×10^{-6}	1.077	—	—	30.6	69.4	—	—
76	1.50	1.833	0.804×10^{-6}	1.082	—	—	33.8	66.2	—	—
76	1.75	1.855	0.795×10^{-6}	1.088	—	—	37.5	62.5	—	—
76	2.00	1.880	0.785×10^{-6}	1.093	—	—	41.7	58.3	—	—
76	2.25	1.908	0.774×10^{-6}	1.096	—	—	46.5	53.5	—	—
76	2.50	1.934	0.764×10^{-6}	1.097	—	—	50.8	49.2	—	—
76	2.75	1.967	0.751×10^{-6}	1.094	—	—	56.5	43.5	—	—
76	3.75	2.039	0.722×10^{-6}	1.078	—	—	68.7	31.3	—	—
76	3.75	2.119	0.690×10^{-6}	1.047	—	—	82.3	17.7	—	—
77	All	2.224	0.649×10^{-6}	1.000	—	—	100.0	—	—	—
85	1.06	1.883	0.873×10^{-6}	1.261	—	22.2	22.4	22.4	33.0	—
85	1.25	1.943	0.841×10^{-6}	1.253	—	23.9	24.2	24.3	27.6	—
85	1.50	2.039	0.791×10^{-6}	1.232	—	26.7	27.4	26.8	19.2	—
85	1.75	2.138	0.738×10^{-6}	1.201	—	29.6	30.4	29.5	10.5	—
86	1.06	2.058	0.742×10^{-6}	1.151	—	22.6	23.0	54.3	—	—
86	1.25	2.087	0.732×10^{-6}	1.156	—	24.3	24.5	51.2	—	—
86	1.50	2.133	0.717×10^{-6}	1.162	—	26.8	27.0	46.3	—	—
86	1.75	2.185	0.699×10^{-6}	1.164	—	29.4	30.0	40.6	—	—
86	2.00	2.247	0.679×10^{-6}	1.161	—	32.8	33.2	33.9	—	—
86	2.25	2.315	0.656×10^{-6}	1.153	—	36.9	36.0	27.1	—	—
86	2.50	2.385	0.633×10^{-6}	1.138	—	40.6	39.7	19.7	—	—
86	2.75	2.455	0.610×10^{-6}	1.119	—	44.5	43.3	12.2	—	—

(1) a working barrel
(2) a plunger
(3) an intake (standing) valve
(4) an exhaust (traveling) valve

The pump is actuated by the sucker-rod string and the surface pumping unit.

Rod-drawn pumps can be divided into three basic types:

(1) tubing pumps
(2) insert (rod) pumps
(3) casing pumps (a large version of insert pumps)

The basic difference between a tubing pump and an insert pump is the manner in which the working barrel is installed. With tubing pumps, the working barrel is connected to the bottom of the tubing and is run into the well as an integral part of the tubing string. With insert pumps, the working barrel is an integral part of the entire subsurface pump assembly and is run as a unit on the sucker-rod string inside of the tubing (or casing) string. Table 5.9 lists the maximum pump (plunger) size that can be run inside the tubing string.

TABLE 5.9
MAXIMUM PUMP SIZE (AFTER BROWN, DAY, AND BYRD)[7]

Pump type	Tubing size, in.			
	1.900	2⅜	2⅞	3½
Tubing one-piece, thin-wall barrel (TW)	1½	1¾	2¼	2¾
Tubing one-piece, heavy-wall barrel (TH)	1½	1¾	2¼	2¾
Tubing liner barrel (TL)	—	1¾	2¼	2¾
Rod one-piece, thin-wall barrel (RW)	1¼	1½	2	2½
Rod one-piece, heavy-wall barrel (RH)	1¹⁄₁₆	1¼	1¾	2¼
Rod liner barrel (RL)	—	1¼	1¾	2¼

TABLE 5.10
SUCKER-ROD DATA (AFTER BROWN, DAY, AND BYRD)[7]

1	2	3	4
Rod size	Metal area, in.^{2}	Rod weight in air, lb/ft	Elastic constant, in./lb-ft E_r
½	0.196	0.72	1.990×10^{-6}
⅝	0.307	1.13	1.270×10^{-6}
¾	0.442	1.63	0.883×10^{-6}
⅞	0.601	2.22	0.649×10^{-5}
1	0.785	2.90	0.497×10^{-6}
1⅛	0.994	3.67	0.393×10^{-6}

(4) *Pump displacement.* The theoretical pump displacement is given by:[7]

$$V = 0.1484\, A_p S_p N \qquad (5.114)$$

where:

V = theoretical pump displacement, b/d
A_p = area of pump plunger, in.^{2}
S_p = effective plunger stroke, in.
N = pump speed, spm

This applies if a pump constant is defined as:[7]

$$K = 0.1484\, A_p \qquad (5.115)$$

Hence, the theoretical pump displacement for a given plunger size and for a given combination of pumping speed and stroke can be determined from:

$$V = K\, S_p N \qquad (5.116)$$

The effective plunger stroke is approximated at 80% of the surface stroke. Thus, the above equation can be written as:

$$V = 0.8K\, SN \qquad (5.117)$$

where S is the surface stroke in inches.

The theoretical pump displacement V refers to the volume of the produced fluid rate (liquid plus gas). It is determined at the intake pressure from Equation 5.4. For the case when pumping slightly compressible fluids such as liquids, it can be considered constant and equal to the surface rate q_{sc}.

(5) *Pumping cycle.* Figure 5.69 shows a schematic of the various stages in a pumping cycle. The cycle is applicable to tubing, insert, or casing pumps.

(6) *Plunger moving down.* In Figure 5.69a, the plunger is moving down near the bottom of the stroke. Fluid is moving up through the open traveling valve while the weight of the fluid column is supported by the standing valve, which is consequently closed.

Nind found that the maximum value of the downward acceleration, which works to increase the load on the sucker-rod string, occurs near the bottom of the stroke.[8] This maximum value is given by:

$$\alpha_1 = \frac{S\,N^2}{70{,}500}(1 \pm c/p) \qquad (5.118)$$

where the plus sign is for conventional units and the minus sign is for air or Mark II units; c/p is the crank-to-pitman ratio.

If it is assumed that the traveling valve closes and the standing valve opens at the instant the downward

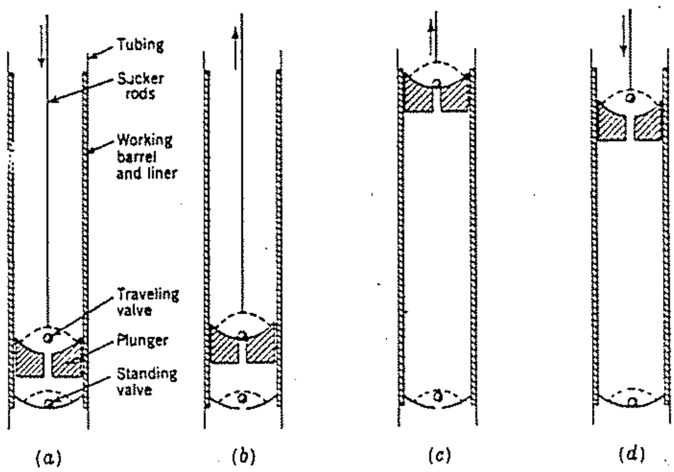

Figure 5.69 The Pumping Cycle: (a) Plunger moving down, near bottom of stroke; (b) plunger moving up, near bottom of stroke; (c) plunger moving up, near top of stroke; (d) plunger moving down, near top of stroke. (after Nind)[8]

acceleration is maximum, a force balance at the same instant yields the peak polished rod load:[8]

PPRL = (weight of fluid column) + (weight of plunger) + (weight of rods) + (acceleration term) + (friction term) − (upthrust from below on plunger)

The friction term and the weight of plunger are small compared to the other terms and, therefore, can be neglected.[7,8] The upthrust from below on the plunger is the pressure of the produced fluid times the plunger area. Hence:

$$PPRL = \frac{62.4\gamma_f D_p (A_p - A_r)}{144} + W_r + \alpha_1 W_r - P_3 A_p \tag{5.119}$$

or:

$$PPRL = \frac{62.4\,\gamma_f D_p A_p}{144} - \frac{62.4\,\gamma_f D_p A_r}{144} + W_r + \alpha_1 W_r - P_3 A_p \tag{5.120}$$

where P_3 is the pump intake pressure (see Figure 5.69).

The first term on the right-hand side of Equation 5.120 is the fluid load on the full plunger area and will be denoted W_f:

$$W_f = \frac{62.4}{144}\gamma_f D_p A_p = 0.433\,\gamma_f D_p A_p \tag{5.121}$$

The second term is the buoyancy force on the rods. This term can be written as:

$$F_b = \left(\frac{62.4\,\gamma_f}{\rho_s}\right)\left(\frac{D_p A_r \rho_s}{144}\right) = \frac{62.4\gamma_f}{490} W_r = 0.1273\,\gamma_f W_r \tag{5.122}$$

where ρ_s is the density of steel (490 lb/ft³).

The buoyancy force appears as a subtractive term in the expression for the peak polished rod load (see Equation 5.120); so, to be on the conservative side, this term should be taken to have its lowest value.[8] A crude with an API gravity of 50° has a specific gravity of 0.78, and in this case, $0.1273\gamma_f$ is equal to 0.1. Hence,

$$F_b = 0.1\,W_r \tag{5.123}$$

Substituting Equations 5.121 and 5.123 into Equation 5.120 gives:

$$PPRL = W_f + 0.9W_r + \alpha_1 W_r - P_3 A_p \tag{5.124}$$

(7) *Plunger moving up.* In Figure 5.69b, the plunger is moving up near the bottom of the stroke. The traveling valve is now closed, and the standing valve is open. The load caused by the fluid column is supported by the rod string.

Nind also found that the maximum value of the upward acceleration, which works to reduce the load on the sucker-rod string, occurs near the top of the stroke.[8] This maximum value is given by:

$$\alpha_2 = \frac{S\,N^2}{70{,}500}(1 \mp c/p) \tag{5.125}$$

where, in this case, the minus sign is for conventional units and the plus sign is for air or Mark II units.

If it is assumed that the traveling valve opens and the standing valve closes at the instant the upward acceleration is maximum, a force balance at the same instant yields the minimum polished rod load:[8]

MPRL = (weight of rods) + (plunger weight) − (friction term) − (acceleration term) − (buoyancy term)

As before, the weight of plunger and the friction term will be neglected. The buoyancy force is given by Equation 5.123. Hence:

$$MPRL = W_r - 0.1W_r - \alpha_2 W_r = 0.9W_r - \alpha_2 W_r \tag{5.126}$$

(8) *Pump size.* The pump (plunger) size is limited by the tubing or casing size and the desired production rate. If the objective is to maximize the production rate from the well, the largest possible plunger size should be used (see Table 5.9). However, if the plunger is too large, unnecessarily high loads may be imposed on the equipment, and plunger undertravel can result in inefficient operation. On the other hand, if the plunger is too small, pumping speeds may be too high, and the increased acceleration effects can result in increased peak loads on the equipment.[7]

5.62 PUMP INTAKE CURVES

5.621 INTRODUCTION

Predicting intake curves for beam pumps is considered for two cases: (1) pumping only liquid, and (2) pumping gas with the liquid. For both cases, it is assumed that the pump is set at the bottom of the well and that the flow-path (tubing or casing) size, pump size, sucker-rod string, and the crank-to-pitman ratio are fixed. For case 2, it is assumed that all associated gas is pumped with the liquid.

The parameter selected for the beam lift system is a combination of the pump speed and stroke length.

Solving Equation 5.124 for P_3 gives:

$$P_3 = \frac{1}{A_p}[W_f + 0.9W_r + \alpha_1 W_r - PPRL] \tag{5.127}$$

The relationship between P_3 and V is implicitly described by Equation 5.127. An explicit relationship can be obtained by substituting the values of PPRL and α_1 in that equation as follows: Substituting Equation 5.112 into Equation 5.110 gives:

$$PPRL = \frac{T}{4} SF\,A_{tr} + 0.5625\,SF\,A_{tr}\sigma_{min} \tag{5.128}$$

Substituting Equation 5.126 into Equation 5.111 gives:

$$\sigma_{min} = \frac{0.9\,W_r}{A_{tr}} - \frac{W_r}{A_{tr}}\alpha_2 \tag{5.129}$$

Substituting Equation 5.125 into the last equation gives:

$$\sigma_{min} = \frac{0.9W_r}{A_{tr}} - \frac{W_r}{A_{tr}}\frac{S\,N^2}{70{,}500}(1 \mp c/p) \tag{5.130}$$

Substituting Equation 5.130 into Equation 5.128 gives:

$$PPRL = \frac{T}{4} SF\,A_{tr} + 0.5063\,SF\,W_r - 0.5625\,SF\,W_r \frac{S\,N^2}{70{,}500}(1 \mp c/p) \tag{5.131}$$

Now, substituting the value of PPRL as given by Equation 5.131 and the value of α_1 as given by Equation 5.118 into Equation 5.127 gives, after some algebraic manipulation:

$$P_3 = \frac{1}{A_p}\left[W_f + (0.9 - 0.5063\ SF)W_r - \frac{T}{4} SF\ A_{tr}\right] + \frac{W_r\ SN^2}{70{,}500\ A_p}\ [1 + 0.5625\ SF \pm (1 - 0.5625\ SF)c/p] \quad (5.132)$$

where the plus sign is for conventional units and the minus sign is for air or Mark II units.

SN^2 in Equation 5.132 can be written as:

$$SN^2 = \frac{(0.8\ KSN)N}{0.8K} \quad (5.133)$$

But (0.8 KSN) is equal to the volume of the produced fluid rate V (see Equation 5.117); hence:

$$SN^2 = \frac{N}{0.8K} V \quad (5.134)$$

Substituting Equation 5.134 into Equation 5.132 gives:

$$P_3 = \frac{1}{A_p}\left[W_f + (0.9 - 0.5063\ SF)W_r - \frac{T}{4} SF\ A_{tr}\right] + \frac{W_r\ N}{56{,}400K\ A_p}\ [1 + 0.5625\ SF \pm (1 - 0.5625\ SF)c/p]V \quad (5.135)$$

Equation 5.135 can be written as:

$$P_3 = a + bV \quad (5.136)$$

where:

$$a = \frac{1}{A_p}\left[W_f + (0.9 - 0.5063\ SF)W_r - \frac{T}{4} SF\ A_{tr}\right] \quad (5.137)$$

$$b = \frac{W_r\ N}{56{,}400K\ A_p}[1 + 0.5625\ SF \pm (1 - 0.5625\ SF)c/p] \quad (5.138)$$

SN^2 also can be written as:

$$SN^2 = \frac{(0.8KSN)^2}{(0.8K)^2S} = \frac{V^2}{(0.8K)^2S} \quad (5.139)$$

Substituting the above value of SN^2 into Equation 5.132 then writing the resulting equation in the form of Equation 5.136 gives:

$$P_3 = a + cV^2 \quad (5.140)$$

where a is given by Equation 5.137 and c is given by:

$$c = \frac{W_r}{45{,}120\ K^2A_pS}[1 + 0.5625\ SF \pm (1 - 0.5625\ SF)c/p)] \quad (5.141)$$

With the assumptions mentioned above, the quantity a will be constant. The quantity b will be constant for each fixed value of N and, in this case, Equation 5.136 is linear, whereas the quantity c will be constant for each fixed value of S and, in this case, Equation 5.140 is quadratic. It should be noted that, with N fixed, the variation of V in Equation 5.136 implies the variation of S only; therefore, it can be stated that P_3 is a linear function of S with a slope equal to (0.8KNb) and an intercept a. On the other hand, with S fixed, the variation of V in Equation 5.140 implies the variation of N only; therefore, it can be stated that P_3 is a quadratic function of N.

Hence, a straight-line relationship between P_3 and V can be obtained for each assumed value of N. Similarly, a quadratic relationship can be obtained for each assumed value of S. If the straight lines or the quadratic curves are plotted to the same scale on the same graph with the IPR curve, their intersection with the IPR curve represents the possible production rates.

The minimum allowable intake pressure (or the maximum allowable production rate) can be determined from the condition that the maximum stress in the top rod must not exceed the allowable stress for the grade of rods used. Substituting Equation 5.116 into Equation 5.115 gives:

$$\sigma_{max} = \frac{PPRL}{A_{tr}} \leq \sigma_a \quad (5.142)$$

or:

$$PPRL \leq \sigma_a A_{tr} \quad (5.143)$$

Substituting Equation 5.131 into the above inequality:

$$\frac{T}{4} SF\ A_{tr} + 0.5063\ SF\ W_r - 0.5625\ SF\ W_r \frac{S\ N^2}{70{,}500} (1 \pm c/p) \leq \sigma_a A_{tr}$$

or:

$$SN^2 \geq \frac{70{,}500}{0.5625\ SF\ W_r(1 \pm c/p)}\left[\left(\frac{T}{4} SF - \sigma_a\right)A_{tr} + 0.5063\ SF\ W_r\right] \quad (5.144)$$

where the minus sign is for conventional units and the plus sign is for the air or Mark II units.

Inequality 5.144 gives the minimum allowable value of SN^2 which, if substituted in Equation 5.132, gives the minimum allowable intake pressure.

5.622 PROCEDURE FOR THE PREPARATION OF TUBING INTAKE CURVES FOR SUCKER-ROD PUMPS (LIQUID ONLY)

The procedure for preparing tubing intake curves for sucker-rod pumps is indeed quite complex, and exact solutions may be questionable. In abandonment of the recommended policy of being exactly sure that all is correct before publishing, this section is presented to encourage others to continue the work by bringing in API calculations, etc. Here is our solution.

Liquids are only slightly compressible; therefore, V in Equations 5.136 and 5.140 can be replaced with surface rate q_{sc}, or:

$$P_3 = a + b\ q_{sc} \quad (5.145)$$

$$P_3 = a + c\ q_{sc}^2 \quad (5.146)$$

Also, γ_f can be considered equal to the value at standard conditions:

$$\gamma_{fsc} = wc\ \gamma_{wsc} + (1 - wc)\gamma_{osc} \quad (5.147)$$

The procedure for constructing intake curves is given as follows.

(1) Decide on the type of surface pumping unit (conventional, air, Mark II unit, etc.)
(2) Select a pump size, a sucker-rod string, and a c/p ratio.
(3) Calculate A_p, K, and W_r. Determine γ_f from Equation 5.147; then, calculate W_f from Equation 5.121.
(4) Calculate a from Equation 5.137. Calculate b as a function of N from Equation 5.138 and c as a function of S from Equation 5.141.
(5) Assume various pump speeds and, for each of these speeds, calculate b; then, plot P_3 vs q_{sc} as given by Equation 5.145.
(6) Assume stroke lengths and, for each of these lengths, calculate c; then plot P_3 vs q_{sc} as given by Equation 5.146.
(7) Plot the stbl/d IPR curve.

Note: The plots of steps 5, 6, and 7 should be made to the same scale on the same graph.

(8) Determine the maximum allowable stress for the grade of rods used; then, calculate the minimum allowable value of SN^2 from Equation 5.144. Use this value of SN^2 to calculate the minimum allowable intake pressure from Equation 5.132. Impose this value of P_3 (horizontal line) on the plot prepared in steps 5, 6, and 7.
(9) Read the rates at the intersection of the pump intake curves (the straight lines of step 5 or the quadratic curves of step 6) with the IPR curve. Read the maximum allowable rate at the intersection of the minimum allowable intake pressure with the IPR curve.
(10) Plot the rate vs S and N. Impose the maximum allowable rate on the same plot.
(11) Select a suitable rate.

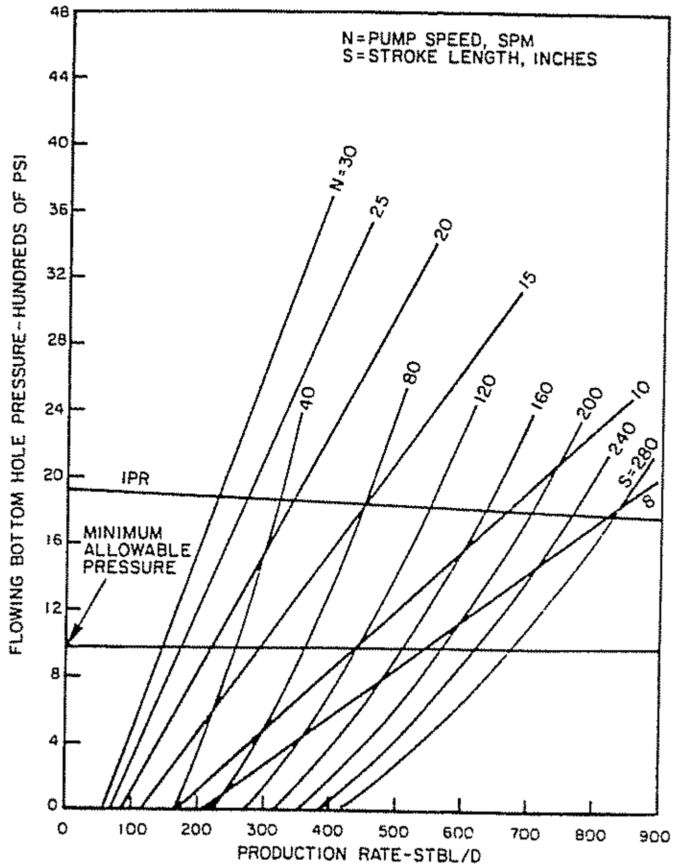

Figure 5.70 Intake Curves for a Beam Pump in Well #1 (Pumping Liquid)

EXAMPLE PROBLEM WELL #1 (LIQUID ONLY)

Well, fluid, and reservoir data are shown in Table 5.1. An insert type of pump with a conventional surface pumping unit is set at the bottom of the well. An API Grade D tapered rod string (rod number 86 in Table 5.7) is used. Calculation of VF with 100% GIP was made in Appendix 5 (Table 5A.1). IPR's in stbl/d and in b/d are shown in Figure 5.8. Results are shown in Figures 5.70 and 5.71.

It is assumed that the pump is set at the bottom of the well and that the tubing size, pump size, sucker-rod string, and the crank-to-pitman ratio are fixed.

Since the objective is to maximize the production rate from the well, the largest possible plunger size will be used. For an insert type of pump with a thin-wall barrel and 2⅞-in. tubing, Table 5.9 shows a 2-in. plunger. Then:

$$A_p = \frac{\pi}{4}(2)^2 = 3.1416 \text{ in.}^2$$

Equation 5.115 gives:

$$K = (0.1484)(3.1416) = 0.4662$$

For rod number 86 and a 2-in. plunger, Table 5.7 shows 32.8% of 1-in., 33.2% of ⅞-in., and 34% of ¾-in. rods. These rods weigh 2.9, 2.22, and 1.63 lb/ft, respectively (see Table 5.10). Then:

$$W_r = 8{,}000(0.328 \times 2.9 + 0.332 \times 2.22 + 0.34 \times 1.63) = 17{,}940 \text{ lb}$$

Since water is produced with oil, a service factor of about 0.9 should be used (see Table 5.8). Then, Equation 5.138 gives:

$$b = \frac{17{,}940\text{ N}}{(56{,}400)(0.4662)(3.1416)}[1 + (0.5625)(0.9) + (1 - 0.5625 \times 0.9)(0.33)] = 0.3625\text{ N} \quad (5.148)$$

and Equation 5.141 gives:

$$c = \frac{17{,}940}{(45{,}120)(0.4662)^2(3.1416)\text{ S}}[1 + (0.5625)(0.9) + (1 - 0.5625 \times 0.9)(0.33)] = 0.972/\text{S} \quad (5.149)$$

Since the 1-in. rod is placed at the top:

$$A_{tr} = \frac{\pi}{r}(1)^2 = 0.7854 \text{ in.}^2$$

Then, Equation 5.137 gives:

$$a = \frac{1}{3.1416}\left[W_f + (0.9 - 0.5063 \times 0.9)(17{,}940) - \frac{(11.5 \times 10^4)}{4}(0.9)(0.7854)\right] = \frac{1}{3.1416}(W_f - 12{,}351) \quad (5.150)$$

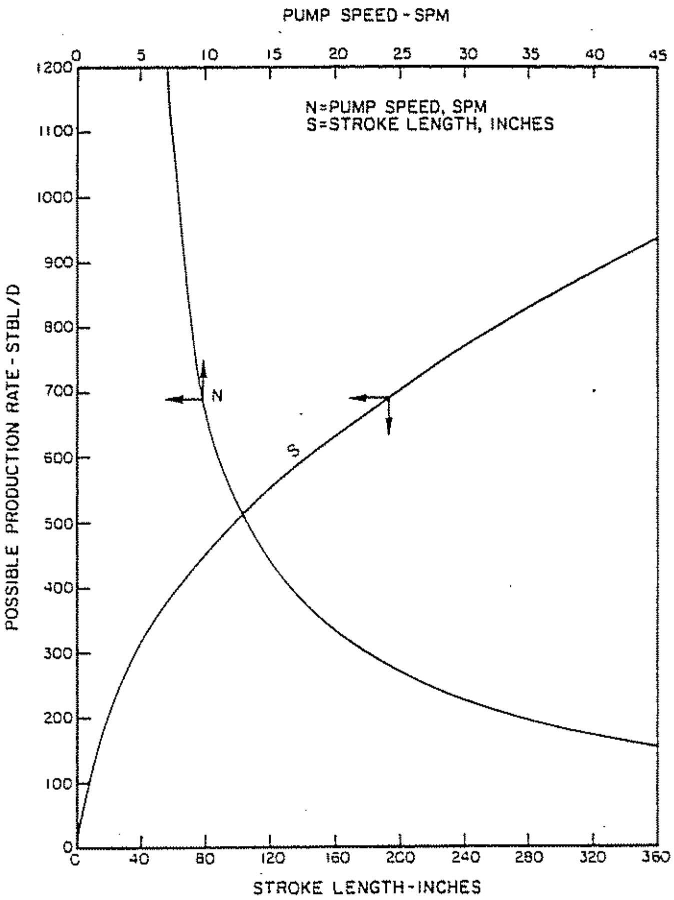

Figure 5.71 Possible Production Rate by Beam Pumping vs N and S for Well #1 (Pumping Liquid)

Since the pump is set at the bottom of the well, the pump intake pressure is equal to the flowing bottom-hole pressure; hence, the stbl/d IPR shown in Figure 5.8 is applicable:

$$\gamma_{osc} = \frac{141.5}{131.5 + 35} = 0.8498$$

Then, Equation 5.147 gives:

$$\gamma_{fsc} = (0.5)(1.074) + (0.5)(0.8498) = 0.9619$$

and Equation 5.121 gives:

$$W_f = (0.433)(0.9619)(8{,}000)(3.1416) = 10{,}468 \text{ lb}$$

Then, Equation 5.150 gives:

$$a = \frac{1}{3.1416}(10{,}468 - 12{,}351) = -600 \text{ psi}$$

With b given by Equation 5.148, Equation 5.145 becomes:

$$P_3 = -600 + (0.3625\ N)q_{sc} \qquad (5.151)$$

and with c given by Equation 5.149, Equation 5.146 becomes:

$$P_3 = -600 + \left(\frac{0.972}{S}\right) q_{sc}^2 \qquad (5.152)$$

By assuming q_{sc}, the intake pressure can be determined from Equation 5.151 for any assumed value of N or from Equation 5.152 for any assumed value of S. These equations were plotted to the same scale in Figure 5.70. The stbl/d IPR curve also was plotted to the same scale in the same figure. The straight lines represent Equation 5.151, and the quadratic curves represent Equation 5.152. Note that the straight lines and the quadratic curves should originate from the same intercept of −600 psi.

If the maximum allowable stress for the rods is taken as 35,000 psi, inequality 5.144 gives:

$$SN^2 \geq 11{,}678$$

Using this value of SN^2 in Equation 5.132 yields:

$$P_3 \geq 980 \text{ psi}$$

This limiting value of P_3 was imposed on Figure 5.70 (horizontal line). For 980-psi flowing bottom-hole pressure, the IPR curve shows 4,350 stbl/d (see Fig. 5.8). Hence, operation of the pump should be anywhere in the region bounded by a minimum intake pressure of 980 psi and a maximum production rate of 4,350 stbl/d.

The rates are represented by the intersection of the pump intake curves (the straight lines or the quadratic curves) with the IPR curve. For example, the well can produce 228 stbl/d with a pump speed of 30 spm (Figure 5.70). The required stroke length for this rate can be directly read from Figure 5.70 or calculated from either Equation 5.117 or Equation 5.152. Using Equation 5.117 (with $V = q_{sc}$) gives:

$$S = \frac{228}{(0.8)(0.4662)(30)} = 20.38 \text{ in.}$$

The required stroke length for other possible rates is shown in Table 5A.33. Possible rate q_p was plotted vs N and S in Figure 5.71. It is evident that the stroke length as well as the pump speed become impractical at high production rates. If the stroke length is limited to a practical value of, say, 180 in., a production rate of 668 stbl/d can be obtained (Figure 5.71). For this rate:

$$N = \frac{668}{(0.8)(0.4662)(180)} = 10 \text{ spm} \qquad \text{(Eq. 5.117)}$$

$$\alpha_1 = \frac{(180)(10)^2}{70{,}500}(1 + 0.33) = 0.3396 \text{ ft/sec}^2 \text{ (Eq. 5.118)}$$

$$\alpha_2 = \frac{(180)(10)^2}{70{,}500}(1 - 0.33) = 0.1711 \text{ ft/sec}^2 \text{ (Eq. 5.125)}$$

$$P_3 = 1{,}800 \text{ psi (IPR curve)}$$

$$PPRL = 10{,}468 + (0.9 + 0.3396)(17{,}940) - (1{,}800)(3.1416) = 27{,}052 \text{ lb}$$

Then:

$$\sigma_{max} = \frac{27{,}052}{0.7854} = 34{,}443 \text{ psi (Eq. 5.110)}$$

Equation 5.126 gives:

$$MPRL = (0.9 - 0.1711)(17{,}940) = 13{,}076 \text{ lb}$$

Then:

$$\sigma_{min} = \frac{13{,}076}{0.7854} = 16{,}649 \text{ psi (Eq. 5.111)}$$

EXAMPLE PROBLEM WELL #2 (LIQUID ONLY)

Well, fluid, and reservoir data are shown in Table 5.1. An insert type of pump with a conventional surface pumping unit is set at the bottom of the well. An API Grade D tapered rod string (rod number 86 in Table 5.7) is used. Calculations of VF with 100% GIP were made in Appendix 5 (Table 5A.2). IPR's in stbl/d and in b/d are shown in Figure 5.9. Refer to Figures 5.72 and 5.73.

The same type of calculations previously made for well #1 were made for this well. The largest possible plunger size was found to be 1.5 in. (Table 5.9). For this plunger size and for rod number 86, the rod-string size was found to be 26.8% of 1-in., 27% of ⅞-in., and 46.2% of ¾-in. (see Table 5.7). A service factor of 0.9 was used.

The relationships between the intake pressure and the flow rate were found to be as follows:

$$P_3 = -4{,}763 + (1.0219\ N)q_{sc} \qquad (5.153)$$

$$P_3 = -4{,}763 + \left(\frac{4.8716}{S}\right)q_{sc}^2 \qquad (5.154)$$

These equations were plotted to the same scale in Figure 5.72. The stbl/d IPR curve also was plotted to the same scale in the same figure. The required stroke length for the possible rates (obtained from Figure 5.72) is shown in Table 5A.34. Figure 5.73 is a plot of the possible rate vs S and N.

For 35,000-psi maximum allowable stress in the top rod, the minimum allowable intake pressure is negative. Hence, the well can be drawn down to zero pressure with safe operations as far as rod stress is concerned.

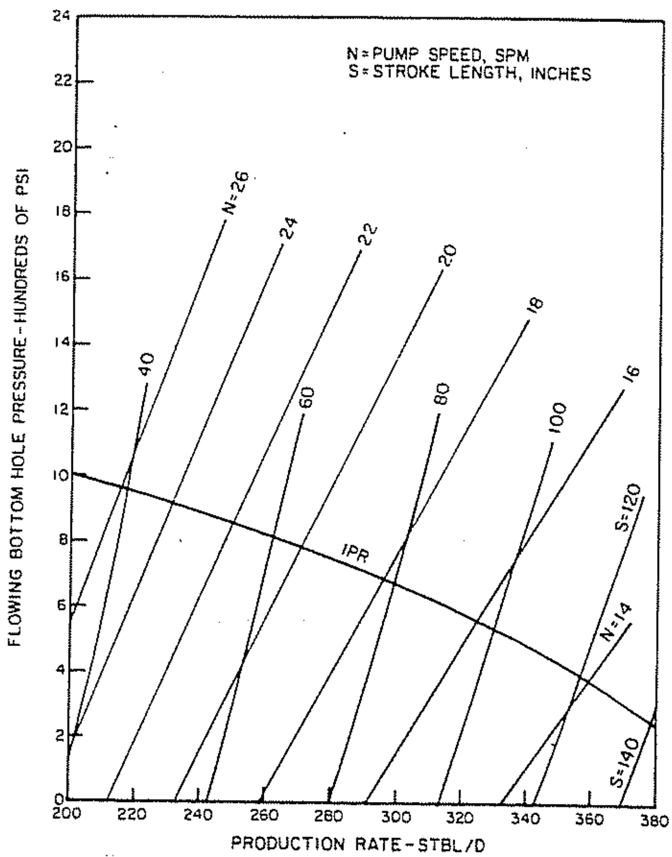

Figure 5.72 Intake Curves for a Beam Pump in Well #2 (Pumping Liquid)

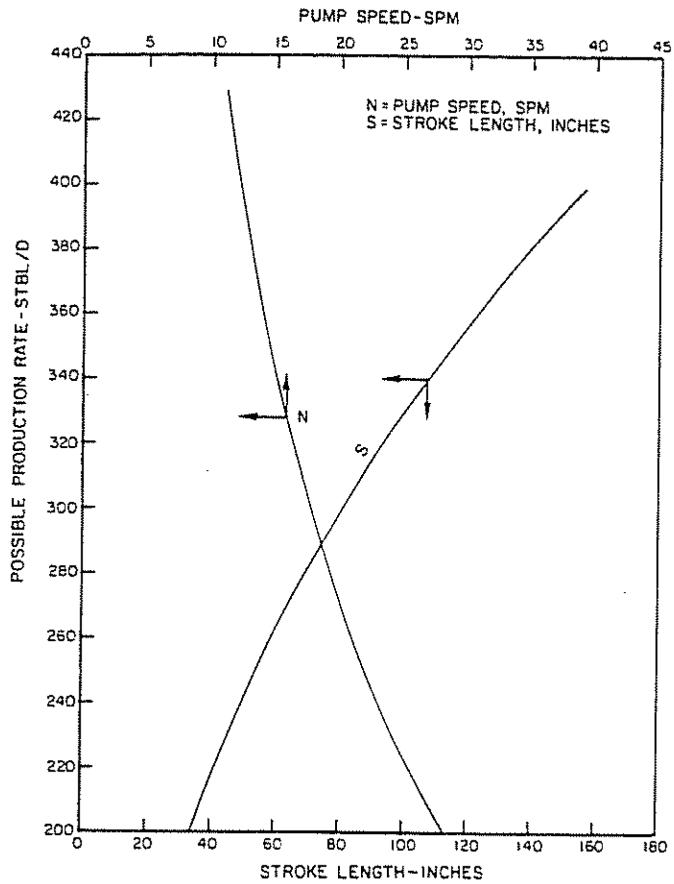

Figure 5.73 Possible Production Rate by Beam Pumping vs N and S for Well #2 (Pumping Liquid)

However, in order to allow a reasonable drawdown, a production rate of 380 stbl/d will be selected. For this rate:

$$S = 140 \text{ in. (Figure 5.73)}$$
$$N = 13 \text{ spm (Equation 5.117)}$$
$$P_3 = 240 \text{ psi (IPR curve)}$$
$$PPRL = 25{,}914 \text{ lb (Equation 5.124)}$$
$$MPRL = 10{,}800 \text{ lb (Equation 5.126)}$$
$$\sigma_{max} = 32{,}994 \text{ psi (Equation 5.110)}$$
$$\sigma_{min} = 13{,}751 \text{ psi (Equation 5.111)}$$

5.623 PREPARATION OF TUBING INTAKE CURVES FOR WELLS PUMPING GAS AND LIQUID

As mentioned previously, V in Equations 5.136 and 5.140 refers to the volume of the produced fluid (liquid plus gas) rate. Therefore, when pumping gas with the liquid, it cannot be considered constant as was done for the case when pumping only liquid but must be determined at the intake pressure from Equation 5.4. Also, the determination of W_f from Equation 5.121 is difficult in this case because γ_f varies between the wellhead and the pump setting depth. However, W_f appears as an additive term in the expression for the peak polished rod load (see Equation 5.120); therefore, to be on the conservative side, γ_f can be considered to have its highest value. A good approximation to γ_f is its value at the bubble-point pressure of the crude:

$$\gamma_{fb} = \frac{350\ wc\ \gamma_{wsc} + 350(1 - wc)\gamma_{osc} + (GLR)(GIP)\rho_{gsc}}{350[wc + (1 - wc)B_{ob}]} \tag{5.155}$$

where:

GIP = the percentage of the GLR pumped with the liquid

B_{ob} = the oil formation volume factor at the bubble point

With this approximation to γ_f, the relationship between P_3 and V will be linear for each fixed value of N (Eq. 5.136) and quadratic for each fixed value of S (Eq. 5.140).

The procedure for constructing intake curves is the same as that outlined previously for the liquid case except that P_3 in this case is plotted vs V instead of q_{sc}, so the possible rates are the intersections of the pump intake curves with the b/d IPR curve instead of the stbl/d IPR curve. However, it is advisable to include the stbl/d IPR curve on the same graph so that the rates can be easily converted to stbl/d.

EXAMPLE PROBLEM WELL #1 (PUMPING GAS)

Since the pump is set at the bottom of the well and all gas is pumped with the liquid, the IPR curves shown in Figure 5.8 and the volume factor data of Table 5A.1 are applicable (see also Figures 5.74 and 5.75).

For this case, the same pump and sucker-rod string used for the liquid case will be used:

$$\rho_{gsc} = (0.0763)(0.7) = 0.0534\ \text{lb/scf}$$

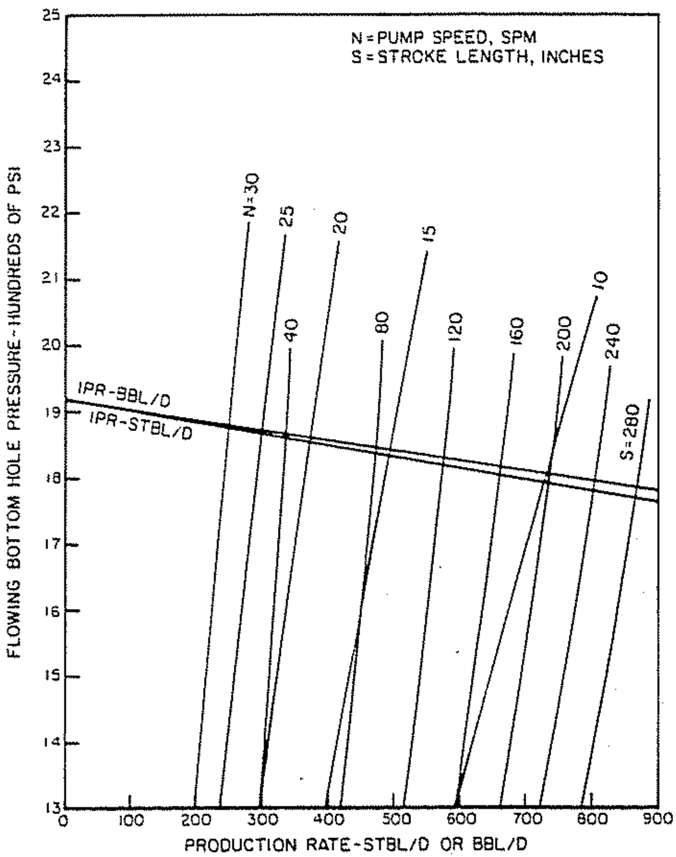

Figure 5.74 Intake Curves for a Beam Pump in Well #1 (Pumping Liquid and Gas)

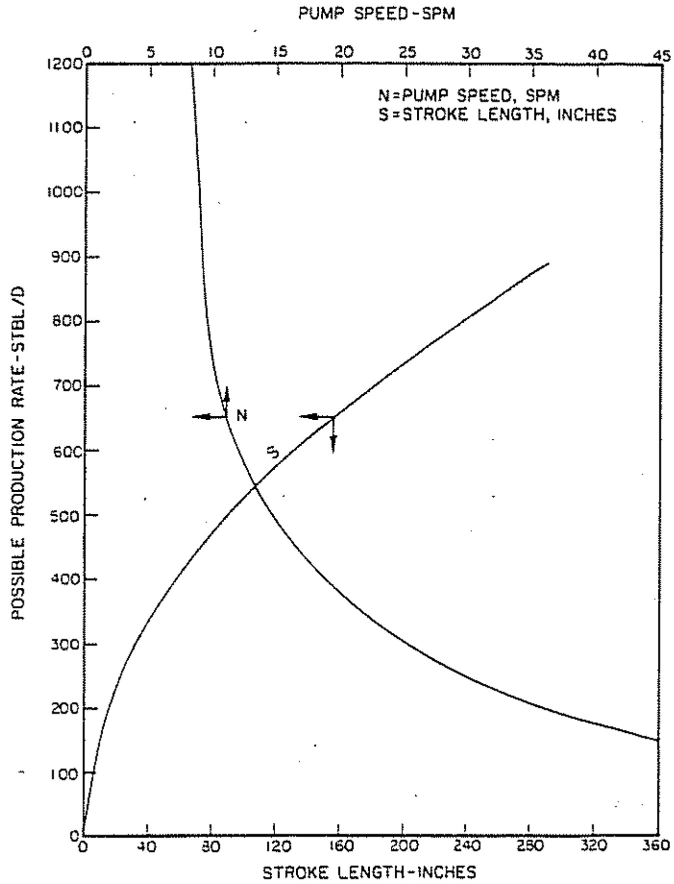

Figure 5.75 Possible Production Rate by Beam Pumping vs N and S for Well #1 (Pumping Liquid and Gas)

The formation volume factor of oil at the bubble-point pressure is about 1.266 bbl/stbo (see Table 5A.1 in Appendix 5). Hence, Equation 5.155 gives:

$$\gamma_{fb} = [(350)(0.5)(1.074) + (350)(0.5)(0.8498) + (200)(0.0534)]/[350\ [0.5 + (0.5)(1.266)]] = 0.8917$$

Then, Equation 5.121 yields:

$$W_f = (0.433)(0.8917)(8{,}000)(3.1416) = 9{,}704\ \text{lb}$$

With this value of W_f, Equation 5.150 gives:

$$a = \frac{1}{3.1416}(9{,}704 - 12{,}351) = -843\ \text{psi}$$

Then, with b given by Equation 5.148, Equation 5.136 becomes:

$$P_3 = -843 + (0.3625\ N)V \tag{5.156}$$

and with c given by Equation 5.149, Equation 5.140 becomes:

$$P_3 = -843 + \left(\frac{0.972}{S}\right)V^2 \tag{5.157}$$

By assuming V, the intake pressure can be determined from Equation 5.156 for any assumed value of N or from Equation 5.157 for any assumed value of S. These equations were plotted to the same scale in Figure 5.74. IPR's in stbl/d and in b/d also were plotted to the same scale in the figure. The straight lines represent Equation 5.156, and the quadratic curves represent Equation 5.157. Note that the straight lines and

the quadratic curves should originate from the same intercept of −843 psi.

For 35,000-psi maximum allowable stress in the top rod, the minimum allowable value of SN^2 is the same as that calculated previously for the liquid case (11,678). Using this value of SN^2 in Equation 5.132 gives:

$$P_3 \geq 736 \text{ psi}$$

For 736-psi flowing bottom-hole pressure, the b/d IPR shows 8,100 b/d (Figure 5.8). Hence, operation of the pump should be anywhere in the region bounded by a minimum intake pressure of 736 psi and a maximum production rate of 8,100 b/d (5,050 stbl/d).

The possible rates in this case are the intersections of the pump intake curves with the b/d IPR curve. For example, the well can produce 250 b/d with a pump speed of 30 spm. This rate can be converted to stbl/d by moving horizontally to the stbl/d IPR to obtain 225 stbl/d. The required stroke length for 250 b/d is:

$$S = \frac{250}{(0.8)(0.4662)(30)} = 22.34 \text{ (Eq. 5.117)}$$

The required stroke length for other possible rates is shown in Table 5A.35. The possible rates were plotted vs N and S in Figure 5.75. It is evident that the stroke length as well as the pump speed become impractical at high production rates. If the stroke length is limited to a practical value of, say, 180 in., a production rate of 700 b/d (625 stbl/d) can be obtained (see Figure 5.75). For this rate:

$$N = \frac{700}{(0.8)(0.4662)(180)} = 10.43 \text{ spm (Eq. 5.117)}$$

$$\alpha_1 = \frac{(180)(10.43)^2}{70{,}500}(1 + 0.33) = 0.3692 \text{ ft/sec}^2 \text{ (Eq. 5.118)}$$

$$\alpha_2 = \frac{(180)(10.43)^2}{70{,}500}(1 - 0.33) = 0.1861 \text{ ft/sec}^2 \text{ (Eq. 5.125)}$$

$P_3 = 1{,}810$ psi (IPR curve)

Equation 5.124 gives:

$$\text{PPRL} = 9{,}704 + (0.9 + 0.3692)(17{,}940) - (1{,}810)(3.1416) = 26{,}787 \text{ lb}$$

Then:

$$\sigma_{\max} = \frac{26{,}787}{0.7854} = 34{,}106 \text{ psi (Eq. 5.110)}$$

Equation 5.126 gives:

$$\text{MPRL} = (0.9 - 0.1861)(17{,}940) = 12{,}807 \text{ lb}$$

Then:

$$\sigma_{\min} = \frac{12{,}807}{0.7854} = 16{,}307 \text{ psi (Eq. 5.111)}$$

EXAMPLE PROBLEM WELL #2 (PUMPING GAS)

For this case, the relationships between the intake pressure and the flow rate were found to be as follows:

$$P_3 = -5{,}070 + (1.0219\,N)V \qquad (5.158)$$

$$P_3 = -5{,}070 + \left(\frac{4.8716}{S}\right)V^2 \qquad (5.159)$$

These equations were plotted to the same scale in Figure 5.76. IPR's in stbl/d and in b/d also were plotted to the same scale in the same figure. The required stroke length for the possible rates (obtained from Fig. 5.76) is shown in Table 5A.36. Figure 5.77 is a plot of the possible rate vs S and N.

For 35,000 psi maximum allowable stress in the top rod, the minimum allowable intake pressure is negative. Hence, the well can be drawn down to zero pressure with safe operations as far as rod stress is concerned.

However, attempts to draw down the well far below the bubble point (940 psi) result in impractically long strokes (see Fig. 5.77) because of expansion of gas. If the stroke length is limited to a practical value of, say, 180 in., a production rate of 467 b/d can be obtained (Fig. 5.77). This rate can be converted to stbl/d by entering the b/d IPR at 467 b/d, then moving horizontally to the stbl/d IPR to obtain 315 stbl/d (Fig. 5.76). For this rate:

$N = 12.36$ spm (Equation 5.117)
$P_3 = 615$ psi (IPR curve)
PPRL $= 25{,}865$ lb (Equation 5.124)
MPRL $= 10{,}217$ lb (Equation 5.126)
$\sigma_{\max} = 32{,}932$ psi (Equation 5.110)
$\sigma_{\min} = 13{,}009$ psi (Equation 5.111)

EXAMPLE PROBLEM #3 USING ACOUSTICAL SURVEYS TO ANALYZE PUMPING WELLS

A well is on sucker rod pump and the following information is known:

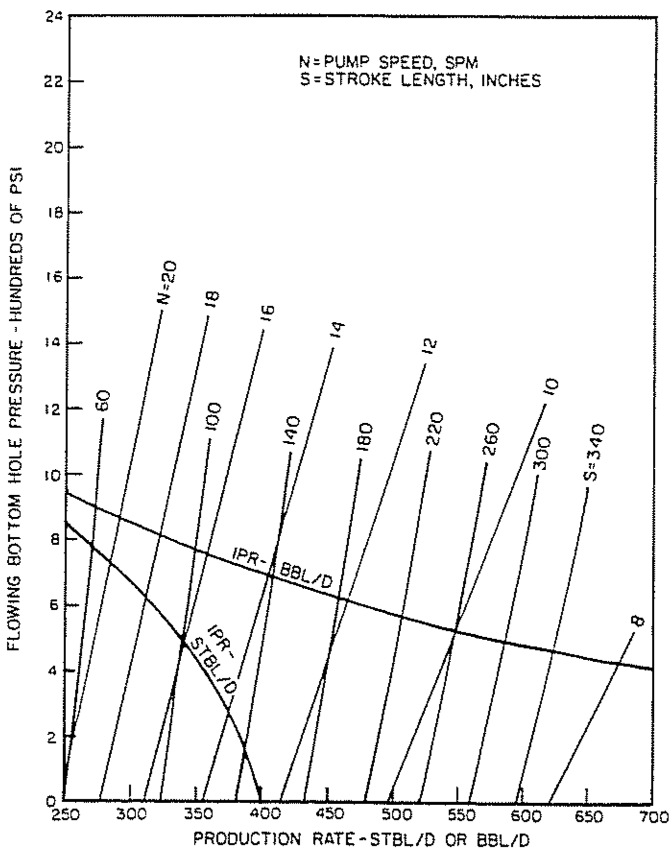

Figure 5.76 Intake Curves for a Beam Pump in Well #2 (Pumping Liquid and Gas)

Given data:

(See Figure 5.78)
6,000 ft of 2⅜-in. OD tubing
2,000 ft of 2-in. ID flow line
Separator pressure = 50 psi
Pump depth = one joint above perforation at 6,000 ft
Well producing only oil
Temperature bottom = 120°F
GOR = 400 scf/bbl
Temperature surface = 80°F
°API = 36
$\gamma_g = 0.7$
5½-in. casing (17 lb/ft)
ID = 4.892 in.

The following test is taken on this well. The well is closed in and a sounding device finds the casing liquid level to be at 4,400 ft from the top with a surface casing pressure of 160 psi. Pressure at depth can be approximated by $P_D = P_S(1 + D/40{,}000)$.

The well is then placed on production and allowed to pump for 24 hr. The rate stabilizes at 50 b/d, and the fluid level is found 5,500 ft from the surface with a casing pressure at the surface of 80 psi. The casing gas is being vented into the flow line at a rate of 15,000 scfd.

Calculate:

Analyze this well and answer the following questions:

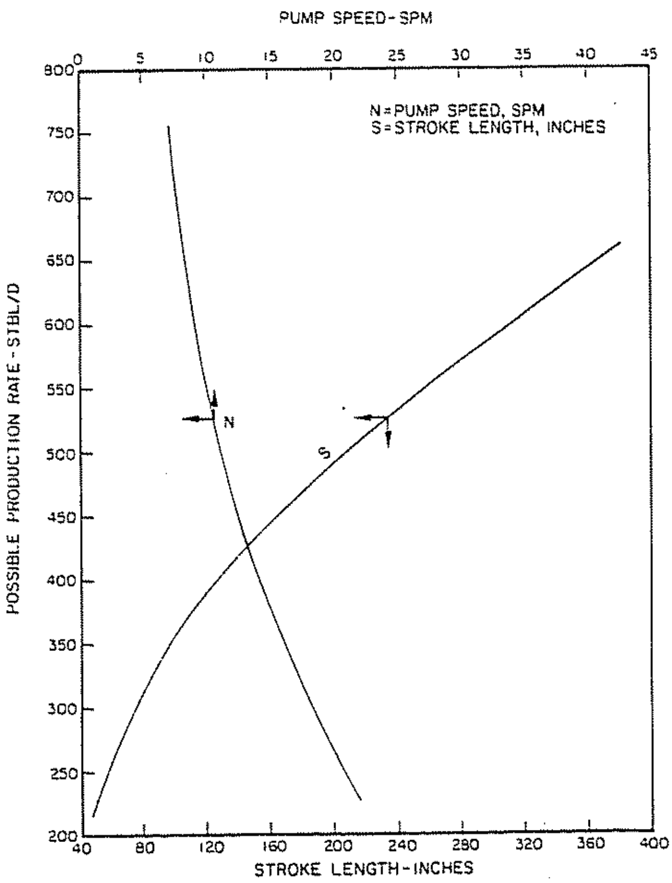

Figure 5.77 Possible Production Rate by Beam Pumping vs N and S for Well #2 (Pumping Liquid and Gas)

(a) Find an average PI.
(b) Prepare an IPR curve according to Vogel's procedure and determine $q_{o_{max}}$.
(c) A low-pressure pickup system of 20 psi is available nearby. How much increase in production would you expect by venting the gas into this system?
(d) Would you suggest that downhole gas separation is satisfactory on this well? Would you expect gas-lock problems?
(e) The separator pressure could be lowered to 25 psi and still function properly. Would you recommend doing this and approximately what rate would you expect, if any?
(f) Would you expect additional pumping problems by attempting to create a lower bottom-hole pressure, which is necessary to increase the flow rate?

Our first objective is to prepare the inflow performance curve for this well making use of the two acoustical surveys in order to obtain the corresponding static wellbore and flowing bottom-hole pressures. In this example the well is producing oil only; hence, the liquid column in the casing is only oil.

However, when the well is producing water and oil, the question arises as to what percentage of water and liquid will be standing in the casing under static (shut-in) and producing conditions. If, for example, the well is making 50% water, what percentage water is expected in the casing? This becomes important because of the differences in gradient between water and oil; therefore, an error will occur in the pressure calculations if this is not known. It is generally accepted that all oil will be standing in the annulus under static conditions with water settling to the bottom. Under pumping conditions it is generally concluded that the same percentage of water and oil being produced will be standing in the annulus.

Obviously, these two assumptions are not exact, but sufficient field tests have been conducted to show that the assumption is reasonably valid. By way of example, assume that the static fluid level is 1,600 ft and the pumping fluid level is 500 ft for a well making 50% water. Find the pressures at bottom neglecting any gas bubbling through the column under pumping conditions.

Water specific gravity = 1.07
Oil specific gravity = 0.845
Water gradient = 0.465 psi/ft
Oil gradient = 0.3658 psi/ft

Solution procedure:

(1) First solution—most widely accepted. Assume all oil in casing; static condition. Assume 50% oil in casing; dynamic condition.

(a) *Static conditions* (1,600-ft column)

Pressure of liquid column = (0.3658)(1,600) = 585 psi

If the gas pressure on top of the liquid column is 178 psi, then $P_{ws} = 585 + 178 = 763$.

(b) *Pumping conditions* (500-ft column)

For 50% water then 50% of 500 ft = 250 ft. For 50% water in the column, the column pressure =

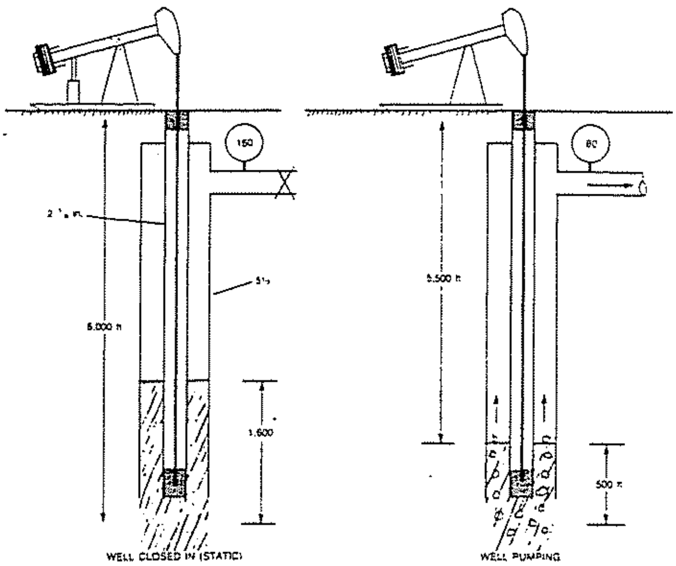

Figure 5.78 Pumping Conditions

(250)(0.465) + (250)(0.3658) = 116.25 + 91.45 = 207.7 psi.

If the pressure on top of the liquid column is 91 psi then P_{wf} = 298.7 psi. If we had assumed all oil, the flowing pressure would be 91 + 500 (0.3658) = 273.9 psi. This would underestimate the flowing pressure by 298.7 − 273.9 = 24.8 psi.

If, under static conditions, we had assumed 50% water were in the 1,600 ft column, the pressure would be:

$$178 + (800)(0.465) + 800\,(0.3568) = 178 + 372 + 285.44 = 835.44 \text{ psi}$$

This also would overpredict the pressure by:

$$835 - 763 = 72 \text{ psi}$$

The correct values for 50% oil and 50% water give a static pressure of 763 psi—assume oil only in column—and a flowing pressure of 299 psi—assume equal oil and water in the column.

Example problem solution (See Figure 5.78):

The example problem is worked in complete detail with the following step-wise procedure.

(1) Find P_{ws} (wellbore static pressure).

A simplified gas-column pressure equation can be used at low surface pressures.

(a) $P = P_{surf}\left(1 + \dfrac{\text{Depth}}{40{,}000}\right) = 160\left(1 + \dfrac{4{,}400}{40{,}000}\right)$

$= 178$ psi

(b) Liquid Column Pressure

$\gamma_0 = 0.845$

Gradient = (0.845)(0.433) = 0.3658 psi/ft

(1,600)(0.3658) = 585 psi

(c) $P_{ws} = 178 + 585 = 763$ psi

(2) Find flowing bottom-hole pressure.

Since a gas rate of 15,000 scfd is being vented, the liquid column in the annulus must be properly corrected. A gradient correction factor can be obtained from the modified S curve shown in Figure 5.79.

This is recent work done by Dr. Podio et al.[17] to improve the original S curve proposed by Gilbert,[18] which is shown in Figure 5.80. A further curve is offered by McCoy[19] and shown in Figure 5.81. In this example, the most recent work of Podio will be used. Note that a gas rate is needed for use in some of these correlations. Measuring a low gas vent rate is not always easy nor always accurate. It is suggested that the gas vent line be closed and that pumping continue. This rise in casing pressure over a period of time is then measured, which allows the calculation of the gas rate.

The following equation can be used to approximate the daily gas production rate:

$$q_{scfd} = \frac{0.68(\text{WFL})(A)(\Delta P_c)}{\Delta t}$$

where:

q_{scfd} = daily gas flow rate, scfd
WFL = depth to liquid level from surface, ft
A = cross-sectional area of annulus, in.^{2}
ΔP = increase in casing pressure, psi
Δt = time required for increase in casing pressure, min

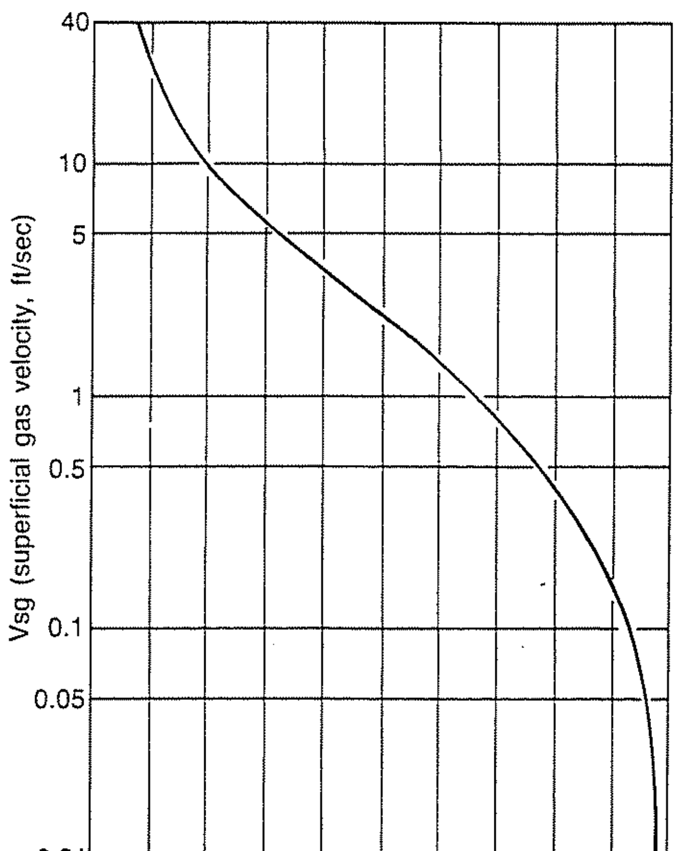

Figure 5.79 Modified S Curve (after Podio)[17]

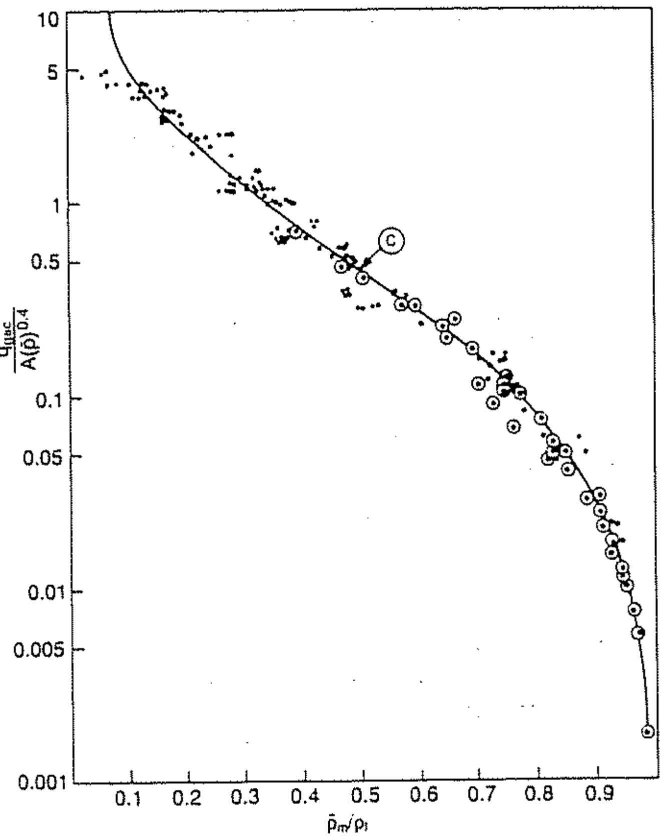

Figure 5.80 The Effect of Gas Rising through a Stationary Liquid Column on the Average Fluid Gradient (after Gipson and Swaim)[13]

(a) Find gas pressure at top of liquid column.

$$P = 80 \times \left(1 + \frac{5{,}500}{40{,}000}\right) = 91 \text{ psi}$$

(b) Find pressure of liquid column with 15,000 scfd of gas bubbling through it. Note that Fig. 5.79 requires knowing the superficial gas velocity.

$$V_{sg} = \frac{47.09\, q\, \overline{ZT}}{A\overline{P}}$$

q = MMscfd = 0.015
$\overline{Z}$ = average compressibility at $\overline{T}$, $\overline{P}$
$\overline{T}$ = average temperature (°R)
$\overline{P}$ = average pressure in liquid column
A = area of annulus (in.^{2})

$$\text{Temperature gradient} = \frac{120 - 80}{6{,}000}$$
$$= 0.00667\text{°F/ft}$$

Temperature at 5,500 ft = 116.7°F

$$\overline{T} = \frac{120 + 116.7}{2} = 118\text{°F}$$

Assume a value of P_{wf} in order to obtain $\overline{P}$. If very little gas is being vented, P_{wf} can be assumed equal to the gas pressure plus the liquid column weight.

Experience shows that as more gas is being vented, the correction factor will be greater; hence, the first assumption can be less than the equivalent static gradient.

Using the equivalent static pressure:

$$\text{assumed } P_{wf} = 91 + (0.3658)(500) = 274 \text{ psi}$$
$$\overline{P} = \frac{91 + 274}{2} = 182.5 \text{ psi}$$
$$Z = 0.975$$
$$\text{Area of annulus} = \frac{\pi}{4}[(4.892)^2 - (2.375)^2]$$
$$= 14.367 \text{ in.}^2$$
$$V_{sg} = \frac{47.09(0.015)(0.975)(578)}{(14.367)(182.5)}$$
$$= 0.152 \text{ ft/sec}$$

Gradient correction factor (GCF) = 0.9 (Fig. 5.79)
Corrected liquid gradient = ((0.9)(0.3658) = 0.3292 psi/ft
P_{wf} = 91 + (500)(0.3292) = 255.6 psi

Additional iterations are not necessary in this example.

(3) Prepare IPR curve.

Note that, for P_{ws} = 763 psi and a GOR of 400 scf/bbl, it is immediately evident that 763 psi is below the bubble-point pressure. Therefore, a Vogel-

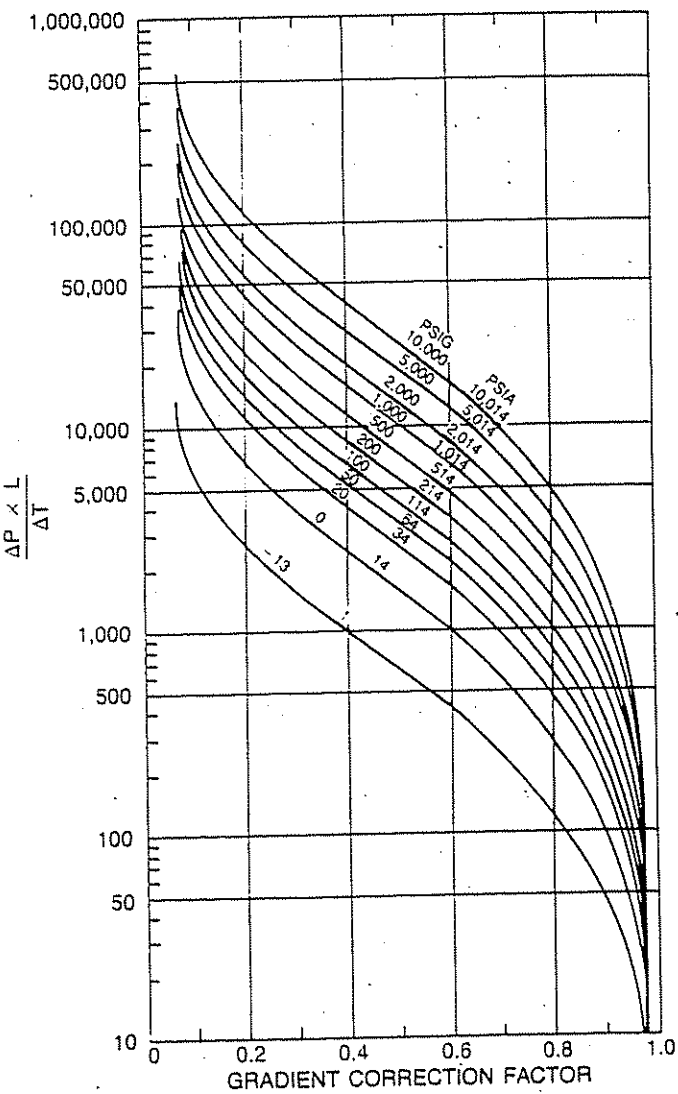

Figure 5.81 Annulus Gradient Correction for Gas Bubbling through a Static Liquid Column (after McCoy)[21]

type IPR curve will result. Using Vogel's equation $q_{o_{max}}$ can be calculated:

$$q_o/q_{max} = 1 - 0.2\left(\frac{P_{wf}}{P_r}\right) - 0.8\left(\frac{P_{wf}}{P_r}\right)^2$$

Substituting obtained values for P_{wf} and P_{ws}:

$$q_{max} = \frac{50}{1 - 0.2\left(\frac{256}{763}\right) - 0.8\left(\frac{256}{763}\right)^2} = 59 \text{ b/d}$$

Plot the IPR curve as noted in Figure 5.82.

Example problem questions.

The questions for the example problem can now be more logically answered by noting the IPR curve.

(a) The average J is found as follows:

$$J = \frac{q}{P_{ws} - P_{wt}} = \frac{50}{763 - 256} = 0.0986 \frac{\text{b/d}}{\text{psi}}$$

If a straight-line PI was assumed for this well, a maximum rate of 0.0986 (763 − 0) = 75 b/d would be obtained and would overpredict the pump-off flow rate by 75 − 59 = 16 b/d.

(b) The IPR curve has been prepared (Figure 5.82).

(c) The low-pressure pickup system of 20 psi would lower the flowing pressure by an additional 60 psi (80 − 20) and increase the flow rate to 53 b/d with a flowing pressure of 196 psi.

(d) Gas separation appears to be reasonably good since 75% of the gas is being vented.

(e) A lowering of the separator pressure to 25 psi would definitely be recommended and should show 1½–2 b/d increase in production.

(f) The flowing bottom-hole pressure could be lowered at least 100 psi to 150 psi more without gas breaking around the end of the tubing string. Most pumping operators prefer to maintain 100 to as high as 300 ft of liquid submergence above the pump. However, there are others who do not hesitate to pump the well off. In some pump-off situations the pump and rod life may be shortened. Experience and individual well conditions should apply to each case.

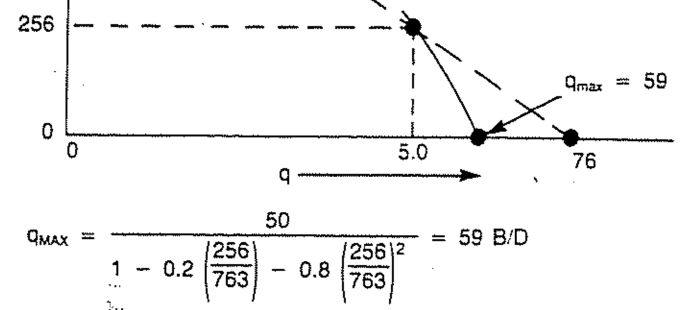

Figure 5.82 Preparing an IPR Curve

5.63 DISCUSSION OF RESULTS—SOCKER-ROD PUMPING

Results of the calculations are shown in Figures 5.70–5.77.

The production rate is shown to decrease with increasing pump speed and this, of course, cannot occur since V is proportional to N (Eq. 5.117). In Figures 5.70, 5.72, 5.74, and 5.76, the intake pressure is shown to decrease with increasing stroke length, and this also cannot occur since P_3 is proportional to S (Eq. 5.132). However, the plots appear logical if they are viewed simultaneously. Because the intake pressure is proportional to SN^2, its variation with N is much greater than its variation with S. This is the reason why higher production rates (or lower intake pressures) can be obtained by simultaneously reducing the pump speed and increasing the stroke length. For example, Figure 5.70 shows that 450 stbl/d can be obtained from well #1 with a pump speed of 15 spm and a stroke length of 80 in., while 825 stbl/d can be obtained by reducing N to 8 spm and increasing S to 280 in.

Pumping gas with the liquid reduces the value of a by reducing the fluid load on the plunger (see Eq. 5.137). This causes the intake curves for the case when pumping only liquid to shift downward by an amount equal to the change in a (compare Figure 5.70 to Figure 5.74 or Figure 5.72 to Figure 5.76). As a result, higher fluid volumes can be obtained by pumping gas with the liquid; however, for intake pressures below the bubble point of the crude, the net liquid rate may be reduced because of free gas entering the working barrel.

5.7 SUMMARY OF RESULTS AND COMPARISONS

For each lift method studied, calculations were made for the two wells shown in Table 5.1. For each well, two cases were considered: (1) pumping only liquid and (2) pumping liquid and gas. In each case, it was assumed that the lift system was set at the bottom of the well and that the wellhead pressure and the size of the flow conduits were fixed. For case 2, it was assumed that all associated gas was pumped with the liquid. Other assumptions are mentioned where applicable. Results of the calculations are summarized in Tables 5.11 and 5.12.

The optimum rates obtained for the various lift methods were based on the same operating conditions, including tubing size, without regard to economic considerations. It was assumed that there is no limit to the number of stages that can be added to an electric pump installation, while the surface operating pressure for hydraulic and jet pumping was limited to the maximum practical value recommended by the manufacturer (4,000 psi). Also, the stroke length for beam pumping was limited to a maximum of 180 in. Production rates by hydraulic piston and jet pumping higher than those shown in the tables can be obtained by increasing the power fluid (or surface operating) pressure. For example, Figure 5.58 shows that the jet pump yields about 2,300 stbl/d before cavitation occurs. How-

TABLE 5.11
COMPARISON OF DIFFERENT LIFT METHODS FOR WELL #1

Lift system	Item	Liquid	Liquid + gas
Electric submer. pump	pump type	Reda, G-180	Reda, G-180
	optimum rate, stbl/d	6,000	4,800
	number of stages	367	275
	horespower, HP	640	425
	intake volume, b/d	6,000	7,250
	discharge volume b/d	6,000	5,300
Hydra. pump	pump type	Kobe, E	Kobe, E
	pump size, in.	$3 \times 2\frac{7}{8}$	$3 \times 2\frac{7}{8}$
	power fluid system	OPF	OPF
	optimum rate, stbl/d	1,975	2,010
	surface operating press, psi	4,000	4,000
	power fluid press, psi	6,600	6,550
	power fluid rate, stbo/d	2,260	2,680
	horsepower, HP	154	183
Jet pump	pump type	Kobe, A	Kobe, A
	nozzle size, in.	0.02	0.025
	optimum rate, stbl/d	880	950
	surface operating press, psi	4,000	4,000
	power fluid rate, stbo/d	1,853	2,250
	power fluid press, psi	6,700	6,600
	horsepower, HP	112	160
Beam pump	surface pump, unit type	conventional	conventional
	subsurface pump type	tubing insert	tubing insert
	plunger size, in.	2	2
	rod string size: 1 in.	32.8%	32.8%
	7/8 in.	33.2%	33.2%
	3/4 in.	34.0%	34.0%
	optimum rate, stbl/d	668	625
	pump speed, spm	10	10.4
	stroke length, in.	180	180
	PPRL, lb	27,052	26,787
	MPRL, lb	13,076	12,807
	maximum stress, psi	34,443	34,106
	minimum stress, psi	16,649	16,307
Gas lift	injection at	bottom	
	flow	tubular	
	optimum rate, stbl/d	2,085	
	total GLR, scf/stbl	1,400	
	injection GLR, scf/stbl	1,200	
	injection rate, Mscfd	2,502	

ever, this rate requires surface operating pressures much greater than 4,000 psi.

Intake curves for the various lift methods are shown in Figures 5.83–5.86. The optimum rate for any lift system is noted by the intersection of its intake curve with the IPR curve. As far as rate is concerned, the obvious choice for well #1 is electrical pumping, while any lift method (except jet pumping) is almost equally suitable for well #2.

Inefficiency of the jet pump is due to its sensitivity to pressure. Inspection of Equation 5.85 shows that a higher power fluid pressure value and a lower discharge pressure value significantly increase the capacity of a jet pump. This can be accomplished by reducing the friction loss through using larger flow conduits. For example, in this study, where a parallel tubing arrangement was used (see Fig. 5.55), a production rate of less than 1000 stbl/d was obtained from well #1 (see Figs. 5.83 and 5.84). Petrie showed that a production rate in excess of 2,000 stbl/d can be obtained from the same well by utilizing the annulus as a return column instead of the tubing.[6] This underscores the importance of the friction loss in jet pumping.

Note, however, that no comparisons were made for different conduit sizes. As for the jet pump, gas lift would benefit from larger flow conduits.[3] The electrical, hydraulic, and beam pumps also would benefit from an increase in size of the flow path but probably to a lesser extent than would gas lift or jet pumping. Therefore, in the final analysis, other conduit sizes (including annular flow for gas lift and hydraulic and jet pumping) would be considered.

For well #2, where more than one lift method is found to be adequate, the final selection of equipment becomes an economical issue such as initial and operating costs of the equipment. Other conditions that must

TABLE 5.12
COMPARISON OF DIFFERENT LIFT METHODS FOR WELL #2

Lift system	Item	Liquid	Liquid + gas
Electric submer. pump	pump type	Reda, A-10	Reda, A-10
	optimum rate, stbl/d	375	300
	number of stages	410	255
	horsepower, HP	36	20
	intake volume, b/d	375	450
	discharge volume, b/d	375	336
Hydra. pump	pump type	fluid-packed	fluid-packed
	pump size, in.	VFR20161613	VFR20161613
	power fluid system	OPF	OPF
	optimum rate, stbl/d	375	290
	surface operating press, psi	2,250	2,550
	power fluid rate, stbo/d	1,135	1,085
	power fluid press, psi	4,775	5,100
	horsepower, HP	44	51
Jet pump	pump type	Kobe, A	Kobe, A
	nozzle size, in.	0.0046	0.0061
	optimum rate, stbl/d	220	250
	surface operating press, psi	4,000	4,000
	power fluid rate, stbo/d	465	610
	power fluid press, psi	6,600	6,550
	horsepower, HP	32	44
Beam pump	surface pump, unit type	conventional	conventional
	subsurface pump type	tubing, insert	tubing, insert
	plunger size, in.	1 1/2	1 1/2
	rod string size: 1 in.	26.8%	26.8%
	7/8 in.	27.0%	27.0%
	3/4 in.	46.2%	46.2%
	optimum rate, stbl/d	380	315
	pump speed, spm	13	13.4
	stroke length, in.	140	180
	PPRL, lb	25,914	25,865
	MPRL, lb	10,800	10,217
	maximum stress, psi.	32,994	32,932
	minimum stress, psi.	13,751	13,009
Gas lift	injection at	bottom	
	flow	tubular	
	optimum rate, stbl/d	347	
	total GLR, scf/stbl	1,000	
	injection GLR, scf/stbl	800	
	injection rate, Mscf/d	278	

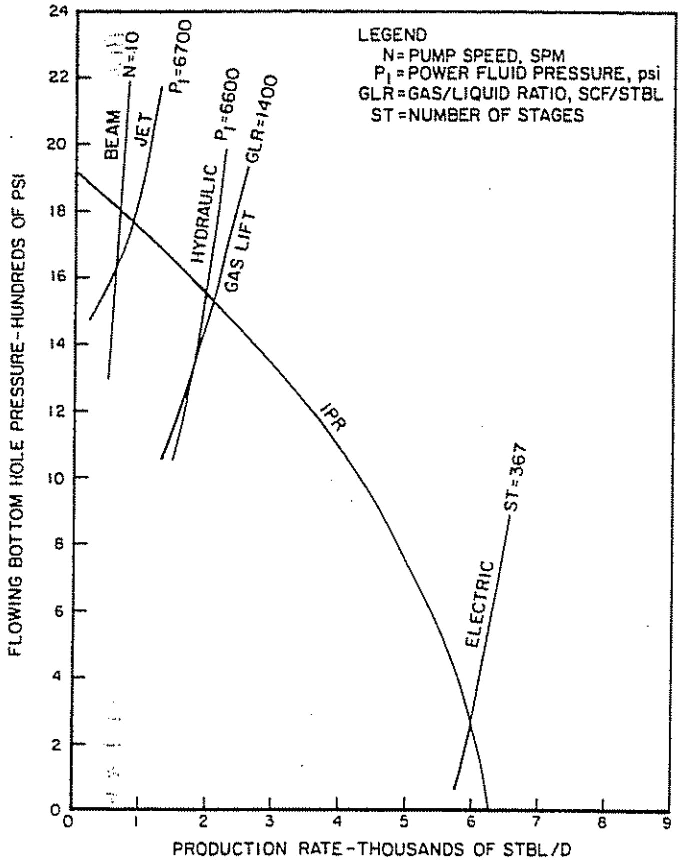

Figure 5.83 Intake Curves for Various Lift Methods in Well #1 (Pumping Liquid)

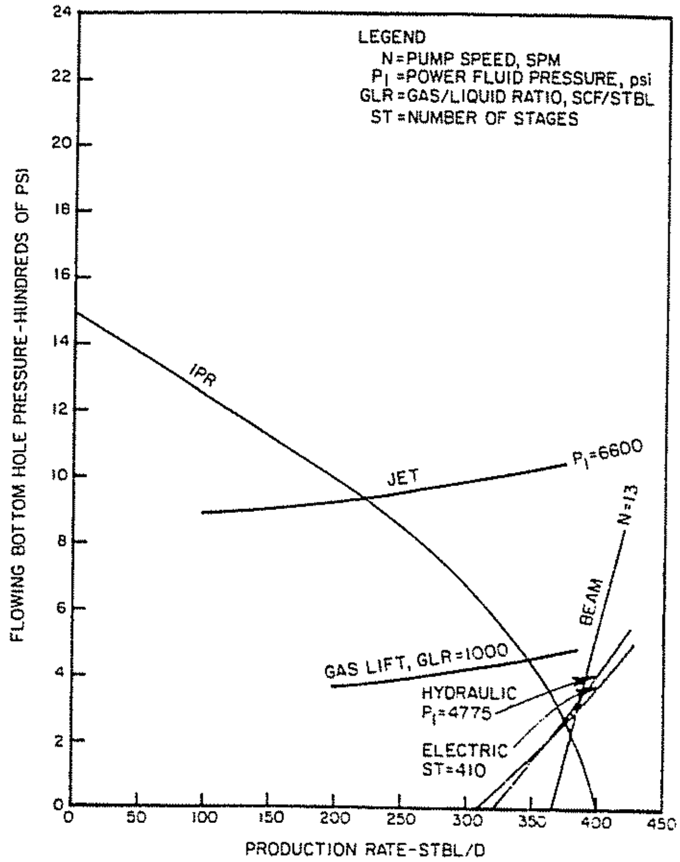

Figure 5.85 Intake Curves for Various Lift Methods in Well #2 (Pumping Liquid)

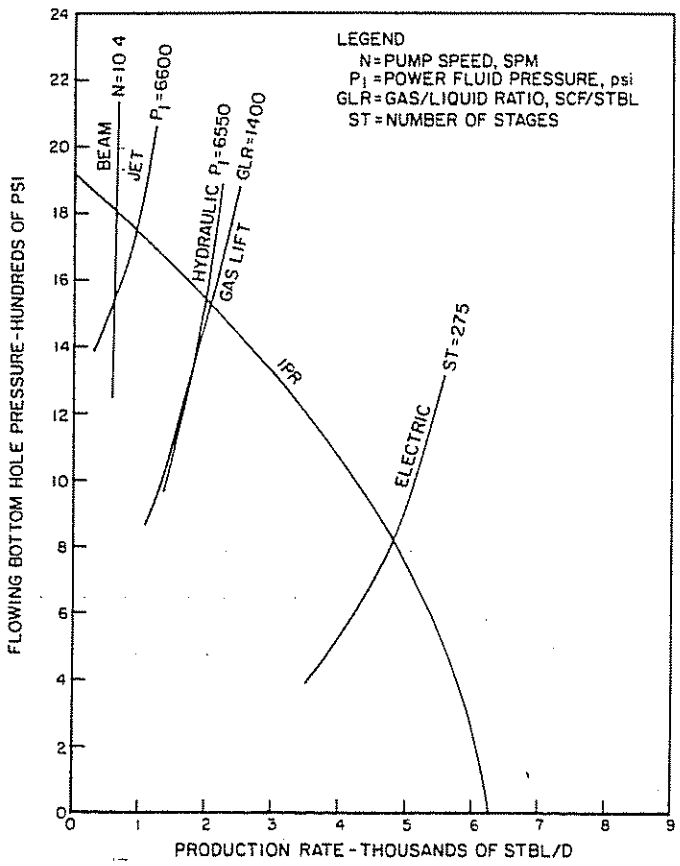

Figure 5.84 Intake Curves for Various Lift Methods in Well #1 (Pumping Liquid and Gas)

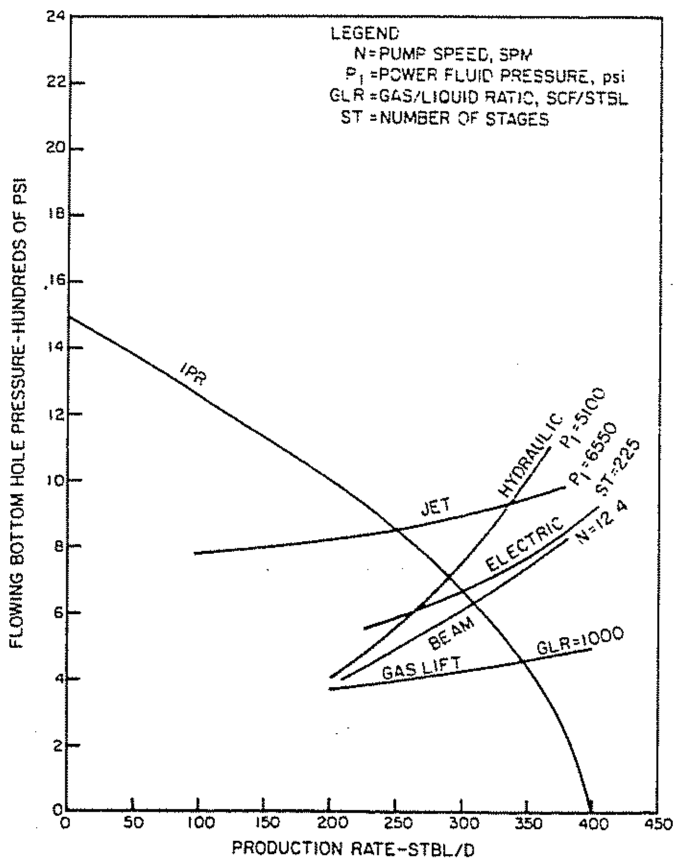

Figure 5.86 Intake Curves for Various Lift Methods in Well #2 (Pumping Liquid and Gas)

be considered include availability of gas or electric power, availability of existing compressor facilities or pumping units, isolated or multiple wells, and physical and environmental restrictions. Detailed discussions of these and other factors were presented by Brown Doll, and Dewan.[2]

These two examples are not intended to specify that one method is always better than another. Rather, only procedures for intake curves are presented. The relative merits of using one method over another must be evaluated for each well or group of wells.

Performance of the various lift methods was investigated through varying only one parameter. However, the method can be used to study the effect of other factors such as wellhead pressure, size of the flow conduits, setting depth of the equipment, and partial pumping of free gas with the liquid. Each of these factors influences performance of the various lift methods to a different degree. As previously mentioned and as far as rate is concerned, gas lift benefits from larger flow conduits. The jet pump is pressure sensitive; hence, its capacity can be improved by increasing size of the flow path. The electric, hydraulic, and beam pumps also gain from an increase in size of the flow path but probably to a lesser extent than does gas lift or jet pumping. Therefore, different conduit sizes should be considered.

The setting depth of the equipment also is important, especially for high-GLR wells. For example, setting an electric pump off bottom results in lower intake pressures and, consequently, larger free gas volumes. This would reduce length (or cost) of the electrical cable but increase the number of stages if gas is pumped. On the other hand, if gas is vented, the complicated process of downhole gas separation becomes necessary. Hence, the pumping or venting of more free gas should be weighed against setting depths.

NOMENCLATURE FOR CHAPTER 5

Latin	
A_e	Gross area of engine piston, in.^{2}
A_j	Nozzle area, in.^{2}
A_p	Gross area of pump piston, in.^{2}
A_r	Area of rods, in.^{2}
A_s	Net throat area, in.^{2}
A_t	Gross area of throat, in.^{2}
A_{tr}	Area of top rod, in.^{2}
bbl	Barrels of fluid
B_g	Gas formation volume factor, bbl/scf
B_o	Oil formation volume factor, bbl/stbo
B_{ob}	Oil formation volume factor at the bubble point, bbl/stbl
B_w	Water formation volume factor, bbl/stbw
c/p	Crank-to-pitman ratio, dimensionless
D	Well depth, ft
d	Days
D_p	Pump setting depth, ft
F_b	Buoyancy force, lb
F_p	Pump friction, psi
G_f	Fluid gradient at any conditions of pressure and temperature, psi/ft
GIP	Percentage of gas injection
GLR	Surface gas-liquid ratio, scf/stbl
GOR	Surface gas-oil ratio, scf/stbo
h	Head per stage, ft
H	Head ratio, dimensionless
hp	Horsepower per stage, HP/stage
H_p	Head ratio at peak efficiency, dimensionless
HP	Horsepower
I_c	Cavitation index
K	Pump constant, min./d/in./bbl
K_j	Nozzle loss coefficient
M	Flow ratio, dimensionless
M_c	Cavitating flow ratio, dimensionless
M_p	Flow ratio at peak efficiency, dimensionless
MPRL	Minimum polished rod load, lb
N	Pump speed, spm
NL	Net lift, ft
P	Pressure, psi
P_1	Power fluid pressure, psi
P_2	Pump discharge pressure, psi
P_3	Pump intake pressure, psi
P_4	Engine discharge pressure, psi
P_b	Bubble-point pressure, psi
P/E	Ratio of net pump piston area to net engine piston area, dimensionless
$(P/E)_{max}$	Maximum allowable P/E ratio, dimensionless
PI	Productivity index, stbl/d/psi
PPRL	Peak polished rod load, lb
$\bar{P}_r$	Average reservoir pressure, psi
P_s	Surface operating pressure, psi
P_{wf}	Flowing bottom-hole pressure, psi
q_1	Actual power fluid rate, stbl/d
q_1'	Engine displacement, stbl/d/SPM
q_1''	Theoretical power fluid rate, stbl/d
q_2	Total liquid rate in production column, stbl/d
q_3'	Pump displacement, b/d/spm
q_3''	Theoretical production rate, b/d
q_{max}	Well potential, stbl/d
q_p	Possible production rate, stbl/d
q_{sc}	Surface production rate, stbl/d
R_s	Solution gas-oil ratio, scf/stbo
R_{sw}	Solution gas-water ratio, scf/stbw
S	Surface stroke, in.
scf	Standard cubic feet
SF	Surface factor
S_p	Effective plunger stroke, in.
spm	Strokes per minute
St	Number of stages
stbl	Stock-tank (surface) barrels of liquid
stbo	Stock-tank (surface) barrels of oil
stbw	Stock-tank (surface) barrels of water
T	Minimum tensile strength, psi
V	Volume of produced fluid rate, b/d
VF	Volume factor, bbl/stbl
W	Weight of produced fluid rate, lb
wc	Reservoir water cut (flowing), fraction
wc_2	Water cut in the production column, fraction
W_f	Fluid load on entire plunger area, lb
W_r	Weight of rods, lbs

Greek	
α_1	Maximum downward acceleration of rods, ft/sec^2
α_2	Maximum upward acceleration of rods, ft/sec^2
γ_1	Specific gravity of power fluid
γ_f	Specific gravity of produced fluid at any conditions of pressure and temperature
γ_{fsc}	Specific gravity of produced fluid at standard conditions
γ_{gsc}	Gas specific gravity at standard conditions
γ_{osc}	Oil specific gravity at standard conditions
γ_{wsc}	Water specific gravity at standard conditions
Δ	Change
η_e	Engine efficiency, percent
η_p	Pump efficiency, percent

Greek	
ρ_{tsc}	Weight of 1 stbl plus associated gas at standard conditions, lb/stbl
ρ_{gsc}	Gas density at standard conditions, lb/scf
ρ_s	Density of steel, lb/ft³
σ_a	Maximum allowable stress for steel, psi
σ_{max}	Maximum stress in the top rod, psi
σ_{min}	Minimum stress in the top rod, psi

REFERENCES

1. Brown, K. E. "Overview of Artificial Lift Methods." *SPE 9979.* SPE of AIME, 1982.
2. ———, T. Doll, and J. T. Dewan. *The Technology of Artificial Lift Methods.* Vol. 2b. Chapter 9. Tulsa, Oklahoma: The Petroleum Publishing Co., 1980.
3. ——— and J. Mach. *The Technology of Artificial Lift Methods.* Vol. 2a. Chapter 3. Tulsa, Oklahoma: The Petroleum Publishing Co., 1980.
4. ——— et al. *The Technology of Artificial Lift Methods.* Vol. 2b. Chapter 4. Tulsa, Oklahoma: The Petroleum Publishing Co., 1980.
5. ——— and P. Wilson. *The Technology of Artificial Lift Methods.* Vol. 2b. Chapter 5. Tulsa, Oklahoma: The Petroleum Publishing Co., 1980.
6. ——— and H. Petrie. *The Technology of Artificial Lift Methods.* Vol. 2b. Chapter 6. Tulsa, Oklahoma: The Petroleum Publishing Co., 1980.
7. ———, J. J. Day, and J. P. Byrd. *The Technology of Artificial Lift Methods.* Vol. 2a. Chapter 2. Tulsa, Oklahoma: The Petroleum Publishing Co., 1980.
8. Nind, T. E. W. *Principles of Oil Well Production.* Chapter 10. New York, New York: McGraw-Hill Book Co., 1964.
9. Brill, J. P. and H. D. Beggs. *Two-Phase Flow in Pipes.* 3d ed. Tulsa, Oklahoma: The University of Tulsa, 1978.
10. McCain, W. D. Jr. *The Properties of Petroleum Fluids.* Tulsa, Oklahoma: The Petroleum Publishing Co., 1973.
11. Standing, M. B. "A General Pressure-Volume-Temperature Correlation for Mixtures of California Oils and Greases." *API Drilling and Production Practice* (1947), 275.
12. ——— and D. L. Katz. "Density of Natural Gases." *Transactions of the AIME* (1942), 140.
13. Vasquez, M. E. "Correlations for Fluid Physical Property Prediction." M. S. Thesis, The University of Tulsa, 1976.
14. Brown, K. E. *The Technology of Artificial Lift Methods.* Vol. 1. Chapter 1. Tulsa, Oklahoma: The Petroleum Publishing Co., 1977.
15. Vogel, J. V. "Inflow Performance Relationship for Solution Gas Drive Wells." *Journal of Petroleum Technology* (January 1968), 83–93.
16. Wilson, P. M. *Introduction to Hydraulic Pumping.* Huntington Park, California: Kobe Inc., 1976.
17. Petrie, H. Personal communication.
18. Byrd, J. P. Personal communication.
19. Podio, A. L., M. J. Tarrillion, and E. T. Roberts. "Laboratory Work Improves Calculations." *Oil & Gas Journal,* August 25, 1980, pp. 137–146.
20. Gipson, Fred, and Howard Swain. "Designed Beam Pumping." Paper presented at the Southwestern Petroleum Short Course, Lubbock, Texas, 1972.
21. McCoy, James N. "Analyzing Well Perfromance XII." DOE Paper #9750 presented at 1981 Production Operations Symposium of the Society of Petroleum Engineers, Oklahoma City, March 1–3, 1981.

Chapter 6

Gas well loading

by J. F. Lea and R. E. Tighe

6.1 NATURAL FLOW FROM GAS WELLS RESTRICTED BY LIQUID LOADING

If a gas well produces liquid, it will likely become a problem producing well in the future because of liquid loading. Liquid loading increases the pressure gradient in the production stream and restricts reservoir drawdown and production. Liquid accumulates in the well because tubing gas velocity becomes too low to surface liquids that are produced or that condense in the production tubing.

Listed below are various liquid unloading methods that are generally applied to gas wells and that are discussed in subsequent sections.

(1) natural flow
  (a) continuous flow (minimum critical velocity)*
  (b) intermittent flow (stop cocking)
(2) assisted gas flow
  (a) plunger lift*
  (b) foams*
  (c) rotative gas lift
  (d) bottom-hole separation schemes
(3) mechanical pumping
  (a) rod pumps*
  (b) hydraulic pumps (jet)
  (c) electric submersible pumps

Methods that may be preferable to others are identified by the asterisks in the preceding list. Some unloading methods or techniques that have marginal application are discussed. They are covered here to bring out features of each application so the operator can compare methods before selecting applications.

Each method is discussed in more detail in subsequent discussions. Information is presented to describe how the method works, when it has application, what specific problems or considerations are involved in this application, and some approach to designing the installation. Some methods are not covered in complete detail but it is hoped the omissions pertain to the more commonly understood operations, with help readily available from equipment manufacturers.

6.11 COMPOSITIONAL CLASSIFICATION OF GAS RESERVOIRS

One of the common factors that can reduce the production of gas wells prematurely is the building of bottom-hole pressure because of liquid accumulations in the tubing. The source of these liquids entering the wellbore can be condensation of liquids from gas in the wellbore or can be from gas and liquid entering the wellbore simultaneously. The type of reservoir and the pressure-volume-temperature (PVT) behavior of the gas and liquids can require different methods of analysis in order to predict gas-well operation and allow estimates of when the gas velocity in the tubing begins to drop below a value too low to bring liquids to the surface.

Figure 6.1 illustrates the features of a typical phase diagram of a hydrocarbon system. The locus of all points where the first bubble of gas appears in a liquid as pressure and temperature change is called the bubble-point line. The line where the first drop of liquid appears in a gas is called the dew-point line. The highest pressure at which a gas can exist is called the cricondenbar, while the highest temperature at which a liquid can exist is the cricondentherm. How source temperatures and pressures are related to such phase diagrams of produced fluids determines how the reservoir fluids may be classified and what amount of liquid may be present in the tubing of a gas well and may be contributing to the vertical flowing pressure gradient. Clark presents additional discussion with excerpts from *World Oil*, March 1953.[1]

Figure 6.2 illustrates the phase envelopes of several hydrocarbon fluid types relative to a source temperature. The fluid types illustrated are classified as dry gas, gas condensate (liquid increases as pressure decreases) volatile oil, and black oil. The location of the source temperature to the critical point of each phase envelope determines the classification. The following illustrates the pressure-temperature path followed as different classifications of fluids are produced and expanded up the tubing.

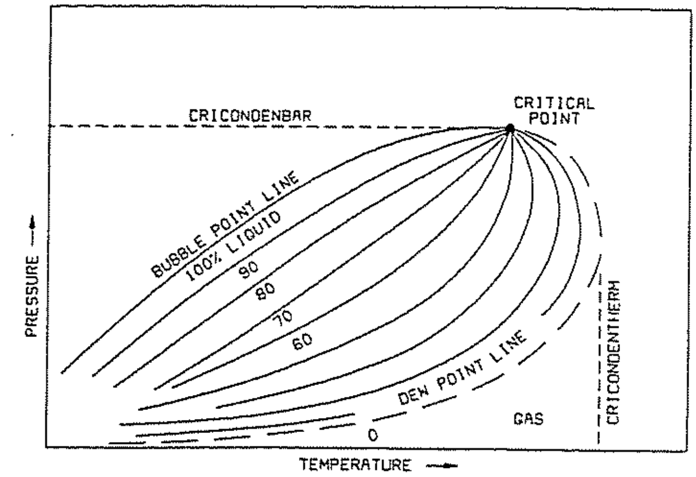

Figure 6.1 Typical Phase Diagram of a System of Hydrocarbon Fluids

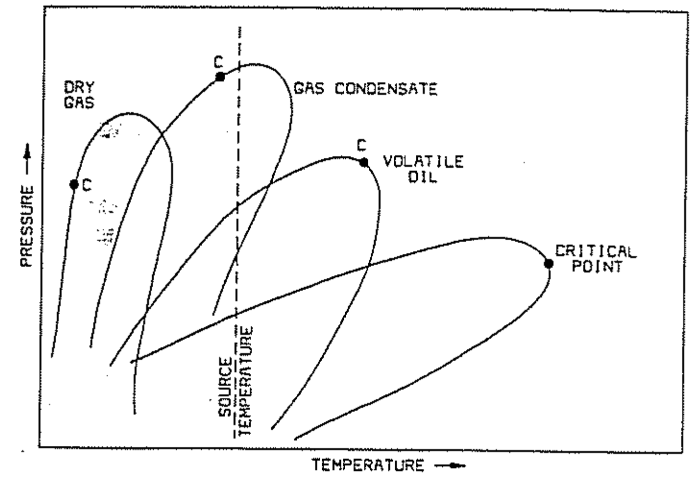

Figure 6.2 Phase Diagram of Several Possible Hydrocarbon Systems Showing Dependence of Definition on Source Temperature

6.111 DRY GAS PHASE DIAGRAM

Figure 6.3 illustrates a phase diagram for a dry gas. A path from bottom hole through the tubing is shown. As the fluid is brought to the surface, the pressure and temperature drop to separator conditions. For the dry gas case, the expansion does not enter the portion of the phase diagram containing some percent of liquid. Generally, most gas wells produce some liquids.

6.112 GAS CONDENSATE PHASE DIAGRAM

The fluid in the reservoir described in Figure 6.4 is initially all gas. If the reservoir fluids remain all-gas but condensation occurs in the tubing, the system can be described as a wet gas system. This could be shown as a tubing pressure drop from the bottom hole to the separator (points 2 or 3) in which condensation begins as the fluid crosses the dew point. If liquids are present at the bottom-hole pressure (BHP), the path could be shown as that from points 2 or 3 to the separator. Note that, if the separator pressure is lowered below the phase envelope (point 4), no liquids would be observed at separator conditions although they would be present in the tubing, contributing to the tubing pressure drop. Condensate reservoirs are often produced with gas cycling to prevent condensation in the reservoir and a subsequent drop in production. The reservoirs can still produce liquids in the tubing as the pressure expands to surface conditions, creating subsequent production problems.

6.113 VOLATILE OILS

Figure 6.5 shows a phase diagram for a volatile oil system. Such systems are characterized by a very rapid change from liquid to gas as the pressure drops near the critical point. After the initial rapid change in liquid volume, the system approaches behavior similar to a black-oil system, demonstrating a fairly linear change in liquid volume with pressure.

6.114 BLACK OIL

In a black-oil type of system (Figure 6.6), as the fluid begins to expand up the tubing, the liquids entering the wellbore contain gas in solution, which breaks out at reduced pressure as the fluid nears the surface. This system is normally modeled for the most commonly used multiphase flow tubing pressure drop models. This type of system is sometimes called an associated gas

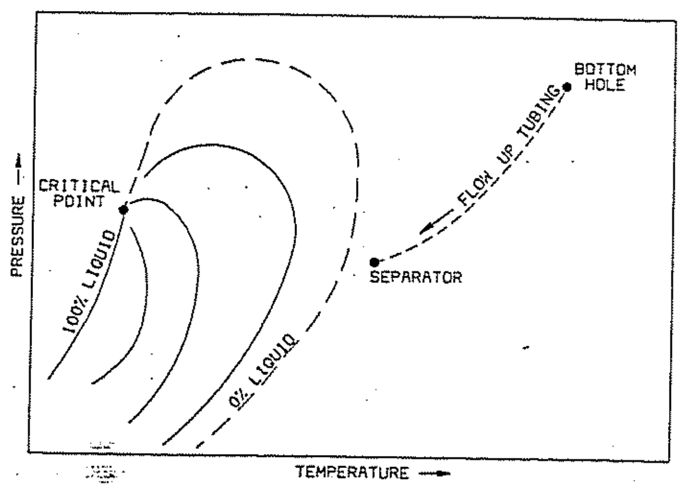

Figure 6.3 Phase Diagram of Dry Gas System

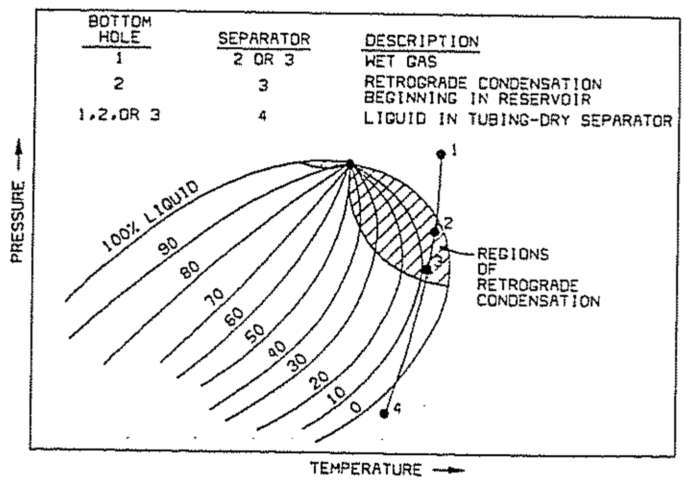

Figure 6.4 Phase Diagram Showing Regions of Retrograde Condensation

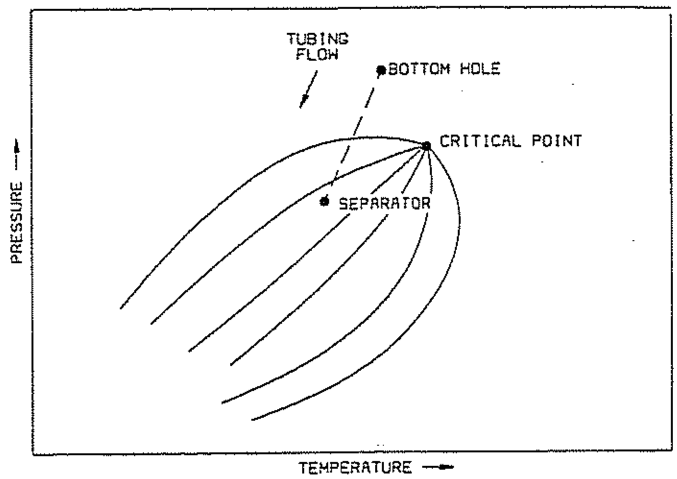

Figure 6.5 Phase Diagram of a Volatile Oil Characterized by a Sharp Drop in Liquid Volume as Pressure Drops Near the Critical Point

system where the reservoir originally consisted of a gas dome with some gas-saturated liquid below the dome. As the gas is depleted, liquids begin to come into the reservoir. For these systems, the change in the percent of liquid is fairly linear with pressure and may be described fairly accurately by existing black-oil PVT correlations such as Standing's[3] or Lasater's[51] correlations for solution GOR and Standing's correlation for formation volume factor.[3]

6.115 TUBING PERFORMANCE

As far as tubing performance is concerned, flash laboratory data for the reservoir fluids would be necessary to determine the approximate phase distribution in the tubing. This of course would assume that the fluids instantaneously followed flash equilibrium. It would then be necessary to make use of some sort of pressure-drop routine that could be a compositional model or an existing multiphase flow correlation with PVT properties input to simulate dry gas, condensate, volatile oil, or black oil. The following sections explain some alternatives available to the engineer to describe flowing tubing performance for a gas well with or without liquids present.

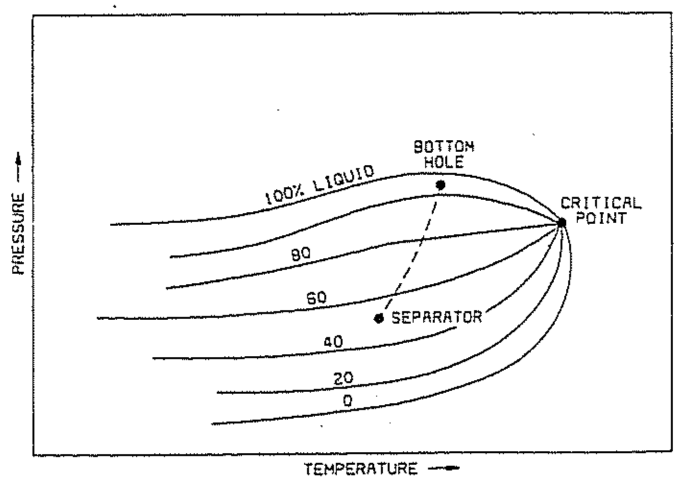

Figure 6.6 Black-Oil Phase Diagram Indicating Increase in Gas Volume as Fluid Expands up the Tubing

6.12 LIQUID LOADING-UNLOADING CONDITIONS FOR GAS WELLS

6.121 LIQUID LOADING CONDITIONS

In most cases, gas wells will produce some liquids. Both hydrocarbons (condensate) and water may condense from the gas stream as the temperature and pressure change during travel to the surface. Liquids may also be produced from the reservoir. When liquids are present, the tubing pressure losses increase primarily because of the weight of the liquid in the gas stream and because of the accumulation of liquids in the lower portion of the tubing. When the gas rate is sufficiently high, the liquids are carried along with the gas. But when the gas rate becomes low, tubing velocity is insufficient to keep liquids from accumulating, and liquid holdup (percent by volume of liquid present) increases. Then, tubing pressure losses increase, and the effective back pressure on the formation increases. The producing rate decreases in some proportion to the increased back pressure. The resulting back pressure on the formation may reach a critical pressure where liquid flow from the formation exceeds the rate at which it can be carried out, and the well dies.

Even wells with very high GLR's (gas-liquid ratios) and small liquid rates can load up if the gas rate is low as the formation pressure is depleted. This condition is typical of very tight-formation (low-permeability) gas wells that produce at low gas rates and have low gas velocities in the tubing. All gas wells that produce liquids, whether in high- or low-permeability formations, will experience liquid loading with reservoir depletion.

The following discussion concerns multiphase-flow tubing-pressure-drop predictions and other criteria that allow prediction of liquid accumulations in the wellbore.

6.122 CONDITIONS FOR NATURAL FLOW

The best way to produce a gas well with minimum expense, equipment, and labor is to maintain natural flow conditions. In natural flow, energy from the gas stream carries the liquid to the surface. This can be accomplished by maintaining satisfactory tubing velocities. If the rate is initially high, the tubing velocities will be adequate to produce steadily without excessive liquid accumulation. Later, it may be necessary and/or economical to reduce the tubing size to maintain adequate tubing velocities. Eventually, for a given tubing size, the rate will decrease so that liquid is produced in slugs, and with further reservoir depletion, the loading and slugging will become more pronounced. At this stage, intermittent well production may be required, or some method of liquid removal may be necessary.

During the intermitting operation, the well is shut in for a period of time to build up pressure in the near-wellbore area and the tubing-casing annulus, assuming the well is not equipped with a bottom-hole packer or if communication has been provided. The

gas volume stored in the pressure buildup will be produced when the well is returned to production—one hopes with enough volume and rate to achieve velocities that will unload the accumulated liquids.

Wells that require intermitting are probably also candidates for other unloading methods. It is suggested that plunger lift or foam be considered for most low-volume/low-permeability gas wells. If the producing formation is a high-permeability reservoir that will produce at significantly higher gas rates as the result of small reductions in bottom-hole pressure, downhole pumps may be an economical method of liquid removal. Plunger lift is a viable unloading method for a wide variety of well conditions, and it is noted that plungers are generally used with 2⅜-in. tubing and therefore should be evaluated before reducing the tubing size to maintain natural flow. Reducing tubing size to maintain flow should be considered when a well will produce for a reasonable time in the future before again reaching critical flow conditions. At the other end of the spectrum, in low-permeability reservoirs, the gas rate will drop sharply in the early life of the well, and it may routinely load with liquids. However, if the liquid is removed, a low-permeability well finally will reach a point where it may flow for a very long time at a low rate.

6.123 PREDICTING WELL PERFORMANCE AND LIQUID LOADING CONDITIONS USING INFLOW, OUTFLOW, AND TUBING PERFORMANCE CURVES

By using multiphase-flow correlations along with inflow curves that represent reservoir flow capacity, curves such as those shown in Figure 6.7 can be generated. The tubing performance (intake) curve is found by fixing the GLR (gas-liquid ratio), depth, surface pressure, etc., and calculating the required bottom-hole pressure at different rates. This curve does not change with time.

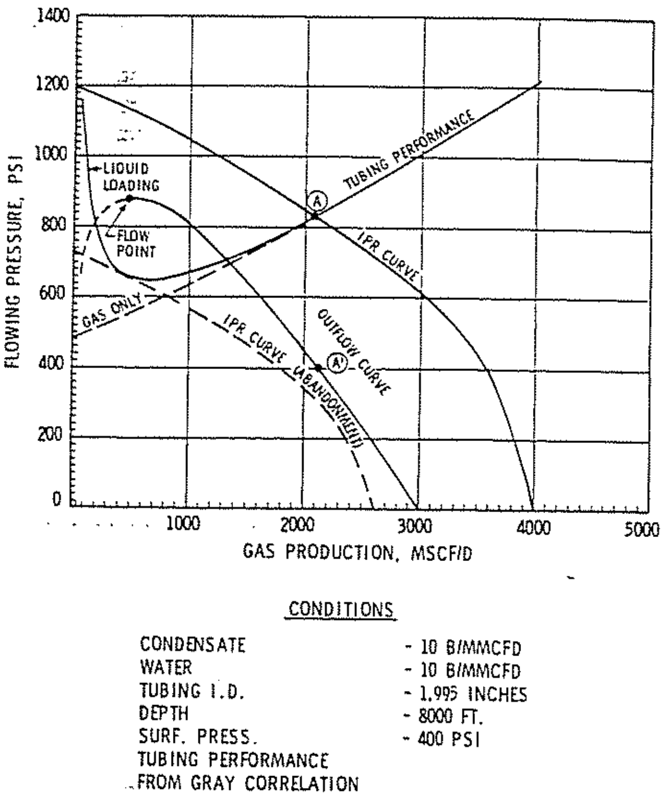

Figure 6.7 Example of Inflow, Outflow, and Tubing Performance for a Gas Well with Some Liquid Production

(1) *Tubing performance curves.* A tubing performance curve as mentioned above must be generated from some sort of multiphase flow computer program or from a set of computer-generated gradient curves. The examples shown here were generated using the Gray correlation developed for gas condensate wells.[4] This type of curve is run at several different rates with a constant GLR, or in this case, with a constant value of 10 bbl/MMcfd condensate and 10 bbl/MMcfd water. The wellhead pressure was input as 400 psi with flow through 1.995-in. ID tubing. Notice that this correlation predicts a minimum flowing BHP around 640 psi and that below about 800 Mcfd the curve turns sharply upward because of liquid loading. These concepts are discussed in more detail in a paper by Greene.[5] Without any liquid the tubing curve would not turn up and the pressure at bottom hole approaches a minimum because of the weight of the gas column plus the surface pressure at zero flow rate. Because of the shape of the multiphase flow tubing performance curve, it is sometimes called a J curve. Note that, for this discussion, the pressure increase from the fixed surface pressure is due to tubing flow, but the pressure change could also include flow-line or wellhead pressure changes referred to a fixed separator pressure. Then, the J curve could be a "system" as opposed to a "tubing" performance curve.

(2) *Inflow performance curve.* The IPR (inflow performance curve) for a gas well is typically found by the so-called back-pressure curve.

$$q = C_1(\overline{P}_R^2 - P_{wf}^2)^n \quad (6.1)$$

where:

q = gas flow rate, Mcfd
C_1 = coefficient determined from well data, Mcfd/psia
$\overline{P}_R$ = shutin static reservoir pressure, psia
n = exponent obtained from well tests that represents the reciprocal of the slope on a log-log plot (will vary because of turbulance)

Normally, the above relationship is obtained from a log-log plot of $(P_R^2 - P_{wf}^2)$ vs q using the well-known four-point back-pressure test. Pseudo-pressure relationships can be used to account for fluid property variations. Stabilized pressure-flow data are easily obtained for such plots if the well has high permeability. However, for less permeable wells, it is more difficult to obtain stabilized data because of the long periods of time required to obtain stabilized flow conditions. For these wells, methods such as the isochronal or modified isochronal well test can be used. These tests are discussed extensively in the literature.[6,7,8] IPR curves also can be prepared from Darcy's Law. Some gas wells, however, have such low permeability that no stabilized flow data can be obtained in a reasonable time. There are methods that predict a stabilized data point from unstabilized data.[9] The calculated stabilized relation-

ships obtained are good only when the stabilized point is predicted to occur, which could be well into the future, leaving no expression for the interim. For very low permeability, well performance predictions can be obtained only by type-curve analysis or by a computer reservoir model.

(3) *Gas producing rate.* By locating the intersection of the IPR curve and the tubing performance curve, the predicted current production can be found, which in Figure 6.7 is about 2.10 MMcfd.

(4) *Outflow curve.* Another way to use the inflow and tubing performance curve is to generate an outflow curve. This can be obtained by subtacting tubing pressure drop from the IPR curve to obtain the outflow curve shown in Figure 6.7. This curve shows the change in surface tubing pressure as a function of rate. Inspection of the curve shows that the last point of possible production is reflected as a *maximum* surface tubing pressure.

(5) *Prediction of critical liquid loading.* The IPR curve that is shown tangent to the tubing performance curve is labeled "abandonment." If the IPR curve declines downward and to the left to this tangent point, this is the last reservoir condition at which the reservoir will flow for the given tubing and surface pressure. At this point, smaller tubing sizes or possibly lowering the surface pressure can be examined with respect to new tubing performance for flowing conditions that will extend the well producing life. However, it may be desirable to go to a positive deliquefication method such as pumping or the use of plungers. Note that the prediction of future producing rates (and IPR curves) requires a future reservoir pressure, $\bar{P}_R$, which under certain conditions can be found from a plot of P/Z vs cumulative production history. This, of course, can be affected by water drive and other considerations. Note that this method will give a straight line for P/Z vs cumulative production for the wells with reasonable permeability and no water influx. For very tight gas wells in which the drainage radius is changing with time (unsteady-state reservoir performance), the method of P/Z vs cumulative production will not plot in a straight line but will curve concavely upward. Again, this would require the use of a reservoir model or the use of type curves for predicting future well performance.

Since the point of tangency between the IPR and the tubing performance curve is the point where the well must be abandoned unless changes are made, this point is termed the flow point by Greene.[5]

6.1234 REDUCING WELLHEAD PRESSURE

Considering the back-pressure relationship to the producing rate of a well, reducing the wellhead pressure should be considered as a means of increasing the flow rate and velocities and for sustaining natural flow. It is also a means of maximizing eventual reservoir depletion. Field situations will determine the options for reducing the well delivery pressure. Often, the options include installation of a compressor and/or to resizing or rearranging flow lines.

Reducing wellhead pressures generally results in more gas production and higher tubing velocities because the gas in-situ volume is greater at lower pressures. This may not be true where a heading well has been "beaned" back to regularize production and reduce erratic liquid unloading. Well performance with surface pressure changes can be evaluated using IPR and tubing performance curves. Example calculations are illustrated in Figure 6.8.

Reducing wellhead pressures can result in significant production increases for high-permeability formations provided the tubing is not too small. The combination of higher rates and a significant increase in ultimate recovery from this type of reservoir will likely support the economics of making changes to reach low wellhead pressures. Usually, the changes have to be considered for a group of several wells or fieldwide applications.

On the other hand, wells producing from very tight reservoirs may not be good candidates for nominal reductions in wellhead pressure considering the expense involved. If the IPR curve is very steep, an additional drawdown increment may not increase well production significantly and whatever increase is initially achieved may be shortlived. Calculations would have to indicate whether the small rate increase would correspond to a significant percent of total recoverable production. However, if the well is having liquid loading problems, the principal benefit would be derived from the gas-volume change in the tubing caused by lower pressure. The expected well performance should be evaluated through reservoir analyses or type curves to generate IPR curves to compare to tubing performance curves.

For compressor sizing and other equipment options, other references should be considered.

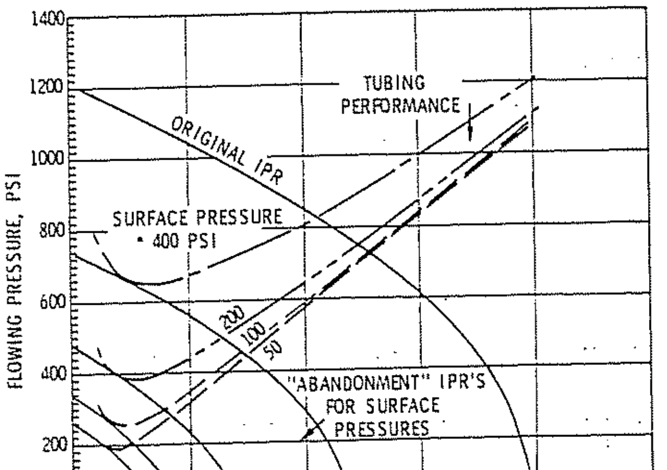

CONDITIONS

CONDENSATE	- 10 B/MMCFD
WATER	- 10 B/MMCFD
TUBING I.D.	- 1.995 INCHES
DEPTH	- 8000 FT.
TUBING PERFORMANCE FROM GRAY CORRELATION	

Figure 6.8 Example of the Effect of Reducing Surface Tubing Pressure on "Abandonment" Conditions

6.1235 TUBING SIZE EFFECTS

Reduction in tubing diameter can extend the life of a gas well with liquid loading problems by increasing the velocity of the gas production. This is a temporary fix because the velocity will gradually diminish with time, but if the application is indicated to provide increased production over a long enough period of time, smaller tubing may be warranted. If, however, plunger lift is indicated as a follow-up, it might be better to initiate plunger lift earlier with, say, 2⅜-in. tubing without making an adjustment in tubing size first to avoid the expense, pulling costs, etc.

An example of the effects of tubing size on tubing performance is shown in Figure 6.9.

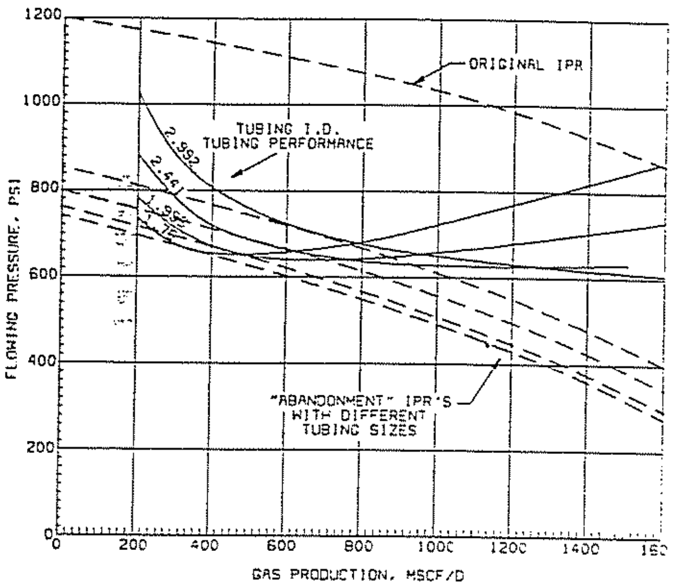

CONDITIONS

CONDENSATE	- 10 B/MMCFD
WATER	- 10 B/MMCFD
TUBING I.D.	- 1.995 INCHES
DEPTH	- 8000 FT
TUBING PERFORMANCE FROM GRAY CORRELATION	

Figure 6.9 Example of the Effect of Tubing ID on "Abandonment" Conditions

6.124 DETECTION OF LIQUID LOADING—BHP ESTIMATES

In a flowing well, the bottom-hole pressure (BHP) must equal the pressure drop in the tubing (or annulus) plus the wellhead pressure. The addition of liquid production to a gas stream increases the tubing pressure gradient. At low gas rates, the gradient is increased a greater percentage than at high gas rates. Therefore, by evaluating the tubing pressure loss for wells producing some liquids and comparing that pressure loss to the expected pressure loss of a flowing dry-gas well, judgments can be made regarding tubing pressure loss caused by liquid production.

Note that, because some free gas will separate from liquids in the wellbore and rise in the annulus, the fluid level in a flowing well will remain depressed to the tubing intake depth except when "heading" occurs or a tubing leak is present. This situation is illustrated under laboratory conditions in Figure 6.10. Flowing conditions are shown in Figures 6.10b and c. The shutin pictures following medium (a) and high-GLR (b) flow have implications regarding plunger-lift cycles discussed later. Note also that, for a flowing well, the wellhead pressure difference between the tubing and the annulus (provided the annulus is closed in, i.e., not producing) represents the flowing pressure loss in the tubing minus the pressure drop in the annulus caused by the gas gradient. The total tubing pressure gradient can be estimated from the surface casing pressure and the calculated weight of the annulus gas column if the liquid level is at the tubing intake. These calculations are usually made assuming a dry-gas gradient in the annulus.

6.1241 CALCULATED BOTTOM-HOLE PRESSURE—STATIC GAS COLUMN

Because the fluid level is depressed to the tubing intake depth while producing, the bottom-hole pressure can be calculated from the shutin annulus pressure from the following relationships:

For a vertical well ($\theta = 90°$, $\sin(\theta) = 1$) the governing equation is:

$$\frac{dP}{dh} = \frac{g\rho_g}{g_c} \tag{6.2}$$

where:

$$\rho_g = \frac{PM}{ZRT}$$

ρ_g = gas density
R = gas constant
T = °R
P = pressure
h = height
M = molecular weight of gas ($M = \gamma_g \times 29$)
γ_g = specific gravity of gas (air = 1.0)

Combining the two equations gives:

$$\frac{dP}{P} = \frac{M\,dh\,g}{ZRT\,g_c} \tag{6.3}$$

$$\int_{P_{wh}}^{P_{BHP}} \frac{dP}{P} = \frac{Mg}{R\,\bar{Z}\bar{T}\,g_c}\int_0^H dh \tag{6.4}$$

This can be integrated to give the following equation expressed in conventional units:

$$P_{BHP} = P_{wh} \exp[0.01875\,\gamma_g\,H/\bar{T}\,\bar{Z}] \tag{6.5}$$

where:

P_{BHP} = bottom-hole pressure, psi
P_{wh} = wellhead pressure (shutin annulus pressure), psi
H = depth, ft
$\bar{T}$ = average temperature in annulus, °R
$\bar{Z}$ = gas compressibility at average conditions

Evaluation of Z makes the calculation iterative. However, estimates of average conditions can provide results of sufficient accuracy for many calculations.

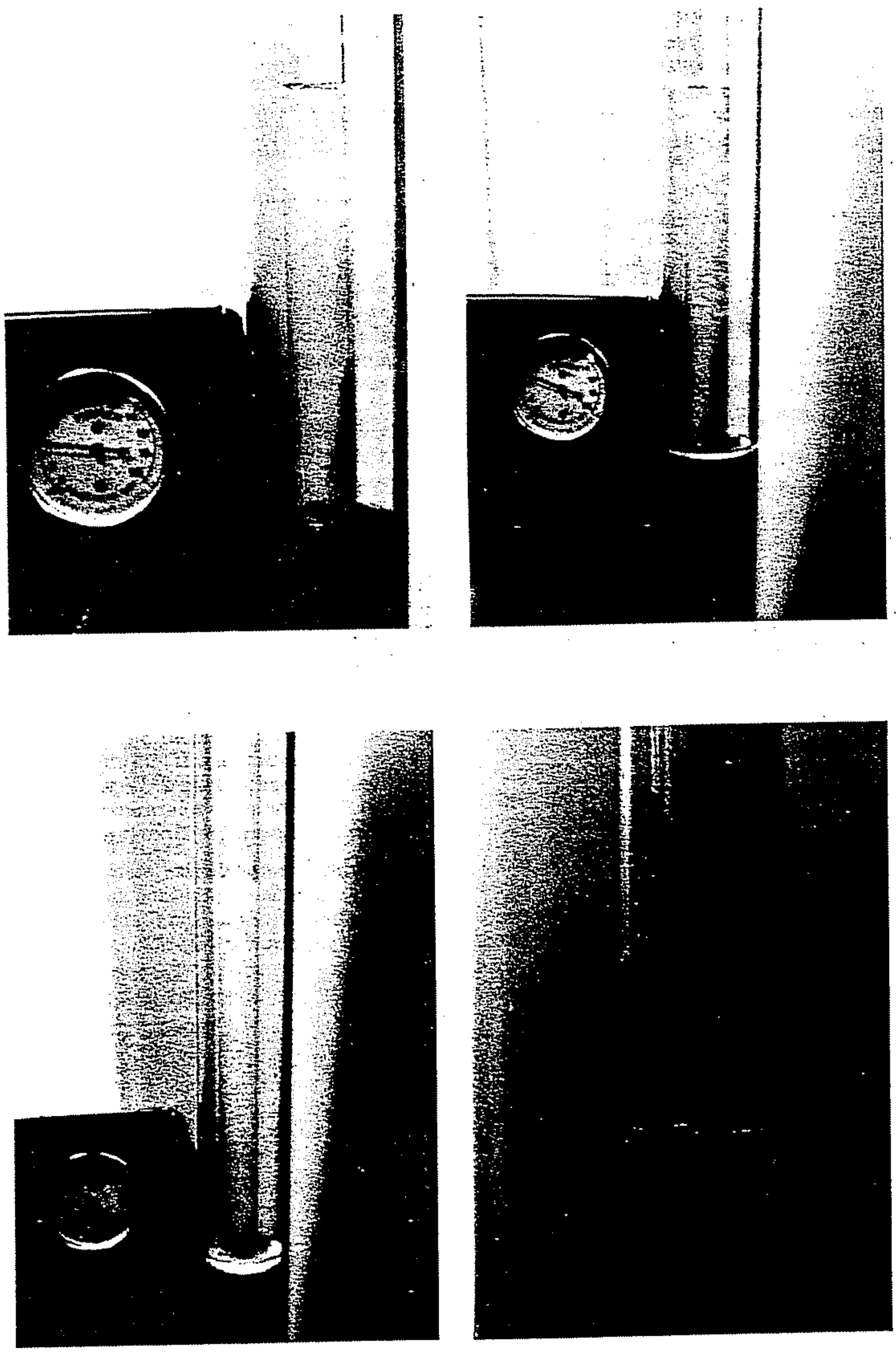

Figure 6.10 Fluid Level in Flowing Wells (Multiphase Flow) (a) Shutin (b) Flow—Low Gas Rate (c) Flow—Slug Flow (d) Shutin, No Leaks > 5,000 GLR

This approach to estimating bottom-hole pressure is applicable to both annulus and tubing, provided the gas column is not flowing—i.e., static. It does permit, however, calculating flowing bottom-hole pressure when the annulus is shut in and flow is through the tubing or vice versa, if applicable. Also, even if the well is flowing but friction is small compared to gravity losses, the expression still gives good approximation.

Another method for calculating static gas gradient is presented by Cullender and Smith and takes into account the variation of temperature with depth and the variation of Z with pressure and temperature.[10] From Equation 6.3:

$$\int_{P_{ts}}^{P_{ws}} \frac{TZ}{P}\,dP = \frac{M}{R}\int_0^H dh = \frac{MH}{R} = 0.01875\,\gamma_g H \quad (6.6)$$

The integral is written in abbreviated notation as:

$$\int_{P_{ts}}^{P_{ws}} \frac{Tt}{P}\,dP = \int_{P_{ts}}^{P_{ws}} I\,dP = 0.01875\,\gamma_g H \quad (6.7)$$

Using a series expansion, the value of the integral is approximated by:

$$2\int IdP = (P_{ms} - P_{ts})(I_{ms} - I_{ts}) + (P_{ws} - P_{ms})(I_{ws} - I_{ms}) \quad (6.8)$$

where:

P_{ms} = pressure at midpoint of well, H/2
P_{ts} = pressure at surface
P_{ws} = pressure at bottom hole
I_{ms} = I evaluated at P_{ms}, $\bar{T}$
I_{ts} = I evaluated at P_{ts}, T_s
I_{ws} = I evaluated at P_{ws}, T_f

The calculation procedure consists of dividing the well into two equal segments of length H/2, finding the pressure P_{ms} at H/2, and using this value to calculate P_{sw}. I_{ts} can be evaluated from known surface conditions. That is:

$$P_{ms} = P_{ts} + \frac{0.01875\,\gamma_g H}{(I_{ms} + I_{ts})} \quad (6.9)$$

$$P_{ws} = P_{ms} + \frac{0.01875\,\gamma_g H}{(I_{ms} + I_{ws})} \quad (6.10)$$

This method is more complicated, yet more accurate than the average pressure and temperature method.

6.1242 FLOWING BOTTOM-HOLE PRESSURE

For a flowing gas well, the velocity is not zero, and ignoring acceleration, the flow equation becomes, for a well inclined at an angle ϕ from the vertical:

$$\frac{dP}{dL} = \frac{g}{g_c}(\rho\cos\phi) + \frac{f\rho V^2}{2g_c d} \quad (6.11)$$

Several methods have been presented for integrating Equation 6.11, depending on the assumption made for handling temperature and Z factor.

(1) *Average pressure and temperature method.* Substituting the expression for gas density in terms of P, T, and Z into Equation 6.13 results in:

$$\frac{dP}{dL} = \frac{PM}{ZRT}\left[\cos\phi + \frac{fV^2}{2g_c d}\right] \quad (6.12)$$

Integration of Equation 6.12, assuming an average temperature in the flow string, evaluating Z at average conditions of pressure and temperature, and using the fact that $\cos\phi$ = TVD/MD, gives:

$$P_{wf}^2 = P_{tf}^2\,\mathrm{EXP}(S_1) + \frac{25\,\gamma_g q^2 \bar{T}\bar{Z} f(\mathrm{MD})\,\mathrm{EXP}[(S_2) - 1]}{S_2 d^5} \quad (6.13)$$

where:

P = psia
$S_1 = 0.0375\,\gamma_g(\mathrm{TVD})/\bar{T}\bar{Z}$
$S_2 = 0.0375\,\gamma_g(\mathrm{MD})/\bar{T}\bar{Z}$
MD = measured depth, ft
TVD = true vertical depth, ft
$\bar{T}$ = °R
q = MMscfd
d = in.
f = f (N_{Re}, ϵ/d) (Jain or Colebrook equation)

The solution procedure is the same as for a shutin well except for evaluation of the friction factor, which requires calculating a Reynolds number and estimating pipe roughness. Iteration is required since Z must be evaluated at an average pressure ($\bar{P} = (P_{tf} + P_{wf})/2$).

Dividing the well into several length increments and using the procedure described earlier will give more accurate results. Actually, any of the methods will give near-identical results if the well is divided into short enough increments for calculations.

Convergence is sometimes obtained faster if iteration is performed on the Z factor rather than on the unknown pressure. The procedure is:

(1) Estimate Z* (Try first estimate of 0.9).
(2) Calculate the unknown pressure using Equation 6.12 with Z = Z*.
(3) Calculate the average pressure, $\bar{P} = (P_{tf} + P_{wf})/2$.
(4) Evaluate Z at $\bar{P}$ and $\bar{T}$.
(5) Compare Z and Z*. If not close enough, set Z* = Z and proceed to step 2. Repeat until abs(Z − Z*)/Z < 0.001 or give tolerance. When the tolerance is met, the pressure from step 2 is the answer.

(2) *Cullender and Smith method.* Derivation of the Cullender and Smith method for vertical flowing gas wells begins with Equation 6.11.[10] The following substitutions are made for velocity:

$$V = q/A \quad (6.14)$$

$$q = q_{sc}\frac{P_{sc}TZ}{T_{sc}PZ_{sc}} \quad (6.15)$$

which gives:

$$\frac{dP}{dL} = \left[\frac{PM\cos\phi}{ZRT}\right] + \left[\frac{MT\,Z^2 P_{sc} f^2 q_{sc}}{RPT_{sc}^2\,2g_c\,d\,A^2}\right] \quad (6.16)$$

or:

$$\frac{P}{ZT}\frac{dP}{dL} = \frac{M}{R}\left[\left(\frac{P}{ZT}\right)^2\cos\phi + c\right] \quad (6.17)$$

where:

$$C = \frac{8\,p_{sc}^2\,q_{sc}\,f}{T_{sc}^2\,g_c\,\pi^2\,d^5} \quad (6.18)$$

which is constant for a given flow rate in a particular pipe size. Separating the variables, substituting field units and the fact that $\cos\phi$ = TVD/MD, and integrating gives:

$$\int_{P_{tf}}^{P_{wt}} \frac{\frac{P}{ZT}\,dP}{\frac{0.001(\mathrm{TVD})}{\mathrm{MD}}\left(\frac{P}{ZT}\right)2 + F^2} = 1{,}875\,\gamma_g(\mathrm{MD}) \quad (6.19)$$

where:

$$F^2 = \frac{0.667\, f\, q_{sc}^2}{d^5} \tag{6.20}$$

Writing Equation 6.18 in abbreviated notation and dividing the well into two increments of length (MD)/2 gives:

Upper half of well:

$$13.75\ \gamma_g(MD) = (P_{mf} - P_{tf})(I_{mf} + I_{tf}) \tag{6.21}$$

Lower half of well:

$$13.75\ \gamma_g(MD) = (P_{wf} + P_{mf})(I_{wf} + I_{mf}) \tag{6.22}$$

where:

$$I = \frac{P/TZ}{\frac{0.001(TVD)}{MD}\left(\frac{P}{ZT}\right)^2 + F^2} \tag{6.23}$$

The solution procedure is similar to that for the static case but is more involved because of the more complicated definition of I. For practical purposes, F can be considered a constant since the only variable in the Reynolds number used in evaluating f is gas viscosity.

Viscosity is a function of pressure, but for simplification of the calculations, it can be evaluated at $\bar{T}$ and the known pressure.

In terms of mass flow rate, the Reynolds number is:

$$N_{Re} = \frac{20{,}011\ \gamma_g\, q_{sc}}{\mu d} \tag{6.24}$$

where:

q_{sc} = gas flow rate, MMscfd
γ_g = gas gravity
μ = gas viscosity, cp
d = pipe inside diameter, in.

6.13 VERTICAL MULTIPHASE FLOW CORRELATIONS FOR PRODUCING GAS WELLS

The prediction of pressure gradients, liquid holdup, and flow patterns during the simultaneous flow of gas and liquid in pipes is necessary for design in both the oil and chemical industry. A tremendous amount of work has been done in this field, and no attempt will be made in this section to thoroughly review the subject. However, good reviews of correlations related to the petroleum industry can be found by K. E. Brown[11] and by Govier and Aziz.[12]

Summarizing briefly, many pressure drop correlations are composed of the sum of three components:

$$\frac{dp}{dL_{total}} = \frac{dp}{dL_{elevation}} + \frac{dp}{dL_{friction}} + \frac{dp}{dL_{acceleration}} \tag{6.25}$$

The elevation pressure gradient term usually dominates the total pressure gradient in multiphase flow situations. The friction term for multiphase flow is usually some sort of two-phase friction factor that varies from one correlation to another. Many correlations ignore the acceleration term, which is usually important only for high rate gas flows.

Most of the more sophisticated correlations have different relationships for the pressure gradient terms, depending on the type of flow regime that is thought to be present. An example flow regime map is shown in Figure 6.11, which is by Duns and Ros.[13] Although other researchers have identified other types of flow regimes such as froth, intermittent, etc., this map has found broad usage. A typical gas well producing some liquids will flow in the mist flow regime at higher gas velocities. At lower gas velocities, liquids accumulate in the wellbore, and slug flow may appear in the bottom of the well. At still lower rates, there could be bubble flow at the bottom of the well with slug flow above. Mist flow could still be evident at the surface of the well where gas velocity is higher because of gas expansion. The onset of liquid accumulation in the well can drastically affect well production as the increased back pressure on the formation reduces flow.

6.131 GAS CONDENSATE WELL PRESSURE DROP PREDICTION

(1) *Compositional models.* For gas condensate systems, it is possible to take available flash vaporization data and construct formation volume factor (B_o) data and solution GOR (R_s) data necessary to input into multiphase flow correlations that are normally run using black-oil PVT correlations. Liquid- and gas-mass fractions and densities can be obtained from flash vaporization data.

In retrograde condensate wells, liquids can build up in the wellbore as the pressure drops coming up the tubing. When using a black-oil model based on describing mass transfer between phases, a finite value of oil rate q_o must be assumed for the stock-tank production rate. For a retrograde condensate well, the value of B_o should be considered by a mathematical technique to assure that the product of q_o B_o is a measure of the in-situ volumetric flow rate. Values of B_o less than one can be calculated to describe a retrograde condensate well.

Also, for a retrograde condensate well, formation volume factors could take on seemingly unrealistic values. Liquid forms as pressure decreases, so free gas $q_o \times (GOR - R_s)$ will decrease. This can be accounted for by suitable values of R_s, the solution GOR (scf/bbl). Another approach is to use a compositional pipe-flow model when dealing with a gas condensate or volatile oil system. Given the total mass flow rate of oil and the composition of the total flow, flash vaporization calculations can be made at selected pressures and temperatures. These calculations will yield values of mass fractions of liquid gas, m_l and m_g, as well as gas and liquid densities. Then, in-situ values of volumetric flow rates can be found from:

$$q_L = \frac{w_t[m_L/(m_L + m_g)]}{\rho_L} \tag{6.26}$$

$$q_g = \frac{w_t[m_g/(m_L + m_g)]}{\rho_g} \tag{6.27}$$

where:

m_L = mass of liquid/moles total flow
m_g = mass of gas/moles total flow
w_t = total mass flow rate

Then, superficial velocities can be calculated, which can be used to calculate values of liquid holdup. To

Note: Some material in Section 6.124 is from course notes prepared by H. D. Beggs.

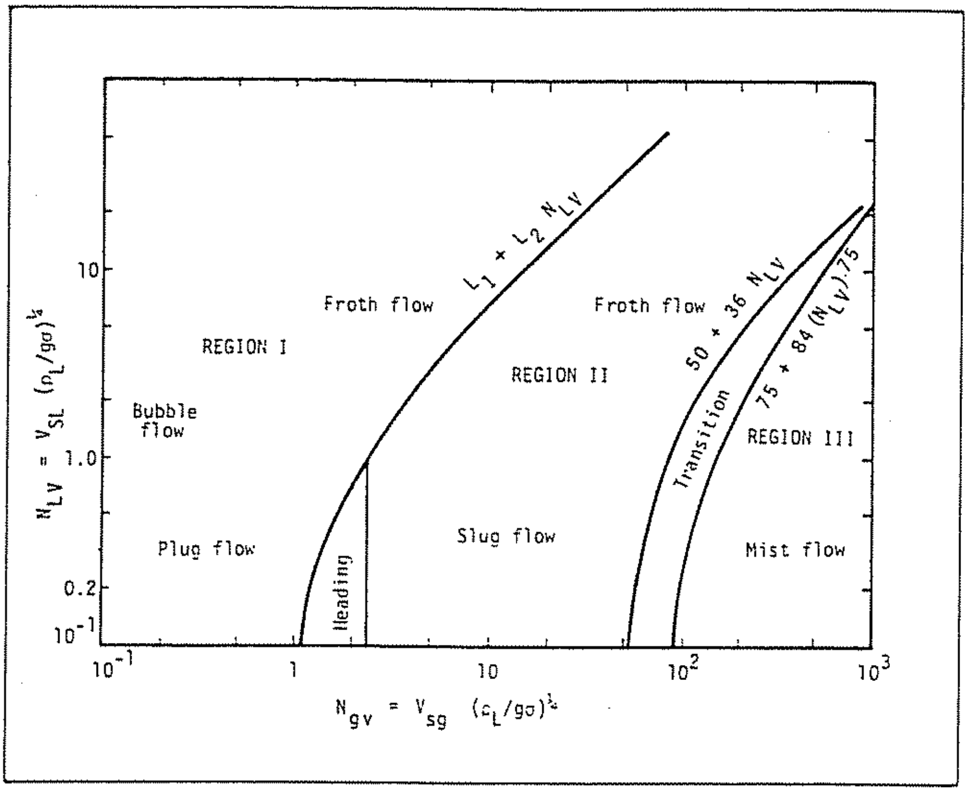

Figure 6.11 Example Flow Regime Map from Duns and Ros as a Function of Dimensionless Superficial Liquid and Gas Velocities[13]

account for slip between the phases, existing holdup or slip correlations usually obtained from experiment must be used. Vertical flow programs normally utilizing correlations can allow input of PVT data, but a lot of computation and accessing of other programs (flash vaporization calculations) would have to be done before using the flow program. The next section describes a more convenient alternative to describing pressure drop in vertical flow with gas condensate fluids.

(2) *The Gray correlation.* A vertical flow correlation for gas condensate wells was developed by H. E. Gray.[4] It is included in the vertical flow package in the computer program described in *API 14b* for sizing subsurface safety valves.

This program uses a pressure balance with a term, ξ, the gas volume fraction obtained from a fit of a few condensate data systems to build a simplified empirical model of a retrograde phenomenon requiring only specific gravity, pressure, and temperature data for input.

The pressure balance equation used is:

$$dP = \frac{g}{q_c}\ \xi\ \rho_g + (1-\xi)\rho_e]\, dh + \frac{f_t\, G^2}{2q_c\, D\, P_{mf}}\, dh + \frac{G^2}{g_c}\, d\left(\frac{1}{\rho_{mi}}\right) \tag{6.28}$$

where ξ, the gas volume fraction, is:

$$\xi = \frac{1 - \exp\left\{-2.314\left[N_V\left(1+\frac{205.0}{N_D}\right)\right]^B\right\}}{R+1} \tag{6.29}$$

$$B = 0.0814\left[1 - 0.0554\ \ln\left(1+\frac{730R}{R+1}\right)\right] \tag{6.30}$$

and:

$$N_V = \frac{\rho_m{}^2 V_{sm}{}^2}{q\ \tau(\rho_e - \rho_g)} \tag{6.31}$$

$$N_D = \frac{g(\rho_e - \rho_g)D^2}{\tau} \tag{6.32}$$

$$R = \frac{V_{so} + V_{sw}}{V_{sg}} \tag{6.33}$$

D = ID of flow conduit
f_t = two-phase flow friction factor
G = mass velocity
h = depth
P = pressure
q = flow rate
R = superficial liquid/gas ratio
S = specific gravity
S_g = gas gravity
t = temperature
V = velocity
ρ = density
τ = mixture surface tension

subscripts:

f = friction effect
g = gas phase
i = inertia effect
l = liquid phase
m = gas/liquid ratio
o = hydrocarbon condensate
s = superficial value
w = freewater phase

The following indicates data ranges over which the Gary correlation was made.[4] Any calculations beyond

the following acceptable guidelines should be viewed with caution:

(1) flow velocities below 50 fps
(2) tubing sizes below 3½ in.
(3) condensate production 50 bbl/MMscf
(4) water production 5 bbl/MMscf

This program was compared to 108 sets of well data. The results were found superior to dry-gas well predictions. The Gray correlation can be used to evaluate gas condensate wells by generating tubing performance J curves and comparing them to reservoir performance. Although the above restrictions should be considered, several calculations made with upward of 300 bbl/MMscf indicated less than 10% error compared to data.

(3) *The Govier-Fogarasi model.*[14] Field data from 102 wells with GLR's ranging from 3,900 to 1.7 million scf/bbl were analyzed. Using standard flash calculations, the phase distributions in the wellbore were determined. An empirical method treating the fluids as single phase with mixture properties and a method accounting for the fluid in the gas core and in the wall film were compared, with both methods showing comparable accuracy. When part of the wellbore flow was predicted to be two-phase and part was predicted to be single phase, the empirical methods worked best.

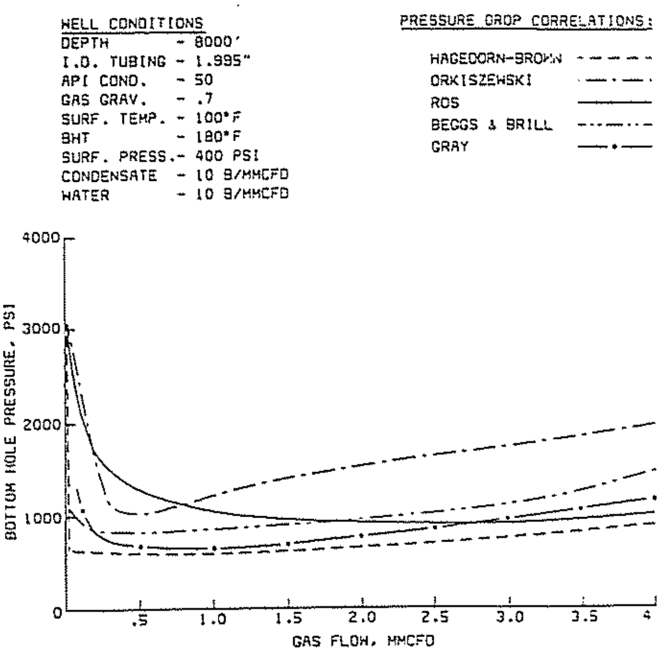

Figure 6.12 Comparison of Some Vertical Flow Pressure-Drop Models

6.132 BLACK-OIL MULTIPHASE-FLOW CORRELATIONS FOR GAS WELLS

Although these correlations were developed primarily for use with black-oil systems, they are sometimes useful in predicting liquid loading conditions for multiphase-flow gas wells. Some of these correlations are based on laboratory data, including air-water data. They may be applicable to gas wells that produce liquids with significant water cuts and wells that produce light-end hydrocarbons.

For example, multiphase-flow correlations that currently find usage can predict the flow regime that the production stream is in and can make calculations accounting for friction, slip, and liquid holdup for each flow regime. Examples are the Ros,[15] Orkiszewski,[16] Beggs and Brill,[17] and Aziz, Govier, and Fogarasi[18] correlations. Additionally, the Hagedorn-Brown correlation[19] (which is not flow-regime dependent) has found wide usage in artificial lift work. If, by comparison to field well data, any of these correlations can reasonably predict loading conditions, the engineer can use the tubing intake curves generated by these correlations and plan appropriate measures such as smaller tubing installations or other lift methods to assist production.

Examination of Figure 6.12 shows a comparison of four multiphase-flow correlations run at typical conditions for a high-GOR well showing the loading up, or J curve characteristics, of each. Also, the Gray correlation for condensate wells[4] is shown for comparison. Unfortunately, there is a fairly wide scatter for the predicted point where the curves begin to turn up. This is probably a typical comparison as far as concerns the disparity between correlations and should be the subject of future research.

The Orkiszewski model was the result of making use of a combination of the best available models when it was developed.[16] The model includes the Griffith-Wallis bubble-flow correlation and the Ros mist-flow correlation with an "improved" slug-flow pressure-drop calculation. In addition, the Orkiszewski model[16] is reported to have been used with good success in a study of liquid loading.[20] However, there are ranges of flow where the Orkiszewski model appears to be in serious error, especially with water production present.

The Ros correlation was developed using some high-GLR laboratory data.[15] Experience or comparison of predictions to some field data remains advisable before general usage of one of the correlations.

6.133 SIMPLIFIED MODELS FOR PREDICTING MINIMUM GAS VELOCITY FOR LIQUID REMOVAL

A simpler approach to predicting safe or "minimum" flow rates to avoid liquid loading in the tubing is based on the concept that gas velocity must be high enough to transport liquid droplets to the surface. Turner et al. made an analysis of the minimum gas velocity necessary for producing liquid droplets from wells and for moving a liquid film up the tubing wall.[21] This study generated a minimal critical velocity criterion using the droplet model and comparing the model to data. Predicted critical velocities were compared to the gas velocity of producing wells at wellhead temperature and pressures.

The critical velocity found by Turner for this droplet model results from simply equating the upward velocity drag on the calculated largest droplets to the downward weight of the droplets.[21] The size of the droplets is calculated from a correlation previously presented by Hinze, which considers shear forces (which tend to shatter the drop) balanced against surface tension forces (which tend to keep the droplet from shattering into smaller droplets).[22] The equations by Turner were developed as follows.[24]

Equating weight to drag for a droplet at terminal velocity:

$$\overset{\text{(weight)}}{g/g_c(\rho_L-\rho_g)\text{vol}}=\overset{\text{(drag)}}{\frac{C_D\,\rho_g\,A_p\,V_t^2}{2g_c}} \tag{6.34}$$

where:

g = local acceleration of gravity, 32.2 ft/s²
g_c = gravitational constant, 32.2 lb_m-ft/lb_p-s²
C_D = drag coefficient, dimensionless
ρ_g = gas density, lb_m/ft^3
ρ_L = liquid density, lb_m/ft^3
V_t = terminal velocity, ft/sec
vol = volume of the droplet, ft³
A_p = projected area of the droplet, ft²

Solving for V_t gives:

$$V_t=6.55\sqrt{\frac{(\rho_L-\rho_g)D}{C_D\,\rho_g}}\text{, ft/sec} \tag{6.35}$$

From Hinze,[22] the relationship between droplet diameter, velocity, and surface tension is:

$$N_{we}=\frac{V_t^2\,\rho_g\,D}{\sigma\,g_c} \tag{6.36}$$

where:

N_{we} = Weber number (used to correlate droplet size)
σ = surface tension, lb_t/ft

Using the above relationship, Turner recommended letting N_{we} = 30 for the larger droplets.[21] Modifying Equation 6.35 to allow input of σ in dynes/cm gives:

$$V_t=\frac{1.59\,\sigma^{1/4}(\rho_L-\rho_g)^{1/4}}{(\rho_g)^{1/2}} \tag{6.37}$$

Following Turner et al.[21] and using the following (approximate average) constants for physical properties:

Water	Condensate
σ = 60 dyne/cm	σ = 20 dyne/cm
T = 120° = 580°R	T = 580°R
ρ_L = 67 lb_m/ft^3	ρ_L = 45 lb_m/ft^3
gas gravity = 0.6	

Adding 20% according to Turner[21] to agree with data gives:

$$V_{g_{water}}=\frac{5.3(\rho_L-0.00279\,P)^{1/4}}{(0.00279\,P)^{1/2}} \tag{6.38}$$

$$V_{g_{condensate}}=\frac{4.03(\rho_L-0.00279\,P)^{1/4}}{(0.00279\,P)^{1/2}} \tag{6.39}$$

The minimum volumetric flow rate to prevent liquid loading for a particular velocity and pipe size may be calculated as:

$$q_g(\min)=\frac{3.06\,V_g\,A}{TZ}P \tag{6.40}$$

where:

$q_{g_{min}}$ = minimum flow rate for continuous liquid removal, MMscfd
V_g = gas velocity, ft/sec
A = conduit area, ft²
Z = gas compressibility factor evaluated at T and the pressure used to calculate V_g
P = pressure, psia

Turner's work suggested that the wellhead pressures be used for evaluation of well liquid loading.[21]

EXAMPLE PROBLEM

A gas well is producing against a fixed wellhead pressure of 1,000 psia through 3½-in. (2.992 ID) tubing. The wellhead temperature is 140°F and the gas gravity is 0–70. Calculate the minimum flow rate to keep the well unloaded. Condensate but no water production is measured.

$$V_{g_{condensate}}=\frac{4.03[45-0.00279(1{,}000)]^{1/4}}{[(1{,}000)(0.00279)]^{1/2}}$$
$$=4.03\left(\frac{2.548}{1.67}\right)=6.15\text{ ft/sec} \tag{6.41}$$

where:

P = 1,000 psi
T = 140°F
γ_g = 0.7
Z = 0.88
A = $\pi D^2/4$ = 0.7854(2.892/12)² = 0.0488 ft²

$$q_{g_{min}}=\frac{3.06(1{,}000)(6.15)(0.0488)}{(600)(0.88)}$$
$$=1.74\text{ MMscfd} \tag{6.42}$$

Turner suggested his model was good up to a liquid rate of about 130 bbl/MMscfd.[21] If both water and condensate are present, the equation for water was suggested for use.

Figure 6.13 shows a tubing performance curve generated from the Duns and Ros correlation.[23] Also plotted on this graph are the superficial gas velocities at the top and bottom of the well. The dash lines are the critical velocities according to Turner et al.[21] Notice that the critical and actual gas velocities intersect at about 0.75 MMcfd using Turner's calculation made at surface conditions. However, the actual and critical velocities cross at about 1.0 MMcfd when Turner's calculation is made at bottom-hole conditions. This shows that the critical required rate can be at bottom-hole conditions. Therefore, in general, critical velocity correlations should be used in conjunction with a pressure-drop correlation to estimate bottom-hole pressure for checking critical velocity at surface and downhole conditions. Also note that the last point of tangency of the tubing performance curve with an IPR curve with a slope of about 45° could be imagined to be about 0.45 MMcfd. This would indicate from this example that Turner's method is conservative when compared to the Ros correlation because it indicates a higher rate than necessary to maintain continuous liquid unloading from inspection of the last possible J curve-IPR curve intersection as shown here. Note that Turner did correct his general theory to agree with surface-collected data,[21] but the physics of the critical flow model indicate it should be used downhole.

Meschack and Ikoku also present an analysis of annular flow with consideration of droplets in the annular

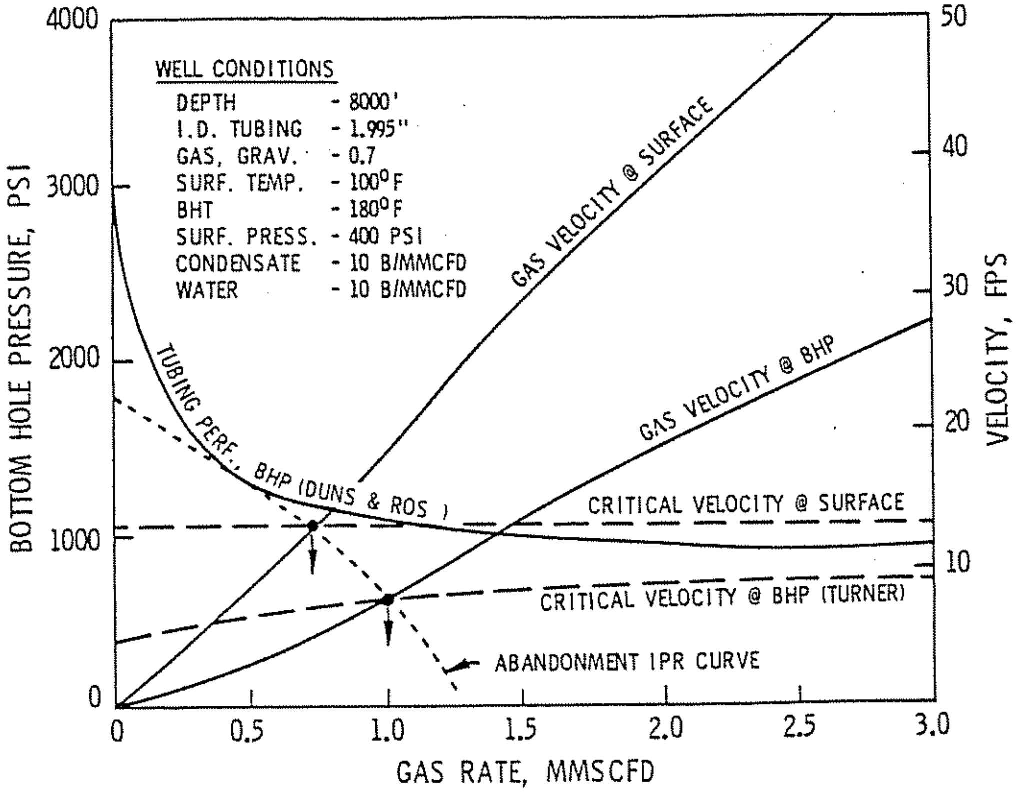

Figure 6.13 Demonstration That Critical Velocity Will Occur at Bottom-Hole Conditions and Not at the Surface

core and the interaction with the liquid film on the tubing.[24] The results indicate the rate of liquids that can be entrained with various gas rates. The results, however, seem to indicate an unrealistically high increase in gas velocity required at low liquid rates. This is an effect apparently apart from the fact that superficial and actual gas velocities differ because of the presence of liquids, as indicated by the authors.

6.134 SUMMARY AND CONCLUSIONS

Prediction of liquid loading conditions in gas wells can be made by stand-alone models, which predict critical velocity, and/or by intersecting tubing performance curves developed with multiphase flow correlations with reservoir IPR curves.

The Turner model, or critical gas velocity, was developed to be applied at wellhead surface conditions and is, in Turner's final form, a function of pressure only.[21] However, it is shown herein that the critical velocity can occur at bottom-hole conditions. Also, the pressure dependence of surface tension of condensate should be used. With the above modifications, the Turner model seems to predict conservatively but may not contain enough physics of the actual situation to be expected to work under broad conditions.

The intersection of tubing curves with IPR curves will predict where the well will flow. Future IPR curves generated from P/Z vs cumulative plots, reservoir models, or type curves can be used to predict future reservoir performance. Where the IPR curve and tubing performance curve become finally tangential indicates the critical flow condition or last possible flow point.

A compositional tubing flow model can be an accurate way of predicting tubing performance for gas condensate production in particular, but the required flash vaporization data is not always available. The Gray correlation was developed to model pressure profiles in gas condensate wells and requires minimum input.[4] Also, Govier and Fogarasi present methods for pressure profile calculations for gas and gas condensate wells as well as presenting a large amount of data.[14]

Other options for generating tubing performance curves include use of one of the petroleum-industry multiphase-flow correlations, which normally are used for calculating pressure drop for wells producing black-oil hydrocarbons, water, and gas.

6.14 OTHER MISCELLANEOUS FLOWING WELL CONSIDERATIONS

6.141 PRESSURE AND RATE CYCLING IN GAS WELLS

In preceding discussions (see Section 6.132), conditions where slugging occurs in multiphase flow wells having low tubing gas velocities (the well would be producing in the slug flow regime) were discussed. It has also been discussed that the fluid level in continuously producing wells is depressed to the tubing intake point. As a consequence of producing a liquid slug at the surface, the tubing back pressure is also reduced, and this will allow annulus gas to feed into the tubing. This further lightens the tubing gradient; still more annulus feeds into the tubing. In this manner, more liquids are removed from the tubing because of the higher gas rate, and the annulus pressure is depleted

to the point where it will not support the normal flowing tubing pressure loss because of incoming production. After blowing down the annulus gas volume, the tubing velocity dies back to the lower rate of incoming production, and liquids will again begin accumulating in the tubing. This causes a pressure buildup cycle wherein increasing liquid holdup in the tubing causes a larger tubing pressure drop, and the casing pressure also increases to support the tubing pressure gradient. The well cycles in terms of pressures and instantaneous gas rates.

At the onset of slugging, the cycle is not pronounced because the slugs are small. However, as the gas rate becomes smaller and the slugs become larger, the cycling becomes more apparent. In tight gas wells, the cycle can become very pronounced because the recovery of the gas rate during the pressure buildup can be very lengthy.

To minimize this form of well cycling, a downhole packer can be used to isolate the annulus volume from the tubing. Use of a packer is recommended for wells of fair-to-good reservoir permeability because the well will stabilize and produce in the future for an extended period of time. Although a tight gas well will see improved flow stabilization with the packer, the future producing rate will likely continue to decline rapidly, and liquid loading will become critical so that other methods of unloading may be preferred. If loading is expected to be critical, other unloading methods such as plunger lift may be better solutions, and the packer would then be removed.

6.142 INTERMITTING OPERATIONS

Intermitting a well enables the stored gas volume to increase the instantaneous production rate and clear liquids from the wellbore. Intermitting, sometimes referred to as "stop cocking" or "blowing down," can be practiced in two ways: (1) the normally pressured well can be opened to the atmosphere, or (2) the well can be shut in for a pressure buildup before opening it to the flow line or, in some cases, the atmosphere. Intermitting the tubing flow to the pit (atmosphere) causes the vented gas to be wasted, and special permission from the proper regulatory agency must be obtained. It does, however, provide the largest instantaneous drawdown and producing rate for any specified starting pressure. It is sometimes used on low-pressure wells. The approach of shutting in for a buildup and then flowing the well to the sales line is generally more desirable since the blowdown gas is not vented.

Intermitting to line pressure is the preferred way for tight-formation gas wells. The pressure buildup rate will usually remain constant (i.e., the rate of pressure increase is steady throughout the buildup period), which indicates the reservoir is still producing normally toward the near-well area.

The buildup pressure that should be reached before the well is put on the production cycle is largely based on experience. A good blowdown cycle will be evident by the closeness of the tubing and casing pressures. A high differential after a period of time sufficient for liquids to reach the surface indicates the accumulated liquid is not being removed. Plunger lift, which is discussed in a following section, might be described as intermitting the well with a seal surface to reduce liquid fallback.

6.2 PLUNGER LIFT

6.21 INTRODUCTION

Plunger lift is a gas-lift method of producing liquids that may or may not require additional injection gas. A plunger-lift installation utilizes a free piston (plunger) to interface between accumulated liquids and the lift gas. A typical equipment arrangement for a plunger-lift installation is shown in Figure 6.14.

Multiphase-flow pressure loss in a low-volume gas well can be due primarily to liquid holdup in the flow stream. In plunger applications, the plunger provides an interface between the liquid slug and the lift gas, thereby minimizing liquid fallback and the resultant holdup in the tubing. These benefits increase the utility of the gas energy, resulting in lowering the multiphase-flow pressure losses and hence lowering the average wellbore pressure.

6.22 THE PLUNGER-LIFT-CYCLE DESCRIPTION

The plunger cycle is termed continuous if the plunger cycles without interruption. The cycle is termed intermittent when the well is shut in for a

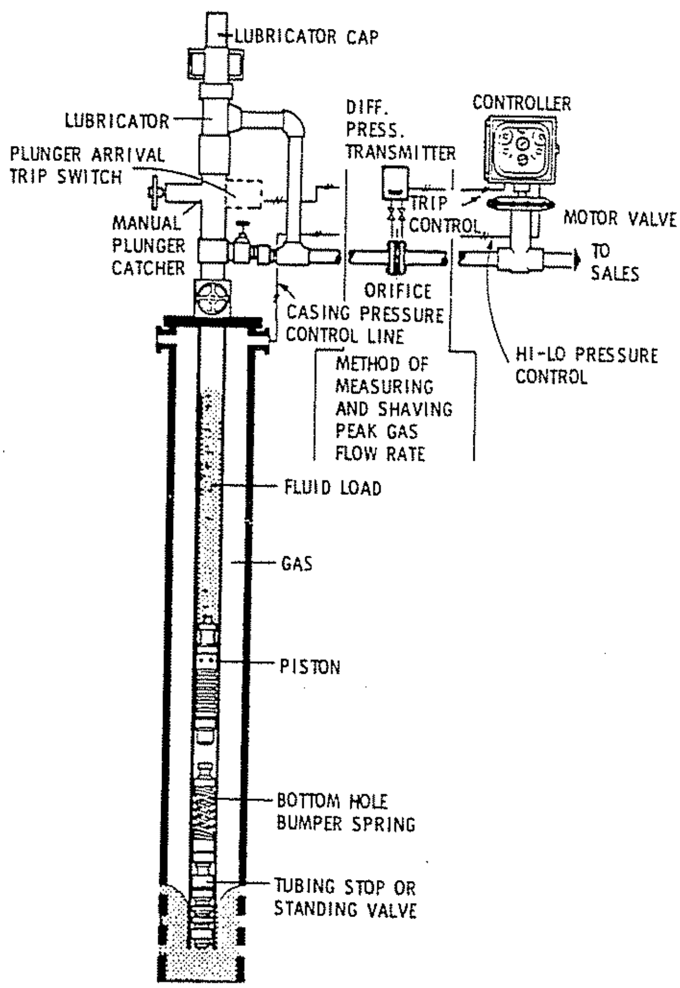

Figure 6.14 Schematic of Plunger Lift Installation

buildup of bottom-hole and casing pressure to lift the liquid slug or if the plunger is held in the wellhead during a production period. Typically, plungers are used on gas wells that have a sufficiently high gas-liquid ratio (GLR) to operate solely with a plunger on formation gas. However, plunger-lift installations can be designed to use makeup injected into the annulus gas when the available produced gas is insufficient. A minimum GLR can be calculated for different conditions but is usually around 3,000–5,000 scf/bbl. Typically with high-GLR wells, the slug size is small and the operating pressures are relatively close to line pressure.

The following example of the plunger cycle is given to further explain the operation and characteristics of a plunger installation. The example is from an actual well. The three cycles shown may be more complex than found in the typical installation, but they serve to bring out several points that can be helpful in examining the production and pressure characteristics of other plunger lift cycles. Refer to the numbered stations on Figure 6.15 to follow the cycle description.

Station 1. The well was initially shut in to build up pressure sufficient to surface the plunger. The tubing is open to the flow line, and the plunger begins to surface with the reduction in tubing pressure. "Top gas" above the plunger and the liquid load is produced.

Station 1'. The liquid slug has arrived at the surface. The liquid slug passes through surface line and fittings and results in a pressure spike on the tubing pressure gauge. Casing pressure decreases as casing gas feeds into the tubing under the plunger.

In this example, the plunger is operated with a time-cycle controller and the well is allowed to produce after plunger arrival with the plunger held at the surface. Tubing pressure continues to decrease as the gas flow rate decreases following plunger arrival. Production of gas after arrival is common when the GLR exceeds the minimum required.

The casing pressure reaches a minimum as gas feeds into the tubing but then begins to increase because of liquid holdup in the tubing, which results from an insufficient gas rate to clear the tubing. The casing pressure must always be higher than the tubing pressure in the flow period in order to support the flowing tubing multiphase pressure gradient.

Station 2. Gas rate has diminished to 200 Mcfd (unsatisfactory low differential reading on the orifice meter for this example) and the well is shut in for a pressure buildup.

Note the sudden increase in tubing pressure as gas and liquid phases separate and the flowing pressure gradient (primarily caused by the liquid holdup in the tubing) is lost. The ensuing gradual tubing-pressure buildup is due to new gas production entering the wellbore. The uniform slope of this buildup indicates that

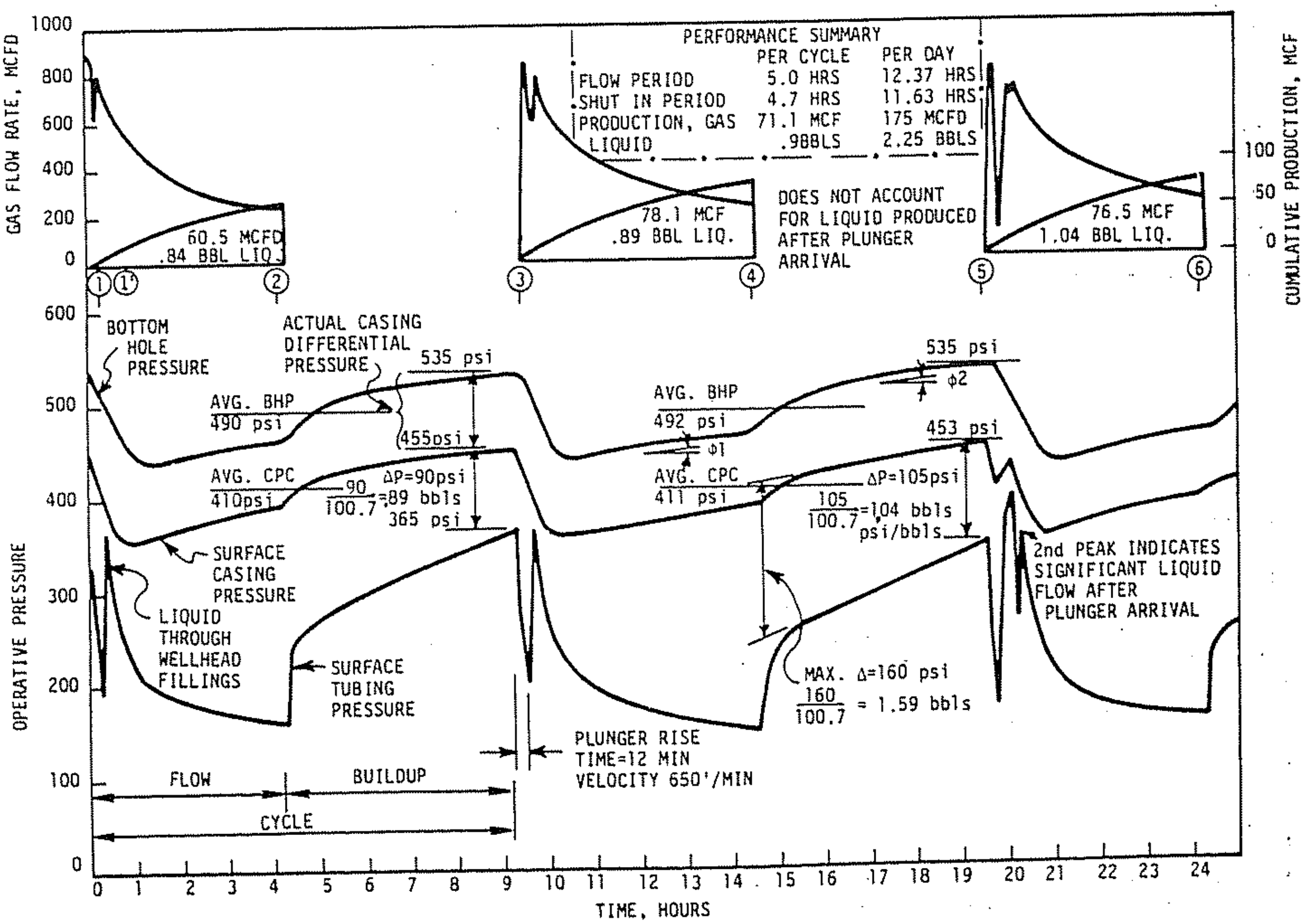

Figure 6.15 Example of Plunger Cycle—Lee Gould Jr. Unit Well No. 1, Wattenberg, Colorado

the well is continuing to build up fairly uniformly throughout the buildup period.

Station 3. Tubing is open to flow. The previous cycle is repeated. Note the indication of plunger travel time (12 min) as shown by the drop in tubing pressure to a minimum value and the sharp peak achieved as the liquid slug reaches the surface line and wellhead fittings, which are in effect "choking" the flow.

The liquid slug size above the plunger may be estimated by dividing the 90-psi differential pressure between the casing and tubing by the equivalent column pressure of 1 bbl of produced fluid in the tubing (for 2⅜-in. tubing, 1 bbl = 258.6 linear ft/bbl × 0.433 psi/ft × 0.8 SpGr = 100.7 psi/bbl). This calculation indicates 0.89 bbl of liquid in the tubing.

Station 4. Flow has diminished to a 200-Mcfd reading on the orifice meter, and the well is shut in for the buildup cycle.

Note that at this time the pressure differential between tubing and casing is 160 psi, which corresponds to a static fluid column of 1.59 bbl of liquid in the tubing (neglecting flowing friction). Based on the buildup in casing pressure during the shutin period, it is estimated that the volumes of gas entering the casing and tubing during the shutin period were 1.75 and 1.13 Mscf, respectively. The associated liquid volume based on a liquid-gas ratio of 13 bbl/MMcf would be 0.024 and 0.015 bbl, respectively, for the casing annulus and tubing. Thus, during the shutin portion of the cycle, 2.87 Mscf of gas and 0.039 bbl of liquid entered the wellbore. This is compared to an average 78 Mscf of gas and 0.9 bbl of liquid produced during the total cycle. The production flow into the wellbore during the shutin period appears to be causing a faster buildup in the tubing pressure compared to the casing pressure. Actually, the more rapid rise in tubing pressure may be due to some liquid draining from the tubing into the annulus. At the end of the buildup period, the casing-tubing differential is 105 psi, indicating 1.04 bbl of liquid remain in the tubing over what is in the casing above the bottom of the tubing. If there is liquid in the annulus above the tubing inlet, it will feed into the tubing under the plunger on the next production cycle. The most reliable way of knowing how much liquid must be produced during the cycle is to measure the liquid on several cycles. Liquid draining from the tubing can be controlled with a tubing standing valve, and/or the amount of liquid in the wellbore can be reduced by decreasing the flow period.

Note that the slope of the buildup lines, both BHP and the surface casing pressure during the shutin period, do not change near the end of the buildup cycle. This constant slope indicates that the gas influx rate into the affected well drainage area is fairly uniform throughout the buildup period, and the long buildup time does not significantly affect the well's production in this tight (low-permeability) reservoir. A slope that leveled off during the shutin period indicates that the buildup cycle would inhibit maximum production expected. The optimum setting for buildup time is the shortest time that provides sufficient pressure to surface the plunger plus liquid slug. Following calculations will quantify the needed pressure.

Station 5. Buildup pressure is complete and the tubing is open to the flow line. Note that there is a second peak on the tubing-pressure recording following the large peak caused by the liquid slug above the plunger passing through restrictions in the surface. The second peak is presumed to indicate some liquid production after plunger arrival (i.e., liquid from the casing annulus or below the tubing feeding into the tubing below the plunger).

Station 6. The flow period is over and the tubing is shut in for the next buildup cycle.

Although the description given above was for a time-cycle controlled plunger operating in a well without a packer, other types of plunger installations have similar characteristics. Other cycles will vary slightly, depending upon the type of cycle controller used and whether the well is equipped with a downhole packer. Where a downhole packer is installed, the formation must supply all of the operating gas during the time the tubing is open for flow. A downhole packer for wells on plunger lift will probably prevent successful operations unless an outside high-pressure gas source is used for the lift gas.

Special wells may require or may show improved operations by a continuous low production of gas from the tubing at all times. This is accomplished by a bypass small-choke arrangement around the time-cycle controller. This permits more liquid entry above the plunger for the next cycle.

6.23 SELECTION OF WELLS FOR APPLICATION OF PLUNGER LIFT

Plunger lift is one preferred method for removing liquids from low-producing-rate gas wells. When the producing rate is in the liquid holdup region of a tubing performance curve, the well begins to produce large liquid slugs (heading) that may require intermitting to clear liquid accumulations from the tubing. These conditions indicate that the well is a good candidate for a plunger installation.

Plunger lift is suited for producing liquid from wells over a wide range of conditions and is capable of producing many wells to satisfactory reservoir depletion pressures. This is particularly true for wells with high GLR's. Higher GLR's allow production with smaller liquid slugs and, hence, lower operating pressures. Tubing size also affects the operating pressure for a given slug size.

The minimum GLR to operate plunger lift is the actual minimum amount of gas in the tubing volume at maximum cycle pressure (in scf) divided by the captured slug (bbl) at average wellbore temperature at which the plunger cycle will still function. The minimum GLR for a plunger lift well can be calculated using gas pressure/volume relationships. As the producing GLR approaches the minimum GLR, the slug size increases for a given amount of production. Since an increase in slug size requires a corresponding increase in operating pressure, it is a matter of economics and field experience to determine if low-GLR wells should or can be produced by some type of method other than plunger lift. If the formation has low permeability and the casing pressure buildup is steady throughout the shutin period, as illustrated in the example, plunger lift is probably the best method for removing small quantities of liquid production.

Another application for plunger lift is its installation in a well that has been treated with injected fluids (stimulated) and that requires some unloading before the well is capable of sustained natural flow. Rigging the well for plunger lift in advance will allow plunger operation during the cleanup period until satisfactory GLR's are reached. When the well has cleaned up sufficiently, the plunger can be captured and the well produced as a naturally flowing well.

Limitations. Provided the GLR remains above the minimum GLR requirement, there should be no limitations to the application of plunger lift except for the number of cycles and, hence, liquid production rate that can be made in a given period of time. In some high-capacity but low-pressure wells, the production increases because of additional back-pressure reduction and may favor the installation of a downhole pump.

Table 6.1 summarizes the advantages and disadvantages of plunger lift installations.

TABLE 6.1
ADVANTAGES AND DISADVANTAGES OF PLUNGER LIFT

Advantages	Disadvantages
Capable of operating over a wide range of well conditions; especially good for high-GLR wells but can be used with wells as low as 3,000–5,000 scf/bbl.	Cannot fully reduce well back pressure to line pressure (i.e., to the potential possible with pumping equipment).
Does not require outside power source.	Cycle performance is somewhat sensitive to changing line pressure.
Downhole equipment can be installed with wire-line equipment.	High permeability but very low pressure formations may lose some production (compared to pumping methods) because of cycle shutin time.
Capable of good reservoir pressure depletion for high GLR wells (average producing pressure may be around 100 psi above line pressure).	
Plunger trips can control paraffin and scale buildup.	

6.24 PLUNGER LIFT DESIGN CALCULATIONS

Many plunger installations have simply started with installing plunger lift equipment and adjusting the controller on a trial-and-error basis. Considerable time may be required to adjust the cycle operation, and the operator should have an experienced background. On the other hand, steady-operation cycle parameters can be based on engineering calculations. This approach will give the designer a good estimate of what is expected from the installation and an understanding of the operation so that he can later analyze performance and make adjustments.

Early methods of design include the procedures of Beeson, Knox, and Stoddard[25] and Foss and Gaul.[26] The Foss and Gaul method is somewhat easier to discuss. Their approach is to assume a slug size and base the maximum pressure of the buildup on the casing pressure required to lift the slug to a given surfacing velocity. After determining the appropriate cycle pressures, the gas requirements of the cycle are calculated using the known volume of the well's tubular goods and the previously calculated pressures. Subsequently, Hacksma modified the presentation of calculated performance to operating curves that are better suited for cycle analyses and optimization.[27] Both investigators were primarily concerned with producing oil wells. More recently, Lea studied the dynamic plunger cycle and the application of plunger lift to unloading gas wells.[28] In addition to developing a dynamic mathematical model, Lea presents data that indicate the Foss and Gaul calculation[26] overpredicts required buildup pressure as far as velocity-related friction pressure drop is concerned. Corrections are given to adjust the Foss and Gaul method to the dynamic cycle. Further discussion of the work by these investigators is given below as an aid in understanding plunger operation and in making design calculations.

6.241 DESIGN CALCULATIONS

Foss and Gaul assume isothermal expansion (at average well temperature) of the lift gas in the casing annulus and a plunger surfacing velocity of 1,000 ft/min to calculate the minimum casing buildup pressure.[26] The base pressure, P_{C-min}, is calculated when the liquid slug and plunger just reach the surface where:

$$PL = P_S + P_{PF} + (P_{LH} + P_{LF})L \quad (6.43)$$

$$P_{C-min} = (1 + D/K) \times PL \quad (6.44)$$

$$P_{C-max} = [(P_{C-min})CPR]\left(1.0 - \frac{\%\ \text{formation gas}}{100}\right) \quad (6.45)$$

$$P_{C-avg} = \frac{P_{C-max} + P_{C-min}}{2} \quad (6.46)$$

where:

PL = sum of static and liquid pressure acting on plunger as it nears the surface, psi
P_{C-min} = casing pressure when liquid slug reaches the surface, psi
P_{C-max} = casing pressure at start of plunger rise cycle, psi (i.e., max. buildup pressure)
P_S = surface line pressure, psi
P_{PF} = pressure required to overcome plunger weight and friction losses, psi (assume 10 psi in design calculations)
P_{LH} = tubing column pressure of liquid slug, psi/bbl
P_{LF} = instantaneous friction loss of liquid, psi/bbl
D = well tubing depth, ft
L = slug volume per cycle, bbl
K = gas friction factor constant
CPR = casing pressure ratio factor assuming all lift gas is supplied by casing gas; this is the ratio of annulus plus tubing volume to annulus volume
$CPR = (SV_A + SV_C)/SVA$

SV_A = specific volume of casing annulus, ft²/lin. ft
SV_C = specific volume of tubing, ft²/lin. ft

The gas friction term is (1 + D/K). Gas friction depends on gas density as defined by pressure term PL and the gas velocity. The gas friction loss h_{fg} is defined by Darcy's pressure drop equation as:

$$h_{fg} = \text{friction pressure loss, psi}$$
$$= F\left(\frac{D}{d}\frac{V^2}{2g}\right)\frac{PL}{144} = \left(f\frac{D}{d}\frac{V^2}{2g}\right)\times\left(\frac{\text{mol}\times\text{wt}\times PL}{ZRT}\right)$$
$$= PL\frac{D}{d}\left(f\frac{V^2}{2g}\frac{\text{mol}\times\text{wt}}{ZRT}\right) = P\ D/K \qquad (6.47)$$

where:

P = PL, pressure term, psi
D = tubing depth, ft
d = tubing ID, ft
K = constant for gas friction (these were apparently adjusted to fit field data by Foss and Gaul and not calculated by formula)

The base casing pressure, P_{C-min} is:

$$P_{C-min} = [PL] + \text{gas friction}$$
$$= [PL] + [PL]\ d/K$$
$$= PL\ (1 + D/K) \qquad (6.48)$$

The P_{C-max} for the case where the plunger lift gas is made up entirely from the annulus is:

$$P_{C-max} = (CPR)\ P_{C-min} \qquad (6.49)$$

(1) *Calculating the gas volume for a specific slug size.* Lift gas fills the tubing as the plunger rises to the surface. The minimum gas volume required to lift the slug is contained in the tubing volume (ft²) and is corrected to operating pressure, P_{C-max}, and the average well temperature. P_{C-max} is used because the minimum quantity of gas produced on each cycle is the top gas above the plunger when the pressure is at P_{C-max}. However, some additional gas may leak past the plunger as it is surfacing.

The normal design procedure is to assume two or more slug sizes and calculate P_{C-min} and P_{C-max} as shown above. The results of this calculation step are presented on a graph such as shown in Figure 6.16. Note that this may be the most useful information that can be obtained from analysis. The maximum casing pressure is required before the tubing is opened and the plunger surfaces. Greater shutin pressure restricts formation flow. Less shutin pressure may not surface the plunger. The minimum casing pressure is not very useful, showing only the pressure as the plunger arrives. Both values are conservative unless they are corrected for gas flow into the well as the plunger surfaces. Next, the volume of gas required for each assumed slug size can be calculated as shown below:

$$VT = \text{absolute volume of tubing, ft}^2$$
$$= SV_T \times \text{tubing depth}$$
$$VG = \text{volume of gas filling tubing at } P_{C-max}\text{, Mscf/cycle}$$
$$= \frac{VT}{1{,}000}\times\frac{P_C}{14.7}\times\frac{(520)}{T}\times\frac{1}{Z}C \qquad (6.50)$$

where:

T = average well temperature, °R
Z = gas compressibility (Refer to *NGSMA Handbook* or other reference)
P_C = pressure of casing, use P_{C-max} for design
$C = 1 + \left(\frac{0.02\ D}{1{,}000}\right)$ = gas slippage correlation factor assuming 2%/1,000 ft slippage from examining Foss and Gaul data

The results of these calculations are presented on a graph of scf/cycle vs slug size as shown on Figure 6.17. Figures 6.16 and 6.17 fully define the cycle parameters for the well data used in the calculations.

The minimum GLR for plunger lift to work is calculated from the slope of the "gas required" line in Figure 6.17. Assuming the gas requirements for 1-bbl and 3-bbl slug sizes have been calculated, the minimum GLR can be calculated as follows:

$$GLR_{min} = [(\text{Mcf/cycle})3\ \text{bbl} - (\text{Mcf/cycle})1\ \text{bbl}] \div (3\ \text{bbl} - 1\ \text{bbl})$$

If the producing GLR is greater than the minimum GLR, the well can operate at any point right of the intersection of the producing GLR line and the gas requirement line as shown on Figure 6.17. The minimum slug size indicated by this calculation must, however, be within the capability of minimum cycle trip time. Minimum trip time for this example is based on 2,000 fpm fall velocity and 1,500 fpm (high) rise velocity. Therefore, trip time is 3.5 min times a well depth of over 1,000. The average trip time may require adjustment in the field because of actual well condition and cycle pressures.

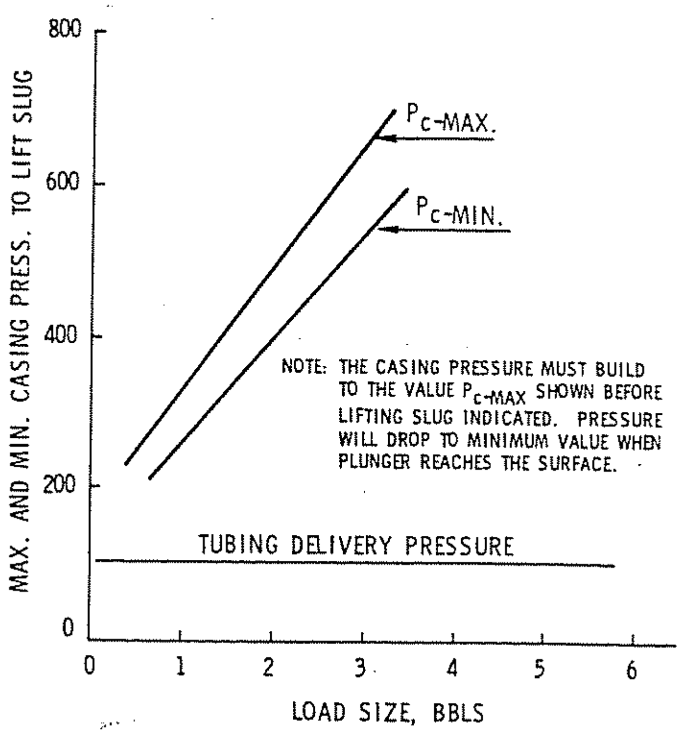

Figure 6.16 Casing Pressure vs Load Size for Plunger Lift in 2⅜-in. Tubing Landed at 7000 ft

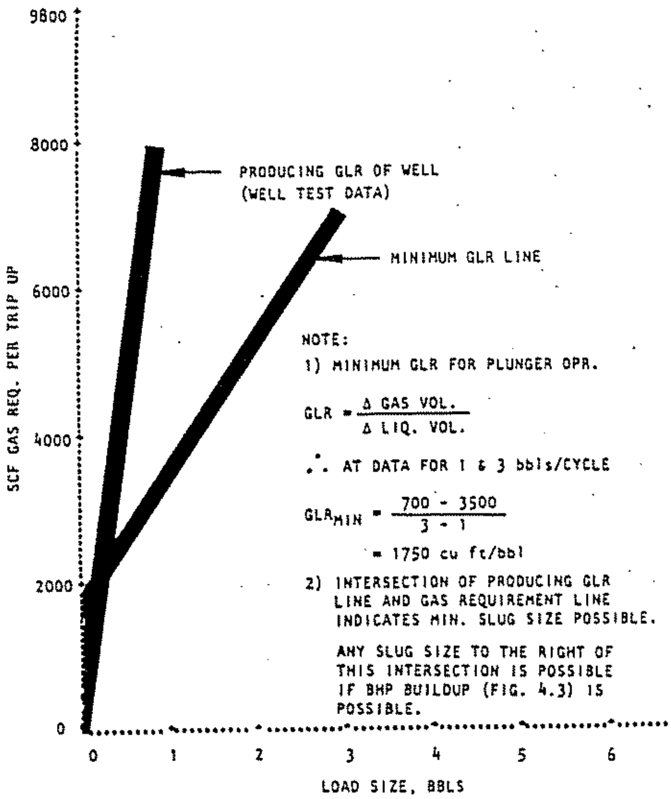

Figure 6.17 Operating and Minimum Gas Requirements for a Plunger Lift Installation

In the original paper by Foss and Gaul, the velocity used to calculate friction terms was 1,000 fpm.[2] Although this was for use in a surface force balance, the value of 1,000 fpm selected was obtained from average rise velocities measured in the field. Lea has developed a program to calculate the actual surfacing velocity based on a dynamic model.[28] This program calculates forces on the plunger and slug (Figure 6.18) equal to mass and acceleration and then integrates as the slug and plunger travel uphole. Assuming both the Foss and Gaul and the Lea methods incorporate an average plunger velocity of 1,000 fpm, the dynamic program gives a lower surfacing velocity and corresponding lower P_{C-min}.

A comparison between the results of the two methods was done by Lea. Lea's work shows how to calculate first hand Foss and Gaul's required casing pressure and then lower the value to the casing pressure required as calculated from the more detailed dynamic method.

(2) *Application of results.* The graph of P_{C-max} vs slug size (see Figure 6.16) is a very useful graph. This graph tells the user what casing pressure the well must build to lift the plunger and slug of liquid before the well is opened at the surface and the plunger is allowed to rise. For instance, if the plunger has been held at the surface and gas has been allowed to flow from the well, the casing pressure is low. When the well is closed in, the casing pressure builds. If the average slug size is, say, 1 bbl, then using Figure 6.16, the casing pressure must be allowed to rise to a value of about 350 psi (using well conditions similar to those used to generate this figure). Anything higher will simply hold unnecessary pressure on the formation, thereby reducing production. Lower values may not surface the plunger and slug.

Figure 6.17 presents the gas required for a single cycle. This graph gives the minimum gas required for a given load size if the plunger is recycled as soon as it reaches the surface without additional gas production while it is at the surface. The natural or producing GLR is also shown. Note that any cycle must operate to the right of the intersection of the required gas curve and the natural well GLR curve. This plot graphically illustrates whether the well has a natural GLR above the minimum required to operate a plunger.

If the selected operating point (slug size) is right of the intersection, the well can be produced following plunger surfacing. For high-GLR wells, it may be typical to select an appropriate slug size, say 2% of tubing volume, and allow sufficient gas flow following plunger surfacing to accumulate the design slug size, assuming no liquid production during the low-volume gas production cycle. After blowing excess gas, shut the well in to begin the lift cycle. A few plunger cycles can provide an estimate of the blowdown period necessary to accumulate near the design slug, to blowdown excess gas, and still not require an excessive buildup time to restore casing pressure to the minimum required to lift the slug.

If the well is initially loaded with liquids around the wellbore, a few short cycles will speed up the unloading and restoration of gas permeability. It is more advisable to begin with a clean well by swabbing out

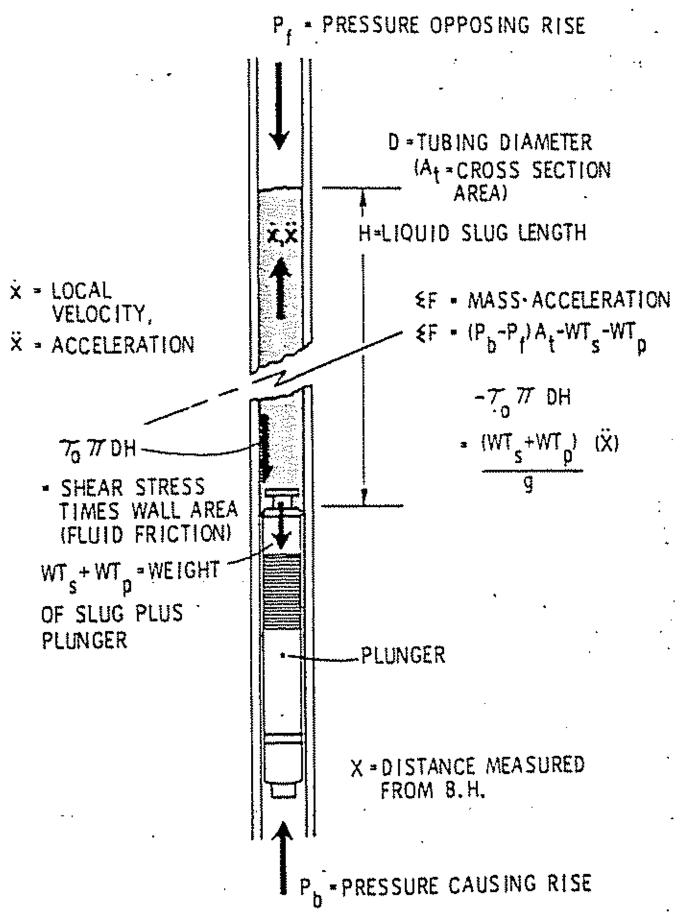

Figure 6.18 Forces Acting on Plunger and Liquid Slug

liquids before commencing plunger operations. However, the buildup pressure before each plunger surfacing must at least reach the P_{C-max} indicated for the slug size. For initial operation, the casing pressure can be allowed to exceed the calculated required well shutin pressure and then gradually be reduced to near-target design values by lowering the pressure in pressure increments (≈10 psi) with perhaps a day between adjustments.

6.25 PLUNGER LIFT EQUIPMENT CONSIDERATIONS

6.251 PLUNGERS

Plungers may be generally classified as (1) solid or (2) bypass plungers. The difference is that the bypass plunger has a passage through the center of the plunger with a shifting valve that is opened by the wellhead lubricator and is closed by the bumper spring when it reaches the bottom. The passage through the plunger allows the plunger to fall faster, thus reducing its chances of sticking in the tubing. Bypass plungers may sometimes fail because of bending of the valve push rod as the plunger strikes the lubricator, particularly if the plunger surfaces dry with a high velocity. Solid plungers, or plungers with the bypass valve removed and the bottom plugged, are generally satisfactory for intermitting wells that have shutin times sufficient for the plunger to fall to bottom (allow about 2 min/1,000 ft in gas and 1 min/100 ft in liquid).[26,29]

Plungers can also be described according to the seal mechanism. Plunger seals may be expanding pads, wobble washers, spiral ribs, or brush types. Figure 6.19 illustrates some types of plungers.

The expanding steel pad type of plunger utilizes a series of interlocking spring-loaded steel pads to provide a liquid seal against the tubing wall. The pads expand on plunger rise to form a tighter seal with the tubing ID. The expanding-steel-pad solid plunger has proven to be effective in many installations. The stainless-steel pads are cast to conform to the nominal ID of the tubing when expanded on the upstroke of the plunger. A cam mechanism in the tool is activated in the lubricator to retract the seals and effect a 0.25-in. reduction in plunger OD for bypass clearance on the tool's downward stroke. It is suited for paraffin removal since it falls through the paraffin in the retracted position and only wipes the tubing on the way up.

The wobble-washer plunger (not shown in Figure 6.19) has twenty-three shifting washers, including ten hard, chrome-plated, mechanically shifted washers, which are spring loaded and placed in the middle of the plunger body to provide a continuous wiping action against the tubing wall. The positive wiping action will also remove paraffin from the tubing wall.

This plunger was offered with a variety in which the bumper spring is fixed to the bottom of the plunger and travels with the plunger each run. The bottom of the bumper spring stops at the seating nipple. This type has the advantage that, when it is caught and removed at the surface, the tubing is completely clear and operations such as running a bottom-hole pressure bomb can be conducted without fishing the bumper spring and standing valve, although the spring adds weight and friction.

The spiral rib and brush types (Figure 6.19) are called turbulent seal types of plungers. The spiral rib type of plunger forms a turbulent seal against the tubing wall as fluid from the wetted wall of the tubing is swept into the recessed areas of the hardened steel spiral packing. Similarly, the brush type of plunger forms a turbulent seal with the bristles against the tubing wall. The brush type is sometimes used in wells with sand or scale problems, but its bristles are subject to rapid wear. Neither the spiral rib nor the brush type of plunger has been as popular as the expanding-steel-pad or wobble-washer plungers.

Most plungers weigh about 10–15 lb in the 2⅜-in. size. The weight is accounted for in design calculations.

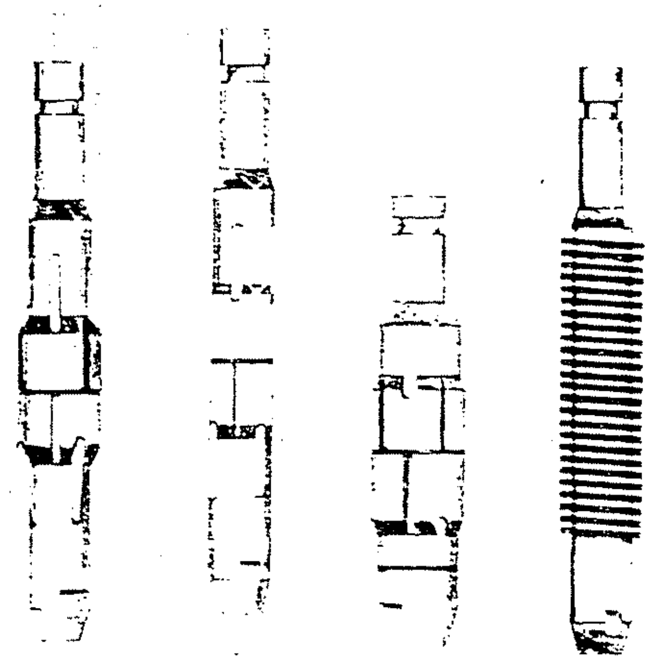

Expanding Blades Activated By Push Rod *Spring-loaded Blades Miniflex* *Brush Plunger*

Figure 6.19 Some Types of Plungers

6.252 LUBRICATORS

Each plunger installation must be equipped with a lubricator mounted above the tubing master valve. The lubricator contains three essential elements: (1) a shock-absorbing spring and striker plate mounted in the top, (2) a plunger-catching device, usually a rod or valve stem mounted on the side of the lubricator, which can be inserted into the bore of the lubricator below the plunger to prevent its downward travel, and (3) an easily removed top to allow removal of the plunger for inspection or replacement.

Generally, it is desirable to use a lubricator that is rigged with two outlets as shown in Figures 6.14 and 6.20. This allows the plunger to rise until it strikes the spring and striker plate near the top outlet, where it remains during production flow. Gas passes around the plunger to the top outlet, but most production flows through the lower outlet below the plunger. The flow line on the bottom outlet may be equipped with a valve or choke so that the pressure at the lower outlet can

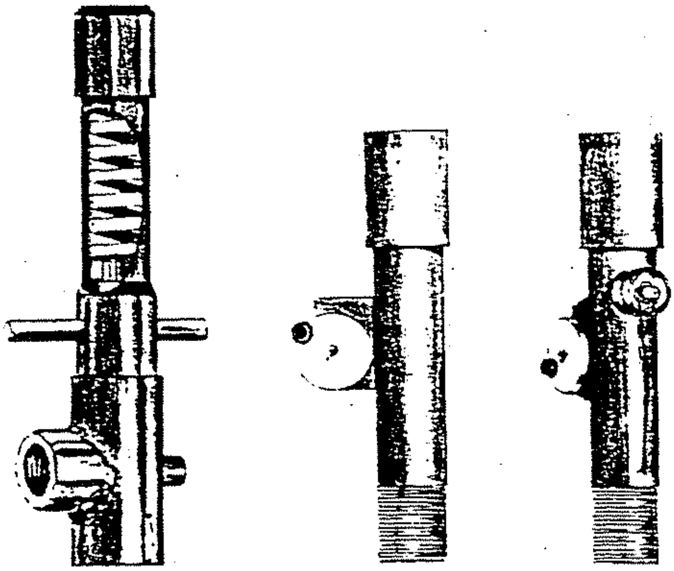

Figure 6.20 Plunger Lift Wellhead Equipment

be set to maintain about 5-psi pressure differential across the plunger. This arrangement accomplishes two objectives: (1) it causes the plunger to travel to the uppermost position in the lubricator so that the bottom outlet is cleared for production flow and the plunger is in position to be captured, and (2) only the top outlet experiences restriction to flow. This is particularly important to minimize the choking effect sometimes seen as the liquid slug passes through the wellhead equipment. Unnecessary choking contributes to liquid fallback, higher pressures, and reduced production.

Most manufacturers can also equip the lubricator with a device to signal plunger arrival. This device can be a magnetic trip switch or a simple lever-probe into the bore of the lubricator (see Figure 6.20). The action of the device can be rigged to capture the plunger or to shut the well in and allow the plunger to fall for another cycle. The latter arrangement is sometimes used initially to unload wells because it does not allow gas production after plunger arrival, thereby saving gas energy for making rapid cycles.

6.253 CYCLE CONTROLS

There are two basic types of primary-cycle control for gas wells: (1) the time-cycle controller, and (2) the high-low pressure controller. An electronic controller incorporating features of the basic controllers is also offered. Moreover, the basic cycle controller can be supplemented with auxiliary controls to limit peak gas flow to keep the recording orifice differential on the chart.

(1) *Time-cycle controller.* The time-cycle controller is more applicable to wells that are capable of long flow periods between plunger cycles—i.e., high-productivity formations where casing pressure may stay, during the flow cycle, at nearly constant pressure before slowly increasing (as seen on the example cycle in Figure 6.15) so that a low set pressure is not clearly defined. Flow periods may be longer than shutin periods. The cycle timer may be a spring-driven, gas-driven, or electronically (battery) driven clock. Timing lugs on the time wheel trip the control switches as they make or break contact.

(2) *High-low pressure controllers.* High-low pressure controllers are easy to adjust and have better characteristics for low-productivity (tight formation) gas wells where casing pressure is easily depleted to a reasonably low pressure. The flow period may be shorter than the shutin period. Moreover, for these low-rate wells, the cycle should be shut in on low pressure before the flow period continues to the point where sizable quantities of liquid accumulate in the tubing. A low gas flow rate provides insufficient velocity for unloading the liquid. The high-low pressure controller is adaptable for use with a plunger trip switch to shut the well in upon plunger arrival. Controllers of this type are effective in unloading stored liquids because the cycle frequency is maximized while lift-gas use is minimized. Once excess liquids have been removed, the controller can be returned to the high-low pressure control scheme.

(3) *Electronic controllers.* The electronic controller is basically a time-cycle control with a digital display of the cycle time. The unit is powered by batteries and uses solid-state circuits for accuracy and longer battery life. Cycle setting is made by entering an ON period (mode) and an OFF period (mode) into the control. Selection for the length of time of each mode is from 1 min to 99 hrs and 99 min. The control then repeats the setting of each mode to form the cycle time. This is a distinct advantage over the mechanical timer, which uses the 24-hr timing wheel where cycles must be divisible into the number of lugs on the wheel. Other equipment includes external sensors such as high-low pressures for casing or tubing, plunger arrival shut off, high-liquid-level shut down, or differential monitors that are connected to the terminal board in the controller panel. These units may be connected in such a way that they will suspend all timing in the off mode, or they may just override the time and switch to the next mode. Any number of sensors can be used on one control at one time. Since these are electric-switch sensors, there are no high-pressure lines connected to the control panel, which is a definite safety feature. Typically, this type of controller operates on a high-low pressure setting, but the time-control feature is utilized to shut the well in if the plunger stalls and the pressure cycle is taking too long for some reason. Also, the line pressure is monitored and the cycle is interrupted if the line pressure is too high for normal plunger rise. This type of controller has proven successful in field operations.

(4) *Intermitting valves.* The intermitting valve is a pneumatic or solenoid control valve that is opened and closed by signals from the cycle controller. The valve is sometimes located in the flow line near the well, or it may be located in the line downstream of the production separator if it is nearby. If the well is equipped with its own gas production unit, it may be desirable to locate both the controller and control valve at the production unit for easy winterization.

(5) *Throttles.* Restricting the rate by choking to eliminate the off-the-chart excursion of the orifice open-

ing is sometimes necessary to get good gas measurement. The initial flow spike is usually short-lived, and installing a larger orifice plate to measure the peak production rate causes much of the remaining gas flow to record very low on the gas chart, a region where meter-reading accuracy also decreases. The problem of getting good orifice meter readings for the flow spike as well as the low flow rates near the end of the flow period can be accomplished by installing an orifice plate sized to read the low flow rate above the first unit on a square-root chart and temporarily choking the well production during peak flow. To do this, another orifice (sometimes a union fitting with an orifice plate and pressure taps) is installed in the flow line (see Fig. 6.14), and a set-point pressure controller monitors the differential reading across the orifice. The controller set point is adjusted to throttle closed the intermitting valve when the meter differential reaches the maximum desired differential chart reading (say, 9 on a square-root chart) and tends to open the intermitting valve when the differential is lower than the set pressure. There are other ways to handle metering problems such as a wide-range differential transducer or a gas turbine meter (if allowed), but the method described above is effective and inexpensive if it controls only a short time spike with much flow reduction.

Choking is sometimes advisable for safety reasons in that if the plunger is ever "blown up" dry it can do damage to the lubricator and the plunger if traveling too fast. This may, in particular, be advisable during the adjustment period and until one is certain that a liquid load will always be above the plunger, since the liquid will act as a cushion upon surface arrival.

(6) *Supervisory instrumentation.* To analyze and optimize a plunger installation, it is necessary to have the production metered and tubing- and casing-pressure history throughout the cycle. If available, 24-hr recording meters are better than multiple-day meters for seeing details in the plunger cycle. Two-pen pressure recorders on the casing and tubing are very helpful in showing a summary of pressure information so that performance can be evaluated on a per-cycle basis or compared to previous cycles when well performance changes or adjustments are made to the plunger cycle. Two-pen pressure recorders are recommended, especially for problem wells.

To facilitate cycle evaluation or to make adjustments on wells with inadequate supervisory instrumentation, a portable testing unit with a 24-hr gas production meter, liquid measurement meters, and a two-pen pressure recorder for annulus and tubing pressure is suggested. Having adequate cycle information to evaluate and adjust plunger cycles will minimize the operator's time and help diagnose well problems or down time.

6.254 CASING SIZE

Casing size, or more specifically, the casing-tubing annulus volume, has a bearing on the maximum casing buildup pressure required to surface the plunger in a liquid slug. When the plunger rises, gas stored in the annulus flows into the tubing to maintain lift pressure under the plunger. This high-pressure casing gas expands on plunger rise as the volume increases from the annulus volume to the annulus plus tubing volume. Therefore, the larger the casing annulus, the lower the buildup pressure has to be to provide the minimum casing pressure required to surface the plunger. This, of course, is accounted for in analyses like the Foss and Gaul method.[26] A minimum casing size of 5½ in. is recommended for wells drilled in fields where plunger lift may have application.

6.255 TUBING SEATING NIPPLE AND STANDING VALVE

It is common to run tubing with the seating nipple at or near the bottom of the tubing in a gas well (see Figures 6.14 and 6.21). This will facilitate subsequent installation of a pump or plunger to unload liquids. If the well is to be placed on plunger lift, a bumper spring (Figure 6.21) can be run on a wire line and landed in the seating nipple. If a seating nipple is not installed in the tubing, it would be necessary to wire line a tubing stop into the well as a seat for the bumper spring. If the well has a seating nipple installed, a plunger with bumper spring attached to the bottom of the plunger can be simply dropped into the tubing when it is time to put the well on plunger lift.

Many wells are equipped with a standing valve (ball and seat) landed in the seating nipple. The purpose of the standing valve is to retain liquid not produced during the flow cycle in the tubing. Otherwise, there is a possibility that liquid, which can be squeezed back in the formation or drop out as the plunger surfaces, may flow from the tubing to the annulus when the well is shut in for the buildup cycle. With the liquid

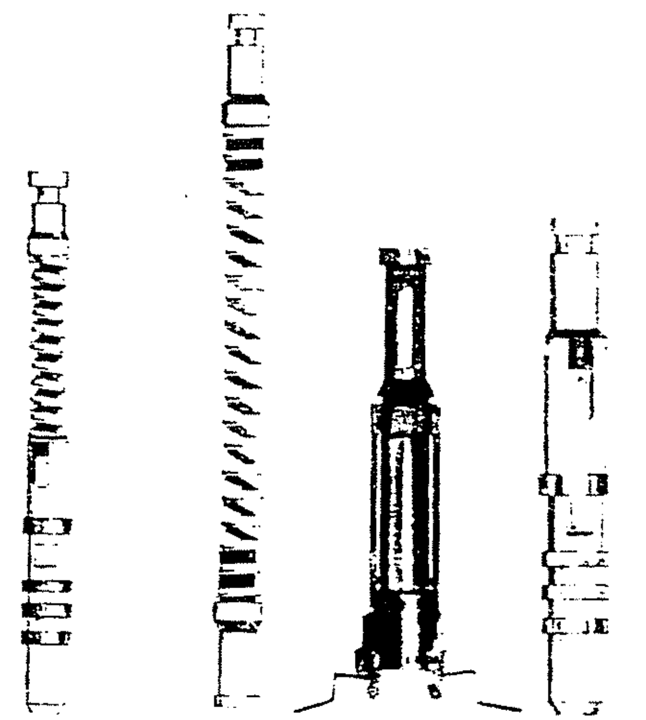

Figure 6.21 Downhole Plunger Lift Equipment Combination Standing Valve with Bumper Bottom-hole Bumper Spring Collar Stop Standing Valve

retained in the tubing, most of the liquid accumulated in the wellbore is above the plunger on the next cycle. Many operators, however, prefer not to use a standing valve, particularly on marginal producers. The reason is that, if a well cannot be kicked off because of a large liquid slug buildup, a well without a standing valve can be shut in until the pressure buildup can be adequate to drive a portion of the liquid back into the formation and the remaining tubing load is then within the operating range of the available pressure. The well can thus be restored to production without swabbing. A good understanding of plunger cycle design and good well-control equipment will largely eliminate upsets of this nature. A standing valve should not be necessary if the tubing is landed at the bottom of the completion interval since essentially all of the liquid will be forced into the tubing.

6.256 TUBING SIZE

Tubing size has a very great influence on cycle buildup pressure and minimum GLR requirements. Figure 6.22 illustrates the effect of tubing size (represented by the bar graphs) on the pressure buildup required to operate plunger lift in a well. Notice that reducing the tubing size in a marginal producing well to increase tubing velocity for continuous flow unloading (production) of liquids is in an opposite direction to using the larger tubing size to minimize the slug height and, hence, pressure buildup on plunger lift installation. Off-the-shelf plungers are available down to 1½-in. tubing size, while 2⅜-in. plungers are the most commonly used size.

The tubing must not have internal upset, and it should always be broached (gauged) to drift diameter if a close tolerance plunger is run. If the tubing has scale or paraffin buildup, or if the tubing is crimped in the slip area, the plunger may not travel freely.

6.257 TUBING LANDING DEPTH

It is best to land the tubing near the bottom of the perforation interval or as low as possible if it is desirable to stay above the perforations. The tubing should be landed a short distance above the completion interval only if salt or scale dissolution and deposition have been experienced in the field. If the tubing is landed at the bottom of the completion zone so that the liquid level does not cover the completion interval during the production cycle, deposits can plug the formation more rapidly.

Sometimes in wells with high fluid levels, the tubing has been landed high so that the resultant slug size is not too large for the available well pressure. Although this may enable the well to operate if the liquid column below the plunger does not reduce flow too much, it does not adequately unload the well because successive cycles cannot remove liquids in the wellbore down to the point where a small amount of fluid covers the completion zone. It is better to land the tubing at the optimum depth and swab or otherwise produce the liquid until the fluid level and gas production reach operating levels.

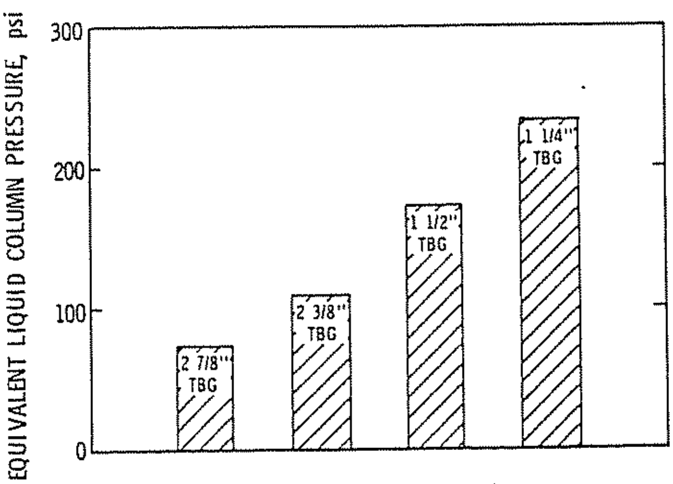

Figure 6.22 Relative Liquid Column Pressure of 1 bbl of Liquid as a Function of Tubing Size

6.26 WELL SYMPTOM ANALYSIS

Observations of casing and tubing pressures throughout the cycle can help identify and correct deficiencies in plunger operation.

(1) *Plunger fails to rise.* This can be seen on the gas chart as restricted gas flow and the pressure recording as a continuing pressure decline of the tubing pressure following the opening of the intermitting valve. This may be due to downhole-plunger sticking or insufficient gas-lift energy. The latter should be suspected if there has been a general increase in the casing-tubing differential on preceding cycles or an increase in line pressure.

(2) *Fast plunger rise and/or abnormally low liquid production.* This condition would indicate the plunger may not be traveling all the way to the bottom. Incomplete travel indicates shutin time is too short or there is a tight spot in the tubing.

Combined with evidence of lubricator damage or plunger damage, this condition would also indicate the liquid slug is too small and/or the buildup pressure is excessive on repetitive cycles. The plunger is surfacing at excessive velocity because of the light liquid load.

(3) *High casing-tubing differential pressure combined with very low flow rate (50–100 Mcfd) gas production.* This condition is somewhat typical of a very tight formation gas well. Gas velocity and volume during the peak flow period following plunger arrival are insufficient to unload liquids under the plunger. Plunger cycles become long and erratic because of variations in the apparent liquid slug size, and the plunger may fail to surface with a normal buildup pressure. The use of a bottom-tubing standing valve should be considered or checked to ensure the tubing is landed near the perforations.

Plunger performance on this type of well has also been improved by using foam surfactant injection in conjunction with the plunger. About 0.1% foam surfactant (usually diluted to make a larger volume for continuous injection) based on the water rate is injected down the annulus. During plunger rise, the turbulence of a gas flow through the liquid, both above and below

the plunger, generates a foam that tends to be more effectively unloaded by the available gas during afterflow. In low-permeability formations, a production increase results from this small improvement in reducing well back pressure, but the principal benefit is more consistent plunger operation. In some very low rate wells (30–40 Mcfd), surfactant injection has deferred abandonment or eliminated the use for much more costly deliquefication methods.

(4) *Buildup analysis.* While referring to Figure 6.23, the following cases can be interpreted from the casing-tubing differential pressure buildup characteristics:

Constant Differential, Case 1:
Constant differential indicates little or no liquid production during the shutin period, and the liquid in the tubing remains in the tubing. The buildup rate is proportional to the gas entering the well; the annulus liquid level is at the bottom of the tubing, and produced gas feeds both tubing and annulus. Differential ΔP_B represents the liquid slug to be lifted on the next cycle.

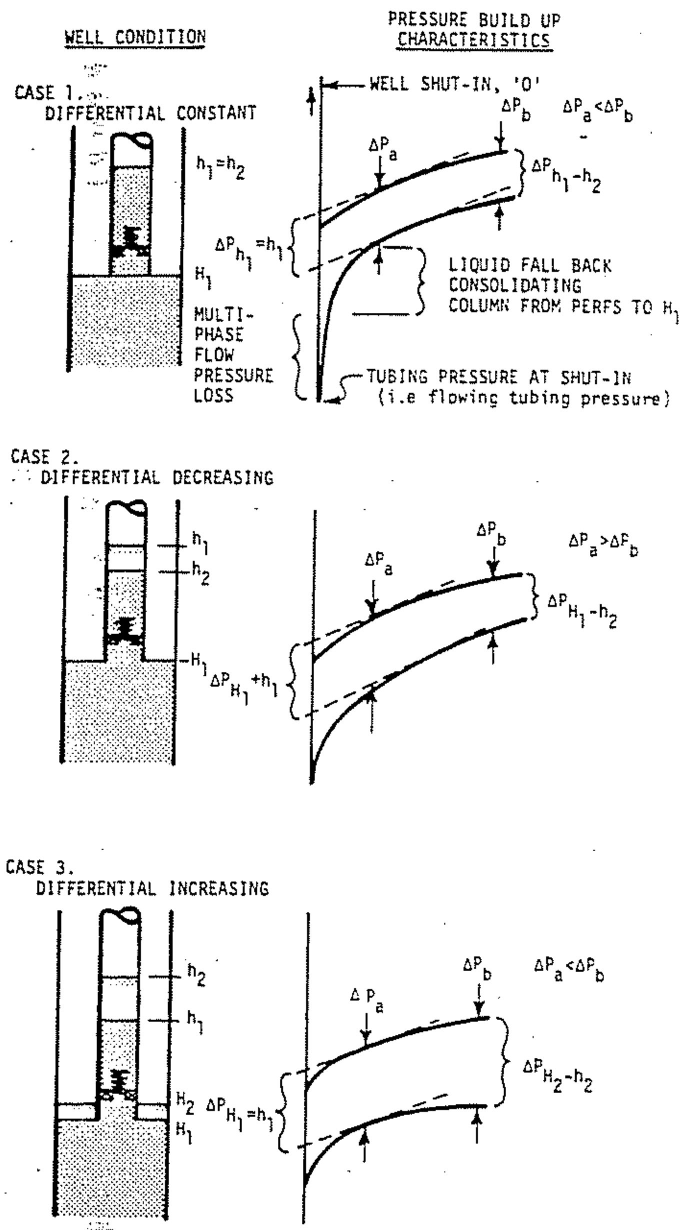

Figure 6.23 Pressure Buildup Analysis

Differential Decreasing, Case 2:
A decrease in the casing-tubing differential during the latter part of the buildup cycle indicates the tubing is losing liquid. Fluid flows back to the annulus (annulus pressure does not change significantly because the annulus capacity is large compared to the tubing capacity), and/or fluid may be pressured into the formation. This can be remedied by landing the tubing near the bottom of the perforation interval, by installing a standing valve at the bottom of the tubing, or by reducing the flow period and making more rapid cycles. All techniques tend to reduce the liquid accumulation in the annulus. To ensure plunger rise on the next cycle, the buildup pressure should allow for the lifting of the liquid column represented by the largest ΔP (ΔP_A) seen during the buildup cycle. If possible, the liquid production should be measured over several cycles to better define the typical load size.

If liquid has been pressure-squeezed into the formation, it will be produced on a subsequent cycle; however, it may not be produced as the next slug. During the production cycle, the liquid squeezed into the formation will flow through the formation permeability channels; thus, it will slowly feed into the wellbore. When liquid is pressured into the wellbore, the permeability to the gas is reduced, and loss of gas flow rate can occur.

Differential Increasing, Case 3:
An increasing differential indicates gas separation to the annulus, and gas pressure increases rapidly in the annulus while the liquid is forced into the tubing. There is possibly a liquid seal on the tubing, which retards gas flow into the tubing such as would be the case when the tubing is landed at the bottom of or below the completion interval. Generally, tubing landed at the bottom of the completion interval will give good gas separation, and pressure forces the liquid into the tubing.

6.3 FOAM UNLOADING OF GAS WELLS

6.31 INTRODUCTION

Foams have several applications in oil-field operations. They are used as a circulating medium for drilling wells and for well cleanouts and as fracturing fluids. These applications differ slightly from the application of foam as a means of removing liquid from producing gas wells. The former applications involve generating the foam at the surface with controlled mixing using only water. In gas-well liquid-removal applications, the liquid-gas-surfactant mixing must be accomplished downhole—often in the presence of both water and liquid hydrocarbons.

The principal benefit of foam as a gas-well deliquefication method is that liquid is held in the bubble film and exposed to more surface area, resulting in less

gas slippage and a low-density mixture. The foam is effective in transporting the liquid to the surface in wells with very low gas rates when liquid holdup would otherwise result in sizable liquid accumulation and/or high multiphase-flow pressure losses. Figure 6.24 shows a laboratory test comparison of tubing-pressure gradient with surfactants vs flowing gradients when surfactants are not used. This figure generally illustrates the potential for pressure-gradient reduction realized with foam and the range of producing conditions where foam has application.

6.32 LIQUID REMOVAL PROCESS

Foam is a particular type of gas and liquid emulsion in which gas bubbles are separated from each other by a liquid film. Surface-active agents (surfactants) are generally employed to reduce the surface tension of the liquid to enable more gas-liquid dispersion. The liquid film between bubbles has two surfactant layers back-to-back, with a liquid contained between them. This method of tying the liquid and gas together can be effective in removing liquid from low-volume gas wells.

Water and liquid hydrocarbons react differently to surfactants. Liquid hydrocarbons do not foam well. This is particularly true for light condensate hydrocarbons. Gas-condensate bubble dispersion can be accomplished, but the resulting foam is not stable and will readily separate. Light hydrocarbon liquids must be continuously agitated to maintain foaming. One reason why hydrocarbons do not foam well is because hydrocarbon molecules are nonpolar and therefore have less molecular attraction forces between molecules. On the other hand, water molecules are polar and can build relatively high film strengths with surfactants. When both water and liquid hydrocarbons are present in the wellbore, foam is created mainly within the water phase, and the water foam assists in carrying along the liquid hydrocarbons. Laboratory observations indicate that, when both water and light hydrocarbon liquids are present, the liquid hydrocarbons tend to

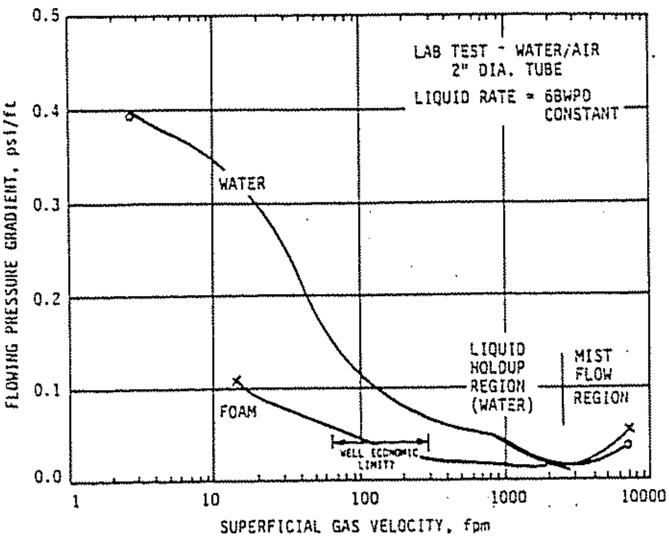

Figure 6.24 Producing Gradients in Lab Column Test at Atmospheric Pressure

emulsify, and the foam is generated in the external water phase.

The percent of gas in the foam mixture at operating pressure and temperature is termed foam quality—i.e., a foam that is 80% gas is called 80-quality foam. Referring to Figure 6.25, the foam appears as a gas-liquid emulsion where the foam quality is less than about 50%. This type of foam or gas dispersion is unstable (gravity forces will separate the liquid and gas phases). At higher foam qualities, the liquid film becomes thinner and distorted because of surface tension. When the foam is nonflowing, it appears in the stable foam form as shown in Figure 6.25 and is relatively stable or persistent. If this foam is caused to flow, a certain minimum stress will be required to overcome the interlocking of the bubble structures. This minimum stress is called a yield point. Thus, foams have an apparent viscosity that is dependent upon the shear rate operating within the moving stream.

Breaking the foam at the surface is accomplished in several ways. Here, foam, if not overly treated with surfactants, will tend to break naturally if it is kept quiescent for a period of time. Liquid drains from the bubble film, and eventually the film ruptures and allows the gas to escape. This is the normal process for foam dissipation. This process may be aided by a further dilution of the surfactant concentration with produced or makeup water. Nonionic surfactants can be heated above their cloud point, indicating a reduction in surfactant solubility and hence lowering the effective surfactant concentration. Surfactants can also be chemically treated with appropriate demulsifier chemicals of the opposite character (see Section 6.364). Liquids are removed in the gas separator.

6.321 UNLOADING TECHNIQUES

Wells are unloaded using two techniques, batch (single-event) treatment or continuous surfactant injection.

(1) *Batch treatment.* Surfactant quantity is based on an estimate of the liquid to be unloaded. Usually, the well is shut in and the liquid load can be determined from the casing-tubing differential. The appropriate surfactant quantity for a 1% surfactant concentration is mixed in 20 gal or more of produced fluid or water and then pumped or lubricated into the tubing. Foam

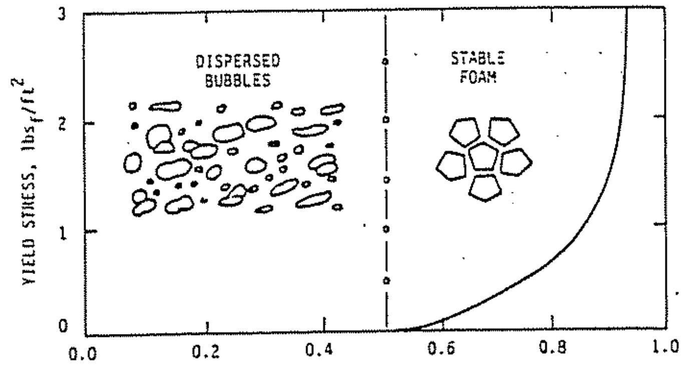

Figure 6.25 Yield Stress Characteristics of Foam

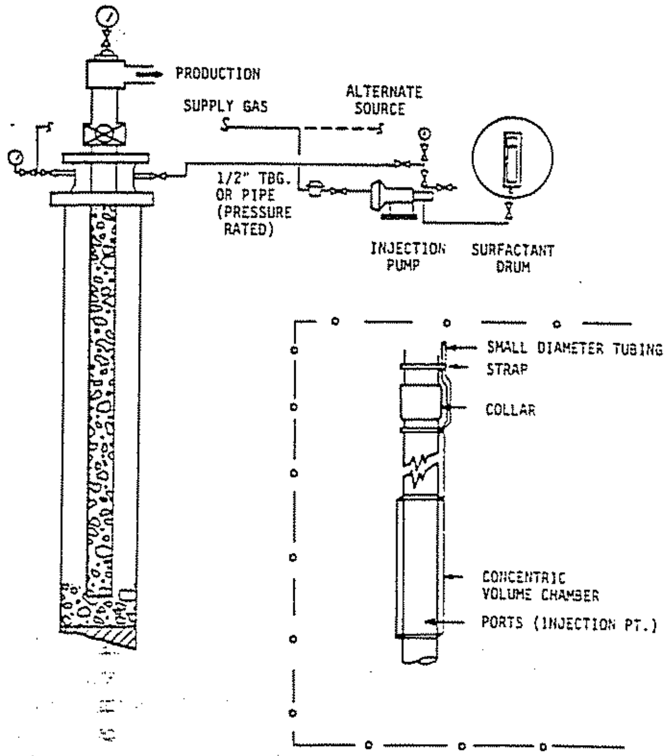

Figure 6.26 Equipment Arrangements for Liquid Surfactant Injection

"soap" sticks can be used in lieu of liquid surfactants. The well is then opened to flow (see Section 6.363).

Batch treatments are best suited to wells that require liquid unloading on an infrequent basis because of the operator's time required to perform batch treating.

(2) *Continuous foam unloading.* Using an appropriate equipment arrangement such as that shown in Figure 6.26, a quantity of surfactant is continuously injected into the wellbore where it mixes with the produced liquid and gas to generate foam. Surfactant injection can be accomplished either down the casing-tubing annulus, or the tubing and the production travels through the alternative path.

6.33 FOAM APPLICATION SELECTION

The application of foam to unloading low-rate gas wells is generally governed by two operating limitations. These limitations are economics and the success of foam surfactants in reducing bottom-hole pressure. Both limits are defined by comparison to other methods of unloading wells. Low-gas-rate wells with producing GLR's between 1,000 and 8,000 ft³/bbl may be among the better candidates for foaming, although there is no upper GLR limit. For high-GLR wells, plunger lift may give better performance—i.e., produce with less bottom-hole pressure than foam. Downhole pumps may be better suited for the lower GLR ranges. The producing gradients expected with foam surfactants are ultimately controlled by the producing rates and well conditions and by the performance of specific surfactants in the well. Lab tests tend to support the assumption that the liquid in the wellbore will form a stable foam ranging between 50 to 85% quality under dynamic conditions. Foam quality appears to vary with the amount

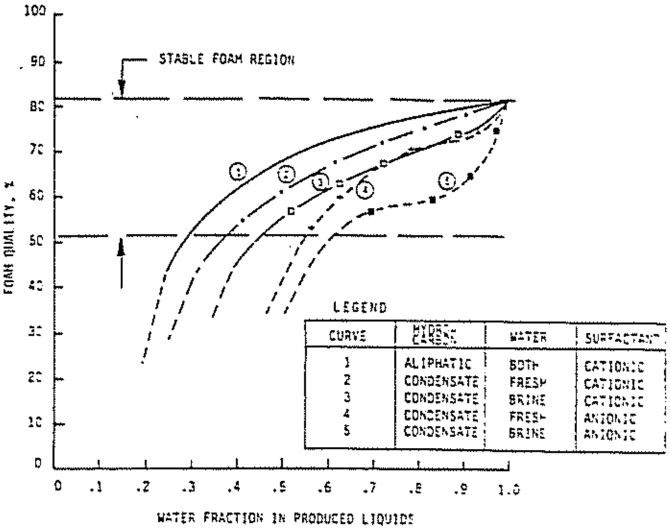

Figure 6.27 Foam Quality in Well Systems

and type of liquids present as shown in Figure 6.27. The viscosity of foam varies with quality and also with the amount and type of surfactant used. Viscosity is reported to vary as a function of foam quality as well as shear rate as shown in Figure 6.28. When quality is above about 52%, foam behaves as a plastic-yield fluid having a plastic viscosity and a yield strength (see Figure 6.25). The yield strength is derived from the interlocking of gas bubbles and the strength of the bubble film.

Foam quality and viscosity can be affected by other surfactant chemicals introduced into the wellbore. Corrosion inhibitors, for example, are packaged with surfactants to make them either water soluble or water dispersible, and they may also contain demulsifiers. Lab tests have evaluated the effect of two filming amine corrosion-inhibitor compounds on foam quality. These tests show that water-dispersible inhibitor with demulsifier chemicals can lower foam quality (up to 10%

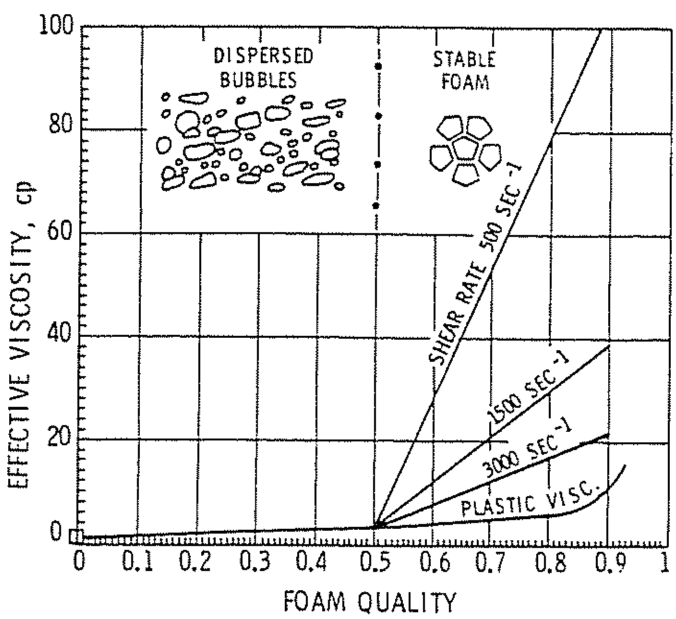

Figure 6.28 Effective Viscosity of Foam as a Function of Quality and Shear Rate (after Blauer, Mitchell, and Kohlhaas)[41]

TABLE 6.2

Advantages	Disadvantages
1. Foam is a very simple and inexpensive method for low-rate wells. Chemical costs are proportional to the liquid-water rate.	1. Surfactant used may result in foam carryover or liquid emulsion problems.
2. No downhole equipment is required. (However, a capillary injection system may be very beneficial to low-rate wells tending to produce in slugs.)	2. The foaming tendency for various systems depends on the amount and type of well fluids and on surfactant effectiveness. Wells producing substantial condensate (say greater than 50% condensate) may not foam.
3. The method is applicable to wells with low gas rate where gas velocities may be on the order of 100 to 1,000 fpm in the production string. The value is about 1,000 fpm for critical velocity in unfoamed wells.	

lower), while the water soluble inhibitor had little effect on foaming. The latter did, however, tend to cause some oil-water emulsion problems.

The economic limitation parameter is a function of chemical costs and equipment costs. Chemical costs are proportional to the liquid (water rate). At some level of water production, chemical costs will approach and exceed the cost of pumping. For example, a well being treated with surfactant costing $8/gal at a concentration of 0.1% will have a chemical cost of 34¢/bbl. It is apparent that the daily cost of a low-liquid-rate well would be minimal.

Use of foaming agents should be curtailed at some locations where experience indicates foam carryover and/or liquid emulsion treating problems are too severe to cope with. Although the cost of surfactant injection equipment is small, the cost for labor, chemicals, additional well equipment, or modification of existing equipment to handle foam carryover and emulsions could be significant.

Foam has also been used in combination with plunger-lift operations to improve the performance and reliability of plunger cycles. Surfactant use on plunger installations appear to be helpful where the gas rate is very low (plunger rise time is long) and/or the gas rate and volume after plunger arrival is insufficient to clear the well of residual liquids unless surfactants are used to minimize gas slippage. This treatment applies to wells where the tubing-casing differential pressure remains relatively high after plunger arrival, thus indicating liquid under the plunger.

Table 6.2 lists some advantages and disadvantages for foam lifting of liquids that should be considered or evaluated before selecting this method for unloading gas wells.

6.34 GENERAL INFORMATION ON FOAMS

The purpose of this section is to provide the reader with some background information on foam surfactants and on the character of foams so he can better understand the liquid removal process and evaluate information supplied by the local chemical company representatives.

6.341 FOAM GENERATION

To produce a useful foam, it is necessary to get a good dispersion of gas and liquid phases (foam generation) and then maintain the bubble film for a useful period of time (foam stability). Foam generation is accomplished through agitation of liquid with gas. This process is enhanced when the surface tension of the liquid is lowered so that gas may more easily disperse throughout the liquid phase. This is part of the role of surfactants. Water has surface tension around 72 dynes/cm, which is generally reduced to the range of 20–35 dynes/cm with surfactants used for foaming. Liquid hydrocarbons also generally have surface tensions in the 20–30 dynes/cm range at lower pressures.

6.342 FOAM STABILITY

Foams begin to deteriorate as soon as they are formed. Excess liquid between surfactant layers drains from the bubble film and results in thinning and weakening of the bubble wall. Liquids in the bubbles below are constantly replenished by the drainage from bubbles above. Also, the bubbles grow as the trapped gas expands until the liquid film becomes thin from drainage and expansion, and eventually the film breaks.

Foam stability can be increased by reducing the liquid drainage rate and by increasing the resiliency of the surfactant layer.[30] Surface and bulk viscosity of the surfactant affects foam generation and stability. A higher viscosity will retard liquid drainage. However, high-bulk viscosities are not attained in dilute solutions of most surfactants, and their surface viscosities are only moderate. Therefore, a surface excess (concentration of surfactant higher than the minimum required to start foaming) of the surfactant is of major importance in producing a stable foam. The surface excess also imparts a property termed surface elasticity. As soon as the bubble expands, the excess concentration is decreased, and an increased surface tension that resists expansion will result; the reverse is true during contraction of the bubble. Thus the surface excess may be sufficient to maintain the surfactant film in spite of some local thinning of the surfactant concentration.

Surfactant effectiveness often passes through a maximum at intermediate surfactant concentrations.[30] A solution that is too dilute will not allow the range of surface effects (surface tension reduction, film elasticity, repair of ruptured bubbles, etc.) required for foaming. A solution that is too concentrated may cause excessive foam stiffness, high apparent foam viscosity, and/or excessive liquid-oil emulsions, as well as increasing the cost of treating the well. Laboratory tests indicate that many surfactants have an optimum effectiveness at about 0.1 to 0.2% concentration in the water phase. (Actually, the concentration should be based on the active quantity of the surfactant in the surfactant mixture as received from the supplier. A surfactant that is 50% active will have 0.5 lb of active ingredient per pound of surfactant. The optimum effectiveness, therefore, may be at 0.5 to 0.1% active concentration in the well fluids.) In water-hydrocarbon liquid mixtures, the optimum water treatment rate can be applied to the total liquid rate. This allows for some surfactant loss to emulsion droplets.

6.343 SURFACTANT TYPES

Surfactant molecules have a water-soluble (hydrophylic) end and a non-water-soluble (hydrophobic) end. Thus, a surfactant contains hydrophylic and lipophylic (oil soluble) constituents that cause the molecule to concentrate at the interface between the water and nonwater phases. When the concentration of the surfactant is such that the interface surface area is completely covered with a maximum number of surfactant molecules, the solute is said to be at its critical concentration. Subsequent additions of the surfactant must enter one of the liquid phases. Therefore, the solubility of the surfactant must be capable of providing a surfactant concentration that will supply surfactants for the large surface area created by dispersed bubbles. Additionally, there are ionic attraction (polar) forces acting between surfactant and liquid molecules, which strengthen the film.

Surfactants can be classified according to their ionic characters as nonionic, cationic, or anionic.[30]

(1) *Nonionic surfactants.* Nonionic surfactants are typically polyoxyethylated compounds of phenols or alcohols. The solubility of most detergents in water increases with temperature, but nonionic types of surfactants are generally more soluble in cool water. As the surfactant solution is heated, the surfactant loses solubility, and the solution becomes cloudy (cloud point). High concentrations of salt and high temperatures decrease the solubility of polyoxyethylated detergents, thus lowering their cloud points. Therefore, members of this series of surfactants with the higher ethyloxy contents (more water soluble) should be used in saline waters. Polyoxyethylated surfactants are available in a homologous series ranging from oil-soluble to water-soluble types. Because they are nonionic, they are relatively unaffected by the activity or chemical nature of the formation brines, and they are used in wells of unknown brine character. They tend to cause less emulsion problems than ionic surfactants. Heating the produced foam above the cloud point (approximately ±150°F) assists in breaking the foam.

(2) *Anionic surfactants.* Anionic surfactants are typically nonionic types of foamers that have undergone a sulfation process during the manufacturing process. The addition of the sulfate radical (SO_4) onto the molecule causes the surfactant to become more polar and anionic in character and increases its solubility in water. Anionic surfactants are excellent water foamers. As with nonionic surfactants, they are available in a homologous series in which the midrange oil-water solubility cut (10–12 carbon atoms) is generally preferred. Some anionic surfactants may be adversely affected by high brine solutions.

(3) *Cationic surfactants.* Cationic surfactants such as quaternary ammonium compounds are effective foaming agents, often performing more effectively in brines than in fresh water. The low-molecular-weight agents of this type are among the most effective agents for foaming mixtures of hydrocarbons and brines, and reportedly, high-molecular-weight quaternaries show some effectiveness in foaming wellbore fluids with high percentages of liquid hydrocarbons. On the other hand, high-molecular-weight quaternaries show a decrease in effectiveness in brine solutions. In some cases, particularly with overtreating, oil and water emulsion problems are created. Figure 6.29 shows the results of one set of laboratory screening tests. This figure demon-

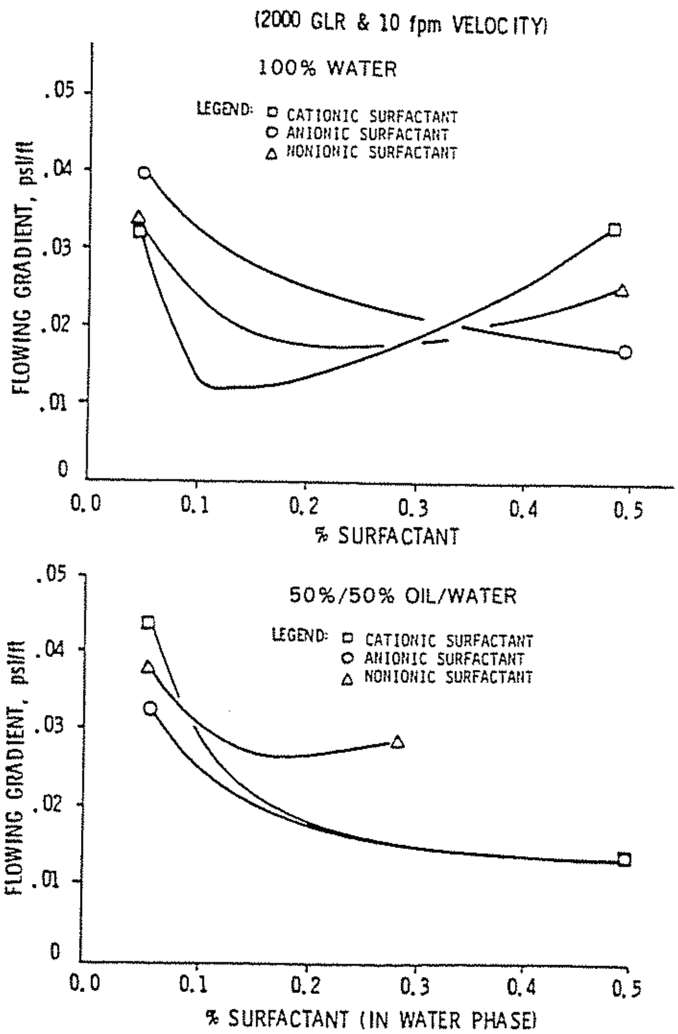

Figure 6.29 Surfactant Screening Test for Air-Water System

strates that the optimum dosage is around 0.15–0.25% for good surfactant compounds and the type of laboratory gradients expected. Ionic and nonionic surfactant performance trends are shown.

(4) *Amphoteric surfactants.* Amphoteric surfactants were found to be good foam surfactants in one laboratory study.[30] Amphoteric compounds exhibit cationic character in an acidic solution, anionic character in basic solutions, and nonionic character in neutral solutions. Reportedly, they are very good foaming agents in high (200°F) temperature tests, with up to 10% salt in solution. At 70°F, their performance in laboratory foam column tests was slightly less favorable than anionic or cationic surfactants.

(5) *Foaming agents for hydrocarbons.* Although hydrocarbons do not foam well, several surfactants are marketed that do improve foam effectiveness with liquid hydrocarbons.

Success has been reported in foaming diesel/condensate following oil frac treatments using a brand-name silicone oil. Laboratory foam tests indicate that the density gradient may be twice as large as a water foam gradient. The onset of water production caused a dissipation of the effectiveness of the silicone oil treatment. The surfactant is marketed as a foam suppressor and apparently behaves as such in a hydrocarbon-water mixture.

Fluorocarbon surfactants are reportedly designed for foaming hydrocarbon liquids to enhance foaming in mixtures of water and hydrocarbon liquids. The benefits of these hydrocarbon foamers has not been fully substantiated by field tests, and they have not shown significant benefit in laboratory tests.

Nonetheless, hydrocarbons do not foam well, and various surfactants offer only limited improvements in foaming characteristics.

6.344 FOAMING TENDENCY AND SURFACTANT BEHAVIOR IN BRINE-CONDENSATE MIXTURES

Why do some water-hydrocarbon liquid mixtures show the ability to foam, and other mixtures do not? Generally speaking, only the water-phase fluid in a water-hydrocarbon mixture produces a stable foam—i.e., foam where the bubble film is sufficiently strong to hold the water and gas in a bubble structure at significantly high gas concentrations. This is because the water molecule is polar and permits a polar hydrogen bond with these surfactants. Foam-surfactant molecules have an oil-loving and a water-loving end, which become oriented at the interface and strengthen the interface film. Hydrocarbons do not foam well because there are no polar bonds with the surfactants; indeed, the principal mechanism for hydrocarbon foam surfactant is to place high-mol wt polymers at the interface to interact with many oil molecules to build viscosity and/or molecular attraction between several oil molecules. This provides some development of film strength although the film is significantly weaker than for water foam films. To successfully foam a well, it is necessary to obtain an effective foam condition in the water phase. If free oil is present, the oil appears to be lifted by the drag forces of the water foam rather than by a foaming tendency in the oil itself.

6.3441 EFFECT OF CONDENSATE (AROMATIC) FRACTION ON FOAMING TENDENCY

A certain amount of the surfactant will react in the system to create an oil-in-water emulsion. Some limited lab work has shown that the emulsion tendency is much higher for low-molecular-weight aromatic and cyclic hydrocarbons than for aliphatic hydrocarbons. As would be expected, an increase in the aromatic (principally toluene) content diminishes the foaming tendency in oil-water mixtures.

Figures 6.29, 6.30 and 6.31 are the result of some laboratory tests showing the column pressure gradient

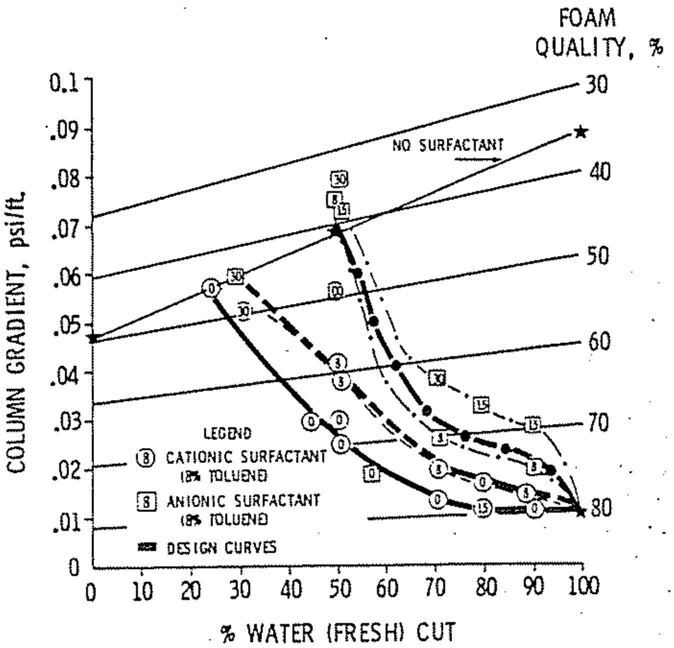

Figure 6.30 Foam Column Test with Condensate and Fresh Water; Superficial Gas Velocity at 60 fpm

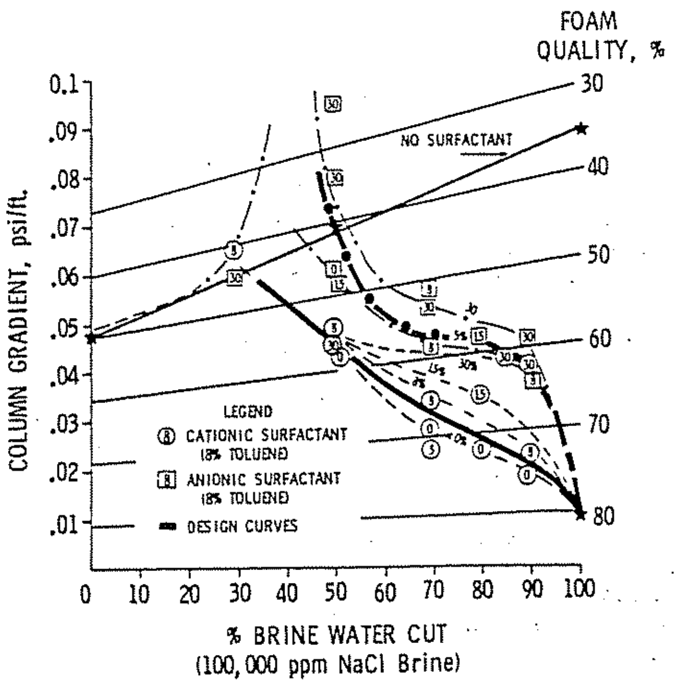

Figure 6.31 Foam Column Test with Condensate and Brine System; Superficial Gas Velocity at 60 fpm

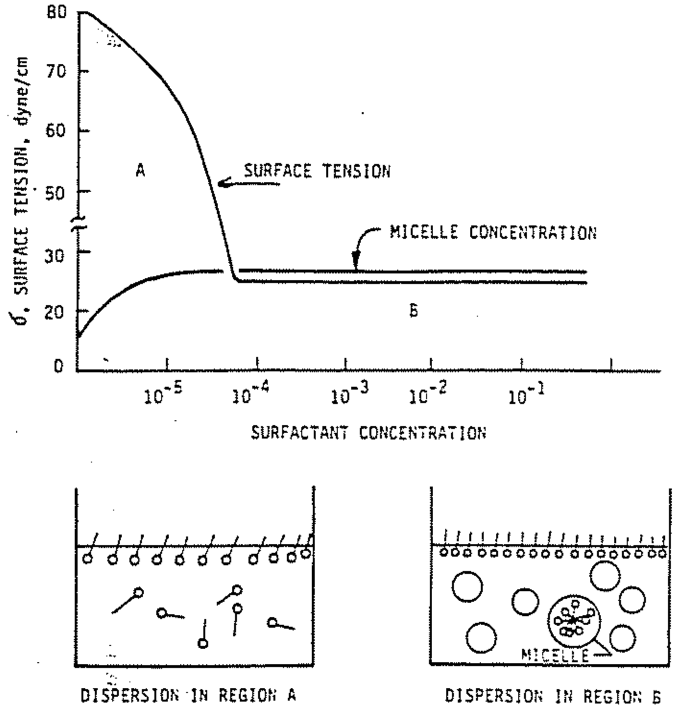

Figure 6.32. Surfactant Dispersion in Well Fluids

and estimated foam qualities for various mixtures of hydrocarbon liquids in both fresh and brine water. The foam quality correlation is based on the gradient observed and on some measurements of foam quality obtained by shutting in the test column and measuring the volume of foam and, subsequently, the liquid components of the dissipated foam. Although the tests were run at very low superficial gas velocities, which may not characterize the true gradient in a field well, the low velocity does diminish the effect of flowing friction and allows a better correlation with foam quality. Based on the data shown in these figures, the foaming tendency of a mixture is good, even to relatively low water cuts, for mixtures containing hydrocarbon liquids with no toluene content. This observation was valid, although one of the hydrocarbon liquids used to represent 0 aromatic content contained 16% heavier aromatics but no benzene or toluene. On the other hand, mixtures with varied light-end aromatic content showed some increase in column gradient as the toluene content increased.

Figure 6.32 shows the theoretical dispersion pattern for foam surfactants in oil-water systems. As a surfactant is added, the surface tension of the water decreases to the point where all of the surface is saturated by a surfactant. Beyond this point, the surface tension is relatively constant at some low value characterized by surfactant constituents. Also, as surfactant concentration increases, more surfactant molecules enter the water phase, and at a critical concentration, the heretofore dispersed surfactant molecules begin to conglomerate in clusters. This point is reached at a much lower surfactant concentration than that required for stabilization of the surface tension and effective foaming. The net result of these interactions in liquid is that a greater abundance of oil is contained in the bubble film, which reduces the film strength and, consequently, foam quality. Also, apparent viscosity of the

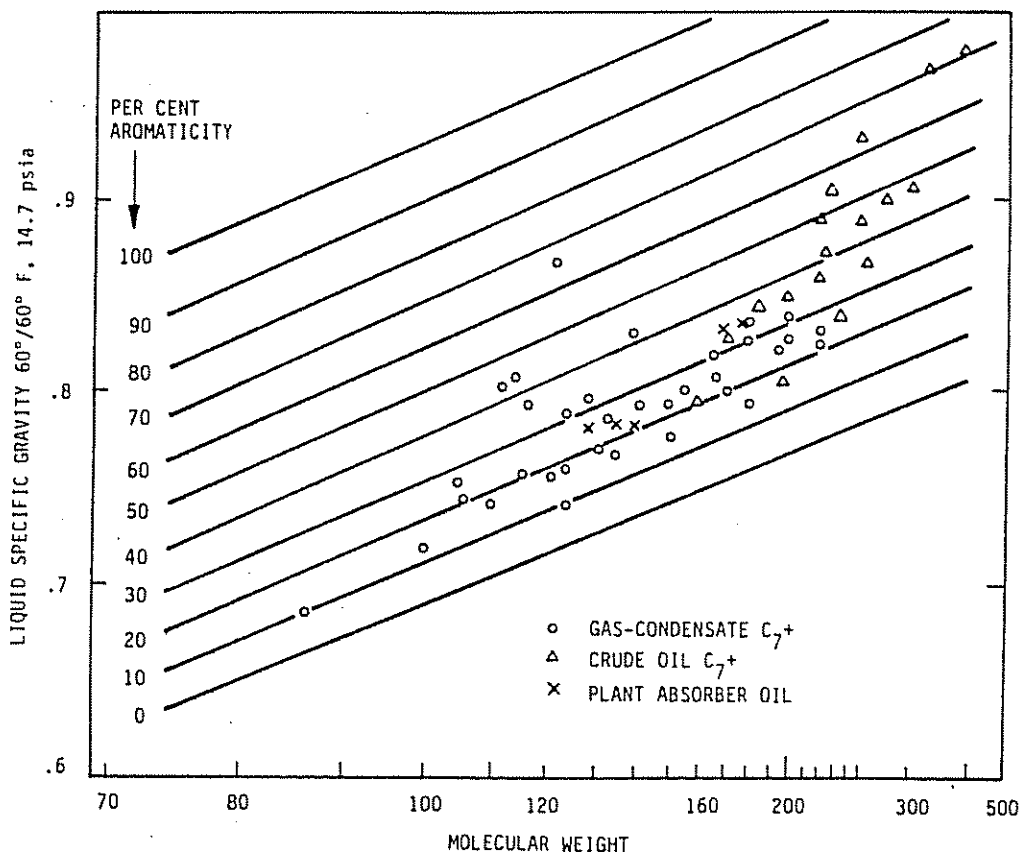

Figure 6.33 Aromatic Content of Hydrocarbon Liquids (after Jacoby)[31]

liquid can increase because of emulsions; this is particularly evident in the midrange water-cut mixtures that exhibited higher pressure gradients than other tests where the liquid contained no surfactant or aromatic hydrocarbons. Figure 6.33 is a general correlation of the percent of aromatics contained in hydrocarbon liquids as a function of specific gravity and average molecular weight of the C_7^+ constituents.[31] This can be used when an analysis of the condensate for aromatic content has not been run. Three condensates were used in the lab tests. All showed about 25% total aromatic content, including 8 to 12% benzene plus toluene fractions. (However, caution should be exercised in extrapolating this information since these samples may have suffered some weathering.)

6.3442 EFFECT OF BRINE ON FOAM TENDENCY

Brine-oil mixtures are associated with field locations where the ability to generate foam has been questioned. Lab tests indicate that brine water with no oil phase present will foam about as well as freshwater. Effective foam quality in an oil-water mixture, however, decreases more rapidly when water salinity is high. In comparing Figures 6.30 and 6.31, the effect of brine rather than freshwater is seen to be a reduced foaming tendency. This effect was more drastic with the anionic surfactant tested, compared to the cationic surfactant. Two things account for brine reaction behavior:

(1) Salts tend to reduce the solubility of surfactants in water.
(2) The critical micelle concentration (concentration of surfactant when micelle formation begins) is reduced.

The water-attracting ends of the surfactant molecule see a reduced number of unassociated water molecules (those without ionic attraction to the disassociated salt ions) to attract the surfactant molecule. As the concentration of the surfactant is increased, the surfactant molecules form micelles (clusters) in the water, each with the oil-attracting ends attracted to the center of the cluster. Thus, in brine waters, a larger number of surfactant micelles tend to be dispersed throughout the fluid. Some of the free hydrocarbon liquid is drawn into the micelle cluster, which causes a greater quantity of oil to be in the water phase.

Investigations by Houth et al. indicate that the surface tension in the methane-water system is slightly lower than the air-water systems.[32] Surface tension also becomes smaller as the pressure of the system increases because of the gas driven into the liquid. Also, there is a slight increase in the surface tension of water as salinity increases.[33] Thus, in summary, the effect of brine solutions is to alter the emulsion tendency for some surfactant-hydrocarbon liquids. The surface tension for wellbore-produced fluids at relatively low pressures should not be significantly different from the air and liquid systems investigated, and the critical control is in the surfactant treatment.

6.35 EQUIPMENT CONSIDERATIONS

6.351 CHEMICAL INJECTION EQUIPMENT

The equipment required for chemical injection is shown in Figure 6.26. Most locations use a gas-powered pump operating off one side of the casing. A pump can be located under a chemical barrel so that the entire pump system can be covered or insulated.

The surfactant may tend to hang up on the tubular walls; therefore, the surfactant solution should be diluted to provide a larger volume to ensure reaching the fluid level, or it should be washed down with additional fluid following surfactant injection. It is recommended that the surfactant be diluted to 1 part in 9 parts of water so that a surfactant dosage of 2 qt of diluted solution per barrel of produced fluid be injected for a surfactant concentration of approximately 0.1%. In winter operations, the diluting liquid can be 50% ethylene glycol.

A better but more expensive injection system is one using a capillary tube strapped to the outside of the production tubing. A chemical injector system is an example of this type of equipment arrangement. The advantage of this type of arrangement is that relatively small quantities of surfactant can be injected with assurance that they will reach the desired downhole injection point. This circumvents problems with fluctuating fluid levels in the annulus.

6.352 TUBULAR GOODS SIZING AND LANDING POSITION

Tubing should be landed at the top of the completion interval. Production flow is generally obtained through the tubing, but it can be obtained through either the tubing or the casing annulus; however, possible casing corrosion must be considered. A selection of which path to use is based on which conduit will give gas velocities in the range of 3 to 12 fps at operating pressure and temperature. There may be some liquid (foam) holdup in larger cross-sectional flow areas (where velocity is in the lower range), particularly when the foam quality is low because of poor surfactant performance or the presence of significant liquid hydrocarbons. In this case, it is probably better to flow up the tubing. Using a multiphase-flow pressure-loss computer program based on the foam system is recommended for estimating producing gradients and selecting the optimum flow path.

6.353 SEPARATION EQUIPMENT

Foam is broken, and the liquid phases are separated in the production separator where the produced fluid is in as near a quiescent state as possible. Therefore, the separator should be relatively large, allowing, one hopes, gas velocities of around 2 fps and 5 min or more holding time for liquids.

Liquid taken from the separator still may have significant oil-water emulsions. If this occurs, it will be desirable to allow additional separation time in a liquid holding tank. If the separator is a three-phase separator, it may be desirable to discharge the water to a holding tank if significant emulsions would otherwise remain in the water going to the pit.

If foam carry over or persistent emulsions continue with existing separation equipment, it may be desirable to chemically treat the produced stream to destroy the foam surfactant activity. Chemical treatment is discussed in Section 6.364.

6.354 INSTRUMENTATION

To evaluate the performance of a well using foam surfactants, it is necessary to have casing and tubing pressures and production data. In a continuously flowing well, the fluid level in the annulus will be at the bottom of the tubing (assuming that the casing is shut in). The casing-tubing differential pressure then reflects the pressure gradient in the tubing; the producing bottom-hole pressure can be calculated. The fluid level will always be at the tubing intake depth in the flowing well, and the casing is shut in because downhole gas separation will fill the annulus with gas (unless a tubing leak is present). However, if the producing rate is so low that surging or slugging occurs, the pressure equilibrium established between the annulus and the tubing may be temporarily upset in proportion to the size of the pressure surges. As a consequence, there may be some liquid or foam accumulation above the tubing intake point when the annulus pressure is recovering from a depressuring cycle (caused by annulus gas production) following the production of a liquid slug.

6.36 OPERATING CONSIDERATIONS

6.361 SURFACTANT SELECTION

Field tests and laboratory screening tests have shown that cationic and anionic surfactants have performed successfully under certain conditions with trends as shown in Figure 6.29. However, condensate and waters differ between fields causing changes in observed trends.

Before using surfactants in the field, it is recommended that a field screening test be performed using samples of produced liquids. Field screening tests show how well the agent foams the produced liquid and the compatibility of the surfactant and produced fluids. The effectiveness of demulsifier chemicals can also be checked.

Shakedown tests. This test consists of placing a known volume of produced liquid into an Erlenmeyer flask with a known quantity of surfactant, covering the flask, and shaking it to agitate the liquid. Observations are made regarding the amount of foam, residual liquids, emulsions, etc.

6.362 WELL PRESSURE CYCLING

Most candidate wells have low gas rates, and liquid is produced in slugs—small slugs if tubing gas velocities are high and larger slugs if velocity is low. Slugging conditions may still be evident in wells using foams. If slugging is severe, gas from the casing will feed into the tubing as tubing pressure decreases slightly because of the production of a slug at the surface. If the casing gas enters the tubing, the tubing gradient becomes still lighter and even more casing gas is depressured into the tubing. Eventually, the casing will depressurize, rendering it incapable of supporting the normal flowing gradient, and the annulus pressure must again be built up. This problem can be acute for tight-gas wells where the recovery of the casing pressure may be slow. In this case, it may be desirable to stabilize casing pressure. A pressure controller on the casing pressure or a differential controller on an orifice meter in the flow line can be used to operate a control valve in the flow line for regulating pressure fluctuations—i.e., preventing excessive lowering of casing pressure. Also, producing the well from below a packer will eliminate surging caused by annulus gas cycling, but the downhole equipment must permit surfactant injection.

6.363 KICKING OFF FLOW WITH SURFACTANTS

Limited field testing indicates that considerable care needs to be exercised in kicking off the well. If not done properly, the well can be overtreated, blown down and killed, or simply not unloaded. The preferred method is to shut the well in and inject 20 gal or more of the diluted surfactant solution to wet the tubular walls and then begin continuous surfactant injection at the treating rate indicated by daily production. Casing and tubing should remain shut in until the casing-tubing differential becomes relatively small (say $\Delta P = 0.04$ psi/ft $\times$ depth). The tubing can be opened for a few minutes at a very low gas rate to mix the liquid and surfactants with the gas. The well can then be opened to the expected flow rate while keeping in mind that the well should not be excessively depleted of the casing pressure, which will be required to support the producing gradient with normal liquid production.

6.364 CHEMICAL TREATMENT PROBLEMS

(1) *Emulsion problems.* Some success in breaking the emulsions has been realized with demulsifier chemicals. Appropriate demulsifier chemicals are usually recommended by chemical companies, and they should be evaluated in bottle tests before use in the well. The chemical is injected to the line upstream of the separator to allow mixing with produced liquids before entering the vessel.

In some cases, wells are treated with other surface-active compounds such as those packaged with corrosion inhibitors. The surfactants may be contributing to emulsion or foam stability problems, and either the foam surfactant or the other treating chemical will have to be changed or the treatment dosage moderated to improve the situation. Further, it may be desirable to discontinue inhibitor treatment for a while in order to be more definite about the cause of severe emulsion problems.

(2) *Foam carryover.* Foam carryover into lines and separators sometimes causes upsets and interferes with level controls. Defoamer chemicals can be effective in suppressing the foam. The defoamer is injected into the flow line upstream of the separator to allow for mixing before the stream reaches the separator. Selecting the type and treatment rate depends on a number of local factors, and tests should be conducted on location with the chemical company representative.

6.4 OTHER FORMS OF ASSISTED NATURAL GAS LIFT

Included in this section are discussions on siphon strings, subsurface liquid diverters (a form of automated siphon string), and rotative gas lift systems. The underlying concept behind all of these deliquefying methods is to develop adequate gas velocity to clear the tubing of liquid. This basic approach is discussed in Section 6.1. The three methods discussed here are variations that are most applicable to producing the liquid to a separate low-pressure collection system or to the atmosphere. In this sense, they are likely to be expensive or wasteful of gas. Nonetheless, they are methods of deliquefication that have enjoyed some popularity and may be useful in some field situations.

6.41 SIPHON-STRING GAS-LIFT SYSTEM

The term siphon string applies to any tubing installed in a gas well for preferentially removing liquids through the tubing while gas is produced from the annulus. Liquids are produced to the surface by natural gas lift. Siphon strings are made of small-diameter tubing (1 in. to 1½ in.), partially because liquid volumes are small but principally because high tubing velocities, which are advantageous for deliquefying operations, can be achieved with relatively low gas rates in small tubulars. Usually the blowdown is sent to a low-pressure system in order to achieve the lift pressure and gas rate necessary for liquid unloading. Frequently, the siphon string is installed inside a larger tubing string, and the producing annulus is the annulus between the two tubing strings, or it may be open as a parallel string.

6.411 CYCLE DESCRIPTION

The siphon-string-equipment arrangement is generally set up as shown in Figure 6.34. Because of the low liquid volumes produced by high-GLR wells at low gas-producing rates, the siphon string is operated on an intermittent cycle. The cycle begins when the siphon string is open to the low-pressure collection system. The reduction in tubing pressure allows the liquid to enter the tubing and wellbore gas to enter behind the liquid and through jet collars or pressure-operated gas-lift valves to aerate the liquid column and supply the lift energy needed to produce the liquid. After the liquid has been produced, the surface siphon-string control valve is closed. Jet-collar or gas-lift valves may or may not be necessary, depending upon well conditions.

6.412 APPLICATIONS

Siphon-string operation is generally applicable to high-GLR, low-liquid-rate wells that have sufficiently high line (casing) pressures to make the pressure differential between casing and siphon-tubing delivery pressures effective in lifting liquid slugs. Siphon strings are usually not employed on wells that require unloading more than once a day. Moreover, the use of siphon strings is much less common today because, in the past, the lift gas was generally vented or wasted. An alternative for wells with low gas rates and sufficient pressure is to equip the well with small-diameter tubing to achieve adequate tubing velocities for continuously unloading the liquids; i.e., all produced gas and liquid is produced through the tubing by natural flow (see Section 6.1). Thus, the principal application for siphon strings is for wells with low bottom-hole pressure where the only significant pressure differential available is obtained by reducing the surface tubing pressure to near-atmospheric pressure. Even this application with current gas prices must be considered only after judging the merits of pumping equipment.

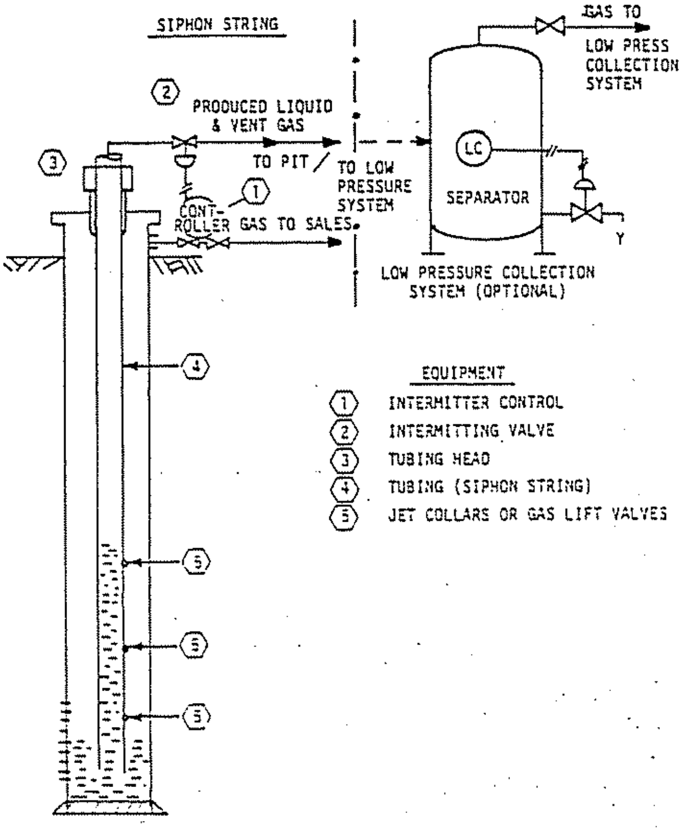

Figure 6.34 Equipment Arrangement for Siphon String Operation in Gas Wells

6.413 DESIGN CONSIDERATIONS

(1) *Tubing size.* Tubing size should be small enough that the designed gas rate is large enough to achieve minimum critical velocity in the tubing. Generally speaking, the recommended minimum gas velocity for the siphon string during unloading is around 1,200 ft/min—i.e., tubing velocity approaching mist-flow conditions. However, see Section 6.133 concerning calculation methods for individual wells.

Small-diameter tubings have relatively low joint strength, and the tensile rating of the joint may limit the tubing depth. Also, if the well has been killed with load fluids and must be swabbed to initiate flow, larger tubing sizes are easier to swab. It would be preferable to not kill the well with load fluids when installing the siphon string; tubing strings can be run with a snubbing unit on low-pressure wells. Frequently, macaroni strings are run inside larger tubing strings. This arrangement also provides some tubing support

when the siphon string is opened for production. Another method for initiating flow in loaded wells equipped with concentric tubing strings is to gas lift with gas from the sales-gas system provided the line pressure is sufficient. The siphon string is discharged to low surface pressure until the well is unloaded and the well is capable of normal blowdown cycles using formation gas.

(2) *Jet collar location and sizing.* It may be necessary to equip the tubing with jet collars (collars that have small holes drilled through the wall to enable gas-lift gas to enter) at appropriate intervals. Holes can also be placed in the tubing by wire line after it is installed if the tubing is large enough to accept the wire-line tools. Design procedures for jet-collar sizing and positioning are given in the following section. Gas-lift valves can be used in lieu of jet collars, but they are unnecessary on intermitting wells since gas will flow through the ports only when the siphon string is open to produce.

(3) *Cycle control.* Siphon strings are normally used on wells in which the liquid production is small and unloading is required only once a day or less. The cycle is usually controlled by a time cycle controller or manually since the cycle is very infrequent. The only way of knowing when to operate the blowdown cycle is to monitor the gas rate. When it falls off, the well should be unloaded. After the daily liquid production rate has been determined, judgment can be made about the time interval between blowdowns.

Design of siphon strings.

(1) jet collar position for intermittent well operation
 (a) determine position of top collar:

h_1 = height of liquid column in inner tubing (liquid from both tubing strings) or height above tubing landing depth based on ΔP

 (b) position of second collar:

$$h_2 = h_1 - 150 \text{ ft}$$

 (c) position of subsequent collars and bottom collar:

$$h_3 = h_2 - 300 \text{ ft}$$
$$h_4 = h_3 - 300 \text{ ft}$$

h (bottom collar) = fluid level depth in casing at start of cycle (i.e., depth of balanced fluid level inside and outside of the tubing string)

If no jet collars are used, the cycle frequency must be watched with caution to present loading with liquid.

(2) sizing jet orifice diameter
 (a) Calculate the required gas rate for minimum critical tubing velocity at flowing tubing pressure and average well temperature. (For approximate design, a critical tubing velocity of 1,200 ft/min can be assumed. This design velocity is intended to put the produced stream in the mist-flow regime, although other criteria for mist flow could be used. When checking tubing-velocities with multiphase flow correlations, select a velocity near the minimum tubing gradient as shown by a plot of rate vs BHP at constant surface pressure and GLR.)
 (b) Correct gas requirement to standard conditions, Mcfd at 14.65 psia and 60°F

$$q_s = q_a \frac{P_a}{P_s} \times \frac{T_s}{T_a} \times \frac{1}{Z}$$

where:

subscript s = standard conditions
a = actual conditions

 (c) Proportion the gas requirement among the number of jet-collar positions, allowing for half of the gas rate to be injected in the bottom of the collar.
 (d) Use the chart in Figure 6.35 to size the jet orifice.

Note: If two holes are to be used per jet position, divide the daily gas rate and size the orifice accordingly.

6.42 SUBSURFACE LIQUID DIVERTER—GAS-LIFT SYSTEM (DIVERTER GAS LIFT)

The subsurface liquid diverter (SLD) is a tool that was available around 1967 to improve the efficiency of producing liquids from gas wells when using gas-lift methods.[34] The SLD allows liquid to be collected in the tubing, which is operated at low pressure. Tubing-pressure-operated gas-lift valves are used in conjunction with the SLD to lift the accumulated liquids to the surface. A schematic equipment arrangement is shown in Figures 6.36 and 6.37. Produced gas in excess of that used for lifting liquids is produced through the casing-tubing annulus. When used in this manner, this system provides downhole automatic control of the siphon-string deliquefication cycle. In this sense, the SLD is not a different method of dewatering a gas well but merely one that has some advantages and disadvantages when compared to the conventional siphon string.

6.421 CYCLE DESCRIPTION

A description of the diverter valve operation is as follows (refer to Figures 6.36 and 6.37): a control spring exerts a downward force on the valve sleeve, tending to keep it open, and a column filled with a control liquid exerts a hydrostatic force upward on the diaphragm connected to the bottom of the sleeve. Since the initial hydrostatic force of the control liquid is greater than the spring force, some additional force is required to open the valve. This is supplied by the produced liquid in the casing, which exerts a downward pressure on the diaphragm. Approximately 2 ft of produced liquid above the ports is required to open the valve. When the valve opens, the liquid is diverted into the tubing string, which operates against low surface pressure. As the fluid level in the casing drops, the force on top of the diaphragm decreases, and the valve closes, keeping gas out of the tubing. The annulus liquid level always remains near the diverter. If possible, the diverter should be installed below the production interval for better gas separation.

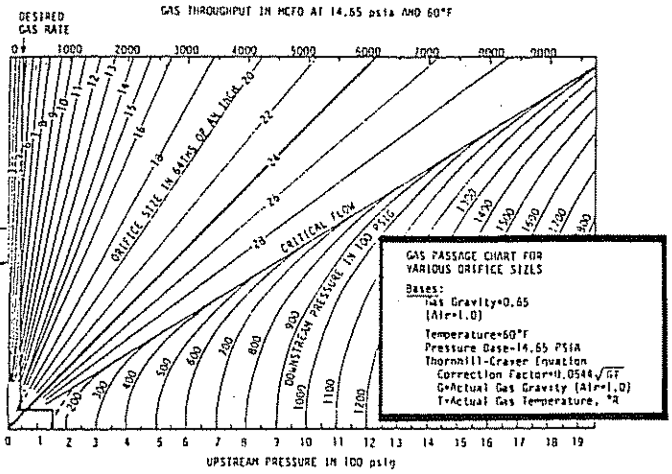

Figure 6.35 Orifice Sizing for Gas-Lift Valves and Jet Collars

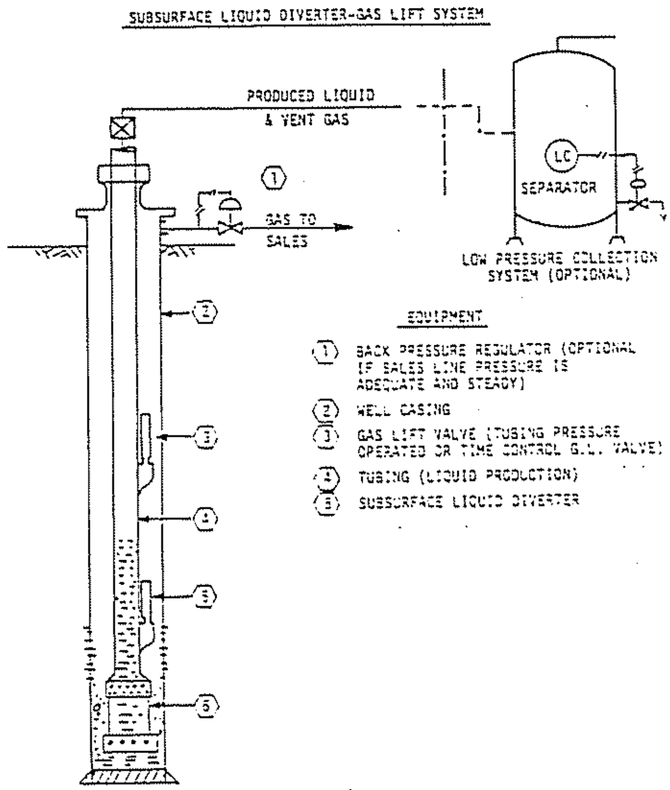

Figure 6.36 Schematic Equipment Arrangement for Diverter Gas Lift "Downhole Separator"

As the liquid is diverted into the tubing, it accumulates until the gas-lift valve opens to gas lift liquids to the surface. The gas-lift system is completely independent of the diverter valve. Gas-lift valves are usually installed a short distance directly above the diverter. Their exact placement depends on the casing-tubing differential pressure available for supporting the liquid column then supplying high pressure gas for the gas lift. Gas-lift valves are opened by increased tubing pressure (tubing-pressure-operated valves) caused by the slug height. They are set by the position of the lower valve and differential pressure required to open it. When a liquid slug is produced at the surface, the tubing pressure is reduced, and the gas-lift valve closes.

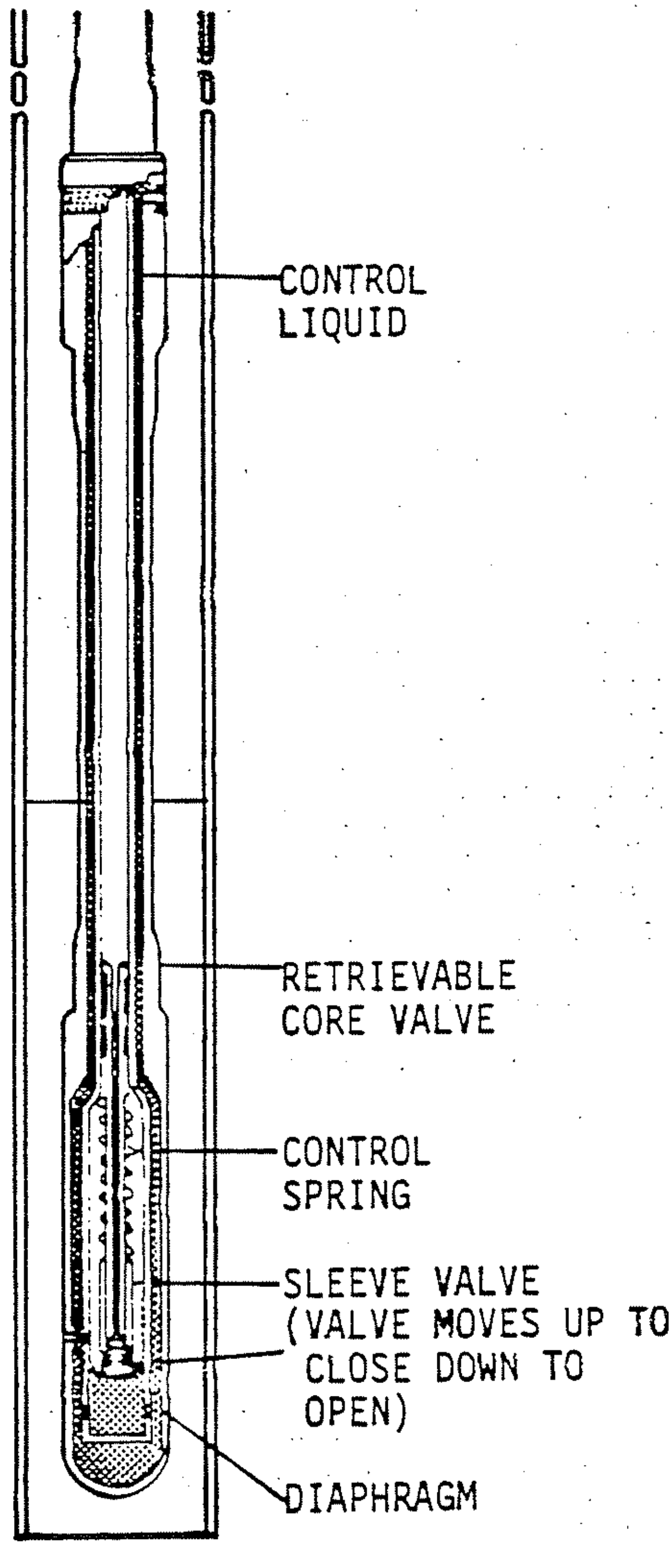

Figure 6.37 Schmatic Subsurface Liquid Diverter

6.422 APPLICATIONS

The SLD–gas-lift system has about the same application criteria as the siphon string. It is best suited to wells that require infrequent blowdown. One advantage of this system over the siphon string is its automatic cycle control for optimum timing of the production cycle. Disadvantages are that more downhole

equipment is required, and the tubing-pressure-operated gas-lift valves sometimes perform poorly in low-pressure wells. Also, it may be necessary to control casing pressure to achieve reliable operation if line-pressure fluctuations cause significant tubing pressure fluctuations.

6.423 DESIGN CONSIDERATIONS

(1) *Gas-lift valves.* The gas-lift valves are the most critical item of equipment, and careful design is required. To select the proper valve design, the tubing pressure under the rising slug must be calculated. The valve-port size and pressure drop can be calculated based on producing tubing pressure and the gas rate required to give a minimum tubing velocity to surface liquids. To have the valves open at the proper tubing pressure, port size must be small. To overcome this restriction in achieving gas rates, several tubing-pressure-operated valves can be placed in the tubing string since the valves will not open until the slug rises above the lower valve. It is recommended that the local gas-lift-valve manufacturer's representative be consulted regarding gas-lift-valve placement and determination of valve opening and closing pressures be made to match his valve specifications. However, Brown and Beggs,[11] Winkler and Smith,[35] and others have provided a general discussion of gas-lift-valve sizing and placement.

A frequently encountered problem when using tubing-pressure-operated valves on low-pressure wells is that the excessive wellhead tubing pressure can prevent the valves from closing. The high tubing pressure accompanying the surfacing liquid slug must decrease rapidly to assure closing of the valves. Excessive back pressure from long and/or small flow lines, flow-line restrictions (chokes, valves, etc.), emulsions, etc., can prevent the valves from closing immediately after the slug has surfaced. This, coupled with the fact that casing pressure is depleted as gas passes into the tubing, makes it difficult to predict the pressure at which the valve would close. Therefore, it is difficult to estimate the amount of lift gas that will be used and/or to control waste.

(2) *Bottom-tubing valve location.* The gas rate should be adequate to lift the slug at an acceptable velocity. Larger tubing will reduce the head pressure of the slug, hence the casing pressure requirement, but it will require more gas rate for effective velocity. Usually, around 1½-in. nominal tubing size is optimum. A maximum permissible slug size can be estimated based on the pressure differential between the surface casing and tubing pressures. The liquid slug above the valve should not represent more than about 75% of this differential pressure. This allows for the flowing friction loss during the gas-lift segment of the cycle.

6.43 CLOSED ROTATIVE GAS-LIFT SYSTEM

In a closed rotative gas-lift system, high-pressure gas from a compressor is delivered to a well (or wells) for lifting fluid. The spent gas and formation gas are returned in a continuous cycle to the compressor for recompression. A rotative gas-lift system may be used

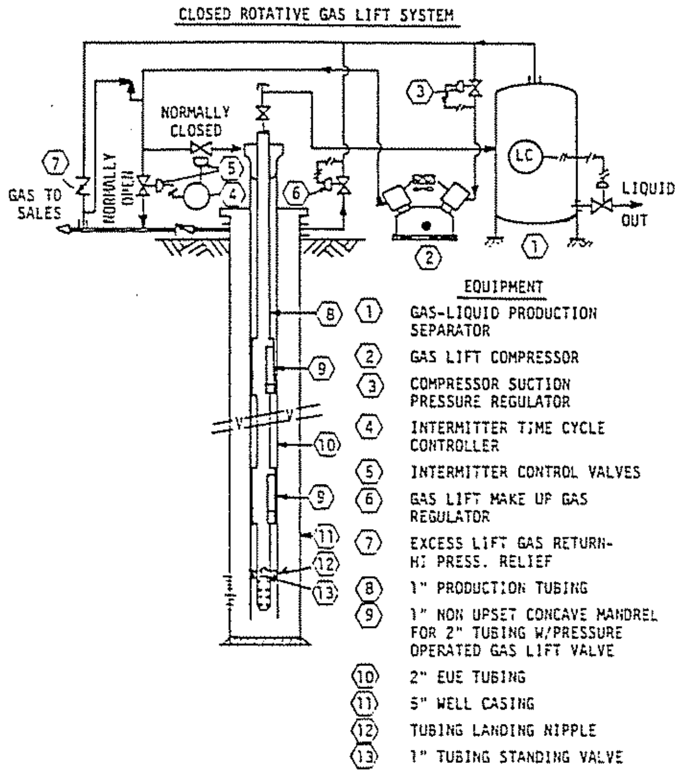

Figure 6.38 Equipment Arrangement for Intermittent Rotative Gas Lift Used in Gas Well Dewatering (after Ziser, Ja. "Unique Gas Lift Hookup Used to Dewater Gas Wells." World Oil, July 1960).

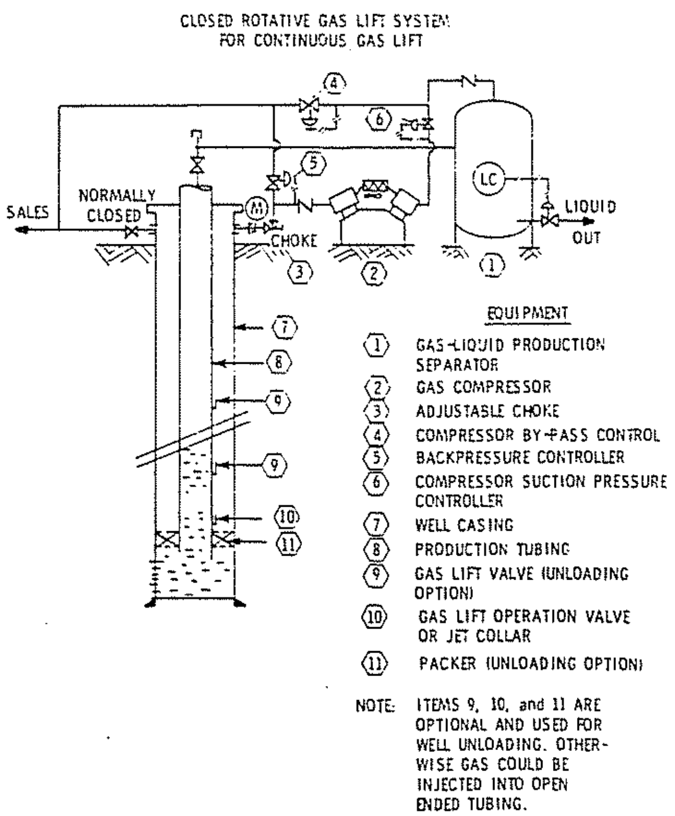

Figure 6.39 Schematic Equipment Arrangement for Continuous Rotative Gas Lift (Supplemental Gas Injection to Maintain Tubing Velocity)

for intermittent or continuous gas lift (supplemental gas injection). A basic use for rotative gas-lift systems is in producing oil wells where a minimum quantity of gas is available. A rotative gas-lift system for deliquefying gas wells is shown in Figure 6.38 for intermitting and Figure 6.39 for continuous.

6.431 CYCLE DESCRIPTION

(1) *Intermittent cycle.* For an intermitting well equipped as shown in Figure 6.38, the cycle begins with an intermitting control, which opens the high-pressure gas line to the annulus between the inner and outer tubing. The high-pressure gas then enters the liquid production tubing through a gas-lift valve or jet collar and lifts the liquid slug. After the liquid slug has surfaced, the compressor discharge is routed to sales. The tubing is allowed to produce naturally to the separator. The tubing gas and some casing gas maintain compressor operating conditions. When the tubing loads again with liquids, the intermitting valve again diverts lift gas to the outer tubing annulus. Usually, the bottom gas-lift valve is designed to open at minimum pressure; thus a jet collar could perform equally well as the gas-lift valve.

The compressor is designed to provide high-pressure gas to remove liquids and eventually, as the well depletes, it may be used to boost the pressure of all produced gas to sales-line pressure. The cycle is usually controlled with a time-cycle intermitter.

If the well is or will be killed with load fluid, it is desirable to kick off flow using the high-pressure gas. It may be necessary to install gas-lift loading/unloading valves to the upper portion of the tubing string. The design of unloading valves is done in the same manner as for continuous-flow gas-lift operations. Otherwise, swabbing or some other unloading method will be required to get the well back on cycle.

(2) *Continuous cycle.* Although the description given above is for intermittent liquid production, a rotative gas-lift system can be used for continuous lifting of liquids, either using concentric tubing strings or by using a single tubing string as shown in Figure 6.39. The latter system is simply a scheme to supplement the natural formation-gas production rate with enough gas to maintain good flow conditions and prevent liquid loading caused by low tubing velocities (see Section 6.1). In this case, the producing bottom-hole pressure is regulated by the multiphase-flow pressure losses in the tubing. The gas injection rate is controlled by a surface choke so that the well maintains a satisfactory producing GLR. The compressor can be sized to handle only the supplemental lift-gas volume (rotative gas lift) or the entire production stream when the wellhead pressure is below sales-line pressure.

A frequently used approach to eliminate swabbing or some other measure to start production from a loaded well is to install a downhole packer and to unload gas-lift valves so that the valve can be initially unloaded, provided a high-pressure gas supply is available. Gas-lift valve manufacturers will provide assistance in making the unloading valve design. Clark[1] and others also discussed valve design.

6.432 APPLICATION

The rotative gas-lift system has applications on any gas well that has low bottom-hole pressure and liquid loading. It has advantages over the siphon-string method in that (1) by using a compressor, the wellhead pressure may be lowered and (2) the well operates without venting or wasting lift gas. Generally, gas lift with compressors is not as efficient as other deliquefication methods such as pumping, and the economics must be evaluated. Rotative gas lift may have advantages where sales-line pressure is high and the lower wellhead pressure provided by the compressor results in significant production gain. The closed rotative lift system, however, is designed for continuous operation, and it is suitable for gas-engine prime movers, which made it a viable scheme for nonelectrified leases.

The rotative gas-lift scheme shown in Figure 6.39 enables the gas to be produced up the casing annulus without multiphase flow losses. This system is ideally suited for edge gas wells where the BHP is approaching a value that is less than sales-line pressure. Eventually, as well production declines, all of the produced gas can be handled by the compressor.

Continuous gas-lift schemes are generally uneconomical compared to pumping methods for dewatering gas wells unless the liquid volume is very high and/or a source of high-pressure gas or the compressor equipment is available. The best candidate wells are high-productivity wells.

6.433 DESIGN CONSIDERATIONS

(1) *Tubing size.* It is important to size the tubing and compressor capacity to provide sufficient gas to achieve critical tubing velocities during the unloading of a slug (see Section 6.133). For intermittent gas-lift wells, this suggests that smaller tubing sizes would be better for low-gas-rate wells. Larger tubing sizes will allow more slug accumulation for a given pressure differential between casing and tubing pressures. Normally, 1½-in. tubing would be the smallest recommended size for continuous lift. The scheme in Figure 6.38 utilized a 2⅜-in. outer tubing and a 1-in. inner tubing. The design procedures given at the end of this discussion show the relationship of these considerations.

(2) *Gas-lift valves.* The lowest gas injection point (just above the landing nipple for the system) has a gas-lift valve designed to open at sales-line pressure. A jet collar can be used instead of a gas-lift valve. Design of jet collars is covered in the section on siphon strings.

Of course any slug volume can be used for the design basis. A smaller slug size will decrease the pressure requirement. The foregoing procedure is based on the maximum liquid-slug size that can be accumulated in the tubing with the available differential pressure. A larger slug would allow more accumulation in the annulus and hence more back pressure on the formation.

The maximum daily liquid rate with intermittent gas lift would approach the predicted inflow rate based on the minimum BHP calculated from the surface casing pressure and the annulus gas gradient. The limita-

ROTATIVE GAS-LIFT DESIGN (INTERMITTENT OPERATION)

	Example
(1) Separator operating pressure is controlled by a gas-lift makeup-gas regulator. This pressure is selected to allow rapid dumping of separator liquids (say between 50 psig and 100 psig).	Separator press. = 80 psig 95 psia Sales-line press. = 270 psig 285 psig
(2) Select a tubing size and determine gas-rate requirement to achieve minimum critical velocity for the chosen separator pressure. Critical velocity can be estimated at 1,200 ft/min for separator pressure = 100 psig.	Select $1\frac{1}{4}$-in. tubing (inside) $2\frac{1}{2}$-in. tubing (outside) $1\frac{1}{4}$-in. tbg. capacity = 0.01039 ft^3/ft Gas rate = 0.01039 ft^3/ft x 1,200 ft/min = 12.4 cfm @ pressure = 17.8 Mcfd @ pressure $17.86 \text{ Mcfd} \times \frac{95}{14.6} \text{ psia} \times \frac{620}{580} = 105 \text{ Mcfd}$ @14.6 psia & 120°F
(3) Calculate max. slug height based on pressure differential between casing and tubing. Assume both casing and tubing to be filled to equilibrium condition before cycle begins; then, all liquid will be displaced into the inside string.	$\Delta P - 270 \text{ psi} - 80 \text{ psi} = 190 \text{ psi}$ $\Delta P = 190 \text{ psi}/0.433 \text{ psi/ft} = 439$ ft filling $2\frac{1}{2}$-in. & $1\frac{1}{4}$-in. tubing Capacity ratio $2\frac{1}{2}$- × $1\frac{1}{4}$-in. tubing where: (1) capacity of $2\frac{1}{2}$ less displacement of $1\frac{1}{4}$-in. = 0.0279 ft^3/ft (2) capacity of $1\frac{1}{4}$-in. = 0.0139 ft^3/ft $\text{Ratio} - \frac{0.0279}{0.0139} = 2.007$ Δh ($1\frac{1}{4}$-in.) = 439 ft × 2.007 = 880 ft
(4) Calculate compressor discharge pressure required by liquid slug. Assume system-flowing-pressure loss at 50% of slug column pressure.	Pd = 1.35 (880 × 0.433 psi/ft) + 80 = 600 psi (suggest 600 psi design press.)
(5) Size compressor: Set compressor suction pressure, allowing for about 25 psi pressure drops across compressor suction-pressure control valve. Calculate overall compression ratio R. From step 2, the gas rate @ 14.6 psia & 60°F, is determined. Use compressor horsepower charts in NGSMA book or estimate for 0.7 SG gas as follows: $Hp = 0.28 (R^{0.2} - 1) \times \text{Mcfd}$ Fuel gas consumption = 0.28 Mcfd/HP The estimated costs of a skim-mounted compressor with safety equipment is approximately $900/HP (as of January, 1983)	Suction pressure: 80 psi (separator) − 25 psi = − 55 psig = − 70 psia Discharge pressure: 600 psia 615 psia Compression ratio: $\frac{615}{70} = 8.8$ For two-stage compressor: $R/\text{stage} = \frac{615}{70} = 2.97$ $HP = 0.28 (8.8^{0.2} - 1) \times 106$ = 16.2 Gas consumption = 0.28 × 16.2 = 4.5 Mcfd
(1) Consider above design case using 1-in. tubing inside 2-in. tubing	
(2) Gas rate for critical velocity tubing capacity = 0.0060 ft^3/ft	0.006 × 1,200-ft min = 7.2 cfm $7.2 \times \frac{1,440}{1,000} \times \frac{95}{14.6} \times \frac{520}{580} = 60.5 \text{ Mcfd}$
(3) Capacity of 2-in. EUG − 0.0217 ft^3/ft Displacement of $1\frac{1}{4}$-in. 0.034 ft^3/ft Capacity of 1-in. = 0.006 ft^3/ft	$\Delta h = 439$ ft $\text{Ratio} = \frac{0.0183}{0.006} = 3.05$ Δh (1-in.) = 439 × 3.05 − 1,340 ft
(4) Required compressor discharge pressure	Pd = 1.35 (1,340 × 0.433) + 80 = 863 psi

tion is that the tubing BHP cannot exceed the producing annulus BHP for continuous gas lift. With intermittent lift, the tubing pressure can temporarily exceed the producing BHP if the tubing contains a standing valve to isolate the tubing pressure from the casing pressure.

(3) *Continuous rotative gas lift.* Design of a continuous rotative gas-lift system (see Figure 6.39) is done in the same manner as continuous natural-gas lift except the compressor requirements must be estimated. Usually, the compressor suction pressure is picked to allow a minimum wellhead pressure, which requires boosting of the excess gas to sale-line pressure. The general procedure would be as follows:

(1) Estimate well inflow performance for prediction of producing rate vs BHP.
(2) Using multiphase flow correlations, investigate the tubing performance curves for various GLR's and tubing sizes.
(3) From the intersection of well IPR and tubing performance curves, pick a design condition based on current and future producing rates.
(4) Compute compressor requirements to match predicted well performance. Note that for gas lift the producing GLR through the tubing is subtracted from the gas-lift GLR determined in step 2 above.
(5) To start production in a dead well, the tubing can be swabbed, or the gas-lift can be used with an unloading sequence of gas-lift valves.

Detailed procedures are shown in the *Technology of Artificial Lift* series, Vol. 2a, and are also given by Winkler and Smith[35] among others.

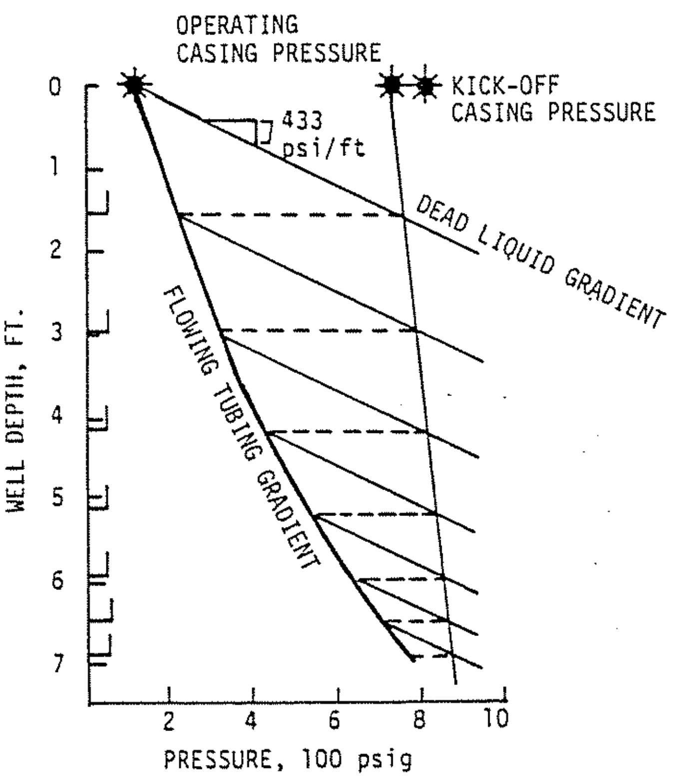

Figure 6.40 Unloading Valve Design Graphical Method—Simplified Schematic

6.5 PUMPING METHODS

6.51 INTRODUCTION

At first glance, it appears to most engineers that a mechanical pumping system that allows liquids to be produced up tubing while gas is produced up the casing annulus would be the optimum method for deliquefying gas wells. The unique feature of pumping methods for deliquefying gas wells is having separate production paths for the gas and the liquid. Such a system eliminates multiphase flow losses, while friction losses are minimized by the usually large annulus flow area. The back pressure on the formation is theoretically reduced to the line pressure plus the pressure gradient of the gas column in the annulus. The well produces at maximum rates and is capable of being produced to the ultimate abandonment pressure. Experience, however, indicates that pumping systems are relatively expensive to install, operate, and maintain in gas-well operations. Pumps are particularly suited to producing low-GLR wells to their lowest reservoir abandonment pressure. Frequently, this application applies to wells nearing abandonment after other deliquefying methods have been discarded.

High-productivity wells respond better to sandface pressure reduction, which is achieved with pumping, than do tight-formation gas wells. In fact, tight-formation (low-permeability) wells may show very small production gains because of the additional drawdown obtained with downhole pumps over that obtainable with natural flow or other gas-lift methods. This is because the pressure decrease is insignificant compared to the already large pressure drawdown between reservoir pressure and wellbore pressure. Of course, this comparison is not valid if the well continually loads and dies with produced liquids and must be deliquefied to produce.

Compared to pumping oil wells, pumping equipment applications used in gas wells generally have some unique characteristics and problems. These are:

(1) Low hydraulic horsepower is required to lift the normally small liquid production rate.
(2) Gas interference in the pump is usually present much of the time.
(3) Gas wells are drilled on wide spacing patterns, and, therefore, they are expensive to electrify for the use of electric-motor prime movers.

These problems are addressed in the discussion relating to the various types of pumping equipment.

6.52 APPLICATION GUIDELINES FOR PUMPING SYSTEMS

Although specific types of pump systems will have specific application criteria, pumps are generally applicable to: (1) any gas well having its production (wellbore pressure drawdown) restricted by liquid accumulation in the wellbore and/or high multiphase-flow pressure losses in the production tubing and (2) the incremental increase in production realized by eliminating the excessive back pressure is sufficient to justify the cost of pump installation and operation.

The better candidate wells will have insufficient GLR's to efficiently operate plunger lift (say GLR's be-

low 5,000 scf/bbl) and/or high-liquid-rates wells (say above 30 bbl of fluid per day) with insufficient gas rates or well pressures to maintain natural flow (Section 6.1) in the tubing. As a rough number, a low-volume flowing gas well with a producing tubing gradient above about 50 psi/1,000 ft of depth should be evaluated for a pump. The gradient can be found from the difference between shutin casing pressure and flowing tubing pressure.

From a mechanical viewpoint, wells in which the pump can be set below perforations for good gas separation will have less gas interference and be more successful. If setting the pump in the casing rathole is not practical, the pump should be equipped with a gas anchor. Similarly, wells equipped with downhole packers are not good candidates since gas must be produced through the pump.

6.53 ROD PUMPS

(1) *Downhole pumps and equipment.* The most common type of pump system for gas wells is the API rod pump. This is because rod pumps are theoretically capable of pumping off all liquid in the wellbore. Also, pumps and service personnel are generally available, and field personnel are generally familiar with the equipment.

(2) *Downhole pumps.* The downhole pump is generally an insert type of pump. Snubbing units can be used to pull low-pressure wells without killing the well with load fluids. The pump should be initially sized for about 70% volumetric efficiency, allowing for gas interference. The recommended practice is to use the longest stroke length with a small-diameter pump in order to have the highest compression ratio and reasonable operating speeds (spm).

(3) *Rod strings.* The design of rod strings and the calculation of pumping-unit operating loads is done in the same manner as for oil wells. Usually at slow pumping speeds, acceleration effects are small and may be neglected.

Computer design programs are available for design of rod-pump installations with beam pumping units.

(4) *Gas anchors.* Where there is considerable free gas in the fluid at the pump intake, it is desirable to prevent as much gas as possible from entering the pump and causing gas locking and fluid pounding. It is generally desirable to set the pump in the rathole below perforations to allow gas-liquid separation to occur in the casing above the pump. However, when this is not possible or when gas interference remains troublesome, gas anchors can be used on the bottom of the tubing. Figure 6.41 illustrates a common type of gas anchor. The well fluid must enter the perforated nipple and travel downward at a low velocity before entering the gas anchor tube. The change in fluid direction and the slow downward travel gives the free-gas bubbles an opportunity to separate and rise to the uppermost ports in the perforated nipple where the gas returns to the casing. The downflow area of the anchor should be as large as practical, providing fluid velocities less than 0.5 ft/sec.

(5) *Rod pumping units.* Rod pumping units are of three types:

(1) beam units
(2) pneumatic units
(3) hydraulic units

MIN. DIP TUBE SIZE

RATE, BPD	SIZE
0-100	3/4"
100-250	1"
>250	1-1/4"& LARGER

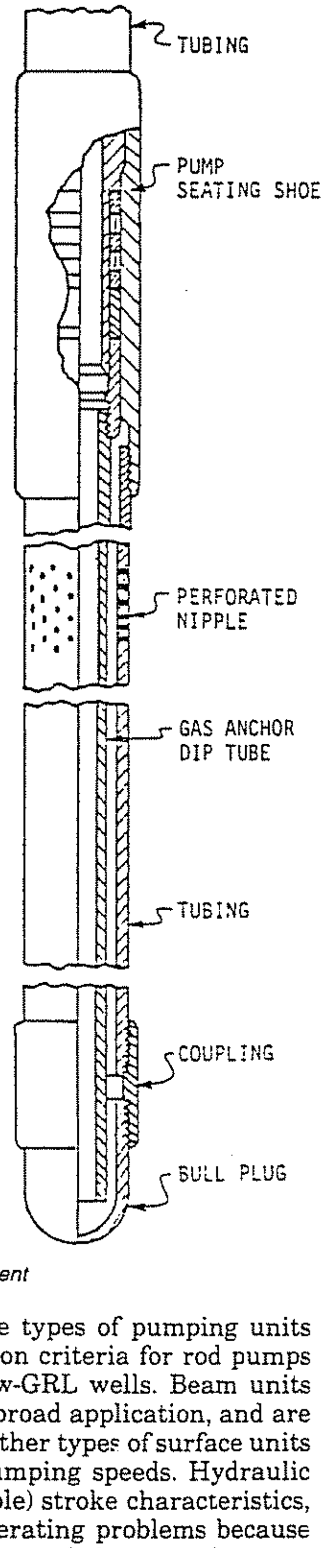

Figure 6.41 Gas Anchor Arrangement

The application for all three types of pumping units follows the general application criteria for rod pumps given in Section 6.52 for low-GRL wells. Beam units are the most common, have broad application, and are probably better suited than other types of surface units for deep wells and faster pumping speeds. Hydraulic units have the best (adjustable) stroke characteristics, but they may have some operating problems because of the high power-oil pressure and they may be more costly to operate. Pneumatic units are specifically designed to operate on nonelectrified leases. This feature alone should give them some application, particularly in tight-gas reservoirs. Because of limited power-cylinder size and the available differential gas pressure, the operating depth (load) with pneumatic units may be less than beam or hydraulic units.

6.531 BEAM PUMPING UNITS

(1) *General description.* The most common pumping unit is the conventional API pumping unit. A crank

and walking beam are used to translate prime mover rotation into reciprocating pump strokes. These units employ counterbalance to minimize horsepower requirements. Beam units normally use electric motors or gas engines as prime movers.

Pump displacement is controlled by changing the drive belt sheave diameter to regulate speed or by changing the position of the pittman arms on the crank to change stroke length. Also, pump-off controllers can be used to match pump displacement with fluid production by stopping and starting the unit if the unit is equipped with an electric-motor prime mover. Pump-off controllers may sense the rod and fluid load and attempt to determine when there is a significant reduction in fluid load. Thus, the effectiveness of pump-off controllers may be diminished as the fluid load decreases as with small plunger diameters and slow pumping speeds.

(2) *Pneumatic beam unit.* A specialized pneumatic-cylinder-powered beam unit is available. The capacity of this unit ranges from about 50 b/d at 3,000 ft to 25 b/d at 5,000 ft.

6.532 PNEUMATIC PUMPING UNITS

Pneumatic pumping units of the type that mount directly over the wellhead are available.

(1) *General description.* The pneumatic pumping unit uses two (or more) pneumatic cylinders. One cylinder is for counterbalance equivalent to the weight of the rods and one-half of the fluid load. A second cylinder is the operating cylinder, which is alternately pressured on the top and bottom of the piston to stroke the rods and pump. The gas supplied to the operating cylinder strokes the piston that supports one-half of the fluid load; i.e., the differential pressure applied against the net piston area equals one-half of the fluid load. The differential pressure could be the differential between the casing and the flow line, in which case the back pressure on the casing is controlled by a throttling control valve. The pressure differential could be between the casing and atmospheric pressure, in which case the spent gas from the operating cylinder is vented. The operating cylinder volume is filled on each stroke with gas at casing pressure. Less gas is used for the atmospheric vent than for the case in which gas is returned to the flow line because the differential pressure is greater. The latter case, however, is not wasteful of produced gas. The applications for specific wells can be evaluated in more detail using design procedures such as those presented in Table 6.3.

(2) *Other operating considerations.* An operating problem that may be encountered is condensation of liquids from the gas causing freeze-ups at throttling valves and liquid collection points in the surface system. These can generally be eliminated by a design in which gas is allowed to reach atmospheric temperature in a separator before it is routed to the unit, or dew-point depressants can be injected. Another problem sometimes encountered is pump stalling if the casing (sales) pressure falls so low that the operating differential pressure is insufficient to stroke the unit. In gas fields where line pressure cycles up and down, frequent adjustments to match operating conditions may be required, and the installation should be designed to hold the maximum well operating pressure that will be needed to pump against the fluid column and the surface tubing pressure.

One unit available utilizes two counterbalance and two operating cylinders to minimize the operating pressure requirements (see Figure 6.42).[36] The unit runs on gas from the well with no outside source of power. The counterbalance charged chamber can be from well gas or from a separate source. Approximate differential pressures to operate the pneumatic pump jack are as follows:[36]

APPROXIMATE DIFFERENTIAL PRESSURE REQUIREMENT REQUIRED TO OPERATE A PNEUMATIC PUMP JACK IN POUNDS PER SQUARE INCH

Depth of pump	Pump size 1-in.	$1\frac{1}{16}$-in.	$1\frac{1}{4}$-in.	$1\frac{1}{2}$-in.
2,000	8	10	18	25
3,000	14	16	24	40
4,000	20	24	32	55
5,000	27	32	40	70
6,000	34	40	50	85
7,000	41	48	60	100

Currently, the largest unit is capable of jacking rods about 7,000 ft deep and weighs about 1,000 lb. The pumps are normally mounted on the wellhead, eliminating a foundation requirement. Additional information on gas required, etc., is available from the manufacture.

Other pneumatic pumping units are configured as conventional beam units that are powered by pneumatic cylinders driven from well gas.

6.533 HYDRAULIC ROD PUMPING UNITS

Vertically mounted hydraulic units can provide the benefits of long stroke length and slow upstroke speed of rod pumps. Hydraulic units have been used to deliquefy gas wells. One version provides for mounting the hydraulic cylinder horizontally where a flexible cable connects the power piston rod to the downhole string. The low-profile horizontal unit is designed to operate in areas where elevated sprinklers are used to irrigate crops.

(1) *General description.* The power-cylinder piston rod attaches to the rod string. The piston moves upward when high-pressure hydraulic oil is applied to the underside of the piston. Piston travel is reversed when a tripping mechanism at the end of the stroke causes the power oil to bypass the cylinder and allows the power fluid to bleed from the cylinder to a receiver vessel. The rod string falls until the lower trip mechanism starts the upstroke cycle unit again. A disadvantage of most hydraulic units is that they do not have a counterbalance feature. In some hydraulic units, high-pressure power oil is supplied by a variable-displacement pump driven by an electric motor or gas engine. The electric-motor-driven units can be intermitted if necessary to match well production. Since the upstroke and downstroke motion is controlled in different ways, the unit can be operated with a slow upstroke speed and a comparatively fast downstroke

TABLE 6.3
APPROXIMATE DESIGN BASIS FOR A PNEUMATIC UNIT

(1) UNIT DATA

6-in. cylinder length, in.	Net stroke, in.	Max. rec'md speed, spm	Displacement per cycle, ft³	Displacement, cfd/cycle
60	54	10	3.53	5,083
50	44	12	2.88	4,147
40	34	15	2.22	3,169

(2) LOAD CALCULATIONS

(A) Counterbalance load

$$CBL = W_{rf} + W_{f/2}$$

where:

W_{rf} = weight of rod string in fluid (use explicit design or approximate rod string weight from Figure 6.43)

$W_f = AP_1$ in.² × 433 psi/ft × depth, ft × SpGr

where:

AP = area of plunger, in.²

(B) Counterbalance cylinder pressure, P_{CB}

$$P_{CB} = \frac{CBL}{A_{CB}}$$

where:

A_{CB} = 54 in.² for 2 ea. – 6-in. cylinders

(C) Operating differential

$$P_D = \frac{\frac{1}{2} W_{f/2} + \text{friction} + \text{acceleration load}}{54}$$

The approximate operating differential can be estimated from Figure 6.44 or by using the above formula. For rough estimating, the friction and acceleration load can be assumed to be about 5–7% of W_f.

(3) GAS REQUIREMENT

(A) Actual displacement volume, V_A

V_A = unit displacement, ft³/cycle × spm × 1,440 min/d = cfd

(B) Gas consumption @ standard conditions, V_s

$$V_s = V_A \times \left(\frac{P_S + 14.7}{14.7}\right) \times \left(\frac{530}{460 + t}\right)$$

where:

P_S = cylinder supply pressure, psig

t = gas inlet temperature, °F

speed. In another (newer) type of hydraulic unit, the power oil is pumped with a variable-displacement pump controlled by an electronic programmable controller.[37] This control of the pump stroke is the principal advantage of a hydraulic unit. Compared to the pneumatic units, the power-oil system provides better lubrication and fewer winterization problems than with pneumatic units.

(2) *Other operating considerations.* Most units have similar operating features and characteristics. One unit uses a spool valve to control the routing of the power fluid. Pump displacement is regulated by the position of the top and bottom ports in the power cylinder, which supply pressure to the spool-valve pilot. One unit uses a four-way valve to route power fluid. The pump stroke is controlled by a cam lever on the polished rod. The upstroke speed on both units can be controlled by adjusting the sheave diameter on the power-oil pump, and hence the power-oil rate.

6.54 HYDRAULIC JET PUMPS

Hydraulic jet pumps are capable of deliquefying gas wells producing less than 150 b/d of liquid.

(1) *General description.* One design uses a downhole jet pump (nozzle and diffuser section) run on a small (1-in.) tubing inside the (2⅜-in.) production tubing and landed in a seating nipple (Figure 6.45).[36] The typical equipment arrangement is shown schematically following this discussion. The high-pressure power fluid is pumped down the annulus between the tubing strings and enters the inside tubing through the jet

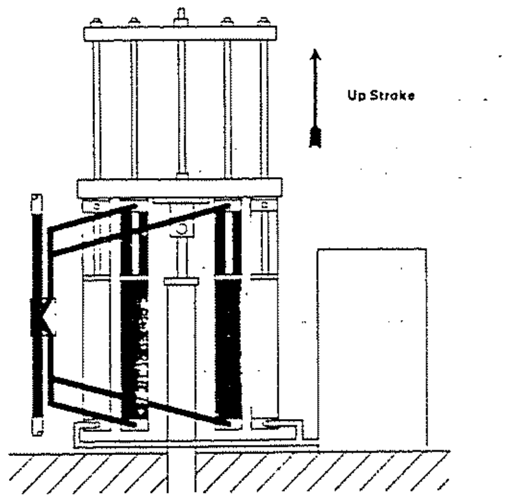

The two inside cylinders are the power cylinders and on the up stroke the well head gas or the high pressure gas is applied to the underneath side of the piston while the sales line gas or the low pressure gas on top of the piston is exhausted to the sales line. On the down stroke the high pressure gas is applied to the top of the pistons and the low pressure gas underneath the pistons is exhausted to the sales line.

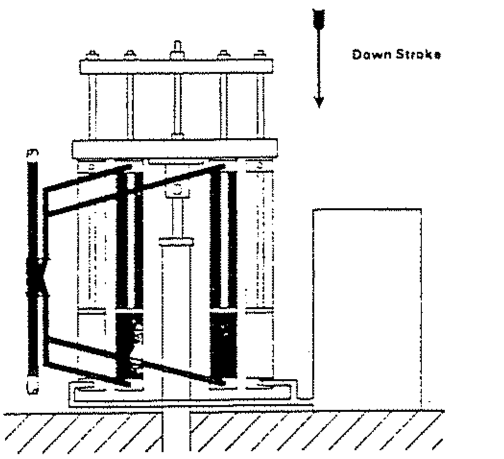

The two outside cylinders are counter balance cylinders. The counter balance gas stored in the counter balance tank is applied underneath the counter balance pistons only, while the top side is vented to atmosphere through filters. The counter balance tank is pressurized with a regulator taking gas from the annulus, with enough pressure to allow the counter balance cylinders to carry all the weight of the rods and one half the weight of the fluid just as a beam unit is balanced. The spool valve reverses the pressure application to the power piston at each end of the stroke and the spool valve is piloted by a reversing rod attached to the piston rod harness.

Figure 6.42 Schematic of Pneumatic Pump Jack Designed to Deliquefy Gas Wells[36]

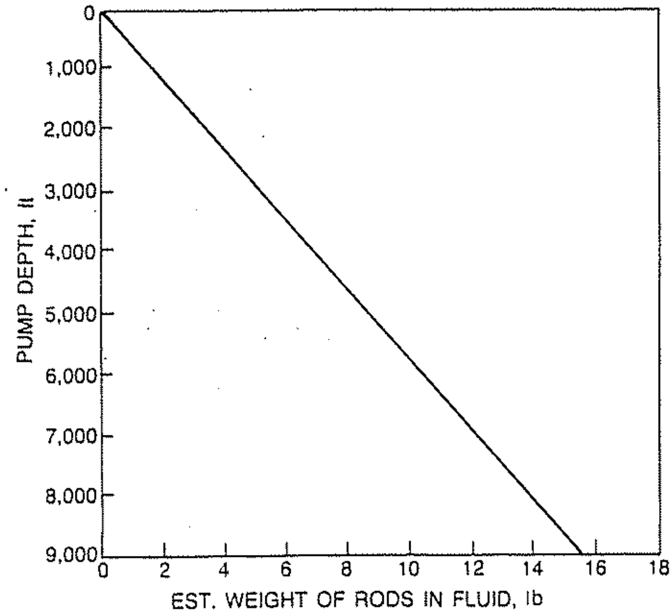

Figure 6.43 Approximate Buoyant Weight of Rod String (≦ 1½-in. Pump Size)

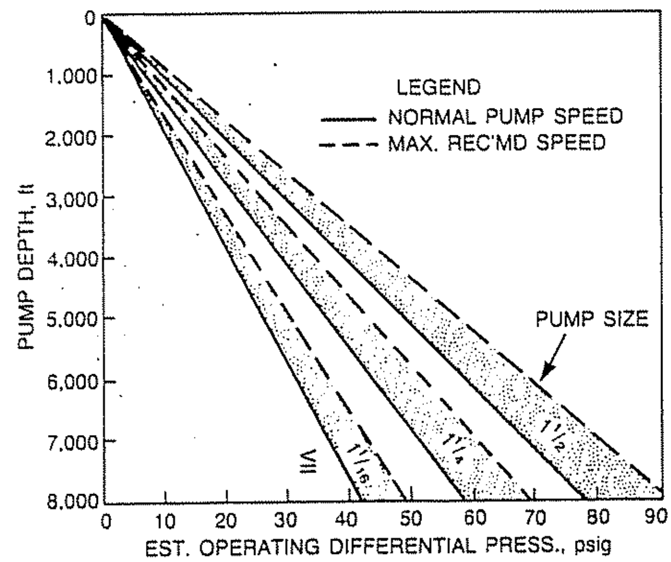

Figure 6.44 Approximate Operating Differential for Pneumatic Pump Jack[36]

nozzle. The pressure of the power fluid is converted to kinetic energy by the nozzle so that a low-pressure area is created around the nozzle throat. Produced fluid is drawn into the throat area and mixed with a high-velocity–low-pressure jet stream. The mixed stream then enters the diffuser area where the kinetic energy is again converted to pressure head. Produced gas is taken from the casing-tubing annulus, while liquids are produced through the small tubing. It is this three-conduit jet arrangement that is unique to one jet-pump system and enables it to effectively produce liquid without forcing gas through the pump. Normally, the casing pressure is allowed to ride on flow-line pressure so that the back pressure on the formation approaches line pressure plus the weight of the gas column in the annulus.

Normally, two limitations that control jet performance are cavitation and choking. Cavitation becomes a problem when the suction pressure at the throat of the jet is below the critical (vapor) pressure of the produced fluid. This limiting pressure criteria is critical for water production but may be less critical for hydrocarbon liquids or water when some free gas is always present. Moreover, it is assumed that the minimum submergence pressure at the pump will be equivalent to line pressure, which is normally 100 psi or more—i.e., above the critical pressure for water at bottom-hole temperature. Choking results when the mixing zone for produced and power fluids backs up to the jet throat inlet, a condition associated with large nozzle/throat area ratios and/or excessive free gas. Either produced water or oil can be used as the power fluid.

(2) *Applications.* The three-conduit jet pump is applicable to wells producing less than 150 b/d (limits

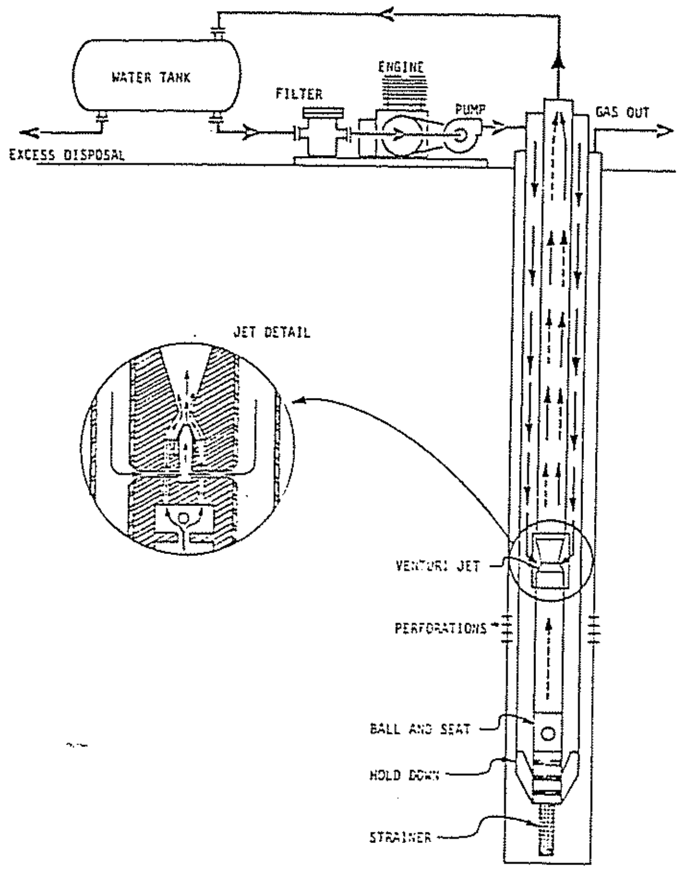

Figure 6.45 Schematic of Jet Pump Designed for Unloading Gas Wells[35]

based on concentric tubing size) from depths above 10,000 ft. The system is capable of operating in wells with small-diameter casing. The downhole pump can be run on coiled tubing. The unit normally operates continuously using an electric motor or gas-engine driver. Sometimes, the pump is operated intermittently by controls that sense gas in the tubing production and activate a timer down-time switch. The jet-pump arrangement discussed herein has considerable potential for operating successfully in a gas-well environment. The main disadvantage of the system is the high cost of the unit.

These units were developed in Canada where they have proved suitable for cold climates if properly housed and also for use in the United States but not for unloading gas wells.

(3) *Other operating considerations.* The system is intended to operate with the fluid level at the pump suction. If the well pumps off, some produced gas is drawn into the jet stream, and performance of the jet deteriorates. If gas production is noticed in the produced stream and the performance of the system is significantly affected, the performance of the jet should be diminished by reducing the power fluid rate to prevent possible cavitation damage and to improve the efficiency. If cavitation occurs, the well's production will fall off sharply, even though power fluid rates may be increased.

The attached curve and design example are given to allow estimates of the general performance of a jet-pump installation (Figures 6.46 and 6.47). The head vs M-ratio curve is an envelope curve for optimum jet-nozzle to throat-area ratios, and the performance of a specific nozzle will only approximate the curve in a narrow operating range. For gas-well deliquefication, M ratios to the left of the graph are used. This requires more power fluid, but the associated nozzle/throat ratio is less sensitive to fluctuations in head pressure, and jet-pump performance is more stable.

The application and design of units for specific wells should be verified with the manufacturer.

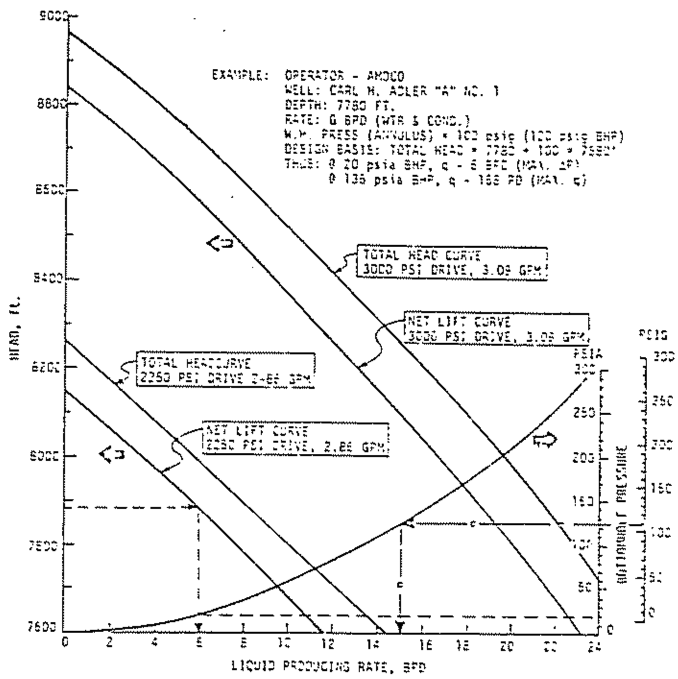

Figure 6.46 Typical Operating Curve for Jet Pump Designed for Unloading Gas Wells

6.55 ELECTRIC SUBMERSIBLE PUMPS

Electric submersible pumps have been used for deliquefying gas wells in special applications. Usually, the applications are in deep wells and/or high-liquid-rate wells. Liquids are pumped through the tubing, and gas is taken from the annulus. If necessary, the pump operation is intermitted to match well inflow and avoid severe pump-off conditions in which no fluid flows to cool the motor. Generally, electric submersible pumps are unattractive compared to other deliquefication methods because of initial cost, operating problems, and expense.

Successful installations for some operators have been reported. Downhole rotary gas separators with a speed or frequency controller for overspeed have been used successfully with a high percent by volume of gas present at pump intake.

Manufacturers are available to advise on sizing and applications.

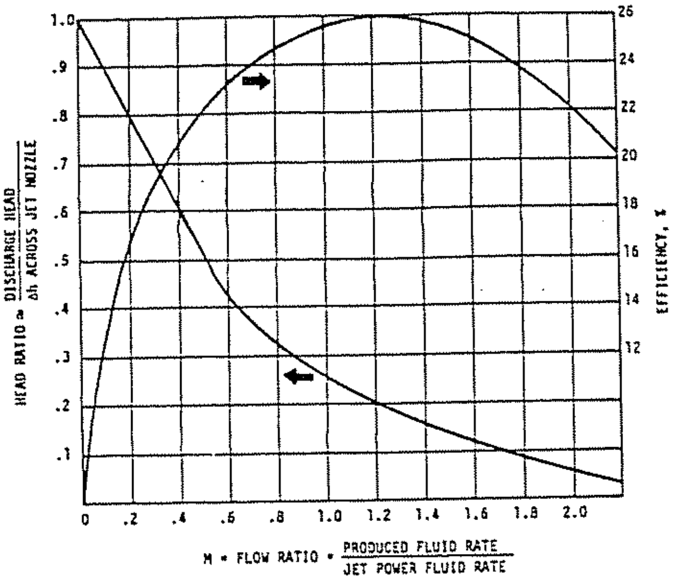

Example Calculation—Jet Pump Design—Rough Estimate

Notes: 1. Manufacturer's have standard jets of various nozzle-to-throat ratios that characterize H and M factors. The manufacturer should be consulted for explicit design.

2. Refer to reference 42 for more detailed design considerations.

Assume: 1. Jet intake submergence pressure = wellhead pressure; therefore, discharge head ≅ tubing depth.

2. Friction losses = 10% of well depth.

3. Power fluid density = produced fluid density.

4. Desired production = 20 b/d from 6,300 ft (7,000 ft with friction losses).

Design	Examples
1. Assume M Ratio M = 0.1–0.2 for depth > 5,000 ft M = 0.2–1.0 for depth < 5,000 ft	1. Let M = 0.1 Q power = 20/0.1 = 200 b/d
2. H Ratio $= \frac{\text{lift pressure required}}{\text{power fluid pressure}}$	2. H Ratio = 0.9 Lift = 7,000 ft × 0.433 psi/ft = 3,031 psi = 3,030/0.9 $P_{surface}$ = 3,368 psi
3. HP = $1.7 \times 10^{-5} \times Q_p \times P_s$ Q = power fluid, b/d P_s = power-fluid surface pressure, psi	3. HP = $1.7 \times 10^{-5} \times 200 \times 3{,}368$ = 11.5 horsepower

Figure 6.47 Jet Pump Operating Parameters

REFERENCES

1. Clark, N. J. *Elements of Petroleum Reservoirs.* Revised Ed. Dallas, Texas: SPE of AIME, 1969.
2. Foss, D. L. and R. B. Gaul. "Plunger-Lift Performance Criteria with Operating Experience—Ventura Avenue Field." *API Drilling and Production Practice* (1965), p. 124–140.
3. Standing, M. B. "A General Pressure-Volume-Temperature Correlation for Mixtures of California Oils and Gasses." *API Drilling and Production Practice* (1947), p. 225.
4. Gray, H. E. "Vertical Flow Correlation in Gas Wells." In *User Manual for API 14B, Subsurface Controlled Safety Valve Sizing Computer Program,* App. B. (June 1974).
5. Greene, W. R. "Analyzing the Performance of Gas Wells." Lubbock, Texas, *25th Annual Southwestern Petroleum Short Course (4/20–21/78) Proceedings.* 1978, p. 129–135.
6. Fetkovich, M. J. *Multipoint Testing of Gas Wells.* SPE Mid-Continent Section, March 17, 1975.
7. Cullender, M. H. "The Isochronal Performance Method of Determining the Flow Characteristics of Gas Wells." *Transactions of the AIME* (1955), p. 204, 137.
8. ERCB. *Gas Well Testing—Theory and Practice.* 4th Ed. Alberta, Canada, 1979.
9. Barr, G. S. and K. Aziz. "The Analysis of Modified Isochronal Tests to Predict the Stabilized Deliverability of Gas Wells Without Using Stabilized Flow Data." *SPE 6134.* New Orleans, Louisiana, October 3–6, 1976, SPE of AIME.
10. Cullender, M. H. and R. V. Smith. "Practical Solution of Gas Flow Equations for Wells and Pipelines with Large Temperature Gradients." *Transactions of the AIME,* 207 (1956).
11. Brown, K. E. and H. D. Beggs. *The Technology of Artificial Lift Methods.* Vol. 1. Tulsa, Oklahoma: PennWell Books, 1977.
12. Govier, G. W. and K. Aziz. *The Flow of Complex Mixtures in Pipes.* New York, New York: Van Nostrand Reinhold Co., 1972.
13. Duns, H. Jr. and N. C. J. Ros. "Vertical Flow of Gas and Liquid Mixtures in Wells." In *Proceedings of the 6th World Petroleum Congress* (1963), p. 451.
14. Govier, E. G. and M. Fogarasi. *Pressure Drop in Wells Producing Gas and Condensate.* Banff, Alberta, Canada, June 11–13, 1975, Petroleum Society of the CIM.
15. Ros, N. C. J. "Simultaneous Flow of Gas and Liquid as Encountered in Well Tubing." *Journal of Petroleum Technology* (October 1961), p. 1037–1049.
16. Orkiszewski, J. "Predicting Two-Phase Pressure Drops in Vertical Pi." *Journal of Petroleum Technology* (June 1967), p. 829–838.
17. Beggs, H. D. and J. P. Brill. "A Study of Two-Phase Flow in Inclined Pipes." *Journal of Petroleum Technology* (May 1973), p. 607–617.
18. Aziz, K., G. W. Govier, and M. Fogarasi. "Pressure Drop in Wells Producing Oil and Gas." *Journal of Canadian Petroleum Technology* (July–September 1972), p. 38–48.
19. Hagedorn, A. R. and K. E. Brown. "Experimental Study of Pressure Gradients Occurring During Continuous Two-Phase Flow in Small-Diameter Vertical Conduits." *Journal of Petroleum Technology* (April 1965), p. 475–484.
20. Libson, T. N. and J. R. Henry. "Case Histories: Identification of and Remedial Action for Liquid Loading in Gas Wells–Intermediate Shelf Gas Play." *Journal of Petroleum Technology* (April 1980), p. 685–693.
21. Turner, R. G., M. G. Hubbard, and A. E. Dukler. "Analysis and Prediction of Minimum Flow Rate for the Continuous Removal of Liquids from Gas Wells." *Journal of Petroleum Technology* (November 1969), p. 1475–1482.
22. Hinze, J. O. "Fundamentals of the Hydrodynamic Mechanism of Splitting in Dispersion Processes." *AIChE Journal,* v. 1, n. 3 (September 1955), p. 28.
23. Lea, J. F. and R. E. Tighe. "Gas Well Operation with Liquid Production." *SPE Preprint 11583.* Oklahoma City, Oklahoma, 1983, SPE of AIME.
24. Meshack I. L. and C. U. Ikoku. "Minimum Gas Flow Rate for Continuous Liquid Removal in Gas Wells." *SPE 10170.* San Antonio, Texas, October 5–7, 1980, SPE of AIME.
25. Beeson, C. M., D. G. Knox, and J. H. Stoddard. "Plunger Lift Correlation Equations and Nomographs." *Paper Sol-G.* New Orleans, Louisiana, October 1955, AIME Petroleum Branch.
26. Foss, D. L. and R. B. Gaul. "Plunger-Lift Performance Criteria with Operating Experience—Ventura Avenue Field." *API Drilling and Production Practice* (1965), p. 124–140.
27. Hacksma, J. D. *Users Guide to Predicting Plunger Lift Performance.* Lubbock, Texas: Southwestern Petroleum Short Course, 1972.
28. Lea, J. F. *Dynamic Analysis of Plunger Lift Operations.* San Antonio, Texas, October 1981, SPE of AIME.
29. Abercrombie, B. "Plunger Lift." In *The Technology of Artificial Lift Methods.* Vol. 2b. Ed. K. E. Brown. Tulsa, Oklahoma: PennWell Publishing Co., 1980.
30. Dunning, H. N. et al. "Foaming Agents for Removal of Liquids from Gas Wells." *Bulletin 05–59–1.* New York, New York: American Gas Association, 1959, 14 pp.
31. Jacoby, R. H. "NGPA Phase Equilibrium Project." In *API Proceedings.* Division of Refining, 1964, p. 288.
32. Hough, E.W. et al. "Interfacial Tensions at Reservoir Pressures and Temperatures; Apparatus and the Water-Methane System." *Transactions of the AIME* (1951), p. 57.

33. Katz, D. L. et al. *Handbook of Natural Gas Engineering.* New York, New York: McGraw-Hill Book Co. Inc., 1959.
34. Ziser, J. A. "Unique Gas Lift Hookup Used to Dewater Gas Wells." *World Oil* (July 1960).
35. Winkler, H. W. and S. S. Smith. *Camco Gas Lift Manual.* Houston, Texas: Camco, 1962.
36. *Oil and Gas Journal.* "New Artificial-Lift Systems Utilize Unique Technology." (February 2, 1976), p. 72–73.
37. Laidlaw, R. N. and P. J. Jespersen. "The HEP Pumping Unit: Performance Characteristics, Potential Applications and Field Trial Results." *Paper 80–31–42.* Calgary, Alberta, Canada, May 25, 1980, Petroleum Society of CIM.
38. *World Oil.* "Venturi Jet Tool Unloads Gas Wells." (November 1979) p. 79.
39. Baker, O. and W. Swerdloff. "Finding Surface Tension of Hydrocarbon Liquids." *Oil and Gas Journal* (January 2, 1956), p. 125.
40. Beauregard, E. M. and P. L. Ferguson. *Petroleum Engineer International* (July 1981).
41. Blauer, R. E., B. J. Mitchell, and C. A. Kohlhaas. "Determination of Laminar, Turbulent, and Transitional Foam Flow Losses in Pipes." *SPE 4885.* April 4–5, 1974, SPE of AIME.
42. Brown, K. E. *Gas Lift Theory and Practice.* Tulsa, Oklahoma: PennWell Publishing Co., 1973.
43. ——*Technology of Artificial Lift Methods.* Vol. 2a. Tulsa, Oklahoma: PennWell Publishing Co., 1981.
44. Camacho, C. A. "A Comparison of Correlations Predicting Pressure Loss in High GLR Wells." M.S. Thesis, University of Tulsa, July 1970.
45. Fancher, G. H. and K. E. Brown. "Predication of Pressure Gradients for Multiphase Flow in Tubing." *SPE Journal* (March 1963), p. 59–69.
46. Gear, C. W. *Numerical Initial Value Problems in Ordinary Differential Equations.* Englewood Cliffs, New Jersey: Prentice-Hall, 1961.
47. Havlena, D. and A. S. Odeh. "The Material Balance as an Equation of a Straight Line." *Transactions of the AIME* (1963).
48. Holiday, C. H. "Automatic Subsurface Liquid Removal from Gas Wells." *SPE 2359.* Charleston, West Virginia, November 7–8, 1968, SPE of AIME.
49. Hutlas, E. J. and W. R. Grandberry. "A Practical Approach to Gas Well Liquid Removal." *SPE 3473.* New Orleans, Louisiana, October 3–6, 1971, SPE of AIME.
50. Katz, K. L. et al. *Handbook of Natural Gas Engineering.* New York, New York: McGraw-Hill Book Co. Inc., 1959.
51. Lasater, J. A. "Bubble Point Pressure Correlations." *Transactions of the AIME* (1958), p. 379.
52. Lebeaux, J. M. and L. F. Sudduth. "Theoretical and Practical Aspects of Free Piston Operation." *Journal of Petroleum Technology* (September 1955), p. 33–35.
53. Moss, E. E. and P. W. Orris. *Liquid Removal From Gas Wells–Lifting with Reservoir Gas.* Southwest Petroleum Shortcourse, April 18–19, 1968.
54. Nichols, Roland. "Dewatering Gas Wells." *Paper 851–42–A.* Amarillo, Texas, April 3–5, 1968, API.
55. Poettman, F. H. and P. G. Carpenter. "The Multiphase Flow of Gas, Oil and Water Through Vertical Flow Strings with Application to the Design of Gas-Lift Installations." *API Drilling and Production Practice* (1952), p. 257–317.
56. Taital, Y., D. Bornea, and A. E. Dukler. "Modeling Flow Pattern Transitions for Steady Upward Gas-Liquid Flow in Vertical Tubes." *AIChE Journal,* v. 26, n. 3 (May 1980), p. 345–354.
57. Thomas, D. C., Amoco Production Research, Private Communication, 1982.

Chapter 7

Coning and fingering of water and gas

by Roberto Aguilera and Luis Acevedo

The difference between coning and fingering has been discussed by Chaney et al.[1] and Arthur[4] and is illustrated on Figure 7.1. Coning of water or gas into an oil well occurs when the flowing pressure gradients established around the wellbore cause the gas or water to flow across the bedding planes as shown in Figure 7.1b. Fingering occurs when the flowing pressure gradients around the wellbore cause gas or water to flow along the bedding planes, as shown in Figure 7.1a.

This chapter will deal with coning and fingering in homogeneous and isotropic reservoirs as well as anisotropic and naturally fractured reservoirs. Although the authors recognize that all problems related to coning cannot be treated realistically with simple analytical solutions, experience indicates that the methods presented in this chapter can give good order-of-magnitude results in many situations. Complications such as irregular boundary conditions, anisotropy, multiphase flow, and variations in production rates can be treated more vigorously with numerical simulators. Unfortunately, these tools are not always available to the practicing petroleum engineer, who must resort then to methods such as those presented in this chapter. Several examples, which can be reproduced readily with hand-calculators, are presented.

7.1 WATER AND GAS CONING

7.11 STABLE AND UNSTABLE CONES

A stable cone[1] occurs when:

(1) a well is produced at a constant rate,
(2) the pressure gradients in the drainage area are constant, and
(3) the flowing pressure gradient is smaller than the gravity forces.

When the flowing pressure gradients become large enough to overcome the gravitational forces, the water or gas form an *unstable* cone, which will advance into the wellbore. Consideration has to be given, consequently, to a delicate balance created between two forces: (1) the gravitational forces caused by the difference of densities between gas, oil, and water; and (2) the pressure gradients that produce the flow of fluids.

7.12 CRITICAL PRODUCTION RATE

Critical production rate is the maximum water-free or gas-free production rate. Above this rate, the flowing pressure drop at the wellbore causes the water or gas to flow into the well. It is important to visualize that, at the critical rate, the cone is stable. However, it is at a position where it may become unstable rather easily, generating consequently an early water or gas breakthrough.

7.13 CONING IN HOMOGENEOUS RESERVOIRS

7.131 MUSKAT AND ARTHUR METHODS

By considering the water and gas-coning conditions presented in Figure 7.2, Muskat[2,3] has related the potential forces set up in the flowing fluid to the differential gravitational forces between the two fluids involved. His equation for coning in a homogeneous reservoir can be written as:

$$\frac{\Delta\Phi}{\Delta\Phi_e} = \frac{\Phi_w - \Phi_z}{\Phi_w - \Phi_e} = 1 - \frac{g\Delta\rho}{\Delta P} h \left(1 - \frac{Z}{h}\right) \qquad (7.1)$$

where:

Φ = velocity potential
Φ_e = potential at drainage radius
Φ_w = potential at the well surface
Φ_z = potential at well radius and at depth Z
g = acceleration of gravity
$\Delta\rho$ = difference in density between two fluids
ΔP = pressure drawdown of producing well, psi
Z = distance of point from selected datum level, ft
h = reservoir thickness, ft

Arthur has generated graphical solutions to Muskat's equation, and these are presented in Figures 7.3 through 7.5.[4] Figure 7.3 shows a cross plot of well penetration (b/h), where b is the penetration of the well

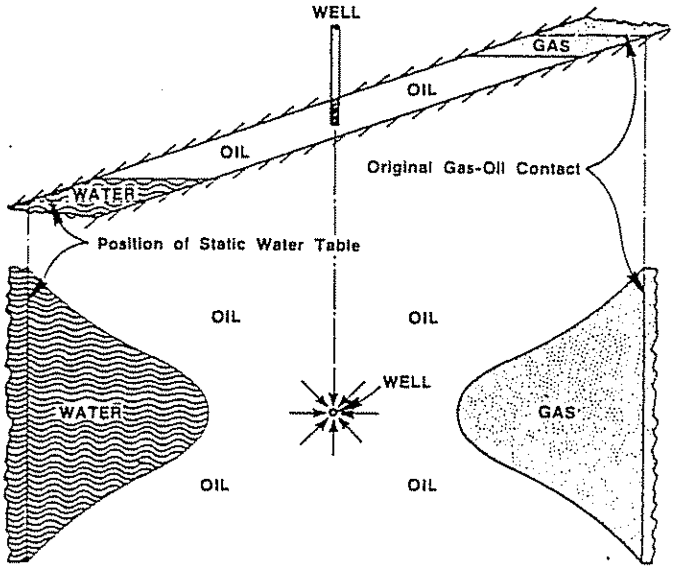

Figure 7.1(a) Water and Gas Fingering[1]

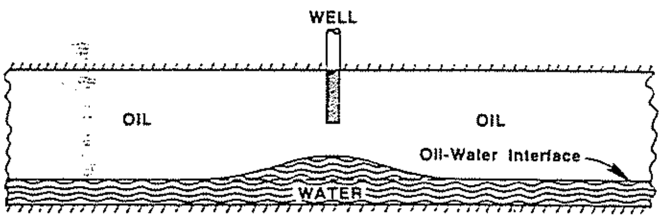

Figure 7.1(b) Water Coning (after Chaney et al.)[1]

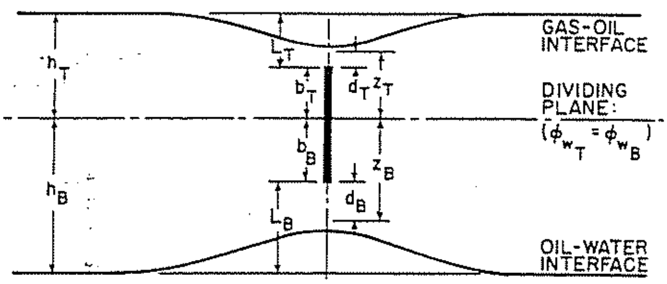

Figure 7.2 Water and Gas-Coning Conditions (after Arthur)[4] *T = top; B = bottom*

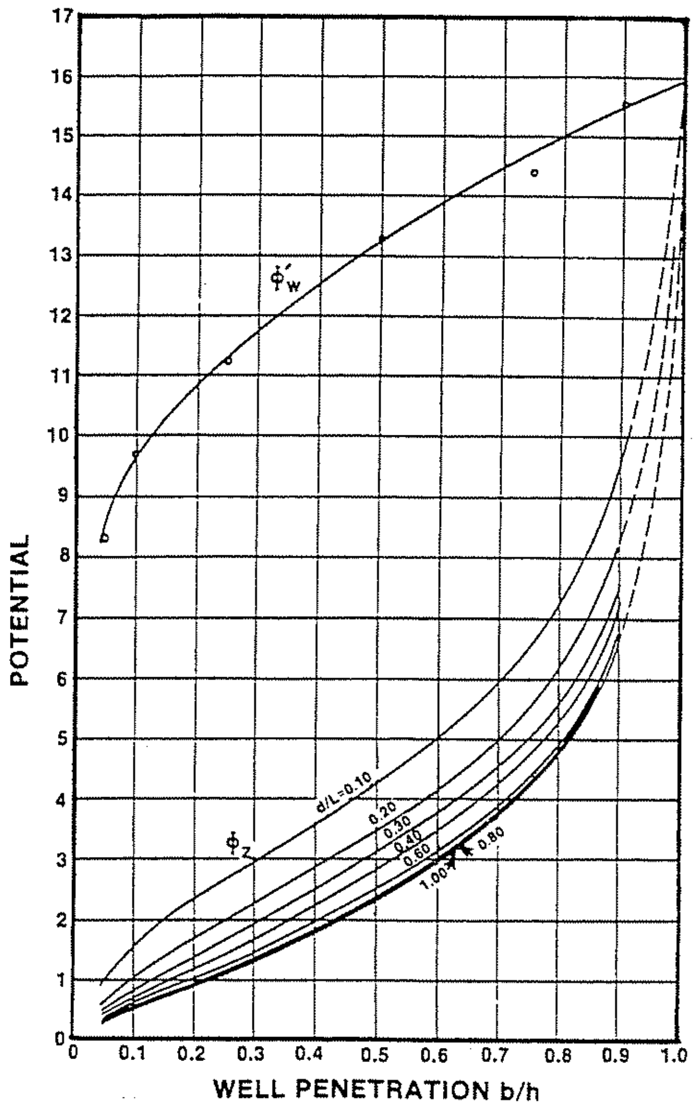

Figure 7.3 Velocity Potential Distribution at Well Radius (after Arthur)[4]
Note: d and L are thicknesses represented on Figure 7-2

in the formation (ft) vs potential at the well surface Φ'_w for a particular value of the well radius (0.001), which is defined by the well radius parameter $r_{DW} = r/2h$. Also cross plotted on the same figure is the well penetration (b/h) vs the potential below the bottom of the well Φ_z. Figure 7.4 shows correction factors that can be applied to Φ_w for values of well radius different from those presented in Figure 7.3.

Figure 7.5 shows velocity potentials Φ_e at drainage radius vs the drainage radius parameter $r_{DE} = r_e/2h$. This figure can be used to obtain potentials Φ_e for reasonable values of drainage radius, r_e.

Arthur's graphical solutions are best illustrated with the following example:[4]

EXAMPLE #1

Given data:

depth of gas-oil contact = 7,535 ft
depth of water-oil contact = 7,695 ft
top of perforations = 7,623 ft
bottom of perforations = 7,685 ft
size of liner = 0.2083 ft
oil gradient in well = 0.325 psi/ft
water gradient in well = 0.425 psi/ft
gas gradient in well = 0.082 psi/ft

A cross section with the above data is presented in Figure 7.6.

Calculate:

Generate maximum pressure drawdowns without conings of water or gas for a well with the characteristics given.

Solution procedure:

To obtain a solution, a horizontal dividing plane must be located such that the potential over the well surface Φ_w is the same for both the upper and lower portions. This dividing plane is located by cross plotting the values of well potential for each portion of the reservoir against the distance of the dividing plane from an arbitrary datum. Figure 7.7 shows the solution of locating the dividing plane and the velocity potential over the well surface for the case of simultaneous coning of water and gas.

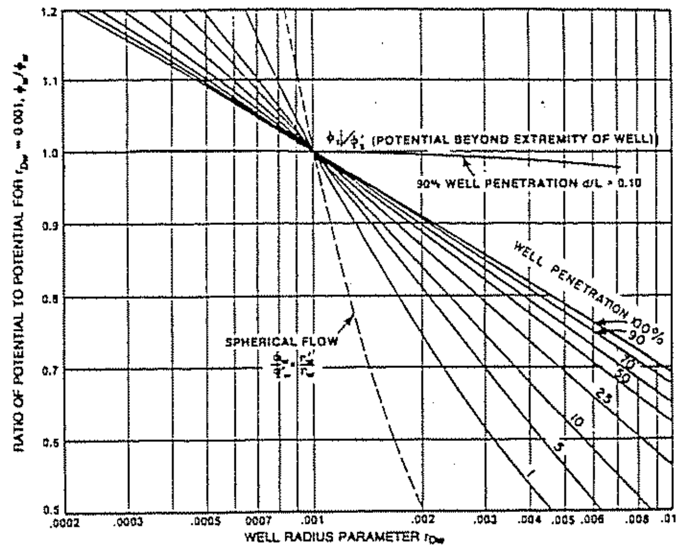

Figure 7.4 Correction Factors for Converting Well Velocity Potential of Figure 7.3 to Velocity Potential for Other Well Radii (after Arthur)[4]

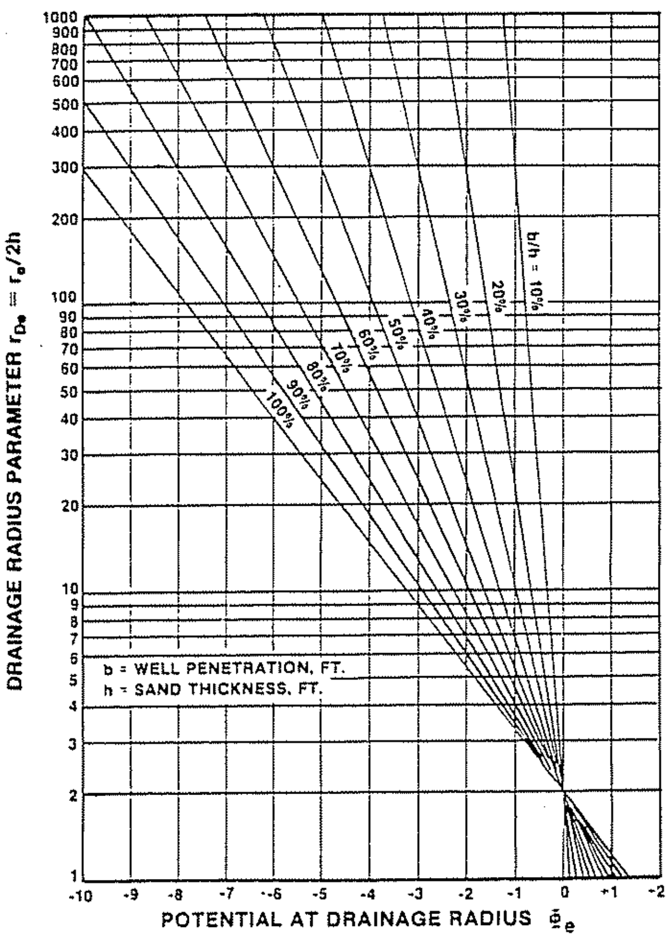

Figure 7.5 Velocity Potential at Drainage Radius (after Arthur)[4]

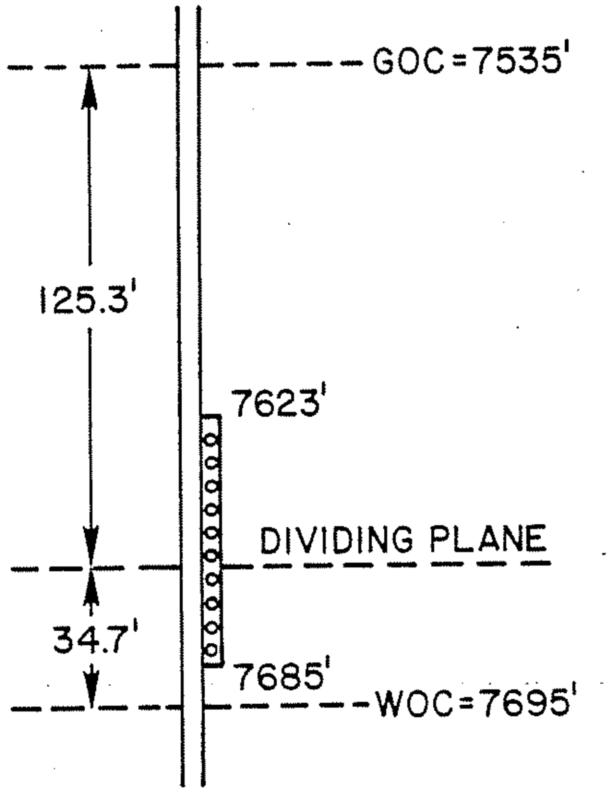

Figure 7.6 Cross Section for Gas and Water Coning (Example #1)

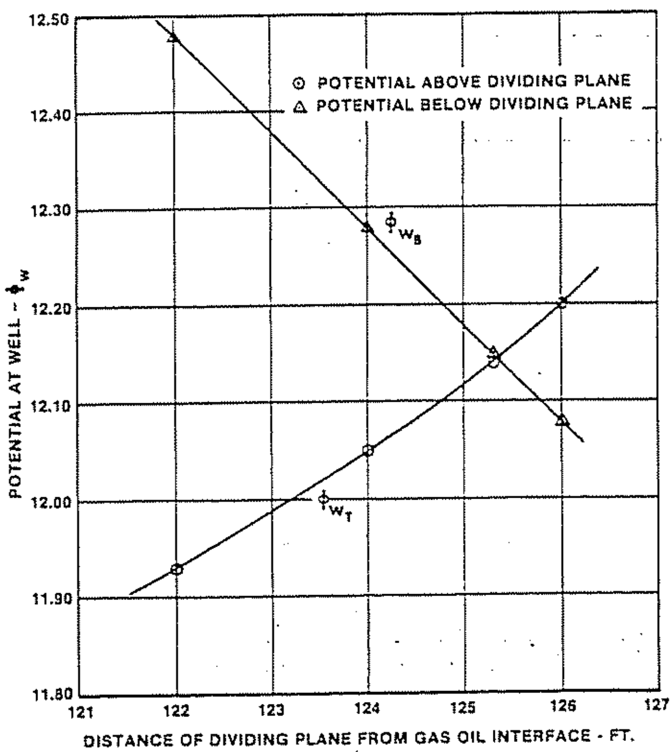

Figure 7.7 Solution of Location of Dividing Plane and Velocity Potential Over Well Surface for Case of Simultaneous Coning of Water and Gas (after Arthur)[4]

The values of the well potential in the top portion, Φ_{wT}, and well potential in the bottom portion, Φ_{wB}, are plotted against the distance of the dividing plane from the gas-oil interface. The curves intercept about 125.35 ft below the gas-oil contact, indicating that this is the proper location of the dividing plane. The potential Φ_w at this point is 12.14.

Arthur has presented the calculation to generate one set of points on Figure 7.7 as follows:[4]

(1) *Calculations above the horizontal dividing plane.* The following is the wellbore radius parameter above the horizontal diving plane r_{DWT}:

$$r_{DWT} = \frac{r_w}{2h_T} = \frac{0.2083}{(2)(125.3)} = 0.000831$$

$$\text{penetration} = \frac{b_T}{h_T} = \frac{125.3 - 88}{125.3} = 29.75\%$$

Notice that 88 ft is the distance between the gas-oil contact and the upper perforation.

The potential at well surface Φ'_{wT} above the horizontal division plane for a radius parameter equal to 0.001 from Figure 7.3 is:

$$\Phi'_{wT} = 11.75$$

Correction factor $C = \Phi_{wT}/\Phi'_{wT}$, or the ratio of potential to potential for $r_{Dw} = 0.001$ from Figure 7.4, is:

$$C = 1.033$$

$$\Phi_{wT} = C \times \Phi'_{wT} = 1.033 \times 11.75 = 12.14$$

(2) *Calculations below the horizontal dividing plane.* Wellbore radius parameter, r_{DWB} is:

$$r_{DWB} = \frac{r_w}{2h_B} = \frac{0.2083}{2(160 - 125.3)} = 0.003$$

$$\text{penetration} = \frac{b_B}{h_B} = \frac{34.7 - 10}{34.7} = 71.2\%$$

Potential at well surface Φ'_{wB} from Figure 7.3 is:

$$\Phi'_{wB} = 14.54$$

Correction factor C from Figure 7–4 is:

$$C = 0.836$$

$$\Phi_{wB} = C \times \Phi'_{wB} = 12.15$$

This is approximately the same number calculated above the horizontal dividing plane. These two points are shown at the intercept of Figure 7.7.

(3) *Water coning calculations.* The reservoir thickness h below the horizontal dividing plane is 34.7 ft as shown in Figure 7.6. The value of b is 24.7 ft, resulting in a penetration of 71.2%.

Values of the potential Φ_z are calculated from Figure 7.3 as a function of d/L, where d is the distance in feet from the end of the perforated interval to point Z, and L is the distance from the end of the perforated interval to the static interface of the two fluids. The ratio d/L can be written as:

$$\frac{d}{L} = \frac{\frac{Z}{h}h - b}{h - b} \tag{7.2}$$

Z/h is the penetration ratio presented in Equation 7.1.

Values of $\Delta\Phi/\Delta\Phi_e$ vs Z/h are presented in Figure 7.8 for various values of drainage radius. As an example, the potential ratio Φ/Φ_e for a Z/h of 0.8 and a drainage radius of 10,000 ft was calculated as follows:

$$\text{ratio}\ \frac{d}{L} = \frac{(0.8)(34.7) - 24.7}{34.7 - 24.7} = 0.306 \text{ from Equation 7.2}$$

The potential at the well radius and at a depth Z was found to be approximately 4.5 from Figure 7.3. The potential Φ_w was calculated in a previous step in this problem to be $\Phi_w = \Phi_{wT} = \Phi_{wB} = 12.15$.

The drainage radius parameter r_{De} is equal to:

$$r_e/2h = 10{,}000/(2 \times 34.7) = 144.1$$

This number was introduced in Figure 7.5 and allowed to calculate a potential at drainage radius Φ_e of −6.3 as a function of the b/h ratio (71.2%).

Inserting the above potentials in Equation 7.1 allows the calculation of $\Delta\Phi/\Delta\Phi_e$ as follows:

$$\frac{\Delta\Phi}{\Delta\Phi_e} = \frac{\Phi_w - \Phi_z}{\Phi_w - \Phi_e} = \frac{12.15 - 4.5}{12.15 - (-6.3)} = 0.4146$$

The above $\Delta\Phi/\Delta\Phi_e$, together with a drainage radius of 10,000 ft and a penetration z/h of 0.8, allows us to plot a data point represented by a circle in Figure 7.8. All curves for different drainage radius were generated in the same fashion discussed above.

The maximum pressure differential without coning is calculated from the equation:

$$\Delta P = \frac{g\,\Delta\rho h}{1 - \left(\frac{\Delta\Phi}{\Delta\Phi_e}\right)_{\frac{Z}{h}=0}} \tag{7.3}$$

where $g\Delta\rho$ is the difference between the water and oil gradients (0.425 − 0.325 = 0.10 psi/ft). The value

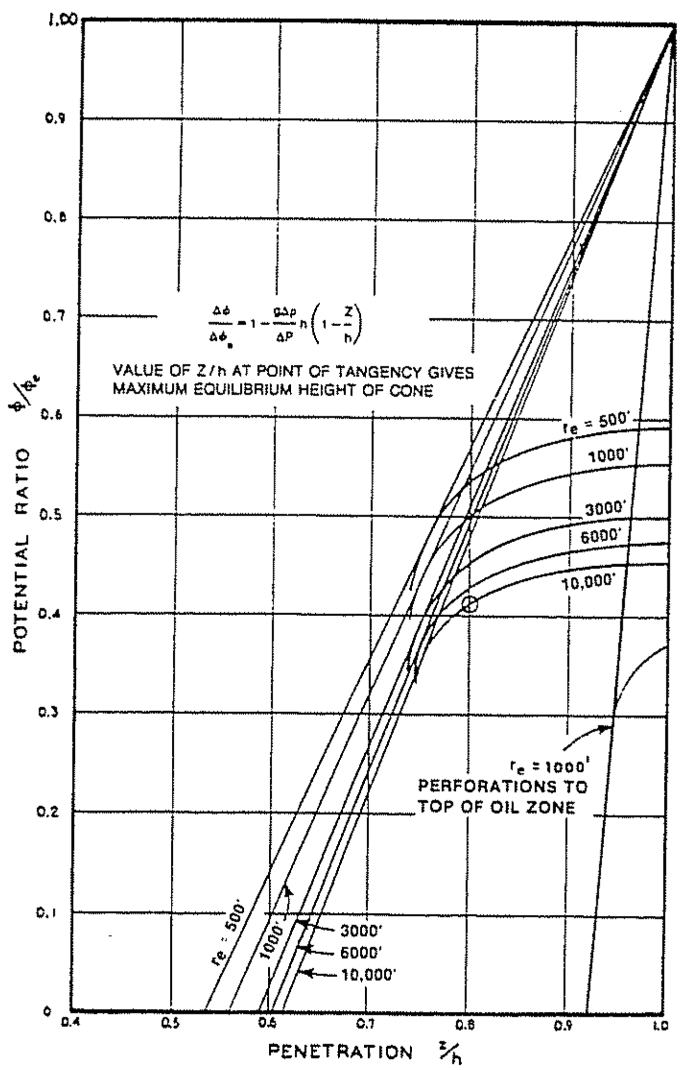

Figure 7.8 Example of Graphical Solution of Equilibrium Height of Water Cone and Maximum Pressure Drawdown Without Water Coning for Selected Values of Drainage Radius (after Arthur)[4]

of $(\Delta\Phi/\Delta\Phi_e)_{z/h=0}$ is calculated from the slope of the tangent for the particular value of drainage radius in Figure 7.8, which is drawn through a Φ/Φ_e and Z/h of 1.0 For example, if r_e = 3,000 ft, the slope is 1/0.41 = 2.439. From Equation 7.1:

$$\left(\frac{\Delta\Phi}{\Delta\Phi_e}\right)_{\frac{Z}{h}=0} = 1 \text{ slope} = -1.439$$

The maximum pressure differential without water coning is calculated from Equation 7.3 as:

$$\Delta P = \frac{(0.10)(34.7)}{1-(-1.439)} = 1.42 \text{ psi}$$

The above pressure differential for a drainage radius of 3,000 ft is represented by a circle in Figure 7.9. The remaining portion of the water coning curve was generated in the same fashion. Notice that the pressure drawdowns that would produce water coning are very small. This is the result of having the lower perforation only 10 ft above the water-oil contact.

(4) *Gas coning calculations.* The reservoir thickness h above the horizontal dividing plane is 125.3 ft. The value of b is 37.4 ft, resulting in a penetration of 29.8%.

The same procedure discussed previously for water-coning has been utilized for the case of gas-coning. Figure 7.10 shows a crossplot of $\Delta\Phi/\Delta\Phi_e$ vs Z/h for various values of drainage radius. The maximum pressure drawdowns without coning of gas are presented in Figure 7.9.

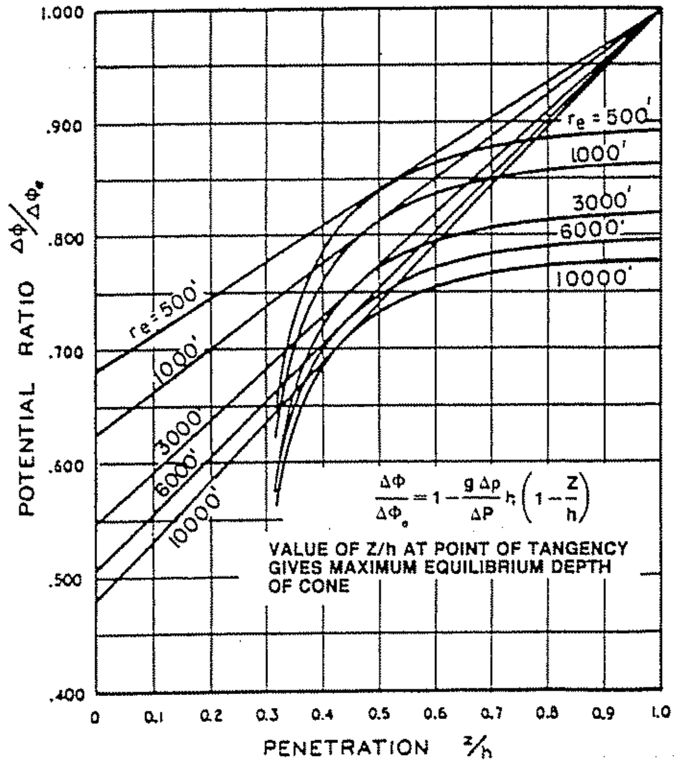

Figure 7.10 Example of Graphical Solution of Equilibrium Depth of Gas Cone and Maximum Pressure Drawdown Without Gas Coning for Selected Values of Drainage Radius (after Arthur)[4]

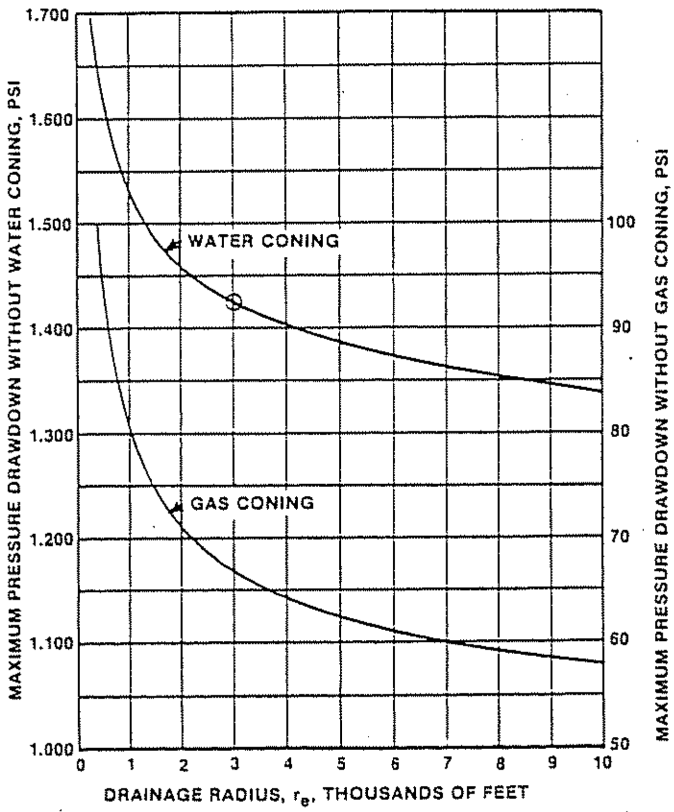

Figure 7.9 Example of Maximum Pressure Drawdown Without Coning of Water and Gas Function of Drainage Radius (after Arthur)[4]

7.132 MEYER AND GARDNER AND PIRSON METHODS

The Meyer and Gardner[5] and Pirson[6] methods consider simplified radial flow of oil under its own gravity head.

(1) *Gas coning.* Figure 7.11 shows gas coning conditions at breakthrough. The well penetrates depth D into a horizontal reservoir of thickness h. The assumption is made that the gas-oil contact is depressed around the wellbore because of radial flow of oil and the pressure differential that results from it. The equation that handles this situation when capillary pressures are neglected can be written as:

$$q_{o_{max}} = 0.001535 \frac{\rho_o - \rho_g}{\ln(r_e/r_w)} \frac{k_o}{\mu_o}[h^2 - (h-D)^2] \quad (7.4)$$

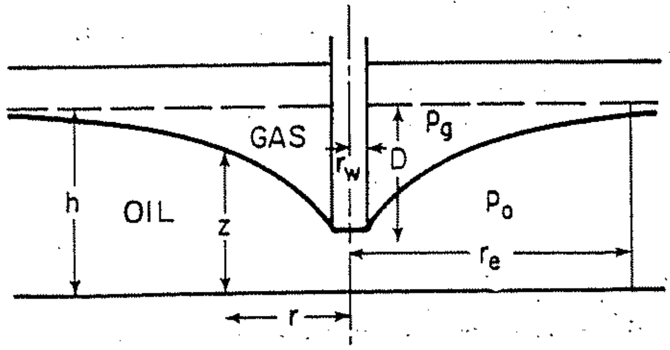

Figure 7.11 Gas Coning (Conditions at Breakthrough) (after Meyer and Gardner[5] and Pirson[6])

where:

$q_{o_{max}}$ = maximum oil rate without gas coning, stb/d
ρ_o = oil density
ρ_g = gas density
r_e = drainage radius, ft
r_w = wellbore radius, ft
k_o = effective permeability to oil, md
μ_o = oil viscosity, cp
h and D = thicknesses represented in Figure 7.11, ft

(2) *Water coning.* Figure 7.12 shows water-coning conditions at breakthrough. The well penetrates a depth D into a horizontal reservoir of thickness h. The assumption is made that the water-oil contact is raised around the wellbore in the form of a cone because of radial flow of oil and the pressure differential that results from it. The equation that handles this situation when capillary pressures are neglected can be written as follows:

$$q_{o_{max}} = 0.001535 \frac{(\rho_w - \rho_o)}{\ln(r_e/r_w)} \frac{k_o}{\mu_o} (h^2 - D^2) \qquad (7.5)$$

where:

ρ_w = the water density

The remaining parameters were defined in the previous section of gas coning.

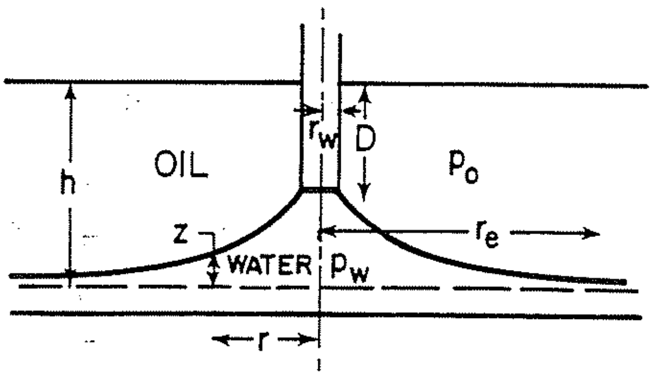

Figure 7.12 Water Coning (Conditions at Water Breakthrough) (after Meyer and Gardner[6] and Pirson[6])

(3) *Simultaneous gas and water coning.* Figure 7.13 shows simultaneous gas and water coning conditions at breakthrough of both fluids. The perforated interval h_c must be placed in such a way as to permit maximum oil production without gas and/or water coning. This can be achieved by obtaining an optimum equilibrium between the well penetration D into a horizontal oil reservoir of thickness h and the completion interval h_c. The well penetration D is calculated from the equation:

$$D = h - (h - h_c) \frac{\rho_o - \rho_g}{\rho_w - \rho_g} \qquad (7.6)$$

Pirson has divided the maximum flow rate ($q_{o_{max}}$) for this case into two components.[6] One is q_{o_w}, which is the maximum oil rate in the absence of water flowing into the well. This rate takes place below the horizontal plane Z_o (Figure 7.13). The other component is q_{o_g}, which is the maximum oil rate without gas breakthrough. This rate takes place above the horizontal plane Z_o, which is given by the relationship:

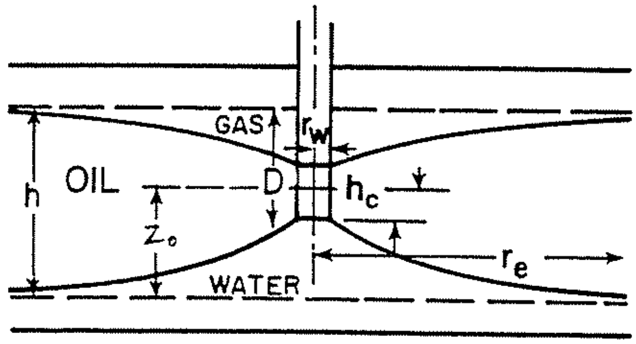

Figure 7.13 Simultaneous Gas and Water Coning (Conditions for Simultaneous Gas and Water Breakthrough) (after Meyer and Gardner[6] and Pirson[6])

$$Z_o = h \left(\frac{\rho_o - \rho_g}{\rho_w - \rho_g} \right) \qquad (7.7a)$$

where all parameters have been defined previously.

The maximum total oil rate without gas or water coning is given by:

$$q_{o_{max}} = q_{o_w} + q_{o_g} \qquad (7.7b)$$

The component q_{o_w} is expressed by the following equation:

$$q_{o_w} = 0.001535 \frac{(\rho_w - \rho_o)}{\ln(r_e/r_w)} \frac{k_o}{\mu_o B_o} \left(\frac{\rho_o - \rho_g}{\rho_w - \rho_g} \right)^2 (h^2 - h_c^2) \qquad (7.8)$$

where B_o is the oil formation volume factor in bbl/stb. The rate q_{o_g} is calculated from the relationship:

$$q_{o_g} = 0.001535 \frac{(\rho_o - \rho_g)}{\ln(r_e/r_w)} \frac{k_o}{\mu_o B_o} \left(1 - \frac{\rho_o - \rho_g}{\rho_w - \rho_g} \right)^2 \times (h^2 - h_c^2) \qquad (7.9)$$

Addition of the above two equations results in the following expression for the maximum total permissible production rate:

$$q_{o_{max}} = 0.001535 \frac{k_o}{\mu_o B_o} \frac{(h^2 - h_c^2)}{\ln(r_e/r_w)} \times \left[(\rho_w - \rho_o) \left(\frac{\rho_o - \rho_g}{\rho_w - \rho_g} \right)^2 + (\rho_o - \rho_g) \left(1 - \frac{\rho_o - \rho_g}{\rho_w - \rho_g} \right)^2 \right] \qquad (7.10)$$

The above equations can be used very easily. However, it must be kept in mind that these are simplified radial-flow formulas, which in general are less accurate than more rigorous methods.

EXAMPLE #2 (HORIZONTAL RESERVOIR WITH A GAS CAP—UNDERLAID BY BOTTOM WATER)

What should be the maximum oil rate to avoid water and gas coning?

Given data:

oil column pay, h = 30 ft
k_o = 80 md
B_o = 1 bbl/stb

$\mu_o = 3$ cp
$\rho_o = 0.85$ g/cc
$\rho_w = 1.1$ g/cc
$\rho_g = 0.3$ g/cc
$r_w = 0.5$ ft
$r_e = 1320$ ft
$h_c = 7$ ft

Calculate:

Find the maximum oil rate to avoid water and gas coning.

Solution procedure:

The well penetration is calculated from Equation 7.6 as follows:

$$D = 30 - (30 - 7)\frac{(0.85 - 0.30)}{(1.10 - 0.30)} = 14.19 \text{ ft}$$

The equilibrium level, Z_o, is calculated from Equation 7.7a:

$$Z_o = 30\frac{(0.85 - 0.30)}{(1.10 - 0.30)} = 20.63 \text{ ft}$$

The maximum oil rate below the horizontal plane Z_o is calculated from Equation 7.8 as follows:

$$q_{o_w} = 0.001535\frac{(1.1 - 0.85)}{\ln(1320/0.5)}\frac{80}{3}\left(\frac{0.85 - 0.30}{1.10 - 0.30}\right)^2 \times (30^2 - 7^2) = 0.522 \text{ b/d}$$

The maximum oil rate above the equilibrium level Z_o is determined from Equation 7.9:

$$q_{o_g} = 0.001535\frac{(0.85 - 0.30)}{\ln(1320/0.5)}\frac{80}{3}\left(1 - \frac{0.85 - 0.30}{1.10 - 0.30}\right)^2 \times (30^2 - 7^2) = 0.237 \text{ b/d}$$

The maximum oil rate, $q_{o_{max}}$, is calculated from Equation 7.7b to be 0.759 b/d. This extremely low rate is the result of the contacts being very close to the perforated interval.

7.133 CRAFT AND HAWKINS METHOD

In the Craft and Hawkins method,[7] the following approximate equations, which were verified using an electric model, are utilized:

$$q_o = \frac{0.00708 k_o h (P_{ws} - P_{wf})}{\mu_o B_o \ln(r_e/r_w)} \times PR \qquad (7.11)$$

$$PR = f\left[1 + 7\sqrt{\frac{r_w}{2fh}}\cos(f \times 90°)\right] \qquad (7.12)$$

where:

PR = productivity ratio
P_{ws} = static well pressure corrected to the middle of the producing interval, psi
P_{wf} = flowing well pressure at the middle of the producing interval, psi
f = fractional penetration

The rest of the nomenclature has been defined previously.

The maximum drawdown without water entering the well is approximated by:

$$\Delta P_{max} = 0.433(\rho_w - \rho_o)\Delta h_{max} \qquad (7.13)$$

where Δh_{max} is the vertical distance between the lowest perforation and the initial water contact.

EXAMPLE #3

Given data:

$\rho_w - \rho_o = 0.48$
fractional penetration = 0.3125 (upper 31.25% of oil column is perforated)
k_o (permeability) = 1,500 md
h (oil-column thickness) = 16 ft
μ_o (oil viscosity) = 0.3 cp
B_o (oil formation volume factor) = 1.4 bbl/stb
r_e (drainage radius) = 1,000 ft
r_w (wellbore radius) = 0.25 ft
$P_{ws} - P_{wf}$ (pressure differential) = 17 psi

Calculate:

Find the maximum rate.

Solution procedure:

The productivity ratio (PR) is calculated with the use of Equation 7.12:

$$PR = 0.3125\left[1 + 7\sqrt{\frac{0.25}{(2)(0.3125)(16)}}\cos(0.3125 \times 90)\right]$$

$PR = 0.618$

The maximum rate is calculated from Equation 7.11:

$$q_o = \frac{0.00708(1{,}500)(16)(17)}{(0.3)(1.4)\ln(1{,}000/0.25)} \times 0.618$$

$$= 512 \text{ stb/d}$$

However, this rate must be reduced since the maximum ΔP without water coning is $(0.433)(0.48)(11) = 2.29$ psi.

7.134 CHANEY ET AL. METHOD

The Chaney et al. approach uses equations similar to those developed by Muskat together with the results of a potentiometric analyzer.[1] The great advantage of this method for the practicing engineer is that the results are presented in a very convenient, graphical form. This method allows one to calculate maximum production rate without generation of coning, where to perforate, and how to make estimates of the production capacity of the well.

The graphical solutions of Chaney et al. are presented in Figures 7.14 through 7.18 for reservoir thickness of 12.5, 25, 50, 75, and 100 ft, respectively, and a drainage radius of 1,000 ft. Each of these figures shows five water-coning curves, which are labeled A, B, C, D, and E, and five gas-coning curves represented by a, b, c, d, and e.

Curves A and a are for the case in which 10% of the net thickness is perforated. Curves B and b are for 20%, curves C and c are for 30%, curves D and d are for 40%, and curves E and e are for the case in which 50% of the net thickness is perforated. These

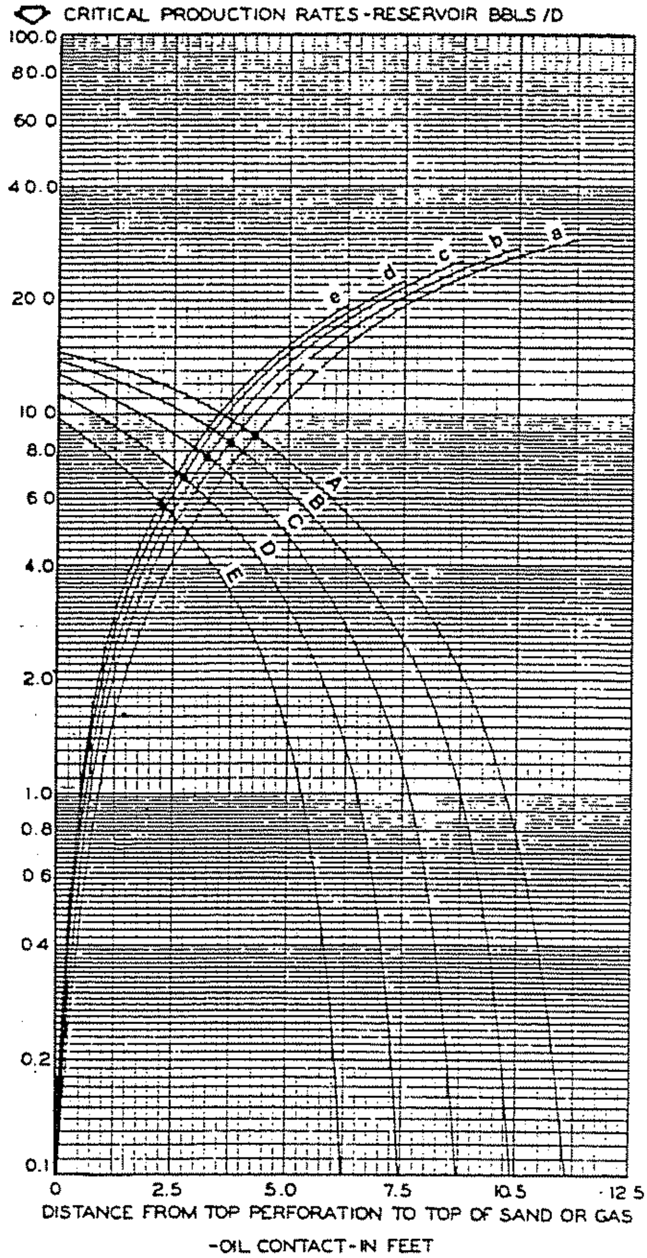

Figure 7.14 Critical-Production-Rate Curves for Sand Thickness of 12.5 ft, Well Radius of 3 in., and Drainage Radius of 1,000 ft. Water Coning Curves: A, 1.25-ft Perforated Interval; B, 2.5 ft; C, 3.75 ft; D, 5.00 ft; and E, 6.25 ft. Gas Coning Curves: a, 1.25-ft Perforated Interval; b, 2.5 ft; c, 3.75 ft; d, 5.00 ft; and e, 6.25 ft (after Chaney et al.)[1]

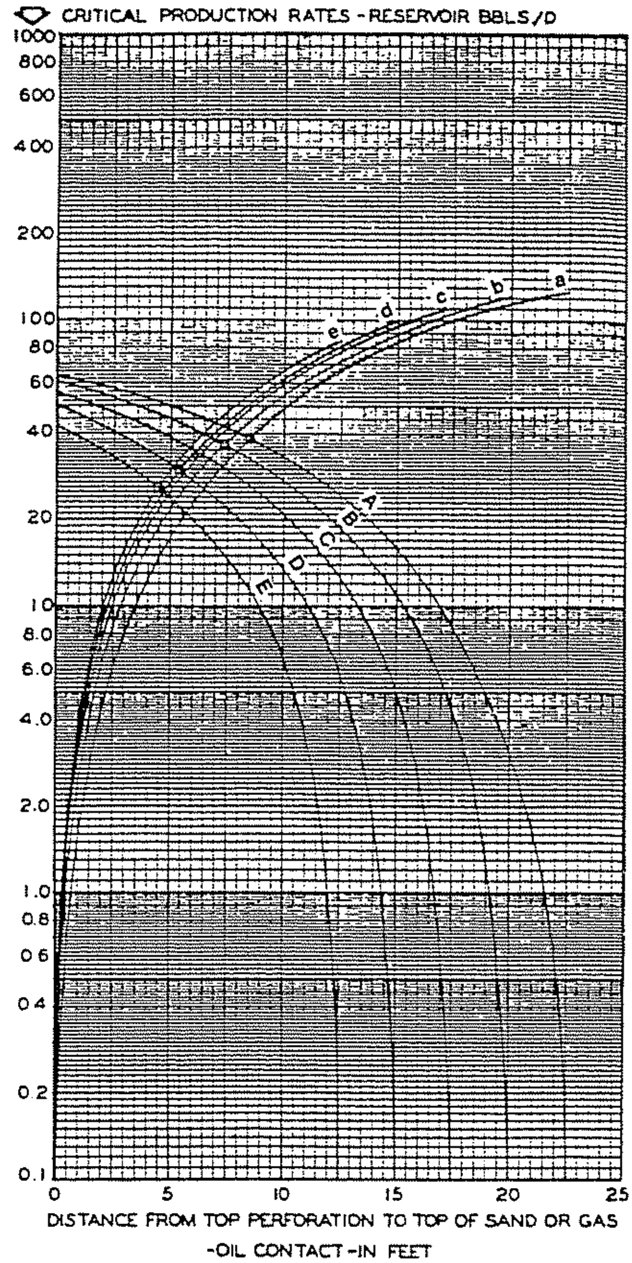

Figure 7.15 Critical-Production-Rate Curves for Sand Thickness of 25 ft, Well Radius of 3 in., and drainage radius of 1,000 ft. Water Coning Curves: A, 2.5-ft Perforated Interval; B, 5 ft; C, 7.5 ft; D, 10 ft; and E, 12.5 ft. Gas Coning Curves: a, 2.5-ft Perforated Interval; b, 5 ft; c, 7.5 ft; d, 10 ft; and e, 12.5 ft (after Chaney et al.)[1]

figures were generated using the following fluid and formation characteristics:

permeability, $k_o = 1{,}000$ md
oil viscosity, $\mu_o = 1$ cp
density difference between oil and water, $\Delta\rho_{o.w} = 0.3$ g/cc
density difference between oil and gas, $\Delta\rho_{og} = 0.6$ g/cc

The results obtained from those figures have to be corrected to take into account variations from the actual values of the fluid and formation characteristics. These corrections are carried out with the use of the following equations.

(1) *Water-coning rates in an oil-water system.*

$$q_{o_{max}} = \frac{0.00333\ k_o \Delta\rho_{o.w}\ q_{curve}}{\mu_o\ B_o} \qquad (7.14)$$

where q_{curve} is the initial production rate in reservoir barrels per day, which is determined from the graphical solutions, $q_{o_{max}}$ is the initial oil rate in stb/d, and k_o is effective permeability to oil in md. Other nomenclature is as defined previously.

(2) *Water-coning rates in a gas-water system.*

$$q_{g_{max}} = \frac{0.00333\ k_g\ \Delta\rho_{g.w}\ q_{curve}}{\mu_g\ B_g} \qquad (7.15)$$

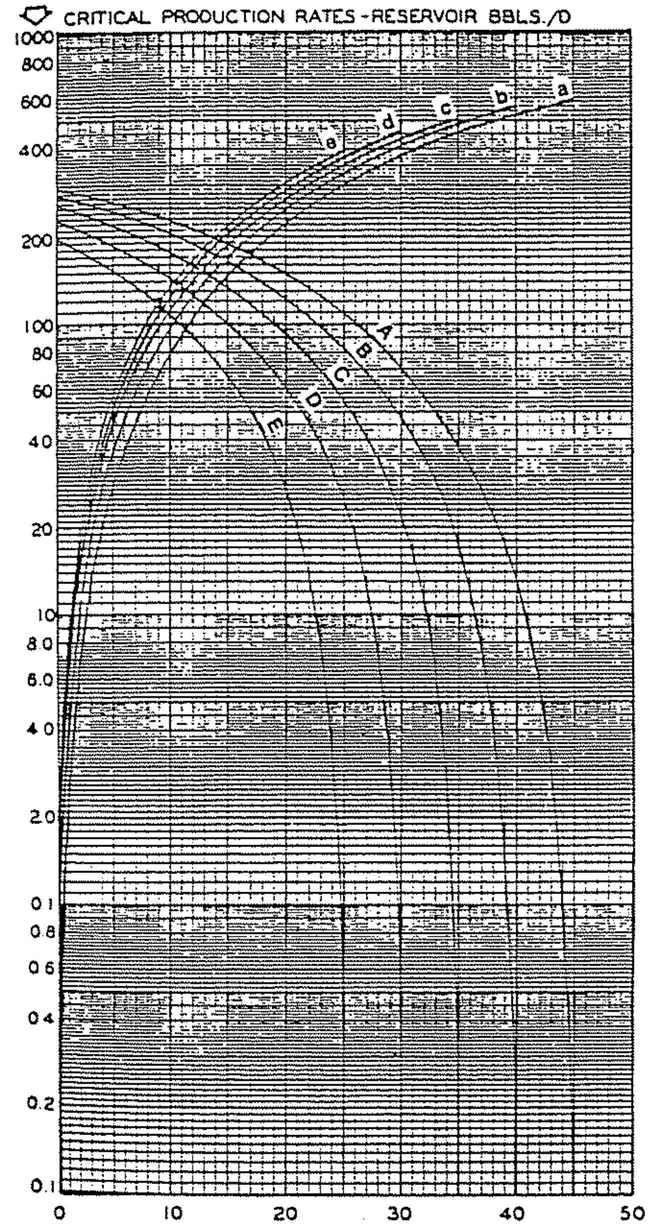

Figure 7.16 Critical-Production-Rate Curves for Sand Thickness of 50 ft, Well Radius of 3 in., and Drainage Radius of 1,000 ft. Water Coning Curves: A, 5-ft Perforated Interval; B, 10 ft; C, 15 ft; D, 20 ft; and E, 25 ft. Gas Coning Curves: a, 5-ft Perforated Interval; b, 10 ft; c, 15 ft; d, 20 ft; and e, 25 ft (after Chaney et al.)[1]

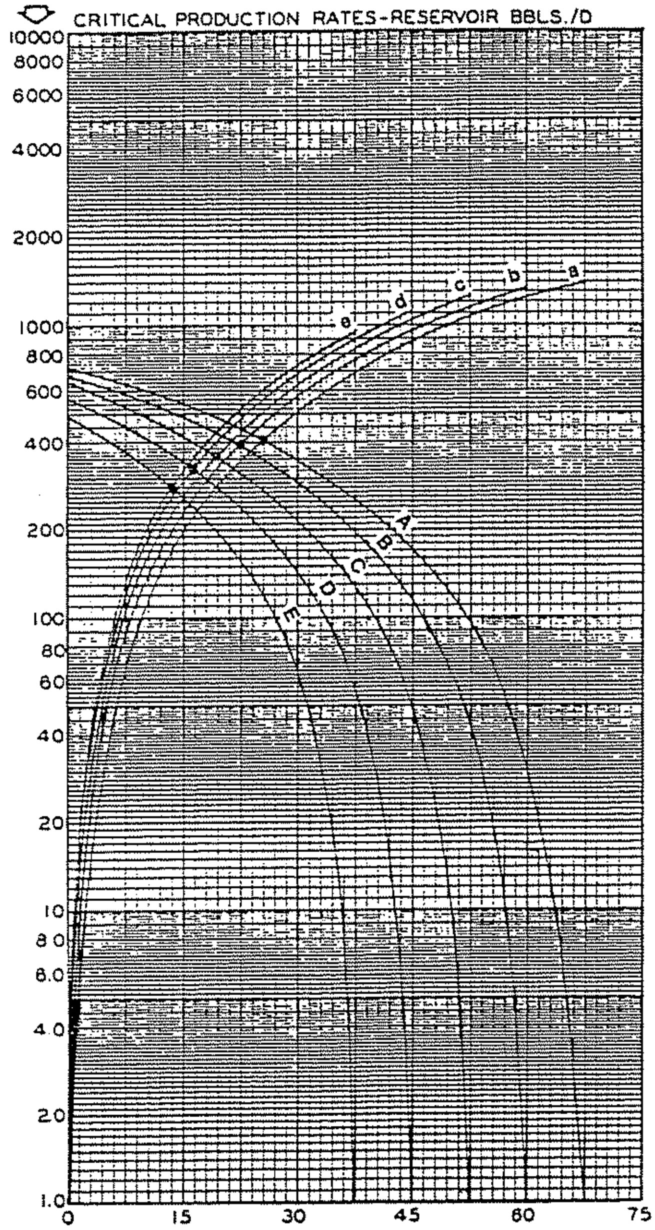

Figure 7.17 Critical-Production-Rate Curves for Sand Thickness of 75 ft, Well Radius of 3 in., and Drainage Radius of 1,000 ft. Water Coning Curves: A, 7.5-ft Perforated Interval; B, 15 ft; C, 22.5 ft; D, 30 ft; and e, 37.5 ft. Gas Coning Curves: a, 7.5-ft Perforated Interval; b, 15 ft; c, 22.5; d, 30 ft; and e, 37.5 ft (after Chaney et al.)[1]

where:

$q_{g_{max}}$ = the maximum gas rate in Mscfd
k_g = effective permeability to gas in md
μ_g = gas viscosity in cp
B_g = gas formation volume factor in reservoir barrels per 1,000 scf of gas.

Other nomenclature is as defined previously.

(3) *Gas-coning rates in an oil-gas system.*

$$q_{o_{max}} = \frac{0.00167\, k_o\, \Delta\rho_{o,g}\, q_{curve}}{\mu_o\, B_o} \tag{7.16}$$

where all nomenclature has been defined previously.

(4) *Production capacity.* Estimates of production capacity can be obtained with the use of Figure 7.19, which shows the maximum pressure drop required to produce at a certain rate for various perforated intervals in a 0.25-ft radius cased borehole with a perforation density of four ¼-in. radius perforations per foot. The assumed drainage radius is 1,000 ft. Different perforated interval curves are shown as follows:

Curve a = 70 ft
b = 60 ft
c = 50 ft
d = 40 ft
e = 30 ft

Curve f = 20 ft
g = 10 ft
h = 5 ft
i = 2½ ft
j = 1.25 ft

The curves were generated based on a permeability of 1 darcy and a viscosity of 1 cp. Consequently, the pressure drop in psi read from Figure 7.19 has to be corrected by multiplying by the correct viscosity in cp and dividing by the correct permeability in darcies. As a general rule, Chaney et al. suggested that, if the corrected pressure drawdown from Figure 7.19 is more than one-half of the available pressure drop or working-pressure drop, a larger interval should be perforated.[1] The working pressure drop is the shutin bottom-hole pressure minus the pressure exerted by the weight of the fluid in the tubing.

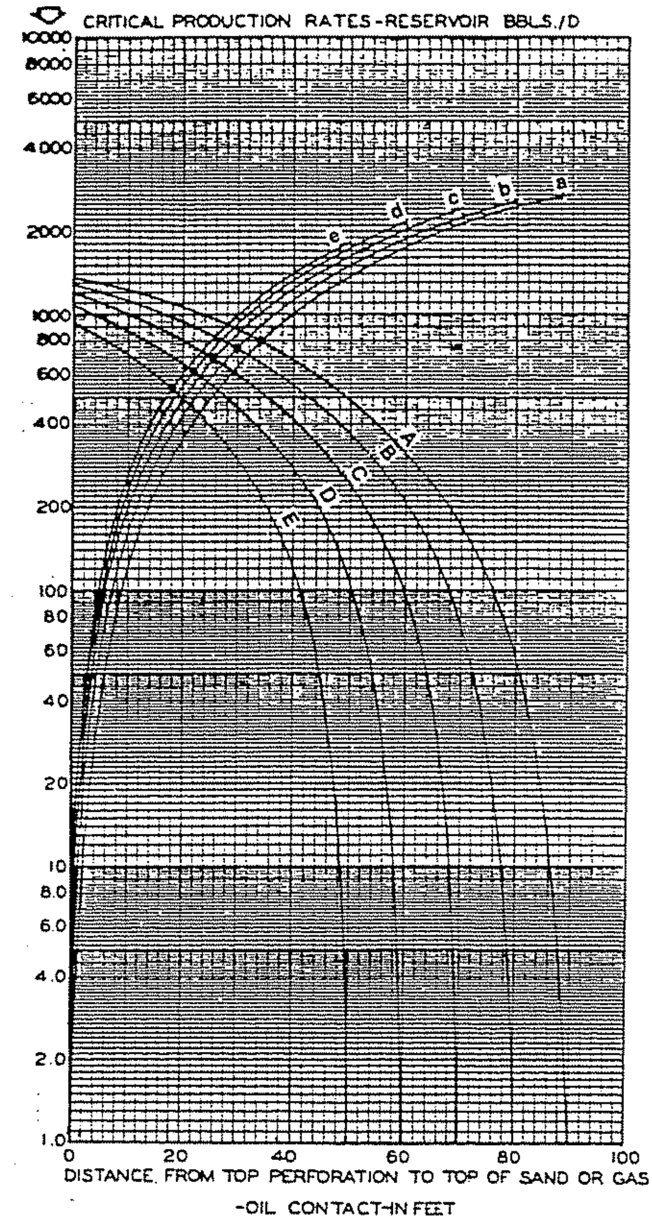

Figure 7.18 Critical-Production-Rate Curves for Sand Thickness of 100 ft, Well Radius of 3 in., and Drainage Radius of 1,000 ft. Water Coning Curves: A, 10-ft Perforated Interval; B, 20 ft; C, 30 ft; D, 40 ft; and E, 50 ft. Gas Coning Curves: a, 10-ft Perforated Interval; b, 20 ft; c, 30 ft; d, 40 ft; and e, 50 ft (after Chaney et al.)[1]

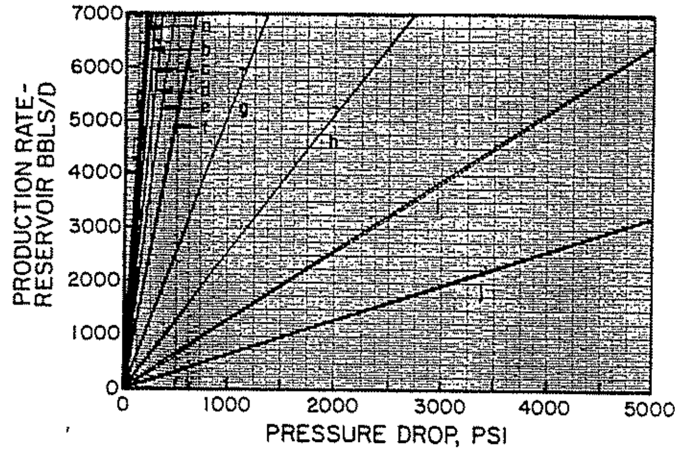

Figure 7.19 Production Rate vs Required Pressure Drop Where the Effective Well Radius is Caused by a Perforation Density of four ¼-in.-Radius Perforations Per Foot. Drainage Radius, 1,000 ft; Well Radius, 0.25 ft; Effective Well Radius, 0.000932 ft. Perforated Interval Curves: a, 70 ft; b, 60 ft; c, 50 ft; d, 40 ft; e, 30 ft; f, 20 ft; g, 10 ft; h, 5 ft; i, 2½ ft; and j, 1.25 ft (after Chaney et al.)[1]

The use of the graphical solutions is clearly explained in the next two examples, which were taken directly from the work of Chaney et al.[1]

EXAMPLE #4

Given data:

These data come from State Lease 1337, Well No. 9, Bateman Lake Field, Louisiana. Figure 7.20 shows the electric log for this well and the perforated interval from 12,119 to 12,123 ft. Additional data are as follows:

depth = 12,118 to 12,134 ft
oil column thickness = 16 ft
drainage radius = 1,000 ft
perforations = top 5 ft
oil viscosity, $\mu_o = 0.3$ cp
density of salt water, $\rho_w = 1.1$ g/cc
density of oil, $\rho_o = 0.62$ g/cc
permeability, $k_o = 1{,}500$ md
oil formation volume factor, $B_o = 1.4$ bbl/stb

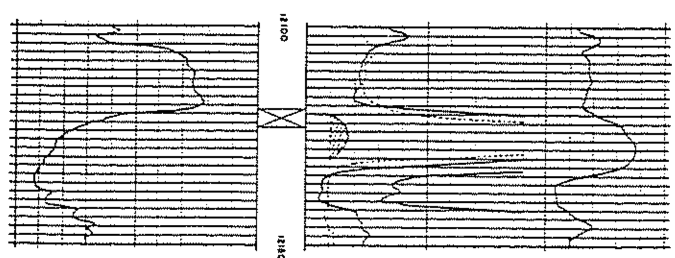

Figure 7.20 Electric Log for Well No. 9, State Lease 1,337; Bateman Lake Field, Louisiana. Potential Test: Perforation Interval, 12,119 to 12,123 ft with Sixteen Shots; 216 b/d, 7/64-in. Choke; Total Pressure, 1,750 psi; Gas-Oil Ratio 800 to 1 (after Chaney et al.)[1]

Solution procedure:

(1) *Critical production rate.* Since no curves are given for a 16-ft oil column thickness, it is necessary to use interpolation. Furthermore, in this case, 5/16 = 31.25% of the oil column thickness is perforated. Since the graphical solutions are for perforated intervals of 10, 20, 30, 40, and 50% of the net thickness, it is necessary also to use interpolation in this case. Chaney et al. have indicated that straight-line interpolation is sufficiently accurate when these graphical solutions are used.[1]

The distance from the top perforation to the top of the reservoir is zero.

From Figure 7.14, for 12.5-ft thickness and a 30% interval, the critical rate is 12.7 reservoir b/d from curve C. For a 40% interval, the critical rate is 11.25 reservoir b/d from curve D.

By straight-line interpolation, the critical production rate for a 12.5-ft oil column with a 31.25% perforated interval would be:

$$12.7 - 0.125\,(12.7 - 11.25) = 12.5 \text{ reservoir b/d}$$

By going through the same procedure from Figure 7.15 for a 25-ft thickness and a 30% interval, the critical rate is 56 reservoir b/d from curve C. For a 40% interval, the critical rate is 50 reservoir b/d. By straight-line interpolation, it is found that the critical rate is 56 − 0.125 (56 − 50) = 55.3 reservoir b/d for a 25-ft net oil thickness with a 31.25% perforated interval.

Interpolating again between the two critical rates calculated above, it is found that, for a net oil thickness of 16 ft with the top 31.25% perforated, the critical rate would be:

$$12.5 + (55.3 - 12.5)\frac{(16 - 12.5)}{(25 - 12.5)} = 24.5 \text{ reservoir b/d}$$

The above critical rate has to be corrected to take into account the actual permeability, viscosity, and densities. This is accomplished with the use of Equation 7.14:

$$q_{o_{max}} = \frac{0.00333(1{,}500)(1.1 - 0.62)(24.5)}{(0.3)(1.4)} = 140 \text{ stb/d}$$

The well was actually produced at a rate of 216 stb/d, which exceeded the critical rate of 140 stb/d. After 12 hr, the well started producing water. One month later, the well was producing 114 stb/d of oil with a water cut of 85% salt water.

(2) *Working pressure drop.* The saltwater gradient is 0.4615 psi/ft. The freshwater gradient is 0.434 psi/ft. The oil gradient is (0.434)(0.62) = 0.2691 psi/ft.

The available pressure drop is (0.4615 − 0.2691) × 12,120.5 = 2,332 psi. Notice that 12,120.5 is the midpoint depth of the perforated interval.

As a general rule, Chaney et al. recommended that the available pressure drops be divided by two in order to calculate a working pressure that takes into account any possible damage around the wellbore, which might increase the pressure drop for a given production rate.[1]

For this example, the working pressure would be 2,332/2 = 1,166 psi.

(3) *Production capability of the well.* The critical rate is equal to 140 × 1.4 = 196 reservoir b/d. From Figure 7.19, it can be seen that, to produce the above rate, a pressure drop of approximately 85 psi is required. To take into account the actual viscosity and permeability, a corrected pressure drop is calculated by multiplying the pressure drop from the curve by the actual viscosity and dividing by the actual permeability—i.e., (85)(0.3)/1.5 darcies = 17 psi.

Since the required pressure drop is 17 psi and the calculated working pressure is 1,666 psi, the well is capable of producing at the critical rate.

EXAMPLE #5

Given data:

These data come from State Lease 1537, Well No. A-1, Eugene Island area, Louisiana. Figure 7.21 shows the electric log of the well. The following information is available:

depth = 11,305 to 11,366 ft
original pressure = 5,225 psi
gas-column thickness = 61 ft
drainage radius = 1,000 ft
perforation = top 30 ft
density of salt water = 1.1 g/cc
density of gas = 0.279 g/cc
viscosity of gas = 0.025 cp
permeability = 200 md
B_g = 0.68 reservoir bbl/1,000 scf

Solution procedure:

(1) *Critical production rate.* Critical production rate is calculated exactly as in the previous example. The perforated interval represents 30/61 = 49.18% of the total gas-column thickness.

From Figure 7.16 for a 50-ft gas formation, the production rates for 40 and 50% perforated intervals are 229 and 198 reservoir b/d. Interpolation for 49.18% perforations results in a critical rate of 200.5 reservoir b/d.

From Figure 7.17 and for a 75-ft gas formation thickness, the interpolated critical rate is 495.7 reservoir b/d. Interpolation for a 61-ft gas column results in a maximum gas rate of 330 reservoir b/d.

The previous rate is corrected to conditions of the example well with the use of Equation 7.15:

$$q_{g_{max}} = \frac{0.00333(200)(1.1 - 0.279)(330)}{(0.025)(0.68)} = 10{,}614 \text{ Mscfd}$$

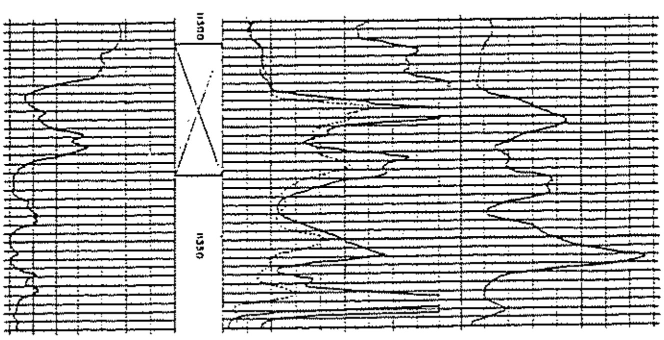

Figure 7.21 Electric Log, Well No. A-1, State Lease 1537, Eugene Island Field, Louisiana. Initial Potential: Perforation Interval 11,305 to 11,335 ft With 117 Shots; 2.5 MMcf Gas/Day; 10/64-in. Choke; Total Pressure, 4,225 lb (after Chaney et al.)[1]

(2) *Working pressure drop.* Depth to the midpoint of the perforated interval is 11,320 ft. The freshwater gradient is 0.434 psi/ft. The saltwater gradient is 0.4615 psi/ft. The gas gradient is $0.434 \times 0.279 = 0.1211$ psi/ft. Consequently, the working pressure drop at the wellbore is:

$$(0.4615 - 0.1211) \times 11{,}320 = 3{,}854 \text{ psi}$$

This pressure is divided by two as recommended by Chaney et al. to take into account possible damage around the wellbore.[1] Upon inclusion of this safety factor, the working pressure drop is calculated to be 1,927 psi.

(3) *Production capability of a well.* The critical production rate, $q_{g_{max}}$, for the previous example is calculated to be 10,614 Mscfd and is equivalent to 7,224 reservoir b/d.

From Figure 7.19 and for 7,224 b/d, a pressure drop of approximately 475 psi is required. The corrected pressure drop would be equal to:

$$(475 \times 0.025)/0.2 = 59.5 \text{ psi}$$

Since the working pressure drop is 1,927 psi and the corrected pressure drop is only 59.5 psi, the well will certainly be capable of producing at the critical rate.

7.14 CONING IN ANISOTROPIC RESERVOIRS

7.141 CONING OF GAS AND WATER

Coning of water or gas into a producing oil well is a result of the pressure equilibrium reached above and below the perforated interval. In order to achieve an equilibrium below the perforated interval, water, the denser fluid, rises until the production pressure drop is counterbalanced by the differential hydrostatic pressure of the cone height; similarly, gas is drawn down toward the perforated interval. The production pressure drop causes the interfacial contact to move across the bedding plane in the form of a cone. This differs from fingering, which occurs along the bedding plane. Figure 7.22 shows the gas and water coning concept.

A stable cone is generated when a well is produced at a constant rate for a sufficiently long period of time that a steady-state condition exists within the drainage system. As long as this steady-state condition exists, the cone height will not change once the cone has stabilized.

An important part in coning theory is the critical production rate, which is the production rate above which the flowing bottom-hole pressure drop causes water or gas to be coned into the wellbore. The critical production rate can thus be visualized as the maximum oil rate allowable without the undesirable coning of water or gas. At the critical production rate, a cone that will cause gas or water to flow into the well with any increase in bottom-hole pressure drop or movement in the static interfacial contacts is formed.

7.142 CHIERICI ET AL. METHOD

The Chierici et al. method for determining the critical oil production rates and the optimum completion interval to maximize oil recovery and recovery rate without gas or water coning makes use of a potentiometric model founded on Muskat's theory of water and gas coning.[8]

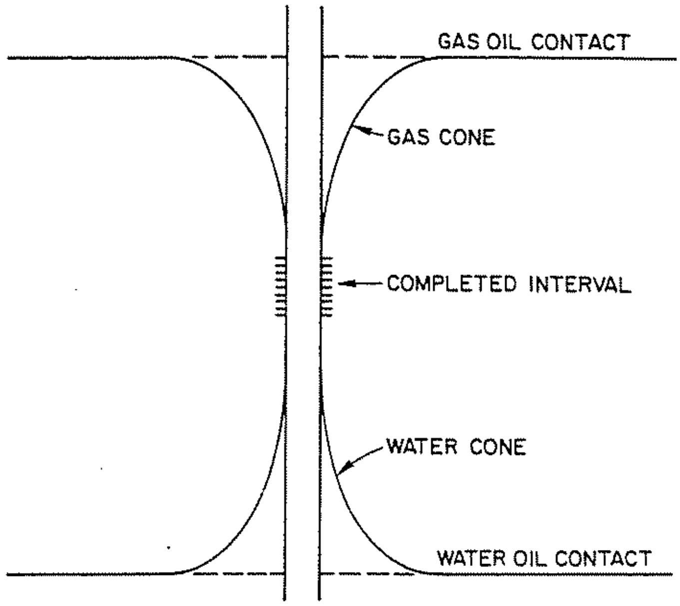

Figure 7.22 Water and Gas Coning

(1) *Critical production rate.* The Chierici et al. method can be used to calculate the critical production rate for a well that has been completed or to optimize the placement and length of the completion interval in order to maximize the critical production rate and thus maximize well economic return.

The Chierici et al. method makes the following assumptions:

(1) The reservoir is homogeneous.
(2) The interfacial contacts are horizontal at static conditions.
(3) Capillary pressure effects are negligible.
(4) The reservoir fluids are incompressible.
(5) The aquifer is of limited size and does not contribute to the reservoir energy.
(6) The gas cap expands slowly; thus the potential gradient is negligible.

The following equations are the basis for the Chierici et al. method. The critical oil production rate for water coning is:

$$q_{oc,w} = 3.073 \times 10^{-3} \left(\frac{h^2 \Delta\rho_{wo}\, k_h}{B_o\, \mu_o}\right) \psi\,(r_{de}, f_b, h_{cw}/h) \quad (7.17)$$

For the critical oil production rate for gas coning:

$$q_{oc,g} = 3.073 \times 10^{-3} \left(\frac{h^2 \Delta\rho_{og}\, k_h}{B_o\, \mu_o}\right) \psi\,(r_{de}, f_b, h_{cg}/h) \quad (7.18)$$

where:

$q_{oc,w}$ = critical oil production rate for a water cone to enter the wellbore, stbo/d
$q_{oc,g}$ = critical oil rate for a gas cone to enter the wellbore, stbo/d
h = total oil column thickness, ft
$\Delta\rho_{wo}$ = oil-water density difference, g/cc
$\Delta\rho_{og}$ = oil-gas density difference, g/cc
k_h = horizontal permeability, md

$$r_{de} = \frac{r_e}{h}\sqrt{\frac{k_h}{k_v}}$$

r_e = drainage radius, ft
k_v = vertical permeability, md
f_b = fraction of the total oil column completed
h_{cw} = distance from the initial water-oil contact to the lowest perforation, ft
h_{cg} = distance from the initial gas-oil contact to the highest perforation, ft
B_o = oil formation volume factor in reservoir bbl/stbo
μ_o = oil viscosity at reservoir condition, cp

If the well is produced at a rate that exceeds the critical rate, water or gas or both will cone into the wellbore. For a given distance to the interfacial contacts, the critical water coning rate is normally the limiting rate because of the smaller available density difference. Both Equations 7.17 and 7.18 indicate that the critical rate is a function of the fluid parameters, rock parameters, and the available coning distance. The critical production rate is related by the function ψ to the dimensionless parameters, r_{de}, f_b, h_{cw}/h and h_{cg}/h, which are defined by the coning system geometry.

Chierici determined values for the function ψ with the use of a potentiometric analyzer. Values of ψ were determined for the following range of dimensionless variables:

$$r_{de} = \frac{r_e}{h}\sqrt{\frac{k_h}{k_v}} \text{ of 5 to 80}$$

$$f_b \text{ of 0.0 to 0.75}$$

$$h_{cw}/h \text{ and } h_{cg}/h \text{ of 0.07 to 0.90}$$

The values of ψ for the previous ranges are shown in Figures 7.23 through 7.29. Each figure is valid for the specified value of r_{de} and contains two groups of curves. One group is for values of h_{cw}/h or h_{cg}/h and is used when only one fluid is coning.

To determine the value of ψ, calculate the value of

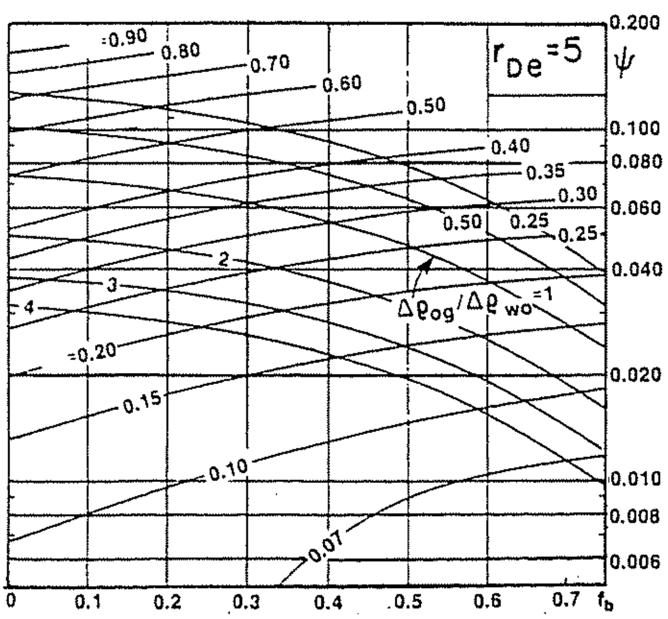

Figure 7.23 Coning correlations for r_{De} = 5 (after Chierici);[8] h_{cw}/h or h_{cg}/h

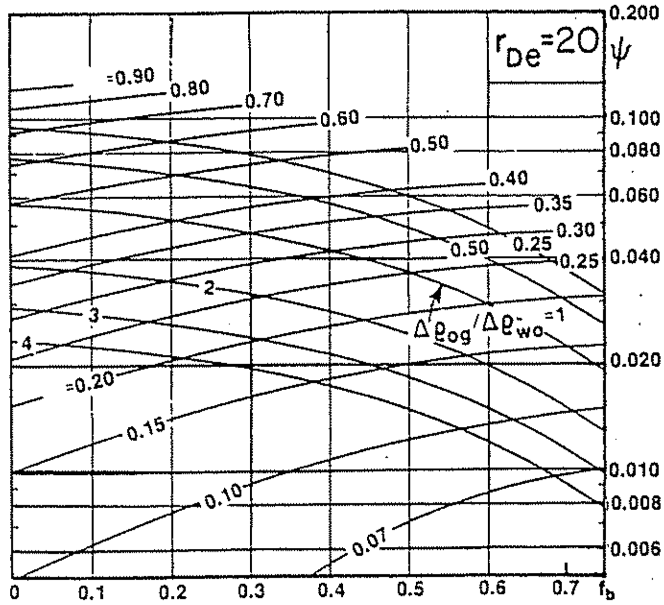

Figure 7.24 Coning correlations for r_{De} = 20 (after Chierici);[8] h_{cw}/h or h_{cg}/h

r_{de} and choose the figure that applies. If the well has been completed, f_b and h_{cw}/h or h_{cg}/h are used, and the value of ψ is found at the intersection of these two values. If both water and gas are present, critical rates should be calculated for both and the lower rate used.

(2) *Optimum completion interval placement.* If the well being evaluated has not been completed, choose a value of f_b, assuming that the well is completed as far away as possible from the fluid contacts. A value of ψ is determined and a critical rate determined. It should be noted that, the lower the f_b, the higher the critical rates. Oil-well productivity data should be used to estimate well potential so that a value of f_b is found where enough well capacity is completed to achieve the critical rate.

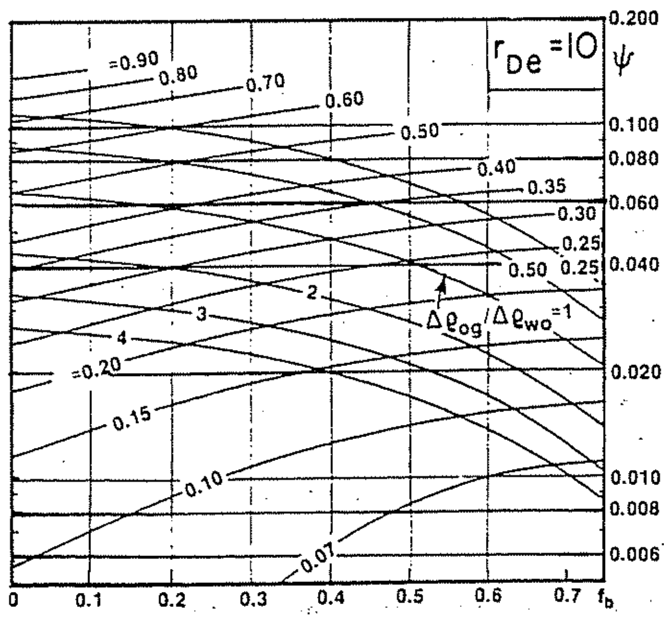

Figure 7.25 Coning correlations for r_{De} = 10 (after Chierici);[8] h_{cw}/h or h_{cg}/h

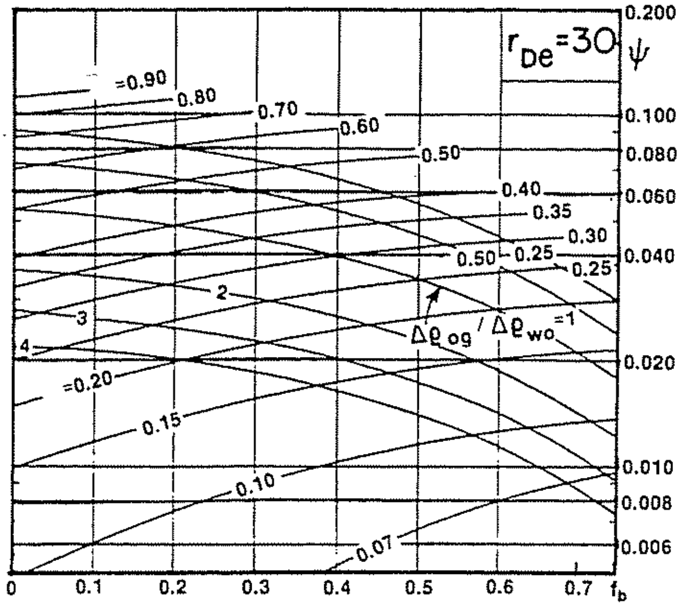

Figure 7.26 Coning correlations for r_{De} = 30 (after Chierici);[8] h_{cw}/h or h_{cg}/h

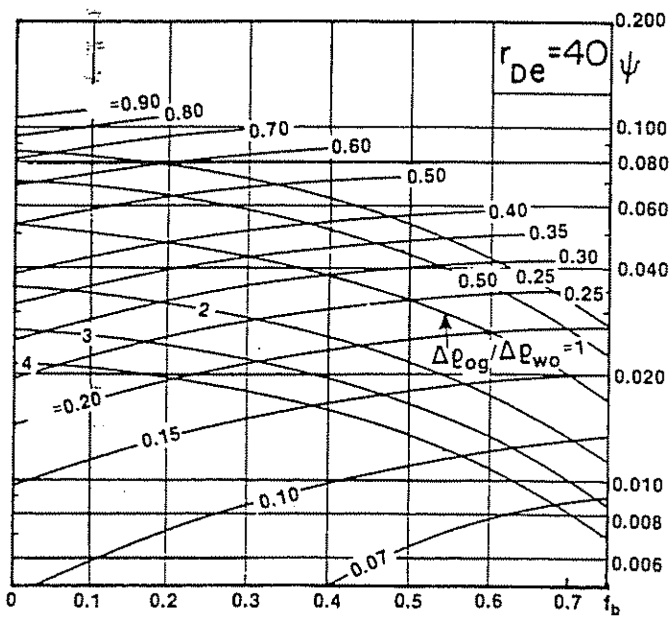

Figure 7.27 Coning correlations for r_{De} = 40 (after Chierici);[8] h_{cw}/h or h_{cg}/h

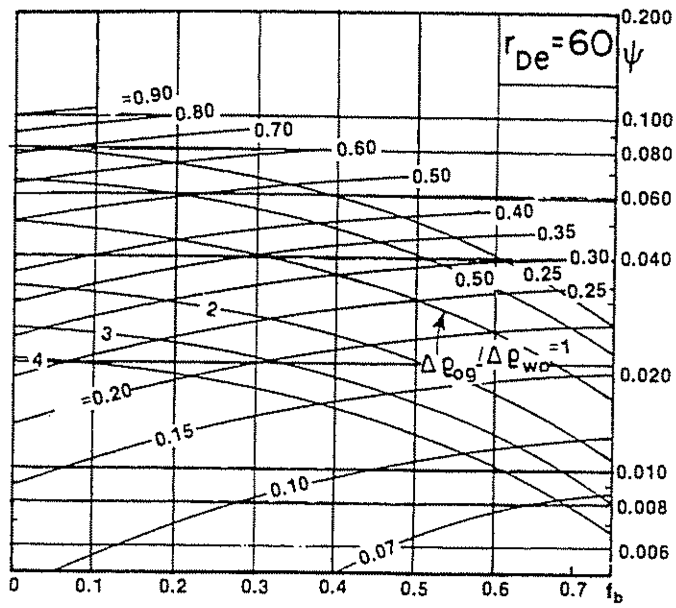

Figure 7.28 Coning correlations for r_{De} = 60 (after Chierici);[8] h_{cw}/h or h_{cg}/h

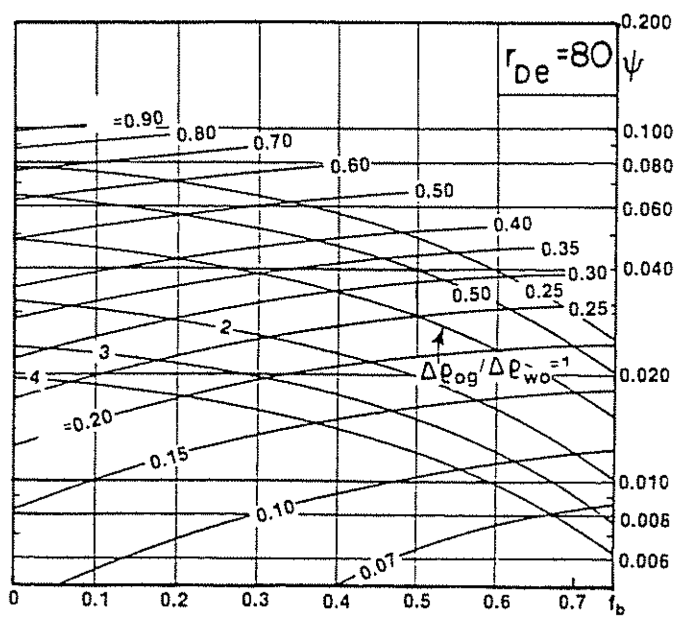

Figure 7.29 Coning correlations for r_{De} = 80 (after Chierici);[8] h_{cw}/h or h_{cg}/h

When both oil or gas coning are possible, the second family of curves in Figures 7.23 through 7.29 must be used. This second family of curves contain values of $\Delta\rho_{og}/\Delta\rho_{wo}$ ranging from 4 to 0.25. The density difference ratio is used as the critical rate, and cone heights are related to density difference.

The values of r_{de} and $\Delta\rho_{og}/\Delta\rho_{wo}$ are determined, a value of f_b is chosen, and a value of h_{cg} can be determined, reading vertically along the chosen value of f_b up to the $\Delta\rho_{og}/\Delta\rho_{wo}$ value. At this point, we have h_{cg}/h and ψ; thus, the critical rate can be calculated. The optimum completion is determined when a match that is based on the perforated interval is found between the critical rate and the well potential. The following examples apply this method in determining the optimum completion and the critical rate.

EXAMPLE #6 (CRITICAL RATE FOR A COMPLETED WELL IN A WATER-OIL SYSTEM) (FIGURE 7.30)

Given data:

total reservoir thickness above the oil-water contact, $h = 40$ ft
drainage radius, $r_e = 1{,}250$ ft
perforated section = top 12 ft
reservoir oil viscosity, $\mu_o = 0.8$ cp
water density, $\rho_w = 1.15$ g/cc
oil density, $\rho_o = 0.65$ g/cc

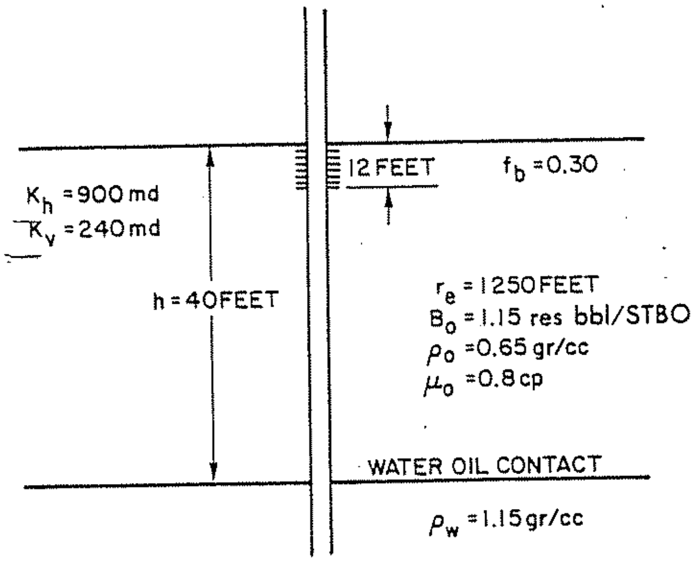

Figure 7.30 Critical Rate in a Completed Well

horizontal permeability, $k_h = 900$ md
vertical permeability, $k_v = 240$ md
oil formation volume factor, $B_o = 1.15$ res. bbl/stbo

Solution procedure:

(1) Determination of r_{de}:

$$r_{de} = \frac{r_e}{h}\sqrt{\frac{k_h}{k_v}} = \frac{1{,}250}{40}\sqrt{\frac{900}{240}} = 60.5$$

(2) Determination of f_b:

$$\frac{12}{40} = 0.30$$

and:

$$\frac{h_{cw}}{h} = \frac{40-12}{40} = 0.70$$

(3) From Figure 7.28:

$$\psi = 0.086$$

(4) Using Equation 7.17, the critical production rate is calculated:

$$q_{oc,w} = 3.073 \times (10^{-3})\, h^2 \left(\frac{\Delta\rho_{wo}}{B_o}\right)\left(\frac{k_h}{\mu_o}\right)\psi$$

$$q_{oc,w} = 3.073 \times (10^{-3})(40^2)\left(\frac{1.15-0.65}{1.15}\right)\left(\frac{900}{0.8}\right)0.086$$

$$q_{oc,w} = 207 \text{ stbo/d}$$

EXAMPLE #7 (CRITICAL PRODUCTION RATE AND OPTIMUM COMPLETION OF A GAS-OIL-WATER SYSTEM) (FIGURE 7.31)

Given data:

oil zone thickness, h = 50 ft
drainage radius, r_e = 1,000 ft
reservoir oil viscosity, μ_o = 1 cp
water density, ρ_w = 1.10 g/cc
oil density, ρ_o = 0.8 g/cc
gas density, ρ_g = 0.2 g/cc
horizontal permeability, k_h = 1,000 md

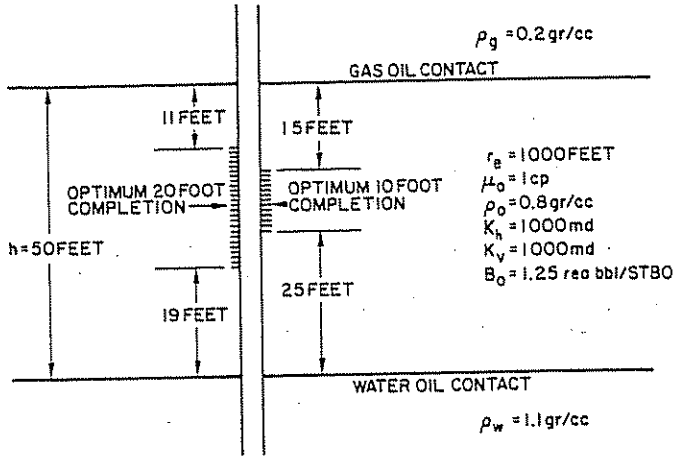

Figure 7.31 Critical Production Rate and Optimum Completion (Example 7.7)

vertical permeability, k_v = 1,000 md
oil formation volume factor, B_o = 1.25 reservoir bbl/stbo

Calculate:

Locate the optimum position of a 10- and 20-ft completion interval and the maximum critical rate.

Solution procedure:

(1) Determination of r_{de}:

$$r_{de} = \frac{r_e}{h}\sqrt{\frac{k_h}{k_v}}$$

$$r_{de} = \frac{1{,}000}{50}\sqrt{\frac{1{,}000}{1{,}000}} = 20$$

(2) For a 10-ft completion interval:

$$f_b = \frac{10}{50} = 0.20$$

(3) $\Delta\rho_{og}/\Delta\rho_{wo} = 0.6/0.3 = 2$

Reading from Figure 7.24 at a value of $f_b = 0.20$ up to $\Delta\rho_{og}/\Delta\rho_{wo} = 2$, values of $h_{cg}/h = 0.30$ and $\Psi = 0.035$ are found. If:

$$h_{cg}/h = 0.3$$

then:

$$h_{cg} = 0.3h$$
$$h_{cg} = (0.30)(50) = 15 \text{ ft}$$

The optimum placement of the 10-ft completion interval is 15 ft from the gas-oil contact; thus, the lowest perforation would be 25 ft from the water-oil contact. The critical rate for this completion interval position is determined from equation 7.18:

$$q_{oc,g} = 3.073(10^{-3})(50^2)\left(\frac{0.6}{1.25}\right)\left(\frac{1{,}000}{1}\right)(0.035)$$

$$q_{oc,g} = 129 \text{ stbo/d}$$

If the completed interval is increased to 20 ft:

$$f_b = \frac{20}{50} = 0.40$$

and:

$$\Delta\rho_{og}/\Delta\rho_{wo} = 2$$

Reading from Figure 7.24 up from $f_b = 0.40$, a value of $h_{cg}/h = 0.22$ and a $\Psi = 0.030$ are found:

$$h_{cg} = 0.22(50) = 11 \text{ ft}$$

The optimum placement of a 20-ft completion would be 11 ft from the gas-oil contact to the top perforation and 19 ft from the water-oil contact to the lowest perforation. The critical rate for the 20-ft completion is:

$$q_{oc,g} = 3.073(10^{-3})(50^2)\left(\frac{0.6}{1.25}\right)\left(\frac{1{,}000}{1}\right)(0.028)$$

$$q_{oc,g} = 104 \text{ stbo/d}$$

It should be noted that, as the completion interval is increased, the critical rate decreases because of the reduction in the allowable cone height. The optimum completion is found when the predicted critical rate can be produced and maintained from the completed interval.

7.143 SOBOCINSKY AND CORNELIUS METHOD[9]

(1) *A correlation for estimating cone development time.* All the previous calculations and concepts do not address the time required to develop a stable cone. Before the cone reaches the critical height, a well can be produced above the critical rate.

A correlation is available for estimating the time-dependent behavior of a cone as it builds up from the static water-oil contact to its stable height. This correlation is based on data from a sand-packed model and a two-dimensional, incompressible system computer model, and it involves dimensionless groups of reservoir and fluid properties.

These dimensionless groups can be used to estimate the performance of water cones not specifically considered in the correlation. The following assumptions and limitations apply to this correlation:

(1) The reservoir is a homogeneous, incompressible system with no gas cap and is produced at a constant rate.
(2) Gravity-to-viscous forces and a geometric scaling group that involves the horizontal-to-vertical permeability ratio are considered. Capillary pressure, oil-water viscosity ratio, and flow geometry are neglected.
(3) The vertical height of a system can be characterized by the oil-zone thickness.
(4) A constant water-oil contact was maintained at the outer radius of the model.

(2) *Z vs t_D method description.* Water-cone breakthrough time and cone-buildup data from both the experimental and computer models were correlated against dimensionless time t_D and dimensionless cone height Z. The correlation is shown in Figure 7.32. The correlating groups, which were developed from the scaling criteria for immiscible displacement, are described by Equations 7.19 and 7.20.

$$Z = \frac{0.00307\Delta\rho_{wo}\, k_h\, h\, h_c}{\mu_o\, q_o\, B_o} \qquad (7.19)$$

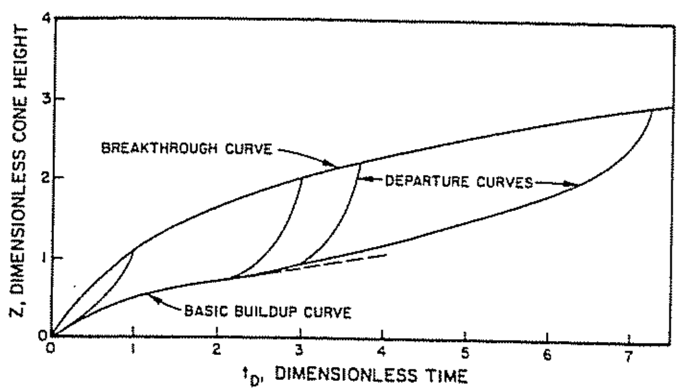

Figure 7.32 Dimensionless Cone Height vs Dimensionless Time

$$t_D = \frac{0.00137\,\Delta\rho_{wo}\, k_h\,(1 + M^{\alpha})t}{\mu_o\, \phi\cdot h\,\eta_k} \qquad (7.20)$$

where:

$\Delta\rho_{wo}$ = water-oil density difference, g/cc
μ_o = oil viscosity, cp
k_h = horizontal permeability, md
h = oil zone thickness, ft
h_c = height of the apex of the water cone above the average water-oil contact, ft
q_o = oil production rate, stb/d
B_o = oil formation volume factor, reservoir bbl/stb
t = time, days
ϕ = porosity
η_k = horizontal to vertical permeability, k_h/k_v
M = water-oil mobility ratio = $\mu_o(k_w)_{or}/\mu_w(k_o)_{wi}$

$$\alpha = 0.5 \text{ for } M < 1$$
$$0.6 \text{ for } 1 < M < 10 \qquad (7.21)$$

The curves in Figure 7.32 describe Z as a function of t_D using smoothed data from the models. The breakthrough curve represents those conditions at which a water cone that builds from static conditions will break into the well when it is produced at a constant and uninterrupted rate. The basic buildup curve traces the apex of the water cone before water breakthrough, while the departure curves describe the rise of the apex as it approaches the well. Note that the slope of the departure curve increases as it approaches the breakthrough curve. This means that the rise of the cone apex accelerates as it nears the well. The four departure curves shown were obtained from laboratory data; departure curves for other breakthrough times can be located by interpolation.

The basic buildup and departure curves apply only to coning situations for which breakthrough conditions fall within the ranges of Figure 7.32. If for specified conditions breakthrough cannot occur, water can be produced by coning only if either the production rate or penetration is increased or the water-oil contact rises.

It is possible to estimate the critical production rate from Figure 7.32. Note from this figure that the dimensionless cone height at breakthrough tends to become asymptotic with dimensionless time at a value of Z greater than 3.0 and less than 4.0. Although the exact asymptotic value for Z_{BT} cannot be obtained from Figure 7.32 or from the data from which it was prepared, it can be assumed that Z_{BT} becomes asymptotic at 3.5.

If we let Equation 7.19 equal 3.5 and insert appropriate values at breakthrough for all factors except q_o, we can calculate q_o to be the critical oil production rate.

(3) *Application of the t_D vs Z correlation in predicting cone development time.* The t_D vs Z correlation method will permit one to estimate whether breakthrough will occur within the limits of Figure 7.32 and, if so, how long it will take for the well to produce water by coning as well as how fast the apex of the cone will rise. Note that the curves in Figure 7.32 are based on limited data only and that predictions made from the correlation of these data are subject to the conditions presented earlier.

To predict the cone behavior of a cone, use the following procedure:

(1) Using Equation 7.19, calculate the dimensionless cone height for breakthrough to determine whether breakthrough will occur within the limits of Figure 7.32 and where the departure curve will lie.
(2) Find the dimensionless time t_D that corresponds to the calculated Z for breakthrough.
(3) Using Equation 7.20, find t, the actual time of breakthrough in days.
(4) Determine the cone height at any time before breakthrough by assuming a cone height less than the breakthrough height by calculating Z from Equation 7.19, determining the corresponding t_D from the basic buildup and appropriate departure curves, and finally by solving Equation 7.20 for time t.

It would be expected that the basic Z and t_D groups would apply also to gas coning, especially if gas compressibility does not change drastically across the drainage system.

EXAMPLE #8

(1) *Breakthrough time calculation* A well has been drilled into a homogeneous oil sand, which is underlain by an aquifer. For the system described below and in Figure 7.33:

Given data:

oil density, $\rho_o = 0.78$ g/cc
oil viscosity, $\mu_o = 1.25$ cp

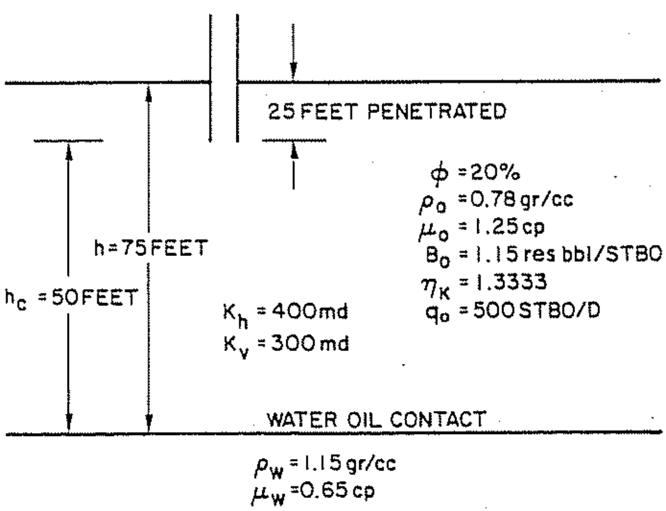

Figure 7.33 Application of Z vs t_d Correlation (Example 7.8)

oil formation volume factor, $B_o = 1.15$ reservoir bbl/stbo
oil production rate, $q_o = 500$ stbo/d
water density, $\rho_w = 1.15$ g/cc
water viscosity, $\mu_w = 0.65$ cp
average porosity, $\phi = 20\%$
penetration thickness = 25 ft
horizontal permeability, $k_h = 400$ md
vertical permeability, $k_v = 300$ md
permeability to water at residual oil, $(k_w)_{or} = 0.58\ k_h$
permeability to oil at connate water, $(k_o)_{wi} = 0.88\ k_h$
oil zone thickness, h = 75 ft
horizontal to vertical permeability ratio $k_h/k_v = \eta_k = 1.3333$

Solution procedure:

Calculate Z:

$$Z = \frac{(0.00307)\Delta\rho_{wo}\, k_h\, h\, h_c}{\mu_o\, q_o\, B_o} = \frac{(0.00307)(0.37)(400)(75)(50)}{(1.25)(500)(1.15)} = 2.37$$

This value of Z indicates that at 500 stbo/d there will be water-cone breakthrough. How long it will take for the cone to break through the dimensionless time at breakthrough t_D is determined from Figure 7.32 to be 4.5.

Rearrange Equation 7.20 to solve for actual breakthrough time t:

$$t = \frac{t_D\, \mu_o\, \phi\, h\, \eta_k}{0.00137\, \Delta\rho_{wo}\, k_h\, (1 + M^{\alpha})} \quad (7.22)$$

M is the water-oil mobility ratio and is defined as:

$$M = \mu_o(k_w)_{or}/\mu_w(k_o)_{wi} = \frac{(1.25)(0.58k_h)}{(0.65)(0.88k_h)} = 1.27 \quad (7.23)$$

For M = 1.27 and from Equation 7.21:

$$\alpha = 0.60$$

Actual time for water-cone breakthrough is calculated as follows:

$$t = \frac{(4.5)(1.25)(0.20)(75)(1.3333)}{(0.00137)(0.37)(400)[1 + (1.27^{0.6})]}$$

= 258 days for the water-cone apex to rise 50 ft and break through

(2) *Cone apex growth rate.* The movement of the apex of the water cone during the 258 days can be determined from the Z and t_D relationship along the basic buildup curve and the appropriate departure curve.

For a 10-ft cone, the time is calculated as follows:

$$Z = (10/50)(2.37) = 0.474$$

From the basic buildup curve in Figure 7.32, t_D = 0.8, so t = (0.8/4.5)(258) = 46 days.

For a 20-ft cone:

$$Z = (20/50)(2.37) = 0.95$$

From Figure 7.32, t_D = 3.3, so t = (3.3/4.5)(2.58) = 189 days.

For a 30-ft cone:

$$Z = (30/50)(2.37) = 1.42$$

From Figure 7.32, t_D = 4.0, so t = 4.0/4.5 (258) = 229 days.

For a 40-ft cone:

$$Z = \frac{40}{50}(2.37) = 1.90$$

From Figure 7.32, t_D = 4.3, so t = 4.3/4.5 (258) = 247 days.

Figure 7.34 shows the growth of the cone apex with time for the previous example.

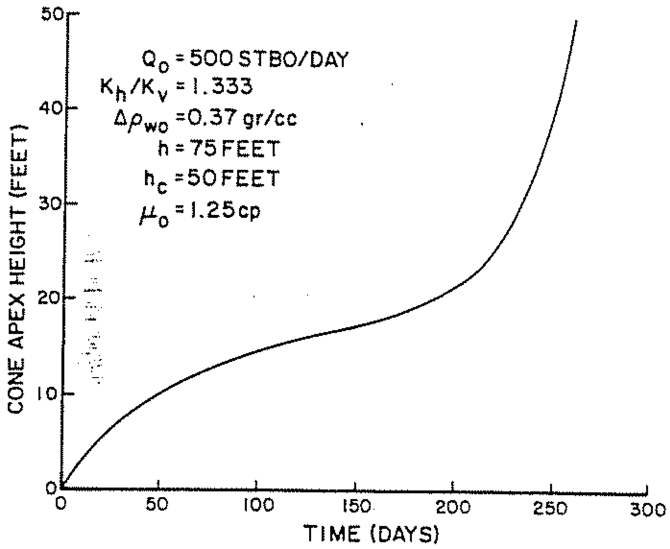

Figure 7.34 Cone Apex Height vs Time

7.15 WATER AND GAS CONING IN FRACTURED RESERVOIRS

The coning of water or gas into a producing oil well is an occurrence that has a large influence on production costs and affects efficient reservoir depletion.

Natural fractures are often found in hard formations such as limestones, dolomites, chalks, low-porosity sandstones, etc., and are mainly generated by rock failure during deformation by folding or faulting. In these hard formations, which normally have low matrix permeabilities relative to the fracture permeabilities, coning of water or gas occurs in the fracture plain. Fractures provide an excellent avenue for reservoir depletion and for water and gas coning.

Water or gas are drawn rapidly into the producing wellbore when drawn into the fracture plain to a critical radius around the wellbore. At this critical radius, the flowing pressure gradient in the oil zone is equal to the static gradient difference between oil and water for water coning or between gas and oil for gas coning. This critical radius is normally smaller for gas than for water coning because of the larger available differential gradient.

7.151 THE BIRKS METHOD[10]

Equivalent single-fracture theory. Before one can make coning calculations, the flowing characteristics of a fractured system must be described. Single-fracture theory, which was described by Baker,[11] can be used to describe multiple fracture flow, including wellbore damage and stimulation effects. While the term coning is used because of the directional properties of fractured reservoirs, a true cone is not developed, but a directionally varying interfacial deformation occurs. Using the single-fissure theory, a correlation can be developed between the bottom-hole flowing pressure drop and the surface flow rate by the following equation:

$$\Delta P = Aq + Bq^2 \tag{7.24}$$

where:

ΔP = bottom-hole flowing pressure drop, psi
A = constant, psi/Mstbo/d
B = Constant, psi/(Mstbo/d)^2

A and B are constants that must be developed for each well. To determine these constants, bottom-hole flowing pressures have to be determined for at least three different flow rates.

As seen in Figure 7.35, a plot is made of $\Delta P/q$ vs q. A best linear fit is made through these points, and constant A is the intercept on the $\Delta P/q$ scale at q = 0. Constant B is the slope of the best linear fit.

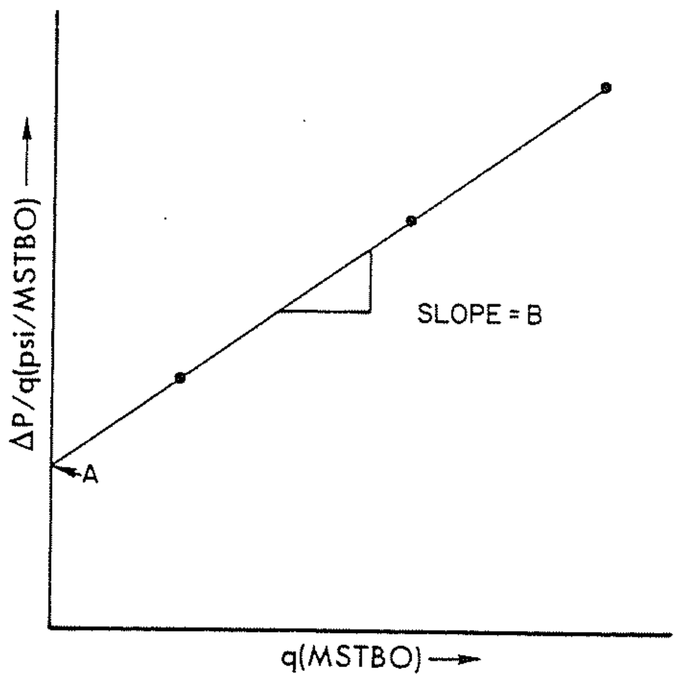

Figure 7.35 q vs $\frac{\Delta P}{q}$ Plot

Aq is the laminar flow pressure-drop component of the total flowing bottom-hole pressure drop.

Bq^2 is kinetic energy and turbulent flow component of the total flowing bottom-hole pressure drop.

The radius in the fracture plain at which flow becomes turbulent is related to the flow rate by the equation:

$$R_t = 0.045 \frac{\rho_o q_o B_o}{\mu_o} \tag{7.25}$$

where:

R_1 = turbulent flow radius, in.
ρ_o = oil density, g/cc
q_o = oil rate, Mstbo/d
B_o = oil formation volume factor, reservoir bbl/stbo
μ_o = oil viscosity, poise

The turbulent flow, critical flow, and drainage radius projections in the fracture plain and vertical plain are seen in Figure 7.36.

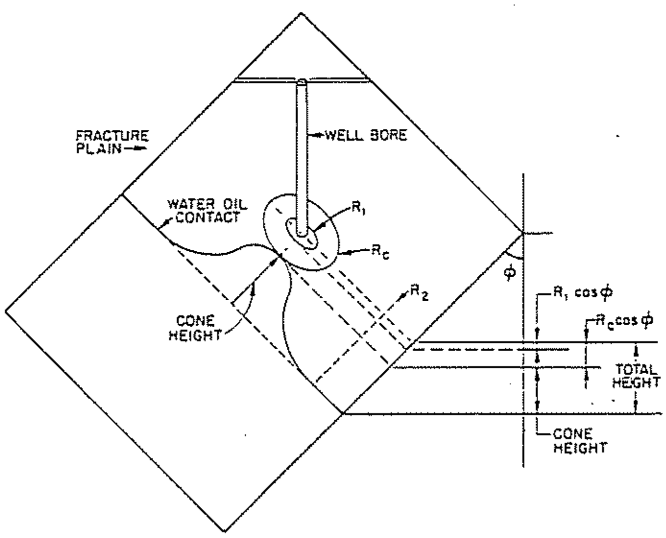

Figure 7.36 Fractured Reservoir Coning System

Constant A is related to the equivalent single fracture width in the laminar flow region by the equation:

$$A = 0.00715 \frac{\mu_o B_o}{F_A^3} \log_{10}\left(\frac{R_2}{R_1}\right) \tag{7.26}$$

where:

F_A = equivalent single fracture width in the laminar flow region, in.
R_2 = drainage radius of the well in the fracture plain in the fracture direction, in.

Once a value of A has been graphically determined, the equivalent single fracture in the laminar flow region F_A is calculated from the equation:

$$F_A = 0.19265\left[\frac{\mu_o B_o}{A} \log_{10}\left(\frac{R_2}{R_1}\right)\right]^{1/3} \tag{7.27}$$

In the stream-lined flow region, the pressure gradient $\frac{dP}{dR}$ is:

$$\left(\frac{dP}{dR}\right) = \frac{0.00715\,\mu_o B_o q_o}{R\,F_A^3 \ln_e(10)} \tag{7.28}$$

At the critical flow radius R_c:

$$\left(\frac{dP}{dR}\right)_{Rc} = (G_w - G_o)\cos\phi \tag{7.29}$$

where:

$\left(\frac{dP}{dR}\right)$ = flowing pressure gradient, psi/ft
G_o = oil gradient, psi/ft
G_w = water gradient, psi/ft
R_c = critical flow radius, ft
ϕ = fracture plain inclination angle measured from the vertical, degrees

Then:

$$R_c = \frac{0.00715\,\mu_o B_o q_o}{F_A^3 (G_w - G_o)\cos\phi \ln_e(10)} \tag{7.30}$$

The vertical component of the critical radius h_{rc} is:

$$h_{rc} = \frac{0.00715\,\mu_o B_o q_o}{F_A^3 (G_w - G_o) \ln_e(10)} \tag{7.31}$$

The water cone height at the critical radius up the fracture plain is:

$$\frac{P_2 - P_c}{(G_w - G_o)\cos\phi} \tag{7.32}$$

where:

P_2 = reservoir pressure at R_2, psi
P_c = reservoir pressure at R_c, psi

The vertical component of the water cone at R_c is:

$$h_{cw} = \frac{P_2 - P_c}{G_w - G_o} \tag{7.33}$$

The pressure drop at R_c is:

$$P_2 - P_c = \frac{0.00715\,\mu_o B_o q_o}{F_A^3} \log_{10}\left(\frac{R_2}{R_c}\right) \tag{7.34}$$

The total allowable distance between the lowest fluid entry point and the static water oil contact is:

$$H_w = h_{rc} + h_{cw} \tag{7.35}$$

In the case of gas coning down a fracture plain, the critical flow radius is:

$$R_c = \frac{0.00715\,\mu_o B_o q_o}{F_A^3 (G_o - G_g)\cos\phi \ln_e(10)} \tag{7.36}$$

where:

G_g = gas gradient, psi/ft

The vertical component of the critical flow radius is:

$$h_{rc} = \frac{0.00715\,\mu_o B_o q_o}{F_A^3 (G_o - G_g) \ln_e(10)} \tag{7.36}$$

The gas-cone height at the critical radius down the fracture plain is:

$$\frac{P_2 - P_c}{(G_o - G_g)\cos\phi} \tag{7.38}$$

The vertical component of the gas cone at R_c is:

$$h_{cg} = \frac{P_2 - P_c}{G_o - G_g} \tag{7.39}$$

The total allowable distance between the highest fluid entry point and the static gas oil contact is:

$$H_g = h_{rc} + h_{cg} \tag{7.40}$$

It must be remembered that as the reservoir is depleted there may be movement of the static water-oil and gas-oil contacts and changes in fracture permeabil-

ity; thus, new calculations of A and B and H_g and H_w are required.

EXAMPLE #9

(1) *Gas-water coning in a fractured reservoir.* Bottom-hole pressure and production rate data for a hypothetical system are used to generate Figure 7.37. The following additional data are used:

Given data:

oil viscosity μ_o = 0.008 poise
oil formation volume factor B_o = 1.15 reservoir bbl/stbo
gas gradient G_g = 0.066 psi/ft
oil gradient G_o = 0.375 psi/ft
water gradient G_w = 0.433 psi/ft
drainage radius in fracture direction = 15,840 in.
gas-oil contact = 8,600 ft
highest perforation = 8,700 ft
lowest perforation = 8,900 ft
water-oil contact = 9,000 ft

As seen in Figure 7.38, constant A is equal to 20 psi/Mstbo/d, and constant B is 5 psi/(Mstbo/d)^2.

Solution procedure:

Calculation of maximum distance for varying flow rates and fracture inclinations were made, the results of which are summarized in Figures 7.39a and 7.39b.

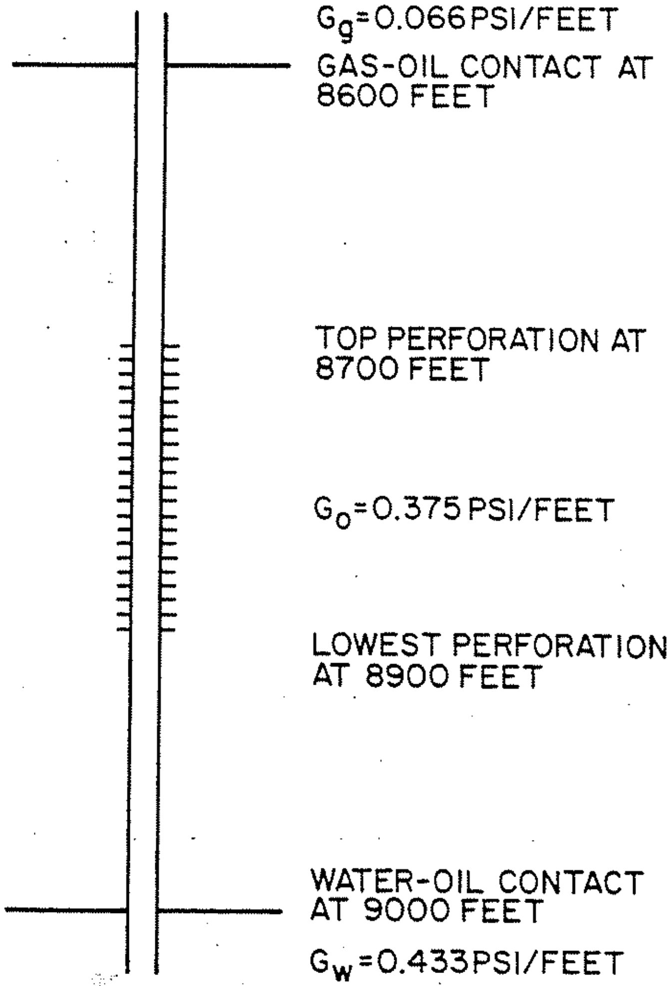

Figure 7.37 Water and Gas Coning in a Fractured Reservoir (Example #9)

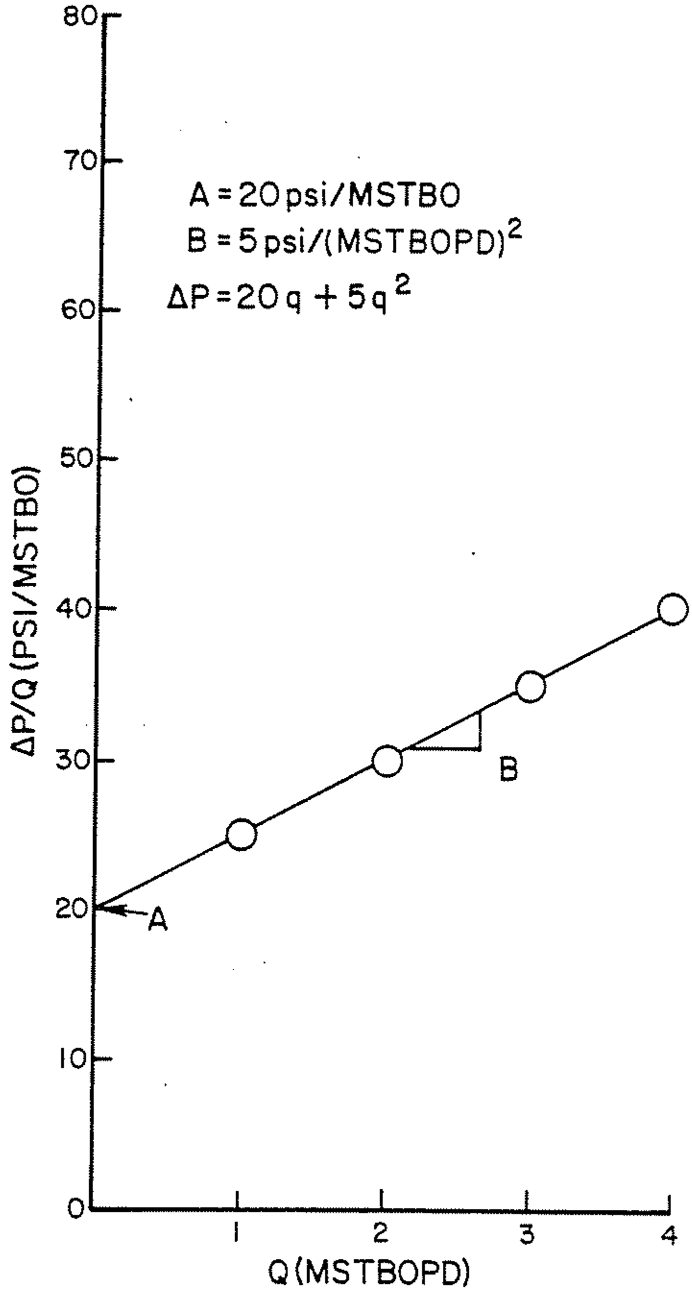

Figure 7.38 q vs q/ΔP

Several angles were used to show the sensitivity to fracture inclination. A determination of the fracture angle can be obtained if a representative whole core can be obtained and analyzed. It should be remembered that whole core recovery in fractured reservoirs tends to be poor, with core recovery representing the least fractured zones and that fracturing can be induced during the coring and core recovery operation.

From Figure 7.39b, it can be seen that, for 100 ft between the lowest perforation and the water oil contact, a maximum rate of about 500 stbo/d to prevent water coning would be allowed because, at 8,900 ft, low fracture angles would be expected. It should be noted that the allowable water coning rate is much lower than the well potential, a characteristic of many naturally fractured reservoirs. The distance

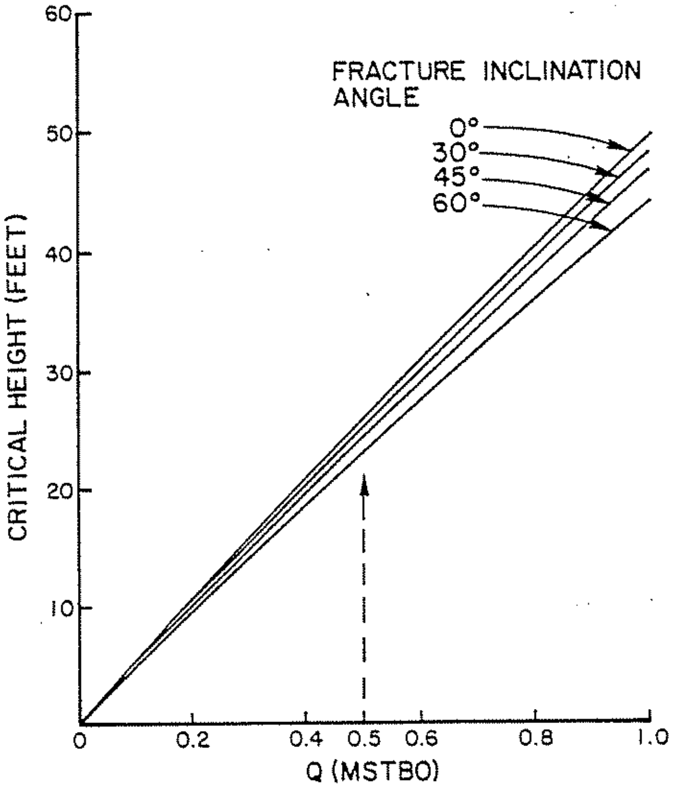

Figure 7.39a Critical h vs q for Gas Coning

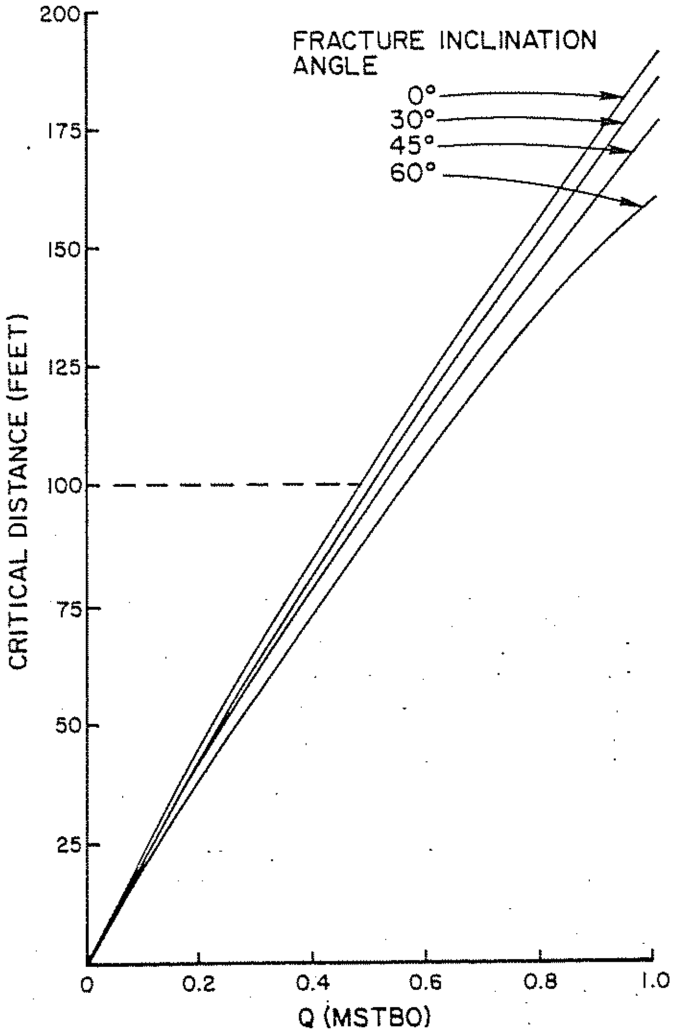

Figure 7.39b Critical h vs q for Water Coning

used was from the lowest perforation. A production log should be used to determine the highest and lowest fluid entry points for coning-rate determination. At this 500-stbo/d allowable rate, the gas-coning distance is about 25 ft, as seen in Figure 7.39a; thus, water coning is, as in most cases, the limiting rate.

(2) *Numerical simulation.* As indicated in the introductory part on water and gas coning, there are certain complications that cannot be treated rigorously with analytical solutions. In these cases, it is wise to resort to numerical simulators. These simulators can handle problems such as anisotropy, multiphase flow, irregular geometry, different production schedules, and various boundary conditions.

In principle, the basic coning equations are written by applying the conservation of mass to each phase, relating flow velocities with pressure by Darcy's Law, and relating pressures across interfaces by means of capillary pressures.[9] The resulting partial differential equations, which describe two-phase incompressible fluid flow for the case of water and oil in a cylindrical section, are:[12]

$$\frac{1}{r}\frac{\partial}{\partial r}\left(r\frac{k_{ro}k_h}{\mu_o}\frac{\partial \Phi_o}{\partial r}\right)+\frac{\partial}{\partial z}\left(\frac{k_{ro}k_z}{\mu_o}\frac{\partial \Phi_o}{\partial z}\right)-B_o q_{vo} = \phi\frac{\partial S_o}{\partial t} \tag{7.41}$$

$$\frac{1}{r}\frac{\partial}{\partial r}\left(r\frac{k_{rw}k_h}{\mu_w}\frac{\partial \Phi_w}{\partial r}\right)+\frac{\partial}{\partial z}\left(\frac{k_{rw}k_z}{\mu_w}\frac{\partial \Phi_w}{\partial z}\right)-B_w q_{vw} = \phi\frac{\partial S_w}{\partial t} \tag{7.42}$$

The potentials are defined as:

$$\Phi_o \equiv P_o - \gamma_o z \tag{7.43}$$

$$\Phi_w \equiv P_w - \gamma_w z \tag{7.44}$$

The pressures in each fluid phase can be related by capillary pressure:

$$P_c = P_o - P_w \tag{7.45a}$$

which is taken to be a function of water saturation alone. Also, the summation of the saturations must be equal to 1.0:

$$S_w + S_o = 1.0 \tag{7.45b}$$

where:

r = radial distance, ft
k_{ro} = relative permeability to oil
k_{rw} = relative permeability to water
k_h = absolute radial (horizontal) permeability (0.00633 × md)
k_z = absolute vertical permeability (0.00633 × md)
μ_o = oil viscosity, cp
μ_w = water viscosity, cp
Φ_o = oil potential, psia
Φ_w = water potential, psia
Z = vertical distance measured positively downward
B_o = oil formation volume factor, ft³/stb
B_w = water formation volume factor, ft³/stb
q_{vo} = oil production, stb/ft³ reservoir-day
q_{vw} = water production, stb/ft³ reservoir-day
S_o = oil saturation, fractional
S_w = water saturation, fractional

P_o = oil pressure, psi
P_w = water pressure, psi
P_c = capillary pressure, psia
ϕ = porosity, fraction
γ_o = specific weight of oil at reservoir conditions, psi/ft
γ_w = specific weight of water at reservoir conditions, psi/ft

The above equations can be written in finite difference form. The resulting algebraic equations can be solved by iterations around a selected grid system.[12-16] Also, the radial node size is varied logorithmically to give good definition of fluids distribution around the wellbore, which is the section where we are interested in more detail.

Van Poollen, Bixel, and Jargon indicated that the implicit rate calculation can be treated by first specifying the total production rate q_t as known.[16] Then, this rate is distributed between water and oil according to the following equations:

$$q_w = q_T \frac{k_{ro}}{\mu_o} \Big/ \left(\frac{k_{ro}}{\mu_o} + \frac{k_{rw}}{\mu_w}\right) \tag{7.46}$$

and:

$$q_o = q_T \frac{k_{rw}}{\mu_w} \Big/ \left(\frac{k_{ro}}{\mu_o} + \frac{k_{rw}}{\mu_w}\right) \tag{7.47}$$

The production rate of the water phase at the time level n + 1 is:

$$q_{w,n+1} = q_{w,n} + dq_w \tag{7.48}$$

where dq_w is the change in production rate during that time step.

If we assume that the total mobility will remain relatively constant during one time step, then:

$$dq_w = \left(\frac{q_t}{(k_{ro}/\mu_o) + (k_{rw}/\mu_w)}\right) \frac{1}{\mu_w} \frac{d(k_{rw})}{dS_w} \Delta_t S_w \tag{7.49}$$

where:

$$\frac{d\,(k_{rw})}{dS_w} = \frac{K_{rw,n+1} - k_{rw,n}}{S_{w,n+1} - S_{w,n}}$$

and $\Delta_t S_w$ is the time derivative of the water saturation.

Implicit relative permeabilities can be determined in the same manner:

$$k_{rw,n+1} = k_{rw,n} + \frac{d\,(k_{rw})}{dS_w} \Delta_t S_w \tag{7.50}$$

Numerical models have been found to simulate the results of coning experiments carried out in the laboratory very well. As an example, MacDonald and Coats[12] have been able to use a numerical simulator to reproduce results obtained by Soengkowo[17] with the use of a physical model. Results from both numerical and physical models are presented in Figures 7.40a and 7.40b. The comparison between the mathematical simulation and the laboratory results is considered to be good.

7.16 REMEDIAL TREATMENTS FOR CONING

Several possibilities can be considered in efforts to reduce the effects of water and/or gas coning, including a reduction of the production rate, infill drilling, improvement in well productivity, recompletions, stop cocking, oil injection, and artificial barriers.

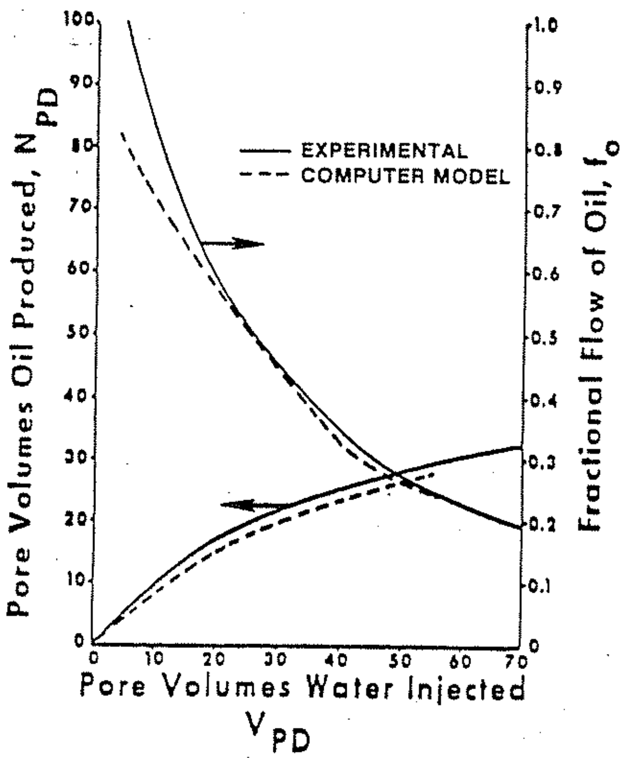

Figure 7.40a Comparison of Physical Model and Numerical Model Results (after Soenkowo)[17]

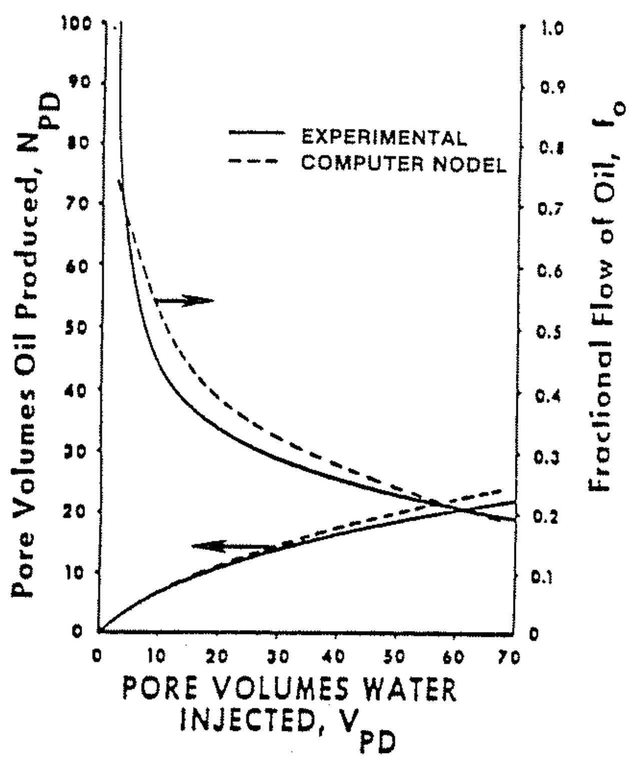

Figure 7.40b Comparison of Physical Model and Numerical Model Results (after Soenkowo)[17]

7.161 REDUCTION OF PRODUCTION RATE

Lowering the rate can reduce the effects of coning by decreasing the pressure drop at the well. This, in turn, reduces dynamic forces around the wellbore and, thus, allows a better gravity segregation of the phases involved.

7.162 INFILL DRILLING

The addition of infill wells in a given reservoir allows the formation of various small cones rather than just a few large ones as shown in the schematic of Figure 7.41.

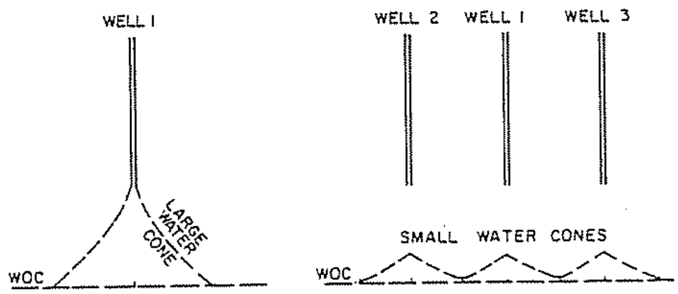

Figure 7.41 Schematic Showing How a Large Number of Wells Can Reduce the Effects of Water Coning

7.163 IMPROVEMENT OF WELL PRODUCTIVITY

In some cases, it is possible to increase well productivity by acidizing or fracturing the reservoir. A fracture can increase the effective wellbore radius, r_{we}, as indicated by the following equation:

$$r_{we} = r_w e^{-S} \tag{7.51}$$

where:

r_w = the wellbore radius
S = the skin

This increase in effective wellbore radius reduces the coning effect by decreasing the pressure drop around the wellbore.

7.164 RECOMPLETIONS

Recompleting wells at higher elevations to increase the distance between the water-oil contact and the lower perforation is a good practice to reduce the effects of water coning.

An example of reducing production rate, improving well productivity by acidizing, and recompleting from upper intervals in a naturally fractured reservoir is provided by the Alamein Field in Egypt.[18] The well, whose logs are shown in Figure 7.42, was perforated initially from 8,235 to 8,255 ft. The distance to the water-oil contact was about 100 ft. Following a 500-gal, 15% hydrochloric acid treatment, the well produced at a rate of 5,200 bbl/day with a drawdown of only 90 psi. This well produced 3 MMstbo before the water cut reached 5%. Later, these perforations were squeezed and the interval from 8,214 to 8,227 ft was opened to production. Following an acid job, the well

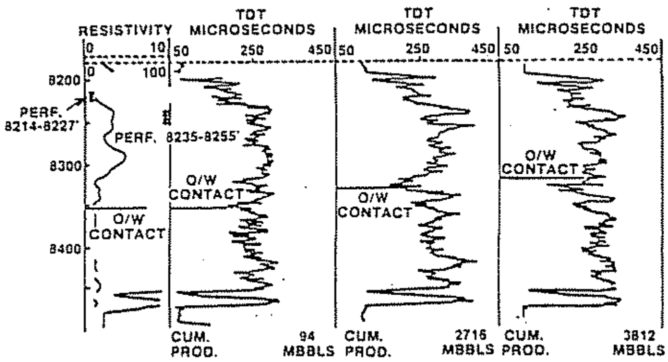

Figure 7.42 Example Well Completion Illustrates Method of Perforating the Top of the Pay Zone, Well Above the Oil-Water Contact (after El Banbi)[18]

produced 3,600 bbl/day with a drawdown of only 46 psi. This well had accumulated 5.9 MMstbo by 1974.

Figure 7.42 also shows the advance of the water table, which was monitored with TDT logs. This information was useful in deciding on recompletions and drilling of additional infill wells.

Conventional buildup interpretation was impossible because of the immediate pressure stabilization obtained in all surveys. Therefore, a multirate test prior to placing the well in continuous production was carried out. This allowed estimates of some reservoir characteristics.

Maximum pressure drawdowns to avoid water coning were calculated using Muskat's equation. Whenever fractures or high-porosity intervals were present below the perforations, the actual drawdown was kept well below the calculated maximum. This approach avoided coning problems.

Figure 7.43 shows the rate sensitivity of the reservoir. As the water cut increases, the well is choked back and there is an immediate decrease in fractional water cut. This minimized the upward movement of water. The well of Figure 7.43 produced about 6 MMbo with less than 5% water cut. This is remarkable for a naturally fractured reservoir with water influx.

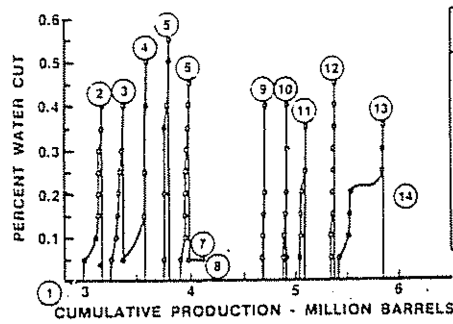

INTERVAL	PROD. RATE b/d
1-2	4955
2-3	4368
3-4	4024
4-5	3352
5-6	2805
6-7	2313
7-8	RECOMPLETE
8-9	3830
9-10	3029
1-11	2430
11-12	2102
12-13	1672
13-14	1485

Figure 7.43 Rate sensitivity of the Alamein Wells is Demonstrated by History of the Example (after El Banbi)[18]

Figure 7.44 shows a cross plot of bottom-hole pressure vs cumulative production. The maximum allowed pressure drop was 108 psi. As the oil rate was reduced, the reservoir pressure increased significantly. Eight years after discovery of the field, the pressure was only 32 psi below the original reservoir pressure.

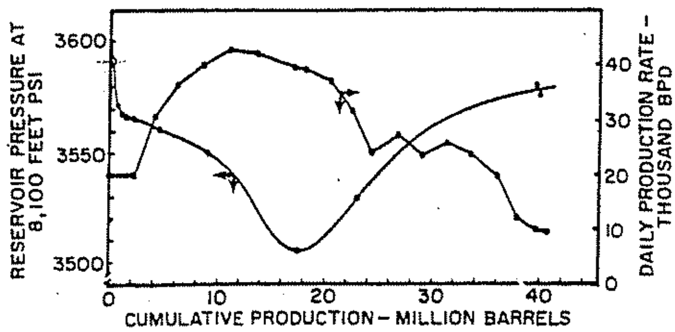

Figure 7.44 BHP vs Cumulative Production Performance for the Entire Alamein Field (after El Banbi)[18]

7.165 STOP COCKING

Stop cocking gives better results in the case of gas than water coning. After the cone breaks in, the well is shut in for a certain period of time. Then, the well is opened to production at a lower rate to prevent a new buildup of the cone. In the case of gas coning, gravity segregation takes place rapidly once the well is shut in. However, in the case of water coning, the segregation might be slower because of the lower density difference between oil and water, as compared with the difference between oil and gas. Furthermore, capillary pressures might retain a portion of the water that has displaced oil, consequently reducing the effective permeability to oil.

7.166 OIL INJECTION

In some cases, it is possible to prevent coning and to increase recoveries by injecting oil near the gas-oil or water-oil contacts. Field experience indicates that this approach might reduce drastically the water-oil or gas-oil ratios.

One problem associated with this approach is that large amounts of oil must be injected to increase the recoveries, and there is always uncertainty with respect to the outcome. For example, in some cases it is necessary to inject 5 bbl of oil to recover 6.

7.167 ARTIFICIAL BARRIERS

Plastics, bitumens, and cement slurries might help to prevent water coning if they penetrate the formation for a considerable distance, generating an artificial barrier. Plastics offer some technical advantages but they are very expensive.

Blocking gelatinous agents can help reduce coning or channeling caused by streaks of high permeability or fractures. A good example of the use of blocking gels has been presented by Mazzocchi and Carter.[19]

Figure 7.45 shows the results of a pilot treatment in which a blocking agent was used in a naturally fractured reservoir in 1971. Actual results compared with extrapolated regression lines clearly indicate that the treatment was highly successful. Oil production increased substantially, while water production followed the same trend projected by the extrapolated regression line. After 28 months of regular water injection, no traces of the gel component were found in the water samples obtained from production wells, indicating the successful application of the gelatinous blocking agent on the edge of this fractured limestone reservoir.

It is important, however, to be very careful when working with gelatinous materials because they tend to decompose because of poor thermal stability. Furthermore, in some cases they are sensitive to metallic ions found in formation fluids.

Karp, Lowe, and Marusov discussed the use of horizontal barriers for controlling water coning.[20] In this procedure, a horizontal fracture is generated by the single-point entry technique. Next, the fracture is opened with a propping agent and filled with cement.

Figure 7.46 shows the time to breakthrough for various barrier radii as reported by Karp, Lowe, and Marusov.[20] Notice that, if the wellbore radius is 0.5 ft, a 10-ft barrier approximately doubles the time to breakthrough. To increase the time to first water breakthrough, it is necessary to build very large barriers.

7.2 WATER AND GAS FINGERING

The difference between fingering and coning was explained with the use of Figure 7.1. Fingering occurs when the flowing pressure gradients around the well-

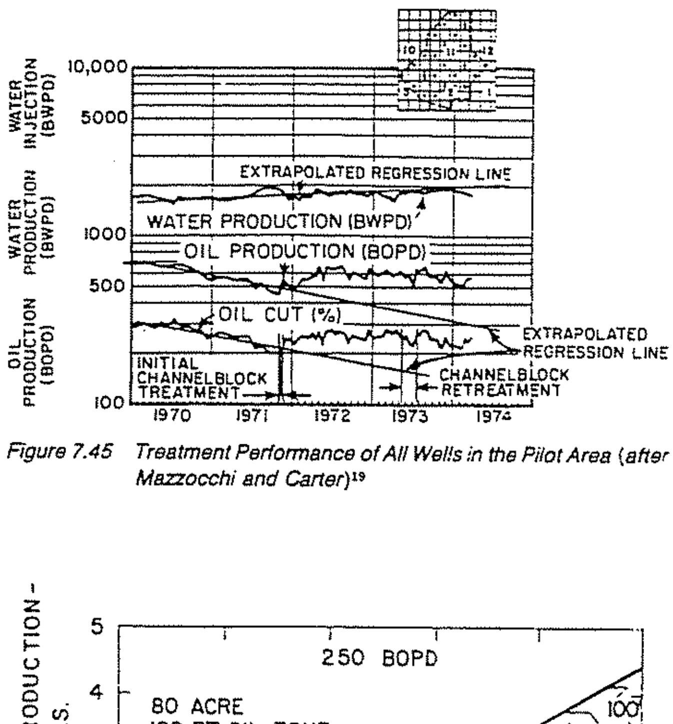

Figure 7.45 Treatment Performance of All Wells in the Pilot Area (after Mazzocchi and Carter)[19]

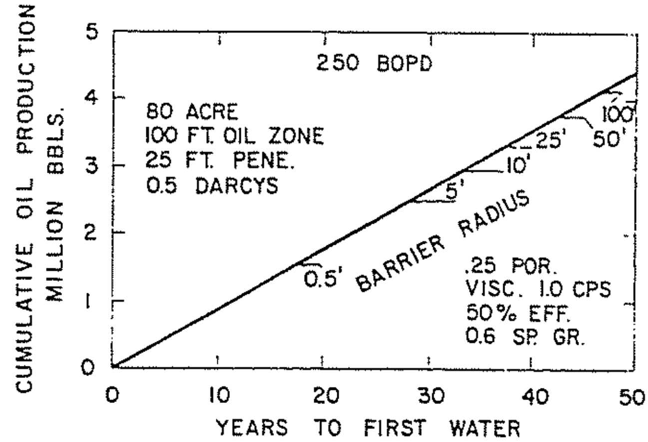

Figure 7.46 Period of Water-Free Oil Production for Various Barrier Radii (after Karp)[20]

bore cause gas or water to flow along the bedding planes. Coning occurs when these gradients cause the gas or water to flow across the bedding planes.

7.21 FINGERING IN HOMOGENEOUS RESERVOIRS

7.211 ARTHUR METHOD

Figure 7.47 shows water-fingering conditions considered by Arthur.[4] The pressure gradient in the flowing fluids generates a water cusp. The assumption is made that two-dimensional radial flow exists. The flow rate, q, is expressed by the equation:

$$q = \frac{2\pi r\, k_o h}{\mu_o} \frac{d\Phi}{dr} \tag{7.52}$$

where:

r = radius, ft
k_o = effective permeability to oil
h = reservoir thickness, ft
μ_o = oil viscosity

and the potential Φ is:

$$\Phi = P - \rho_o g z$$

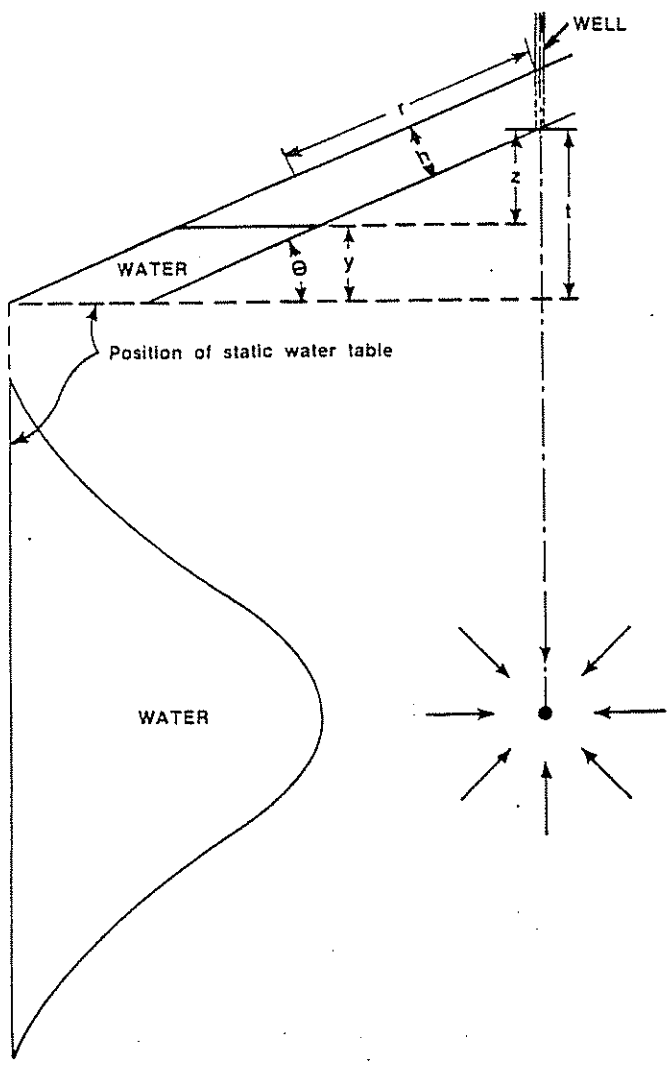

Figure 7.47 Water Fingering Conditions

where:

P = pressure, psi
ρ_o = oil density
g = acceleration of gravity
z = distance of point from selected datum level, ft

The velocity potential Φ takes into account the effect of gravity and corrects the pressures at various points in the system.

A *stable* finger occurs when the differential gravitational force between water and oil is equal to the pressure gradient at the top of the water surface. A stable finger occurs when:

$$\Delta\Phi = \Delta P - \Delta\rho g\,(t - \frac{dZ}{dr} r) \tag{7.53}$$

where t is the vertical distance of the well from the static water level in feet.

Combining the above two equations allows the calculation of the minimum distance that a finger can approach without breaking through into the well. This minimum distance r_{min} is given by the equation:

$$r_{min} = \frac{\Delta P}{\Delta\rho\, g \sin\theta\, \ln(r_e/r_w)} \tag{7.54}$$

The minimum vertical distance t_{min} that a well can be located above the static water-oil contact without fingering is given by:

$$t_{min} = \frac{\Delta\rho}{\Delta\rho g}\left(\frac{1 + \ln(r_e/r_{min})}{\ln(r_e/r_w)}\right) \tag{7.55}$$

where:

r_e = drainage radius
r_w = wellbore radius

Notice that the above equations are of the same form as those presented by Birks for calculating water coning in naturally fractured reservoirs. The following example illustrates the use of the above equations.

EXAMPLE #10

Given data:

The differential weight between water and oil $\Delta\rho g$ is equal to 0.14 psi/ft. The reservoir dip θ is 5.74° and the well radius is 0.333 ft.

Calculate:

Find the minimum height of the well above the water table to avoid flow of water into the well for a pressure differential of 40 psi and a drainage radius of 600 ft.

Solution procedure:

The minimum radius is calculated from Equation 7.54 to be:

$$r_{min} = \frac{40}{(0.14)(\sin 5.74)\ln(600/0.333)} = 381.1 \text{ ft}$$

The minimum vertical distance t_{min} is calculated from Equation 7.55 as follows:

$$t_{min} = \frac{40}{0.14}\left(\frac{1 + \ln(600/381.1)}{\ln(600/0.333)}\right) = 55.4 \text{ ft}$$

7.212 PIRSON METHOD

In the Pirson method, a tilted, uniform, and isotropic reservoir is considered as shown in Figure 7.48.[6] When dynamic equilibrium is reached and the drive velocity is constant and uniform, a "planar flow" is reached, with flow lines parallel to the structure.

The reservoir dip is α, and the angle made by the surface of liquid separation with the direction X is β. In a gas-cap-expansion reservoir, the constant velocity generates components v_g and v_o in the gas and oil phases, respectively. These flow components are parallel to the interface.

The gas cap will tend to finger into the oil zone when $dZ/dX = 0$; i.e., when the interface tends to become parallel to the structure. Pirson has shown that, for the case of gas-oil, this condition is reached at a critical velocity and is given by the following relationship:[6]

$$v_c = g(\rho_o - \rho_g)\frac{\sin\alpha}{\frac{\mu_o}{k_o} - \frac{\mu_g}{k_g}} = \frac{\rho_o - \rho_g}{1.033}\,\frac{\sin\alpha}{\frac{\mu_o}{k_o} - \frac{\mu_g}{k_g}} \qquad (7.56)$$

where k_o and k_g are the effective permeabilities to oil and gas, respectively, in md.

For the case of water fingering, the critical velocity, v_c, is given by:

$$v_c = g(\rho_w - \rho_o)\frac{\sin\alpha}{\frac{\mu_w}{k_w} - \frac{\mu_o}{k_o}} = \frac{\rho_w - \rho_o}{1.033}\,\frac{\sin\alpha}{\frac{\mu_w}{k_w} - \frac{\mu_o}{k_o}} \qquad (7.57)$$

7.22 VISCOUS FINGERING IN WATER DRIVES

Van Meurs and van der Poel presented a method to predict recovery in water-drive reservoirs involving viscous fingering.[21] These analytical solutions have allowed the reproduction of experiments carried out in the laboratory with different mobilities.

Figure 7.49 shows an idealized picture of viscous fingering with three flow areas. The sizes of these areas are characterized by their oil and water saturations. The immobile water of area 3 is expressed as S_{wm}, the residual oil saturation as S_{or}, the size of area 2 as $S_w - S_{wm}$, and the size of area 1 as $S_o - S_{or}$, or $1 - S_{or} - S_w$. Oil flows in area 1 unhindered, water flows in area 2, and oil and water are immobile in area 3. The system is horizontal and homogeneous, and steady-state conditions prevail. By assuming that the phases are incompressible, van Meurs and van der Poel developed the following equations for fractional flow:[21]

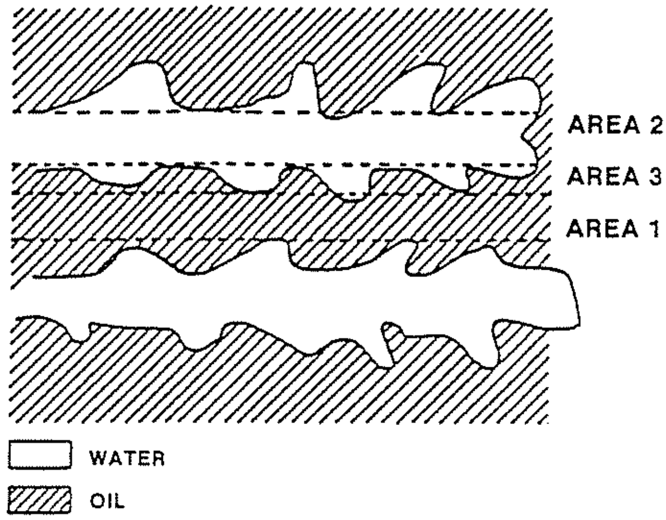

Figure 7.49 Idealized Picture of Viscous Fingering Showing the Various Flow Areas (after van Meurs and van der Poel)[21]

$$f_w = \frac{q_w}{q_t} = \frac{M(S_w - S_{wm})}{(M-1)(S_w - S_{wm}) + B} \qquad (7.58)$$

where:

$$B = 1 - S_{or} - S_{wm} \qquad (7.59)$$

$$M = \text{mobility} = \mu_w/\mu_o \qquad (7.60)$$

Figure 7.50 shows a schematic representation of water saturations through the linear system prior to breakthrough. The critical water saturation S_c at the cutoff point X_c is given by:

$$S_c = S_{wm} + \left(\frac{B\,S_{wm}}{M-1}\right)^{0.5} \qquad (7.61)$$

The oil recovery at breakthrough is given as a function of mobility M, S_{wm}, and the constant B by the following equation:

$$N_{pb} = \frac{\{[(M-1)\,B\,S_{wm}]^{0.5} + B\}^2}{MB} \qquad (7.62)$$

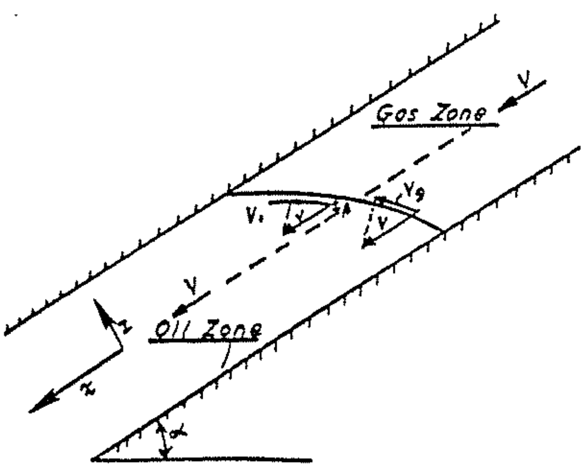

Figure 7.48 Gas-Cap Expansion With Fluid Flow Deflections at Gas-Oil Contact (after Pirson)[6]

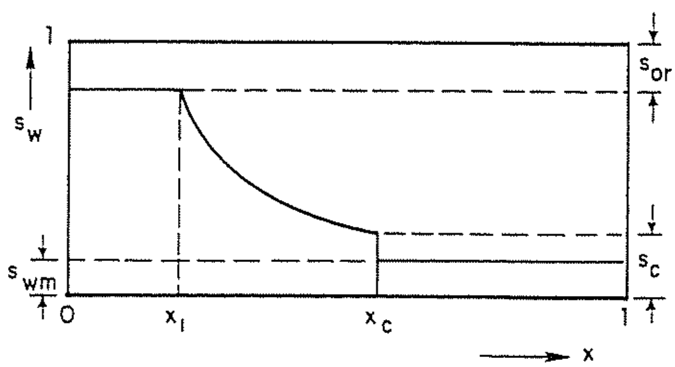

Figure 7.50 Schematic Representation of Water Saturations Through the Liner System Prior to Breakthrough (after van Meurs and van der Poel)[21]

The position X_1 of the critical distance in which all the movable oil has been swept out at breakthrough is given by:

$$X_1 = \frac{W_i}{BM} \quad (7.63)$$

where W_i is the cumulative water injected. The fractional water cut at breakthrough f_i is given by:

$$f_i = \frac{M}{M-1}\left[1-\left(\frac{B}{MW_i}\right)^{0.5}\right] \quad (7.64)$$

and the ultimate recovery, N_{pv}, is:

$$N_{pv} = S_{wm} + B\left\{\frac{M - f_i^2(M-1)}{[M - f_i(M-1)]^2}\right\} \quad (7.65)$$

Finally, by considering steady state, a time relationship between water injected and oil produced is developed:

$$W_i = \frac{\int q\,dt}{\phi L} \quad (7.66)$$

Land has shown that van Meurs and van der Poel's equations can be developed directly from the Buckley-Leverett approach by considering straight-line relative permeability curves as shown in Figure 7.51.[22] From this figure, it can be seen that:

$$k_{ro} = 1 - S_{or} - S_w \quad (7.67)$$

and:

$$k_{rw} = S_w - S_{wm} \quad (7.68)$$

If the above equations for relative permeabilities are included in Buckley-Leverett's relationship:

$$f_w = \frac{k_{rw}/\mu_w}{k_{rw}/\mu_w + k_{ro}/\mu_o} \quad (7.69)$$

it is found that:

$$f_w = \frac{M(S_w - S_{wm})}{(M-1)(S_w - S_{wm}) + B}$$

which is the same as Equation 7.58.

EXAMPLE #11

This illustration is taken directly from the work of Smith.[23]

Given data:

A horizontal, linear system contains oil and has a cross-sectional area of 1 ft² and a length of 1,000 ft.

$q = 10$ ft³/hr
$\mu_o = 10$ cp
$\mu_w = 1$ cp
$S_{wi} = 0.20$
$\phi = 0.25$
$S_{wm} = 0.15$
$B_o = 1.00$
$M = \mu_o/\mu_w = 10$
$S_{or} = 0.20$

Calculate:

Find the performance under waterflooding.

Solution procedure:

(1) Total oil in the system = N = 1.00(1,000)(0.25) × (1 − 0.20) = 200 ft³
(2) $B = 1 - S_{or} - S_{wm} = 1 - 0.20 - 0.15 = 0.65$
(3) Calculate the oil produced at breakthrough:

$$N_{pb} = \frac{[0.65 + \sqrt{(10-1)(0.15)(0.65)}\,]^2}{10\,(0.65)} = 0.39$$

(4) At breakthrough, the position of the critical distance at which all the movable oil has been swept out is:

$$X_1 = \frac{W_i}{BM} = \frac{0.39}{0.65(10)}$$
$$= 0.06 \text{ or } 60 \text{ ft from the inlet end}$$

(5) Calculate the water cut at breakthrough:

$$f_i = \frac{10}{10-1}\left\{1 - \left[\frac{0.65}{10(0.39)}\right]^{0.5}\right\} = 0.657$$

(6) The ultimate recovery at a water cut of 0.98:

$$N_{pv} = 0.15 + 0.65\frac{[10 - 0.657^2(10-1)]}{[10 - 0.657(10-1)]^2} = 0.740$$

(7) To include the time relationship with the water injected and the oil produced:

$$W_i = \frac{\int q\,dt}{\phi L} = \frac{10t}{0.25(1,000)} = 0.04t$$

It would then be a direct problem to generate the performance curves as a function of time or of cumulative oil produced.

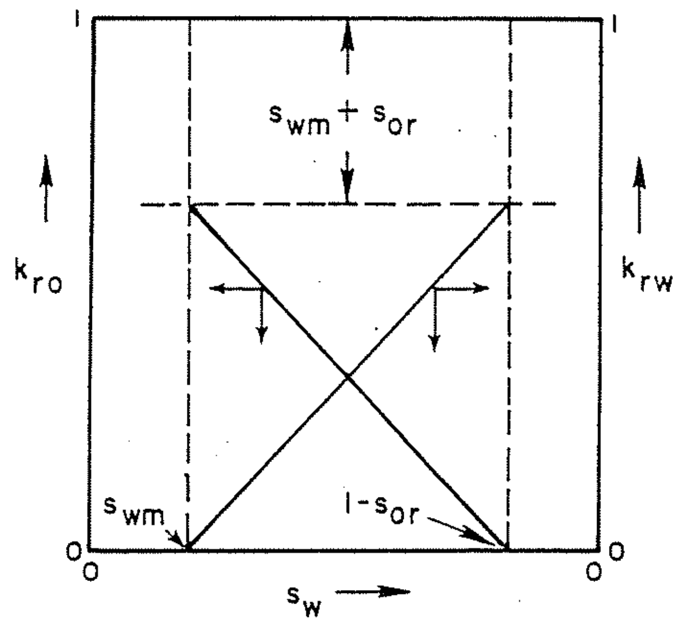

Figure 7.51 Relative Permeability Curves Preassumed for the Viscous Fingering Immiscible Displacement Theory

7.221 FINGERING IN ANISOTROPIC RESERVOIRS

It is important to determine the degree of anisotropy to avoid premature problems of gas or water channel-

ing. Radioactive tracers and interference pressure analysis are powerful tools for determining preferential orientation of natural fractures or direction of streaks of high permeability. In the case of natural fractures, aerial photography, landsat information, and oriented cores can become very powerful tools.

(1) *Radioactive tracers.* Flagg et al.,[24] Mardock and Watson,[25] and Alberts et al.[26] have discussed the use of radioactive traces for determining permeability profiles and orientation of streaks of high permeability.

(2) *Pressure interference.* Pressure interference analysis can determine fracture orientation in naturally fractured reservoirs. Delineation of fractured trends is very important for proper selection of injection patterns in secondary recovery projects. It is also very important in early stages of development for proper location and drilling of deviated holes.

(3) *Elkins and Skov method.* Elkins and Skov used pressure interference successfully for determining fracture orientation in the Spraberry field of Texas.[27] They assumed that pressure drawdown at a new well, which was caused by constant single-phase production of another well in a horizontal reservoir of constant thickness with anisotropic permeability, expanded in an elliptical form with length/width varying as the square root of the ratio of permeability along and at right angles to the fracture trend. This pressure drawdown is given by the equation:

$$P_i - P = \frac{-q\mu B}{4\pi\sqrt{k_X k_y}\, h\, 1.127} E_i \times \left[-\frac{\dfrac{(x-x_o)^2}{k_X} + \dfrac{(y-y_o)^2}{k_y}}{\dfrac{4t}{\phi\mu c}\, 6.32} \right] \qquad (7.70)$$

where:

$(x - x_o)$ = distance from producing well to pressure point in x direction, ft
$(y - y_o)$ = distance from producing well to pressure point in y direction, ft
P_i = initial pressure, psi
P = pressure at x and y at time t, psi
k_X = effective permeability in x direction, darcies
k_y = effective permeability in y direction, darcies
t = time, days
q = rate, stb/d
μ = viscosity, cp
c = total compressibility, psi^{-1}

Equation 7.70 is solved by trial and error, assuming effective compressibility of rock and fluids and permeabilities in the x and y directions, until a "good match" between calculated and measured pressure drop in the observation wells is obtained.

A good match usually can be obtained. However, a more precise match can be obtained by the least-squares method using the following sequence (Elkins and Skov):[27]

(1) x and y coordinates of all production and pressure observation wells are calculated.

(2) The coordinates are rotated to an assumed fracture orientation since the axis in Equation 7.70 corresponds to directions of maximum and minimum permeability.

(3) $\Sigma q_i E_i (-\_\_\_\_)$ is calculated for each pressure observation using assumed values of diffusivity in the new x and y directions, and the associated values of $\sqrt{k_x k_y}$ and P_i are determined by the least-square method.

(4) Modify the fracture orientation and diffusivities in the x and y directions successively until a set of these factors is obtained such that any further change increases the sum of squares of the difference between measured and calculated pressures of the individual observation wells.

The previous approach was used successfully by Elkins and Skov for delineating major fracture trends in the Spraberry field, Texas (Figures 7.52 and 7.53). Seventy complete sets of calculations involving 155 producing wells and fifty-five new wells were carried out. The results are presented in Figure 7.53 in the form of fracture orientation by area and by lease in the Driver area. Figure 7.54 shows the effects of changing magnitude of permeability ratio in the calculations.

(4) *Kazemi, Seth, and Thomas method.* Kazemi, Seth, and Thomas extended the Warren and Root model for pressure drawdown and buildup to interpret interference test results by numerical and analytical means.[28] This study determined interference drawdown in an observation well while an adjacent well was producing at a constant rate (Figure 7.55).

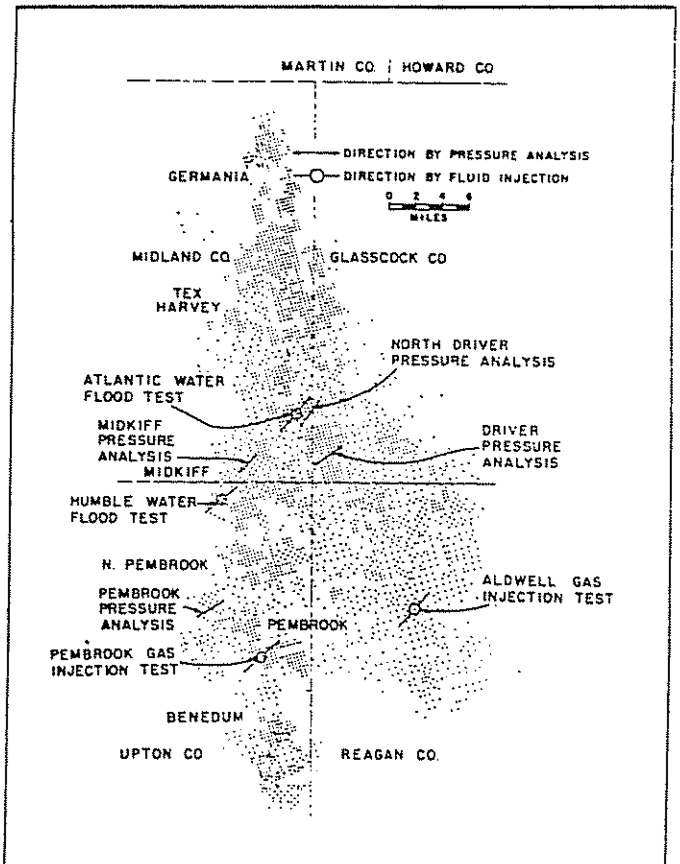

Figure 7.52 Fracture Orientation, Spraberry Trend (after Elkins and Skov)[27]

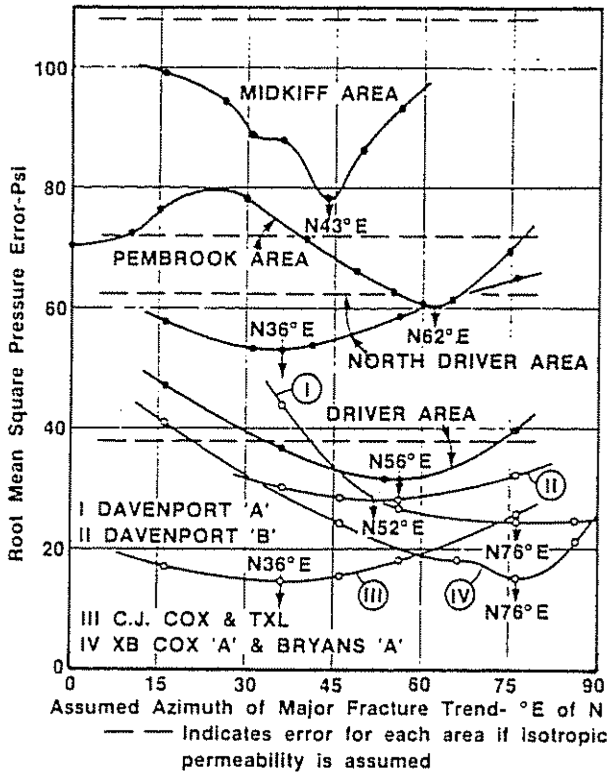

Figure 7.53 Fracture Orientation by Area and by Lease in the Driver Area (after Elkins and Skov)[27]

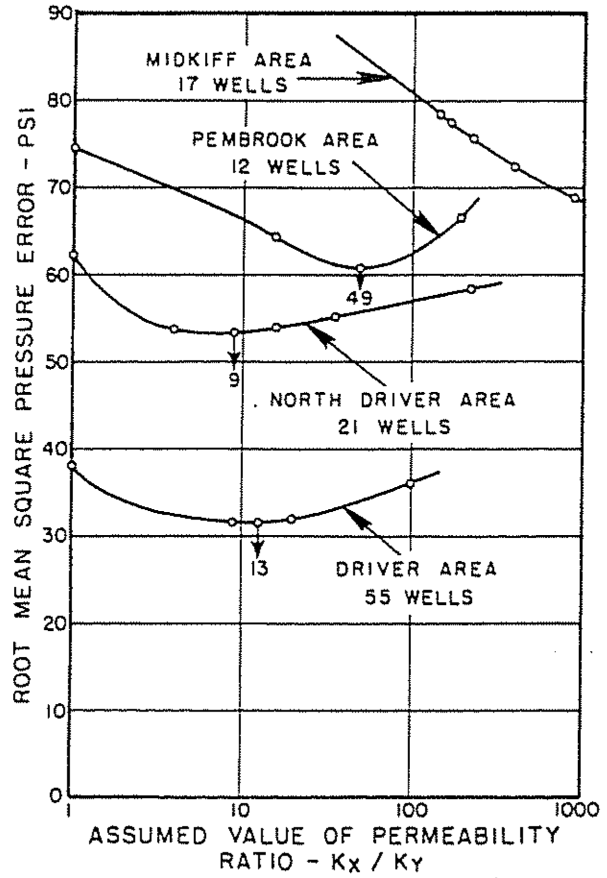

Figure 7.54 Effects of Changing Magnitude of Permeability Ratio– k_x/k_y (after Elkins and Skov)[27]

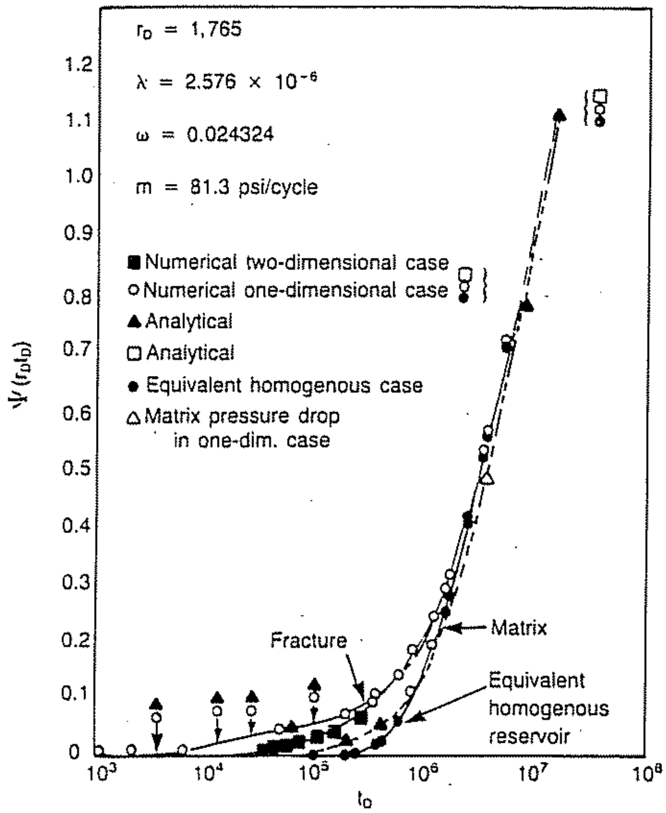

Figure 7.55 Comparison of Interference Drawdown for Five Mathematical Models Representing a Naturally Fractured Reservoir (after Kazemi, Seth, and Thomas)[25]

The curves indicate that the Warren and Root one-dimensional model gives an interference drawdown:

$$\Psi(r_D, t_D) = P_D(r_D, t_D) = \text{Dimensionless pressure}$$

$$= (P_i - P) \Big/ \left(\frac{141.2\, q\mu B}{kh}\right) \quad (7.71)$$

which is reasonably close to that obtained from a more realistic two-dimensional vertical model.

Figure 7.55 further shows that an equivalent homogeneous model of the same radial dimension with a volumetrically weighted average porosity and a permeability that is equal to the total flow capacity (kh_t) divided by the thickness of the formation fails to approximate the correct answers for early times. For instance, for a typical value of t_D for interference tests ($t_D = 4 \times 10^5$), the Warren and Root model gives an interference drawdown $\Psi = 0.111$, and the equivalent homogeneous model gives $\Psi = 0.026$. The pressure drop is calculated from the equation:

$$\Delta P = 0.87\, m\Psi \quad (7.72)$$

Consequently, for an m of 81.3 psi/cycle, the pressure drop predicted by the Warren and Root model is 8 psi as compared with 2 psi predicted by the equivalent homogeneous model. The difference is too large and indicates that the equivalent homogeneous model is not adequate for early analysis.

Figure 7.55 shows that at larger times all solutions converge to the same value. Consequently, interference tests with late pressure responses can be analyzed using the familiar point-source solution as applied to an equivalent homogeneous model.

(5) *Type curves.* Type curves are valuable tools for analyzing anisotropic formations, including fractured reservoirs containing parallel vertical fractures.[29] The permeability perpendicular to the fracture planes represents essentially the matrix permeability. The permeability in the fracture direction would be higher than the matrix permeability. The idea behind this approach is essentially the same one presented by Elkins and Skov.[27]

The pressure (x, y, t) caused by a line-source well at origin is represented by (Papadopulus):[30]

$$\sqrt{k_{xx}k_{yy}-k_{xy}^2}\,\frac{h(P_i-P_{x,y,t})}{141.2qB\mu} = -\tfrac{1}{2}Ei\left[\frac{-\phi\mu c}{0.00105t}\left(\frac{k_{xx}y^2+k_{yy}x^2-2k_{xy}xy}{k_{xx}k_{yy}-k_{xy}^2}\right)\right] \quad (7.73)$$

$$k_{XX} = \tfrac{1}{2}\,\{(k_{xx}+k_{yy})+[(k_{xx}-k_{yy})^2+4k_{xy}^2]^{1/2}\} \quad (7.74)$$

$$k_{YY} = \tfrac{1}{2}\,\{(k_{xx}+k_{yy})-[(k_{xx}-k_{yy})^2+4k_{xy}^2]^{1/2}\} \quad (7.75)$$

$$\theta = \arctan\left(\frac{k_{XX}-k_{xx}}{k_{xy}}\right) \quad (7.76)$$

where:

k_{XX} = maximum principal permeability, md
k_{xx}, k_{yy}, k_{xy} = components of the permeability tensor, md
k_{YY} = minimum principal permeability, md
θ = angle between x and X axis, positive in counterclockwise direction from x axis

The use of type curves for pressure interference in anisotropic formations will be illustrated with one example from a watered-out formation (Ramey).

EXAMPLE #12

Given data:

Figure 7.56 shows a net isopach map and well pattern used in the test. Figure 7.57 shows the well pattern, well designation, and well coordinates using an injector well as origin. An injection test rather than a production test was selected because of the low production characteristics of the well. The well pattern was a nine spot. Table 7.1 shows the interference test data. The solution is presented only for wells 5-E, 1-E, and 1-D, which form the northeast part of the pattern.

Figure 7.58 shows the water-injection interference data in log-log coordinates. Figure 7.59 represents the analytical solution for the conventional line source solution represented by the equation shown in the figure. Figure 7.59 is also a solution to Equation 7.73, where the dimensionless quantities are defined as follows:

$$P_D = \frac{\sqrt{k_{xx}k_{yy}-k_{xy}^2}}{141.2qB\mu}\,h(P_i-P_{x,y,t}) \quad (7.77)$$

$$\frac{t_D}{r_D^2} = \left(\frac{0.000264t}{\phi\mu c}\right)\left(\frac{k_{xx}k_{yy}-k_{xy}^2}{k_{xx}y^2+k_{yy}x^2-2k_{xy}xy}\right) \quad (7.78)$$

The log-log crossplot of Figure 7.58 shows that the ΔP for well 5-E is consistently lower than that for well 1-D.

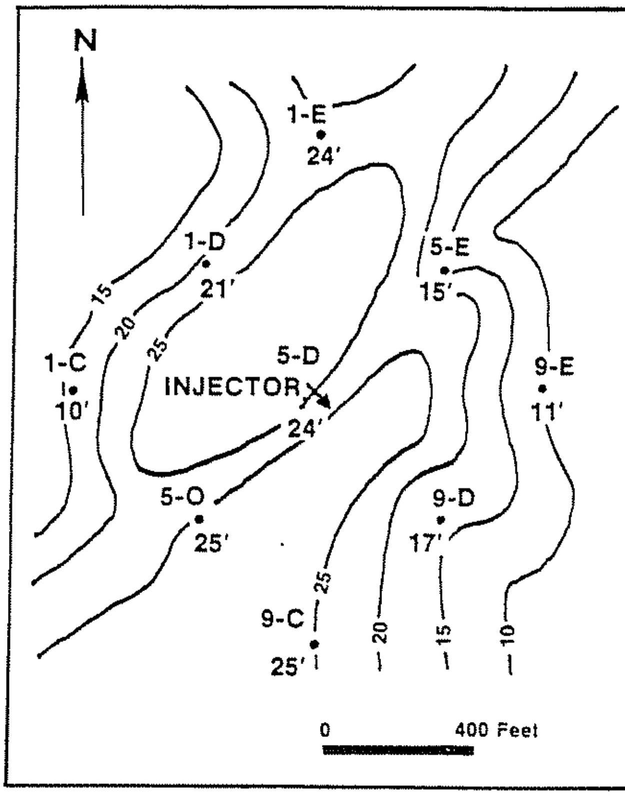

Figure 7.56 Net Sand Isopach (after Ramey)[29]

Figure 7.60 shows a type curve match for the three wells. Notice, however, that the time scales have been displaced to correlate with well 1-E data. The vertical lines in the figure indicate 100-hr time for each well. Notice that, in this procedure, the pressures are aligned at the same scale, and the time scale is adjusted until the observation data match. From Figure 7.60, $\Delta P = 10$ psi at $P_D = 0.26$ for all three wells. At 100 hr, the t_D/r_D^2 values are read from Figure 7.60 to be:

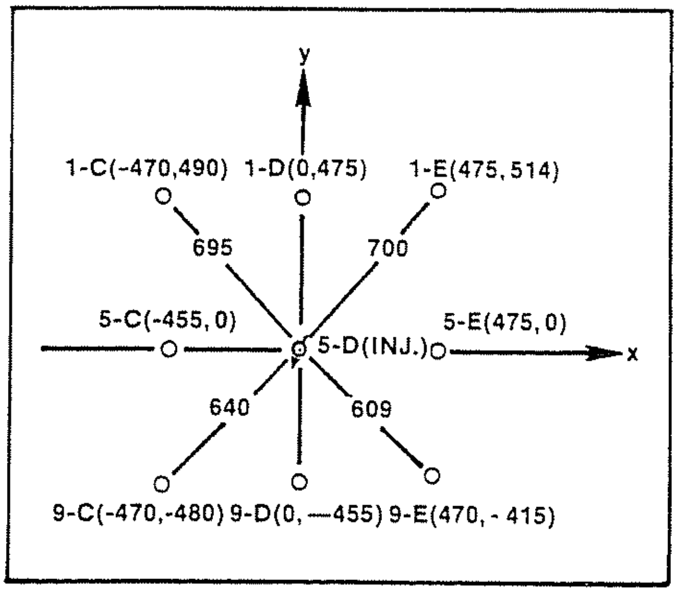

Figure 7.57 Field Example Well Pattern (Distances and Coordinates in Feet) (after Ramey)[29]

TABLE 7.1
FIELD EXAMPLE INTERFERENCE TEST DATA (AFTER RAMEY)[25]

$i_w = 115$ stb/d	$c_i = 3.7 \times 10^{-6}$
$h = 25$ ft	$c_o = 7.5 \times 10^{-6}$
$B_w = 1$ reservoir bbl/stb	oil gravity 36° API at 60°F
$\mu_w = 1$ cp	formation temperature = 72°F
$\phi = 20\%$	initial pressure = 240 psi
$c = 8 \times 10^{6}$ psi^{-1}	$r_w = 0.563$ ft mean; open hole shot with nitro
$c_w = 3.3 \times 10^{-6}$	

Injection well data: total depth 1,011 ft; completed with 2-in. EUE tubing, bottom-hole packer
Pressure data (ΔP is pressure rise above initial pressure)

Well 1-C		Well 1-D		Well 1-E		Well 5-C	
t, hr	ΔP, psi	t, hr	ΔP, psi	t, hr	ΔP, psi	t, hr	ΔP, psi
		23.5	6.7	27.5	3	47	10
		28.5	7.2	47	5	71	17.2
		51	15	72	11	94	24
		77	20	95	13	113	25.1
		95	25	115	16	124	26
		119	24	125	16	146	24
113	22	125	23.2	142	13	192	17
125	22	141	19	192	10	210	15
146	19	163	18	215	10	240	15.2
195	16	188	14	240	6	260	14
215	14	215	12	295	5.8	285	13
249	14	265	10				
295	11	290	10				

Well 5-E		Well 9-C		Well 9-D		Well 9-E	
t, hr	ΔP, psi	t, hr	ΔP, psi	t, hr	ΔP, psi	t, hr	ΔP, psi
21	4	24	4	23.5	8.2	21	3
47	11	47	8	28.5	9.3	47	3
72	16.3	72	13	51	17	71	3
94	21.2	94	17.7	75	23.2	94	10
115	22	115	18	95	27.2	115	12.5
122	25	126	18	120	27	125	13
140	22.3	145	17	143	21	143	12.8
188	19.2	194	11	190	16	195	13
210	18	215	13	215	14	215	13
285	15	245	11	270	13	240	10
		295	10	285	12	295	10

Well	t_D/r_D^2	(ft)
I-E	0.70	700
5-E	1.10	475
I-D	1.40	475

Equation 7.77 is used to calculate:

$$P_D = \frac{\sqrt{k_{xx}k_{yy} - k_{xy}^2}\,(25)(10)}{141.2(115)(1)(1)} = 0.26$$

$$k_{xx}k_{yy} - k_{xy}^2 = 285.3 \text{ md}^2$$

Equation 7.78 is used to write three more equations as follows:

well 5-E (x = 475 ft, y = 0)

$$1.10 = \frac{(0.000264)(100)(285.3)}{\phi\mu c\, k_{yy}\, 475^2} \tag{7.79}$$

well 1-E (x = 475 ft, y = 514 ft)

$$0.70 = \frac{(0.000264)(100)(258.3)}{\phi\mu c\,[(k_{xx})(514)^2 + (k_{yy})(475)^2 - (2k_{xy})(475)(514)]} \tag{7.80}$$

well 1-D (x = 0, y = 475 ft)

$$1.40 = \frac{(0.000264)(100)(285.3)}{\phi\mu c\, k_{xx}\, 475^2} \tag{7.81}$$

Solving simultaneously we obtain:

$$k_{xx} = 15.2 \text{ md}$$
$$k_{yy} = 19.4 \text{ md}$$
$$k_{xy} = 3.12 \text{ md}$$
$$\phi\mu c = 1.57 \times 10^{-6} \text{ cp/psi}$$

The value of $\phi\mu c$ can calculate c from known $\phi = 0.20$ and $\mu = 1$ cp. In this case, the compressibility c is 7.85×10^{-6} psi^{-1}, which compares well with the value $c = 8 \times 10^{-6}$ psi^{-1} presented in the Table 7.1.

With the previous information, it is possible to calculate the principal permeabilities and their orientations with the use of Equations 7.74 to 7.76 as follows:

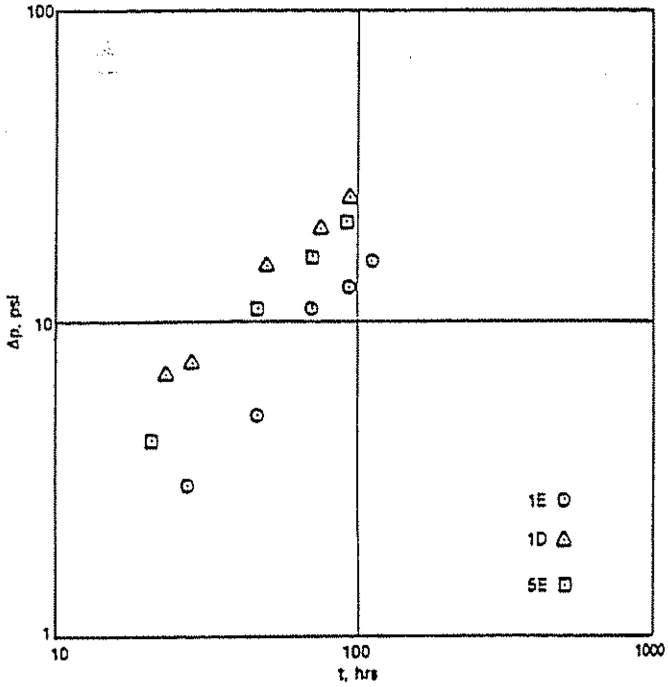

Figure 7.58 Water Injection Interference Data (after Ramey)[29]

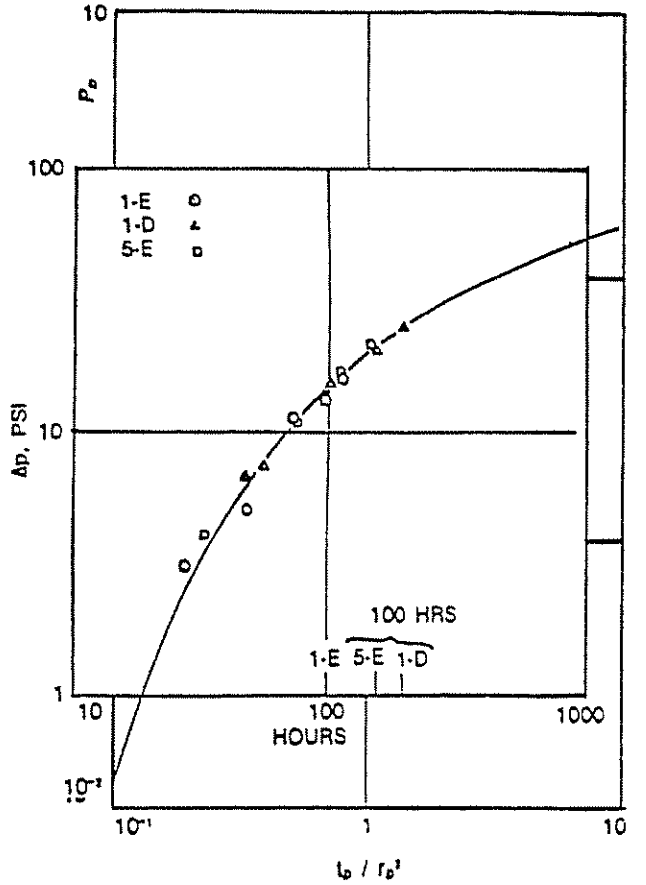

Figure 7.60 Type Curve Match for Anisotropic-Case Water Injection (after Ramey)[29]

$$k_{XX} = \tfrac{1}{2}\{15.2 + 19.4 + [(15.2 - 19.4)^2 + 4(3.12)^2]^{1/2}\}$$
$$= 21.1 \text{ md}$$
$$k_{YY} = \tfrac{1}{2}\{15.2 + 19.4 - [(15.2 - 19.4)^2 + 4(3.12)^2]^{1/2}\}$$
$$= 13.5 \text{ md}$$
$$\theta = \arctan\left(\frac{21.1 - 15.2}{3.12}\right) = \arctan 1.89$$
$$\theta = 62.1$$

Figure 7.57 shows that the X axis was chosen as a line passing through wells 5-C, 5-D, and 5-E. Figure 7.56 shows that true north is in the direction from well 5-D to 1-E. The angle subtended by wells 1-E, 5-D, 5-E is equal to $\sin^{-1}(514/700) = 47.2°$, as shown in Figure 7.61. Consequently, the major permeability axis lies in the direction N14.8°W.

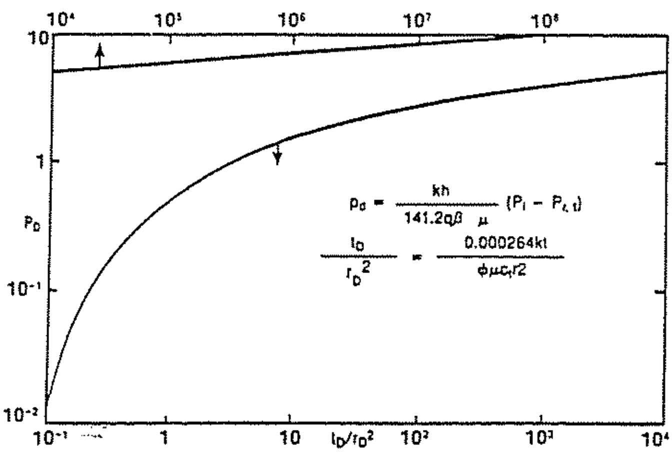

Figure 7.59 Continuous Line-Source Solution Type Curve

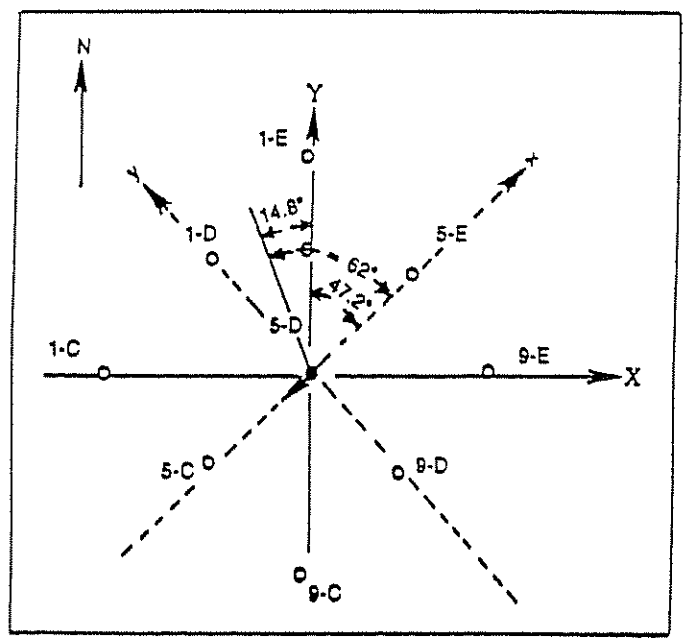

Figure 7.61 Evaluation of Angle With Respect to North

REFERENCES

1. Chaney, P. et al. "How to Perforate Your Well to Prevent Water and Gas Coning." *Oil and Gas Journal* (May 7, 1956), p. 108–114.
2. Muskat, M. *The Flow of Homogeneous Fluids Through Porous Media.* Boston, Massachusetts: International Human Resources Development Corporation, 1982.
3. Muskat, M. *Physical Principles of Oil Production.* Boston, Massachusetts: International Human Resources Development Corporation, 1982.
4. Arthur, M. G. "Fingering and Coning of Water and Gas in Homogeneous Oil Sands." *Transactions of the AIME* (1944–45), p. 183–199.
5. Meyer, H. L., and A. O. Gardner. "Mechanics of Two Immiscible Fluids in Porous Media." *Journal of Applied Physics,* v. 25, n. 11, p. 1400ff.
6. Pirson, S. J. *Oil Reservoir Engineering.* Huntington, New York: Robert E. Krieger Publishing Company, 1977.
7. Craft, B. C. and M. F. Hawkins. *Applied Petroleum Reservoir Engineering.* Englewood Cliffs, New Jersey: Prentice-Hall Inc., 1959.
8. Chierici et al. "A Systematic Study of Gas and Water Coning by Potentiometric Models." *Journal of Petroleum Technology* (August 1964), p. 923–929.
9. Sobocinski, D. P. and A. J. Cornelius. "A Correlation for Predicting Water Coning Time." *Journal of Petroleum Technology* (May 1965), p. 594–600.
10. Birks, J. "Coning Theory and Its Use in Predicting Allowable Producing Rates of Wells in a Fissured Limestone Reservoir." *Iranian Petroleum Institute Bulletin,* n. 12 and 13 (December 1970), p. 470–480.
11. Baker, W. J. "Flow in Fissured Formations." In *Proceedings of the 4th World Petroleum Congress—Section II/E.* Vol. 2, 1954, p. 379–393.
12. MacDonald, R. C. and K. H. Coats. "Methods for Numerical Simulation of Water and Gas Coning." *Transactions of the AIME,* v. 249 (1970).
13. Blair, P. M. and C. F. Weinaug. "Solution of Two-Phase Flow Problems Using Implicit-Difference Equations." *SPE Journal* (1969), p. 417–424.
14. Spivak, A. and K. H. Coats. "Simulation Techniques for Two- and Three-Phase Coning Studies." *SPE Journal* (September 1970), p. 257–267.
15. Letkeman, J. P. and R. L. Ridings. "A Numerical Coning Model." *SPE 2812.* February 5, 6, 1970, SPE of AIME.
16. van Poollen, H. K., H. C. Bixel, and J. R. Jargon. "Reservoir Modeling." *Oil and Gas Journal,* reprint (1969, 1970, 1971), p. 42.
17. Soengkowo, I. "Model Studies of Water Coning in Petroleum Reservoirs with Natural Water Drives." Ph.D. Thesis, University of Texas at Austin, May 1969.
18. El Banbi, H. A. "Carbonate Field Developed to Recover 37% Primary Oil." *World Oil* (October 1974), p. 139–141.
19. Mazzocchi, E. F. and K. M. Carter. "Pilot Application of a Blocking Agent—Weyburn Unit, Saskatchewan." *Journal of Petroleum Technology* (September 1974), p. 973–978.
20. Karp, J. C., D. K. Lowe, and N. Marusov. "Horizontal Barriers for Controlling Water Coning." *Transactions of the AIME,* v. 225 (1962), p. 784.
21. van Meurs, P. and C. van der Poel. *"A Theoretical Description of Water Drive Process Involving Viscous Fingering."* SPE Reprint Series No. 2A. 1973 Revision. p. 226–235.
22. Land N. Personal communication with Charles R. Smith.
23. Smith, C. R. *Mechanics of Secondary Oil Recovery.* New York, New York: Reinhold Publishing Corporation, 1960.
24. Flagg, A. H. et al. *"Radioactive Tracers in Oil Production Problems.* SPE Reprint Series No. 2A.
25. Mardock, E. S. and J. W. Watson. "Use of Radioactive Iodine as a Tracer in Waterflood Operations." *Transactions of the AIME,* v. 201 (1954), p. 209.
26. Alberts, A. A. et al. "Application of Radioisotopes to Subsurface Surveys." *SPE 398-G.* San Antonio, Texas, October 17–20, 1954, SPE of AIME.
27. Elkins, L. F. and A. M. Skov. "Determination of Fracture Orientation from Pressure Interference." *Transactions of the AIME,* v. 219 (1960), p. 301–304.
28. Kazemi, H., M. S. Seth, and G. W. Thomas. "The Interpretation of Interference Tests in Naturally Fractured Reservoirs with Uniform Fracture Distribution. *SPE Journal* (December 1969), p. 463–472.
29. Ramey, H. J. "Interference Analysis for Anisotropic Formations—A Case History." *Journal of Petroleum Technology* (October 1975), p. 1290–1298.
30. Papadopulus, I. S. "Nonsteady Flow to a Well in an Infinite Anisotropic Aquifer." In *Symposium of the International Association of Science Hydrology,* Dubrovinik, Yugoslavia, 1965.
31. Aguilera, Roberto. *Naturally Fractured Reservoirs.* Tulsa, Oklahoma: PennWell Publishing Co., 1980, p. 306.

Appendix 2.1
Working graphs

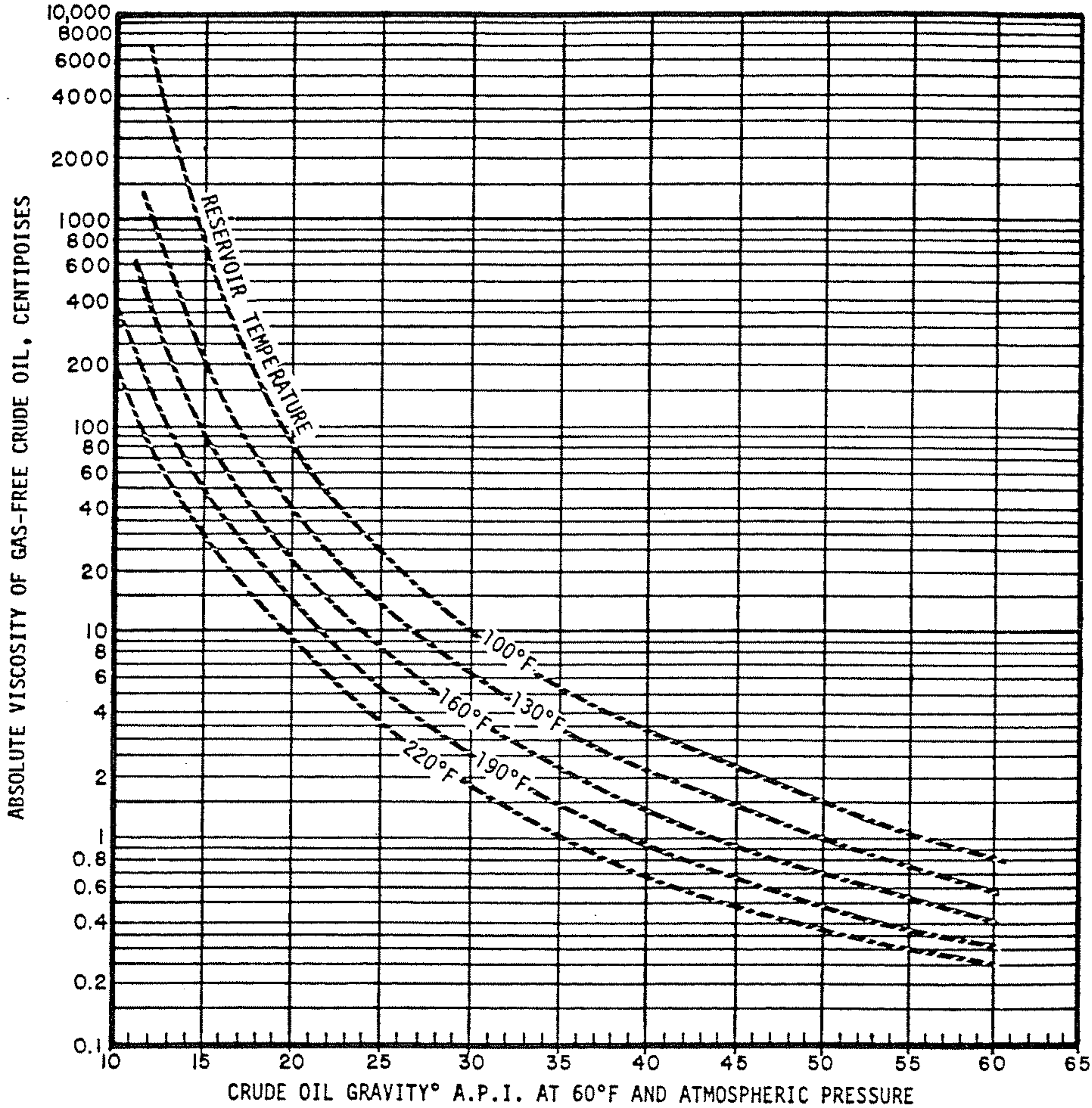

Figure 2.1(1) Viscosity of Gas-free Crude Oil

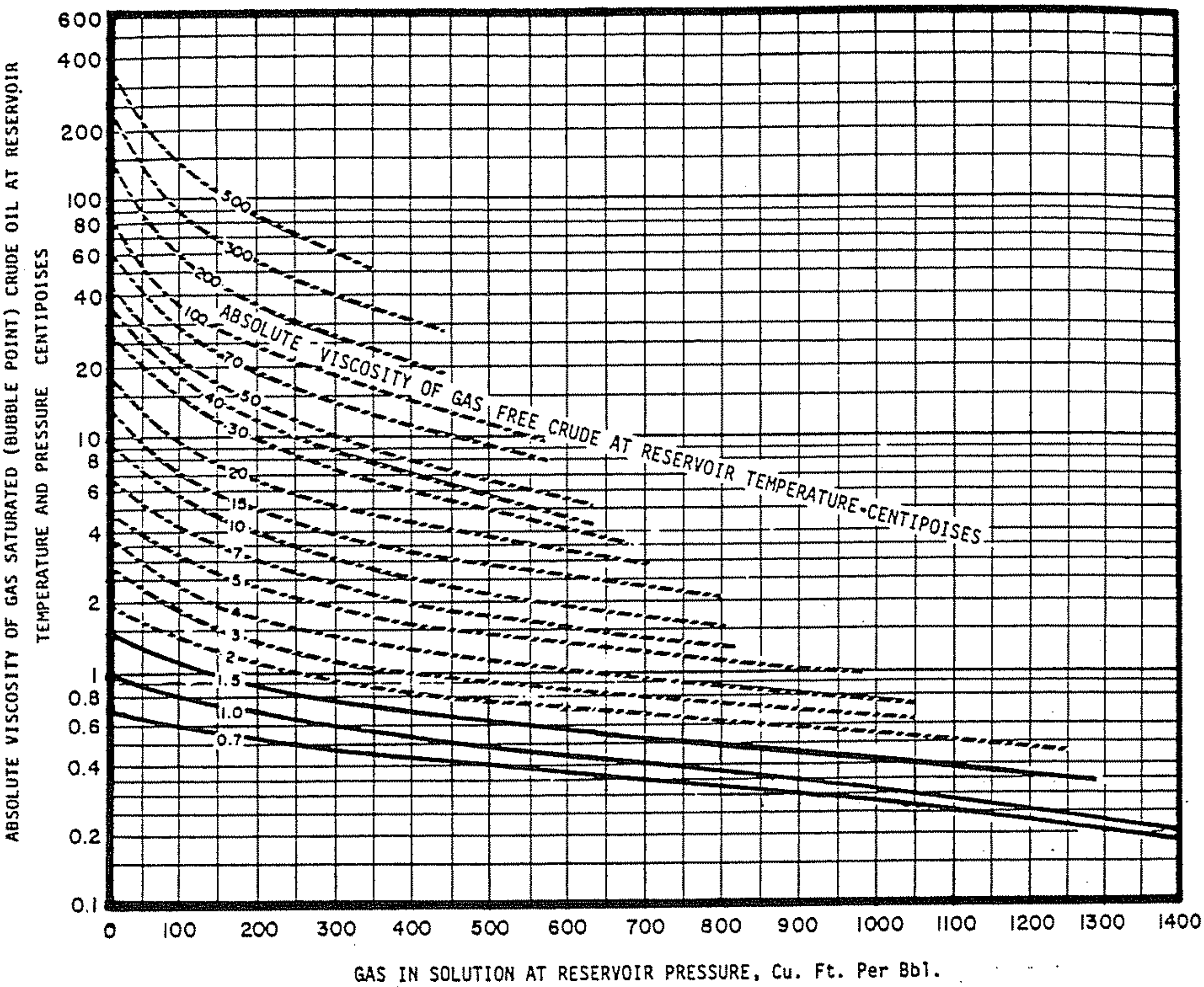

Figure 2.1(2) Viscosity of Gas-saturated Oil

EXAMPLE

REQUIRED:
Bubble point pressure at 200°F of a liquid having a gas-oil ratio of 350 CFB, a gas gravity of 0.75, and a tank oil gravity of 30°API.

PROCEDURE:
Starting at the left side of the chart, proceed horizontally along the 350 CFB line to a gas gravity of 0.75. From this point drop vertically to the 30°API line. Proceed horizontally from the tank oil gravity scale to the 200°F line. The required pressure is found to be 1930 PSIA.

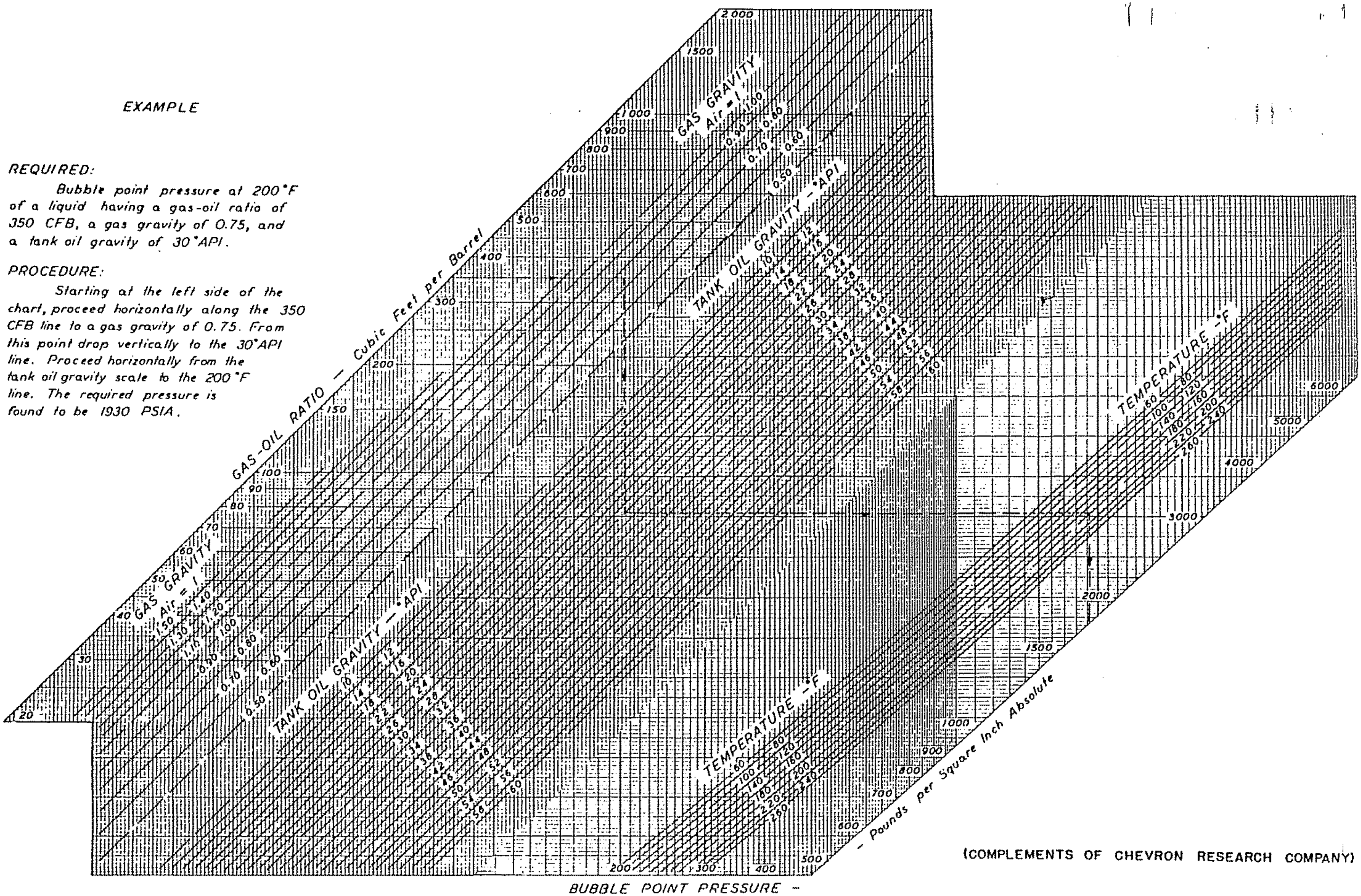

Figure 2.1(3) Properties of natural hydrocarbon mixtures of gas and liquid bubble point pressure

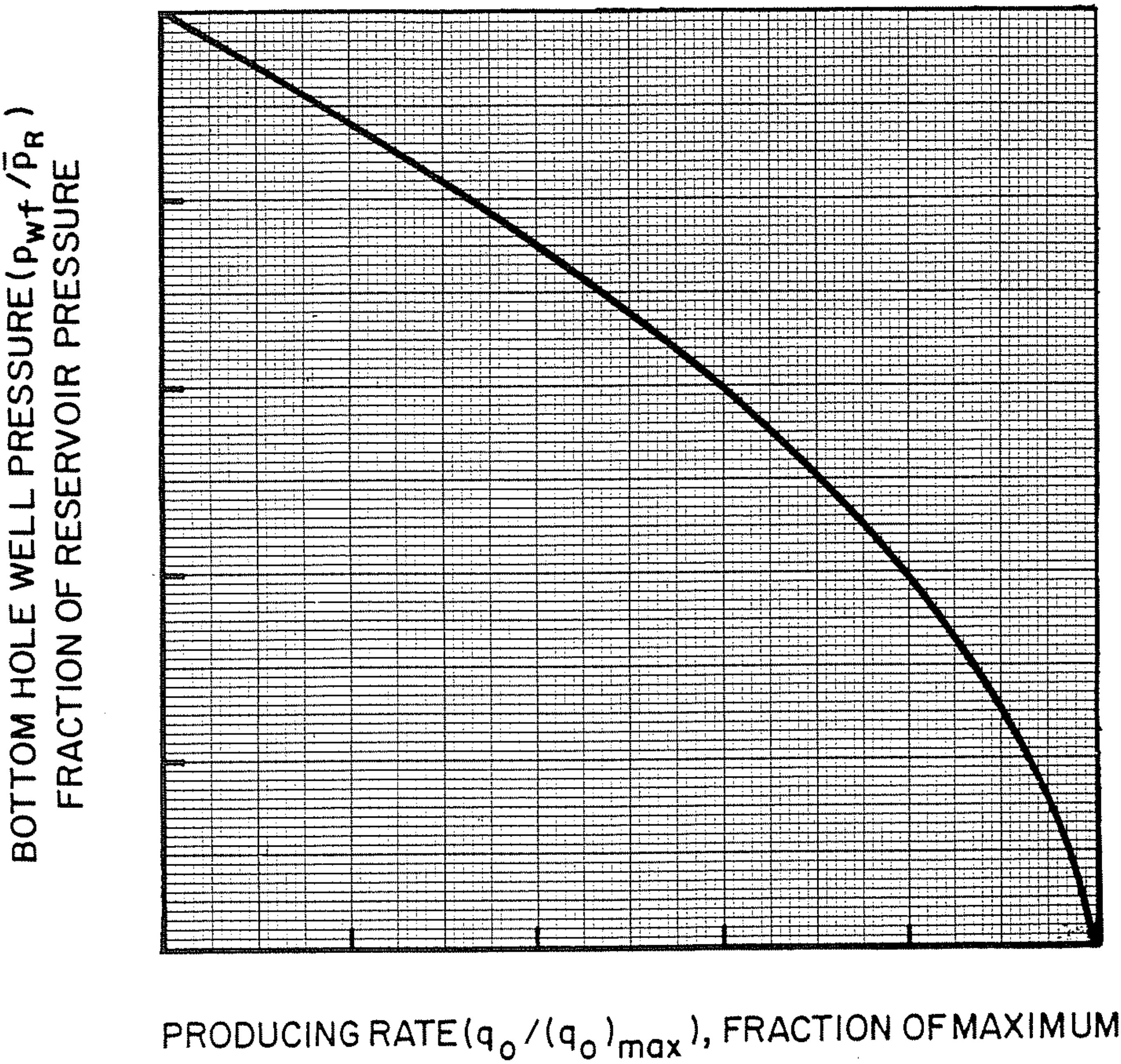

Figure 2.1(5) Inflow Performance Relationship for Solution-Gas Drive Reservoirs (after Vogel)[8]

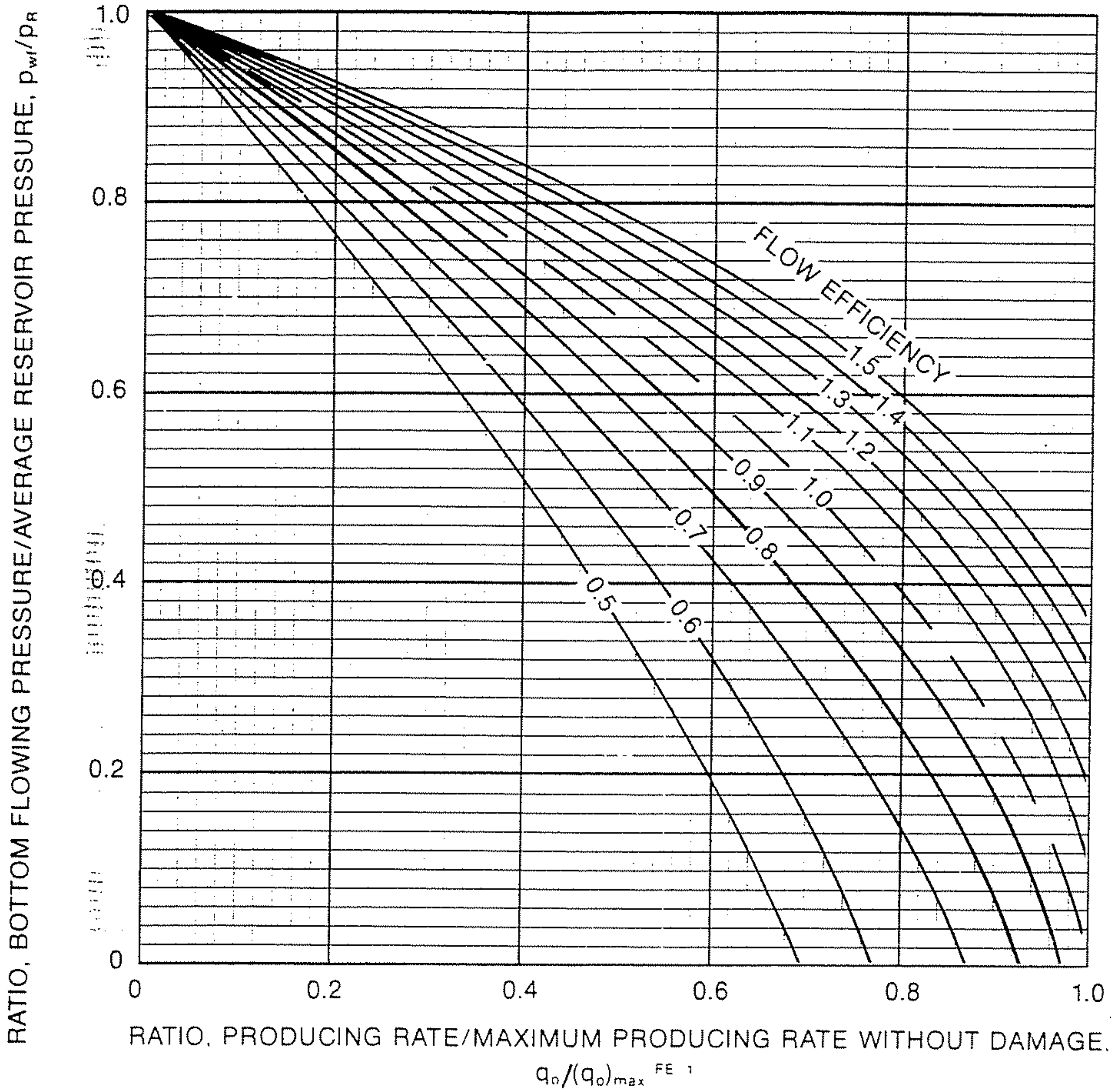

Figure 2.1(6) Standing's Correlation for Wells with FE Values not Equal to 1

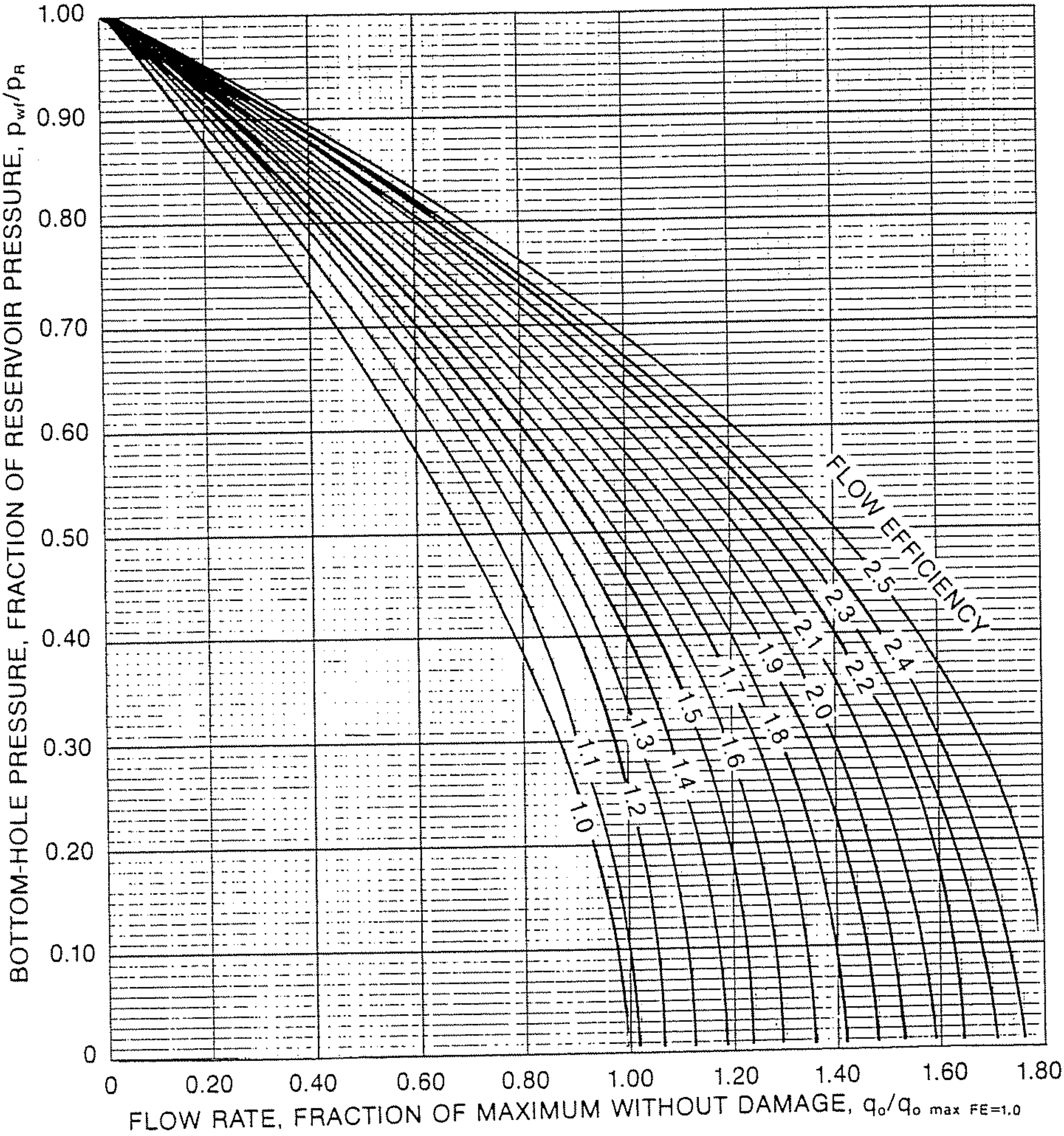

Figure 2.1(7) Harrison's Extension of Standing's Work to Include Other FE Values

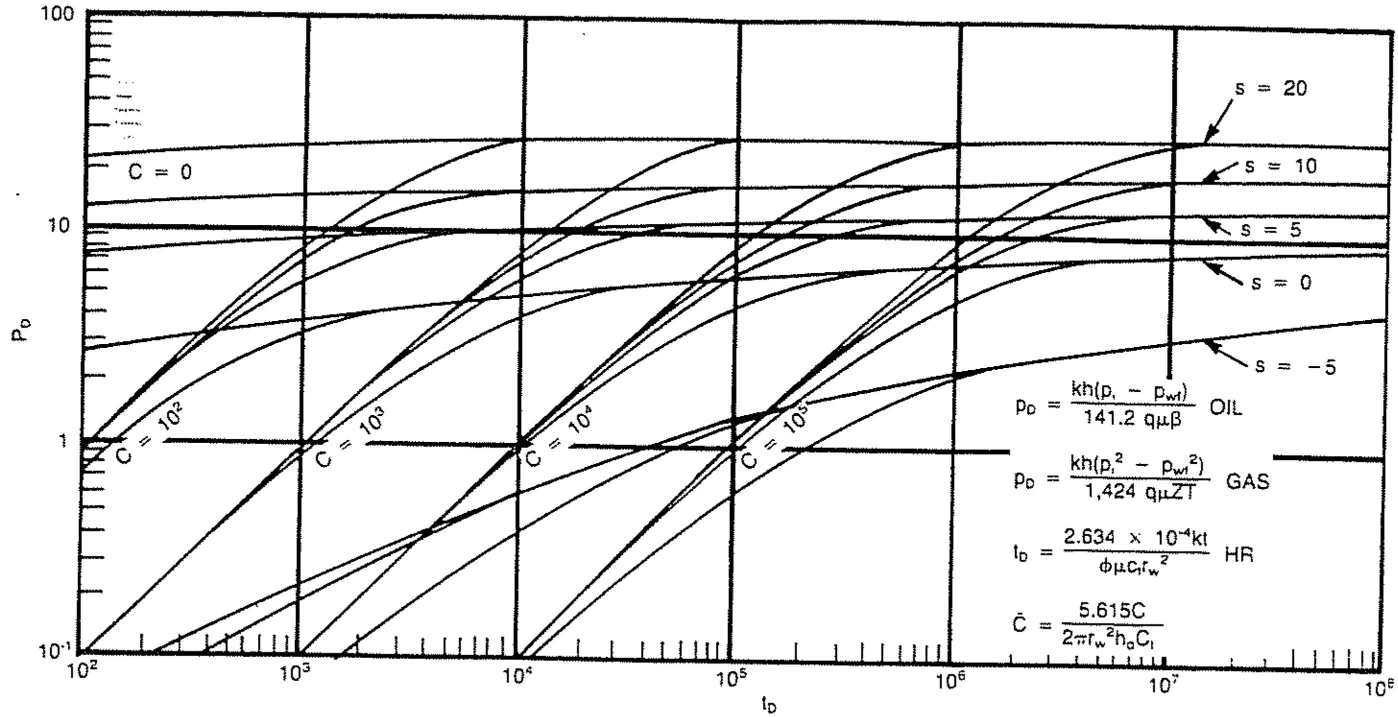

Figure 2.1(8) P_D vs t_D for Well with Storage and Skin Effect (after Agarwal, Al-Hussainy, and Ramey)[35]

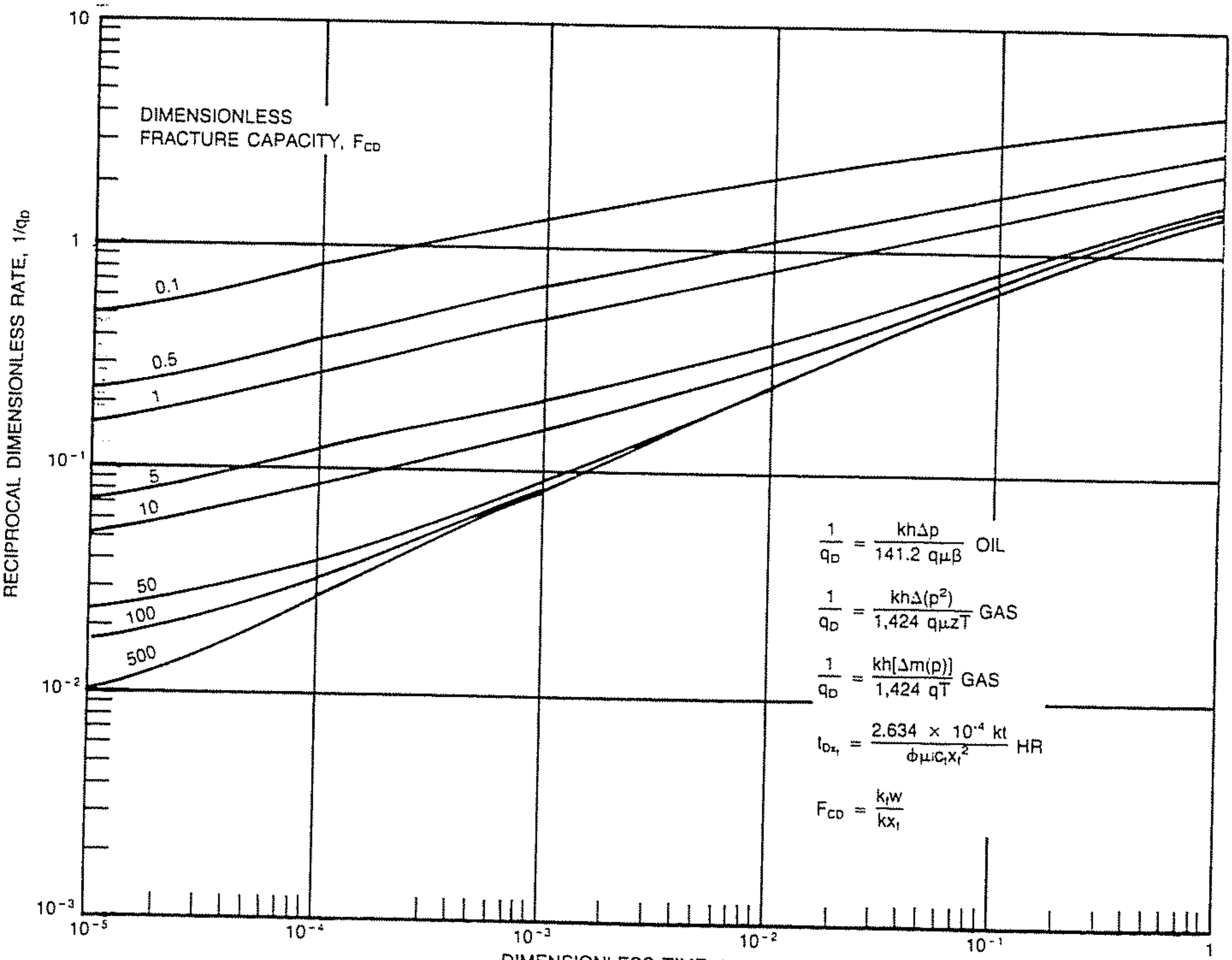

Figure 2.1(9) Log-Log Type Curves for Finite Capacity Vertical Fractures (Constant Wellbore Pressure) (after Agarwal, Carter, and Pollock)[36]

Appendix 4.1
Horizontal flowing pressure gradients

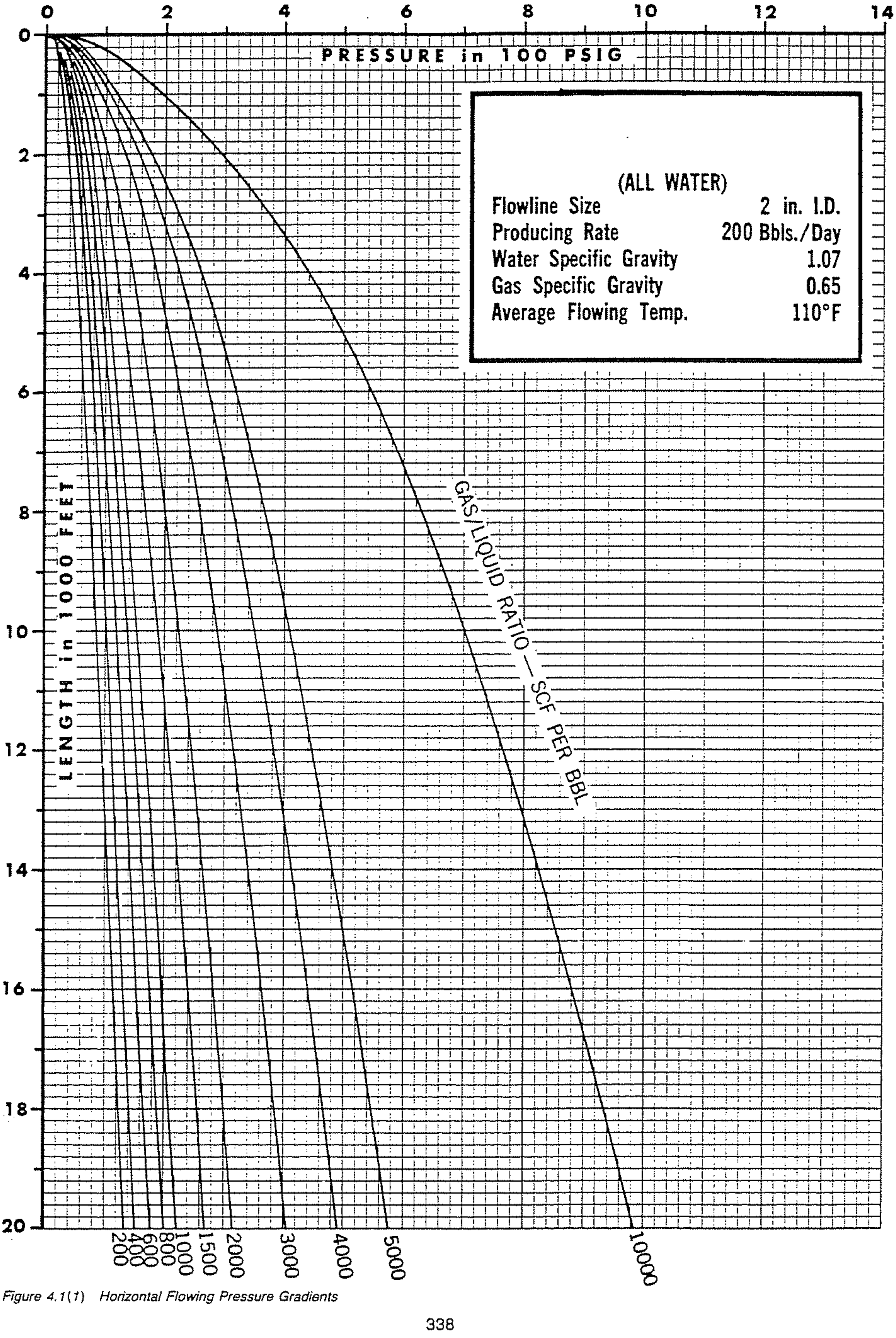

Figure 4.1(1) Horizontal Flowing Pressure Gradients

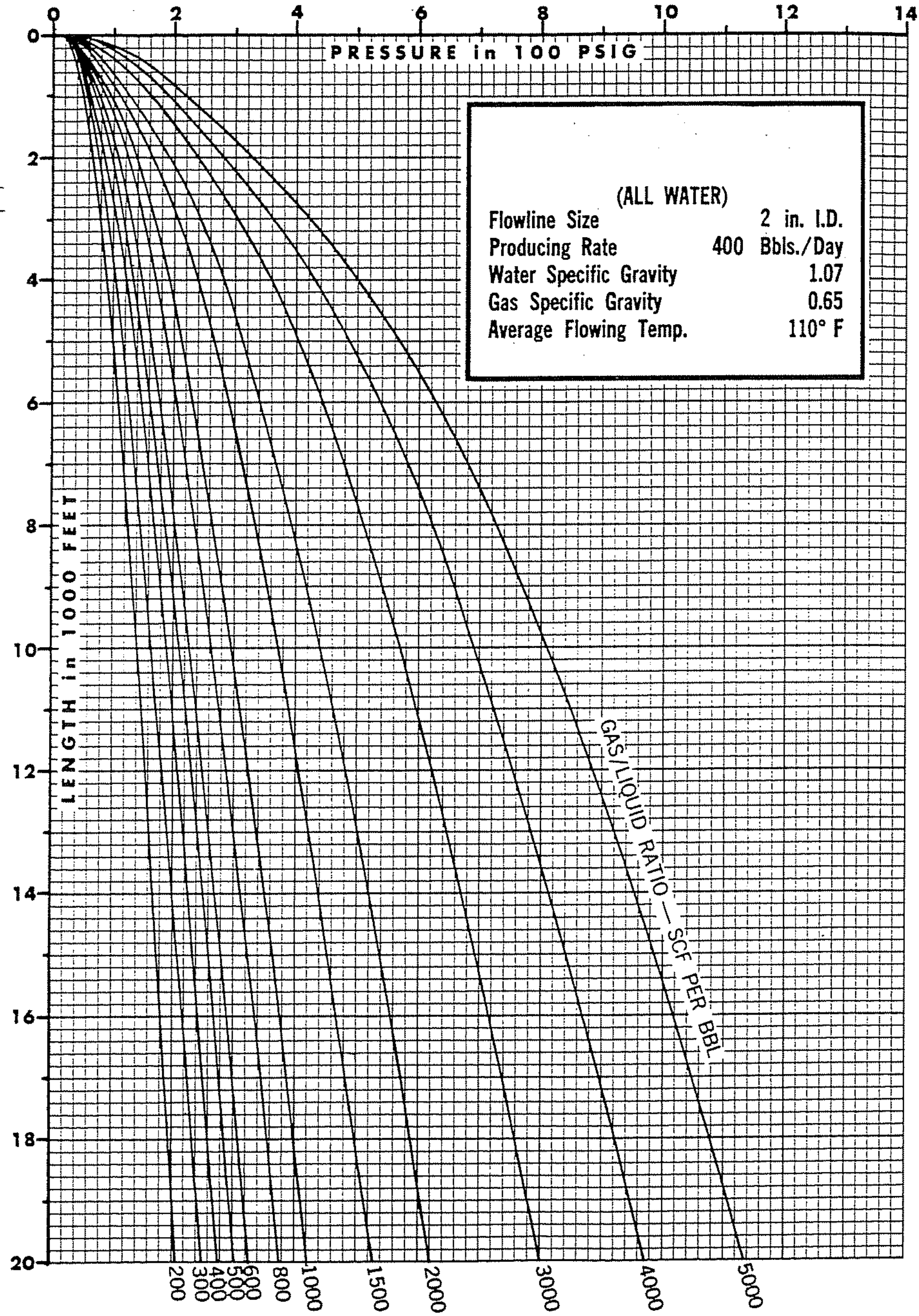

Figure 4.1(2) Horizontal Flowing Pressure Gradients

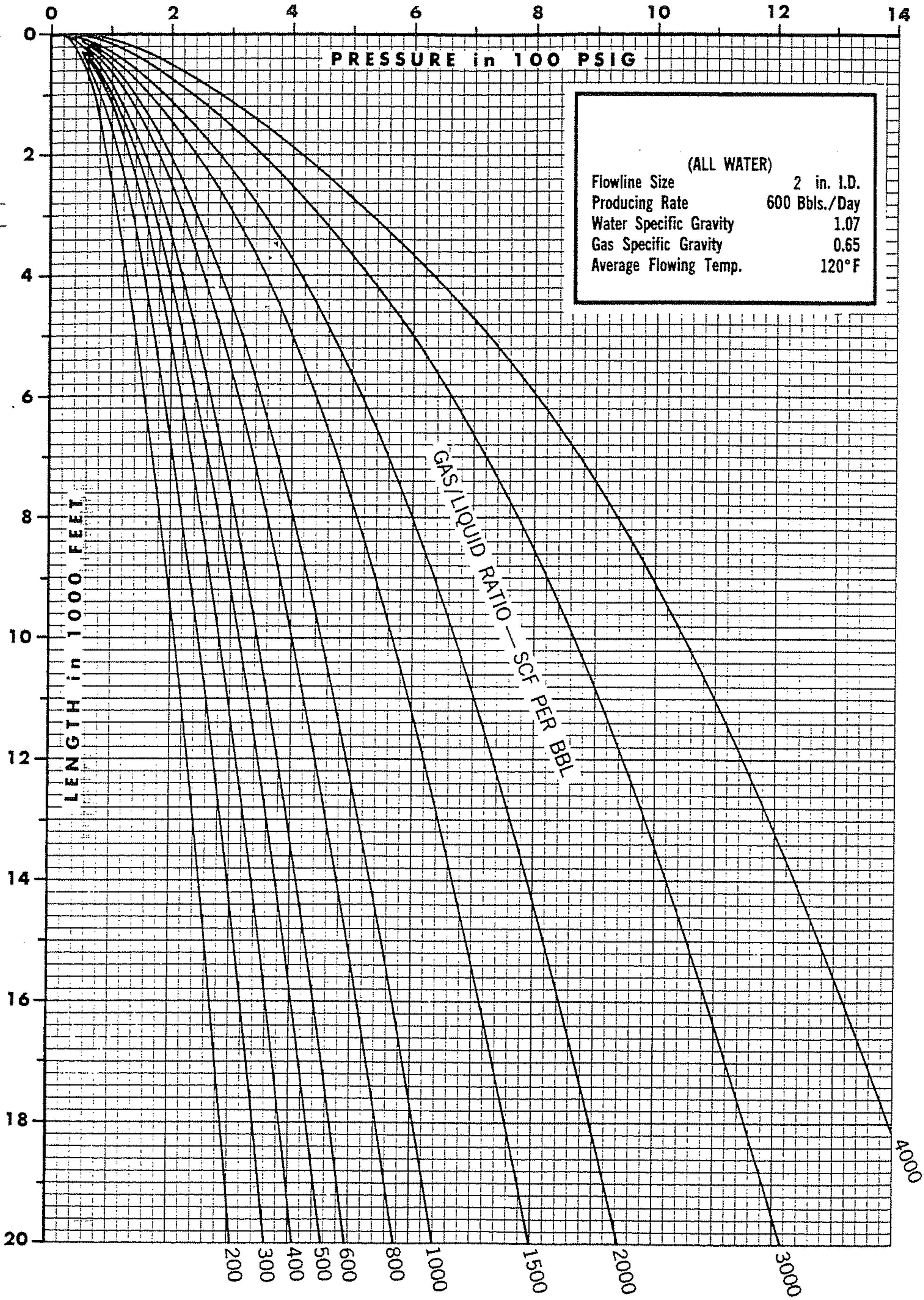

Figure 4.1(3) Horizontal Flowing Pressure Gradients

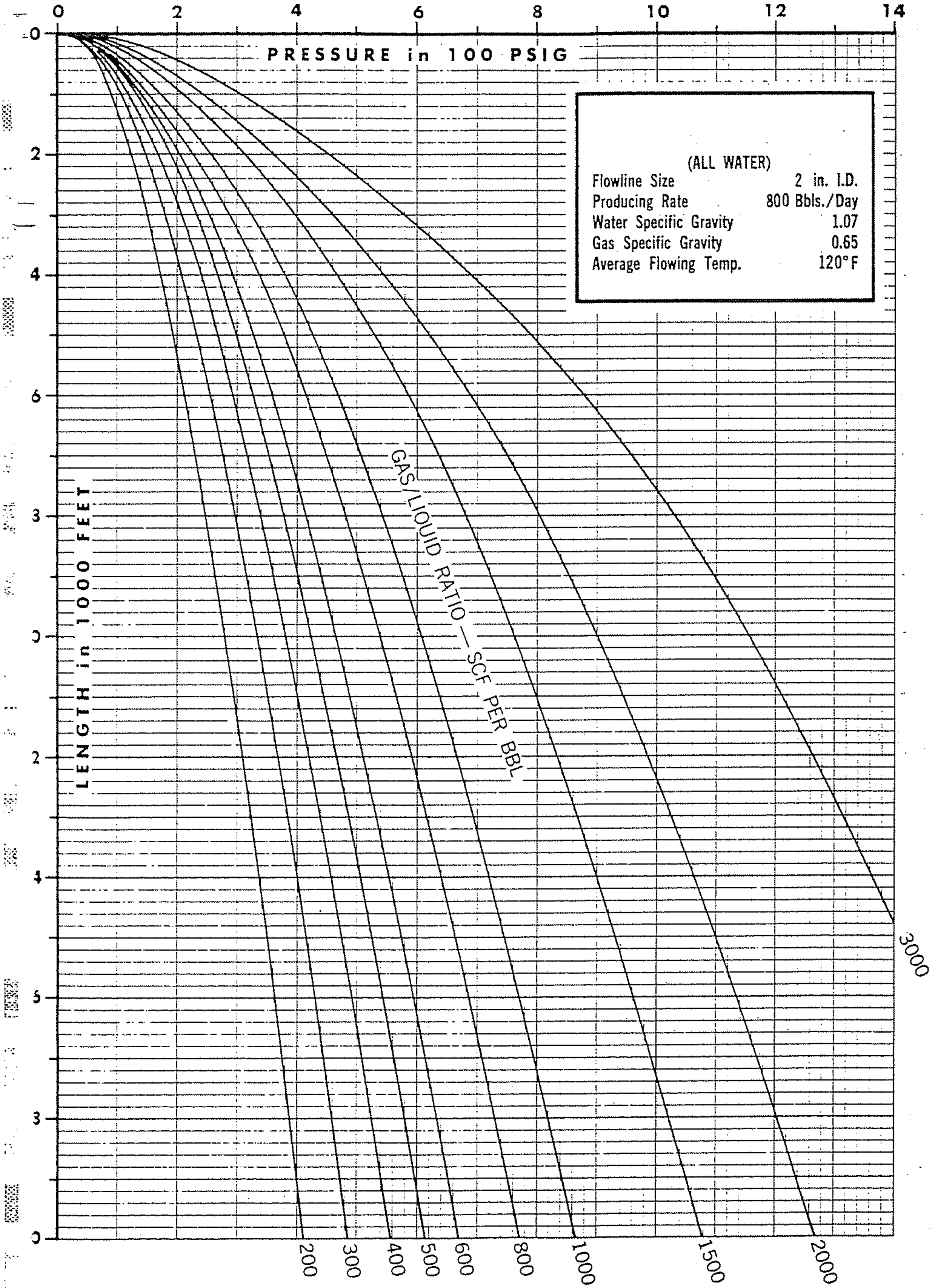

Figure 4.1(4) Horizontal Flowing Pressure Gradients

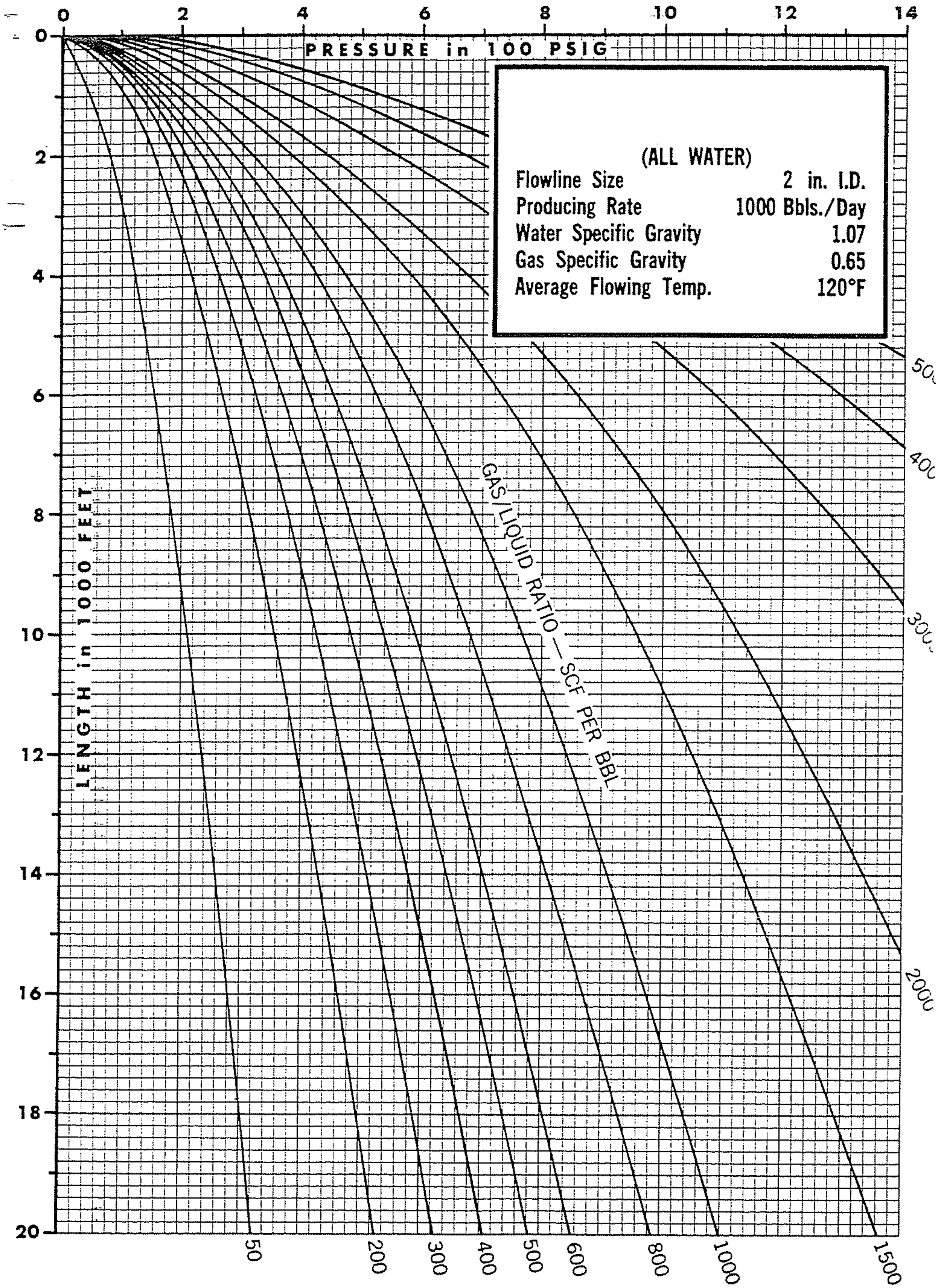

Figure 4.1(5) Horizontal Flowing Pressure Gradients

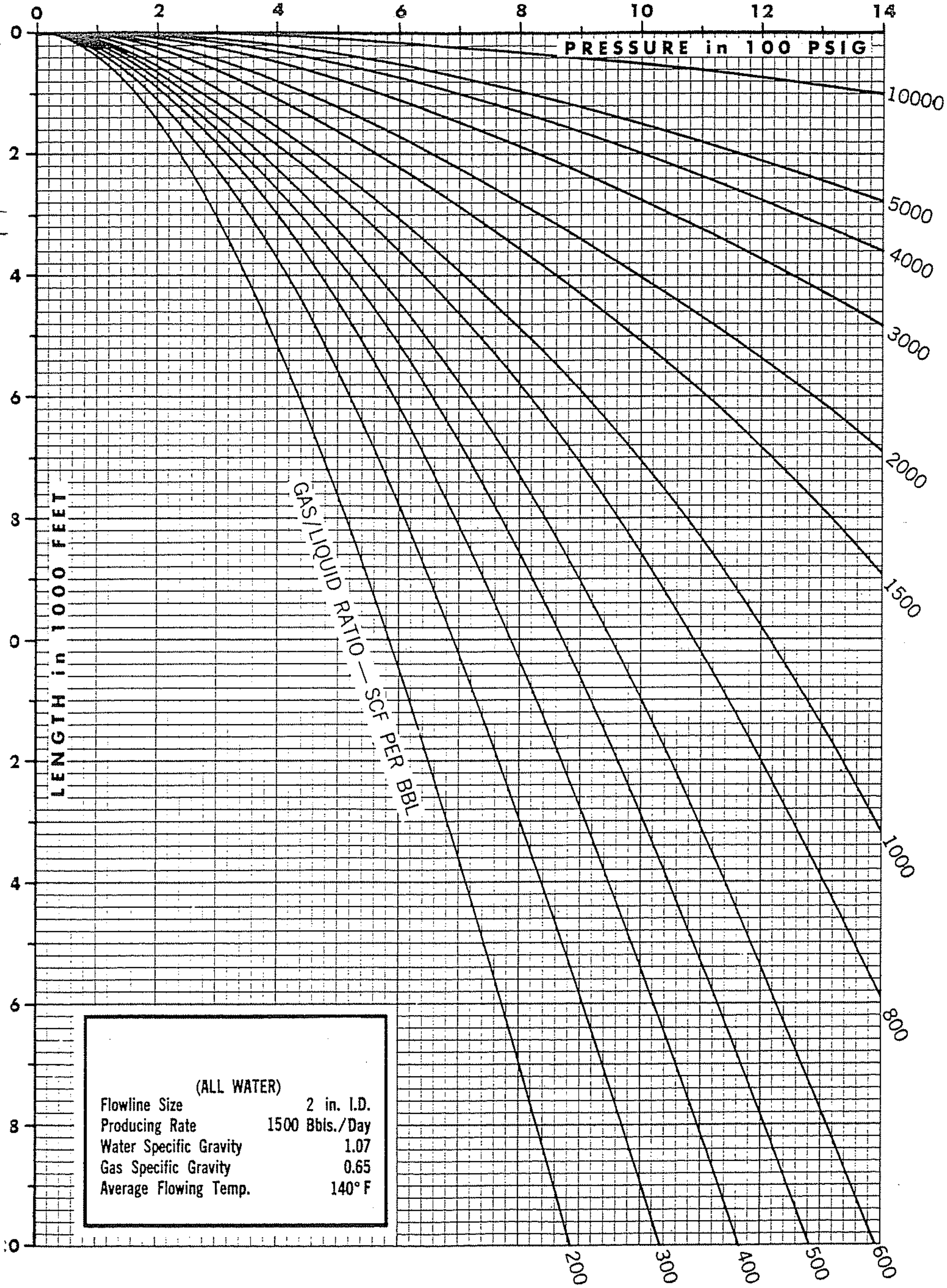

Figure 4.1(6) Horizontal Flowing Pressure Gradients

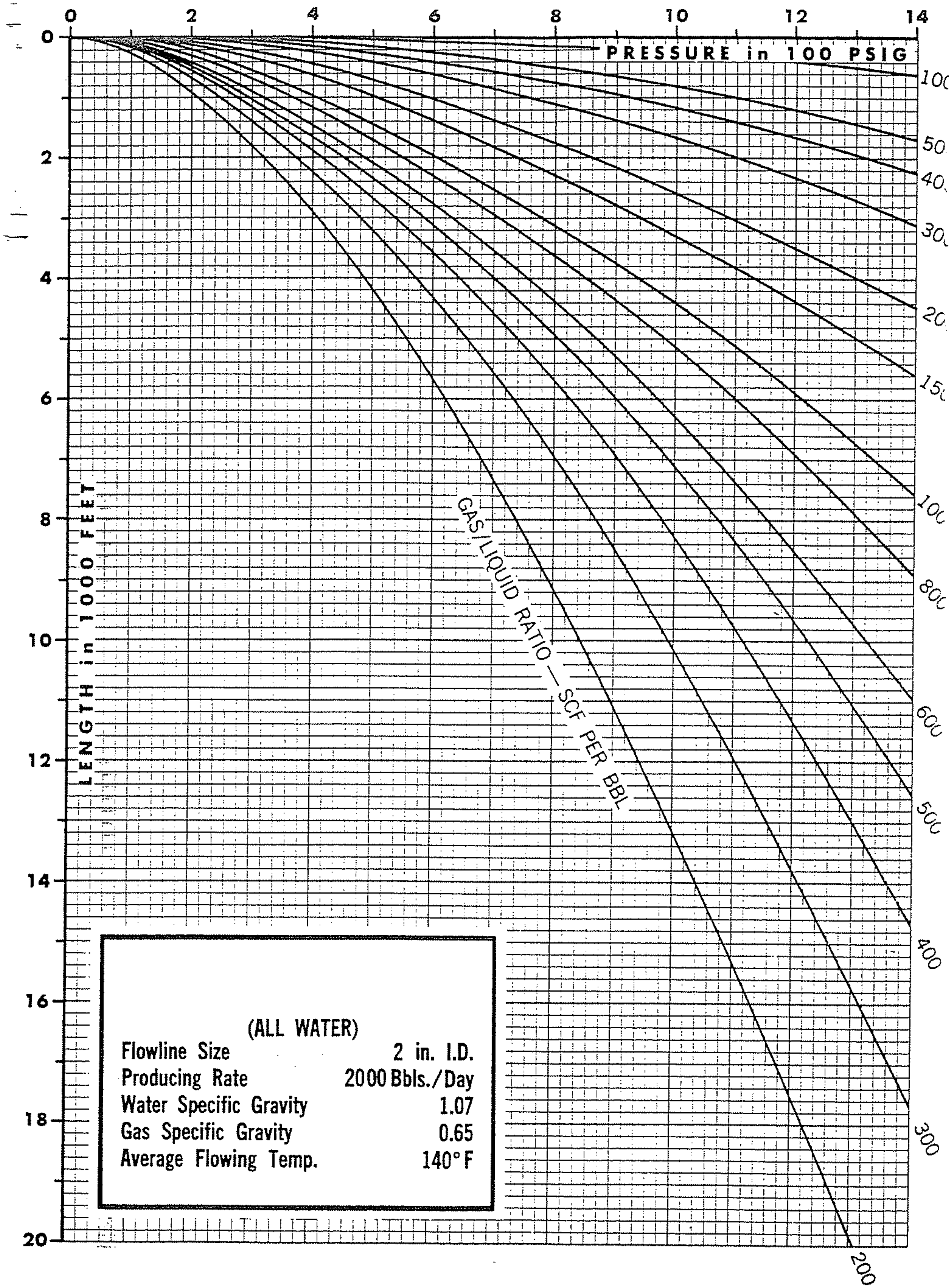

Figure 4.1(7) Horizontal Flowing Pressure Gradients

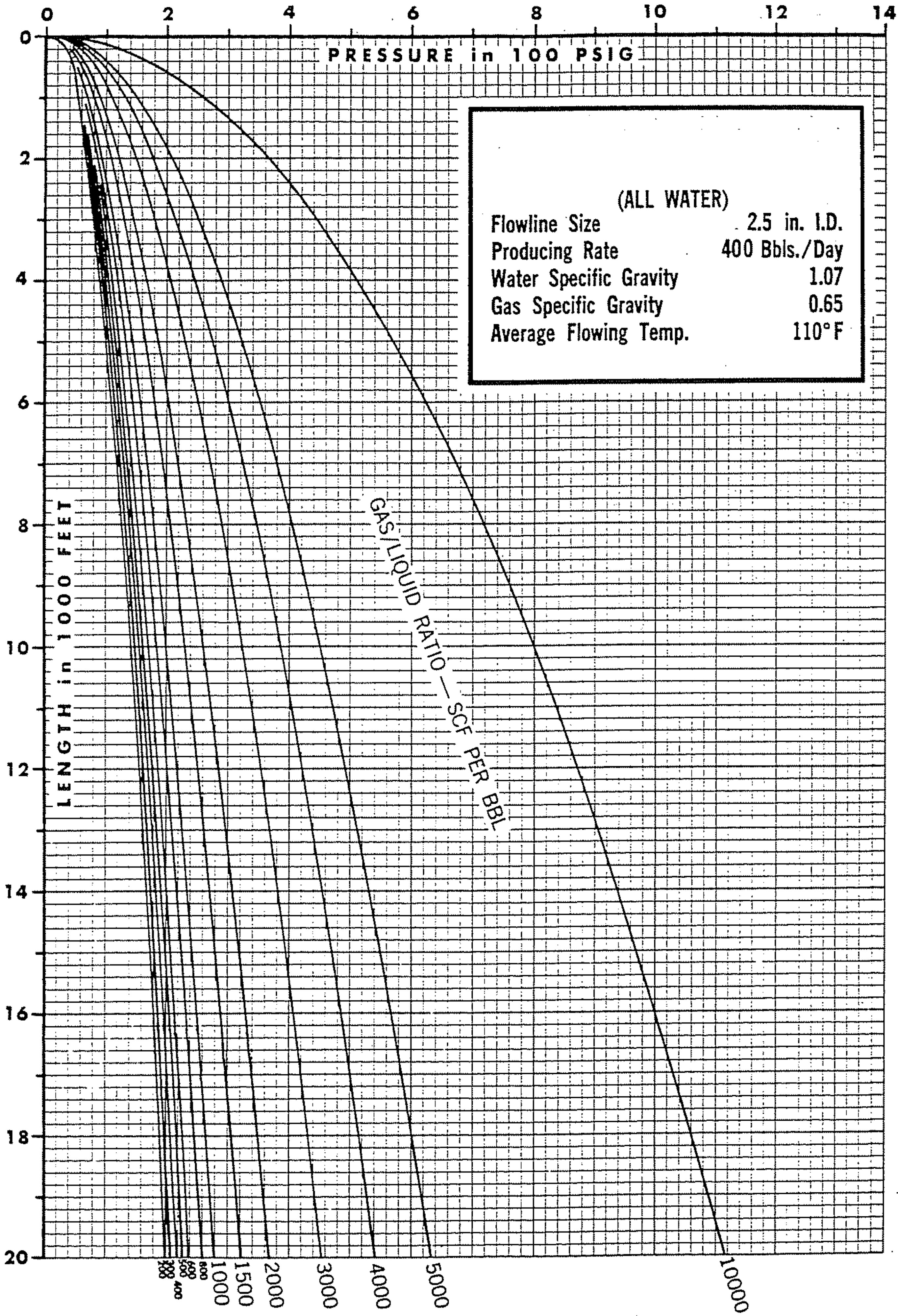

Figure 4.1(8) Horizontal Flowing Pressure Gradients

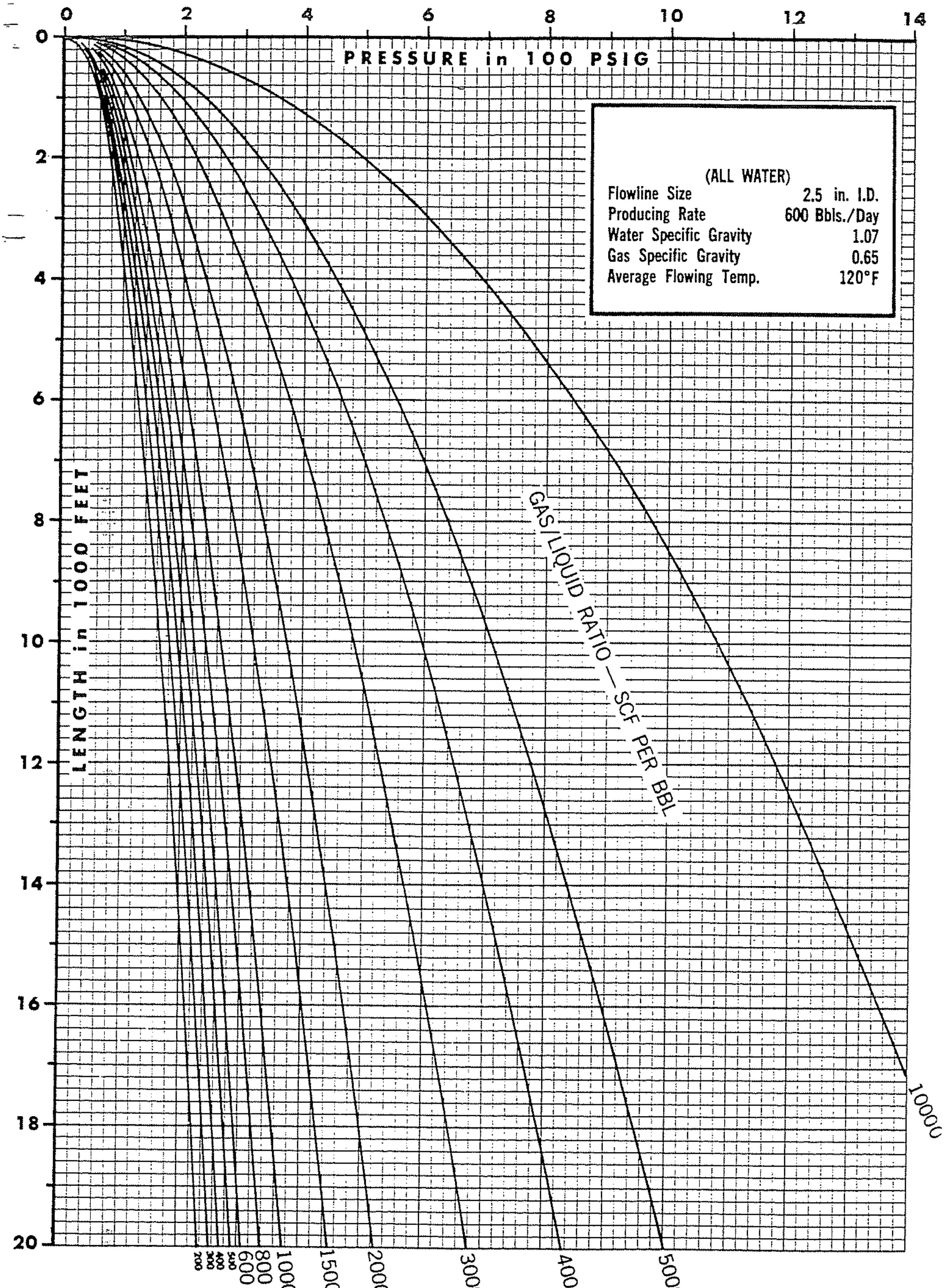

Figure 4.1(9) Horizontal Flowing Pressure Gradients

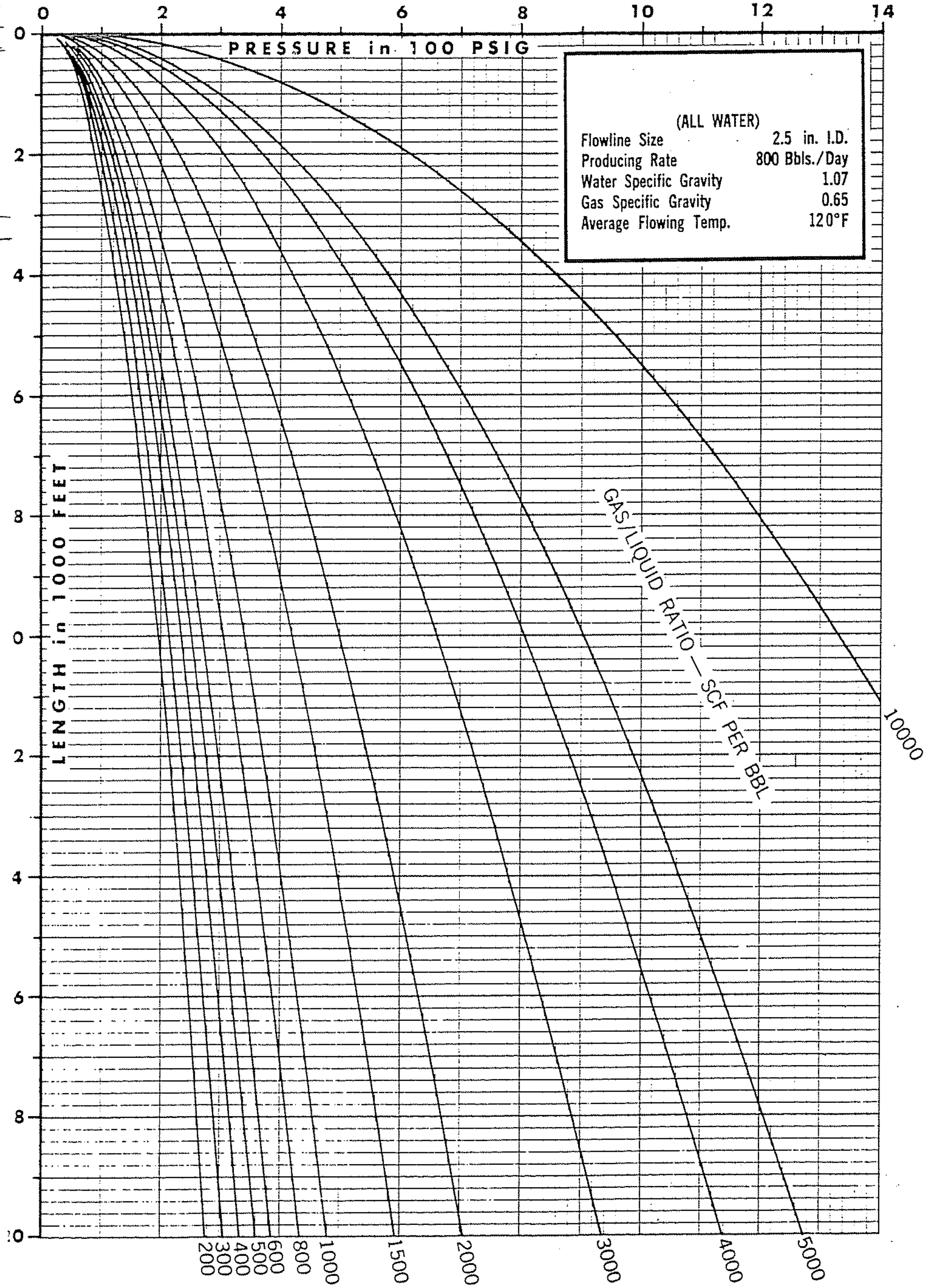

Figure 4.1(10) Horizontal Flowing Pressure Gradients

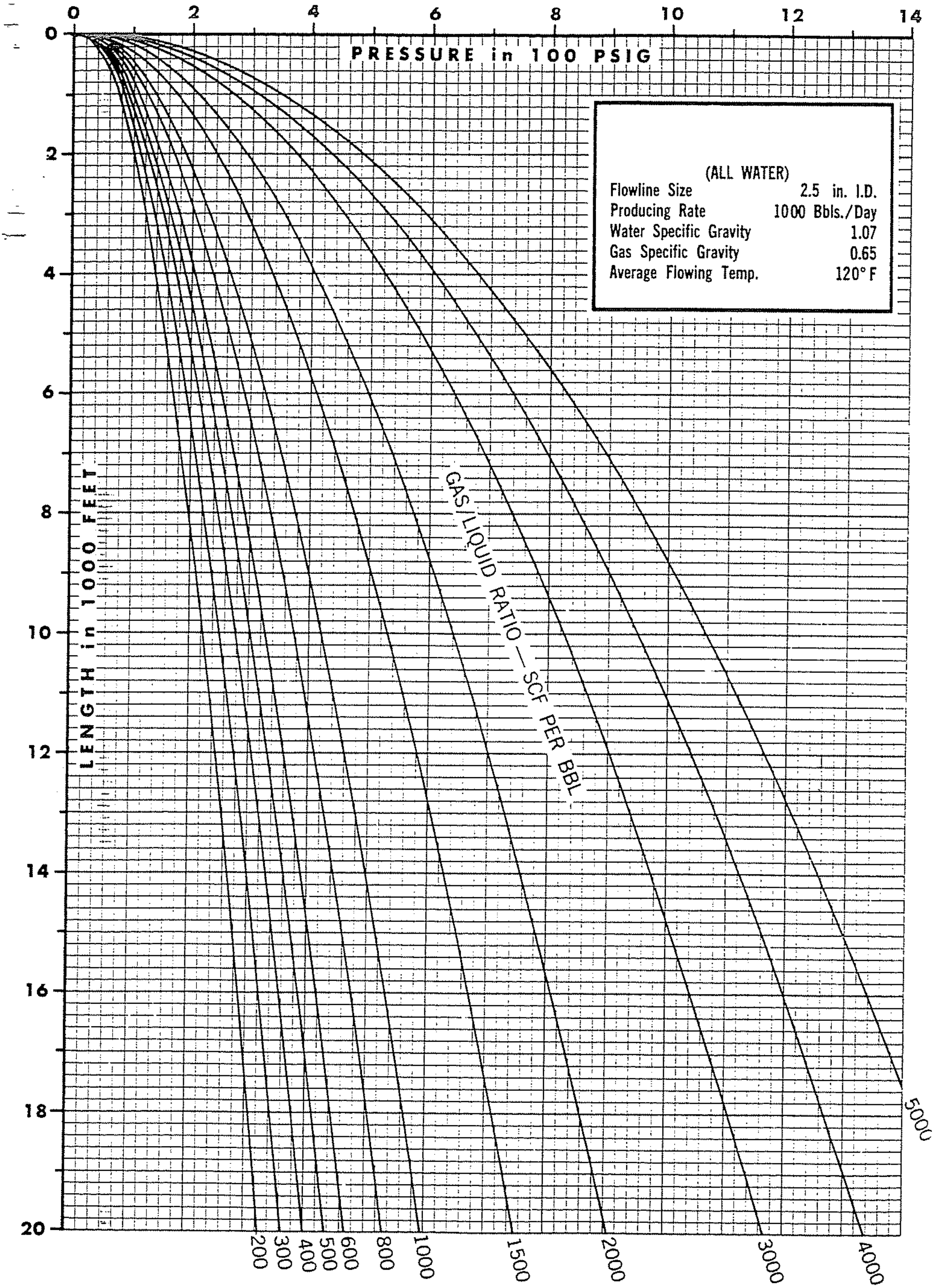

Figure 4.1(11) Horizontal Flowing Pressure Gradients

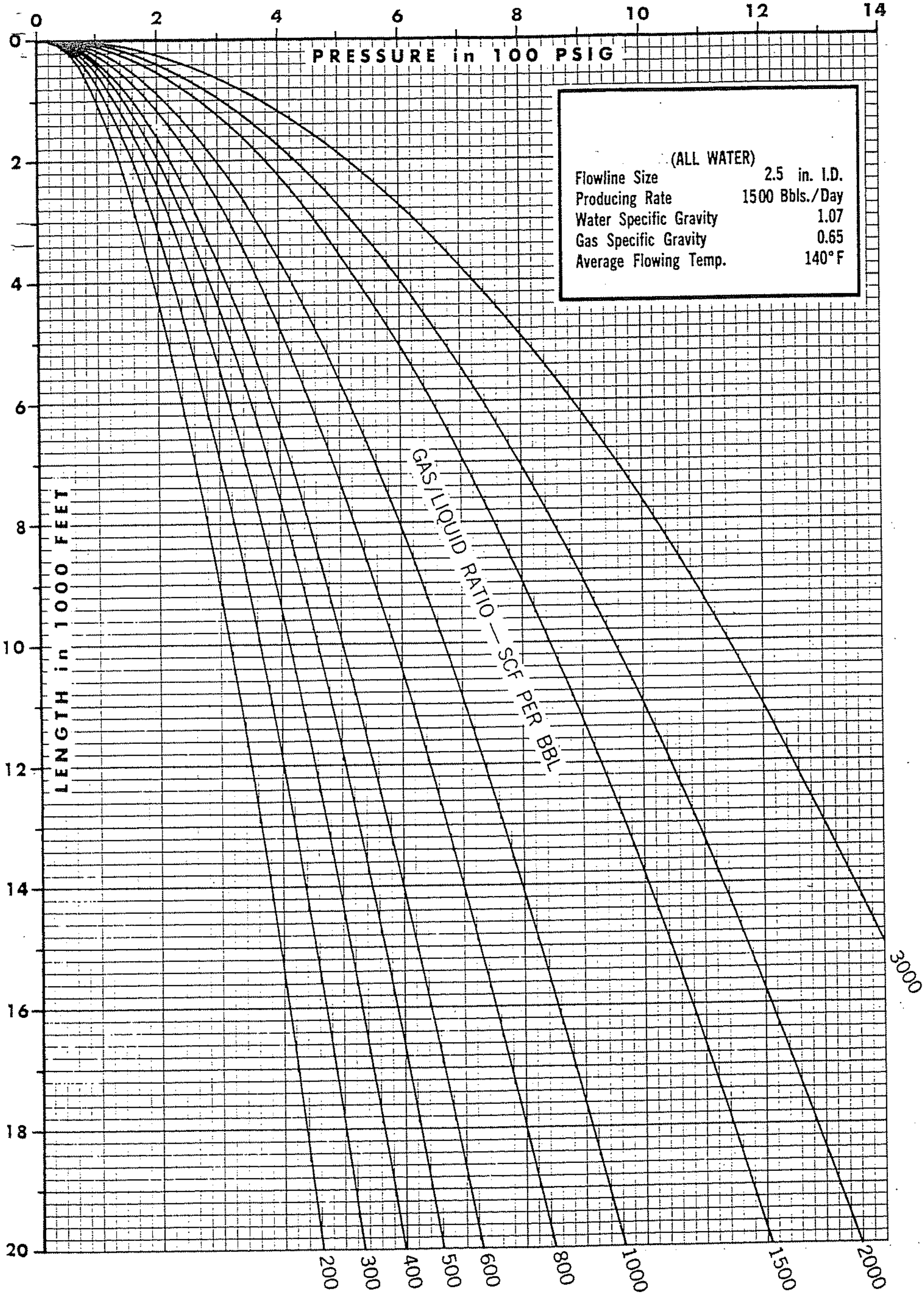

Figure 4.1(12) Horizontal Flowing Pressure Gradients

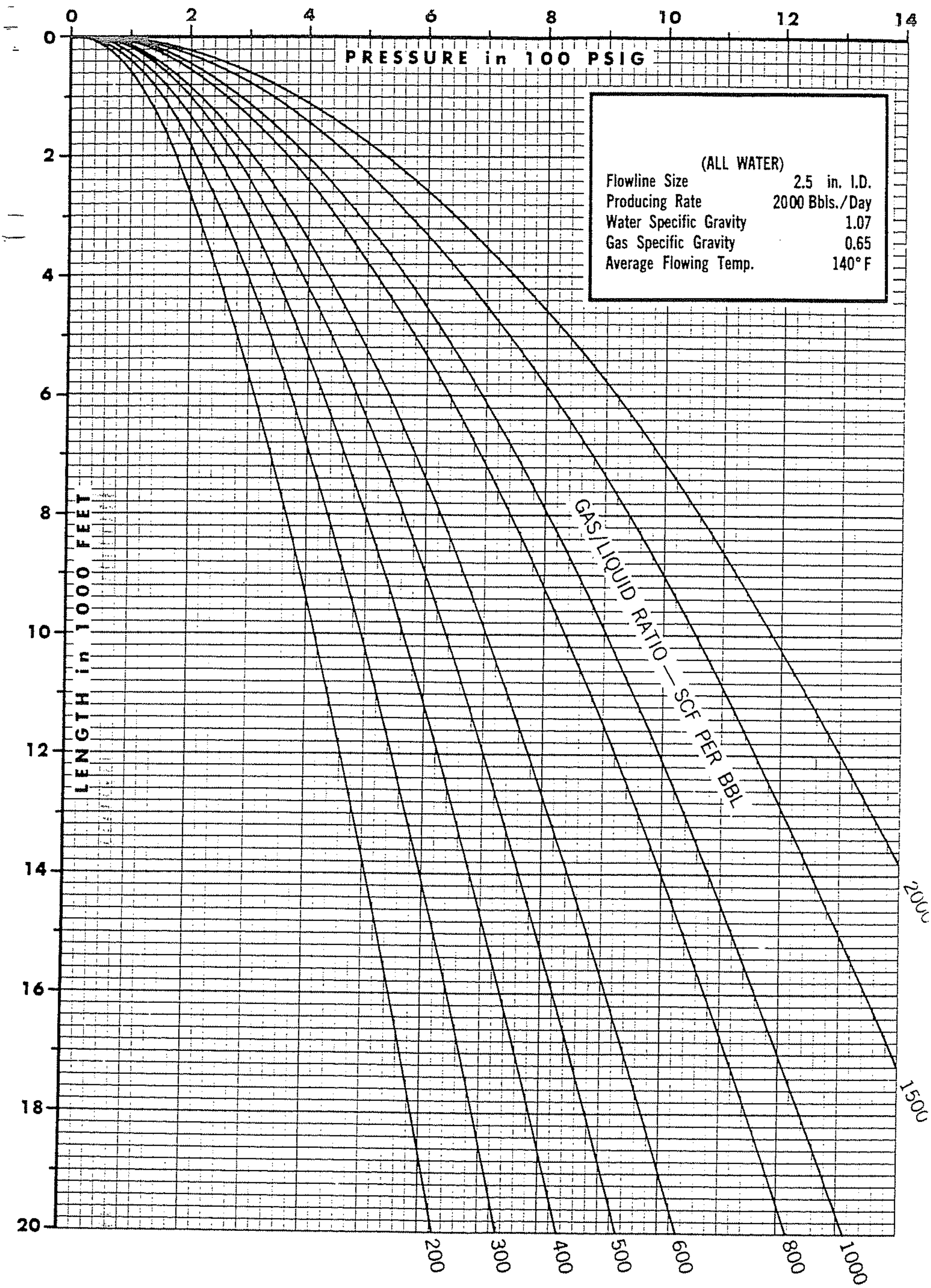

Figure 4.1(13) Horizontal Flowing Pressure Gradients

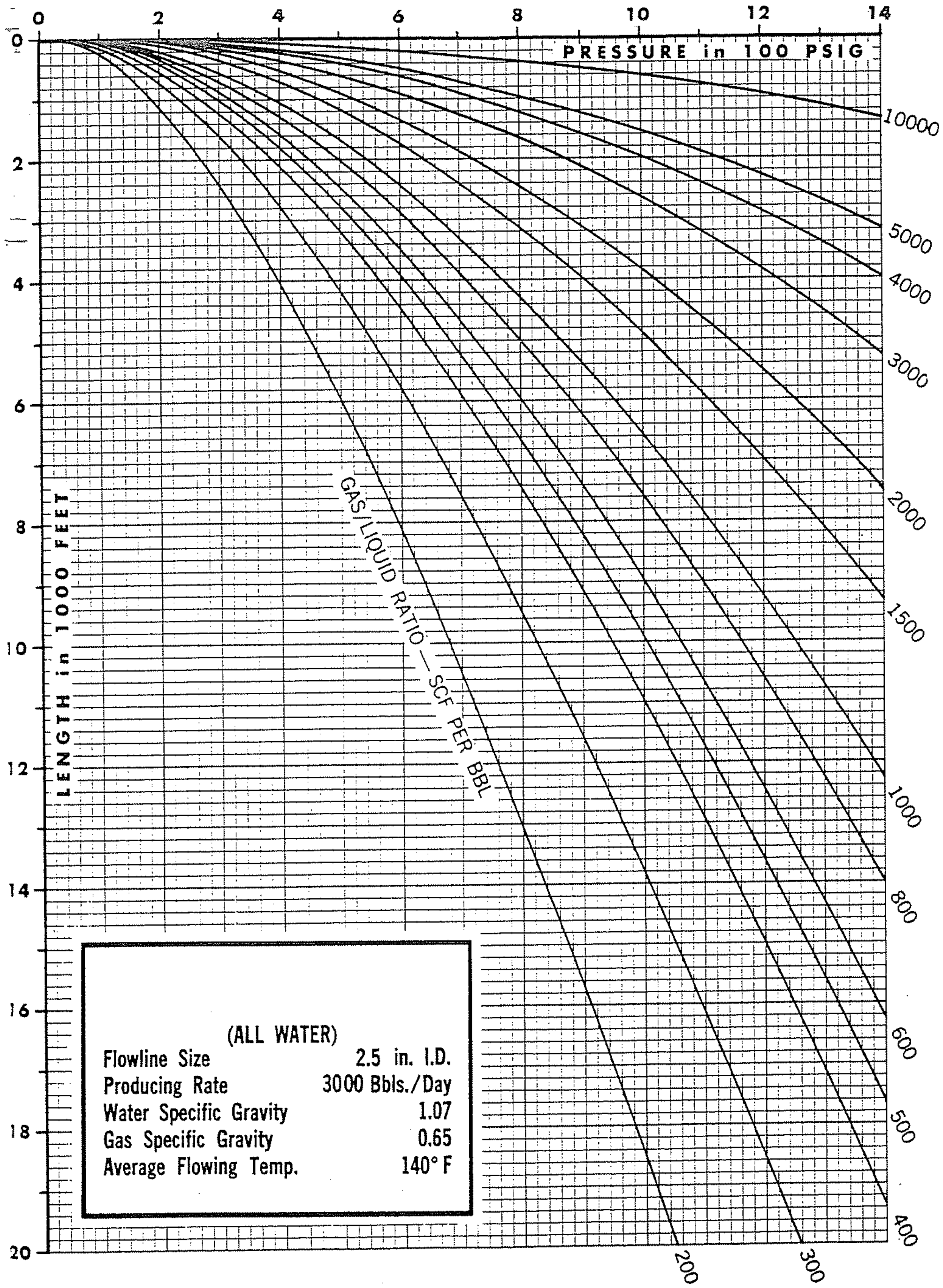

Figure 4.1(14) *Horizontal Flowing Pressure Gradients*

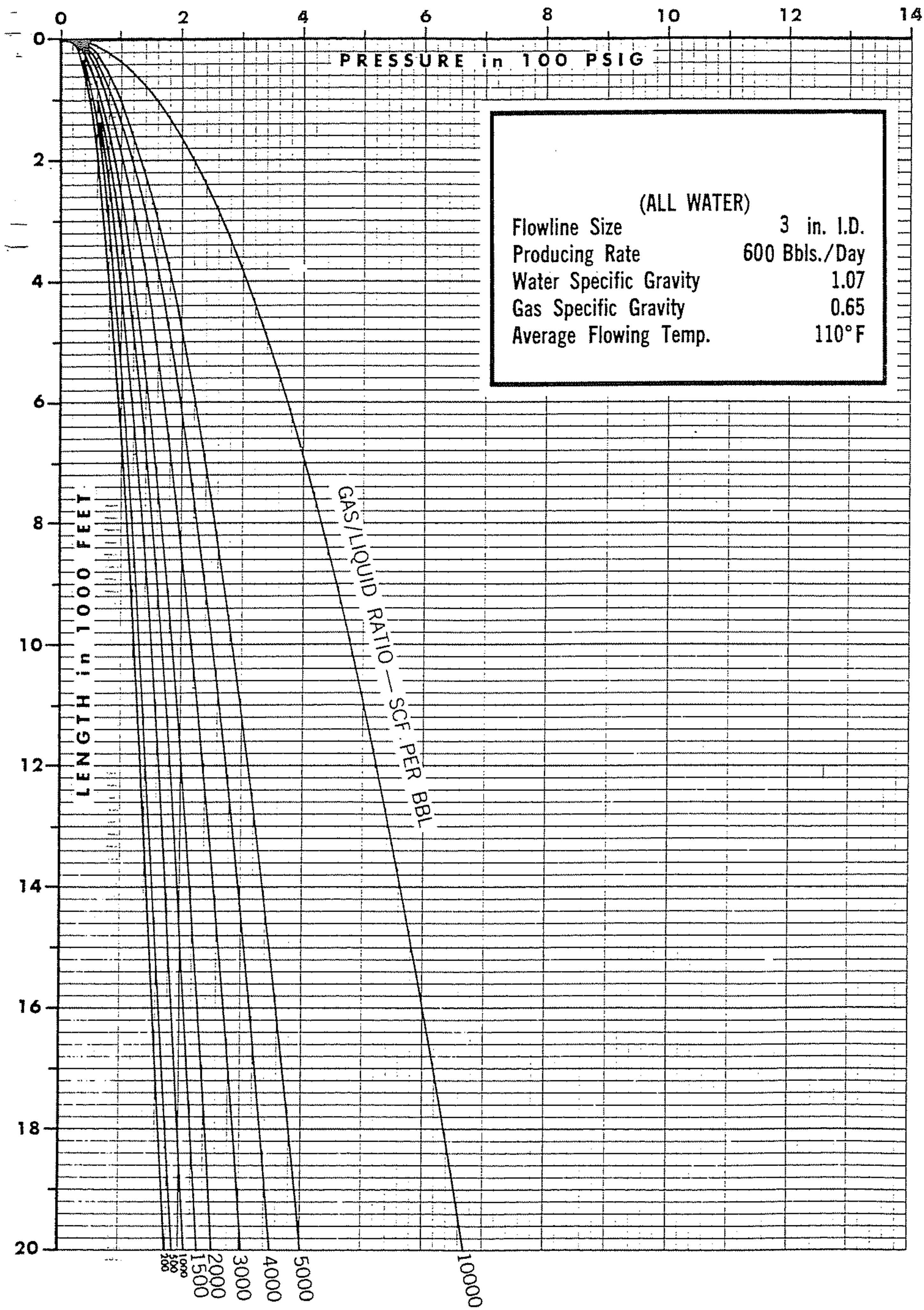

Figure 4.1(15) Horizontal Flowing Pressure Gradients

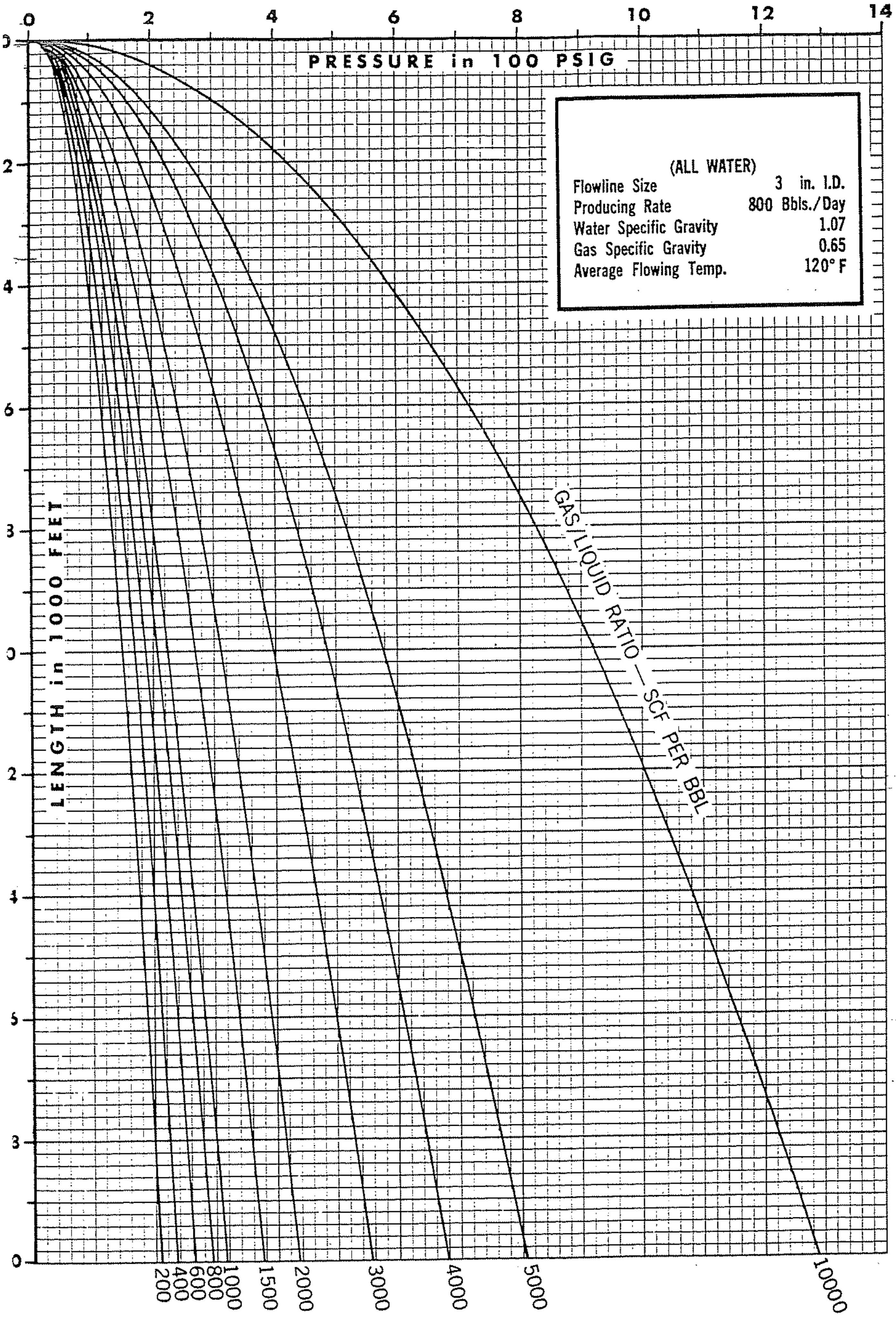

:ure 4.1(16) *Horizontal Flowing Pressure Gradients*

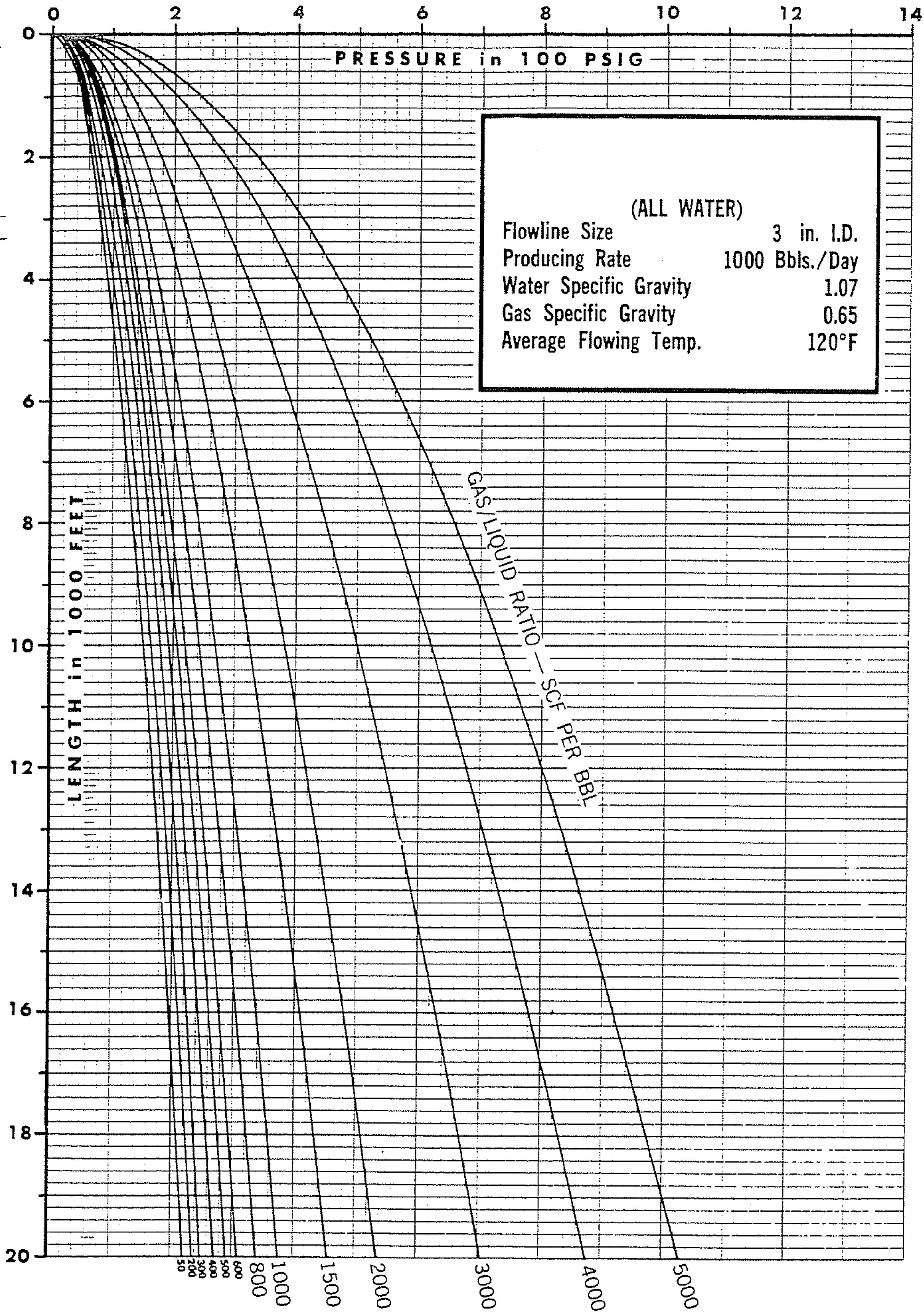

Figure 4.1(17) Horizontal Flowing Pressure Gradients

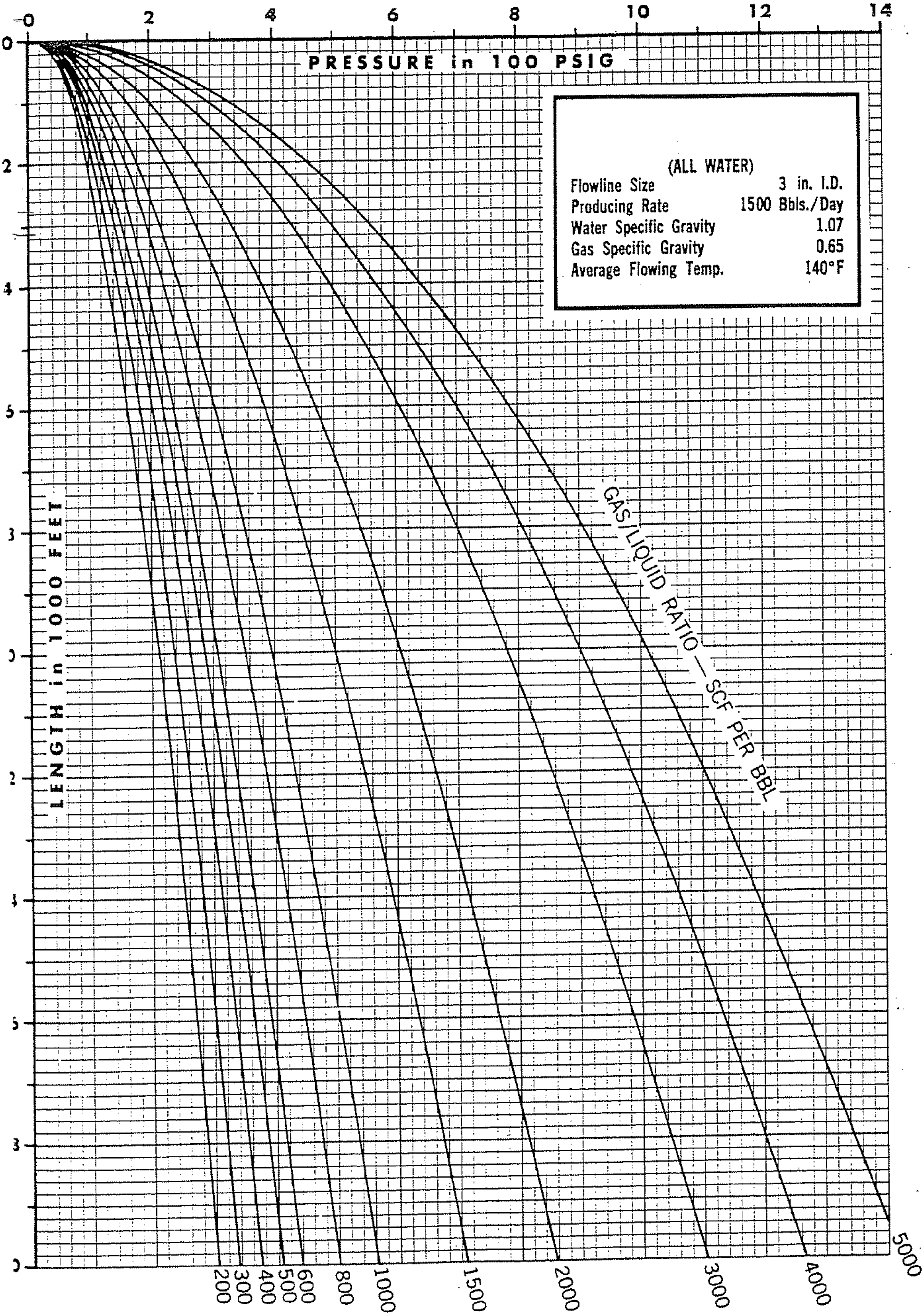

Figure 4.1(18) Horizontal Flowing Pressure Gradients

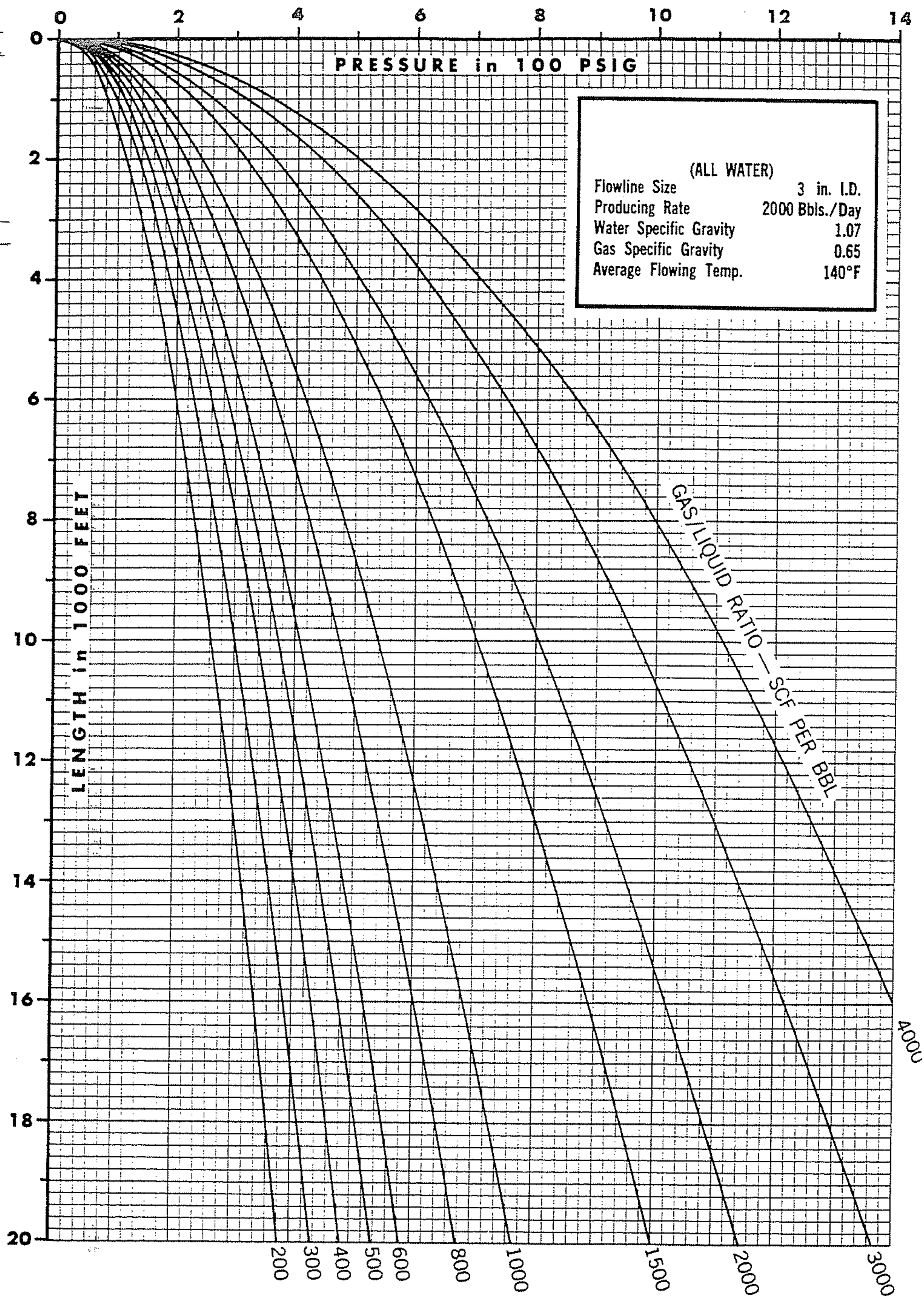

Figure 4.1(19) Horizontal Flowing Pressure Gradients

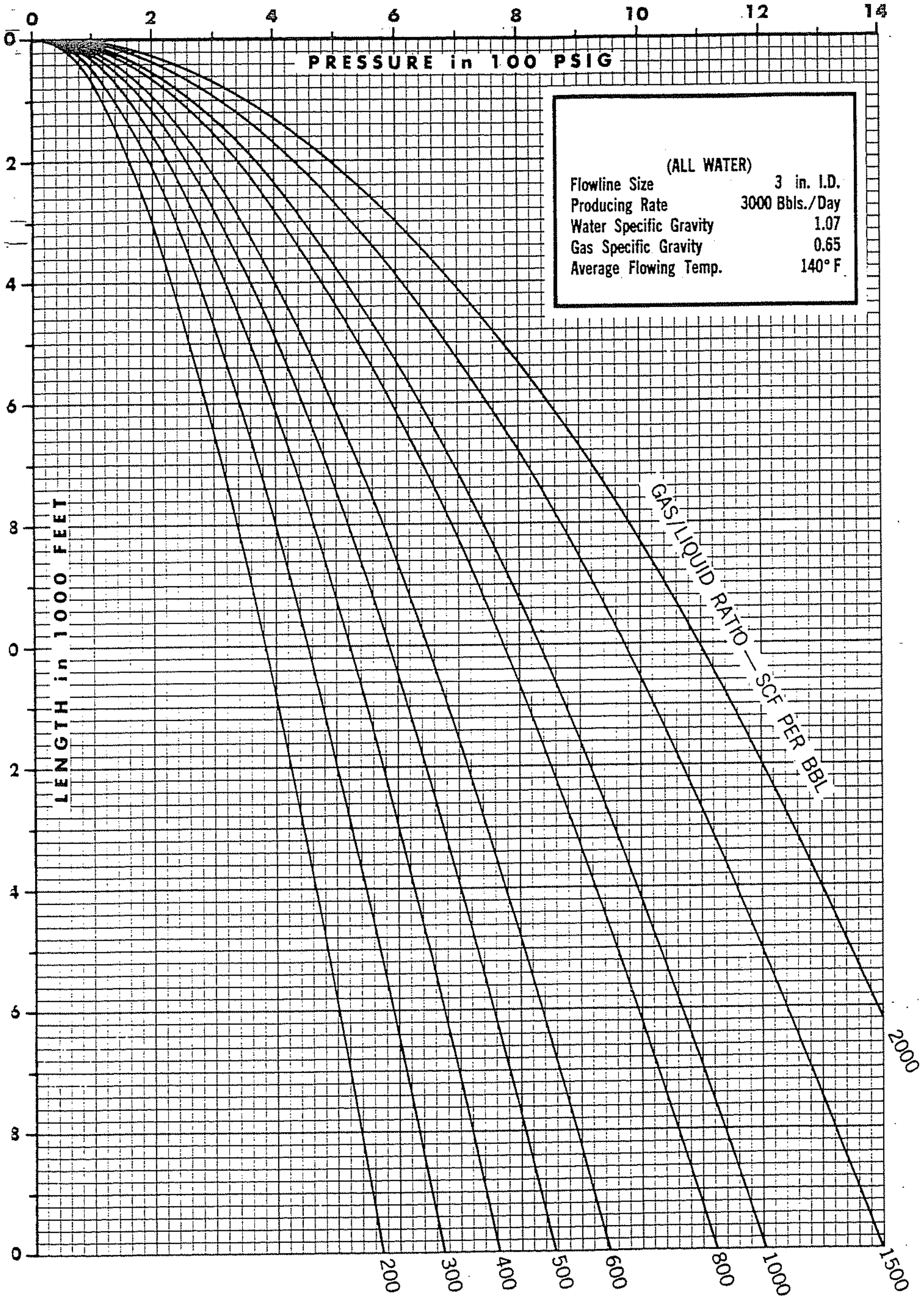

gure 4.1(20) Horizontal Flowing Pressure Gradients

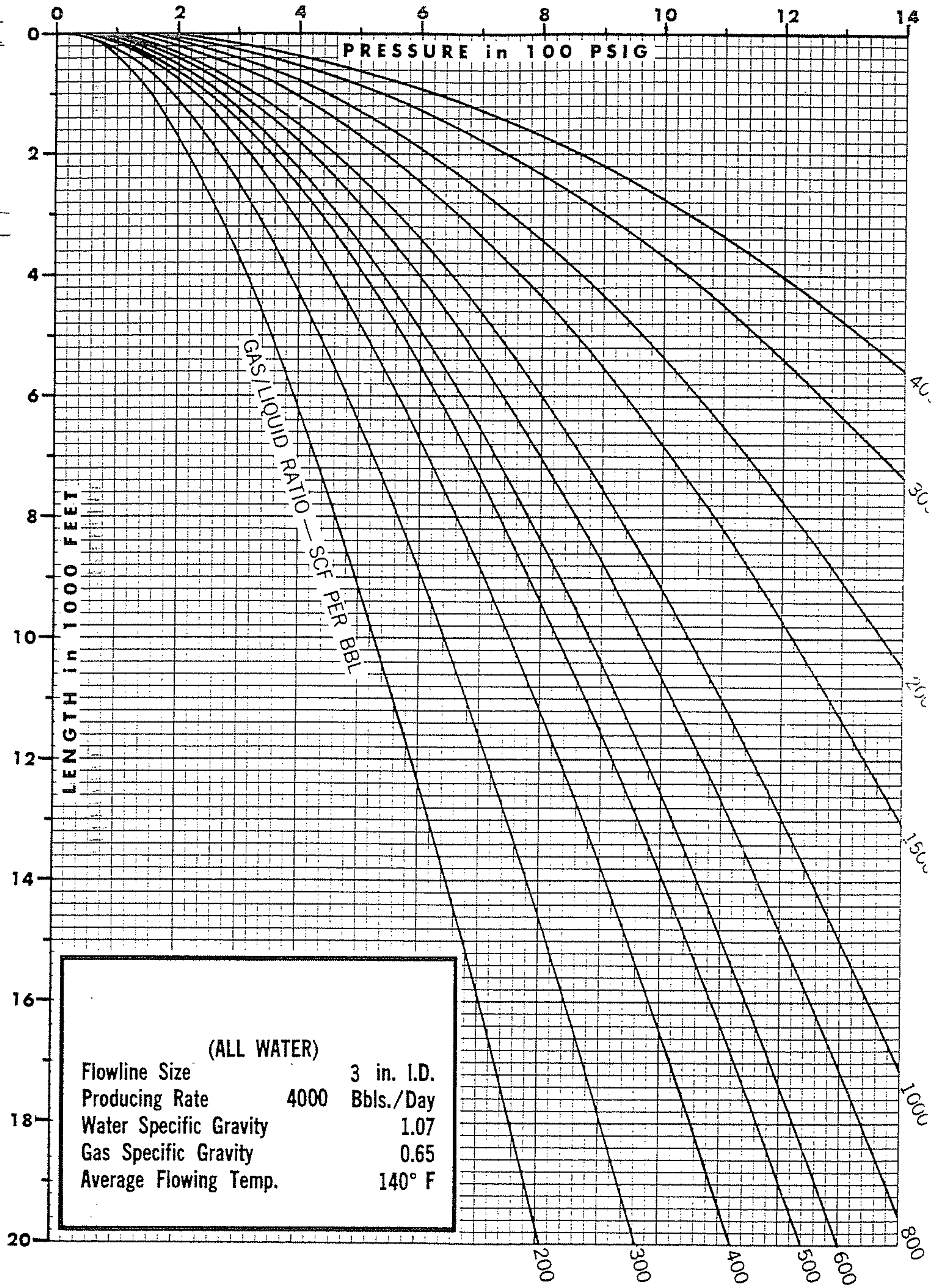

Figure 4.1(21) Horizontal Flowing Pressure Gradients

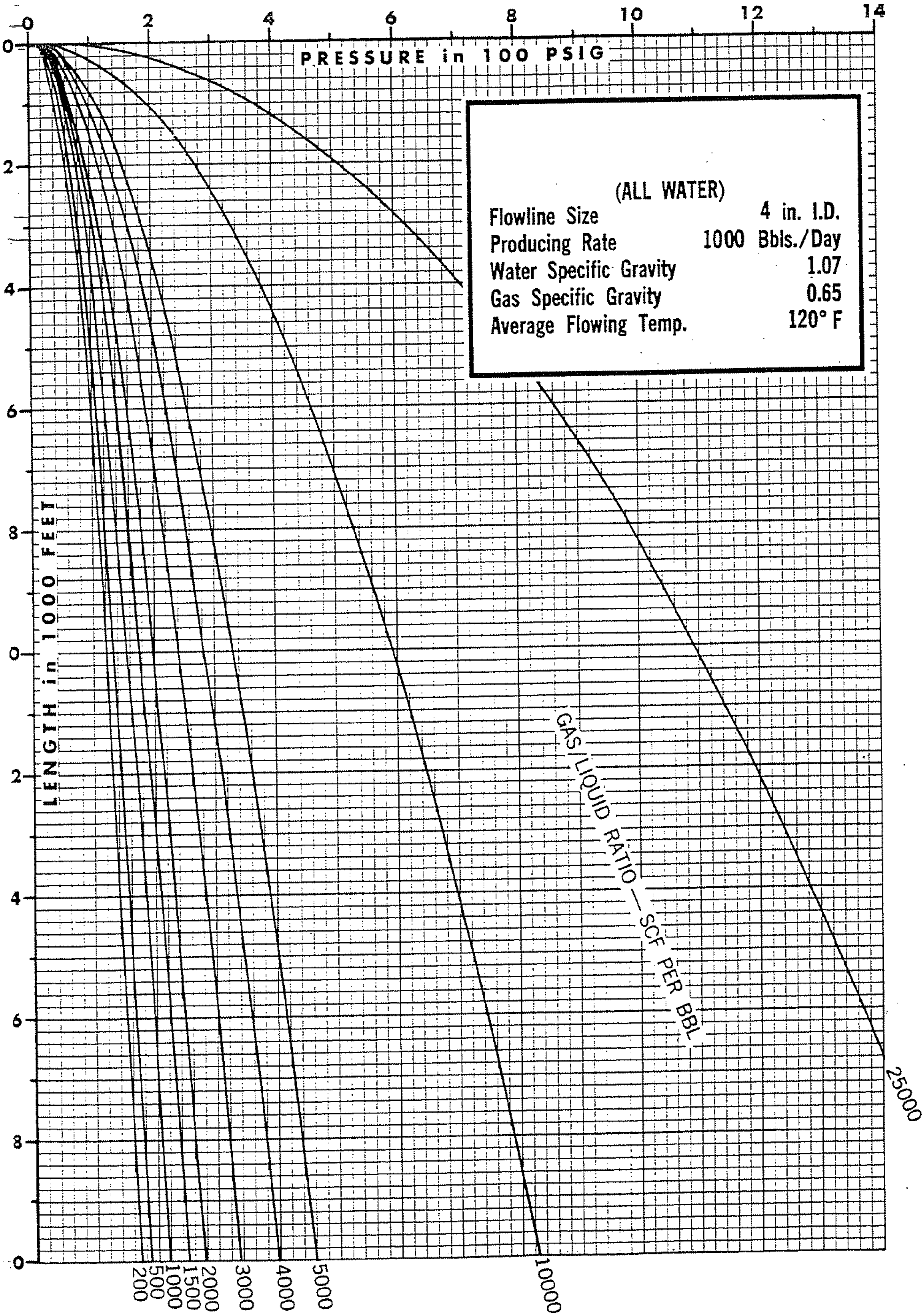

Figure 4.1(22) Horizontal Flowing Pressure Gradients

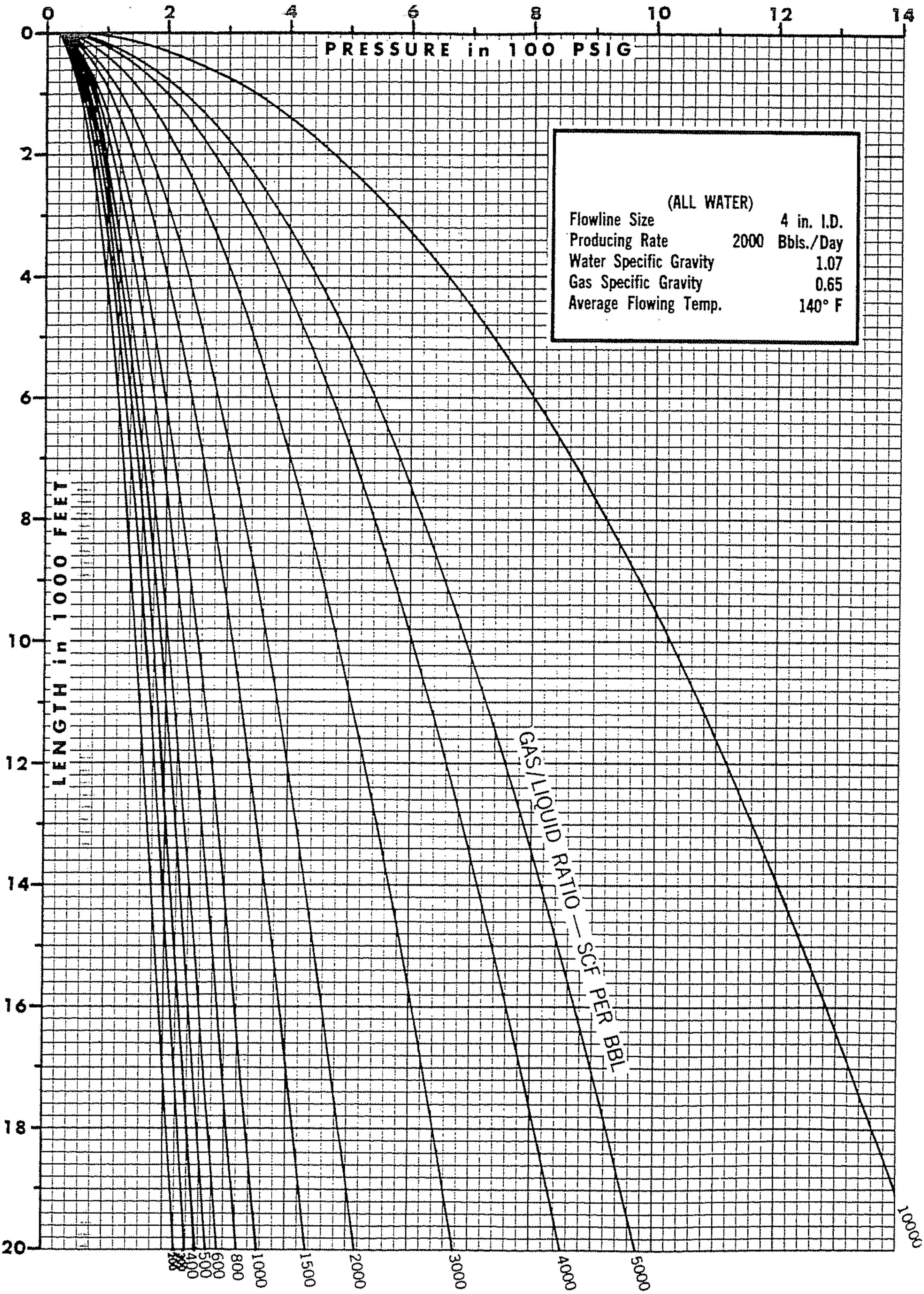

Figure 4.1(23) Horizontal Flowing Pressure Gradients

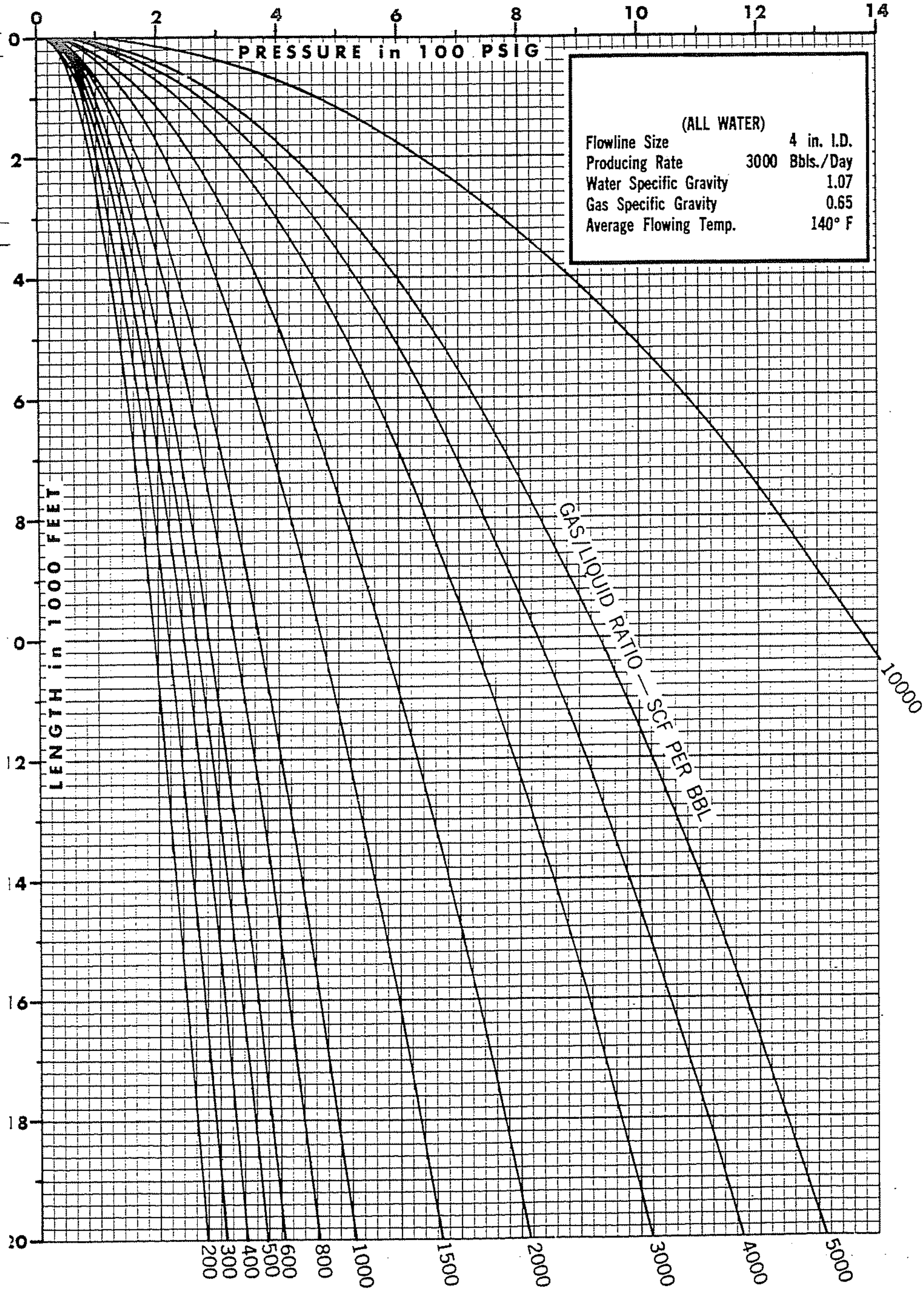

Figure 4.1(24) Horizontal Flowing Pressure Gradients

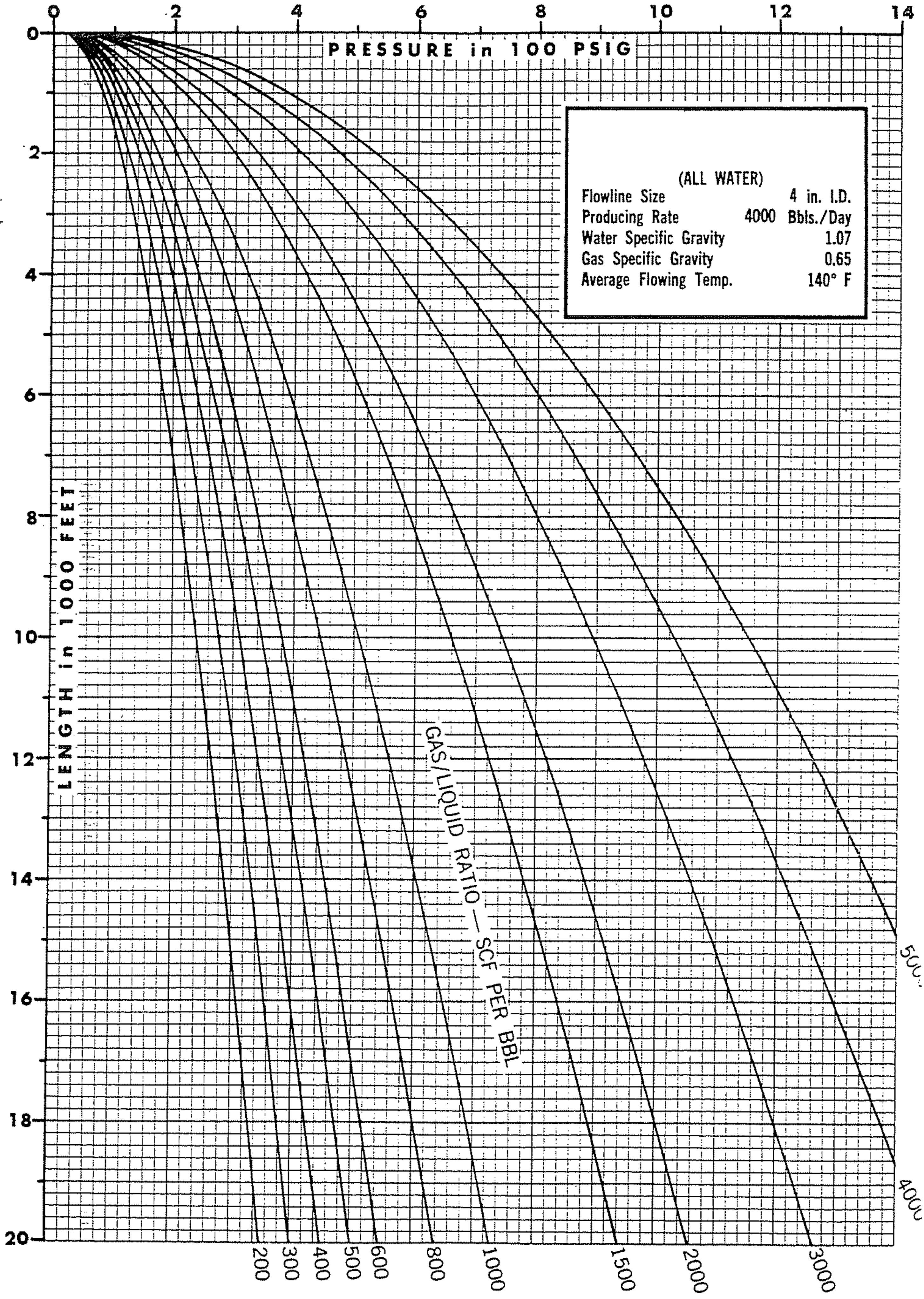

Figure 4.1(25) Horizontal Flowing Pressure Gradients

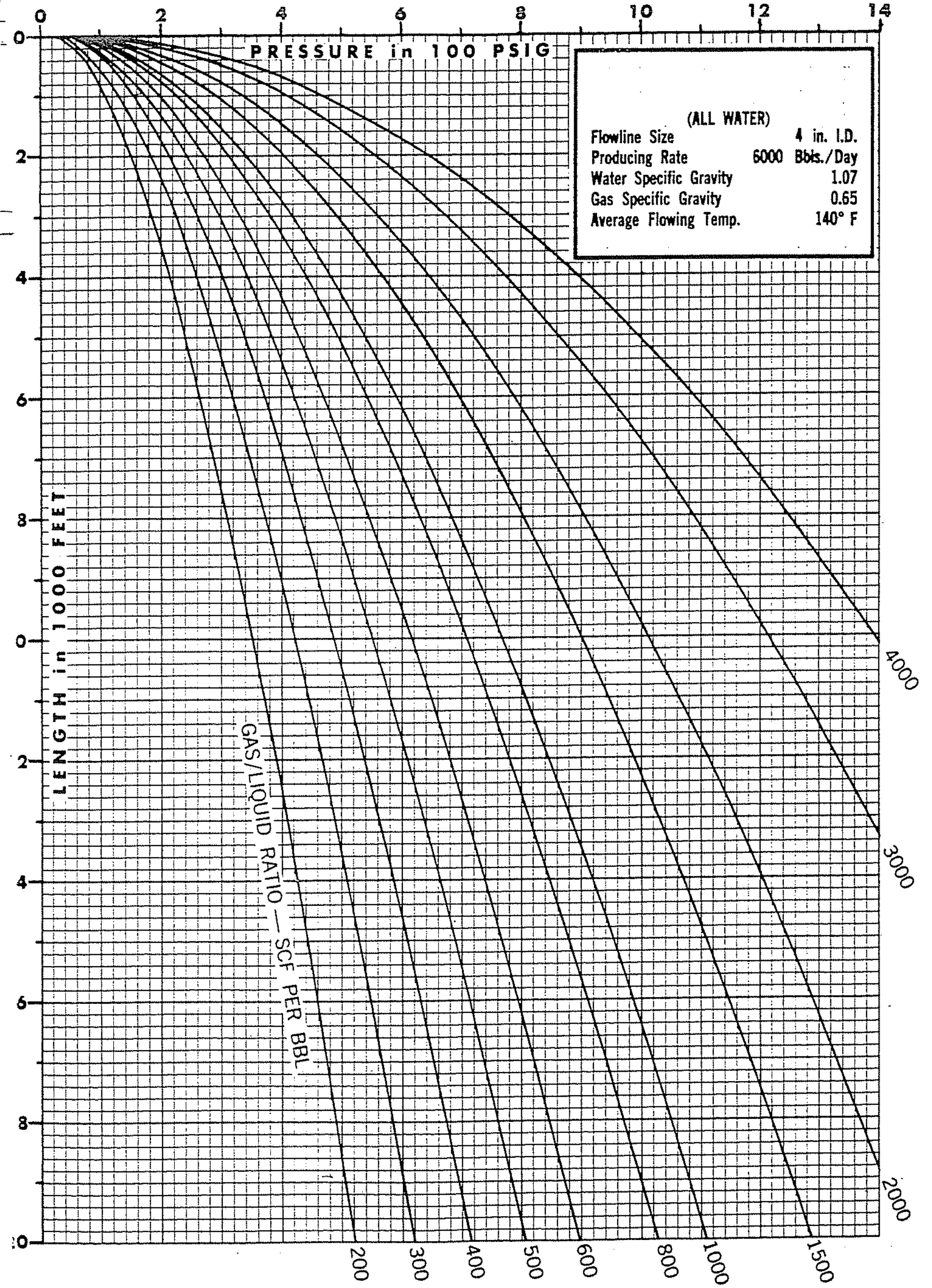

Figure 4.1(26) Horizontal Flowing Pressure Gradients

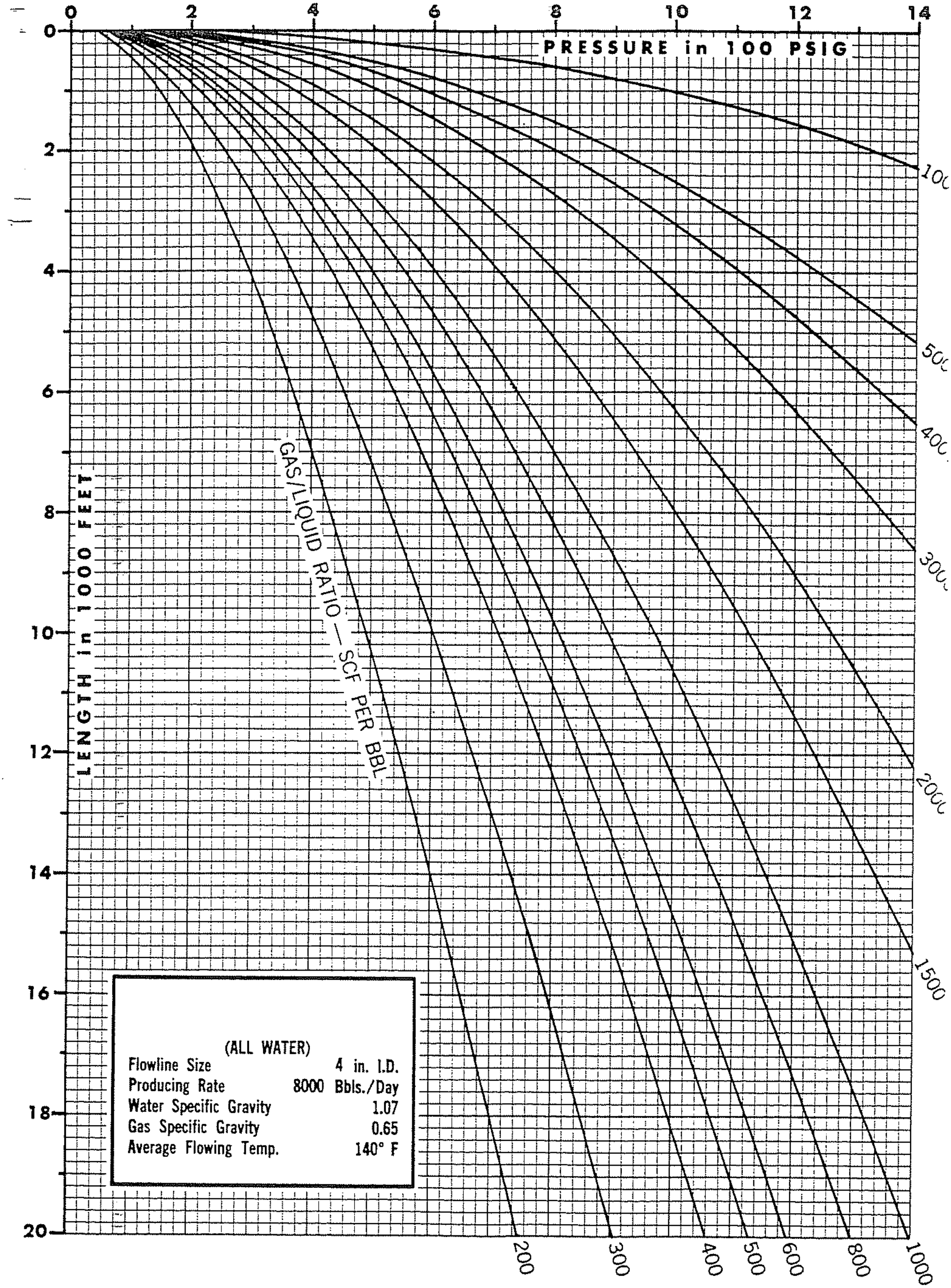

Figure 4.1(27) Horizontal Flowing Pressure Gradients

Appendix 4.2
Vertical flowing pressure gradients

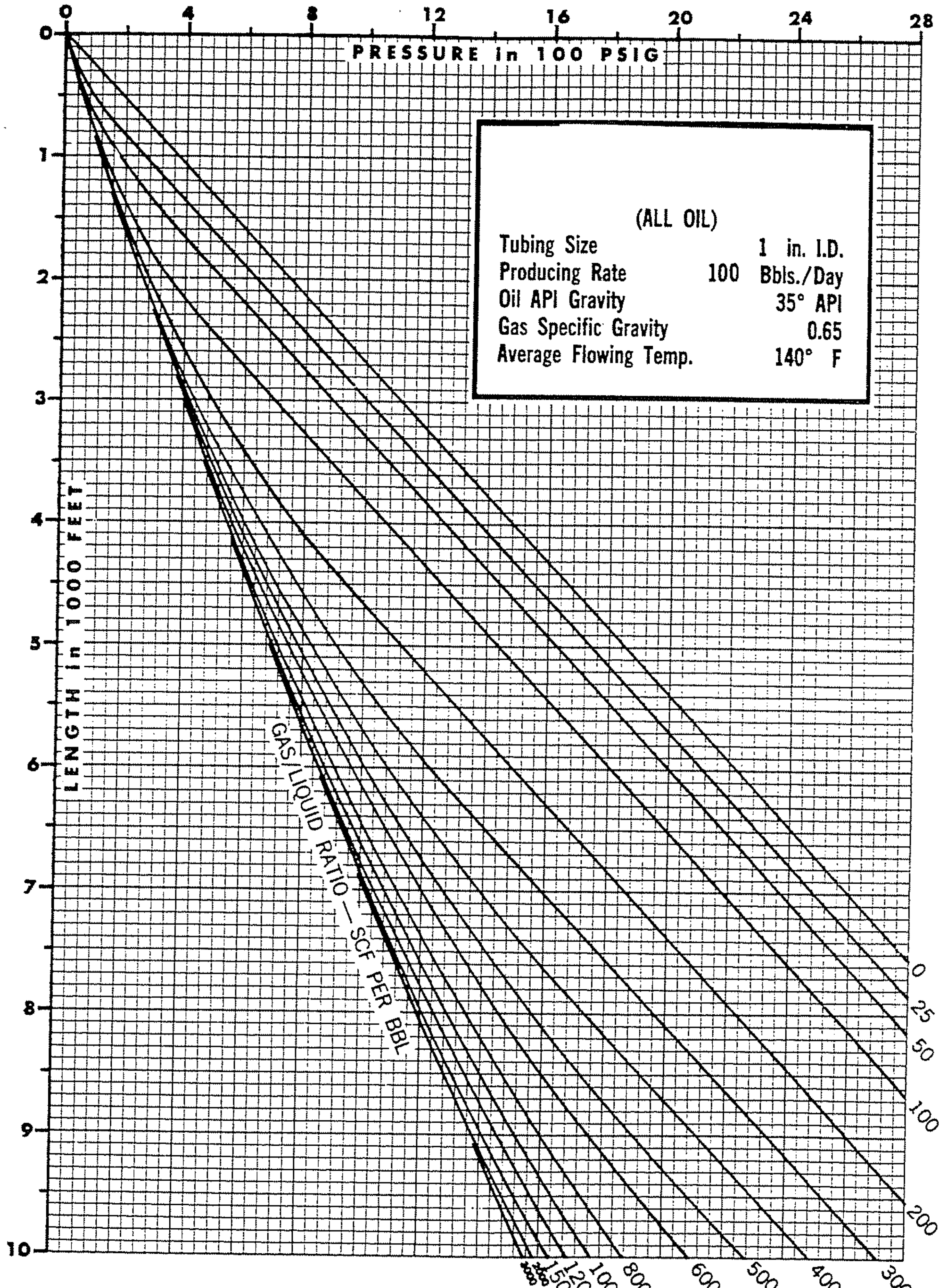

Figure 4.2(1) Vertical Flowing Pressure Gradients

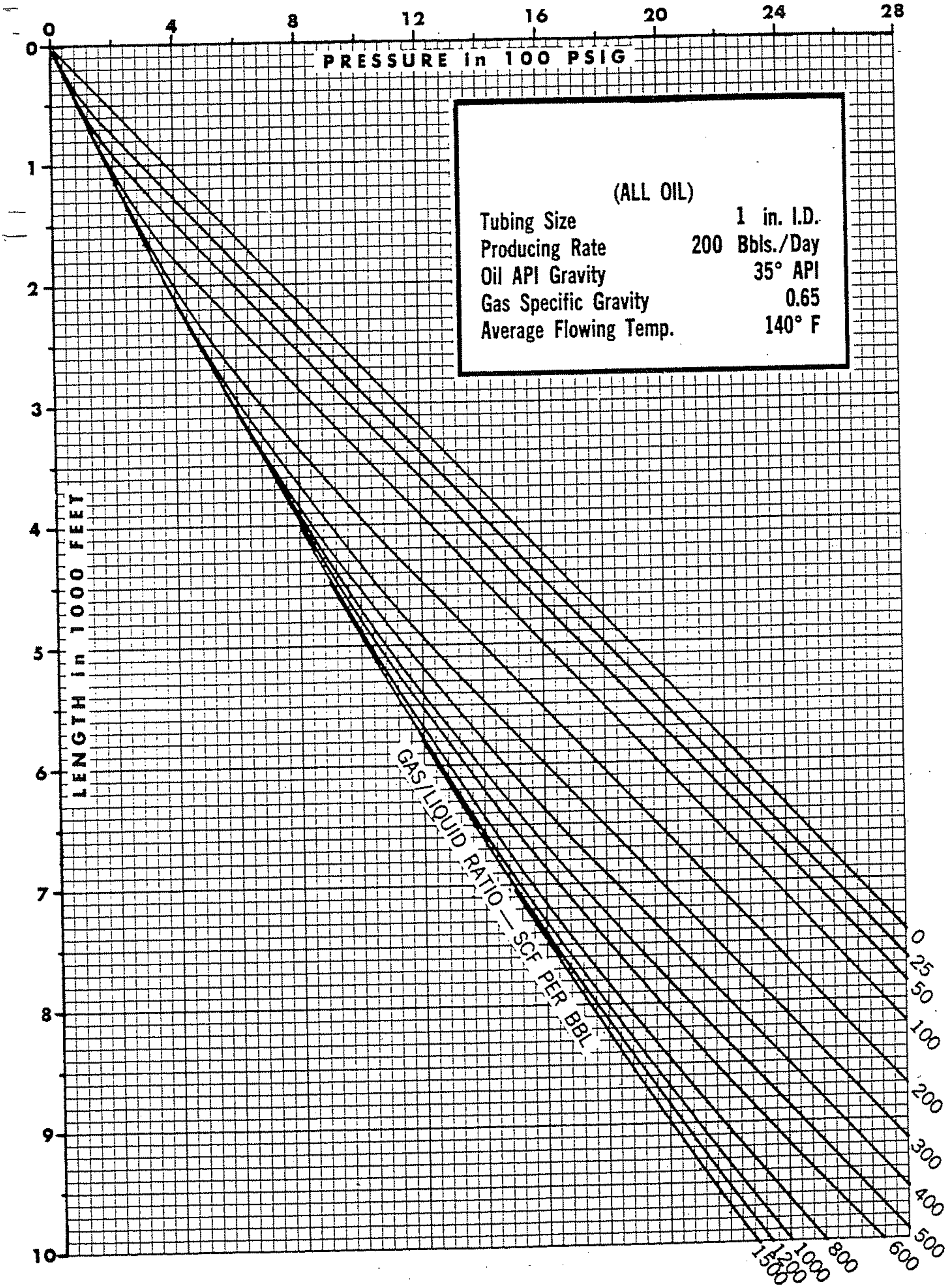

Figure 4.2(2) Vertical Flowing Pressure Gradients

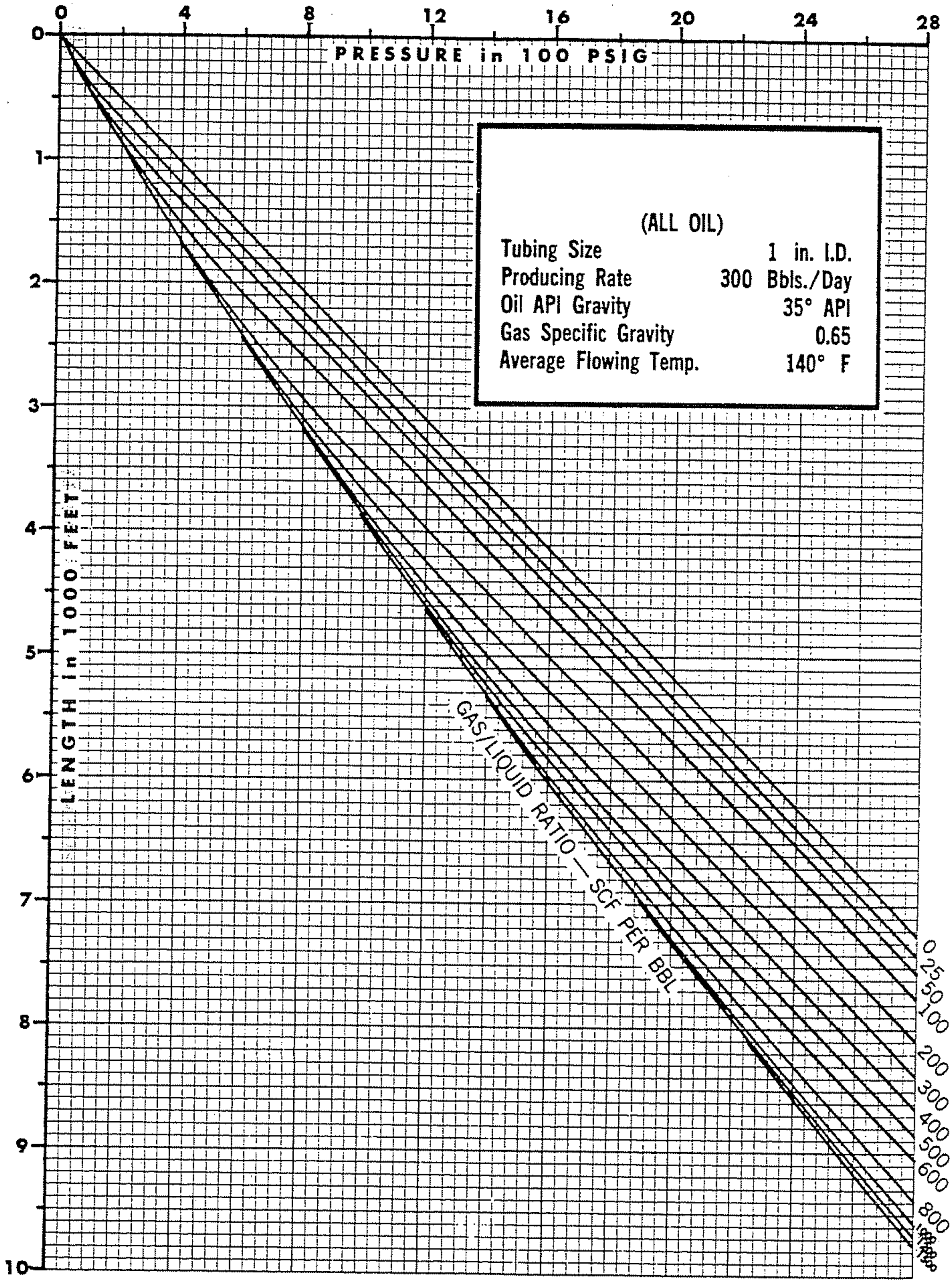

Figure 4.2(3) Vertical Flowing Pressure Gradients

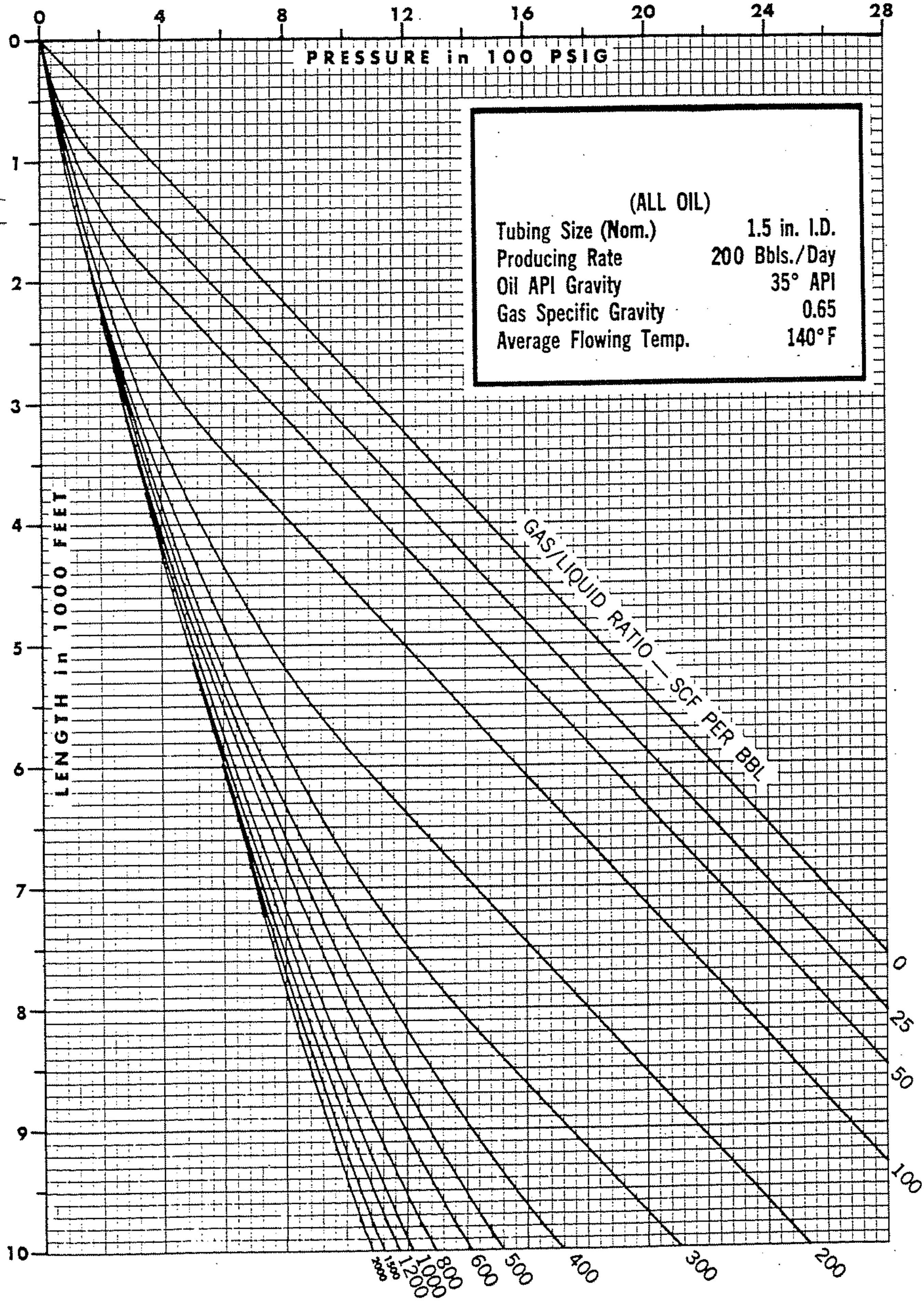

Figure 4.2(4) Vertical Flowing Pressure Gradients

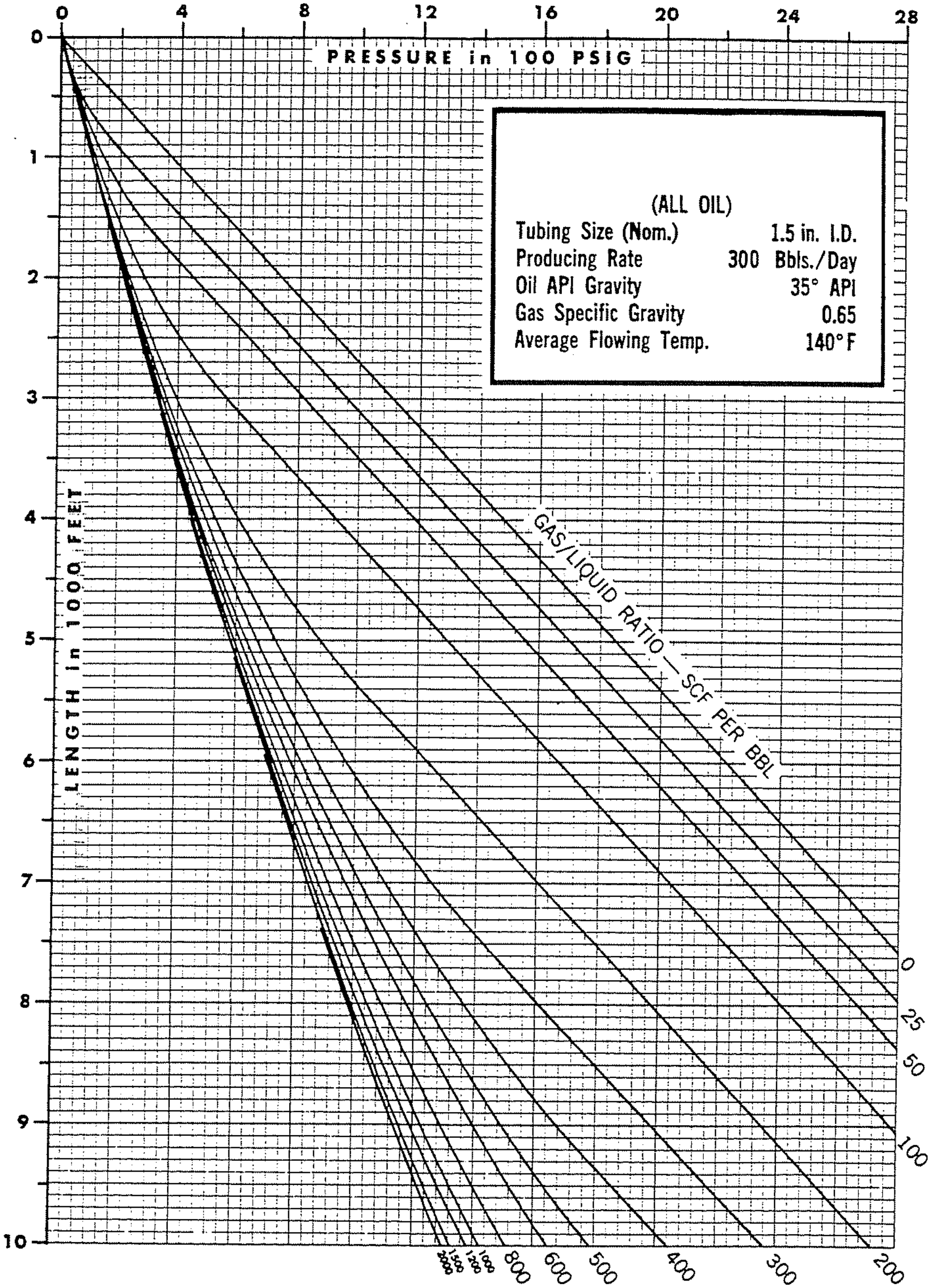

Figure 4.2(5) Vertical Flowing Pressure Gradients

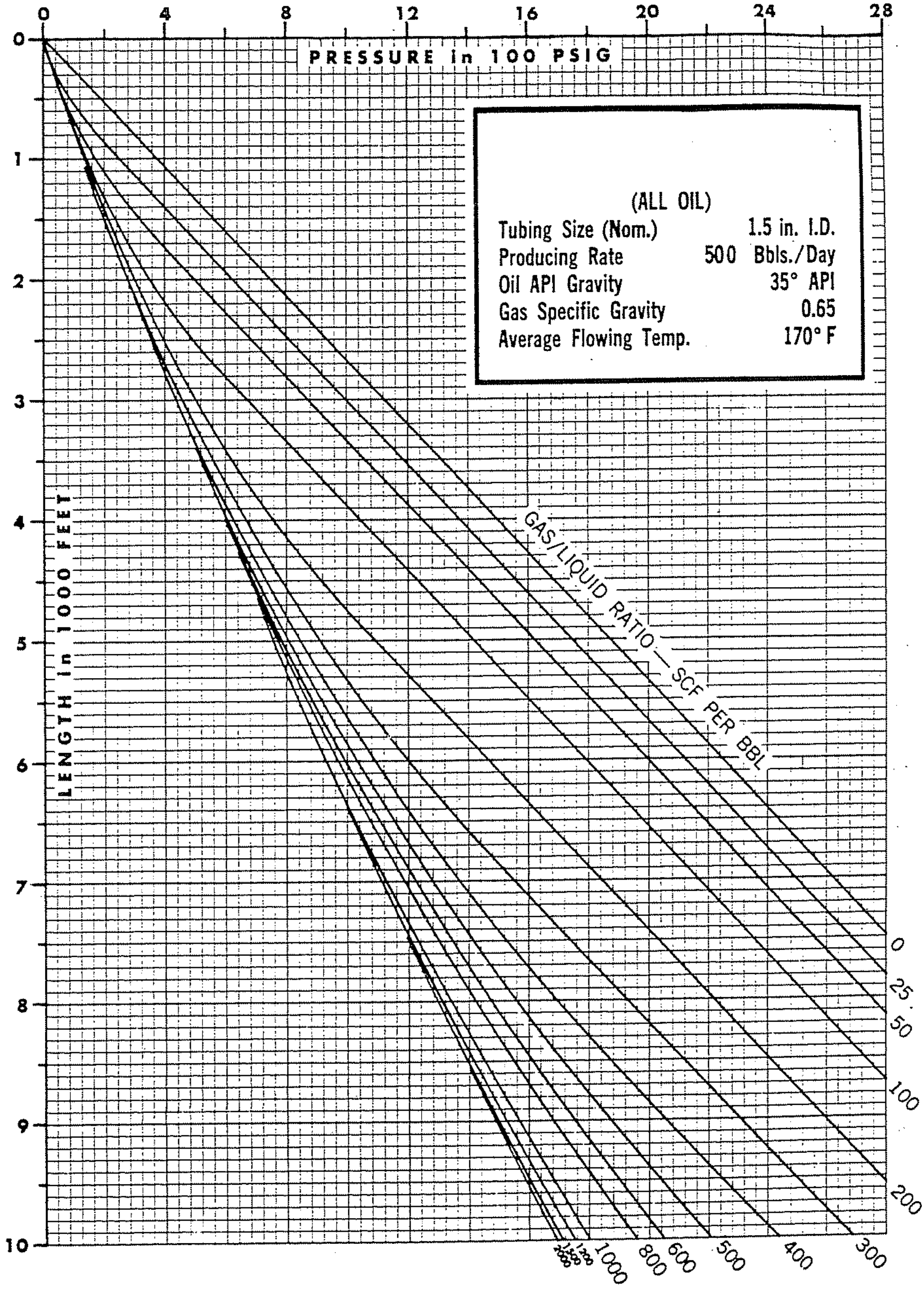

Figure 4.2(6) Vertical Flowing Pressure Gradients

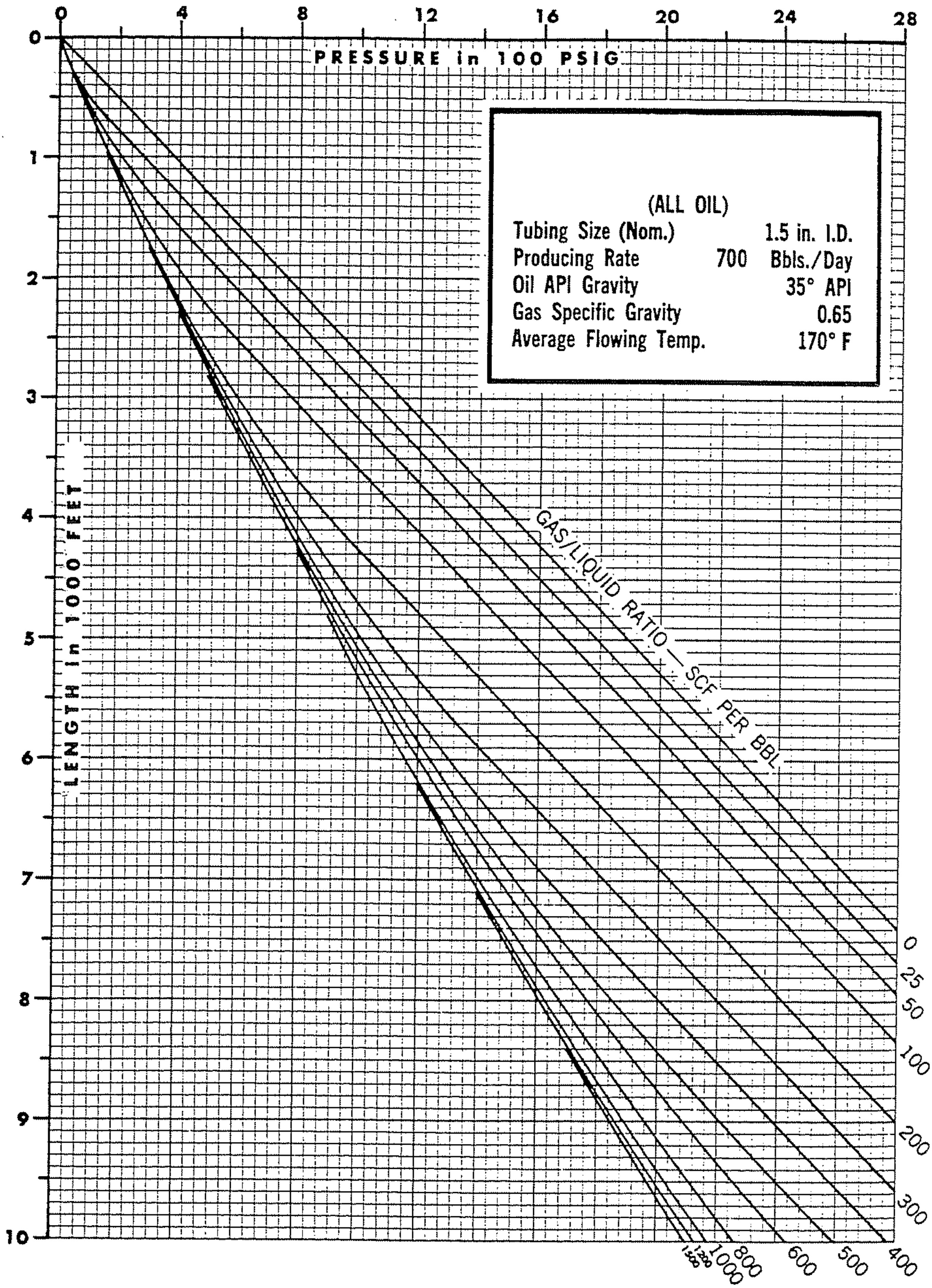

Figure 4.2(7) Vertical Flowing Pressure Gradients

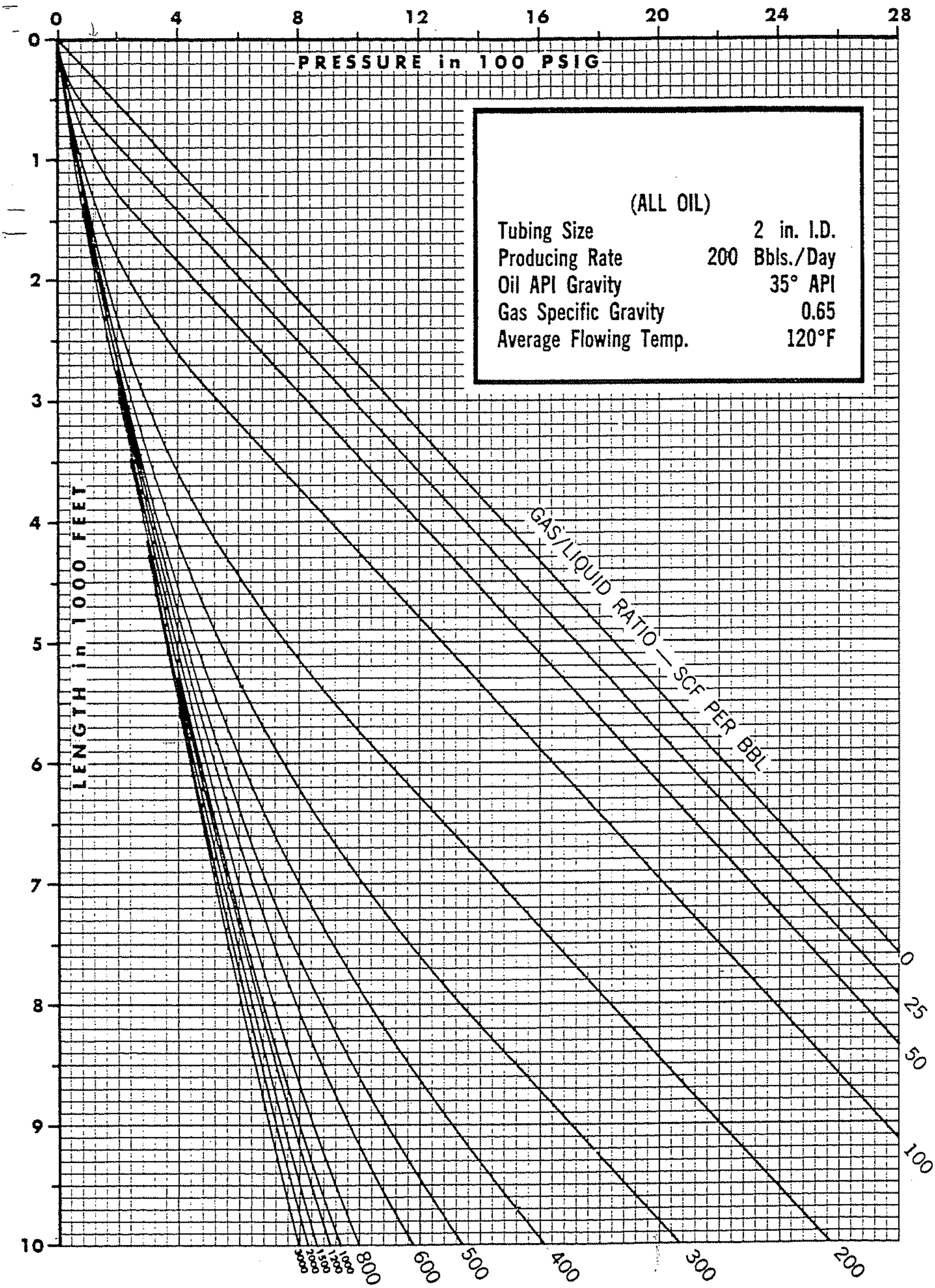

Figure 4.2(8) Vertical Flowing Pressure Gradients

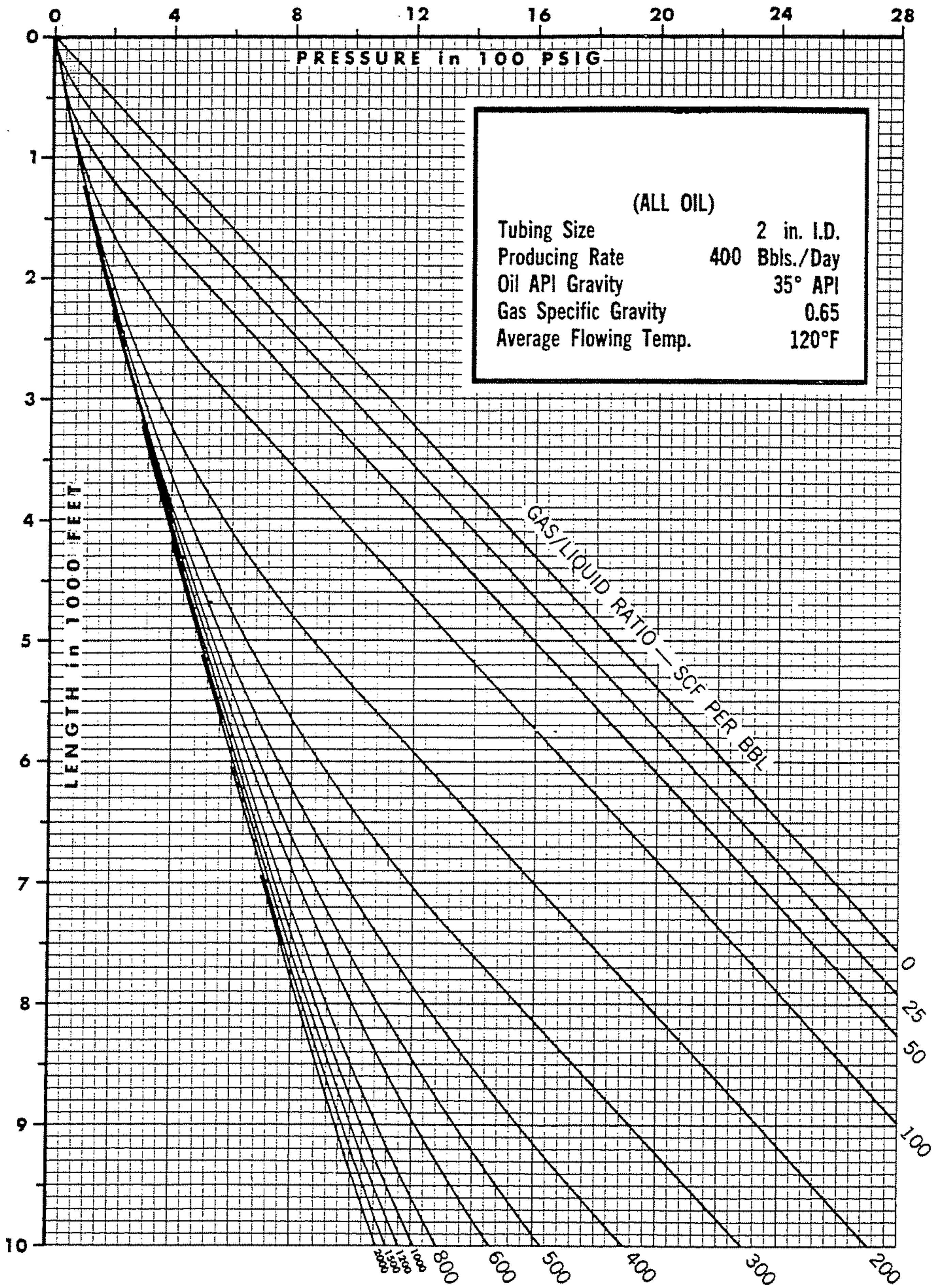

Figure 4.2(9) Vertical Flowing Pressure Gradients

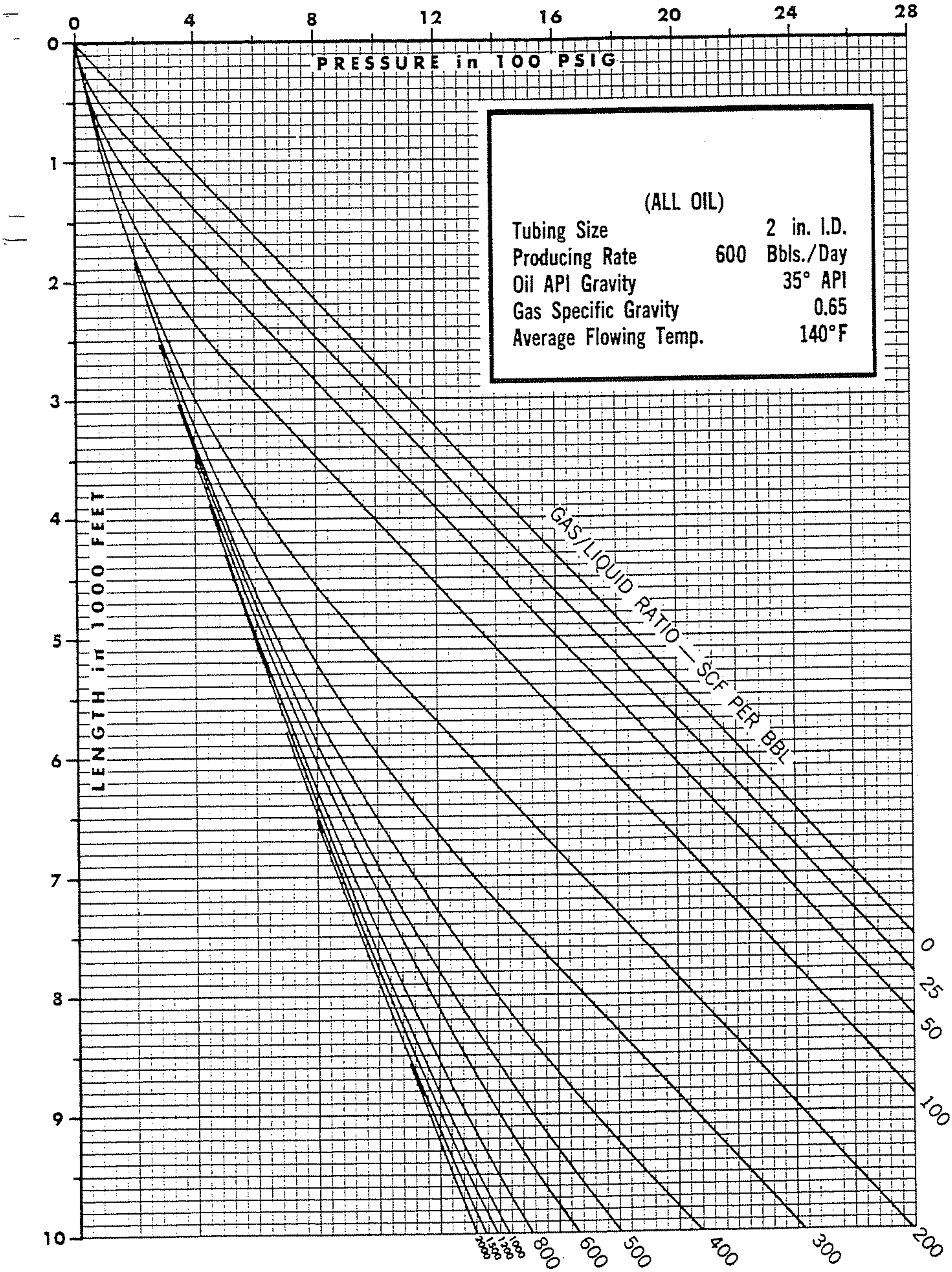

Figure 4.2(10) Vertical Flowing Pressure Gradients

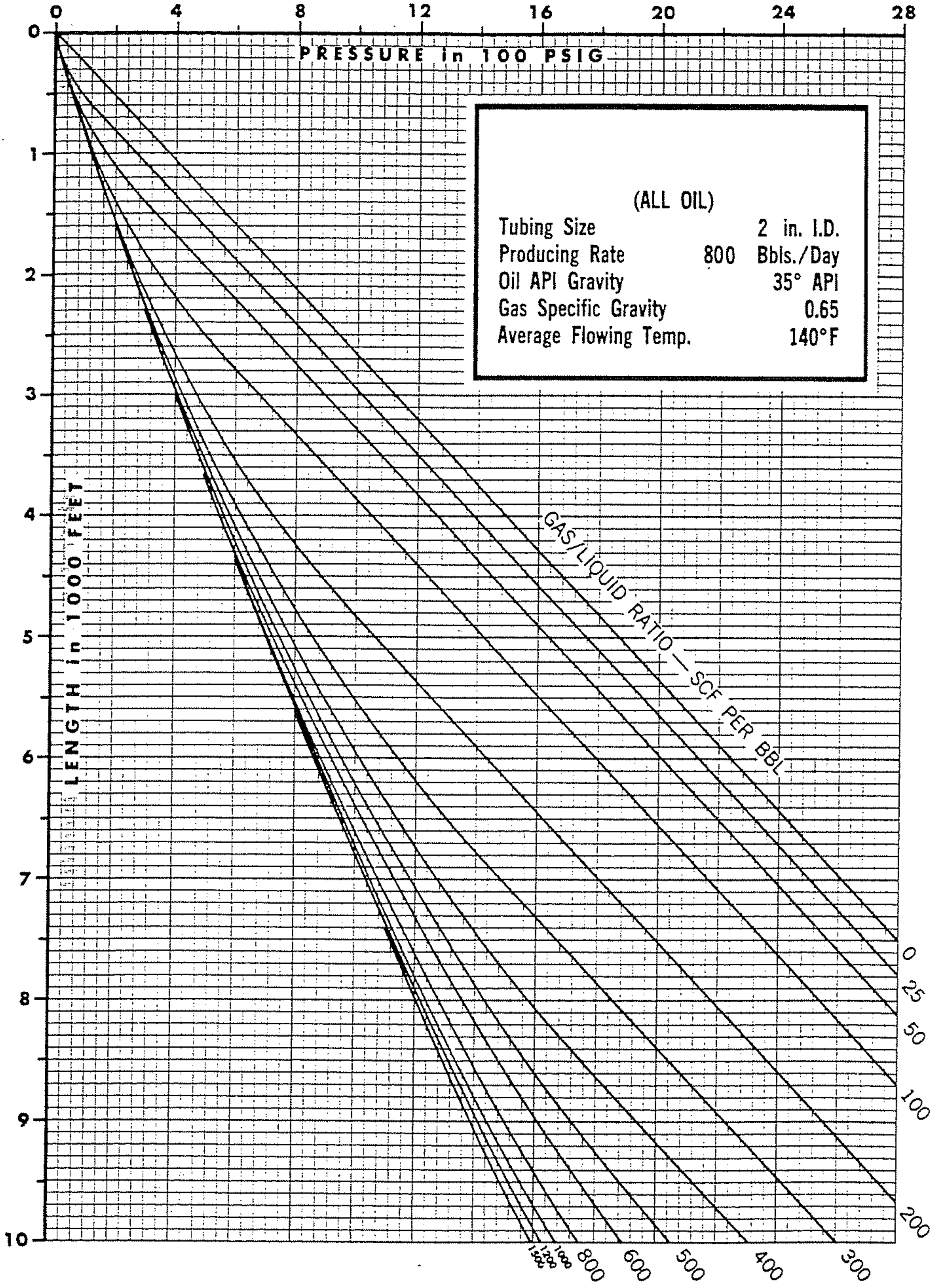

Figure 4.2(11) Vertical Flowing Pressure Gradients

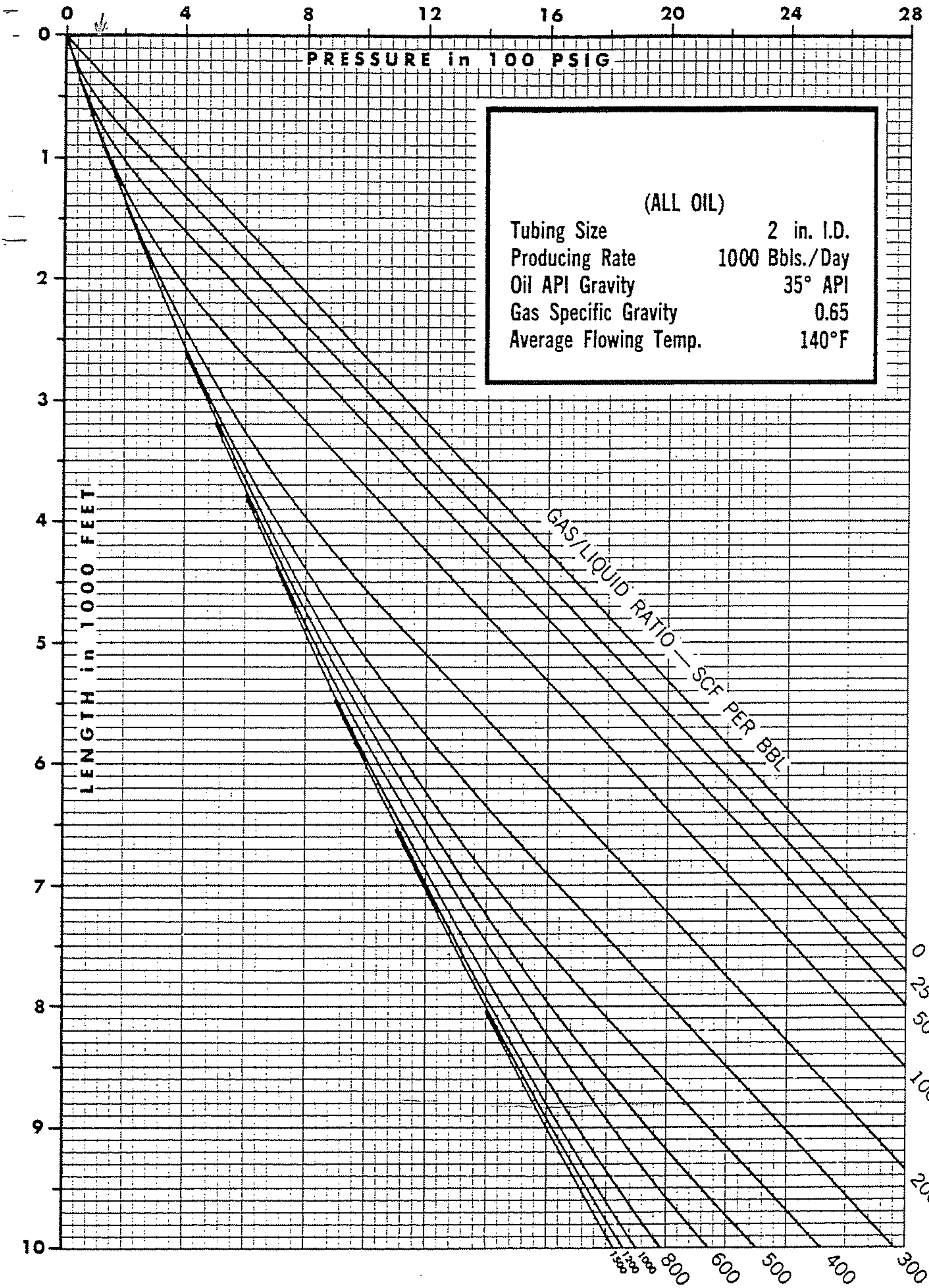

Figure 4.2(12) Vertical Flowing Pressure Gradients

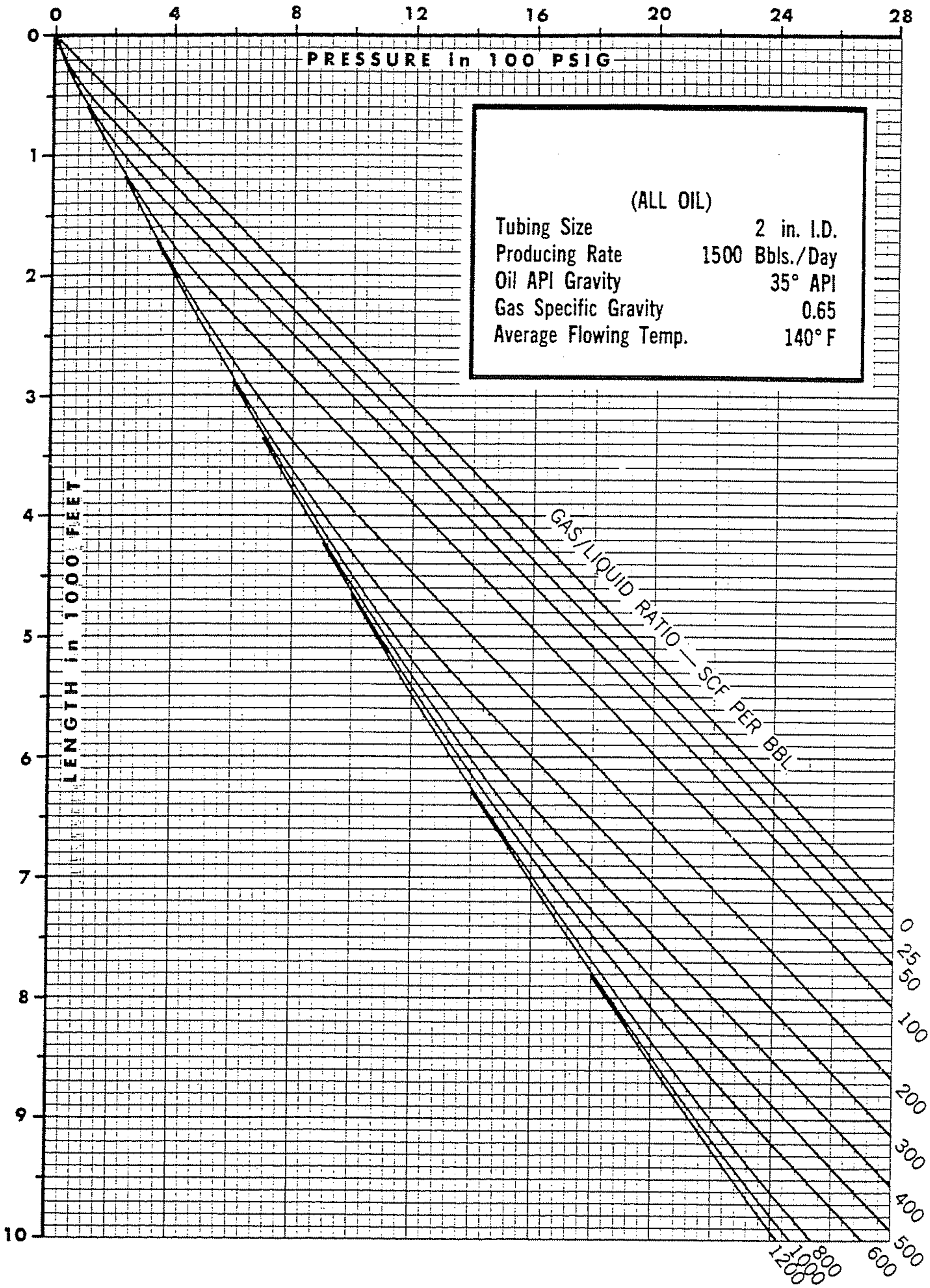

Figure 4.2(13) Vertical Flowing Pressure Gradients

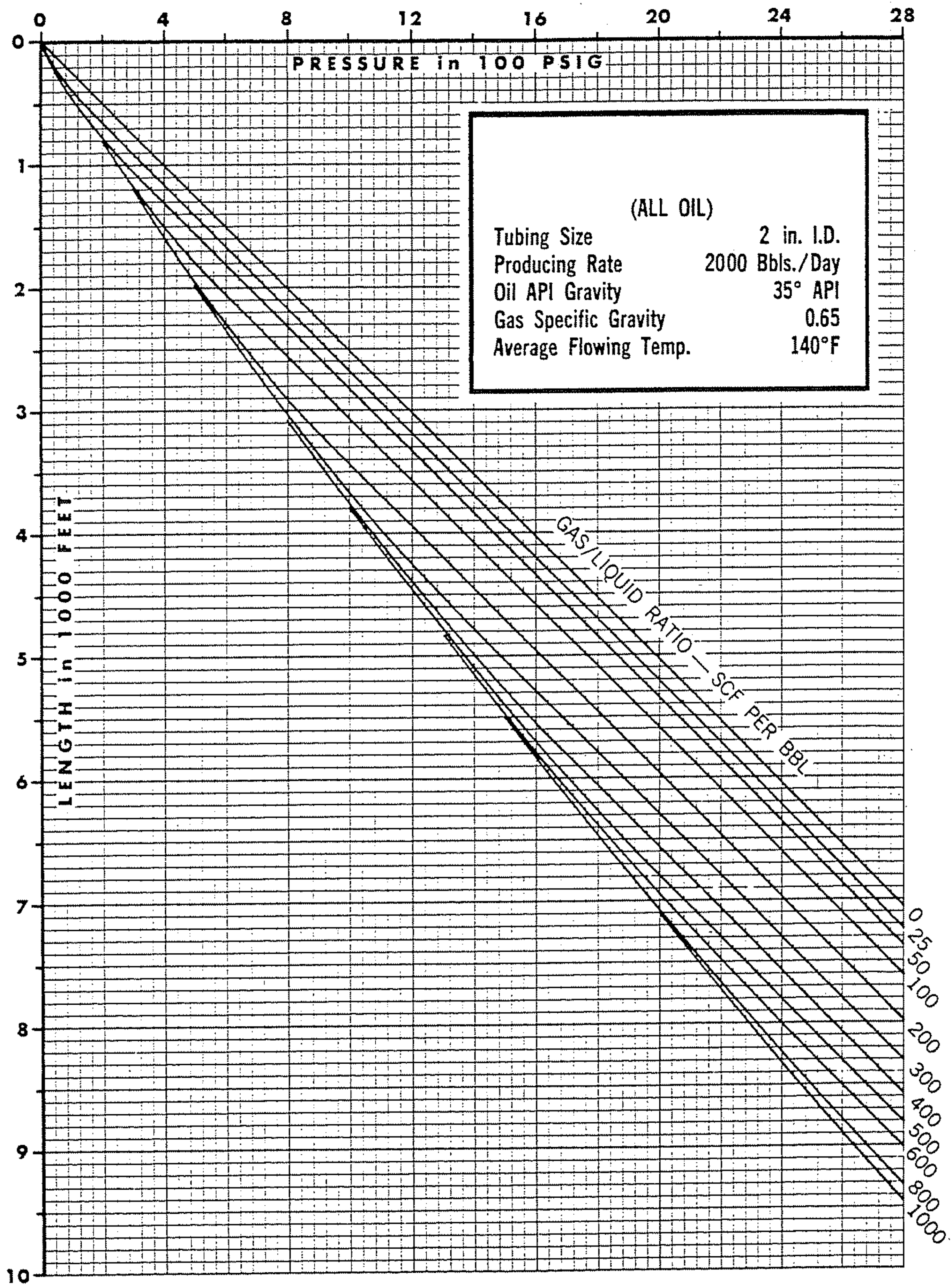

Figure 4.2(14) Vertical Flowing Pressure Gradients

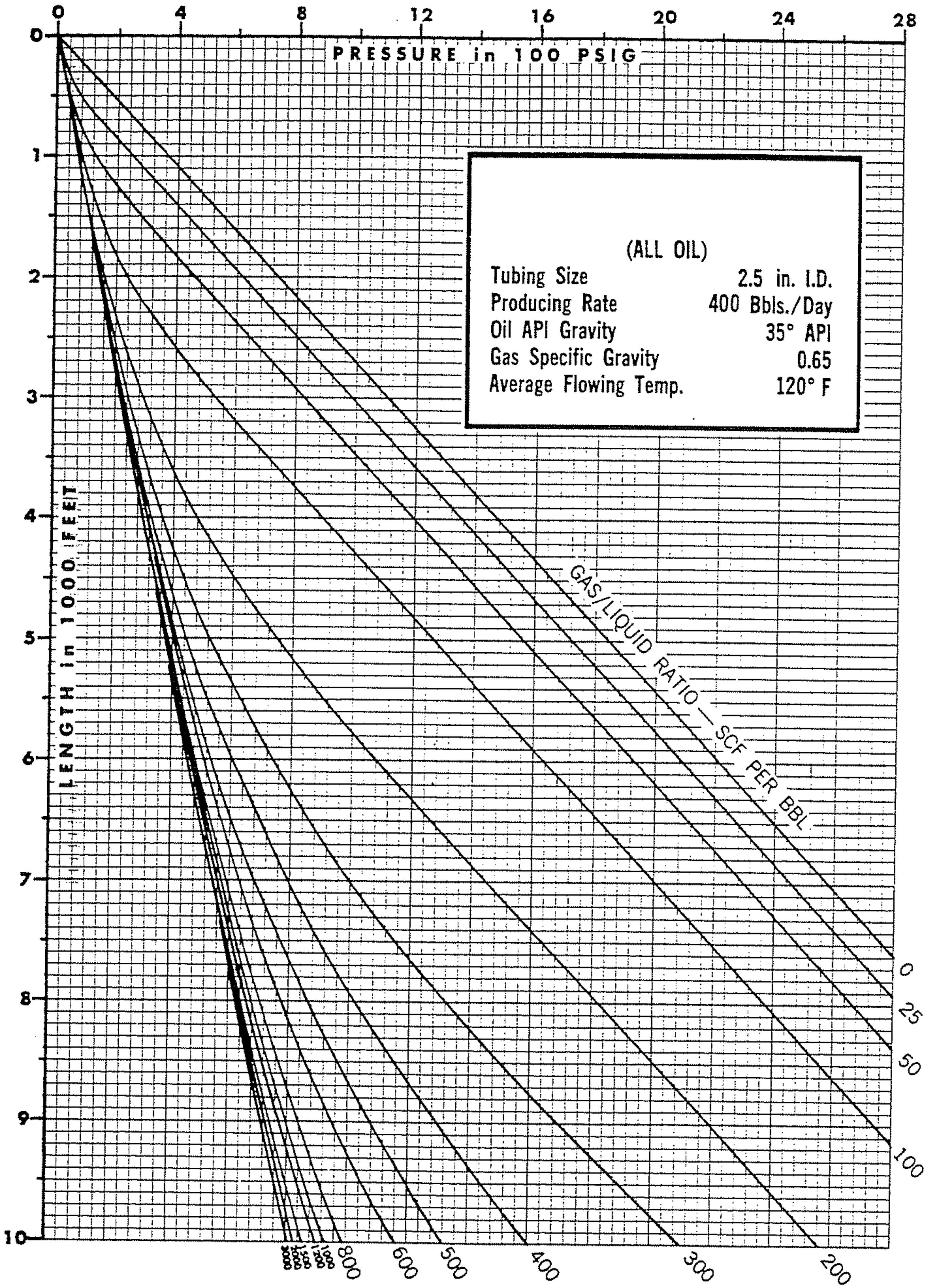

Figure 4.2(15) Vertical Flowing Pressure Gradients

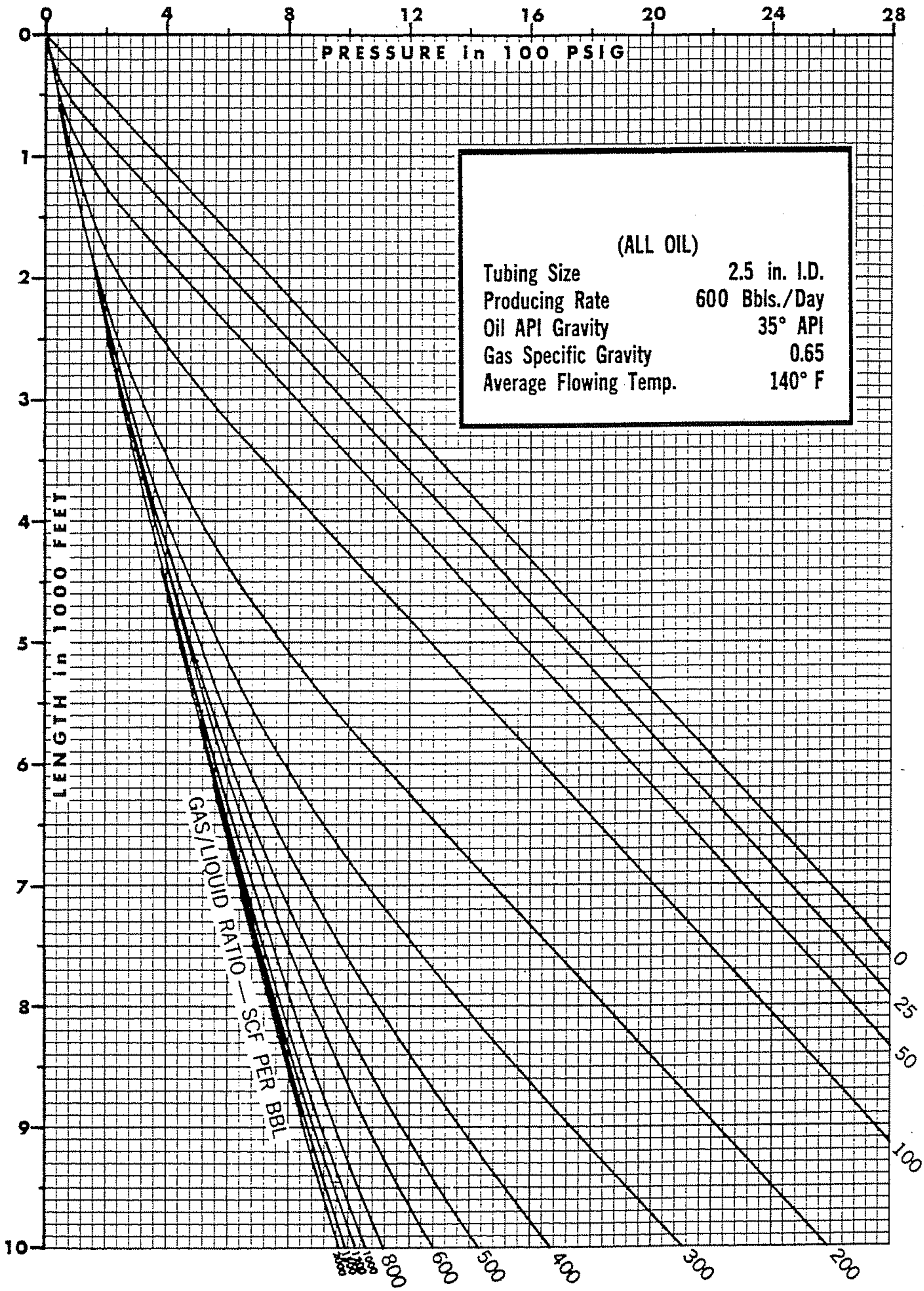

Figure 4.2(16) Vertical Flowing Pressure Gradients

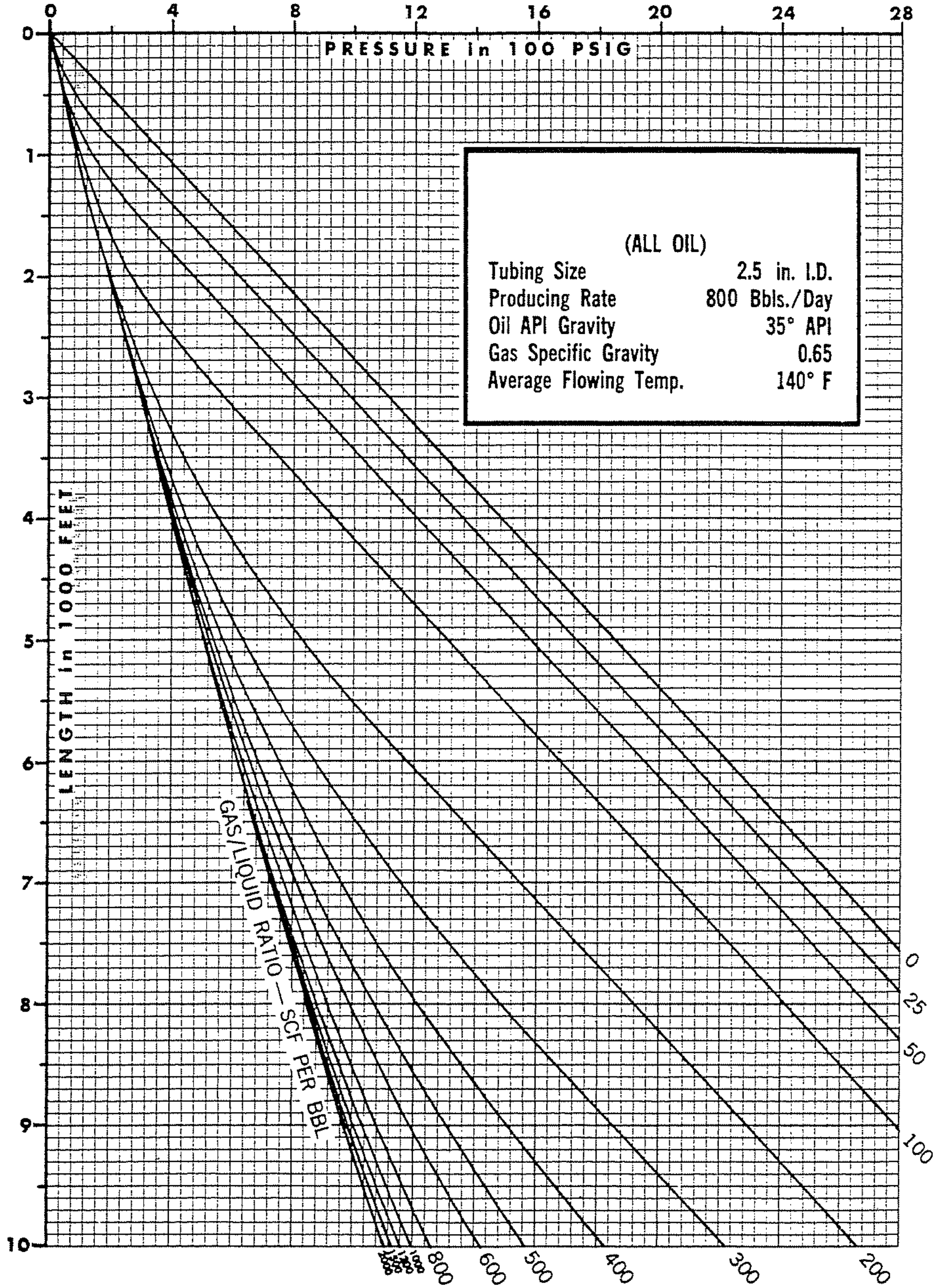

Figure 4.2(17) Vertical Flowing Pressure Gradients

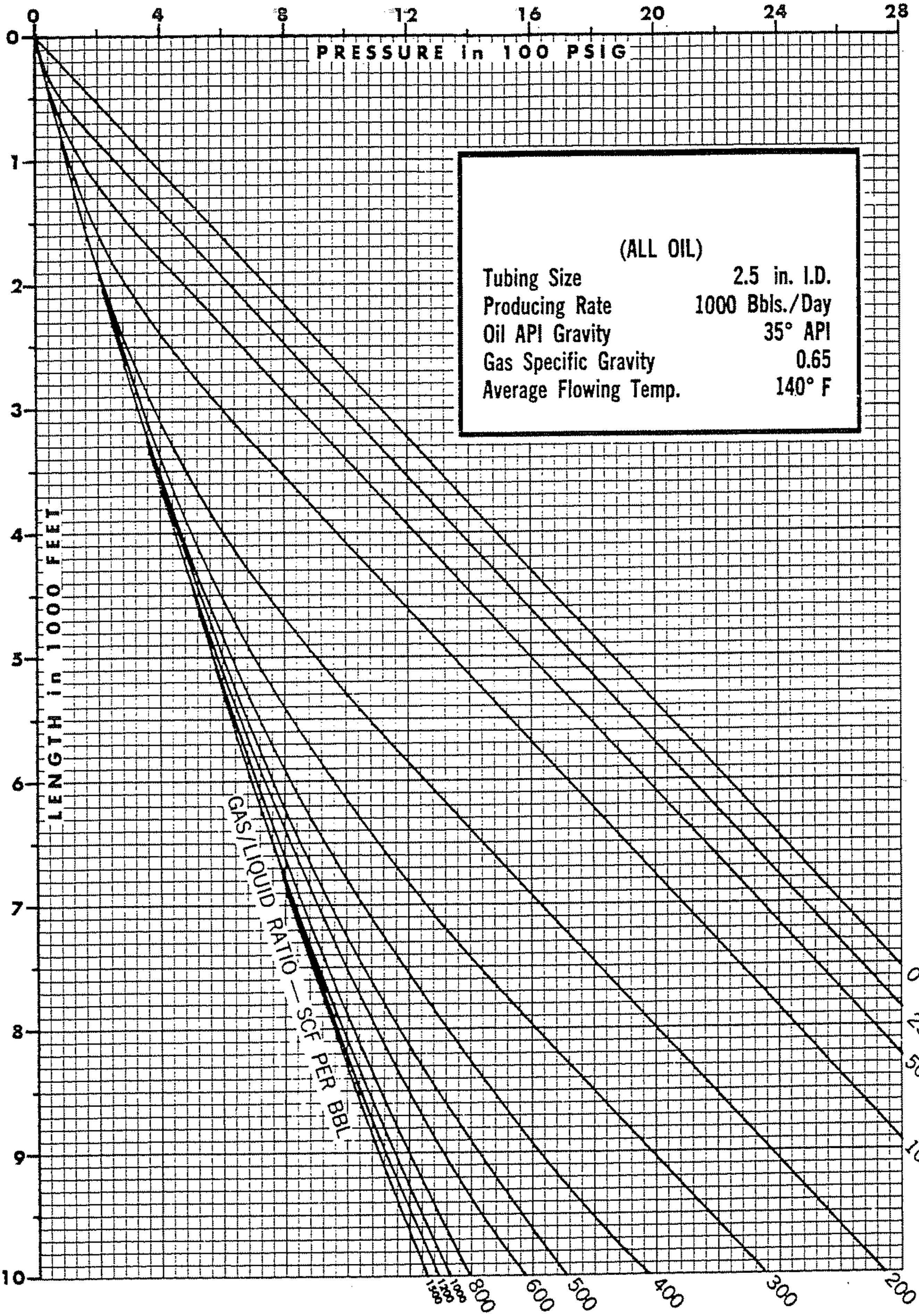

Figure 4.2(18) Vertical Flowing Pressure Gradients

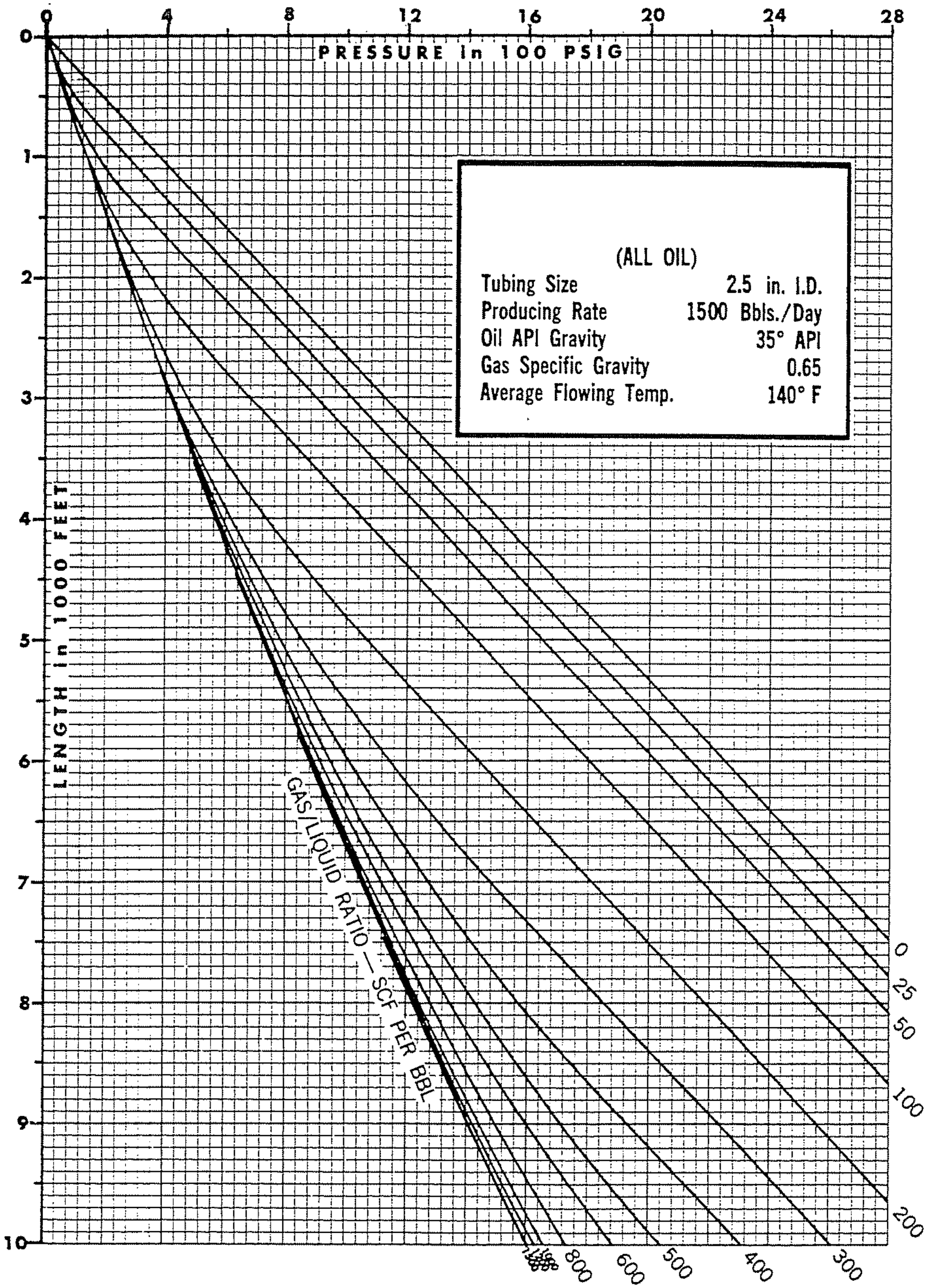

Figure 4.2(19) Vertical Flowing Pressure Gradients

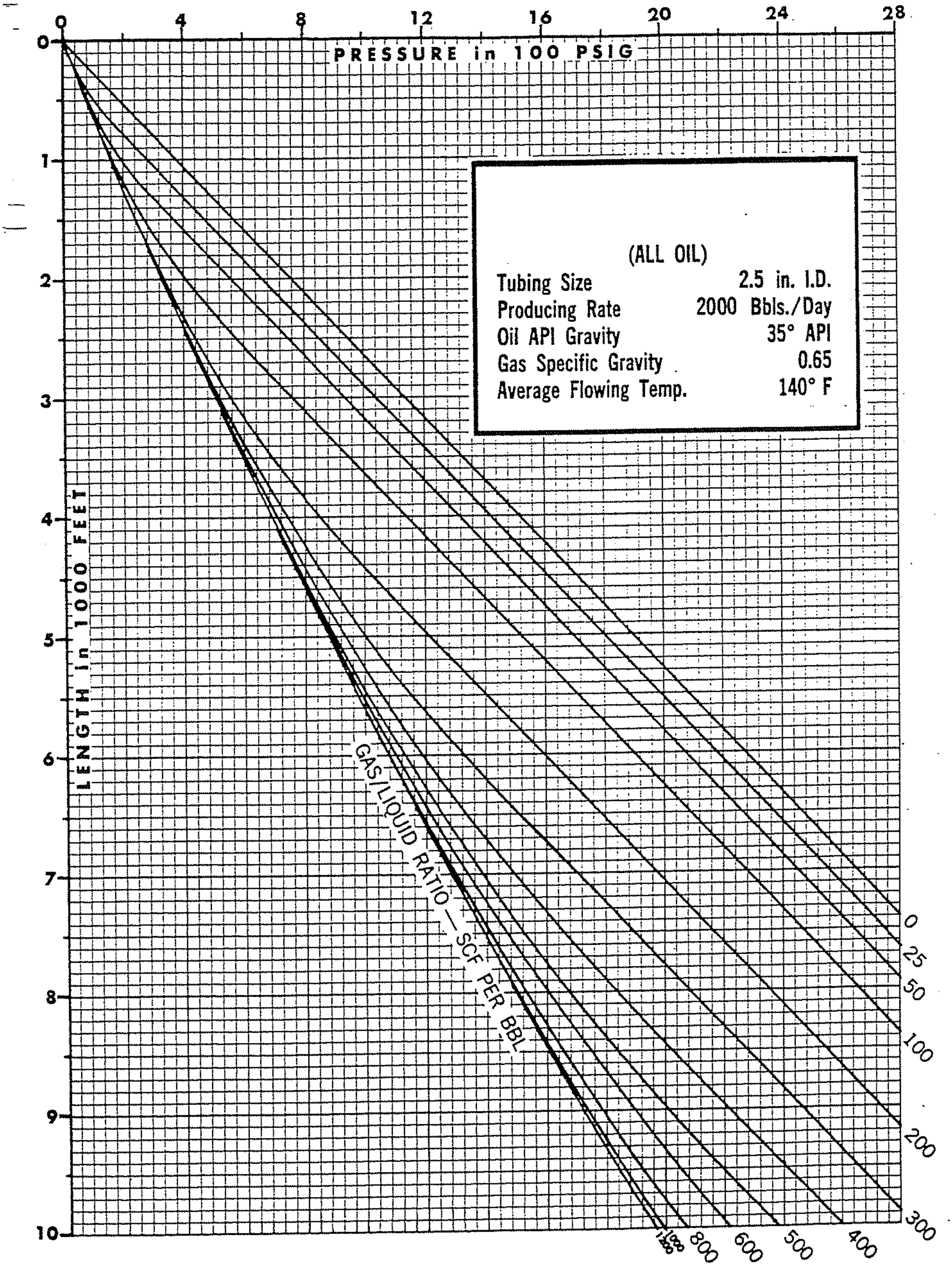

Figure 4.2(20) Vertical Flowing Pressure Gradients

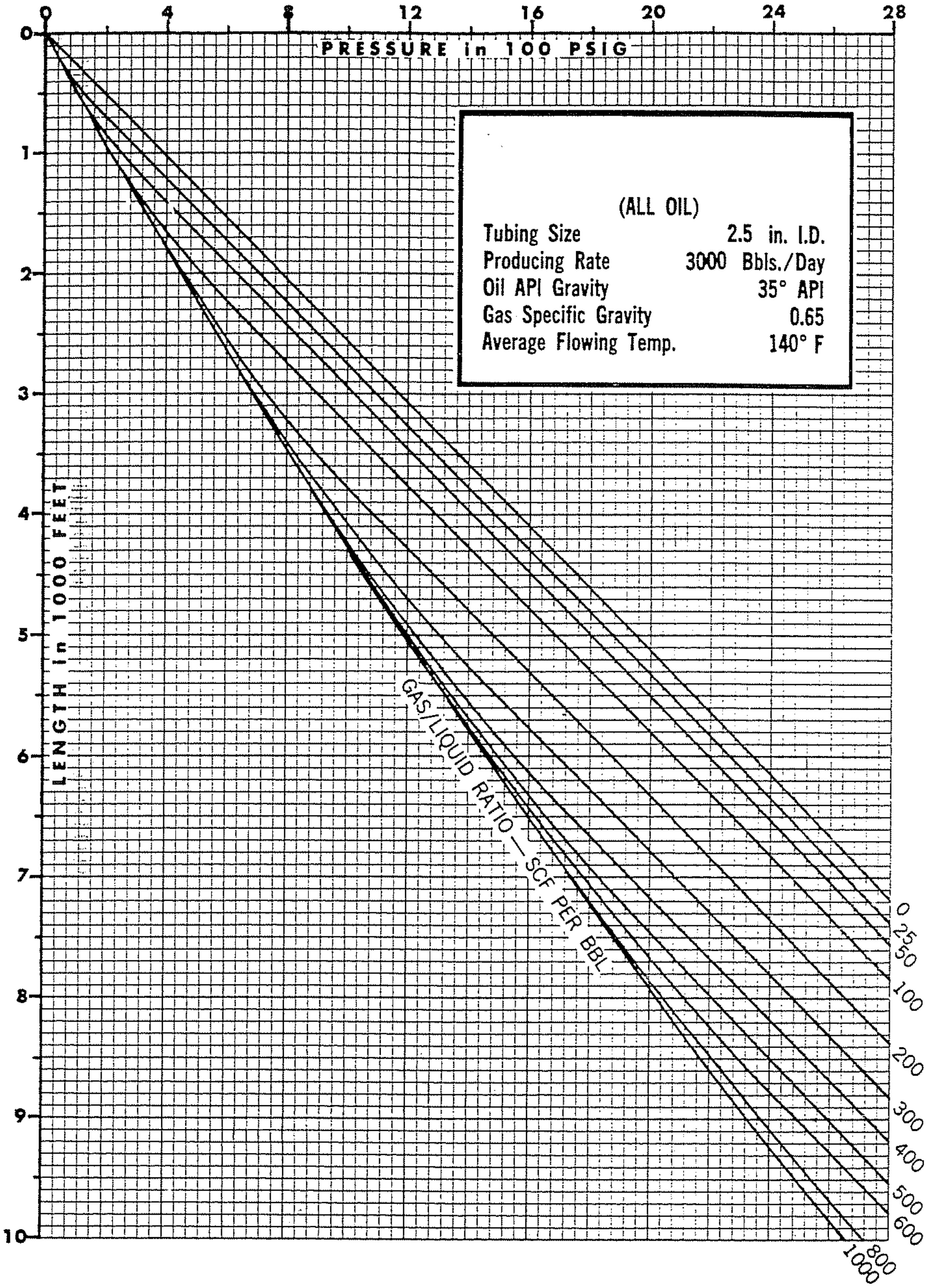

Figure 4.2(21) Vertical Flowing Pressure Gradients

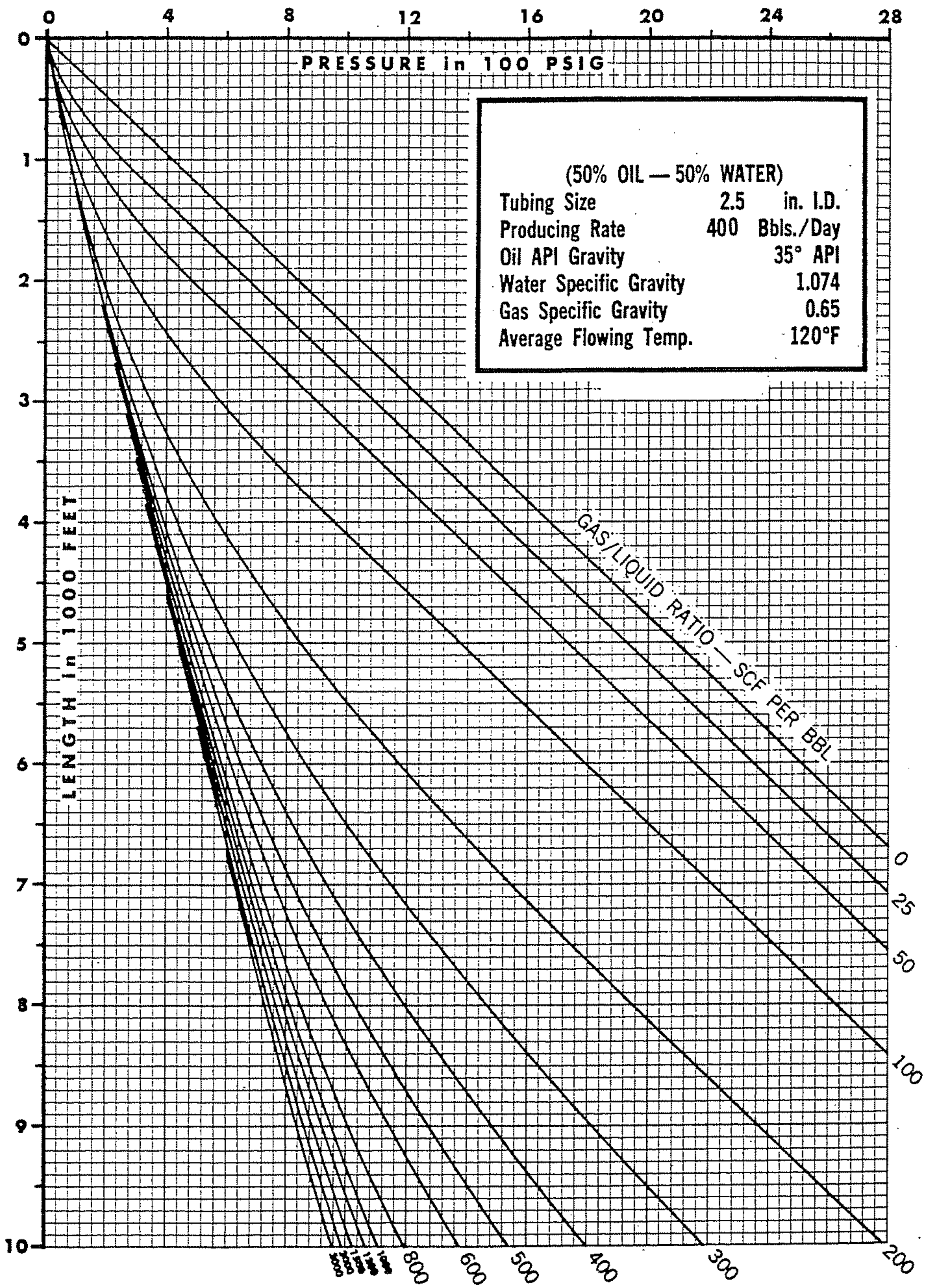

Figure 4.2(22) Vertical Flowing Pressure Gradients

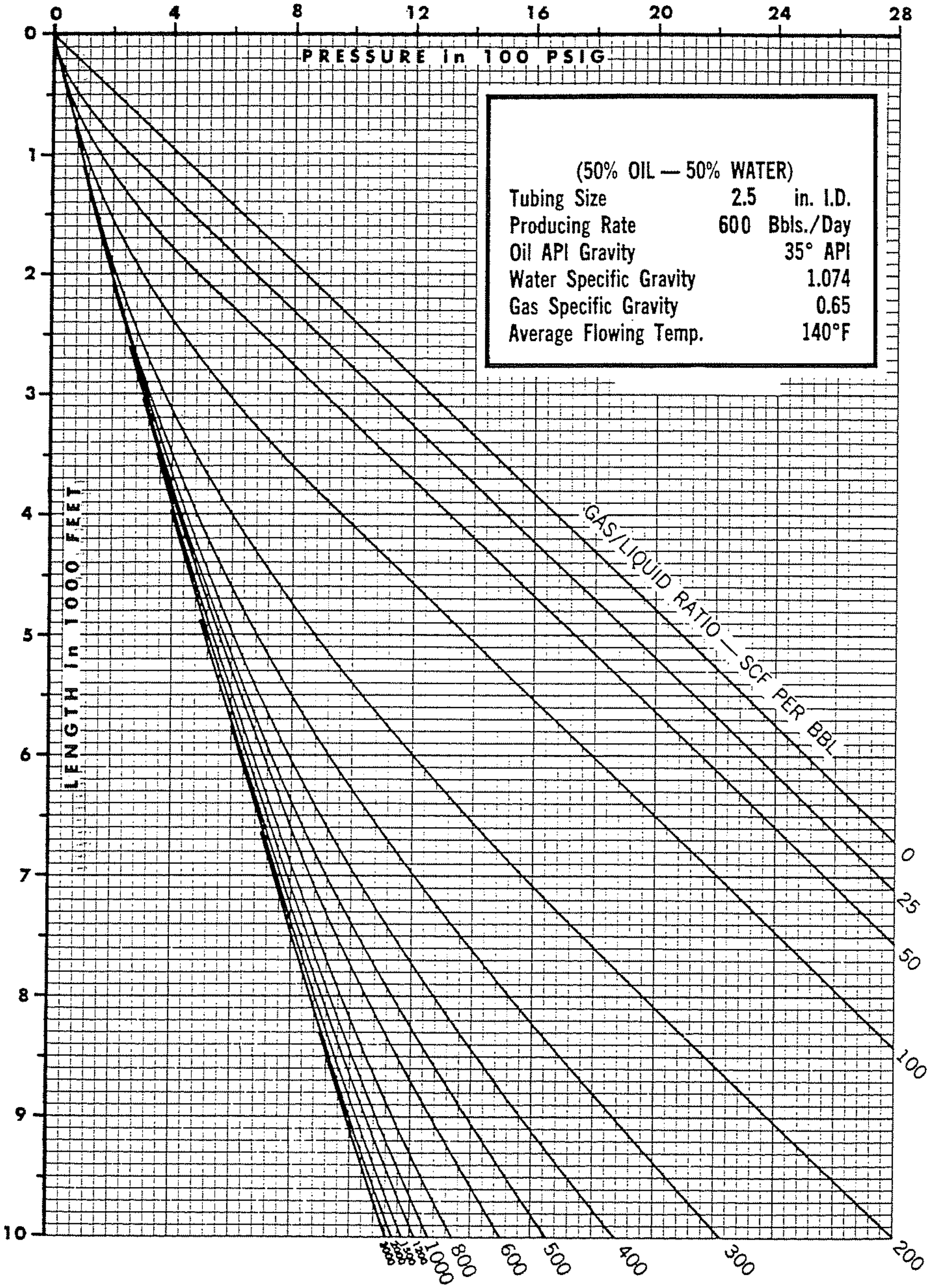

Figure 4.2(23) Vertical Flowing Pressure Gradients

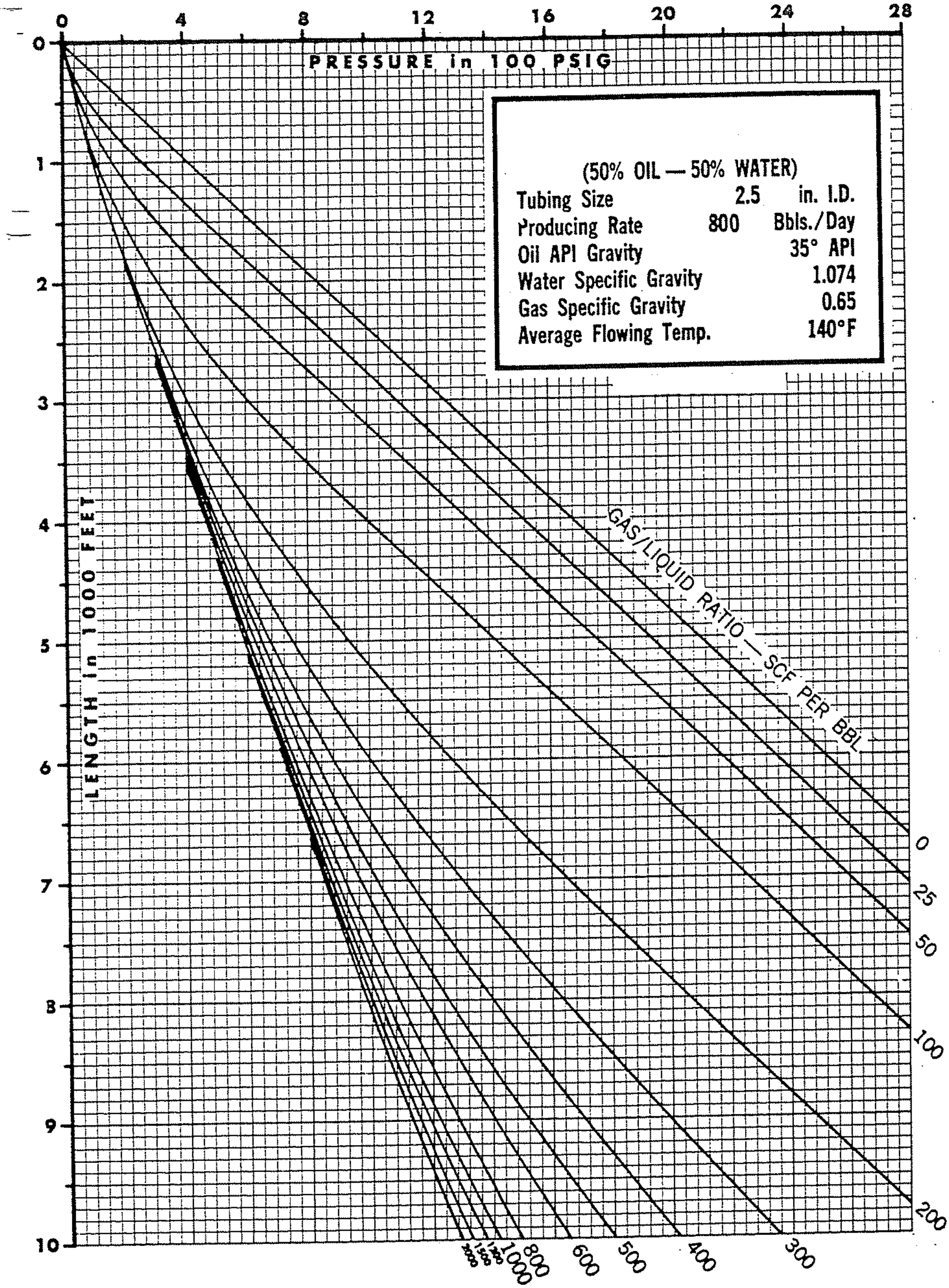

Figure 4.2(24) Vertical Flowing Pressure Gradients

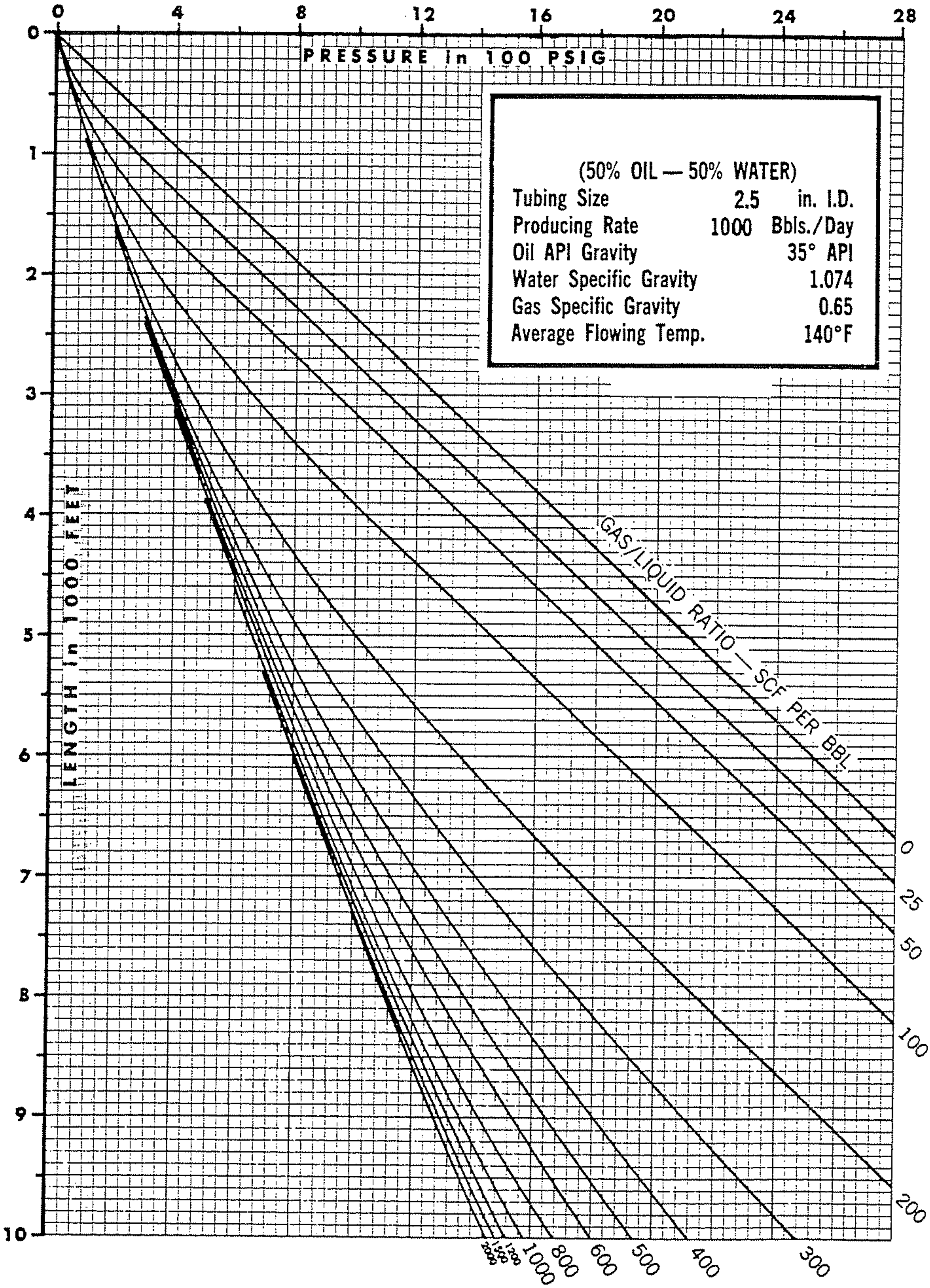

Figure 4.2(25) Vertical Flowing Pressure Gradients

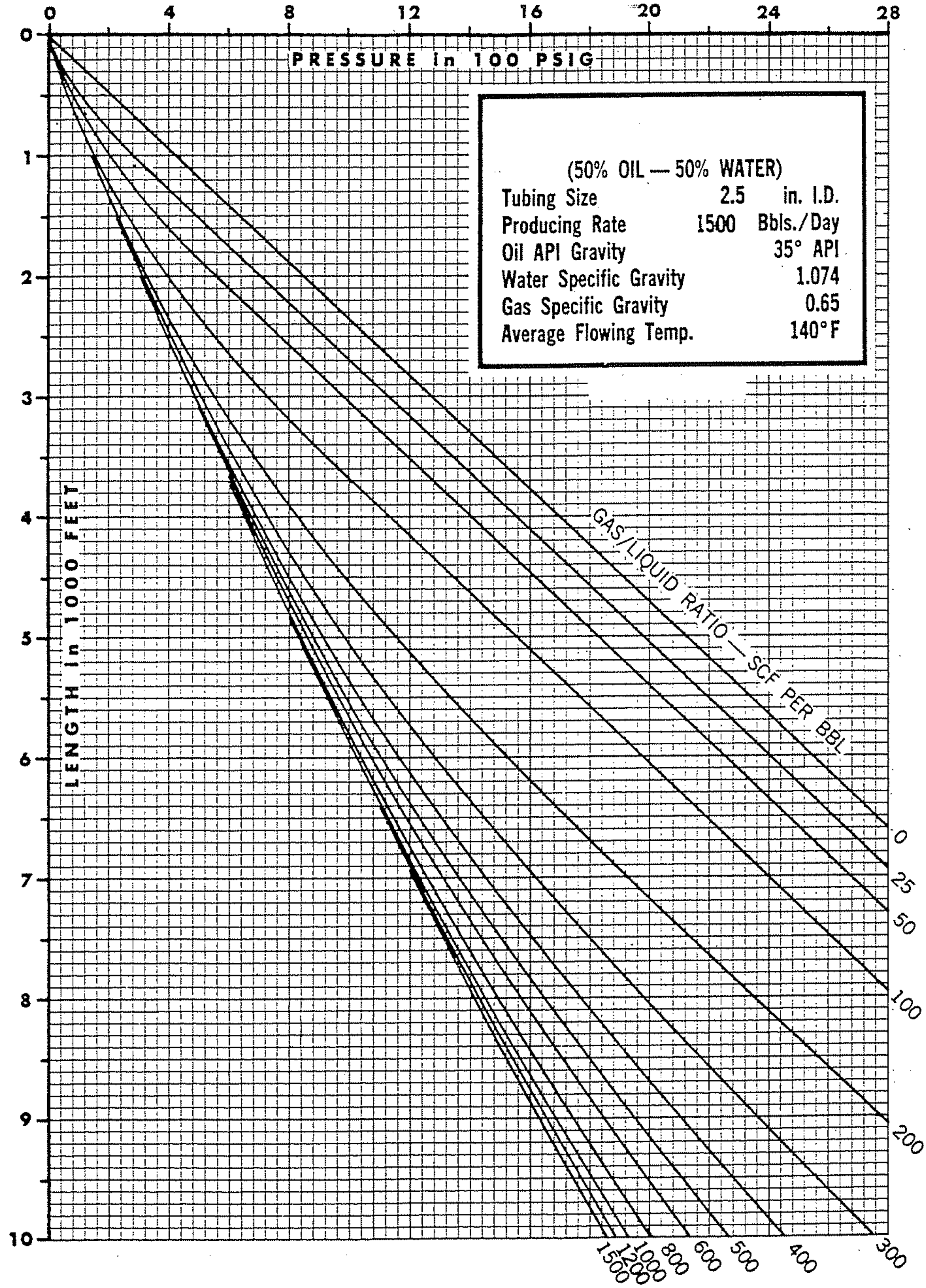

Figure 4.2(26) Vertical Flowing Pressure Gradients

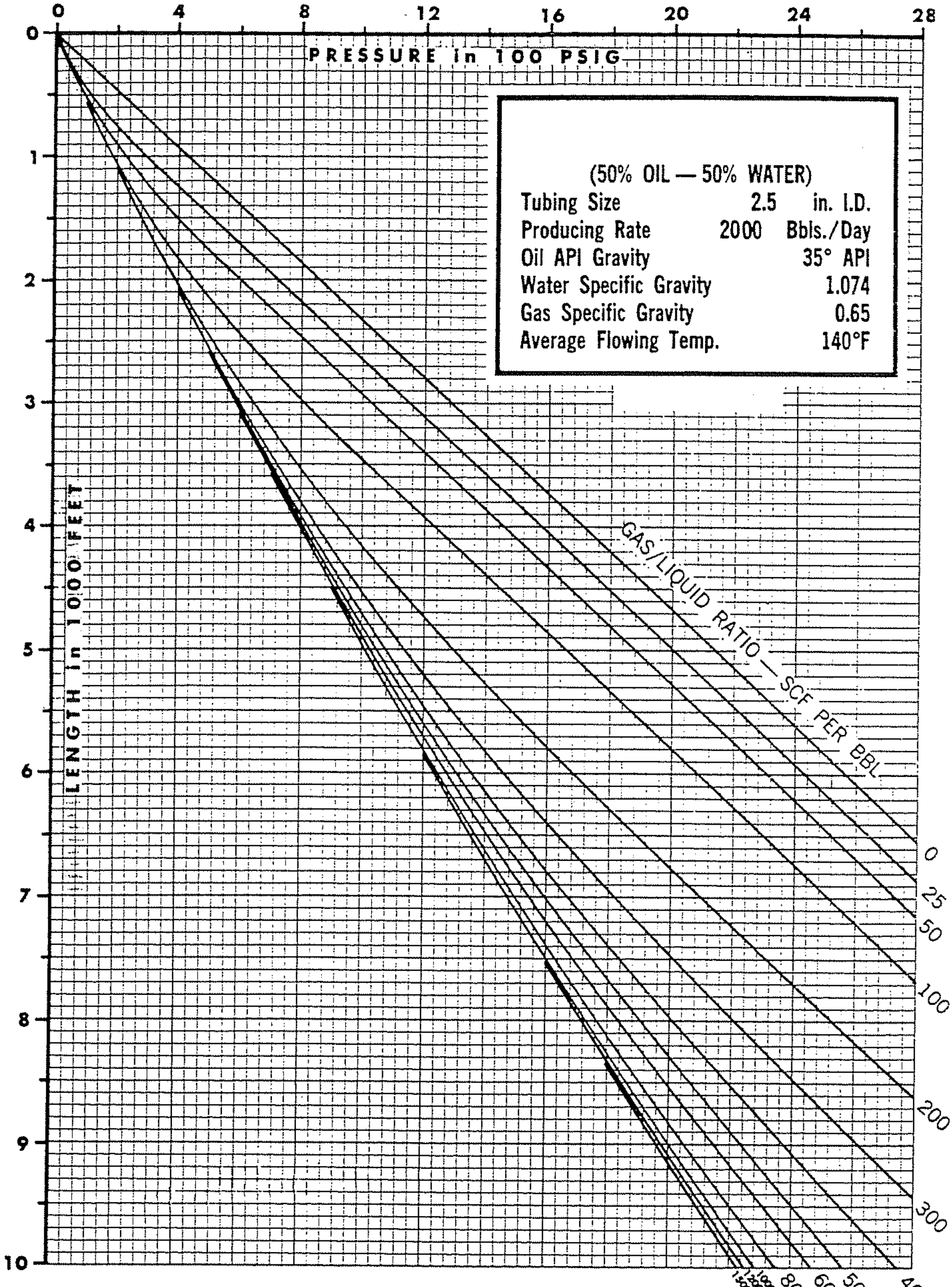

Figure 4.2(27) Vertical Flowing Pressure Gradients

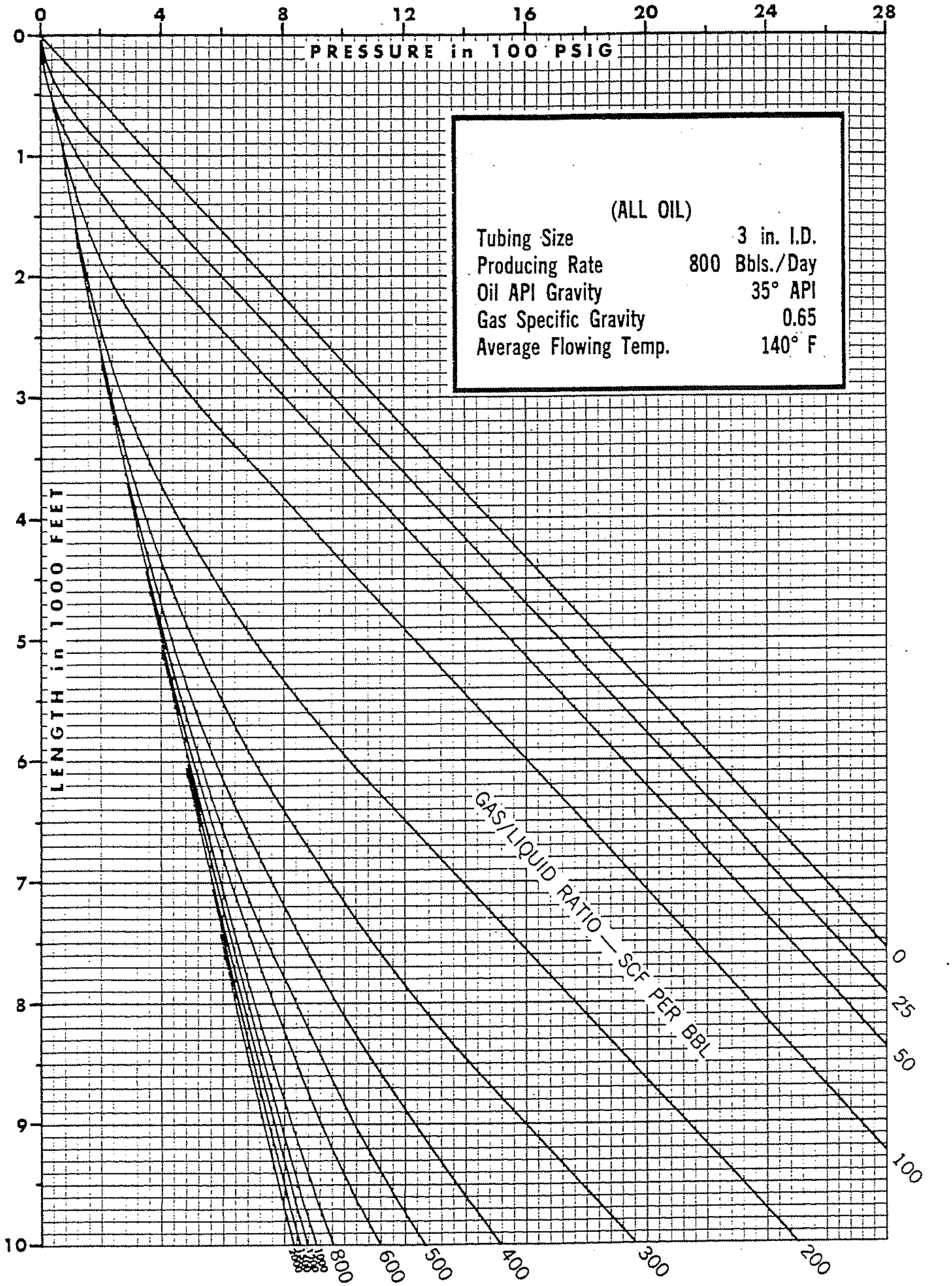

Figure 4.2(28) Vertical Flowing Pressure Gradients

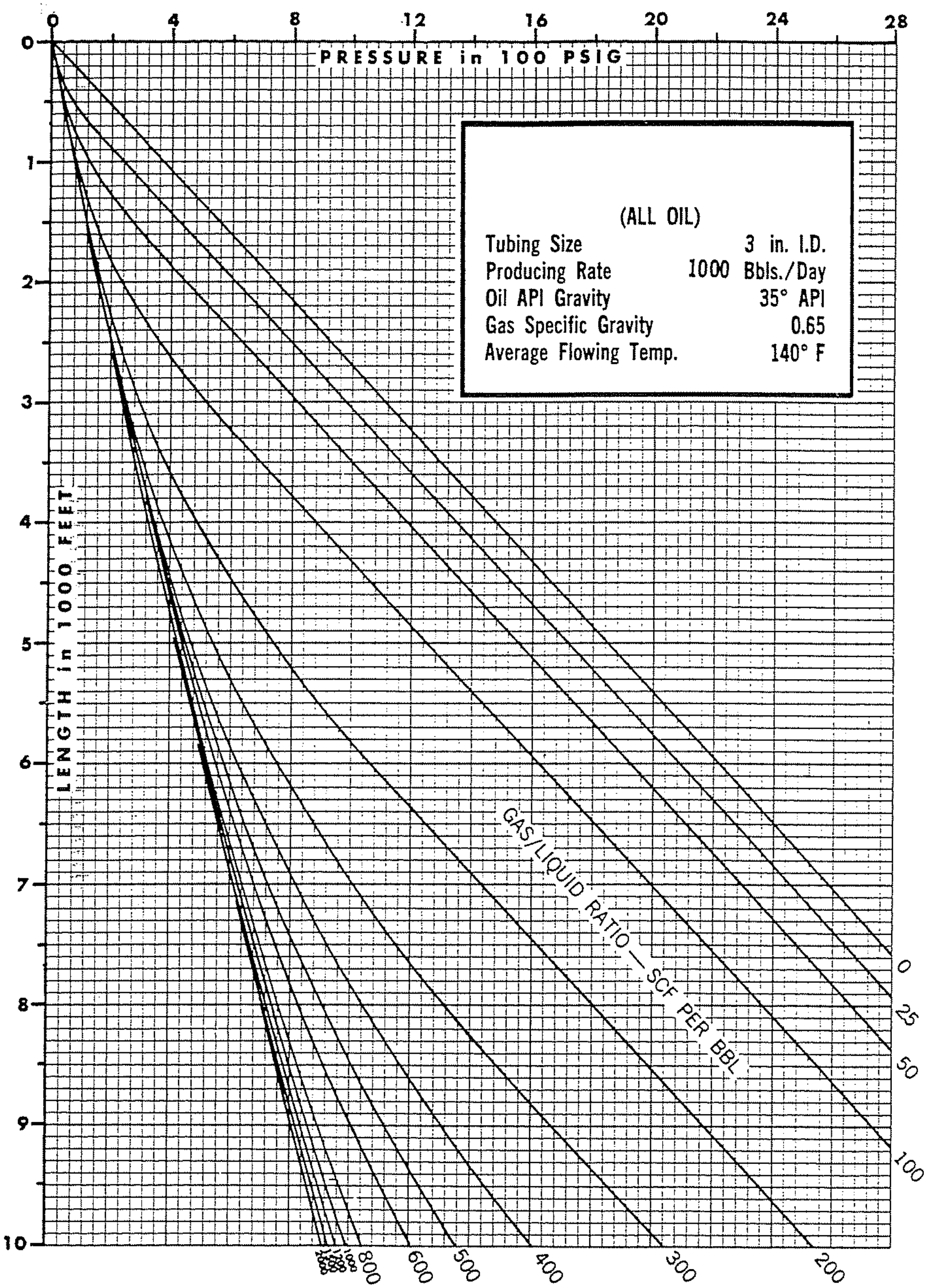

Figure 4.2(29) Vertical Flowing Pressure Gradients

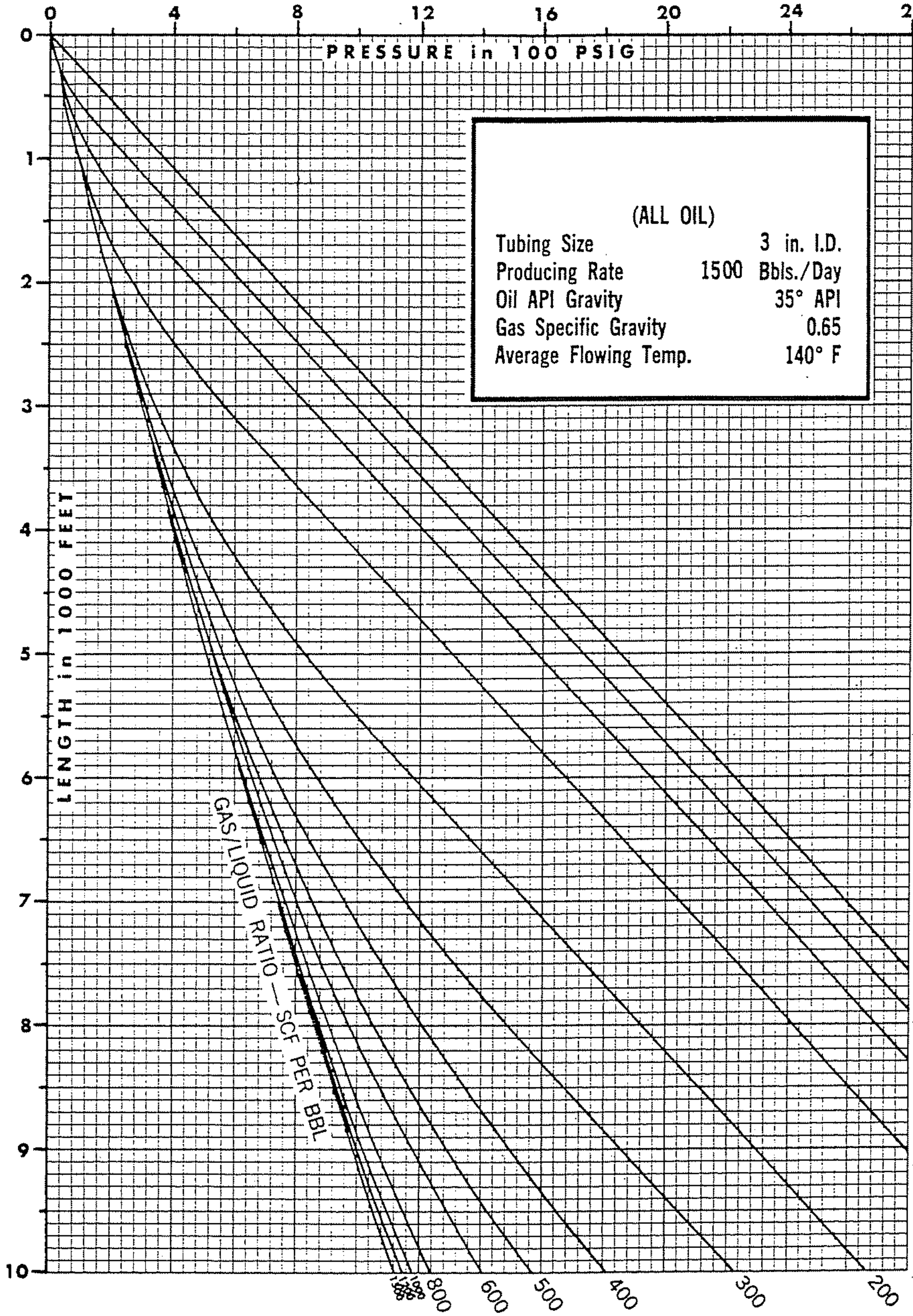

Figure 4.2(30) Vertical Flowing Pressure Gradients

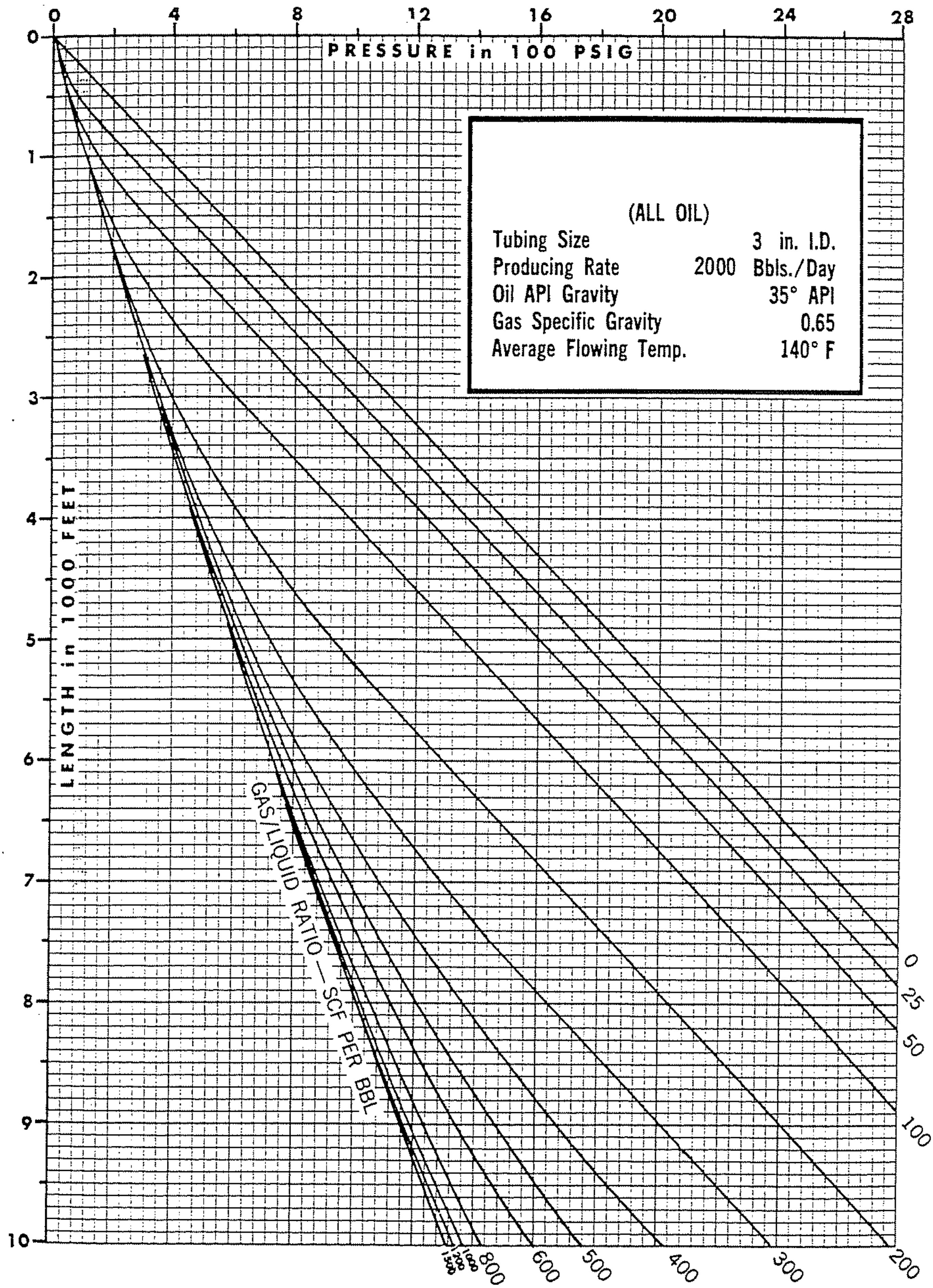

Figure 4.2(31) Vertical Flowing Pressure Gradients

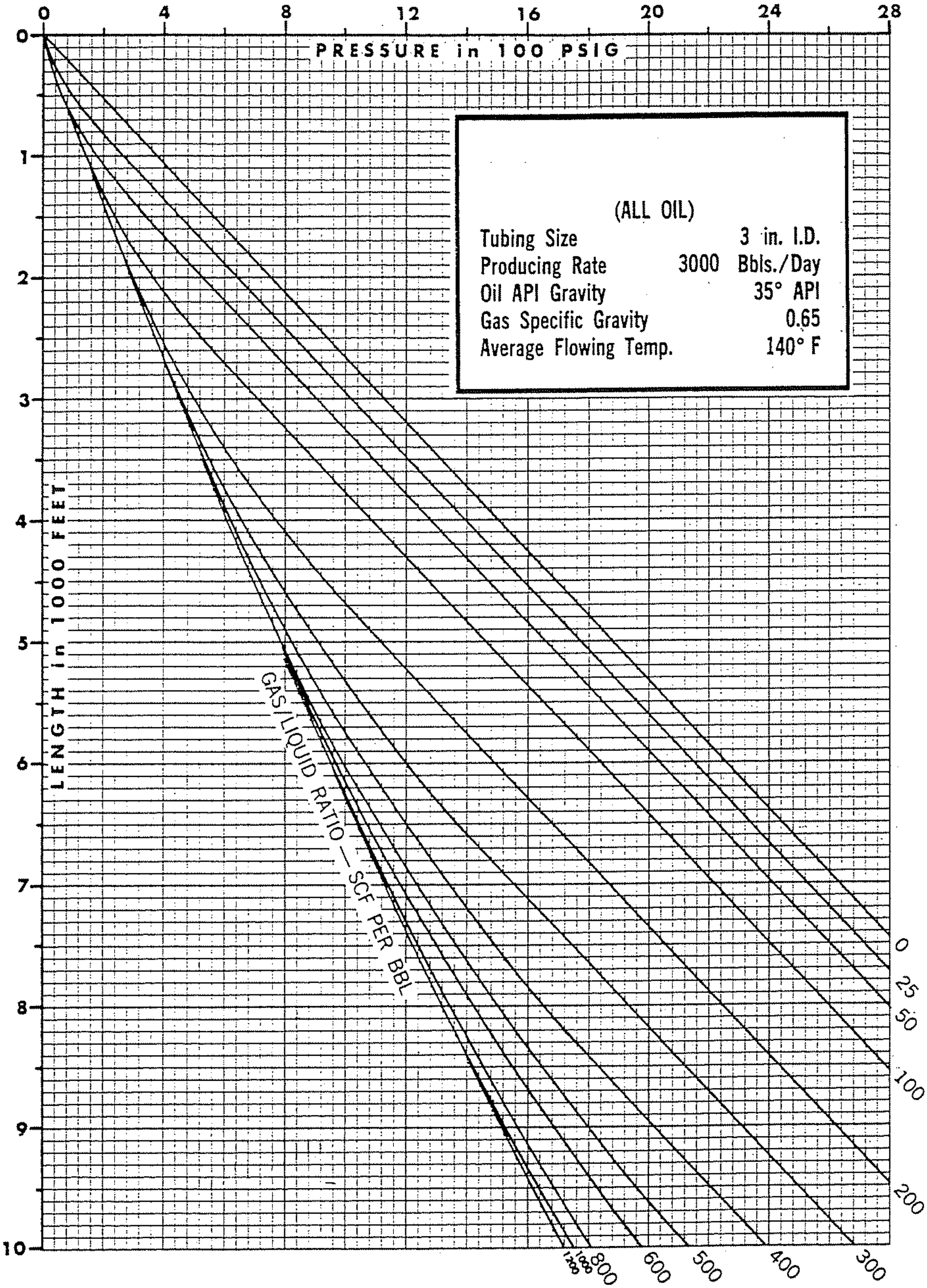

Figure 4.2(32) Vertical Flowing Pressure Gradients

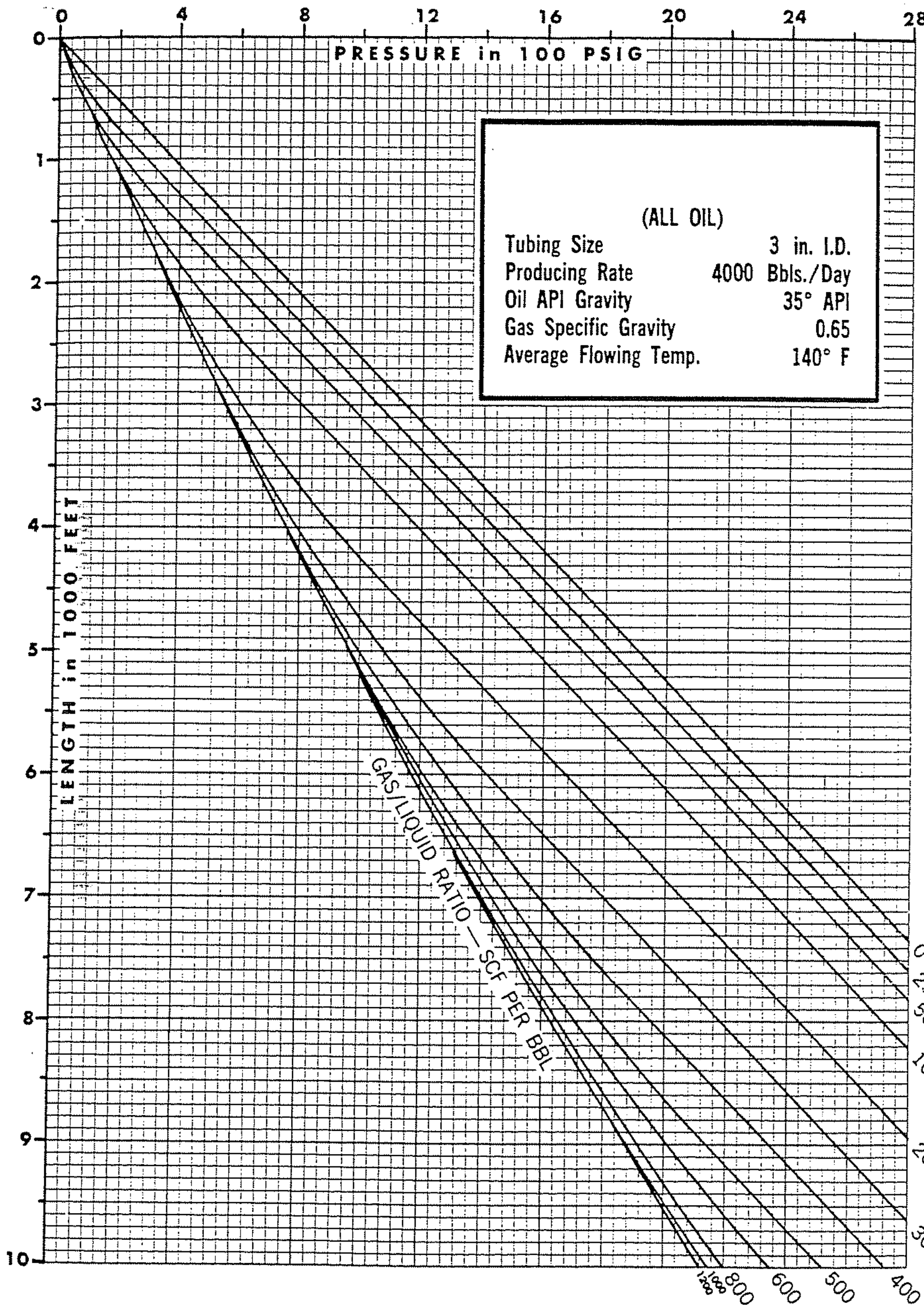

Figure 4.2(33) Vertical Flowing Pressure Gradients

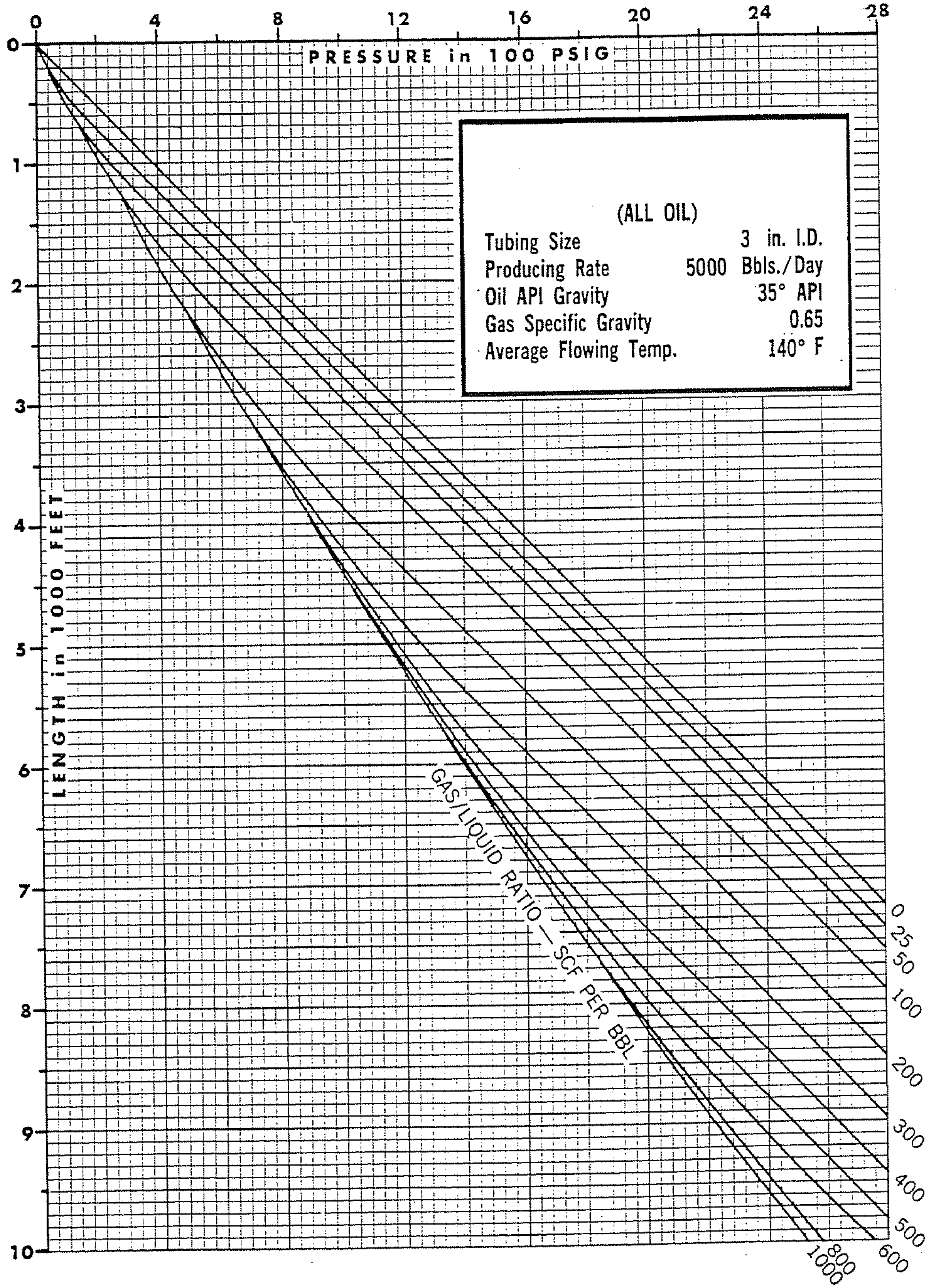

Figure 4.2(34) Vertical Flowing Pressure Gradients

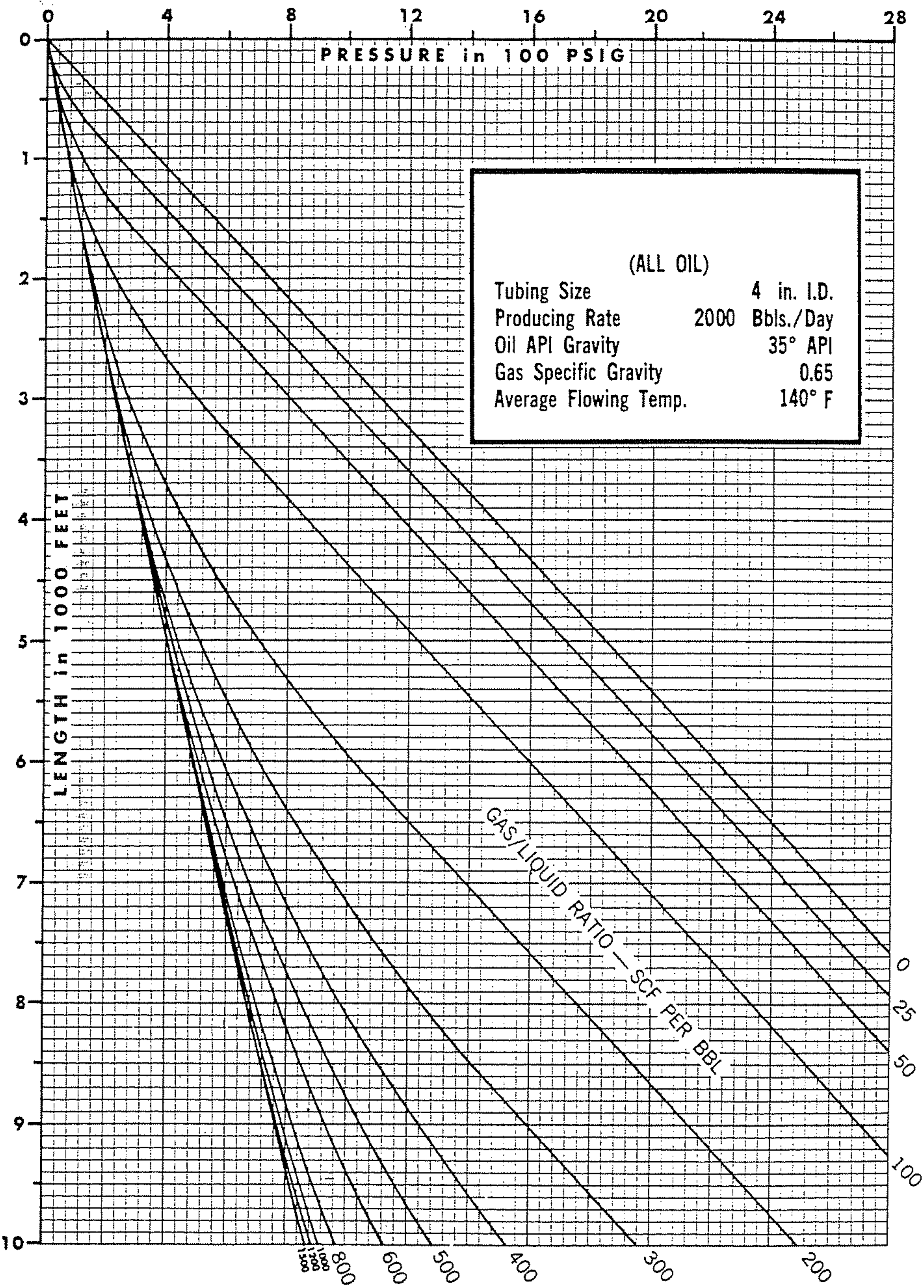

Figure 4.2(35) Vertical Flowing Pressure Gradients

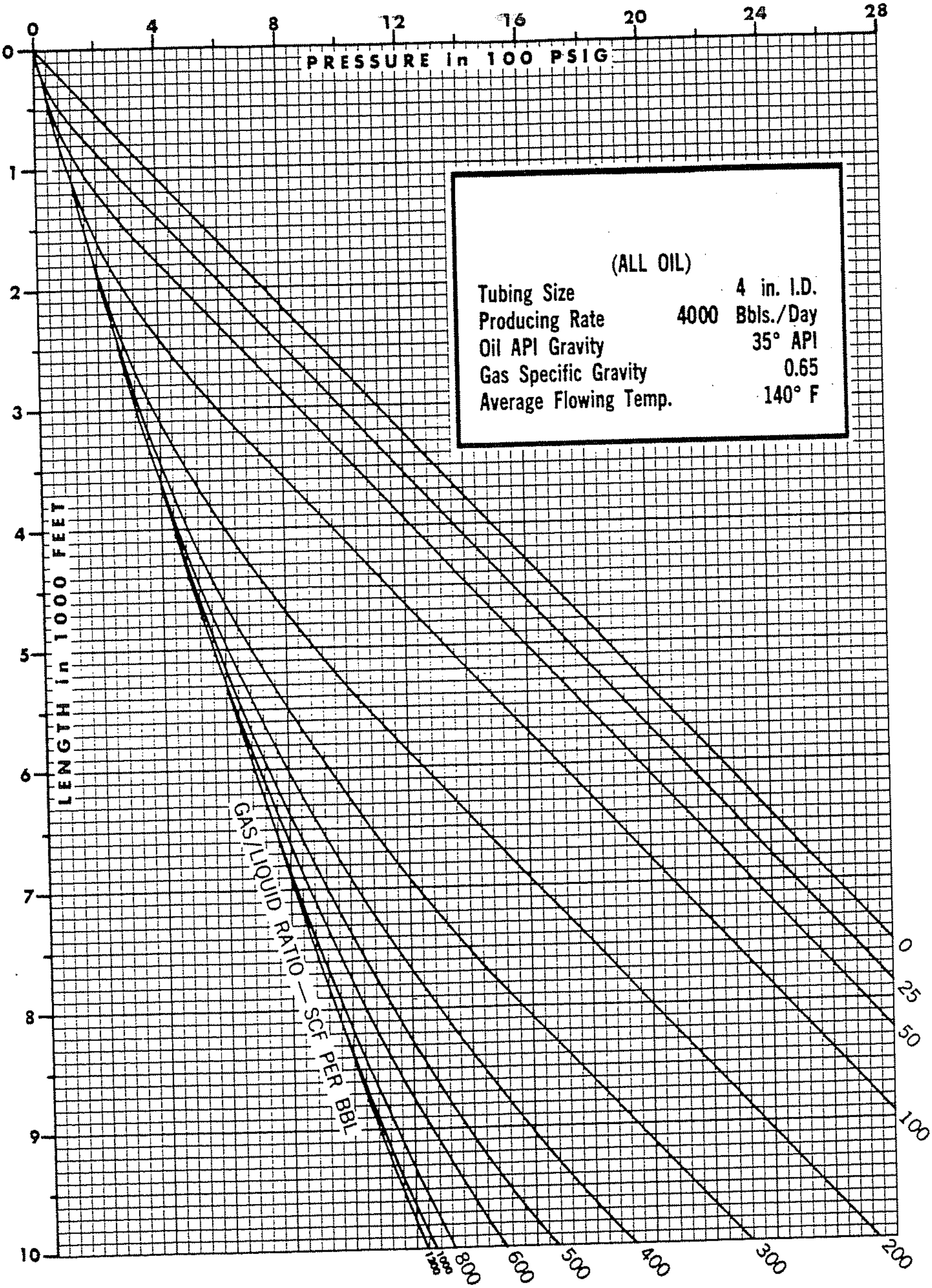

Figure 4.2(36) Vertical Flowing Pressure Gradients

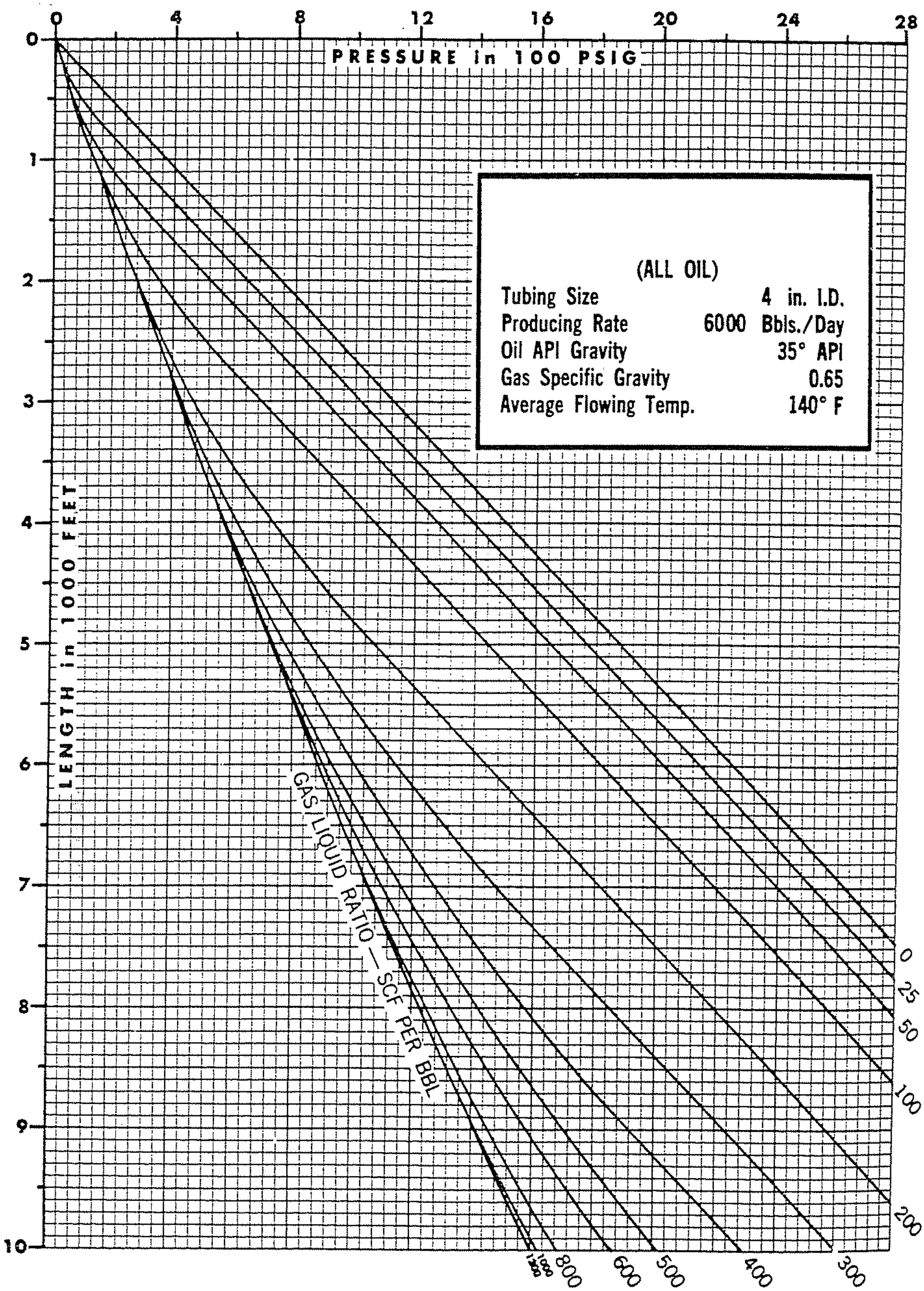

Figure 4.2(37) Vertical Flowing Pressure Gradients

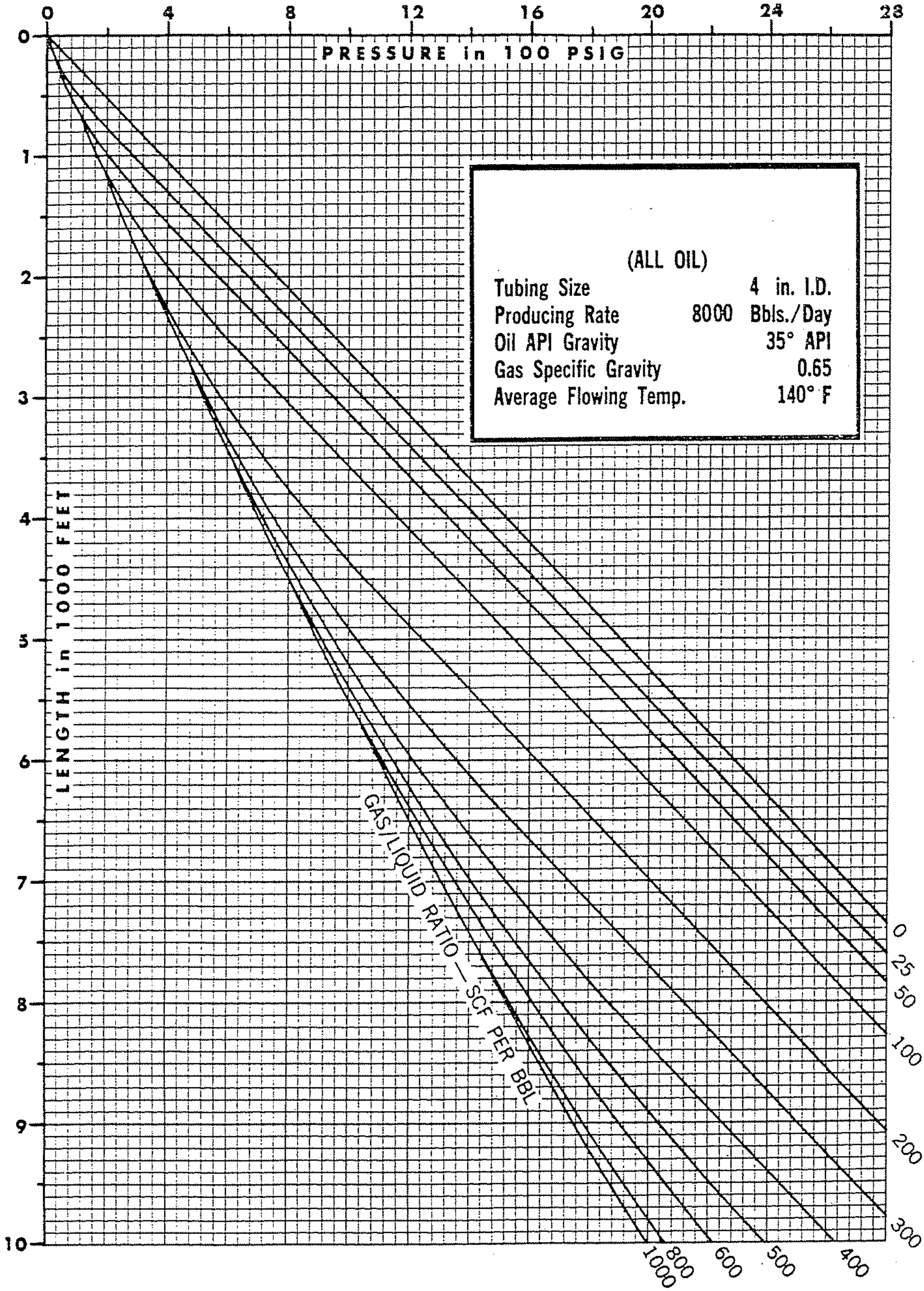

Figure 4.2(38) Vertical Flowing Pressure Gradients

Appendix 4.3
"Design criteria for selecting velocity type subsurface safety valves"*

by H. D. Beggs, J. P. Brill, E. P. Kanu, and C. A. Paz-y-Mino

Application Example

In order to demonstrate the application of the correlations and equations resulting from this study, an example is worked for the selection of bean size and number of spacers for the Camco A-3, 2-⅜ SSSV. A hypothetical well is chosen which has the following characteristics:

Well depth = 10,000 ft (3048 m)
Tubing diameter = 1.995 in. I.D. (50.7 mm)
Surface temperature = 110° (43° C)
Bottom-hole temperature = 270°F (132° C)
Oil gravity = 35° API (0.85)
Gas gravity = 0.65
Avg. reservoir pressure = 3000 psia (20685 k Pa)

The well is presently equipped with a SSSV located at 3000 ft (914 m) below the surface containing a 20/64 in. bean. A recent production test on the well resulted in the following data:

$q_o = 700$ STB/D (0.00129 m³/s),

$q_g = 280$ Mscfd (0.092 m³/s),

Flowing tubing pressure = 300 psia (2069 k Pa)

It is desired to equip the well with a SSSV which will allow a normal production rate of 800 STB/D at the same GOR. The procedure outlined in the flow chart (Fig. 1) is to be followed. The assumption is made that the Productivity Index is independent of flow rate.

Solution for the Camco A-3 Valve

STEP 1. $q_o = 700$ STB/D (0.00129 m³/s)
$q_g = 280$ Mscfd (0.092 m³/s)
$P_{tf} = 300$ psia (2069 k Pa)

STEP 2. Using the Orkiszewski two-phase vertical flow correlation, the pressure downstream of the SSSV (3000 ft) is 688.4 psia. (4747 k Pa). Calculation of the pressure drop across the SSSV presently installed is an iterative procedure, since the discharge coefficient correlation is based on conditions upstream of the SSSV.

Trial 1. Estimate Δp = 10 psi (69 k Pa)

$A_B = 0.000532$ ft² (4.94E-5 m²)
$v_{sLB} = 93.73$ ft/sec (28.57 m/s)
$v_{sgB} = 97.68$ ft/sec (29.77 m/s)
$v_{mB} = 191.41$ ft/sec (58.34 m/s)
$\rho_m = 25.33$ lb$_m$/ft³ (405.79 kg/m³)

$$R_D = \frac{20/64}{1.995} = \frac{0.3125}{1.995} = 0.1566$$

$V_D = 1.042$

$C_D = C_o + C_1 R_D + C_2 R_D^2 + C_3 V_D$

From Table 4,

$C_0 = 0.5417$
$C_1 = 3.8749$
$C_2 = -10.4536$
$C_3 = 0$
$C_D = 0.5417 + 3.8749 (0.1566) - 10.4536 (0.1566)^2$
$C_D = 0.892$
$\Delta p = \rho_m v_{mB}^2/2 g_c C_d^2 = 125.77$ psi (867.2 k Pa)

This is not close enough to the estimated Δp of 10 psi. Using the calculated Δp as the next estimated Δp resulted in convergence at Δp = 113.3 psi in two more iterations. The pressure upstream of the SSSV is then 688.4 + 113.3 = 801.7 psia. The calculated P_{wf} is 2528.2 psia (17432 k Pa) at 10,000 ft. (3048 m).

STEP 3. $J = \dfrac{q_o}{P_{ws} - P_{wf}} = \dfrac{700}{3000 - 2528.2}$

STEP 4. Select a pressure differential across the new SSSV to be installed of 150 psi. (1034 k Pa).

STEP 5. The desired normal production rate is to be 800 STB/D (0.00147 m³/s). The closure rate must be between 110 and 150% of the normal production rate, therefore the pressure drop calculations were made using

$q_o = 800 (1.25) =$ STB/D (0.00184 m³/s)

STEP 6. For $q_o = 1000$ STB/D, $P_{wf} = P_{wf} - \dfrac{q_o}{J} = 3000$

Using the Orkiszewski method, the SSSV upstream pressure is 707 psia. A bean size must be selected such that the pressure drop across the bean at a flow rate of 1000 STB/D is less than 150 psi. Using the discharge coefficient equation, it was found that a bean size of 24/64 in. would give a C_D = 0.900 and Δp = 120.3 psi (829.5 k Pa). The flowing wellhead pressure is then

* Reprinted by permission of the American Society of Mechanical Engineers, ASME 80-Pet-52, presented in New Orleans, LA, February 1980.

calculated to be 178 psia, (1227 k Pa), which is greater than 50 psi (345 k Pa) and is therefore satisfactory.

STEP 7. For the 2⅜ in. (60.33 mm) Camco valve available, the spring force data obtained by making two measurements of force vs deflection resulted in the following equations:

For the 12 lb_f/in. spring: $F_s = 13.51 + 5.84N$
For the 30 lb_f/in. spring: $F_s = 41.63 + 13.5N$

The spring force required to allow the SSSV close at a Δp of 120.3 psi is calculated from Eq. (4) for the Camco A-3 valve.

$$\Delta p = 2.0107\ F_s + 16.4073$$
$$F_s = \frac{120.3 - 16.4073}{2.0107} = 51.67\ lb_f\ (229.83N)$$

Selecting a 30 lb_f spring, the number of spacers required is

$$N = \frac{F_s - 41.63}{13.5} = \frac{51.67 - 41.63}{13.5} = 0.744$$

Therefore

$$N = 1 \text{ spacer.}$$

Using 1 spacer will require a pressure drop to close of

$$\Delta p = 2.0107\ F_s + 16.4073$$
$$\Delta p = 2.0107\ (41.63 + 13.5\ (1) + 16.4073$$
$$\Delta p = 127 \text{ psi } (876 \text{ k Pa})$$

Therefore, the SSSV will not close at a producing rate of exactly 1000 STB/D (0.00184 m^3/s). Using a trial and error procedure, it was determined that the producing rate required to produce a Δp of 127 psi is 1030 STB/D. This rate is within the limits required as it is only (100) (1030)/800 = 129% of the desired producing rate.

The completed design then calls for a 2⅜-in. (60.33 mm) Camco A-3 valve equipped with a 24/64 in. (9.53 mm) bean and a 30 lb_f/in. spring with 1 spacer to be installed. The SSSV will then close when the wells producing rate exceeds 1030 STB/D (0.0019 m^3/s).

Appendix 4.4
Vertical injection pressure gradients

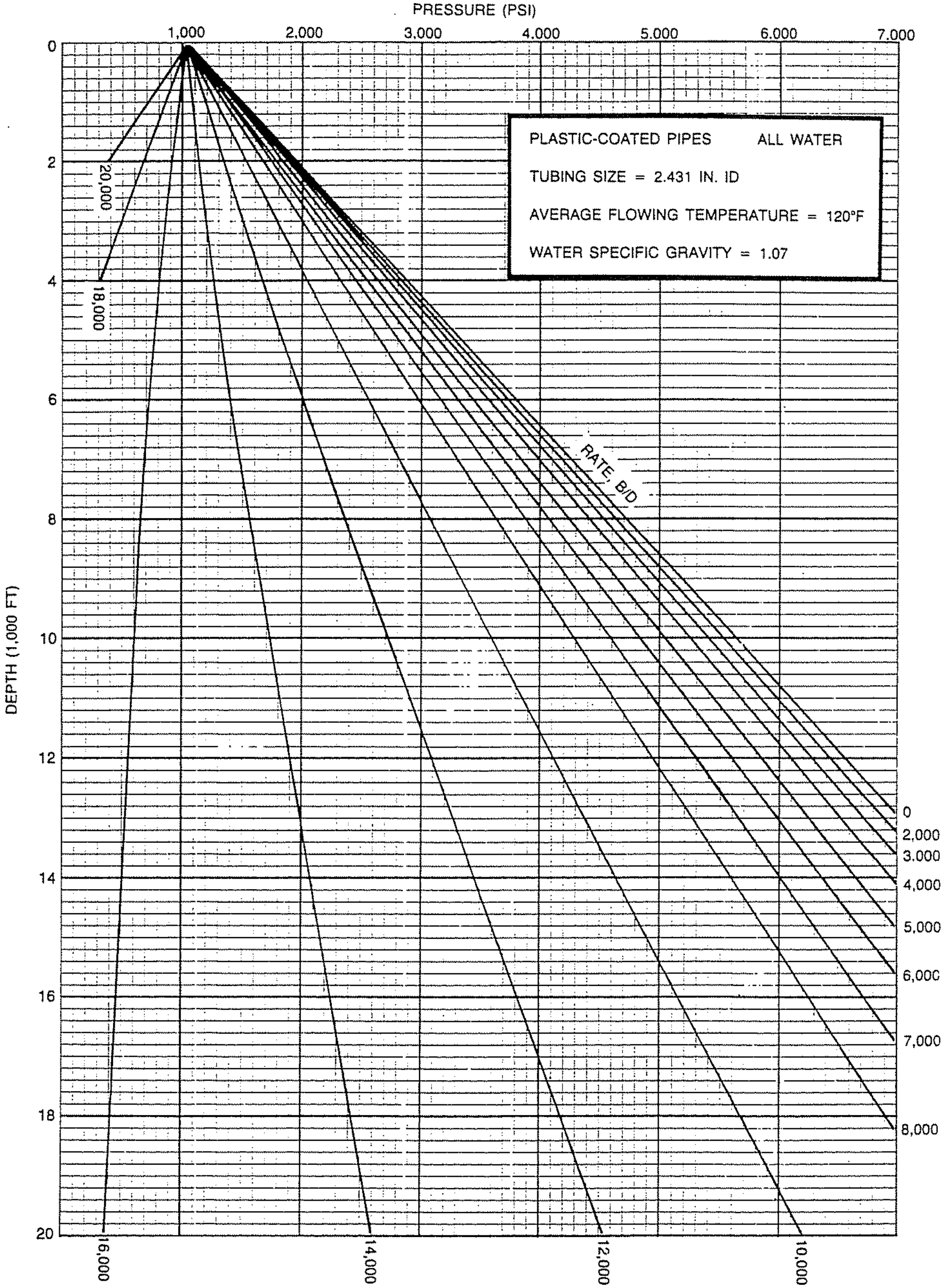

Figure 4.4(1) Vertical Injection Pressure Gradients

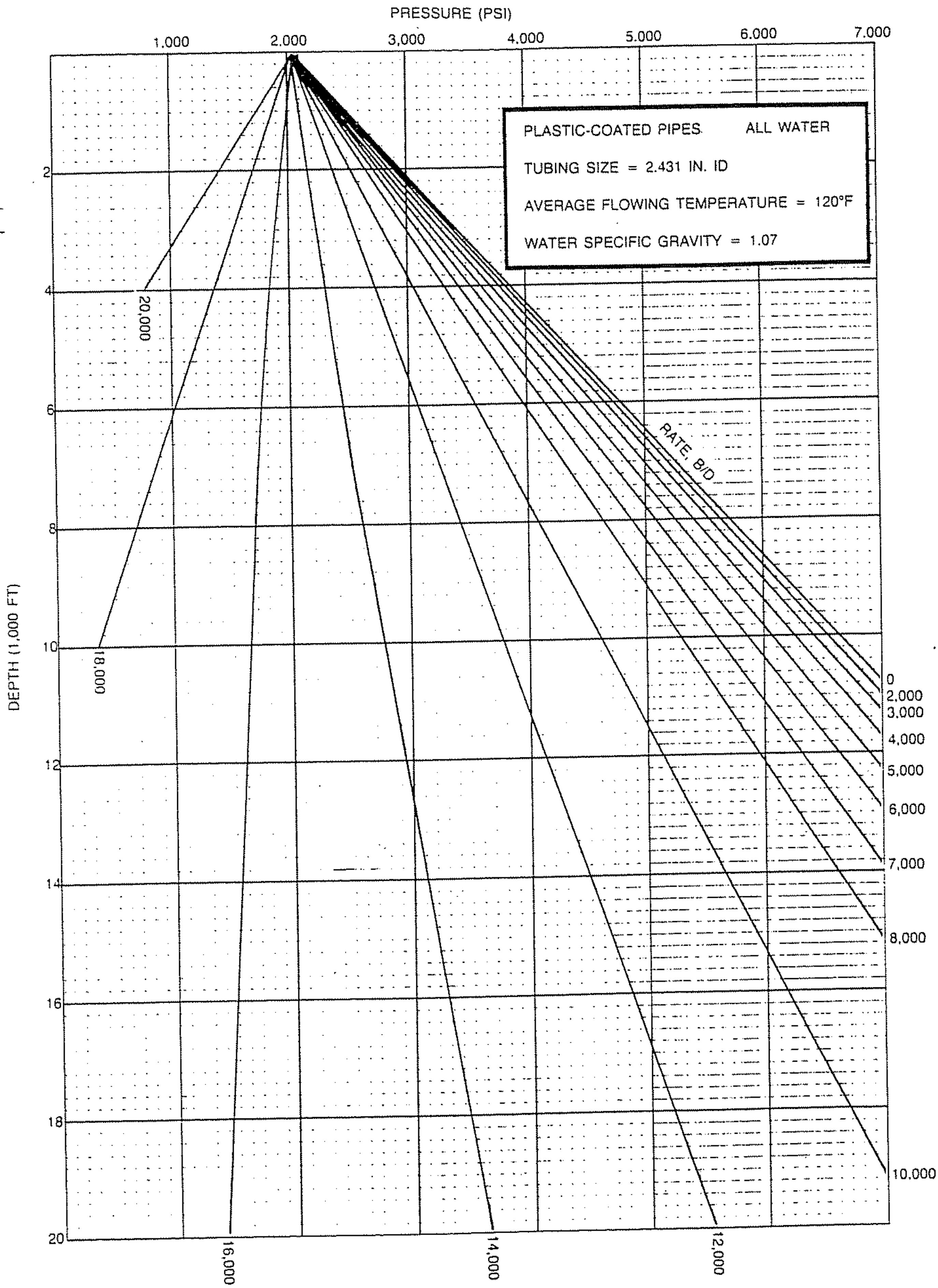

Figure 4.4(2) Vertical Injection Pressure Gradients

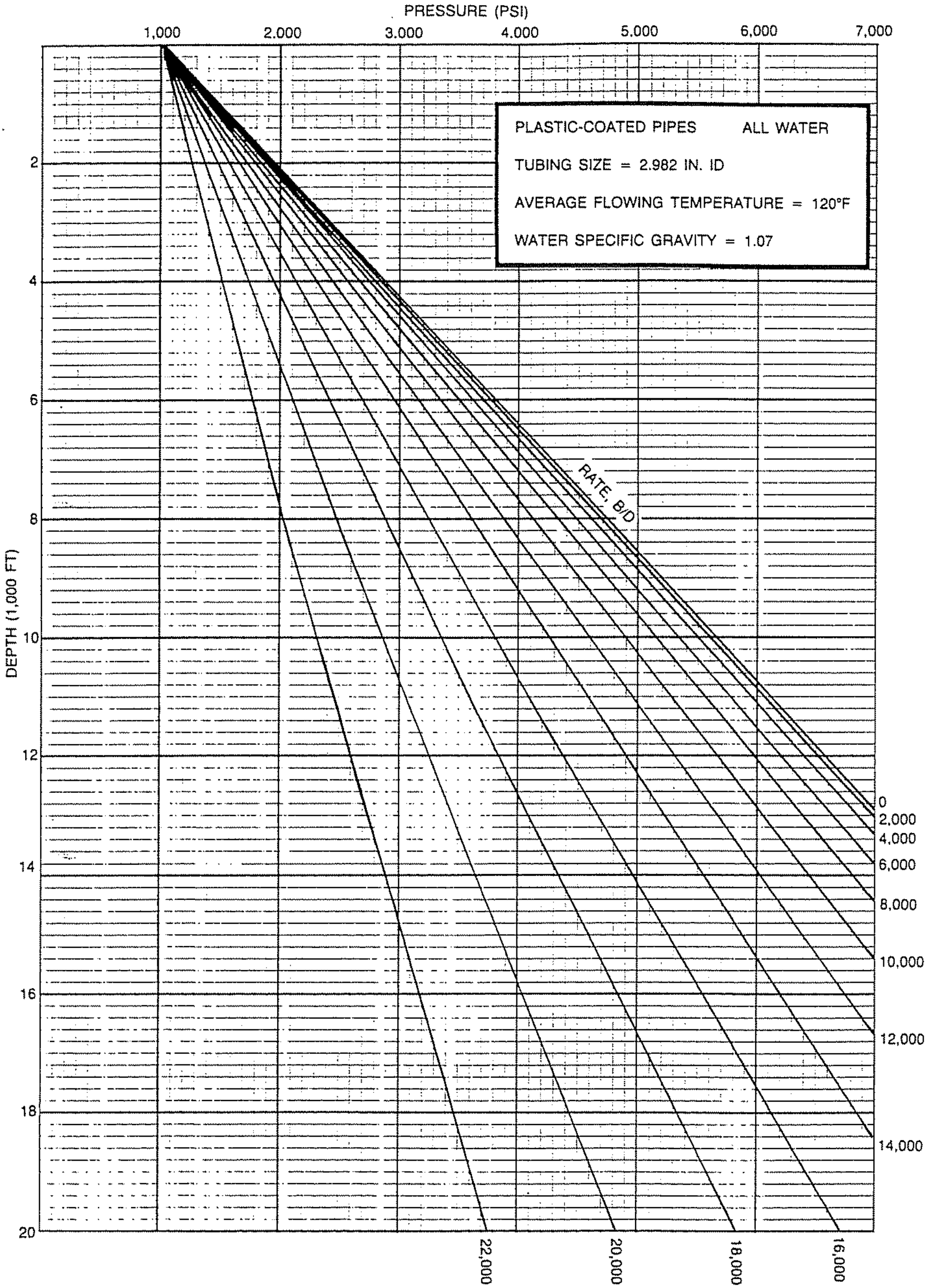

Figure 4.4(3) Vertical Injection Pressure Gradients

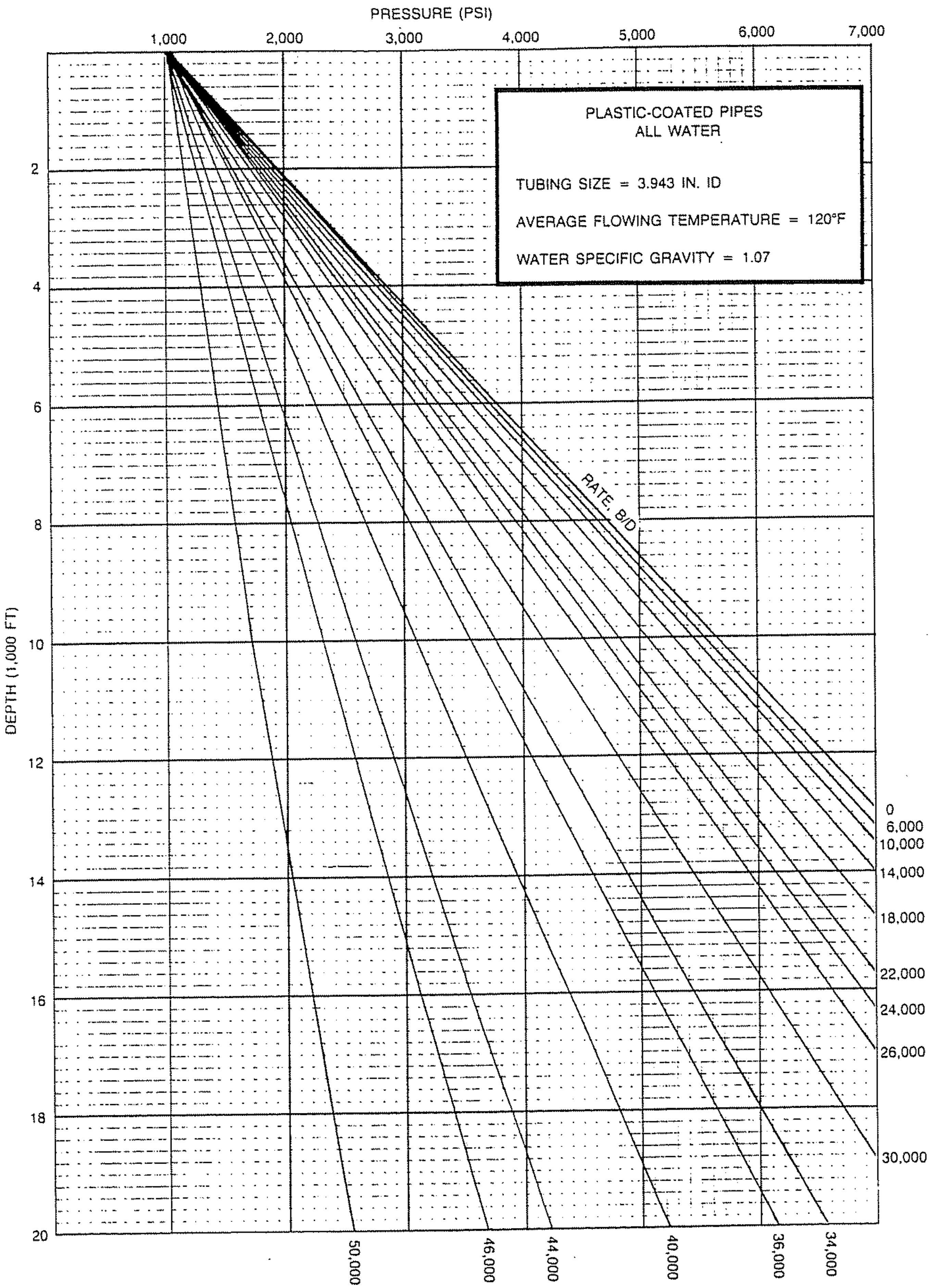

Figure 4.4(4) Vertical Injection Pressure Gradients

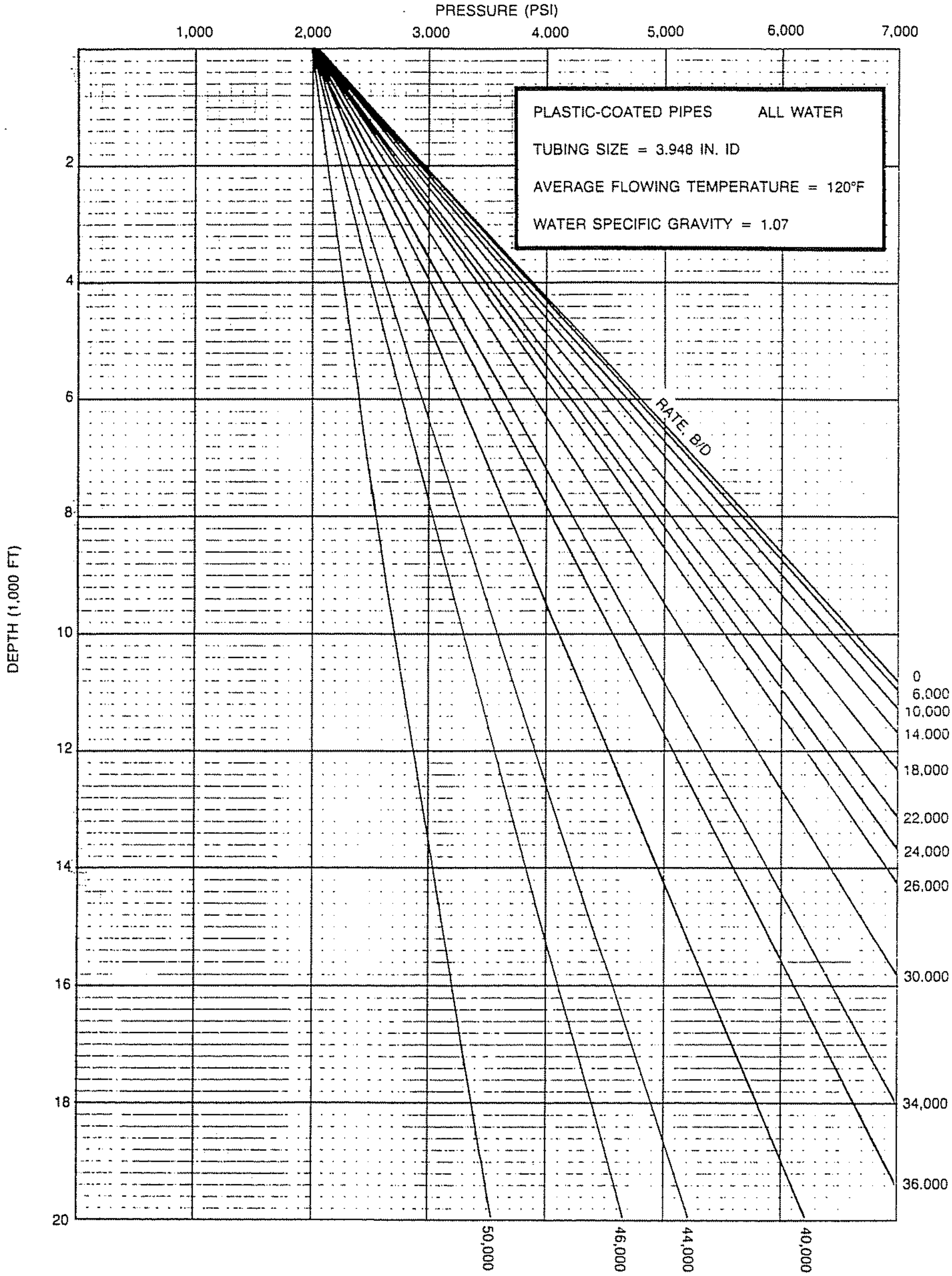

Figure 4.4(5) Vertical Injection Pressure Gradients

Appendix 4.5
Vertical flowing gas injection gradients

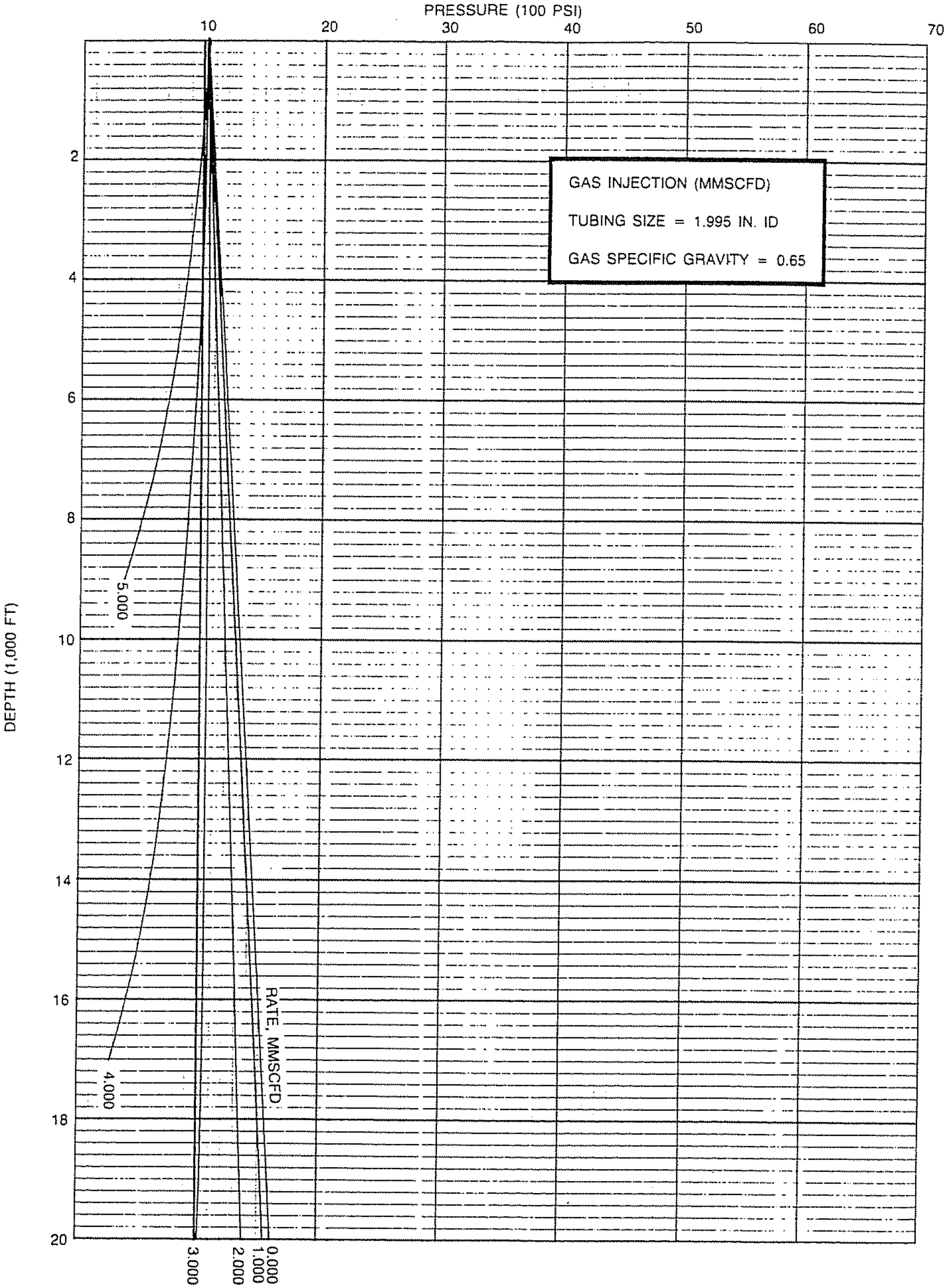

Figure 4.5(1) Vertical Flowing Gas Gradients

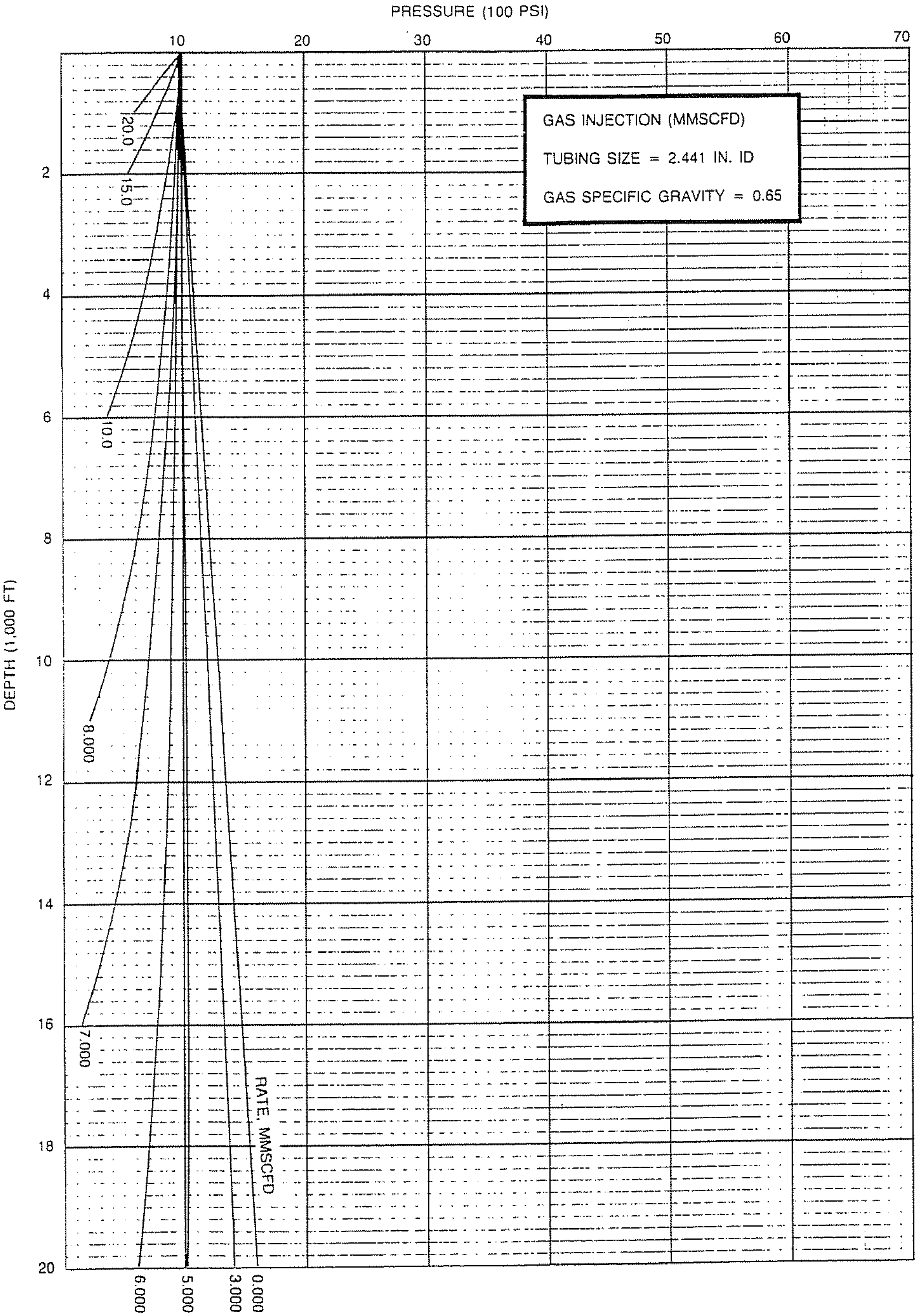

Figure 4.5(2)   Vertical Flowing Gas Gradients

Appendix 4.6
Vertical flowing gas production gradients

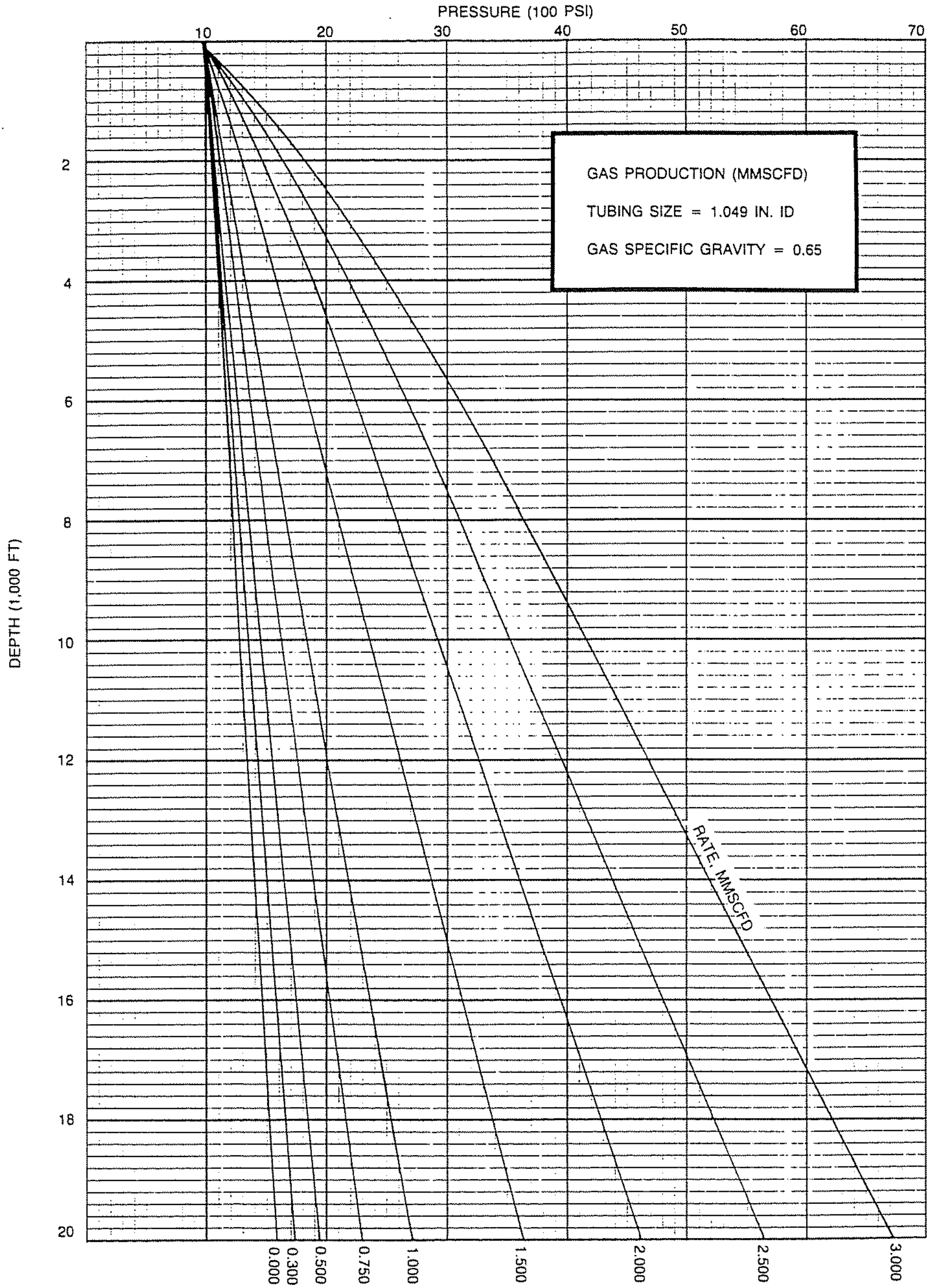

Figure 4.6(1) Vertical Flowing Gas Gradients

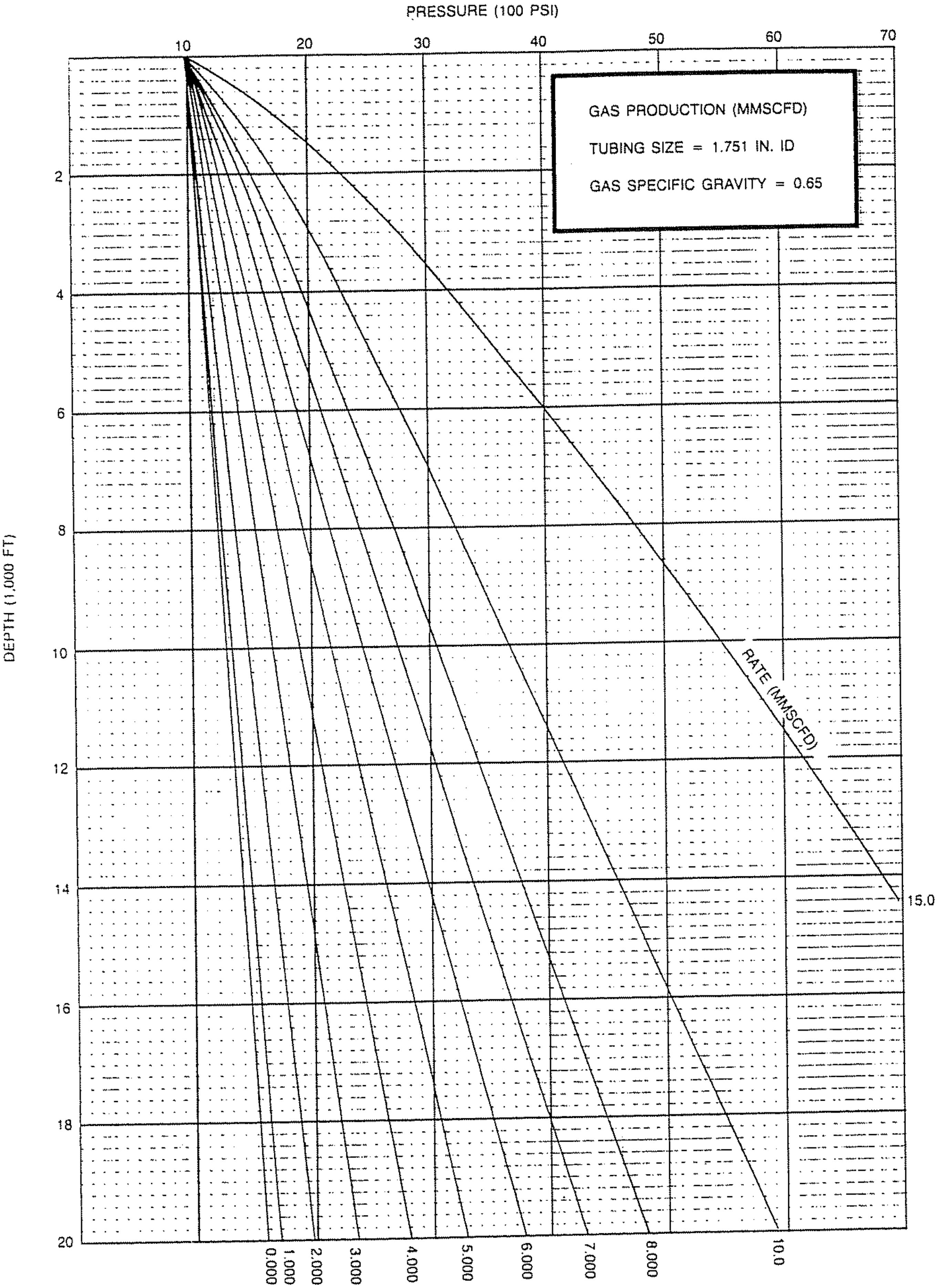

Figure 4.6(2) Vertical Flowing Gas Gradients

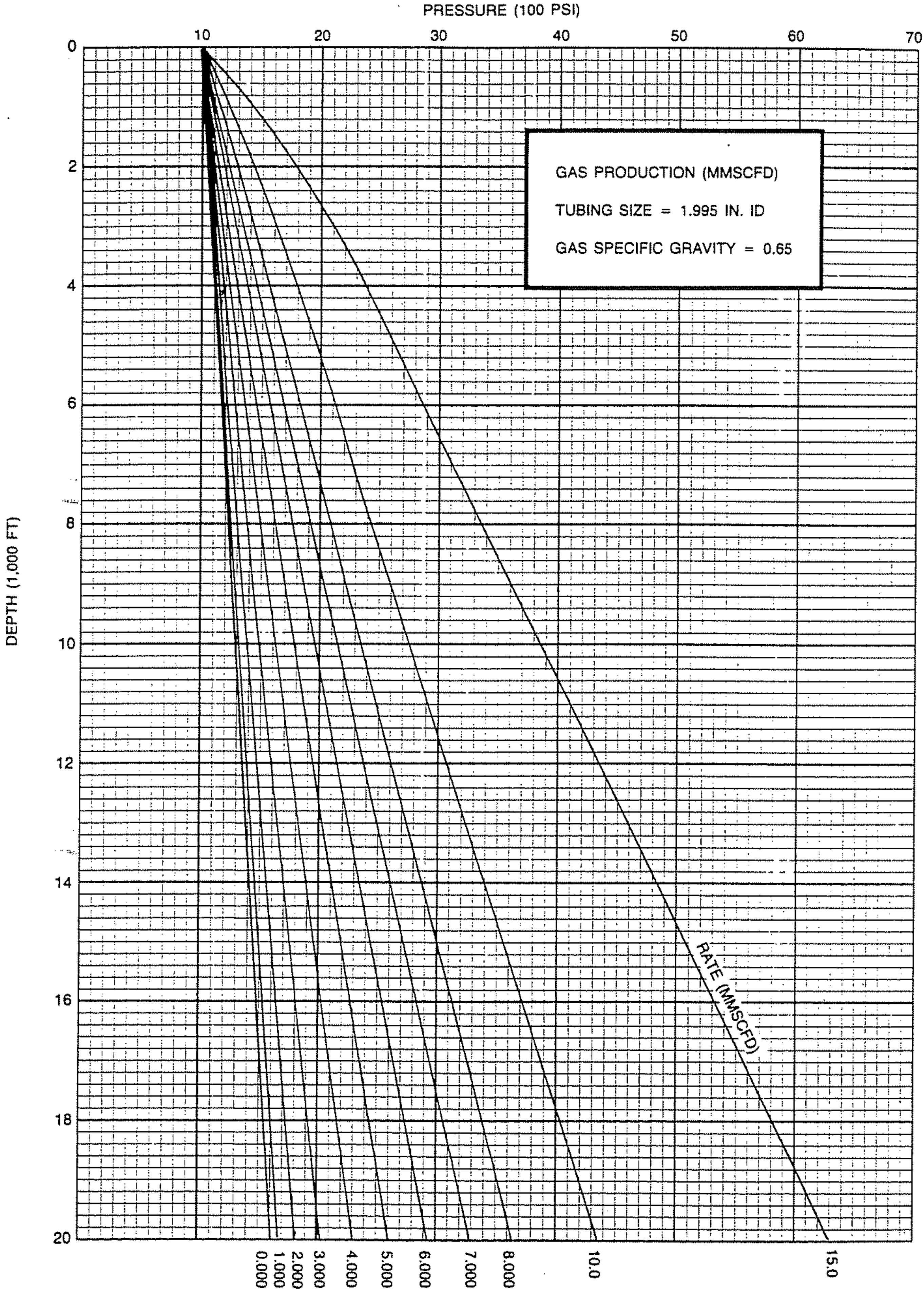

Figure 4.6(3) Vertical Flowing Gas Gradients

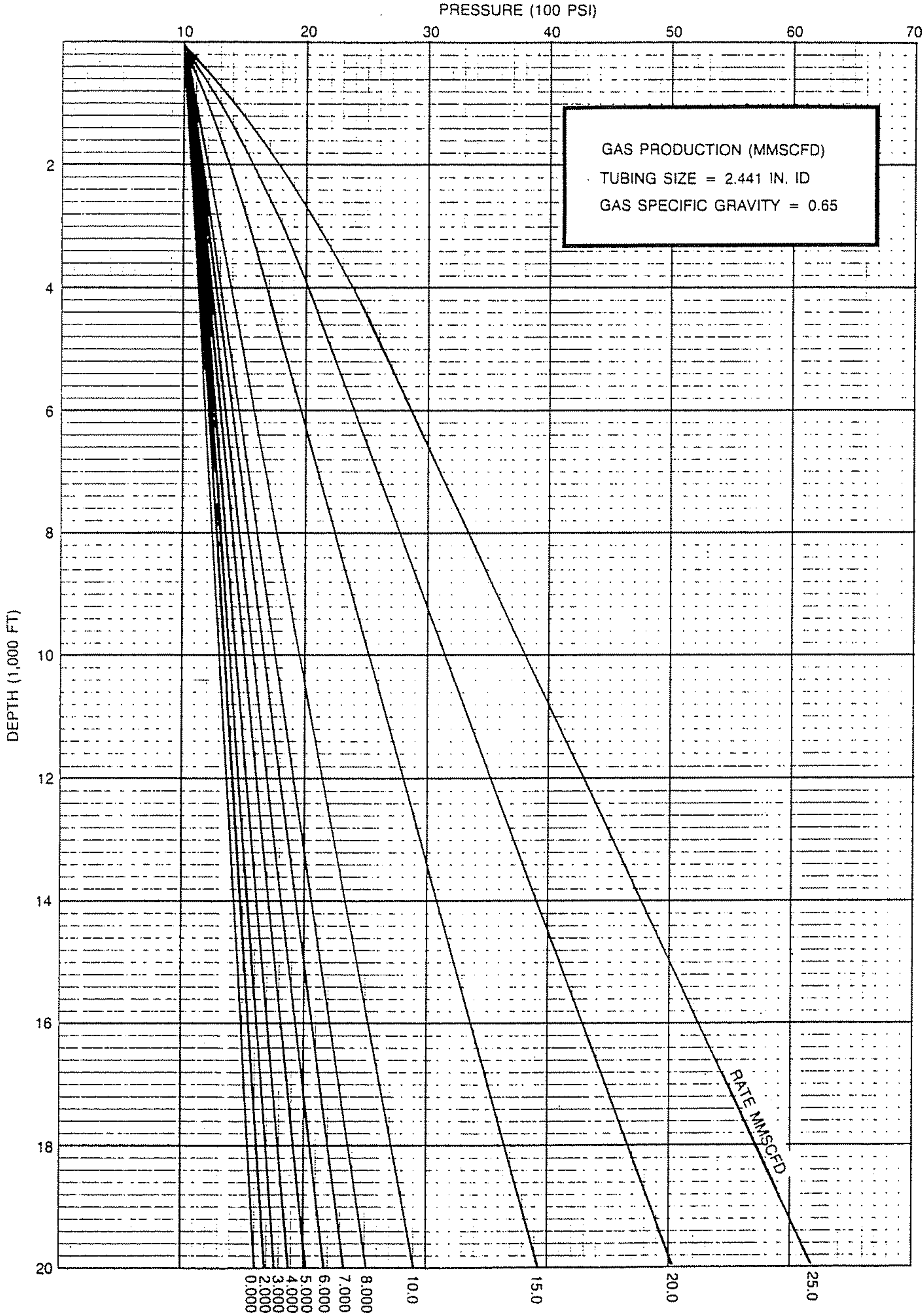

Figure 4.6(4) Vertical Flowing Gas Gradients

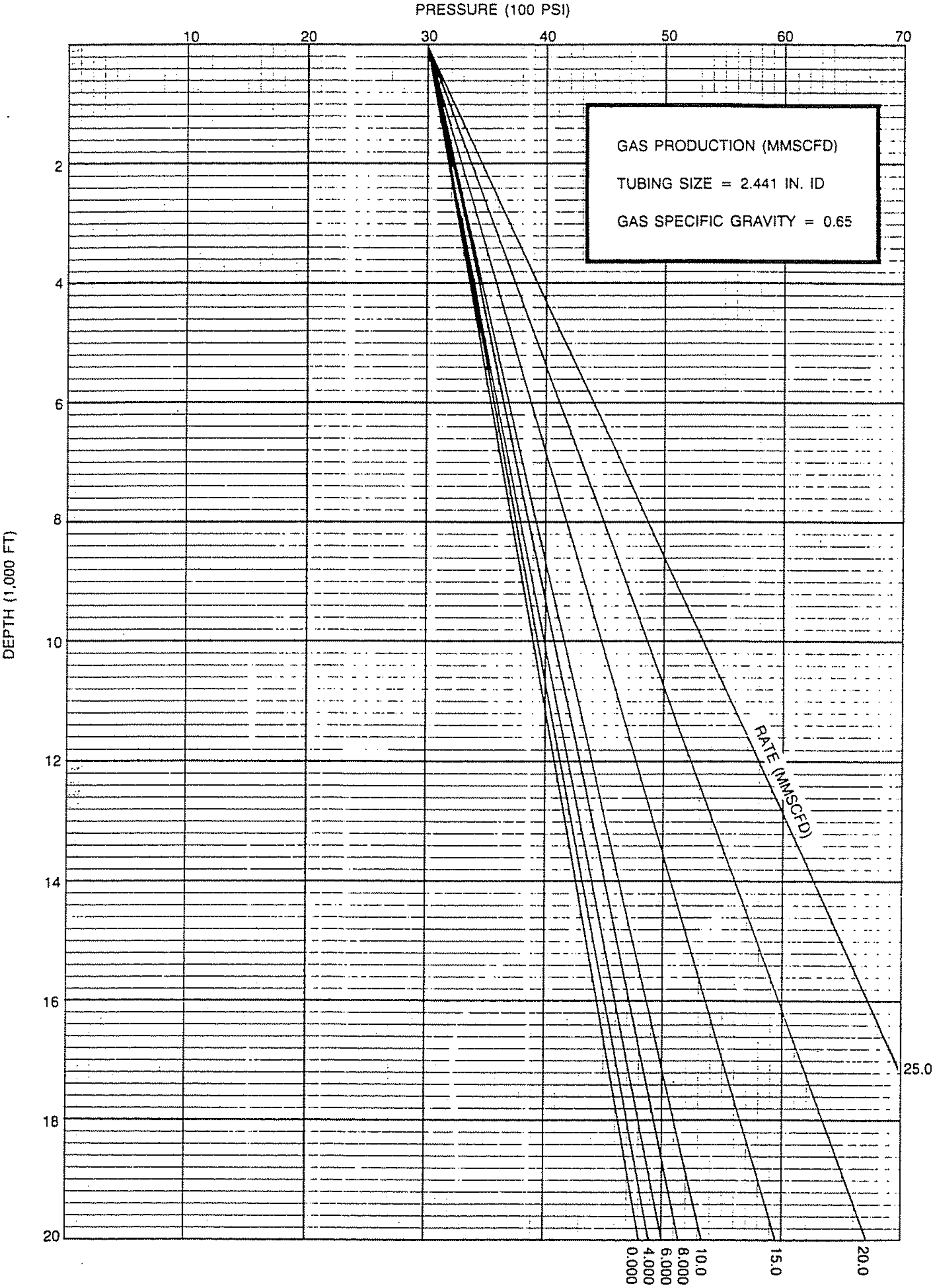

Figure 4.6(5) Vertical Flowing Gas Gradients

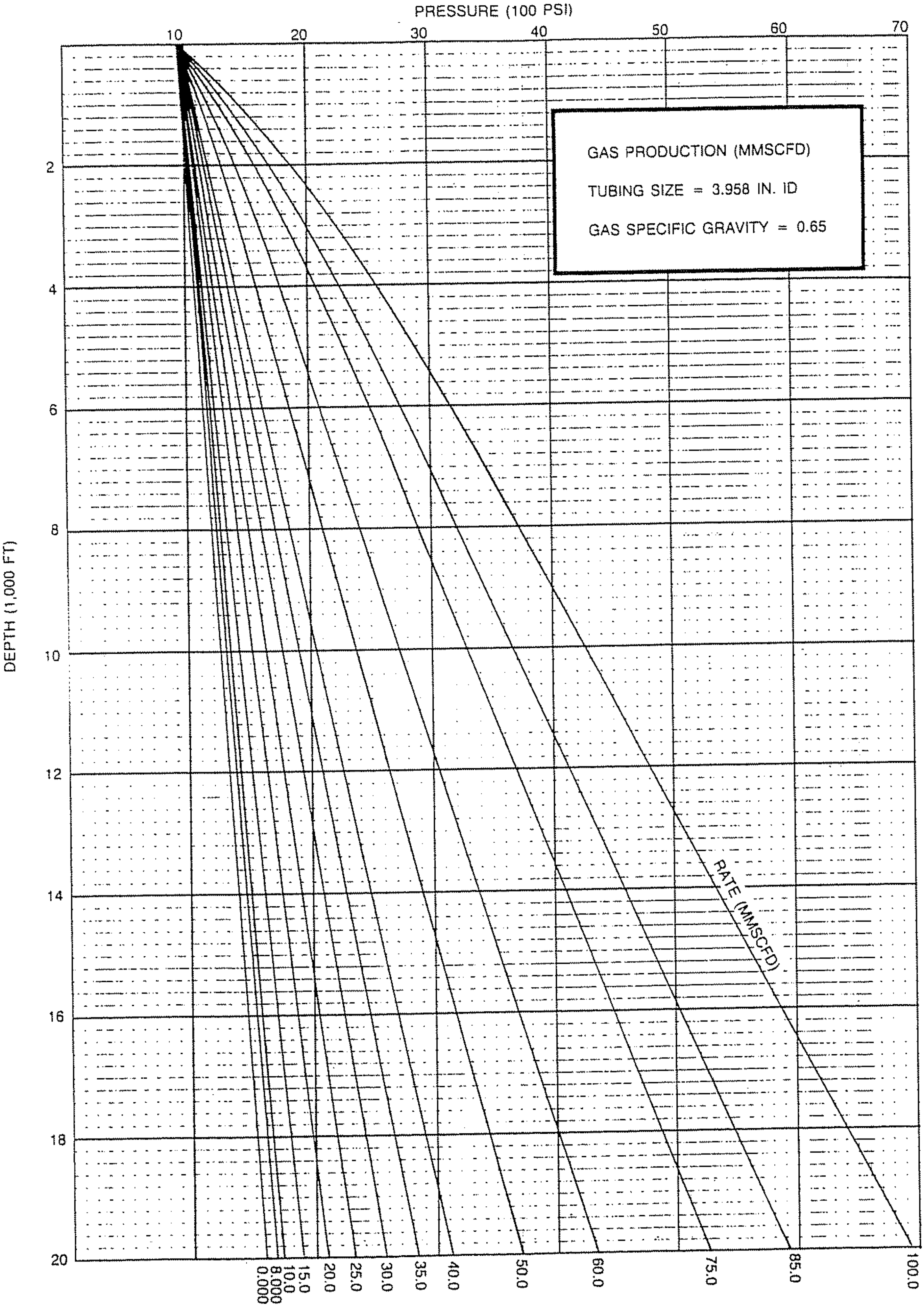

Figure 4.6(6) Vertical Flowing Gas Gradients

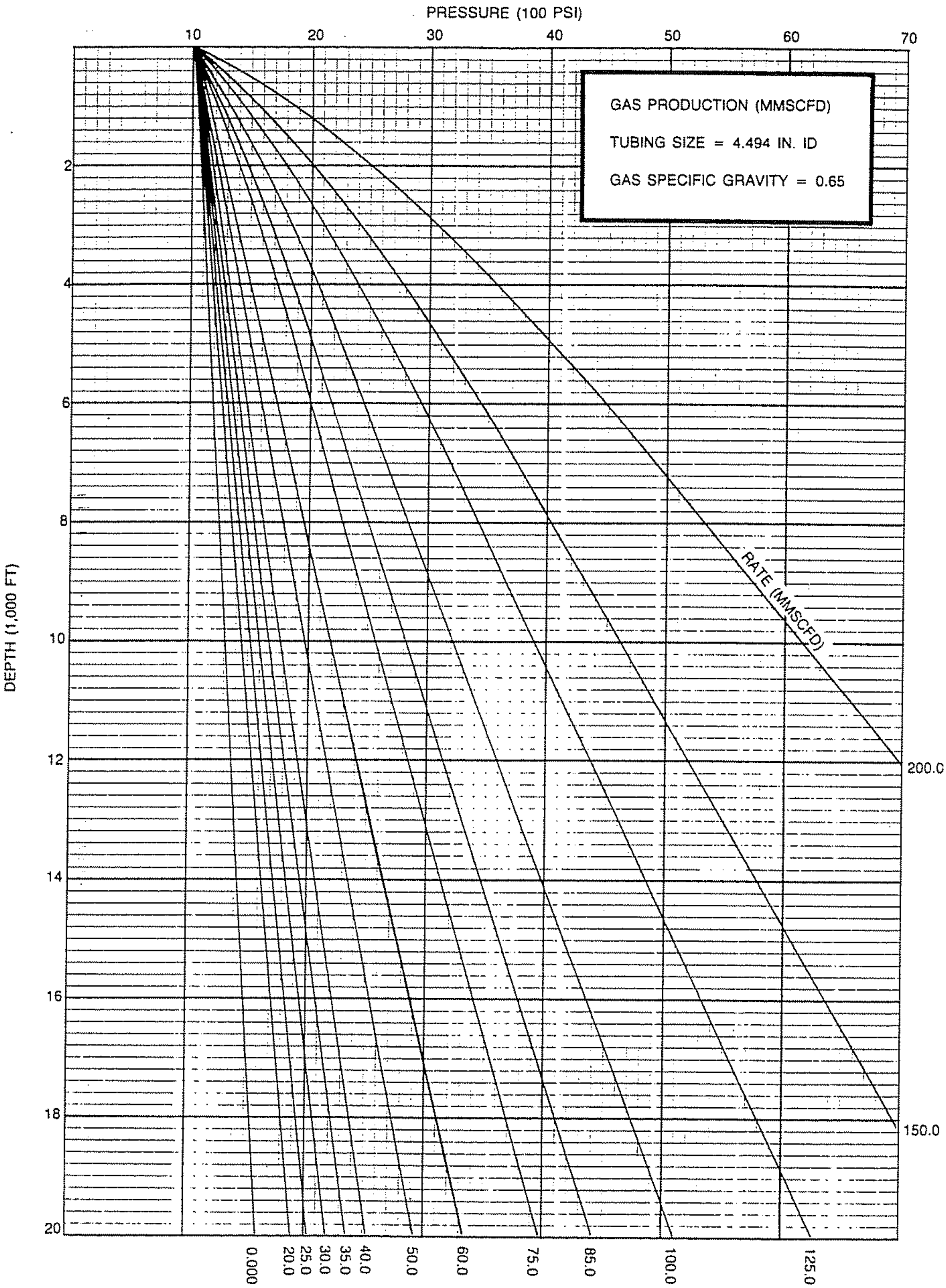

Figure 4.6(7) Vertical Flowing Gas Gradients

Appendix 4.7
Working graphs

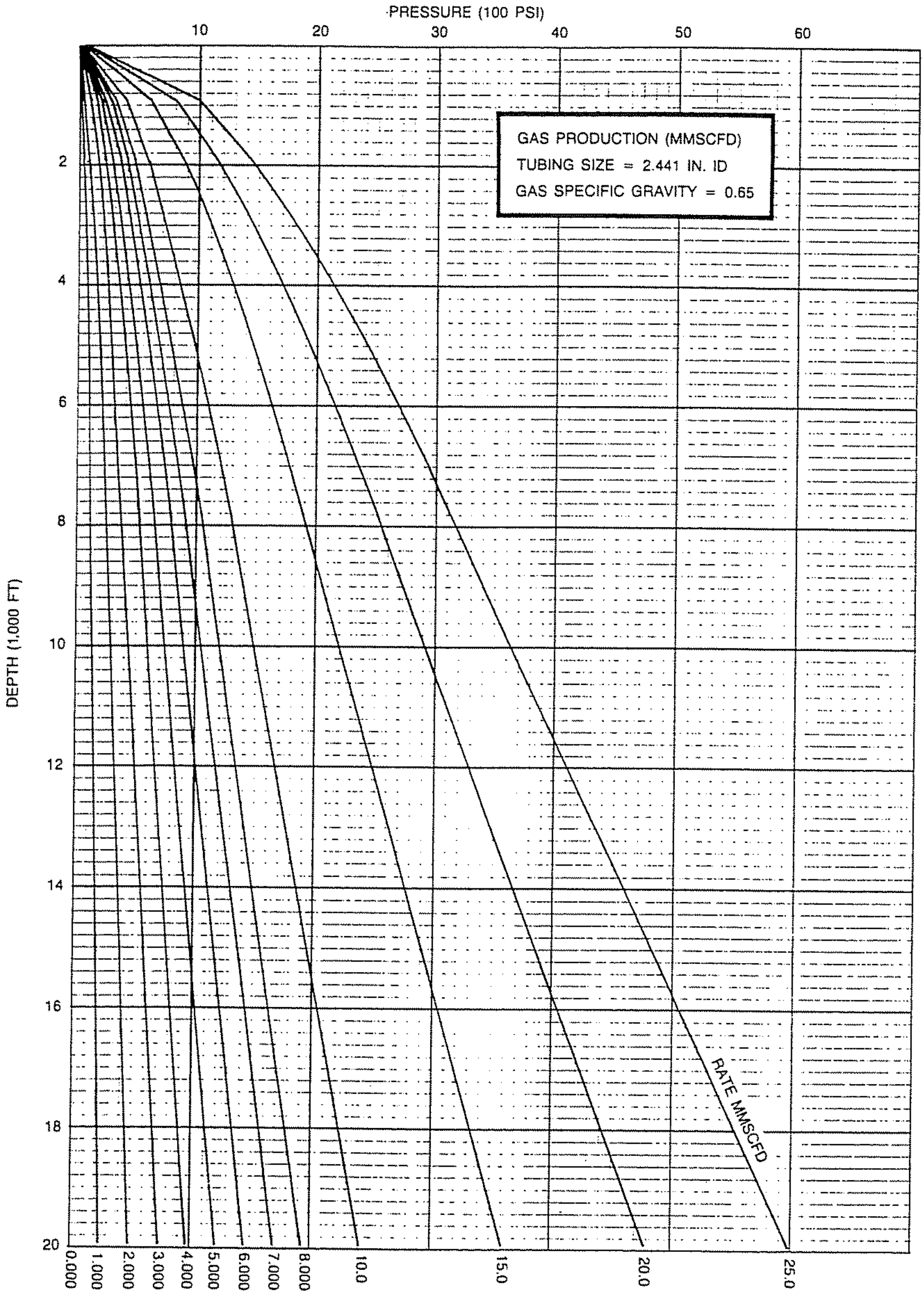

Figure 4.7(1) Vertical Flowing Gas Gradients (*Gas Production, MMscfd; Tubing Size, 2.441-in. ID; Gas Specific Gravity, 0.65*)

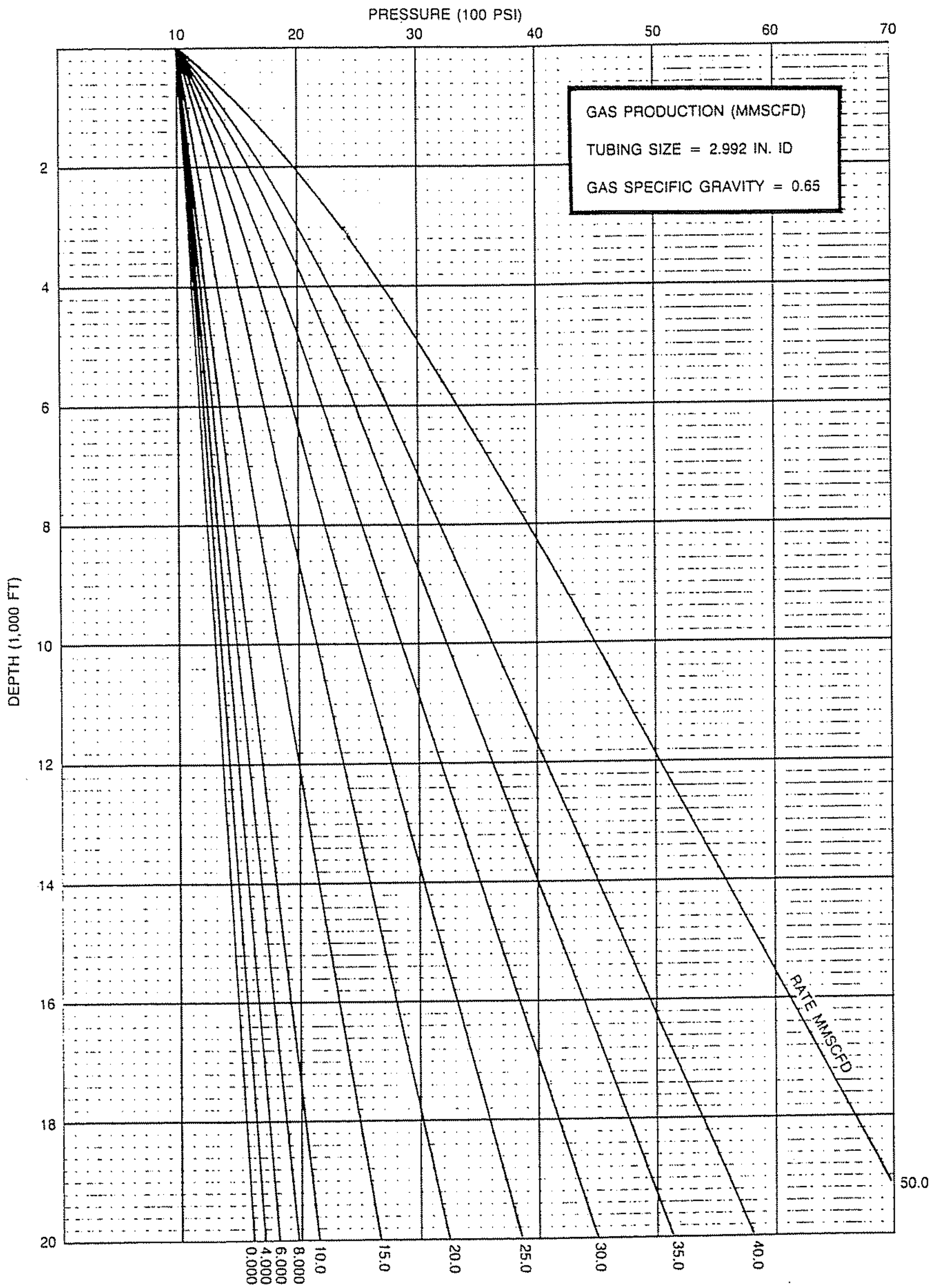

Figure 4.7(2) Vertical Flowing Gas Gradients (*Gas Production, MMscfd; Tubing Size, 2.992-in. ID; Gas Specific Gravity, 0.65*

EXAMPLE

REQUIRED:

Formation volume at 200°F of a bubble point liquid having a gas-oil ratio of 350 CFB, a gas gravity of 0.75, and a tank oil gravity of 30 °API.

PROCEDURE:

Starting at the left side of the chart, proceed horizontally along the 350 CFB line to a gas gravity of 0.75. From this point drop vertically to the 30°API line. Proceed horizontally from the tank oil gravity scale to the 200°F line. The required formation volume is found to be 1.22 barrel per barrel of tank oil.

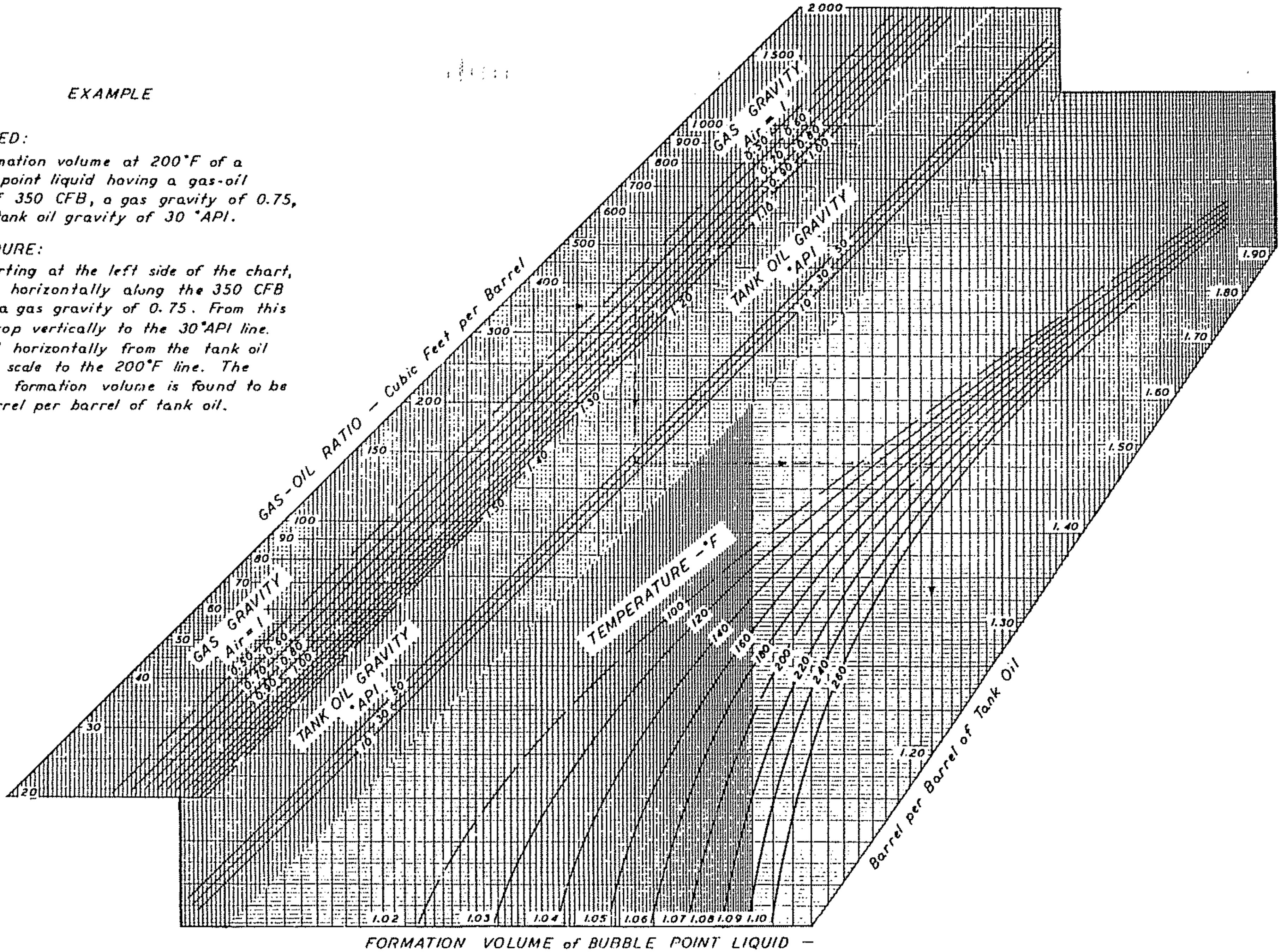

Figure 4.7(3) Properties of natural hydrocarbon mixtures formation volume of bubble point liquid. (Courtesy Chevron Research Company).

Appendix 4.8
Equation summary

by Carl Granger and Hai-Zui Meng

I. Oil IPR Equations
  A. Darcy's Law
  B. Vogel; Test Data; $P_r \leq P_b$
  C. Combination Vogel—Darcy; Test Data
    (1) For test when P_{wf} test $> P_b$
    (2) For test when P_{wf} test $< P_b$
  D. Jones IPR

II. Gas IPR Equations
  A. Darcy's Law (Gas)
  B. Jones' Gas IPR

III. Back-Pressure Equation

IV. Transient Period Equations
  A. Time to Pseudo-Steady-State
  B. Oil IPR (Transient)
  C. Gas IPR (Transient)

V. Completion Pressure Drop Equations
  A. Gravel-Packed Wells
    (1) Oil Wells
    (2) Gas Wells
  B. Open Perforation Pressure Drop
    (1) Oil Wells
    (2) Gas Wells

I. Oil IPR Equations

A. Darcy's Law

$$q_o = \frac{7.08 \times 10^{-3}\, kh\,(\overline{P}_r - \overline{P}_{wf_s})}{\overline{\mu}_o\, \overline{B}_o\,[\ln(r_e/r_w) - 3/4 + S]} \qquad \text{(Eq. 1a)}$$

$$J = \frac{q}{\overline{P}_r - \overline{P}_{wf_s}} = \frac{q}{\Delta P}$$

$$= \frac{7.08 \times 10^{-3}\, kh}{\overline{\mu}_o\, \overline{B}_o\,[\ln(r_e/r_w) - 3/4 + S]} \qquad \text{(Eq. 1b)}$$

$$AOF = (J)(\overline{P}_r - 0) \qquad \text{(Eq.1c)}$$

where:

q = b/d
AOF = absolute open flow potential, b/d
k = oil permeability, md
h = net vertical formation thickness, ft
$\overline{P}_r$ = average formation pressure (shutin BHP), psi
$\overline{P}_{wf_s}$ = average flowing bottom-hole pressure at sandface, psi
$\overline{\mu}_o$ = average viscosity, cp
$\overline{B}_o$ = formation volume factor, rb/stb
r_e = drainage radius, ft
r_w = wellbore radius, ft
S = skin factor (dimensionless)
PI = productivity index, b/d/psi

B. Vogel; Test Data; $\overline{P}_r \leq P_b$:

$$q_o/q_{o_{max}} = 1 - 0.2\left(\frac{P_{wf_s}}{\overline{P}_r}\right) - 0.8\left(\frac{P_{wf_s}}{\overline{P}_r}\right)^2 \qquad \text{(Eq. 2)}$$

C. Combination Vogel = Darcy; $\overline{P}_r > P_b$; Test Data

(1) For test when $P_{wf_{test}} > P_b$:

$$J = \frac{q}{\overline{P}_r - P_{wf_s}} \qquad \text{(Eq.3a)}$$

$$q_b = J\,(\overline{P}_r - P_b) \qquad \text{(Eq. 3b)}$$

$$q_{o_{max}} = q_b + \frac{J \times P_b}{1.8} \qquad \text{(Eq. 3c)}$$

Points on IPR curve:

For $P_{wf} > P_b$:

$$q_o = J\,(\overline{P}_r - P_{wf}) \qquad \text{(Eq. 3d)}$$

For $P_{wf} < P_b$:

$$q_o = q_b + \left[q_{o_{max}} - q_b\right] \times \left[1 - 0.2\left(\frac{P_{wf}}{P_b}\right) - 0.8\left(\frac{P_{wf}}{P_b}\right)^2\right] \qquad \text{(Eq. 3e)}$$

(2) For test when $P_{wf_{test}} < P_b$:

$$J = \frac{q}{(\overline{P}_r - P_b) + \frac{P_b}{1.8}\left[1 - 0.2\left(\frac{P_{wf}}{P_b}\right) - 0.8\left(\frac{P_{wf}}{P_b}\right)^2\right]} \qquad \text{(Eq. 3f)}$$

$$q_b = J(\overline{P}_r - P_b) \quad \text{(Eq. 3g)}$$

$$q_{o_{max}} = q_b + \frac{(J)(P_b)}{1.8} \quad \text{(Eq. 3h)}$$

Points on IPR curve:

For $P_{wf} > P_b$:

$$q_o = (J)(\overline{P}_r - P_{wf}) \quad \text{(Eq. 3i)}$$

For $P_{wf} < P_b$:

$$q_o = q_b + [q_{max} - q_b]\left[1 - 0.2 \times \left(\frac{P_{wf}}{P_b}\right) - 0.8\left(\frac{P_{wf}}{P_b}\right)^2\right] \quad \text{(Eq. 3j)}$$

where:

q_o = flow rate, b/d
q_b = flow rate at bubble point
P_b = bubble-point pressure
$q_{o_{max}}$ = maximum flow rate (Vogel or Combination)
J = productivity index, b/d/psi

D. Jones IPR

$$P_r - P_{wf_s} = aq^2 + bq \quad \text{(Eq. 4a)}$$

$$P_r - P_{wf_s} = \left\{\frac{2.30 \times 10^{-14}\,\beta\, B_o^2 \rho}{h_p^2\, r_w}\right\} q^2 + \left\{\frac{\mu_o B_o [\ln(0.472(r_e/r_w) + S]}{7.08 \times 10^{-3}\, kh}\right\} q \quad \text{(Eq. 4b)}$$

$$AOF = \frac{-b \pm \sqrt{b^2 + 4a(P_r - 0)}}{2a} \quad \text{(Eq. 4c)}$$

where:

$$a = \frac{2.30 \times 10^{-14}\,\beta\, B_o^2\, \rho}{h_p^2\, r_w}$$

$$b = \frac{\mu_o B_o [\ln(0.472\, r_e/r_w) + S]}{7.08 \times 10^{-3}\, kh}$$

q = flow rate, b/d
$\overline{P}_r$ = average reservoir pressure (shutin BHP), psi
P_{wf_s} = flowing BHP at sandface, psi
β = turbulence coefficient, ft^{-1}

$$\beta = \frac{2.33 \times 10^{10}}{k^{1.201}} \quad \text{(after Katz)}$$

B_o = formation volume factor, rb/stb
ρ = fluid density, lb/ft³
h_p = perforated interval, ft
μ_o = viscosity, cp
r_e = drainage radius, ft
r_w = wellbore radius, ft
S = skin factor (dimensionless)
k_o = oil permeability, md
a = turbulence term
b = Darcy flow term

II. Gas IPR Equations

A. Darcy's Law (Gas)

$$q_g = \frac{703 \times 10^{-6}\, kh\,(\overline{P}_r^2 - P_{wf_s}^2)}{\overline{\mu}_o \overline{T}\,\overline{Z}\,[\ln(r_e/r_w) - 3/4 + S + a'q]} \quad \text{(Eq. 5)}$$

where:

q_g = flow rate, mcfd
k = gas permeability, md
h = net vertical thickness, ft
$\overline{P}_r$ = average formation pressure (shutin BHP), psia
P_{wf_s} = sandface flowing BHP, psia
μ_o = viscosity, cp
T = temperature, °R (°F + 460)
Z = supercompressibility (dimensionless)
r_e = drainage radius, ft
r_w = wellbore radius, ft
S = skin factor (dimensionless)

B. Jones' Gas IPR (General Form)

$$\overline{P}_r^2 - P_{wf_s}^2 = aq^2 + bq \quad \text{(Eq. 6a)}$$

$$\overline{P}_r^2 - P_{wf_s}^2 = \frac{3.16 \times 10^{-12}\,\beta\gamma_g\, TZ}{h_p^2\, r_w} q^2 + \frac{1.424 \times 10^3\, \mu_o TZ\,[\ln[0.472(r_e/r_w)] + S]}{kh} q \quad \text{(Eq. 6b)}$$

$$AOF = \frac{-b \pm \sqrt{b^2 + 4a(\overline{P}_r^2)}}{2a} \quad \text{(Eq. 6c)}$$

where:

$$a = \frac{3.16 \times 10^{-12}\,\beta\,\gamma_g\, TZ}{h_p^2\, r_w}$$

$$b = \frac{1.424 \times 10^3\, \mu_g TZ\,[\ln[0.472(r_e/r_w] + S]}{kh}$$

q = flow rate, mcfd
a = turbulence term
b = Darcy flow term
$\overline{P}_r$ = reservoir pressure (shutin BHP), psia
P_{wf_s} = sandface flowing BHP, psia
β = turbulence coefficient, ft^{-1}

$$\beta = \frac{2.33 \times 10^{10}}{k^{1.201}}$$

γ_g = gas specific gravity (dimensionless)
T = reservoir temperature, °R (°F + 460)
Z = supercompressibility (dimensionless)
h_p = perforated interval, ft
μ_o = viscosity, cp
r_e = drainage radius, ft
r_w = wellbore radius, ft

III. Back-Pressure Equation

$$q_g = C(\overline{P}_r^2 - P_{wf_s}^2)^n \quad \text{(Eq. 7)}$$

where:

$$C = \frac{703 \times 10^{-6}\, kh}{\mu_o\, TZ[\ln(r_e/r_w) - 3/4 + S]}$$

n = 0.5 < n < 1.0
q_g = flowrate, mcfd
k = gas permeability, md
h = net vertical thickness, ft
$\overline{P}_r$ = average formation pressure (shutin BHP), psia
P_{wf_s} = sandface flowing BHP, psia
μ_o = viscosity, cp

T = temperature, °R (°F + 460)
Z = supercompressibility (dimensionless)
r_e = drainage radius, ft
r_w = wellbore radius, ft
S = skin factor (dimensionless)

IV. Transient Period Equations

A. Time to Pseudo-Steady-State

$$t_{stab} = (948)\left(\frac{\phi\, \mu_o\, C_t\, r_e^2}{k}\right) \qquad \text{(Eq. 8)}$$

where:

ϕ = porosity (fraction)
μ_o = viscosity, cp
C_t = total system compressibility, psi^{-1}
r_e = drainage radius
k = permeability, md
t_{stab} = time for pressure transient to reach r_e, hrs

B. Oil IPR (Transient)

$$q_o = \frac{kh\,(\overline{P}_r - P_{wf_s})}{162.6\, \mu_o\, B_o \left[\log\left(\frac{kt}{\phi\, \mu\, C_t\, r_w^2}\right) - 3.23 + 0.87\, S\right]} \qquad \text{(Eq. 9)}$$

where:

k = oil permeability, md
h = wet vertical thickness, ft
μ = viscosity, cp
B_o = formation volume factor, rb/stb
t = time of interest; $t < t_{stab}$ (hrs)
ϕ = porosity (fraction)
C_t = total system compressibility
r_w = wellbore radius, ft
S = skin factor (dimensionless)

C. Gas IPR (Transient)

$$q_g = \frac{kh\,(\overline{P}_r^2 - P_{wf_s}^2)}{1{,}638\, \mu\, TZ \left[\log\left(\frac{kt}{\phi\, \mu\, C_t\, r_w^2}\right) - 3.23 + 0.87\, S\right]} \qquad \text{(Eq. 10)}$$

where:

q_g = flow rate, mcfd
k = gas permeability, md
$\overline{P}_r$ = reservoir pressure (shutin BHP), psia
P_{wf} = flowing bottom-hole pressure at sandface, psia
μ = viscosity, cp
T = temperature, °R (°F + 460)
Z = supercompressibility (dimensionless)
t = time of interest; $t < t_{stab}$ (hrs)
ϕ = porosity (fraction)
C_t = total system compressibility
r_w = wellbore radius, ft
S = skin factor (dimensionless)

V. Completion Pressure Drop Equations

A. Gravel-Packed Wells

(1) Oil Wells (General)

$$P_{wf_s} - P_{wf} = \Delta P = aq^2 + bq \qquad \text{(Eq. 11a)}$$

$$\Delta P = \frac{9.08 \times 10^{-13}\, \beta\, B_o^2\, \rho_o\, L}{A^2}\, q^2 + \frac{\mu_o\, B_o\, L}{1.127 \times 10^{-3}\, k_G A}\, q \qquad \text{(Eq. 11b)}$$

where:

$$a = \frac{9.08 \times 10^{-13} \beta\, B_o^2\, \rho_o\, L}{A^2}$$

$$b = \frac{\mu_o\, B_o\, L}{1.127 \times 10^{-3}\, kA}$$

q = flow rate, b/d
P_{wf} = pressure well flowing (wellbore), psi
P_{wf_s} = flowing BHP at sandface, psi
β = turbulence coefficient, ft^{-1}

For GP wells:

$$\beta = \frac{1.47 \times 10^7}{k_G^{0.55}}$$

B_o = formation volume factor, rb/stb
ρ_o = oil density, lb/ft^3
L = length of linear flow path, ft
A = total area open to flow, ft^2
(A = area of 1 perforation × shot density × perforated interval)
k_G = permeability of gravel, md

(2) Gas Wells (General)

$$P_{wf_s}^2 - P_{wf}^2 = aq^2 + bq \qquad \text{(Eq. 12a)}$$

$$P_{wf_s}^2 - P_{wf}^2 = \frac{1.247 \times 10^{-10}\, \beta\, \gamma_g\, TZL}{A^2}\, q^2 + \frac{8.93 \times 10^3\, \mu_g TZL}{k_G A}\, q \qquad \text{(Eq. 12b)}$$

where:

$$a = \frac{1.247 \times 10^{-10} \beta\, \gamma_g\, TZL}{A^2}$$

$$b = \frac{8.93 \times 10^3\, \mu_g TZL}{k_G A}$$

q = flow rate, mcfd
P_{wf_s} = flowing pressure at sandface, psia
P_{wf} = flowing bottom-hole pressure in wellbore, psia
β = turbulence factor, ft^{-1}

$$\beta = \frac{1.47 \times 10^7}{k_G^{0.55}}$$

γ_g = gas specific gravity (dimensionless)
T = temperature, °R (°F + 460)
Z = supercompressibility (dimensionless)
L = linear flow path
A = total area open to flow
(A = area of 1 perforation × shot density × perforated interval)
μ_g = gas viscosity, cp

B. Open Perforation Pressure Drop

(1) Oil Wells (General)

$$P_{wf_s} - P_{wf} = aq^2 + bq = \Delta P \qquad \text{(Eq. 13a)}$$

$$\Delta P = \left(\frac{2.30 \times 10^{-14}\, \beta\, B_o^2\, \rho_o \left(\frac{1}{r_p} - \frac{1}{r_c}\right)}{L_p^2} \right) q_2 + \left(\frac{\mu_o\, B_o (\ln r_c/r_p)}{7.08 \times 10^{-3} L_p\, k_p} \right) q \qquad \text{(Eq. 13b)}$$

where:

$$a = \frac{2.30 \times 10^{-14} \beta\, B_o^2\, \rho_o \left(\frac{1}{r_p} - \frac{1}{r_c}\right)}{L_p^2}$$

$$b = \frac{\mu_o\, B_o\, (\ln r_c/r_p)}{7.08 \times 10^{-3}\, L_p\, k_p}$$

q_o = flow rate/perforation (q/perforation), b/d

β = turbulence factor, ft^{-1}

$$\beta = \frac{2.33 \times 10^{10}}{k_p^{1.201}}$$

B_o = formation volume factor, rb/stb
ρ_o = oil density, lb/ft^3
L_p = perforation tunnel length, ft
μ_o = oil viscosity, cp
k_p = permeability of compacted zone, md
$k_p = 0.1k$ formation if shot overbalanced
0.4k formation if shot underbalanced
r_p = radius of perforation tunnel, ft
r_c = radius of compact zone, ft
($r_c = r_p + 0.5$ in.)

(2) Gas Wells (General)

$$P_{wf_s}{}^2 - P_{wf}{}^2 = aq^2 + bq \qquad \text{(Eq. 14a)}$$

$$P_{wf_s}{}^2 - P_{wf}{}^2 = \left(\frac{3.16 \times 10^{-12} \beta\, \gamma_g\, TZ \left(\frac{1}{r_p} - \frac{1}{r_c}\right)}{L_p^2} \right) q^2 + \left(\frac{1.424 \times 10^3\, \mu_g\, TZ (\ln r_c/r_p)}{k_p\, L_p} \right) q \qquad \text{(Eq. 14b)}$$

where:

$$a = \frac{3.16 \times 10^{-12} \beta \gamma_g\, TZ \left(\frac{1}{r_p} - \frac{1}{r_c}\right)}{L_p^2}$$

$$b = \frac{1.424 \times 10^3\, \mu_g\, TZ\, (\ln r_c/r_p)}{k_p\, L_p}$$

q = flow rate/perforation (q/perforation), mcfd

β = turbulence factor, ft^{-1}

$$\beta = \frac{2.33 \times 10^{10}}{k_p^{1.201}}$$

γ_g = gas specific gravity (dimensionless)
T = temperature, °R (°F + 460)
Z = supercompressibility factor (dimensionless)
r_c = radius of compact zone, ft
($r_c = r_p + 0.5$ in.)
r_p = radius of perforation, ft
L_p = perforation tunnel length, ft
μ_g = gas viscosity, cp
k_p = permeability of compacted zone, md
$k_p = 0.1k$ formation if shot overbalanced
0.4k formation if shot underbalanced

Appendix 5.1
Calculation data

TABLE 5A.1
VF DATA AT VARIOUS PRESSURES FOR THE FLUID OF WELL #1
(T = 170°F, R_{sw} = 0, B_w = 1.0)

P	R_s	B_o	B_g	VF
200	27.9	1.0631	0.0155	3.9210
400	64.4	1.0782	0.0076	2.3197
600	105	1.0953	0.0050	1.7900
800	148.4	1.1141	0.0038	1.5302
1,000	194.2	1.1343	0.0030	1.3733
1,200	241.9	1.1557	0.0025	1.2718
1,400	291.3	1.1783	0.0021	1.2025
1,600	342.2	1.2019	0.0018	1.1533
1,800	394.3	1.2266	0.0015	1.1175
2,000*	400	1.2259	—	1.1129
2,200	400	1.2227	—	1.1114
2,400	400	1.2201	—	1.1101
2,600	400	1.2179	—	1.1090
2,800	400	1.2160	—	1.1080
3,000	400	1.2144	—	1.1072
3,200	400	1.2129	—	1.1058
3,400	400	1.2117	—	1.1058
3,600	400	1.2106	—	1.1053
3,800	400	1.2096	—	1.1048
4,000	400	1.2087	—	1.1043
4,200	400	1.2078	—	1.1039
4,400	400	1.2071	—	1.1036
4,600	400	1.2064	—	1.1032
4,800	400	1.2058	—	1.1029
5,000	400	1.2052	—	1.1026

* Above the bubble-point pressure

TABLE 5A.2
VF DATA AT VARIOUS PRESSURES FOR THE FLUID OF WELL #2
(T = 167°F)

P	R_s	B_o	B_g	VF
200	31.1	1.0554	0.0157	3.7216
400	71.6	1.0788	0.0077	2.0639
600	116.8	1.0975	0.0050	1.5176
800	165.2	1.1180	0.0037	1.2483
1,000*	200	1.1315	—	1.1315
1,200	200	1.1277	—	1.1277
1,400	200	1.1249	—	1.1249
1,600	200	1.1229	—	1.1229
1,800	200	1.1213	—	1.1213
2,000	200	1.1200	—	1.1200
2,200	200	1.1190	—	1.1190
2,400	200	1.1181	—	1.1181
2,600	200	1.1174	—	1.1174
2,800	200	1.1168	—	1.1168
3,000	200	1.1162	—	1.1162
3,200	200	1.1157	—	1.1157
3,400	200	1.1153	—	1.1153
3,600	200	1.1149	—	1.1149
3,800	200	1.1146	—	1.1146
4,000	200	1.1143	—	1.1143
4,200	200	1.1140	—	1.1140
4,400	200	1.1138	—	1.1138
4,600	200	1.1136	—	1.1136
4,800	200	1.1134	—	1.1134
5,000	200	1.1132	—	1.1132

* Above the bubble-point pressure

TABLE 5A.3
CALCULATION OF IPR'S FOR THE RESERVOIR OF WELL #1
(q_{max} = 6,267, PI = 5, $\overline{P}_r$ = 1,920, P_b = 1,820)

P_{wf}	q_{sc}	VF	V
1,900	100	1.1139	111
1,800	686	1.1175	766
1,700	1,227	1.1342	1,391
1,600	1,741	1.1533	2,008
1,500	2,228	1.1759	2,620
1,400	2,687	1.2025	3,232
1,300	3,120	1.2340	3,850
1,200	3,525	1.2718	4,483
1,100	3,903	1.3175	5,143
1,000	4,354	1.3733	5,842
900	4,578	1.4425	6,604
800	4,874	1.5302	7,459
700	5,144	1.6410	8,441
600	5,386	1.7900	9,641
500	5,601	2.0009	11,207
400	5,788	2.3197	13,427
300	5,949	2.8532	16,973
200	6,082	3.9210	23,848

TABLE 5A.4
CALCULATION OF IPR'S FOR THE RESERVOIR OF WELL #2
(q_{max} = 400, PI = 0.4, $\overline{P}_r$ = 1,500, P_b = 940)

P_{wf}	q_{sc}	VF	V
1,400	40	1.1249	45
1,300	80	1.1262	90
1,200	120	1.1277	135
1,100	160	1.1294	181
1,000	200	1.1315	226
900	237	1.1607	275
800	266	1.2483	332
700	293	1.3629	400
600	317	1.5176	481
500	338	1.7359	586
400	356	2.0639	735
300	371	2.6093	970
200	384	3.7216	1,428
100	393	6.9272	2,724

TABLE 5A.5
INTAKE PRESSURE FOR AN ELECTRIC SUBMERSIBLE PUMP IN WELL #1 (PUMPING LIQUID)

			P_3 for assumed number of stages of					
q_{sc}	P_2	h	150	175	200	250	300	350	400
3,500	3,777	37	1,465	1,080	695	−76	−846	−1,617	−2,387
4,000	3,890	35.5	1,672	1,302	933	193	−546	−1,285	−2,025
4,500	4,017	34	1,893	1,539	1,185	477	−232	−940	−1,648
5,000	4,160	32.2	2,147	1,812	1,476	806	135	−535	−1,206
5,500	4,315	29.9	2,447	2,136	1,824	1,202	579	−44	−666
6,000	4,487	27.5	2,769	2,482	2,196	1,623	1,059	478	−95
6,500	4,763	24.8	3,124	2,866	2,608	2,091	1,575	1,058	542
7,000	4,876	21.4	3,539	3,316	3,093	2,647	2,202	1,756	1,310

TABLE 5A.6
HORSEPOWER REQUIREMENT FOR POSSIBLE RATES FROM WELL #1 WITH AN ELECTRIC PUMP (PUMPING LIQUID)

St	q_p	hp	HP	$\Delta q_p/\Delta St$
150	3,075	1.66	240	12.5
175	3,700	1.72	290	9.1
200	4,190	1.79	344	8.1
250	4,950	1.82	438	5.9
300	5,480	1.83	528	4.5
350	5,880	1.83	616	3.6
400	4,180	1.82	700	—

TABLE 5A.7
INTAKE PRESSURE FOR AN ELECTRIC SUBMERSIBLE PUMP IN WELL #2 (PUMPING LIQUID)

			P_3 for assumed number of stages of					
q_{sc}	P_2	h	150	200	250	300	350	400
50	2,724	21.6	1,567	1,181	796	410	24	−362
100	2,726	21.5	1,573	1,189	805	421	37	−347
150	2,727	21.2	1,590	1,212	833	454	76	−303
200	2,728	20.8	1,613	1,241	870	498	127	−245
250	2,730	19.9	1,664	1,309	953	598	242	−113
300	2,734	18.8	1,726	1,390	1,055	719	383	47
350	2,737	17.5	1,800	1,487	1,174	862	549	237
400	2,741	16.2	1,873	1,583	1,294	1,005	715	426

TABLE 5A.8
HORSEPOWER REQUIREMENT FOR POSSIBLE RATES FROM WELL #2 WITH AN ELECTRIC SUBMERSIBLE PUMP
(PUMPING LIQUID)

St	q_p	hp	HP	$\Delta q_p/\Delta St$
200	120	0.0800	13.2	2.2
250	230	0.0942	19.4	1.3
300	295	0.0997	24.6	0.84
350	337	0.1034	29.9	0.66
400	370	0.1066	35.2	—

TABLE 5A.9
CALCULATION OF THE NUMBER OF STAGES FOR AN ELECTRICAL PUMP IN WELL #1
(PUMPING 3,000 stbl/d WITH ALL GAS)

i	$P_{3,i}$	$\bar{P}_{3,i}$	$\overline{VF}_i$	$\bar{V}_i$	$\bar{h}_i$	ΔSt_i	St_i
0	3,178*	—	—	—	—	—	—
1	3,128	3,153	1.1066	3,319	37.5	3.4	3.4
2	3,078	3,103	1.1068	3,320	37.5	3.4	6.8
3	3,028	3,053	1.1070	3,321	37.5	3.4	10.2
4	2,978	3,003	1.1072	3,322	37.5	3.4	13.6
5	2,928	2,953	1.1074	3,322	37.5	3.4	17
6	2,878	2,903	1.1076	3,323	37.5	3.4	20.4
7	2,828	2,853	1.1078	3,323	37.5	3.4	23.8
8	2,778	2,803	1.1080	3,324	37.5	3.4	27.2
9	2,728	2,753	1.1082	3,325	37.4	3.4	30.6
10	2,678	2,703	1.1084	3,325	37.4	3.4	34
11	2,628	2,653	1.1078	3,326	37.4	3.5	37.5
12	2,578	2,603	1.1089	3,327	37.4	3.5	41
13	2,528	2,553	1.1092	3,328	37.4	3.5	44.5
14	2,478	2,503	1.1095	3,328	37.4	3.5	48
15	2,428	2,453	1.1097	3,329	37.4	3.5	51.5
16	2,378	2,403	1.1100	3,330	37.4	3.5	55
17	2,328	2,353	1.1103	3,331	37.4	3.5	58.5
18	2,278	2,303	1.1107	3,332	37.4	3.5	62
19	2,228	2,253	1.1110	3,333	37.4	3.5	64.4
20	2,178	2,203	1.1113	3,334	37.4	3.5	69
21	2,128	2,153	1.1117	3,335	37.4	3.5	72.5
22	2,078	2,103	1.1121	3,336	37.4	3.5	76
23	2,028	2,053	1.1125	3,338	37.4	3.5	79.5
24	1,978	2,003	1.1129	3,339	37.4	3.5	83
25	1,928	1,953	1.1133	3,340	37.4	3.5	86.5
26	1,878	1,903	1.1138	3,341	37.4	3.5	90
27	1,828	1,853	1.1145	3,342	37.4	3.5	93.5
28	1,778	1,803	1.1172	3,352	37.4	3.5	97
29	1,728	1,753	1.125	3,375	37.3	3.5	100.5
30	1,678	1,703	1.1336	3,401	37.3	3.5	104
31	1,628	1,653	1.1427	3,428	37.2	3.6	107.6
32	1,578	1,603	1.1527	3,458	37.1	3.6	111.2
33	1,528	1,553	1.1634	3,490	37	3.7	114.9
34	1,478	1,503	1.1751	3,525	36.9	3.7	118.6
35	1,428	1,453	1.1877	3,563	36.8	3.8	122.4
36	1,378	1,403	1.2015	3,605	36.7	3.8	126.2
37	1,328	1,353	1.2165	3,649	36.6	3.9	130.1
38	1,278	1,303	1.2329	3,699	36.4	3.9	134
40	1,228	1,253	1.2507	3,752	36.3	4	138
41	1,178	1,203	1.2705	3,811	36.1	4.1	142.1
42	1,128	1,153	1.2919	3,876	35.9	4.2	146.3
43	1,078	1,103	1.3158	3,948	35.7	4.3	150.6
44	1,028	1,053	1.3149	4,026	35.4	4.4	155
45	978	1,003	1.3712	4,114	35.2	4.5	159.5
46	928	953	1.4034	4,210	34.9	4.7	164.2
47	878	903	1.4400	4,320	34.5	4.9	169.1
48	828	853	1.4806	4,442	34.2	5	174.1
49	778	803	1.5269	4,581	33.7	5.3	179.4
50	728	753	1.5772	4,732	33.2	5.5	184.9
51	678	703	1.6368	4,910	32.5	5.9	190.8

* Discharge pressure

TABLE 5A.9 (*Continued*)

i	$P_{3,i}$	$\bar{P}_{3,i}$	$\overline{VF}_i$	$\bar{V}_i$	$\bar{h}_i$	ΔSt_i	St_i
52	628	653	1.7030	5,109	31.7	6.2	197
53	578	603	1.7842	5,353	30.6	6.8	203.8
54	528	553	1.8752	5,626	29.3	7.4	211.2
55	478	503	1.9924	5,977	27.6	8.4	219.6
56	428	453	2.1232	6,370	25.5	9.7	229.3
57	378	403	2.306	6,918	22	12.2	241.5
58	328	353	2.5026	7,508	17.9	16.2	257.7

TABLE 5A.10
INTAKE PRESSURE FOR AN ELECTRICAL SUBMERSIBLE PUMP IN WELL #1 (PUMPING LIQUID AND GAS)

		Interpolated values of P_3 for number of stages of								
q_{sc}	P_2	150	175	200	250	300	350	400	450	500
3,500	3,340	1,293	1,012	777	467	345	—	—	—	—
4,000	3,115	1,538	1,246	991	624	449	378	328	—	—
4,500	3,698	1,824	1,525	1,256	833	591	492	446	443	—
5,000	3,887	2,156	1,871	1,593	1,121	800	633	563	534	—
5,500	4,093	2,516	2,255	1,995	1,497	1,105	850	718	660	—
6,000	4,308	2,910	2,679	2,448	1,989	1,551	1,206	974	846	785
6,500	4,536	3,358	3,163	2,968	2,580	2,194	1,812	1,470	1,215	1,050
7,000	4,773	3,821	3,663	3,506	3,192	2,879	2,568	2,259	1,953	1,659

— is negative pressure

TABLE 5A.11
CALCULATION OF HORSEPOWER FOR AN ELECTRIC PUMP IN WELL #1 (PUMPING 3,370 STBL/D WITH ALL GAS)

i	$P_{3,i}$	$\bar{P}_{3,i}$	$\overline{VF}_i$	$\bar{V}_i$	$\overline{hp}_i$	$\bar{h}_i$	ΔHP_i	HP_i
0	3,298*	—	—	—	—	—	—	—
1	3,248	3,273	1.1062	3,728	1.73	36.3	5.49	5.49
2	3,198	3,223	1.1064	3,729	1.73	36.3	5.49	10.98
3	3,148	3,173	1.1066	3,729	1.73	36.3	5.49	16.47
4	3,098	3,123	1.1067	3,730	1.73	36.3	5.49	21.96
5	3,048	3,073	1.1069	3,730	1.73	36.3	5.49	27.45
6	2,998	3,023	1.1071	3,731	1.73	36.3	5.49	32.94
7	2,948	2,973	1.1073	3,732	1.73	36.3	5.49	38.43
8	2,898	2,923	1.1075	3,732	1.73	36.3	5.49	43.92
9	2,848	2,873	1.1077	3,733	1.73	36.3	5.49	49.41
10	2,798	2,823	1.1079	3,634	1.73	36.3	5.49	54.90
11	2,748	2,773	1.1081	3,734	1.73	36.3	5.49	60.39
12	2,698	2,723	1.1084	3,735	1.73	36.3	5.49	65.88
13	2,648	2,673	1.1086	3,736	1.73	36.3	5.50	71.38
14	2,598	2,623	1.1088	3,737	1.73	36.3	5.50	76.88
15	2,548	2,573	1.1091	3,738	1.73	36.3	5.50	82.38
16	2,498	2,523	1.1094	3,739	1.73	36.3	5.50	87.88
17	2,448	2,473	1.1096	3,740	1.73	36.3	5.50	93.38
18	2,398	2,423	1.1099	3,740	1.73	36.3	5.50	98.88
19	2,348	2,373	1.1102	3,742	1.73	36.3	5.50	104.38
20	2,298	2,323	1.1105	3,743	1.73	35.3	5.50	109.88
21	2,248	2,273	1.1109	3,744	1.73	36.3	5.50	115.38
22	2,198	2,223	1.1112	3,745	1.73	36.3	5.50	120.88
23	2,148	2,173	1.1116	3,746	1.73	36.3	5.50	126.38
24	2,098	2,123	1.1119	3,747	1.73	36.3	5.51	131.89
25	2,047	2,073	1.1123	3,749	1.73	36.3	5.51	137.40
26	1,998	2,023	1.1127	3,750	1.73	36.3	5.51	142.91
27	1,948	1,973	1.1129	3,751	1.73	36.3	5.51	148.42
28	1,894	1,923	1.1134	3,752	1.73	36.3	5.51	153.93
29	1,848	1,873	1.1136	3,753	1.73	36.3	5.51	159.44
30	1,798	1,823	1.1155	3,759	1.73	36.2	5.52	164.96
31	1,748	1,773	1.1218	3,780	1.73	36.2	5.53	170.49
32	1,698	1,723	1.1301	3,808	1.74	36.1	5.56	176.05

* Discharge pressure

TABLE 5A.11 (*Continued*)

i	$P_{3,i}$	$\bar{P}_{3,i}$	$\overline{VF}_i$	$\bar{V}_i$	$\overline{hp}_i$	$\bar{n}_i$	ΔHP_i	HP_i
33	1,648	1,673	1.139	3,838	1.74	36	5.58	181.63
34	1,598	1,623	1.1486	3,871	1.74	35.9	5.61	187.24
35	1,548	1,573	1.1590	3,906	1.75	35.8	5.64	192.88
36	1,498	1,523	1.1703	3,944	1.75	35.7	5.67	198.55
37	1,448	1,473	1.1826	3,985	1.76	35.6	5.71	204.26
38	1,398	1,423	1.1959	4,030	1.76	35.4	5.75	210.01
39	1,348	1,373	1.2104	4,079	1.77	35.3	5.78	215.79
40	1,298	1,323	1.2262	4,132	1.77	35.1	5.83	216.62
41	1,248	1,273	1.2435	4,191	1.78	34.9	5.87	227.49
42	1,238	1,243	1.2546	4,228	1.78	34.8	1.18	228.67

TABLE 5A.12
HORSEPOWER REQUIREMENTS FOR POSSIBLE RATES FROM WELL #1 WITH AN ELECTRIC PUMP (PUMPING LIQUID AND GAS)

St	q_p	P_3	P_2	HP	$\Delta q_p/\Delta St$
150	3,370	1,238	3,298	229	9.1
175	3,760	1,137	3,429	272	8.1
200	4,100	1,045	3,551	314	6.5
250	4,610	892	3,740	393	4.8
300	4,950	775	3,868	464	3.5
350	5,150	695	3,947	521	2.3
400	5,275	645	4,000	575	0.9
450	5,350	615	4,030	653	0.2
500	5,380	602	4,042	786	—

TABLE 5A.13
INTAKE PRESSURE FOR AN ELECTRIC SUBMERSIBLE PUMP IN WELL #2 (PUMPING LIQUID AND GAS)

		P_3 for number of stages of					
q_{sc}	P_2	150	200	250	300	350	400
50	2,396	1,329	975	655	316	250	—
100	2,257	1,197	850	562	356	220	157
150	2,190	1,150	812	542	356	238	190
200	2,153	1,145	818	561	387	284	228
250	2,132	1,182	870	617	446	349	298
300	2,122	1,239	947	694	522	426	378
350	2,121	1,310	1,042	791	615	514	462
400	2,121	1,406	1,171	937	745	627	563
450	2,124	1,542	1,350	1,159	970	808	707

TABLE 5A.14
HORSEPOWER REQUIREMENT FOR POSSIBLE RATES FROM WELL #2 WITH AN ELECTRIC PUMP (PUMPING LIQUID AND GAS)

St	q_p	P_3	P_2	HP	$\Delta q_p/\Delta St$
150	140	1,140	2,200	9.7	2.14
200	247	860	2,133	15.1	1.00
250	297	680	2,122	19.4	0.56
300	325	560	2,119	23.3	0.30
350	340	495	2,121	26.2	0.14
400	347	455	2,121	29	—

TABLE 5A.15
INTAKE PRESSURE FOR A HYDRAULIC PUMP IN WELL #1 (PUMPING LIQUID)

			P_3 for assumed power fluid pressures of									
q_{sc}	P_2	F_p	4,500	5,000	5,500	6,000	6,500	7,000	7,500	8,000	8,500	9,000
400	3,200	110	2,159	1,721	1,283	845	408	—	—	—	—	—
800	3,273	131	2,314	1,876	1,438	1,000	453	125	—	—	—	—
1,200	3,387	205	2,595	2,154	1,716	1,278	840	402	—	—	—	—
1,600	3,541	279	2,945	2,507	2,069	1,631	1,193	755	318	—	—	—
2,000	3,735	378	3,396	2,958	2,520	2,082	1,645	1,207	769	331	—	—
2,400	3,971	506	3,951	3,513	3,075	2,637	2,199	1,761	1,324	886	448	10
2,800	4,249	677	4,623	4,185	3,747	3,309	2,871	2,434	1,996	1,558	1,120	682
3,200	4,572	850	5,379	4,941	4,503	4,066	3,628	3,190	2,752	2,314	1,876	1,439
3,600	4,950	935	6,144	5,707	5,269	4,831	4,393	3,955	3,517	3,080	2,641	2,204

TABLE 5A.16
HORSEPOWER REQUIREMENT FOR POSSIBLE RATES FROM WELL #1 WITH A HYDRAULIC PUMP (PUMPING LIQUID)

P_1	q_p	N	q_1	P_s	HP	$\Delta q_p/\Delta HP$
5,000	650	10	744	2,221	28	15
5,500	1,190	18	1,362	2,777	64	10.3
6,000	1,590	25	1,819	3,337	103	7.7
6,500	1,920	30	2,197	3,903	146	6.4
7,000	2,220	34	2,540	4,477	193	5
7,500	2,470	38	2,826	5,052	243	4.4
8,000	2,710	42	3,101	5,635	297	3.7
8,500	2,925	45	3,347	6,221	354	3.3
9,000	3,125	49	3,576	6,811	414	—

TABLE 5A.17
INTAKE PRESSURE FOR A HYDRAULIC PUMP IN WELL #2 (PUMPING LIQUID)

			P_3 for assumed power pressures of					
q_{sc}	P_2	F_p	3,500	3,750	4,000	4,250	4,500	4,750
50	2,727	52	1,394	931	468	—	—	—
100	2,741	97	1,516	1,053	590	127	—	—
150	2,159	156	1,675	1,212	749	286	—	—
200	2,783	202	1,828	1,365	900	439	—	—
250	2,812	260	2,020	1,557	1,094	631	168	—
300	2,847	327	2,244	1,781	1,318	855	392	—
350	2,887	406	2,505	2,042	1,579	1,116	653	190
400	2,934	454	2,725	2,262	1,799	1,336	873	410

TABLE 5A.18
HORSEPOWER REQUIREMENT FOR POSSIBLE RATE FROM WELL #2 WITH A HYDRAULIC PUMP (PUMPING LIQUID)

P_1	q_p	N	q_1	P_s	HP	$\Delta q_p/\Delta HP$
3,500	47	18.7	142	860	2.1	15.25
3,750	137	54.5	415	1,124	8	10.38
4,000	220	87.4	666	1,405	16	7.23
4,250	280	111.3	848	1,684	24.3	5.49
4,500	330	131.2	1,000	1,963	33.4	4.38
4,750	372	147.9	1,127	2,242	43	—

TABLE 5A.19
POWER FLUID PRESSURE FOR A HYDRAULIC PUMP IN WELL #1 (PUMPING 400 stbl/d WITH ALL GAS)

P_3	VF	N	%RS	F_p	q_1	q_2	GOR_2	WC_2	P_2	P_1
200	3.9210	24.36	45.95	273	1,795	2,195	40	0.09	3,175	6,846
300	2.8532	17.72	33.44	193	1,306	1,706	53	0.12	3,122	6,538
400	2.3197	14.41	27.19	153	1,062	1,462	63	0.14	3,098	6,332
500	2.0009	12.53	23.45	131	916	1,316	72	0.15	3,082	6,162
600	1.7900	11.12	20.98	116	819	1,219	78	0.16	3,072	6,010
700	1.6410	10.19	19.23	106	751	1,151	84	0.17	3,065	5,871
800	1.5302	9.50	17.93	99	700	1,100	89	0.18	3,052	5,723
900	1.4425	8.96	16.91	93	660	1,060	93	0.19	3,047	5,591
1,000	1.3733	8.53	16.10	89	629	1,029	97	0.19	3,042	5,463
1,100	1.3175	8.18	15.44	85	603	1,003	100	0.20	3,038	5,337
1,200	1.2718	7.90	14.91	82	582	982	102	0.20	3,035	5,213
1,300	1.2340	7.67	14.46	80	565	965	105	0.21	3,033	5,091
1,400	1.2025	7.47	14.10	78	550	950	107	0.21	3,030	4,970
1,500	1.1759	7.30	13.78	76	538	938	108	0.21	3,029	4,852
1,600	1.1533	7.16	13.52	75	527	927	110	0.22	3,027	4,732
1,700	1.1342	7.04	13.29	73	519	919	111	0.22	3,025	4,613
1,800	1.1175	6.94	13.10	72	512	912	112	0.22	3,024	4,495
1,900	1.1139	6.92	13.10	72	510	910	113	0.22	3,024	4,380
2,000	1.1129	6.91	13	72	510	910	113	0.22	3,024	4,265

TABLE 5A.20
INTAKE PRESSURE FOR A HYDRAULIC PUMP IN WELL #1 (PUMPING LIQUID AND GAS)

	Interpolated values of P_3 for power fluids pressures of								
q_{sc}	4,500	5,000	5,500	6,000	6,500	7,000	7,500	8,000	8,500
400	1,795	1,375	971	607	317	162	—	—	—
800	1,946	1,584	1,195	849	562	378	280	225	179
1,200	2,324	1,888	1,496	1,142	845	624	477	385	320
1,600	2,739	2,304	1,870	1,504	1,185	930	737	598	495
2,000	3,277	2,842	2,408	1,975	1,605	1,308	1,068	880	734
2,400	3,926	3,491	3,057	2,623	2,192	1,777	1,486	1,242	1,042
2,800	4,677	4,242	3,807	3,372	2,939	2,507	2,078	1,705	1,444
3,200	—	—	4,578	4,143	3,707	3,273	2,839	2,407	1,977
3,600	—	—	—	4,881	4,405	4,010	3,576	3,142	2,710

TABLE 5A.21
HORSEPOWER REQUIREMENT FOR POSSIBLE RATES FROM WELL #1 WITH A HYDRAULIC PUMP (PUMPING LIQUID AND GAS)

P_1	q_p	P_3	VF	N	q_1	P_s	HP	$\Delta q_p/\Delta HP$
4,500	530	1,830	1.1150	9.18	676	1,659	19.1	16.17
5,000	1,020	1,740	1.1272	17.85	1,316	2,209	49.4	10.32
5,500	1,405	1,665	1.1405	24.88	1,834	2,781	86.7	7.25
6,000	1,700	1,610	1.1513	30.39	2,240	3,346	127.4	5.97
6,500	1,955	1,560	1.1619	35.27	2,599	3,849	170.1	4.45
7,000	2,180	1,510	1.1734	39.72	2,927	4,435	220.7	3.70
7,500	2,390	1,470	1.1833	43.92	3,236	5,042	277.4	2.94
8,000	2,570	1,430	1.1940	47.65	3,511	5,672	338.6	2.58
8,500	2,750	1,390	1.2053	51.47	3,793	6,332	408.3	—

TABLE 5A.22
INTAKE PRESSURE FOR A HYDRAULIC PUMP IN WELL #2
(PUMPING LIQUID AND GAS)

	Interpolated values of P_3 for power fluid pressures					
q_{sc}	3,500	3,750	4,000	4,250	4,500	4,750
50	1,285	843	506	310	210	150
100	1,457	998	640	430	315	240
150	1,644	1,185	805	570	440	360
200	1,890	1,430	1,015	735	585	490
250	2,196	1,740	1,285	950	780	660
300	2,533	2,074	1,617	1,240	1,020	870
350	2,942	2,481	2,019	1,560	1,340	1,140

TABLE 5A.23
HORSEPOWER REQUIREMENT FOR POSSIBLE RATES FROM WELL #2 WITH A HYDRAULIC PUMP (PUMPING LIQUID AND GAS)

P_1	q_p	P_3	VF	N	q_1	P_s	HP	$\Delta q_p/\Delta HP$
3,500	66	1,335	1.1257	29.53	225	862	3	12.67
3,750	142	1,150	1.1285	63.69	485	1,131	9	7.86
4,000	197	1,010	1.1301	88.48	674	1,406	16	5.13
4,250	238	895	1.1645	110.15	840	1,682	24	2.75
4,500	260	825	1.2238	126.47	964	1,956	32	1.89
4,750	277	765	1.2838	141.34	1,077	2,232	41	—

TABLE 5A.24
INTAKE PRESSURE FOR A JET PUMP IN WELL #1 (PUMPING LIQUID)

		P_3 for assumed power fluid pressures of						
q_{sc}	P_2	6,000	7,000	8,000	9,000	10,000	11,000	12,000
400	3,169	1,825	1,350	875	400	—	—	—
800	3,314	2,038	1,563	1,088	613	138	—	—
1,200	3,542	2,375	1,900	1,425	950	475	0	—
1,600	3,855	2,836	2,361	1,886	1,411	936	461	—
2,000	4,256	3,428	2,953	2,478	2,003	1,528	1,053	578
2,400	4,750	4,156	3,681	3,206	2,731	2,256	1,781	1,306
2,800	5,343	5,031	4,556	4,081	3,606	3,131	2,656	2,181

TABLE 5A.25
HORSEPOWER REQUIREMENTS FOR THE POSSIBLE RATES FROM WELL #1 WITH A JET PUMP (PUMPING LIQUID)

P_1	q_p	q_1	P_s	HP	$\Delta q_p/\Delta HP$
6,000	450	947	3,198	52	5.3
7,000	1,030	2,168	4,354	161	3.2
8,000	1,425	3,000	5,588	285	2.2
9,000	1,740	3,663	6,923	431	1.6
10,000	2,010	4,232	8,361	601	1.3
11,000	2,255	4,757	9,874	797	1.0
12,000	2,470	5,200	11,386	1,007	—

TABLE 5A.26
INTAKE PRESSURE FOR A JET PUMP IN WELL #2 (PUMPING LIQUID)

		Intake pressure for assumed power fluid pressures of					
q_{sc}	P_2	5,500	6,000	6,500	7,000	7,500	8,000
50	2,727	1,409	1,172	934	697	459	222
100	2,735	1,421	1,183	946	708	471	233
200	2,761	1,460	1,222	985	747	510	272
300	2,800	1,518	1,281	1,043	806	568	331
400	2,853	1,596	1,359	1,121	884	646	409
500	2,920	1,694	1,456	1,219	981	744	506
600	2,999	1,811	1,573	1,336	1,098	861	623
700	3,091	1,947	1,710	1,472	1,235	997	760
800	3,197	2,103	1,886	1,628	1,391	1,153	916
900	3,317	2,280	2,042	1,805	1,567	1,330	1,092

TABLE 5A.27
HORSEPOWER REQUIREMENTS FOR POSSIBLE RATES FROM WELL #2 WITH A JET PUMP (PUMPING LIQUID)

P_1	q_p	q_1	P_s	HP	$\Delta q_p/\Delta HP$
5,500	40	84	2,862	4	7.91
6,000	127	267	3,381	15	5.57
6,500	205	432	3,906	29	4.50
7,000	268	564	4,436	43	3.71
7,500	320	674	4,973	57	2.86
8,000	360	758	5,513	71	—

TABLE 5A.28
POWER FLUID PRESSURE FOR A JET PUMP IN WELL #1 (PUMPING 200 stbl/d WITH ALL GAS)

P_3	VF	q_1	q_2	GOR_2	wc_2	P_2	P_1
500	1.9899	838	1,038	43	0.096	3,066	8,467
600	1.7767	748	948	47	0.106	3,061	8,243
700	1.6256	684	884	51	0.113	3,059	8,024
800	1.5134	637	837	54	0.120	3,057	7,808
900	1.4274	601	801	57	0.125	3,056	7,594
1,000	1.3598	573	773	59	0.129	3,054	7,379
1,100	1.3057	550	750	62	0.133	3,053	7,164
1,200	1.2618	531	731	63	0.137	3,051	6,949
1,300	1.2257	516	716	65	0.140	3,050	6,735
1,400	1.1957	503	703	66	0.199	3,049	6,521
1,500	1.1708	493	693	67	0.144	3,044	6,295
1,600	1.1499	484	684	68	0.146	3,043	6,082
1,700	1.1323	477	677	69	0.148	3,043	5,870
1,800	1.1175	471	671	70	0.149	3,042	5,657

TABLE 5A.29
INTAKE PRESSURE FOR A JET PUMP IN WELL #1 (PUMPING LIQUID AND GAS)

	Interpolated valves of P_3 for power fluid pressures of						
q_{sc}	6,000	7,000	8,000	9,000	10,000	11,000	12,000
400	1,702	1,243	800	422	221	120	86
800	1,932	1,483	1,070	719	478	343	272
1,200	2,310	1,838	1,426	1,068	788	594	469
1,600	2,822	2,351	1,881	1,491	1,170	919	737
2,000	3,470	2,998	2,528	2,060	1,648	1,338	1,093
2,400	4,253	3,781	3,310	2,840	2,373	1,909	1,569
2,800	—	4,699	4,227	3,757	3,287	2,820	2,355

TABLE 5A.30
HORSEPOWER REQUIREMENTS FOR THE POSSIBLE RATES FROM WELL #1 WITH A JET PUMP (PUMPING LIQUID AND GAS)

P_1	q_p	P_3	VF	q_1	P_s	HP	$\Delta q_p/\Delta HP$
6,000	630	1,815	1.1162	1,480	3,233	81	4.1
7,000	1,090	1,730	1.1276	2,587	4,398	193	2.5
8,000	1,420	1,665	1.1381	3,402	5,654	327	1.7
9,000	1,690	1,615	1.1470	4,081	7,025	487	1.2
10,000	1,925	1,560	1.1578	4,692	8,517	679	0.96
11,000	2,140	1,515	1.1674	5,259	10,095	903	0.78
12,000	2,325	1,430	1.1754	5,753	11,661	1,140	—

TABLE 5A.31
INTAKE PRESSURE FOR A JET PUMP IN WELL #2 (PUMPING LIQUID AND GAS)

	Interpolated values of P_3 for power fluid pressures of					
q_{sc}	5,500	6,000	6,500	7,000	7,500	8,000
50	1,297	1,060	833	621	413	270
100	1,294	1,056	832	626	434	300
150	1,305	1,068	843	640	460	330
200	1,327	1,090	867	670	490	360
300	1,397	1,160	930	730	570	430
400	1,488	1,252	1,015	810	645	520
500	1,605	1,369	1,133	910	735	600
600	1,745	1,509	1,275	1,040	850	710
700	1,908	1,672	1,437	1,202	—	—

TABLE 5A.32
HORSEPOWER REQUIREMENTS FOR POSSIBLE RATES FROM WELL #2 WITH A JET PUMP (PUMPING LIQUID AND GAS)

P_1	q_p	P_3	VF	q_1	P_s	HP	$\Delta q_p/\Delta HP$
5,500	85	1,295	1.1263	202	2,871	10	6.21
6,000	172	1,075	1.1274	408	3,394	24	4.25
6,500	240	885	1.1721	592	3,925	40	2.14
7,000	285	720	1.3367	802	4,471	61	1.21
7,500	320	580	1.5525	1,046	5,039	90	0.68
8,000	345	465	1.8260	1,326	5,637	127	—

TABLE 5A.33
REQUIRED STROKE LENGTH FOR POSSIBLE RATES FROM WELL #1 WITH A CONVENTIONAL BEAM PUMP (PUMPING LIQUID)

N	q_p	S
25	272	29.17
20	338	45.31
15	448	80.07
10	665	178.28
8	818	274.13

TABLE 5A.34
REQUIRED STROKE LENGTH FOR POSSIBLE RATES FROM WELL #2 WITH A CONVENTIONAL BEAM PUMP (PUMPING LIQUID)

N	q_p	S
26	216	39.60
24	231	45.86
22	250	54.16
20	271	64.59
18	296	78.38
16	325	96.82
14	359	122.23

TABLE 5A.35
REQUIRED STROKE LENGTH FOR POSSIBLE RATES FROM WELL #1 WITH A CONVENTIONAL BEAM PUMP (PUMPING LIQUID AND GAS)

N	q_p — bbl/d	q_p — stbl/d	S
30	250	225	22.34
25	300	275	32.17
20	374	335	50.13
15	492	440	87.94
10	732	645	196.25

TABLE 5A.36
REQUIRED STROKE LENGTH FOR POSSIBLE RATES FROM WELL #2 WITH A CONVENTIONAL BEAM PUMP (PUMPING LIQUID AND GAS)

N	q_p — bbl/d	q_p — stbl/d	S
20	266	225	63.41
18	321	260	85.02
16	357	277	106.37
14	403	295	137.23
12	464	315	184.33
10	548	332	257.33
8	673	352	395.03

Index

A

acceleration component (for pipe flow), 71, 73
Al-Hussainy, 50
Arthur coning method, 295–299
Arthur fingering method, 319
artificial barrier (remedial treatment for coning), 318
artificial lift, 3, 185–248: Nodal systems analysis, 185, 187; design of system, 185; analysis of system, 185; mechanical pumping system, 185–187, 189; gas lift system, 191, 193, 196–199; system components, 185; solution position in Nodal systems analysis, 187
assisted gas flow, 249: plunger lift, 249; foam, 249; rotative gas lift, 249; bottom-hole separation, 249
Aziz correlation, 73

B

back-pressure equation, 425–427
bailed sample (from formation), 125–126
beam pump, 230–234, 245–247, 288–289: components, 230; surface pumping unit, 230–231; sucker rod string, 231; subsurface pump, 231, 233; displacement, 233; plunger size, 233–234; pumping cycle, 233; size, 234; for gas well, 288–289
Beggs and Brill correlation, 73
Birks coning method, 312–316
black oil (gas well), 250–251; multiphase flow correlation, 259
bottom-hole flowing pressure (for composite inflow performance relationship curves), 30–32, 186–187
bottom-hole position (for solution of Nodal systems analysis), 89–92, 196
bottom-hole pressure, 76, 254–257, 333–335: gas well, 254–257; static, 254–257; flowing, 256–257
bottom-hole restriction, 3
bottom-hole separation (gas well), 249
bottom-hole/wellhead combination position (for solution of Nodal systems analysis), 94–95
brine effect (on foaming tendency), 279
brine-oil mixture, 279
bubble-point liquid, 332
bubble-point pressure factor, 8–9, 332

C

casing pressure (effects of in gas lift), 197–198
cavitation (jet pump), 221–222
Chaney *et al.* coning method, 301–306
chemical injection (of foam), 279
chemical treatment problems, 280: emulsion, 280; foam carryover, 280
Chierici *et al.* coning method, 306–310
choke, 1–4, 78, 80, 159–160, 185: site of, 1; gas flow through, 78, 80; surface, 78, 80; multiphase flow through, 78, 80; pressure drop at, 159–160
choking, 74–75
circular drainage area, 23
circulating pack, 129–130
combination tubing flow, 91–92
completion pressure drop equations, 134, 425, 427–428: gravel-packed well, 425, 427; open perforation well, 425, 428
component effect, 1
composite inflow performance relationship curve, 31–35
Compositional model (of pressure drop prediction), 257–258
compressibility, 44–49, 55–57: oil at isothermal conditions, 44; gas, 45, 55–57; water, 45–47; formation or rock, 46; effect of dissolved gas on water compressibility, 57; pore-volume, 47–49
compressibility factor (natural gas), 55–57
compression ratio, 1
compressor (feasibility study), 119, 121
computer programming, 2, 178–183
coning and fingering (of water and gas), 295–327
coning/channeling, 4
coning of water and gas, 295–318; homogeneous reservoir, 295–306; anisotropic reservoir, 306–312; fractured reservoir, 312–316; remedial treatments for, 316–318
continuous flow (gas well), 249
core (conventional), 3, 6, 125
Couto's procedure, 23–24, 39: for flow efficiency not equal to 1.0, 23–24
Craft and Hawkins coning method, 301
critical production rate, 295
criticality of liquid loading (gas well), 254
Cullender and Smith method (flowing bottom-hole pressure in gas well), 256

D

Darcy's law, 5–18, 425–426
dead well, 75
deliverability curve, 67
depletion stage (of solution gas-drive reservoir), 39–40
depletion (well), 3, 39–40; of solution gas-drive reservoir, 39–40
design criteria (safety valve selection), 405–406
detection of liquid loading (gas well), 254–257
deviation angle (of directionally drilled well), 80

differential pressure (effects of in gas lift), 198–199
dimensionless area (jet pump), 220
dimensionless flow rate (jet pump), 220
dimensionless head (jet pump), 220
dimensionless type curves, 63
directionally drilled well, 75–78
displacement 211–212, 233: pump, 211–212; engine, 212; beam pump, 233
diverter gas lift. *See* subsurface liquid diverter.
downhole restriction, 1
drainage area, 6–7, 10
drillstem test, 3
dry-gas-phase diagram, 250
Duns and Ros correlation, 73

E
Eckmier, 43
electric submersible pump, 245–247, 249, 292–293; gas well, 249, 292–293
electrical centrifugal pump, 185–186, 189, 199–210; submersible, 186, 189, 199–210
elevation/static component (for pipe flow), 71–72, 78
Elkins and Skov fingering method, 322–323
enhanced recovery project, 69
equation summary, 425–428
equipment scheduling (producing), 182
Ertle's equation, 62

F
Fetkovitch plot, 24, 36
Fetkovitch procedure, 36–38
Fetkovitch three- or four-point tests, 24–30
fingering of water and gas, 318–326: homogeneous reservoir, 319–320; in water drives, 320–321; anisotropic reservoir, 321–326. *See also* coning and fingering (of water and gas).
finite-capacity fractures (type curve for), 68
finite capacity (vertical fractures), 336
Flanigan correlation, 75, 78
flow-after-flow tests, 24
flow efficiency, 335
flow line, 3, 92, 94, 169, 173, 185, 197: effect of change in size, 94; horizontal ocean floor, 169, 173; restriction in, 185; effects of size in gas lift, 197
flow rate, 1–4, 32, 49, 185, 335: determination of, 3; calculation of at certain bottom-hole pressures, 32; vs. producing time, 49
flow regime, 43–50
flowing pressure gradients, 337–403
fluid property options (in pipeline design), 160
foam (used in gas well), 249, 272–280; liquid removal process, 273; unloading techniques (batch or continuous), 273–274; application selection, 274–275; generation of, 275; stability of, 275–276; surfactant types, 276–279; foaming tendency and surfactant behavior (in brine-condensate mixtures), 277; condensate (aromatic) fraction effect on foaming tendency, 277–279; brine effect on foaming tendency, 279; equipment, 279–280; chemical injection, 279; tubular goods, 279; separator, 279–280; surfactant selection, 280; instrumentation, 280; starting well flow, 280; well pressure cycling, 280; chemical treatment problems, 280
foam generation (for use in gas well), 275
foam stability, 275–276
foaming tendency factors, 277–279
formation sand consolidation, 125, 131–132: systems, 132
formation volume factor, 47, 332
four-point test plot, 24, 60–61: for gas well, 60–61
fracture capacity, 336
fracture flow capacity, 64–65
friction component (for pipe flow), 71–73
friction factor correlation, 72–73
functional node/position, 102–111
future production inflow performance relation curves, 36

G
gas availability, 175
gas condensate reservoir, 69, 250: phase diagram, 250
gas flow through choke, 80
gas holdup, 72–73, 78, 81–85: for horizontal flow, 78; in multiphase flow, 81–85
gas inflow performance relationships equations, 425–427
gas injection, 117–118, 413–415
gas lift, 1, 170, 172, 176, 191, 193, 196–197, 245–247, 281–282: system graphs, 170; performance curves, 172, 176; sensitivity analysis, 197; siphon string system, 281–282
gas-liquid ratio, 338–364, 366–403
gas locking, 3, 189
gas mole fraction, 8
gas-oil ratio, 332
gas-oil separation, 1–2. *See also* separator.
gas production, 120, 253, 417–424, 429–432: rate of, 253
gas pumping, 227, 287–293: application guidelines, 287–288; rod pumps, 288; beam pumps, 288–289; pneumatic pumps, 289–291; hydraulic rod pumps, 289–290; hydraulic jet pumps, 290–293; electric submersible pumps, 292–293
gas reservoir compositional classification, 249–250
gas velocity prediction for liquid removal (gas well), 259–261
gas well, 3–4, 118–124, 249–294, 425, 427–428: loading, 4, 123–124, 249–294; Nodal systems analysis of, 118–123
gathering system map (optimization), 183
Govier-Fogarasi model (pressure drop prediction), 259
gravel-pack design/criteria, 125–134: gravel size, 126; gravel selection, 126–127; screen slot size, 127; screen diameter, 127; screen centralizer, 127–128; well preparation, 128–129; gravel placement, 129; circulating pack, 129–130; squeeze pack, 130; squeeze-circulating pack combination, 130; slurry volume, 130; blank circulating pack, 130; fluids for, 130–131
gravel-packed well, 1–2, 124–149, 425, 427: Nodal systems analysis of, 124–149; well flow path, 133; bringing into production, 145–149
gravel placement, 130
gravel/sand packing systems, 133
gravel size, 126
gravity pack fluids, 130–131
Gray correlation (pressure drop prediction), 258–259
Gulf Coast area, 2

H
Hagedorn and Brown correlation, 73
Harrison's extension of Standing's correlation, 20–21, 335
Hasan's equation, 16–17
head per stage, 200–201
heading/slugging. *See* slugging/heading.
holdup correlation for horizontal flow, 78, 83–85
horizontal flow, 2, 75, 78–79, 173, 192, 337–364
horizontal flow line inlet pressure, 173
horizontal flowing pressure gradients, 192, 337–364
horizontal multiphase flow (in pipes), 75, 78–79
horizontal multiphase flow gradient curves, 75
horsepower requirement, 202, 206, 212, 223, 434–442
hydraulic jet pump (gas well), 249, 290–293. *See also* hydraulic pump.
hydraulic pump, 185, 189, 210–220, 245–247, 249, 289–293: power fluid systems, 210–211; tubing arrangements, 211; P/E ratio, 211; displacement, 211–212; friction, 212; pressure calculation, 212; horsepower requirement, 212; pump intake curves, 212–213; jet pump, 249, 290–293; rod pump, 289–290

hydraulic rod pump (gas well), 249, 289–290. *See also* hydraulic pump.
hydrocarbon mixture, 332

I
improvement effects on well flow rate, 92
inclined flow, 2, 75–78
inclined multiphase flow (in pipes), 75–78
infill drilling (remedial treatment for coning), 317
inflow equations, 5–50
inflow performance relationship, 3, 5–70, 90–91, 185, 191, 252–253, 333, 434: curve, 3, 5, 30, 32–70, 90–91, 252–253, 434; artificial lift, 50–63, 185, 333
inflow performance relationship (artificial lift), 50–63, 185, 333: gas well, 50–63; gas drive reservoir, 333
inflow performance relationship curve, 3, 5, 30, 32–70, 90–91, 252–253, 434: reservoir pressure below bubble-point pressure, 33–35; reservoir pressure above bubble-point pressure, 33–34; future production, 36–43; transient (oil flow), 43; transient (gas well), 61–63; fractured wells, 63–69; tight gas wells, 63, 65–69; computation of, 67–69; construction of, 90–91; gas well with liquid, 252–253; calculation of, 434
injection pressure, 198, 407–415: effect of in gas lift, 198; gradients, 407–415
injection pressure gradients, 407–415
injection well (Nodal systems analysis of), 112–118: water injection, 112–117; gas injection, 117–118
instrumentation (for foaming chemical injection), 279
intake pressure, 2, 434, 436–441
intermittent flow (gas well), 249, 262
IPR. *See* inflow performance relationship.
isochronal tests, 24

J
jet pump, 220–229, 245–247: components, 220; dimensionless area, 220; dimensionless flow rate, 220; dimensionless head, 220; efficiency, 220–222; cavitation, 221; power fluid rate and pressure, 245–247. *See also* hydraulic jet pump (gas well).
Jones, Blount, and Glaze equation, 26–28
Jones inflow performance relationship equation, 425–426

K
Kazemi, Seth, and Thomas fingering method, 322–323

L
late transient flow, 43
lift mechanism, 185. *See also* gas lift.
linear flow plot, 65
liquid flow behavior, 83–85
liquid inventory (of pipeline), 161
liquid loading (gas well), 69, 249, 251–257: prediction of criticality, 253; detection of, 254–257
liquid pounding, 189
liquid pumping, 203–205. *See also* liquid-gas pumping.
liquid-gas pumping, 205–210, 216–220, 226–229, 238–244

M
mandrel spacing (effects of in gas lift), 199
manifold position (for Nodal systems analysis), 175–177
material balance calculation, 36
mechanical pumping, 185–187, 189, 199–220, 245–247, 249, 289–293: systems, 185–187, 189; electrical centrifugal pump, 185–186, 189, 199–210; electric submersible pump, 245–247, 249, 292–293; hydraulic rod pump, 249, 289–290; hydraulic jet pump, 249, 290–293
Meyer and Gardner coning method, 299–301
molecular weight, 8
multiphase flow, 3–4, 13–15, 71–86, 257–261: in pipes, 71–86; correlations for producing gas wells, 257–261
multiphase flow correlations (for producing gas wells), 257–261: pressure drop prediction (gas condensate well), 257–259; black oil, 259; minimum gas velocity prediction for liquid removal, 259–261
multiphase flow in pipes, 71–86: vertical, 73–75; horizontal, 75, 78–79; inclined, 75–78; flow-through restrictions, 78, 80
multipoint test (plot), 60
Muskat coning method, 295
Muskat's relationship, 38

N
natural flow (gas well), 249–262: continuous flow, 249; intermittent flow, 249, 262; tubing performance, 251
Nodal analysis. *See* Nodal systems analysis.
Nodal plot, 2–3
Nodal systems analysis, 1–3, 87–184: Nodal plot, 2–3. *See also* inflow performance relationship.
node outflow pressure curve, 74
noncircular drainage area, 23

O
ocean-floor completion (Nodal systems analysis), 169–178: equipment on ocean floor, 169–170; wellhead pressure, 170–171; production analysis, 170
ocean-floor equipment (for well completion), 169–170: riser pipe, 169, 171; flow line (horizontal), 169, 173; surface platform, 170
oil formation volume factor, 6, 45
oil gravity, 332: gravity of oil, 332; gravity of gas, 332
oil inflow performance relationship equations, 425–427
oil injection (remedial treatment for coning), 318
oil production system (integrated, Nodal systems analysis), 178–183: component selection, 180; production life, 180; production modeling, 180; production spoke evaluation, 180; production cost, 180; numerical simulation of subsystems, 181–182
oil well, 142–145, 425, 427–428: gravel-packed, 142–145
oil well (gravel-packed), 142–145
open perforation well, 425, 428. *See also* perforation (well).
optimization (of production). *See* inflow performance relationship *and* Nodal systems analysis.
Orkiszewski correlation, 73
Orkiszewski method (two-phase vertical flow correlation), 405–406
Orkiszewski model, 259
outflow curve (gas well), 253

P
P/E ratio (net pump piston area/net engine piston area), 211
perforated well (Nodal systems analysis), 149–159
perforation shot density, 2, 135, 140, 145–158
perforation (well), 1–22, 90, 135, 140, 145–158: shot density, 2, 135, 140, 145–158; cleanout, 129; Nodal systems analysis, 149–159
permeability, 5–6, 10–11, 59: effect on turbulent term, 59
Petrobras method, 30
pigging characteristics (in pipeline design), 84–85, 160–161
pipe size selection, 3
pipeline design, 5, 81–85, 90, 159–169: piping system optimization, 5, 90; flow capacity, 159–169; liquid related problems, 159; pressure drop prediction, 81–82, 159; pressure gradient options, 159; choke pressure drop prediction, 159–160; fluid property options, 160; slug characteristics prediction, 160; pigging characteristics prediction, 160–161
pipeline pressure drop, 159
Pirson coning method, 299–301
Pirson fingering method, 320
pivot point method, 39–43

plunger, 233–234, 249, 262–272: beam pump, 233–234; gas lift, 249, 262–272; lift equipment, 268–272
plunger lift equipment, 268–272: solid plunger, 268; bypass plunger, 268; lubricator, 268; cycle controls, 269–270; casing, 270; tubing seating nipple, 270; standing valve, 270–271; tubing, 271
plunger lift (gas well), 249, 262, 272: cycle description, 262–264; selection of wells for application, 264–265; design, 265–268; equipment, 268–272; solid plunger, 268; bypass plunger, 268; lubricator, 268–269; cycle controls, 269–270; casing, 270; tubing seating nipple, 270; standing valve, 270–271; tubing, 271; well symptom analysis, 271–272
pneumatic pump (for gas well), 289–291
porous media, 2 *et passim*
post-fracture well testing, 63–64
power fluid systems, 210–211, 222–223, 438, 441
prefracture well testing, 63
pressure calculation (for hydraulic pump), 212
pressure discontinuity, 102
pressure drop, 64–65, 150–159, 257–259, 425, 427–428: after fracturing, 64–65; in open perforation well, 150–159; prediction (gas condensate well), 257–259; equations, 425, 427–428
pressure drop equations, 425, 427–428
pressure drop (in open perforation well), 150–159: in pipeline, 159; choke, 159–160
pressure drop prediction (gas condensate well), 257–259: compositional model, 257–258; Gray correlation, 258–259; Govier-Fogarasi model, 259
pressure gradient options (in pipeline design), 159
pressure interference (in fingering), 322
pressure loss, 2–3, 26, 81–85, 88, 174, 179. *See also* pressure drop.
pressure profile (for damaged well producing by solution gas drive), 19
pressure/rate cycling (gas well), 261–262
pressure-saturation relationship, 18
pressure traverse (for pumping system), 186–187
procedure (Nodal systems analysis), 89–183
produced sample (from formation), 125–126
producing rate, 333–334
producing zone thickness, 5–6
production cost, 180
production gradients, 417–424, 429–432
production life, 180
production modeling, 180
production optimization. *See* Nodal systems analysis.
production spoke evaluation, 180
production systems analysis. *See* Nodal systems analysis.
productive capacity (well), 5
productivity index (estimation of), 12–18, 36–37
pseudo-steady-state flow, 43
pump friction, 212
pump intake, 186, 202–203, 212–213, 223, 234–235: pressure, 186; curves, 202–203, 212–213, 223, 234–235
pump intake curves, 202–203, 212–213, 223, 234–235
pump intake pressure, 186
pump selection, 206
pump setting off bottom hole, 190–191
pumping cycle (beam pump), 233

R

radial flow, 25
radioactive tracer method (for fingering), 322
radius of drainage, 6–7
Ramey, 50, 324–326: fingering method, 324–326
Ramey fingering method, 324–326
recompletion (remedial treatment for coning), 317
remedial treatments (for coning), 317–318: infill drilling, 317; well productivity improvement, 317; recompletion, 317; stop-cocking, 318; oil injection, 318; artificial barriers, 318
reservoir component, 90
reservoir position (for Nodal systems analysis), 98–100
reservoir pressure, 6–7, 33–35, 40–41, 333–335: below bubble-point pressure (composite curves for), 33–35; envelope construction using pivot point method, 40–41
reservoir pressure below bubble-point pressure (composite curves for), 33–35
reservoir pressure envelope (construction of using pivot point method), 40–41
reservoir simulation, 5, 69
resin sand slurry (for sand control), 125, 131–132
restrictions (multiphase flow in pipes), 78, 80
rigorous solution, 175–177
riser inlet pressure, 172, 174–175
riser pipe, 169, 171–172, 174–175: inlet pressure, 172, 174–175
rod and pump data (for artificial lift), 232
rod pump (gas well), 249, 288
Ros and Gray correlation, 73
rotative gas lift system, 249, 281, 284–287: cycle description, 285; application, 285; design, 285–287
rubber sleeve core, 125

S

safety valve, 1, 3, 104–111, 185, 405–406: velocity actuated, 105–107, 109–110; pressure actuated/operated, 110–111; design criteria, 405–406; velocity type, subsurface, 405–406
sand control, 124–149: gravel pack, 125–131; design criteria, 125–131; formation sand consolidation, 131; resin sand slurry, 131–132
screen, 127–128: design for gravel pack, 127–128; centralizer, 128
screen centralizer, 128
screen design (for gravel pack), 127–128
Secenov's coefficient for methane, 46
sensitivity analysis (of gas lift system), 197
separation (gas-oil), 1–2. *See also* separator.
separator, 1–3, 92–98, 185, 197–198, 279–280: pressure, 1; equipment, 1–2; position for Nodal systems analysis, 95–98; pressure effects of in gas lift, 197–198; foam-liquid, 279–280
separator (foam-liquid), 279–280
separator position (for Nodal systems analysis), 95–98
separator pressure, 1, 197–198: effects of in gas lift, 197–198
shot density calculation, 141
sidewall core, 125
single-phase liquid flow, 5–15
siphon string gas lift system, 281–282: cycle description, 281; application, 281; design, 281–282
size (beam pump), 234
skin effect/damage, 3, 336
slotted liner, 127
slug characteristics (in pipeline design), 83–85, 160
slug flow conditions (at pipeline outlet), 83–85, 161–169, 177–178
slugging/heading, 1, 83–85, 177, 261–262
slurry volume (for gravel pack), 130
Sobocinsky and Cornelius coning method, 310–312
solubility (natural gas in water), 46
solution position/node (for Nodal systems analysis), 1, 87–89, 102: bottom hole, 89–92; wellhead, 92–94; bottom-hole/wellhead combination, 94–95; separator, 95–98; reservoir, 98–100, taper, 100–102
squeeze pack, 130
stable flow, 74
stable cone, 295
stage calculation, 435–436
stage determination, 205–206

Standing's correlation, 38–39, 44, 334–335
Standing's procedure (for flow efficiency not equal to 1.0), 18–23
Standing's work (errors from extrapolation), 19
states of flow. *See* flow regime.
static gas column, 194, 254–256: pressure, 194
stock tank, 3 *et passim*
stop-cocking (remedial treatment for coning), 318
storage effect, 336
stripper well production, 186
stroke length requirement, 442
submersible pump, 186, 189, 199–210: performance curves, 202; selection, 203
subsurface liquid diverter (for assisted gas lift system), 281–284: cycle description, 282–283; application, 283–284; design, 284
subsurface pump (beam pump), 231, 233
sucker rod, 185, 189, 231, 244–247: string for beam pump, 231; pump, 244–247
sucker rod pump, 244–247
sucker rod string (beam pump), 231
surface choke, 78, 80, 102–104: multiphase flow through, 78, 80; gas flow through, 80
surface platform, 170
surface pumping unit (beam pump), 230–231
surfactants (for foam generation), 276–280: nonionic, 276; anionic, 276; cationic, 276–277; amphoteric, 277; foaming agents, 277; condensate (aromatic) fraction effect on foaming tendency, 277–279; foaming tendency and behavior in brine-condensate mixtures, 277; dispersion in well fluids, 278; starting well flow, 280; selection, 280

T
tandem square-foot buildup plot, 66
taper position (for Nodal systems analysis), 100–102
tapered string, 100–102
three- or four-point tests, 24–30
tight gas well performance, 63, 65–69
time to pseudo-steady-state equation, 425, 427
transient flow, 43
transient period equations, 425, 427
troubleshooting (gas lift well), 271–272
tubing, 2–4, 68–69, 73–74, 91, 93–94, 121–123, 135, 137, 185–187, 189–200, 203–204, 206–210, 213–220, 223–229, 234–247, 251–252, 254, 260–261. *See also* tubing intake/node outflow curves, tubing intake pressure, tubing performance, tubing size, *and* tubing string.
tubing intake curve. *See* tubing intake/node outflow curves.
tubing intake/node outflow curves, 3, 73–74, 135, 137, 185–187, 189–200, 203–204, 206–210, 213–220, 223–229, 234–247: pressure, 185–187, 203–204; preparation of, 189–200, 203–204, 206–210, 213–220, 223–229, 234–244
tubing intake pressure, 185–187, 203–204
tubing performance, 68–69, 251–252, 260–261: curve, 69, 252, 260–261; gas well, 251, 260–261; gas well with liquid, 252
tubing performance curve, 69, 252, 260–261: gas well with liquid, 252; gas well, 260–261
tubing size, 1, 4, 121–123, 197–198, 254: selection of, 1, 4, 121–122; effects of, 121–123; effects of in gas lift, 197–198; effects on gas well natural flow, 254
tubing string, 91, 94, 185: flow, 91, 94; flow restriction, 185
tubular goods (for foaming chemical injection), 279
turbulence term, 58–59
turbulent flow, 8–9, 11
two-phase flow. *See* multiphase flow.
type curve (fingering in anisotropic reservoir), 324
type curve matching, 63–64, 67

U
Uhri and Blount procedure, 39–43
unstable cone, 295

V
van Meurs and van der Poel fingering method, 320–321
vertical flowing gas gradient, 120–122, 137
vertical flowing gas injection gradients, 413–415
vertical flowing gas production gradients, 417–424, 429–432
vertical flowing pressure gradients, 188, 195, 365–403, 433
vertical injection pressure gradients, 407–412
vertical multiphase flow (in pipes), 73–75
vertical pressure traverse, 80
viscosity, 6, 52–54, 116, 274, 330–331: natural gas, 52–54; water, 116; foam, 274; gas-free crude oil, 6, 330; gas saturated oil, 6, 331
Vogel correlation, 92
Vogel procedure, 37–38
Vogel test data, 425–426
Vogel's equation, 13–14, 30–31
volatile oils (gas well), 250–251
volume factor, 190

W
Warren and Root fingering model, 323
water cut (effects of in gas lift), 198
water injection well, 112–117
well capability, 3
well completion technique, 1–3
well file, 2
well performance, 4
well preparation (for gravel pack), 128–129
well pressure cycling (for foam use in gas wells), 280
well productivity, 3, 317: improvement (remedial treatment for coning), 317
well productivity improvement (remedial treatment for coning), 317
well selection (for plunger lift application), 264–265
well test interpretation, 26–28
wellbore pressure, 336
wellbore restriction (of flow), 25
wellhead position (for Nodal systems analysis in gas lift), 92–94, 193, 196
wellhead pressure, 1–2, 77, 122, 171, 253: flowing well, 77; effects of, 122, 171; reduction of, 253
wellhead separation, 1–2. *See also* separator.